# THE METALLIFEROUS SEDIMENTS OF THE ATLANTIS II DEEP (RED SEA)

Tea Elisa Laurila

Thesis submitted to the
Faculty of Graduate and Postdoctoral Studies
in partial fulfillment of the requirements
for the Doctorate in Philosophy degree in Earth Sciences

Department of Earth Sciences
Faculty of Science
University of Ottawa

© Tea Elisa Laurila, Ottawa, Canada, 2015

## Abstract

The Atlantis II Deep is a location of modern submarine hydrothermal activity along the slowly spreading Red Sea rift axis. Venting of high-temperature hydrothermal fluids, similar to those associated with black smokers, takes place in a brine pool and has led to the accumulation of 90 Mt (dry, salt free) of stratiform, metalliferous sediment. The conditions of mineralization are unique in the modern oceans, but have been widely suggested as a possible analog of some important ancient stratiform base metal ore deposits. This study shows that many of the proposed genetic models for these ancient deposits may be highly simplified and do not take into account rapid diagenetic transformations, widespread non-equilibrium processes, and many other aspects of metal deposition.

Sediment cores of the Atlantis II muds were last studied more than 30 years ago. High-resolution sampling and careful re-examination of the mineralogy and geochemistry of the sediments, using modern analytical techniques has significantly improved the understanding of the different processes responsible for the formation of the finely layered metallifeous sediments. The geochemistry of the individual layers is controlled by highly variable detrital, hydrogenic and hydrothermal input. Primary depositional pathways from the brine pool are the main control on basin-wide metal distribution (e.g., increasing Cu/Zn away from the vents) including variable enrichment in trace metals via scavenging from the brine pool and from the enriched pore waters. Cu and Zn have been deposited not only as sulfides but also with poorly crystalline Si-Fe-(oxy)hydroxides. A significant proportion of the original non-sulfide Cu and Zn are diagenetically transformed into sulfides, but also

carbonates and clays, in large part reflecting sulfide deficient pore waters. Negative $\delta^{34}S$ values, previously unrecognized in the sulfide- and metal-rich units, indicate a source of bacteriogenic sulfide. Syn-diagenetic processes also appear to have been responsible for the sharp laminations in the sediments, as well as distinctive zoning of carbonate and clay minerals around the vent source. The early diagenetic transformations observed in the Atlantis II Deep may not be preserved in the ancient rock record but nevertheless have important implications for metal deposition in some of the world's largest and richest base metal ore deposits.

**Résumé**

La zone hydrothermale active Atlantis II Deep se situe le long de l'axe du rift de la Mer Rouge. La remontée de fluides hydrothermaux de haute température associés aux sources hydrothermales de type "fumeur noir" dans le bassin de saumures a conduit à l'accumulation progressive de 90 mégatonnes (sèches, sans sel) de sédiments stratifiés métallifères. En dépit de leur caractère unique dans les océans actuels, les sédiments métallifères d'Atlantis II Deep sont un analogue possible à plusieurs anciens dépôts stratiformes de minerai de métaux communs. Notre étude démontre que les modèles génétiques proposés pour ces anciens dépôts peuvent être largement simplifiés et qu'ils ne prennent pas en compte les transformations diagénétiques rapides, les phénomènes transitoires diffus, ainsi que de nombreux autres aspects des processus de dépôts métalliques.

Des échantillons de boue d'Atlantis II ont été étudiés il y a plus de 30 ans. Un échantillonnage de haute résolution combiné à un réexamen détaillé de la minéralogie et de la géochimie des sédiments en recourant à des techniques d'analyse modernes a permis de considérablement améliorer la compréhension des différents processus responsables de la formation des sédiments métallifères finement stratifiés. La géochimie de chaque strate est ainsi contrôlée par des paramètres détritiques, hydrogéniques et hydrothermaux très variables. Les processus primaires de dépôts dans le bassin de saumures constituent la principale cause de la présence de métaux à l'échelle du bassin (e.g. une augmentation du rapport Cu/Zn avec la distance aux zones de diffusion). Ils incluent un enrichissement variable en métaux traces par adsorption dans le bassin de saumures et les eaux interstitielles.

Le cuivre et le zinc ne se déposent pas uniquement sous forme de sulfures mais également d'(oxy)hydroxydes Si-Fe faiblement cristallisés. Une part importante de ces (oxy)hydroxydes sont transformés en sulfures de manière diagénétique mais également en carbonates et argiles, traduisant la présence d'eaux interstitielles pauvres en sulfures. Les valeurs négatives de $\delta^{34}S$, non observées initialement dans les échantillons riches en sulfures et en métaux révèlent une source de sulfures bactériogéniques. Des processus syn-diagénétiques semblent également jouer un rôle dans le laminage fin des sédiments ainsi que dans la zonation des carbonates et des minéraux argileux autour de la zone de diffusion. Les transformations diagénétiques précoces observées à Atlantis II Deep ne sont sans doute pas

préservées dans les roches anciennes mais conservent toutefois une implication importante dans les dépôts de certains des plus grands et plus riches gisements de métaux au monde.


## Acknowledgements

This thesis is a result of a 5-year journey that has physically taken me around the world, given me opportunity to meet fantastic people and, most importantly, taught me a lot about myself. In retrospect, I can only say that it has been the greatest years of my life so far and I am grateful for the people who shared the good times with me and helped me through the downtimes. I have learned to love science, how to establish questions, solve problems and make statements, but also perseverance, how to keep on working hard regardless of feeling inadequate, frustrated or discouraged, and patience; sometimes it just takes “as long as it takes” , instead of how long I want it to take.

Firstly I want to acknowledge my supervisor Mark Hannington for bearing with me and my occasional breakdowns and for patiently red-inking my scribbles, one pen after another. Your trust in me carried me over the times, when my trust in myself was somewhere sub-zero. Your amazing editorial skills made my random thoughts, triangle diagrams and “yeah buts” into a piece of work that I am very proud of; I hope you can be as well. Especially I want to thank you for encouraging me even with the most insane ideas. You did well to hide your doubts and let me to crash to the wall all on my own after surveying the literature in an attempt to prove myself right. Those times were lots of work, but full of joy and passion about my very own “eureka” moments. Occasionally they also paid off scientifically.

The rest of the acknowledgements go to my family, co-workers and friends. Without your endless support I would not have been able to accomplish any of this. Mum, Dad, Teemu and Colin, thank you for standing right there by me; it never felt like there is a whole ocean between us even if this was the case most of the time. Thank you for being the perfect, even if innocent, target to unload my worries and grumpiness and for bearing with me while helping to extinguish urgent fires I managed to light up with my ignorance regarding many practical necessities. Mum and Dad, your unconditional love for me is the foundation for my courage to explore the world following the emerging opportunities, such as this, and my capability to ignore the upcoming face-plants. Kiitos myös Terhille, Essille, Piialle, Hennalle, Ollille, Jampalle, Hannalle, Artolle, Ilkalle, Juhalan, Lehtimäen ja Fagerlundin porukoille, ja monille muille Suomen taustavaikuttajille!

Thank you Sven Petersen for help with the science, lessons for climbing in Kernlager, and most importantly for being the nice person you are. Big thanks to Isobel Yeo for being my family and mental support in Kiel, as well as Thor, Nico, Froukje, Tom, Dominik, and the whole FB4 crowd for all the scientific and non-scientific communication that made staying in Kiel pleasurable. Jeff Hedenquist is acknowledged for being the inspiration to start a PhD in economic geology. Scientific discussion with him, Jim Franklin, Paul Spry, Thomas Monecke, Wayne Goodfellow, Andrey Bekker and many others greatly helped me to understand what is, or rather could be, the location of the Atlantis II Deep in the world of ancient deposits. Those discussions were the fuel to keep me reading and plotting. I also want to thank the people at the University of Turku, especially Krister Sundblad, Jeremy Woodard and Timo Kilpeläinen. Dieter Garbe-Schönberg and Matt Leybourne are thanked for co-operation with laboratory work.

Merci bien, Florent Szitkar et Mélanie Cousineau, pour la traduction de résumé. Mélanie also for help with sulfur extractions, and for the chats over a cup of coffee that kept me a human being in the midst of cumulating insanity. At the university of Ottawa, special thanks go to Fritz and Fabio, you are the best, I am glad we ate all those chicken wings. Huge thanks to Harry, Micha, Zuza, Hayden, Lilian, Agata, Sophia and Ed for doing random stuff with me during the past 5 years; hopefully to be continued into the future. Thanks to the Detonators, and all my swing dancing friends for being awesome. Thank you pastor Paul Donison for help in my search for truth, righteousness and peace in the world, and for Lisa Marie and Brian for encouragement and prayers.

## Table of Contents


**Chapter 1**
**Introduction** 1
1. Motivation and Approach 2
2. Geological Background 6
*2.1 The brine pool* 8
*2.2 Precipitation in the brine pool* 14
*2.3 Sedimentation and sediment stratigraphy* 16
3. Contents of the Thesis 22
4. Contributions from Others 28
References 30
Figure Captions 36
Tables 38
Figures 39

**Chapter 2**
**A New Look at the Mineralogy of the Atlantis II Deep Metalliferous Sediments** 42
1. Introduction 43
2. Sediment Stratigraphy 46
3. Detailed Mineralogy of the Atlantis II Sediments: Previous Work 48
4. Sampling and Methodology 58
5. Results 62
*5.1 Detrital minerals* 65
*5.2 Authigenic minerals* 67
*5.3 Normative mineralogy* 78
*5.4 Sequential leaching experiments* 82
*5.5 Effects of core storage* 87
6. Discussion and Conclusions 90
*6.1 Formation of Fe and Mn minerals* 91
*6.2 Fate of surface-active particles* 93
*6.3 Primary sulfide and sulfate deposition* 94
*6.4 Silica, clays and hydrothermal carbonates* 96
*6.5 Effects of diagenesis and hydrothermal alteration* 99
*6.6 Implications for ore geology* 100
References 104
Figure Captions 113
Tables 127
Figures 143
Appendices 160

**Chapter 3**
**Trace Metal Distribution in the Atlantis II Deep Sediments** 172
1. Introduction 173
*1.1 Geologic setting and depositional environment* 174
*1.2 Sediment stratigraphy* 178
2. Sampling and Methods 181
3. Results 183
*3.1 Classification of sample types* 183
*3.2 Sulfur* 185
*3.3 Non-ferrous base metals* 186
*3.4 Trace metals* 186
*3.5 Proximal versus distal enrichments and depletions* 189
4. Discussion 191
*4.1 Distribution of reduced sulfur* 191
*4.2 Importance of non-sulfidic components* 192
*4.3 Possible controls on Cu/Zn ratios* 194
*4.4 Pathways of enrichment of trace metals* 196
*4.5 Links to the evolution of the Deep* 200
*4.6 Mass balances of metals* 202
5. Summary and Conclusions 204
References 207
Figure Captions 214
Tables 225
Figures 233
Appendices 248

**Chapter 4**
**Early Depositional History of Metalliferous Sediments in the Atlantis II Deep: Evidence from Rare Earth Element Geochemistry** 259
1. Introduction 260
*1.1 Geological setting* 262
*1.2 Depositional environment* 263
*1.3 Stratigraphy of the Atlantis II sediments* 266
2. Sampling and Methods 269
3. Results 272
*3.1 REE geochemistry of the stratigraphic units* 275
*3.2 REE geochemistry of the different layer types* 277

4. Discussion 280
*4.1 Sources of REE in the Atlantis II sediments* 280
*4.2 Factors affecting the concentrations of REE in the Atlantis II sediments* 282
*4.3 Variations in sources of REE during the evolution of the brine pool* 285
*4.4 Comparison with other modern and ancient hydrothermal systems* 287
5. Conclusions 290
References 292
Figure Captions 299
Tables 304
Figures 311
Appendices 321

**Chapter 5**
**Sources of Reduced Sulfur and the Formation of Sulfides in the Atlantis II Sediments: Evidence from Sulfur Isotope Data** 327
1. Introduction 328
2. Depositional Environments 329
*2.1 Characteristics of the brine pool* 330
*2.2 Pathways of sulfur and metal deposition* 331
*2.3 Diagenesis* 334
*2.4 Sulfate precipitation* 335
3. Methodology 336
*3.1 Sampling and geochemical analysis* 336
*3.2 Mineralogy* 337
*3.3 Sulfur isotope analyses* 339
4. Results 341
5. Discussion 345
*5.1 Sulfides* 345
*5.2 Anhydrite and barite* 347
6. Conclusions 350
References 352
Figure Captions 357
Tables 363
Figures 367

**Chapter 6**
**Comparison of the Atlantis II Deep to Ancient Stratiform Ore Deposits** 376
1. Introduction 377
2. Summary: Setting and Conditions of Deposition in the Atlantis II Deep 377
*2.1 Tectonic setting* 377
*2.2 Depositional environment and conditions of mineralization* 378
3. The Geological Record of Other Stratiform Base-Metal Ore Deposits 382
*3.1 Volcanogenic massive sulfide deposits* 385
*3.2 Sedimentary exhalative deposits* 388
*3.3 Atypical stratiform base metal deposits* 391
4. Comparisons with the Atlantis II Deep 394
*4.1 Geologic settings and sizes of deposits* 394
*4.2 Metal sources and hydrothermal deposition* 397
*4.3 Origins of the brines* 400
*4.4 Role of anoxia and euxinia* 401
*4.5 Fate of metals in the brine pool environment* 404
*4.6 Origin of banding in laminated ores* 406
5. Conclusions 407
References 411
Figure Captions 423
Tables 427
Figures 431

**Chapter 7**
**Conclusions** 437

**Appendices:**
Appendix A: Compilation of MESEDA data 445
Appendix B: Sampling for this study 448
Appendix C: Total chemistry for all samples and PCA 568
Appendix D: Normative mineralogy 581
Appendix E: Mineral characterization and mineral chemistry 583
Appendix F: XRF-core scans 639

# CHAPTER 1

## INTRODUCTION

## 1. Motivation and Approach

Hydrothermal activity is an important process influencing the composition of the Earth's crust, hydrosphere and atmosphere (Ohmoto et al., 2006; Lyons et al., 2006; Bekker et al., 2010). Near the surface, it is commonly caused by magmatic heating of water that causes mobilization and deposition of metals, such as at hydrothermal vent sites on the ocean floor (Von Damm, 1990; Rona and Scott, 1993). In some circumstances, hydrothermal exhalation may lead to formation of significant mineral deposits. These processes may be observed directly on the modern seafloor greatly improving the understanding of the formation of volcanogenic massive sulfide (VMS) deposits and other exhalative mineralization associated with volcanic vents (Ohmoto, 1996; Hannington et al., 1995; Hannington, 2014). However, modern analogs of sedimentary exhalative (SEDEX) massive sulfide deposits have not been widely recognized despite the importance of this class of deposit in the geological record (Goodfellow and Lydon, 2007). The metalliferous sediments in the Atlantis II Deep, situated on the slowly spreading axis of the Red Sea rift, are the only well-documented example of exhalative sedimentary ores on the modern seafloor, making it a unique natural laboratory for the study of this type of deposit. The style of mineralization in the Atlantis II Deep, which involves deposition mainly from a highly metal-enriched brine pool, is widely considered to be an analog for many ancient sediment-hosted base metal ores (Large et al., 1996; Peter and Goodfellow, 1996; Kato et al., 1998; Johnson and Skinner, 2003; Grenne and Slack, 2005; Huston et al., 2006; Tornos et al., 2008). However, most studies of the metalliferous sediments in the Atlantis II Deep were published more than 30 years ago (e.g., Degens and Ross, 1969; Bäcker and Richter, 1973;

Shanks and Bischoff, 1980, Pottorf and Barnes, 1983). Since then, our understanding of processes involved in seafloor hydrothermal activity, including fluid compositions, aspects of chemical sedimentation, and biological interactions, have greatly improved. At the same time, major advances have been made in analytical techniques for characterizing the mineralogy and geochemistry of the associated mineral deposits, including dramatically improved detection limits, a more comprehensive suite of elements, smaller sample sizes and methods to deal with the high salt contents of the sediments that necessitated washing of the cores in earlier studies.

The metalliferous sediments of the Atlantis II Deep constitute by far the largest "ore" deposit known on the modern seafloor, measuring more than 90 Mt (2.1% Zn, 0.5% Cu and significant amount of precious metals, 41 ppm Ag and 0.5 ppm Au: Guney et al., 1988; Bertram et al., 2011), and the first place where a serious attempt at commercial recovery of the valuable metals was conducted back in 1979 in form of a pre-pilot mining test (Amann, 1985; Guney et al., 1988). The deposit comprises a ~20 m-thick succession of metalliferous sediment, covering an area of about 70 $km^2$ and overlain by a dominantly anoxic, stratified brine pool. Metals precipitate in the anoxic part of the brine pool as sulfides, forming a laterally extensive plume, and as oxide particles in higher levels of the brine pool. Both types of particles "rain down" over large areas forming the metalliferous sediments of the Deep. The chemically and physically distinct layers and laminae are typical of number of stratiform sediment-hosted base metal ore deposits, including SEDEX ores and banded iron formations (BIF). The dynamics of the sedimentation process are poorly understood in

ancient deposits and best studied in an active hydrothermal system − the main goal of the research presented in this thesis.

In 2010, a long-forgotten archive of more than 400 of the original cores from the Atlantis II Deep was discovered in the repository of the Helmholtz Centre for Ocean Research in Kiel, Germany (GEOMAR). This presented the unique opportunity to undertake a modern study of the only known example of active metal deposition in a brine pool environment and the type locality for sedimentary-exhalative ore formation. At the same time, a three-leg expedition to the Red Sea was organized during 2011 with the German research vessel *RV Poseidon* as part of a co-operative project between GEOMAR and the King Abdullah University in Jeddah, Saudi-Arabia. I was fortunate to get on opportunity to visit this unique area of the global ocean by participating on the first leg during which new bathymetric data was collected, shedding light on the transition from rifting to seafloor spreading in the Red Sea (Augustin et al., 2014).

Among the major questions addressed in this study is the origin of the fine layering of the chemical sediments, which are deposited from what has been widely considered to be a compositionally uniform brine pool. The origin of mineralogically and chemically distinct laminae during diagenesis is examined but also new evidence for rapid changes in the composition of the brine pool and primary precipitation over the 15,000-year history of sedimentation in the Deep. Among those variations is the deposition of metals (Fe, Zn, and Cu) both in sulfide minerals and in non-sulfidic particles, mainly Si- and Fe-rich

(oxy)hydroxides that scavenge metals as they are deposited. This study is the first to demonstrate the importance of non-sulfide deposition of metals in the sediments of the Atlantis II Deep and possibly in other ancient mineralized basins where metals>$H_2S$. A problem in past studies is that evidence for primary non-sulfide deposition of metals, is almost totally lost within the first few meters of burial (or <5000 years), where metals are incorporated by diagenetic sulfide. Therefore, preservation of this potentially important step in ore formation is limited in the rock record. I also examine the origin of metal zoning with respect to proximity to known or inferred vent sites in the Atlantis II Deep. This important aspect of seafloor mineralization is a key tool in mineral exploration, but it is apparent from the study of the Atlantis II cores that not all of the factors influencing metal zonation in a brine pool setting are properly understood. In particular, I consider how evolving pore water composition has a dramatic effect on the variation of trace metals with depth in the sediment, with proximity to the vents source(s), and at the basin scale. The input of sediment from different sources also is examined using high-precision REE geochemistry, linking the major changes in basin history to the variations in trace metal input to give insights to the variation in trace metals recorded in ancient stratiform brine-pool type ore deposits.

Among the challenges in early studies of the Atlantis II cores was the scale of the sampling, which typically combined many different layer types into much thicker units, thus losing the fine resolution necessary to understand the depositional processes. This study introduced an entirely new sampling protocol aimed specifically at the origins of the fine layering. I

paid particular attention to the problems of core storage, using novel sequential leach techniques to establish the mineralogical siting (primary versus secondary) of nearly the full suite of elements analyzed. Prior to this study, fewer than 600 multielement chemical analyses have been published in the peer-reviewed literature in 45 years. Only a few dozen cores have been sampled in detail, and in almost all cases fewer than 20 elements were analyzed. Some key elements, such as Sb and Hg, were analyzed in only a handful of samples; for many elements, virtually no data have been published (Be, Bi, Br, Cs, F, Hf, In, Li, Nb, Rb, Sc, Se, Sn, Ta, Te, Th, Tl, U, W, Y, the PGEs plus Re and Os, and high precision REE). The analyses, which include results for 67 elements, are now the most complete for any sample suite from the AII Deep.

## 2. Geological Background

The Red Sea is a ~2000-km long (17-28°N) nascent ocean basin created by wedge-like extension between the Arabian and African continental plates. It has evolved from early continental breakup (presently happening north of ~25°N, where spreading rates are ~0.5 cm/year), to ocean spreading, which is most evolved in the South where spreading rates are ~1 cm/year faster (Cochran and Martinez, 1988). The basin is 250-450 km wide and characterized by a shallow and wide main trough with a deep and narrow segmented axial trough in the middle, where new tholeiitic basalts are extruding (Cochran, 1983). The Atlantis II Deep is one of the main segments of the axial trough at latitude (~21°N) where the spreading rate is ~1.1 cm/year (Cochran and Martinez, 1988). Based on different interpretation of geophysical data (seismic, gravity and magnetic surveys), the estimates for

beginning of ocean spreading in the Red Sea have varied from ~5 Ma (e.g., Cochran, 2005) to >10 Ma (Izzeldin, 1987). More recently, Augustin et al. (2014) suggested that spreading started at 8 Ma and that the rifting to spreading transition likely evolved from initial rifting by segment initiation followed by rapid propagation (Taylor et al., 1995).

Altogether there are 26 deeps in the Red Sea rift valley (Scholten et al., 2000; Figure 1.1.). Some deeps are floored by basalts, some by evaporites; some have brine at the bottom, others do not. Metalliferous sediments and even sulfide-rich chimneys (Kebrit Deep: Blum and Puchelt, 1991) have been found in some basins, whereas others have no mineralization (Gurvich, 2006). The configurations of the deeps are mainly determined by the local tectonics and have developed independently from each other and in unique ways (Pierret et al., 2001). For example, some deeps have been covered by brine since the time of their formation; others have periodically drained due to tectonic activity. Some brine pools formed from cold brine sourced only from the evaporites; others are products of hydrothermal circulation. The large metal endowment of the Atlantis II Deep is due to the presence of a well-developed brine pool at this site for at least 15,000 years, punctuated by at least two episodes of high-temperature hydrothermal venting from ~11.7 to ~8.6 ka and ~5.9 ka to present (Gurvich, 2006 and references therein).

The Atlantis II Deep is by far the most metal enriched of all the deeps and contains the hottest brine. It is about 5 km wide and 14 km long and surrounded by steep bathymetric barriers that confine the sediment and brine to one large basin and four sub-basins (Figures

1.1 and 1.2). It is floored by basalts, but Miocene evaporites that are abundant in the Red Sea sedimentary strata outcrop at the flanks. The depth is greatest in the Southwest Basin (~2200 m), where the current hydrothermal venting is taking place. The well laminated metalliferous sediments at the bottom of the basin have been interpreted to indicate that sedimentation happens mainly as "rainout" from the brine pool (Shanks and Bischoff, 1977, 1980). Epigenetic features (Zierenberg and Shanks, 1983) are found in the sediments in the Southwest Basin and have been considered among the best evidence for the location of the vent sites, but are of minor importance in terms of the total volume of mineralized material in the basin. Relevant details of the geological background are provided in each of the chapters of this thesis. An overview of the properties of the brine pool, the different sediment types, the sedimentary stratigraphy, and the evolution of the Deep is provided in this Chapter.

**2.1 The brine pool**

Although there has been little recent research on the metalliferous sediments, the brine pool has been well studied. The stratified brine pool has a thickness of ~150 m, including ~100 m of anoxic and hot (~70°C) Lower Brine and ~50 m of progressively more seawater-like Upper Brine. A ~100 m "transitional layer" overlies the brine pool (Swift et al., 2012). The current brine pool consists of six layers with different temperatures and salinities resulting from double-diffusive convection of heat and salt (Anschutz et al., 1998). Salt diffuses through the interfaces at a slower rate than heat, thus creating homogenous convection cells within the brine pool. The lowermost brine (Lower Brine) has a volume of

~4 $km^3$ and is the most saline (~28 wt.% NaCl), anoxic and devoid of reduced sulfur (Anschutz et al., 1998). The temperature of the lower brine increased by 12°C during the last ~40 years and was 68.3°C when last measured in 2008 (Swift et al., 2012). This Lower Brine has a mean thickness of ~76 m (Anschutz et al., 1998) but reaches ~135 m at the deepest parts in the Southwest Basin. The Upper Brine consists of 2-5 convective layers (according to different authors and at different times in the past 30-40 years). These layers are progressively cooler, more oxidized and less saline with proximity to the overlying seawater, and they have a temperature from~57 to 43°C (Swift et al., 2012).

The compositions of individual layers of brine are relatively uniform throughout the basin, although temporal variations in the concentrations of metal are recognized in different parts of the Atlantis II Deep (Hartmann, 1985). During high stands of the Lower Brine, it may "spill over" barriers created by bottom topography and flow into distal areas such as the North Basin of the Atlantis II Deep, but also into the Chain A and B and Discovery Deeps. The latter are situated south of the Atlantis II Deep at the same water depth (~2200 m), but they are isolated from it by barriers reaching to a minimum depth of ~1950 m. At present, the surface of the Lower Brine is situated below this depth and therefore contained entirely within the Atlantis II Deep. During formation of the first sulfide-rich metalliferous sediment (SU1, see below), the Lower Brine rose to 260 m above the seafloor; during formation of SU2 the brine level reached 210 m above the bottom of the Southwest Basin (Bäcker and Richter, 1973).

The current Lower Brine is enriched in Na, K, Ca and Cl, which are mainly leached from evaporites, and metals (e.g., ~65 ppm Fe, 90 ppm Mn, 5 ppm Zn: Anschutz et al., 2000), which are mainly from deep hydrothermal circulation into the basement basalts. The brine is depleted in Mg, $SO_4^{2-}$, I, $O_2$, F and $NO_3$, compared to seawater, and deficient in $H_2S$, although the presence of $H_2S$ has been inferred from blackening of brass messengers (Miller et al., 1966). Sulfide also has been found in the Lower Brine in particulate form (Hartmann, 1985). Shanks and Bischoff (1977) attributed the low concentrations of reduced sulfur to oxidation during recovery of the sampling device. Sulfate is present at high concentrations in the whole brine pool (~850 ppm in the Lower Brine: Anschutz et al., 2000), with increasing concentration towards the Red Sea Deep Water (2960 ppm $SO_4$: Bäcker and Schoell, 1972). Sulfate-reducing bacteria have been found in the Upper Brine and in particular at the chemocline overlying the sterile Lower Brine (Trüper, 1969; Fiala et al., 1990).

Measured concentrations of the major elements (Fe, Mn and Si) show little temporal variation in the Lower brine, whereas the minor elements (e.g., Cu and Co) have changed significantly. Hartmann (1985) studied the temporal variation in the composition of the brine pool at various times between 1966 and 1977. Copper concentrations varied more than two orders of magnitude, whereas Zn and Fe concentrations showed almost no variation. However, longer term variations in the chemistry of the brine pool can be inferred from details of the mineralogy and geochemistry of the metalliferous sediments

presented in this thesis including major episodes of euxinia, anoxia (low $H_2S$) and sub-oxic conditions in the Lower Brine.

Current hydrothermal input is thought to be localized mainly within the central part of the Southwest Basin as indicated by the chemistry of the brine pool (Hartmann, 1973) and sedimentary pore water (Henricks et al., 1969; Anschutz et al., 2000), the presence of epigenetic features (e.g., anhydrite veining in sediment cores: Zierenberg and Shanks, 1983) and the bulk compositions of the sediment (Appendix A.3; see also Bertram et al., 2011). However, the exact location(s) of the present-day hydrothermal venting are not known. At the beginning of the hydrothermal venting (~15,000 years ago: Hackett and Bischoff, 1973; Shanks and Bischoff, 1980), the location of the hydrothermal vents is thought to have been in the northeast, shifting to the Southwest Basin during formation of unit CO at ~6 to 8 Ma ago (Bäcker and Richter, 1973)

The chemical and isotopic compositions of the brine(s) reflect different sources of elements, including seawater (i.e., elements transported into the Deep by surface-active particles via redox cycling at the chemoclines), non-hydrothermal brines leached from the evaporites and shales in the surrounding Red Sea sedimentary strata, and hydrothermal venting (Schoell and Faber, 1978; Dupre et al., 1988; Anschutz et al., 1995; Pierret et al., 2001; Figure 1.2). $CaCO_3$ is undersaturated in the anoxic brine (with pH ~5.5; Shanks and Bischoff, 1977), which results in dissolution of biogenic pelagic detritus entering the brine pool. As a result, the Lower Brine is highly enriched in Ca. In contrast, biogenic silica and

detrital siliciclastic components are rather insoluble in the brines. Nevertheless, the Lower Brine has about two orders of magnitude higher silica than the Red Sea Deep Water and pore water has a Si concentration about an order of magnitude higher than the Red Sea Deep Water (Anschutz and Blanc, 1995a). Silica is thought to have been mainly introduced into the Lower Brine by hydrothermal venting, whereupon it is diffused to seawater or deposited in the sediment (Anschutz and Blanc, 1995a).

Hydrothermal venting is by far the most important source of elements in the current brine pool. Various attempts have been made to reconstruct the composition of the source fluid based on isotopic studies as well as mass balance (i.e., variation in the temperature and dissolved solid contents in the different brine layers: Blanc et al., 1995; Anschutz and Blanc, 1996). However, the exact composition of the hydrothermal fluid is still not known. It is clearly influenced by interaction with both the surrounding Miocene evaporites and the basaltic basement rocks (e.g., Dupré et al., 1988; Anschutz et al., 1995). Fluid inclusion data in veins indicate that the hydrothermal fluids have reached black smoker temperatures (up to 403°C: Ramboz et al., 1988), high salinities (up to 32 wt.% NaCl) and presumably also high metal contents during circulation through the surrounding sediments and underlying mid-ocean ridge basalts (Oudin et al., 1984; Ramboz et al., 1988; Missack et al., 1989). The hydrothermal fluid vents into the Deep at ~100-200°C (Shanks and Bischoff, 1977; Pottorf and Barnes, 1983, and ref. therein; Cole, 1988), but the metal concentrations of these lower temperature vent fluids are presumably still high because of the high salinities (Shanks and Bischoff, 1977; Pottorf and Barnes, 1983). The metal ratios in the metalliferous sediment

are very similar to those of black smoker fluids at mid-ocean ridges (Fe:Zn:Cu = ~10:1:0.3: Bischoff and Manheim, 1969; Von Damm, 1990), although the metal-to-sulfur ratios are much higher.

Shanks and Bischoff (1980) identified an organic carbon source that may be related to sulfate-reducing bacteria living the Upper Brines (Trüper, 1969; Fiala et al., 1990). Schmidt et al. (2003) studied the stable isotopic compositions of hydrocarbons dissolved in the brines and concluded that higher hydrocarbons are produced by thermal degradation of organic matter but methane is of abiogenic origin (most likely secondary high temperature processes, as in black smokers). However, the high methane contents (up to >6000 nmol/l) in the brine are due to efficient trapping and accumulation in the stratified brine pool, rather than an unusually large mass flux from the hydrothermal vents, although boiling and phase separation also likely influenced the hydrocarbon gas content of the brines (Schmidt et al., 2003). Schoell and Stahl (1972) determined that the Lower Brine has a uniform $\delta^{13}C$ (-7.0 ± 0.5‰), distinctly different from Red Sea Deep Water (-1.5‰). They interpreted the low $\delta^{13}C$ in the Lower Brine to represent juvenile mantle-derived carbon and the higher values in the Upper Brine layers as mixtures of the two end-members. However, Anschutz et al. (1998) concluded that it is not possible to explain the observed salinity and temperature changes in the Atlantis II brine pool during 1966-1992 by purely diffusive processes or simple mixing of the Lower Brine with the Upper Brine. Oxygen and hydrogen isotopes also do not fit to a mixing line with salinity (Blanc et al., 1995). Anschutz et al. (1998) suggested that cold brines entered the Deep from above and supplied most of the

salt in the Upper Brines, with little influence on the Lower Brine. These cold brines also have been suggested as a source of some of the metals in the Atlantis II Deep (especially Zn as it is abundant in the Red Sea black shales: Pottorf and Barnes, 1983), but there is little evidence to properly assess this.

**2.2 Precipitation in the brine pool**

The presence of the stratified brine pool prevents most elements, and most importantly metals from escaping the basin, and they are efficiently deposited in the sediments at the bottom of the Deep (Bignell et al., 1976; Gurvich, 2006). This is in contrast to mid-ocean ridge hydrothermal systems, where most of the metals (>90%: Converse et al., 1984) are dispersed to the open ocean with minor deposition from hydrothermal plumes (Baker et al., 1985). Minor elements have particularly complex patterns of enrichment and depletion in the sediments, reflecting a range of depositional processes that are the focus of this study.

Sulfides and (oxy)hydroxides are the main authigenic components in the sediments, and they precipitate in the current brine pool in a number of ways. During periods of anoxic brine, such as the present-day, sulfides precipitate from the hydrothermal fluids before and immediately after venting into the Lower Brine. Sulfides are mainly deposited proximal to the vent source but also as finer particles further away from the vents. Large sulfide grains predominate in the area close to the inferred vents, whereas smaller and poorly crystalline sulfides are typical in vent distal sediments; the latter are thought to deposit mainly as fall-out from a laterally extensive neutrally buoyant plume forming in the Lower Brine

(Hartmann, 1973, 1985; Schoell, 1976). Bacterial sulfate reduction in the Upper Brine and at the chemocline overlying the Lower Brine are also thought to contribute to basin-wide deposition of fine sulfide particles (Trüper, 1969; Shanks and Bischoff, 1980; this study). In the current brine pool, non-hydrothermal sulfide deposition is subordinate to hydrothermal sulfide deposition, but it is clear from the present study that it has been more important in the past, particularly during periods of lower hydrothermal activity.

Fe-(oxy)hydroxides, such as ferrihydrite, form mainly at the chemocline overlying the Lower Brine and in the Upper Brine. Mn-(oxy)hydroxides precipitate mainly in the upper part of the Upper Brine, where oxygen is increasingly available (Hartmann, 1985; Butuzova et al., 1990; Blanc et al., 1998; Taitel-Goldman and Singer, 2002). Presently Mn-oxides and (oxy)hydroxides dissolve in the anoxic Lower Brine and may accumulate only on the flanks of the Deep where the Upper Brine directly overlies the seafloor. Times of more oxic Lower Brine are indicated by the presence of Mn-oxides in the sediment. Fe-(oxy)hydroxides, on the contrary, may settle through the current Lower Brine in a metastable form, accumulate on the bottom of the deep and become preserved in the sedimentary record. (Oxy)-hydroxides incorporate some trace elements into their structure at formation (e.g., U), whereas other elements (e.g., REE) are continuously scavenged onto their surfaces from the ambient environment. The results of the present study show that precipitation of Mn-(oxy)hydroxides near the top of the brine pool causes them to become enriched in elements derived from seawater, but they dissolve while settling through the brines thus transporting elements from seawater into the Lower Brine (especially Mo and REE).

Because the Lower Brine is highly enriched in metals but devoid of reduced sulfur (e.g., Brewer and Spencer, 1969; Shanks and Bischoff, 1977), non-ferrous metals (Zn, Cu, Co, Ag etc.) are adsorbed onto the Fe-(oxy)hydroxides and possibly other surface active particles that settle through the brine into the sediments (e.g., Badaut et al., 1992; Schwertmann et al., 1998; Taitel-Goldman and Singer, 2002; Taitel-Goldman et al., 2004). High Si concentrations, which are typical of the Lower Brine (26 ppm: Anschutz and Blanc, 1995a), help to stabilize the surface active particles by creating Fe-O-Si bonds that cause clustering (e.g., Cornell et al., 1987). Several studies have suggested that after co-deposition, many of the adsorbed elements are desorbed and released to the pore water as the amorphous material gradually becomes more crystalline, forming minerals such as goethite, siderite and smectite (Anschutz and Blanc, 1995b; Taitel-Goldman et al., 2004). This process is examined in the present study, which focuses on the mineralogical and geochemical transitions in the sediments from the bottom of the Lower Brine to progressively deeper sediments and with proximity to the known vent sites.

**2.3 Sedimentation and sediment stratigraphy**

Sedimentation in the Atlantis II Deep began at least ~25,000 years ago (Hackett and Bischoff, 1973), and the hydrothermal activity started about 15,000 year ago (Shanks and Bischoff, 1980). The total sedimentation rate in the Atlantis II Deep has varied from <20 cm/ka (i.e., background sedimentation) to >2 m/Ka mainly as hydrothermal sedimentation. Background sedimentation in the Atlantis II Deep comprises pelagic biogenic components

(~80%) and detrital siliciclastic components (~20%) with high aluminum content (Ku et al., 1969; Stoffers and Ross, 1974). The sedimentation rate of these components in the Deep is 15-20 cm/ka, compared to detrital sedimentation rates of 2-15 cm/ka for the Red Sea as a whole (Ku et al., 1969). The sedimentation rate is higher proximal to the vent source than in the distal parts of the basin, and the composition of the sediment also changes from sulfide- and sulfate-rich proximal to the vents to more carbonate-, clay- and oxide-rich distal to the vents.

Hydrothermal sedimentation in the Deep is ~1 m/Ka (Table 1.1), corresponding to ~1 mm/yr. Interstitial fluid content is up to 95 vol.%, and the minerals are very fine grained (50-80% <2 μm). The most metal-rich sediment contains <10 vol.% background sediment. The majority comprise mainly Fe-(oxy)hydroxides (~40 vol.%), a siliceous component consisting of Si-Fe-(oxy)hydroxides and clays (~20 vol.%), hydrothermal carbonates (~10 vol.%), sulfides (<10 vol.%), and minor sulfates, Mn-oxides and other non-sulfidic metal-bearing minerals. Although initially deposited as homogenous layers, the authigenic sediments at depth in the cores are typically delicately banded in bright colors of red, yellow, orange and green, as well as pitch black. Bischoff (1969) defined a number of different facies according to the dominant mineralogy (Fe-montmorillonite, goethite, sulfide, manganosiderite, anhydrite, manganite). Different proportions of these minerals also define the finer-scale layering identified in the present study. Sulfate-rich layers are a dominant host for non-ferrous metals in the sediments, although authigenic clay-rich layers and hydrothermal carbonate layers also are enriched in metal.

The stratigraphy of the Atlantis II sediments was defined by Bäcker and Richter (1973), who distinguished 5 units based on 78 sedimentary cores (Table 1.1 and Figure 1.3). The different units range from 1 to 12 meters in thickness and reflect major changes in the bulk sediment geochemistry related to changes in the location and intensity of hydrothermal activity and the amount of hydrothermal versus background sedimentation. Variations in the physical properties of the sediment (e.g., color, grain size) are closely linked to these chemical differences but also reflect a gradual decrease in pore-water content down stratigraphy.

The lowermost stratigraphic unit, referred to as the detrital oxidic pyritic unit (DOP) started to form ~25,000 years ago (Ku et al., 1969) and is composed mostly of a mixture of biogenic pelagic detritus (marl consisting of foraminifera, pteropods, nanofossils), inorganic carbonate and siliciclastic terrigenous detrital material with rare clasts of basalt (Chase, 1969; Stoffers and Ross, 1974; Anschutz and Blanc, 1995c). Limonitic and manganite-bearing layers and disseminated sulfides are present and become more abundant up stratigraphy from the lowermost sediments, recording the beginning of hydrothermal activity ~15,000 years ago. Zn-sulfides first appear at the top of the DOP unit (Blanc et al., 1998). They have a negative $\delta^{34}S$ signature, typical of reduced sulfide produced by bacterial sulfate reduction (Nakai and Jensen, 1964). However, the presence of manganite in DOP indicates formation when the brine was more oxidized than it is now, allowing Mn-oxides to accumulate at the bottom of the Deep. In the northeast parts of the Deep, the DOP unit is

cut by vertical anhydrite veins indicating the presence of a hydrothermal vent source in this part of the Deep early in the history of the basin (North Passage or East Basin, Figure 1.1).

The beginning of hydrothermal activity in the northeast part of the Deep was marked by the formation of the first sulfide- and metal-rich unit SU1 (~12-8.6 Ka), which directly overlies the DOP (Bäcker and Richter, 1973). SU1 comprises Si- and Fe-bearing clays (e.g., montmorillonite, nontronite), oxides and hydroxides, carbonates, anhydrite, rare barite and abundant sulfides (Bischoff, 1969; Bäcker and Richter, 1973; Pottorf and Barnes, 1983). The clays are typically red-brown in color. Anhydrite is found as crosscutting veins but also as sill-like bodies up to several meters thick. The horizontal extent of the anhydrite sills is poorly defined as they can be traced from core to core only in a few cases. The $\delta^{34}S$ values of sulfides are +5 per mill (Shanks and Bischoff, 1980; Zierenberg and Shanks, 1988), consistent with a hydrothermal source for the sulfide (e.g., Seal, 2006).

The end of SU1 formation and the beginning of formation of the central oxidic (CO) unit is marked by a rather sharp interface with red clays and iron oxides. The central oxidic (CO) unit was formed from ~8.6 to 5.9 Ka and consists mainly of amorphous to well-crystallized oxides and hydroxides of manganese and iron, carbonates, and locally abundant anhydrite; minor disseminated sulfides are also present. The formation of the CO unit records a time of intense tectonic activity, during which the location of the vent source shifted to the Southwest Basin (Bäcker and Richter, 1973). The brine pool was more oxidized at this time, as evidenced by precipitation of Mn-OOH minerals on the bottom of the Deep (presently

Mn is precipitated only at the flanks of the Deep where the reduced Lower Brine is absent). Hydrothermal sedimentation composed of various Mn- and Fe-OOH minerals was greatest during the formation of the CO unit, but little Cu, Zn or sulfide were deposited, implying that low-temperature hydrothermal venting was dominant. The $\delta^{34}S$ values of the sulfides indicate the involvement of both hydrothermal and biogenic sulfur (Kaplan et al., 1969; Shanks and Bischoff, 1980). Where silicates are present at higher than average concentration, this unit is referred to as the central oxidic siliceous unit (COS). In the Southwest Basin, the lower part of the CO unit is the only place where euhedral magnetite and silicates such as pyroxene are found. This assemblage is thought to have formed as a result of heating of Fe-(oxy)hydroxides and/or hematite by the intrusion of a basaltic sill about 6,000 years ago (Zierenberg and Shanks, 1983).

Deposition of the CO unit was terminated around 5.9 Ka by the outbreak of hydrothermal activity in the Southwest Basin and the beginning of formation of the second sulfidic unit (SU2). Fe-oxides and anhydrite found at the base of SU2 gradually give way to Fe- and Mn-carbonates (±anhydrite) up stratigraphy and finally to abundant sulfides. The ratios Cu/Zn and (Cu+Zn)/sulfide in the sediment also increase upwards within this unit. However, sulfides, including pyrite, sphalerite and chalcopyrite, are less common in SU2 than in SU1, and sphalerite/pyrite and Zn/Cu ratios are higher (Blanc et al., 1998; Gurvich, 2006). The $\delta^{34}S$ of the sulfides is again indicative of a dominantly hydrothermal source for sulfide (Shanks and Bischoff, 1980). As in SU1, anhydrite is found as vertical veins and sill-like bodies; where sulfates are abundant, SU2 is referred to as the oxidic anhydritic unit (OAN)

or sulfidic oxidic anhydritic unit (SOAN). The clays are often green, in contrast to typically red-brown clays in unit SU1.

The topmost unit, referred to as the amorphous silicic unit (AM), is composed mainly of poorly crystalline Si-Fe-OOH phases. It has very high pore water content and a graditional interface with the overlying brine pool. The AM unit is separated from SU2, almost basin-wide, by a bright orange lepidocrocite horizon (Bäcker and Richter, 1973) that is interpreted to have formed around 3.6 Ka ago during the intrusion of an oxidized, bottom-hugging brine into the Lower Brine, sourced from outside the Deep (Taitel-Goldman et al., 2002). Where the lepidocrocite horizon is absent, the transition between SU2 and AM is gradational. Mineralogically, the AM unit resembles the CO unit (i.e., dominated by various Si-Fe-OOH compounds that were likely precursors for the more crystalline oxides in CO; Taitel-Goldman and Singer, 2001, 2002), but has higher metal contents (e.g., Gurvich, 2006). Blanc et al. (1998) considered the AM unit to be a continuation of SU2 due to the similarity in bulk composition. In proximity to the inferred vent source(s), the AM unit has higher sulfide concentration and is referred to as the sulfidic amorphous siliceous unit (SAM).

Various sedimentary structures are abundant in the Atlantis II muds. The dominant feature is layering or lamination (down to <1 mm thick). Contacts may be sharp, irregular or faulted, and the layering may be horizontal or inclined. The interfaces between layers are typically diffuse in the upper strata becoming sharper with depth in the sediment. The origin of

these features, which are typical of many fine-grained or chemical sedimentary rocks, are a major focus of the thesis, and are interpreted in terms of abrupt changes in sedimentation, diagenetic processes, and the overall evolution of the basin. Brecciation is a common feature. Clasts of soft sediment have been displaced locally, although longer distance transport also has occurred (e.g., clasts of genetically unrelated material coexisting in the same cores). Clasts may be rounded or angular and compositionally homogenous or have internal structure, like laminations. Contacts between clasts and the matrix may be sharp or diffuse. In some places soft, laminated clasts occur in layered mud with sharp cross-cutting relationships. The breccias are interpreted to result from mass gravity transport, movement from the flanks to the deep or other mass movements related to faulting (earthquakes with magnitude >5 have been measured in the area: Boulos et al., 1987). The breccias are especially common in the CO unit, which formed at a time of frequent tectonic activity that may partly explain the high sediment accumulation rates within this unit (Daggett et al., 1986). Moreover, hydrothermal fluid flow has been linked to faulting (Bischoff, 1969; Pottorf and Barnes, 1983), suggesting temporal and spatial correlation between hydrothermal pulses and mass flow events.

## 3. Contents of the Thesis

This thesis comprises 4 papers (published and in preparation) dealing respectively with the sedimentology and mineralogy, trace metal chemistry, rare earth element (REE) chemistry, and sulfur isotopic compositions of the Atlantis II sediments. The last chapter summarizes the conclusions and also considers the implications of the findings for ancient ore deposits.

As noted above, though the Atlantis II Deep has been studied extensively since its discovery in 1964 (Miller, 1964), the last 20-30 years of research have focused mainly on the brine pool and not the sediments. Until now, the current understanding of the origin of the metalliferous sediments has relied on only the earliest studies (Degens and Ross, 1969; Pottorf and Barnes, 1983; Shanks and Bischoff, 1980; Zierenberg and Shanks, 1983, 1988). Because of sample handling at the time, which included washing of the sediment to remove salt, many of these studies underestimated the proportions of certain constituents such as non-sulfidic Cu and Zn phases. Few studies were supported by the type of high precision geochemical analyses that are readily available today. Despite the importance of the Atlantis II Deep as the only modern analog of brine pool deposition of metals, key questions remained concerning the origin of the fine layering, the distribution and mineralogical siting of certain trace and precious metals, the depositional pathways in the brine pool, as well as the importance of non-hydrothermal sources of trace elements and sulfur.

The samples included in this study are part of a large archive of original sediment cores from the Atlantis II Deep located at the Helmholtz Centre for Ocean Research Kiel, GEOMAR. This archive contains 486 sedimentary cores (Appendix A) recovered during the MESEDA (MEtalliferous SEdiments Atlantis II) project initiated to assess the feasibility of commercial recovery of metals from of the Atlantis II Deep that involved 3 cruises during 1977-1981. Additionally some sedimentary cores from Valdivia cruises 1 and 3 (during 1971 and 1972, respectively) are stored in the archive, including cores from outside the Atlantis II brine covered area. The locations of the cores were based on, then state-of-the-art, ITT

satellite navigation device on board Valdivia and a Decca Hi-fix system with two radio transmitters installed at two different points on the coasts, with precision of ± 30 m. All samples studied here come from sedimentary cores recovered with a “kasten corer”, a 6-m long device with a 15 x 15 cm square corer. For recovery of long cores, several boxes would be screwed together. Directly after recovery, the cores were split in two. One half was studied on board; the other half was packed in waterproof plastic cases (100 x 15 x 7 cm) and sent to the research laboratory of Preussag AG to be systematically analyzed for various physical and chemical properties (Steinkamp and Schumann, 1974). At Preussag, the cores were stored in a cooled warehouse. Later these boxes were moved to the GEOMAR “Kernlager”, a general storage house at ambient temperature.

Appendix B describes 42 cores chosen for detailed logging (including XRF core scanning of some sections; cf. Appendix F), photography, and sampling to include samples from all parts of the Deep and all stratigraphic units. Altogether 1000 small volume samples were collected and include sediments from all parts of the Deep and from all stratigraphic units since the beginning of sedimentation ~25,000 years ago up to the topmost sediment that was still forming at the time of collection (Appendix B). All samples, including wet, dried and powdered varieties, are currently located at GEOMAR. A subset of 100 samples from 9 cores were studied in detail to address specific questions about mineralogy and geochemistry, including by X-ray diffraction (XRD), scanning electron microscopy (SEM) and electron probe microanalysis (EPMA) on thin sections of dried intact samples as well as polished blocks of mineral separates. The mineralogical siting of specific trace metals was

further examined by field emission (FE) SEM and synchrotron X-ray Fluorescence (XRF). The study also includes the first full spectrum multi-element geochemical analysis (67 elements) of any samples from the Atlantis II sediments, with an emphasis on the compositions of the different layer types. Four-step sequential leaching experiments were also conducted on 33 representative samples to better characterize the mineralogy of the sediments.

A quantitative assessment of the mineralogy of the different layer types is presented in Chapter 2, based on re-logging of selected cores, petrography, sequential leaches, and the bulk compositions of different sample types. The mineral chemistry of well-crystallized phases was examined in order to better understand the principal phases carrying the trace metals. Primary mineral precipitates from the anoxic metal-rich brine are identified, some for the first time, that were deposited in the sediments together with background biogenic-detrital material. A clear distinction is also made between components precipitated directly as sulfides and those adsorbed onto surface-active particles, mainly Fe-(oxy)hydroxides, settling through the brine pool. The link between this rainout of particles and the crude layering of the uppermost sediments, which are saturated in brine, is examined, and the crystallinity of the different phases and origin of the lamination with depth and decreasing pore water content in the cores is explored. The fate of metals originally in poorly crystalline phases or in pore water and subsequently incorporated in diagenetic sulfides, and to a lesser extent in carbonates and authigenic clays, is also examined, together with the mineral compositions.

In Chapter 3 the different processes controlling trace metal distribution in the Atlantis II sediments are considered, including precipitation directly from the high-temperature hydrothermal fluids and enrichment in diagenetically growing sulfides. A clear link is established between metal concentrations in the sediments and co-deposition from the brine with surface-active Fe- and Si-rich particles. We identify a number of different non-hydrothermal sources of metals, including seawater (e.g., Mo), pelagic phytoplankton (Ni) and detrital input (Cr). An unexpected increase in the Cu/Zn ratio of the sediments with distance from the vent source(s) is observed and discussed with reference to mineralogical data presented in Chapter 2. The chemical dataset (67 elements) is the most comprehensive of any study currently available in the literature. Typically fewer than 20 elements have been analyzed in previous studies, mostly by techniques with much higher detection limits, lower precision, and requiring much larger sample sizes. Moreover, in almost all previous studies samples were washed prior to analysis to remove salt, resulting in significant losses of water-soluble components and fine particles that would have passed the filters used in those studies. The new data presented in this study shed new light on the importance of non-sulfidic deposition and diagenetic scavenging in controlling the spatial distribution of trace metals in the Deep. These results have implications for ancient ore deposits formed in stratified brine-pool environments, but where the evidence of the primary precipitation pathways has not been preserved.

Major events in the brine pool, leading to the observed distribution of metals in the sediments are further assessed in Chapter 4 with the aid of rare earth elements (REE).

Detrital silicic sedimentation is identified as the main REE source for most of the sediments in the Atlantis II Deep, similar to BIF, with variable contributions from hydrothermal vent fluids and seawater. The record of REE deposition is used here to trace the evolution of the basin from the early stage with no hydrothermal activity, through stages of high- and low-temperature activity, until the present day. A clear decrease in REE content of the sediments is identified with time, which is attributed to massive draw-down of REE from the early brine pool at the beginning of hydrothermal activity.

Chapter 5 examines the spatial and temporal variation in the abundance and isotopic composition of sulfur in the metalliferous sediment. For the first time, isotopic evidence for bacterial sulfate reduction is found in the sulfide- and metal-rich stratigraphic units. This record is preserved in metal sulfates derived from the oxidation of fine-grained diagenetic sulfides that have never been analyzed for $\delta^{34}S$. Additional evidence for bacterial sulfate reduction in the pore waters is found in layer-type anhydrite that has higher $\delta^{34}S$ than any of the possible sources of $SO_4$.

The final chapter of the thesis compares the various properties of the Atlantis II Deep metalliferous sediments to other modern and ancient ore deposits that are thought to have formed under similar conditions and possibly in a similar environment. In particular, the finely laminated metalliferous sediments of the Atlantis II Deep are compared to SEDEX and brine-pool type VMS deposits, non-sulfide Zn deposits, BIF and arsenic- and gold-rich sediment-hosted pyritic gold ores, such as in the Carlin trend.

## 4. Contributions From Others

This study was financially supported by the Canadian Mining Industry Organization (CAMIRO), through a Natural Sciences and Engineering Research Council - Collaborative Research and Development (NSERC-CRD), a NSERC Discovery grant to Mark Hannington, by a Society of Economic Geologists (SEG-Canada) research grant, and support from individual laboratories, including the Canadian Light Source (CLS). The cruise to the Red Sea was organized and funded by GEOMAR – Helmholtz Centre for Ocean Science Kiel.

All core logging, sampling, sample preparation, mineralogical and a majority of the chemical analyses were carried out by me at GEOMAR, CAU Kiel, and the University of Ottawa. Sven Petersen assisted with locating and retrieving cores from the core storage and provided the access to his laboratory for logging and sampling. Anna Krätchell helped with the compilation and presentation of the historical data. Core scanning was done by Simon Jost at the University of Kiel as a part of his B.Sc. thesis. Thin section preparation was done by Jiri (George) Mrazek at the University of Ottawa. Grain mounts of sulfides were prepared by me at GEOMAR and for non-sulfides by Judith Price at CANMET. All XRD, XRF, and SEM studies, including EPMA mapping and analysis, were performed by me at the University of Ottawa and at GEOMAR, with the assistance of Glenn Poirier (Ottawa) and Mario Thöner (GEOMAR). Synchrotron-XRF analyses at the Canadian Light Source were supervised by Renfei Feng and Darren Hunter, who greatly helped to optimize the analytical procedures at the beamline 07B2-1 (VESPERS). The chemical analyses at the University of Kiel were

conducted by me (dissolution of samples into liquids), with the assistance from Ulrike Westernströer, who did the final ICP-OES and ICP-MS analyses of the samples. Additional chemical data by a variety of techniques were provided by Activation Laboratories, Ancaster, Ontario. All sample preparation for carbon, sulfur, and $\delta^{34}S$, including sulfide and sulfate extractions using the sulfur extraction line of Mélanie Cousineau, were done by me. The final analyses were performed by the Hatch Laboratories at the University of Ottawa. The sequential leaching experiments were conducted at ALS Laboratories in Vancouver, Canada, under the direction of Matthew Leybourne.

## References


Anschutz, P. and Amann, H., 1985, Development of ocean mining in the Red Sea. *Mar. Mining* 5(2), p. 103-116.

Anschutz, P. and Blanc, G., 1995a, Geochemical dynamics of the Atlantis II Deep (Red Sea): silica behavior. *Mar. Geol*. 128, p. 25-36

Anschutz, P. and Blanc, G., 1995b, Chemical mass balances in metalliferous deposits from the Atlantis II Deep (Red Sea). *Geochim. Cosmochim. Acta* 59, p. 4205-4218.

Anschutz, P. and Blanc, G., 1995c, Diagenetic evolution of the DOP facies from the Atlantis II Deep (Red Sea), evidence of early hydrothermal activity. *Oceanol. Acta* 18 (N°1), p. 105-112.

Anschutz, P. and Blanc, G., 1996, Heat and salt fluxes in the Atlantis II Deep (Red Sea). *Earth Planet. Sci. Lett.* 142, p. 147-159.

Anschutz, P., Blanc, G. and Stille, P., 1995, Origin of fluids and the evolution of the Atlantis II deep hydrothermal system, Red Sea: Strontium isotope study. *Geochim. Cosmochim. Acta* 59 (23), p. 4799-4808.

Anschutz, P., Turner, J. S. and Blanc, G., 1998, The development of layering, fluxes through double-diffusive interfaces, and location of hydrothermal sources of brines in the Atlantis II Deep: Red Sea. *Jour. Geophys. Res*. 103 (C12), p. 27809-27819.

Anschutz, P., Blank, G., Monnin, C. and Boulècue, J., 2000, Geochemical dynamics of the Atlantis II Deep (Red Sea): II. Composition of metalliferous sediment pore waters. *Geochim. Cosmochim. Acta* 64 (23), p. 3995-4006.

Augustin, N., Devey, C. W., van der Zwan, F. M., Feldens, P., Tominaga, M., Bantan, R. A. and Kwasnitschka, T., 2014, The rifting to spreading transition in the Red Sea. *Earth Planet. Sci. Lett.* 395, p. 217-230.

Badaut, D. Decarreau, A, and Besson, G., 1992, Ferripyrophyllite and related Fe 3+ - rich 2:1 clays in recent deposits of Atlantis II Deep, Red Sea. *Clay min*. 27, p. 227-244.

Baker E. T., Lavelle, J. W. and Massoth, G. J., 1985, Hydrothermal particle plumes over the southern Juan de Fuca Ridge. *Nature* 316 (6026), p. 342-344.

Bekker A., Slack J., Planavsky N., Krapež B., Hofmann A., Konhauser K. O. and Rouxel O. J., 2010, Iron formation: The sedimentary product of a complex interplay among mantle, tectonic, oceanic, and biospheric processes*. Econ. Geol*. 105, p. 467–508.

Bertram, C., Krätschell, A., O'Brien, K., Brückmann, W., Proelss, A. and Rehdanz, K., 2011, Metalliferous sediments in the Atlantis II Deep—Assessing the geological and economic resource potential and legal constraints. *Res. Policy* 36, p. 315-329.

Bignell, R. D., Cronan, D. S. and Tooms, J. S., 1976, Metal dispersion in the Red Sea as an aid to marine geochemical exploration. *Inst. Mining Metall. Trans*. 84 (B), p. 274-278.

Bischoff, J. L., 1969. Red Sea geothermal brine deposits: their mineralogy, chemistry and genesis, *in* Degens, E. T. and Ross, D. A., eds., *Hot Brines and Recent Heavy Metal Deposits in the Red Sea*, Springer-Verlag, New York. p. 368-406.

Bischoff, J. L. and Manheim, F. T., 1969, Economic potential of the Red Sea heavy metal deposit, *in* Degens, E. T. and Ross, D. A., eds., *Hot Brines and Recent Heavy Metal Deposits in the Red Sea*. Springer-Verlag, New York. p. 535-541.

Blanc, G., Boulègue, J., and Michard, A., 1995, Isotope composition of the Red Sea hydrothermal end-member. *Isot. Geochem*. 320 (IIa), p. 1187-1193.

Blanc, G., Anschutz, P. and Pierret, M-C., 1998, Metalliferous sedimentation in the Atlantis II Deep: a geochemical insight, *in* Purser, B. H. and Bosence Dan, W. J., eds., *Sedimentation and Tectonics in Rift Basins: Red Sea – Gulf of Aden*, Springer. p. 505-520.

Blum, N. and Puchelt, H., 1991, Sedimentary-hosted polymetallic massive sulfide deposits of the Kebrit and Shaban Deeps, Red Sea. *Min. Deposita* 26, p. 217-227.

Bonatti, E., 1985, Punctiform initiation of seafloor spreading in the Red Sea during transition from a continental to an oceanic rift. *Nature* 316, p. 33-37.

Boulos, F. K., Morgan, P. and Toppozada, T. R., 1987, Microearthquake studies in Egypt carried out by Geological Survey of Egypt. *Journal of Geodynamics* 7, p. 227-249.

Brewer, P. G. and Spencer, D. W., 1969, A note on the chemical composition of the Red Sea Brines. *in* Degens, E. T. and Ross, D. A., eds., *Hot Brines and Recent Heavy Metal Deposits in the Red Sea*. Springer-Verlag, New York. p. 174-179.

Butuzova, G. Yu., Drits, V. A., Morozov, A. A., Gorschkov, A. I., 1990, Process of formation of iron- manganese oxyhydroxides in the Atlantis-II and Thetis Deeps of the Red Sea. *Spec. Publs. int. Ass. Sediment.* 11, p. 57-72.

Bäcker, H. and Schoell, M., 1972, New deeps with brines and metalliferous sediments in the Red Sea. *Nature (phys. Sci.)* 240, p. 153-158.

Bäcker, H. and Richter, H., 1973, Die rezente hydrothermal-sedimentärelagerstätte Atlantis II-tier im Roten Meer. *Geol. Rundsch.* 62, p. 697-740.

Chase, R. L., 1969, Basalt from the axial trough of the Red Sea, *in* Degens, E. T. and Ross, D. A., eds., *Hot Brines and Recent Heavy Metal Deposits in the Red Sea*. Springer-Verlag, New York. p. 122-128.

Cochran, J. R., 1983, A Model for Development of Red Sea. *Am. Assoc. Pet. Geol. Bull*. 67(1), p. 41-69.

Cochran, J. R., 2005, Northern Red Sea: Nucleation of an oceanic spreading center within a continental rift. *Geochem. Geophys. Geosyst*. 6 (3), Q03006, 34 p.

Cochran, J. R. and Martinez, F., 1988, Evidence from the northern Red Sea on the transition from continental to oceanic rifting, *in* Le Pichon, X. and Cochran, J. R, eds., *The Gulf of Suez and Red Sea Rifting*. *Tectonophysics* 153, p. 25-53.

Cole, T. G., 1988, The nature and origin of smectite in the Atlantis II Deep, Red Sea. *Can. Min*. 26, p. 755-763.

Converse, D. R., Holland, H. D. and Edmond, J. M., 1984, Flow rates in the axial hot springs of the East Pacific Rise (21°N): implications for the heat budget and the formation of massive sulfides. *Earth Planet. Sci. Iett*. 69, p. 159-175.

Cooke, D. R., Bull, S. W., Large, R. R. and McGoldrick, P. J., 2000, The Importance of Oxidized Brines for the Formation of Australian Proterozoic Stratiform Sediment-Hosted Pb-Zn (Sedex) Deposits. *Econ. Geol. Bull.* 95 (1), p. 1-18.

Cornell, R. M., Giovanoli, R., and Schindler, P. W., 1987, Effect of silicate species on the transformation of ferrihydrite into goethite and hematite in alkaline media. *Clays clay mdaggetiner.* 35 (1), p. 21-28.

Daggett, P. M., Morgan, P., Boulos, F. K., Hennin, S. F., El-Sherif, A. A., El-Sayed, A. A., Basta, N. Z. and Melek, Y. S., 1986, Seismicity and active tectonics on the Egyptian Red Sea margin and northern Red Sea. *Tectonophysics* 125, p. 313-324.

Degens, E. T. and Ross, D. A., 1969, *Hot Brines and Recent Heavy Metal Deposits in the Red Sea*. Springer-Verlag, New York Inc., 600 p.

Dupré, B., Blanc, G., Boulègue, J. and Allègre, J., 1988, Metal remobilization at a spreading centre studied using lead isotopes. *Nature* 333, p. 165-167.

Fiala, G., Woese, C. R., Langworthy, T. A. and Stetter, K. O., 1990, *Flexistipessinusarabici*, a novel genus and species of eubacteria occurring in the Atlantis II Deep brines of the Red Sea. *Arch. Microbiol*. 154, p. 120-126.

Goodfellow, W. D., and Lydon, J. W., 2007, Sedimentary exhalative (SEDEX) deposits. *In* Goodfellow, W. D., ed., *Mineral Deposits of Canada: A Synthesis of Major Deposit Types, District Metallogeny, the Evolution of Geological Provinces, and Exploration Methods*. Geol. Ass. Canada, Mineral Deposits Division, Spec. Publ. 5, p. 163-183.

Grenne, T. and Slack, J. F., 2005, Geochemistry of jasper beds from the Ordovician Løkken ophiolite, Norway: origin of proximal and distal siliceous exhalites*. Econ. Geol*. 100, p. 1511-1527.

Guney, M., Al-Marhoun, M. A. and Nawab, Z. A., 1988, Metalliferous sub-marine sediments of the Atlantis II – Deep, Red Sea. *CIM Bulletin* 81, p. 33-39.

Gurvich, E. G., 2006, *Metalliferous Sediments of the World Ocean: Fundamental Theory of Deep-Sea Hydrothermal Sedimentation*, Springer, Heidelberg. 423 p.

Hackett, J. and Bischoff, J. L., 1973, New data on the stratigraphy, extent, and geologic history of the red sea geothermal deposits. *Econ. Geol*., 68, p. 553-564.

Hannington, M. D., 2014, Volcanogenic Massive Sulfide Deposits, *in* Scott, S. D., ed., Chapter 13.18, The Geochemistry of Ore Deposits. *In* Holland, H. D. and Turekian, K. K., eds., *Treatise on Geochemistry* 28. Elsevier-Pergamon, Oxford. p. 463-488.

Hannington, M. D., Jonasson, I. R., Herzig, P. M. and Petersen, S., 1995, Physical and chemical processes of seafloor mineralization. *In* Humphris, S., Fornari, D., and Zierenberg, R., eds., *Physical, Chemical, Biological and Geological Interactions within Hydrothermal Systems*. AGU Monograph 91, p. 115-157.

Hartmann, M., 1973, Untersuchungen von suspendiertem Material in den Hydrothermallaugen des Atlantis-II-Tiefs. *Geol. Rundsch*. 62, p. 742-754.

Hartmann, M., 1985, Atlantis-II-Deep geothermal brine system: Chemical processes between hydrothermal brines and Red Sea deep water. *Mar. Geol*. 64, p. 157-177.

Hendricks, R. L., Reisbick, F. B., Mahaffey, E. J., Roberts, D. B. and Peterson, M. N. A., 1969, Chemical composition of sediments and interstitial brines from the Atlantis II, Discovery and Chain Deeps. *in* Degens, E. T. and Ross, D. A., eds., *Hot Brines and Recent Heavy Metal Deposits in the Red Sea*. Springer-Verlag, New York. p. 407-440.

Huston, D. L., Stevens, B., Southgate, P. N., Muhling, P. and Wyborn, L., 2006, Australian Zn-Pb-Ag ore-forming systems: a review and analysis. *Econ. Geol*. 101, p. 1117-1157.

Izzeldin, A. Y., 1987, Seismic, gravity and magnetic surveys in the central part of the Red-Sea – their interpretation and implications for the structure and evolution of the Red-Sea. *Tectonophysics* 143, p. 269-306.

Johnson, C. A. and Skinner, B. J., 2003, Geochemistry of the Furnace magnetite bed, Franklin, New Jersey, and the relationship between stratiform iron oxide ores and stratiform zinc oxide-silicate ores in the New Jersey Highlands. *Econ. Geol*. 98, p. 837-854.

Kaplan, I. R., Sweeney, R. E. and Nissenbaum, A., 1969, Sulfur isotope studies on Red Sea geothermal brines and sediments, *in* Degens, E. T. and Ross, D. A., eds., Hot Brines and Recent Heavy Metal Deposits in the Red Sea: Springer-Verlag, New York. p. 474-498.

Kato, Y., Ohta, I., Tsunematsu, T., Watanabe, Y., Isozaki, Y., Maruyama, S and Imai, N., 1998, Rare earth element variations in mid-Archean banded iron formations: Implications for the chemistry of ocean and continent and plate tectonics. *Geochim. Cosmochim. Acta* 62 (21/22), p. 3475-3497.

Ku, T. L., Thurber, D. L. and Mathieu, G. G., 1969, Radiocarbon chronology of Red Sea sediments, *in* Degens, E. T. and Ross, D. A., eds., *Hot Brines and Recent Heavy Metal Deposits in the Red Sea*. Springer-Verlag, New York. p. 348-359.

Large, R. R., Bodon, S., Davidson, G. J. and Cooke, D., 1996, The chemistry of BHT ore formation – one of the keys to understanding the difference between SEDEX and BHT deposits *in* Pongratz, J. and Davidson, G. J., eds., *New Developments in Broken Hill Type Deposits*; Proceedings of a Workshop Held at CODES, University of Tasmania, July 1996, p. 105-111.

Lyons, T. W., Gellatly, A. M., McGoldrick, P. J. and Kah, L. C., 2006, Proterozoic sedimentary exhalative (SEDEX) deposits and links to evolving global ocean chemistry, *in* Kesler, S. E., and Ohmoto, H., eds., *Evolution of Early Earth's Atmosphere, Hydrosphere, and Biosphere—Constraints from Ore Deposits. Geol. Soc. Amer*. *Memoir* 198, p. 169-184.

Miller, A. R., 1964, Highest salinity in the world ocean? *Nature* 203, p. 590.

Miller, A. R., Densmore, D. C., Degens, E. T., Hathaway, J. C., Manheim, F. T., McFarlin, P. F., Pocklington, R. and Jokela, A., 1966, Hot brines and recent iron deposits in deeps of the Red Sea. *Geochim. Cosmochim. Acta* 30, p. 341-359.

Missack, E., Stoffers, P. and El Goresy, A., 1989, Mineralogy, parageneses, and phase relations of copper-iron sulfides in the Atlantis II Deep, Red Sea. *Mineral. Deposita* 24, p. 82-91.

Nakai, N. and Jensen, M. L., 1964, The kinetic isotope effect in the bacterial reduction and oxidation of sulfur. *Geochim. Cosmochim. Acta* 28 (12), p. 1893-1912.

Ohmoto, H., 1996, Formation of volcanic massive sulfide deposits: The Kuroko perspective. *Ore. Geol. Rev*. 10, p .135-177.

Ohmoto, H., Watanabe, Y., Yamaguchi, K. E., Naraoka, H., Haruna, M., Kakegawa, T., Hayashi, K. and Kato, Y., 2006, Chemical and biological evolution of early Earth: Constraints from banded iron formations, *in* Kesler, S. E. and Ohmoto, H., eds., *Evolution of Early Earth's Atmosphere, Hydrosphere, and Biosphere – Constraints from Ore Deposits*. *Geol. Soc. Amer*. Memoir, v. 198, p. 291-331.

Oudin, E., Thisse, Y. and Ramboz, C., 1984, Fluid inclusion and mineralogical evidence for high temperature saline hydrothermal circulation in the Red Sea metalliferous sediments: Preliminary results. *Mar. Mining* 5 (1), p. 3-31.

Peter, J. M. and Goodfellow, W. D., 1996, Mineralogy, bulk and rare earth element geochemistry of massive sulphide-associated hydrothermal sediments of the Brunswick Horizon, Bathurst Mining Camp, New Brunswick. *Can. J. Earth Sci*. 33, p. 252-283.

Pierret, M. C., Clauer, N., Bosch, D., Blanc, G. and France-Lanord, C., 2001, Chemical and isotopic ($^{87}Sr/^{86}Sr$, $\delta^{18}O$, $\delta D$) constraints to the formation processes of Red-Sea brines. *Geochim. Cosmochim. Acta* 65 (8), p. 1259-1275.

Pottorf, R. J. and Barnes. H. L., 1983, Mineralogy, geochemistry, and ore genesis of hydrothermal sediments from the Atlantis II Deep, Red Sea. *Econ. Geol. Monograph* 5, p. 198-223.

Ramboz, C., Oudin, E. and Thisse, Y., 1988, Geyser-type discharge in Atlantis II Deep, Red Sea: Evidence of boiling from fluid inclusions in epigenetic anhydrite. *Can. Mineral*. 26, p. 765-786.

Rona, P. A. and Scott, S. D., 1993, A special issue on sea-floor hydrothermal mineralization; new perspectives: preface. *Econ. Geol*. 88 (8), p. 1933-1973.

Schmidt, M., Botz, R., Faber, E., Schmitt, M., Poggenburg, J., Garbe-Schönberg, D. and Stoffers, P., 2003, High-resolution methane profiles across anoxic brine–seawater boundaries in the Atlantis-II, Discovery, and Kebrit Deeps (Red Sea). *Chem. Geol*. 200, p. 359-375.

Schoell, M. and Stahl, W., 1972, The carbon isotopic composition and the concentration of dissolved anorganic carbon in the Atlantis II Deep brines/Res Sea. *Earth Planet. Sci. Lett*. 15, p. 206-211.

Schoell, M. 1976. Heating and convection within the Atlantis II Deep geothermal system of the Red Sea. Proc. Second United Nations symposium on the development and use of geothermal resources 1, p. 583-590.

Schoell, M. and Faber, E., 1978, New isotopic evidence for the origin of Red Sea brines. *Nature* 275, p. 436-438.

Scholten, J. C., Stoffers, P., Garbe-Schönberg, D. and Moammar, M., 2000, Hydrothermal mineralization in the Red Sea. *In* Cronan, D. S., eds., *Handbook of Marine Mineral Deposits.* CRC-Press, Boca Raton, p. 369-395.

Schwertmann, U., Friedl, J., Stanjek, H., Murad, E. and Bender Koch, C., 1998, Iron oxides and smectites in sediments from the Atlantis II Deep, Red Sea. *Eur. J. Mineral.* 10, p. 953-967.

Seal, R. R., 2006, Sulfur isotope geochemistry of sulfide minerals. *Rev. Mineral. Geochem*. 61, p. 633-677.

Shanks, W. C. and Bischoff, J. L., 1977, Ore transport and deposition in the Red Sea geothermal system: a geochemical model. *Geochim. Cosmochim. Acta* 41, p. 1507-1519.

Shanks, W. C. and Bischoff, J. L., 1980, Geochemistry, sulfur isotope composition and accumulation rates of Red Sea geothermal deposits. *Econ. Geol*. 75, p. 445-459.

Skinner, B. J., White, D. E., Rose, H. J. and Mays, R. E., 1967, Sulfides associated with the Salton Sea geothermal brine. *Econ. Geol.* 62, p. 316-330.

Solomon, M., Tornos, F., Large, R. R., Badham, J. N. P., Both, R. A. and Khin Zaw., 2004, Zn–Pb–Cu volcanic-hosted massive sulphide deposits: criteria for distinguishing brine pool-type from black smoker-type sulphide deposition. *Ore Geol. Rev*. 25, p. 259-283.

Steinkamp, K., Schumann, D., 1974, The Chemical Composition of Sediment Cores Recovered During Valdivia Cruises VA01 and VA03 from the Atlantis II Deep (Red Sea): Unpublished Cruise Report 1.11.1974, Series CL, Preussag, Hannover, 155 p.

Stoffers, P. and Ross, D. A., 1974, Sedimentary history of the Red Sea, (ch. 23), *in*, Whitmarsh, R. B., Weser, O. E., Ross, D. A., *et al., Initial Reports of the Deep Sea Drilling Project* 23, Washington (U.S. Government Printing Office), p. 849-865.

Swift, A., Bower, A. S. and Schmitt, R., 2012, Vertical, horizontal, and temporal changes in temperature in the Atlantis II and Discovery hot brine pools, Red Sea. *Deep Sea Res*. I, 64, p. 118-128.

Taitel-Goldman, N. and Singer, A., 2001, High-resolution transmission electron microscopy study of newly formed sediments in the Atlantis II Deep, Red Sea. *Clays Clay Miner.* 49 (2), p. 174-182.

Taitel-Goldman, N. and Singer, A., 2002, Metastable Si-Fe phases in hydrothermal sediments of Atlantis II Deep: Red Sea. *Clay Miner*. 37, p. 235-248.

Taitel-Goldman, N., Koch, C. B. and Singer, A., 2002, Lepidocrocite in hydrothermal sediments of the Atlantis II and Thetis Deeps, Red Sea. *Clays Clay Miner*. 50 (2), p. 186-197.

Taitel-Goldman, N., Koch, C. B. and Singer, A., 2004, Si-associated goethite in hydrothermal sediments of the Atlantis II and Thetis Deeps, Red Sea. *Clays Clay miner*. 52(1), p.115-129.

Tornos, F., Solomon, M., Conde, C. and Spiro, B. F., 2008, Formation of the Tharsis Massive Sulfide Deposit, Iberian Pyrite Belt: Geological, Lithogeochemical, and Stable Isotope Evidence for Deposition in a Brine Pool. *Econ. Geol*. 100, p. 185-214.

Trüper, H. G., 1969, Bacterial sulfate reduction in the Red Sea hot brines, *in* Degens, E. T. and Ross, D. A., eds., *Hot Brines and Recent Heavy Metal Deposits in the Red Sea*. Springer-Verlag, New York. p. 263-271.

Von Damm, K. L., 1990, Seafloor hydrothermal activity; black smoker chemistry and chimneys. *Annu. Rev. Earth Planet. Sci*. 18, p. 173-204.

Zierenberg, R. A. and Shanks, W. C., 1983, Mineralogy and geochemistry of epigenetic features in metalliferous sediments, Atlantis II Deep, Red Sea. *Econ. Geol*. 78, p. 57-72.

Zierenberg, R. A. and Shanks, W. C., 1988, Isotopic studies of epigenetic features in metalliferous sediment, Atlantis II Deep, Red Sea. *Can. Min*. 26, p. 737-753.

## Figure Captions

Figure 1.1. Location of the Atlantis II Deep and some other well-studied deeps in the Red Sea rift axis. The deeps with hot (>30°C) brine are marked in red, and the deeps without brine are marked in green. On the left, the locations of cores sampled for this study are indicated. Triangles mark the pore-water sampling locations of Anschutz et al. (2000), and squares mark the locations of cores studied by Oudin and Cocherie (1988), Oudin et al. (1984) and Ramboz et al. (1988), which are referred to in the text.

Figure 1.2. Schematic cross-section through the Atlantis II Deep sediments and brine pool. The present thickness of the sedimentary strata is about 20 m, and the sediments are overlain by about 200 m of brine (modified after Pottorf and Barnes, 1983, and Zierenberg and Shanks, 1988). Metals and other elements in the brines have four main sources: S1) background sedimentation that brings biogenic pelagic and detrital silicic material into the Deep; S2) hot hydrothermal brines formed by seawater circulation through evaporites and underlying basalts; S3) cold, near-bottom brines that enter the Deep from dissolution of evaporites (their exact contribution to the element budget is not known); S4) seawater. Elements from seawater are brought into the Deep via Mn- and Fe-OOH precipitation-dissolution cycling through the chemocline. By far most of the metals in the brine and sediment are derived from hot hydrothermal fluids. Metals precipitate out of these fluids according to four different pathways: P1) in sub-seafloor veins and conduits as high-temperature sulfides and anhydrite; P2) as sulfide particles in plume fallout; P3) adsorbed onto non-sufidic particles that settle through the Lower Brine; P4) as diagenetic sulfides.

The basin has a width of 5 km; the bottom of the Deep is at approximately 2200 m depth and the transition from the Lower Brine to the upper brines is at 2050 m.

Figure 1.3. Stratigraphic column of Atlantis II sediment (based on 78 cores: Bäcker and Richter, 1973). The main stratigraphic units are shown on the left. The uppermost units AM and SU2 are limited to the Southwest Basin where the current vent source is located and subunits SAM, SOAN and OAN are identified. Units SU1 and DOP units are missing in the central part of the Southwest Basin due to the presence of a basaltic sill in this part of the Deep. The CO and COS units are found basin-wide. Some special features are identified at their specific stratigraphic level (*italics*).

Table 1.1. Physical, chemical and mineralogical properties of the stratigraphic units of the Atlantis II metalliferous sediments (modified from Bäcker and Richter, 1973).

| Unit and thickness | Age (Ka) | Sedimentat-ion rate | Mineralogy | Specific enrichment |
|---|---|---|---|---|
| AM (*SAM)* Amorphous-Siliceous 3.5 (1-4) m | last 3.6 | 97 cm/ka ~4,700 t/a tot. 17 Mt | Amorphous Si-Fe-OOH, goethite, Fe-smectite, Mn-siderite; SW basin: sulfides, Fe-oxides, anhydrite; elevated areas: Mn-OOH | Zn, Cd, Ag, Co, Sb |
| Lepidocrocite horizon | | | | |
| SU2 (*SOAN/OAN*) Sulfidic 4 *(*2-12) m | 5.9-3.6 | 174 cm/ka ~8,800 t/a tot. 20 Mt | Sphalerite (common almost everywhere), pyrite (rare), Fe-OOH, green silicates, anhydrite (barite rare), Fe- and Mn-carbonates. | Zn, Pb, As, Cd, Hg, Tl, Ba, Mo, V, Cr |
| Layer of anhydrite | | | | |
| CO *(COS*) Central Oxidic 6 (1-11) m | ~8.6-5.9 | 222 cm/ka ~12,000 t/a tot. 32 Mt | Goethite, rare sulfides, carbonates, Mn-OOH minerals and Mn-oxides, poorly crystalline Fe-OOH, hematite, anhydrite and euhedral magnetite | Mn, Fe, K, Ba, Mo, Rb, Cs; low S |
| Red silicate layers with Fe-oxides | | | | |
| SU1 Sulfidic* 3.8 (1-4) m | ~11.7-8.6 | 123 cm/ka ~5,800 t/a tot. 18 Mt | Fe-clays, red-brown silicates, abundant sulfides: pyrite, chalcopyrite, sphalerite, Mn-siderite, hematite, anhydrite (rare barite) | Si, Cu, Ag, As, S, P, Ni, Tl, W |
| Pyrite much more abundant at the top of DOP than at the bottom | | | | |
| DOP Detrital-Oxidic-Pyritic* 2.5 (1-6) m | ~25-~11.7 | 19 cm/ka | Mixture of detrital-biogenic material with Fe- and Mn-rich layers, pyrite increase up, where sphalerite appears, Fe-OOH, anhydrite, basalt fragments | Ca, Al, Ti, Sr, Cr, Sc, HFSE, Li, Nb, Ta, Th and REEs |

Names in *italics* refer to sub-units, mainly found in the Southwest Basin: SAM= Sulfidic-Amorphous-Siliceous unit; SOAN=Sulfidic-Oxidic-Anhydritic unit; OAN=Oxidic-Anhydritic unit; COS=Central-Oxidic-Siliceous unit

*= Absent in the SW Basin

The ages of the units are from Hackett and Bischoff (1973) and Shanks and Bischoff (1980). Thickness of the units varies spatially depending on depth and distance from the hydrothermal vent source; averages from Bäcker and Richter (1973) are used to calculate the average sedimentation rates. Gurvich (2006) determined the deposition rates of dry salt-free ore material ($g/cm^2/Ka$) for the different units and sub-basins according to chemical analyses of 71 sedimentary cores and calculated the average deposition rates (t/a) for each unit. Total tonnage (dry, salt free) is calculated according to average deposition rate multiplied by age.

Figure 1.1

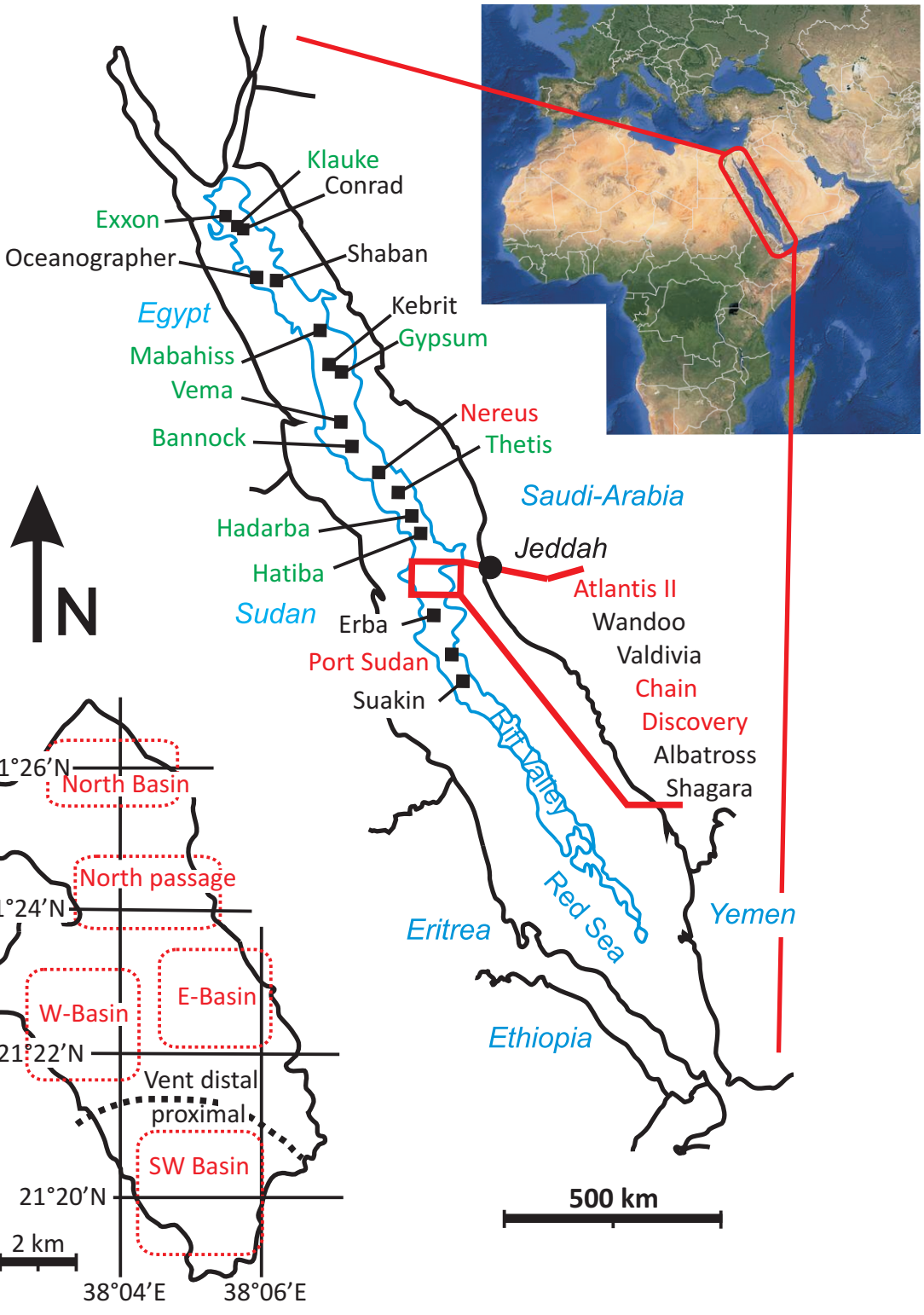
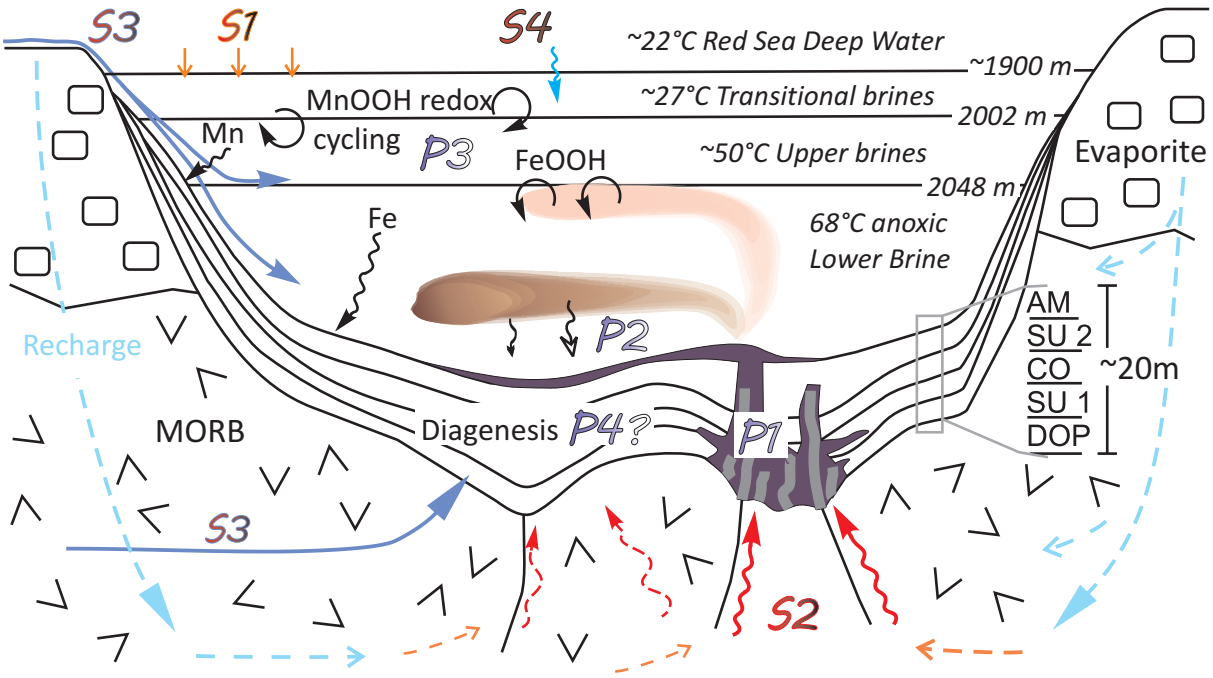

Klauke
Conrad
Exxon
Oceanographer
Shaban
Egypt
Kebrit
Gypsum
Mabahiss
Vema
Nereus
Bannock
Thetis
Saudi-Arabia
Hadarba
Jeddah
Hatiba
Atlantis II
Sudan
Erba
Wandoo
Valdivia
Port Sudan
Chain
Suakin
Discovery
Albatross
Shagara
Rift valley
Red Sea
Yemen
Eritrea
Ethiopia
N
500 km
21°26'N
North Basin
North passage
21°24'N
W-Basin
E-Basin
21°22'N
Vent distal
proximal
SW Basin
21°20'N
2 km
38°04'E
38°06'E

Figure 1.2



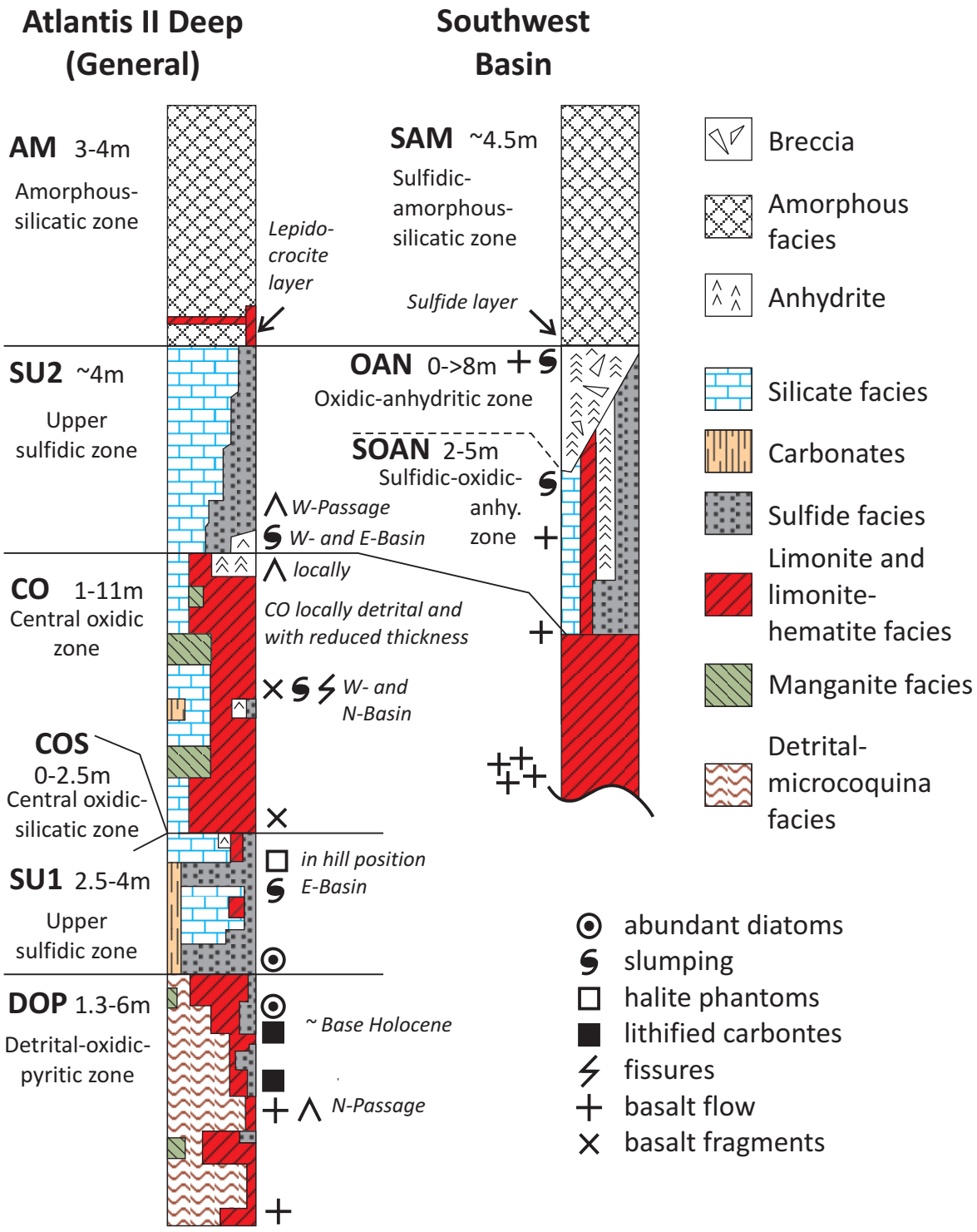

**Sources of elements:**

- *S1* Biogenic-siliciclastic detrital
- *S2* Metal-rich hydrothermal fluid
- *S3* Sinking brines or non-hydrothermal brines from below
- *S4* Seawater via MnOOH/MnO transport

**Precipitation environments:**

- *P1* Fluid conduits (Anhydrite + sulfides)
- *P2* Hydrothermal plume (mainly sulfides)
- *P3* Transitional brines (Fe at low $fO_2$; Mn at shallower and higher $fO_2$
- *P4?* Diagenesis/replacement

Figure 1.3


Atlantis II Deep (General)
Southwest Basin
AM 3-4m
Amorphous-silicatic zone
Lepido-crocite layer
SAM ~4.5m
Sulfidic-amorphous-silicatic zone
Sulfide layer
SU2 ~4m
Upper sulfidic zone
OAN 0->8m
Oxidic-anhydritic zone
SOAN 2-5m
Sulfidic-oxidic-anhy. zone
W-Passage
W- and E-Basin
locally
CO 1-11m
Central oxidic zone
CO locally detrital and with reduced thickness
W- and N-Basin
COS 0-2.5m
Central oxidic-silicatic zone
in hill position
E-Basin
SU1 2.5-4m
Upper sulfidic zone
DOP 1.3-6m
Detrital-oxidic-pyritic zone
~ Base Holocene
N-Passage
Breccia
Amorphous facies
Anhydrite
Silicate facies
Carbonates
Sulfide facies
Limonite and limonite-hematite facies
Manganite facies
Detrital-microcoquina facies
abundant diatoms
slumping
halite phantoms
lithified carbontes
fissures
basalt flow
basalt fragments

# CHAPTER 2

## A NEW LOOK AT THE MINERALOGY OF THE ATLANTIS II DEEP METALLIFEROUS SEDIMENTS

In preparation for Marine Geology

## 1. Introduction

The Atlantis II Deep is situated on the slowly spreading Red Sea rift axis at about 2.2 km water depth (Figure 2.1). It was one of the first known locations of present-day metal deposition associated with seafloor hydrothermal activity (e.g., Miller, 1964; Miller et al., 1966; Degens and Ross, 1969) and is by far the largest known hydrothermal mineral deposit on the seafloor (~90 Mt of salt-free ore material: Guney et al., 1988). The metals are contained in a ~20 meter-thick fine-grained and laminated sedimentary succession composed of oxides, sulfides, silicates, carbonates, and poorly crystalline material that cover an area of about 70 $km^2$ on the floor of the Deep. The bottom of the Deep is occupied by a stratified brine pool (Figure 2.2). The lowermost brine has a volume of ~4 $km^3$ and is extremely saline (~27 wt.% NaCl), hot (~68°C in 2008: Swift et al., 2012), anoxic and devoid of reduced sulfur (Anschutz et al., 1998). At the deepest part of the basin the thickness of the Lower Brine is 135 m. It is overlain by ~50 m of Upper Brine (Swift et al., 2012), which comprises a number of sub-layers that are progressively more seawater-like with height above the Lower Brine.

The thin layers of metalliferous mud at the bottom of the Deep have formed by the settling of mainly Fe-(oxy)hydroxide and lesser sulfide particles from the brine pool during periods of hydrothermal venting into the Deep (Shanks and Bischoff, 1977, 1980). During high-temperature hydrothermal activity sulfide precipitation has been dominant, with temperatures reaching ~100-200°C close to the seafloor near the vent location(s) (Shanks and Bischoff, 1977; Pottorf and Barnes, 1983, and ref. therein; Cole, 1988;). Zn-sulfides

formed at or close to the seafloor near the vents; Cu-sulfides were precipitated below the brine-sediment interface due to cooling of deeper hydrothermal fluid from ~350°C (Zierenberg and Shanks, 1983; Oudin et al., 1984; Ramboz et al., 1988; Missack et al., 1989). Sulfides (dominantly sphalerite) also precipitated from cooled hydrothermal fluid vented into the brine pool, creating a plume within the Lower Brine (Hartmann, 1973, 1985; Schoell, 1976). The precipitation of Fe-(oxy)hydroxides occurs mainly at the interface between the Lower Brine and more oxidized Upper Brine (Figure 2.2), and Mn-(oxy)hydroxides precipitate only within the Upper Brine layers, where oxygen is increasingly available, and are deposited only on the flanks of the Deep. However, during times of diminished hydrothermal activity and more oxidized Lower Brine, Mn-(oxy)hydroxides also have been deposited basin-wide (Butuzova et al., 1990; Blanc et al., 1998). Despite the abundant chemical sedimentation, the texture of the Atlantis II sediments is distinct from that of cherts, due to the large contribution of clastic components.

In contrast to MOR hydrothermal systems, where most of the metals are dispersed to the open ocean by buoyant hydrothermal plumes (Baker et al., 1985), metals in the Atlantis II brine pool have been efficiently deposited in the sediments at the bottom of the Deep (Bignell et al., 1976; Gurvich, 2006). This style of metal accumulation is not known anywhere else on the modern seafloor but has been widely suggested as an analog for many stratiform sediment-hosted metal deposits on land (e.g., Johnson and Skinner, 2003; Solomon et al., 2004; Tornos, 2008; Ohmoto et al., 2006; Goodfellow and Lydon, 2007). Nonferrous metal concentrations in the sediments are lower than in sulfide deposits

formed at open ocean MOR hydrothermal vents because of dilution by the efficiently deposited Fe and by other sedimentary material. However, the bulk metal ratios in the Atlantis II sediment (Fe:Zn:Cu = ~10:1:0.3: Bischoff and Manheim, 1969) are similar to those of MOR black smokers fluids (Von Damm, 1990). Metal-to-sulfide ratios are much higher (~10 in Atlantis II compared to ~1 in black smoker fluids), reflecting the high concentrations of metals in the brines. Because the Lower Brine is highly enriched in metals but devoid of reduced sulfur (e.g., Brewer and Spencer, 1969; Shanks and Bischoff, 1977; Anschutz et al., 2000), nonsulfide deposition of metals is also important (Laurila et al., 2014a).

A number of different descriptions and classifications of the sediments in the Atlantis II Deep have been published by Bischoff (1969a), Bäcker and Richter (1973) and, more recently, by Blanc et al. (1998). Although the early studies had access to relatively fresh core material, the emphasis was on coarse, unit-scale stratigraphy. The small grain sizes (60% <2 μm: Bäcker and Richter, 1973), abundant amorphous material, and the finely laminated character of the sediments complicated the sampling and mineral identification and led to considerable uncertainty in the interpretation of the primary mineralogy. Samples used for mineralogical studies were typically washed with distilled water to remove salt, and in the process many very fine-grained and water-soluble phases were also unexpectedly lost (e.g., Bischoff, 1969a; Weber-Diefenbach, 1977; Shanks and Bischoff, 1980; Butuzova, 1984). In this study, we have used small samples to examine the differences between the fine laminae and to resolve short-term (down to ~annual) variations in the deposition. The

samples were dried but not washed, thus preserving water-soluble compounds and other phases that likely passed the 0.45 μm filters commonly used in previous studies.

## 2. Sediment Stratigraphy

The stratigraphy of the Atlantis II sediments was defined by Bäcker and Richter (1973), who distinguished 5 units based on 78 sedimentary cores (Table 2.1 and Figure 2.3). The different units range from 1 to 12 meters in thickness and reflect changes in the intensity and location of hydrothermal activity over thousands of years. According to the compositions of the oldest sediments, venting was initially located in the northeast part of the Atlantis II Deep about 15,000 years ago (Shanks and Bischoff, 1980) but has since shifted to the Southwest Basin. The part of the Deep referred to as "proximal" to inferred vents is shown in Figure 2.1.

The lowermost stratigraphic unit, referred to as the detrital oxidic pyritic unit (DOP), is composed mostly of siliciclastic and biogenic detrital material. Limonitic and manganitic layers and disseminated sulfides are present and become more abundant up stratigraphy, recording the change from normal marine to dominantly hydrothermal sedimentation (Blanc et al., 1998; Laurila et al., 2014b). The DOP unit is overlain by the first sulfidic unit (SU1), which was formed during the period when hydrothermal venting was located in the northeast part of the Deep (Figure 2.1: Bäcker and Richter, 1973).

SU1 comprises Fe- and Si-bearing clays (e.g., nontronite, montmorillonite), oxides and (oxy)hydroxides, carbonates, anhydrite, rare barite and abundant sulfides (Bischoff, 1969a; Bäcker and Richter, 1973; Pottorf and Barnes, 1983). The DOP unit and SU1 are absent, or at least inaccessible, in the Southwest Basin due to intrusion of a basaltic sill. The top of SU1 is marked by a rather sharp interface with the overlying central oxidic (CO) unit, which consists mainly of amorphous to well-crystallized Mn- and Fe-(oxy)hydroxides, carbonates, and locally abundant anhydrite; minor disseminated sulfides are also present. The formation of the CO unit recorded a time of intense tectonic activity (e.g., marked by brecciation of the sediment; e.g., Figure 2.4A), during which the location of the vent source shifted to the Southwest Basin (Bäcker and Richter, 1973; Gurvich, 2006). The brine pool was more oxidized at this time, as evidenced by precipitation of Mn-oxides; presently Mn-oxides precipitate only at the flanks of the Deep where the reduced Lower Brine is absent and the transitional oxic brines directly overlie the seafloor. Hydrothermal sedimentation (composed of Mn- and Fe-OOH) was greatest during the formation of the CO unit, but little Cu, Zn or reduced sulfide species were deposited, implying that low-temperature hydrothermal venting was dominant. In the northern and eastern parts of the Deep, there is a significant silicate component (authigenic clays) and CO is referred to as the central oxidic siliceous (COS) unit.

Deposition of CO was terminated by the outbreak of higher-temperature hydrothermal activity in the Southwest Basin, which is marked by the formation of the second sulfidic unit (SU2). Sulfides are less common in SU2 than in SU1, and the Cu/Zn ratio is lower (Blanc et

al., 1998; Gurvich, 2006; Laurila et al., 2014a), but Fe-(oxy)hydroxides and anhydrite found at the base of SU2 gradually give way to Fe- and Mn-carbonates (±anhydrite) up stratigraphy and finally to abundant sulfides, similar to SU1. The ratio of Cu/Zn and total metals-to-sulfur in the sediment also increase upwards (Blanc et al., 1998).

The topmost unit, referred to as the amorphous siliceous unit (AM), is composed mainly of poorly crystalline Si-Fe-rich phases. Mineralogically, the AM unit resembles the CO unit. It is dominated by Si-Fe-(oxy)hydroxides that are thought to have been the precursors of more crystalline oxides now in CO (Taitel-Goldman and Singer, 2002), but it is saturated with brine (up to 95 wt.%) and has higher metal contents (Gurvich, 2006). Blanc et al. (1998) considered the AM unit to be a continuation of SU2 due to the similarity in bulk composition. However, the AM unit is separated from SU2 almost basin-wide by a bright orange lepidocrocite horizon (Bäcker and Richter, 1973; Figure 2.4B) that is interpreted to have formed during the intrusion of an oxidized, bottom hugging brine from outside the Deep into the Lower Brine (Taitel-Goldman et al., 2002). Where the lepidocrocite horizon is absent, the transition between SU2 and AM is gradational. In the vent proximal (southwest) part of the Deep, AM is locally referred to as the sulfidic amorphous siliceous (SAM) unit, and SU2 is subdivided into the oxidic anhydritic (OAN) or sulfidic oxidic anhydritic (SOAN) unit (e.g., Figure 2.4C).

## 3. Detailed Mineralogy of the Atlantis II Sediments: Previous Work

The bulk composition of the Atlantis II metalliferous sediments (4 upper units) includes ~10 vol% of detrital biogenic carbonate, silica, and volcanic-derived or terrigenous silicates (i.e., normal deep-sea sediment of the Red Sea: Ku et al., 1969; Stoffers and Ross, 1974). The authigenic component (90 vol%) includes mainly Fe-(oxy)hydroxides (~40 vol%), a siliceous component consisting of Si-Fe-(oxy)hydroxides and clays (~20 vol%), hydrothermal carbonates (~10 vol%), sulfides (<10 vol%), and minor sulfates, Mn-oxides and other nonsulfidic metal-bearing minerals (Table 2.2). The different layer types throughout the basin are mainly characterized by different proportions of these minerals. Bischoff (1969a) defined a number of different facies according to the dominant mineralogy (Fe-smectite, goethite, sulfide, manganosiderite, anhydrite, manganite). Rarely, the different facies comprise almost monomineralic layers. Their distribution among the stratigraphic units is illustrated in Figure 2.3 (from Bäcker and Richter, 1973) and examples different petrographic relationships from this study are shown in Figure 2.4.

The normal pelagic component of the sediment in the Red Sea consists mainly of biogenic carbonates (~80 vol%), including aragonitic pteropod shells, calcitic foraminiferal tests, and coccoliths, with minor radiolarian silica tests (Stoffers and Ross, 1974; Figure 2.4D). Terrigenous clastic material and minor volcanogenic components, such as quartz, feldspar and clays, comprise the remainder. Altered volcanic ash (montmorillonite, cristobalite, and devitrified volcanic glass) were documented by Stoffers and Ross (1974). Normal sedimentation rates in the Red Sea were on the order of 10 cm/1000 yr during the last 20,000 years (Ku et al., 1969); deposition in the Atlantis II Deep included both normal Red

Sea sedimentation and mass wasting from the flanks. This type of sediment dominates the DOP unit (i.e., at the beginning of hydrothermal activity when biogenic detrital carbonate was thickly deposited at the bottom of the Deep: Anschutz and Blanc, 1995a; Blanc et al., 1998). However, carbonate detritus dissolves in the current Lower Brine (Bischoff, 1969; Blanc et al., 1998) and generally is not abundant in the metalliferous sediments (<10 vol%). Biogenic input of silica was restricted to a short period in the early history of the Deep, ~12,000-9,000 years ago, when radiolaria from the Indian Ocean had brief access to the Red Sea due to globally high sea level (Goll, 1969). The silica tests have a good preservation potential compared to biogenic calcite, even in the hydrothermally altered sediments, due to low solubility in low-pH brine, and some metal-rich horizons contain abundant silica tests (Bischoff, 1969a).

Biogenic and siliciclastic detrital material (i.e., background sedimentation) has been deposited throughout the history of the Deep, but input from hydrothermal sources has been variable. The total sedimentation rate during hydrothermal activity is estimated to have been ~100-120 cm/1000 yr (Shanks and Bischoff, 1980) or ~1 mm of authigenic sediment per year, which corresponds closely to the thickness of many of the finer layers observed in the metalliferous muds (e.g., Figure 2.4D, E, F). Fe-(oxy)hydroxides and authigenic clays were the dominant hydrothermal precipitates in sediments formed during periods of low-temperature hydrothermal activity. A variety of poorly crystalline compounds, suggested to have been precursors for various Fe-oxides and clay minerals (Butuzova et al., 1990; Taitel-Goldman and Singer, 2002), are still present in the Atlantis II

sediments (e.g., brown and orange layers in Figure 2.4D and E and green layers in 2.4F). Ferrihydrite, goethite (±limonite), lepidocrocite, and variably crystalline hematite and magnetite have been described in other facies of the Atlantis II sediments, but these have been difficult to identify with certainty because of the poorly crystalline nature of the material and the presence of fine-grained multicomponent mixtures (Bischoff, 1969a; Pottorf, 1980; Knedler, 1985; Butuzova et al., 1988, 1990; Schwertmann et al., 1998). Akaganeite and wüstite also have been filtered from samples of the Lower Brine (Holm et al., 1983). Hartmann (1973) found abundant particulate Fe-(oxy)hydroxides in the Lower Brine and especially at the contact with the Upper Brine. Taitel-Goldman and Singer (2001) suggested that euhedral feroxyhyte (δ-FeOOH) grains, only a few hundred nanometers in diameter, found in the sediment might have formed in the Upper Brine.

Butuzova et al. (1990) and Blanc et al. (1998) suggested the main differences in Fe-(oxy)hydroxide mineralogy of the sediments are due to diagenetic transformation of ferrihydrite, originally formed in the brine pool, to goethite (or hematite in closest proximity to the vents: Bischoff, 1969b; Zierenberg and Shanks, 1983) in a process that has been well documented experimentally (e.g., Schwertmann and Murad, 1983). Although goethite is commonly considered the most important Fe-bearing mineral in the Atlantis II sediments, studies by Schwertmann et al. (1998) and Taitel-Goldman and Singer (2001, 2002) suggested that the high Si concentration in the Lower Brine may have initially retarded goethite formation (cf. Cornell et al., 1987). Schwertmann et al. (1998) also suggested that previous studies underestimated the amount of nano-hematite, due to the

similarity of its XRD pattern to that of goethite. It is generally agreed that diagenesis has increased the crystallinity and grain size of the Fe-(oxy)hydroxide minerals (e.g., Blanc et al., 1998; Taitel-Goldman and Singer, 2002; cf. Taitel-Goldman et al., 2004). It remains unclear to what degree the Fe minerals may have been affected by the sample processing or core storage, but significant differences in Fe mineralogy are always observed between different layer types and therefore likely represent primary variations in the mineralogy.

Well-crystallized manganite is the most common Mn-oxide mineral in the Atlantis II sediments, but groutite, todorokite and the Zn-bearing woodruffite also have been described (Bischoff, 1969a). Manganite can remain metastable in the sediment long after deposition (Diem and Stumm, 1984) and is still present in the metalliferous muds today. However, the Mn-oxide minerals are only common in the CO unit (e.g., Figure 2.4D) and rare elsewhere. Some coarse-grained Mn-oxide layers were suggested by Bischoff (1969a) to have formed by alteration of pre-existing carbonate layers, but Bäcker and Richter (1973) considered the coarser Mn-oxide grains to represent recrystallization during core storage.

Authigenic clays or their precursors formed in the brine pool and in pore waters (Zierenberg and Shanks, 1983; Butuzova, 1984). The most common authigenic clays belong to the smectite group, and these have been studied extensively (e.g., Bischoff, 1972; Goulart, 1976; Cole, 1983, 1988; Cole and Shaw, 1983a; Badaut et al, 1985; Schwertmann et al., 1998; Taitel-Goldman and Singer, 2002: Appendix 2.1). They are mainly composed of Fe and Si, with rare Mg-rich clays at the immediate vent proximity (Cole, 1988) with Na, Ca or K in

the interlayers. Fe-smectite was described as the most common authigenic clay by Bischoff (1969a) and Bäcker and Richter (1973). Other trace clays include vermiculite (Singers and Stoffers, 1981), kerolite (Cole and Shaw, 1983b), talc and chlorite (Zierenberg and Shanks, 1983), and ferripyrophyllite-like minerals (Badaut et al., 1992). In the high-temperature part of the Deep, few published analyses indicate that smectite is compositionally saponite. The clay becomes more iron-rich with distance away from the vents (less than 1 km), where end-member nontronite is dominant (Zierenberg and Shanks, 1983). Most early workers recognized the highly variable crystallinity of the clays (e.g., Badaut et al., 1985); more recently it has been suggested that the majority of the crystalline clays formed during diagenesis rather than by primary precipitation in the brine pool (Badaut et al., 1992; Taitel-Goldman and Singer, 2001, 2002; cf. Taitel-Goldman et al., 2004). The importance of diagenetic changes in the clay mineralogy is supported by Anschutz and Blanc (1995b) who noted a sharp decrease in the Si concentration of the pore fluids during early diagenesis, which was interpreted to reflect the formation of clays and other minerals that crystallized out of the amorphous Si-Fe-(oxy)hydroxides. The recrystallization of the clay minerals during diagenesis is also reflected by changes in the clay mineralogy, from trioctahedral $Fe^{2+}$-smectite in the upper strata to $Fe^{3+}$-clays in the lower strata (Badaut et al., 1985, 1992). Zierenberg and Shanks (1983, 1988) and Singer and Stoffers (1987) concluded that Fe-rich clays (e.g., nontronite) are more common higher in the strata, whereas Mg-rich clays are more abundant at depth. Authigenic silicates also have been found in subvertical anhydrite veins associated with the highest-temperature venting. The silicate minerals in these epigenetic features include Mg-rich smectite, talc, kerolite, and chlorite, but also locally

amphibole, pyroxene, garnet and sphene (Cole and Shaw, 1983b; Zierenberg and Shanks, 1983). The latter (amphibole, pyroxene, garnet and sphene) are thought to have formed by contact metamorphism associated with the intrusion of the basaltic sill (Hackett and Bischoff, 1973; Zierenberg and Shanks, 1983). Heating of the sediments, either by diffusive upflow of hydrothermal fluids or intrusion of basaltic sills, also has directly influenced the Fe mineralogy (e.g., local transformation of hematite to magnetite: Zierenberg and Shanks, 1983).

Authigenic carbonates occur as a minor phase in all of the sediments and are locally abundant (Blanc et al., 1998). Most are solid-solutions between rhodocrosite and siderite, with variable proportions of Mn, Fe, and Ca ("manganosiderite" facies of Bischoff, 1969a, and Bäcker and Richter, 1973). The manganosiderite facies, which includes ankerite and kutnohorite, is interpreted to have formed diagenetically by replacement of biogenic calcium carbonate, as carbonates cannot precipitate in the Lower Brine (Bischoff, 1969a). Other pathways of authigenic carbonate formation were discussed by Blanc et al. (1998) and include (autocatalytic or bacterial) reduction of Fe- and Mn-oxides simultaneously with organic matter oxidation. Dolomite is less common, although many of the carbonates contain minor Mg (Bischoff, 1969a; Blanc et al., 1998). Zn- and Cu-bearing carbonates also have been described by Oudin et al. (1984), Butuzova (1984) and Gurvich (2006).

Amorphous silica and chalcedony have been found in the sediment, but due to slow kinetics of silica precipitation, are unlikely to have precipitated directly from the hydrothermal fluids

during cooling (Ohmoto et al., 1983; Campbell et al., 1988). Anschutz and Blanc (1995b) suggested that silica is brought into the Lower Brine from hydrothermal and detrital sources but removed from the brine pool by molecular diffusion through the chemocline and by deposition into the sediments. Deposition happens mainly with Fe-(oxy)hydroxides as a Si-Fe gel. During diagenesis, celadonite-like or nontronite-like minerals composed mainly of Fe and Si (±K) crystallized out of the Si-Fe gel (Butuzova, 1984; Taitel-Goldman and Singer, 2002) and the residual Si may have remained as amorphous silica in the sediment (Bischoff, 1969a).

Pyrite and sphalerite are the most commonly reported sulfide minerals in the Atlantis II sediments (Pottorf and Barnes, 1983); chalcopyrite is present but less common. All of the sulfides occur as disseminations in a fine-grained matrix of authigenic Fe-(oxy)hydroxides, clays, carbonates, anhydrite and other phases. In the topmost sediments of the AM unit, where there is a very high interstitial brine content (down to about 1 m), the sulfides are mainly X-ray amorphous (Hartmann, 1973; Brockamp et al., 1978), strongly suggesting that the well-crystallized sulfides deeper in the cores formed during diagenesis, as proposed by Weber-Diefenbach (1977) and Butuzova (1984). In other units, the sulfides are also very fine-grained (50-80% <2 μm), but larger grains with diameters of a few tens of μm up to a few hundred μm are not uncommon, becoming more abundant at depth and especially in or near veins (Pottorf and Barnes, 1983). Some of the coarser grains have textures suggesting precipitation directly from the cooling hydrothermal fluids (Pottorf and Barnes, 1983; Missack et al., 1989).

Pyrite formed both during low-temperature hydrothermal activity (in the DOP and CO units), along with Fe- and Mn-(oxy)hydroxides, and also during higher-temperature hydrothermal venting (SU1 and SU2). It occurs as (i) framboids, (ii) spongy yellow pyrite, and (iii) euhedral pyrite (Pottorf and Barnes, 1983). Marcasite is found rarely. Framboidal pyrite is most abundant in the lowermost units and distal from the currently known vent sources; it is absent in the sulfide veins. Sphalerite and chalcopyrite were formed during increased hydrothermal activity and mainly deposited in SU1, SU2 and AM and are most abundant in black sulfidic layers (e.g., Figure 2.4G). Sphalerite is dominant; marmatite (very Fe-rich sphalerite) has been identified (Stephens and Wittkopp, 1969; Butuzova, 1984) but wurtzite has not been found. Sphalerite in the veins has significantly higher Fe contents than sphalerite in the laminated sediment, consistent with formation at higher temperature (Stephens and Wittkopp 1969; Pottorf and Barnes, 1983). Although commonly found rimming chalcopyrite (e.g., Pottorf and Barnes, 1983), suggesting formation during the waning stages of high-temperature hydrothermal activity, the opposite also has been found (Stephens and Wittkopp, 1969) consistent with pulsed high-temperature hydrothermal activity (cf. Ramboz et al., 1988; Missack et al., 1989). In addition to chalcopyrite, the Cu-sulfides include intermediate solid solution (ISS or cubic cubanite), and isocubanite, as well as covellite, chalcocite, digenite and djurleite (Pottorf and Barnes, 1983). Pyrrhotite is found as large grains (up to 150 µm) in sediments closest to the hydrothermal vents and likely formed at high temperatures. The presence of other iron monosulfide(s), such as amorphous FeS, mackinawite or greigite also has been inferred from rapid reaction in cold

HF (Pottorf and Barnes, 1983). Overall, the ratios of Zn- and Cu-sulfides to Fe-sulfides are high compared to most seafloor massive sulfide deposits (cf. Hannington et al., 1995, 2005).

A number of authors have described nonsulfidic metal-rich minerals from the Atlantis II sediments (e.g., chrysocolla and atacamite: Bischoff, 1969a; Butuzova, 1984; Gurvich, 2006; Zn-rich oxyhydroxides and carbonates, such as woodruffite and hydrozincite: Bischoff, 1969a; Oudin et al., 1984). Most are likely secondary minerals that formed during core storage and sample preparation (see below). However, Zn-enrichment of Fe-(oxy)hydroxide particles from the Lower Brine (Hartmann, 1973) strongly supports the suggestion that Zn (and probably minor Cu) were deposited in the sediments by adsorption onto Fe-OOH.

Sulfates are locally abundant in the sediments, and anhydrite, barite, gypsum and bassanite have been described from many of the cores (Zierenberg and Shanks, 1983; Blanc et al., 1998; e.g., Figure 2.4C and H). Anhydrite is found as subvertical, cross-cutting veins in sediment cores taken near the locations of hydrothermal venting and especially in the lower strata (Zierenberg and Shanks, 1983). Anhydrite also has precipitated directly from the brines, most likely pore water (see below), forming massive, stratabound, sill-like bodies that may reach several meters in thickness and hundreds of meters in strike length (Bäcker and Richter, 1973). The massive beds of anhydrite are most common in the area of active hydrothermal venting, but they are also found in the distal part of the Deep. The gypsum and bassanite that have been reported in the sediments would be unstable in the Atlantis II brines and likely formed during core storage. Barite is undersaturated in the

Lower Brine (Shanks and Bischoff, 1977) and is mainly found on the flanks of the basin and on highs that reach the upper brines (e.g., Sval'nov et al., 1984).

## 4. Sampling and Methodology

For this study, one hundred samples were taken from 9 brine-saturated sediment cores collected in the southern 2/3 of the basin (Figure 2.1). All cores were collected during the *R/V Valdivia* cruise 29 in 1980. Cores that contain all 5 lithostratigraphic units were selected to study the differences between sedimentary units as well as spatial variations across the deep. The selected cores are 5 to ~12 m long, and most are from depths of >2100 m (cores 495 and 546 are from 2076 and 2013 m, respectively). After recovery, the cores were split, and one half was sealed and stored in a cool warehouse. When reopened in 2010, the archived cores were in excellent condition and still moist, although the cut surfaces were, in many cases, encrusted with salt and had a thin layer of surface oxidation. When the crystalline salt and surface oxidation were removed, the remarkably delicate layering of the sediments could be readily logged and sampled. Figures 2.3 and 2.4 show the large variation in textures and mineralogy over very short vertical intervals.

In order to correlate fine-scale layering with mineralogical and chemical changes, representative cores were scanned using an automated energy-dispersive X-ray fluorescence (XRF) scanner at the University of Kiel (AVAATEC Scanner). Two cores were chosen from the northern part of the Deep where the sections are most condensed: core Va29-229 at depth intervals 300-500 cm and 600-800 cm and core Va22-275 at a depth

interval 500-600 cm (cf. Jost, 2014). The relative intensity of X-ray peaks for selected elements were measured on the untreated surfaces of the cores at 2 mm intervals with slit size 2 mm down core and 12 mm cross core. Runs were done at 10 keV and 30 keV with 1250 and 2000 mA, respectively, and count times of 10 seconds. No filter was used during the 10 keV run; a Pd filter was used for the 30 keV run. Absolute concentrations could not be reliably determined, owing to the highly variable physical properties of the sediment, such as density and brine content (e.g., Tjallingii et al., 2006). However, the scans match observed variations in the core logs, even at a fine scale (Figure 2.5).

After re-logging the cores, samples were collected using <2 cm-diameter minicores; in some cases samples were cut from the core box with a spatula. This approach is much more detailed than in previous studies, which were mostly based on composite samples several 10s of cm up to 1 m in length (e.g., Henricks et al., 1969; Bäcker and Richter, 1973; Shanks and Bischoff, 1980; Gurvich, 2006). Individual samples were dried at 40°C, during which pore water was evaporated. This contrasts with earlier studies in which samples were washed to remove salt before mineralogical or chemical analyses.

The mineralogy of the samples was determined by a combination of petrographic study, X-ray diffraction (XRD), and electron microbeam techniques. XRD analyses were carried out at the University of Ottawa on a PANanalytical XRD system, using Phillips X'Pert system analytical software to identify the minerals present. Due to the abundance of salt and poorly crystalline phases and the fine grain sizes, typically only the most abundant Fe-

mineral was resolved. Polished thin sections of the samples were prepared at the University of Ottawa from undisturbed sediment. ~2 x 3 cm blocks were dried in air and impregnated in epoxy to preserve the sedimentary structures. The thin sections were examined in reflected and transmitted light and using a JEOL 6610LV scanning electron microscope (SEM) at the University of Ottawa. Spot analyses of discrete mineral phases were performed using the energy dispersive spectrometer of the SEM and by element mapping using the JEOL 8230 SuperProbes, both at University of Ottawa and GEOMAR. The microanalytical data for different phases are summarized in Tables 2.3 and 2.4, but the precision of the analyses of the very fine-grained material generally does not permit positive identification of the minerals. Several samples were studied further using a Field Emission SEM (JSM-7500F FE-SEM) at the University of Ottawa and by synchrotron-XRF (VESPER beamline at the Canadian Light Source) in an attempt to resolve the residence of Au in As-rich pyrite. Details of these methods are discussed further below.

The mineralogical data were compared to the normative mineralogy of the different layer types determined from the bulk compositions of individual samples. The chemical analyses were performed at the University of Kiel; powdered samples were dissolved in a multistep table-top procedure using HF-$HNO_3$-HCl-$HClO_4$ (described in Garbe-Schönberg, 1993) and analyzed by inductively coupled plasma (ICP) optical emission spectrometry (OES, Spectro Ciros SOP) for major elements (Al, Ti, P, Na, K) and by ICP mass spectrometry (MS, Agilent 7500cs) for trace elements (As, Ag, Cd, Ni, Cr, Th, Hf, Zr, Y, Sc, V, Cs, Li, Nb, Ta and REE). Splits of the samples were also analyzed by Activation Laboratories, Ancaster, Ontario,

following fusion with sodium-peroxide to achieve total dissolution; these samples were analyzed by ICP-OES (Varian Vista) for Fe, Si, Ca, Mg, and by ICP-MS (Perkin Elmer Sciex ELAN) for Mn, Ba, Cu, Zn, Pb, Co, Mo, Ga, Ge, Tl, V, W, U, Se, Sn, Sr, Rb, In and B (plus Be, Bi and Te, which were not detected, except 6.3 ppm Bi in one sample). The samples were also analyzed by instrumental neutron activation (INA) for Au, Sb and Br (plus Ir, which was not detected); by cold vapor flow-injection (FIMS) for Hg; by ion selective electrode (ISE) for fluoride; by coulometry for carbonate carbon; and by infrared detection (IR) after combustion at 550°C for sulfate sulfur. At the University of Ottawa (Hatch Laboratories) samples were analyzed for total N, O, C and S after combustion at 1800°C using an Elementar VarioEL III elemental analyzer. Reduced sulfur was calculated from total and oxidized sulfur concentrations, and organic carbon was calculated from total and oxidized carbon concentrations. Because some sulfate has undoubtedly originated from oxidation of sulfide during core storage (see below), the amount of reduced sulfur is a minimum value and the sulfate a maximum. The primary data were recalculated to “salt-free” compositions using the sodium concentration as a proxy for the amount of NaCl and assuming all Na is bound to halite. The full data set is reported in Laurila et al. (2014a) and Appendix C.

Finally, a series of sequential leaching experiments was performed on selected samples at ALS Laboratories in Vancouver. Four leaching steps were performed: with distilled water, which dissolves the secondary salts and secondary sulfates; with ammonium acetate (0.1 M buffered to pH 4.7-4.9), which mainly dissolves calcite and dolomite but not the authigenic carbonates (e.g., Fe-Mn carbonates); with cold hydroxylamine hydrochloride (0.1 M

$NH_2OH{\cdot}HCl$ in 0.01 M $HNO_3$), which dissolves mainly amorphous Mn- and Fe-(oxy)hydroxides (Tessier et al., 1979; Hall et al., 1996; Hlavay et al., 2004); and with hot hydroxylamine hydrochloride (0.25 M $NH_2OH{\cdot}HCl$ in 0.025 M $HNO_3$ at 60°C), which dissolves the residual Mn- and Fe-(oxy)hydroxides (e.g., ferrihydrite, goethite and lepidocrocite) but not hematite or magnetite. The behaviour of the different phases was monitored by analyzing the major and trace element concentrations by ICP in the leachates after each step.

## 5. Results

Both the core logs and XRF scans highlight the fine mm-scale layering and variable mineralogy of the sediments (Figures 2.3, 2.4, and 2.5). Figure 2.5A gives an example of the variations in bulk composition in just 1 m of sediment in the upper (unit SU2 to AM) and lower strata (unit SU1 to COS) from core 229, which is located in the far north of the Deep (see Figure 2.1 for location). The chemical variations in the upper strata reflect mainly diffuse layering, typical of AM, whereas layering in the lower strata is characterized by sharp changes in the K, Si and Fe contents of different laminae. The high Cu and Zn concentrations in SU1 in this core correspond to a time when the hydrothermal venting was located in the north of the Deep; Cu and Zn are much lower in SU2 and AM because the main hydrothermal venting is now located far away from this core, in the southwest. Figure 2.5B shows the transition from COS to SU2 in a 1-m interval from core 275, also in the northern part of the Deep. Bulk sampling of the COS previously indicated uniformly high concentrations of Fe and low Mn (Laurila et al., 2014a), but the core scans show alternating

layers of Fe then Mn enrichment at the cm scale (see also Figure 2.4D). This may corresponds to previously unrecognized rapid changes in the chemistry of the brine pool. In Figure 2.5B, as many as five episodes of Mn-oxide deposition appear to have occurred over an interval of less than 20 cm.

Whereas the uppermost sediments are characterized by diffuse lamination (e.g., Figure 2.4B and upper section of Figure 2.5A), well-defined laminations are common in the lower strata (e.g., Figures 2.4D, E, F, G and lower section of Figure 2.5A). Figure 2.6A (sample 373-734 from DOP) shows a typical 5-mm thick hard layer of Fe-(oxy)hydroxides with millimeter-scale laminae of different colors (orange, yellow, brownish red). Sulfidic layers are typically darker grey to black bands (e.g., sample 495-859 from SU1: Figure 2.4G and Figure 2.6B). Although chalcopyrite and sphalerite occur as small anhedral sulfide grains, and pyrite is found as larger, commonly more euhedral crystals in sample 495-859 (Figure 2.6B), most of the metals in the sulfidic layers occur in the "matrix" (see below). The sulfidic component imparts a dark color to the sediment even in very small quantities (as low as a few percent). Other samples with a large hydrothermal component comprise submillimeter, metal-enriched laminae (e.g., dark grey layers in sample 495-777 from SU1: Figure 2.6C) that contain abundant silica tests in a hydrothermal carbonate- and clay-rich matrix. Most sulfidic layers also contain anhydrite (e.g., sample 264-907 from SU1: Figure 2.6D). Other layers are green in color and contain fewer and smaller sulfide grains (Figure 2.4F); clays are common in these layers and pore water content is typically higher. The lighter, mm-scale

bands (Figure 2.6B) are composed mainly of detrital material, including relict biogenic calcite, intermixed with minor hydrothermal components.

The different layer types can also be classified according to their bulk compositions (Figure 2.7: Laurila et al., 2014a). Layers that are largely detrital in origin contain abundant biogenic calcite (Figure 2.7A) and abundant $Al_2O_3$ in aluminosilicates (Figure 2.7B). The Fe-oxide-rich layers, which may also include Fe-rich clays and Fe-bearing carbonates but not sulfides, all plot close to $Fe_2O_3$ in Figure 2.7B. The sulfate-rich layers contain both anhydrite and abundant secondary sulfates that were originally present in the cores as sulfides (see below). These samples contain the most base-metal sulfides and plot in the metal-rich corners of Figures 2.7B and C. The clay-rich layers plot in the lower left of Figure 2.7A because they contain neither abundant carbonate nor sulfate.

In the cores taken closest to the known areas of hydrothermal venting, there is a marked increase in anhydrite with decreasing carbonate (linked to the higher temperatures associated with hydrothermal venting). These samples contain the most sulfide, with lesser amounts of authigenic clays. We have classified these samples according to their metal-to-sulfur ratios: high sulfur, high metal (HSHM); high sulfur, low metal (HSLM); low sulfur, high metal (LSHM); and low sulfur, low metal (LSLM) (Figure 2.7). The mineralogy of the HSHM samples is dominated by Zn and Cu sulfides and sulfate; HSLM samples include mainly Fe sulfides and sulfate. LSLM samples contain abundant Fe-(oxy)hydroxides and authigenic clays as well as anhydrite. Although LSHM samples have very low sulfide they have high

nonferrous metal concentrations and contain a number of nonsulfidic metal-bearing minerals that are described below.

The different layer types with different bulk compositions are found in all of the stratigraphic units but in varying proportions. This complicated previous attempts to classify the mineralogy of the sediments, because mineralogically different layers at the centimeter scale were typically grouped together as one “facies” characterizing a particular stratigraphic unit. Calcite-rich, detrital layers are most abundant in DOP, whereas hydrothermal carbonates are most abundant in samples from CO; clay-rich layers are most common in CO, COS and SU2; metal-rich layers (both HSHM and LSHM) are found in SU1, SU2, AM, SOAN (>35% of samples) and especially in SAM (100% of samples). Metal-poor but sulfur-rich (HSLM) samples are mainly from the lower units, OAN and SU1, reflecting mainly diagenetic pyrite; anhydrite-rich layers are most common in SOAN but also SU1.

## 5.1 Detrital minerals

### 5.1.1 Detrital silicates

The terrigenous clastic components of the sediments are resistant to hydrothermal alteration and well preserved in almost all layers. Detrital silicates account for about 20-45 vol% of the background sediment but never account for more than 5 vol.% of the clay-rich and sulfate-rich samples. The terrigenous clastic component of the carbonate-rich samples is more variable, owing to dissolution of the biogenic carbonate component and, in some cases, precipitation of authigenic carbonate. Quartz, feldspar, rock fragments, and mica

were readily identifiable under SEM (e.g., Figures 2.8, 2.9 and 2.10). More rarely heavy minerals (zircon, titanite) were also identified by SEM in most sediment types (samples 264-474 and 373-734: Table 2.3). Unlike the authigenic silicate components (see below), the detritial silicates are generally well crystallized.

### 5.1.2 Detrital carbonates

Biogenic detritus is the main source of calcite in all samples and can be readily discriminated from later hydrothermal carbonate (Mn-Fe-rich) by the well-preserved fossil textures (e.g., Figure 2.8). Calcite comprises 30-65 vol% of the layers with the most abundant detritus, and Mg-carbonate <10 vol% (present as Mg-rich calcite and dolomite). Sulfur- and metal-rich samples contain only minor amounts of calcite. Dolomite is present in both the terrigenous and authigenic constituents of the Red Sea sediment (Stoffers and Ross, 1974), and it is more resistant to hydrothermal alteration than calcite. Locally it is found in the cores of zoned, hydrothermal Fe-Mn-rich carbonates (see below).

### 5.1.3 Biogenic silica

Radiolarian tests, which are resistant to alteration, are preserved even in sediment with a strong hydrothermal overprint (e.g., SU1), commonly in discrete laminae (e.g., Figures 2.6C and 2.9A). Layers enriched in radiolarian tests are highly porous and appear to have acted as thin aquifers for the hydrothermal fluids. This is evident in the distinctive Zn and S enrichment of the fossil-bearing horizons (Figure 2.10). Pseudomorphs of silica tests are common in these layers, replaced or infilled by clay minerals (possibly associated with dissolution and reprecipitation of silica). Figures 2.9A and B show radiolaria that have been

dissolved and infilled with clays (dark areas) and the silica framework replaced by Fe-(oxy)hydroxides (lighter areas). In Figure 2.9C, a radiolarian test has been replaced by an unidentified nonsulfide Zn-(oxy)hydroxide(?) phase (up to 57 wt.% Zn: see sample 495-859 below and in Table 2.3).

## 5.2 Authigenic minerals

### 5.2.1 Fe-oxides and (oxy)hydroxides

Fe-oxides and (oxy)hydroxides are the major components of most sediment, but the poor crystallinity, extremely small grain size, and the extent of post-depositional alteration make positive identification of the minerals generally difficult. In thin section, the Fe-(oxy)hydroxides are commonly interstitial to more crystalline phases or occur in diffuse patches of Fe-enrichment in a poorly crystalline matrix of Si, Ca, Na, Cl, O (e.g., Figures 2.9B and 2.10). The diffuse nature of the Fe-enrichment is consistent with the suggestion of Taitel-Goldman and Singer (2002) that the Fe-rich layers were originally deposited as amorphous precipitates and later crystallized during diagenesis. The bulk composition of the Fe-(oxy)hydroxides include subequal amounts of Fe and O with a few percent of minor elements (e.g., Si, K, Cl or S; samples 373-734, 495-859 and 264-474: Table 2.3). Some Fe-(oxy)hydroxides are notably enriched in other metals. Figure 2.11A shows an EPMA element map of a cluster of rounded Fe-(Si)-OOH particles in sample 503-912 that are depleted in S but nevertheless enriched in Ag, As, and Cd compared to the matrix.

Layers with bright red, yellow and orange colors typically have the highest Fe-contents. The macroscopic color variations reflect the relative abundance of Fe-(oxy)hydroxides and clays. Unexpectedly, darker reddish brown layers commonly have a high clay content (see below). However, in most samples it was not possible to correlate color with a consistent mineralogy, indicating that most layers are mixtures. X-ray diffraction of the different Fe-rich layers indicates a wide range of Fe-hydroxides among the better crystallized phases (e.g., samples 373-798 and 334-757: Table 2.5). The bright yellow layers commonly contain goethite (α-FeOOH), orange layers contain lepidocrocite (γ-FeOOH), and dark red layers sometimes contain hematite ($Fe_2O_3$). Akaganeite (β-FeOOH), which is the only Fe-(oxy)hydroxide mineral that may contain Cl in its structure, was also identified (sample 503-889: Table 2.5). Sample 421-870 was bright orange at the time of sampling but became brownish during sample preparation, typical of lepidocrocite (Schwertmann and Cornell, 2000). Other layers, which were bright yellow (sample 421-223) turned dark red after drying in air and crushing; XRD showed that sample 421-223 was mainly composed of goethite. Sample 503-626 was bright red and remained so during sample preparation; it also consisted mainly of goethite. The variations in color might be explained by variations in grain size. Schwertmann and Cornell (2000) showed that a decrease in grain size from ~2 to 0.2 μm causes goethite to become notably darker, although the presence of minor hematite intermixed with goethite has the same effect. Sample 334-757, located in the lower sediments close to the known hydrothermal venting, was the only sample where hematite was positively identified by XRD. Magnetite was not identified.

Larger grains of Fe-oxides, up to ~30 µm in size, are found as minor phases in all types of samples, including sulfur- and metal-rich samples (Figure 2.9D), hydrothermally altered detrital samples (Figure 2.9E), and anhydrite samples (Figure 2.9F). Some well-crystallized Fe-oxides (e.g., in Figure 2.9E) have bulk compositions resembling goethite or hematite (~67% Fe and ~33% O) with notable rims that are enriched in Zn (>5 wt.%) and Si (~15 wt.%) (sample 495-859: Table 2.3). This may indicate that the precursor Fe-(oxy)hydroxides crystallized out of Si-Fe-OOH gel with adsorbed Zn, but did not accommodate Zn into their structure.

### 5.2.2 Mn-(oxy)hydroxides

The Mn-rich layers are extremely fine grained and soft (Figures 2.4D and 2.5B) and Mn is likely present as amorphous Mn-(oxy)hydroxides. Black Mn-staining is locally found in adjacent layers suggesting that some of the Mn has likely migrated out of the Mn-rich layers. Crystalline manganite (MnOOH) is also locally abundant, especially in samples from the CO unit (e.g., identified by XRD in sample 495-569: Table 2.5). In contrast to DOP, in which much of the Mn is present as carbonate, samples from CO contain significantly more Mn than can be bound to carbonate (e.g., samples 373-265 and 495-569, which contain ~32 and 27 wt.% Mn, respectively, and only 0.5 and 2.3 wt.% $CO_2$: Chapter 3 and Laurila et al., 2014a). Samples containing abundant Mn-oxides generally do not contain abundant Fe-(oxy)hydroxides, confirming that conditions suitable for precipitation of Mn alternated with conditions of Fe deposition (as in Figures 2.4D and 2.5B). At two locations in core Va22-275 (e.g., 580-585 cm) very high Fe and Mn values overlap, indicating that Mn- and Fe-

(oxy)hydroxides are mixed or that alternating Mn- and Fe-rich layers are very thin (about the spot size of the core scanner, i.e., < 2 mm).

### 5.2.3 Authigenic clays

Clay-rich layers are found in all stratigraphic units. These layers typically have a greenish color (Figure 2.4A, upper part, and 2.4F), are very fine grained, and commonly are saturated with water with a high salt content. During drying (at 40°C), some of the clay-rich samples took several weeks to become completely dry. Although the typical color of the clay-rich layers is greenish, some of the clay-rich layers in SU1 are red-brown (Figure 2.4H).

The clay mineralogy is dominated by amorphous and poorly crystalline phases, that dominate the fine-grained matrix of many sediments. Authigenic clays are readily distinguished from detrital silicates (most abundant in DOP) by their much lower Al/(Fe+Mg) (Singer and Stoffers, 1981; Schwertmann et al., 1998; sample 264-474: Table 2.3 and Figure 2.12). Authigenic clays are most common in the upper 3 units, especially in unit COS and in cores from the distal part of the Deep. Clays and clay-rich layers are also present in the metal-rich units, and some clays in SU1 and SU2 have high metal contents (sample 264-474 in unit SU2: Table 2.3). As noted above, clay-rich material commonly infills and partly replaces siliceous tests, suggesting that it may have crystallized out of the pore water during diagenesis.

The abundant pore water in the clay-rich layers likely accounts for the high $K_2O$ content (~2.5 wt.%) of the clay-rich samples (Appendix 3.1 and Appendix C), but some authigenic

clays also may contain K in their interlayers (Badaut et al., 1985). In particular, Butuzova (1984) suggested that some of these K-rich clays may have formed from the K-rich pore water during diagenesis. Other previous studies mainly reported clays with <0.5 wt.% $K_2O$ (Bischoff, 1969a; Singer and Stoffers, 1981; 1987; Zierenberg and Shanks, 1983; Badaut et al., 1985; Cole, 1988; Schwertmann et al., 1998), although Bischoff (1972), Badaut et al. (1992), and Taitel-Goldman and Singer (2001) all found clays with higher $K_2O$.

The clay-rich horizons are also notably enriched in Fe (Figure 2.7 and Appendix 3.1) partly because of co-deposition with Fe-(oxy)hydroxides but also because of the presence of Fe-rich smectite (e.g., sample 264-474, Table 2.3). The latter is thought to have been typical of clays precipitated directly from the brine pool (Zierenberg and Shanks, 1983, 1988; Cole, 1988). SEM spot analyses of the dark areas in Figure 2.9B (sample 373-734: Table 2.3) indicate ~45% O, ~20-30 wt.% Fe, 10-15 wt.% Si, and up to 15 wt.% combined Mg, Al and K, which is approximately the composition of authigenic clays found in other studies of the Atlantis II sediments (e.g., Appendix 2.1 and Figure 2.12). Three clay-rich samples from an anhydrite-rich core proximal to the inferred vent sites in the SW Basin (core 617) have whole-rock concentrations of MgO as high as ~6-8 wt.% with low $CO_2$ (i.e., thus excluding dolomite: Appendix C.1). Mg-rich smectite has been described as the main epigenetic clay associated with hydrothermal venting in the Deep (e.g., Cole, 1988).

SEM spot analyses indicate variable but locally high Zn concentrations in some clays (e.g., up to a few wt.% percent at the arrow in Figure 2.9G; sample 495-777: Table 2.3). In low-

sulfide, high-metal (LSHM) samples, almost all clays contain at least a few percent metals (e.g., up to 5 wt.% Zn in sample 264-474: Table 2.3). Similar metal-enrichment has been documented in other studies (Appendix 2.1).

### 5.2.4 Hydrothermal carbonates

Most carbonates in the lighter colored layers (e.g., Figure 2.6B) are calcite with well-preserved fossil textures, but in the darker layers biogenic calcite is replaced by very small grains of Fe-Mn-carbonates that are dark or opaque (Figure 2.9H). Hydrothermal carbonates are mainly Ca-Mn-Fe solid solutions (Figure 2.13) and commonly have well developed crystal forms (Figure 2.9I). Fe-Mn-rich carbonates commonly are found rimming earlier carbonates (especially Mg-rich calcite or dolomite: Figure 2.9J), with the rims containing as much as ~40 wt.% Fe, ~8 wt.% Mn, and ~5 wt.% Ca (i.e., manganosiderite: Table 2.3). Hydrothermal carbonates are common in CO and DOP, and in a few samples from SU1 and SU2, but they are not abundant in cores closest to the inferred hydrothermal vents. In some Mn-rich samples from DOP (e.g., sample 495-889, which contains 9.3 wt.% Mn and 11 wt.% $CO_2$: Appendix C.1), much of the Mn is bound to carbonate. The composition of the carbonates changes from Mn- to Fe-dominated with proximity to the known vents, reflecting the stronger hydrothermal influence.

Siderite is present in some of these samples, commonly in association with pyrite. Many hydrothermal Fe-Mn carbonates contain a few percent of Zn (sample 495-777 in Figure 2.9G and Table 2.3), especially in the low-sulfur samples. However, there appears to be little correlation between the carbonate concentration and the bulk Cu and Zn contents of

the sediments (e.g., samples 503-516 and 503-987 from the same core have similar $CO_2$ contents of 3.5 and 4.5 wt.%, respectively, but different metal concentrations of 3.4 and 1.2 wt.% Zn+Cu, respectively: Appendix C.1). Abundant hydrothermal carbonate appears to have formed mainly by infiltration of hydrothermal fluids into the sediment or from diagenetic reactions with pore fluids (e.g., Figure 2.10). Generally, sulfate-rich samples have no calcite and low $CO_3$-content, especially in vent proximal cores; however, a few have unexpectedly high hydrothermal carbonate contents (e.g., samples 334-83, 334-612, 557-388, 503-7, 503-509).

### 5.2.5 Amorphous silica

It is unclear how much silica was precipitated directly from solution or was derived from the poorly crystalline assemblage of Si-Fe-(oxy)hydroxides and authigenic clays. Although Anschutz and Blanc (1993) observed the direct transformation of radiolarian tests to chalcedony, most of the siliceous fossils in our samples were not dissolved even by strong hydrothermal alteration (e.g., sample 495-777 from SU1: Figure 2.10). Increasing Si with depth in the cores (from less than 7 wt.% Si in AM to >9 wt.% in SU1 and DOP: Table 2.1) and high $SiO_2/Fe_2O_3$ ratios in the lower strata (e.g., in samples 503-516 and 546-318: Appendix C.1) suggest that silica was being deposited rather than dissolved during diagenesis (Laurila et al., 2014a).

### 5.2.6 Sulfides and associated trace minerals

In all sediments, the darkest bands generally contain the most sulfides (e.g., sample 495-859 in Figures 2.4G and 2.6B). They are most abundant in the vent-proximal sediments, in

AM and SU2 and in the lower sulfidic unit (SU1) in the distal part of the Deep. Sulfide-rich layers in the cores closer to the known areas of venting (e.g., sample 334-513) contain both Cu- and Zn-sulfides; far from the known vents the sulfides are dominated by pyrite (e.g., sample 387-575). Some sulfide-rich layers in the proximal cores are black in color and distinctly granular, especially in unit SU1. These have been the focus of previous studies of the ore mineralogy because of the large grain sizes (Stephens and Wittkopp, 1969; Pottorf and Barnes, 1983; Oudin et al., 1984; Missack et al., 1989). However, most of the samples from other units have no or few sulfide grains that are detectable with a normal petrographic microscope. Samples that are highly sulfidic comprise millimeter-scale, metal-enriched laminae (e.g., sample 495-859 from SU1: Figure 2.4G) that contain Cu- and Zn-sulfides (up to 100 µm) but also diffuse patches of metal enrichment in the "matrix" in which no grains can be clearly discriminated under SEM (Figure 2.10). Composite grains of both chalcopyrite and sphalerite are common (Figures 2.11C and 2.14A). Sphalerite is less common in the studied samples, mainly due to alteration during core storage (e.g., Figures 2.14B and C; see below). Where present, the sphalerite grains show strong Fe/Zn zonation and high Cd concentrations (Figure 2.11C, upper part). Most of the analyzed grains in this study had low Fe contents (Table 2.4) compared to many earlier studies (Figure 2.16). The Cd concentration in sphalerite based on bulk compositions of the sediment and assuming stoichiometric substitution is ~0.2 wt.% (Figure 2.15B); the Hg content is ~30 ppm (Figure 2.15C). Where visible, the larger chalcopyrite grains have exsolution lamellae with variable Fe/Cu ratios (Figures 2.9K and 2.11B), similar to the ISS previously documented by Pottorf and Barnes (1983) and Missack et al. (1989). In a number of samples, chalcopyrite is notably

enriched in Ag (Figures 2.11B and C). Assuming that all of the Ag in the samples is present in chalcopyrite, it is possible to estimate the Ag content of chalcopyrite from the bulk compositional data (Figure 2.15). Stoichimetric substitution of Ag in chalcopyrite would correspond to a concentration in chalcopyrite of ~0.3 wt.% Ag (Figure 2.15A). Galena is not present in the samples from this study.

Pyrite is most commonly found as clusters of tiny (<1 μm) grains (e.g., similar to framboids: Figures 2.14D, E) but also as large (up to 200 μm) sub- to euhedral crystals (Figure 2.11E). The grain size of the pyrite generally increases with depth in the cores, with more and more densely clustered grains (e.g., Figures 2.14E and F) found at depth. Brockamp et al. (1978) showed that the pyrite framboids have locally grown around a nucleus of Fe-rich particles (in some cases Fe-monosulfide). Coarse subhedral to euhedral pyrite is found only in sediment closest to the known vents in SU1 and SU2. Some of these grains may have been mechanically transported from the vent source (cf. Pottorf and Barnes, 1983), but some have continued to grow in the sediment, as indicated by distinctive As-rich rims (Figure 2.11F). The framboidal pyrite (Figure 2.11H) typically has much higher trace metal concentrations than the coarse euhedral pyrite (e.g., Figure 2.11E), which may reflect scavenging of metals from enriched pore fluids or changing pore water composition during diagenetic growth. The highest As contents in the rims (up to 1.6 wt.%, sample 503-912: Table 2.4) are about 4 times higher than in the cores. This sample also has the highest bulk gold content measured in our study (3.8 ppm Au: Table 3.2 and Appendix C.1), strongly suggesting a correlation between the occurrence of As-rich pyrite and Au. Other trace

elements, such as Ni, Mo and Se are present in pyrite but are not notably enriched in the As-rich rims (see Appendix E.2_4).

In an attempt to determine the residence of the Au in the Atlantis II sediments, several anomalous sulfide-rich samples were studied under the FE-SEM, a surface technique, and with powerful X-rays by synchrotron-XRF, a deeply penetrating technique. The studied samples showed no evidence of Au nanoparticles on their surfaces under FE-SEM. The high-energy X-rays of the synchrotron penetrate ~100 µm into the sample, thus increasing the volume of the material accessible to analysis. The presence of even a few Au nanoparticles in this volume would likely be detected by this method (Basto et al., 1995; Brugger et al., 2012; cf. Dobosz, 2012). Figure 2.17 shows the synchrotron-XRF maps of two samples targeted for the detection of Au, one containing a grain of As-rich pyrite (sample 503-912) and another containing individual grains of chalcopyrite, secondary Cu and Zn phases, and authigenic clay (sample 268-985). Unfortunately, the Fe, As, and Au maps in the pyrite sample completely overlap, precluding the detection of Au. The Kβ1 peaks of Zn at 9572 eV and As at 11726 eV directly overlap with the Lα1 and Lβ peaks of Au (9713 and 11441 eV, respectively), and the doubling peaks of Fe (12807 and 14115 eV) raise the background around the Lγ1 peak of Au at 13381 eV. However, the authigenic clay in 268-985 shows the distinct Lγ1 peak of Au that does not match the doubling peak of Fe at the same energy. The lack of correlation with Fe in this grain is a good indication of possible nonsulfide Au enrichment, but no other evidence of submicroscopic gold was found.

### 5.2.7 Nonsulfidic metal-bearing minerals

A variety of nonsulfidic minerals in the metalliferous sediment are distinctly rich in metals. Some are primary precipitates (e.g., carbonates and metal-enriched clays), whereas others clearly formed during core storage, either by oxidation of pre-existing sulfide minerals or by direct precipitation from metal-enriched pore fluids in the recovered cores (e.g., metal sulfate or metal salts: see below). A number of cores in SU2 contain sediment with abundant metal-enriched clays (e.g., 508-512 cm in core 495 in Figure 2.3). These include dark green layers with low sulfide content but high metals with a distinctive “greasy” feel at the time of sampling, indicative high primary pore water content now seen as abundant salt crystals. Some metal-rich clays (e.g., sample 495-777, Figure 2.9G) contain up to 5 wt.% Zn with no sulfur (Table 2.3). This is interpreted to reflect metal deposition via adsorption onto poorly crystalline Si-Fe-OOH, followed by incorporation in diagenetic clays. To a lesser extent, similar metal enrichment is found in carbonates, sulfates, and chlorides (e.g., Figure 2.11D and Table 2.3).

### 5.2.8 Sulfates

Anhydrite is the dominant sulfate mineral in the metalliferous sediment and occurs as disseminated grains, discordant veins, and locally as massive beds. Some layers of almost pure anhydrite are typically well consolidated and fine-grained (Figures 2.4C and H); they may be up to 2 m in thickness, although most are less than a few 10s of cm thick. Some layers are part of laterally extensive sill-like bodies, up to a few hundred meters wide, that are interpreted to have crystallized from pore water during magmatic heating (Shanks and Bischoff, 1977).

Figures 2.9F and L show the typical texture of anhydrite layers. In some cases, clusters of anhydrite have coprecipitated with hydrothermal clays and Fe-(oxy)hydroxides and locally with minor barite and sulfides. Commonly, however, sulfides are absent, and most of the nonferrous metals (up to ~1 wt.% Zn) are associated with clays and other nonsulfide minerals, as noted above. Thin anhydrite beds (<2 cm: e.g., Figure 2.4C) commonly have diffuse contacts with the adjacent layers, suggesting that they crystallized along zones within porous layers in the sediment. These layers are typically found in groups (multiple thin layers) rather than single coherent beds. Epigenetic veins of anhydrite proximal to the inferred upflow zones in the SW Basin have been studied in detail by Zierenberg and Shanks (1983), Oudin et al. (1984), and Ramboz et al. (1988). In contrast to the massive and disseminated anhydrite, the veins are often metal-enriched and contain abundant sulfides (Stephens and Wittkopp, 1969; Pottorf and Barnes, 1983; Zierenberg and Shanks, 1983; Oudin et al., 1984).

Barite is a minor phase (<2 vol%) and most common in cores close to the inferred locations of the hydrothermal vents. Barite appears to have grown within the sediments, most likely from interaction with hydrothermal fluids, similar to the authigenic carbonates. Typically it has a distinctly crystalline habit (Figure 2.9D). Strontium, the only significant trace element in barite, is present at concentrations of 4-5 wt.% (e.g., sample 495-777: Table 2.3).

**5.3 Normative mineralogy**

Using the qualitative mineralogy of the studied samples as a guide, the normative abundance of minerals in the Atlantis II sediments can be estimated from their bulk chemical composition (Appendix D). Figure 2.18 is a summary of the normative mineralogy of the Atlantis II sediments in this study showing the relative proportions of the major components of different layer types plus the weight percent of sulfide and nonsulfide metal-bearing minerals. After correcting for the salt content, the siliciclastic detrital component was calculated according to immobile element concentrations (e.g., Al, Zr, Ti, Sc). Good correlations between Sc and the Al, Si and K concentrations ($r^2$=0.97, 0.80 and 0.50, respectively) allow us to estimate the detrital component of the samples by assuming that the ratios of these elements are constant and similar to those of average shale (e.g., using the Sc/element ratio of PAAS from Taylor and McLennan, 1985). The total amount of Al, Mg, K, Si, Fe, and Ca bound to detrital minerals in each sample estimated in this way is listed in g/kg in Table 2.6. Detrital layers contain about 35 wt.% siliciclastic material, on average. In all other layer types, the siliciclastic detrital component is typically less than 10 wt.% (and <5 wt.% in the clay-rich and anhydrite-rich layers). Most of the silica in the samples can be accounted for by a detrital component containing 63 wt% $SiO_2$. Non-detrital silica accounts for about 10-15 wt.% of all sample types, except the Mn-oxide and anhydrite samples that typically contain <2 wt.% residual $SiO_2$.

In samples with molar $CO_3$>$SO_4$, Ca was first attributed to calcite, then anhydrite; in samples with molar $SO_4$>$CO_3$, Ca was first attributed to anhydrite, then calcite. Any residual Ca is assumed to be present in clays. In many carbonate-rich samples molar Ca is less than or

equal to the molar $CO_3$. In the $CO_3$-rich (calcite and detrital silicate rich) samples (Table 2.6), the residual $CO_3$ correlates well with residual Mg ($r^2$=0.57), consistent with the presence of dolomite. The amount of dolomite in these samples is estimated from the residual Mg concentration and reported as end-member $MgCO_3$. Other samples contained minor dolomite. Any residual $CO_3$ after calcite (and dolomite) formation was first attributed to $MnCO_3$ (according to the bulk Mn content) and the remainder to $FeCO_3$. Non-zero residual carbonate is always less than 1 percent of the total. Table 2.6 shows that the layers rich in detrital carbonate contain as much as 65 wt.% carbonate minerals (~90% biogenic calcite and ~10% Mg-carbonate). The most carbonate-rich of the hydrothermal layers contain about 20 wt.% authigenic Fe- and Mn-carbonate, with minor Ca-carbonate. Other metal-rich layers typically contain ~10 wt.% authigenic carbonate, and clay-rich layers <5 wt.% carbonate (both detrital and authigenic). Residual Mn after forming Mn-carbonate is assumed to be present as Mn-oxides and amount to <2.2 wt.% MnO for all samples except in the most Mn-rich layers.

The most metal-rich layers contain about 15 wt.% anhydrite as expected from the high temperatures proximal to the inferred vent sites. The clay-rich layers, which are more distal, contain only about 5 wt.% anhydrite (some $CaSO_4$ may be secondary gypsum: see below). The amount of sulfate present as barite is never more than a few percent. The maximum concentration in all of the samples is 1.6 wt.% Ba or 2.7 wt.% as barite (the average for all samples is 0.14 wt.% Ba). As a result, $BaSO_4$ is not reported in Table 2.6. Many samples have a higher molar amount of $SO_4$ than Ca and Ba combined, indicating the

presence of other sulfates. These are mainly secondary metal sulfates formed during core storage.

The reduced sulfur content of the samples is mainly present as pyrite and chalcopyrite, and was first attributed to $CuFeS_2$, then $FeS_2$. Although sphalerite was rarely found under the microscope, for the purposes of the normative calculation we assume that all Zn that is now present as secondary Zn-sulfates was originally deposited as sphalerite. A strong co-enrichment with trace metals normally associated with sphalerite (e.g., Cd: Laurila et al., 2014a) confirms that much of the Zn in the samples was originally present as sphalerite. Therefore, the sulfur in residual sulfate after the formation of anhydrite was attributed first to ZnS, and any remaining sulfur was attributed to pyrite. In a number of samples insufficient residual sulfate was present to account for all of the Zn, leaving a nontrivial component of residual Zn (Table 2.6).

The detrital layers contain about 2 wt.% pyrite and 0.5 wt.% of other sulfides. Clay-rich samples contain about 1 wt.% pyrite and 1 wt.% of other sulfides. The hydrothermal carbonate samples contain about 10 wt.% sulfides, mostly pyrite. Metal-rich layers contain about 15 wt.% sulfides, on average, with subequal amounts of pyrite, chalcopyrite, and Zn-sulfide. An important observation is that there is more Zn in the samples than can be accounted for by the residual sulfur after the formation of anhydrite and the other sulfides. In 7 of the samples, the total amount of sulfur was far less than that needed to bind all Zn and Cu as sulfides, strongly suggesting the presence of abundant nonsulfidic Zn and Cu

minerals. All Fe remaining after the formation of pyrite, chalcopyrite and siderite is reported as $Fe_2O_3$ and is assumed to be present mostly in Fe-(oxy)hydroxides and authigenic clays (most probably nontronite). Clay-rich samples contain ~40 wt.% of non-detrital, non-carbonate $Fe_2O_3$; sulfate-rich and hydrothermal carbonate samples contain ~25 wt.%. Detrital layers, as well as anhydrite layers, typically contain less than 3 wt.% $Fe_2O_3$.

After correcting for the salt content of the sample, the total of the normative minerals are close to 100 wt.% for most sample types, except the clay-rich samples (totals of <75 wt.%: Table 2.6). The latter presumably reflects a large proportion of water still in the clays that was not analyzed.

**5.4 Sequential leaching experiments**

Sequential leaching experiments were performed on a representative subset of 33 samples to better characterize the proportions of nonsulfide minerals in the different sample types (e.g., Tessier et al., 1979; Hall et al., 1996; Hlavay et al., 2004; Cappuyns et al., 2007). The first leaching step was done with distilled water, which dissolves anhydrite, secondary salts and secondary sulfates (especially halite, sylvite, and metal sulfates, $MeSO_4 \bullet nH_2O$). The second step was an ammonium acetate leach, which mainly dissolves calcite and dolomite, some Cu- and Zn-carbonates, but not the Fe- or Mn-carbonates. The third step used cold hydroxylamine hydrochloride, which dissolves Mn- and Fe-(oxy)hydroxides and authigenic Fe-Mn-carbonates (e.g., manganosiderite), but the most insoluble carbonates (e.g., siderite)

remain in the residue. The fourth step treated the samples with hot (60 °C) hydroxylamine hydrochloride, which dissolves the residual Mn- and Fe-(oxy)hydroxides; ferrihydrite, goethite and lepidocrocite are leached but not crystalline Fe-oxide minerals such as hematite and magnetite. The behaviour of the different sample types was monitored by analyzing the leachates after each step. The pH of the first leachate decreased rapidly in some samples (due to dissolution of acid-producing compounds, such as metal-sulfates), whereas in the carbonate-buffered and/or metal-poor samples, the pH of the leachate solution remained near neutral. Table 2.7 shows the cumulative proportions of different elements dissolved by all 4 steps from the different sample types. The leachate data for each step normalized to 100% are reported for the different sample types in Tables 2.8, 2.9 and 2.10; the whole dataset is given in Appendix 2.2.

The total of dissolved elements in the first leaching step for all sample types correlates well with Na, confirming that most of the leachable components in this step (e.g., Ca, Mg and K) were contained in the salt fraction of the samples. The ratios of the major cations (Ca:K:Mg:Mn) in the leachates are similar to that of the Lower Brine and pore water (Anschutz et al., 2000; Pierret et al., 2001). Most of the anhydrite was also removed by the first leaching step, except in the anhydrite-rich samples, in which total dissolution of the anhydrite was not achieved until the second leach (Table 2.10). The first leachates may have become saturated with $CaSO_4$ quite quickly or the kinetics of anhydrite dissolution may have been sluggish in the pure water. Dissolution of anhydrite also might have been greater in the samples that experienced pH decrease during the first step (e.g., as a result of

metal-sulfate dissolution). Only 50% of the Ba was leached overall, indicating the presence of insoluble barite but also Ba in leachable phases (possibly carbonate). Almost all Sr was leached in steps 1 and 2, indicating that it was mainly present in anhydrite. The concentration of Mn in the first leachate varied greatly between sample types, but some Mn compound(s) were clearly soluble.

In the clay-rich samples, an average of 9% of the total Fe was removed by the complete leaching procedure; 14% of the Fe in the hydrothermal carbonate samples was removed. The majority of the elements leached from the carbonate-rich samples were from carbonate dissolution in step 2. In the detrital carbonate-rich samples, as much as ~90% of the Ca was dissolved (up to 15 wt.% from sample 421-825: Table 2.8). In the samples with highest calcite content (samples 421-825 and 495-557), Ca was the major component leached in steps 1 to 3, and the total molar amount of elements dissolved correlates with the molar amount of carbonate, indicating that all other elements leached were also present in carbonate. Samples 546-180 and 503-889 have high $CO_3$ contents (Appendix C.1) but lacked calcite, so they were less affected by the second leaching step. Despite the high Fe content of these samples (Table 2.8), the Fe (and Mn) were only leached during steps 3 and 4; most of the Fe was not leached, and 36% of the Mn remained undissolved in sample 503-889. For some Mn-rich samples (e.g., 495-569), the total of Mn leached during steps 2-4 was much larger than the molar amount of $CO_3$, consistent with the abundant non-carbonate Mn (soluble Mn-oxides). In some carbonate-rich samples, a large proportion of

the Cu and Zn was apparently bound to carbonate, although these minerals account for only a small fraction of the total metal in the Atlantis II sediments.

Very little of the Fe-(oxy)hydroxides identified by XRD as goethite appears to have been leached by cold or hot hydroxylamine hydrochloride. Only 1% of the Fe in sample 495-569, which contains abundant goethite according to XRD, was found in any of the leachates. This may be explained by the presence of extremely fine-grained and insoluble "nano-hematite", which is difficult to distinguish from goethite by XRD (e.g., as previously noted by Schwertmann et al., 1998). Samples in which akageneite and lepidocrocite were identified by XRD have the largest leachable Fe contents (Table 2.5). In the clay-rich samples (Table 2.9), ~20% of the total Mg and ~40% of the total K was not leached after all 4 steps, confirming the presence of K-rich clay minerals or other insoluble phases with a high K content (e.g., jarosite).

Although sulfides are resistant to the sequential leaches, abundant Zn (and to a lesser extent Cu) was found in all of the leachates due to the presence of soluble efflorescent salts. A strong correlation ($r^2$=0.61) between non-anhydrite $SO_4$ and total dissolved metals in the sulfate-rich samples during the first leaching step is also consistent with the presence of metal sulfates, especially $ZnSO_4$. The amount of metal dissolved by distilled water also correlates well with the measured pH of the first leachate ($r^2$=0.80 for Cu and 0.63 for Zn for 33 samples; Appendix 2.2). Trace metals normally associated with sphalerite (e.g., Cd) were dissolved with Zn during the first and second leaching steps in all samples, confirming that

much of the leachable Zn in the samples was likely originally present as sphalerite. Although many of the samples contained abundant pore water brine, the maximum contribution of the pore water to the Zn content of the samples is only about 1 wt.% (cf. Anschutz et al., 2000).

In the high-sulfide samples (HSHM, Cu-rich: Table 2.10), only 20% of the Cu was leached, along with 30% of the Pb but almost all of the Zn, as noted above, due to major dissolution of secondary $ZnSO_4$ at the first leaching step. A minor amount of Cu in the first leachate also suggests the presence of secondary Cu sulfates or chlorides. In contrast, only ~40% of the Zn was leached from the low-sulfide, high-metal samples (LSHM) in the first step. This suggests the presence of insoluble Zn-rich nonsulfide minerals in these samples. In all samples, about half of the Ni and Co were leached by the final step, but less than 10% of the As, Mo, Sb, Ga, and Sn (most likely in insoluble pyrite: Table 2.7). In the Cu-rich samples, Ag was not leached, consistent with the high Ag content of insoluble chalcopyrite; the behavior of Ag and Cu in each step of the sequential leaches confirms the mineralogical siting of Ag inferred from the X-ray mapping. High-sulfide and low-metal samples (HSLM) contain on average ~30% more sulfide than other samples (Figure 2.17) but significantly less Zn and Cu; Au, As, Ga, Sb, and Mo in these samples report to the residue with insoluble pyrite (Appendix 2.2). Pb in the HSLM samples is also retained in the residue, although the total concentrations are low.

In 90% of the samples Au was insoluble (Table 2.7), most likely present in clays and insoluble sulfides. Leachable Au was detected in 4 samples after the first leach, suggesting that in these few cases Au was present in secondary salts or weakly adsorbed onto clays; 73% of the gold was leached from sample 373-8 (with a total gold content of 575 ppb Au, salt free) and 39% of the gold from sample 495-362 (total gold content of 1041 ppb Au) (Appendix 2.2). Both samples come from the two uppermost units, which contain abundant nonsulfide metal compounds. However, these samples did not contain significant leachable Zn and Cu compared to other samples, suggesting that the leachable Au was not necessarily present in secondary metal-sulfates.

**5.5 Effects of core storage**

The uppermost sediment of the Atlantis II Deep is saturated with pore water (up to 95 vol.%: Hendricks et al., 1969); the amount decreases down stratigraphy but remains significant in all strata. The pore water is compositionally similar to the Lower brine in terms of pH, Eh, and $SO_4$ concentration, but lower in carbonate and higher in metals (Craig, 1969; Hendricks et al., 1969; Schoell and Stahl, 1972; Anschutz et al., 2000). Core recovery exposed this brine-saturated sediment to atmospheric pressure, oxygen and cooler temperatures. Sphalerite, which was found in abundance in the early studies (Pottorf and Barnes, 1983), was reported less and less frequently in later studies of similar cores that had been stored for as little as 10 years (e.g., Missack et al., 1989). Our data confirm that the sphalerite was almost entirely replaced by water-soluble Zn-sulfates during storage.

Although the core boxes were sealed to prevent dehydration and oxidation, after ~30 years of core storage, desiccation, formation of salt crusts, recrystallization of anhydrite to gypsum, and oxidation on the cut surfaces were all evident. In the re-logged cores, these effects varied significantly between boxes but also according to the original mineralogy of the sediments, most importantly the amount of sulfides and the presence of carbonate (especially calcite), which apparently buffered the pH of the pore fluids in carbonate-rich cores during storage. In this study we noticed that colors of the Fe-rich layers (bright red, orange, yellow), for the most part, were unchanged by core storage, according to comparison with photos taken immediately after core recovery. Some originally dark and sulfide-rich layers became lighter during core storage, acquiring red, yellow or grey tints.

In addition to NaCl, the main secondary minerals were efflorescent salts, a group of compounds with the general formula $Me^{2+}SO_4 \bullet nH_2O$ that are commonly formed by sulfide oxidation. The conditions in the cores during formation of the salts were likely similar to acid mine drainage (e.g., Hammarstrom et al. 2005). Bacterial activity might also have contributed to sulfide-oxidation. The pH of the first leachate in the sequential leaching of samples with abundant metal sulfates was between 3.8 and 6.4 (Appendix 2.2); a number of samples had pHs <3.8, down to 2.5 (i.e., lower than the acid leach in step 2). Well-buffered samples with a higher carbonate content (e.g., sample 421-825; Appendix 2.2) had pHs in the first leachate of between 6.4 and 7.8. These samples apparently did not experience significant sulfide oxidation or the formation of acidic pore fluids during core storage. Significant amounts of sphalerite were only preserved in the cores that contained

sufficient carbonate to buffer against acid generation. Most of the preserved grains of sphalerite had low Fe contents (Table 2.4) compared to sphalerite analyzed in many earlier studies (e.g., Figure 2.16). This might be due to preferential dissolution of the sphalerite with high Fe contents during core storage (cf. Perez and Dutrizac, 1991). In sample 264-474, which contains little sulfur and almost no sulfides, Zn apparently formed Cl-salts or oxides rather than sulfates (with up to 46 wt.% Zn, 33 wt.% Cl and 21 wt.% O: Table 2.3). In other samples, secondary Zn and Cu-carbonates were formed (Gurvich, 2006). Oudin et al. (1984) previously reported large (up to 0.5 mm in diameter) grains of hydrozincite ($Zn_5(OH)_6(CO_3)_2$) in the pore water-rich upper part of one core just a few years after it was collected. Cu- and Fe-sulfides were less strongly affected by core storage than the Zn-sulfides; this may be due to the formation of an Fe-(oxy)hydroxide armor on the chalcopyrite and pyrite (e.g., Figure 2.11B; cf. Rosso and Vaughan, 2006; Holmström and Öhlander, 2001). Figure 2.14G shows a large grain of primary chalcopyrite partly replaced by secondary metal-sulfates, that may be pseudomorphing anhydrite that has now dissolved. Figure 2.14H shows a similar feature infilled by secondary Pb-oxide and/or chloride minerals.

It is noteworthy that when bulk samples were collected in 1979 and conventional methods of sulfide mineral recovery by froth flotation were attempted, recoveries were on the order of 60-70% for Zn and Cu, as sphalerite and chalcopyrite (Nawab, 1984). However, metal-bearing phases in the sediments are clearly not limited to sulfides and all of the minerals are highly susceptible to oxidation and leaching, including the formation of water-soluble salts. These observations might suggest that metals could be more effectively recovered by

a combination of leaching and flotation of the sulfides. Purposeful attempts to hasten the oxidation of the sediments might also lead to significant improvements in metal recovery by leaching.

## 6. Discussion and Conclusions

The formation of the metalliferous sediments in the Atlantis II Deep involved a number of different precipitation pathways, including direct precipitation in the brine pool during mixing and cooling of the hydrothermal fluids, diagenetic recrystallization, hydrothermal alteration of the sediments in permeable layers and subseafloor deposition. The causes of nonferrous metal precipitation include mainly temperature decrease and/or redox change as high-temperature fluids enter the brine pool (or when sinking cold brines mix with hotter brines). The main controls on the sedimentary layering at the scale of the major sedimentary units have involved input from hydrothermal and detrital sources at the basin or sub-basin scale (~millenial changes in the stratigraphic units). The present study has revealed important mineralogical differences between sedimentary layers at a finer scale and more local controls on precipitation (~annual variations in element fluxes and diagenetic effects responsible for fine layering). Precipitation in and deposition from the brine pool is the first order control on the layering of the sediment. It is likely that multiple vents have existed both in the Northeast and in the Southwest Basins, and their activity may have varied from dormant to robustly active at yearly to hundred-year time scales (similar to MOR black smoker systems: Hannington et al., 2005). Such rapid changes in the hydrothermal outflow have been inferred from the composition of particulate matter in the

Lower Brine (Hartmann, 1973, 1985). During periods of "short-term" intense hydrothermal activity, deposition of sulfidic particles occurs almost basin-wide, but ten years later they may be entirely absent in the brine (Hartmann, 1985). The dispersion patterns may also have been influenced by currents in the >100 m deep brine pool (Bäcker, 1976).

The following sections discuss the origin of the dominant Fe- and Mn minerals in the sediments, the fate of primary sulfide and sulfate minerals, and the effects of diagenesis and alteration on the formation of delicately banded sediments. The Chapter concludes with a discussion of the significance of some of these observations for the mineralogical layering and origin of similarly banded textures in some ancient ores.

### 6.1 Formation of Fe and Mn minerals

The precise mineralogy of the Fe-rich primary precipitates in the Atlantis II sediments has been the subject of numerous studies (Blanc et al., 1998; Taitel-Goldman and Singer, 2001). The dominant Fe precipitation occurred in the brine pool via oxidation of reduced Fe to Fe-OOH at the chemocline. Taitel-Goldman and Singer (2001) suggested that the variety of minerals formed (e.g., goethite, ferrihydrite, hematite) may reflect formation in different parts of the brine pool, whereas Blanc et al. (1998) concluded that the differences were mainly due to diagenesis. The primary precipitate was most likely a non-crystalline Si-Fe-OOH compound that was flocculated and stabilized by Si-Fe-O bonds, followed by diagenetic transformation to more crystalline Fe-oxides, silica, and clays (Cornell et al., 1987; Schwertmann et al., 1998; Taitel-Goldman and Singer, 2001). Taitel-Goldman and

Singer (2002a, 2002b) reproduced these particles in the laboratory and found that the high ionic strength and high Si concentration of the Lower Brine (26 ppm: Anschutz and Blanc, 1995b) likely contributed to their stability in the brine pool. Data from this study show that the particles were likely deposited as a poorly crystalline Fe-Si "gel" that infilled and cemented the already crystalline particles of the sediments, in part replacing pre-existing phases during burial. The sequential leach experiments did not dissolve Fe in steps that would have removed Fe-OOH minerals like goethite or ferrihydrite, suggesting that a more stable phase is now present in the cores. This observation is consistent with Mossbauer data from Schwertmann et al. (1998) that suggested much of the Fe is now present as nano-hematite. However, they failed to produce nano-hematite in the laboratory under conditions simulating the Atlantis II Deep.

Currently Mn-(oxy)hydroxides dissolve in the Lower Brine, and most of the Mn is diffused out of the basin up to kilometers from the Deep (Bignell et al., 1976, Gurvich, 2006). Discrete layers of Mn-oxides are present in the older strata (especially in units CO, but also in DOP) indicating times of more oxidized Lower Brine. This study shows that Fe- and Mn-enrichments alternate at the scale of individual laminae, most likely because of short-term fluctuations in the Lower Brine, similar to what is observed in other anoxic basins (e.g., Black Sea, Cariaco Basin: Lewis and Landing, 1991; Yarincik et al., 2000), as well as in some lakes (Davison, 1993) and tailings ponds (Holmström and Öhlander, 2001). Although Mn-(oxy)hydroxides are locally abundant, most of the Mn in samples from this study is in

hydrothermal carbonate, in some cases precipitated from the $CO_3$ originally in biogenic calcite dissolved by the low pH brines.

### 6.2 Fate of surface-active particles

Numerous authors have shown that surface-active particles that are formed at the chemocline between the Lower Brine and the more oxidized upper brines scavenge metals as they descend through the brine pool (Ryan, 1969; Hartmann, 1973, 1985; Danielson et al., 1980). Fe-(oxy)hydroxides, in particular, adsorb metals from the ambient fluid, especially in the presence of $SO_4$ (Webster et al., 1998), and this has been suggested as an important pathway for nonferrous metal deposition, in particular Zn, in the Atlantis II sediments (Weber-Diefenbach, 1977; Butuzova, 1984; Laurila et al., 2014a). Data presented here support the suggestion that the descending particles were mainly poorly crystalline Si-Fe-OOH phases and carried Zn to the seafloor. However, the detailed composition or structure of the surface-active particles remain poorly known.

Anschutz et al. (2000) and Laurila et al. (2014a) showed that metals adsorbed onto the particles are released to the uppermost sedimentary pore water following deposition, resulting in high dissolved metal concentrations in the uppermost brine-saturated sediment (i.e., AM unit). The increase in dissolved metals in the pore waters is coincident with a decrease in Si and Fe, which has been interpreted to reflect the formation of well-crystallized Si- and Fe-bearing minerals (especially clays) during early diagenesis (Anschutz and Blanc, 1995b). The nonferrous base metals precipitated mainly as sulfides, and the

remaining cations (e.g., Mg, Al, K and Ca) were incorporated into clay interlayers or other minerals. In the absence of reduced sulfur, we suggest that a significant proportion of the total metal was also incorporated into nonsulfide phases, including carbonates and clays. The high metal contents of the nonsulfidic, clay-rich layers in SU2 are interpreted to reflect scavenging of metals onto diagenetic clays from metal-rich pore water. Direct observations of metal-enrichment in the amorphous Fe-Si-rich rims of more crystalline minerals is also evidence of continuing precipitation of metals during diagenesis. Samples with abundant nonsulfide metal enrichment are more common higher in the strata, whereas sulfides are dominant in the units SU1 and DOP. This might be due to diagenesis and hydrothermal alteration with burial or more reduced Lower Brine during the early history of the Deep.

**6.3 Primary sulfide and sulfate deposition**

Some sulfide-rich layers in cores proximal to the inferred vents in the SW Basin, especially in unit SU1, contain large (up to 100 µm) sulfide grains (Stephens and Wittkopp, 1969; Pottorf and Barnes, 1983; Oudin et al., 1984; Missack et al., 1989). One interpretation of the larger sulfide grains is that they formed at high temperatures (>300°C) in subseafloor feeder zones and were transported mechanically into the vent proximal sediment. While these were the focus of many previous studies, the most abundant sulfides in the sediments either settled from the brine pool or formed in the sedimentary pore water and grew diagenetically during burial.

Cooling of the fluids below about 350°C before entering the brine pool was the main cause of sulfide precipitation in the subseafloor veins. High-temperature fluids in the veins at ~10 m depth had temperatures of close to 400°C (Ramboz et al., 1988, Oudin et al., 1984). The temperatures decreased to ~100°C in the upper sediments (e.g., Cole, 1988) and ~70°C in the brine pool. In the current upflow zone, most of the dissolved $H_2S$ in the hydrothermal fluid is apparently exhausted before the fluids vent into the Lower Brine. No reduced sulfur has been detected in the Lower Brine, thus limiting the amount of metal precipitated as sulfide minerals at the seafloor or in the plume (Manheim, 1974; Hartmann, 1985; Anschutz et al., 2000; Pierret et al., 2001). As a result, significant metal remains dissolved in the Lower Brine, and any addition of $H_2S$ causes rapid precipitation of sulfides according to their solubilities (Figure 2.19: Shanks and Bischoff, 1977). The distribution of different sulfide phases in the sediments, with respect to the location of the inferred hydrothermal vents, is generally consistent with the saturation states of the respective minerals in the Lower Brine; first chalcopyrite, and then sphalerite, dominate close to the vent sources, whereas Fe-sulfides are more common further away. However, an increase in the Cu/Zn ratio in the sediments away from the main vents also has been noted (Laurila et al., 2014a), which may reflect nonsulfide metal deposition in the distal part of the Deep.

Although previous studies concluded that almost all sulfide was precipitated from the brine pool or upwelling hydrothermal fluids, this study suggests that the precipitation of sulfide minerals within the sediment column has been much more important. Pyrite, in particular, is not stable in the current brine pool (Shanks and Bischoff, 1977), not found as plume

particles (Hartmann, 1973), and is rare in the uppermost sediment (e.g., Bischoff, 1969a; Brockamp et al., 1978) but abundant in some deeper units. In accordance with the common framboidal texture, the pyrite is interpreted to have formed mainly after burial (Sweeney and Kaplan, 1973; this study).

Anhydrite formed both in high-temperature subseafloor veins (e.g., Zierenberg and Shanks, 1983, 1988; Oudin et al., 1984; Ramboz 1988) and as discrete layers in the sediment (Bäcker and Richter, 1973; Zierenberg and Shanks, 1983, 1988). The latter are thought to have formed from pore water, which is nearly saturated with respect to anhydrite (Figure 2.19: Shanks and Bischoff, 1977; Zierenberg and Shanks, 1988). Ca concentrations are >10 times Red Sea Deep water (Anschutz et al., 2000), enabling formation of such bodies simply by heating of the pore water above ~130°C (Figure 2.20, from Blount and Dickson, 1969). The ~50°C temperature increase in the pore water required to precipitate anhydrite may have been due to fracturing associated with tectonic disturbances (Shanks and Bischoff, 1977), intrusion of the basaltic sill (Zierenberg and Shanks, 1983), or diffusion of higher-temperature fluids into the sediments close to the vent source (indicated by clay formation temperatures higher than the Lower Brine: Zierenberg and Shanks, 1988). Diffuse boundaries between the anhydrite layers and adjacent layers observed in this study are consistent with formation by heating of pore fluids without significant chemical mass transfer or replacement.

**6.4 Silica, clays and hydrothermal carbonates**

After a few meters of burial, Si is released from the metastable Fe-Si-rich particles deposited from the brine pool and co-crystallizes with Fe to form authigenic clays. Previous studies have identified the clays as tri- or dioctahedral Fe-rich smectites. Cole (1983, 1988) and Zierenberg and Shanks (1988) confirmed that the composition of the smectites (Fe/Mg ratio) correlates well with their formation temperatures (determined by $\delta^{18}O$ thermometry and modelled by Zierenberg and Shanks, 1988). They found that brine pool precipitates formed at low temperatures are Fe-rich whereas epigenetic clays found in vertical veins in closest proximity to the vents are commonly Mg-rich and formed at higher temperatures (~160-200°C), in contrast to expected Fe-enrichment in higher-temperature fluids. Most of the clays observed in this study were either amorphous or poorly crystalline. Taitel-Goldman and Singer (2002) found similar poorly crystalline phases only a few hundred nm in size in the uppermost sediments. However, most of these particles would have passed the 0.45 μm filters used in other studies and therefore have not been widely recognized. Such clays are known to bind significant metals into their structures (Hein et al., 1979; Schlegel and Manceau, 2006), and the leaching experiments of the present study confirm that they likely played an important role in the enrichment of metals and other elements in the sediments (Figure 2.18).

The notable color change of the clay-rich layers from green in SU2 to red-brown in SU1, is similar to the color change observed during experimental synthesis of Fe(III) smectites by aging silica gels in the presence of $Fe^{2+}$-sulfate (Decarreau and Bonnin, 1986). In the experiments, the color change was accompanied by slight decrease in pH and dramatic

drop in dissolved $SiO_2$ and Fe concentrations similar to the change seen across the interface from the Lower brine into the sedimentary pore water of the Atlantis II sediments (Anschutz and Blanc, 1995b; Anschutz et al., 2000). The observed changes are similar to the "diagenetic segregation" of Fe and Si proposed to explain the separate Fe- and Si-rich layers in banded cherts (e.g., Lowe, 1999), and contrasts with models of differential settling of Fe- and Si-rich particles from the water column (cf. Stefurak et al., 2014). Observations in this study, including the presence of silica infilling detrital biogenic particles or as rims around other grains, strongly suggest that silica was mobile within the sediment during diagenesis. Increasing Si with depth in the cores also suggests that silica was being deposited rather than dissolved during diagenesis (Laurila et al., 2014a). Some samples from which calcite has been dissolved (e.g., sample 503-516) have a high Si content, suggesting that the hydrothermal fluids that dissolved the calcite were responsible for silica deposition. In some samples, Si content correlates with certain trace element enrichments (in particular Au, As, Ga and Ba: Laurila et al., 2014a), suggesting that hydrothermal fluids responsible for silica deposition also introduced these elements.

Most of the carbonates in the hydrothermal layers are Fe- and Mn-carbonates with compositions that vary from Mn- to Fe-dominated with proximity to the inferred vent sites (Figure 2.13). A notable transition from Ca-rich to Mn-rich and finally Fe-rich carbonate is seen in the $CO_3$-rich samples within several kilometers of the vent source (Figure 2.13). As calcite is dissolved by hydrothermal fluids, the proportion of Mn and Fe in carbonate increases. Although Fe- and Mn-carbonates are undersaturated in the current Lower Brine

(e.g., Bischoff, 1969a; Blanc et al., 1998), and so are largely absent in AM and SU1, they are common in the lower strata, consistent with diagenetic formation rather than deposition directly from the brine pool.

### 6.5 Role of diagenesis and hydrothermal alteration in the origin of fine laminations

Comparison of individual laminae in samples from different depths in the cores show that the fine layering changes from diffuse to well-defined with depth, eventually developing sharp interfaces and large chemical differences between adjacent laminae (Figure 2.5). This is considered to be due to diagenetic recrystallization of most minerals within a few meters of burial (i.e., a few thousand years at ~1 m/Ka). Where reduced sulfur was introduced (e.g., by upward diffusion from vent proximal sources: Anschutz et al., 2000), sulfide minerals (especially sphalerite) formed in the fluid-saturated sediment. Where pore water contained insufficient reduced sulfur to precipitate sulfide minerals, nonsulfidic metal-bearing minerals, mostly authigenic clays, formed.

Diagenetic enrichment of metals was particularly important in sections with enhanced permeability associated with dissolution of biogenic calcite or where higher permeability layers were present (e.g., layers rich in radiolaria in SU1). Bischoff (1969a) and Kaplan et al. (1969) noted early in the study of the cores that the detrital layers are locally metal-enriched, suggesting replacive mineralization at the locus of post-depositional fluid flow. Because the hot fluids are not particularly buoyant, owing to their high salinity, lateral migration into permeable aquifer horizons may have been particularly common. And the

higher heat capacity of the brine compared to seawater may have promoted mineralization of the permeable layers over great distances. Some of the laminae in the deeper strata show evidence of stronger (darker) and weaker (light) hydrothermal alteration. The light color is due to generally coarser-grained detrital components, whereas the darker colors reflect locally abundant sulfides, and many samples show evidence of replacement textures in association with dissolution of biogenic detritus and infilling of radiolaria tests.

### 6.6 Implications for ore geology

The Atlantis II Deep is a unique natural laboratory for the study of processes that may have been involved in formation of a number of important stratiform ore deposits. Several models for banded iron formation (BIF) deposition involve primary precipitation of Fe-(oxy)hydroxides and silica that were then diagenetically transformed to goethite and finally to hematite (e.g., Grenne and Slack, 2003; Klein, 2005), similar to that suggested here for the Atlantis II sediments. Detailed examination of the fine layering of the Atlantis II metalliferous sediments in this study shows that they are formed by a combination of chemical and clastic deposition. The formation of mm-scale laminae in BIF has been the subject of considerable debate. Our study suggests mineralogical and chemical segregation during diagenesis contributed to the fine layering of the Atlantis II sediments, a process that has been described for some iron formation (e.g., Lowe, 1999; Grenne and Slack, 2003). In this model, the presence of fine banding does not require rapid changes in the water-column chemistry. Instead, the predominance of ferric Fe-(oxy)hydroxides as primary precipitates in the Atlantis II Deep is a consequence of a stratified water column with a

mostly stable chemocline between the Lower and Upper brines. Transiently oxidized conditions produced many alternating layers of Fe- and Mn-(oxy)hydroxides in some units (e.g., during CO) suggesting that changes in the water column may have significant influence on formation of the layering under specific conditions.

Metal deposition from brine pools has been widely suggested as an explanation for the finely laminated sulfide ores in many volcanic- and sediment-hosted base metal deposits (e.g., VMS and SEDEX: Solomon et al., 2004; Tornos, 2008; Goodfellow and Lydon, 2007). The abundance of reduced sulfur (volcanic sulfur in VMS and bacteriogenic sulfide in euxinic basins that host SEDEX) results in most metal being deposited as sulfides, in contrast to the Atlantis II Deep. This reflects the high metals/$H_2S$ ratio of the Atlantis II hydrothermal fluids, resulting from the high salinity of the brines. The end-member fluids contain more metal than sulfur, in contrast to typical MOR hydrothermal vents (Von Damm, 1990). However, the abundance of chalcopyrite and lack of galena in the sulfide fraction of the Atlantis II sediments and the correspondingly high Cu/Zn and Zn/Zn+Pb ratios (compared to SEDEX deposits) reflects the equilibration of the hydrothermal fluids with a dominantly basaltic MOR-type basement with little sedimentary influence (Huston and Large, 1987; Franklin, 1996; Barrie and Hannington, 1999). The typical zonation in VMS and SEDEX from vent complex sulfides → bedded sulfide and carbonate ore → distal carbonates and siliceous exhalites (e.g., Lydon, 1996; Goodfellow and Lydon, 2007) is not observed, although there is evidence for lateral migration of fluids into permeable horizons adjacent to the upflow zone of the Atlantis II Deep. Rather a more uniform distribution of minerals away from the vent

source appears to be typical of the brine pool depositional environment. Absolute concentrations of Fe in the sediment actually increase away from the vent source as proximal deposition of sulfides, hydrothermal carbonate, and anhydrite become less important. However, some changes in mineralogy are similar to those expected for vent proximal environments of both VMS and SEDEX deposits, such as the common zonation from Ca±Mg-dominated to Mn-Fe-dominated carbonates with increasing hydrothermal influence (e.g., Lady Loretta: Large and McGoldrick, 1998).

The possibility of nonsulfidic primary precipitation followed by transformation to sulfides, as in the Atlantis II sediment, is rarely considered in models of stratiform base metal ore deposits. One exception is the stratiform hypogene nonsulfide Zn deposits (Hitzman et al., 2003), for example Franklin and Sterling Hill in the New Jersey Highlands (Johnson and Skinner, 2003). However, many of these deposits are so highly metamorphosed that it remains unclear whether the metallic minerals were deposited without sulfur or if all the sulfur was removed during metamorphism (e.g., Broken Hill: Large et al., 1996; Huston et al., 2006; Spry et al., 2007). Evidence for metal deposition as nonsulfidic particles also may have been lost early in the diagenetic history, as observed in the Atlantis II sediments, replaced by sulfides within only a few thousand years of deposition. The predominance of incompletely crystallized phases in the brine pool and in the youngest sediment of the Atlantis II Deep (e.g., AM unit) means that diagenetic reactions cannot be modelled by equilibrium processes involving stable minerals. This may also be true of some BIF and SEDEX ores.

In the Atlantis II sediment, the primary hydrothermal precipitates are often lower in trace metals than the later diagenetic phases. In particular, diagenetic pyrite is significantly enriched in As, and possibly Au, most likely as a consequence of diagenetic growth in metal-enriched pore fluid. The As-rich rims on diagenetic pyrite in the Atlantis II sediments are strikingly similar to the arsenian pyrite in a number of important sediment-hosted gold deposits (e.g., Carlin and SEDEX: Emsbo et al., 1999, 2000; Large et al., 2007, 2009, 2013, but also VMS: Huston et al., 1992, 1993).

## References


Anschutz, P. and Blanc, G., 1993. L'histoire sédimentologique de la fosse Atlantis II (mer Rouge). Les apports de la micropaleontology. C*. R. Acad. Sci., Paris, Sér.* II, 317, p. 1303-1308.

Anschutz, P. and Blanc, G., 1995a, Diagenetic evolution of the DOP facies from the Atlantis II Deep (Red Sea): evidence of early hydrothermal activity. *Oceanol. Acta* 18 - N°1, p. 105-112.

Anschutz, P. and Blanc, G., 1995b, Geochemical dynamics of the Atlantis II Deep (Red Sea): silica behavior. *Mar. Geol.* 128, p. 25-36

Anschutz, P., Turner, J. S. and Blanc, G., 1998, The development of layering, fluxes through double-diffusive interfaces, and location of hydrothermal sources of brines in the Atlantis II Deep: *Red Sea. Jour. Geophys. Res.* 103 (C12), p. 27809-27819.

Anschutz, P., Blank, G., Monnin, C. and Boulècue, J., 2000, Geochemical dynamics of the Atlantis II Deep (Red Sea): II. Composition of metalliferous sediment pore waters: *Geochim. Cosmochim. Acta* 64 (23), p. 3995–4006.

Badaut, D, Besson, G, Decarreau, A. and Rautureau, R., 1985, Occurrence of a ferrous trioctahedral smectite in recent sediments of Atlantis II Deep, Red Sea. *Clay Miner.* 20, p. 389-404.

Badaut, D. Decarreau, A. and Besson, G., 1992, Ferripyrophyllite and related $Fe^{3+}$-rich 2:1 clays in recent deposits of Atlantis II Deep, Red Sea. *Clay Miner*. 27, p. 227-244.

Baker E. T., Lavelle, J. W. and Massoth, G. J., 1985, Hydrothermal particle plumes over the southern Juan de Fuca Ridge. *Nature* 316 (6026), p. 342-344.

Barrie, C. T. and Hannington, M. D., 1999, Classification of VMS deposits based on host rock compositions, *in* Barrie, C. T. and Hannington, M. D., eds., *Volcanic-Associated Massive Sulfide Deposits: Processes and Examples in Modern and Ancient Settings*. Rev. Econ. Geol. 8, p. 1-13.

Basto, M. J., Figueiredo, M. O., Legrand, F., Chevallier, P., Melo, Z. and Ramos, M. T., 1995, Gold assessment in micas by XRF using synchrotron radiation. *Chem. Geol*. 124, p. 83-90.

Bertram, C., Krätschell, A., O'Brien, K., Brückmann, W., Proelss, A. and Rehdanz, K., 2011, Metalliferous sediments in the Atlantis II Deep—Assessing the geological and economic resource potential and legal constraints. *Res. Pol.* 36, p. 315-329.

Bignell, R. D., Cronan, D. S. and Tooms, J. S., 1976, Metal dispersion in the Red Sea as an aid to marine geochemical exploration. *Inst. Mining Metall. Trans.* 84 (B), p. 274-278.

Bischoff, J. L., 1969a, Red Sea geothermal brine deposits: their mineralogy, chemistry and genesis, *in* Degens, E. T. and Ross, D. A., eds., *Hot Brines and Recent Heavy Metal Deposits in the Red Sea*. Springer-Verlag, New York, p. 368-406.

Bischoff, J. L., 1969b, Goethite-hematite stability relations with relevance to sea water and the Red Sea brine system, *in* Degens, E. T. and Ross, D. A., eds., Hot Brines and Recent Heavy Metal Deposits in the Red Sea: Springer-Verlag, New York, p. 402-406.

Bischoff, J. L., 1972, A ferroan nontronite from the Red Sea geothermal system. *Clay Clay Miner.* 20, p. 217- 223.

Bischoff, J. L. and Manheim, F. T., 1969, Economic potential of the Red Sea heavy metal deposit, *in* Degens, E. T. and Ross, D. A., eds., *Hot Brines and Recent Heavy Metal Deposits in the Red Sea*. Springer-Verlag, New York, p. 535-541.

Blanc, G., Anschutz, P. and Pierret, M-C., 1998, Metalliferous sedimentation in the Atlantis II Deep: a geochemical insight, *in* Purser, B. H. and Bosence Dan, W. J., eds., *Sedimentation and Tectonics in Rift Basins: Red Sea – Gulf of Aden*. Chapman & Hall, London, p. 505-520.

Blount, C. W. and Dickson, F. W., 1969, The solubility of anhydrite ($CaSO_4$) in NaCl-$H_2O$ from 100 to 450°C and 1 to 1000 bars. *Geochim. Cosmochim. Acta* 33, p. 227-245.

Brewer, P. G., Riley, J. P. and Culkin, F., 1965, The chemical composition of the hot salty water from the bottom of the Red Sea. *Deep-Sea Res.* 12, p. 497-503.

Brewer, P. G. and Spencer, D. W., 1969, A note on the chemical composition of the Red Sea Brines. *in* Degens, E. T. and Ross, D. A., eds., *Hot Brines and Recent Heavy Metal Deposits in the Red Sea*. Springer-Verlag, New York, p. 174-179.

Brockamp, O., Goulart, E., Harder, H. and Heydemann, A., 1978, Amorphous copper and zinc sulfides in the metalliferous sediments of the Red Sea. *Contr. Mineral. Petrol.* 68, p. 85-88.

Brugger, J., Pring, A., Reith, F., Ryan, C., Etschmann, B., Liu, W., O'Neill, B. and Ngothai, Y., 2010, Probing ore deposits formation: New insights and challenges from synchrotron and neutron studies. *Rad. Phys. Chem.* 79, p. 151-161.

Butuzova, G. Y., 1984, Mineralogy and certain aspects of ore-bearing sediment genesis in the Red Sea; Part II, General processes of mineralization and ore-formation in the Atlantis II Deep. *Lithology and Mineral Resources* 19(4), p. 293-311.

Butuzova, G. Y., Gorshkov, A. I., Drits, V. A., Morozov, A. A. and Sivtsov, A. V., 1988, Mineralogy and formation processes of oxidized Fe and Mn substances in the Red Sea rift zone. Part I, ore mineralogy. *Lith. Min. Res.* 23 (4), p. 318-329. (Translation from Litologiya i Poleznye Iskopaemye 1988, vol. 4, p. 21-35).

Butuzova, G. Y., Drits, V. A., Morozov, A. A. and Gorschkov, A. I., 1990, Process of formation of iron- manganese oxyhydroxides in the Atlantis-II and Thetis Deeps of the Red Sea. *Int. Assoc. Sediment, Spec. Publ.* 11, p. 57-72.

Bäcker, H., 1976, Facies und chemische Zusammensetzung rezenter Ausfäblungen aus Mineralquellen im Roten Meer. *Geol. Jahrb.* D17, p. 151-172.

Bäcker, H. and Richter, H., 1973, Die rezente hydrothermal-seidimentärelagerstätte Atlantis II-tier im Roten Meer. *Geol. Rundsch.* 62, p. 697-740.

Campbell, A. C., Palmer, M. R., Klinkhammer, G. P., Bowers, T. S., Edmond, J. M., Lawrence, J. R., Casey, J. F., Thompson, G., Humphris, S., Rona, P. and Karson, J. A., 1988, Chemistry of hot springs on the Mid-Atlantic Ridge. *Nature* 335, p. 514-519.

Cappuyns, V., Swennen, R. and Niclaes, M., 2007, Application of the BCR sequential extraction scheme to dredged pond sediments contaminated by Pb-Zn mining: a combined geochemical and mineralogical approach. *J. Geochem. Explor.* 93, p. 78-90.

Cole, T. G., 1983, Oxygen isotope geothermometry and origin of smectite in the Atlantis II Deep, Red Sea. *Earth Planet. Sci. Lett.* 66, p. 166-176.

Cole, T. G., 1988, The nature and origin of smectite in the Atlantis II Deep, Red Sea, *Can. Mineral.* 26, p. 755-763.

Cole, T. G. and Shaw, H. F., 1983a, The nature and origin of authigenic smectites in some recent marine sediments. *Clay Miner.* 18, p. 239-252.

Cole, T. G. and Shaw, H. F., 1983b, Kerolite associated with anhydrite in sediments from the Atlantis II Deep, Red Sea. *Clay Miner*. 18, p. 325-331.

Cook, N. J., Ciobanu, C. L., Pring, A., Skinner, W., Shimizu, M., Danyushevsky, L., Saini-Eidukat, B. and Melcher, F., 2009, Trace and minor elements in sphalerite: A LA-ICPMS study. *Geochim. Cosmochim. Acta*. 73 (16), p. 4761-4791.

Cornell, R. M., Giovanoli, R. and Schindler, P. W., 1987, Effect of silicate species on the transformation of ferrihydrite into goethite and hematite in alkaline media. *Clay Clay Miner.* 35 (1), p. 21-28.

Craig, H., 1969, Geochemistry and origin of the Red Sea brines, *in* Degens, E. T. and Ross, D. A., eds., *Hot Brines and Recent Heavy Metal Deposits in the Red Sea*. Springer-Verlag, New York, p. 208-242.

Danielson, L. G., Dryssen, D. and Graneli, A., 1980, Chemical investigations of Atlantis II and Discovery brines in the Red Sea. *Geochim. Cosmochim. Acta* 44, p. 2051-2065.

Davison, W., 1993, Iron and manganese in lakes. *Earth-Sci. Rev.* 34, p. 119-163.

Decarreau, A. and Bonnin, D., 1986, Synthesis and crystallogenesis at low temperature of Fe(III)-smectites by evolution of coprecipitated gels: experiments in partially reducing conditions. *Clay Miner*. 20, p. 861-877.

Degens, E. T. and Ross, D. A., 1969, *Hot Brines and Recent Heavy Metal Deposits in the Red Sea*. Springer-Verlag Inc., New York, 600 p.

Diem, D. and Stumm, W., 1984, Is dissolved $Mn^{2+}$ being oxidized by $O_2$ in absence of Mn-bacteria or surface catalyst?. *Geochim. Cosmochim. Acta*. 48, p. 1571-1573.

Dobosz, A. N., 2012, *Characterization of Carlin-type auriferous arsenian pyrite from the Goldstrike property using EMP, SIMS, and VESPERS synchrotron µ-XRF: constraints to ore deposition mechanisms*. M.Sc. Thesis, Queen's University, Kingston, Ontario, Canada.

Emsbo, P., Hutchinson, R. W., Hofstra, A. H., Volk, J. A., Bettles, K. H., Baschuk, G. J. and Johnson, C. A., 1999, Syngenetic Au on the Carlin trend: Implications for Carlin-type deposits. *Geology* 27 (1), p. 59-62.

Emsbo, P., 2000, Gold in sedex deposits. *Rev. Econ. Geol.* 13, p. 427-437.

Franklin, J. M., 1996, Volcanic-associated massive sulphide base metals, *in* Eckstrand, O. R., Sinclair, W. D. and Thorpe, R. I., eds., *Geology of Canadian Mineral Deposit Types*. Geology of Canada 8, Geological Survey of Canada, p. 158-183.

Garbe-Schönberg, D., 1993, Simultaneous determination of thirty-seven trace elements in twenty-eight international rock standards by ICP-MS. *Geostand. Newslett.* 17 (1), p. 81-97.

Goulart, E. P., 1976, different smectite types in sediments of the Red Sea. *Geol. Jahrb. B*. D17, p. 135-149.

Goll, R. M., 1969, Radiolaria: The history of a brief invasion, *in* Degens, E. T. and Ross, D. A., eds., *Hot Brines and Recent Heavy Metal Deposits in the Red Sea*, Springer-Verlag, New York, p. 306-312.

Goodfellow, W. D. and Lydon, J. W., 2007, Sedimentary exhalative (SEDEX) deposits, *in* Goodfellow, W. D., ed., *Mineral deposits of Canada: A synthesis of Major Deposit*

*Types, District Metallogeny, the Evolution of Geological Provinces, and Exploration Methods*. Geol. Assoc. Can., Spec. Publ. 5, p. 163-183.

Grenne, T. and Slack, J. F., 2003, Bedded jaspers of the Ordovician Løkken ophiolite, Norway: seafloor deposition and diagenetic maturation of hydrothermal plume-derived silica-iron gels. *Miner. Deposita* 38, p. 625-639.

Guney, M., Al-Marhoun, M. A. and Nawab, Z. A., 1988, Metalliferous sub-marine sediments of the Atlantis-II-Deep, Red Sea. *CIM Bulletin* 81, p. 33-39.

Gurvich, E. G., 2006, *Metalliferous Sediments of the World Ocean: Fundamental Theory of Deep-Sea Hydrothermal Sedimentation.* Springer, Heidelberg, 423 p.

Hackett, J. P. and Bischoff, J. L., 1973, New data on the stratigraphy, extent, and geologic history of the Red Sea geothermal deposits. *Econ. Geol*. 68, p. 553-564.

Hall, G. E. M., Vaive, J. E., Beer, R. and Hoashi, M., 1996, Selective leaches revisited, with emphasis on the amorphous Fe oxyhydroxides phase extraction. *J. Geochem. Explor.* 56, p. 59-78.

Hammarstrom, J. M., Seal II, R. R., Meier, A. L. and Kornfeld, J. M., 2005, Secondary sulfate minerals associated with acid drainage in the eastern US: recycling of metals and acidity in surficial environments. *Chem. Geol*. 215, p. 407-431.

Hannington, M. D., Jonasson, I. R., Herzig, P. M. and Petersen, S., 1995, Physical and chemical processes of seafloor mineralization, *in* Humphris, S., Fornari, D. and Zierenberg, R., eds., *Physical, Chemical, Biological and Geological Interactions within Hydrothermal Systems*. AGU Monograph 91, p. 115-157.

Hannington, M. D., de Ronde, C. E. J. and Petersen, S., 2005, Modern sea-floor tectonics and submarine hydrothermal systems, *in* Hedenquist, J. F., Thompson, J. F. H., Goldfarb, R. J. and Richards, J. P., eds., *100th Anniversary Volume of Econ. Geol.*, p. 111-142.

Hartmann, M., 1973, Untersuchungen von suspendiertem Material in den Hydrothermallaugen des Atlantis-II-Tiefs*, Geol. Rundsch*. 62, p. 742-754.

Hartmann, M., 1985, Atlantis-II-Deep geothermal brine system: Chemical processes between hydrothermal brines and Red Sea deep water, *Mar. Geol*. 64, p. 157-177.

Hein, J. R., Ross, C. R. and Yeh, H., 1979, Mineralogy and diagenesis of surface sediments from Domes area A, B and C, *in* Bischoff, J. L. and Piper, D. Z., eds., *Marine Geology and Oceanography of the Pacific Manganese Nodule Province*. Plenum, New York, p. 365-396.

Hendricks, R. L., Reisbick, F. B., Mahaffey, E. J., Roberts, D. B. and Peterson, M. N. A., 1969, Chemical composition of sediments and interstitial brines from the Atlantis II, Discovery and Chain Deeps, *in* Degens, E. T. and Ross, D. A., eds., *Hot Brines and Recent Heavy Metal Deposits in the Red Sea*. Springer-Verlag, New York, p. 407-440.

Hitzman, M. W., Reynolds, N. A., Sangster, D. F., Allen, C. R. and Carman, C. E., 2003, Classification, genesis, and exploration guides for nonsulfide Zinc deposits. *Econ. Geol*. 98, p. 685-714.

Hlavay, J., Prohaska, T., Weisz, M., Wenzel, W. W. and Stingeder, G. J., 2004, Determination of trace elements bound to soils and sediment fractions. *Pure Appl. Chem*. 76 (2), p. 415-442. (IUPAC Technical Report)

Holm, N. G., Dowler, M. J., Wadsten, T. and Arrhenius, G., 1983, β-FeOOH·$Cl_n$ (akaganéite) and $_{Fe1-x}$O (wüstite) in hot brine from the Atlantis II Deep (Red Sea) and the uptake of amino acids by synthetic β-FeOOH·$Cl_n$. *Geochim. Cosmochim. Acta* 47, p. 1465-1470.

Holmström, H. and Öhlander, B., 2001, Layers rich in Fe- and Mn-oxyhydroxides formed at the tailings-pond water interface, a possible trap for trace metals in flooded mine tailings. *J. Geochem. Explor*. 74, p. 189-203.

Huston, D. L. and Large, R. R., 1987, Genetic and exploration significance of the zinc ratio (100 Zn/(Zn + Pb)) in massive sulfide systems. *Econ. Geol.* 82, p. 1521-1539.

Huston, D. L., Bottrill, R. S., Creelman, R., A., Zaw, K., Ramsden, T. R., Rand, S. W., Gemmel, J. B., Jablonski, B., Sie, S. H. and Large, R. R., 1992, Geologic and geochemical controls on the mineralogy and grain size of gold-bearing phases, eastern Australian volcanic-hosted massive sulfide deposits. *Econ. Geol.* 87, p. 542-563.

Huston, D. L., Sie, S. H., Suter, G. F. and Ryan, C. G., 1993, The composition of pyrite in volcanogenic massive sulfide deposits as determined with the proton microprobe. *Nucl. Instrum. Methods* B75, p. 531-534.

Huston, D. L., Stevens, B., Southgate, P. N., Muhling, P. and Wyborn, L., 2006, Australian Zn-Pb-Ag ore-forming systems: a review and analysis. *Econ. Geol.* 101, p. 1117-1157.

Johnson, C. A. and Skinner, B. J., 2003, Geochemistry of the Furnace magnetite bed, Franklin, New Jersey, and the relationship between stratiform iron oxide ores and stratiform zinc oxide-silicate ores in the New Jersey Highlands. *Econ. Geol.* 98, p. 837-854.

Jost, S., 2014, *High-resolution XRF Core Scanning of Metalliferous Sediments from the Atlantis II Deep (Red Sea)*, B.Sc. Thesis, University of Kiel, Germany.

Kaplan, I. R., Sweeney, R. E. and Nissenbaum, A., 1969, Sulfur isotope studies on Red Sea geothermal brines and sediments, *in* Degens, E. T. and Ross, D. A., eds., *Hot Brines and Recent Heavy Metal Deposits in the Red Sea*. Springer-Verlag, New York, p. 474-498.

Klein, C., 2005, Some Precambrian banded iron-formations (BIFs) from around the world: Their age, geologic setting, mineralogy, metamorphism, geochemistry, and origin. *Amer. Min.* 90, p. 1473-1499.

Knedler, K. E., 1985, *A geochemical and $^{57}$Fe Mossbauer investigation of East Pacific Rise and the Red Sea metalliferous sediments and other selected marine sedimentary deposits,* Ph.D. thesis, Victoria University of Wellington, New Zealand, 356 pp.

Ku, T. L., Thurber, D. L. and Mathieu, G. G., 1969, Radiocarbon chronology of Red Sea sediments, *in* Degens, E. T. and Ross, D. A., eds., *Hot Brines and Recent Heavy Metal Deposits in the Red Sea*. Springer-Verlag, New York, p. 348-359.

Large, R.R. and McGoldrick, P. J., 1998, Lithogeochemical halos and geochemical vectors to stratiform sediment hosted Zn-Pb-Ag deposits, 1. Lady Loretta Deposit, Queensland. *J. Geochem. Explor*. 63, p. 37-56.

Large, R. R., Bodon, S., Davidson, G. J. and Cooke, D., 1996, The chemistry of BHT ore formation – one of the keys to understanding the difference between SEDEX and BHT deposits, *in* Pongratz, J. and Davidson, G. J., eds., *New Developments in Broken Hill Type Deposits*. Proceedings of a Workshop Held at CODES, University of Tasmania, July 1996, p. 105-111.

Large, R. R., Maslennikov, V. V., Robert, F., Danyushevsky, L. V. and Chang, Z., 2007, Multistage sedimentary and metamorphic origin of pyrite and gold in the giant Sukhoi Log deposit, Lena Gold Province, Russia. *Econ. Geol.* 102, p. 1233-1267.

Large, R. R., Danyushevsky, L., Hollit, C., Maslennikov, V., Meffre, S., Gilbert, S., Bull, S., Scott, R., Emsbo, P., Thomas, H., Singh, R. and Foster, J., 2009, Gold and trace element zonation in pyrite using a laser imaging technique: Implications for the timing of gold in orogenic and Carlin-style sediment-hosted deposits. *Econ. Geol.* 104, p. 635-668.

Large, R. R., Meffre, S., Burnett, R., Guy, B., Bull, S., Gilbert, S., Goemann, K. and Danyushevsky, L., 2013, Evidence for an intrabasinal source and multiple concentration processes in the formation of the Carbon Leader Reef, Witwatersrand Supergroup, South Africa. *Econ. Geol. Bull*. 108 (6), p. 1215-1241.

Laurila, T. E., Hannington, M. D., Petersen, S. and Garbe-Schönberg, D., 2014a, Trace metal distribution in the Atlantis II Deep (Red Sea) sediments, *Chem. Geol.* 386, p. 80-100.

Laurila, T. E., Hannington, M. D., Petersen, S. and Garbe-Schönberg, D., 2014b, Early depositional history of metalliferous sediments in the Atlantis II Deep of the Red Sea: Evidence from rare earth element geochemistry. *Geochim. Cosmochim. Acta* 126, p. 146-168.

Lewis, B. L. and Landing, W. M., 1991, The biogeochemistry of manganese and iron in the Black Sea. *Deep-sea res.* 38 (2), p. 5773-5803.

Lowe, D. R., 1999, Petrology and sedimentology of cherts and related silicified sedimentary rocks in the Swaziland Supergroup, *in* Lowe, D. R. and Byerly, G.R., eds., *Geologic Evolution of the Barberton Greenstone Belt, South Africa*. Geol. Soc. Am. Special Paper 329, p. 83-114.

Lydon, J. W., 1996, Sedimentary exhalative sulphides (Sedex), *in* Eckstrand, O. R., Sinclair, W. D. and Thorpe, R. I., eds., *Geology of Canadian Mineral Deposit Types*. Geology of Canada 8, Geological Survey of Canada, p. 130-152.

Miller, A. R., 1964, Highest salinity in the world ocean? *Nature* 203, p. 590.

Miller, A. R., Densmore, D. C., Degens, E. T., Hathaway, J. C., Manheim, F. T., McFarlin, P. F., Pocklington, R. and Jokela, A., 1966, Hot brines and recent iron deposits in deeps of the Red Sea, *Geochim. Cosmochim. Acta* 30, p. 341-359.

Missack, E., Stoffers, P. and El Goresy, A., 1989, Mineralogy, parageneses, and phase relations of copper-iron sulfides in the Atlantis II Deep, Red Sea. *Miner. Deposita* 24, p. 82-91.

Manheim, F. T., 1974, Red Sea geochemistry (ch. 38), *in* Whitmarsh, R. B., Weser, O. E., Ross, D. A., *et al., Initial Reports of the Deep Sea Drilling Project,* v. 23, Washington (U.S. Government Printing Office) p. 975-998.

Nawab, Z. A., 1984, Red Sea mining: a new era. *Deep-sea Res.* 31, p. 813-822.

Ohmoto, H., Mizukami, M., Drummond, S. E., Eldridge, C. S., Pisutha-Arnond, V. and Lenagh, T. C., 1983, Chemical processes of Kuroko formation. *Econ. Geol. Monogr*. 5, p. 570-604.

Ohmoto, H., Watanabe, Y., Yamaguchi, K. E., Naraoka, H., Haruna, M., Kakegawa, T., Hayashi, K. and Kato, Y., 2006, Chemical and biological evolution of early Earth: Constraints from banded iron formations, *in* Kesler, S. E. and Ohmoto, H., eds.,

*Evolution of Early Earth's Atmosphere, Hydrosphere, and Biosphere – Constraints from Ore Deposits*. Geol. Soc. Am. Mem. 198, p. 291-331.

Oudin, E., 1987, Trace element and precious metal concentrations in East Pacific Rise, Cyprus and Red Sea submarine sulfide deposits, *in* Teleki, P. G., Dobson, M. R., Moore, J. R. and Stackelberg, U., eds., Marine Minerals: Advances in Research and Resource Assessment strategies: Proceedings of the NATO Advanced Research Workshop, Series C, 194, p. 349-362.

Oudin, E., Thisse, Y. and Ramboz, C., 1984, Fluid inclusion and mineralogical evidence for high temperature saline hydrothermal circulation in the Red Sea metalliferous sediments: Preliminary results. *Mar. Mining* 5 (1), p. 3-31.

Perez, I. P. and Dutrizac, J. E., 1991, The effect of the iron content of sphalerite on its rate of dissolution in ferric sulphate and ferric chloride media. *Hydrometallurgy* 26, p. 211-232.

Pierret, M. C., Clauer, N., Bosch, D., Blanc, G. and France-Lanord, C., 2001, Chemical and isotopic ($^{87}Sr/^{86}Sr$, $\delta^{18}O$, $\delta D$) constraints to the formation processes of Red-Sea brines. *Geochim. Cosmochim. Acta* 65 (8), p. 1259-1275.

Pottorf, R. J., 1980, *Hydrothermal sediments of the Red Sea, Atlantis II Deep - A model for massive sulfide-type ore deposits.* Unpubl. Ph.D. dissert., Pennsylvania State Univ., 193 p.

Pottorf, R. J. and Barnes. H. L., 1983, Mineralogy, geochemistry, and ore genesis of hydrothermal sediments from the Atlantis II Deep, Red Sea. *Econ. Geol. Monograph* 5, p. 198-223.

Ramboz, C., Oudin, E. and Thisse, Y., 1988, Geyser-type discharge in Atlantis II Deep, Red Sea: Evidence of boiling from fluid inclusions in epigenetic anhydrite. *Can. Mineral*. 26, p. 765-786.

Rosso, K. M. and Vaughan, D., 2006, Reactivity of sulfide mineral surfaces. *Rev. Mineral. Geochem.* 61, p. 557-607.

Ryan, W. B. F, Thorndic, E. M., Ewing, M. and Ross, D. A., 1969, Suspended matter in the Red Sea brines and its detection by light scattering, *in* Degens, E. T. and Ross, D. A., eds., *Hot Brines and Recent Heavy Metal Deposits in the Red Sea*. Springer-Verlag, New York, p. 153-157.

Schlegel M. L. and Manceau A., 2006, Evidence for the nucleation and epitaxial growth of Zn phyllosilicate on montmorillonite. *Geochim. Cosmochim. Acta* 70, p. 901-917.

Schoell, M., 1976, Heating and convection within the Atlantis II Deep geothermal system of the Red Sea. Proc. Second United Nations symposium on the development and use of geothermal resources 1, p. 583-590.

Schoell, M. and Stahl, W., 1972, The carbon isotopic composition and the concentration of dissolved anorganic carbon in the Atlantis II Deep brines/Res Sea. *Earth Planet. Sci. Lett.* 15, p. 206-211.

Schwertmann, U. and Murad, E., 1983, Effect of pH on the formation of goethite and hematite from ferrihydrite. *Clay Clay Miner*. 31 (4), p. 277-284.

Schwertmann, U. and Cornell, R. M., 2000, Iron Oxides in the Laboratory: Preparation and Characterization (2nd edition). Wiley-VCH Verlag GmbH, D-69469 Weinheim, 204 p.

Schwertmann, U., Friedl, J., Stanjek, H., Murad, E. and Bender Koch, C., 1998, Iron oxides and smectites in sediments from the Atlantis II Deep, Red Sea. *Eur. J. Mineral.* 10, p. 953-967.

Shanks, W. C. and Bischoff, J. L., 1977, Ore transport and deposition in the Red Sea geothermal system: a geochemical model. *Geochim. Cosmochim. Acta* 41, p. 1507-1519.

Shanks, W. C. and Bischoff, J. L., 1980, Geochemistry, sulfur isotope composition and accumulation rates of Red Sea geothermal deposits. *Econ. Geol*. 75, p. 445-459.

Singer, A. and Stoffers, P., 1981, Hydrothermal vermiculite from the Atlantis II Deep, Red Sea. *Clay Clay Miner.* 29 (6), p. 454-458.

Singer, A. and Stoffers, P., 1987, Mineralogy of a hydrothermal sequence in a core from the Atlantis II Deep, Red Sea. *Clay Miner*. 22, p. 251-267.

Solomon, M., Tornos, F., Large, R. R., Badham, J. N. P., Both, R. A. and Zaw, K., 2004, Zn-Pb-Cu volcanic-hosted massive sulphide deposits: criteria for distinguishing brine pool-type from black smoker-type sulphide deposition. *Ore Geol. Rev*. 25, p. 259-283.

Spry, R. G., Heimann, A., Messerly, J. D. and Houk, R. S., 2007, Discrimination of metamorphic and metasomatic processes at the Broken Hill Pb-Zn-Ag deposit, Australia: rare earth element signatures of garnet-rich rocks. *Econ. Geol*. 102, p. 471-494.

Steinkamp, K. and Schumann, D., 1974, The Chemical Composition of Sediment Cores Recovered During Valdivia Cruises VA01 and VA03 from the Atlantis II Deep (Red Sea). Unpublished cruise report 1.11.1974, Series CL, Preussag, Hannover, 155 p.

Stefurak, E. J. T., Lowe, D. R., Zentner, D. and Fischer, W. W., 2014, Primary silica granules—A new mode of Paleoarchean sedimentation. *Geology* 42 (4), p. 283-286.

Stephens, J. D. and Wittkopp, R. W., 1969, Microscopic and electron beam microprobe study of sulfide minerals in Red Sea mud samples, *in* Degens, E. T. and Ross, D. A., eds., *Hot Brines and Recent Heavy Metal Deposits in the Red Sea*, Springer-Verlag, New York, p. 441-447.

Stoffers, P. and Ross, D. A., 1974, Sedimentary history of the Red Sea, (ch. 23), *in* Whitmarsh, R. B., Weser, O. E., Ross, D. A., *et al*., *Initial Reports of the Deep Sea Drilling Project*, v. 23, Washington (U.S. Government Printing Office) p. 849-865.

Sval'nov V. N., Strizhov, V. P., Bogdanov, Y, A. and Isayeva, A. B., 1984, Hydrothermal barite crust on basalts in the Atlantis II Deep (Red Sea). *Oceanology* 24 (6), p. 716-720.

Sweeney, R. E. and Kaplan, I. R., 1973, Pyrite framboid formation: Laboratory synthesis and marine sediments. *Econ. Geol.* 68 (5), p. 618-634.

Swift, A., Bower, A. S. and Schmitt, R., 2012, Vertical, horizontal, and temporal changes in temperature in the Atlantis II and Discovery hot brine pools, Red Sea, *Deep Sea Res. I* 64, p. 118-128.

Taitel-Goldman, N. and Singer, A., 2001, High-resolution transmission electron microscopy study of newly formed sediments in the Atlantis II Deep, Red Sea. *Clay Clay Miner.* 49 (2), p. 174-182.

Taitel-Goldman, N. and Singer, A., 2002a, Metastable Si-Fe phases in hydrothermal sediments of Atlantis II Deep, Red Sea. *Clay Miner.* 37, p. 235-248.

Taitel-Goldman, N. and Singer, A., 2002a, Synthesis of clay-sized iron oxides under marine hydrothermal conditions. *Clay Miner.* 37, p. 719-731.

Taitel-Goldman, N., Koch, C. B. and Singer, A., 2002, Lepidocrocite in hydrothermal sediments of the Atlantis II and Thetis Deeps, Red Sea*. Clay Clay Miner.* 50 (2), p. 186-197.

Taitel-Goldman, N., Koch, C. B. and Singer, A., 2004, Si-associated goethite in hydrothermal sediments of the Atlantis II and Thetis Deeps, Red Sea. *Clay Clay Miner.* 52 (1), p. 115-129.

Taylor, S. R. and McLennan, S. M., 1985, *The Continental Crust: Its Composition and Evolution*. Blackwell, Oxford, 312 p.

Tessier, A., Campbell, P. G. C. and Blsson, M., 1979, Sequential extraction procedure for the speciation of particulate trace metals. *Anal. Chem.* 51 (7), p. 844-851.

Tjallingii, R., Röhl, U., Kölling, M. and Bickert, T., 2006, Influence of the water content on X-ray fluorescence core scanning measurements in soft marine sediments. *Geochem. Geophy. Geosyst.* 8 (2), p. 1-12.

Tornos, F., Solomon, M., Conde, C. and Spiro, B., 2008, The formation of the Tharsis massive sulfide deposit, Iberian Pyrite Belt: geological, lithogeochemical, and stable isotope evidence for deposition in a brine pool. *Econ. Geol.* 103, p. 185-214.

Von Damm, K. L., 1990, Seafloor hydrothermal activity; black smoker chemistry and chimneys. *Annu. Rev. Earth Planet. Sci.* 18, p. 173-204.

Weber-Diefenbach, K., 1977, Geochemistry and diagenesis of recent heavy metal ore deposits at the Atlantis II Deep (Red Sea), *in* Klemm, D. D. and Schneider, H. J., eds., *Time and Strata-bound Ore Deposits*. Springer-Verlag, Berlin, p. 419-436.

Webster, J. G., Swedlund, P. J. and Webster, K. S., 1998, Trace metal absorption onto an acid mine drainage iron (III) oxy hydroxy sulfate. *Environ. Sci. Technol.* 32 (10), p. 1361-1368.

Yarincik, K. M., Murray, R. W., Lyons, T. W., Peterson, L. C. and Haug, G. H., 2000, Oxygenation history of bottom waters in the Cariaco Basin, Venezuela, over the past 578,000 years: Results from redox-sensitive metals (Mo, V, Mn, and Fe), *Paleoceanography* 15 (5), p. 593-604.

Zierenberg, R. A. and Shanks, W. C., 1983, Mineralogy and geochemistry of epigenetic features in metalliferous sediments, Atlantis II Deep, Red Sea. *Econ. Geol.* 78, p. 57-72.

Zierenberg, R. A. and Shanks, W. C., 1988, Isotopic studies of epigenetic features in metalliferous sediment, Atlantis II Deep, Red Sea. *Can. Mineral.* 26, p. 737-753.

## Figure Captions

Figure 2.1. Location of the Atlantis II Deep and other brine filled basins on the Red Sea rift axis. Deeps with hot brines are shown in red font; other brine filled basins are indicated in green. The sub-basins and core locations of various studies are shown on the left. The inferred present-day hydrothermal vent source(s) are located in the SW Basin. The proximal and distal parts of the Deep with respect to the currently active venting are approximately delineated by Zn concentrations of >2.5 wt.% (bulk core, salt-free, based on unpublished data on 497 cores from the MESEDA I-III projects: Bertram et al., 2011). The lower stratigraphic units are missing in the SW Basin.

Figure 2.2. Schematic cross section through the Atlantis II Deep sediments and brine pool. The present thickness of the sedimentary strata is about 20 m, and the sediments are overlain by a 150- to 180-m deep stratified brine pool. The brine pool consists mainly of a lower anoxic layer and an upper brine which comprises a number of sub-layers that are progressively more seawater-like with height above the Lower Brine (modified after Zierenberg and Shanks, 1988; Swift et al., 2012). Metals and other elements in the brines have four main sources (cf. Laurila et al., 2014b): S1) background sedimentation that brings biogenic pelagic and detrital silicic particles into the Deep; S2) hot hydrothermal brines formed by seawater circulation through evaporites and underlying basalts; S3) cold, bottom-hugging brines that react with the surrounding sediments (evaporites, shales) before entering the Deep from above or below; S4) Red Sea Deep Water. Elements from seawater are brought into the Deep via redox driven Mn- and Fe-(oxy)hydroxide

precipitation-dissolution cycling at the chemoclines. By far most of the metals in the brine and sediment are derived from hot hydrothermal fluids. Metals precipitate out of these fluids according to four different pathways: P1) in sub-seafloor veins and conduits as high-temperature sulfides; P2) as sulfidic plume fall-out; P3) adsorbed onto surface active Si-Fe-(oxy)hydroxide particulates settling through the metal-rich Lower Brine; P4) incorporation in sulfides during diagenesis.

Figure 2.3. Example of a 4-meter long section of the metalliferous sediment just outside the SW Basin (core 495 at depth 5 to 9 m). The core includes sediment from unit DOP to SU2; the latter is compositionally gradational with the overlying AM unit. Lamination becomes more pronounced with depth in the core below SU2. On the right is a schematic illustration of the stratigraphy of the Atlantis II sediment (based on 76 cores: Bäcker and Richter, 1973). The SAM, SOAN and OAN units are typically found in the Southwest Basin, whereas the SU1 and DOP units are missing in the central part of the Southwest Basin due to the presence of a basaltic sill in this part of the Deep. The CO and COS units are found basin-wide.

Figure 2.4. Photographs of typical characteristics of the Atlantis II metalliferous sediment, all scale bars are 2 cm. A) An example of brecciated mud; the top part of the photograph consists mainly of clays (green), whereas the lower part is dominated by Fe-(oxy)hydroxides (from unit COS in core 373 at 460-500 cm). B) Gradational and diffuse lamination typical of the upper strata. The orange band is the lepidocrocite horizon that separates SU2 from AM (core 373 at 10-50 cm). C) Bright red Fe-(oxy)hydroxide and grey anhydrite-rich layers from

a vent proximal core 617 at 358-398 cm (unit OAN). The top part of the photograph shows sub-vertical veins of anhydrite. D) Finely-laminated sediment in unit CO composed mainly of Si-Fe-(oxy)hydroxides interlayered with hydrothermal carbonates and Mn-(oxy)hydroxides. The dark grey layer, at an angle to the fine laminations, is composed mainly of Mn-(oxy)hydroxide. The white layer is composed of detrital silicates and biogenic calcite. The top part of the photograph shows alternating layers of Fe- (red) and Mn-(oxy)hydroxides (dark grey); from core 495 at depth 560-600 (Figure 2.3). E) Finely-laminated Fe-(oxy)hydroxides in unit DOP (core 373 at 789-797 cm). The different colors are due to variations in the abundance of different minerals (esp. clays) mixed with the Fe-(oxy)hydroxides. The yellowish layers (top and bottom of photo) contain abundant detrital material, whereas brighter orange and red laminae have a higher proportion of Fe-(oxy)hydroxide minerals. F) Finely-laminated section from unit DOP containing abundant authigenic clays (green layers; core 421 at 878-886 cm). Red, yellow and brown laminae are dominated by Fe-(oxy)hydroxides with carbonates; light beige laminae are dominated by detrital components. Sharp contacts between laminae are typical of the lower stratigraphy; diffuse lamination is more typical in the upper strata (shown in B). G) Interlayered sulfide (dark) and detrital sediment (light) in unit SU1 (core 495 at 858-866 cm; detail from Figure 2.3). The right-hand side of the core shows the effect of surface oxidation during core storage; this was removed on the left side of the core to reveal the well-preserved layering. H) Layer of anhydrite in unit SU1 (core 387 at 500-507 cm) showing a sharp contact with the underlying sediment.

Figure 2.5. Representative scans using the XRF core scanner of two cores from the northern part of the Deep (see Fig. 2.1 for location). Relative abundances (total counts) of different elements are plotted along the lengths of the two cores. The stratigraphic units are shown according to the original core logging (unpublished MESEDA data; cf. Steinkamp and Schumann, 1974). A) Dramatic variations are seen in the abundances of different elements at two different depths in core Va29-229 (300-400 cm and 700-800 cm). K correlates with Si in the upper part of the core (most likely as authigenic clays) but not in the lower strata where there may be more detrital input. Cu correlates with total sulfur in the sulfidic section, but not in the clay-rich section in SU1. Fe concentrations reflect the change from diffuse to sharp lamination with burial (i.e., amplitude of variation in concentration increases due to segregation of Fe between adjacent laminae). B) Core Va22_275 (on right) includes two sections with high Mn concentration and low Fe. In some sections, the core scans show alternating layers of Fe then Mn enrichment at the cm scale (see also Figure 2.4D). In other sections with low total Mn counts, Mn concentration correlates with Fe, most likely in authigenic carbonates. Ca, Si and K correlate with Al in the section dominated by detrital sediment. Zn adsorption onto Fe-(oxy)hydroxides is suggested by correlation between Zn and Fe. Open spaces in the core (cracks) are indicated by low concentrations of all elements. See Appendix F for larger images and data from Va29-229 at 400-500 cm and 600-700 cm.

Figure 2.6. Close-up photographs in normal and transmitted light of fine, millimeter-scale layering in metalliferous sediment of the Atlantis II Deep (scale bar is 5 mm). A) Sample

from a laminated Fe-(oxy)hydroxide-rich layer in unit DOP (373-734). The different colors (from light yellow to bright orange and darker red) mainly reflect the proportion of Fe-(oxy)hydroxides and authigenic clays, although changes in Fe-mineralogy might also be important. B) Laminated detrital- and sulfide-rich sediment from unit SU1 (495-859; Figure 2.4G). Lighter bands contain abundant fossiliferous calcite; darker bands are mixtures of detrital components and sulfidic components. Cracks that distort the primary layering are lined with darker minerals suggesting that they represent primary upflow of pore fluids. Alternatively they may have formed during drying and sample preparation. C) Sulfide-rich section (495-777) in unit SU1. Darker layers are sulfide-rich; lighter layers contain abundant biogenic detrital silica but are enriched in metals owing to their high permeability (see Figure 2.10). Alteration on microfractures may be evidence of fluid migration between permeable layers. White areas are void space. D) Sulfide and metal-rich sample from unit SU1 (core 264 at 907 cm) showing an example of disseminated anhydrite (white) typical of cores from proximity to known venting.

Figure 2.7. Classification of the Atlantis II Deep sediments according to major metal and nonmetal contents (modified from Laurila et al., 2014a). The samples considered in this study comprise three main types identified during core logging from the mineralogy of the sediments, and their bulk chemical compositions. Carbonate-rich samples that contain mostly biogenic carbonate are largely detrital in origin and plot close to calcite in (A). These samples contain abundant $Al_2O_3$ in aluminosilicates (B), which are also detrital. The clay-rich samples plot in the lower left of (A) because they contain neither abundant $CO_3$ nor $SO_4$;

they are not particularly Ca-rich, although the clay fraction may contain Ca. Many of the clay-rich samples and carbonate-rich samples are Fe-rich (B), which reflects the abundance of Fe-(oxy)hydroxides (Laurila et al., 2014b) and also the presence of both Fe-rich clays (e.g., nontronite) and Fe-bearing carbonates; accordingly Fe-content cannot be used to discriminate between mineralogically different samples. The sulfate-rich samples contain both anhydrite and abundant secondary sulfates that were originally present in the cores as sulfides (see text for discussion). These samples contain the most base-metal sulfides and plot in the metal-rich corners of (B) and (C). Reduced sulfur (i.e., sulfur remaining in the samples as sulfides) was calculated from total sulfur minus sulfate sulfur (C). Although the calculated sulfide contents are minimum values, because of oxidation to sulfate, they generally match the published mineralogy of the cores and our own re-logging. Samples with the most sulfide and sulfate can be classified according to their metal-to-sulfur ratios: high sulfur, high metal (HSHM); high sulfur, low metal (HSLM); low sulfur, high metal (LSHM); and low sulfur, low metal (LSLM). The mineralogy of the HSHM samples is dominated by Zn and Cu sulfides and sulfate; HSLM samples include mainly Fe sulfides and sulfate. LSLM samples contain abundant Fe-(oxy)hydroxides and authigenic clays as well as anhydrite. LSHM samples have very low reduced sulfur but high nonferrous metal concentrations and contain a number of nonsulfidic metal-bearing minerals (see text for discussion). (Cu*2+Zn+Pb)*15 in (C) and (Cu+Zn+Pb*10+Cd*100) in (B) are examples of different proxies for nonferrous sulfides. (Al*2+Ca+Fe)*7 in (C) is a proxy for detrital components, anhydrite, and Fe-oxyhydroxides. The compositions of the samples are plotted in moles; different scalars are applied for ease of visualization.

Figure 2.8. Backscattered electron image of a biogenic detrital layer from sample 495-859 (white layer in Figure 2.6B). Examples are shown of detrital particles: a detrital aluminosilicate (A), detrital biogenic calcite (B) and detrital biogenic silica (C), as well as of authigenic particles: sulfide grains (D), carbonates (E), and metal-bearing clay-rich components (F). Scale bar is 100 μm.

Figure 2.9. Backscattered electron images of detrital and authigenic components in different layer types of the chemical-clastic sediments of the Atlantis II Deep. A) Radiolaria fossil replaced by authigenic minerals (clays and carbonate) from a detrital and granular sulfide-rich section (264-907) in unit SU1. Arrows indicate detrital clays (sheet-like biotite grain) and detrital silica. B) Densely packed radiolaria tests infilled with authigenic clays (dark areas) from a laminated Fe-rich section (373-734) in unit SU1. The silica framework of the fossils is replaced by Fe-(oxy)hydroxide minerals (light areas). C) Large composite particle composed of Zn (up to ~45 wt.%), oxygen (~25-45 wt.%) and S, Cl, Ca (up to ~7 wt.% each), from 495-859 in unit SU1 (shown in Figure 2.6B). The arrows indicate authigenic clays. The rounded shape implies infill and replacement of a circular fossil. Secondary minerals formed during core storage are unlikely, since abundant calcite is still present in the sample and would have buffered against pH decrease. D) Crystals of authigenic barite in a sulfide-rich section 495-777 in unit SU1 shown in Figure 2.6C. The arrow points to a Fe-(oxy)hydroxide particle. E) Large Fe-oxide grain (goethite or hematite) with a thin rim of Si-Fe-(oxy)hydroxide containing ~6% of Zn and ~0.6% S. The arrow shows coexisting calcite,

which would not have been preserved if the nonsulfidic phases were formed during core storage. From the same sample shown in C. F) Anhydrite crystals in an anhydrite bed from sample 503-254 in unit SOAN; downward arrows indicate Fe-(oxy)hydroxides, which are the most Zn-rich minerals in this sample (~1 wt.% Zn). Horizontal arrow (lower right corner) indicates a barite crystal. G) Zn-rich authigenic clay (arrow) containing ~5 wt.% Zn and remnant of radiolarian (bottom of photo) in a sulfide-rich section of sample 495-777 from unit SU1. H) Authigenic Fe-Mn(-Ca)-carbonates (arrows) in the same sample (495-777). The carbonates are commonly zoned with Fe-rich rims. I) Euhedral (cubic) authigenic Fe-Mn(-Ca) carbonate in sulfide-rich section (264-907) in unit SU1. The brightest grain is pyrite; arrow indicates authigenic clay. J) Zoned carbonate with dolomite core and rim of authigenic Fe-Mn(-Ca) carbonate from 495-859 in unit SU1. Arrows indicate pyrite grains. K) Coarse-grained chalcopyrites with exsolution lamellae from a granular sulfide-rich section (264-907) in unit SU1. The arrow points to authigenic clay (dark large grain) and carbonate. L) Detail of anhydrite in (F). The arrow points to microscopic authigenic clay containing ~1 wt.% Zn. All scale bars are 40 μm except in F, for which the scale bar is 400 μm.

Figure 2.10. EPMA element maps of a sulfide-rich section 495-777 from SU1 (shown in Figure 2.6C). SEM= backscattered electron SEM image. NL= Normal light photomicrograph taken with a stereographic microscope and external light from above. RL= Reflected light photomicrograph. The scale bar is 100 microns in all images. Aluminum is a proxy for detrital aluminosilicate minerals (including feldspar, mica and rock fragments), Na for salt (and also apparently detrital aluminosilicates, as the highest Na correlates with Al, likely in

feldspar). The highest Ca concentrations correspond to calcite, but this layer (lower part of the image) also contains abundant Fe and O, most likely in authigenic carbonate. The highest Si concentrations correlate with a permeable layer (upper part of the image) with abundant siliceous microfossils and detrital clays. This layer also has high Zn and Cu concentrations, with moderate S enrichment (10-20 wt.% S). Zn enrichment is confined to the middle of the S-rich band (a few tens of percent Zn), whereas Cu enrichment is found at the margins of the band. Na is also enriched in the permeable layer, consistent with the presence of salt, including metal-salts.

Figure 2.11. EPMA element maps of selected authigenic sulfide and nonsulfide particles in polished grain mounts. A, F and G are from sample 503-912 in the lower SU1 (3.8 ppm Au and ~17 wt.% Zn+Cu: this study); B, C, D, E, and H are from sample 268-985 in unit CO (21 ppm Au and ~17 wt.% Zn+Cu: Oudin, 1987). Scale bars are 20 µm, except 50 µm in B and E. A) Cluster of Fe-rich authigenic clay particles (devoid of S). The clays contain more Ag, As and Cd than the matrix. The highest As is found in pyrite inclusions (bright S-rich spots in the clays); the highest Ag and Cd are found in three Zn- and Cu-rich nonsulfidic particles. B) Grain of chalcopyrite showing clear Cu-rich exsolution lamellae and a Fe-Zn enriched rim. A tiny inclusion of sphalerite is seen in the middle of the grain. C) Composite grain of sphalerite and chalcopyrite showing the distribution of trace elements between these minerals. Cd is enriched in sphalerite and Ag in chalcopyrite. Sphalerite is zoned with varying Cd and Fe contents. D) Nonsulfidic metal-enriched particle (most likely a metal-chloride) containing little or no Fe but high Cu, Zn, and Cd. The Cu concentrations are ~45

wt.% and the Zn content is <10 wt.%. E) Euhedral pyrite with low As content (<0.4 wt.%) based on counting statistics and comparison with microprobe data (Table 2.4). The relative concentrations of Fe, As, and S are illustrated in this image in grey scale. F) Cluster of rounded (diagenetic?) pyrite grains with distinctive As-rich rims. The highest measured As content is 1.6 wt.% As: Table 2.4). G) Cluster of smaller As-rich pyrite grains from the lower strata. H) Chalcopyrite that has been strongly altered during core storage.

Figure 2.12. Compositions of clay minerals based on SEM spot analyses (Table 2.3), compared to data from previous studies (Appendix 2.1). Nontronite is the most common authigenic clay, but Mg-rich clays are found in proximity to the known vents. Figure 2.12. Compositions of clay minerals based on SEM spot analyses (Table 2.3), compared to data from previous studies (Appendix 2.1). Nontronite is the most common authigenic clay, but Mg-rich clays are found in proximity to the known vents.

Figure 2.13. Compositions of carbonate minerals based on normative mineralogy (see text for discussion and Table 2.6). Detrital carbonate-rich samples plot close to the Ca+Mg corner, consistent with the abundance of calcite and dolomite in these samples. Other carbonate-rich samples, with a low detrital component, span the compositional field from Ca-Mg rich to Mn and Fe rich, consistent with the inferred compositions of hydrothermal carbonate. Trend A represent increasing hydrothermal influence and decreasing total carbonate. Trend B represent changes in the hydrothermal carbonate from vent distal to proximal. Normative carbonate in all other hydrothermal samples (sulfate-rich) plot along

the Fe-Mn line, closer to Fe than Mn, consistent with the presence of Fe-rich authigenic carbonate. Nine samples analyzed by SEM are listed in Table 2.3. Precise compositional data is not available in the literature for the Atlantis II carbonates.

Figure 2.14. Reflected light photomicrographs of selected sulfide minerals from sample 268-985 in unit CO (A, B, C, G) and from sample 503-912 in lower SU1 (D, E, F, H). Scale bars are 50 µm, except in G, which is 200 µm. A) Typical composite sphalerite-chalcopyrite grain. B and C) Partly dissolved sphalerite grains resulting from oxidation during core storage. In B the original shape of the grain is hardly visible, whereas in C sphalerite has been partly replaced by secondary phases. D to F show different forms of diagenetic pyrite. D and E) Cluster of framboidal pyrite grains of different size. F) Single rounded grains of pyrite (nodular?) apparently composed of tight clusters of smaller pyrite grains. G) Rounded grain of chalcopyrite rimmed and surrounded by Fe-rich and Zn-rich nonsulfide alteration. The rectangular outline may be a relict anhydrite crystal (see H). H) Nonsulfidic, Pb-rich particle (grey) and small pyrite grains (white) with As-rich rims. The rectangular shape of the alteration halo in G and H is a rather common occurrence in the samples and may reflect secondary metal-sulfates that are pseudomorphing dissolved anhydrite or salt.

Figure 2.15. Biplots of Ag versus Cu and Cd and Hg versus Zn concentration in bulk sediment samples from the Atlantis II Deep (Appendix C.1). If all Ag is present in chalcopyrite (e.g., see Figure 2.11B and C), then the Ag content of chalcopyrite is ~0.3 wt.% Ag (best fit trendline). If all Cd and Hg are present in sphalerite (as is typically found in exhalative ores;

e.g., Cook et al., 2009), we can estimate the Cd and Hg concentrations in sphalerite to be ~0.2 wt.% and ~30 ppm, respectively.

Figure 2.16. Range of Fe contents in sphalerite from metalliferous sediments of the Atlantis II Deep. Lower and upper limit of the boxes mark minimum and maximum values, respectively, the dotted line indicates averages. Sphalerite grains in this study (1; from a distal core 495 in unit SU1, see Table 2.4) had low Fe-content compared to earlier studies (2-5 are EPMA data from Pottorf and Barnes, 1983; 6 is semi-quantitative data from Stephens and Wittkopp, 1969), which might be due to their greater resistance against dissolution during core storage. 2) Unit SOAN, 3) unit CO, 4) late sphalerite in unit OAN, 5) early sphalerite in unit OAN, 6) marmatite in sulfide facies sample. All samples came from cores in the Southwest Basin.

Figure 2.17. X-ray fluorescence element map of co-existing As-rich pyrite and nonsulfide particles in polished grain mounts from sample 503-912 (upper) and 268-985 (lower). The upper shows a pyrite grain rimmed by a secondary nonsulfide Zn phase (up to 15 wt.% Zn). The lower map shows a chalcopyrite grain surrounded by similar nonsulfide Zn phase, a separate Cu-Zn-rich (up to 45 wt.% Cu) phase (chloride?), two authigenic clay minerals, and a small Mn mineral. The scale bars are 50 microns in both images. In 503-912 (upper image), Zn and Cu in the S-XRF maps correlate with the surface expressions of the target grains, but Fe and As concentrations reflect the penetration of X-rays below the sample surface. The Fe, As, and Au maps in this sample completely overlap, precluding the

detection of Au. In 268-985 (lower image), one of the authigenic clay minerals shows the distinct Lγ1 peak of Au that does not match the doubling Kα peak of Fe at the same energy (Fe Kα x2). The lack of correlation with Fe and As in this grain is a good indication of possible nonsulfide Au enrichment, possibly below the surface.

Figure 2.18. Summary of the normative mineralogy of the Atlantis II metalliferous sediments (data from Table 2.6). The proportions of major minerals in different layer types are shown in the left panel. NaCl refers to salt crystallized from pore water in the samples during drying. The relative abundance of sulfide and nonsulfide Cu and Zn minerals (residual components) in the different samples are shown in the middle panel. The total amount of sulfide and nonsulfide Cu and Zn minerals (in wt.%) are indicated in the right panel.

Figure 2.19. Saturation state of the Lower Brine in different minerals according to Shanks and Bischoff (1977), using the brine composition of Brewer et al. (1965), Miller et al. (1966) and Brewer and Spencer (1969). The Cu concentration in the Lower Brine used in this diagram (0.26 ppm Cu) is much higher than measured in 1971 (~0.03-0.12 ppm: Hartmann, 1973), 1977 (~0.0005 ppm: Hartmann, 1985) and during 1985 (0.005 ppm: Anschutz et al., 2000). However, the dissolved Zn concentration in the Lower Brine has remained relatively constant (2-5.3 ppm, according to the cited references). These data suggest that all Cu introduced to the Lower Brine is rapidly precipitated as chalcopyrite, whereas Zn remains in solution to much lower temperatures.

Figure 2.20. Anhydrite solubility in the pure $H_2O$-NaCl-$CaSO_4$ system as a function of temperature (at 1000 bars) according to Blount and Dickson (1969). Anhydrite may precipitate in the Atlantis II sediments either by cooling of high temperature (hydrothermal) fluid or heating of pore water.

Table 2.1. Physical, chemical and mineralogical properties of the stratigraphic units of the Atlantis II metalliferous sediments (modified from Bäcker and Richter, 1973, Shanks and Bischoff, 1980, Blanc et al., 1998 and Laurila et al., 2014b).

| | thick-ness (m) | Age (ka) | depo-sition rate m/ka | Na Cl wt. % | Fe Si wt.% | Ca $CO_2$ wt.% | $S_{tot}$ $S_{red}$ wt. % | Cu Zn wt.% | Al Ba Mn wt.% | |
|---|---|---|---|---|---|---|---|---|---|---|
| AM (*SAM*) Amorphous-Siliceous | 3.5 (1-4) | last 3.6 | 0.97 | 55 | 23.8 6.8 | 4.9 1.8 | 5.3 1.6 | 0.88 3.2 | 0.57 0.08 0.72 | Amorphous Si-Fe-OOH, goethite, Fe-smectite, Mn-siderite; SW basin: sulfides, Fe-oxides, anhydrite; elevated areas: MnOOH |
| Lepidocrocite horizon | | | | | | | | | | |
| SU2 (*OAN /SOAN*) Up-per Sulfidic | 4 (2-12) | 5.9-3.6 | 1.74 | 45 | 16.2 8.2 | 8.4 3.1 | 8.0 1.5 | 0.45 2.3 | 0.70 0.16 0.63 | Sphalerite (common almost everywhere), pyrite (rare), Fe-OOH, green silicates, anhydrite (barite rare), Fe- and Mn-carbonates |
| Layer of anhydrite | | | | | | | | | | |
| CO (*COS*) Central Oxidic | 6 (1-11) | ~8.6-5.9 | 2.22 | 42 | 22.6 7.9 | 5.7 6.6 | 1.4 0.6 | 0.25 0.69 | 1.27 0.15 4.3 | Goethite, Fe-OOH, rare sulfides, carbonates, MnOOH minerals and Mn-oxides, limonite, hematite, anhydrite and rare euhedral magnetite (SW basin) |
| Red silicate layers with Fe-oxides | | | | | | | | | | |
| SU1 Lower Sulfidic* | 3.8 (1-4) | ~11.7 -8.6 | 1.23 | 29 | 17.0 9.3 | 6.5 8.0 | 9.0 3.1 | 0.92 2.7 | 1.15 0.22 1.3 | Fe-clays, red-brown silicates, abundant sulfides: pyrite, chalcopyrite, sphalerite, Mn-siderite, hematite, anhydrite (rare barite) |
| Pyrite much more abundant at the top of DOP than at the bottom | | | | | | | | | | |
| DOP Det-rital-Oxidic-Pyritic* | 2.5 (1-6) | ~25-~11.7 | 0.19 m/ka | 26 | 13.2 9.1 | 13.4 16.5 | 3.6 1.8 | 0.23 1.1 | 2.36 0.08 1.3 | Mixture of detrital-biogenic material with upward increasing pyrite content; limonitic and manganitic layers, rare sphalerite, Fe-OOH, anhydrite, rare basalt fragments |

Names in *italics* refer to sub-units, mainly found in the Southwest Basin: SAM= Sulfidic-Amorphous-Siliceous unit; SOAN=Sulfidic-Oxidic-Anhydritic unit; OAN=Oxidic-Anhydritic unit; COS=Central-Oxidic-Siliceous unit. *= Absent in the SW Basin. The ages of the units are derived from Hackett and Bischoff (1973), Shanks and Bischoff (1980) and Gurvich (2006). Thicknesses of the units are averages from Bäcker and Richter (1973) and used to calculate the average sedimentation rates.

Table 2.2. Minerals found previously in the Atlantis II metalliferous sediments (silicic-detrital minerals, such as plagioclase and zircon, are excluded).

| Mineral name | Ideal formula | abundance[1] | Reference |
|---|---|---|---|
| **Silicates** | | | |
| Nontronite (di-oct.) | $(CaO_{0.5},Na)_{0.3}Fe^{3+}{}_2(Si,Al)_4O_{10}(OH)_2 \cdot nH_2O$ | ~20% | Badaut et al., 1985 |
| Montmorillonite (di-octahedral) | $(Na,Ca)_{0.33}(Al,Mg)_2(Si_4O_{10})(OH)_2 \cdot nH_2O$ | ~10% | Bischoff, 1969a |
| Saponite (tri-oct.) | $(Ca_{0.5},Na)_{0.33}(Mg,Fe^{+2})_3(Si,Al)_4O_{10}(OH)_2 \cdot 4H_2O$ | ~2% | Cole, 1988 |
| Celadonite | $K(Mg,Fe^{2+})(Fe^{3+},Al)[Si_4O_{10}](OH)_2$ | tr. | Badaut et al., 1985 |
| Vermiculite | $(MgFe,Al)_3(Al,Si)_4O_{10}(OH)_2 \cdot 4H_2O$ | tr. | Singers and Stoffers, 1981 |
| Glauconite | $(K,Na)(Fe^{3+},Al,Mg)_2(Si,Al)_4O_{10}(OH)_2$ | tr. | Badaut et al., 1985 |
| Ferripyrophyllite | $Si_4Fe^{3+}{}_20_{10}(OH)_2$ | tr. | Badaut et al., 1992 |
| Annite | $KFe_3{}^{2+}AlSi_3O_{10}(OH,F)_2$ | tr. | Badaut et al., 1985 |
| Ilvaite | $CaFe^{2+}{}_2Fe^{3+}Si_2O_7O(OH)$ | tr. | Oudin et a., 1984 |
| Talc | $Mg_3Si_4O_{10}(OH)_2$ | tr. | Oudin et a., 1984 |
| Kerolite | $(Mg,Ni)_3Si_4O_{10}(OH)_2 \cdot H_2O$ | tr. | Cole and Shaw, 1983b |
| Chrysotile | $Mg_3(Si_2O_5)(OH)_4$ | tr. | Singer and Stoffers, 1987 |
| Chlorite | $(Mg,Fe)_3(Si,Al)_4O_{10}(OH)_2 \cdot (Mg,Fe)_3(OH)_6$ | tr. | Singer and Stoffers, 1987 |
| Amphibole | $[Mg,Fe,Al,Ca,Na)Si_8O_{22}(OH)_2$ | tr. | Zierenberg and Shanks, 1983 |
| Actinolite (amph.) | $Ca_2(Mg,Fe^{2+})Si_8O_{22}(OH)_2$ | tr. | Oudin et a., 1984 |
| Andradite (garnet) | $Ca_3Fe_2Si_3O_{12}$ | tr. | Zierenberg and Shanks, 1983 |
| Illite | $(K,H_3O)(Al,Mg,Fe)_2(Si,Al)_4O_{10}[(OH)_2,(H_2O)]$ | tr. | Anschutz and Blanc, 1995b |
| Kaolinite | $Al_2Si_2O_5(OH)_4$ | tr. | Anschutz and Blanc, 1995b |
| **Oxides and (oxy)hydroxides** | | | |
| *Goethite* | α-FeO(OH) | ~30% | Butuzova et al., 1990 |
| Limonite | $FeO(OH) \cdot nH_2O$ | ~10% | Bischoff, 1969b |
| Ferrihydrite | $Fe^{3+}{}_2O_3 \bullet 0.5(H_2O)$ | ~10% | Butuzova et al., 1990 |
| *Hematite* | $Fe_2O_3$ | ~5% | Pottorf and Barnes, 1983 |
| *Lepidocrocite* | γ-FeO(OH) | ~2% | Butuzova et al., 1990 |
| Feroxyhyte | δ-FeO(OH) | tr. | Taitel-Goldman and Singer, 2001 |
| *Akaganeite* | β-FeO(OH,Cl) | tr. | Holm et al., 1983 |
| Wüstite | FeO | tr. | Holm et al., 1983 |
| Mushketovite | $Fe_3O_4$ | tr. | Oudin et a., 1984 |
| Magnetite | $Fe_3O_4$ | tr. | Zierenberg and Shanks, 1983 |
| Maghemite | $\gamma\text{-}Fe_2O_3$ | tr. | Butuzova, 1984 |
| Chamosite | $(Fe^{2+},Mg)_{2.3}(Fe^{3+}, Al)_{0.7}(Si,Al)O_5(OH)_9$ | tr. | Pottorf and Barnes, 1983 |
| *Amorph. Si* | $SiO_2$ | ~2% | Anschutz and Blanc, 1995a |
| Calcedony | $SiO_2$ | ~2% | Anschutz and Blanc, 1995a |
| Quartz | $SiO_2$ | ~2% | Anschutz and Blanc, 1995a |
| *Manganite* | γ-MnOOH | ~5% | Butuzova et al., 1990 |
| Groutite | α-MnOOH | tr. | Butuzova et al., 1990 |
| Todorokite | $(Mn,Mg,Ca,Ba,K,Na)_2Mn_3O_{12} \cdot 3H_2O.$ | tr. | Butuzova et al., 1990 |
| Buserite | $Na_4Mn_{14}O_{27} \cdot 21H_2O$ | tr. | Butuzova et al., 1988 |
| **Carbonates** | | | |
| *"manganosiderite"* | $(Mn,Fe)CO_3$ (varying amount of Fe-Mn) | ~10% | Bischoff, 1969a |

| | | | |
|---|---|---|---|
| *Siderite* | $FeCO_3$ | ~10% | Anschutz and Blanc, 1995b |
| Rhodochrosite | $MnCO_3$ | ~10% | Anschutz and Blanc, 1995b |
| *Calcite/Aragonite* | $CaCO_3$ | ~10% | Bischoff, 1969a |
| *Dolomite* | $(Ca,Mg)CO_3$ | ~2% | Anschutz and Blanc, 1995b |
| *Ankerite* | $Ca(Fe,Mg,Mn)(CO_3)_2$ | tr. | Anschutz and Blanc, 1995b |
| Kutnohorite | $Ca(Mn,Mg,Fe)(CO_3)_2$ | tr. | Anschutz and Blanc, 1995b |
| Smithsonite | $ZnCO_3$ | tr. | Oudin et al., 1984 |
| Hydrozincite | $Zn_5(OH)_6(CO_3)_2$ | tr. | Oudin et al., 1984 |
| **Sulfates** | | | |
| *Anhydrite* | $CaSO_4$ | ~10% | Pottorf and Barnes, 1983 |
| *Barite* | $BaSO_4$ | tr. | Sval'nov et al., 1984 |
| *Gypsum* | $CaSO_4 \cdot 2H_2O$ | tr. | Pottorf and Barnes, 1983 |
| Bassanite | $CaSO_4 \cdot 0.5H_2O$ | tr. | Zierenberg and Shanks, 1983 |
| **Sulfides** | | | |
| Amorp. sulfides | metal-S | ~10% | Brockamp et al., 1978 |
| *Pyrite* | $FeS_2$ | ~10% | Pottorf and Barnes, 1983 |
| *Sphalerite* | ZnS | ~10% | Pottorf and Barnes, 1983 |
| *Chalcopyrite* | $CuFeS_2$ | ~5% | Missack et al., 1989 |
| Marcasite | $FeS_2$ | tr. | Pottorf and Barnes, 1983 |
| Pyrrhotite | FeS | tr. | Pottorf and Barnes, 1983 |
| Greigite | $Fe_3S_4$ | tr. | Pottorf and Barnes, 1983 |
| Mackinawite | $(Fe,Ni)_{1+x}S$ | tr. | Pottorf and Barnes, 1983 |
| Marmatite | (Zn,Fe)S | tr. | Stephens and Wittkopp, 1969 |
| Argentite | AgS | tr. | Weber-Diefenbach, 1977 |
| Galena | PbS | tr. | Oudin et al., 1984 |
| ISS | (Cu,Fe)S | tr. | Missack et al., 1989 |
| Isocubanite | $CuFe_2S_3$ | tr. | Oudin et al., 1984 |
| Covellite | CuS | tr. | Missack et al., 1989 |
| Chalcocite | $Cu_2S$ | tr. | Pottorf and Barnes, 1983 |
| Digenite | $Cu_9S_5$ | tr. | Pottorf and Barnes, 1983 |
| Djurleite | $Cu_{31}S_{16}$ | tr. | Pottorf and Barnes, 1983 |
| Valleriite | $(Fe^{2+},Cu)_4(Mg,Al)_3S_4(OH,O)_6$ | tr. | Pottorf and Barnes, 1983 |
| Cu sulfosalts | e.g., tetrahedr. $Cu_{12}Sb_4S_{13}$; enarg. $Cu_3AsS_4$ | tr. | Butuzova, 1984 |
| **Nonsulfides** | | | |
| Cu thiosalts | e.g., $CuS_2O_3$ | tr. | Butuzova, 1984 |
| Atacamite | $Cu_2Cl(OH)_3$ | tr. | Gurvich, 2006 |
| Ferrofranklinite | $(Fe,Zn,Mn)\cdot(Fe,Mn)_2O_4$ | tr. | Butuzova, 1984 |
| Chrysocolla | $(Cu,Al)_2H_2Si_2O_5(OH)_4 \cdot nH_2O$ | tr. | Butuzova, 1984 |
| Woodruffite | $(Zn,Mn^{2+})Mn^{4+}{}_5O_{12} \bullet 4(H_2O)$ | tr. | Bischoff, 1969a |

[1] Estimate of the abundance of the mineral in a typical sample containing the mineral. Only one reference is cited for each mineral, although most the minerals have been found in multiple studies. Font italics indicates minerals found in this study.

Table 2.3. Representative semiquantitative spot analyses (SEM-EDX) of nonsulfide minerals in the Atlantis II Deep metalliferous sediments. All analyses are normalized to 100%.

| **Detrital minerals*** | Sample | O | Si | Ca | Mg | K | Al | Na | Cl | Mn | Fe | S | Cu | Zn | Pb | As | Ti | Zr | Br | Ba | Sr |
|---|---|---|---|---|---|---|---|---|---|---|---|---|---|---|---|---|---|---|---|---|---|
| plagioclase[1] | 264-474 | 52.1 | 28.0 | 2.0 | | | 10.6 | 6.8 | | | 0.6 | | | | | | | | | | |
| plagioclase[1] | 495-859 | 53.4 | 29.5 | | | | 9.2 | 7.9 | | | | | | | | | | | | | |
| plagioclase[1] | 495-777 | 55.3 | 27.6 | 0.4 | | | 9.2 | 7.6 | | | | | | | | | | | | | |
| mica[2] | 495-859 | 52.5 | 20.9 | | 0.7 | 7.4 | 14.8 | 0.8 | | | 2.9 | | | | | | | | | | |
| titanite | 264-474 | 50.9 | | | | | | | | | 1.3 | | | | | | 47.8 | | | | |
| zircon | 373-734 | 37.1 | 14.2 | | | | | | | | 2.0 | | | | | | | 46.7 | | | |
| calcite[3] | 495-859 | 58.0 | 0.5 | 41.5 | | | | | | | | | | | | | | | | | |
| calcite[3] | 495-859 | 55.7 | 1.3 | 41.1 | 0.5 | | | | | | 0.7 | | | | | | | | 0.7 | | |
| dolomite[4] | 495-859 | 58.3 | 2.8 | 23.3 | 11.4 | | 0.9 | | | | 3.3 | | | | | | | | | | |
| dolomite[4] | 495-859 | 60.7 | | 24.3 | 15.0 | | | | | | | | | | | | | | | | |
| $SiO_2$ | 495-859 | 57.1 | 42.9 | | | | | | | | | | | | | | | | | | |
| $SiO_2$ | 495-777 | 62.5 | 36.9 | | | | | | 0.6 | | | | | | | | | | | | |
| **Authigenic minerals** | | | | | | | | | | | | | | | | | | | | | |
| hematite | 373-734 | 27.3 | | | | | | | | | 70.9 | | | | | 0.63 | 1.9 | | | | |
| goethite | 495-859 | 32.7 | | | | | | | | | 67.3 | | | | | | | | | | |
| Zn-rich FeOOH | 373-734 | 42.8 | 2.7 | | | 0.3 | 0.8 | | 2.0 | | 48.3 | 1.0 | | 2.0 | | | | | | | |
| Zn-rich FeOOH | 264-474 | 33.6 | 2.5 | | | 0.7 | | | 7.0 | | 47.9 | 0.6 | | 7.6 | | | | | | | |
| Fe-rich clay | 373-734 | 27.9 | 9.5 | 0.7 | | | 2.0 | 1.3 | 9.9 | | 45.8 | 3.0 | | | | | | | | | |
| nontronite[5] | 373-734 | 46.7 | 10.8 | | 0.9 | 1.1 | 2.9 | 1.6 | 3.5 | | 31.3 | 1.1 | | | | | | | | | |
| nontronite[5] | 264-474 | 40.9 | 19.5 | | 0.9 | 2.8 | 0.6 | | 6.6 | | 23.3 | | | 5.3 | | | | | | | |
| nontronite[5] | 264-474 | 46.0 | 21.4 | | 1.1 | 2.6 | 0.6 | | 3.2 | | 23.0 | | | 2.2 | | | | | | | . |
| Mg-rich clay | 495-859 | 50.0 | 23.1 | 7.2 | 9.6 | 0.2 | 1.8 | 1.1 | | | 7.0 | | | | | | | | | | |
| FeOOH; Zn-rich rim | 495-859 | 16.4 | 13.6 | 1.5 | 3.0 | 1.8 | 5.7 | | 0.7 | | 50.2 | 0.6 | | 6.4 | | | | | | | |
| Zn-rich nonsulfide | 264-474 | 35.0 | 10.1 | | | 1.5 | 0.7 | | 6.5 | | 37.7 | | | 7.4 | | 1.20 | | | | | |
| Zn-rich nonsulfide | 264-474 | 26.9 | 8.6 | | 2.2 | 1.4 | 0.4 | 6.2 | 7.0 | 0.5 | 35.6 | 4.6 | | 6.7 | | | | | | | |
| Zn-rich nonsulfide | 495-777 | 37.1 | 21.5 | 0.7 | | | 1.5 | | 12.0 | | 8.8 | 8.7 | 2.8 | 7.0 | | | | | | | |
| Zn-rich nonsulfide | 495-777 | 38.0 | 21.4 | 1.0 | 5.6 | | 4.2 | | 3.6 | 0.6 | 9.0 | 7.4 | 1.7 | 7.5 | | | | | | | |
| Zn-rich nonsulfide | 264-474 | 44.6 | 22.0 | | | 2.4 | | 4.1 | 1.9 | | 18.0 | | | 7.0 | | | | | | | |
| Zn-rich nonsulfide | 264-474 | 39.4 | 10.6 | | 5.2 | 2.0 | | 5.2 | 4.5 | 0.8 | 19.2 | 8.9 | | 4.4 | | | | | | | |
| Fe-Mn carbonate | 495-859 | 49.6 | 0.5 | 7.7 | 1.2 | | | | | 10.1 | 31.0 | | | | | | | | | | |
| Fe-Mn carbonate | 495-859 | 50.9 | 0.5 | 6.1 | 0.9 | | | | | 7.4 | 34.2 | | | | | | | | | | |
| Fe-Mn carbonate | 503-254 | 56.1 | 0.6 | 1.3 | 1.1 | | | | | 6.7 | 34.2 | | | | | | | | | | |
| Fe-Mn carbonate | 495-777 | 50.7 | 0.5 | 4.8 | 1.1 | | | | 0.6 | 5.7 | 36.7 | | | | | | | | | | |
| Fe-Mn carbonate | 495-777 | 30.8 | 4.2 | 4.3 | | | 1.1 | | 1.6 | 7.2 | 45.6 | 1.6 | | 3.7 | | | | | | | |
| Fe-Mn carbonate | 264-907 | 43.3 | 1.5 | 4.9 | 1.3 | | 0.5 | | 0.4 | 7.6 | 39.6 | | | 0.9 | | | | | | | |

| **Secondary minerals** | Sample | O | Si | Ca | Mg | K | Al | Na | Cl | Mn | Fe | S | Cu | Zn | Pb | As | Ti | Zr | Br | Ba | Sr |
|---|---|---|---|---|---|---|---|---|---|---|---|---|---|---|---|---|---|---|---|---|---|
| Cu-chloride | 495-777 | 20.7 | 1.0 | | | | | | 19.1 | 0.5 | 1.8 | 0.8 | 56.1 | | | | | | | | |
| Cu-chloride | 495-777 | 23.0 | | | | | | | 17.2 | | 2.2 | | 57.6 | | | | | | | | |
| Zn-chloride | 264-474 | 20.9 | | | | | | | 33.4 | | | | | 45.7 | | | | | | | |
| Pb-chloride | 264-474 | 22.7 | 2.9 | | | 2.2 | | | 18.3 | | 4.3 | | | 4.2 | 45.6 | | | | | | |
| Pb-chloride | 264-474 | 30.1 | 8.2 | | | 1.2 | | | 4.1 | | 9.9 | | | 1.9 | 44.2 | 0.40 | | | | | |
| **Sulfates** | | | | | | | | | | | | | | | | | | | | | |
| Zn-sulfate | 495-859 | 26.6 | 1.2 | 1.1 | | | | | 6.4 | | 0.8 | 6.9 | | 57.0 | | | | | | | |
| Zn-sulfate | 495-859 | 28.4 | 1.1 | 3.3 | | | | | 5.9 | | 0.8 | 6.3 | | 54.4 | | | | | | | |
| barite | 503-254 | 29.5 | | | | | | | | | | 14.1 | | | | | | | | 52.1 | 4.4 |
| barite | 264-474 | 30.3 | | | | | | 1.6 | 1.1 | | 1.6 | 13.6 | | | | | | | | 47.0 | 4.9 |
| anhydrite | 503-254 | 49.1 | | 27.1 | | | | | | | | 23.8 | | | | | | | | | |
| anhydrite | 503-254 | 49.8 | | 26.3 | | | | | | | 0.5 | 23.3 | | | | | | | | | |

* Close to stoichiometric composition: [1] plagioclase, [2] mica, [3] calcite, [4] dolomite, [5] nontronite,

Table 2.4. Representative semiquantitative spot analyses (SEM-EDX/EPMA) of sulfide minerals in the Atlantis II Deep metalliferous sediments. All analyses are normalized to 100%

| Sulfides | Sample | O | Si | Ca | Fe | S | Cu | Zn | As | Au | Sb | Ni | Ga |
|---|---|---|---|---|---|---|---|---|---|---|---|---|---|
| pyrite | 264-907 | | | | 45.0 | 55.0 | | | | | | | |
| pyrite | 495-859 | | 0.4 | 0.6 | 46.5 | 52.5 | | | | | | | |
| chalcopyrite | 264-907 | | | | 38.4 | 36.9 | 24.7 | | | | | | |
| chalcopyrite | 264-907 | | | | 40.5 | 36.7 | 22.8 | | | | | | |
| sphalerite | 495-859 | | | | 1.5 | 31.7 | | 66.8 | | | | | |
| sphalerite | 495-859 | 2.2 | | | 0.9 | 30.5 | | 66.3 | | | | | |
| rim on pyrite[1] | 503-912 | | <0.01 | | 46.3 | 52.2 | 0.1 | 0.2 | 0.29 | <0.010 | <0.013 | 0.01 | <0.013 |
| rim on pyrite[1] | 503-912 | | 0.1 | | 43.9 | 50.8 | 0.1 | 0.1 | 1.31 | 0.05 | <0.013 | 0.04 | <0.013 |
| rim on pyrite[1] | 503-912 | | 0.9 | | 42.1 | 43.8 | 0.4 | 0.8 | 1.61 | 0.04 | 0.02 | 0.05 | <0.013 |
| rim on pyrite[1] | 503-912 | | 0.5 | | 41.8 | 38.8 | 0.5 | 2.2 | 0.39 | <0.010 | 0.02 | 0.02 | <0.013 |

[1] See Figure 2.11F

Table 2.5. Munsell color code and mineralogy of selected layers of sediment from the Atlantis II Deep.

| Sample name | Color when sampled | Munsell color code | Color after drying | Munsell color code | strat. unit | Mineralogy (XRD) | Fe wt.% |
|---|---|---|---|---|---|---|---|
| 334-757 | bright med. red | 10R 4/8 | red orange | 10R 6/6 | SU2 | Hematite | 21.1 |
| 503-626 | bright red | 10R 5/6 | yellow brown | 5YR 5/5 | CO | Goethite | 41.0 |
| 495-569 (Mn-rich) | dark red brown | 10R 3/5 | yellow brown | 10YR 5/3 | CO | Goethite[1] (+Manganite) | 14.1 |
| 373-798 | medium yellow | 10YR 8/10 | dark yellow orange | 10YR 6/6 | DOP | Goethite | 41.8 |
| 421-223 | bright yellow | 10YR 8/14 | med. brown | 5YR 4/5 | CO | Goethite | 30.8 |
| 495-557 | yellow grey | 10YR 6/4 | yellow brown | 10YR 5/5 | CO | Goethite[1] | 29.3 |
| 421-870 | bright orange | 5YR 6/14 | pale orange | 10YR 7/6 | DOP | Lepidocrocite | 40.5 |
| 495-934 | light brown | 5YR 6/6 | light green grey | 5GY 8/1 | DOP | Ankerite | 4.0 |
| 495-1195 | green brown | 10YR 5/6 | pale olive | 10Y 6/2 | DOP | Ankerite | 5.6 |
| 495-1088 | reddish grey | 10R 4/3 | bluish grey | 5B 7/1 | DOP | Ankerite | 4.1 |
| 495-867 | grey | 10YR 5/2 | light green grey | 5GY 8/1 | SU1 | Ankerite | 6.6 |
| 495-777 | greyish black | N2 | med. grey | 5Y 4/1 | SU1 | Ankerite | 19.1 |
| 503-75 | grey | 5PB 4/2 | pale green | 10Y 8/2 | SU2 | Jarosite[2] | 6.4 |
| 373-555 | dark grey | N3 | med. grey | N5 | SU1 | Pyrite | 11.0 |
| 387-466 | dark grey | N3 | pale brown grey | 10Y 6/2 | SU1 | Pyrite[2] | 22.7 |
| 503-889 (Mn-rich) | purple grey | 5P 4/2 | dark yellow orange | 10YR 6/6 | SU1 | Akaganeite[2] | 37.3 |
| 546-311 | brownish black | 5YR 3/1 | dark yellow brown | 10YR 6/4 | SU1 | Siderite (Akaganeite) | 37.1 |

[1] Only 1 % of the total iron was dissolved during leaching with weak acids that should have dissolved goethite, suggesting that the Fe-oxides may be nano-hematite.

[2] These three samples contained 14.1-27.1 % of Fe in soluble form. Whereas jarosite and pyrite are insoluble in weak acids, akageneite is soluble.

Table 2.6. Normative mineralogy (g/kg) of 100 sedimentary samples from the Atlantis II Deep (see text for details).

| | | | | Carbonates | | | | | Sulfates | | Sulfides | | | Oxides | | Residual elements | | | | | | | Tot. |
|---|---|---|---|---|---|---|---|---|---|---|---|---|---|---|---|---|---|---|---|---|---|---|---|
| Sample number | Unit | Na Cl | Detrital | Ca $CO_3$ | Mg $CO_3$ | Mn $CO_3$ | Fe $CO_3$ | res. $CO_3$ | Ca $SO_4$ | res. $SO_4$ | Cpy | Py | Sph | Mn O | $Fe_2O_3$ | Ca O | Mg O | $SiO_2$ | $Al_2O_3$ | $K_2O$ | Zn | Cu | tot. (%) |
| $CO_3$-rich (calcite, detrital silicates); "detrital layers" in the text | | | | | | | | | | | | | | | | | | | | | | | |
| 373-780 | DOP | 226 | 218 | 430 | 43 | 89 | 0 | 0 | 0 | 0 | 0 | 5 | 13 | 5 | 59 | 0 | 0 | 28 | 0 | 5 | 1 | 0 | 90 |
| 421-825* | DOP | 185 | 458 | 322 | 22 | 7 | 42 | 2 | 0 | 0 | 2 | 66 | 8 | 0 | na | 0 | 0 | 2 | 0 | 0 | 0 | 0 | 93 |
| 495-1088 | DOP | 110 | 433 | 358 | 71 | 5 | 26 | 12 | 0 | 0 | 1 | 25 | 4 | 0 | na | 0 | 0 | 0 | 1 | 0 | 0 | 0 | 94 |
| 495-1195 | DOP | 0 | 439 | 307 | 75 | 8 | 49 | 13 | 0 | 0 | 1 | 28 | 1 | 0 | na | 0 | 0 | 16 | 5 | 0 | 0 | 0 | 94 |
| 495-582 | CO | 154 | 246 | 562 | 33 | 67 | 9 | 2 | 0 | 0 | 0 | 7 | 2 | 0 | na | 0 | 0 | 0 | 0 | 0 | 0 | 0 | 93 |
| 495-757 | SU1 | 196 | 361 | 313 | 58 | 16 | 67 | 0 | 0 | 0 | 2 | 54 | 26 | 0 | na | 0 | 0 | 27 | 4 | 2 | 0 | 4 | 93 |
| 495-867 | SU1 | 184 | 337 | 415 | 50 | 13 | 74 | 0 | 0 | 0 | 4 | 24 | 11 | 0 | 17 | 0 | 0 | 18 | 3 | 2 | 0 | 1 | 97 |
| 495-934 | DOP | 128 | 389 | 454 | 53 | 7 | 6 | 0 | 0 | 0 | 2 | 13 | 2 | 0 | 13 | 0 | 0 | 0 | 0 | 0 | 0 | 0 | 94 |
| 546-252 | CO | 191 | 435 | 373 | 27 | 23 | 21 | 0 | 0 | 0 | 0 | 7 | 10 | 0 | 19 | 0 | 0 | 0 | 0 | 0 | 0 | 0 | 91 |
| 546-385 | DOP | 132 | 410 | 451 | 25 | 13 | 57 | 0 | 0 | 0 | 1 | 17 | 1 | 0 | 9 | 0 | 0 | 0 | 0 | 0 | 0 | 0 | 98 |
| 557-502 | DOP | 87 | 331 | 556 | 40 | 9 | 4 | 0 | 0 | 0 | 1 | 8 | 3 | 0 | 1 | 0 | 0 | 0 | 0 | 0 | 0 | 0 | 95 |
| 557-608 | DOP | 120 | 249 | 624 | 29 | 8 | 1 | 0 | 0 | 0 | 0 | 5 | 0 | 0 | 31 | 0 | 0 | 0 | 0 | 0 | 0 | 0 | 95 |
| 557-753 | DOP | 132 | 272 | 594 | 22 | 9 | 0 | 0 | 0 | 0 | 1 | 5 | 1 | 2 | 12 | 0 | 0 | 0 | 0 | 1 | 0 | 0 | 92 |
| 557-795 | DOP | 111 | 210 | 642 | 32 | 8 | 10 | 0 | 0 | 0 | 0 | 5 | 0 | 0 | 27 | 0 | 0 | 0 | 0 | 0 | 0 | 0 | 93 |
| 617-508 | SOAN | 207 | 312 | 361 | 24 | 0 | 0 | 0 | 0 | 0 | 4 | 14 | 9 | 0 | 122 | 0 | 1 | 66 | 3 | 0 | 0 | 0 | 92 |
| $CO_3$-rich (authigenic carbonate); "hydrothermal carbonate layers" in the text | | | | | | | | | | | | | | | | | | | | | | | |
| 373-515 | COS | 505 | 34 | 74 | 0 | 50 | 9 | 0 | 0 | 0 | 4 | 56 | 10 | 0 | 311 | 0 | 13 | 151 | 0 | 21 | 7 | 0 | 75 |
| 387-261 | CO | 308 | 388 | 89 | 0 | 37 | 168 | 0 | 0 | 0 | 4 | 63 | 17 | 0 | na | 0 | 12 | 63 | 1 | 6 | 0 | 0 | 88 |
| 421-160 | SU2 | 654 | 25 | 78 | 0 | 46 | 32 | 0 | 0 | 0 | 9 | 55 | 12 | 0 | 287 | 0 | 14 | 138 | 0 | 27 | 17 | 0 | 74 |
| 421-496 | SU1 | 327 | 152 | 64 | 0 | 89 | 136 | 0 | 0 | 0 | 2 | 60 | 2 | 0 | 166 | 0 | 13 | 58 | 0 | 10 | 1 | 0 | 76 |
| 421-520 | SU1 | 518 | 66 | 125 | 0 | 14 | 0 | 0 | 0 | 0 | 4 | 96 | 3 | 16 | 262 | 0 | 13 | 122 | 0 | 23 | 2 | 0 | 75 |
| 421-870 | DOP | 434 | 126 | 28 | 0 | 4 | 1 | 0 | 0 | 0 | 0 | 32 | 5 | 0 | 547 | 0 | 7 | 50 | 0 | 7 | 0 | 0 | 82 |
| 495-548 | SU2 | 451 | 79 | 67 | 0 | 61 | 146 | 0 | 0 | 0 | 5 | 54 | 13 | 0 | 258 | 0 | 11 | 91 | 3 | 16 | 2 | 0 | 83 |
| 495-557* | CO | 273 | 152 | 184 | 0 | 60 | 4 | 0 | 0 | 0 | 1 | 156 | 10 | 0 | 299 | 0 | 7 | 15 | 0 | 5 | 0 | 0 | 91 |
| 495-599 | CO | 351 | 182 | 279 | 0 | 79 | 50 | 0 | 0 | 0 | 1 | 217 | 4 | 0 | na | 0 | 12 | 77 | 0 | 15 | 0 | 0 | 92 |
| 503-516* | COS | 341 | 560 | 0 | 0 | 11 | 33 | 0 | 0 | 0 | 52 | 0 | 8 | 1 | 0 | 0 | 0 | 124 | 3 | 1 | 11 | 0 | 80 |
| 503-889* | SU1 | 77 | 44 | 63 | 0 | 53 | 221 | 0 | 0 | 0 | 39 | 69 | 70 | 0 | 261 | 0 | 7 | 6 | 2 | 1 | 0 | 0 | 95 |
| 546-180* | AM | 537 | 36 | 45 | 0 | 53 | 37 | 0 | 0 | 0 | 6 | 40 | 11 | 0 | 280 | 0 | 25 | 157 | 2 | 17 | 0 | 0 | 73 |
| 546-229 | SU2 | 382 | 41 | 53 | 0 | 108 | 199 | 0 | 0 | 0 | 30 | 38 | 23 | 0 | 120 | 0 | 24 | 117 | 8 | 11 | 0 | 0 | 81 |
| 546-311 | SU1 | 102 | 55 | 52 | 0 | 96 | 269 | 0 | 0 | 0 | 30 | 29 | 9 | 0 | 244 | 0 | 11 | 9 | 1 | 0 | 0 | 0 | 82 |
| 557-255 | CO | 352 | 370 | 23 | 0 | 62 | 89 | 0 | 0 | 0 | 6 | 54 | 15 | 0 | 91 | 0 | 9 | 39 | 0 | 5 | 0 | 0 | 79 |

| | | | | Carbonates | | | | | Sulfates | | Sulfides | | | Oxides | | Residual elements | | | | | | | Tot. |
|---|---|---|---|---|---|---|---|---|---|---|---|---|---|---|---|---|---|---|---|---|---|---|---|
| Sample number | Unit | Na Cl | Detrital | Ca $CO_3$ | Mg $CO_3$ | Mn $CO_3$ | Fe $CO_3$ | res. $CO_3$ | Ca $SO_4$ | res. $SO_4$ | Cpy | Py | Sph | Mn O | $Fe_2O_3$ | Ca O | Mg O | $SiO_2$ | $Al_2O_3$ | $K_2O$ | Zn | Cu | tot. (%) |
| Clay-rich | | | | | | | | | | | | | | | | | | | | | | | |
| 373-210 | SU2 | 659 | 20 | 0 | 0 | 13 | 0 | 0 | 37 | 0 | 4 | 6 | 0 | 4 | 246 | 41 | 20 | 275 | 2 | 44 | 2 | 0 | 71 |
| 373-798 | DOP | 499 | 86 | 20 | 0 | 16 | 0 | 0 | 0 | 0 | 1 | 1 | 3 | 0 | 590 | 18 | 13 | 17 | 0 | 12 | 13 | 0 | 78 |
| 373-8* | AM | 666 | 57 | 38 | 0 | 6 | 0 | 0 | 0 | 0 | 9 | 13 | 15 | 0 | 266 | 56 | 15 | 146 | 2 | 35 | 7 | 0 | 68 |
| 373-93 | SU2 | 605 | 69 | 97 | 0 | 5 | 0 | 0 | 0 | 0 | 8 | 5 | 8 | 0 | 282 | 36 | 14 | 156 | 2 | 28 | 8 | 0 | 72 |
| 387-174 | SU2 | 663 | 24 | 0 | 0 | 6 | 5 | 0 | 59 | 0 | 2 | 7 | 0 | 0 | 306 | 38 | 25 | 362 | 0 | 39 | 14 | 0 | 87 |
| 387-302 | CO | 353 | 48 | 7 | 0 | 19 | 0 | 0 | 0 | 0 | 1 | 0 | 2 | 0 | 648 | 19 | 5 | 70 | 1 | 7 | 3 | 0 | 83 |
| 421-223 | CO | 600 | 27 | 43 | 0 | 14 | 0 | 0 | 0 | 0 | 2 | 2 | 4 | 0 | 438 | 18 | 8 | 29 | 0 | 20 | 9 | 0 | 61 |
| 421-362* | COS | 659 | 33 | 44 | 0 | 13 | 0 | 0 | 0 | 0 | 16 | 40 | 15 | 0 | 263 | 54 | 13 | 161 | 4 | 27 | 0 | 0 | 71 |
| 495-113 | AM | 138 | 26 | 0 | 0 | 8 | 9 | 0 | 79 | 0 | 4 | 2 | 0 | 0 | 420 | 31 | 10 | 127 | 3 | 25 | 14 | 0 | 74 |
| 495-362 | SU2 | 527 | 33 | 0 | 0 | 9 | 16 | 0 | 84 | 0 | 15 | 0 | 0 | 0 | 354 | 37 | 10 | 136 | 3 | 22 | 13 | 1 | 72 |
| 495-693 | COS | 527 | 79 | 0 | 0 | 16 | 12 | 0 | 39 | 0 | 5 | 0 | 0 | 0 | 372 | 24 | 9 | 173 | 0 | 23 | 1 | 0 | 75 |
| 503-407 | COS | 375 | 16 | 10 | 0 | 9 | 0 | 0 | 0 | 0 | 3 | 2 | 2 | 0 | 731 | 12 | 4 | 25 | 2 | 7 | 0 | 1 | 83 |
| 503-671* | COS | 615 | 31 | 22 | 0 | 8 | 0 | 0 | 0 | 0 | 3 | 21 | 16 | 0 | 213 | 45 | 20 | 286 | 0 | 48 | 0 | 0 | 74 |
| 503-680* | COS | 545 | 39 | 14 | 0 | 33 | 0 | 0 | 0 | 0 | 20 | 9 | 14 | 0 | 412 | 33 | 14 | 175 | 1 | 23 | 0 | 7 | 81 |
| 557-289 | CO | 465 | 17 | 0 | 0 | 21 | 0 | 0 | 27 | 0 | 14 | 0 | 0 | 0 | 573 | 8 | 9 | 29 | 3 | 13 | 12 | 0 | 71 |
| Mn-rich | | | | | | | | | | | | | | | | | | | | | | | |
| 373-265 | CO | 528 | 81 | 11 | 0 | 0 | 0 | 0 | 0 | 0 | 1 | 55 | 1 | 419 | na | 0 | 0 | 0 | 0 | 23 | 0 | 0 | 59 |
| 495-569* | CO | 250 | 103 | 50 | 3 | 0 | 0 | 0 | 0 | 0 | 1 | 47 | 2 | 345 | 163 | 0 | 3 | 8 | 0 | 3 | 0 | 0 | 73 |
| 495-889 | DOP | 359 | 175 | 167 | 22 | 69 | 0 | 0 | 0 | 0 | 9 | 161 | 43 | 77 | 188 | 0 | 0 | 52 | 7 | 10 | 0 | 0 | 105 |
| Anhydrite | | | | | | | | | | | | | | | | | | | | | | | |
| 373-586* | SU1 | 44 | 8 | 0 | 0 | 1 | 3 | 0 | 766 | 110 | 0 | 0 | 6 | 0 | 14 | 0 | 0 | 17 | 0 | 0 | 0 | 1 | 88 |
| 387-502 | SU1 | 28 | 5 | 0 | 0 | 1 | 3 | 0 | 789 | 82 | 0 | 0 | 3 | 0 | 12 | 0 | 0 | 4 | 0 | 0 | 0 | 0 | 86 |
| 503-235 | SOAN | 79 | 6 | 0 | 0 | 1 | 0 | 0 | 925 | 58 | 0 | 0 | 5 | 1 | 1 | 0 | 1 | 1 | 0 | 2 | 0 | 0 | 98 |
| 503-266 | SOAN | 163 | 8 | 0 | 0 | 8 | 29 | 0 | 709 | 39 | 0 | 0 | 3 | 0 | 27 | 0 | 1 | 7 | 0 | 0 | 0 | 1 | 80 |
| 617-551 | SOAN | 143 | 22 | 0 | 0 | 2 | 39 | 0 | 873 | 20 | 0 | 0 | 9 | 0 | 15 | 0 | 4 | 21 | 1 | 1 | 0 | 1 | 101 |
| 617-875* | SOAN | 247 | 44 | 0 | 0 | 2 | 18 | 0 | 553 | 39 | 0 | 0 | 45 | 0 | 103 | 0 | 12 | 76 | 5 | 1 | 0 | 7 | 94 |
| $SO_4$-rich (high sulfide and high metals; Cu-rich); “metal- and sulfide-rich layers” in the text | | | | | | | | | | | | | | | | | | | | | | | |
| 334-612 | SOAN | 539 | 35 | 101 | 0 | 2 | 1 | 0 | 148 | 0 | 28 | 2 | 0 | 0 | 332 | 0 | 13 | 158 | 4 | 18 | 31 | 0 | 84 |
| 387-398* | SU1 | 437 | 166 | 0 | 0 | 8 | 100 | 2 | 115 | 0 | 73 | 102 | 118 | 0 | na | 0 | 5 | 201 | 6 | 6 | 0 | 0 | 110 |
| 387-466* | SU1 | 351 | 105 | 0 | 0 | 34 | 396 | 0 | 97 | 0 | 46 | 68 | 61 | 0 | na | 0 | 10 | 89 | 5 | 5 | 0 | 0 | 102 |
| 387-490 | SU1 | 145 | 84 | 0 | 0 | 16 | 103 | 0 | 19 | 0 | 36 | 20 | 9 | 0 | 506 | 0 | 3 | 5 | 2 | 2 | 0 | 5 | 82 |
| 421-678 | DOP | 389 | 174 | 0 | 0 | 24 | 182 | 0 | 54 | 0 | 76 | 155 | 80 | 0 | na | 0 | 6 | 137 | 7 | 6 | 0 | 0 | 103 |
| 495-777 | SU1 | 247 | 137 | 0 | 0 | 33 | 154 | 0 | 58 | 0 | 43 | 179 | 35 | 0 | 44 | 0 | 9 | 150 | 6 | 3 | 0 | 0 | 91 |
| 546-5 | AM | 563 | 35 | 0 | 0 | 37 | 47 | 0 | 33 | 0 | 41 | 0 | 29 | 0 | 396 | 0 | 21 | 122 | 10 | 16 | 14 | 9 | 84 |

| | | | | Carbonates | | | | | Sulfates | | Sulfides | | | Oxides | | Residual elements | | | | | | | Tot. |
|---|---|---|---|---|---|---|---|---|---|---|---|---|---|---|---|---|---|---|---|---|---|---|---|
| Sample number | Unit | Na Cl | Detrital | Ca $CO_3$ | Mg $CO_3$ | Mn $CO_3$ | Fe $CO_3$ | res. $CO_3$ | Ca $SO_4$ | res. $SO_4$ | Cpy | Py | Sph | Mn O | $Fe_2O_3$ | Ca O | Mg O | $SiO_2$ | $Al_2O_3$ | $K_2O$ | Zn | Cu | tot. (%) |
| 557-388 | SU1 | 318 | 138 | 0 | 0 | 44 | 232 | 0 | 99 | 0 | 59 | 115 | 93 | 0 | na | 0 | 9 | 121 | 11 | 5 | 0 | 0 | 108 |
| 617-148* | SAM | 542 | 40 | 0 | 0 | 5 | 16 | 0 | 167 | 0 | 48 | 49 | 71 | 0 | 251 | 0 | 13 | 128 | 6 | 17 | 0 | 0 | 93 |
| 617-396 | OAN | 368 | 285 | 0 | 0 | 4 | 83 | 0 | 73 | 0 | 7 | 0 | 11 | 0 | 161 | 0 | 65 | 132 | 3 | 2 | 1 | 9 | 84 |
| 617-9 | SAM | 600 | 46 | 0 | 0 | 6 | 7 | 0 | 139 | 0 | 38 | 2 | 12 | 0 | 330 | 0 | 12 | 119 | 6 | 19 | 24 | 0 | 76 |
| $SO_4$-rich samples (high sulfide and high metals; Zn-rich); “metal- and sulfide-rich layers” in the text | | | | | | | | | | | | | | | | | | | | | | | |
| 334-513* | SAM | 496 | 48 | 0 | 0 | 8 | 47 | 0 | 221 | 0 | 25 | 61 | 107 | 0 | 205 | 0 | 14 | 84 | 4 | 9 | 0 | 0 | 101 |
| 334-757* | SOAN | 506 | 37 | 0 | 0 | 2 | 16 | 0 | 128 | 0 | 4 | 44 | 77 | 0 | 271 | 0 | 19 | 155 | 6 | 10 | 0 | 0 | 90 |
| 334-83* | SAM | 497 | 35 | 130 | 0 | 5 | 0 | 0 | 271 | 0 | 10 | 10 | 0 | 0 | 200 | 3 | 8 | 97 | 2 | 14 | 23 | 0 | 78 |
| 373-555 | SU1 | 437 | 165 | 0 | 0 | 15 | 153 | 9 | 113 | 0 | 62 | 64 | 131 | 0 | na | 0 | 7 | 193 | 4 | 6 | 0 | 0 | 114 |
| 373-751 | SU1 | 308 | 122 | 0 | 0 | 51 | 269 | 13 | 98 | 0 | 48 | 60 | 100 | 0 | na | 0 | 10 | 90 | 8 | 4 | 0 | 0 | 104 |
| 387-80* | SU2 | 558 | 36 | 74 | 0 | 4 | 0 | 0 | 167 | 0 | 13 | 8 | 0 | 0 | 222 | 2 | 10 | 117 | 3 | 19 | 20 | 0 | 68 |
| 421-740* | DOP | 608 | 49 | 0 | 0 | 22 | 23 | 0 | 41 | 0 | 3 | 19 | 22 | 0 | 218 | 0 | 19 | 273 | 0 | 26 | 22 | 0 | 75 |
| 495-240 | AM | 704 | 49 | 0 | 0 | 14 | 0 | 0 | 96 | 0 | 10 | 0 | 0 | 4 | 426 | 23 | 9 | 97 | 2 | 21 | 15 | 12 | 75 |
| 495-484 | SU2 | 578 | 38 | 26 | 0 | 5 | 23 | 0 | 165 | 0 | 25 | 19 | 0 | 0 | 277 | 0 | 10 | 156 | 6 | 25 | 32 | 0 | 77 |
| 503-155 | SOAN | 542 | 44 | 0 | 0 | 3 | 20 | 0 | 126 | 0 | 10 | 35 | 30 | 0 | 174 | 0 | 13 | 178 | 4 | 50 | 0 | 0 | 74 |
| 503-7 | SAM | 585 | 36 | 151 | 0 | 3 | 0 | 0 | 154 | 0 | 14 | 6 | 0 | 0 | 358 | 4 | 10 | 109 | 2 | 22 | 20 | 0 | 87 |
| 503-912* | SU1 | 400 | 108 | 0 | 0 | 22 | 30 | 0 | 105 | 0 | 73 | 125 | 216 | 0 | na | 0 | 6 | 118 | 11 | 4 | 0 | 0 | 118 |
| 503-946 | DOP | 388 | 80 | 0 | 0 | 35 | 76 | 0 | 185 | 0 | 11 | 37 | 36 | 0 | 232 | 0 | 8 | 53 | 3 | 4 | 0 | 0 | 82 |
| 557-173* | SU2 | 667 | 50 | 0 | 0 | 4 | 24 | 0 | 126 | 0 | 33 | 43 | 53 | 0 | 218 | 0 | 15 | 196 | 9 | 29 | 44 | 0 | 89 |
| 557-227 | SU2 | 550 | 23 | 0 | 0 | 16 | 1 | 0 | 167 | 0 | 6 | 32 | 52 | 0 | 172 | 0 | 12 | 153 | 6 | 19 | 10 | 0 | 74 |
| 557-9 | SAM | 624 | 34 | 0 | 0 | 6 | 17 | 0 | 207 | 0 | 37 | 2 | 12 | 0 | 232 | 0 | 12 | 121 | 4 | 24 | 38 | 0 | 73 |
| 617-650 | SOAN | 409 | 70 | 0 | 0 | 5 | 29 | 0 | 192 | 0 | 31 | 39 | 73 | 0 | 195 | 0 | 11 | 140 | 9 | 6 | 0 | 0 | 92 |
| 617-787 | SOAN | 364 | 45 | 0 | 0 | 7 | 14 | 0 | 277 | 0 | 7 | 42 | 37 | 0 | 270 | 0 | 8 | 120 | 7 | 3 | 0 | 0 | 90 |
| $SO_4$-rich samples (high sulfide and low metals); “sulfide-rich layers” in the text | | | | | | | | | | | | | | | | | | | | | | | |
| 373-672 | SU1 | 551 | 23 | 0 | 0 | 16 | 0 | 0 | 76 | 0 | 4 | 13 | 0 | 3 | 374 | 0 | 13 | 202 | 1 | 22 | 9 | 0 | 75 |
| 387-575* | SU1 | 322 | 70 | 0 | 0 | 8 | 73 | 0 | 254 | 0 | 15 | 152 | 13 | 0 | na | 0 | 3 | 220 | 2 | 12 | 0 | 0 | 85 |
| 503-758 | OAN | 407 | 60 | 0 | 0 | 15 | 67 | 0 | 101 | 0 | 7 | 191 | 18 | 0 | na | 0 | 4 | 334 | 3 | 7 | 0 | 0 | 83 |
| 503-807* | SU1 | 319 | 93 | 0 | 0 | 21 | 34 | 0 | 107 | 0 | 20 | 154 | 10 | 0 | 61 | 0 | 4 | 242 | 3 | 13 | 0 | 0 | 78 |
| 503-987 | DOP | 195 | 421 | 0 | 0 | 8 | 112 | 0 | 7 | 0 | 3 | 378 | 16 | 0 | 8 | 0 | 4 | 8 | 2 | 0 | 0 | 0 | 100 |
| 546-318 | SU1 | 202 | 101 | 0 | 0 | 9 | 45 | 0 | 130 | 0 | 1 | 63 | 1 | 0 | na | 0 | 7 | 489 | 4 | 3 | 0 | 0 | 85 |
| 617-395 | OAN | 442 | 58 | 49 | 0 | 2 | 19 | 0 | 259 | 0 | 1 | 28 | 0 | 0 | 209 | 0 | 73 | 121 | 4 | 10 | 8 | 0 | 83 |
| $SO_4$-rich samples (low sulfide and high metals); “metal-rich layers” in the text | | | | | | | | | | | | | | | | | | | | | | | |
| 334-312* | SAM | 523 | 38 | 0 | 0 | 4 | 21 | 0 | 217 | 0 | 20 | 34 | 25 | 0 | 307 | 0 | 7 | 118 | 5 | 15 | 29 | 0 | 85 |
| 421-80* | SU2 | 555 | 29 | 168 | 0 | 20 | 72 | 0 | 86 | 0 | 37 | 3 | 0 | 0 | 272 | 0 | 10 | 126 | 4 | 23 | 24 | 0 | 85 |
| 546-92* | AM | 616 | 25 | 0 | 0 | 55 | 44 | 0 | 63 | 0 | 0 | 7 | 49 | 0 | 327 | 0 | 29 | 162 | 7 | 21 | 0 | 10 | 87 |

| | | | | Carbonates | | | | | Sulfates | | Sulfides | | | Oxides | | Residual elements | | | | | | | Tot. |
|---|---|---|---|---|---|---|---|---|---|---|---|---|---|---|---|---|---|---|---|---|---|---|---|
| Sample number | Unit | NaCl | Detrital | $CaCO_3$ | $MgCO_3$ | $MnCO_3$ | $FeCO_3$ | res. $CO_3$ | $CaSO_4$ | res. $SO_4$ | Cpy | Py | Sph | MnO | $Fe_2O_3$ | CaO | MgO | $SiO_2$ | $Al_2O_3$ | $K_2O$ | Zn | Cu | tot. (%) |
| 617-799* | SOAN | 359 | 91 | 0 | 0 | 6 | 47 | 0 | 408 | 0 | 18 | 0 | 75 | 0 | 116 | 0 | 12 | 64 | 4 | 2 | 20 | 3 | 97 |
| $SO_4$-rich samples (low sulfide and low metals) | | | | | | | | | | | | | | | | | | | | | | | |
| 495-809* | SU1 | 590 | 52 | 180 | 0 | 7 | 9 | 0 | 90 | 0 | 1 | 4 | 0 | 0 | 252 | 0 | 20 | 335 | 0 | 29 | 11 | 0 | 98 |
| 503-140* | SOAN | 548 | 22 | 0 | 0 | 3 | 13 | 0 | 208 | 0 | 2 | 31 | 28 | 0 | 166 | 0 | 14 | 160 | 2 | 48 | 0 | 3 | 74 |
| 503-509 | COS | 451 | 14 | 316 | 0 | 33 | 111 | 0 | 181 | 0 | 9 | 0 | 0 | 0 | 274 | 0 | 9 | 108 | 1 | 16 | 4 | 0 | 107 |
| 503-626 | COS | 466 | 16 | 0 | 0 | 10 | 3 | 0 | 70 | 0 | 0 | 13 | 2 | 0 | 573 | 0 | 5 | 49 | 1 | 12 | 0 | 1 | 76 |
| 546-267* | SU1 | 351 | 64 | 0 | 0 | 14 | 40 | 0 | 123 | 0 | 4 | 16 | 4 | 0 | 356 | 0 | 17 | 148 | 1 | 8 | 0 | 2 | 80 |
| 617-220* | OAN | 315 | 21 | 0 | 0 | 0 | 0 | 0 | 470 | 0 | 3 | 31 | 2 | 1 | 17 | 0 | 81 | 146 | 1 | 5 | 0 | 0 | 78 |

Sample number includes core number and sampling depth in the core (cm); asterisk indicates samples with sequential leaching data. Stratigraphic units are according to Bäcker and Richter (1973) (Figure 2.3: Table 2.1). See text for additional discussion of sample types. NaCl (according to Na-concentration) is the amount of salt before the salt-free calculation, and is not included in the total. The detrital component is the sum of $Al_2O_3$, MgO, $K_2O$, $SiO_2$, $Fe_2O_3$, and CaO (g/kg). Res.= residual, Cpy= Chalcopyrite, Py= Pyrite, Sph= Sphalerite, tot.= total of all components. All values are in g/kg, except total is in wt.%. The total is the sum of all calculated mineralogical components; low values are mainly due to lack of precision in estimates of the oxygen contained in the poorly crystalline phases. Residual CaO, MgO, $Al_2O_3$, and $K_2O$ are bound to authigenic clays. Residual Cu and Zn are contained in nonsulfidic minerals. $Fe_2O_3$ is all Fe (mainly in Fe-oxyhydroxides) not accounted for by detrital, carbonate and sulfide fractions. na= insufficient Fe to account for all detrital Fe-silicate, siderite and Fe-sulfides (i.e., normative concentration would be slightly negative).

Table 2.7. Cumulative percent of elements leached by all 4 steps of the sequential leaching experiments on different types of Atlantis II sediments (see text for discussion).

| | Fe | Al | Mg | K | Ca | Mn | Sr | Ba | Cu | Zn | Pb | Cd | Ag | Tl | Ni | Se | Co | Br |
|---|---|---|---|---|---|---|---|---|---|---|---|---|---|---|---|---|---|---|
| Clay-rich | 9 | 9 | 78 | 55 | 114 | 89 | 117 | 79 | 83 | 97 | 62 | 98 | 112 | 71 | 42 | 79 | 52 | 159 |
| $CO_3$-rich (detrital) | 5 | 2 | 35 | 24 | 105 | 100 | 120 | 11 | 27 | 85 | 53 | 72 | 5 | 30 | 52 | 31 | 50 | 111 |
| $CO_3$-rich (authigenic) | 14 | 2 | 78 | 57 | 86 | 81 | 105 | 89 | 29 | 77 | 22 | 107 | 48 | 73 | 31 | 57 | 41 | 135 |
| Mn-rich | 1 | 2 | 56 | 72 | 97 | 81 | 97 | 65 | 34 | 74 | 4 | 30 | 111 | 84 | 25 | 225 | 33 | 130 |
| $SO_4$-rich | 11 | 9 | 65 | 82 | 109 | 96 | 102 | 62 | 60 | 105 | 54 | 108 | 58 | 53 | 60 | 89 | 61 | 120 |
| | | | | | | | | | | | | | | | | | | |
| | As | Mo | Sb | Sn | W | V | Rb | Cs | Au* | Cr | Ga | Te | U | Y | P | B | Li | |
| Clay-rich | 3 | 3 | 6 | 7 | 0 | 22 | 20 | 7 | 2/4 | 57 | 8 | 31 | 44 | 47 | 7 | 33 | 85 | |
| $CO_3$-rich (detrital) | 19 | 13 | 16 | 1 | 3 | 14 | 18 | 10 | n.d | 9 | 4 | 48 | 59 | 39 | 77 | 28 | 20 | |
| $CO_3$-rich (authigenic) | 1 | 1 | 1 | 7 | 0 | 11 | 36 | 15 | n.d | 30 | 12 | 42 | 20 | 47 | 1 | 27 | 67 | |
| Mn-rich | 1 | 5 | 4 | 1 | 1 | 32 | 45 | 17 | n.d. | 11 | 76 | 43 | 14 | 17 | 2 | 37 | 62 | |
| $SO_4$-rich | 5 | 2 | 6 | 17 | 1 | 11 | 30 | 14 | 2/23 | 7 | 6 | 41 | 40 | 53 | 13 | 30 | 79 | |

The proportions leached are according to bulk chemistry in Laurila et al. (2014b). Values greater than 100% reflect cumulative error of ICP-MS analyses in the dilute leachates. Ti, Zr, Ge, Hg, Hf, Nb, Ta, Th, Be, Bi, I and In were analyzed, but the leached concentrations were consistently below detection. The detection limit for gold was 50 ppb, and it was detected only in 4 of 92 leachates, all after the first dissolution step; two in the clay-rich samples (373-8 and 495-362; average 56% of 340 ppb Au leached) and two in $SO_4$-rich samples (546-180 and 334-83; average 18% of 270 ppb Au leached). The complete results are given in Appendix 2.2.

Table 2.8. Step-wise sequential leaching results for representative samples of detrital-, authigenic carbonate- and Mn-rich sediments in the Atlantis II Deep (numbers are the percentage of each element leached during each step).

| | Ca | K | Mg | Mn | Fe | Cu | Zn | Pb | Cd | Ag | As | Ni |
|---|---|---|---|---|---|---|---|---|---|---|---|---|
| 421-825; detrital (high $CaCO_3$ and Al) sample | | | | | | | | | | | | |
| **Bulk composition** | **12.2** | **1.2** | **1.3** | **0.3** | **4.5** | **0.0** | **0.4** | **22** | **5** | **1** | **90** | **87** |
| 1st leach (%) | 9 | 20 | 7 | 4 | 0 | 0 | 1 | 0 | 2 | 0 | 0 | 0 |
| 2nd leach (%) | 87 | 3 | 16 | 91 | 1 | 10 | 76 | 16 | 68 | 0 | 10 | 35 |
| 3rd leach (%) | 3 | 0 | 10 | 4 | 1 | 0 | 4 | 1 | 2 | 0 | 3 | 7 |
| 4th leach (%) | 1 | 1 | 2 | 2 | 3 | 16 | 3 | 37 | 1 | 4 | 5 | 9 |
| Total | 100 | 24 | 35 | 100 | 5 | 27 | 85 | 53 | 72 | 5 | 19 | 52 |
| 495-557; authigenic carbonate rich sample | | | | | | | | | | | | |
| **Bulk composition** | **5.9** | **0.7** | **0.6** | **2.1** | **21.3** | **0.0** | **0.4** | **25** | **1** | **1** | **120** | **34** |
| 1st leach (%) | 23 | 49 | 21 | 0 | 0 | 0 | 0 | 0 | 3 | 31 | 0 | 0 |
| 2nd leach (%) | 75 | 5 | 40 | 75 | 0 | 53 | 78 | 25 | 92 | 0 | 1 | 6 |
| 3rd leach (%) | 3 | 0 | 8 | 21 | 0 | 6 | 7 | 1 | 3 | 13 | 0 | 4 |
| 4th leach (%) | 0 | 1 | 2 | 4 | 1 | 18 | 4 | 31 | 2 | 10 | 0 | 3 |
| Total | 100 | 55 | 71 | 100 | 1 | 77 | 89 | 57 | 99 | 54 | 1 | 13 |
| 546-180; authigenic carbonate-rich sample | | | | | | | | | | | | |
| **Bulk composition** | **0.9** | **0.8** | **0.7** | **1.2** | **11.2** | **0.1** | **0.5** | **105** | **31** | **14** | **64** | **3** |
| 1st leach (%) | 66 | 58 | 77 | 21 | 0 | 0 | 17 | 0 | 75 | 95 | 1 | 11 |
| 2nd leach (%) | 9 | 4 | 7 | 14 | 1 | 55 | 52 | 7 | 23 | 0 | 1 | 29 |
| 3rd leach (%) | 11 | 0 | 4 | 29 | 5 | 4 | 8 | 0 | 2 | 1 | 0 | 12 |
| 4th leach (%) | 14 | 0 | 6 | 36 | 9 | 11 | 7 | 22 | 0 | 3 | 0 | 14 |
| Total | 100 | 63 | 94 | 100 | 14 | 70 | 84 | 29 | 100 | 100 | 1 | 66 |
| 503-889; authigenic carbonate-rich sample | | | | | | | | | | | | |
| **Bulk composition** | **2.5** | **0.2** | **0.5** | **2.3** | **34.4** | **1.2** | **2.5** | **397** | **16** | **18** | **122** | **88** |
| 1st leach (%) | 57 | 15 | 28 | 23 | 0 | 0 | 31 | 0 | 74 | 0 | 0 | 19 |
| 2nd leach (%) | 5 | 3 | 6 | 8 | 2 | 24 | 21 | 13 | 20 | 0 | 0 | 8 |
| 3rd leach (%) | 6 | 6 | 8 | 11 | 4 | 0 | 8 | 1 | 5 | 0 | 0 | 1 |
| 4th leach (%) | 11 | 8 | 14 | 21 | 8 | 1 | 6 | 6 | 1 | 0 | 0 | 1 |
| Total | 78 | 32 | 55 | 64 | 14 | 26 | 66 | 20 | 100 | 0 | 0 | 30 |
| 503-516; authigenic carbonate-rich sample | | | | | | | | | | | | |
| **Bulk composition** | **1.5** | **1.4** | **0.8** | **0.3** | **3.4** | **1.2** | **1.5** | **277** | **98** | **85** | **99** | **52** |
| 1st leach (%) | 56 | 27 | 15 | 41 | 0 | 0 | 30 | 0 | 53 | 0 | 1 | 13 |
| 2nd leach (%) | 19 | 4 | 2 | 33 | 1 | 4 | 51 | 29 | 21 | 0 | 17 | 18 |
| 3rd leach (%) | 3 | 0 | 0 | 20 | 9 | 2 | 4 | 13 | 2 | 0 | 7 | 9 |
| 4th leach (%) | 1 | 1 | 0 | 6 | 9 | 7 | 2 | 25 | 0 | 1 | 18 | 5 |
| Total | 78 | 32 | 17 | 100 | 19 | 13 | 86 | 66 | 77 | 1 | 42 | 46 |
| 495-569; Mn-rich sample | | | | | | | | | | | | |
| **Bulk composition** | **1.8** | **0.5** | **0.4** | **20.0** | **10.6** | **0.0** | **0.4** | **89** | **0** | **0** | **50** | **17** |
| 1st leach (%) | 60 | 67 | 29 | 0 | 0 | 1 | 0 | 0 | 4 | 72 | 0 | 0 |
| 2nd leach (%) | 34 | 4 | 16 | 2 | 0 | 23 | 54 | 4 | 20 | 1 | 0 | 7 |
| 3rd leach (%) | 2 | 1 | 6 | 43 | 0 | 1 | 8 | 0 | 4 | 5 | 0 | 9 |
| 4th leach (%) | 1 | 1 | 5 | 36 | 1 | 8 | 11 | 0 | 2 | 23 | 0 | 9 |
| Total | 97 | 72 | 56 | 81 | 1 | 34 | 74 | 4 | 30 | 100 | 1 | 25 |

Bulk compositions are in wt.% (Ca, K, Mg, Mn, Fe) and ppm (Pb, Cd, Ag, As, Ni). Tabulated data are the percentage of each element reporting to the different leachates. Totals were

normalized to 100%. The complete dataset for all elements and samples is given in Appendix 2.2.

Table 2.9. Step-wise sequential leaching results for representative samples of clay-rich sediments in the Atlantis II Deep (numbers are the percentage of each element leached during each step).

| | Ca | K | Mg | Mn | Fe | Cu | Zn | Pb | Cd | Ag | As | Ni |
|---|---|---|---|---|---|---|---|---|---|---|---|---|
| 495-362; clay-rich | | | | | | | | | | | | |
| **Bulk composition** | **2.5** | **1.1** | **0.3** | **0.1** | **11.8** | **0.26** | **0.63** | **160** | **2** | **8** | **88** | **0** |
| 1st leach (%) | 91 | 54 | 61 | 31 | 0 | 1 | 39 | 0 | 69 | 95 | 0 | 39 |
| 2nd leach (%) | 9 | 5 | 5 | 23 | 1 | 71 | 50 | 34 | 29 | 0 | 2 | 0 |
| 3rd leach (%) | 0 | 0 | 3 | 22 | 5 | 11 | 7 | 13 | 2 | 3 | 0 | 0 |
| 4th leach (%) | 0 | 1 | 3 | 6 | 4 | 4 | 3 | 32 | 0 | 2 | 0 | 0 |
| Total | 100 | 60 | 71 | 81 | 10 | 86 | 99 | 78 | 100 | 100 | 3 | 39 |
| 503-671; clay-rich | | | | | | | | | | | | |
| **Bulk composition** | **1.6** | **1.9** | **0.5** | **0.2** | **6.0** | **0.04** | **0.07** | **5** | **0** | **1** | **21** | **0** |
| 1st leach (%) | 93 | 39 | 76 | 81 | 0 | 4 | 56 | 0 | 24 | 87 | 2 | 0 |
| 2nd leach (%) | 7 | 3 | 6 | 12 | 0 | 75 | 27 | 21 | 4 | 0 | 2 | 0 |
| 3rd leach (%) | 0 | 0 | 0 | 5 | 1 | 10 | 10 | 10 | 2 | 0 | 0 | 0 |
| 4th leach (%) | 0 | 0 | 0 | 2 | 1 | 11 | 7 | 16 | 2 | 4 | 0 | 0 |
| Total | 100 | 42 | 82 | 100 | 2 | 100 | 100 | 47 | 32 | 91 | 4 | 0 |
| 373-8; clay-rich | | | | | | | | | | | | |
| **Bulk composition** | **1.9** | **1.2** | **0.4** | **0.1** | **6.3** | **0.11** | **0.58** | **222** | **1** | **1** | **60** | **0** |
| 1st leach (%) | 93 | 64 | 69 | 42 | 0 | 0 | 39 | 0 | 29 | 98 | 1 | 73 |
| 2nd leach (%) | 6 | 4 | 4 | 25 | 1 | 69 | 52 | 45 | 67 | 0 | 5 | 0 |
| 3rd leach (%) | 0 | 0 | 2 | 27 | 7 | 10 | 6 | 16 | 3 | 1 | 0 | 0 |
| 4th leach (%) | 0 | 0 | 2 | 6 | 6 | 4 | 2 | 23 | 1 | 1 | 1 | 0 |
| Total | 100 | 69 | 78 | 100 | 14 | 83 | 100 | 84 | 100 | 100 | 7 | 73 |
| 503-680; clay-rich | | | | | | | | | | | | |
| **Bulk composition** | **1.4** | **1.1** | **0.4** | **0.7** | **13.4** | **0.33** | **0.17** | **225** | **1** | **1** | **134** | **0** |
| 1st leach (%) | 92 | 54 | 73 | 16 | 0 | 0 | 5 | 0 | 4 | 76 | 0 | 0 |
| 2nd leach (%) | 7 | 4 | 5 | 16 | 0 | 63 | 54 | 2 | 83 | 0 | 0 | 0 |
| 3rd leach (%) | 1 | 0 | 1 | 40 | 4 | 10 | 13 | 2 | 5 | 1 | 0 | 0 |
| 4th leach (%) | 0 | 0 | 1 | 10 | 3 | 6 | 5 | 26 | 0 | 8 | 0 | 0 |
| Total | 100 | 58 | 80 | 81 | 8 | 78 | 77 | 30 | 93 | 85 | 1 | 0 |

Bulk compositions are in wt.% (Ca, K, Mg, Mn, Fe) and ppm (Pb, Cd, Ag, As, Ni). Tabulated data are the percentage of each element reporting to the different leachates. Totals were normalized to 100%. The complete dataset for all elements and samples is given in Appendix 2.2.

Table 2.10. Step-wise sequential leaching results for sulfate-rich samples in the Atlantis II Deep (numbers are the percentage of each element leached during each step).

| | Ca | K | Mg | Mn | Fe | Cu | Zn | Pb | Cd | Ag | As | Ni |
|---|---|---|---|---|---|---|---|---|---|---|---|---|
| Average of 7 Zn-rich high sulfur and high metal samples | | | | | | | | | | | | |
| **Bulk composition** | **2.3** | **0.8** | **0.4** | **0.2** | **7.4** | **0.4** | **3.0** | **618** | **149** | **92** | **167** | **20** |
| 1st leach (%) | 90 | 58 | 60 | 73 | 0 | 18 | 91 | 9 | 94 | 60 | 1 | 45 |
| 2nd leach (%) | 9 | 5 | 3 | 6 | 1 | 34 | 12 | 40 | 6 | 0 | 2 | 10 |
| 3rd leach (%) | 0 | 0 | 1 | 9 | 4 | 6 | 2 | 10 | 0 | 1 | 1 | 5 |
| 4th leach (%) | 0 | 0 | 2 | 4 | 4 | 5 | 1 | 10 | 0 | 4 | 1 | 3 |
| Total | 100 | 64 | 66 | 93 | 9 | 63 | 105 | 70 | 100 | 65 | 4 | 63 |
| Average of 3 Cu-rich high sulfur and high metal samples | | | | | | | | | | | | |
| **Bulk composition** | **2.3** | **0.7** | **0.4** | **0.5** | **9.8** | **1.1** | **3.1** | **970** | **170** | **146** | **275** | **59** |
| 1st leach (%) | 80 | 52 | 53 | 48 | 0 | 3 | 86 | 1 | 90 | 7 | 0 | 22 |
| 2nd leach (%) | 7 | 7 | 4 | 5 | 1 | 9 | 11 | 19 | 7 | 0 | 1 | 4 |
| 3rd leach (%) | 4 | 0 | 4 | 22 | 8 | 2 | 2 | 3 | 2 | 1 | 0 | 2 |
| 4th leach (%) | 5 | 0 | 4 | 15 | 10 | 6 | 1 | 6 | 1 | 4 | 1 | 2 |
| Total | 95 | 60 | 65 | 89 | 19 | 20 | 100 | 30 | 100 | 12 | 3 | 30 |
| Average of 4 low sulfur and high metal samples | | | | | | | | | | | | |
| **Bulk composition** | **3.4** | **0.8** | **0.5** | **0.4** | **9.9** | **0.4** | **2.3** | **676** | **59** | **49** | **80** | **12** |
| 1st leach (%) | 78 | 53 | 62 | 37 | 0 | 3 | 50 | 1 | 82 | 59 | 1 | 16 |
| 2nd leach (%) | 18 | 4 | 5 | 22 | 2 | 52 | 39 | 39 | 15 | 0 | 3 | 21 |
| 3rd leach (%) | 2 | 0 | 2 | 21 | 5 | 4 | 5 | 4 | 1 | 1 | 0 | 11 |
| 4th leach (%) | 2 | 1 | 4 | 15 | 7 | 5 | 2 | 21 | 0 | 8 | 2 | 6 |
| Total | 100 | 58 | 73 | 95 | 14 | 64 | 96 | 64 | 98 | 68 | 5 | 54 |
| Average of 3 high sulfur and low metal samples | | | | | | | | | | | | |
| **Bulk composition** | **3.2** | **0.9** | **0.3** | **0.4** | **5.4** | **0.3** | **0.6** | **0** | **63** | **73** | **458** | **28** |
| 1st leach (%) | 92 | 1 | 74 | 97 | 1 | 74 | 98 | 0 | 98 | 32 | 1 | 96 |
| 2nd leach (%) | 8 | 0 | 2 | 2 | 2 | 3 | 2 | 1 | 2 | 0 | 2 | 2 |
| 3rd leach (%) | 0 | 0 | 0 | 0 | 4 | 2 | 0 | 2 | 0 | 1 | 1 | 0 |
| 4th leach (%) | 0 | 1 | 0 | 0 | 4 | 1 | 0 | 6 | 0 | 1 | 8 | 0 |
| Total | 100 | 3 | 76 | 100 | 10 | 81 | 100 | 9 | 100 | 35 | 12 | 98 |
| Average of 4 low sulfur and low metal samples | | | | | | | | | | | | |
| **Bulk composition** | **4.2** | **1.1** | **1.3** | **0.2** | **8.4** | **0.1** | **0.4** | **0** | **5** | **6** | **65** | **4** |
| 1st leach (%) | 81 | 52 | 52 | 81 | 0 | 40 | 72 | 18 | 90 | 71 | 1 | 41 |
| 2nd leach (%) | 18 | 4 | 4 | 8 | 0 | 19 | 12 | 23 | 8 | 0 | 2 | 4 |
| 3rd leach (%) | 0 | 0 | 0 | 5 | 1 | 5 | 3 | 14 | 1 | 3 | 0 | 2 |
| 4th leach (%) | 0 | 0 | 0 | 3 | 1 | 4 | 1 | 13 | 1 | 13 | 1 | 2 |
| Total | 100 | 57 | 57 | 97 | 3 | 68 | 88 | 69 | 100 | 87 | 4 | 49 |
| Average of 2 anhydrite samples | | | | | | | | | | | | |
| **Bulk composition** | **17.0** | **0.1** | **0.3** | **0.1** | **4.0** | **0.3** | **1.3** | **248** | **54** | **15** | **123** | **12** |
| 1st leach (%) | 23 | 61 | 40 | 52 | 0 | 22 | 60 | 1 | 88 | 3 | 1 | 26 |
| 2nd leach (%) | 70 | 10 | 1 | 12 | 2 | 31 | 28 | 28 | 9 | 0 | 2 | 21 |
| 3rd leach (%) | 6 | 1 | 1 | 11 | 5 | 3 | 5 | 7 | 1 | 3 | 1 | 9 |
| 4th leach (%) | 0 | 1 | 2 | 9 | 6 | 2 | 1 | 15 | 0 | 12 | 2 | 3 |
| Total | 100 | 73 | 46 | 84 | 13 | 57 | 94 | 51 | 97 | 18 | 5 | 61 |

Bulk compositions are in wt.% (Ca, K, Mg, Mn, Fe) and ppm (Pb, Cd, Ag, As, Ni). Tabulated data are the percentage of each element reporting to the different leachates. Totals were normalized to 100%. The complete dataset for all elements and samples is given in Appendix 2.2.

Figure 2.1

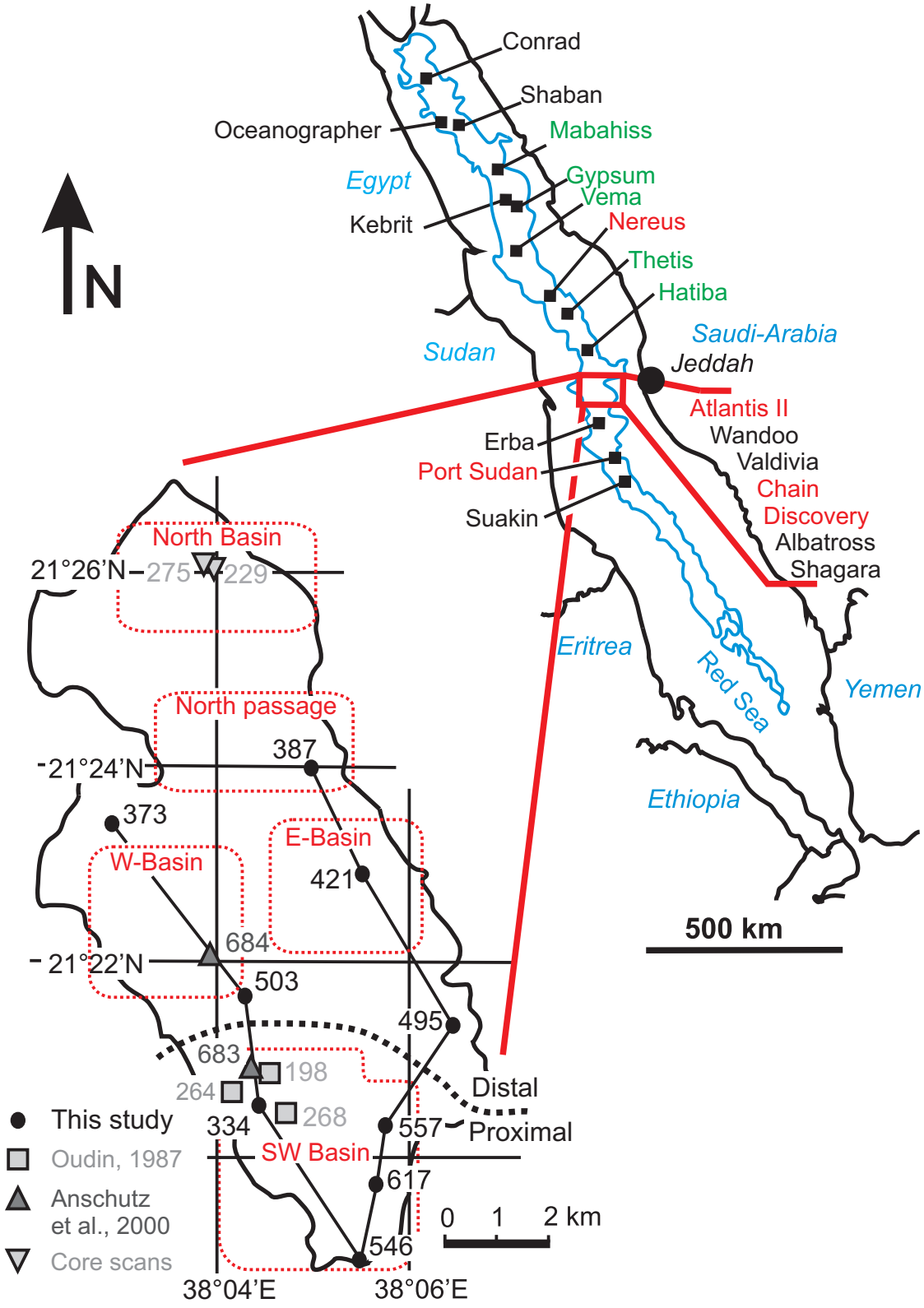
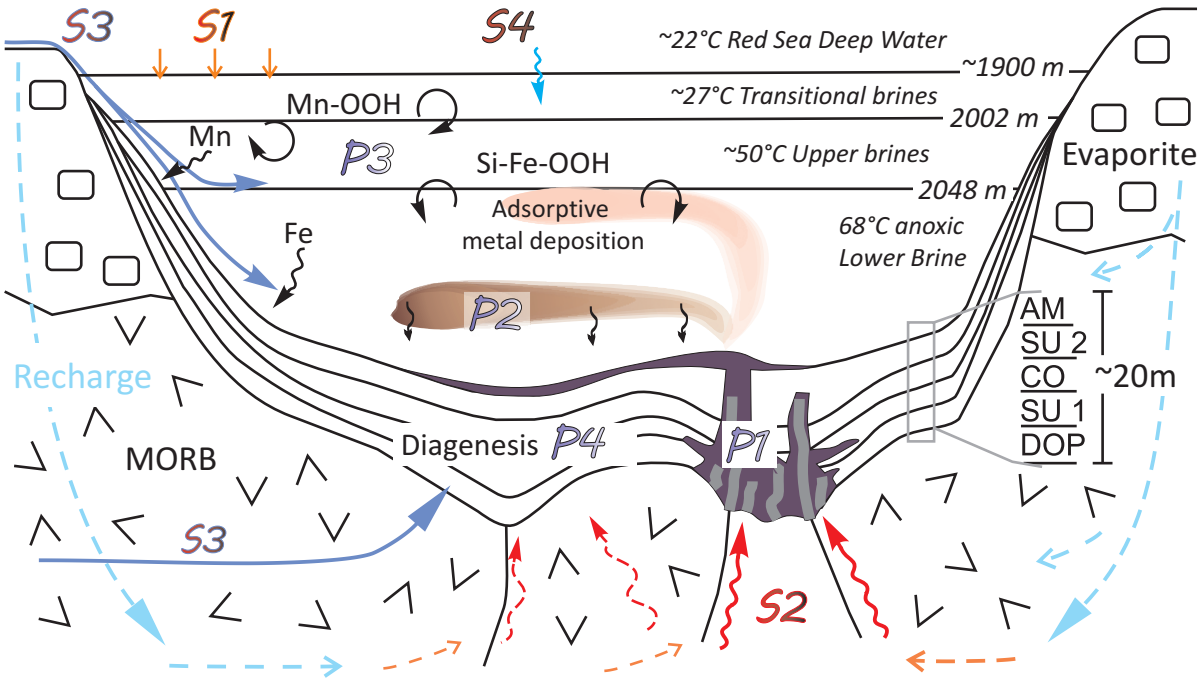

Conrad
Shaban
Oceanographer
Mabahiss
Egypt
Gypsum
Vema
Kebrit
Nereus
Thetis
Hatiba
Saudi-Arabia
Sudan
Jeddah
Atlantis II
Wandoo
Erba
Valdivia
Port Sudan
Chain
Suakin
Discovery
Albatross
Shagara
N
North Basin
21°26'N
275
229
Eritrea
Red Sea
Yemen
North passage
387
21°24'N
373
Ethiopia
E-Basin
W-Basin
421
500 km
684
21°22'N
503
495
683
198
264
Distal
268
This study
334
557
Proximal
Oudin, 1987
SW Basin
Anschutz
et al., 2000
617
0 1 2 km
Core scans
546
38°04'E
38°06'E

Figure 2.2




**Sources of elements:**

- S1 Biogenic-siliciclastic detrital
- S2 Metal-rich hydrothermal fluid
- S3 Sinking brines or non-hydrothermal brines from below
- S4 Seawater via MnOOH/MnO transport

**Precipitation environments:**

- P1 Fluid conduits (Anhydrite + sulfides)
- P2 Hydrothermal plume (mainly sulfides)
- P3 Transitional brines (Fe at low $fO_2$; Mn at shallower and higher $fO_2$)
- P4 Diagenetic recrystallization of amorphous compounds (sulfides, clays, carbonates)

Figure 2.3

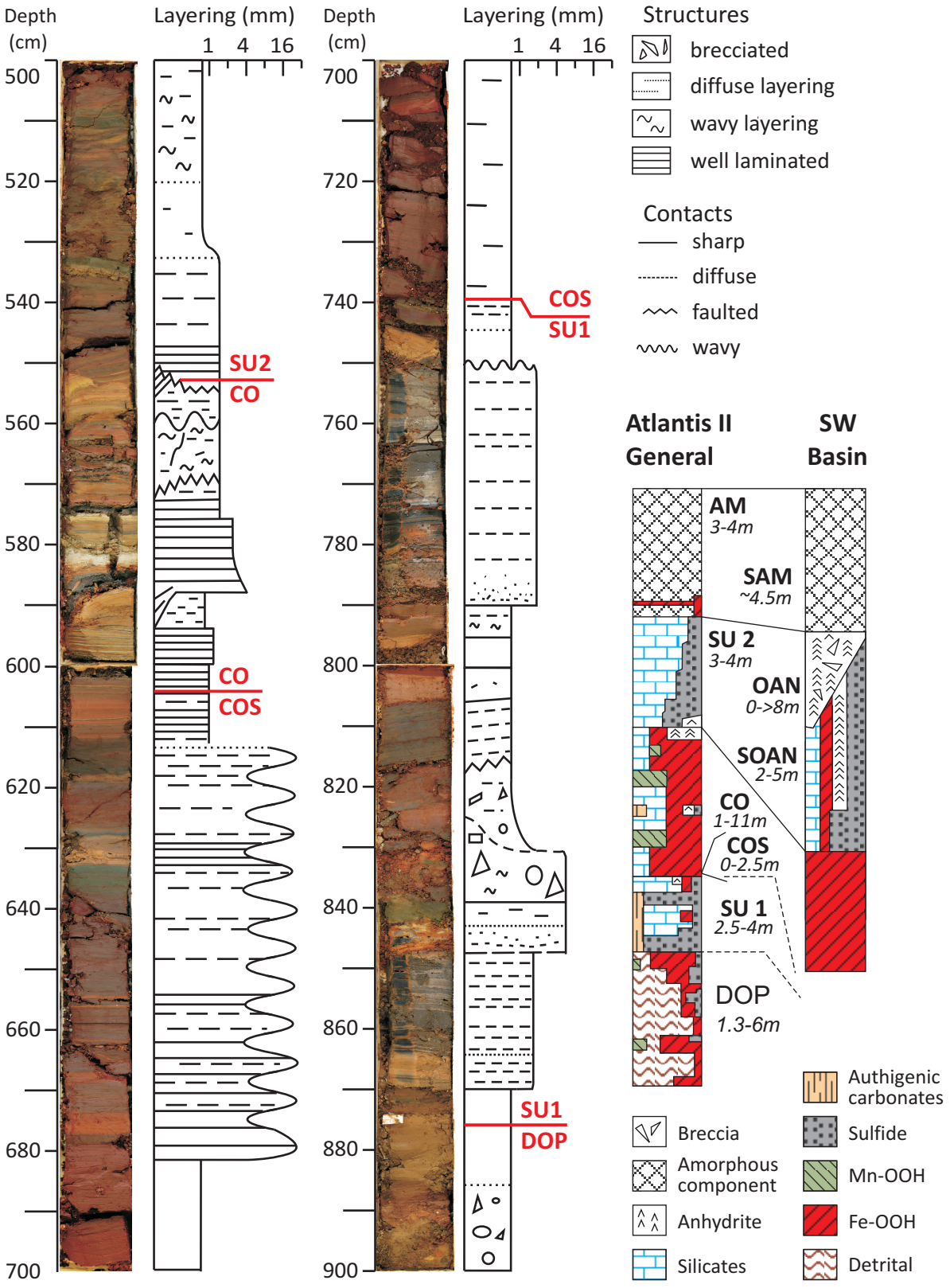
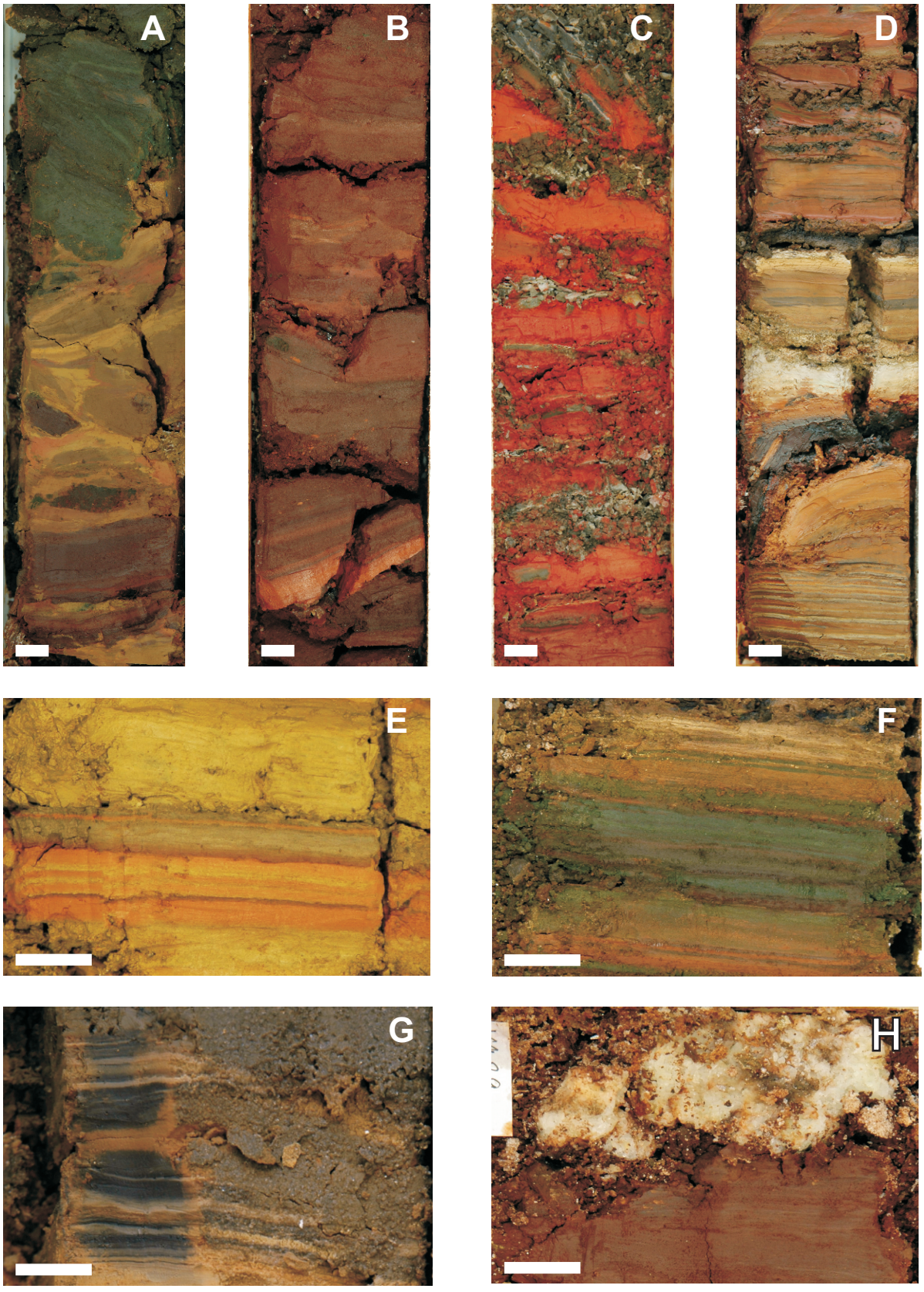

Depth (cm)
Layering (mm)
1 4 16
500
520
540
560
580
600
620
640
660
680
700
SU2
CO
CO
COS
700
720
740
760
780
800
820
840
860
880
900
COS
SU1
SU1
DOP
Structures
brecciated
diffuse layering
wavy layering
well laminated
Contacts
sharp
diffuse
faulted
wavy
Atlantis II General
SW Basin
AM
3-4m
SAM
~4.5m
SU 2
3-4m
OAN
0->8m
SOAN
2-5m
CO
1-11m
COS
0-2.5m
SU 1
2.5-4m
DOP
1.3-6m
Breccia
Amorphous component
Anhydrite
Silicates
Authigenic carbonates
Sulfide
Mn-OOH
Fe-OOH
Detrital

Figure 2.4



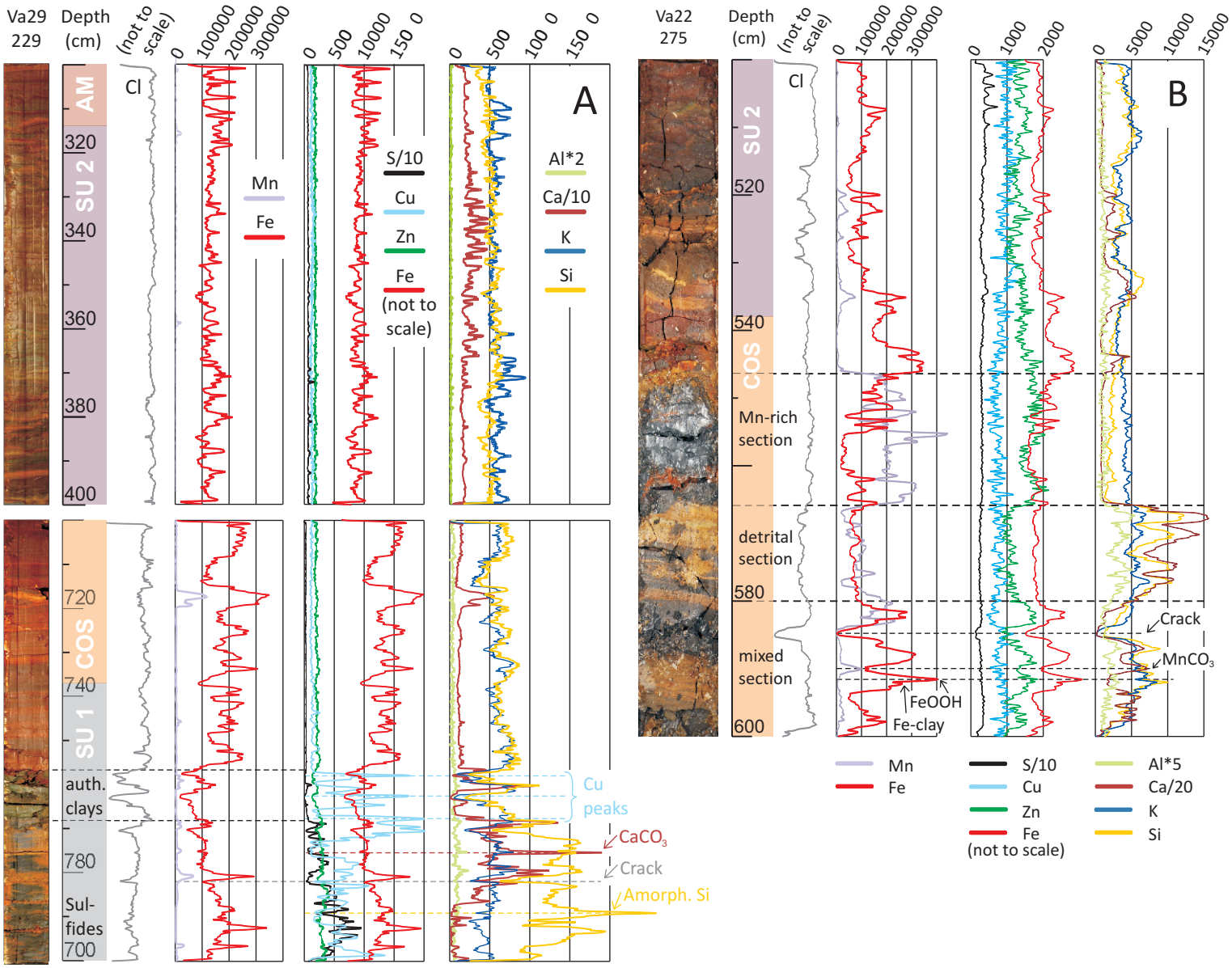

Va29 229
Depth (cm)
(not to scale)
Cl
AM
SU 2
320
340
360
380
400
Mn
Fe
S/10
Cu
Zn
Fe (not to scale)
A
Al*2
Ca/10
K
Si
720
COS
740
SU 1
auth. clays
780
Sul-fides
700
Cu peaks
CaCO3
Crack
Amorph. Si
Va22 275
Depth (cm)
(not to scale)
Cl
SU 2
520
540
COS
Mn-rich section
detrital section
580
mixed section
600
FeOOH
Fe-clay
B
Crack
MnCO3
Mn
Fe
S/10
Cu
Zn
Fe (not to scale)
Al*5
Ca/20
K
Si

Figure 2.5

Figure 2.6

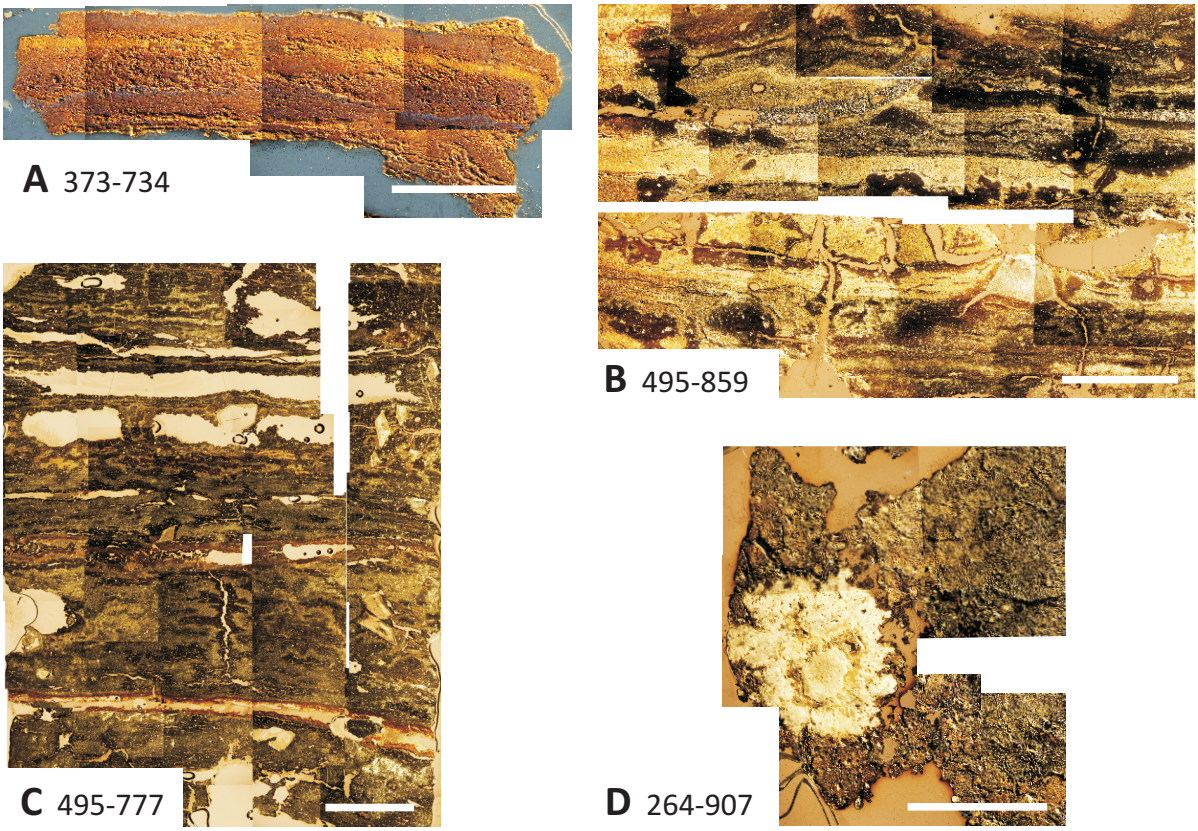


Figure 2.7

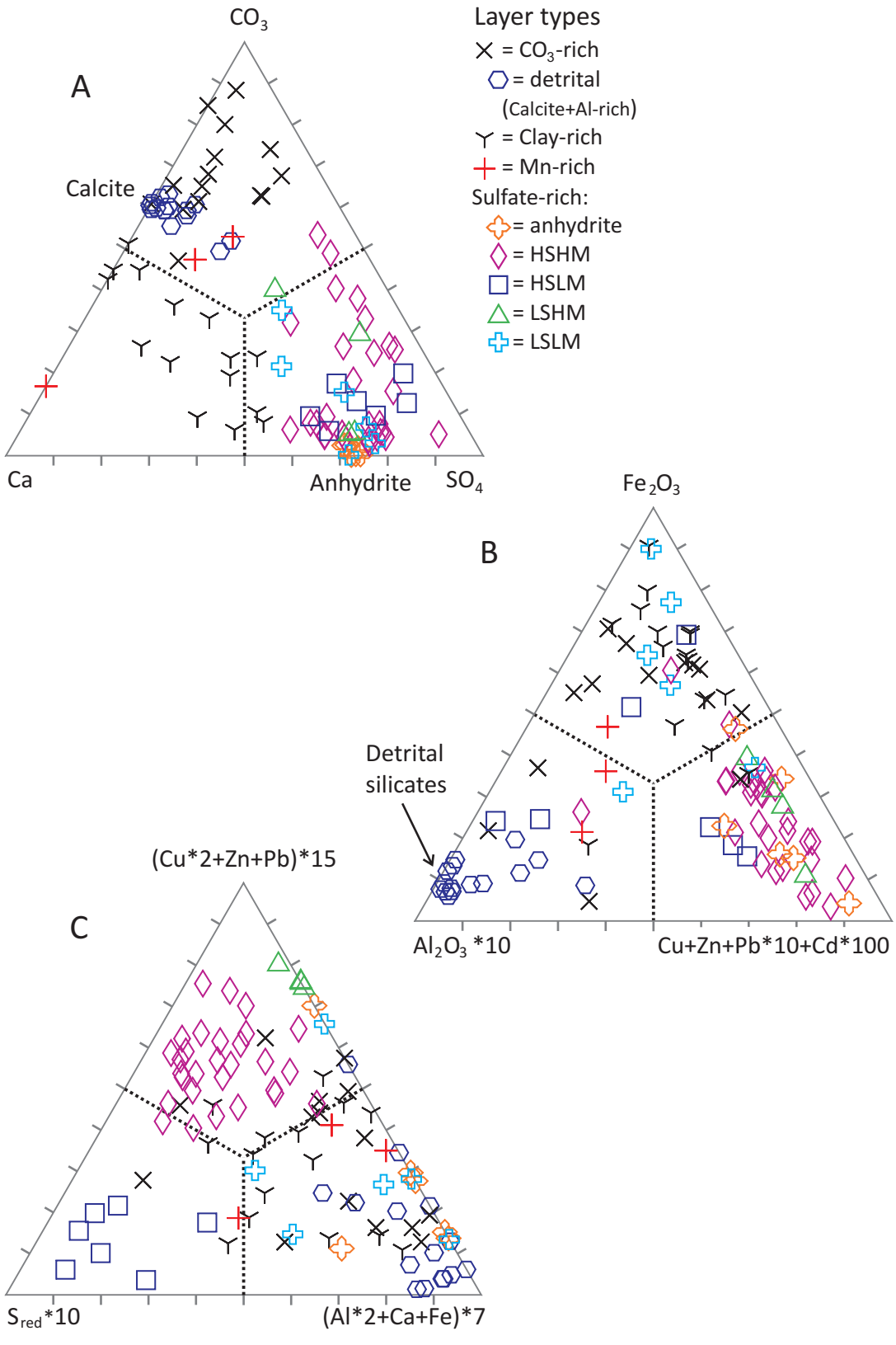

A
$CO_3$
Calcite
Ca
Anhydrite
$SO_4$
Layer types
= $CO_3$-rich
= detrital
(Calcite+Al-rich)
= Clay-rich
= Mn-rich
Sulfate-rich:
= anhydrite
= HSHM
= HSLM
= LSHM
= LSLM
B
$Fe_2O_3$
Detrital
silicates
$Al_2O_3$ *10
Cu+Zn+Pb*10+Cd*100
C
(Cu*2+Zn+Pb)*15
$S_{red}$*10
(Al*2+Ca+Fe)*7

Figure 2.8

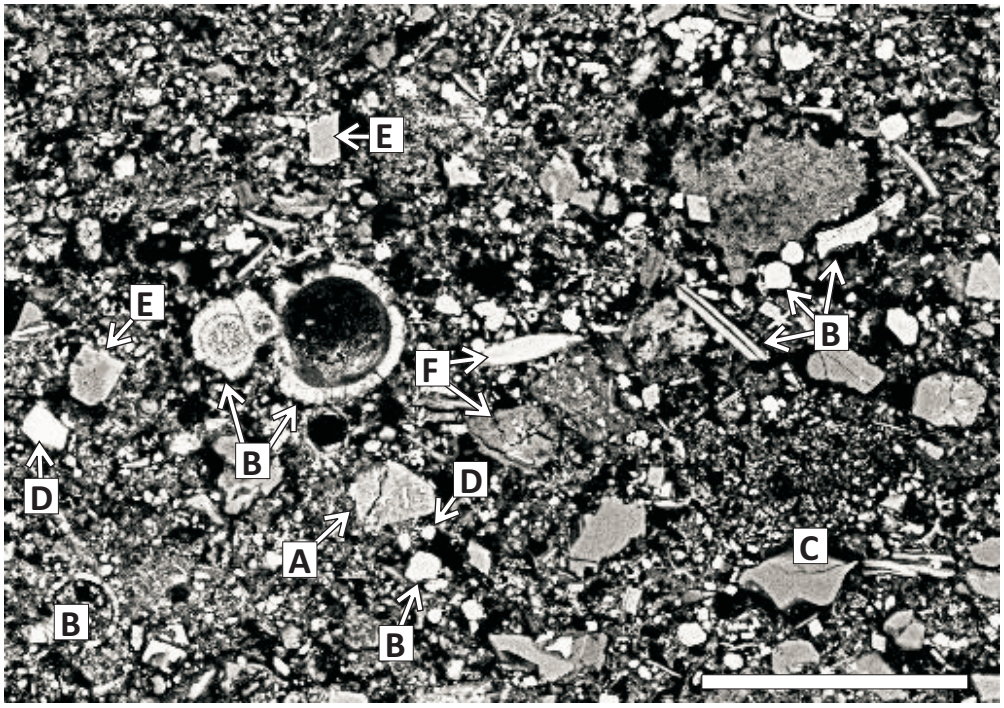


Figure 2.9

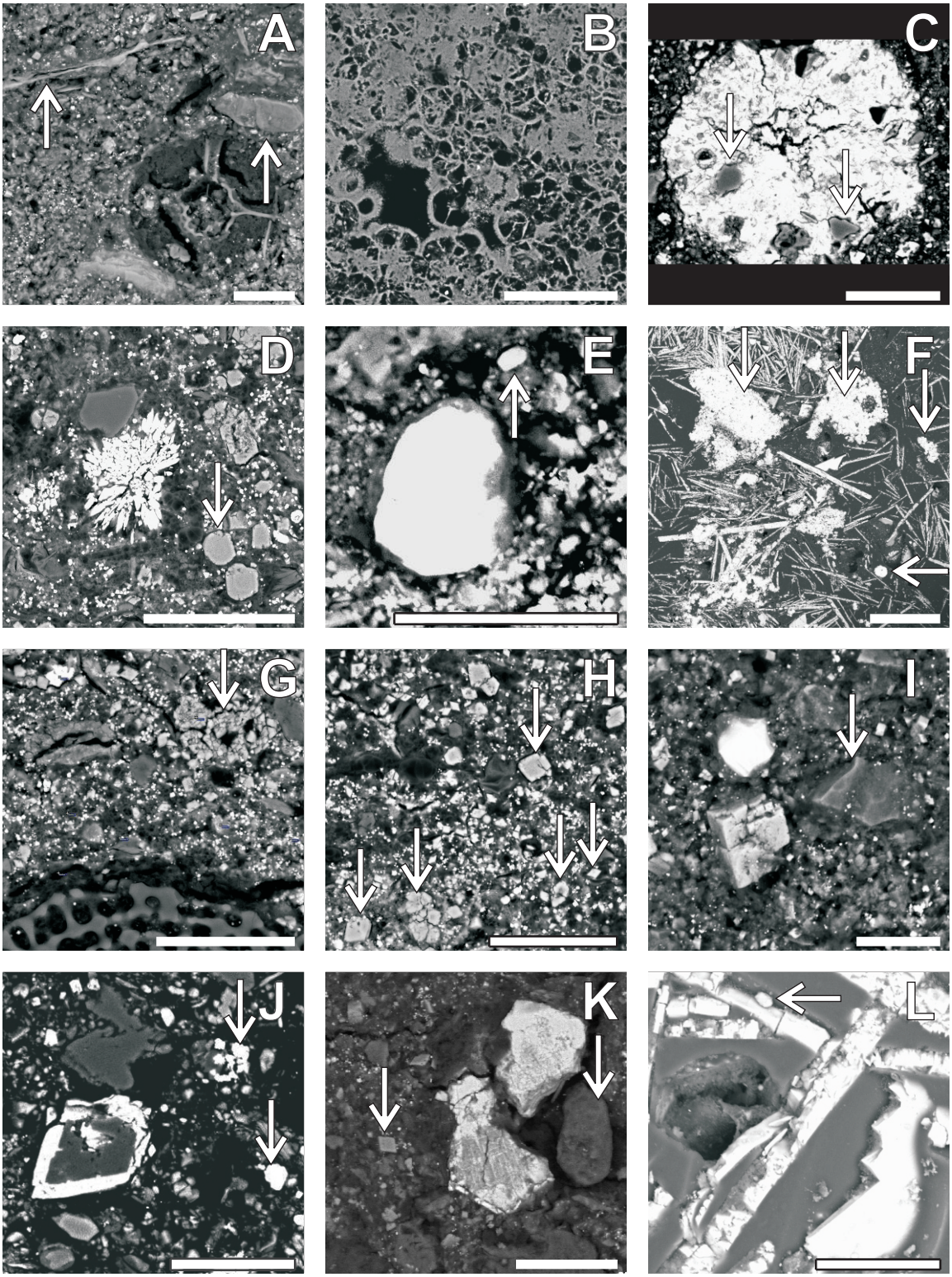


Figure 2.10

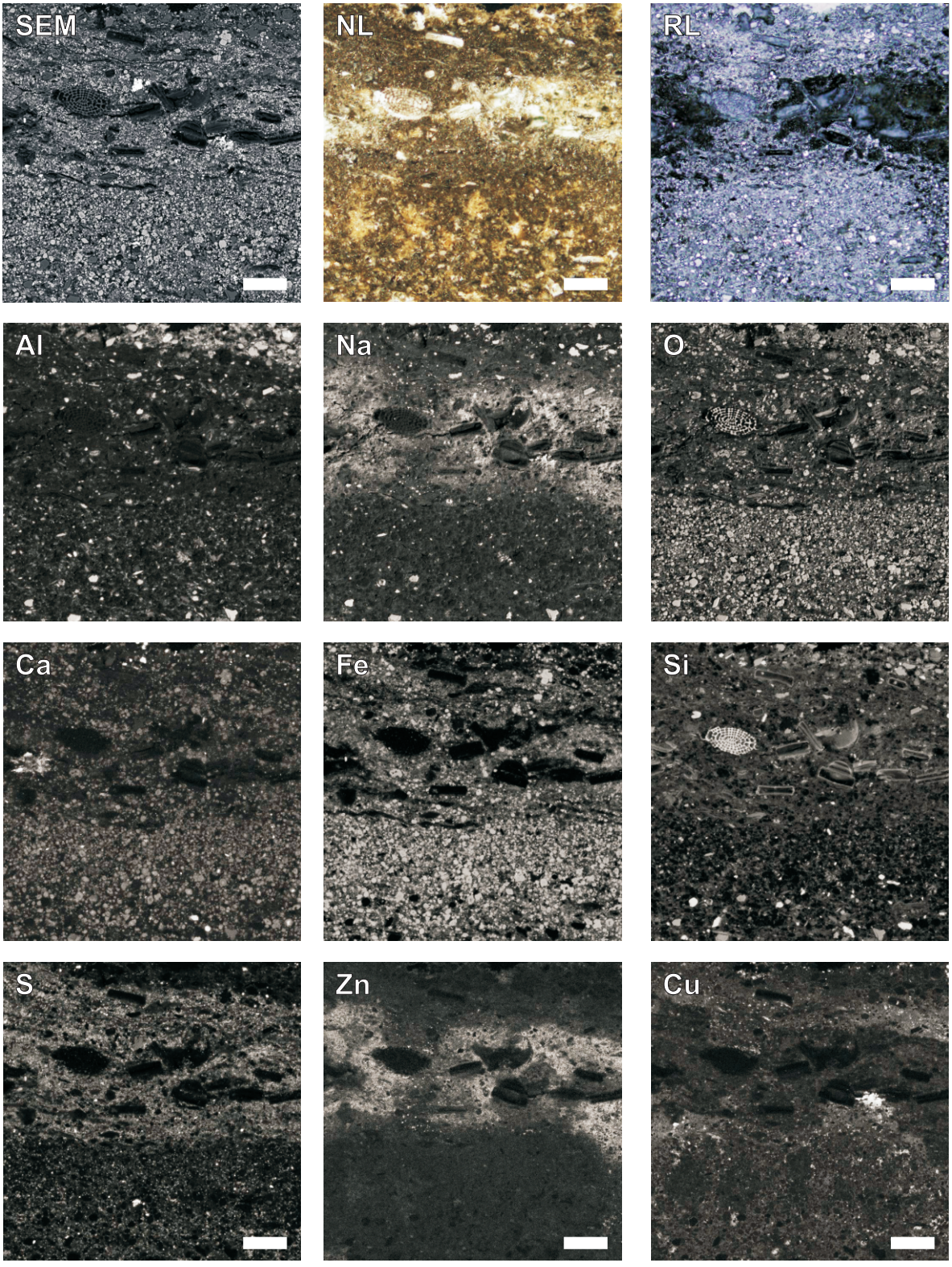


Figure 2.11

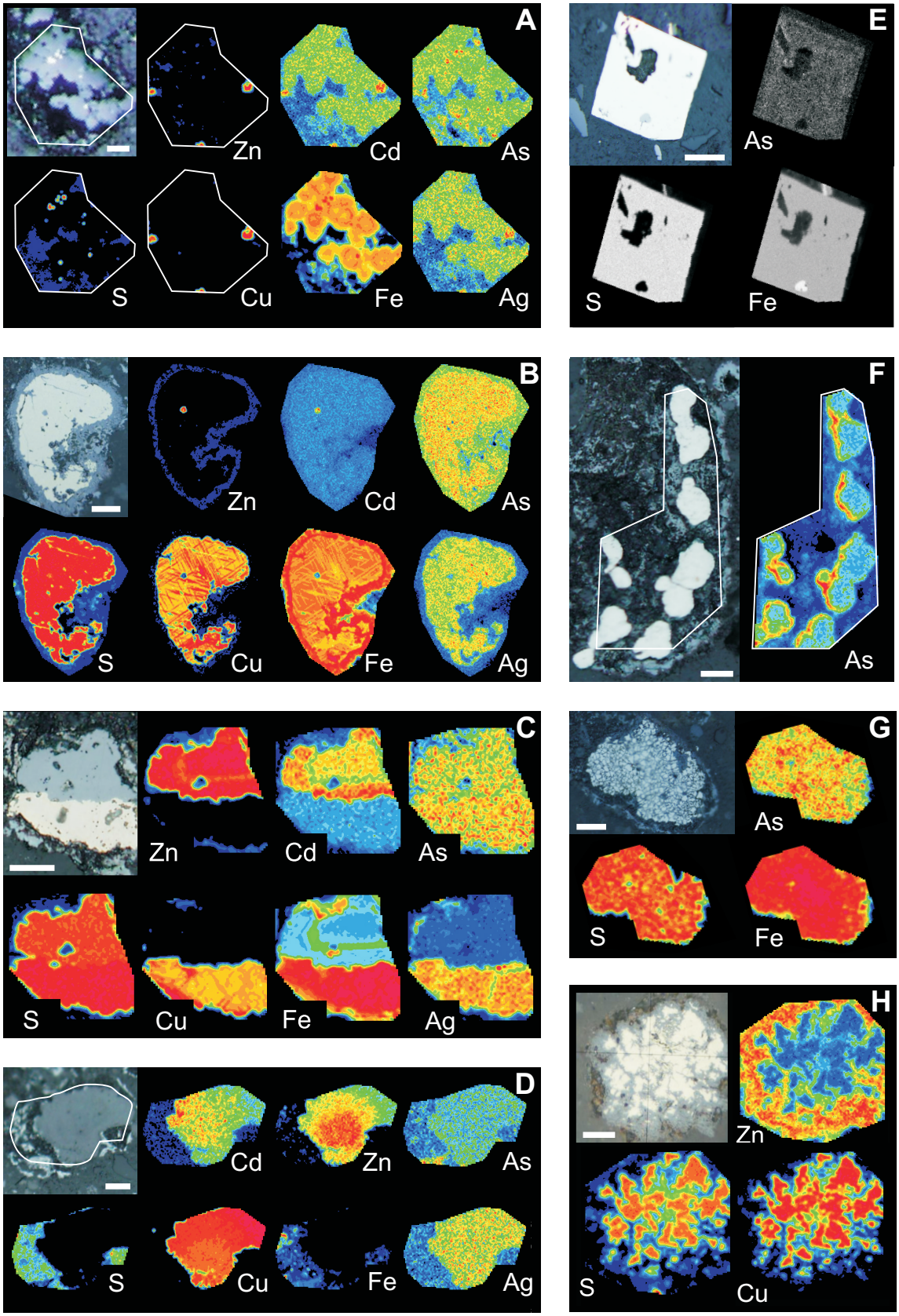

A
Zn
Cd
As
S
Cu
Fe
Ag
E
As
S
Fe
B
Zn
Cd
As
S
Cu
Fe
Ag
F
As
C
Zn
Cd
As
S
Cu
Fe
Ag
G
As
S
Fe
D
Cd
Zn
As
S
Cu
Fe
Ag
H
Zn
S
Cu

Figure 2.12

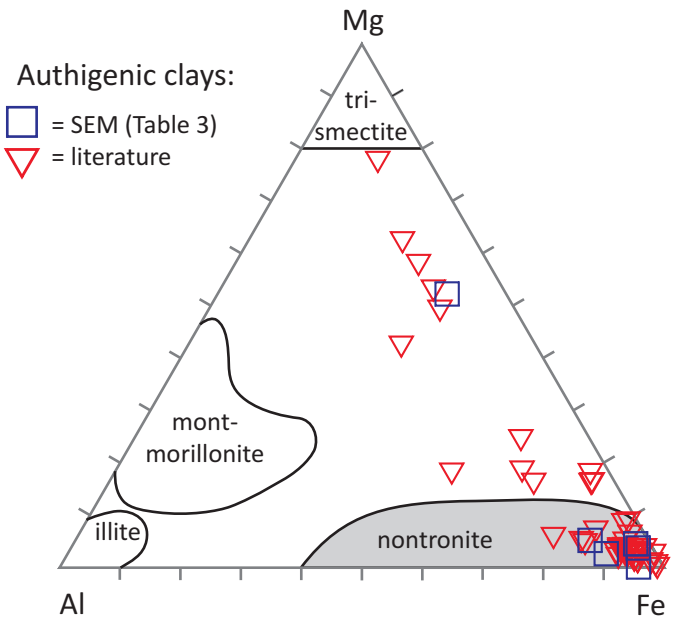



Figure 2.13

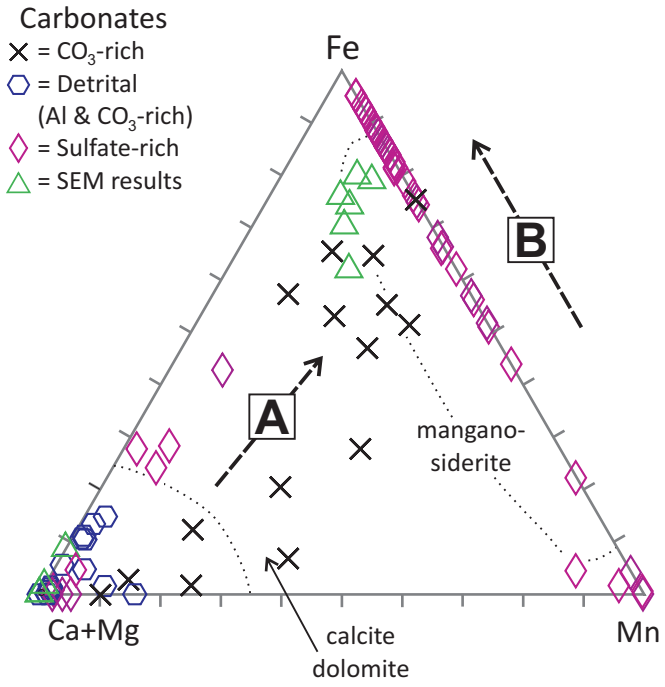


Figure 2.14

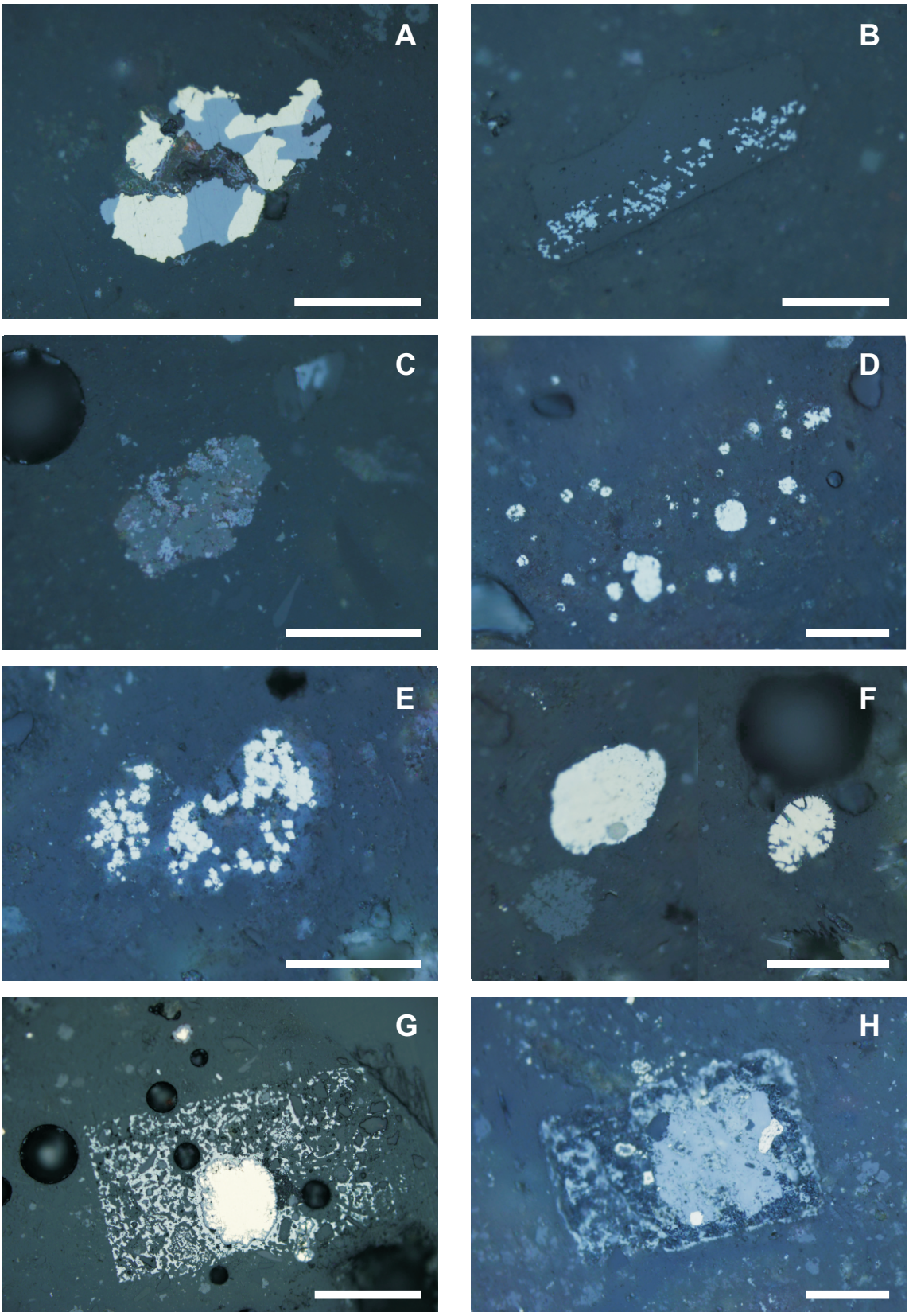


Figure 2.15

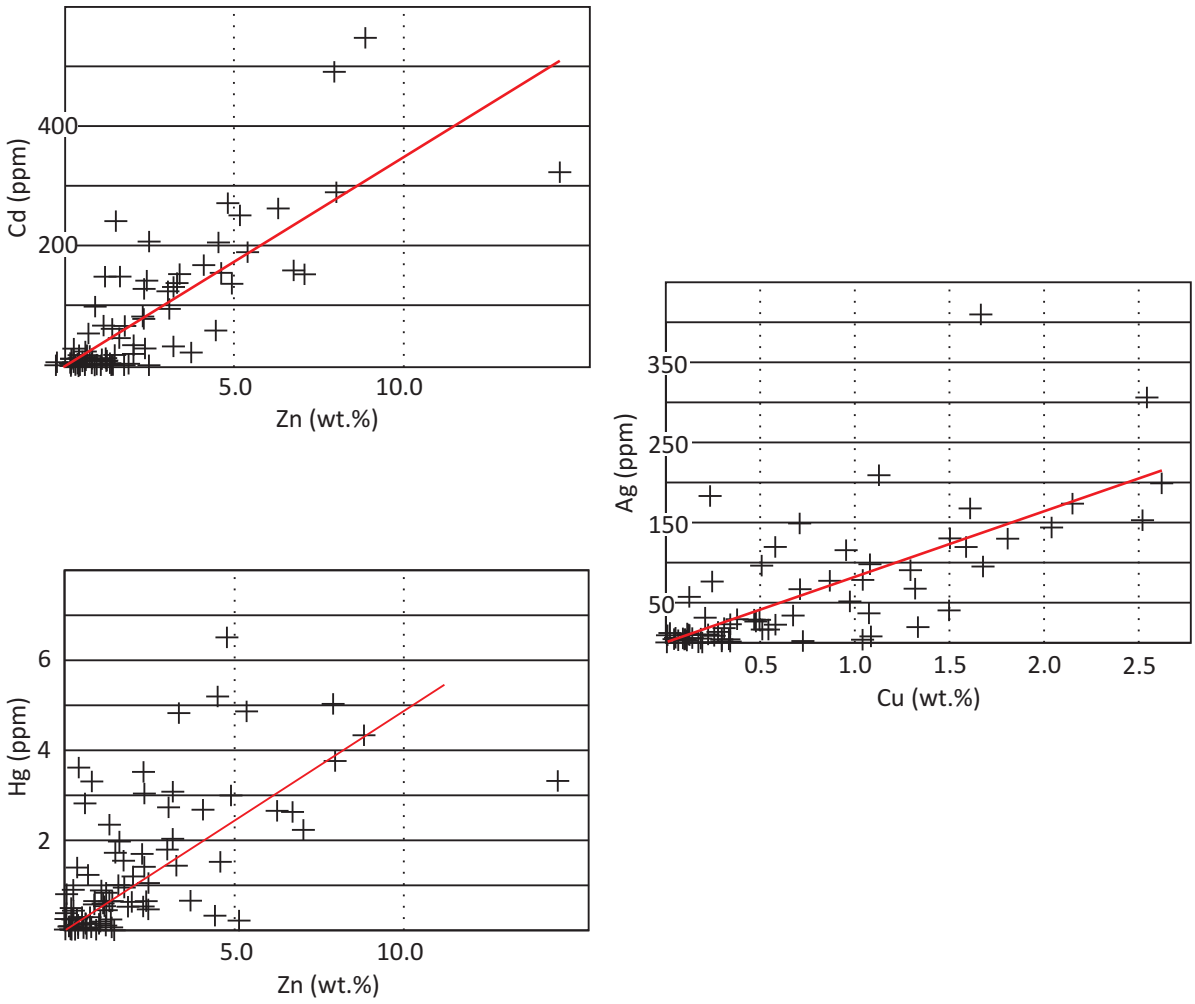



Figure 2.16

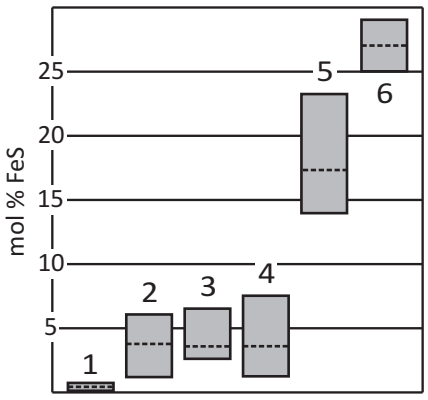


Figure 2.17

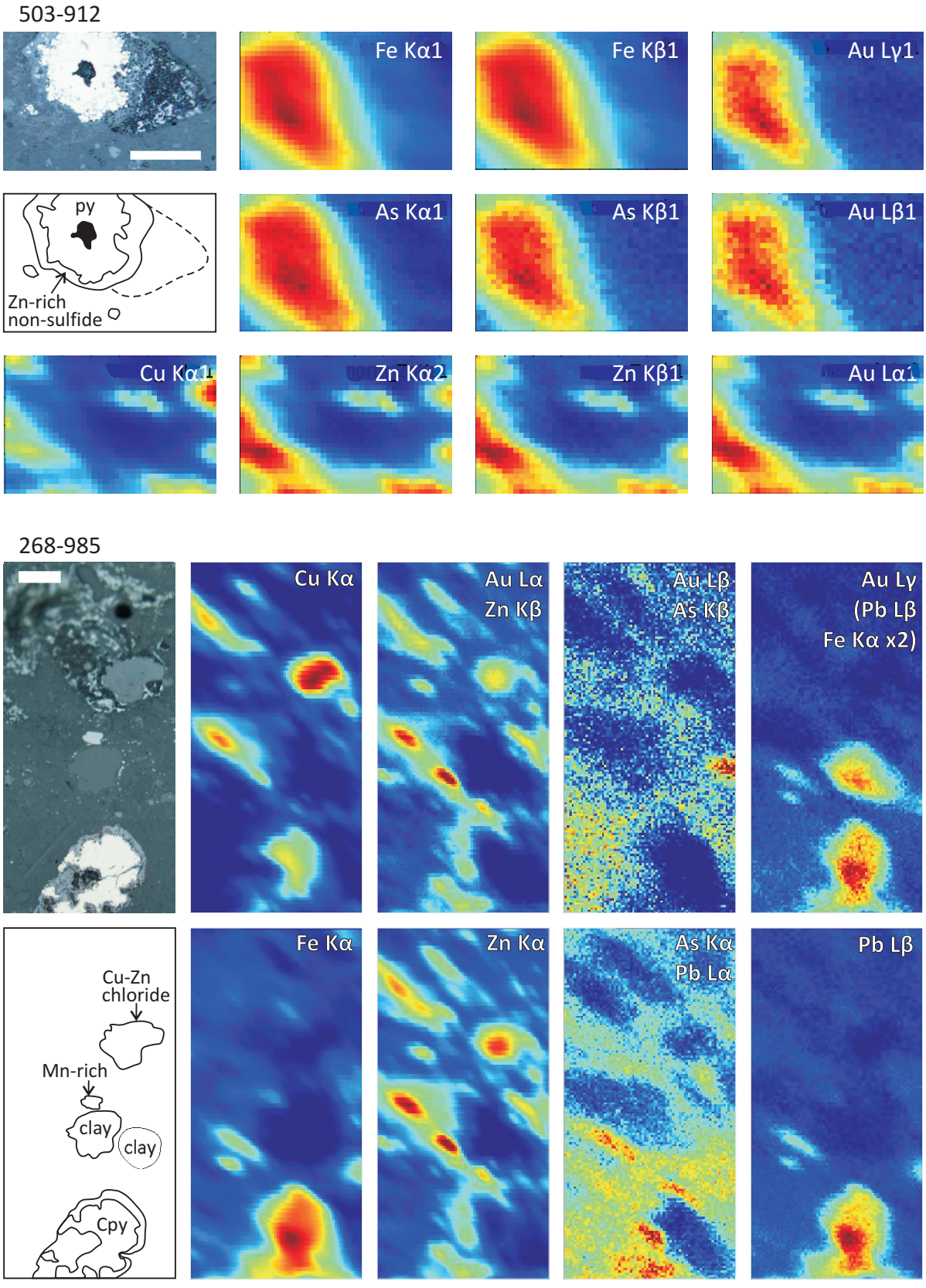

503-912
Fe Kα1
Fe Kβ1
Au Lγ1
py
Zn-rich
non-sulfide
As Kα1
As Kβ1
Au Lβ1
Cu Kα1
Zn Kα2
Zn Kβ1
Au Lα1
268-985
Cu Kα
Au Lα
Zn Kβ
Au Lβ
As Kβ
Au Lγ
(Pb Lβ
Fe Kα x2)
Cu-Zn
chloride
Mn-rich
clay
clay
Cpy
Fe Kα
Zn Kα
As Kα
Pb Lα
Pb Lβ

Figure 2.18

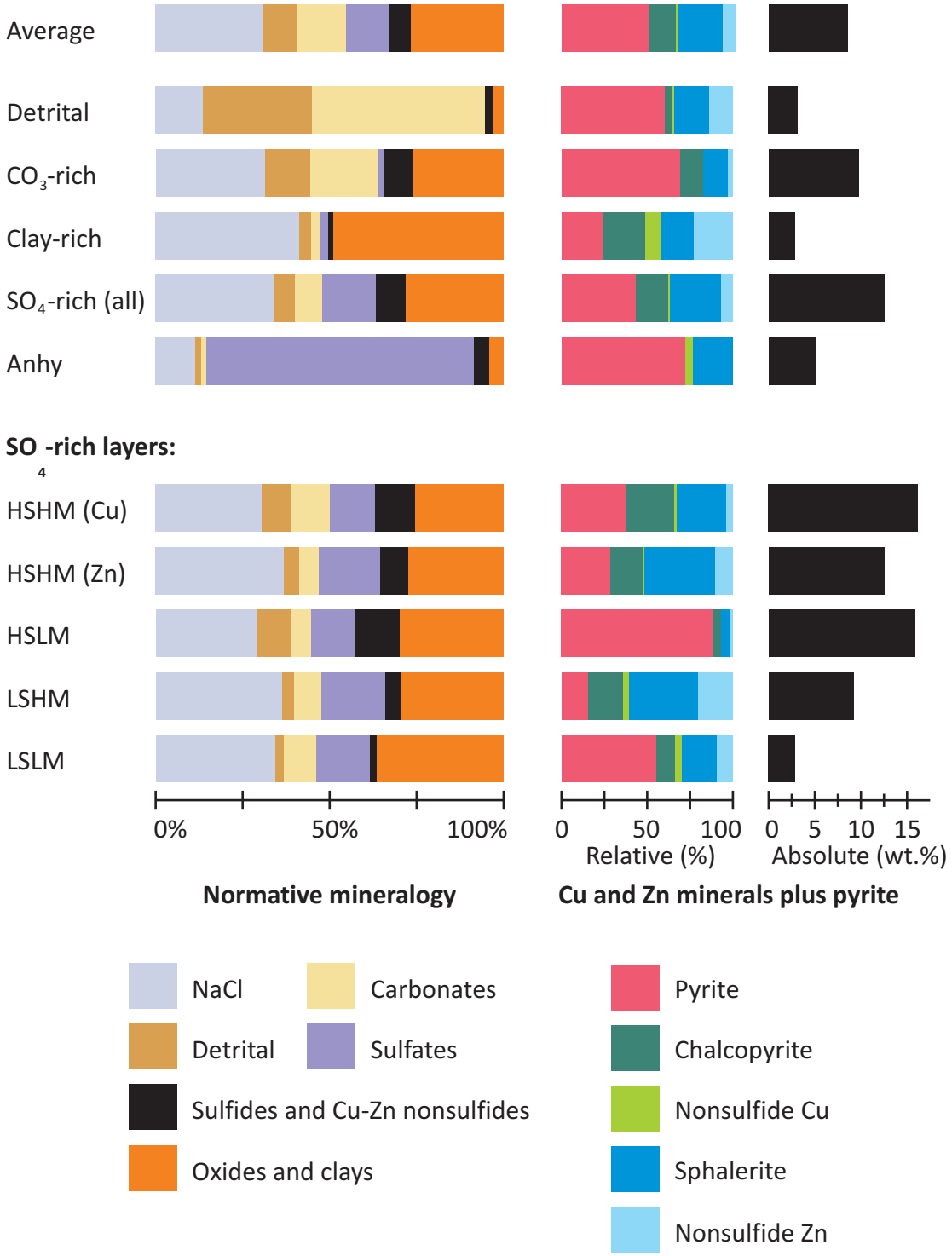

Average
Detrital
$CO_3$-rich
Clay-rich
$SO_4$-rich (all)
Anhy
SO -rich layers:
4
HSHM (Cu)
HSHM (Zn)
HSLM
LSHM
LSLM
0%
50%
100%
0
50
100
Relative (%)
0
5
10
15
Absolute (wt.%)
Normative mineralogy
Cu and Zn minerals plus pyrite
NaCl
Carbonates
Detrital
Sulfates
Sulfides and Cu-Zn nonsulfides
Oxides and clays
Pyrite
Chalcopyrite
Nonsulfide Cu
Sphalerite
Nonsulfide Zn

Figure 2.19

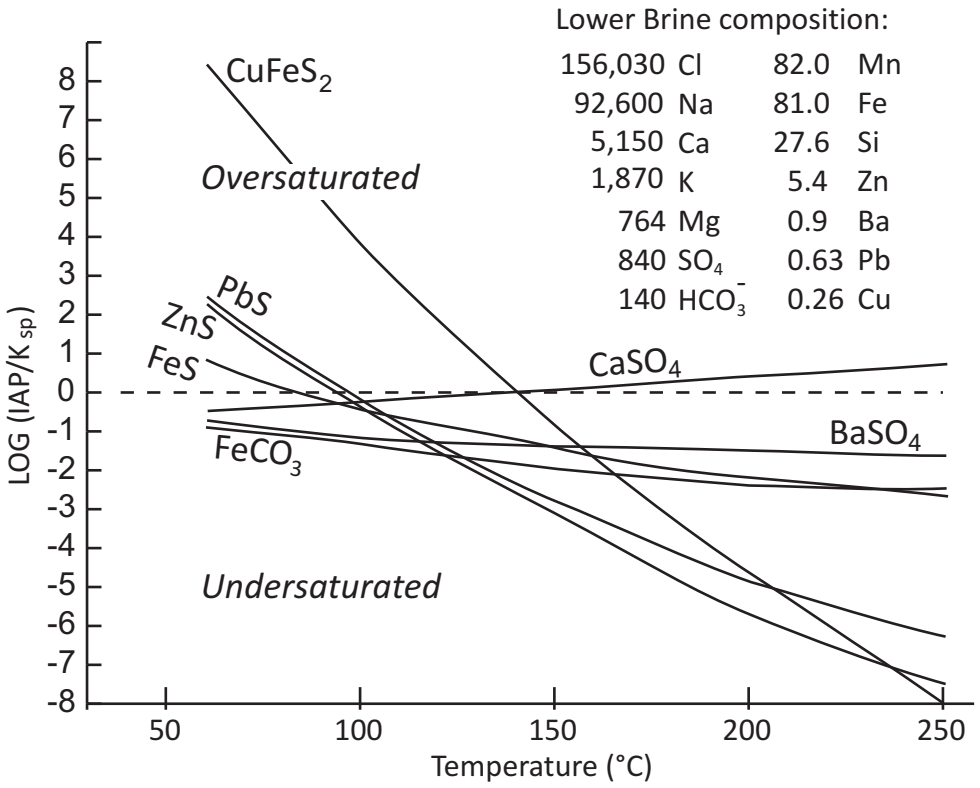
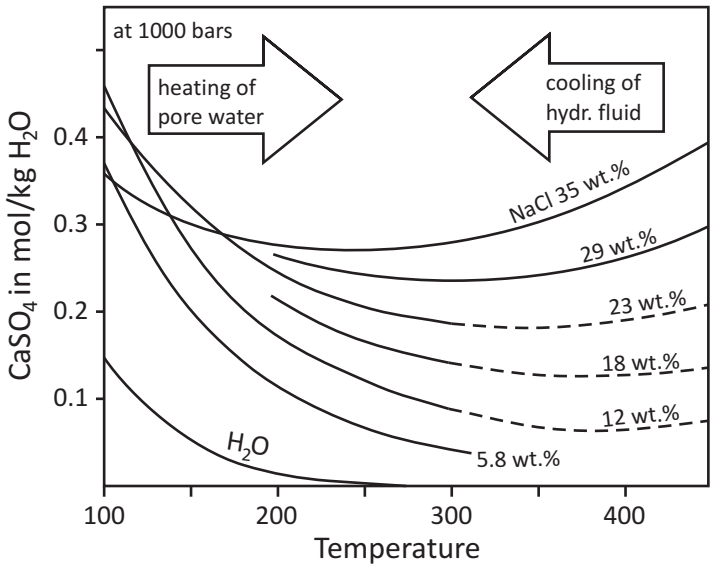



Figure 2.20



Appendix 2.1. Review of previously published data on the clay mineralogy of sediments of the Atlantis II Deep.

| Mineralogy | $SiO_2$ | $Al_2O_3$ | $Fe_2O_3$ | FeO | MgO | CaO | $Na_2O$ | $K_2O$ | MnO | Zn | Cu | Cl | S | Location | Facies/unit | Treatment | Reference |
|---|---|---|---|---|---|---|---|---|---|---|---|---|---|---|---|---|---|
| nontronite[1] | 39.8 | 2.1 | 34.8 | | 1.4 | 0.6 | 0.7 | 0.2 | tr. | 4.2 | 1.3 | | | SW basin- ~1 km from venting | SSA | BCD | Cole, 1988 |
| nontronite[1] | 36.8 | 2.0 | 32.0 | | 1.4 | 0.6 | 4.2 | 0.2 | tr. | 3.2 | 0.9 | | | SW basin- ~1 km from venting | SSA | BCD | Cole, 1988 |
| nontronite[1] | 37.5 | 2.0 | 32.5 | | 1.4 | 0.4 | 3.1 | 0.2 | tr. | 4.4 | 1.0 | | | SW basin- ~1 km from venting | SSA | BCD | Cole, 1988 |
| nontronite[1] | 36.0 | 1.7 | 28.9 | | 1.6 | 0.7 | 2.4 | 0.6 | tr. | 2.7 | 0.5 | | | SW basin- ~1 km from venting | SSA | BCD | Cole, 1988 |
| nontronite[1] | 36.3 | 1.7 | 29.3 | | 1.6 | 0.6 | 2.4 | 0.6 | tr. | 3.2 | 1.1 | | | SW basin- ~1 km from venting | SSA | BCD | Cole, 1988 |
| nontronite[1] | 40.4 | 2.2 | 29.2 | | 1.3 | 0.5 | 2.6 | 0.3 | tr. | 3.7 | 0.6 | | | SW basin- vent proximal (~120°C) | SSA | BCD | Cole, 1988 |
| nontronite[1] | 38.1 | 2.1 | 29.1 | | 1.6 | 0.8 | 3.1 | 0.2 | 0.1 | 3.8 | 0.9 | | | SW basin- vent proximal (~180°C) | SSA | BCD | Cole, 1988 |
| nontronite | 46.4 | 0.3 | 32.9 | | 0.4 | 0.1 | 3.9 | 0.1 | tr. | 0.4 | 0.3 | | | SW basin- ~1 km from venting | SCO | BCD | Cole, 1988 |
| saponite | 46.6 | 5.0 | 8.2 | | 23.5 | 0.8 | 3.6 | tr. | tr. | 0.2 | 0.1 | | | SW basin- vent proximal (~180°C) | SSSO | BCD | Cole, 1988 |
| saponite | 40.6 | 5.3 | 12.7 | | 19.2 | 0.3 | 6.6 | tr. | tr. | 0.2 | tr. | | | SW basin- vent proximal (~180°C) | SSSO | BCD | Cole, 1988 |
| saponite | 52.7 | 3.3 | 4.2 | | 27.9 | 0.2 | 2.1 | tr. | tr. | 0.2 | tr. | | | SW basin- vent proximal (~180°C) | SSSO | BCD | Cole, 1988 |
| vermiculite clays | 45.6 | 9.9 | 10.6 | 1.3 | 17.0 | 0.6 | 0.7 | 0.2 | 0.1 | tr. | tr. | | | SW basin | | water <2µm | Singer and Stoffers, 1981 |
| vermiculite clays | 54.3 | 9.5 | 15.7 | | 6.1 | 0.8 | 0.3 | 0.2 | 0.2 | tr. | tr. | | | SW basin | | water <2µm | Singer and Stoffers, 1981 |
| vermiculite clays | 38.9 | 7.4 | 24.3 | 2.6 | 8.9 | 1.7 | 0.7 | 0.4 | 0.2 | 0.5 | 0.2 | | | SW basin | | water <2µm | Singer and Stoffers, 1981 |
| vermiculite clays | 37.4 | 7.7 | 31.3 | tr. | 8.6 | 0.9 | 1.1 | 0.2 | 0.2 | 0.1 | 0.6 | | | SW basin | | water <2µm | Singer and Stoffers, 1981 |
| ferrous smectite | 24.5 | 2.4 | 46.2 | | 1.1 | 2.7 | 1.6 | 0.3 | 0.3 | 10.2 | 1.2 | 0.1 | 6.0 | SW basin | | water | Badaut et al., 1985 |
| ferri-pyrophyllite[1] | 46.5 | 1.2 | 42.7 | | 1.7 | 1.5 | tr. | 1.0 | | 1.5 | | 1.2 | 2.7 | SW basin | SOAN | water | Badaut et al., 1992 |
| celadonite-hydro-ferri-pyrophyllite[1] | 56.4 | | 34.4 | | 3.0 | 0.3 | tr. | 4.1 | | 1.1 | | 0.3 | 0.4 | SW basin | SOAN | water | Badaut et al., 1992 |
| celadonite-hydro-ferri-pyrophyllite[1] | 49.6 | 1.3 | 39.3 | | 1.8 | 2.6 | tr. | 2.0 | | tr. | | 0.4 | 3.1 | E basin | SU1 | water | Badaut et al., 1992 |

| Mineralogy | $SiO_2$ | $Al_2O_3$ | $Fe_2O_3$ | FeO | MgO | CaO | $Na_2O$ | $K_2O$ | MnO | Zn | Cu | Cl | S | Location | Facies/unit | Treatment | Reference |
|---|---|---|---|---|---|---|---|---|---|---|---|---|---|---|---|---|---|
| celadonite-hydro-ferripyrophyllite[1] | 52.6 | 0.5 | 39.2 | | 2.0 | 0.8 | tr. | 3.0 | | tr. | | 0.3 | 1.8 | E basin | SU1 | water | Badaut et al., 1992 |
| nontronite[1] | 51.8 | 1.4 | 41.0 | | 1.6 | 1.7 | 1.3 | 1.4 | | tr. | | tr. | tr. | W basin | SU2 | water | Badaut et al., 1992 |
| ferripyrophyllite | 56.1 | tr. | 40.7 | | 1.5 | 0.5 | tr. | 1.1 | | tr. | | tr. | tr. | W basin | SU1 | water, $CO_3$ dissolution | Badaut et al., 1992 |
| nontronite[1] | 27.3 | 2.1 | 28.4 | 4.7 | 1.2 | 4.5 | 0.6 | 1.3 | 0.8 | 1.4 | 0.7 | | | E basin | | water | Bischoff, 1972 |
| same sample as above | 36.4 | 2.1 | 26.2 | 4.8 | 1.5 | 0.5 | 2.8 | 0.3 | 1.1 | 1.5 | 0.6 | | | E basin | | EDTA+ BCD | Bischoff, 1972 |
| nontronite[1] | 29.3 | 1.9 | 32.9 | 7.0 | 0.8 | 1.8 | 0.7 | 0.5 | 0.3 | 4.4 | 0.8 | | | E basin | | water | Bischoff, 1972 |
| same sample as above | 38.1 | 2.8 | 22.9 | 7.7 | 1.0 | 0.2 | 2.3 | 0.6 | tr. | 3.9 | 1.0 | | | E basin | | EDTA+ BCD | Bischoff, 1972 |
| nontronite[1] | 30.9 | 1.8 | 32.2 | 4.1 | 1.4 | 7.0 | 0.8 | 0.3 | 1.6 | 2.2 | 0.6 | | | W basin | | water | Bischoff, 1972 |
| same sample as above | 39.0 | 2.6 | 23.1 | 5.9 | 1.3 | 0.5 | 2.7 | 1.4 | 0.3 | 2.1 | 0.8 | | | W basin | | EDTA+ BCD | Bischoff, 1972 |
| nontronite[1] | 28.9 | 1.9 | 32.4 | 3.9 | 1.3 | 6.7 | 1.0 | 0.8 | 0.8 | 1.8 | 0.4 | | | N basin | | water | Bischoff, 1972 |
| same sample as above | 32.9 | 2.3 | 30.5 | 3.1 | 1.3 | 0.5 | 3.0 | 0.8 | 0.3 | 1.7 | 0.4 | | | N basin | | EDTA+ BCD | Bischoff, 1972 |
| nontronite | 43.7 | 1.6 | 30.0 | | 2.1 | | | | 0.1 | tr. | tr. | | | E basin | COS | water | Brockamp et al., 1978 |
| nontronite | 46.7 | 1.3 | 21.5 | | 5.2 | | | | 0.1 | 0.4 | 0.2 | | | SW Basin | OAN | water | Brockamp et al., 1978 |
| nontronite | 44.7 | 1.3 | 30.0 | | 1.3 | | | | 0.1 | 0.2 | 0.1 | | | SW Basin | SAM | water | Brockamp et al., 1978 |
| nontronite | 44.7 | 1.3 | 30.8 | | 1.6 | | | | 0.1 | 0.1 | tr. | | | Central Ridge | CO | water | Brockamp et al., 1978 |
| smectite | | 2.2 | 12.9 | | 1.0 | | | | | | | | | SW basin | | BCD | Schwertmann et al., 1998 |
| smectite | | 2.7 | 16.9 | | 1.2 | | | | | | | | | SW basin | | BCD | Schwertmann et al., 1998 |
| smectite | | 2.9 | 11.5 | | 1.1 | | | | | | | | | SW basin | | BCD | Schwertmann et al., 1998 |
| smectite | | 2.3 | 10.1 | | 4.6 | | | | | | | | | SW basin | | BCD | Schwertmann et al., 1998 |
| smectite | | 3.6 | 7.4 | | 16.8 | | | | | | | | | SW basin | | BCD | Schwertmann et al., 1998 |
| nontronite + hemat. | 21.8 | 1.8 | 58.2 | | 5.0 | 0.1 | 0.1 | 0.1 | 0.2 | tr. | tr. | | | SW basin | Smectite facies | water <2µm | Singer and Stoffers, 1987 |

| Mineralogy | $SiO_2$ | $Al_2O_3$ | $Fe_2O_3$ | FeO | MgO | CaO | $Na_2O$ | $K_2O$ | MnO | Zn | Cu | Cl | S | Location | Facies/unit | Treatment | Reference |
|---|---|---|---|---|---|---|---|---|---|---|---|---|---|---|---|---|---|
| nontronite + hemat. | 24.5 | 1.6 | 52.1 | | 6.1 | 0.1 | 0.1 | 0.1 | 0.1 | tr. | 0.3 | | | SW basin | Mixed facies | water <2µm | Singer and Stoffers, 1987 |
| smectite + poorly crystaline FeOOH | 26.4 | 4.3 | 37.9 | | 3.9 | 0.1 | 0.2 | 0.1 | 0.2 | tr. | tr. | | | SW basin | Sulfide facies | water <2µm | Singer and Stoffers, 1987 |
| Fe-rich vermiculite | 4.9 | 0.7 | 82.2 | | 0.5 | 0.1 | tr. | 0.1 | tr. | 1.0 | 0.7 | | | SW basin | Fe-oxide facies | water <2µm | Singer and Stoffers, 1987 |
| vermiculite-chrysotile | 14.5 | 1.2 | 70.1 | | 8.4 | 0.3 | 0.1 | 0.2 | tr. | tr. | 0.3 | | | SW basin | Fe-oxide facies | water <2µm | Singer and Stoffers, 1987 |
| Fe-rich chlorite | 22.4 | 2.4 | 51.3 | | 14.0 | 0.1 | 0.1 | 0.1 | tr. | tr. | 0.3 | | | SW basin | Fe-oxide facies | water <2µm | Singer and Stoffers, 1987 |
| vermiculite | 9.0 | 1.5 | 83.2 | | 1.4 | 1.1 | tr. | 0.2 | tr. | tr. | 0.2 | | | SW basin | Fe-oxide facies | water <2µm | Singer and Stoffers, 1987 |
| vermiculite, chrysotile and talc | 28.5 | 2.7 | 48.2 | | 11.7 | 0.3 | 0.2 | 0.4 | tr. | tr. | tr. | | | SW basin | Mixed facies | water <2µm | Singer and Stoffers, 1987 |
| smectite to vermiculite | 41.0 | 5.7 | 13.5 | | 23.8 | 2.6 | 0.1 | 0.3 | tr. | tr. | tr. | | | SW basin | Anhydrite facies | water <2µm | Singer and Stoffers, 1987 |
| vermiculite chlorite most important | 40.0 | 4.0 | 22.5 | | 22.5 | 1.3 | 1.1 | 0.2 | tr. | tr. | tr. | | | SW basin | Anhydrite facies | water <2µm | Singer and Stoffers, 1987 |

Mineralogical data is based on various methods, including XRD, Mössbauer spectroscopy, Fourier Transform Infra Red spectroscopy (FTIR), Differential thermal analyses (DTA), Differential thermal gravimetry (DTG), Transmission electron microscopy (TEM) and Scanning electron microscopy (SEM). Chemistry is bulk chemistry determined by various elemental analyses after varying amount of leaching treatments. [1] = Clay mineralogy could not be solved explicitly; data most closely corresponds to this mineral. Tr. = element was analyzed, but concentration was below detection or found in trace amounts (<0.05 wt.%). Facies: SSA = Sulfide-Silicate-Amorphous; SCO = Silicate-Carbonate-Oxide; SSSO= Sulfate-Sulfide-Silicate-Oxide (Cole, 1988); SOAN = Sulfidic-Oxidic-Anhydritic unit, SU1 = Lower Sulfidic unit; SU2 = Upper Sulfidic unit; COS = Central Oxidic-Silicatic unit; OAN = Oxidic-Anhydritic unit; SAM = Sulfidic-Amorphous-Silicatic unit; CO = Central-Oxidic unit (Figure 1.3). Treatments: water = washing with distilled water; BCD= bicarbonate-buffered citrate/dithionite (Mehra, O. P. and Jackson, M. L., 1960, Iron oxide removal from soils and clays by a dithionite-citrate system buffered with sodium bicarbonate. *Proc. Nat. Conf. Clays Clay Minerals* 7, p. 317-327); EDTA= Ethylene-diamine-tetra-acetic acid (to remove carbonates); $CO_3$-dissolution = carbonates were dissolved with unknown method.

Appendix 2.2. Results of analysis of leachates from four-step sequential leaching experiments on selected sample of metalliferous sediment from the Atlantis II Deep.

| | | | Au | Ag | As | Cd | Co | Cr | Ga | Mn | Mo | Ni | Rb | Sb | Se | Sn | Sr | Te | Tl | U |
|---|---|---|---|---|---|---|---|---|---|---|---|---|---|---|---|---|---|---|---|---|
| | | *Det.L.* | *0.05* | *0.002* | *0.01* | *0.01* | *0.05* | *0.05* | *0.05* | *0.10* | *0.001* | *0.05* | *0.01* | *0.005* | *0.02* | *0.005* | *0.05* | *0.005* | *0.005* | *0.005* |
| **Sample no** | **Sample type** | **Leach** [1] | ppm | ppm | ppm | ppm | ppm | ppm | ppm | ppm | ppm | ppm | ppm | ppm | ppm | ppm | ppm | ppm | ppm | ppm |
| 334-83 | HSHM (Zn) | 1 | 0.05 | 13.4 | 0.39 | 38.3 | 11.9 | n.d. | n.d. | 461 | 0.97 | 0.72 | 1.39 | 0.02 | 1.20 | n.d. | 187 | 0.011 | 1.11 | n.d. |
| 334-83 | HSHM (Zn) | 2 | n.d. | 0.02 | 0.71 | 4.15 | 12.8 | n.d. | n.d. | 138 | 0.13 | 1.00 | 0.21 | 0.22 | 0.28 | n.d. | 24.4 | n.d. | 0.70 | 0.58 |
| 334-83 | HSHM (Zn) | 3 | n.d. | 0.09 | 0.04 | 0.28 | 9.9 | 0.1 | 0.13 | 351 | 0.01 | 0.96 | 0.11 | n.d. | n.d. | n.d. | 43.2 | 0.018 | 0.33 | 0.13 |
| 334-83 | HSHM (Zn) | 4 | n.d. | 0.21 | 0.17 | 0.05 | 4.9 | 0.1 | 0.25 | 130 | 0.04 | 0.57 | 0.16 | 0.05 | 0.03 | n.d. | 26.1 | 0.005 | 0.22 | 0.14 |
| 334-83 | HSHM (Zn) | orig. | 0.24 | 11.4 | 59.8 | 38.9 | 61.7 | 2.5 | 4.40 | 1240 | 43.0 | 5.83 | 9.00 | 5.40 | 2.60 | 3.1 | 288 | 0.100 | 4.10 | 2.40 |
| 334-513 | HSHM (Zn) | 1 | n.d. | 12.8 | 1.78 | 601 | 24.5 | n.d. | n.d. | 920 | 0.36 | 2.17 | 2.30 | 0.44 | 2.35 | 0.037 | 134 | 0.014 | 3.77 | 0.01 |
| 334-513 | HSHM (Zn) | 2 | n.d. | 0.16 | 7.08 | 17.9 | 9.8 | n.d. | n.d. | 87 | 0.23 | 1.66 | 0.58 | 8.63 | 0.48 | n.d. | 18.6 | 0.012 | 3.25 | 0.55 |
| 334-513 | HSHM (Zn) | 3 | n.d. | 2.55 | 1.01 | 0.46 | 2.8 | 0.1 | 0.07 | 477 | 0.03 | 0.41 | 0.12 | 1.28 | n.d. | n.d. | 20.5 | 0.021 | 0.71 | 0.04 |
| 334-513 | HSHM (Zn) | 4 | n.d. | 38.0 | 6.21 | 0.15 | 2.0 | 0.1 | 0.81 | 298 | 0.13 | 0.35 | 0.18 | 3.80 | 0.08 | n.d. | 10.4 | n.d. | 0.71 | 0.15 |
| 334-513 | HSHM (Zn) | orig. | 0.87 | 428 | 304 | 564 | 114 | 2.5 | 8.70 | 1860 | 121 | 14.0 | 8.60 | 161 | 3.10 | 1.1 | 166 | 0.100 | 17.4 | 4.90 |
| 334-757 | HSHM (Zn) | 1 | n.d. | 32.4 | 0.66 | 134 | 43.4 | n.d. | n.d. | 389 | 0.07 | 4.62 | 0.67 | 0.02 | 2.02 | n.d. | 158 | 0.008 | 0.77 | 0.06 |
| 334-757 | HSHM (Zn) | 2 | n.d. | 0.09 | 0.23 | 3.16 | 2.0 | n.d. | n.d. | 25 | 0.04 | 0.25 | 0.18 | 0.10 | 0.25 | n.d. | 15.8 | 0.029 | 0.57 | 0.18 |
| 334-757 | HSHM (Zn) | 3 | n.d. | 0.30 | n.d. | 0.06 | 0.4 | 0.1 | n.d. | 2 | tr. | 0.06 | 0.06 | n.d. | n.d. | n.d. | 4.5 | 0.014 | 0.18 | 0.02 |
| 334-757 | HSHM (Zn) | 4 | n.d. | 0.33 | 0.04 | 0.01 | 0.4 | 0.1 | 0.22 | 2 | 0.03 | 0.08 | 0.16 | 0.03 | 0.04 | n.d. | 2.6 | n.d. | 0.34 | 0.03 |
| 334-757 | HSHM (Zn) | orig. | 0.57 | 28.2 | 82.9 | 124 | 61.9 | 2.5 | 9.00 | 491 | 75.0 | 6.88 | 6.90 | 8.40 | 2.10 | 1.3 | 159 | 0.100 | 4.20 | 2.70 |
| 387-80 | HSHM (Zn) | 1 | n.d. | 15.0 | 0.42 | 15.9 | 23.5 | n.d. | n.d. | 802 | 0.04 | 3.66 | 0.84 | 0.01 | 1.37 | n.d. | 163 | 0.007 | 2.27 | 0.12 |
| 387-80 | HSHM (Zn) | 2 | n.d. | 0.03 | 0.15 | 0.47 | 1.2 | n.d. | n.d. | 39 | 0.04 | 0.22 | 0.12 | 0.14 | 0.16 | n.d. | 15.1 | 0.005 | 0.92 | 0.51 |
| 387-80 | HSHM (Zn) | 3 | n.d. | 0.05 | n.d. | 0.01 | 1.0 | 0.1 | n.d. | 8 | tr. | 0.10 | 0.05 | n.d. | n.d. | n.d. | 3.9 | 0.014 | 0.30 | 0.07 |
| 387-80 | HSHM (Zn) | 4 | n.d. | 0.15 | 0.03 | n.d. | 1.0 | 0.1 | 0.12 | 4 | 0.03 | 0.12 | 0.09 | 0.03 | 0.09 | n.d. | 0.6 | n.d. | 0.22 | 0.07 |
| 387-80 | HSHM (Zn) | orig. | 0.31 | 12.6 | 60.7 | 14.9 | 43.9 | 2.5 | 5.00 | 861 | 49.0 | 6.24 | 12.6 | 5.10 | 2.70 | 1.1 | 143 | 0.100 | 6.50 | 1.80 |
| 503-912 | HSHM (Zn) | 1 | n.d. | 0.26 | 3.08 | 175 | 86.1 | n.d. | 0.22 | 6000 | 0.61 | 73.8 | 2.58 | 0.14 | 4.48 | 0.013 | 81.6 | 0.023 | 0.43 | 0.11 |
| 503-912 | HSHM (Zn) | 2 | n.d. | 0.16 | 4.10 | 29.6 | 10.0 | n.d. | 0.15 | 338 | 0.49 | 7.09 | 2.32 | 1.25 | 0.95 | n.d. | 12.3 | 0.011 | 5.50 | 1.33 |
| 503-912 | HSHM (Zn) | 3 | n.d. | 0.68 | 1.20 | 1.10 | 0.4 | 0.1 | 0.52 | 124 | 0.19 | 0.87 | 0.09 | 0.13 | n.d. | n.d. | 2.1 | 0.012 | 0.18 | 0.17 |
| 503-912 | HSHM (Zn) | 4 | n.d. | 3.58 | 2.98 | 0.37 | 0.3 | 0.1 | 3.54 | 43 | 0.37 | 0.78 | 0.14 | 0.49 | 0.04 | n.d. | 0.3 | n.d. | 0.81 | 0.18 |
| 503-912 | HSHM (Zn) | orig. | 2.25 | 91.6 | 532 | 193 | 119 | 9.0 | 32.2 | 6330 | 257 | 92.6 | 10.8 | 89.1 | 6.60 | 0.25 | 90.0 | 0.100 | 25.0 | 3.20 |
| 421-740 | HSHM (Zn) | 1 | n.d. | 4.16 | 1.04 | 9.34 | 6.9 | n.d. | 0.12 | 4050 | 2.16 | 4.09 | 5.63 | 0.22 | 1.50 | 0.007 | 115 | 0.016 | 5.46 | n.d. |
| 421-740 | HSHM (Zn) | 2 | n.d. | tr. | 1.56 | 0.53 | 0.7 | n.d. | n.d. | 341 | 1.78 | 0.40 | 1.30 | 0.17 | 0.24 | n.d. | 10.6 | 0.006 | 1.25 | 0.18 |
| 421-740 | HSHM (Zn) | 3 | n.d. | 0.02 | 1.09 | 0.02 | 0.6 | 0.1 | n.d. | 30 | 0.11 | 0.36 | 0.12 | 0.07 | n.d. | n.d. | 0.3 | 0.009 | 0.11 | 0.01 |
| 421-740 | HSHM (Zn) | 4 | n.d. | 0.20 | 1.77 | n.d. | 0.5 | 0.2 | 0.12 | 13 | 0.24 | 0.28 | 0.13 | 0.26 | 0.08 | n.d. | 0.1 | n.d. | 0.07 | 0.05 |
| 421-740 | HSHM (Zn) | orig. | 0.52 | 3.99 | 37.6 | 8.34 | 11.9 | 8.3 | 5.10 | 4030 | 49.0 | 6.72 | 23.1 | 9.40 | 1.20 | 2.4 | 98.0 | 0.100 | 7.60 | 0.60 |
| 557-173 | HSHM (Zn) | 1 | n.d. | 19.4 | 0.78 | 101 | 26.2 | n.d. | n.d. | 418 | 0.12 | 1.85 | 2.18 | 0.04 | 2.13 | 0.11 | 147 | 0.008 | 2.82 | 0.01 |
| 557-173 | HSHM (Zn) | 2 | n.d. | 0.04 | 1.70 | 4.83 | 12.2 | n.d. | n.d. | 38 | 0.05 | 1.86 | 0.46 | 0.52 | 0.40 | n.d. | 16.6 | 0.011 | 1.44 | 0.47 |
| 557-173 | HSHM (Zn) | 3 | n.d. | 0.98 | 0.22 | 0.22 | 7.2 | 0.1 | n.d. | 35 | 0.01 | 0.78 | 0.14 | 0.05 | n.d. | n.d. | 2.2 | 0.007 | 0.67 | 0.08 |
| 557-173 | HSHM (Zn) | 4 | n.d. | 7.19 | 0.81 | 0.11 | 3.5 | 0.1 | 0.36 | 12 | 0.04 | 0.38 | 0.20 | 0.21 | 0.09 | n.d. | 0.5 | n.d. | 0.59 | 0.08 |
| 557-173 | HSHM (Zn) | orig. | 0.79 | 69.4 | 91.4 | 96.1 | 109 | 2.5 | 7.80 | 590 | 27.0 | 10.1 | 13.6 | 14.7 | 3.00 | 0.25 | 136 | 0.100 | 13.8 | 1.20 |

| Sample no | Sample type | Leach [1] | Au | Ag | As | Cd | Co | Cr | Ga | Mn | Mo | Ni | Rb | Sb | Se | Sn | Sr | Te | Tl | U |
|---|---|---|---|---|---|---|---|---|---|---|---|---|---|---|---|---|---|---|---|---|
| 387-398 | HSHM (Cu) | 1 | n.d. | 0.40 | 2.08 | 235 | 46.9 | n.d. | 0.05 | 654 | 3.16 | 14.0 | 3.98 | 0.16 | 2.26 | 0.11 | 104 | 0.020 | 2.95 | 0.01 |
| 387-398 | HSHM (Cu) | 2 | n.d. | 0.08 | 6.76 | 36.7 | 5.9 | n.d. | 0.15 | 112 | 0.81 | 3.95 | 1.89 | 2.83 | 0.73 | 0.007 | 70.9 | 0.014 | 9.99 | 0.61 |
| 387-398 | HSHM (Cu) | 3 | n.d. | 0.07 | 0.81 | 6.62 | 1.4 | 0.1 | 0.07 | 976 | 0.09 | 1.31 | 0.14 | 0.38 | 0.07 | n.d. | 92.7 | 0.024 | 0.35 | 0.01 |
| 387-398 | HSHM (Cu) | 4 | n.d. | 1.24 | 13.6 | 4.33 | 1.7 | 0.3 | 2.97 | 323 | 1.28 | 1.59 | 0.28 | 2.54 | 0.17 | n.d. | 85.7 | 0.007 | 3.15 | 0.14 |
| 387-398 | HSHM (Cu) | orig. | 1.78 | 172 | 395 | 276 | 162. | 13.6 | 24.5 | 2100 | 213 | 111 | 13.9 | 54.2 | 5.30 | 16.3 | 497 | 0.100 | 50.9 | 1.70 |
| 387-466 | HSHM (Cu) | 1 | n.d. | 0.15 | 0.86 | 101 | 28.2 | n.d. | 0.09 | 3060 | 0.06 | 10.6 | 3.31 | 0.02 | 1.60 | 0.15 | 49.5 | 0.005 | 2.24 | 0.01 |
| 387-466 | HSHM (Cu) | 2 | n.d. | 0.04 | 1.17 | 5.25 | 1.7 | n.d. | 0.05 | 358 | 0.08 | 0.85 | 1.48 | 0.14 | 0.49 | n.d. | 31.1 | 0.031 | 5.19 | 1.08 |
| 387-466 | HSHM (Cu) | 3 | n.d. | 0.02 | 0.09 | 3.24 | 0.4 | 0.1 | 0.08 | 1380 | 0.01 | 0.35 | 0.10 | n.d. | n.d. | n.d. | 15.5 | 0.007 | 0.16 | 0.01 |
| 387-466 | HSHM (Cu) | 4 | n.d. | 0.31 | 0.22 | 2.22 | 0.4 | 0.3 | 0.15 | 2760 | 0.05 | 0.36 | 0.13 | 0.04 | 0.04 | n.d. | 7.7 | n.d. | 0.66 | 0.02 |
| 387-466 | HSHM (Cu) | orig. | 0.73 | 77.4 | 277 | 109 | 103 | 9.4 | 14.6 | 10500 | 83.0 | 43.7 | 10.9 | 21.2 | 4.30 | 2.1 | 116 | 0.100 | 31.8 | 3.40 |
| 617-148 | HSHM (Cu) | 1 | n.d. | 40.20 | 0.80 | 126 | 62.2 | n.d. | n.d. | 896 | 0.19 | 5.98 | 4.46 | 0.06 | 2.07 | 0.31 | 193 | 0.010 | 2.54 | 0.03 |
| 617-148 | HSHM (Cu) | 2 | n.d. | 0.03 | 1.35 | 5.62 | 13.7 | n.d. | n.d. | 60 | 0.20 | 1.34 | 1.53 | 1.17 | 0.24 | n.d. | 32.2 | 0.008 | 3.13 | 1.24 |
| 617-148 | HSHM (Cu) | 3 | n.d. | 3.10 | 0.10 | 0.23 | 5.7 | 0.1 | n.d. | 61 | 0.02 | 0.97 | 0.18 | 0.08 | n.d. | n.d. | 35.9 | 0.016 | 0.46 | 0.30 |
| 617-148 | HSHM (Cu) | 4 | n.d. | 19.3 | 0.52 | 0.06 | 4.5 | 0.1 | 0.77 | 28 | 0.06 | 0.81 | 0.19 | 0.35 | 0.06 | n.d. | 11.4 | n.d. | 0.50 | 0.29 |
| 617-148 | HSHM (Cu) | orig. | 0.85 | 188 | 152 | 124 | 164 | 2.5 | 8.90 | 1070 | 95.0 | 21.0 | 13.3 | 38.1 | 2.20 | 0.25 | 227 | 0.100 | 18.0 | 5.60 |
| 334-312 | LSHM | 1 | n.d. | 37.2 | 0.57 | 76.8 | 44.9 | n.d. | n.d. | 531 | 0.13 | 4.56 | 1.09 | 0.01 | 1.64 | n.d. | 162 | n.d. | 4.94 | 0.01 |
| 334-312 | LSHM | 2 | n.d. | tr. | 0.57 | 3.22 | 7.5 | n.d. | n.d. | 36 | 0.12 | 1.04 | 0.22 | 0.32 | 0.33 | n.d. | 19.7 | 0.007 | 2.83 | 0.87 |
| 334-312 | LSHM | 3 | n.d. | 2.29 | 0.03 | 0.18 | 6.4 | 0.1 | n.d. | 38 | 0.01 | 0.83 | 0.09 | n.d. | n.d. | n.d. | 24.1 | 0.010 | 1.36 | 0.16 |
| 334-312 | LSHM | 4 | n.d. | 7.96 | 0.13 | 0.04 | 4.3 | 0.1 | 0.32 | 27 | 0.04 | 0.56 | 0.15 | 0.05 | n.d. | n.d. | 15.0 | n.d. | 1.22 | 0.24 |
| 334-312 | LSHM | orig. | 0.50 | 71.0 | 87.4 | 73.7 | 120 | 2.5 | 6.90 | 803 | 71.0 | 12.3 | 9.00 | 10.1 | 3.00 | 50.6 | 215 | 0.100 | 22.6 | 3.50 |
| 421-80 | LSHM | 1 | n.d. | 24.4 | 0.42 | 13.0 | 10.8 | n.d. | n.d. | 1330 | 0.24 | 1.32 | 2.68 | 0.01 | 1.38 | 0.10 | 159 | 0.011 | 3.60 | n.d. |
| 421-80 | LSHM | 2 | n.d. | 0.02 | 0.55 | 1.35 | 15.0 | n.d. | n.d. | 577 | 0.08 | 1.60 | 0.49 | 0.24 | 0.37 | n.d. | 18.9 | 0.007 | 1.83 | 0.69 |
| 421-80 | LSHM | 3 | n.d. | 0.03 | n.d. | 0.07 | 4.6 | n.d. | 0.06 | 1165 | 0.01 | 0.84 | 0.10 | n.d. | n.d. | n.d. | 2.1 | 0.014 | 0.43 | 0.02 |
| 421-80 | LSHM | 4 | n.d. | 2.11 | 0.20 | 0.01 | 4.3 | 0.1 | 0.23 | 1190 | 0.06 | 0.76 | 0.18 | 0.05 | 0.07 | n.d. | 1.2 | 0.005 | 0.41 | 0.24 |
| 421-80 | LSHM | orig. | 0.57 | 29.4 | 82.0 | 12.4 | 65.2 | 2.5 | 6.20 | 4210 | 77.0 | 9.82 | 16.2 | 8.70 | 1.20 | 0.25 | 143 | 0.100 | 9.60 | 2.50 |
| 617-799 | LSHM | 1 | n.d. | 0.55 | 0.22 | 67.2 | 7.1 | n.d. | n.d. | 348 | 0.66 | 0.15 | 0.06 | 0.08 | 0.68 | n.d. | 154 | 0.006 | 0.03 | n.d. |
| 617-799 | LSHM | 2 | n.d. | 0.03 | 7.11 | 20.8 | 58.2 | n.d. | 0.12 | 1160 | 0.35 | 8.33 | 0.06 | 8.55 | 3.04 | 0.006 | 71.8 | 0.020 | 0.07 | 0.29 |
| 617-799 | LSHM | 3 | n.d. | 0.76 | 0.78 | 0.40 | 17.0 | 0.1 | n.d. | 279 | 0.01 | 2.87 | 0.03 | 0.65 | 0.21 | n.d. | 7.2 | 0.013 | 0.04 | 0.02 |
| 617-799 | LSHM | 4 | n.d. | 10.4 | 6.75 | 0.10 | 3.3 | 0.3 | 0.53 | 79 | 0.16 | 0.68 | 0.05 | 0.99 | 0.11 | n.d. | 6.5 | n.d. | 0.10 | 0.25 |
| 617-799 | LSHM | orig. | 0.96 | 76.5 | 83.8 | 97.4 | 103 | 7.5 | 11.1 | 1730 | 35.0 | 18.5 | 3.40 | 28.0 | 2.90 | 0.25 | 279 | 0.100 | 3.20 | 2.60 |
| 546-92 | LSHM | 1 | n.d. | 22.0 | 0.39 | 40.4 | 17.7 | n.d. | 0.09 | 3150 | 0.07 | 0.85 | 1.31 | 0.01 | 1.66 | n.d. | 115 | n.d. | 0.66 | n.d. |
| 546-92 | LSHM | 2 | n.d. | 0.11 | 0.27 | 14.4 | 17.4 | n.d. | n.d. | 919 | 0.01 | 1.07 | 0.24 | 0.05 | 0.47 | n.d. | 11.7 | n.d. | 0.41 | 0.68 |
| 546-92 | LSHM | 3 | n.d. | 0.15 | 0.04 | 0.98 | 12.0 | 0.1 | 0.27 | 3780 | tr. | 1.03 | 0.12 | n.d. | 0.05 | n.d. | 1.5 | 0.014 | 0.23 | 0.04 |
| 546-92 | LSHM | 4 | n.d. | 0.18 | 0.01 | 0.17 | 7.6 | 0.2 | 0.56 | 2300 | 0.01 | 0.73 | 0.19 | 0.02 | 0.06 | n.d. | 0.8 | n.d. | 0.18 | 0.35 |
| 546-92 | LSHM | orig. | 0.47 | 19.7 | 65.1 | 52.7 | 89.7 | 2.5 | 7.30 | 9990 | 27.0 | 7.32 | 7.70 | 6.70 | 2.10 | 0.25 | 103 | 0.100 | 2.50 | 3.00 |
| 387-575 | HSLM | 1 | n.d. | 19.9 | 5.73 | 72.8 | 36.6 | 0.1 | 0.12 | 2480 | 0.77 | 25.5 | 1.96 | 1.72 | 0.68 | 0.29 | 225 | 0.007 | 0.59 | 0.71 |
| 387-575 | HSLM | 2 | n.d. | 0.05 | 16.0 | 1.49 | 0.9 | n.d. | n.d. | 67 | 3.21 | 0.59 | 0.88 | 1.13 | 0.14 | n.d. | 79.7 | 0.006 | 0.72 | 0.32 |
| 387-575 | HSLM | 3 | n.d. | 0.76 | 11.6 | 0.03 | 0.1 | 0.2 | 0.21 | 5 | 0.68 | 0.08 | 0.17 | 0.67 | n.d. | n.d. | 90.9 | 0.015 | 5.48 | 0.02 |
| 387-575 | HSLM | 4 | n.d. | 1.02 | 39.6 | 0.01 | 0.1 | 0.3 | 0.75 | 6 | 1.89 | 0.08 | 0.20 | 1.40 | 0.03 | n.d. | 64.6 | n.d. | 8.72 | 0.04 |
| 387-575 | HSLM | orig. | 2.29 | 65.1 | 558 | 66.5 | 43.9 | 11.2 | 23.3 | 2550 | 204 | 27.5 | 12.1 | 70.1 | 3.20 | 1.8 | 850 | 0.100 | 30.4 | 3.00 |
| 503-75 | HSLM | 1 | n.d. | 43.0 | 2.94 | 96.6 | 34.1 | 0.3 | 0.20 | 4210 | 0.84 | 21.6 | 1.77 | 0.58 | 0.72 | 0.15 | 167 | 0.010 | 0.20 | 0.49 |
| 503-75 | HSLM | 2 | n.d. | 0.08 | 12.2 | 1.84 | 0.7 | n.d. | n.d. | 97 | 1.80 | 0.46 | 0.64 | 1.66 | 0.11 | n.d. | 60.7 | 0.013 | 0.30 | 0.05 |

| Sample no | Sample type | Leach [1] | Au | Ag | As | Cd | Co | Cr | Ga | Mn | Mo | Ni | Rb | Sb | Se | Sn | Sr | Te | Tl | U |
|---|---|---|---|---|---|---|---|---|---|---|---|---|---|---|---|---|---|---|---|---|
| 503-75 | HSLM | 3 | n.d. | 0.85 | 2.30 | 0.02 | 0.1 | 0.2 | 0.16 | 3 | 0.27 | 0.07 | 0.11 | 0.39 | n.d. | n.d. | 74.9 | 0.015 | 6.79 | 0.01 |
| 503-75 | HSLM | 4 | n.d. | 0.92 | 44.2 | n.d. | 0.1 | 0.2 | 0.32 | 3 | 3.10 | 0.08 | 0.11 | 1.78 | 0.08 | n.d. | 28.6 | n.d. | 6.45 | 0.01 |
| 503-75 | HSLM | orig. | 2.18 | 108 | 458 | 87.8 | 38.3 | 8.2 | 21.5 | 4170 | 1820 | 22.1 | 7.70 | 70.5 | 2.00 | 0.80 | 976 | 0.100 | 24.5 | 4.70 |
| 503-807 | HSLM | 1 | n.d. | 11.6 | 3.74 | 40.4 | 45.8 | 0.1 | 0.27 | 7630 | 0.27 | 33.8 | 0.93 | 0.94 | 0.72 | n.d. | 80.3 | 0.013 | 0.26 | 1.03 |
| 503-807 | HSLM | 2 | n.d. | 0.02 | 5.45 | 0.76 | 1.0 | n.d. | n.d. | 167 | 0.86 | 0.76 | 0.73 | 0.36 | 0.13 | n.d. | 39.5 | 0.014 | 0.72 | 0.26 |
| 503-807 | HSLM | 3 | n.d. | 0.55 | 5.54 | 0.01 | 0.1 | 0.2 | 0.13 | 12 | 0.33 | 0.10 | 0.15 | 0.30 | n.d. | n.d. | 40.0 | 0.015 | 6.47 | 0.02 |
| 503-807 | HSLM | 4 | n.d. | 0.88 | 21.9 | n.d. | 0.1 | 0.2 | 0.42 | 7 | 1.08 | 0.12 | 0.17 | 0.58 | 0.04 | 0.016 | 19.8 | n.d. | 9.12 | 0.04 |
| 503-807 | HSLM | orig. | 1.46 | 45.3 | 356 | 36.2 | 52.6 | 9.8 | 26.7 | 6620 | 116 | 34.3 | 14.0 | 39.5 | 4.80 | 0.90 | 494 | 0.100 | 40.3 | 2.70 |
| 546-267 | LSLM | 1 | n.d. | 7.06 | 0.35 | 16.2 | 1.8 | n.d. | 0.06 | 2110 | 0.04 | 0.40 | 2.42 | 0.01 | 0.94 | 0.027 | 93.9 | 0.006 | 3.08 | 0.01 |
| 546-267 | LSLM | 2 | n.d. | 0.01 | 0.33 | 3.28 | 0.8 | n.d. | n.d. | 485 | 0.02 | 0.22 | 0.62 | 0.08 | 0.32 | n.d. | 22.5 | 0.020 | 2.43 | 0.82 |
| 546-267 | LSLM | 3 | n.d. | 1.80 | 0.01 | 0.41 | 0.4 | n.d. | n.d. | 730 | 0.01 | 0.12 | 0.11 | n.d. | n.d. | n.d. | 105 | 0.010 | 0.28 | 0.12 |
| 546-267 | LSLM | 4 | n.d. | 5.52 | 0.08 | 0.08 | 0.3 | 0.1 | 0.31 | 519 | 0.02 | 0.13 | 0.22 | 0.01 | 0.04 | n.d. | 56.4 | n.d. | 0.16 | 0.19 |
| 546-267 | LSLM | orig. | 0.76 | 16.7 | 176 | 18.0 | 9.8 | 7.2 | 19.1 | 4220 | 91.0 | 5.26 | 11.1 | 18.9 | 2.10 | 0.25 | 314 | 0.100 | 7.20 | 5.10 |
| 617-220 | LSLM | 1 | n.d. | 2.10 | 0.39 | 2.59 | 13.6 | n.d. | n.d. | 749 | 0.14 | 1.22 | 3.50 | 0.03 | 0.62 | n.d. | 178 | 0.007 | 0.31 | 0.06 |
| 617-220 | LSLM | 2 | n.d. | tr. | 0.67 | 0.14 | 1.1 | n.d. | n.d. | 49 | 0.36 | n.d. | 0.42 | 0.02 | 0.26 | n.d. | 82.7 | 0.026 | 0.05 | 0.12 |
| 617-220 | LSLM | 3 | n.d. | 0.04 | 0.17 | n.d. | 0.6 | n.d. | n.d. | 2 | 0.04 | 0.08 | 0.01 | n.d. | n.d. | n.d. | 1.0 | 0.005 | 0.01 | 0.03 |
| 617-220 | LSLM | 4 | n.d. | 0.29 | 0.29 | n.d. | 0.4 | 0.1 | 0.13 | 1 | 0.10 | 0.07 | 0.03 | 0.04 | 0.08 | n.d. | 0.2 | n.d. | tr. | 0.03 |
| 617-220 | LSLM | orig. | 0.21 | 3.51 | 31.7 | 2.55 | 29.4 | 2.5 | 5.80 | 831 | 20.0 | 2.50 | 4.20 | 4.30 | 0.40 | 0.25 | 209 | 0.100 | 0.40 | 1.30 |
| 495-809 | LSLM | 1 | n.d. | 1.18 | 0.61 | 0.23 | 1.6 | n.d. | n.d. | 1315 | 0.25 | 0.35 | 3.69 | 0.06 | 1.06 | 0.32 | 193 | 0.008 | 3.66 | n.d. |
| 495-809 | LSLM | 2 | n.d. | n.d. | 0.56 | 0.02 | 0.3 | n.d. | n.d. | 140 | 0.14 | 0.09 | 1.06 | 0.05 | 0.23 | n.d. | 17.4 | 0.018 | 0.82 | 0.22 |
| 495-809 | LSLM | 3 | n.d. | 0.01 | 0.19 | n.d. | 0.3 | 0.1 | n.d. | 20 | 0.01 | 0.08 | 0.12 | n.d. | n.d. | n.d. | 0.5 | 0.011 | 0.07 | 0.01 |
| 495-809 | LSLM | 4 | n.d. | 0.04 | 0.29 | n.d. | 0.3 | 0.2 | n.d. | 14 | 0.02 | 0.11 | 0.14 | 0.07 | 0.03 | n.d. | 0.1 | n.d. | 0.04 | 0.04 |
| 495-809 | LSLM | orig. | 0.10 | 1.30 | 18.8 | 0.25 | 6.1 | 2.5 | 2.80 | 1430 | 13.0 | 2.50 | 29.7 | 3.60 | 1.60 | 0.60 | 176 | 0.100 | 5.20 | 0.70 |
| 503-140 | LSLM | 1 | n.d. | 0.55 | 0.41 | 1.14 | 48.0 | n.d. | n.d. | 584 | 0.02 | 7.49 | 4.20 | 0.03 | 1.28 | n.d. | 227 | 0.006 | 4.84 | 0.58 |
| 503-140 | LSLM | 2 | n.d. | n.d. | 0.28 | 0.05 | 2.5 | n.d. | n.d. | 32 | 0.02 | 0.42 | 0.97 | 0.05 | 0.13 | n.d. | 13.4 | 0.008 | 0.55 | 0.19 |
| 503-140 | LSLM | 3 | n.d. | 0.01 | 0.01 | n.d. | 0.2 | 0.1 | n.d. | 1 | tr. | 0.05 | 0.17 | n.d. | 0.02 | n.d. | 1.8 | 0.020 | 0.06 | 0.02 |
| 503-140 | LSLM | 4 | n.d. | 0.04 | 0.15 | n.d. | 0.1 | 0.1 | 0.11 | 1 | 0.02 | n.d. | 0.33 | 0.04 | 0.09 | 0.006 | 1.4 | n.d. | 0.05 | 0.02 |
| 503-140 | LSLM | orig. | 0.15 | 0.60 | 34.6 | 1.10 | 51.6 | 2.5 | 5.50 | 622 | 15.0 | 7.53 | 29.8 | 2.80 | 2.00 | 0.25 | 208 | 0.100 | 5.90 | 1.00 |
| 421-825 | detrital | 1 | n.d. | 0.01 | 0.44 | 0.08 | 0.5 | 0.1 | n.d. | 96 | 1.42 | 0.43 | 2.82 | 0.29 | 0.55 | n.d. | 84.4 | 0.006 | 0.29 | 0.17 |
| 421-825 | detrital | 2 | n.d. | n.d. | 9.37 | 3.29 | 20.3 | n.d. | 0.11 | 2350 | 0.10 | 30.2 | 1.53 | 0.61 | 2.94 | n.d. | 546 | 0.022 | 0.39 | 4.45 |
| 421-825 | detrital | 3 | n.d. | 0.01 | 3.04 | 0.09 | 5.1 | 0.3 | n.d. | 96 | 0.01 | 6.27 | 0.40 | 0.28 | 0.28 | n.d. | 10.8 | 0.015 | 0.08 | 0.01 |
| 421-825 | detrital | 4 | n.d. | 0.05 | 4.36 | 0.04 | 5.1 | 1.1 | 0.17 | 39 | 0.04 | 7.90 | 1.08 | 0.37 | 0.22 | n.d. | 2.2 | 0.005 | 0.09 | 0.49 |
| 421-825 | detrital | orig. | tr. | 1.48 | 90.4 | 4.87 | 62.6 | 71.5 | 8.50 | 2570 | 12.0 | 86.5 | 32.1 | 9.90 | 13.0 | 1.6 | 537 | 0.100 | 2.80 | 8.60 |
| 495-557 | CO2-rich | 1 | n.d. | 0.40 | 0.22 | 0.02 | 0.1 | 0.1 | n.d. | 81 | 11.9 | n.d. | 3.10 | 0.01 | 0.50 | n.d. | 91.8 | 0.009 | 0.21 | 0.03 |
| 495-557 | CO2-rich | 2 | n.d. | 0.01 | 0.82 | 0.58 | 3.7 | n.d. | 0.65 | 16550 | 0.11 | 1.93 | 1.55 | 0.04 | 0.42 | n.d. | 145 | 0.008 | 0.51 | 1.04 |
| 495-557 | CO2-rich | 3 | n.d. | 0.17 | n.d. | 0.02 | 1.4 | 0.1 | 0.23 | 4560 | 0.01 | 1.36 | 0.17 | n.d. | n.d. | n.d. | 2.5 | 0.014 | 0.03 | 0.01 |
| 495-557 | CO2-rich | 4 | n.d. | 0.13 | n.d. | 0.01 | 1.1 | 0.2 | 0.08 | 929 | 0.02 | 1.18 | 0.46 | 0.01 | 0.03 | n.d. | 0.5 | n.d. | 0.03 | 0.22 |
| 495-557 | CO2-rich | orig. | tr. | 1.32 | 120 | 0.63 | 24.8 | 16.7 | 3.90 | 21000 | 123 | 34.1 | 14.1 | 3.80 | 1.40 | 1.4 | 214 | 0.100 | 0.90 | 5.80 |
| 546-180 | CO2-rich | 1 | 0.05 | 14.6 | 0.41 | 24.2 | 4.9 | n.d. | 0.08 | 2830 | 0.42 | 0.28 | 3.00 | 0.01 | 1.37 | n.d. | 99.7 | 0.005 | 0.58 | n.d. |
| 546-180 | CO2-rich | 2 | n.d. | 0.06 | 0.43 | 7.43 | 6.0 | n.d. | 0.07 | 1905 | 0.02 | 0.72 | 0.57 | 0.11 | 0.42 | 0.007 | 14.8 | 0.025 | 0.33 | 0.83 |
| 546-180 | CO2-rich | 3 | n.d. | 0.19 | n.d. | 0.49 | 2.8 | 0.1 | 0.15 | 3930 | tr. | 0.30 | 0.15 | n.d. | n.d. | n.d. | 2.0 | 0.015 | 0.07 | 0.01 |
| 546-180 | CO2-rich | 4 | n.d. | 0.53 | 0.11 | 0.13 | 3.1 | 0.2 | 0.32 | 4860 | 0.02 | 0.36 | 0.19 | 0.02 | 0.05 | n.d. | 1.8 | n.d. | 0.06 | 0.29 |

| Sample no | Sample type | Leach [1] | Au | Ag | As | Cd | Co | Cr | Ga | Mn | Mo | Ni | Rb | Sb | Se | Sn | Sr | Te | Tl | U |
|---|---|---|---|---|---|---|---|---|---|---|---|---|---|---|---|---|---|---|---|---|
| 546-180 | CO2-rich | orig. | 0.31 | 14.3 | 64.4 | 30.7 | 31.4 | 2.5 | 4.30 | 11700 | 21.0 | 2.50 | 10.6 | 6.50 | 2.30 | 0.25 | 99.0 | 0.100 | 1.20 | 3.70 |
| 503-889 | CO2-rich | 1 | n.d. | 0.01 | 0.09 | 12.7 | 58.6 | n.d. | 0.15 | 5470 | 0.01 | 17.0 | 1.02 | tr. | 0.21 | 0.012 | 37.5 | 0.013 | 3.72 | 0.01 |
| 503-889 | CO2-rich | 2 | n.d. | tr. | 0.41 | 3.37 | 22.7 | n.d. | 0.08 | 1910 | 0.03 | 7.31 | 0.44 | 0.03 | 0.21 | n.d. | 6.1 | 0.006 | 3.21 | 1.36 |
| 503-889 | CO2-rich | 3 | n.d. | 0.01 | 0.02 | 0.77 | 2.7 | n.d. | 0.12 | 2600 | tr. | 1.10 | 0.12 | n.d. | n.d. | n.d. | 6.1 | 0.015 | 0.41 | 0.04 |
| 503-889 | CO2-rich | 4 | n.d. | 0.02 | n.d. | 0.24 | 2.5 | 0.2 | 0.22 | 4990 | 0.02 | 1.07 | 0.18 | 0.01 | 0.04 | n.d. | 5.5 | n.d. | 0.42 | 0.07 |
| 503-889 | CO2-rich | orig. | 0.23 | 17.7 | 122 | 15.5 | 218 | 5.5 | 5.50 | 23400 | 82.0 | 87.8 | 5.10 | 19.0 | 1.80 | 0.25 | 67.0 | 0.100 | 10.9 | 9.20 |
| 503-516 | CO2-rich | 1 | n.d. | 0.12 | 0.70 | 51.8 | 5.2 | 0.1 | 0.05 | 1620 | 6.99 | 6.75 | 4.87 | 0.35 | 0.71 | 0.033 | 96.6 | n.d. | 0.78 | 0.02 |
| 503-516 | CO2-rich | 2 | n.d. | 0.03 | 16.6 | 20.8 | 5.7 | n.d. | 0.11 | 1285 | 0.73 | 9.51 | 2.17 | 2.11 | 0.93 | n.d. | 53.3 | 0.008 | 0.88 | 4.91 |
| 503-516 | CO2-rich | 3 | n.d. | 0.14 | 6.46 | 1.72 | 3.2 | 0.2 | 0.06 | 796 | 0.14 | 4.78 | 0.39 | 1.20 | 0.03 | n.d. | 32.3 | 0.029 | 0.24 | 0.04 |
| 503-516 | CO2-rich | 4 | n.d. | 0.92 | 17.9 | 0.41 | 1.8 | 0.3 | 0.93 | 241 | 0.59 | 2.76 | 0.90 | 2.43 | 0.11 | n.d. | 44.6 | 0.005 | 0.21 | 0.32 |
| 503-516 | CO2-rich | orig. | 0.86 | 85.4 | 99.1 | 97.6 | 29.9 | 51.5 | 17.8 | 3450 | 43.0 | 52.0 | 36.5 | 27.7 | 6.10 | 0.25 | 435 | 0.240 | 11.2 | 8.20 |
| 495-362 | Clay-rich | 1 | 0.19 | 8.60 | 0.40 | 1.21 | 2.2 | 0.1 | n.d. | 234 | 1.15 | 0.14 | 0.50 | 0.04 | 1.06 | n.d. | 168 | 0.008 | 0.50 | n.d. |
| 495-362 | Clay-rich | 2 | n.d. | 0.02 | 2.06 | 0.52 | 4.0 | n.d. | n.d. | 172 | 0.11 | 0.31 | 0.13 | 0.56 | 0.38 | n.d. | 35.9 | 0.008 | 0.65 | 1.15 |
| 495-362 | Clay-rich | 3 | n.d. | 0.24 | 0.10 | 0.03 | 3.8 | 0.1 | n.d. | 167 | tr. | 0.37 | 0.07 | 0.01 | n.d. | n.d. | 4.2 | 0.016 | 0.25 | 0.18 |
| 495-362 | Clay-rich | 4 | n.d. | 0.22 | 0.35 | n.d. | 2.4 | 0.1 | 0.22 | 43 | 0.02 | 0.24 | 0.13 | 0.11 | 0.09 | n.d. | 0.5 | n.d. | 0.19 | 0.24 |
| 495-362 | Clay-rich | orig. | 0.49 | 7.66 | 88.2 | 1.58 | 28.2 | 2.5 | 5.10 | 759 | 33.0 | 2.50 | 13.1 | 8.20 | 2.00 | 0.25 | 175 | 0.100 | 3.80 | 3.10 |
| 503-671 | Clay-rich | 1 | n.d. | 1.09 | 0.37 | 0.06 | 1.4 | n.d. | n.d. | 1530 | 0.33 | 0.23 | 5.74 | 0.03 | 1.03 | 0.078 | 198 | n.d. | 2.13 | n.d. |
| 503-671 | Clay-rich | 2 | n.d. | n.d. | 0.33 | 0.01 | 0.6 | n.d. | n.d. | 230 | 0.08 | 0.16 | 1.26 | 0.36 | 0.05 | n.d. | 21.0 | n.d. | 0.46 | 0.21 |
| 503-671 | Clay-rich | 3 | n.d. | tr. | n.d. | n.d. | 0.4 | 0.1 | n.d. | 86 | 0.01 | 0.09 | 0.17 | 0.01 | n.d. | n.d. | 5.1 | 0.014 | 0.05 | 0.02 |
| 503-671 | Clay-rich | 4 | n.d. | 0.05 | 0.03 | n.d. | 0.3 | 0.1 | n.d. | 34 | 0.02 | 0.07 | 0.24 | 0.07 | 0.05 | n.d. | 2.7 | n.d. | 0.03 | 0.03 |
| 503-671 | Clay-rich | orig. | 0.07 | 1.25 | 20.8 | 0.25 | 4.7 | 2.5 | 2.40 | 1550 | 17.0 | 2.50 | 48.8 | 5.30 | 0.40 | 0.25 | 160 | 0.100 | 2.70 | 0.40 |
| 373-8 | Clay-rich | 1 | 0.14 | 1.41 | 0.48 | 0.17 | 4.2 | n.d. | n.d. | 417 | 2.21 | 0.67 | 3.32 | 0.04 | 1.20 | 0.016 | 203 | 0.010 | 1.03 | n.d. |
| 373-8 | Clay-rich | 2 | n.d. | n.d. | 3.10 | 0.40 | 7.5 | n.d. | n.d. | 242 | 0.20 | 1.43 | 0.56 | 0.30 | 0.29 | n.d. | 20.5 | n.d. | 0.66 | 0.50 |
| 373-8 | Clay-rich | 3 | n.d. | 0.01 | 0.19 | 0.02 | 5.9 | 0.1 | 0.07 | 268 | 0.01 | 1.23 | 0.17 | 0.01 | 0.11 | n.d. | 1.9 | 0.020 | 0.20 | 0.08 |
| 373-8 | Clay-rich | 4 | n.d. | 0.02 | 0.66 | n.d. | 3.4 | 0.1 | 0.23 | 59 | 0.04 | 0.84 | 0.22 | 0.08 | n.d. | 0.007 | 0.6 | n.d. | 0.14 | 0.11 |
| 373-8 | Clay-rich | orig. | 0.19 | 1.32 | 59.7 | 0.60 | 34.9 | 2.5 | 3.70 | 984 | 26.0 | 7.84 | 13.1 | 3.00 | 3.00 | 1.3 | 183 | 0.100 | 3.20 | 1.30 |
| 503-680 | Clay-rich | 1 | n.d. | 0.61 | 0.24 | 0.05 | 1.6 | n.d. | n.d. | 1135 | 0.25 | 0.25 | 4.72 | 0.01 | 0.80 | n.d. | 182 | n.d. | 1.52 | n.d. |
| 503-680 | Clay-rich | 2 | n.d. | n.d. | 0.32 | 0.97 | 8.0 | n.d. | n.d. | 1110 | 0.06 | 2.32 | 0.77 | 0.10 | 0.23 | n.d. | 68.3 | 0.015 | 1.28 | 0.48 |
| 503-680 | Clay-rich | 3 | n.d. | 0.01 | n.d. | 0.06 | 3.8 | 0.1 | 0.19 | 2850 | 0.01 | 1.36 | 0.10 | n.d. | n.d. | n.d. | 35.9 | 0.014 | 0.16 | 0.08 |
| 503-680 | Clay-rich | 4 | n.d. | 0.06 | 0.12 | n.d. | 1.8 | 0.1 | 0.14 | 697 | 0.07 | 0.72 | 0.15 | 0.02 | 0.02 | n.d. | 17.7 | n.d. | 0.06 | 0.20 |
| 503-680 | Clay-rich | orig. | 0.16 | 0.80 | 134 | 1.17 | 30.4 | 2.5 | 3.40 | 7110 | 97.0 | 12.0 | 16.2 | 14.4 | 1.40 | 0.25 | 307 | 0.100 | 3.40 | 2.70 |
| 495-569 | Mn-rich | 1 | n.d. | 0.20 | 0.10 | 0.01 | 0.1 | 0.1 | n.d. | 70 | 10.6 | n.d. | 2.91 | tr. | 0.52 | n.d. | 80.7 | 0.012 | 0.20 | 0.01 |
| 495-569 | Mn-rich | 2 | n.d. | tr. | 0.19 | 0.05 | 2.7 | n.d. | 0.13 | 4050 | 0.05 | 1.18 | 0.41 | 0.02 | 0.22 | n.d. | 21.5 | 0.012 | 0.48 | 1.40 |
| 495-569 | Mn-rich | 3 | n.d. | 0.01 | n.d. | 0.01 | 2.3 | n.d. | 3.24 | 86500 | 0.59 | 1.51 | 0.14 | 0.03 | 0.07 | n.d. | 9.1 | 0.016 | 0.04 | 0.57 |
| 495-569 | Mn-rich | 4 | n.d. | 0.06 | n.d. | n.d. | 1.8 | 0.1 | 6.44 | 72300 | 2.65 | 1.42 | 0.22 | 0.08 | 0.09 | n.d. | 6.6 | n.d. | 0.04 | 0.49 |
| 495-569 | Mn-rich | orig. | tr. | 0.25 | 50.0 | 0.25 | 20.9 | 11.7 | 13.0 | 200000 | 292 | 16.7 | 8.20 | 3.70 | 0.40 | 0.80 | 121 | 0.100 | 0.90 | 17.4 |
| 373-586 | anhy | 1 | n.d. | 0.04 | 0.80 | 17.1 | 5.3 | n.d. | n.d. | 218 | 0.24 | 3.43 | 0.56 | 0.04 | 0.32 | n.d. | 136 | n.d. | 0.28 | 0.02 |
| 373-586 | anhy | 2 | n.d. | 0.01 | 0.78 | 0.35 | 0.5 | n.d. | n.d. | 18 | 0.19 | 0.90 | 0.22 | 0.14 | 0.39 | 0.005 | 419 | 0.018 | 0.48 | 0.09 |
| 373-586 | anhy | 3 | n.d. | 0.07 | 0.84 | 0.09 | 0.1 | 0.1 | 0.08 | 6 | 0.19 | 0.06 | 0.02 | 0.11 | 0.05 | n.d. | 57.0 | 0.019 | 0.58 | 0.02 |
| 373-586 | anhy | 4 | n.d. | 0.21 | 0.75 | 0.04 | 0.1 | 0.1 | 0.08 | 2 | 0.30 | 0.06 | 0.02 | 0.13 | 0.05 | n.d. | 12.9 | n.d. | 0.38 | 0.01 |
| 373-586 | anhy | orig. | 0.25 | 4.04 | 89.8 | 15.1 | 11.2 | 2.5 | 3.60 | 270 | 50.0 | 7.02 | 1.40 | 7.80 | 1.20 | 77.1 | 490 | 0.100 | 2.50 | 0.10 |

| Sample no | Sample type | Leach [1] | Au | Ag | As | Cd | Co | Cr | Ga | Mn | Mo | Ni | Rb | Sb | Se | Sn | Sr | Te | Tl | U |
|---|---|---|---|---|---|---|---|---|---|---|---|---|---|---|---|---|---|---|---|---|
| 617-875 | anhy | 1 | n.d. | 1.14 | 0.37 | 72.8 | 7.9 | n.d. | n.d. | 201 | 0.84 | 0.62 | 0.09 | 0.02 | 0.80 | 0.030 | 129 | 0.014 | 0.03 | n.d. |
| 617-875 | anhy | 2 | n.d. | tr. | 5.48 | 14.5 | 23.6 | n.d. | 0.05 | 152 | 0.37 | 4.88 | 0.04 | 0.81 | 1.04 | 0.008 | 198 | 0.024 | 0.03 | 0.24 |
| 617-875 | anhy | 3 | n.d. | 1.06 | 1.17 | 0.62 | 10.1 | 0.1 | n.d. | 159 | 0.05 | 2.94 | 0.03 | 0.10 | 0.16 | n.d. | 10.3 | 0.031 | 0.03 | 0.03 |
| 617-875 | anhy | 4 | n.d. | 4.61 | 4.59 | 0.11 | 2.6 | 0.2 | 0.55 | 141 | 0.22 | 0.95 | 0.04 | 0.23 | 0.11 | n.d. | 3.4 | 0.007 | 0.04 | 0.15 |
| 617-875 | anhy | orig. | 0.55 | 25.3 | 156 | 93.1 | 64.4 | 2.5 | 9.90 | 831 | 53.0 | 16.3 | 2.60 | 9.40 | 2.20 | 0.25 | 279 | 0.100 | 2.00 | 1.60 |

Appendix 2.2. Continuation. Four-step sequential leaching results for metalliferous sediments from the Atlantis II Deep (Red Sea).

| | | V | W | Y | Cu | Zn | Pb | Fe | Ba | Ca | Al | Mg | K | P | B | Br | Cs | Li | REE | pH |
|---|---|---|---|---|---|---|---|---|---|---|---|---|---|---|---|---|---|---|---|---|
| | *Det.L.* | *0.05* | *0.001* | *0.005* | *0.05* | *0.20* | *0.01* | *5* | *0.05* | *10* | *1* | *1* | *5* | *5* | *2* | *2* | *0.005* | *0.05* | | |
| **Sample no** | **Leach[1]** | ppm | ppm | ppm | ppm | ppm | ppm | ppm | ppm | ppm | ppm | ppm | ppm | ppm | ppm | ppm | ppm | ppm | ppm | ppm |
| 334-83 | 1 | n.d. | 0.004 | n.d. | 31 | 7420 | 0 | 175 | 5 | 43900 | n.d. | 1760 | 5350 | n.d. | 16 | 290 | 0.01 | 5.63 | 0.04 | 5.9 |
| 334-83 | 2 | 2.0 | 0.002 | 0.14 | 1175 | 3150 | 55 | 438 | 69 | 5770 | 24 | 95 | 295 | n.d. | n.d. | 4 | n.d. | 0.41 | 0.59 | 4.8 |
| 334-83 | 3 | 3.0 | n.d. | 0.06 | 183 | 565 | 32 | 4340 | 391 | 100 | 124 | 61 | 33 | n.d. | 4 | 2 | n.d. | 1.42 | 0.38 | 2.2 |
| 334-83 | 4 | 2.6 | 0.003 | 0.05 | 65 | 217 | 52 | 3820 | 239 | 30 | 121 | 55 | 41 | n.d. | 2 | n.d. | 0.01 | 0.64 | 0.36 | 1.7 |
| 334-83 | orig. | 39 | 3.1 | 0.70 | 1720 | 11700 | 217 | 73900 | 1130 | 45800 | 2142 | 2800 | 7759 | 240 | 80 | 186 | 0.40 | 10.4 | 2.45 | |
| 334-513 | 1 | n.d. | 0.005 | 0.05 | 17 | 36700 | 109 | 205 | 4 | 33300 | 3 | 1570 | 3760 | n.d. | 6 | 189 | 0.01 | 4.94 | 0.27 | 5.7 |
| 334-513 | 2 | 2.0 | 0.013 | 0.25 | 244 | 4620 | 841 | 739 | 97 | 2770 | 83 | 98 | 214 | 21 | n.d. | 3 | 0.01 | 0.14 | 1.51 | 4.8 |
| 334-513 | 3 | 0.7 | n.d. | 0.08 | 113 | 613 | 105 | 4550 | 202 | 320 | 142 | 160 | 17 | n.d. | n.d. | 2 | n.d. | 0.23 | 0.44 | 2.4 |
| 334-513 | 4 | 0.7 | 0.005 | 0.07 | 687 | 353 | 129 | 4860 | 122 | 170 | 271 | 266 | 20 | 19 | n.d. | n.d. | 0.01 | 0.18 | 0.48 | 1.6 |
| 334-513 | orig. | 50 | 3.7 | 0.90 | 4420 | 36500 | 1710 | 97200 | 534 | 33800 | 3221 | 4700 | 5403 | 320 | 40 | 117 | 0.41 | 6.60 | 4.37 | |
| 334-757 | 1 | n.d. | 0.006 | 0.09 | 230 | 29900 | 71 | 83 | 4 | 20100 | 1 | 2220 | 3290 | n.d. | 4 | 216 | n.d. | 5.53 | 0.98 | 3.8 |
| 334-757 | 2 | 2.0 | 0.003 | 0.05 | 76 | 1360 | 101 | 173 | 49 | 860 | 5 | 108 | 230 | n.d. | n.d. | 2 | n.d. | 0.12 | 0.57 | 4.8 |
| 334-757 | 3 | n.d. | 0.001 | 0.03 | 27 | 103 | 21 | 1370 | 55 | 20 | 90 | 36 | 25 | n.d. | n.d. | 3 | n.d. | 0.07 | 0.22 | 2.3 |
| 334-757 | 4 | n.d. | 0.005 | 0.02 | 20 | 45 | 23 | 1670 | 39 | 5 | 173 | 80 | 51 | n.d. | n.d. | n.d. | n.d. | 0.08 | 0.21 | 1.5 |
| 334-757 | orig. | 37 | 6.6 | 0.50 | 608 | 25500 | 249 | 104000 | 201 | 19500 | 3162 | 6000 | 5776 | 290 | 40 | 139 | 0.24 | 6.97 | 3.06 | |
| 387-80 | 1 | n.d. | 0.006 | 0.09 | 1055 | 8370 | 41 | 68 | 7 | 27900 | n.d. | 2220 | 5800 | n.d. | 8 | 307 | 0.01 | 7.40 | 0.33 | 4.1 |
| 387-80 | 2 | 2.0 | 0.002 | 0.08 | 375 | 458 | 83 | 182 | 49 | 2680 | 3 | 105 | 329 | n.d. | n.d. | 6 | n.d. | 0.25 | 0.38 | 4.8 |
| 387-80 | 3 | 0.4 | n.d. | 0.03 | 81 | 76 | 13 | 1930 | 26 | 40 | 87 | 10 | 17 | n.d. | 2 | 2 | n.d. | 0.16 | 0.20 | 2.1 |
| 387-80 | 4 | 0.3 | 0.003 | 0.02 | 43 | 34 | 11 | 1410 | 4 | 5 | 76 | 13 | 30 | n.d. | n.d. | n.d. | 0.01 | 0.09 | 0.23 | 1.5 |
| 387-80 | orig. | 30 | 3.3 | 0.60 | 2060 | 8960 | 183 | 72200 | 101 | 24900 | 2100 | 3100 | 9133 | 200 | 50 | 196 | 0.63 | 9.60 | 2.34 | |
| 503-912 | 1 | n.d. | 0.014 | 0.40 | 1550 | 95100 | 23 | 33 | 2 | 18600 | 6 | 2430 | 1860 | n.d. | 5 | 84 | 0.08 | 5.71 | 2.95 | 5.3 |
| 503-912 | 2 | 2.0 | 0.012 | 0.32 | 13100 | 10350 | 318 | 522 | 21 | 3260 | 22 | 105 | 562 | n.d. | n.d. | 4 | 0.18 | 0.22 | 2.57 | 4.8 |
| 503-912 | 3 | 0.9 | 0.001 | 0.21 | 474 | 415 | 102 | 2190 | 14 | 140 | 163 | 35 | 18 | n.d. | n.d. | 2 | 0.01 | 0.05 | 1.67 | 2.0 |
| 503-912 | 4 | 1.2 | 0.009 | 0.09 | 209 | 190 | 97 | 2070 | 3 | 30 | 102 | 15 | 16 | n.d. | n.d. | n.d. | 0.03 | 0.10 | 1.07 | 1.6 |
| 503-912 | orig. | 93 | 8.1 | 2.10 | 15100 | 87500 | 1250 | 38100 | 70 | 21500 | 9213 | 3700 | 4412 | 370 | 50 | 95 | 0.80 | 8.63 | 12.8 | |
| 421-740 | 1 | 0.8 | 0.006 | 0.01 | 99 | 14350 | 8 | 56 | 15 | 5480 | 1 | 4030 | 5420 | 32 | 15 | 331 | 0.10 | 11.8 | 0.08 | 4.8 |
| 421-740 | 2 | 3.0 | 0.006 | 0.34 | 148 | 1745 | 114 | 266 | 13 | 620 | 3 | 256 | 450 | 303 | n.d. | 9 | 0.09 | 0.55 | 2.26 | 4.8 |

| Sample no | Leach[1] | V | W | Y | Cu | Zn | Pb | Fe | Ba | Ca | Al | Mg | K | P | B | Br | Cs | Li | REE | pH |
|---|---|---|---|---|---|---|---|---|---|---|---|---|---|---|---|---|---|---|---|---|
| 421-740 | 3 | 30 | 0.003 | 0.05 | 34 | 156 | 33 | 1910 | 1 | 20 | 17 | 11 | 27 | 242 | n.d. | 2 | 0.02 | 0.11 | 0.37 | 2.3 |
| 421-740 | 4 | 16 | 0.013 | 0.07 | 25 | 64 | 19 | 1540 | 0 | 5 | 15 | 11 | 23 | 242 | n.d. | n.d. | 0.02 | 0.06 | 0.52 | 1.6 |
| 421-740 | orig. | 292 | 6.9 | 0.70 | 434 | 14600 | 187 | 67200 | 30 | 5600 | 1318 | 4800 | 11032 | 1331 | 40 | 240 | 2.21 | 12.8 | 4.44 | |
| 557-173 | 1 | n.d. | 0.003 | 0.02 | 82 | 25400 | 16 | 44 | 10 | 14400 | 2 | 2170 | 5790 | n.d. | 9 | 323 | 0.01 | 7.78 | 0.10 | 5.7 |
| 557-173 | 2 | 2.0 | 0.005 | 0.18 | 414 | 3810 | 194 | 344 | 56 | 1040 | 45 | 147 | 441 | 24 | n.d. | 7 | 0.01 | 0.32 | 0.83 | 4.8 |
| 557-173 | 3 | 1.4 | n.d. | 0.05 | 254 | 618 | 44 | 3750 | 17 | 40 | 202 | 48 | 29 | n.d. | 3 | 3 | n.d. | 0.43 | 0.30 | 2.2 |
| 557-173 | 4 | 1.3 | 0.005 | 0.04 | 236 | 277 | 41 | 3390 | 4 | 10 | 209 | 54 | 51 | 9 | n.d. | n.d. | 0.01 | 0.23 | 0.31 | 1.6 |
| 557-173 | orig. | 35 | 5.4 | 0.60 | 3740 | 26600 | 530 | 61900 | 88 | 13100 | 2991 | 3300 | 10369 | 270 | 40 | 397 | 0.71 | 9.69 | 2.79 | |
| 387-398 | 1 | n.d. | 0.011 | 0.06 | 17 | 38800 | 4 | 27 | 7 | 20900 | 8 | 1410 | 3210 | n.d. | 6 | 130 | 0.12 | 4.14 | 0.30 | 6.4 |
| 387-398 | 2 | 3.0 | 0.010 | 0.80 | 322 | 7560 | 195 | 890 | 291 | 1700 | 77 | 250 | 574 | 63 | n.d. | 6 | 0.16 | 0.18 | 4.92 | 4.8 |
| 387-398 | 3 | 3.8 | 0.002 | 0.27 | 16 | 1265 | 20 | 5980 | 413 | 1000 | 193 | 200 | 27 | n.d. | n.d. | 2 | 0.02 | 0.24 | 1.57 | 2.7 |
| 387-398 | 4 | 3.9 | 0.017 | 0.29 | 1475 | 1170 | 109 | 5070 | 490 | 280 | 349 | 71 | 37 | 85 | n.d. | n.d. | 0.04 | 0.14 | 2.19 | 1.5 |
| 387-398 | orig. | 82 | 10.2 | 2.90 | 14300 | 44700 | 1280 | 51500 | 2160 | 23300 | 10048 | 3600 | 6682 | 570 | 40 | 109 | 1.23 | 8.97 | 14.8 | |
| 387-466 | 1 | n.d. | 0.004 | 0.06 | 24 | 27100 | 1 | 94 | 7 | 12800 | 5 | 1880 | 2950 | n.d. | 6 | 131 | 0.08 | 6.07 | 0.44 | 6.4 |
| 387-466 | 2 | 2.0 | 0.006 | 0.65 | 430 | 2680 | 79 | 1930 | 127 | 1430 | 20 | 119 | 434 | n.d. | n.d. | 3 | 0.13 | 0.15 | 5.85 | 4.8 |
| 387-466 | 3 | 1.4 | n.d. | 0.14 | 2 | 413 | 2 | 11650 | 62 | 1330 | 27 | 292 | 19 | n.d. | n.d. | 2 | 0.01 | 0.35 | 1.18 | 4.2 |
| 387-466 | 4 | 3.0 | 0.003 | 0.30 | 16 | 312 | 19 | 26200 | 26 | 2690 | 108 | 570 | 23 | n.d. | 2 | n.d. | 0.02 | 0.87 | 3.35 | 2.5 |
| 387-466 | orig. | 76 | 6.5 | 2.50 | 10300 | 26600 | 590 | 147000 | 247 | 21600 | 7579 | 5500 | 5873 | 780 | 40 | 111 | 0.95 | 11.7 | 18.5 | |
| 617-148 | 1 | n.d. | 0.006 | 0.21 | 728 | 24500 | 38 | 23 | 6 | 25800 | 7 | 3370 | 4940 | n.d. | 15 | 261 | 0.03 | 8.73 | 0.84 | 5.3 |
| 617-148 | 2 | 2.0 | 0.002 | 0.57 | 1655 | 2120 | 292 | 371 | 150 | 1720 | 43 | 156 | 424 | n.d. | n.d. | 6 | 0.02 | 0.35 | 2.26 | 4.8 |
| 617-148 | 3 | 1.4 | n.d. | 0.16 | 386 | 284 | 84 | 2880 | 258 | 60 | 218 | 32 | 21 | n.d. | 2 | 3 | 0.01 | 0.09 | 0.76 | 2.1 |
| 617-148 | 4 | 1.1 | 0.003 | 0.11 | 525 | 145 | 64 | 2520 | 98 | 10 | 185 | 41 | 29 | n.d. | n.d. | n.d. | 0.01 | 0.05 | 0.70 | 1.5 |
| 617-148 | orig. | 41 | 6.4 | 1.30 | 7620 | 22000 | 1040 | 96800 | 573 | 23300 | 3028 | 4000 | 8443 | 240 | 40 | 283 | 0.61 | 10.6 | 6.80 | |
| 334-312 | 1 | n.d. | 0.004 | 0.02 | 375 | 21600 | 8 | 46 | 6 | 28300 | n.d. | 1620 | 4410 | n.d. | 15 | 240 | 0.01 | 6.88 | 0.08 | 5.3 |
| 334-312 | 2 | 2.0 | 0.002 | 0.12 | 1105 | 2740 | 163 | 442 | 41 | 5850 | 35 | 79 | 271 | n.d. | n.d. | 4 | n.d. | 0.22 | 0.48 | 4.8 |
| 334-312 | 3 | 1.1 | n.d. | 0.05 | 223 | 580 | 46 | 4040 | 192 | 70 | 130 | 19 | 29 | n.d. | 3 | 3 | n.d. | 0.26 | 0.24 | 2.2 |
| 334-312 | 4 | 1.3 | 0.002 | 0.05 | 142 | 292 | 66 | 3710 | 119 | 20 | 179 | 27 | 47 | n.d. | 2 | n.d. | 0.01 | 0.17 | 0.38 | 1.6 |
| 334-312 | orig. | 43 | 4.6 | 0.70 | 3370 | 22000 | 501 | 115000 | 549 | 31300 | 2869 | 2500 | 7683 | 330 | 80 | 165 | 0.42 | 9.44 | 3.23 | |
| 421-80 | 1 | n.d. | 0.002 | n.d. | 109 | 7470 | 1 | 161 | 16 | 17100 | 2 | 2140 | 6390 | n.d. | 14 | 346 | 0.01 | 7.62 | 0.04 | 6.2 |
| 421-80 | 2 | 2.0 | 0.002 | 0.11 | 4310 | 2560 | 69 | 746 | 48 | 1280 | 25 | 199 | 503 | n.d. | 2 | 9 | 0.01 | 0.50 | 0.47 | 4.8 |
| 421-80 | 3 | 0.5 | n.d. | 0.04 | 38 | 306 | 5 | 7260 | 6 | 790 | 29 | 126 | 23 | n.d. | 2 | 2 | n.d. | 0.73 | 0.15 | 2.6 |
| 421-80 | 4 | 0.8 | 0.004 | 0.08 | 240 | 199 | 54 | 8790 | 2 | 810 | 169 | 133 | 38 | n.d. | 2 | n.d. | 0.01 | 0.60 | 0.46 | 1.7 |
| 421-80 | orig. | 29.0 | 5.6 | 0.50 | 5650 | 10500 | 190 | 106000 | 78 | 17500 | 2180 | 3000 | 10836 | 430 | 80 | 240 | 0.72 | 10.8 | 2.30 | |
| 617-799 | 1 | n.d. | 0.001 | 0.01 | 2 | 3520 | 4 | 10 | 3 | 50600 | 1 | 1450 | 1220 | n.d. | n.d. | 140 | n.d. | 3.37 | 0.06 | 6.8 |
| 617-799 | 2 | 2.0 | 0.005 | 0.72 | 1380 | 43500 | 1090 | 3810 | 15 | 35500 | 589 | 213 | 149 | n.d. | n.d. | 6 | n.d. | 0.76 | 4.56 | 4.8 |
| 617-799 | 3 | 0.9 | 0.001 | 0.50 | 65 | 3720 | 44 | 3100 | 128 | 940 | 274 | 107 | 26 | 26 | n.d. | 2 | n.d. | 0.31 | 2.08 | 2.5 |
| 617-799 | 4 | 1.2 | 0.004 | 0.51 | 170 | 799 | 219 | 6550 | 389 | 160 | 766 | 345 | 42 | 134 | n.d. | n.d. | n.d. | 0.29 | 3.48 | 1.7 |
| 617-799 | orig. | 39 | 3.2 | 2.40 | 3700 | 45300 | 1470 | 73100 | 5970 | 79700 | 6444 | 5900 | 3471 | 400 | 20 | 153 | 0.19 | 5.91 | 10.5 | |
| 546-92 | 1 | n.d. | 0.001 | n.d. | 8 | 4580 | 0 | 150 | 12 | 7030 | n.d. | 6360 | 4880 | n.d. | 24 | 486 | n.d. | 6.05 | 0.04 | 6.2 |
| 546-92 | 2 | 2.0 | 0.002 | 0.08 | 2230 | 4510 | 62 | 453 | 20 | 560 | 32 | 408 | 368 | n.d. | 2 | 8 | n.d. | 0.32 | 0.29 | 4.8 |
| 546-92 | 3 | 1.6 | n.d. | 0.03 | 231 | 1200 | 10 | 6250 | 7 | 380 | 48 | 197 | 42 | n.d. | 4 | 3 | n.d. | 0.66 | 0.17 | 2.3 |
| 546-92 | 4 | 3.0 | 0.002 | 0.06 | 262 | 534 | 140 | 8100 | 2 | 400 | 213 | 220 | 66 | n.d. | 4 | n.d. | n.d. | 0.80 | 0.37 | 1.6 |

| Sample no | Leach[1] | V | W | Y | Cu | Zn | Pb | Fe | Ba | Ca | Al | Mg | K | P | B | Br | Cs | Li | REE | pH |
|---|---|---|---|---|---|---|---|---|---|---|---|---|---|---|---|---|---|---|---|---|
| 546-92 | orig. | 37 | 3.4 | 0.50 | 3730 | 12700 | 543 | 101000 | 47 | 7500 | 2223 | 7000 | 8202 | 440 | 80 | 354 | 0.32 | 8.52 | 1.97 | |
| 387-575 | 1 | 0.2 | 0.008 | 0.50 | 2530 | 5900 | 1 | 437 | 9 | 45600 | 190 | 1620 | 92 | n.d. | 6 | 75 | 0.08 | 5.35 | 6.38 | 3 |
| 387-575 | 2 | 3.0 | 0.009 | 0.05 | 142 | 155 | 2 | 369 | 55 | 10700 | 14 | 41 | 35 | n.d. | n.d. | 5 | 0.07 | 0.18 | 1.14 | 4.8 |
| 387-575 | 3 | 3.0 | n.d. | 0.05 | 69 | 13 | 9 | 1210 | 192 | 90 | 34 | 1 | 31 | 9 | n.d. | 2 | 0.02 | n.d. | 0.58 | 2.1 |
| 387-575 | 4 | 2.0 | 0.009 | 0.04 | 50 | 7 | 32 | 990 | 315 | 10 | 31 | 2 | 68 | 23 | n.d. | n.d. | 0.03 | n.d. | 0.61 | 1.5 |
| 387-575 | orig. | 189 | 5.4 | 1.40 | 3430 | 6060 | 636 | 50100 | 4740 | 52900 | 4992 | 2400 | 10059 | 600 | 40 | 141 | 1.02 | 7.25 | 11.5 | |
| 503-75 | 1 | 0.4 | 0.014 | 0.36 | 997 | 7180 | 3 | 1160 | 22 | 20600 | 161 | 1660 | 130 | n.d. | 4 | 80 | 0.06 | 4.34 | 10.2 | 2.5 |
| 503-75 | 2 | 3.0 | 0.010 | 0.01 | 32 | 155 | 9 | 1430 | 186 | 420 | 5 | 36 | 26 | 9 | n.d. | 4 | 0.04 | 0.09 | 1.15 | 4.8 |
| 503-75 | 3 | 4.3 | 0.001 | 0.05 | 26 | 8 | 17 | 2500 | 243 | 20 | 14 | 1 | 35 | 7 | n.d. | 3 | 0.01 | n.d. | 0.69 | 2.1 |
| 503-75 | 4 | 2.7 | 0.012 | 0.02 | 23 | 4 | 35 | 2580 | 208 | 5 | 14 | 1 | 60 | 60 | n.d. | n.d. | 0.01 | n.d. | 0.35 | 1.5 |
| 503-75 | orig. | 181 | 6.696 | 1.20 | 1380 | 7020 | 437 | 38000 | 9340 | 19200 | 4147 | 2100 | 5203 | 750 | 20 | 108 | 0.66 | 5.49 | 13.1 | |
| 503-807 | 1 | 0.5 | 0.012 | 1.19 | 3690 | 4870 | 1 | 264 | 5 | 24700 | 285 | 2280 | 51 | 6 | 4 | 86 | 0.04 | 5.61 | 17.2 | 3 |
| 503-807 | 2 | 3.0 | 0.006 | 0.08 | 141 | 109 | 5 | 279 | 241 | 750 | 25 | 58 | 35 | n.d. | n.d. | 4 | 0.04 | 0.13 | 2.33 | 4.8 |
| 503-807 | 3 | 4.6 | 0.002 | 0.05 | 91 | 12 | 14 | 1350 | 95 | 30 | 80 | 2 | 19 | n.d. | n.d. | 2 | 0.01 | n.d. | 0.88 | 2.1 |
| 503-807 | 4 | 2.3 | 0.016 | 0.02 | 59 | 5 | 46 | 1330 | 165 | 10 | 73 | 2 | 43 | 8 | n.d. | n.d. | 0.01 | n.d. | 0.77 | 1.5 |
| 503-807 | orig. | 193 | 7.8 | 2.00 | 4820 | 4730 | 1030 | 73500 | 4460 | 24300 | 6563 | 3000 | 10909 | 590 | 30 | 133 | 1.03 | 7.94 | 24.1 | |
| 546-267 | 1 | n.d. | 0.007 | n.d. | 16 | 320 | 0 | 42 | 6 | 24200 | 3 | 4750 | 3420 | n.d. | 10 | 259 | 0.02 | 4.40 | 0.04 | 6.5 |
| 546-267 | 2 | 2.0 | 0.006 | 0.11 | 456 | 403 | 22 | 198 | 125 | 2180 | 8 | 386 | 315 | n.d. | n.d. | 7 | 0.04 | 0.23 | 0.90 | 4.8 |
| 546-267 | 3 | 2.1 | n.d. | 0.09 | 132 | 133 | 10 | 3220 | 1150 | 250 | 112 | 95 | 23 | n.d. | n.d. | 2 | 0.01 | 0.14 | 0.54 | 2.3 |
| 546-267 | 4 | 3.7 | 0.008 | 0.12 | 94 | 60 | 35 | 3070 | 587 | 150 | 99 | 61 | 49 | n.d. | n.d. | n.d. | 0.01 | 0.10 | 0.95 | 1.5 |
| 546-267 | orig. | 78 | 34.7 | 0.90 | 1590 | 1710 | 165 | 182000 | 2750 | 25400 | 4097 | 7600 | 6691 | 600 | 50 | 223 | 1.02 | 7.65 | 6.10 | |
| 617-220 | 1 | n.d. | 0.001 | 0.23 | 394 | 1025 | 11 | 44 | 0 | 51300 | 3 | 4230 | 3550 | 5 | 6 | 163 | 0.06 | 3.96 | 1.07 | 3.9 |
| 617-220 | 2 | 2.0 | 0.001 | 0.17 | 80 | 77 | 5 | 91 | 1 | 51000 | 7 | 276 | 234 | n.d. | n.d. | 7 | 0.03 | 0.63 | 1.11 | 4.8 |
| 617-220 | 3 | 0.3 | n.d. | 0.09 | 24 | 14 | 1 | 296 | 0 | 450 | 38 | 59 | n.d. | 16 | n.d. | 3 | n.d. | 0.12 | 0.32 | 2.1 |
| 617-220 | 4 | 0.1 | 0.002 | 0.04 | 12 | 3 | 1 | 237 | 1 | 40 | 27 | 75 | n.d. | 14 | n.d. | n.d. | n.d. | 0.07 | 0.20 | 1.6 |
| 617-220 | orig. | 21 | 0.250 | 0.70 | 611 | 1080 | 19 | 16600 | 2 | 95300 | 1638 | 33700 | 4112 | 140 | 20 | 188 | 0.16 | 8.48 | 2.75 | |
| 495-809 | 1 | 0.3 | 0.004 | 0.01 | 17 | 3990 | 0 | 75 | 6 | 18300 | 4 | 3730 | 5850 | 26 | 9 | 335 | 0.06 | 11.1 | 0.11 | 5.2 |
| 495-809 | 2 | 2.0 | 0.004 | 0.22 | 50 | 691 | 9 | 70 | 6 | 1830 | 4 | 277 | 554 | 99 | n.d. | 9 | 0.10 | 0.61 | 2.93 | 4.8 |
| 495-809 | 3 | 9.7 | n.d. | 0.04 | 9 | 117 | 3 | 808 | 2 | 30 | 11 | 15 | 41 | 51 | n.d. | 2 | 0.02 | 0.14 | 0.41 | 2.5 |
| 495-809 | 4 | 4.8 | 0.004 | 0.07 | 14 | 70 | 4 | 854 | 0 | 10 | 16 | 17 | 31 | 58 | n.d. | n.d. | 0.02 | 0.10 | 1.06 | 1.5 |
| 495-809 | orig. | 229 | 3.4 | 0.70 | 188 | 4340 | 23 | 75700 | 22 | 17400 | 1800 | 5400 | 12710 | 750 | 40 | 244 | 2.89 | 11.9 | 6.65 | |
| 503-140 | 1 | n.d. | 0.002 | 0.16 | 1150 | 9090 | 48 | 62 | 1 | 30900 | 34 | 2550 | 5450 | n.d. | 16 | 309 | 0.04 | 19.9 | 0.50 | 3.6 |
| 503-140 | 2 | 2.0 | 0.002 | 0.01 | 102 | 489 | 41 | 89 | 4 | 1770 | 33 | 141 | 410 | n.d. | n.d. | 8 | 0.05 | 0.93 | 0.07 | 4.8 |
| 503-140 | 3 | 0.1 | n.d. | n.d. | 25 | 51 | 91 | 383 | 3 | 10 | 43 | 2 | 95 | n.d. | n.d. | 2 | 0.01 | 0.05 | 0.05 | 2.2 |
| 503-140 | 4 | n.d. | n.d. | n.d. | 22 | 19 | 41 | 414 | 2 | 5 | 47 | 2 | 108 | n.d. | n.d. | n.d. | 0.01 | n.d. | 0.06 | 1.5 |
| 503-140 | orig. | 25 | 0.250 | 0.20 | 1330 | 8480 | 296 | 63300 | 26 | 28100 | 1308 | 3900 | 22227 | 100 | 50 | 234 | 1.51 | 24.7 | 0.99 | |
| 421-825 | 1 | 0.3 | 0.001 | n.d. | 1 | 24 | 0 | 15 | 4 | 11800 | 4 | 860 | 2330 | n.d. | 10 | 87 | 0.03 | 2.54 | 0.04 | 7.8 |
| 421-825 | 2 | 5.0 | 0.004 | 2.76 | 51 | 3230 | 3 | 246 | 9 | 111500 | 227 | 2110 | 318 | 407 | 2 | 4 | 0.13 | 0.68 | 15.5 | 4.9 |
| 421-825 | 3 | 11 | n.d. | 0.19 | 1 | 183 | 0 | 619 | 1 | 4200 | 125 | 1340 | 45 | 361 | n.d. | 3 | 0.03 | 0.38 | 0.83 | 3.5 |
| 421-825 | 4 | 14 | 0.002 | 2.57 | 80 | 140 | 8 | 1580 | 1 | 680 | 336 | 248 | 135 | 249 | n.d. | n.d. | 0.05 | 0.59 | 15.2 | 1.6 |
| 421-825 | orig. | 215 | 0.250 | 14.2 | 489 | 4230 | 22 | 45200 | 142 | 122000 | 32621 | 13000 | 11877 | 1331 | 50 | 85 | 2.41 | 20.5 | 70.3 | |
| 495-557 | 1 | n.d. | 0.001 | n.d. | 0 | 18 | 0 | 79 | 2 | 14000 | 3 | 1150 | 3610 | n.d. | 16 | 175 | 0.03 | 4.60 | 0.04 | 7.7 |

| Sample no | Leach[1] | V | W | Y | Cu | Zn | Pb | Fe | Ba | Ca | Al | Mg | K | P | B | Br | Cs | Li | REE | pH |
|---|---|---|---|---|---|---|---|---|---|---|---|---|---|---|---|---|---|---|---|---|
| 495-557 | 2 | 3.0 | 0.002 | 1.59 | 82 | 3180 | 6 | 77 | 3 | 46200 | 61 | 2220 | 380 | 52 | 2 | 3 | 0.04 | 0.77 | 7.20 | 4.9 |
| 495-557 | 3 | 4.3 | n.d. | 0.13 | 9 | 298 | 0 | 861 | 0 | 1560 | 67 | 436 | 21 | n.d. | n.d. | 2 | 0.01 | 0.22 | 0.63 | 3.1 |
| 495-557 | 4 | 2.7 | 0.001 | 0.37 | 29 | 144 | 8 | 1200 | 0 | 220 | 257 | 95 | 57 | n.d. | n.d. | n.d. | 0.03 | 0.22 | 2.77 | 1.6 |
| 495-557 | orig. | 199 | 1.6 | 4.60 | 156 | 4090 | 25 | 213000 | 36 | 58600 | 9586 | 5500 | 7382 | 900 | 120 | 125 | 0.82 | 9.95 | 24.2 | |
| 546-180 | 1 | n.d. | 0.005 | n.d. | 2 | 896 | 0 | 38 | 25 | 6340 | n.d. | 5540 | 4860 | n.d. | 17 | 416 | 0.03 | 5.60 | 0.04 | 6.6 |
| 546-180 | 2 | 2.0 | 0.002 | 0.12 | 526 | 2730 | 8 | 836 | 45 | 900 | 21 | 486 | 351 | 10 | 2 | 10 | 0.02 | 0.38 | 0.57 | 4.8 |
| 546-180 | 3 | 2.1 | n.d. | 0.03 | 40 | 447 | 0 | 5560 | 7 | 1070 | 12 | 314 | 32 | n.d. | 2 | 3 | 0.01 | 0.25 | 0.14 | 2.7 |
| 546-180 | 4 | 2.2 | 0.002 | 0.13 | 105 | 387 | 23 | 9730 | 3 | 1330 | 53 | 405 | 41 | n.d. | 2 | n.d. | 0.02 | 0.33 | 0.62 | 1.8 |
| 546-180 | orig. | 46 | 3.3 | 0.50 | 956 | 5280 | 105 | 112000 | 82 | 9000 | 1907 | 7200 | 8369 | 510 | 80 | 310 | 0.67 | 8.39 | 2.60 | |
| 503-889 | 1 | n.d. | n.d. | 0.02 | 49 | 1200 | 0 | 24 | 0 | 14300 | n.d. | 1380 | 281 | n.d. | 11 | 31 | 0.02 | 2.60 | 0.10 | 6.9 |
| 503-889 | 2 | 2.0 | 0.001 | 0.78 | 2990 | 799 | 50 | 6730 | 2 | 1370 | 9 | 280 | 52 | n.d. | n.d. | 3 | 0.03 | 0.36 | 4.50 | 4.8 |
| 503-889 | 3 | 0.6 | n.d. | 0.27 | 32 | 308 | 5 | 13250 | 2 | 1470 | 2 | 391 | 114 | n.d. | 2 | 2 | 0.01 | 0.62 | 1.71 | 2.9 |
| 503-889 | 4 | 1.6 | 0.001 | 0.40 | 103 | 245 | 25 | 28400 | 1 | 2660 | 24 | 713 | 158 | n.d. | 3 | n.d. | 0.02 | 1.15 | 2.51 | 2.5 |
| 503-889 | orig. | 49 | 2.0 | 3.20 | 12300 | 3880 | 397 | 344000 | 15 | 25300 | 4525 | 5000 | 1916 | 1611 | 70 | 37 | 0.41 | 8.51 | 15.6 | |
| 503-516 | 1 | n.d. | 0.003 | n.d. | 6 | 3170 | 0 | 5 | 16 | 8300 | 3 | 1140 | 3730 | n.d. | 14 | 178 | 0.12 | 5.53 | 0.04 | 7 |
| 503-516 | 2 | 3.0 | 0.005 | 2.47 | 492 | 5460 | 80 | 433 | 421 | 2790 | 77 | 133 | 507 | 384 | 2 | 4 | 0.25 | 0.38 | 16.4 | 4.8 |
| 503-516 | 3 | 5.2 | n.d. | 0.51 | 200 | 395 | 36 | 2930 | 304 | 400 | 162 | 23 | 40 | 120 | 2 | 2 | 0.06 | 0.33 | 2.75 | 2.3 |
| 503-516 | 4 | 4.0 | 0.006 | 1.13 | 816 | 193 | 68 | 3220 | 445 | 180 | 186 | 26 | 88 | 165 | n.d. | n.d. | 0.09 | 0.57 | 8.28 | 1.5 |
| 503-516 | orig. | 136 | 3.2 | 12.2 | 11900 | 10700 | 277 | 34000 | 3290 | 14900 | 33179 | 7800 | 13766 | 1001 | 60 | 158 | 3.82 | 21.6 | 61.9 | |
| 495-362 | 1 | n.d. | 0.003 | n.d. | 14 | 2450 | 0 | 166 | 16 | 25400 | n.d. | 2000 | 5950 | n.d. | 20 | 354 | n.d. | 4.82 | 0.04 | 6.7 |
| 495-362 | 2 | 2.0 | 0.001 | 0.14 | 1830 | 3170 | 55 | 853 | 177 | 2410 | 27 | 176 | 549 | n.d. | 2 | 7 | n.d. | 0.71 | 0.53 | 4.8 |
| 495-362 | 3 | 2.5 | 0.002 | 0.05 | 273 | 421 | 20 | 5930 | 36 | 60 | 105 | 87 | 53 | n.d. | 4 | 2 | n.d. | 2.51 | 0.26 | 2.2 |
| 495-362 | 4 | 1.7 | 0.001 | 0.04 | 97 | 161 | 51 | 5250 | 5 | 10 | 134 | 87 | 70 | n.d. | 3 | n.d. | 0.01 | 1.30 | 0.38 | 1.6 |
| 495-362 | orig. | 37 | 4.0 | 0.50 | 2560 | 6290 | 160 | 118000 | 227 | 24900 | 2065 | 3300 | 10999 | 320 | 80 | 223 | 0.55 | 11.5 | 2.86 | |
| 503-671 | 1 | n.d. | 0.004 | n.d. | 15 | 427 | 0 | 62 | 19 | 19000 | 2 | 3640 | 7360 | n.d. | 7 | 394 | 0.08 | 11.6 | 0.04 | 7.1 |
| 503-671 | 2 | 2.0 | 0.002 | 0.04 | 275 | 204 | 1 | 71 | 44 | 1330 | 2 | 269 | 537 | n.d. | n.d. | 10 | 0.09 | 0.57 | 0.20 | 4.8 |
| 503-671 | 3 | 1.8 | n.d. | 0.01 | 38 | 76 | 0 | 450 | 35 | 20 | 5 | 17 | 30 | n.d. | n.d. | 3 | 0.02 | 0.14 | 0.09 | 2.1 |
| 503-671 | 4 | 1.2 | 0.003 | 0.02 | 40 | 56 | 1 | 443 | 18 | 10 | 8 | 18 | 43 | n.d. | n.d. | n.d. | 0.03 | 0.09 | 0.17 | 1.5 |
| 503-671 | orig. | 17 | 5.3 | 0.20 | 368 | 680 | 5 | 59700 | 94 | 16400 | 896 | 4800 | 18783 | 90 | 90 | 243 | 3.38 | 13.0 | 0.78 | |
| 373-8 | 1 | n.d. | 0.002 | n.d. | 4 | 2290 | 1 | 57 | 33 | 20300 | 1 | 2420 | 8010 | n.d. | 32 | 409 | 0.01 | 8.33 | 0.04 | 6.9 |
| 373-8 | 2 | 3.0 | 0.001 | 0.19 | 764 | 3050 | 99 | 749 | 60 | 1410 | 27 | 152 | 452 | 17 | 2 | 5 | 0.01 | 0.62 | 0.66 | 4.8 |
| 373-8 | 3 | 2.6 | n.d. | 0.06 | 113 | 335 | 36 | 4450 | 11 | 80 | 97 | 78 | 40 | n.d. | 4 | 3 | 0.01 | 1.95 | 0.33 | 2.3 |
| 373-8 | 4 | 1.2 | 0.002 | 0.05 | 45 | 139 | 51 | 3740 | 3 | 10 | 95 | 63 | 44 | 8 | 2 | n.d. | 0.01 | 0.92 | 0.39 | 1.6 |
| 373-8 | orig. | 23 | 2.8 | 0.60 | 1110 | 5830 | 222 | 63200 | 109 | 19300 | 2004 | 3500 | 12439 | 220 | 80 | 245 | 0.81 | 13.5 | 3.29 | |
| 503-680 | 1 | n.d. | 0.007 | n.d. | 3 | 84 | 0 | 35 | 46 | 14000 | n.d. | 3010 | 6000 | n.d. | 20 | 298 | 0.07 | 8.87 | 0.04 | 7.1 |
| 503-680 | 2 | 2.0 | 0.003 | 0.12 | 2060 | 920 | 5 | 330 | 461 | 1140 | 17 | 215 | 393 | n.d. | 2 | 8 | 0.06 | 0.48 | 0.34 | 4.8 |
| 503-680 | 3 | 1.0 | n.d. | 0.05 | 325 | 222 | 4 | 5620 | 290 | 110 | 35 | 37 | 18 | n.d. | 3 | 3 | 0.02 | 0.12 | 0.29 | 2.2 |
| 503-680 | 4 | 1.7 | 0.003 | 0.10 | 184 | 90 | 58 | 4150 | 154 | 50 | 31 | 25 | 25 | n.d. | 2 | n.d. | 0.02 | 0.09 | 0.62 | 1.6 |
| 503-680 | orig. | 26 | 3.4 | 0.60 | 3290 | 1700 | 225 | 134000 | 1350 | 14100 | 1711 | 4100 | 11108 | 270 | 70 | 233 | 1.42 | 12.9 | 3.65 | |
| 495-569 | 1 | n.d. | 0.001 | n.d. | 2 | 16 | 0 | 38 | 8 | 11000 | n.d. | 1020 | 3310 | n.d. | 18 | 155 | 0.03 | 3.63 | 0.05 | 7.7 |
| 495-569 | 2 | 2.0 | n.d. | 0.27 | 39 | 2400 | 3 | 53 | 25 | 6210 | 50 | 552 | 176 | n.d. | 3 | 3 | 0.02 | 0.23 | 0.89 | 4.8 |
| 495-569 | 3 | 8.6 | n.d. | 0.01 | 2 | 343 | 0 | 80 | 25 | 440 | 1 | 222 | 30 | n.d. | 17 | 2 | 0.01 | 0.26 | 0.04 | 5.2 |

| Sample no | Leach[1] | V | W | Y | Cu | Zn | Pb | Fe | Ba | Ca | Al | Mg | K | P | B | Br | Cs | Li | REE | pH |
|---|---|---|---|---|---|---|---|---|---|---|---|---|---|---|---|---|---|---|---|---|
| 495-569 | 4 | 11.0 | 0.002 | 0.13 | 14 | 509 | 0 | 1100 | 8 | 230 | 82 | 167 | 30 | n.d. | 14 | n.d. | 0.02 | 0.21 | 0.54 | 3.5 |
| 495-569 | orig. | 67 | 0.59 | 2.40 | 166 | 4430 | 89 | 106000 | 102 | 18400 | 6163 | 3500 | 4943 | 470 | 140 | 124 | 0.48 | 6.95 | 11.9 | |
| 373-586 | 1 | n.d. | 0.007 | 0.04 | 556 | 3310 | 2 | 56 | 3 | 34900 | 2 | 277 | 388 | n.d. | 2 | 17 | 0.02 | 0.84 | 0.23 | 4.4 |
| 373-586 | 2 | 2.0 | 0.004 | 0.07 | 401 | 122 | 26 | 77 | 2 | 175500 | 6 | 7 | 66 | n.d. | n.d. | 4 | 0.02 | 1.07 | 0.50 | 4.7 |
| 373-586 | 3 | 0.3 | n.d. | 0.02 | 45 | 14 | 11 | 430 | 6 | 21900 | 21 | 2 | 9 | 5 | n.d. | 3 | 0.01 | 0.29 | 0.12 | 2.1 |
| 373-586 | 4 | 0.1 | 0.007 | 0.01 | 19 | 10 | 8 | 330 | 49 | 1460 | 10 | 2 | 5 | n.d. | n.d. | n.d. | 0.01 | n.d. | 0.06 | 1.5 |
| 373-586 | orig. | 10 | 1.1 | 0.20 | 1290 | 3860 | 137 | 11900 | 175 | 216000 | 769 | 400 | 62 | 110 | 20 | 21 | 0.11 | 2.52 | 1.34 | |
| 617-875 | 1 | n.d. | 0.005 | 0.01 | 7 | 7880 | 0 | 31 | 3 | 44700 | 3 | 723 | 622 | n.d. | n.d. | 79 | n.d. | 1.62 | 0.08 | 6.5 |
| 617-875 | 2 | 3.0 | 0.007 | 0.36 | 1515 | 11950 | 134 | 1840 | 4 | 93200 | 244 | 77 | 79 | n.d. | n.d. | 5 | n.d. | 0.47 | 3.02 | 4.8 |
| 617-875 | 3 | 2.5 | 0.002 | 0.45 | 138 | 2060 | 25 | 4540 | 13 | 3260 | 312 | 130 | 15 | 21 | n.d. | 2 | n.d. | 0.23 | 2.28 | 2.4 |
| 617-875 | 4 | 2.6 | 0.006 | 0.30 | 82 | 534 | 87 | 6350 | 137 | 440 | 419 | 261 | 23 | 61 | n.d. | n.d. | n.d. | 0.17 | 2.55 | 1.7 |
| 617-875 | orig. | 79 | 3.9 | 1.40 | 5060 | 22900 | 358 | 67200 | 750 | 124000 | 4864 | 6200 | 1574 | 500 | 10 | 90 | 0.12 | 3.57 | 8.34 | |

[1] = Leachate number. Leachates are: 1) distilled water (dissolves secondary salts and secondary sulfates); 2) 0.1 M ammonium acetate buffered to pH 4.7-4.9 (dissolves calcite and dolomite but not authigenic Fe-Mn carbonates); 3) cold 0.1 M hydroxylamine hydrochloride in 0.01 M $HNO_3$ (dissolves mainly amorphous Mn- and Fe-oxyhydroxides); 4) 60°C, 0.25 M hydroxylamine hydrochloride in 0.025 M $HNO_3$ (dissolves residual Mn- and Fe-oxyhydroxides, but not hematite or magnetite). The behaviour of the different phases was monitored by analyzing the major and trace element concentrations by ICP in the leachates after each step. "orig." = chemistry according to total dissolution (Appendix C). Det. L. = Detection limit; Tr. = traces detected (less than half of the smallest number that can be expressed in the column); n.d. = not detected. Sequential leaching experiments were performed at ALS Laboratories in Vancouver.

# CHAPTER 3

## TRACE METAL DISTRIBUTION IN THE ATLANTIS II DEEP SEDIMENTS

Published in Laurila, T. E., Hannington, M. D., Petersen, S. and Garbe-Schönberg, D., 2014, Chemical Geology 386, p. 80-100.

## 1. Introduction

The Atlantis II Deep, situated in the Red Sea rift valley, is one of the first locations where seafloor hydrothermal activity was detected (Miller, 1966; Degens and Ross, 1969). It also contains by far the largest known hydrothermal mineral deposit on the seafloor (Guney et al., 1988). The metals have accumulated in a ~20 meter-thick sedimentary succession composed of finely laminated beds of oxides, carbonates, sulfides, silicates and other poorly-crystalline phases. The sediments are overlain by about 4 $km^3$ of hot (~68°C), anoxic, metal-rich brine, covering an area of about 60 $km^2$, from which most of the metals have precipitated. This style of metal accumulation is not known anywhere outside the Red Sea but has been widely invoked in the genetic models of many ancient stratiform metal deposits (e.g., Large et al., 1996; Johnson and Skinner, 2003; Solomon et al., 2004; Tornos et al., 2008; Ohmoto et al., 2006; Goodfellow and Lydon, 2007).

The metalliferous sediments of the Atlantis II Deep have been studied extensively since 1969, but comprehensive multi-element analyses by modern ICP-MS techniques have never been published. Fewer than 600 chemical analyses of the sediments are known, most with incomplete trace element data, despite more than 500 sediment cores having been taken. The most recent cores from the 1980s were relocated in a repository in Germany and re-opened for this study. Previous work on these cores mostly analyzed composite samples (~1 m intervals) in attempts to represent the bulk facies or entire stratigraphic units (unpublished data from the MESEDA I-III projects; Bertram et al., 2011). This paper reports the first modern geochemical data on the metalliferous sediments in 20 years (since

Anschutz and Blanc, 1995a), including one of the few comprehensive suites of trace elements (67 elements), and is the first to target the fine layering of the sediments at the scale of centimeters. While the spatial distribution of the major metals, Cu and Zn, has been well established from bulk assays of the cores, little has been known about the trace metal distribution in the Atlantis II sediments. We present detailed trace element data for the different stratigraphic units and reconstruct the sequence of mineralizing processes that led to the observed trace metal zoning in the basin. It has been known for a long time that the precious metals, for example, have high concentrations in some cores and are a potentially important resource in the Atlantis II Deep (e.g., Oudin et al., 1984), but the major controls on Au and Ag enrichment are unknown. The present study provides some of the first insights into the controls on trace metal distribution, detailing the behaviour with respect to the evolution of the basin, the diagenetic history of the sediments, and the zoning with respect to hydrothermal sources. The latter has major implications for understanding brine-pool sedimentation and exploration for mineral deposits thought to have formed in such an environment.

**1.1 Geologic setting and depositional environment**

The Atlantis II Deep is an axial trough situated in the middle of the slowly spreading Red Sea rift, which is opening at a rate of ~1.1 cm/year at this latitude (Cochran and Martinez, 1988). It has a depth of about 2200 m and is surrounded by bathymetric barriers that confine the sediment and brine to one large basin and 4 sub-basins (Fig. 3.1). The current composition of the brine reflects contributions from different sources: Red Sea deep water,

leaching of surrounding Miocene evaporites, and hydrothermal circulation in the underlying basalts and/or normal Red Sea sediments (Schoell and Faber, 1978; Zierenberg and Shanks, 1986; Dupré et al., 1988; Anschutz et al., 1995a; Pierret et al., 2001). The brine pool is interpreted to have developed early in the history of the Deep (Oudin and Cocherie, 1988), prior to the first major hydrothermal activity, which began at least 15,000 years ago (Hackett and Bischoff, 1973; Shanks and Bischoff, 1980).

Hydrothermal fluids at close to black smoker temperatures (~350°C: Zierenberg and Shanks, 1983; Oudin et al., 1984; Ramboz et al., 1988; Missack et al., 1989) are circulated through the sedimentary succession and underlying mid-ocean ridge basalt (MORB), resulting in exchange of elements with surrounding strata before venting into the brine pool (Shanks and Bischoff, 1977; Pottorf and Barnes, 1983 and ref. therein; Cole, 1988). The exact composition of the hydrothermal fluid is not known (see e.g., Anschutz et al., 1995; Blanc et al., 1995; Anschutz and Blanc, 1995a, 1996) but is clearly influenced by interaction with both Miocene evaporites in the sedimentary strata (Dupré et al., 1988) and the basaltic basement rocks (Pottorf and Barnes, 1983). Salinities up to 32 wt.% NaCl have been measured in fluid inclusions in vein anhydrite (Oudin et al., 1984; Ramboz et al., 1988). These salinities are about 5-10 times higher than in any other modern seafloor hydrothermal system (Von Damm, 1990; Douville et al., 1999).

Figure 3.2 shows a schematic cross section through the present-day Atlantis II Deep sediments and brine pool. The deepest part of the brine pool is metal-rich, anoxic, devoid of

reduced sulfur, hot (68.3°C when last measured in 2008: Swift et al., 2012) and extremely saline (~28 wt.% NaCl). This Lower Brine has a mean thickness of ~76 m (Anschutz et al., 1998) and is ~135 m thick at the deepest parts in the Southwest Basin. It is overlain by a number of cooler brine layers (2-5 layers ranging in temperature from ~57°C to 43°C, according to different authors: e.g., Swift et al., 2012) that are more oxidized and less saline and together have a combined thickness of ~50 m (hereafter collectively referred to as the Upper Brine). Metals are enriched in the brine pool by hydrothermal input, but the exact locations of the present-day hydrothermal venting are not known. According to epigenetic features (e.g., anhydrite veining in sediment cores: Zierenberg and Shanks, 1983), historical Cu and Zn assay data (Fig. 3.1; see also Bertram et al., 2011), pore water chemistry (Henricks et al., 1969; Anschutz et al., 2000), and the chemistry of the brine pool itself (Hartmann, 1973), current hydrothermal input is thought to be localized mainly within the central part of the Southwest Basin.

In contrast to MOR hydrothermal systems, where most of the metals are dispersed to the open ocean and are deposited from plumes many kilometers away from the vent sites (Baker et al., 1985), metals from venting in the Atlantis II Deep are efficiently deposited in the sediments at the bottom of the brine pool (Bignell et al., 1976; Gurvich, 2006). Other major influences on the compositions of the sediments include background Red Sea sedimentation (i.e., biogenic pelagic and siliciclastic detrital input), scavenging from seawater (i.e., elements transported into the Deep by surface-active particles), deposition from non-hydrothermal brines that originate from the surrounding evaporites, and

diagenetic enrichment (Fig. 3.2). Fe and Mn are precipitated from the brines as various oxides and hydroxides (hereafter referred to collectively as Mn- and Fe-OOH). Although deposition of metals such as Cu and Zn is highly efficient, the abundance of Fe-OOH minerals as well as sedimentation from other sources dilute the base and precious metal grades compared to mineral deposits formed at open ocean hydrothermal vents. Although the grades of the deposits are different, the bulk metal ratios (Fe:Zn:Cu) in the Atlantis II sediment (~10:1:0.3) are similar to those of MOR black smokers fluids (Von Damm, 1990).

Before the beginning of hydrothermal activity in the Atlantis II Deep, the composition of the brine was likely similar to brine pools in other deeps in the Red Sea (e.g., Hartmann et al., 1998). These deeps have a number of characteristics typical of well-studied anoxic basins in the global oceans (e.g., Cariaco Trench: Jacobs et al., 1987; Tyro and Bannock Basins: De Lange et al., 1990; Framvaren Fjord: Yao and Millero, 1995). The water bodies in the deeps are typically at ambient temperatures, variably saline, and often euxinic owing to the action of sulfate-reducing bacteria. In the Atlantis II Deep, hydrothermal activity started to change the composition of the brine ~15,000 years ago (Shanks and Bischoff, 1980) and has continued to do so until the present time. Recent changes in the salinity, temperature, and layering of the brine pool are discussed in Ramboz and Danis (1990), Blanc and Anschutz (1995), Anschutz and Blanc (1996), Anschutz et al. (1998), and Swift et al. (2012). Below, we examine how some of these changes have affected the trace metal distribution in the underlying metalliferous sediments at the scale of stratigraphic units (representing

thousands of years of sedimentation) down to individual laminae (e.g., approximately annual based on sedimentation rates of ~1 m/Ka or ~1 mm/year: Table 3.1).

**1.2 Sediment stratigraphy**

The stratigraphy of the Atlantis II Deep sediments was defined by Bäcker and Richter (1973), who distinguished 5 units based on studies of 78 sedimentary cores (Table 3.1). The different units range from 1 to 12 meters in thickness and reflect major changes in the bulk mineralogy. Variations in the physical properties of the sediment (e.g., color, grain size) are closely linked to these chemical differences but also reflect a gradual decrease in pore-water content down stratigraphy. Changes in the intensity and location of hydrothermal activity over time also have influenced the major chemical differences between units. According to the compositions of the oldest sediments, venting was initially located in the northeast part of the Atlantis II Deep but is now centered in the Southwest Basin (Bäcker and Richter, 1973).

The lowermost stratigraphic unit, referred to as the detrital oxidic pyritic unit (DOP) started to form ~25,000 years ago (Ku et al., 1969) and is composed mostly of a mixture of biogenic pelagic and siliciclastic detrital material with rare clasts of basalt (Chase, 1969; Stoffers and Ross, 1974; Anschutz and Blanc, 1995c). Fe-oxyhydroxide- and manganite-bearing layers and disseminated sulfides are present and become more abundant up stratigraphy, recording the beginning of hydrothermal activity in the Atlantis II Deep. The DOP unit is overlain by the first sulfidic unit (SU1), which was deposited during the period when

hydrothermal venting was located in the northeast part of the Deep (Fig. 3.1: Bäcker and Richter, 1973). The DOP and SU1 are absent (or at least inaccessible due to intrusion of a basaltic sill) in the central part of the Southwest Basin. SU1 comprises clays (e.g., montmorillonite, nontronite), oxides and hydroxides, carbonates, anhydrite, rare barite and abundant sulfides (Bischoff, 1969; Bäcker and Richter, 1973; Pottorf and Barnes, 1983). The top of SU1 is marked by a rather sharp interface with the overlying central oxidic (CO) unit, which consists mainly of amorphous to well-crystallized oxides and hydroxides of Mn and Fe, carbonates, and locally abundant anhydrite; minor disseminated sulfides are also present. The formation of the CO unit records a time of intense tectonic activity, during which the location of the vent source shifted to the Southwest Basin (Bäcker and Richter, 1973). The brine pool was more oxidized at this time, as evidenced by precipitation of Mn-OOH on the bottom of the Deep. Manganese is part of the "stock" of metals in the brine pool, accumulated over time when the pool is reduced and then deposited at times when it is more oxidized. Presently Mn is precipitated only at the flanks of the Deep where the anoxic Lower Brine is absent and the more oxic Upper Brine directly overlies the seafloor (Hartmann, 1985). Hydrothermal sedimentation (composed of various Mn- and Fe-OOH minerals) was greatest during the formation of the CO unit, but little Cu, Zn or reduced sulfide species were deposited, implying that low-temperature hydrothermal venting was dominant.

Deposition of the CO unit was terminated by the outbreak of hydrothermal activity in the Southwest Basin and the beginning of formation of the second sulfidic unit (SU2). Sulfides

are less common in SU2 than in SU1, and the concentrations of Cu and Zn, as well as the Cu/Zn ratio, are lower (Blanc et al., 1998; Gurvich, 2006). Fe-OOH and anhydrite found at the base of SU2 gradually give way to Fe- and Mn-carbonates (±anhydrite) up stratigraphy and finally to abundant sulfides. The ratio of Cu/Zn and total metals to sulfur in the sediment also increase upwards within this unit. The topmost unit, referred to as the amorphous silicic unit (AM), is composed mainly of poorly crystalline Si-Fe-OOH phases. The AM unit is separated from SU2, almost basin-wide, by a bright orange lepidocrocite horizon (Bäcker and Richter, 1973) that is interpreted to have formed during down-welling of an oxidized brine sourced from outside the Deep (Taitel-Goldman et al., 2002). Where the lepidocrocite horizon is absent, the transition between SU2 and AM is gradational. Mineralogically, the AM unit resembles the CO unit (i.e., dominated by various Si-Fe-OOH compounds that were likely precursors for more crystalline oxides in CO; Taitel-Goldman and Singer, 2001, 2002), but it is saturated with brine (up to 95 wt.%) and has higher metal contents (e.g., Gurvich, 2006). Blanc et al. (1998) considered the AM unit to be a continuation of SU2 due to the similarity in bulk composition.

Each of the stratigraphic units consists of many beds and fine layers that range from centimeters to millimeters in thickness. A number of subunits (e.g., SAM, SOAN, OAN, COS: Table 3.1) are also recognized. Laurila et al. (2014) showed that some chemical differences between individual layers are much greater than between different stratigraphic units. The transitions are commonly very sharp, implying that these small-scale changes in sedimentation were abrupt.

## 2. Sampling and Methods

For this study, one hundred samples were taken from 9 brine-saturated sediment cores collected in the southern 2/3 of the Deep (Fig. 3.1). All cores were collected during the *R/V Valdivia* cruise 29 in 1980. After recovery, the cores were split, with one half being sealed in plastic wrap and stored in a cool (max. 15°C) warehouse. When reopened in 2010, the archived cores were in excellent condition and still moist, although the cut surfaces were in many cases encrusted with salt and had a thin layer of surface oxidation. This crystalline salt and surface oxidation were removed before logging and sampling.

Most of the cores are from >2100 m depth (cores 495 and 546 are from 2076 and 2013 m, respectively) and are 5 to ~12 m long. The locations of samples in each core and the boundaries of stratigraphic units (according to original core logging directly after recovery) are shown in Figure 3.3. The analyzed samples come from all 5 lithostratigraphic units and were selected to study the geochemical differences between sedimentary layer types as well as spatial variations across the Deep. After re-logging, samples were collected using <2 cm-diameter minicores; in some cases samples were cut from the core box with a spatula. This sampling is more detailed than in most previous studies of the Atlantis II cores (e.g., Henricks et al., 1969; Bäcker and Richter, 1973; Steinkamp and Schumann, 1974; Shanks and Bischoff, 1980) that used composite samples of up to several 10s of cm in length, combining many layers. Our samples were dried at 40°C, during which pore water was evaporated and the salt preserved. After drying, all samples contained variable amounts of

salt (from a few up to 70 wt.% based on Na concentrations). This also contrasts with earlier studies in which samples were washed and filtered to remove salt before chemical analyses. Dry samples were pulverized in an agate ball mill, and the powders were dissolved in HF-$HNO_3$-HCl-$HClO_4$ in a multi-step bench-top procedure at the University of Kiel, described in Garbe-Schönberg (1993). Analysis of the major elements was by ICP-OES (SpectroCiros SOP); trace elements were analyzed by ICP-MS (Agilent 7500cs). Additional chemical data were obtained from Activation Laboratories, Ancaster, Ontario, by ICP-OES and ICP-MS after fusion of the samples with sodium-peroxide and total dissolution of the fused sample. Some elements were also determined at Activation Laboratories by instrumental neutron activation analysis (INAA) and various single-element techniques. Special attention was paid to the possibility of interferences in the ICP analyses due to the high salt content of the samples. All samples were diluted to 50 ml solutions (a factor of 500 times), resulting in final salt concentrations in solution of <0.1%, thus minimizing any interferences. Possible interferences were calculated from actual formation rates in synthetic solutions analyzed with each sample batch and the measured values were corrected accordingly. We also directly compared the analytical results by ICP-MS to instrumental analysis of the same samples by neutron activation, which showed no statistically significant differences for elements prone to interferences by ICP. Details of the methods used for each element are given in Appendix 3.1.

The major element and trace metal data are reported in Table 3.2, recalculated to “salt-free” compositions using the sodium concentration as a proxy for the amount of NaCl and

assuming all Na is bound to halite. Sulfur is reported as sulfate sulfur and reduced sulfur (calculated from total sulfur and sulfate). Because some sulfate has undoubtedly originated from oxidation of sulfide during core storage (see below), the amount of reduced sulfur is a minimum value and the sulfate a maximum. None of the samples contained significant organic carbon, thus only carbonate carbon is reported in Table 3.2. Data for 25 elements are reported in Table 3.2; data for 53 elements are given in Appendix 3.1. Complete REE data were previously reported in Laurila et al. (2014).

## 3. Results

### 3.1 Classification of sample types

The samples in this study can be classified according to 3 main types (carbonate-rich, sulfate-rich, and clay-rich) based on core logging, previously published data on the mineralogy of the cores, and bulk chemical compositions (Fig. 3.4). Carbonate-rich samples that contain mostly biogenic carbonate are interpreted to be largely detrital in origin. These samples also contain abundant $Al_2O_3$ in aluminosilicates, which are also detrital. The $SO_4$-rich samples are anhydrite-rich but may also contain abundant secondary sulfates that were originally present in the cores as sulfides. Both the anhydrite and the sulfides were formed by hydrothermal activity, but much of the sulfide has since oxidized to sulfate; therefore, all sulfate in the samples is attributed to hydrothermal deposition. Gypsum content is minor (e.g., Zierenberg and Shanks, 1983). The clay-rich samples plot in the lower left of Figure 3.4A because they contain neither abundant $CO_3$ nor $SO_4$ (Table 3.2); they are not particularly Ca-rich, although the clay fraction may contain Ca (Fig. 3.4B). Many of the clay-

rich samples and carbonate-rich samples are also Fe-rich (Fig. 3.4C), which reflects the abundance of Fe-(oxy)hydroxides in the samples but also the presence of both Fe-rich clays (e.g., nontronite) and Fe-bearing carbonates. Laurila et al. (2014) previously noted from a study of REE that the detrital input is greatest in Al-rich samples, and the hydrothermal input is greatest in non-ferrous base metal- and sulfur-rich samples. Carbonate- and clay-rich samples were mainly formed during stages of low hydrothermal activity and/or distal to the vents, whereas sulfate-rich samples could only have been formed proximal to the vents where anhydrite (and sulfide) precipitation was caused by nearby hydrothermal activity.

Most samples nearest to the $SO_4$ corner of Figure 3.4A (n=52) contain, on average, >4 times more non-ferrous base metals than the other sample types. These samples are further classified according to their metal and sulfide contents into high sulfide, high metal samples (HSHM); low sulfide, high metal samples (LSHM); high sulfide, low metal samples (HSLM) and low sulfide, low metal samples (LSLM). Because of the different forms of sulfur now in the sediments, we use a "base metal sulfide index", hereafter referred to as BMI (=Cu*2+Zn+Pb in moles), rather than reduced S to estimate the hydrothermal component in our samples. BMI is equivalent to the amount of sulfur that would be needed to bind all the non-ferrous base metals in the sample as common sulfide minerals (chalcopyrite, sphalerite and galena). Pyrite is not included in BMI because the proportion of Fe in sulfides versus oxides cannot be estimated. Some of the pyrite has formed by direct hydrothermal precipitation in the sediments and is recognized by its euhedral shape, whereas other pyrite

in the samples formed diagenetically and therefore is not directly related to hydrothermal activity (e.g., Pottorf and Barnes, 1983). Thirty-four samples were classified as having high metal contents, with BMI values >0.4 mol/kg. Twenty-nine of these samples have sulfide contents >0.1 mol/kg and are referred to as high-sulfide, high-metal type (HSHM); four have much lower sulfide contents (<0.1 mol/kg) and are referred to as low-sulfide, high-metal type (LSHM). Thirteen samples were classified as having low metal contents, with BMI values <0.4 mol/kg. Seven of these samples have sulfide contents >0.4 mol/kg and are referred to as high-sulfide, low-metal type (HSLM, dominantly pyritic); the remainder are classified as low-sulfide, low-metal type (LSLM). Six samples that contain >50 wt.% anhydrite were classified as anhydrite samples.

**3.2 Sulfur**

The total sulfur concentrations in our samples vary from 0.25 to 24 wt.% (0.08-7.4 mol/kg); the averages for the different stratigraphic units vary from 1.3 to 7.7 wt.% (0.4-2.4 mol/kg) (Table 3.3). The amount of reduced sulfur remaining in the samples varies from <0.01 to 14 wt.% in individual samples (Table 3.2) and from 0.48 to 2.43 wt.% (0.15-0.76 mol/kg) between stratigraphic units (Table 3.3). The stratigraphic units with high base metal contents (SU1, SU2 and AM; BMI >0.5 mol/kg) have a higher total sulfur content than the units with low base metal contents (CO and DOP; BMI <0.25 mol/kg), but the ratio of reduced/oxidized sulfur is generally lower. This mainly reflects the abundance of anhydrite in proximal hydrothermal samples and also sulfide oxidation during core storage, which was greatest in the samples with high metal contents. On average our samples contain >3 times

more oxidized than reduced sulfur (even if the 6 anhydrite samples are omitted). In 58 out of 100 samples, the molar abundance of $SO_4$ is greater than that of Ca + Ba (locally barium concentrations are up to 1.6 wt.%, but barite accounts for only a small fraction of the total $SO_4$), confirming that other sulfates are present, and in particular metal-sulfates formed during core storage.

### 3.3 Non-ferrous base metals

The concentrations of Cu in individual samples range from 45 to 26200 ppm (Table 3.2), with average concentrations in different stratigraphic units ranging from 0.23 to 1.0 wt.% (Table 3.3). SU1 has the highest concentration of Cu (~1.0 wt.%), but AM is almost as rich (0.9 wt.%). Samples from SU2 contain ~0.5 wt.% Cu, and the units DOP and CO contain ~0.25 wt.%. The concentrations of Zn in individual samples range from 250 to 146,000 ppm, with average concentrations in different units from 0.7 to 3.2 wt.%. The AM unit, SU1 and SU2 are the most Zn rich (3.2 wt.%, 2.7 wt.% and 2.3 wt.%, respectively). The sulfide- and metal-poor unit, CO, has the highest Cu/Zn ratio (0.36), and Cu/Zn ratios increase up-section with increasing hydrothermal influence (i.e., from DOP to SU1 and to CO and from SU2 to AM; Table 3.3). The concentrations of Pb in individual samples range from 0.5 to 3400 ppm, with average concentrations in different units from 0.02 to 0.12 wt.%. Average Pb concentrations decrease in the order AM > SU1 > SU2 > CO > DOP, although high values in individual samples have a large influence on the averages.

### 3.4 Trace metals

There is a general co-enrichment of the trace metals in all of the sediments (Figure 3.5; cf. Appendix C.2 for PCA), but they correlate rather poorly with total sulfur, reduced sulfur, and iron due to the abundance of anhydrite (and other sulfates), pyrite, and non-sulfidic Fe-minerals. Certain trace metals are more strongly correlated with each other. Inspection of Figure 3.5 reveals two distinct groups: (1) Hg, Ag, and Cd, which correlate better with Zn, and (2) Mo, As, Ga, and Tl, which correlate well with Cu. Sb is strongly correlated with Ag, Cd and Hg, but also with other elements. Cobalt and Pb are also correlated equally well with both groups. Ni is more strongly correlated with Mo, As, Ga and Tl than with Hg, Ag and Cd. As expected, the predominantly detrital element Cr (Laurila et al., 2014), as well as Ni and V, are enriched in DOP. The AM unit contains the most Sb, Hg, Cd, Pb and Co; SU1 contains the most Mo, As, Ga, Tl, Ni and Au (Table 3.3).

The concentrations of Au in all of the samples range from <2 to 3760 ppb; Ag concentrations range from <0.5 to 850 ppm. However, the precious metals have very different distributions within different stratigraphic units (Table 3.3). Au concentrations are high and rather homogenous within SU1, SU2 and AM (average values of 1.35 ppm, 1.0 ppm and 1.2 ppm Au, respectively). The units with low base metals, CO and DOP, have generally very low concentrations of Au (<0.25 ppm). Ag is highly concentrated in AM (147 ppm), and to a lesser extent in SU1 and SU2 (70 ppm and 51 ppm, respectively), whereas CO and DOP contain only 11 ppm and 16 ppm, respectively.

Figure 3.6 shows the enrichment of trace metals, normalized to BMI, in the AM unit compared to the average of all sedimentary units. The enrichments and depletions in different stratigraphic units relative to each other are shown in Figure 3.7. Ag, Cd and Hg are highly enriched in AM (more than double the concentrations in other units), but Mo, As, Ni and V are depleted. Ag, Cd, Hg and Pb also show decreasing concentration relative to the base metal sulfides from the uppermost to the lowermost units. Mo, As, Ga and Tl show the opposite trend, increasing with depth, particularly in the three upper units. The CO unit is highly enriched in these elements. Co and Sb concentrations are variable, whereas Au concentrations are generally in proportion to base metals in all stratigraphic units (Au/BMI ~1: Figure 3.6 and 3.7). The concentrations of Ni, Cr and V increase relative to base metals down stratigraphy, with the highest concentrations in the low base metal units, CO and DOP, as noted above.

The absolute concentrations of the different trace elements in different sample types are illustrated in Figure 3.8; the relative enrichments are shown in Figure 3.9. Mo, As and Ga are strongly co-enriched in all sample types and show similar enrichment with sulfide content. Hg, Ag, Cd, and Pb are more highly enriched in the metal-rich samples and not necessarily in the high sulfide samples (e.g., LSHM>HSLM, pyritic). HSLM samples, which contain abundant pyrite but low base metals (low BMI values; cf. Pottorf and Barnes, 1983), are enriched in Mo, As, Ga, Au, Tl and Sb (Figure 3.9). LSLM samples are relatively depleted in Hg, Ag and Cd but not As, Au, Tl and Sb, and they are enriched in Mo, Ga and V, mainly in diagenetic pyrite (cf. Pottorf and Barnes, 1983; Missack et al., 1989).

Ni, Cr and V are also enriched in samples with diagenetic pyrite (Figure 3.9), most probably related to episodes of low hydrothermal activity and major input from non-hydrothermal sources (Backer and Richter, 1973; Shanks and Bischoff, 1980). In particular, Ni is interpreted to have a non-hydrothermal source related to biological pathways (see discussion). Cr is brought to the basin by silicic detrital input (see also Laurila et al., 2014). V appears to have been derived mainly from seawater and diagenetically adsorbed by pyrite and phosphorus-bearing detritus, according to its poor correlation with the hydrothermal elements (Fig. 3.5).

**3.5 Proximal versus distal enrichments and depletions**

The vent proximal sediments of the Atlantis II Deep are highly enriched in non-ferrous metals and sulfides due to precipitation directly from the hydrothermal fluids (Table 3.4 and Fig. 3.10). Sediments that are distal to the present-day vent source(s) have lower sulfide and non-ferrous metal concentrations, but relatively more diagenetic pyrite (Sweeney and Kaplan, 1973; Pottorf and Barnes, 1983). The latter is evidence for non-hydrothermal source(s) of reduced sulfur in the distal part of the Deep (cf. Zierenberg and Shanks, 1988). In the vent proximal sediments, hydrothermal sulfides formed in vein conduits due to cooling of the hydrothermal fluids from >300°C (Oudin et al., 1984) and also as "plume fallout" from the lower part of the Lower Brine. Today, the Lower Brine is essentially devoid of reduced sulfur but still enriched in dissolved metals (e.g., ~5 ppm Zn and >65 ppm Fe: Manheim, 1974; Anschutz et al., 2000).

Four of the 9 cores selected for this study were taken in the Southwest Basin, close to the inferred location of the presently active hydrothermal vents (within 3 km: Fig. 3.1). Cores taken outside this area are considered to be distal from the current vent source (up to 8 km). When comparing these cores, we excluded samples from units SU1 and DOP, which were either absent or inaccessible in the Southwest Basin due to the intrusion of a basaltic sill. Average concentrations of metals in samples of AM, SU2, and CO in cores from the different parts of the Deep are listed in Table 3.4. Samples from cores taken close to the inferred vent(s) in the Southwest Basin contain on average more sulfur than the samples from the distal part of the Deep (7.1 wt.% S or 2.2 mol/kg versus 3.7 wt.% S or 1.2 mol/kg). Although the calculated amount of reduced sulfur is a minimum value for the original sulfide content of the samples, the ratio of reduced sulfur to total sulfur is lower in the proximal part of the Deep (0.18 versus 0.24) due to abundant anhydrite close to the areas of venting.

Except for Cr and V, all of the trace metals correlate positively with Zn and Cu; Mo, As, Ga, Au, Tl, and Sb show a stronger correlation with pyrite content. A comparison of trace metal enrichment in proximal versus distal cores (Fig. 3.11) shows that Hg, Ag, Cd and Pb are enriched relative to the base metals proximal to the vent source (within 3 km), whereas Mo, As and Ga, as well as Ni, Cr and V are enriched relative to the base metals at greater distance from the vents (3-7 km). Figure 3.12 (uppermost panel) shows an unexpected increase in the Cu/Zn ratio of the sediments with distance from the recent vent source,

although at lower Cu and Zn concentrations. Some metals decrease rapidly away from the vent source (e.g., Ag), some more gradually (e.g., As), and some are more widely distributed within the Deep (e.g., Au).

## 4. Discussion

### 4.1 Distribution of reduced sulfur

Most of the non-ferrous metals in the Atlantis II sediments are contained in the sulfide fraction. Shanks and Bischoff (1977) discussed several origins for the abundant sulfides in SU1 and SU2. They noted that the sulfide contents are greatest in proximity to the vent source in all stratigraphic units and appear to correlate with increased brine flux. They argued that the brine flux was an order of magnitude greater during the formation of SU1 and SU2 than it is today. However, if the metal/$H_2S$ ratio of the hydrothermal fluid was the same as it is today (inferred to be high because of the abundance of Fe-OOH and low pyrite content of most of the sediments), there would have been insufficient sulfur to deposit all the metals as sulfides. Shanks and Bischoff (1977, 1980) and Pottorf and Barnes (1983) also considered whether bacterial sulfate reduction could be a more plausible source of reduced sulfur. Shanks and Bischoff (1980) and Simoneit et al. (1987) showed that organic carbon input was higher during the periods of increased hydrothermal activity due to bacterial growth in the Upper Brine. However, bacterial sulfate reduction was deemed unlikely as a major source of sulfide because the $\delta^{34}S$ values of the minerals are typical of hydrothermal sulfides (~5‰) in all metalliferous units (SU1, SU2 and AM), because there is no isotopic difference between sulfate in pore water and the Lower Brine (Kaplan et al., 1969; Pottorf

and Barnes, 1980; Zierenberg and Shanks, 1986), and because bacteria were not found in the sediment or the Lower Brine (Trüper, 1969; Watson and Waterbury, 1969). Other studies concluded that sulfide oxidation rather than sulfate reduction was likely in the Upper Brine and also in the sediment (Kaplan et al., 1969). More recent discoveries of bacterial activity in the sediment (Siam et al., 2012) suggest diagenetic sulfate reduction is an important process and may account for some of the abundant framboidal pyrite in the sediment cores (Chapter 2).

**4.2 Importance of non-sulfidic components**

In previous studies of sediment cores from the Atlantis II Deep, it is clear that many water-soluble compounds were lost because the samples were washed before analysis and many fine particles would have passed the 0.45 μm filters commonly used in those studies (e.g., Steinkamp and Schumann, 1974; Shanks and Bischoff, 1980). Our data, which are from samples that were not washed, allow direct comparison with the older analyses. Particularly interesting are the differences in metal concentrations for the different stratigraphic units. Zn and Cu concentrations are unexpectedly ~50% lower in unwashed samples of SU2 (this study) compared to data for washed samples (summarized in Gurvich, 2006; Appendix 3.2). Zn and Cu concentrations are ~20% lower in our samples of SU1. In contrast, Zn concentrations in the AM unit, which is chemically similar to SU1 and SU2, are ~40% higher in our unwashed samples, and Cu concentrations are ~80% higher. These discrepancies are explained by loss of anhydrite during washing of the samples from SU1 and SU2, evident in the significantly lower Ca contents in the data compiled by Gurvich

(2006) and resulting in higher reported metal grades in these units; whereas samples from AM contained abundant fine particles and water-soluble metallic compounds leading to lower metal concentrations reported in the literature compared to our unwashed samples. The high metal contents of the samples from AM could not have been due to evaporated metal-rich pore water alone, as the Zn and Cu concentrations in the most metal-rich pore water are only 58 ppm and 1 ppm, respectively (Anschutz et al., 2000) and if evaporated would contribute only ~100 ppm of Zn and ~2 ppm of Cu to the metal content of the unwashed muds (in a sample with 50 wt.% NaCl).

Washing of the samples has led to over-estimation of the abundance of insoluble sulfides in the sediments and under-estimation of the non-sulfide metal content, especially in the uppermost cores. A number of different non-sulfidic metallic components have been found in the Atlantis II sediments, including woodruffite [$(Zn,Mn)_2Mn_5O_{12}\cdot 4(H_2O)$], hydrozincite [$Zn_5(CO_3)_2(OH)_6$], Cu-chlorides [e.g., atacamite, $Cu_2Cl(OH)_3$], chrysocolla [$(Cu,Al)_2(HSi_2O_5)(OH)_4\cdot n(H_2O)$], and abundant water-soluble efflorescent salts (Bischoff, 1969; Oudin et al., 1984; Weber-Diefenbach, 1977; Gurvich, 2006; Chapter 2). Much of the metal-rich non-sulfidic component of the sediment is likely secondary. Pottorf and Barnes (1983) examined the cores relatively soon after they were taken and reported sphalerite as the most abundant sulfide mineral. However, after longer core storage, Missack et al. (1989) reported that sphalerite was much less common, probably due to oxidation and dissolution.

The importance of primary non-sulfidic metal compounds in the sediments is less certain. Zn-enrichment in Fe-OOH particles from the Lower Brine (Hartmann, 1973) strongly suggests that Zn (with minor Cu and other trace metals) was deposited in the sediments by adsorption onto poorly crystalline Fe-OOH and Si-Fe-OOH compounds. It has been well documented that Fe-OOH minerals such as ferrihydrite, schwertmannite, and goethite can efficiently scavenge Cu, as well as Zn and Pb, from solutions at pHs similar to the Lower Brine (~5.5), especially in the presence of sulfate (Webster et al., 1998). Ali and Dzombak (1996) attributed this to the formation of surface complexes such as $FeOH{\cdot}CuSO_4$. We suggest that a significant portion of the metals (especially Zn) were similarly scavenged from the brine, and this process accounts for the sharp increase in the metal concentrations of the pore water at the transition from the Lower Brine into the top of the AM unit (Anschutz et al., 2000; Fig. 3.13). During diagenesis metals released from poorly crystalline Si-Fe-OOH compounds were incorporated into non-sulfidic minerals, such as clays and carbonates, where the amount of reduced sulfide was insufficient to precipitate all metals as sulfides. Comparing our analyses of samples from the AM unit to data from previous studies (Gurvich, 2006; Appendix 3.2), it is evident that as much as 30% of the Zn metal might have been present in water-soluble phases or at least very fine-grained particles lost during washing of the samples.

### 4.3 Posible controls on Cu/Zn ratios

The higher Cu/Zn ratio in sediments from the distal part of the Deep (Figs. 3.10 and 3.12) is the opposite of that expected for seafloor hydrothermal systems in which temperature is

the dominant control on Cu and Zn solubility (e.g., Sangster, 1972; Large, 1992; Large et al., 2001; Hannington, 2014). The metal-poor unit, CO, also has a high Cu/Zn ratio (Table 3.3). These observations require copper deposition in the distal part of the Deep and during more oxidized conditions in the brine pool, or higher rates of Zn than Cu precipitation (both sulfidic and non-sulfidic) in proximity to the vents, as noted above.

Direct measurements in the Lower Brine (Hartmann, 1985 and references therein; Anschutz et al., 2000; Pierret et al., 2001) show significant variability in Cu concentration (e.g., ~0.2 ppm in 1966, 0.03 ppm in 1971 and 1976, ~0.001 ppm in 1977, 0.005 ppm in 1985 and 0.24 ppm in 1992), while the concentration of Zn has remained rather constant (2.0-5.3 ppm). The higher Cu concentrations in 1966 and 1992 may reflect pulses of higher-temperature venting, which are recorded as higher Cu/Zn ratios in the distal sediments. However, precipitation of Cu-sulfides in the distal sediments requires a source of reduced sulfur. Some of the reduced sulfur may be supplied by sulfate-reducing bacteria living at the chemocline and in the Upper Brine (Trüper, 1969). This is proportionately more important in the distal rather than proximal part of the Deep. An alternative explanation for the high Cu/Zn ratios may be that metal complexing in the distal part of the basin is somehow different from that controlling Cu and Zn solubility in open ocean hydrothermal systems (i.e., dominantly as chloride complexes), although this seems unlikely given the high salinity of the brine. The high (Cu+Zn)/S ratio of sediments to the northeast of the current location of hydrothermal venting (Fig. 3.10), suggests another possible explanation for the high Cu/Zn ratios of these sediments. A number of authors (e.g., Webster et al., 1998) have

shown that adsorption of Cu to Fe-OOH is more efficient than adsorption of Zn, which could lead to high Cu/Zn ratios in sediments formed by non-sulfide deposition of metals. It is noteworthy that cores from shallower water depths (546, 495) are especially rich in Cu, possibly because the brine interface (at ~2000 m depth), where Fe-OOH formation mainly occurs, is much closer to the seafloor.

### 4.4 Pathways of enrichment of trace metals

Trace metal distribution in the sediments of the Atlantis II Deep is controlled by three main processes: (1) cooling of hydrothermal fluids below the seafloor and during venting into the brine pool; (2) adsorption onto surface-active particles, in particular Si-Fe-(oxy)hydroxides, and deposition from the brine pool; (3) incorporation into diagenetic sulfides (Fig. 3.14). Although the deep hydrothermal fluids have never been sampled, most authors agree that by far the most important source of trace metals in the brine and sediment is the hydrothermal venting (Shanks and Bischoff, 1977; Pottorf and Barnes, 1983; Gurvich, 2006). Proximal to the inferred vents, metals are deposited with sulfides and on surface-active particles – the latter then incorporated into diagenetically forming (mainly Zn and Cu) sulfides – as indicated by the strong correlations between different trace metals and Cu and Zn in the sediments and the behaviour of metals in the pore waters (e.g., Anschutz et al., 2000). Because the Lower Brine has high concentrations of dissolved metals but low reduced sulfur, adsorption by non-sulfide particles in the brine pool is particularly important (e.g., Hartmann, 1973, 1985). Deposition of surface-active particles at the bottom of the brine pool and release of metals from the poorly crystalline phases causes

the uppermost sedimentary pore water to become highly enriched in Cu and Zn relative to the Lower Brine (Fig. 3.13).

A sharp decrease in the Si concentration of the pore fluids during early diagenesis is interpreted to reflect the formation of clays and other minerals that crystallize out of the Si-Fe-(oxy)hydroxide gels (Anschutz and Blanc, 1995b). The breakdown of Fe-(oxy)hydroxides also increases the concentration of Fe and the Eh of the pore fluid, which may promote the formation of clays (cf. Decarreau and Bonnin, 1986). The high concentrations of metals in pore water near the surface of the sediment decrease abruptly within ~5 m of burial (Fig. 3.13). Dissolved Cu decreases rapidly, incorporated in insoluble sulfides, whereas Zn and Cd decrease more gradually in accordance with mineral solubility. Zn-rich carbonates (Oudin et al., 1984; Chapter 2) and metal-bearing clays (e.g., Bischoff, 1972; Singer and Stoffers, 1987; Cole, 1988; Chapter 2; see also Hein et al., 1979; Schlegel and Manceau, 2006) also formed during burial, although Brockamp et al. (1978) interpreted the high metal contents in clay-rich samples as mixtures of clays and amorphous sulfides. Thus, diagenetic transformation of non-sulfidic particles to sulfides is considered to have played an important role in the generation of sulfides in the sulfidic units compared to the AM unit, consistent with mineral textures in SU2 that are indicative of diagenetic growth (e.g., Pottorf and Barnes, 1983; Blanc et al., 1998; Chapter 2.).

Proximal to the inferred vents, especially in the most recent sediments (AM), Cd, Ag, Hg (± Sb) are deposited with Zn in sulfides and also incorporated into diagenetically forming Zn-

rich minerals (Fig. 3.6). Pb is also deposited basin-wide with sulfides, in proportion to Zn and Cu, but at low concentrations compared to mineral deposits associated with mid-ocean ridge hydrothermal systems (e.g., Hannington et al., 2005). Whereas sphalerite and chalcopyrite are common in the vent proximal environment, pyrite is the dominant sulfide in the distal part of the Deep. Close to the vents, it commonly occurs as sub- to euhedral grains (e.g., Pottorf and Barnes, 1983; Oudin et al., 1984; Missack et al., 1989); in the more distal sediments, the pyrite is typically framboidal, consistent with diagenetic growth (Sweeney and Kaplan, 1973; Berner, 1984). The euhedral pyrite has low trace metal concentrations, whereas diagenetic pyrite is commonly enriched in Mo, As, and Ga (e.g., Fig. 3.8). The enrichment of these elements, relative to base metals, also increases with depth in the three uppermost units due to continued adsorption by pyrite (Fig. 3.7). Au and Tl are deposited mainly with sulfides close to the vent source but also appear to have been adsorbed by pyrite in distal sediments, suggested by the strong correlation with Mo, As and Ga (Fig. 3.5). This is similar to the observed co-enrichment of Au and Tl in diagenetic pyrite associated with many sediment-hosted ore deposits (e.g., Fleet and Mumin, 1997; Emsbo et al., 1999; Graham et al., 2009; Large et al., 2013).

Other trace elements that are enriched in the samples dominated by detrital components (e.g., Ni, Cr, V in clay- and $CO_3$-rich samples) are poorly correlated with hydrothermal elements (Fig. 3.5) and are interpreted to have been at least partly enriched via non-hydrothermal pathways. These elements cluster in Figure 3.6 along the lower dotted line. Although Ni correlates with the hydrothermal elements better than V and Cr, the low total

Ni concentration (typically less than contemporaneous pelagic sediments: Chester and Hughes, 1967) and relative enrichment in the clay-rich and $CO_3$-rich samples (Fig. 3.9) as well in the DOP (Fig. 3.7) suggest that hydrothermal sources of Ni have not been important. Whereas Cr is mostly detrital (Laurila et al., 2014), Ni and V may have been partly transported from seawater into the Lower Brine via Fe- or Mn-OOH cycling at the chemoclines (cf. Berrang and Grill, 1974; Trefry and Metz, 1989; Calvert and Pedersen, 1993). These elements are present in the lowermost oxic-pyritic unit, which formed before the hydrothermal venting commenced, and in this unit represent background elements enriched from seawater. Ni, Cr and V also form organo-metallic complexes and may have had a biological pathway into the basin. Oceanic phytoplankton that enters the Deep with background sedimentation is a major bioconcentrator for Ni ($10^3$-$10^4$ enrichment relative to seawater and containing up to 10 ppm Ni: Wang and Wood, 1984) and may be a significant source of Ni in the Atlantis II Deep. As the organic matter breaks down in the Lower Brine, the Ni is adsorbed onto Fe-(oxy)hydroxides and eventually sulfides (cf. Rose and Bianchi-Mosquera, 1993). This would have been especially important in the earliest brines, which likely had a higher pH and Eh (inferred from mineralogy and REE concentrations: Blanc et al., 1998; Laurila et al., 2014), and may explain the high Ni content of the lowermost units (Table 3.3). V was also apparently incorporated in phosphorus-bearing pelagic detritus (e.g., Emerson and Huested, 1991), evidenced by the correlation between V and P (Fig. 3.5). Once deposited, the Ni and V were likely incorporated into diagenetic pyrite, as in black shales (e.g., Large et al., 2013). Mo and As also were likely enriched by this pathway. The correlation between Cu and Ni (Fig. 3.5) suggests that some of the processes contributing to

high Cu/Zn ratios in distal sediments may also be involved in Ni deposition. In contrast to Ni, Co shows a much closer relationship to the hydrothermal components of the sediments (Figs. 3.5 and 3.6; cf. Manheim and Lane-Bostwick, 1988).

Figure 3.15, which shows the distribution of trace metals in the AM unit, illustrates how metals are currently being deposited from the brine pool. The plot compares the enrichments and depletions of elements in AM relative to other units (i.e., normalized to the base metal sulfide index, BMI=Cu*2+Zn+Pb, in the whole strata) and relative to distance from the vent source(s). The plotted values for Ag show that it is enriched in AM compared to all other strata and also enriched in the most proximal cores, whereas Mo is relatively depleted in AM compared to other strata and enriched in distal cores. Proximal to the vent source(s) and especially in AM, the deposition of trace metals is dominated by Zn and Cu sulfides as well as non-sulfides, whereas in the distal cores trace metal enrichment is mainly controlled by pyrite. The different pathways of removal of metal from the Lower Brine appear to control the trace metal distribution throughout the Atlantis II Deep.

**4.5 Links to the evolution of the Deep**

The non-ferrous base metal contents of the sediments are complexly related to episodes of high-temperature hydrothermal activity (DOP to SU1 and SU2 to AM), the amount of reduced sulfur in the brine pool, and to changes in the Eh and pH of the brine. The upper part of the lowermost unit (DOP) marks the beginning of hydrothermal activity (a in Fig. 3.16) where pyrite is abundant and later sphalerite appears (Bäcker and Richter, 1973).

Sedimentation during the initial hydrothermal activity was characterized by high $S_{red}$/metal, linked to production of reduced sulfide by bacterial sulfate reduction (Shanks and Bischoff, 1980). At this stage, all metals introduced to the brine by hydrothermal venting were efficiently precipitated as sulfides (cf. Jacobs et al., 1987; Lyons and Severmann, 2006). During SU1 formation (b to c in Fig. 3.16) more metals than reduced sulfur were introduced into the brine, causing the decrease in the $S_{red}$/metal ratio of the sediments. By the end of SU1, the initial reservoir of $H_2S$ in the brine pool was exhausted, the Lower Brine had become completely anoxic, and there was no significant bacterial activity in the Lower Brine (similar to the current conditions).

Despite the waning hydrothermal activity during the formation of CO (Shanks and Biscoff, 1980), precipitation of abundant Fe- and Mn-OOH from the brine pool resulted in the highest mass accumulation rates in the history of the Deep (Table 3.1). The unexpectedly high Cu/Zn ratios in CO were possibly related to pulses of higher-temperature hydrothermal venting (Pottorf and Barnes, 1983). The transition from CO to SU2 and the outbreak of renewed hydrothermal activity in the Southwest (d in Fig. 3.16) was marked by basin-wide precipitation of sphalerite (Blanc et al., 1998). A low Cu/Zn ratio in these sediments is interpreted to be due to Cu precipitation below the seafloor during the initial stages of hydrothermal activity and higher concentrations of Zn in the hydrothermal fluids reaching the seafloor. As the conduits became sealed, the Cu/Zn ratio of the fluid that reached the brine pool increased and this is reflected in the composition of the sediment (from d to the present day in Fig. 3.16).

The evolution of the brine pool also played a role in the distribution of certain trace metals in the sediments. Non-hydrothermal sources of trace metals were most important during the formation of DOP (elements from background sedimentation) and CO (elements from seawater). Increased solubility of metals such as Hg, Ag, and Cd during formation of the CO unit (possibly due to higher $fO_2$ and pH) may have resulted in diffusive release of these metals from the brine pool and deposition away from the Atlantis II Deep (e.g., Bignell, 1976). In contrast, enrichment of As and Ga in the CO unit (Fig. 3.7) appears to reflect increasing efficiency of adsorption onto Si-Fe-OOH with increasing pH (e.g., Pierce and Moore, 1982). Periods of enhanced hydrothermal activity (SU2, SU1, and AM) were dominated by efficient co-deposition of trace metals with sulfides. As the stock of reduced sulfur was exhausted at the end of SU1 and SU2 (Fig. 3.16), metal deposition was mainly by adsorption onto non-sulfidic particles.

**4.6 Mass balances of metals**

The Atlantis II Deep represents a unique opportunity to assess the balances between hydrothermal metal fluxes and sediment deposition in a brine pool environment. The known metals in the Atlantis II Deep, which include an established resource of 1.89 Mt Zn, 0.43 Mt Cu, 3750 t Ag, and 47 t Au (Guney et al., 1988), accumulated over a period of about 15,000 yrs, implying a mass flux of at least 125 t/yr Zn, 28 t/yr Cu, 250 kg/yr Ag and 3 kg/yr Au. The standing pool of Zn in the Lower Brine (~4 $km^3$= ~4 Bt) is about 20,000 tons (based on a concentration of ~5 ppm Zn: Manheim, 1974; Anschutz et al. 2000), which is ~1% of the total Zn contained in the sediments. Some trace metals, such as Pb, have high solubility

in the Lower Brine (as much as 4.9 ppm in some samples of pore fluid: Anschutz et al., 2000). If we assume that the concentration of Pb in the brine pool is no more than 0.6 ppm (one of the lowest measured concentrations: Manheim, 1974), the Lower Brine would contain ~2500 t of Pb, which is about 30% of the total Pb content of the sediments (~8,000 t: Bischoff and Manheim, 1969). Some of this Pb may be lost by diffusion through the chemocline into seawater (cf. Bignell, 1976). Ni and Co concentrations are also high in the Lower Brine (0.4 and 0.16 ppm, respectively: Manheim, 1974), representing as much as ~50% of the total Ni and ~8% of the total Co in the Deep (assuming the 90 Mt of bulk sediment has Ni and Co grades similar to the average of all samples in this study, 36 and 91 ppm, respectively).

Most other trace and precious metal concentrations in the Lower Brine are not known, but the high concentrations in the sediment suggest that they are rather efficiently deposited. If we assume 100% efficiency of deposition in the metalliferous sediments and a hydrothermal flux of brine equivalent to that estimated from heat balances (~670 kg/s: Anschutz and Blanc, 1996) we can estimate a minimum concentration for many of these trace metals in the high-temperature hydrothermal fluids. Most of the Zn, Cu, Ag and Au in the sediments (1.89 Mt Zn, 0.43 Mt Cu, 3750 t Ag, and 47 t Au) are contained in the metal-rich units SU1, SU2 and AM that were deposited during approximately 9,000 years of hydrothermal activity (Table 3.1). Therefore, at least ~0.2 Mt of Zn was deposited per 1,000 years, requiring a hydrothermal fluid that contained at least 11 ppm Zn. The concentrations of Cu, Ag and Au would have been 2.4 ppm Cu, 21 ppb Ag and 0.26 ppb Au, which are

remarkably close to the concentrations in black smoker fluids at MORs (e.g., Von Damm, 1990, and estimated concentrations of Au from Hannington et al., 1999). However, considering the high salinity of the Atlantis II brine, the calculated concentrations of metals are rather low and the total metals-to-sulfur ratio likely very high. This contrasts with black smoker fluids, in which the ratio of metals to reduced sulfur is ~1:1.

## 5. Summary and Conclusions

A careful re-examination of metalliferous sediment in archived cores from the Atlantis II Deep has provided a better understanding of possible controls on metal deposition in anoxic and sulfide-deficient brine-pool settings. Valuable metals from the hydrothermal activity in the Atlantis II Deep have been efficiently deposited during periods of high hydrothermal activity and venting into the anoxic brine pool. These episodes have alternated with periods of absent or low-temperature hydrothermal activity, which were characterized by background sedimentation or Fe- and Mn-OOH deposition, respectively. Considerable variation in the deposition of metals is related to processes taking place in the brine pool during its evolution (e.g., Fig. 3.14 and 3.15), including cooling of hydrothermal fluids close to the vents, either in the fluid conduits or in the particle plume, and adsorption onto surface-active Si-Fe-OOH particles. Zn and Cu deposition has been most important close to the hydrothermal vent source(s), and includes both sulfide deposition and deposition by adsorption onto abundant non-sulfidic particles. An unexpected increase in the Cu/Zn ratio of the sediments with distance from the vent source(s) may reflect pulses of higher-temperature venting and increased Cu fluxes to the brine pool or more efficient

adsorption of Cu to Fe-OOH particles in the distal brine. Most trace metals precipitate from the cooling of hydrothermal fluids in proximity to the vents, notably Ag, Cd, and Hg, which are incorporated in vent-proximal Cu and Zn sulfides. Mo, As, and Ga also appear to be adsorbed directly from the pore water by diagenetically forming pyrite, including in the more distal sediments. Elements that have a number of different precipitation pathways (e.g., Au, Sb, Tl), as well as elements that have a high concentration in the brine (e.g., Pb), are widely distributed within the Deep (Fig. 3.14).

Newly deposited particles are rapidly recrystallized during initial burial (within a few meters, or few thousand years). Proximal to the vent source, where pore water is highly enriched in metals such as Zn, diagenetically forming sulfides, including sphalerite, incorporate trace metals such as Cd and Hg. In the more distal sediments, pyrite is the main diagenetically forming sulfide and has a high affinity for trace metals such as As, Mo, Ga, Tl and Au. Reduced sulfur needed for diagenetic sulfide formation is largely from the hydrothermal source; farther from the vents, it is produced by chemical or bacterial reduction of pore water sulfate, or it might be brought into the system from other non-hydrothermal sources (e.g., cold brines that reacted with black shales in the surrounding strata: Pottorf and Barnes, 1983). After about 5 meters of burial, metal concentrations in the modern pore water are generally below those in the Lower Brine (Fig. 3.13: Anschutz et al., 2000).

The metalliferous sediments of the Atlantis II Deep have been considered a modern analog of a variety of stratabound ore deposits, in particular sedimentary exhalative massive sulfide deposits (SEDEX) and some volcanic-hosted massive sulfide (VMS) deposits. Typical models of brine pool-type deposits consider that the brine pool was mainly a trap for exhaling metals, resulting in broadly uniform deposition of all metals in the sediments (e.g., Solomon et al., 2004; Tornos et al., 2008; Goodfellow and Lydon, 2007). However, analysis of trace metal zoning in the Atlantis II sediments shows considerable variation related to processes taking place in the brine pool. Co-deposition of Zn with primary Si-Fe-OOH particles also is recognized as a major process in the sulfide-deficient brine pool of the Atlantis II Deep and may have implications for the formation of some important stratiform Zn oxide-silicate deposits (e.g., Johnson and Skinner, 2003).

## References


Ali, M. A. and Dzombak, D. A., 1996, Interactions of copper, organic acids, and sulfate in goethite suspensions. *Geochim. Cosmochim. Acta* 60, p. 5045-5053.

Anschutz, P. and Blanc, G., 1995a, Chemical mass balances in metalliferous deposits from the Atlantis II Deep (Red Sea). *Geochim. Cosmochim. Acta* 59, p. 4205-4218.

Anschutz, P. and Blanc, G., 1995b, Geochemical dynamics of the Atlantis II Deep (Red Sea): silica behavior. *Mar. Geol.* 128, p. 25-36

Anschutz, P. and Blanc, G., 1995c, Diagenetic evolution of the DOP facies from the Atlantis II Deep (Red Sea): evidence of early hydrothermal activity. *Oceanol. Acta* 18, p. 105-112.

Anschutz, P. and Blanc, G., 1996, Heat and salt fluxes in the Atlantis II Deep (Red Sea). *Earth Planet. Sci. Lett.* 142, p. 147-159.

Anschutz, P. and Blanc, G., Stille, P., 1995, Origin of fluids and the evolution of the Atlantis II deep hydrothermal system, Red Sea: Strontium isotope study. *Geochim. Cosmochim. Acta* 59, p. 4799-4808.

Anschutz, P., Turner, J. S. and Blanc, G., 1998, The development of layering, fluxes through double-diffusive interfaces, and location of hydrothermal sources of brines in the Atlantis II Deep: Red Sea. *Jour. Geophys. Res.* 103, p. 27809-27819.

Anschutz, P., Blank, G., Monnin, C. and Boulècue, J., 2000, Geochemical dynamics of the Atlantis II Deep (Red Sea): II. Composition of metalliferous sediment pore waters: *Geochim. Cosmochim. Acta* 64, p. 3995-4006.

Baker E. T., Lavelle, J. W. and Massoth, G. J., 1985, Hydrothermal particle plumes over the southern Juan de Fuca Ridge. *Nature* 316, p. 342-344.

Berner, R. A., 1984, Sedimentary pyrite formation: An update. *Geochim. Cosmochim. Acta* 48, p. 605-615.

Berrang, P. G. and Grill, E. V., 1974, The effect of manganese oxide scavenging on molybdenum in Saanich Inlet, British Columbia. *Mar. Chem*. 2, p. 125-148.

Bertram, C., Krätschell, A., O'Brien, K., Brückmann, W., Proelss, A. and Rehdanz, K., 2011, Metalliferous sediments in the Atlantis II Deep - Assessing the geological and economic resource potential and legal constraints. *Res. Policy* 36, p. 315-329.

Bignell, R. D., Cronan, D. S. and Tooms, J. S., 1976, Metal dispersion in the Red Sea as an aid to marine geochemical exploration. *Inst. Mining Metall. Trans*. 84 (B), p. 274-278.

Bischoff, J. L., 1969, Red Sea geothermal brine deposits: their mineralogy, chemistry and genesis, *in* Degens, E. T. and Ross, D. A., eds., *Hot Brines and Recent Heavy Metal Deposits in the Red Sea*, Springer-Verlag, New York, p. 368-406.

Bischoff, J. L., 1972, A ferroan nontronite from the Red Sea geothermal system. *Clays Clay Miner.* 20, p. 217-223.

Bischoff, J. L. and Manheim, F. T., 1969, Economic potential of the Red Sea heavy metal deposit, *in* Degens, E. T. and Ross, D. A., eds., *Hot Brines and Recent Heavy Metal Deposits in the Red Sea*, Springer-Verlag, New York, p. 535-541.

Blanc, G. and Anschutz, P., 1995, New hydrographic situation in the Atlantis II Deep hydrothermal brine system. *Geology* 23, p. 543-546.

Blanc G., Boulègue J. and Michard A., 1995, Isotope compositions of the Red Sea hydrothermal end-member. *C. R. Acad. Sci*. 320, p. 1187-1193.

Blanc, G., Anschutz, P. and Pierret, M-C., 1998, Metalliferous sedimentation in the Atlantis II Deep: a geochemical insight, *in* Purser, B. H. and Bosence D. W. J., eds., *Sedimentation and Tectonics in Rift Basins: Red Sea – Gulf of Aden.* Chapman & Hall, London, p. 505-520.

Brockamp, O., Goulart, E., Harder, H. and Heydemann, A., 1978, Amorphous copper and zinc sulfides in the metalliferous sediments of the Red Sea. *Contr. Mineral. Petrol.* 68, p. 85-88.

Bäcker, H. and Richter, H., 1973, Die rezente hydrothermal-seidimentärelagerstätte Atlantis II-tier im Roten Meer. *Geol. Rundsch.* 62, p. 697-740.

Calvert, S. E. and Pedersen, T. F., 1993, Geochemistry of Recent oxic and anoxic marine sediments: Implications for the geological record, *in* Parkes, R. J., Westbroek, P. and de Leeuw, J. W., eds., *Marine Sediments, Burial, Pore Water Chemistry, Microbiology and Diagenesis*. Mar. Geol. 113, p. 67-88.

Chase, R. L., 1969, Basalt from the axial trough of the Red Sea, *in* Degens, E. T. and Ross, D. A., eds., *Hot Brines and Recent Heavy Metal Deposits in the Red Sea*, Springer-Verlag, New York, p. 122-128.

Chester, R. and Hughes, M. J., 1967, A chemical technique for the separation of ferro-manganese minerals, carbonate minerals and adsorbed trace elements from pelagic sediments. *Chem. Geol.* 2, p. 249-262.

Cochran, J. R. and Martinez, F., 1988, Evidence from the northern Red Sea on the transition from continental to oceanic rifting, *in* Le Pichon, X. and Cochran, J. R., eds., *The Gulf of Suez and Red Sea Rifting*. Tectonophysics 153, p. 25-53.

Cole, T. G., 1988, The nature and origin of smectite in the Atlantis II Deep, Red Sea. *Can. Mineral.* 26, p. 755-763.

De Lange, G. J., Middelburg, J. J., van der Weijden, C. H., Catalano, G., Luther, G. W., III, Hydes, D. J., Woittiez, J. R. W. and Klinkhammer, G. P., 1990, Composition of anoxic hypersaline brines in the Tyro and Bannock Basins, eastern Mediterranean. *Mar. Chem.* 31, p. 63-88.

Decarreau, A. and Bonnin, D., 1986, Synthesis and crystallogenesis at low temperature of Fe(III)-smectites by evolution of coprecipitated gels: experiments in partially reducing conditions. *Clay Miner*. 20, p. 861-877.

Degens, E. T. and Ross, D. A., 1969, *Hot Brines and Recent Heavy Metal Deposits in the Red Sea*. Springer-Verlag Inc., New York, 600 p.

Douville, E., Bienvenu, P., Charlou, J. L., Donval, J. P. Fouquet, Y., Appriou, P. and Gamo, T., 1999, Yttrium and rare earth elements in fluids from various deep-sea hydrothermal systems. *Geochim. Cosmochim. Acta* 63, p. 627-643.

Dupré, B., Blanc, G., Boulègue, J. and Allègre, J., 1988, Metal remobilization at a spreading centre studied using lead isotopes. *Nature* 333, p. 165-167.

Emerson, S. R. and Huested, S. S., 1991, Ocean anoxia and the concentrations of molybdenum and vanadium in seawater. *Mar. Chem*. 34, p. 177-196.

Emsbo, P., Hutchinson, R. W., Hofstra, A., Volk, J. A, Bettles, K. H., Baschuk, G. J. and Johnson, C. A., 1999, Syngenetic Au on the Carlin trend: Implications for Carlin-type deposits. *Geology* 27, p. 59-62.

Fleet, M. E. and Mumin, A. H., 1997, Gold-bearing arsenian pyrite and marcasite and arsenopyrite from Carlin trend gold deposits and laboratory synthesis. *Am. Mineral.* 82, p. 182-193.

Garbe-Schönberg, D., 1993, Simultaneous determination of thirty-seven trace elements in twenty-eight international rock standards by ICP-MS. *Geostand. Newslett*. 17, p. 81-97.

Goodfellow, W. D. and Lydon, J. W., 2007, Sedimentary exhalative (SEDEX) deposits, *in* Goodfellow, W. D., ed., *Mineral deposits of Canada: A synthesis of major deposit types, district metallogeny, the evolution of geological provinces, and exploration methods*. Geol. Assoc. Can., Spec. Publ. 5, p. 163-183.

Graham, G. E., Kelley, K. D., Slack, J. F. and Koenig, A. E., 2009, Trace elements in Zn–Pb–Ag deposits and related stream sediments, Brooks Range Alaska, with implications for Tl as a pathfinder element. *Geochem. Explor. Environ. Analysis* 9, p. 19-37.

Guney, M., Al-Marhoun, M. A. and Nawab, Z. A., 1988, Metalliferous sub-marine sediments of the Atlantis II – Deep, Red Sea. *CIM Bulletin* 81, p. 33-39.

Gurvich, E. G., 2006, *Metalliferous Sediments of the World Ocean: Fundamental Theory of Deep-Sea Hydrothermal Sedimentation.* Springer, Heidelberg, 423 p.

Hackett, J. and Bischoff, J. L., 1973, New data on the stratigraphy, extent, and geologic history of the red sea geothermal deposits. *Econ. Geol.* 68, p. 553-564.

Hannington, M. D., 2014, Volcanogenic Massive Sulfide Deposits, *in* Scott, S. D., ed., Chapter 13.18, *The Geochemistry of Ore Deposits*, *in* Holland, H. D. and Turekian, K. K., eds., *Treatise on Geochemistry* 28, Elsevier-Pergamon, Oxford, p. 463-488.

Hannington, M. D., de Ronde, C. E. J. and Petersen, S., 2005, Modern sea-floor tectonics and submarine hydrothermal systems, *in* Hedenquist, J. F., Thompson, J. F. H., Goldfarb, R. J. and Richards, J. P., eds., 100th Anniversary Volume of Econ. Geol., p. 111-142.

Hannington, M. D., Poulsen, H., Thompson, J. and Sillitoe, R., 1999, Volcanogenic gold and epithermal- style mineralization in the VMS environment, *in* Barrie, C. T. and Hannington, M. D., eds., *Volcanic Associated Massive Sulfide Deposits: Processes and Examples in Modern and Ancient Settings*. Rev. Econ. Geol. 8, p. 325-356.

Hartmann, M., 1973, Untersuchungen von suspendiertem Material in den Hydrothermallaugen des Atlantis-II-Tiefs. *Geol. Rundsch.* 62, p. 742-754.

Hartmann, M., 1985, Atlantis-II-Deep geothermal brine system: Chemical processes between hydrothermal brines and Red Sea deep water. *Mar. Geol.* 64, p. 157-177.

Hartmann, M., Scholten, J. C., Stoffers, P. and Wehner, F., 1998, Hydrographic structure of brine-filled deeps in the Red Sea – new results from the Shaban, Kebrit, Atlantis II, and Discovery Deep. *Mar. Geol*. 144, p. 311-330.

Hein, J. R., Ross, C. R. and Yeh, H., 1979, Mineralogy and diagenesis of surface sediments from Domes area A, B and C, *in* Bischoff, J. L. and Piper, D. Z., eds., *Marine Geology and Oceanography of the Pacific Manganese Nodule Province*. Plenum, New York, p. 365-396.

Hendricks, R.L., Reisbick, F.B., Mahaffey, E.J., Roberts, D.B. and Peterson, M.N.A., 1969, Chemical composition of sediments and interstitial brines from the Atlantis II, Discovery and Chain Deeps, *in* Degens, E. T. and Ross, D. A., eds., *Hot Brines and Recent Heavy Metal Deposits in the Red Sea*, Springer-Verlag, New York, p. 407-440.

Jacobs, L., Emerson, S. and Huested, S. S., 1987, Trace metal geochemistry in the Cariaco Trench. *Deep Sea Res*. 34, p. 965-981.

Johnson, C. A. and Skinner, B. J., 2003, Geochemistry of the Furnace magnetite bed, Franklin, New Jersey, and the relationship between stratiform iron oxide ores and stratiform zinc oxide-silicate ores in the New Jersey Highlands. *Econ. Geol*. 98, p. 837-854.

Kaplan, I. R., Sweeney, R. E. and Nissenbaum, A., 1969, Sulfur isotope studies on Red Sea geothermal brines and sediments *in* Degens, E. T. and Ross, D. A., eds., *Hot Brines and Recent Heavy Metal Deposits in the Red Sea*, Springer-Verlag, New York, p. 474-498.

Ku, T. L., Thurber, D. L. and Mathieu, G. G., 1969, Radiocarbon chronology of Red Sea sediments, *in* Degens, E. T. and Ross, D. A., eds., *Hot Brines and Recent Heavy Metal Deposits in the Red Sea*, Springer-Verlag, New York, p. 348-359.

Large, R. R., 1992, Australian volcanic-hosted massive sulfide deposits: features, styles, and genetic models. *Econ. Geol.* 87, p. 471-510.

Large, R. R., Bodon, S., Davidson, G. J. and Cooke, D., 1996, The chemistry of BHT ore formation – one of the keys to understanding the difference between SEDEX and BHT deposits, *in* Pongratz, J. and Davidson, G. J., eds., *New Developments in Broken Hill Type Deposits*. Proceedings of a Workshop Held at CODES, University of Tasmania, July 1996, p. 105-111.

Large, R. R., McPhie, J., Gemmell, J. B., Herrmann, W. and Davidson, G. J., 2001, The spectrum of ore deposit types, volcanic environments, alteration halos, and related exploration vectors in submarine volcanic successions: Some examples from Australia. *Econ. Geol.* 96, p. 913-938.

Large, R. R., Meffre, S., Burnett, R., Guy, B., Bull, S., Gilbert, S., Goemann, K. and Danyushevsky, L., 2013, Evidence for an intrabasinal source and multiple concentration processes in the formation of the Carbon Leader Reef, Witwatersrand Supergroup, South Africa. *Econ. Geol.* 108, p. 1215-1241.

Laurila, T. E., Hannington, M. D., Petersen, S. and Garbe-Schönberg, D., 2014, Early depositional history of metalliferous sediments in the Atlantis II Deep of the Red Sea: Evidence from rare earth element geochemistry. *Geochim. Cosmochim. Acta* 126, p. 146-168.

Lyons, T. W. and Severmann, S., 2006, A critical look at iron paleoredox proxies: New insights from modern euxinic marine basins. *Geochim. Cosmochim. Acta* 70, p. 5698-5722.

Manheim, F. T., 1974, Red Sea geochemistry (ch. 38), *in* Whitmarsh, R. B., Weser, O. E., Ross, D. A., et al*., Initial Reports of the Deep Sea Drilling Project,* v. 23, Washington (U.S. Government Printing Office) p. 975-998.

Manheim, F. T. and Lane-Bostwick, C. M., 1988, Cobalt in ferromanganese crusts as a monitor of hydrothermal discharge on the Pacific sea floor. *Nature* 335, p. 59-62.

Miller, A. R., Densmore, C. D., Degens, E. T., Hathaway, J. C., Manheim, F. T., McFarlin, P. F., Pocklington, R. and Jokela A., 1966, Hot brines and recent iron deposits in deeps of the Red Sea. *Geochim. Cosmochim. Acta* 30, p. 341-359.

Missack, E., Stoffers, P. and El Goresy, A., 1989, Mineralogy, parageneses, and phase relations of copper-iron sulfides in the Atlantis II Deep, Red Sea. *Mineral. Deposita* 24, p. 82-91.

Ohmoto, H., Watanabe, Y., Yamaguchi, K. E., Naraoka, H., Haruna, M., Kakegawa, T., Hayashi, K. and Kato, Y., 2006, Chemical and Biological Evolution of Early Earth: Constraints from Banded Iron Formations, *in* Kesler, S. E. and Ohmoto, H., eds., *Evolution of Early Earth's Atmosphere, Hydrosphere, and Biosphere – Constraints from Ore Deposits*. Geol. Soc. Amer. Memoir 198, p. 291-331.

Oudin, E., 1987, Trace element and precious metal concentrations in East Pacific Rise, Cyprus and Red Sea submarine sulfide deposits, *in* Teleki, P. G., Dobson, M. R., Moore, J. R. and Stackelberg, U., eds., *Marine Minerals: Advances in Research and Resource Assessment strategies.* Proceedings of the NATO Advanced Research Workshop, Series C 194, p. 349-362.

Oudin, E. and Cocherie, A., 1988, Fish debris record the hydrothermal activity in the Atlantis II Deep sediments (Red Sea). *Geochim. Cosmochim. Acta* 52, p. 177-184.

Oudin, E., Thisse, Y. and Ramboz, C., 1984, Fluid inclusion and mineralogical evidence for high temperature saline hydrothermal circulation in the Red Sea metalliferous sediments: Preliminary results. *Mar. Mining* 5, p. 3-31.

Pierce, M. L. and Moore, C. B., 1982, Adsorption of arsenite and arsenate on amorphous iron hydroxide. *Water Res.* 16, p. 1247-1253.

Pierret, M. C., Clauer, N., Bosch, D., Blanc, G. and France-Lanord, C., 2001, Chemical and isotopic ($^{87}Sr/^{86}Sr$, $\delta^{18}O$, $\delta D$) constraints to the formation processes of Red-Sea brines. *Geochim. Cosmochim. Acta* 65, p. 1259-1275.

Pottorf, R. J. and Barnes, H. L., 1983, Mineralogy, geochemistry, and ore genesis of hydrothermal sediments from the Atlantis II Deep, Red Sea. *Econ. Geol. Monograph* 5, p. 198-223.

Ramboz, C. and Danis, M., 1990, Superheating in the Red Sea? The heat-mass balance of the Atlantis II Deep revisited. *Earth Planet. Sci. Lett.* 97, p. 190-210.

Ramboz, C., Oudin, E. and Thisse, Y., 1988, Geyser-type discharge in Atlantis II Deep, Red Sea: Evidence of boiling from fluid inclusions in epigenetic anhydrite. *Can. Mineral.* 26, p. 765-786.

Rose, A. W. and Bianchi-Mosquera, G. C., 1993, Adsorption of Cu, Pb, Zn, Co, Ni, and Ag on goethite and hematite: A control on metal mobilization from red beds into stratiform copper deposits. *Econ. Geol*. 88, p. 1226-1236.

Sangster, D. F., 1972, Precambrian volcanogenic massive sulphide deposits in Canada: A review. *Canada Geol. Survey Paper* 72-22, 44 p.

Schlegel M. L. and Manceau A., 2006, Evidence for the nucleation and epitaxial growth of Zn phyllosilicate on montmorillonite. *Geochim. Cosmochim. Acta* 70, p. 901-917.

Schoell, M. and Faber, E., 1978, New isotopic evidence for the origin of Red Sea brines. *Nature* 275, p. 436-438.

Shanks, W. C. and Bischoff, J. L., 1977, Ore transport and deposition in the Red Sea geothermal system: a geochemical model. *Geochim. Cosmochim. Acta* 41, p. 1507-1519.

Shanks, W. C. and Bischoff, J. L., 1980, Geochemistry, sulfur isotope composition and accumulation rates of Red Sea geothermal deposits. *Econ. Geol*. 75, p. 445-459.

Siam, R., Mustafa, G. A., Sharaf, H., Moustafa, A., Ramadan, A. R., Antunes, A., Bajic, V. B., Stingl, U., Marsis, N. G. R., Coolen, M. J. L., Sogin, M., Ferreira, A. J. S. and Dorry, H. E., 2012, Unique prokaryotic consortia in geochemically distinct sediments from Red Sea Atlantis II and Discovery Deep brine pools. *PLoS ONE 7* (8), e42872.

Simoneit, B. R. T., Grimalt, J. O., Hayes, J. M. and Hartman, H., 1987, Low temperature hydrothermal maturation of organic matter in sediments from the Atlantis II Deep, Red Sea. *Geochim. Cosmochim. Acta* 51, p. 879-894.

Singer, A. and Stoffers, P., 1987, Mineralogy of a hydrothermal sequence in a core from the Atlantis II Deep, Red Sea. *Clay Miner*. 22, p. 251-267.

Solomon, M., Tornos, F., Large, R. R., Badham, J. N. P., Both, R. A. and Zaw, K., 2004, Zn-Pb-Cu volcanic-hosted massive sulphide deposits: criteria for distinguishing brine pool-type from black smoker-type sulphide deposition. *Ore Geol. Rev*. 25, p. 259-283.

Steinkamp, K. and Schumann, D., 1974, The Chemical Composition of Sediment Cores Recovered During Valdivia Cruises VA01 and VA03 from the Atlantis II Deep (Red Sea): Unpublished Cruise Report 1.11.1974, Series CL, Preussag, Hannover, 155 p.

Stoffers, P. and Ross, D. A., 1974, Sedimentary history of the Red Sea, (ch. 23), *in* Whitmarsh, R. B., Weser, O. E., Ross, D. A., *et al*., *Initial Reports of the Deep Sea Drilling Project*, v. 23, Washington (U.S. Government Printing Office) p. 849-865.

Sweeney, R. E. and Kaplan, I. R., 1973, Pyrite framboid formation: Laboratory synthesis and marine sediments. *Econ. Geol*. 68, p. 618-634.

Swift, A., Bower, A. S. and Schmitt, R., 2012, Vertical, horizontal, and temporal changes in temperature in the Atlantis II and Discovery hot brine pools, Red Sea. *Deep Sea Res.* 64, p. 118-128.

Taitel-Goldman, N. and Singer, A., 2001, High-resolution transmission electron microscopy study of newly formed sediments in the Atlantis II Deep, Red Sea. *Clay Clay Miner.* 49, p. 174-182.

Taitel-Goldman, N. and Singer, A., 2002, Metastable Si-Fe phases in hydrothermal sediments of Atlantis II Deep: Red Sea. *Clay Miner*. 37, p. 235-248.

Taitel-Goldman, N., Koch, C. B. and Singer, A., 2002, Lepidocrocite in hydrothermal sediments of the Atlantis II and Thetis Deeps, Red Sea. *Clay Clay Miner*. 50, p. 186-197.

Tornos, F., Solomon, M., Conde, C. and Spiro, B. F., 2008, Formation of the Tharsis massive sulfide deposit, Iberian Pyrite Belt: Geological, lithogeochemical, and stable isotope evidence for deposition in a brine pool. *Econ. Geol.* 103, p. 185-214.

Trefry, J. H. and Metz, S., 1989, Role of hydrothermal precipitates in geochemical cycling of vanadium. *Nature* 342, p. 531-533.

Trüper, H. G., 1969, Bacterial sulfate reduction in the Red Sea hot brines, *in* Degens, E. T. and Ross, D. A., eds., *Hot Brines and Recent Heavy Metal Deposits in the Red Sea*, Springer-Verlag, New York, p. 263-271.

Von Damm, K. L., 1990, Seafloor hydrothermal activity; black smoker chemistry and chimneys. *Annu. Rev. Earth Planet. Sci.* 18, p. 173-204.

Wang, H.-K. and Wood, J. M., 1984, Bioaccumulation of nickel by algae. *Environ. Sci. Technol.* 18, p. 106-109.

Watson, S. W. and Waterbury, J. B., 1969, The Sterile Hot Brines of the Red Sea, *in* Degens, E. T. and Ross, D. A., eds., *Hot Brines and Recent Heavy Metal Deposits in the Red Sea*, Springer-Verlag, New York, p. 272-281.

Weber-Diefenbach, K., 1977, Geochemistry and diagenesis of recent heavy metal ore deposits at the Atlantis II Deep (Red Sea), *in* Klemm, D. D. and Schneider, H. J., eds., *Time and Strata-bound Ore Deposits*. Springer-Verlag, Berlin, p. 419-436.

Webster, J. G., Swedlund, P. J. and Webster, K. S., 1998, Trace metal absorption onto an acid mine drainage iron (III) oxy hydroxy sulfate. *Environ. Sci. Technol.* 32, p. 1361-1368.

Yao, W. and Millero, F. J., 1995, The chemistry of the anoxic waters in the Framvaren Fjord, Norway. *Aq. Chem.* 1, p. 53-88.

Zierenberg, R. A. and Shanks, W. C., 1983, Mineralogy and geochemistry of epigenetic features in metalliferous sediments, Atlantis II Deep, Red Sea. *Econ. Geol*. 78, p. 57-72.

Zierenberg, R. A. and Shanks, W. C., 1986, Isotopic constraints on the origin of the Atlantis II, Suakin and Valdivia brines, Red Sea. *Geochim. Cosmochim. Acta* 50, p. 2205-2214.

Zierenberg, R. A. and Shanks, W. C., 1988, Isotopic studies of epigenetic features in metalliferous sediment, Atlantis II Deep, Red Sea. *Can. Mineral.* 26, p. 737-753.

## Figure Captions

Figure 3.1. Location of the Atlantis II Deep in the Red Sea rift axis. On the left, the sub-basins are indicated. Sediment cores are indicated by the numbers; the blue line is a fence of cores used to examine metal zonation within the basin. The location of the inferred present-day hydrothermal vent source(s) (proximal part of the Deep) is delineated by whole-core bulk concentrations of Zn >2.5 wt.% in all units. Contoured data are averages of all metal assays in each of 497 cores (salt-free, based on washed core samples: unpublished data from the MESEDA I-III projects; Bertram et al., 2011). The cores varied in length from <1 to 20 m and thus represent variable parts of the stratigraphy; the lower stratigraphic units are missing in the SW Basin. Four of the 9 cores selected for this study are within 3 km of the inferred location of the presently active hydrothermal vents and referred to as proximal; cores outside this area (up to 8 km from the current vent source) are referred to as distal.

Figure 3.2. Schematic cross-section through the Atlantis II Deep sediments and brine pool. The present thickness of the sedimentary strata is about 20 m, and the sediments are overlain by about 200 m of brine (modified after Pottorf and Barnes, 1983, and Zierenberg and Shanks, 1988). Metals and other elements in the brines have four main sources: S1) background sedimentation that brings biogenic pelagic and detrital silicic material into the Deep; S2) hot hydrothermal brines formed by seawater circulation through evaporites and underlying basalts; S3) cold, near-bottom brines that enter the Deep from dissolution of evaporites (their exact contribution to the element budget is not known); S4) seawater.

Elements from seawater are brought into the Deep via Mn- and Fe-OOH precipitation-dissolution cycling through the chemocline. By far most of the metals in the brine and sediment are derived from hot hydrothermal fluids. Metals precipitate out of these fluids according to four different pathways: P1) in sub-seafloor veins and conduits as high-temperature sulfides and anhydrite; P2) as sulfide particles in plume fallout; P3) adsorbed onto non-sufidic particles that settle through the Lower Brine; P4) as diagenetic sulfides. The basin has a width of 5 km; the bottom of the Deep is at approximately 2200 m depth and the transition from the Lower Brine to the upper brines is at 2050 m.

Figure 3.3. Sample distribution in the 9 cores used for this study. The core number is indicated above the stratigraphic column, and core locations are indicated in Figure 3.1. Numbers inside the columns are sampling depths in cm below the top of the core. Colors of the sections reflect different stratigraphic units (details in Table 3.1). The SAM, SOAN and OAN units are most commonly found in the Southwest Basin, whereas the SU1 and DOP units are missing in the central part of the Southwest Basin due to the presence of a basaltic sill in this part of the Deep. The CO and COS units are found basin-wide.

Figure 3.4. Classification of the Atlantis II Deep sediments according to major metal and nonmetal contents. The samples considered in this study comprise three main types identified during core logging, from previously published data on the mineralogy of the sediments, and their bulk chemical compositions. The carbonate-rich samples contain mostly biogenic detrital carbonate and detrital aluminosilicates (A). The sulfate-rich

samples contain mostly anhydrite but may also contain abundant secondary sulfates that were originally present in the cores as sulfides. Reduced sulfur (i.e., sulfur remaining in the samples as sulfides) was calculated from total sulfur minus sulfate sulfur (B). Although the calculated sulfide contents are minimum values, because of oxidation to sulfate, they generally match the published mineralogy of the cores and our own re-logging. The clay-rich samples plot in the lower left of (A) because they contain neither abundant $CO_3$ nor $SO_4$; they are not particularly Ca-rich, although the clay fraction may contain Ca (B). Many of the clay-rich samples and carbonate-rich samples are Fe-rich (C), which reflects the abundance of Fe-(oxy)hydroxides and also the presence of both Fe-rich clays (e.g., nontronite) and Fe-bearing carbonates. In B, the non-ferrous base metal contents of the samples are expressed as Cu*2+Zn+Pb in moles (BMI, equivalent to the amount of sulfur needed to bind all the non-ferrous base metals in the sample as common the sulfide minerals, chalcopyrite, sphalerite and galena). Samples with high metal contents (BMI values >0.4 mol/kg) are subdivided into high-sulfide, high-metal type (HSHM) and low-sulfide, high-metal type (LSHM) (Table 3.2). Samples with low metal contents (BMI values <0.4 mol/kg) are subdivided into high-sulfide, low-metal type (HSLM) and low-sulfide, low-metal type (LSLM). Six samples that contain >50 wt.% anhydrite were classified as anhydrite samples. The compositions of the different samples types are plotted in moles. (Al*2+Ca+Fe)*7 is a proxy for detrital components, anhydrite, and Fe-oxyhydroxides. (Cu*2+Zn+Pb)*15 and (Cu+Zn+Pb*10+Cd*100) are examples of different proxies for nonferrous sulfides. Different scalars are applied for ease of visualization.

Figure 3.5. Pearson correlation coefficients (r) for major and trace elements in all 100 samples considered in this study. Values for dominantly hydrothermal elements are grouped in the lower panel; values for other elements are in the upper panel. $S_{ox}$=Sulfate sulfur, $S_{red}$=Sulfide sulfur ($S_{tot}$ minus $S_{ox}$). Correlations with r >0.5 (r2 >0.25) are significant at 99% confidence. Element pairs that are not shown have r <0.4 (=r2<0.16). Values of the Pearson correlation coefficient for all element pairs are listed in Appendix 3.3. Results for principal component analysis are given in Appendix C.2.

Figure 3.6. Plot of trace metal enrichment in samples from the AM unit compared to the average of all stratigraphic units. $TM_{AM}$ refers to the average concentration of the metal in the AM unit (Y-axis); $TM_{Average}$ is the average concentration for all stratigraphic units (X-axis). BMI is the corresponding base metal sulfide index (BMI=Cu*2+Zn+Pb in moles). The plot shows that elements like Ag, Cd and Hg are highly enriched in AM, whereas Ni, Mo and As are depleted compared to other stratigraphic units. Elements dominantly sourced from hydrothermal fluids cluster along the upper dotted line; elements mainly associated with the non-hydrothermal sources plot along the lower dotted line.

Figure 3.7. Relative enrichments and depletions of selected trace metals (normalized to the base metal sulfide index: BMI=Cu*2+Zn+Pb in moles) in the different stratigraphic units. $TM_{Unit}$ refers to the average concentration of the metal in all samples from the unit; $BMI_{Unit}$ is the average base metal index for the unit. $TM_{Average}$ is the average concentration of the metal in all stratigraphic units; $BMI_{Average}$ is the base metal index for all stratigraphic units.

Mo, As and Ga show a trend of increasing concentration relative to the base metal sulfides from AM to CO, reflecting uptake into diagenetically growing pyrite. Hg, Ag, and Cd show a trend of decreasing concentration relative to base metal sulfides from AM to lower units reflecting mainly primary deposition with surface active particles in AM (and subsequent diagenetic incorporation to sulfides). Ni, Cr, and V show a trend of increasing concentration with depth and are highly enriched in the units with lower hydrothermal influence (CO and DOP), especially in the lowermost DOP. The plotted data are given in Appendix 3.4.

Figure 3.8 A) Average concentrations of trace metals in different sample types from all stratigraphic units. Some elements are scaled by a factor of 10 for clarity. Mo, As and Ga are strongly co-enriched in pyritic samples (i.e., HSLM samples defined in the text). Au, Tl, and Sb show co-enrichment in both pyritic and high-metal samples (i.e., Cu- and Zn-rich HSHM and LSHM samples defined in the text). Hg, Ag, Cd, Pb and Co show the highest concentrations in the high metal samples. The boxes and whiskers show the average (dashed line), 25th and 75th percentiles, and minimum and maximum values for each element. B) Absolute concentrations of trace metals in different sample types from all stratigraphic units (some elements are scaled by a factor of 10 for clarity). Mo, As and Ga are strongly co-enriched in all samples types, with the highest concentrations in the high-sulfur samples. Au, Tl, and Sb show co-enrichment in both high-sulfur and high-metal samples. Hg, Ag, Cd, and Pb are distributed unevenly between different sample types, with the highest concentrations in the high metal samples. Ni, Cr, and V are associated with

background sedimentation and are enriched in the detrital- and pyrite-dominated samples. Co distribution resembles that of both detrital and hydrothermal elements.

Figure 3.9. A) Relative enrichments and depletions of selected trace metals in the different sample types from all stratigraphic units (normalized to the base metal sulfide index: BMI=Cu*2+Zn+Pb in moles). $TM_{Sample}$ refers to the average concentration of the metal in all samples of the respective sample type; $BMI_{Sample}$ is the average base metal index for the sample type. $TM_{Average}$ is the average concentration of the metal in all sample types; $BMI_{Average}$ is the base metal index for all sample types. The construction is similar to Figure 3.7. Because pyrite is not considered in the BMI, the enrichment of trace metals in the HSLM samples is exaggerated. As seen in Figure 3.7, Mo, As, Ga, and Au, Tl and Sb behave very differently from Hg, As, Cd and Pb, reflecting their removal from the brine pool by different processes responsible for the formation of different sample types. The plotted data are given in Appendix 3.4. B) Plot showing the degree of correlation between the concentrations of different trace metals, the abundance of pyrite (Chapter 3.2.), and the concentrations of Zn and Cu in all samples. All of the trace metals, except Cr and V, correlate positively with concentrations of Zn and Cu, due to their common (hydrothermal) source, and especially those elements that are deposited proximal to the vent source (Hg, Ag, Cd, Pb). Other trace metals (Mo, As, Ga, Au, Tl, Sb) show a stronger correlation with pyrite, which is more abundant distal to the vent source.

Figure 3.10. Maps of the Atlantis II Deep showing the distribution of Zn, Cu, Ag, Cu/Zn, $S_{red}$, (Cu+Zn)/S, CaO, $CO_2$, and Fe/Mn in 453 selected cores of the three uppermost sedimentary units (AM, SU2, CO). The contoured area corresponds to that shown in Figure 3.1; contoured data are average values of all samples taken at 1-m intervals in each core. The assays are based on salt-free, washed core samples (unpublished data from the MESEDA I-III projects and Bertram et al., 2011); $S_{red}$ is acid-soluble sulfide. Zn, Cu, Ag and $S_{red}$ are all enriched in the SW, close to the location of the inferred vents. (Cu+Zn)/S ratios are highest farther away from the vents, highlighting the importance of non-sulfide deposition of Cu and Zn in the basin. See Appendix A.3 for larger maps of more elements.

Figure 3.11. Relative enrichments and depletions of selected trace metals (normalized to the base metal sulfide index: BMI=Cu*2+Zn+Pb in moles) in all samples from the three uppermost units of the proximal and distal cores. $TM_{Proximal}$ refers to the average concentration of the metal in all samples from all proximal cores (up to 3 km from the inferred vent source: Fig. 3.1); $TM_{Distal}$ refers to the average concentration of the metal in all samples from all distal cores (3-7 km). The relative enrichments are obtained by dividing average BMI-normalized trace metal concentrations in vent distal cores by BMI-normalized trace metal concentrations in the proximal cores. Values of 1 correspond to equal concentration in proximal and distal cores; values less than 1 correspond to relative enrichment proximal to the vent(s), and values greater than 1 correspond to relative enrichment distal to the vent(s). The plotted data are given in Appendix 3.4.

Figure 3.12. Metal concentrations in the three uppermost units, which are found basin-wide, at different distances from the inferred vent sources in the Southwest Basin (core locations are indicated in Fig. 3.1). Values are averages for sulfur-rich samples ($SO_4$-rich samples in this study, according to Fig. 3.4) and samples from units SU2, SOAN, OAN, SAM from Oudin (1987). Cu/Zn ratios show an unexpected increase with distance from the vent(s), whereas total metal concentrations generally decrease. Silver is mainly deposited in proximity to the vent(s), whereas As is transported further away. High concentrations of Au are found both proximal to and distal to the vent(s).

Figure 3.13. Concentrations of selected elements in pore water in a vent proximal core (683, see Fig. 3.1 for location: after Anschutz et al., 2000; Anschutz and Blanc, 1995b for Si). Concentrations of Fe, K and Sr are given in mmol/l; Si, Pb, Cd, Cu and Zn are in µmol/l. The concentrations of Pb are almost constant in the Lower Brine and pore water, similar to K and Sr. Si concentration decreases by an order of magnitude from the Lower Brine to the uppermost pore water due to the crystallization of clay minerals from poorly crystallized Si-Fe-OOH (cf. Anschutz and Blanc, 1995b; Anschutz et al., 2000). This releases adsorbed metals (e.g., Cu, Zn and Cd) into the pore water resulting in the observed increase in concentrations. A gradual decrease in the pore fluid concentration of metals with depth reflects the formation of stable minerals, most importantly sulfides. Zn concentrations are almost two orders of magnitude higher than Cu; however, Cu shows a more dramatic increase from the brine into the pore water of the uppermost part of AM and a larger decrease in concentration with depth. See text for discussion

Figure 3.14. Summary of different pathways of trace metal enrichment in the sediments of the Atlantis II Deep. Most of the metals in the Deep are from hydrothermal fluids vented into the brine pool, from which deposition may occur in a number of different ways. A portion of almost all trace metals (and the largest proportion of base metals) is precipitated as sulfide by cooling of the hydrothermal fluids either below the seafloor or within the proximal plume. Close to the vents, Zn, Cd, Ag, Hg (± Sb) are also deposited with surface-active particles (mainly Si-Fe-OOH) and then incorporated into diagenetically forming (mainly Zn and Cu) sulfides. At greater distance from the vents, Mo, As, and Ga, in particular, are adsorbed by diagenetically growing pyrite. Cu is also deposited in the distal environment, which partly accounts for the increasing Cu/Zn ratio away from the vents. Co, Ni and Pb have high solubility in the brine (Manheim, 1974; Anschutz et al., 2000), but may be deposited basin-wide with both hydrothermal and diagenetic sulfides. Au, Tl, and Sb are incorporated in sulfides deposited close to the vent source but also in distal pyrite. Mo, and to a much lesser extent some other trace metals such as Ni, are also added to the brine pool and sediments by Fe-Mn-redox cycling across the seawater-brine interface.

Figure 3.15. Deposition of metals from the current brine as reflected in the composition of the AM unit. The plot compares the relative enrichments and depletions of elements in AM compared to other units (normalized to the base metal sulfide index, BMI=Cu*2+Zn+Pb in the whole strata) from Figure 3.6 and the enrichments and depletions with distance from the inferred present-day vent source(s) from Figure 3.11. The plotted values for Ag show

that it is enriched in AM compared to all other strata and also enriched in the most proximal cores. In contrast, Mo is relatively depleted in AM compared to other strata but more enriched in distal cores than in proximal cores. The deposition of trace metals with non-sulfides (common in AM) is more important proximal to the vent source(s), whereas in distal cores trace metals are mainly controlled by pyrite.

Figure 3.16. Summary of the stratigraphic variation in non-ferrous base metals and reduced sulfur in metalliferous sediments of the Atlantis II Deep. The plotted data for sediments are from Table 3.3; data for $S_{red}$ are minimum values, as discussed in the text. The inferred composition of the brine during formation of the corresponding unit (green and grey lines on the right) are according to Kaplan et al. (19690, Shanks and Bischoff (1980) and Blanc et al. (1998), and only given for reference to general evolution of the Atlantis II Deep. The upper part of the lowermost unit (DOP) marks the beginning of hydrothermal activity (a) where pyrite is abundant and later sphalerite appears. Sedimentation during the initial hydrothermal activity was characterized by high $S_{red}$/metal. During SU1 (b to c) more metals than reduced sulfur were introduced into the brine, causing the decrease in the $S_{red}$/metal ratio of the sediments. The transition from CO to SU2 and the outbreak of renewed hydrothermal activity in the Southwest (d) was marked by basin-wide precipitation of Zn. A low Cu/Zn ratio in these sediments is interpreted to be due to Cu precipitation below the seafloor during the initial stages of hydrothermal activity and higher concentrations of Zn in the hydrothermal fluids reaching the seafloor. As the conduits became sealed, the Cu/Zn

ratio of the fluid that reached the brine pool increased and this is reflected in the composition of the sediment (from d to the present day).

Table 3.1. Physical, chemical and mineralogical properties of the stratigraphic units of the Atlantis II metalliferous sediments (modified from Bäcker and Richter, 1973).

| Unit and thickness | Age (Ka) | Sedimentat-ion rate | Mineralogy | Specific enrichment |
|---|---|---|---|---|
| AM (*SAM)* Amorphous-Siliceous 3.5 (1-4) m | last 3.6 | 97 cm/ka ~4,700 t/a tot. 17 Mt | Amorphous Si-Fe-OOH, goethite, Fe-smectite, Mn-siderite; SW basin: sulfides, Fe-oxides, anhydrite; elevated areas: Mn-OOH | Zn, Cd, Ag, Co, Sb |
| Lepidocrocite horizon | | | | |
| SU2 (*SOAN/OAN*) Sulfidic 4 *(*2-12) m | 5.9-3.6 | 174 cm/ka ~8,800 t/a tot. 20 Mt | Sphalerite (common almost everywhere), pyrite (rare), Fe-OOH, green silicates, anhydrite (barite rare), Fe- and Mn-carbonates. | Zn, Pb, As, Cd, Hg, Tl, Ba, Mo, V, Cr |
| Layer of anhydrite | | | | |
| CO *(COS*) Central Oxidic 6 (1-11) m | ~8.6-5.9 | 222 cm/ka ~12,000 t/a tot. 32 Mt | Goethite, rare sulfides, carbonates, Mn-OOH minerals and Mn-oxides, poorly crystalline Fe-OOH, hematite, anhydrite and euhedral magnetite | Mn, Fe, K, Ba, Mo, Rb, Cs; low S |
| Red silicate layers with Fe-oxides | | | | |
| SU1 Sulfidic* 3.8 (1-4) m | ~11.7-8.6 | 123 cm/ka ~5,800 t/a tot. 18 Mt | Fe-clays, red-brown silicates, abundant sulfides: pyrite, chalcopyrite, sphalerite, Mn-siderite, hematite, anhydrite (rare barite) | Si, Cu, Ag, As, S, P, Ni, Tl, W |
| Pyrite much more abundant at the top of DOP than at the bottom | | | | |
| DOP Detrital-Oxidic-Pyritic* 2.5 (1-6) m | ~25-~11.7 | 19 cm/ka | Mixture of detrital-biogenic material with Fe- and Mn-rich layers, pyrite increase up, where sphalerite appears, Fe-OOH, anhydrite, basalt fragments | Ca, Al, Ti, Sr, Cr, Sc, HFSE, Li, Nb, Ta, Th and REEs |

Names in *italics* refer to sub-units, mainly found in the Southwest Basin: SAM= Sulfidic-Amorphous-Siliceous unit; SOAN=Sulfidic-Oxidic-Anhydritic unit; OAN=Oxidic-Anhydritic unit; COS=Central-Oxidic-Siliceous unit. *= Absent in the SW Basin

The ages of the units are from Hackett and Bischoff (1973) and Shanks and Bischoff (1980). Thickness of the units varies spatially depending on depth and distance from the hydrothermal vent source; averages from Bäcker and Richter (1973) are used to calculate the average sedimentation rates. Gurvich (2006) determined the deposition rates of dry salt-free ore material ($g/cm^2/Ka$) for the different units and sub-basins according to chemical analyses of 71 sedimentary cores and calculated the average deposition rates (t/a) for each unit. Total tonnage (dry, salt free) is calculated according to average deposition rate multiplied by age.

Table 3.2. Major and trace element compositions of cores from the Atlantis II Deep (salt-free basis).

| | Element | | | Fe | Mn | Si | Al | $CO_2^*$ | Ca | Ba | $S_{red}$ | $SO_4$ | Cu | Zn |
|---|---|---|---|---|---|---|---|---|---|---|---|---|---|---|
| | Method | | | 2 | 1 | 2 | 9 | 5 | 2 | 1 | 7 | 6 | 1 | 1 |
| | Detection limit | | | 0.05 | 4e-4 | 0.01 | 0.01 | 0.01 | 0.01 | 3 | - | 0.3 | 2 | 30 |
| Sample ID | Sample type | Unit | Corr. | wt. % | wt. % | wt. % | wt. % | wt. % | wt. % | wt.% | wt. % | wt. % | wt. % | wt. % |
| 373-8 | Clay-rich | AM | 3.0 | 18.9 | 0.3 | 8.5 | 0.60 | 1.9 | 5.8 | 0.033 | 1.92 | 1.5 | 0.33 | 1.75 |
| 373-93 | Clay-rich | SU2 | 2.5 | 20.1 | 0.3 | 9.3 | 0.70 | 4.5 | 6.8 | 0.108 | 0.97 | 0.8 | 0.28 | 1.33 |
| 373-210 | Clay-rich | SU2 | 2.9 | 17.3 | 1.0 | 13.5 | 0.26 | 0.5 | 4.1 | 0.011 | 0.92 | 2.6 | 0.16 | 0.25 |
| 373-265 | Clay-rich | CO | 2.1 | 2.8 | 32.5 | 2.2 | 0.62 | 0.5 | 3.2 | 0.573 | 0.41 | n.d. | 0.03 | 0.18 |
| 373-798 | Clay-rich | DOP | 2.0 | 41.8 | 0.7 | 3.3 | 0.70 | 1.5 | 2.4 | 0.004 | 1.52 | n.d. | 0.03 | 1.47 |
| 387-174 | Clay-rich | SU2 | 3.0 | 21.5 | 0.4 | 17.6 | 0.22 | 0.4 | 4.5 | 0.025 | 1.03 | 4.2 | 0.07 | 1.40 |
| 387-302 | Clay-rich | CO | 1.5 | 45.6 | 0.9 | 4.7 | 0.49 | 1.0 | 1.9 | 0.008 | 0.40 | n.d. | 0.05 | 0.45 |
| 421-223 | Clay-rich | CO | 2.5 | 30.8 | 0.7 | 2.2 | 0.24 | 2.5 | 3.2 | 0.227 | 0.57 | n.d. | 0.06 | 1.21 |
| 421-362 | Clay-rich | COS | 2.9 | 19.0 | 0.6 | 8.5 | 0.48 | 2.4 | 5.8 | 0.036 | 1.91 | 5.0 | 0.58 | 2.36 |
| 495-113 | Clay-rich | AM | 2.4 | 29.5 | 0.1 | 6.7 | 0.39 | 0.7 | 4.7 | 0.019 | 0.03 | 5.6 | 0.14 | 1.37 |
| 495-362 | Clay-rich | SU2 | 2.1 | 25.0 | 0.2 | 7.3 | 0.44 | 1.0 | 5.3 | 0.048 | 0.23 | 5.9 | 0.54 | 1.33 |
| 495-693 | Clay-rich | COS | 2.1 | 26.4 | 0.2 | 10.4 | 0.63 | 1.0 | 3.2 | 0.012 | 0.55 | 2.7 | 0.17 | 0.06 |
| 503-407 | Clay-rich | COS | 1.6 | 51.3 | 0.4 | 1.6 | 0.24 | 0.8 | 1.3 | 0.012 | 0.31 | 0.5 | 0.12 | 0.16 |
| 503-671 | Clay-rich | COS | 2.6 | 15.5 | 0.4 | 14.3 | 0.23 | 1.3 | 4.3 | 0.024 | 1.04 | 1.8 | 0.10 | 0.18 |
| 503-680 | Clay-rich | COS | 2.2 | 29.5 | 1.6 | 9.3 | 0.38 | 1.8 | 3.1 | 0.297 | 0.17 | 2.0 | 0.72 | 0.37 |
| 557-289 | Clay-rich | CO | 1.9 | 40.6 | 1.0 | 1.9 | 0.33 | 0.8 | 1.6 | 0.062 | 0.79 | 1.9 | 0.51 | 1.23 |
| 373-515 | $CO_3$-rich | COS | 2.0 | 25.3 | 2.4 | 8.1 | 0.31 | 5.6 | 3.1 | 0.019 | 0.34 | 1.0 | 0.13 | 1.41 |
| 373-780 | $CO_3$-rich | DOP | 1.3 | 5.5 | 4.6 | 7.7 | 1.89 | 24.5 | 18.2 | 0.007 | 0.60 | 1.3 | 0.01 | 0.94 |
| 387-261 | $CO_3$-rich | CO | 1.4 | 13.5 | 1.8 | 14.3 | 3.45 | 13.9 | 5.3 | 0.159 | 0.95 | 2.0 | 0.13 | 0.20 |
| 421-160 | $CO_3$-rich | SU2 | 2.9 | 25.1 | 2.2 | 7.2 | 0.24 | 6.9 | 3.2 | 0.006 | 4.71 | 1.2 | 0.30 | 2.48 |
| 421-496 | $CO_3$-rich | SU1 | 1.5 | 24.1 | 4.3 | 7.2 | 1.29 | 13.2 | 3.3 | 0.022 | 0.27 | n.d. | 0.08 | 0.27 |
| 421-520 | $CO_3$-rich | SU1 | 2.1 | 23.3 | 1.3 | 7.6 | 0.58 | 6.0 | 5.3 | 0.010 | 0.36 | n.d. | 0.15 | 0.37 |
| 421-825 | $CO_3$-rich | DOP | 1.2 | 5.5 | 0.3 | 13.5 | 4.01 | 17.8 | 15.0 | 0.017 | n.d. | 9.9 | 0.06 | 0.52 |
| 421-870 | $CO_3$-rich | DOP | 1.8 | 40.5 | 0.2 | 6.0 | 1.05 | 1.4 | 1.7 | 0.007 | 0.15 | 0.5 | 0.01 | 0.38 |
| 495-548 | $CO_3$-rich | SU2 | 1.8 | 30.6 | 2.9 | 6.6 | 0.83 | 12.8 | 3.1 | 0.088 | 0.15 | 1.3 | 0.18 | 1.02 |
| 495-557 | $CO_3$-rich | CO | 1.4 | 29.3 | 2.9 | 5.1 | 1.32 | 10.6 | 8.1 | 0.005 | 0.03 | 1.8 | 0.02 | 0.56 |
| 495-569 | $CO_3$-rich | CO | 1.3 | 14.1 | 26.7 | 3.4 | 0.82 | 2.3 | 2.5 | 0.014 | 0.03 | 1.1 | 0.02 | 0.59 |
| 495-582 | $CO_3$-rich | CO | 1.2 | 2.1 | 3.2 | 6.8 | 2.02 | 29.7 | 23.6 | 0.350 | 0.07 | 0.7 | 0.01 | 0.11 |
| 495-599 | $CO_3$-rich | CO | 1.5 | 13.8 | 3.8 | 8.9 | 1.57 | 17.9 | 12.0 | 0.031 | 0.12 | 0.9 | 0.03 | 0.36 |
| 495-757 | $CO_3$-rich | SU1 | 1.2 | 6.3 | 0.8 | 11.8 | 3.33 | 20.0 | 14.2 | 0.146 | n.d. | 11.2 | 0.48 | 1.77 |
| 495-867 | $CO_3$-rich | SU1 | 1.2 | 6.6 | 0.6 | 10.7 | 3.12 | 23.3 | 18.1 | 0.029 | n.d. | 4.9 | 0.25 | 0.76 |
| 495-889 | $CO_3$-rich | DOP | 1.6 | 21.8 | 9.3 | 7.5 | 1.91 | 11.2 | 7.5 | 0.320 | 0.37 | 6.1 | 0.31 | 1.24 |
| 495-934 | $CO_3$-rich | DOP | 1.1 | 4.0 | 0.3 | 10.9 | 3.35 | 23.3 | 20.0 | 0.016 | 0.10 | 1.9 | 0.07 | 0.16 |
| 495-1088 | $CO_3$-rich | DOP | 1.1 | 4.1 | 0.2 | 12.6 | 3.83 | 21.8 | 16.3 | 0.022 | n.d. | 4.2 | 0.04 | 0.27 |
| 495-1195 | $CO_3$-rich | DOP | 1.2 | 5.6 | 0.4 | 13.6 | 4.11 | 21.1 | 14.3 | 0.038 | n.d. | 4.4 | 0.04 | 0.07 |
| 503-516 | $CO_3$-rich | COS | 1.5 | 5.2 | 0.5 | 22.2 | 5.04 | 3.5 | 2.3 | 0.500 | 3.47 | 0.8 | 1.81 | 1.62 |
| 503-889 | $CO_3$-rich | SU1 | 1.1 | 37.3 | 2.5 | 1.6 | 0.49 | 16.1 | 2.7 | 0.002 | n.d. | 7.8 | 1.33 | 0.42 |
| 546-180 | $CO_3$-rich | AM | 2.2 | 24.2 | 2.5 | 8.4 | 0.41 | 5.9 | 1.9 | 0.018 | 0.38 | 2.8 | 0.21 | 1.14 |
| 546-229 | $CO_3$-rich | SU2 | 1.6 | 24.3 | 5.1 | 6.7 | 0.78 | 16.7 | 2.3 | 0.021 | 0.75 | 5.7 | 1.04 | 2.30 |
| 546-252 | $CO_3$-rich | CO | 1.2 | 5.3 | 1.1 | 12.7 | 3.61 | 19.8 | 16.9 | 0.012 | 0.18 | 1.6 | 0.01 | 0.65 |
| 546-311 | $CO_3$-rich | SU1 | 1.1 | 37.1 | 4.6 | 2.0 | 0.55 | 19.7 | 2.3 | 0.024 | 0.12 | 1.2 | 1.04 | 0.26 |
| 546-385 | $CO_3$-rich | DOP | 1.2 | 7.3 | 0.6 | 9.3 | 3.52 | 24.5 | 19.9 | 0.010 | 0.13 | 2.2 | 0.02 | 0.07 |
| 557-255 | $CO_3$-rich | CO | 1.5 | 16.8 | 2.9 | 12.6 | 3.21 | 7.9 | 2.6 | 0.079 | 0.34 | 3.9 | 0.20 | 1.61 |
| 557-502 | $CO_3$-rich | DOP | 1.1 | 2.5 | 0.4 | 9.0 | 2.80 | 27.1 | 23.8 | 0.021 | 0.26 | 1.0 | 0.02 | 0.18 |
| 557-608 | $CO_3$-rich | DOP | 1.1 | 3.8 | 0.4 | 5.9 | 2.07 | 29.3 | 26.1 | 0.010 | 0.29 | n.d. | 0.01 | 0.03 |
| 557-753 | $CO_3$-rich | DOP | 1.2 | 2.5 | 0.4 | 7.1 | 2.25 | 27.4 | 25.0 | 0.009 | 0.13 | 0.5 | 0.03 | 0.04 |
| 557-795 | $CO_3$-rich | DOP | 1.1 | 3.9 | 0.4 | 5.3 | 1.68 | 30.7 | 26.7 | 0.006 | 0.25 | n.d. | 0.00 | 0.03 |

| Sample ID | Sample type | Unit | Corr. | Fe | Mn | Si | Al | $CO_2^*$ | Ca | Ba | $S_{red}$ | $SO_4$ | Cu | Zn |
|---|---|---|---|---|---|---|---|---|---|---|---|---|---|---|
| 617-508 | $CO_3$-rich | SOAN | 1.3 | 10.9 | 0.3 | 12.2 | 2.89 | 17.2 | 15.9 | 0.024 | 0.45 | 2.9 | 0.12 | 0.62 |
| 334-612 | HSHM | SOAN | 2.2 | 24.3 | 0.1 | 8.4 | 0.50 | 1.0 | 5.3 | 0.064 | 1.98 | 10.4 | 0.95 | 3.08 |
| 387-398 | HSHM | SU1 | 1.8 | 9.2 | 0.4 | 14.3 | 1.79 | 4.3 | 4.1 | 0.384 | 5.98 | 27.6 | 2.54 | 7.95 |
| 387-466 | HSHM | SU1 | 1.5 | 22.7 | 1.6 | 7.2 | 1.17 | 16.3 | 3.3 | 0.038 | 5.01 | 16.2 | 1.59 | 4.10 |
| 387-490 | HSHM | SU1 | 1.2 | 42.7 | 0.8 | 2.7 | 0.85 | 4.5 | 0.9 | 0.010 | 0.51 | 5.5 | 1.08 | 0.61 |
| 421-678 | HSHM | DOP | 1.6 | 16.9 | 1.2 | 11.5 | 1.90 | 7.8 | 2.4 | 0.046 | 4.41 | 28.8 | 2.62 | 5.39 |
| 495-240 | HSHM | AM | 3.4 | 30.0 | 0.3 | 6.0 | 0.54 | 0.5 | 4.5 | 0.039 | 0.32 | 6.8 | 1.50 | 1.50 |
| 495-777 | HSHM | SU1 | 1.3 | 19.1 | 1.5 | 11.0 | 1.50 | 7.1 | 2.3 | 0.091 | 4.42 | 24.5 | 1.50 | 2.34 |
| 546-5 | HSHM | AM | 2.3 | 31.6 | 1.7 | 6.7 | 0.86 | 3.2 | 1.1 | 0.085 | 1.39 | 5.3 | 1.61 | 3.39 |
| 557-388 | HSHM | SU1 | 1.5 | 15.4 | 2.1 | 9.7 | 1.76 | 10.5 | 3.5 | 0.029 | 4.72 | 25.5 | 2.04 | 6.29 |
| 617-9 | HSHM | SAM | 2.5 | 24.8 | 0.3 | 6.9 | 0.73 | 0.5 | 4.3 | 0.140 | 1.45 | 11.0 | 1.32 | 3.21 |
| 617-148 | HSHM | SAM | 2.2 | 21.2 | 0.2 | 7.2 | 0.66 | 0.8 | 5.1 | 0.125 | 4.22 | 19.2 | 1.66 | 4.81 |
| 617-396 | HSHM | OAN | 1.6 | 17.7 | 0.2 | 14.5 | 2.64 | 3.3 | 3.4 | 0.002 | 0.54 | 6.2 | 1.07 | 0.81 |
| 334-83 | HSHM | SAM | 2.0 | 14.7 | 0.2 | 5.6 | 0.43 | 1.0 | 9.1 | 0.225 | 1.77 | 19.1 | 0.34 | 2.33 |
| 334-513 | HSHM | SAM | 2.0 | 19.3 | 0.4 | 5.3 | 0.64 | 2.1 | 6.7 | 0.106 | 4.56 | 28.0 | 0.88 | 7.25 |
| 334-757 | HSHM | SOAN | 2.0 | 21.1 | 0.1 | 8.3 | 0.64 | 0.7 | 4.0 | 0.041 | 2.91 | 16.8 | 0.12 | 5.17 |
| 373-555 | HSHM | SU1 | 1.8 | 11.0 | 0.7 | 13.8 | 1.65 | 7.1 | 4.1 | 0.625 | 5.04 | 25.2 | 2.15 | 8.87 |
| 373-751 | HSHM | SU1 | 1.4 | 15.2 | 2.4 | 7.8 | 1.48 | 13.1 | 3.5 | 0.026 | 1.64 | 25.9 | 1.68 | 6.75 |
| 387-80 | HSHM | SU2 | 2.3 | 16.3 | 0.2 | 6.5 | 0.48 | 0.6 | 5.6 | 0.023 | 2.21 | 11.8 | 0.47 | 2.03 |
| 421-740 | HSHM | DOP | 2.6 | 17.2 | 1.0 | 14.2 | 0.34 | 1.7 | 1.4 | 0.008 | 1.39 | 5.1 | 0.11 | 3.73 |
| 495-484 | HSHM | SU2 | 2.4 | 21.9 | 0.2 | 8.4 | 0.66 | 1.3 | 5.2 | 0.022 | 1.64 | 11.6 | 0.87 | 3.20 |
| 503-7 | HSHM | SAM | 2.4 | 25.8 | 0.2 | 6.1 | 0.42 | 1.0 | 5.8 | 0.038 | 0.85 | 10.9 | 0.49 | 2.02 |
| 503-155 | HSHM | SOAN | 2.2 | 15.1 | 0.1 | 9.6 | 0.61 | 0.9 | 3.9 | 0.011 | 0.60 | 16.4 | 0.34 | 1.99 |
| 503-912 | HSHM | SU1 | 1.7 | 6.4 | 1.1 | 8.7 | 1.54 | 2.0 | 3.6 | 0.012 | 4.02 | 47.2 | 2.52 | 14.6 |
| 503-946 | HSHM | DOP | 1.6 | 22.1 | 1.7 | 4.8 | 0.87 | 4.2 | 5.8 | 0.707 | 1.47 | 20.4 | 0.38 | 2.42 |
| 557-9 | HSHM | SAM | 2.7 | 18.4 | 0.3 | 6.6 | 0.51 | 0.9 | 6.2 | 0.036 | 1.10 | 15.7 | 1.29 | 4.53 |
| 557-173 | HSHM | SU2 | 3.0 | 18.6 | 0.2 | 10.6 | 0.90 | 1.1 | 3.9 | 0.026 | 3.27 | 14.2 | 1.13 | 8.01 |
| 557-227 | HSHM | SU2 | 2.2 | 13.1 | 0.7 | 7.8 | 0.50 | 0.6 | 5.0 | 0.005 | 2.25 | 16.9 | 0.22 | 4.45 |
| 617-650 | HSHM | SOAN | 1.7 | 17.8 | 0.2 | 8.6 | 1.06 | 1.3 | 6.0 | 0.010 | 2.07 | 24.2 | 1.08 | 4.93 |
| 617-787 | HSHM | SOAN | 1.6 | 21.7 | 0.3 | 6.9 | 0.74 | 0.8 | 8.3 | 0.143 | 0.86 | 28.0 | 0.24 | 2.48 |
| 373-672 | HSLM | SU1 | 2.2 | 26.7 | 1.0 | 10.1 | 0.25 | 0.6 | 2.9 | 0.010 | 6.43 | 5.3 | 0.13 | 0.88 |
| 387-575 | HSLM | SU1 | 1.5 | 7.4 | 0.4 | 12.3 | 0.74 | 3.1 | 7.8 | 0.699 | 4.40 | 32.1 | 0.51 | 0.89 |
| 503-75 | HSLM | OAN | 1.7 | 6.4 | 0.7 | 17.4 | 0.70 | 3.1 | 3.2 | 1.576 | 4.49 | 26.2 | 0.23 | 1.18 |
| 503-807 | HSLM | SU1 | 1.5 | 10.8 | 1.0 | 14.0 | 0.96 | 2.1 | 3.6 | 0.656 | 8.06 | 9.8 | 0.71 | 0.70 |
| 503-987 | HSLM | DOP | 1.2 | 20.1 | 0.4 | 12.7 | 3.80 | 4.6 | 2.1 | 0.057 | 13.9 | 23.1 | 0.12 | 1.09 |
| 546-318 | HSLM | SU1 | 1.3 | 4.9 | 0.4 | 25.8 | 1.09 | 2.1 | 4.3 | 1.605 | 1.54 | 14.4 | 0.02 | 0.06 |
| 617-395 | HSLM | OAN | 1.8 | 16.6 | 0.1 | 7.4 | 0.70 | 1.2 | 8.3 | 0.003 | 1.81 | 18.3 | 0.04 | 0.79 |
| 334-312 | LSHM | SAM | 2.1 | 24.1 | 0.2 | 6.6 | 0.60 | 0.9 | 6.6 | 0.115 | n.d. | 17.8 | 0.71 | 4.61 |
| 421-80 | LSHM | SU2 | 2.3 | 23.9 | 0.9 | 6.8 | 0.49 | 4.9 | 3.9 | 0.018 | n.d. | 6.1 | 1.27 | 2.36 |
| 546-92 | LSHM | AM | 2.6 | 26.3 | 2.6 | 8.3 | 0.58 | 3.8 | 2.0 | 0.012 | n.d. | 10.4 | 0.97 | 3.31 |
| 617-799 | LSHM | SOAN | 1.6 | 11.4 | 0.3 | 5.7 | 1.01 | 2.0 | 12.4 | 0.932 | 0.20 | 36.2 | 0.58 | 7.07 |
| 495-809 | LSLM | SU1 | 2.4 | 18.5 | 0.3 | 17.2 | 0.44 | 2.1 | 4.2 | 0.005 | 0.92 | 6.3 | 0.05 | 1.06 |
| 503-140 | LSLM | SOAN | 2.2 | 14.0 | 0.1 | 8.1 | 0.29 | 0.6 | 6.2 | 0.006 | n.d. | 22.4 | 0.29 | 1.88 |
| 503-509 | LSLM | COS | 1.8 | 24.8 | 1.6 | 5.5 | 0.19 | 8.1 | 7.8 | 0.162 | 0.16 | 12.8 | 0.19 | 0.40 |
| 503-626 | LSLM | COS | 1.9 | 41.0 | 0.5 | 2.8 | 0.19 | 0.5 | 2.1 | 0.322 | n.d. | 7.3 | 0.11 | 0.15 |
| 546-267 | LSLM | SU1 | 1.5 | 28.1 | 0.7 | 8.8 | 0.63 | 2.0 | 3.9 | 0.424 | 0.01 | 11.6 | 0.25 | 0.26 |
| 617-220 | LSLM | OAN | 1.5 | 2.4 | 0.1 | 7.4 | 0.24 | n.d. | 13.9 | n.d. | 0.56 | 35.5 | 0.09 | 0.16 |
| 373-586 | ANHY | SU1 | 1.0 | 1.2 | 0.0 | 1.0 | 0.08 | 0.1 | 22.6 | 0.018 | n.d. | 65.7 | 0.13 | 0.40 |
| 387-502 | ANHY | SU1 | 1.0 | 1.0 | 0.1 | 0.3 | 0.01 | 0.2 | 23.3 | 0.002 | n.d. | 64.2 | 0.04 | 0.21 |
| 503-235 | ANHY | SOAN | 1.1 | 0.1 | 0.1 | 0.2 | 0.02 | 0.0 | 27.3 | 0.503 | n.d. | 71.6 | 0.02 | 0.33 |
| 503-266 | ANHY | SOAN | 1.2 | 3.3 | 0.4 | 0.5 | 0.05 | 1.4 | 20.9 | 0.417 | 0.48 | 54.3 | 0.05 | 0.20 |
| 617-551 | ANHY | SOAN | 1.2 | 3.1 | 0.1 | 1.6 | 0.24 | 1.6 | 25.8 | 0.020 | n.d. | 64.5 | 0.14 | 0.63 |
| 617-875 | ANHY | SOAN | 1.3 | 8.9 | 0.1 | 4.8 | 0.65 | 0.8 | 16.5 | 0.100 | n.d. | 47.4 | 0.67 | 3.04 |

Table 3.2. continuation. Major and trace element compositions of cores from the Atlantis II Deep (salt-free basis). All values are in ppm, except Au and Hg in ppb.

| | Element | Mo | As | Ga | Au | Tl | Sb | Hg | Ag | Cd | Pb | Co | Ni | Cr | V |
|---|---|---|---|---|---|---|---|---|---|---|---|---|---|---|---|
| | Method | 1 | 8 | 1 | 3 | 1 | 3 | 4 | 8 | 8 | 1 | 1 | 8 | 8 | 1 |
| | Det. lim. | 1 | 2 | 1 | 2 | 0.1 | 0.1 | 5 | 1 | 1 | 0.8 | 0.2 | 10 | 5 | 5 |
| Sample ID | Sample type | | | | | | | | | | | | | | |
| 373-8 | Clay-rich | 78 | 179 | 11 | 575 | 10 | 9 | 1546 | 4 | n.d. | 665 | 105 | 23 | n.d. | 69 |
| 373-93 | Clay-rich | 76 | 178 | 8 | 357 | 4 | 11 | 644 | 13 | 2 | 248 | 61 | n.d. | 14 | 74 |
| 373-210 | Clay-rich | 79 | 123 | 9 | 206 | 17 | 6 | 241 | n.d. | n.d. | 154 | 30 | n.d. | n.d. | 32 |
| 373-265 | Clay-rich | 216 | 138 | 24 | n.d. | 12 | 9 | n.d. | n.d. | n.d. | 375 | 173 | 36 | n.d. | 140 |
| 373-798 | Clay-rich | 268 | 137 | 3 | n.d. | 3 | 7 | n.d. | 1 | 17 | 32 | 27 | 33 | 18 | 98 |
| 387-174 | Clay-rich | 119 | 112 | 6 | n.d. | 6 | 6 | 65 | 11 | 61 | 56 | 18 | n.d. | n.d. | 39 |
| 387-302 | Clay-rich | 269 | 1145 | 2 | n.d. | 1 | 9 | 119 | 2 | 11 | 115 | 9 | 21 | n.d. | 88 |
| 421-223 | Clay-rich | 153 | 71 | 1 | 90 | 3 | n.d. | 115 | 4 | 12 | 40 | 28 | n.d. | n.d. | 28 |
| 421-362 | Clay-rich | 100 | 147 | 15 | 719 | 18 | 16 | 1412 | 22 | 41 | 605 | 119 | 28 | n.d. | 65 |
| 495-113 | Clay-rich | 119 | 186 | 9 | 375 | 8 | 8 | 242 | n.d. | n.d. | 199 | 36 | n.d. | n.d. | 70 |
| 495-362 | Clay-rich | 70 | 187 | 11 | 1041 | 8 | 17 | 2348 | 16 | 3 | 338 | 60 | n.d. | n.d. | 78 |
| 495-693 | Clay-rich | 127 | 156 | 9 | 362 | 4 | 20 | 381 | n.d. | n.d. | 58 | 24 | n.d. | 12 | 127 |
| 503-407 | Clay-rich | 320 | 153 | 3 | 85 | <1 | 6 | 32 | 1 | n.d. | 21 | 13 | n.d. | n.d. | 69 |
| 503-671 | Clay-rich | 44 | 54 | 6 | 185 | 7 | 14 | 312 | 3 | n.d. | 12 | 12 | n.d. | n.d. | 44 |
| 503-680 | Clay-rich | 213 | 295 | 7 | 352 | 7 | 32 | 1395 | 2 | 3 | 495 | 67 | 26 | n.d. | 57 |
| 557-289 | Clay-rich | 314 | 185 | 17 | 795 | 10 | 22 | 835 | 16 | 7 | 118 | 94 | n.d. | n.d. | 66 |
| 373-515 | $CO_3$-rich | 156 | 233 | 6 | 449 | 3 | 18 | 649 | n.d. | n.d. | 193 | 38 | 20 | n.d. | 51 |
| 373-780 | $CO_3$-rich | 12 | 24 | 8 | n.d. | 2 | 2 | 14 | n.d. | 1 | 39 | 19 | 29 | 33 | 101 |
| 387-261 | $CO_3$-rich | 32 | 188 | 11 | 108 | 4 | 3 | 496 | 4 | 1 | 67 | 18 | 39 | 54 | 158 |
| 421-160 | $CO_3$-rich | 119 | 76 | 5 | n.d. | 13 | 3 | 466 | 2 | n.d. | 318 | 43 | 28 | n.d. | 38 |
| 421-496 | $CO_3$-rich | 174 | 55 | 6 | 59 | <1 | 1 | 118 | n.d. | n.d. | 13 | 19 | 22 | 22 | 88 |
| 421-520 | $CO_3$-rich | 112 | 101 | 5 | 114 | 2 | 11 | 260 | 1 | n.d. | 23 | 15 | 14 | n.d. | 60 |
| 421-825 | $CO_3$-rich | 15 | 111 | 10 | n.d. | 3 | 12 | 293 | 2 | 6 | 27 | 77 | 106 | 88 | 264 |
| 421-870 | $CO_3$-rich | 175 | 76 | 4 | n.d. | 1 | 4 | 25 | n.d. | 3 | 4 | 14 | 20 | 30 | 237 |
| 495-548 | $CO_3$-rich | 144 | 198 | 16 | 115 | 3 | 16 | 144 | 5 | 1 | 211 | 37 | 40 | 12 | 109 |
| 495-557 | $CO_3$-rich | 169 | 165 | 5 | n.d. | 1 | 5 | 51 | 2 | 1 | 34 | 34 | 47 | 23 | 274 |
| 495-569 | $CO_3$-rich | 390 | 67 | 17 | n.d. | 1 | 5 | 44 | n.d. | n.d. | 119 | 28 | 22 | 16 | 89 |
| 495-582 | $CO_3$-rich | 7 | 6 | 8 | 24 | <1 | n.d. | 47 | n.d. | 1 | n.d. | 9 | 20 | 34 | 93 |
| 495-599 | $CO_3$-rich | 59 | 38 | 8 | 28 | 1 | 4 | 128 | n.d. | n.d. | n.d. | 15 | 29 | 27 | 111 |
| 495-757 | $CO_3$-rich | 54 | 108 | 14 | 458 | 11 | 22 | 950 | 26 | 66 | 406 | 70 | 60 | 51 | 115 |
| 495-867 | $CO_3$-rich | 32 | 42 | 12 | 221 | 5 | 7 | 293 | 8 | 14 | 185 | 36 | 47 | 48 | 126 |
| 495-889 | $CO_3$-rich | 215 | 194 | 15 | 334 | 10 | 19 | 448 | 18 | 8 | 271 | 83 | 55 | 27 | 148 |
| 495-934 | $CO_3$-rich | 14 | 20 | 10 | 58 | 2 | 3 | 101 | 3 | 1 | 31 | 27 | 50 | 52 | 111 |
| 495-1088 | $CO_3$-rich | 18 | 21 | 10 | n.d. | 2 | 3 | 75 | 2 | 1 | 36 | 25 | 42 | 55 | 120 |
| 495-1195 | $CO_3$-rich | 20 | 30 | 11 | 41 | 1 | 3 | 91 | 2 | n.d. | 28 | 26 | 44 | 60 | 149 |
| 503-516 | $CO_3$-rich | 65 | 151 | 27 | 1300 | 17 | 42 | 1974 | 130 | 148 | 421 | 45 | 79 | 78 | 207 |
| 503-889 | $CO_3$-rich | 89 | 132 | 6 | 253 | 12 | 21 | 3618 | 19 | 17 | 430 | 236 | 95 | 6 | 53 |
| 546-180 | $CO_3$-rich | 45 | 139 | 9 | 673 | 3 | 14 | 597 | 31 | 66 | 227 | 68 | n.d. | n.d. | 100 |
| 546-229 | $CO_3$-rich | 81 | 111 | 28 | 1513 | 13 | 29 | 1699 | 78 | 81 | 1037 | 252 | 41 | 9 | 129 |
| 546-252 | $CO_3$-rich | 5 | 14 | 10 | n.d. | 4 | 1 | 36 | 9 | 16 | 4 | 45 | 38 | 58 | 94 |
| 546-311 | $CO_3$-rich | 13 | 17 | 5 | 96 | 4 | 1 | 93 | 3 | 4 | 819 | 66 | 49 | 8 | 56 |
| 546-385 | $CO_3$-rich | 30 | 39 | 8 | n.d. | 0 | 1 | 58 | n.d. | 1 | 1 | 46 | 45 | 54 | 120 |
| 557-255 | $CO_3$-rich | 32 | 47 | 11 | 134 | 12 | 3 | 996 | 23 | 45 | 465 | 41 | 36 | 58 | 145 |
| 557-502 | $CO_3$-rich | 5 | 50 | 7 | 34 | 1 | 2 | 32 | n.d. | 2 | 16 | 19 | 43 | 47 | 100 |
| 557-608 | $CO_3$-rich | 6 | 49 | 5 | 39 | <1 | 2 | 17 | n.d. | 1 | n.d. | 22 | 46 | 33 | 81 |
| 557-753 | $CO_3$-rich | 2 | 19 | 6 | n.d. | <1 | 1 | 251 | n.d. | n.d. | n.d. | 23 | 48 | 58 | 383 |
| 557-795 | $CO_3$-rich | 2 | 46 | 5 | n.d. | <1 | 2 | 12 | n.d. | n.d. | 7 | 10 | 30 | 30 | 88 |

| Sample ID | Sample type | Mo | As | Ga | Au | Tl | Sb | Hg | Ag | Cd | Pb | Co | Ni | Cr | V |
|---|---|---|---|---|---|---|---|---|---|---|---|---|---|---|---|
| 617-508 | $CO_3$-rich | 6 | 22 | 9 | 161 | 1 | 3 | 160 | 9 | 9 | 55 | 60 | 36 | 45 | 77 |
| 334-612 | HSHM | 85 | 231 | 12 | 1018 | 13 | 27 | 2734 | 115 | 94 | 794 | 148 | 11 | n.d. | 102 |
| 387-398 | HSHM | 379 | 703 | 44 | 3166 | 91 | 96 | 5034 | 306 | 491 | 2277 | 288 | 198 | 24 | 146 |
| 387-466 | HSHM | 128 | 427 | 22 | 1126 | 49 | 33 | 2681 | 119 | 167 | 909 | 159 | 67 | 14 | 117 |
| 387-490 | HSHM | 82 | 280 | 10 | 249 | 9 | 37 | 2820 | 8 | 23 | 442 | 53 | 51 | 9 | 101 |
| 421-678 | HSHM | 203 | 647 | 37 | 1753 | 96 | 39 | 4867 | 199 | 189 | 1655 | 315 | 157 | 27 | 143 |
| 495-240 | HSHM | 176 | 416 | 11 | 777 | 11 | 58 | 1723 | 40 | 241 | 1284 | 164 | 32 | n.d. | 71 |
| 495-777 | HSHM | 310 | 802 | 48 | 2047 | 89 | 60 | 3522 | 130 | 128 | 2100 | 157 | 113 | 22 | 141 |
| 546-5 | HSHM | 105 | 259 | 23 | 1654 | 12 | 23 | 4828 | 168 | 152 | 1153 | 122 | 13 | 13 | 183 |
| 557-388 | HSHM | 247 | 608 | 42 | 2964 | 51 | 52 | 2656 | 144 | 262 | 1775 | 242 | 106 | 22 | 117 |
| 617-9 | HSHM | 130 | 185 | 16 | 1448 | 27 | 20 | 3081 | 67 | 131 | 847 | 232 | 25 | n.d. | 90 |
| 617-148 | HSHM | 208 | 332 | 19 | 1853 | 39 | 83 | 6511 | 410 | 271 | 2272 | 358 | 46 | n.d. | 90 |
| 617-396 | HSHM | 13 | 143 | 16 | 1381 | 3 | 6 | 3309 | 36 | 11 | 107 | 138 | 35 | 41 | 106 |
| 334-83 | HSHM | 86 | 119 | 9 | 484 | 8 | 11 | 529 | 23 | 78 | 432 | 123 | 12 | n.d. | 78 |
| 334-513 | HSHM | 240 | 604 | 17 | 1727 | 35 | 320 | 19455 | 850 | 1121 | 3398 | 227 | 28 | n.d. | 99 |
| 334-757 | HSHM | 152 | 168 | 18 | 1157 | 9 | 17 | 217 | 57 | 251 | 504 | 125 | 14 | n.d. | 75 |
| 373-555 | HSHM | 288 | 613 | 37 | 2434 | 65 | 104 | 4335 | 174 | 548 | 2221 | 259 | 162 | 24 | 110 |
| 373-751 | HSHM | 399 | 893 | 37 | 2154 | 47 | 94 | 2631 | 95 | 159 | 1995 | 185 | 130 | 20 | 145 |
| 387-80 | HSHM | 111 | 137 | 11 | 708 | 15 | 12 | 1197 | 28 | 34 | 414 | 99 | 14 | n.d. | 68 |
| 421-740 | HSHM | 125 | 96 | 13 | 1318 | 19 | 24 | 659 | 10 | 21 | 478 | 30 | 17 | 21 | 746 |
| 495-484 | HSHM | 142 | 194 | 18 | 923 | 25 | 19 | 2034 | 77 | 31 | 748 | 214 | 23 | n.d. | 90 |
| 503-7 | HSHM | 183 | 233 | 9 | 890 | 16 | 15 | 1380 | 28 | 19 | 574 | 160 | 15 | n.d. | 72 |
| 503-155 | HSHM | 50 | 121 | 14 | 717 | 15 | 18 | 632 | 1 | 2 | 748 | 131 | 20 | n.d. | 72 |
| 503-912 | HSHM | 429 | 888 | 54 | 3755 | 42 | 149 | 3321 | 153 | 323 | 2086 | 199 | 154 | 15 | 155 |
| 503-946 | HSHM | 87 | 168 | 11 | 327 | 12 | 22 | 649 | 29 | 141 | 291 | 45 | 41 | 9 | 132 |
| 557-9 | HSHM | 99 | 198 | 14 | 2460 | 28 | 31 | 5198 | 90 | 205 | 2277 | 187 | 35 | n.d. | 77 |
| 557-173 | HSHM | 81 | 275 | 23 | 2388 | 42 | 44 | 3764 | 209 | 289 | 1596 | 328 | 30 | n.d. | 105 |
| 557-227 | HSHM | 109 | 208 | 19 | 1567 | 24 | 25 | 325 | 10 | 58 | 530 | 55 | 15 | n.d. | 163 |
| 617-650 | HSHM | 68 | 312 | 24 | 1998 | 12 | 35 | 2997 | 98 | 136 | 760 | 317 | 27 | 11 | 113 |
| 617-787 | HSHM | 153 | 293 | 15 | 1236 | 5 | 23 | 1050 | 76 | 207 | 689 | 122 | 18 | n.d. | 75 |
| 373-672 | HSLM | 147 | 291 | 12 | 419 | 13 | 22 | 577 | 6 | n.d. | 218 | 17 | n.d. | n.d. | 287 |
| 387-575 | HSLM | 301 | 822 | 34 | 3376 | 45 | 103 | 650 | 96 | 98 | 938 | 65 | 41 | 17 | 279 |
| 503-75 | HSLM | 307 | 773 | 36 | 3678 | 41 | 119 | 537 | 183 | 148 | 737 | 65 | 37 | 14 | 305 |
| 503-807 | HSLM | 170 | 524 | 39 | 2146 | 59 | 58 | 1232 | 67 | 53 | 1514 | 77 | 50 | 14 | 284 |
| 503-987 | HSLM | 94 | 373 | 13 | 167 | 30 | 26 | 885 | 9 | 10 | 328 | 45 | 86 | 72 | 193 |
| 546-318 | HSLM | 46 | 191 | 8 | 440 | 4 | 11 | 804 | 12 | 5 | 15 | 3 | n.d. | 19 | 167 |
| 617-395 | HSLM | 68 | 108 | 12 | 589 | 1 | 11 | 66 | 4 | 3 | 36 | 61 | n.d. | n.d. | 124 |
| 334-312 | LSHM | 149 | 183 | 14 | 1048 | 47 | 21 | 1522 | 149 | 155 | 1050 | 252 | 26 | n.d. | 90 |
| 421-80 | LSHM | 173 | 185 | 14 | 1277 | 22 | 20 | 3040 | 66 | 28 | 428 | 147 | 22 | n.d. | 65 |
| 546-92 | LSHM | 70 | 170 | 19 | 1220 | 7 | 17 | 1436 | 51 | 137 | 1415 | 234 | 19 | n.d. | 96 |
| 617-799 | LSHM | 55 | 131 | 17 | 1498 | 5 | 44 | 2232 | 119 | 152 | 2294 | 161 | 29 | 12 | 61 |
| 495-809 | LSLM | 32 | 46 | 7 | 254 | 13 | 9 | 193 | 3 | n.d. | 57 | 15 | n.d. | n.d. | 559 |
| 503-140 | LSLM | 33 | 77 | 12 | 328 | 13 | 6 | 525 | 1 | 2 | 656 | 114 | 17 | n.d. | 55 |
| 503-509 | LSLM | 128 | 169 | 4 | 69 | 1 | 7 | 118 | n.d. | n.d. | 104 | 8 | n.d. | n.d. | 26 |
| 503-626 | LSLM | 258 | 133 | 2 | 82 | 1 | 6 | 56 | 2 | 2 | 26 | 4 | n.d. | n.d. | 51 |
| 546-267 | LSLM | 140 | 271 | 29 | 1170 | 11 | 29 | 438 | 26 | 28 | 254 | 15 | 8 | 11 | 120 |
| 617-220 | LSLM | 29 | 46 | 8 | 300 | 1 | 6 | 91 | 5 | 4 | 27 | 43 | n.d. | n.d. | 31 |
| 373-586 | ANHY | 52 | 94 | 4 | 264 | 3 | 8 | 72 | 4 | 16 | 143 | 12 | 7 | n.d. | 10 |
| 387-502 | ANHY | 6 | 12 | 1 | 11 | <1 | 1 | 11 | n.d. | n.d. | 7 | 2 | n.d. | n.d. | n.d. |
| 503-235 | ANHY | 2 | 4 | <1 | 40 | 1 | 1 | 24 | n.d. | n.d. | 44 | 14 | n.d. | n.d. | 7 |
| 503-266 | ANHY | 17 | 18 | 1 | 56 | 1 | 2 | 65 | 6 | 11 | 95 | 20 | n.d. | n.d. | 12 |
| 617-551 | ANHY | 16 | 86 | 3 | 232 | 1 | 6 | 145 | 5 | 13 | 139 | 57 | 7 | n.d. | 25 |
| 617-875 | ANHY | 70 | 207 | 13 | 731 | 3 | 12 | 1793 | 34 | 124 | 476 | 86 | 22 | n.d. | 105 |

Sample ID consists of the core number (locations in Fig. 3.1) and sampling depth (cm below the top of the core). Sample types are according to Fig. 3.4: Clay-rich, carbonate-rich ($CO_3$-rich), and $SO_4$-rich (all other samples). Thirty-three $SO_4$-rich samples are classified as having high metal contents, with BMI values >0.4 mol/kg. Twenty-nine of these samples have sulfide contents >0.1 mol/kg and are referred to as high-sulfide, high-metal type (HSHM); four have much lower sulfide contents (<0.1 mol/kg) and are referred to as low-sulfide, high-metal type (LSHM). Thirteen samples are classified as having low metal contents, with BMI values <0.4 mol/kg. Seven of these samples have sulfide contents >0.4 mol/kg and are referred to as high-sulfide, low-metal type (HSLM); six have much lower sulfide contents and are referred to as low-sulfide, low-metal type (LSLM). Six samples that contain >50 wt.% anhydrite were classified as anhydrite samples (ANHY). Unit descriptions are in Table 3.1. Corr. is the salt correction according to the amount of NaCl in the sample (assuming all Na is present as NaCl). Analysis methods are: 1=Fusion followed by inductively coupled plasma (ICP) mass spectrometry (MS), 2=Fusion followed by ICP optical emission spectrometry (OES), 3=Instrumental neutron activation (INAA), 4=Cold vapour flow injection mercury analysis (FIMS), 5=Coulometry (*carbonate carbon as $CO_2$; samples did not contain significant organic carbon: Appendix 3.1), 6=Infrared detection (IR) after combustion at 550°C (sulfate sulfur), 7=Total sulfur (determined by thermal conductivity after combustion at 1800°C) minus sulfate sulfur determined by method 6, 8=Four-acid leach followed by ICP-MS, 9=Four-acid leach followed by ICP-OES. Methods 1-6 were performed at Activation Laboratories, method 7 at the Hatch Laboratories (University of Ottawa), and methods 8-9 at the University of Kiel. n.d.= not detected.

Table 3.3. Average concentrations of metals (and sulfur) in samples from the different stratigraphic units of the Atlantis II Deep (salt-free basis; see Table 3.1)

| Unit | n | Fe % | Mn % | Cu % | Zn % | Mo ppm | As ppm | Ga ppm | Au ppb | Tl ppm | Sb ppm | Hg ppb | Ag ppm | Cd ppm | Pb ppm | Co ppm | Ni ppm | Cr ppm | V ppm | Cu/ Zn | $S_{tot}$ mol | $S_{red}$ mol | BMI mol |
|---|---|---|---|---|---|---|---|---|---|---|---|---|---|---|---|---|---|---|---|---|---|---|---|
| AM | 13 | 23.8 | 0.7 | 0.88 | 3.2 | 130 | 246 | 14 | 1168 | 19 | 49 | 3696 | 159 | 234 | 1215 | 174 | 25 | 13 | 91 | 0.28 | 1.66 | 0.51 | 0.77 |
| SU2 | 28 | 16.2 | 0.6 | 0.45 | 2.3 | 87 | 169 | 14 | 970 | 11 | 19 | 1162 | 49 | 70 | 509 | 107 | 24 | 20 | 83 | 0.19 | 2.48 | 0.48 | 0.50 |
| CO | 20 | 22.6 | 4.3 | 0.25 | 0.7 | 153 | 178 | 10 | 319 | 5 | 12 | 484 | 17 | 24 | 182 | 41 | 34 | 40 | 99 | 0.36 | 0.43 | 0.19 | 0.19 |
| SU1 | 22 | 17.0 | 1.3 | 0.92 | 2.7 | 165 | 360 | 22 | 1235 | 28 | 42 | 1687 | 70 | 141 | 856 | 100 | 76 | 20 | 154 | 0.34 | 2.80 | 0.98 | 0.71 |
| DOP | 17 | 13.2 | 1.3 | 0.23 | 1.1 | 76 | 124 | 10 | 452 | 11 | 10 | 530 | 27 | 29 | 216 | 50 | 52 | 42 | 189 | 0.21 | 1.13 | 0.56 | 0.23 |

Abbreviations: n=Number of samples analyzed from each unit. $S_{tot}$=Total sulfur determined by thermal conductivity after combustion, $S_{red}$=Total sulfur minus sulfate sulfur (Table 3.2). BMI=Base metal sulfide index (2*Cu+Zn+Pb in moles). Averages (arithmetic mean values) were calculated by assigning concentrations below detection a value equivalent to half the detection limit before correction to a salt-free basis.

Table 3.4. Average concentrations of metals and sulfur in all samples from the three uppermost units of proximal and distal cores from the Atlantis II Deep (salt-free basis).

| | n | Fe % | Mn % | Cu % | Zn % | Mo ppm | As ppm | Ga ppm | Au ppb | Tl ppm | Sb ppm | Hg ppb | Ag ppm | Cd ppm | Pb ppm | Co ppm | Ni ppm | Cr ppm | V ppm | Cu / Zn | $S_{tot}$ mol | $S_{red}$ mol | BMI mol |
|---|---|---|---|---|---|---|---|---|---|---|---|---|---|---|---|---|---|---|---|---|---|---|---|
| Distal | 35 | 21 | 2.6 | 0.34 | 1.09 | 134 | 192 | 10 | 455 | 9 | 15 | 691 | 19 | 23 | 303 | 62 | 20 | 12 | 86 | 0.31 | 1.16 | 0.27 | 0.27 |
| Proximal | 26 | 18 | 0.8 | 0.66 | 3.14 | 95 | 184 | 15 | 1126 | 14 | 33 | 2523 | 106 | 147 | 873 | 151 | 22 | 13 | 96 | 0.21 | 2.21 | 0.40 | 0.69 |

The location of cores taken from the proximal part of the basin (334, 546, 557, 617) and from the distal part of the basin (373, 387, 421, 495, 503) are shown in Figure 3.1. We excluded samples from units SU1 and DOP, which are either absent or inaccessible due to intrusion of a basaltic sill in the Southwest Basin. Abbreviations: n=Number of samples in this category. $S_{tot}$=Total sulfur determined by thermal conductivity after combustion, $S_{red}$=Total sulfur minus sulfate sulfur (Table 3.2). BMI=Base metal sulfide index (2*Cu+Zn+Pb in moles). Averages (arithmetic mean values) were calculated by assigning concentrations below detection a value equivalent to half the detection limit before correction to a salt-free basis.

Figure 3.1

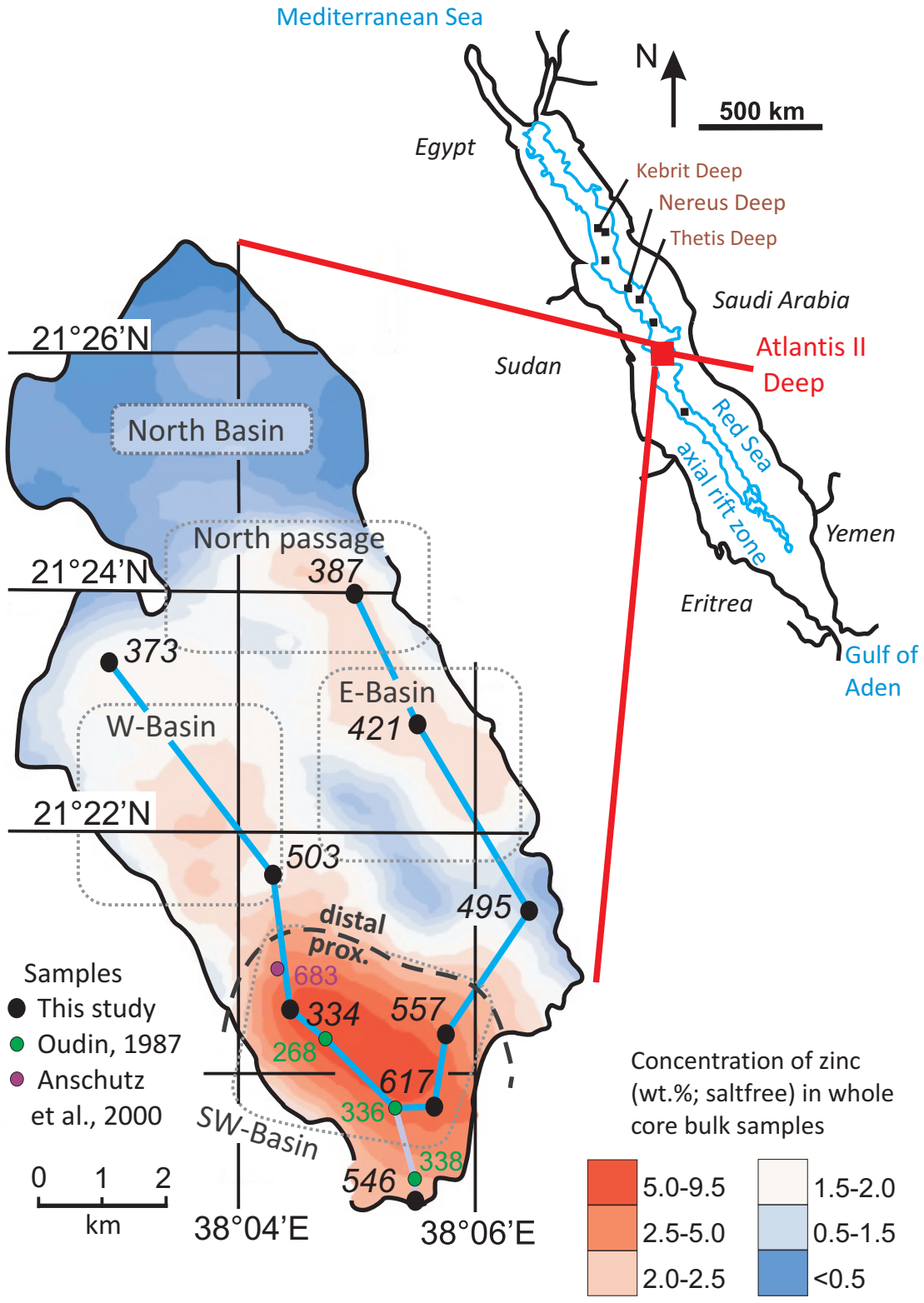
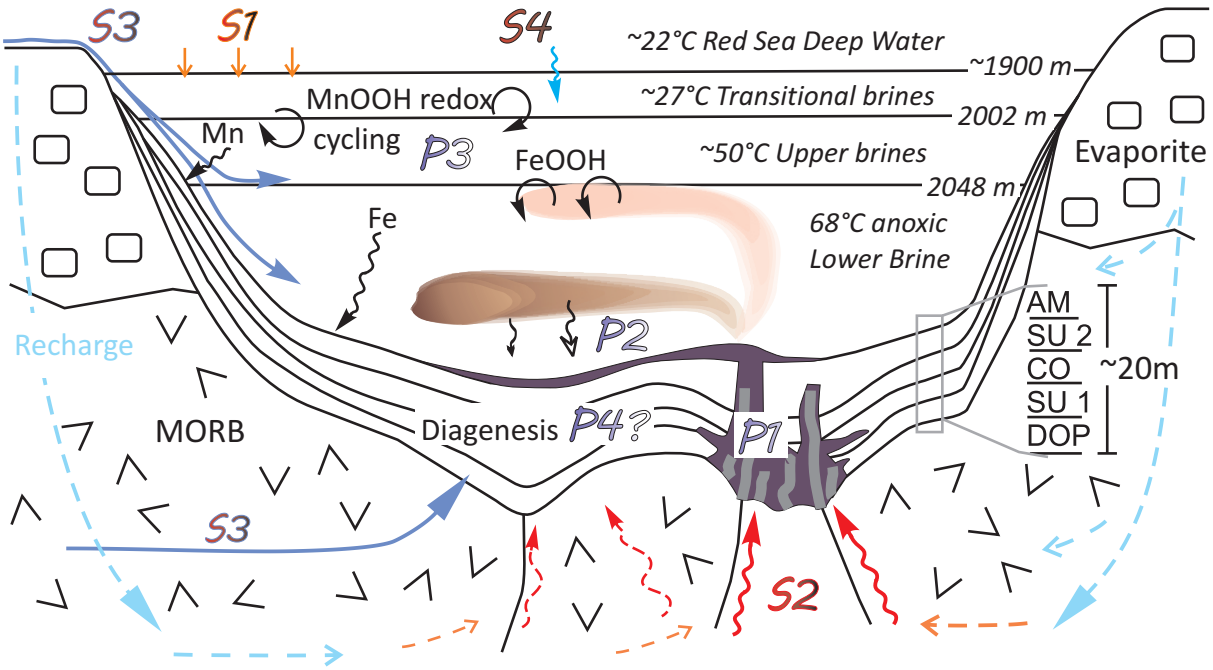

Mediterranean Sea
N
500 km
Egypt
Kebrit Deep
Nereus Deep
Thetis Deep
Saudi Arabia
Atlantis II Deep
Sudan
Red Sea axial rift zone
Yemen
Eritrea
Gulf of Aden
21°26'N
North Basin
North passage
21°24'N
387
373
E-Basin
421
W-Basin
21°22'N
503
495
distal
prox.
683
334
557
268
617
336
338
546
SW-Basin
Samples
This study
Oudin, 1987
Anschutz et al., 2000
0 1 2
km
38°04'E
38°06'E
Concentration of zinc (wt.%; saltfree) in whole core bulk samples
5.0-9.5
2.5-5.0
2.0-2.5
1.5-2.0
0.5-1.5
<0.5

Figure 3.2




**Sources of elements:**

- S1 Biogenic-siliciclastic detrital
- S2 Metal-rich hydrothermal fluid
- S3 Sinking brines or non-hydrothermal brines from below
- S4 Seawater via MnOOH/MnO transport

**Precipitation environments:**

- P1 Fluid conduits (Anhydrite + sulfides)
- P2 Hydrothermal plume (mainly sulfides)
- P3 Transitional brines (Fe at low $fO_2$; Mn at shallower and higher $fO_2$
- P4? Diagenesis/replacement

Figure 3.3

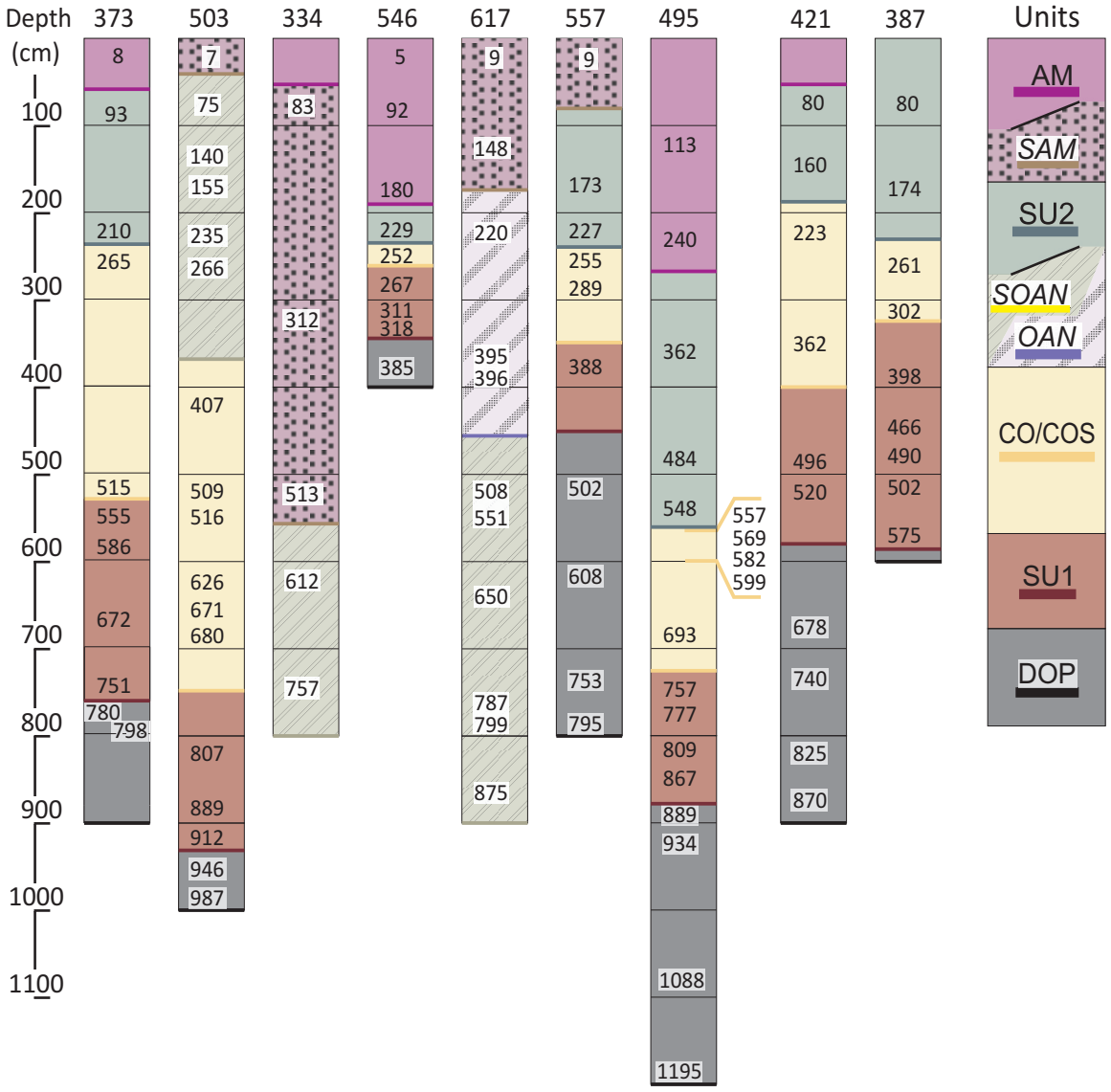
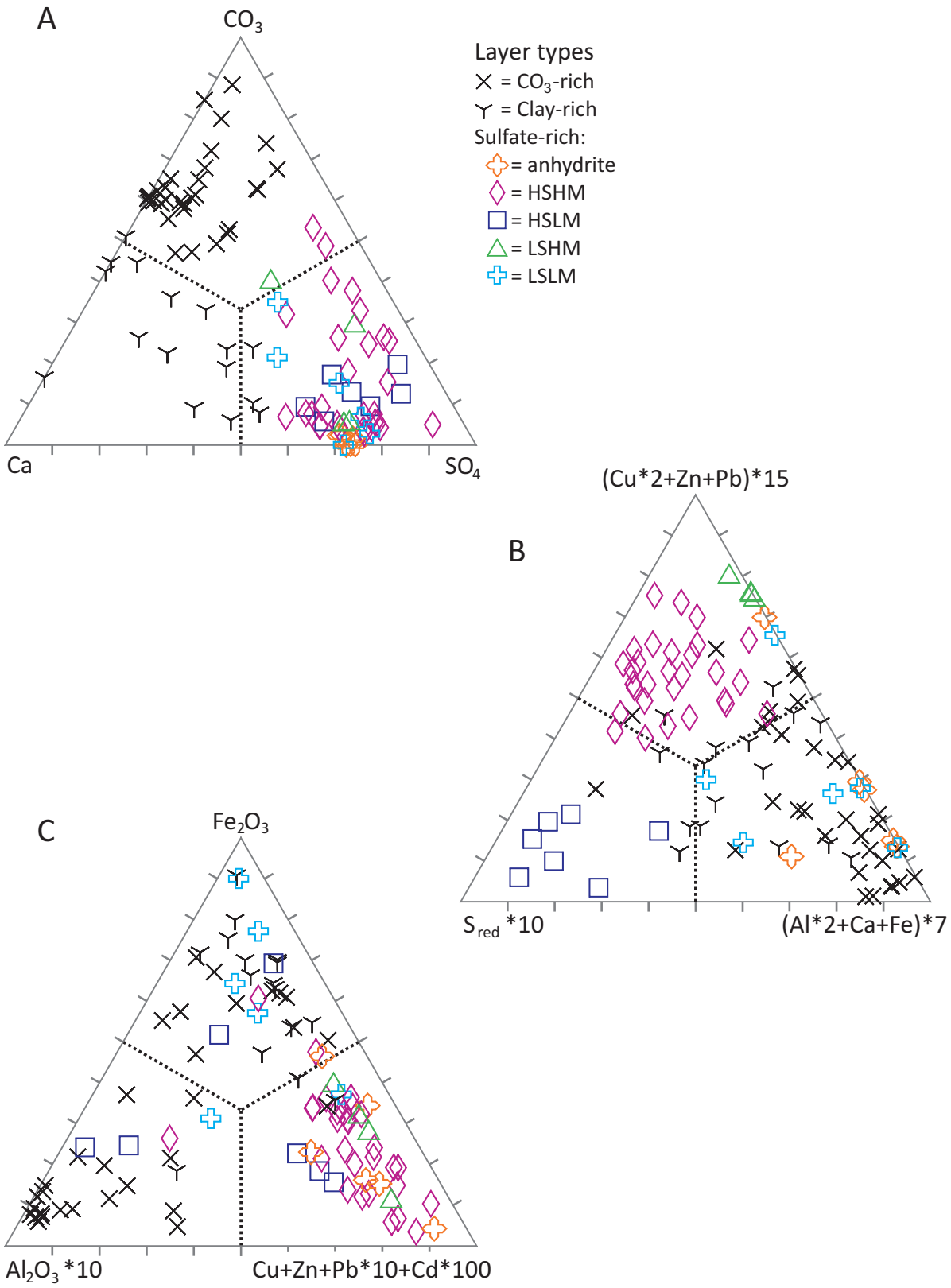

Depth
(cm)
100
200
300
400
500
600
700
800
900
1000
1100
373
8
93
210
265
515
555
586
672
751
780
798
503
7
75
140
155
235
266
407
509
516
626
671
680
807
889
912
946
987
334
83
312
513
612
757
546
5
92
180
229
252
267
311
318
385
617
9
148
220
395
396
508
551
650
787
799
875
557
9
173
227
255
289
388
502
608
753
795
495
113
240
362
484
548
557
569
582
599
693
757
777
809
867
889
934
1088
1195
421
80
160
223
362
496
520
678
740
825
870
387
80
174
261
302
398
466
490
502
575
Units
AM
SAM
SU2
SOAN
OAN
CO/COS
SU1
DOP

Figure 3.4


A
CO3
Ca
SO4
Layer types
= CO3-rich
= Clay-rich
Sulfate-rich:
= anhydrite
= HSHM
= HSLM
= LSHM
= LSLM
B
(Cu*2+Zn+Pb)*15
Sred *10
(Al*2+Ca+Fe)*7
C
Fe2O3
Al2O3 *10
Cu+Zn+Pb*10+Cd*100

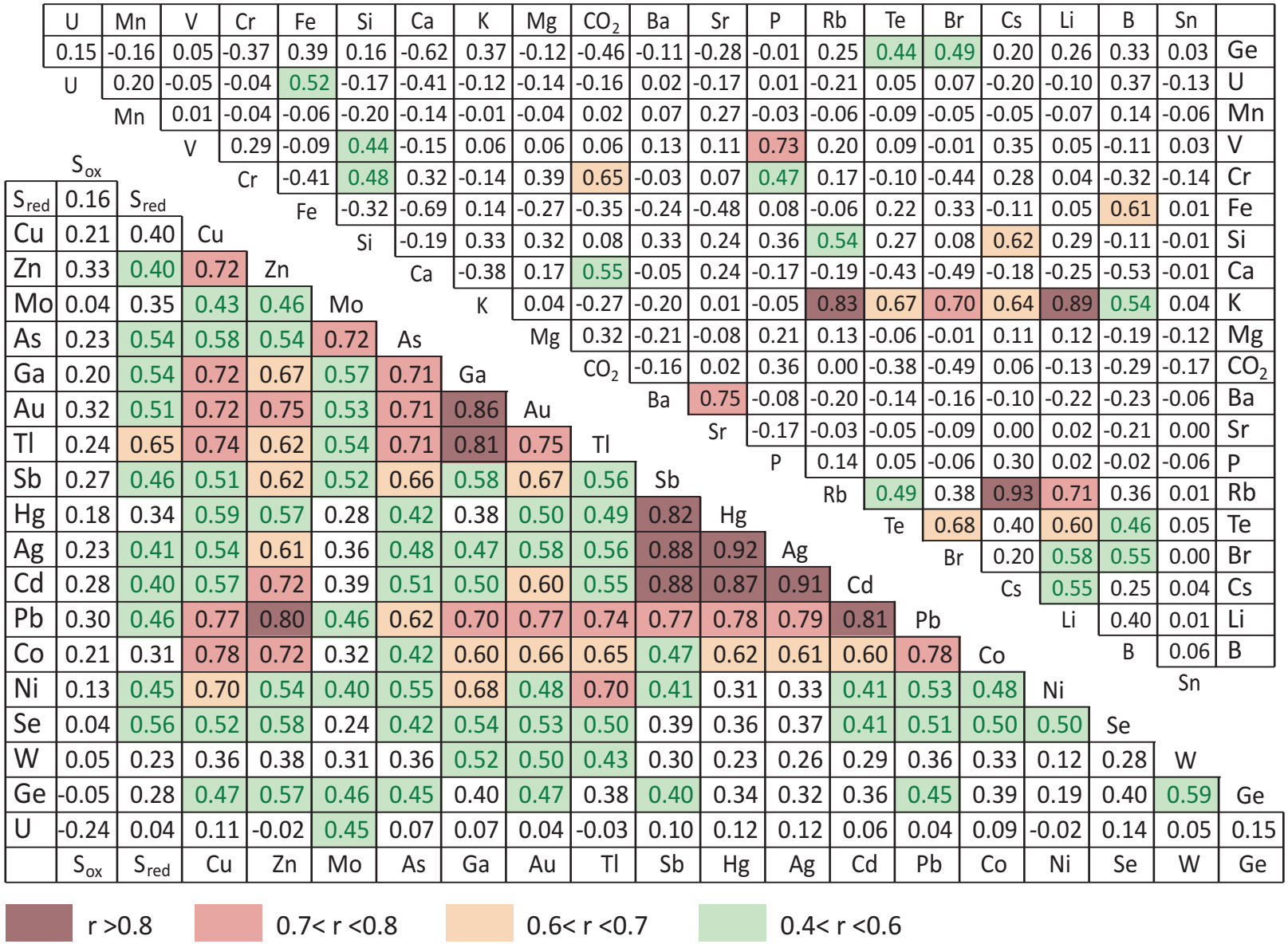

U Mn V Cr Fe Si Ca K Mg $CO_2$ Ba Sr P Rb Te Br Cs Li B Sn
0.15 -0.16 0.05 -0.37 0.39 0.16 -0.62 0.37 -0.12 -0.46 -0.11 -0.28 -0.01 0.25 0.44 0.49 0.20 0.26 0.33 0.03 Ge
U 0.20 -0.05 -0.04 0.52 -0.17 -0.41 -0.12 -0.14 -0.16 0.02 -0.17 0.01 -0.21 0.05 0.07 -0.20 -0.10 0.37 -0.13 U
Mn 0.01 -0.04 -0.06 -0.20 -0.14 -0.01 -0.04 0.02 0.07 0.27 -0.03 -0.06 -0.09 -0.05 -0.05 -0.07 0.14 -0.06 Mn
V 0.29 -0.09 0.44 -0.15 0.06 0.06 0.06 0.13 0.11 0.73 0.20 0.09 -0.01 0.35 0.05 -0.11 0.03 V
Cr -0.41 0.48 0.32 -0.14 0.39 0.65 -0.03 0.07 0.47 0.17 -0.10 -0.44 0.28 0.04 -0.32 -0.14 Cr
Fe -0.32 -0.69 0.14 -0.27 -0.35 -0.24 -0.48 0.08 -0.06 0.22 0.33 -0.11 0.05 0.61 0.01 Fe
Si -0.19 0.33 0.32 0.08 0.33 0.24 0.36 0.54 0.27 0.08 0.62 0.29 -0.11 -0.01 Si
Ca -0.38 0.17 0.55 -0.05 0.24 -0.17 -0.19 -0.43 -0.49 -0.18 -0.25 -0.53 -0.01 Ca
K 0.04 -0.27 -0.20 0.01 -0.05 0.83 0.67 0.70 0.64 0.89 0.54 0.04 K
Mg 0.32 -0.21 -0.08 0.21 0.13 -0.06 -0.01 0.11 0.12 -0.19 -0.12 Mg
$CO_2$ -0.16 0.02 0.36 0.00 -0.38 -0.49 0.06 -0.13 -0.29 -0.17 $CO_2$
Ba 0.75 -0.08 -0.20 -0.14 -0.16 -0.10 -0.22 -0.23 -0.06 Ba
Sr -0.17 -0.03 -0.05 -0.09 0.00 0.02 -0.21 0.00 Sr
P 0.14 0.05 -0.06 0.30 0.02 -0.02 -0.06 P
Rb 0.49 0.38 0.93 0.71 0.36 0.01 Rb
Te 0.68 0.40 0.60 0.46 0.05 Te
Br 0.20 0.58 0.55 0.00 Br
Cs 0.55 0.25 0.04 Cs
Li 0.40 0.01 Li
B 0.06 B
Sn
$S_{ox}$ $S_{red}$ Cu Zn Mo As Ga Au Tl Sb Hg Ag Cd Pb Co Ni Se W Ge
$S_{red}$ 0.16
Cu 0.21 0.40
Zn 0.33 0.40 0.72
Mo 0.04 0.35 0.43 0.46
As 0.23 0.54 0.58 0.54 0.72
Ga 0.20 0.54 0.72 0.67 0.57 0.71
Au 0.32 0.51 0.72 0.75 0.53 0.71 0.86
Tl 0.24 0.65 0.74 0.62 0.54 0.71 0.81 0.75
Sb 0.27 0.46 0.51 0.62 0.52 0.66 0.58 0.67 0.56
Hg 0.18 0.34 0.59 0.57 0.28 0.42 0.38 0.50 0.49 0.82
Ag 0.23 0.41 0.54 0.61 0.36 0.48 0.47 0.58 0.56 0.88 0.92
Cd 0.28 0.40 0.57 0.72 0.39 0.51 0.50 0.60 0.55 0.88 0.87 0.91
Pb 0.30 0.46 0.77 0.80 0.46 0.62 0.70 0.77 0.74 0.77 0.78 0.79 0.81
Co 0.21 0.31 0.78 0.72 0.32 0.42 0.60 0.66 0.65 0.47 0.62 0.61 0.60 0.78
Ni 0.13 0.45 0.70 0.54 0.40 0.55 0.68 0.48 0.70 0.41 0.31 0.33 0.41 0.53 0.48
Se 0.04 0.56 0.52 0.58 0.24 0.42 0.54 0.53 0.50 0.39 0.36 0.37 0.41 0.51 0.50 0.50
W 0.05 0.23 0.36 0.38 0.31 0.36 0.52 0.50 0.43 0.30 0.23 0.26 0.29 0.36 0.33 0.12 0.28
Ge -0.05 0.28 0.47 0.57 0.46 0.45 0.40 0.47 0.38 0.40 0.34 0.32 0.36 0.45 0.39 0.19 0.40 0.59
U -0.24 0.04 0.11 -0.02 0.45 0.07 0.07 0.04 -0.03 0.10 0.12 0.12 0.06 0.04 0.09 -0.02 0.14 0.05 0.15
r >0.8
0.7< r <0.8
0.6< r <0.7
0.4< r <0.6

Figure 3.5

Figure 3.6

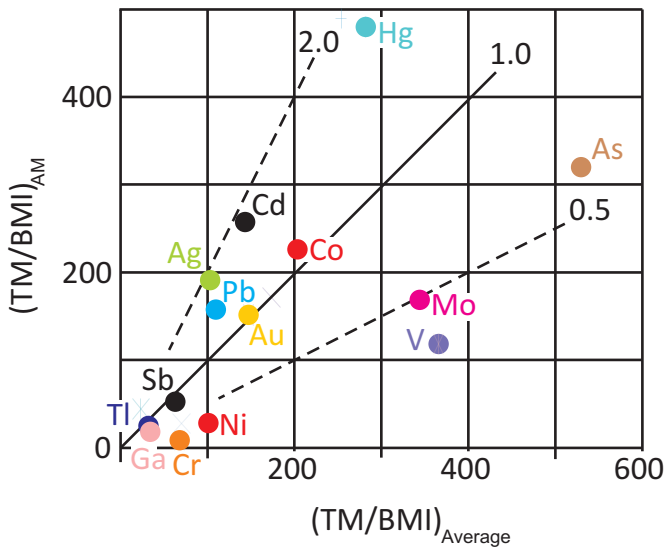

2.0
1.0
0.5
Hg
As
Cd
Co
Ag
Pb
Au
Mo
V
Sb
Tl
Ni
Ga
Cr
400
200
0
200
400
600
(TM/BMI)AM
(TM/BMI)Average

Figure 3.7

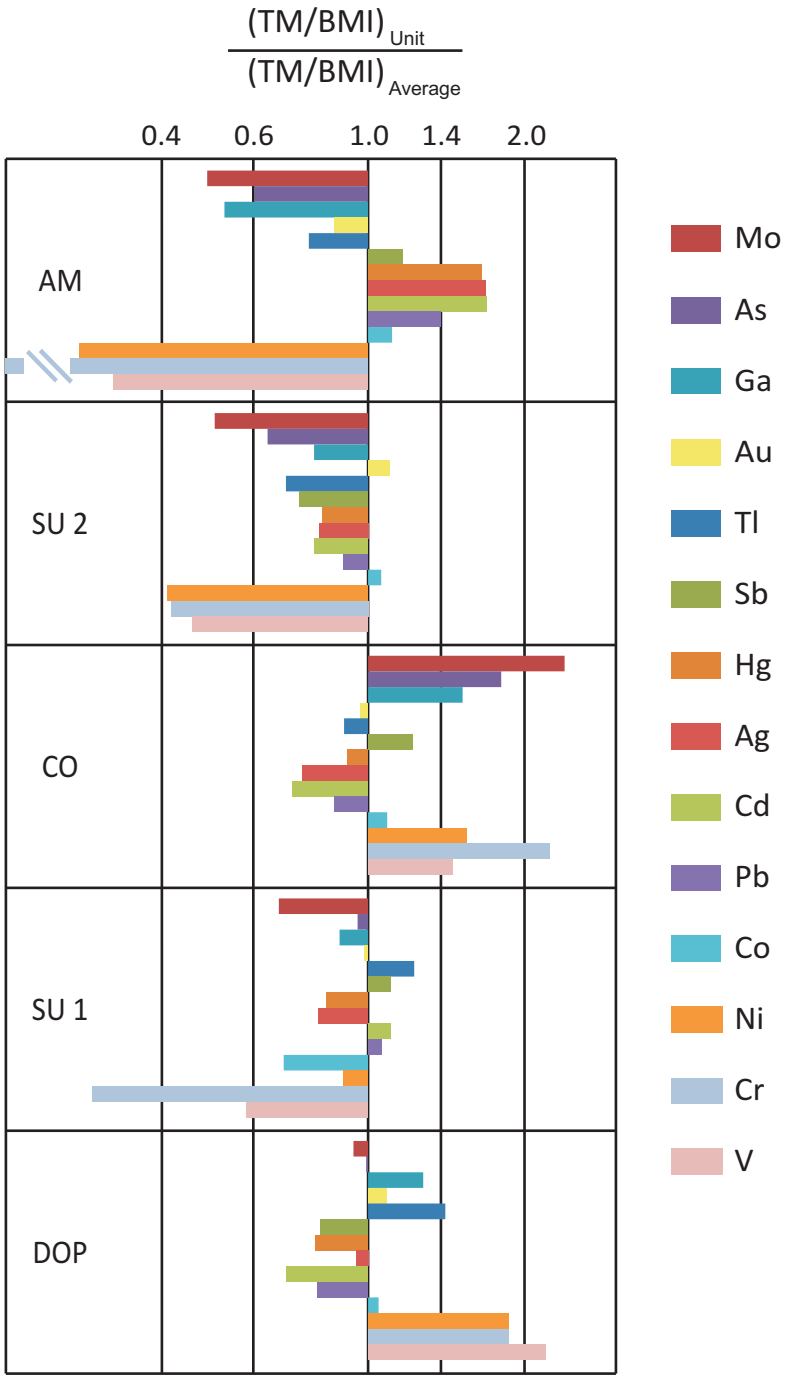

(TM/BMI) Unit
(TM/BMI) Average
0.4
0.6
1.0
1.4
2.0
AM
SU 2
CO
SU 1
DOP
Mo
As
Ga
Au
Tl
Sb
Hg
Ag
Cd
Pb
Co
Ni
Cr
V

Figure 3.8

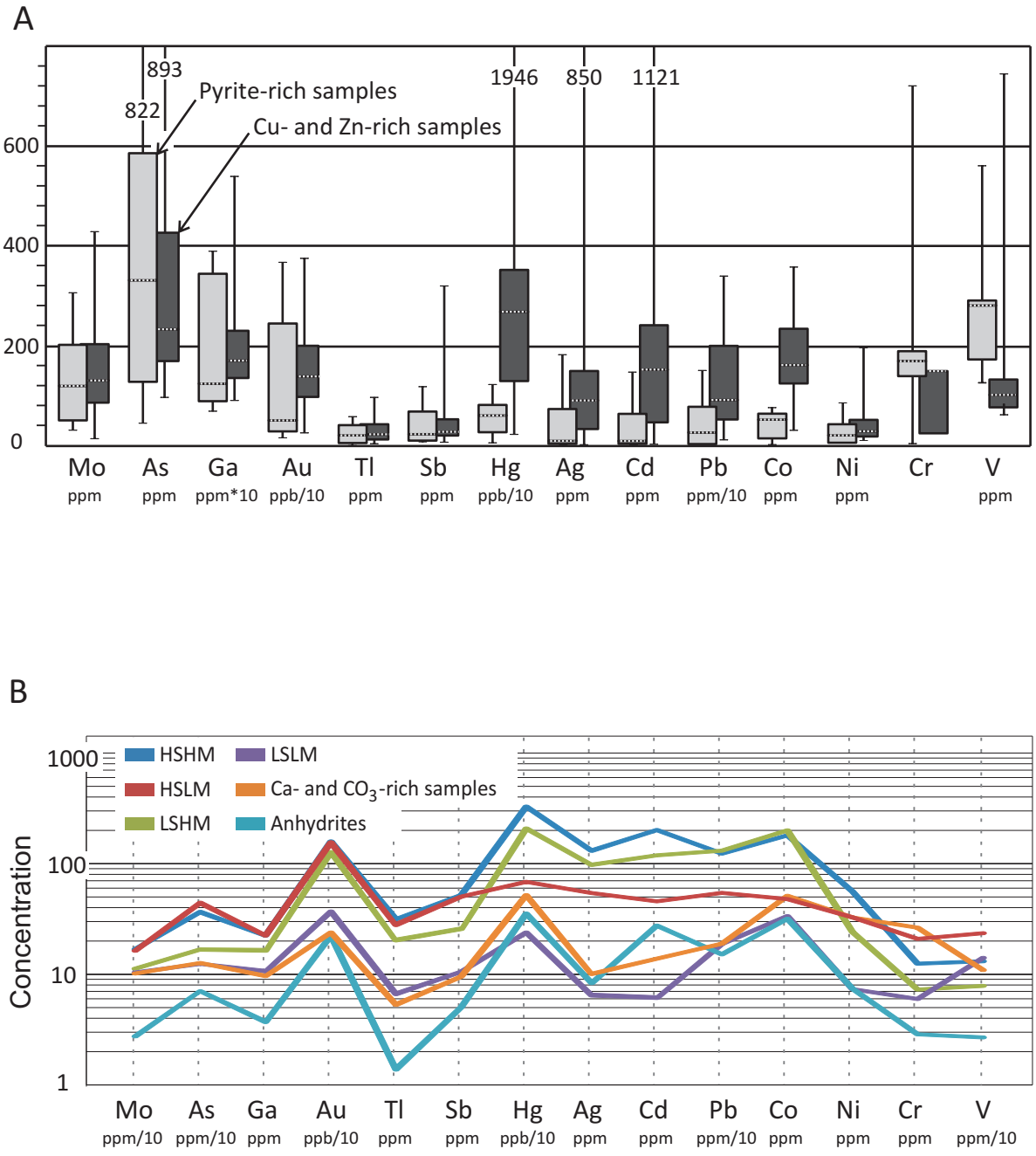

A
893
822
Pyrite-rich samples
Cu- and Zn-rich samples
1946
850
1121
600
400
200
0
Mo ppm
As ppm
Ga ppm*10
Au ppb/10
Tl ppm
Sb ppm
Hg ppb/10
Ag ppm
Cd ppm
Pb ppm/10
Co ppm
Ni ppm
Cr
V ppm
B
HSHM
LSLM
HSLM
Ca- and CO3-rich samples
LSHM
Anhydrites
1000
100
10
1
Concentration
Mo ppm/10
As ppm/10
Ga ppm
Au ppb/10
Tl ppm
Sb ppm
Hg ppb/10
Ag ppm
Cd ppm
Pb ppm/10
Co ppm
Ni ppm
Cr ppm
V ppm/10

Figure 3.9

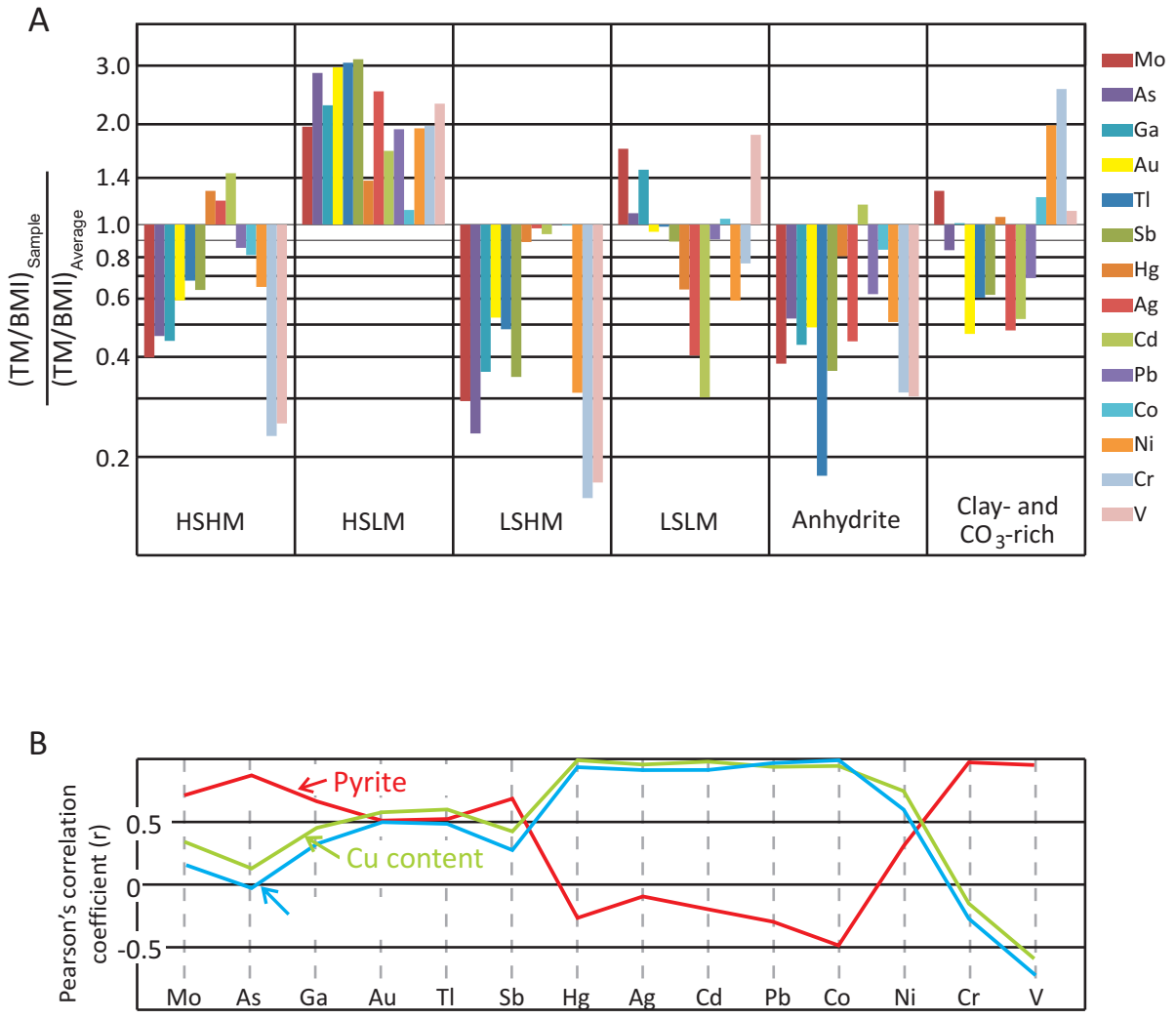

A
3.0
2.0
1.4
1.0
0.8
0.6
0.4
0.2
(TM/BMI)Sample / (TM/BMI)Average
HSHM
HSLM
LSHM
LSLM
Anhydrite
Clay- and CO3-rich
Mo
As
Ga
Au
Tl
Sb
Hg
Ag
Cd
Pb
Co
Ni
Cr
V
B
Pearson's correlation coefficient (r)
0.5
0
-0.5
Pyrite
Cu content
Mo
As
Ga
Au
Tl
Sb
Hg
Ag
Cd
Pb
Co
Ni
Cr
V

Figure 3.10

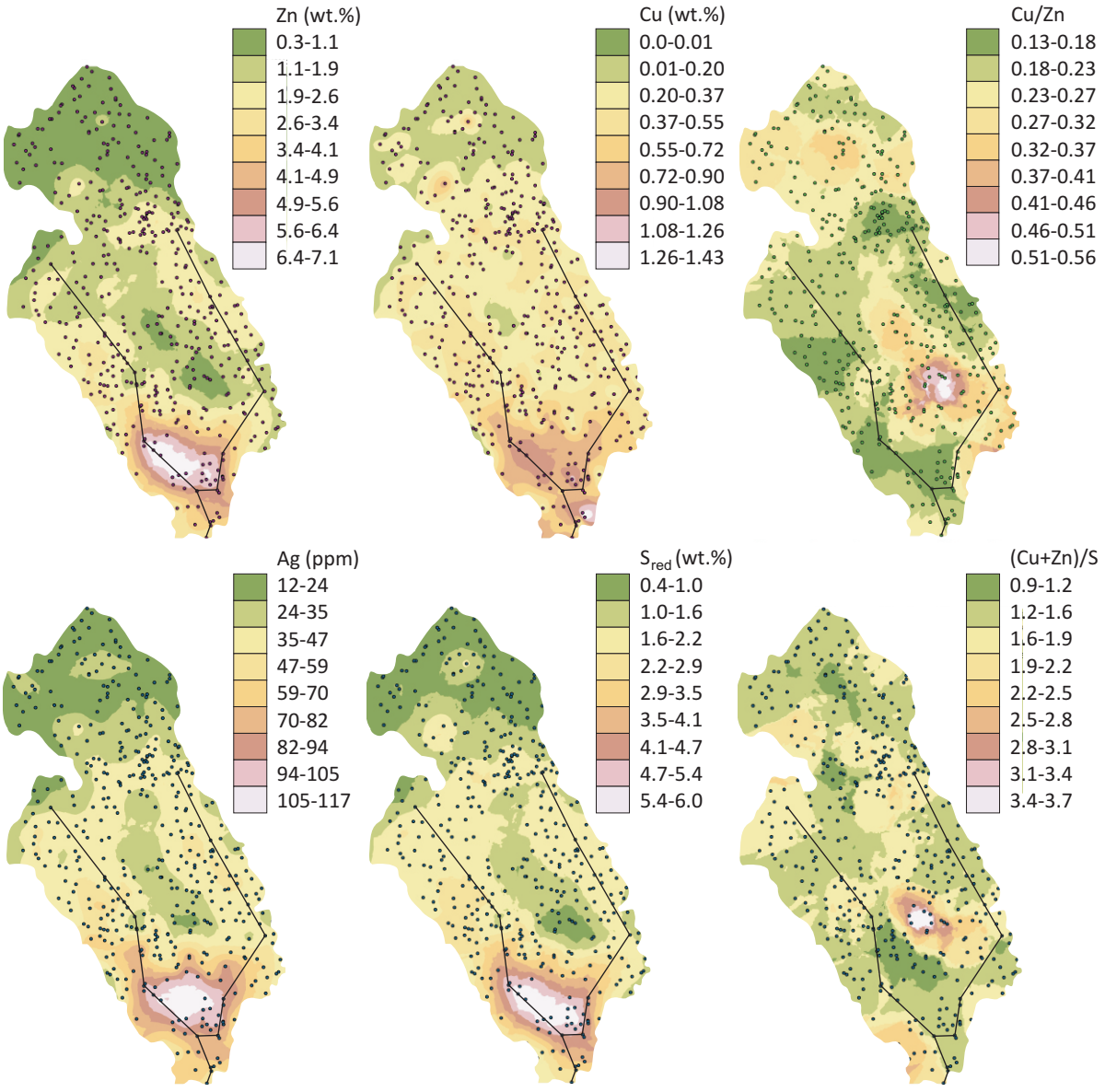

Zn (wt.%)
0.3-1.1
1.1-1.9
1.9-2.6
2.6-3.4
3.4-4.1
4.1-4.9
4.9-5.6
5.6-6.4
6.4-7.1
Cu (wt.%)
0.0-0.01
0.01-0.20
0.20-0.37
0.37-0.55
0.55-0.72
0.72-0.90
0.90-1.08
1.08-1.26
1.26-1.43
Cu/Zn
0.13-0.18
0.18-0.23
0.23-0.27
0.27-0.32
0.32-0.37
0.37-0.41
0.41-0.46
0.46-0.51
0.51-0.56
Ag (ppm)
12-24
24-35
35-47
47-59
59-70
70-82
82-94
94-105
105-117
$S_{red}$ (wt.%)
0.4-1.0
1.0-1.6
1.6-2.2
2.2-2.9
2.9-3.5
3.5-4.1
4.1-4.7
4.7-5.4
5.4-6.0
(Cu+Zn)/S
0.9-1.2
1.2-1.6
1.6-1.9
1.9-2.2
2.2-2.5
2.5-2.8
2.8-3.1
3.1-3.4
3.4-3.7

Figure 3.11

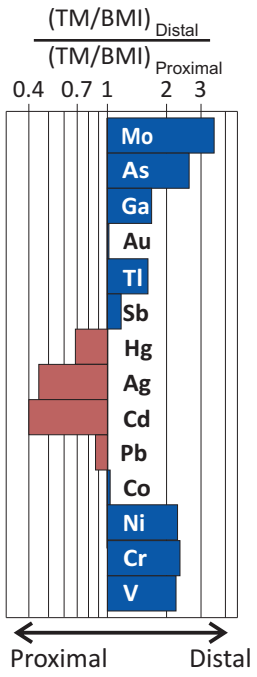



Figure 3.12

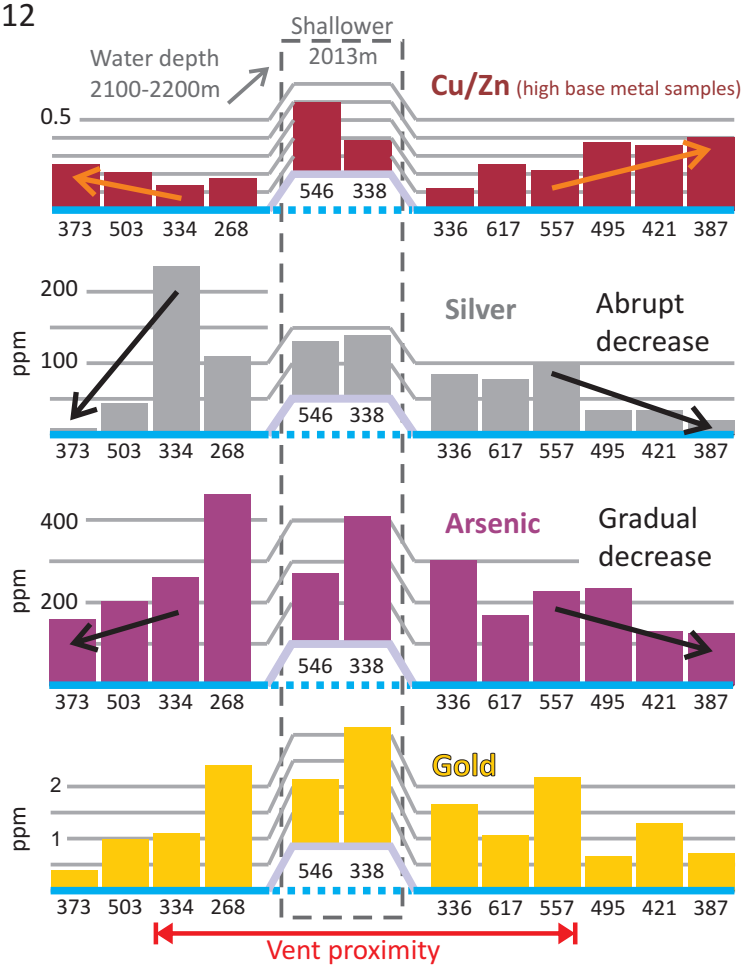


Figure 3.13

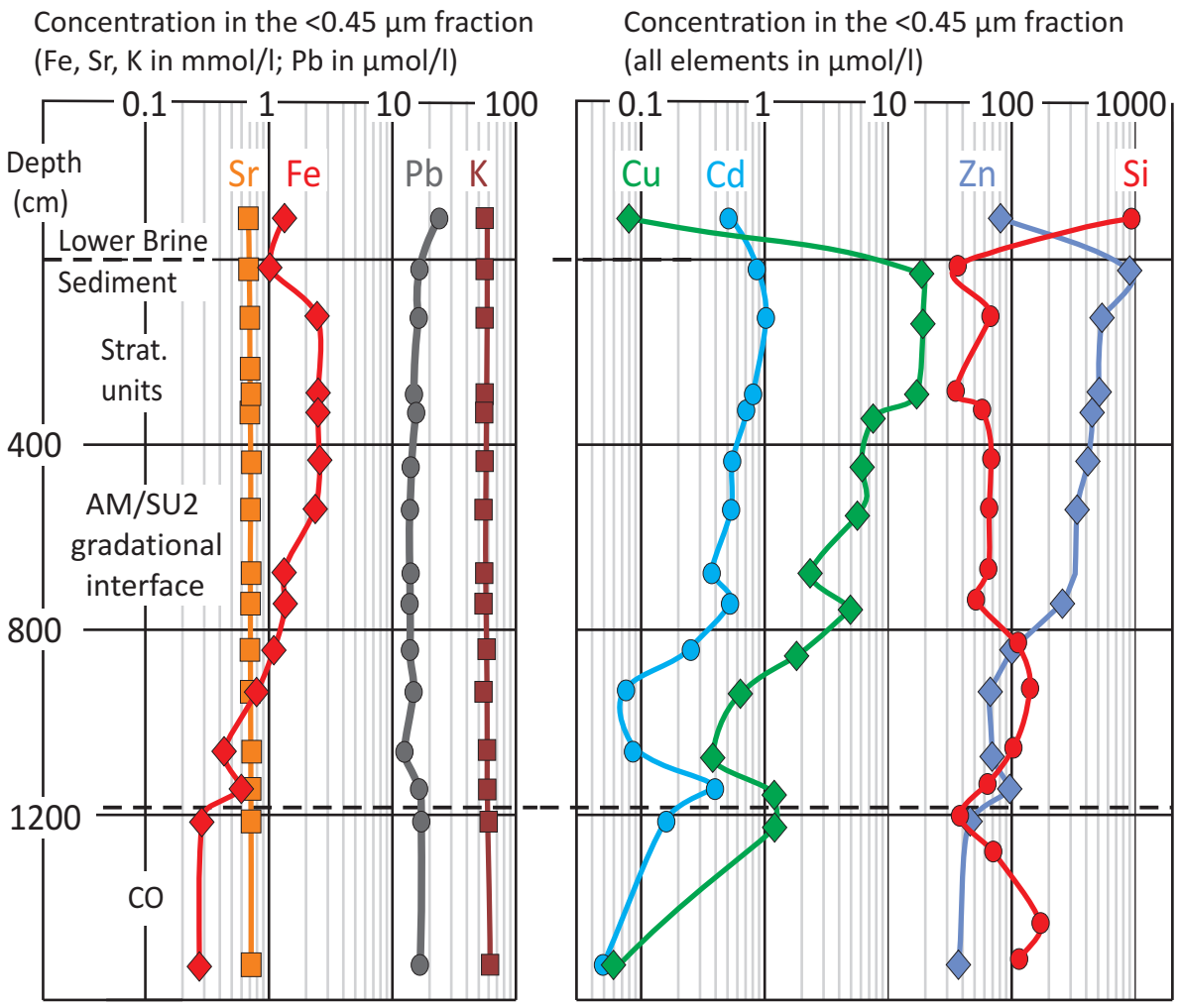

Concentration in the <0.45 µm fraction
(Fe, Sr, K in mmol/l; Pb in µmol/l)
Concentration in the <0.45 µm fraction
(all elements in µmol/l)
0.1
1
10
100
1000
Depth
(cm)
Sr
Fe
Pb
K
Cu
Cd
Zn
Si
Lower Brine
Sediment
Strat.
units
400
AM/SU2
gradational
interface
800
1200
CO

Figure 3.14

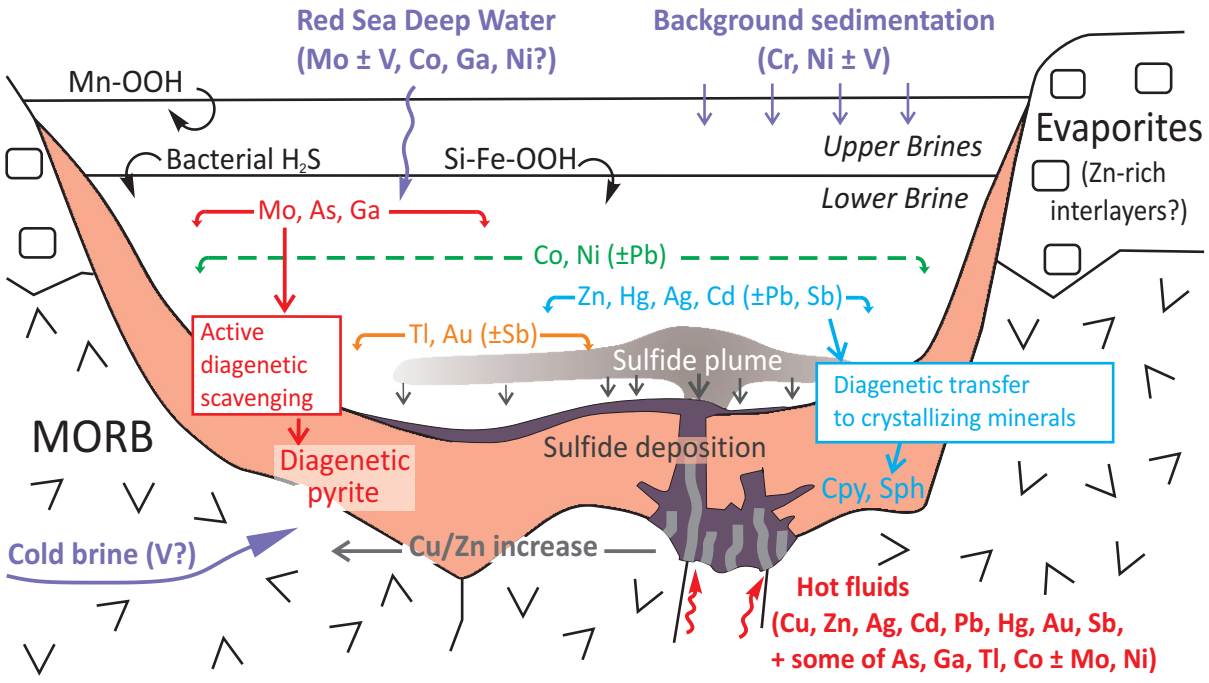

Red Sea Deep Water
(Mo ± V, Co, Ga, Ni?)
Background sedimentation
(Cr, Ni ± V)
Mn-OOH
Bacterial $H_2S$
Si-Fe-OOH
Upper Brines
Lower Brine
Evaporites
(Zn-rich
interlayers?)
Mo, As, Ga
Co, Ni (±Pb)
Zn, Hg, Ag, Cd (±Pb, Sb)
Active
diagenetic
scavenging
Tl, Au (±Sb)
Sulfide plume
Diagenetic transfer
to crystallizing minerals
MORB
Diagenetic
pyrite
Sulfide deposition
Cpy, Sph
Cu/Zn increase
Cold brine (V?)
Hot fluids
(Cu, Zn, Ag, Cd, Pb, Hg, Au, Sb,
+ some of As, Ga, Tl, Co ± Mo, Ni)

Figure 3.15

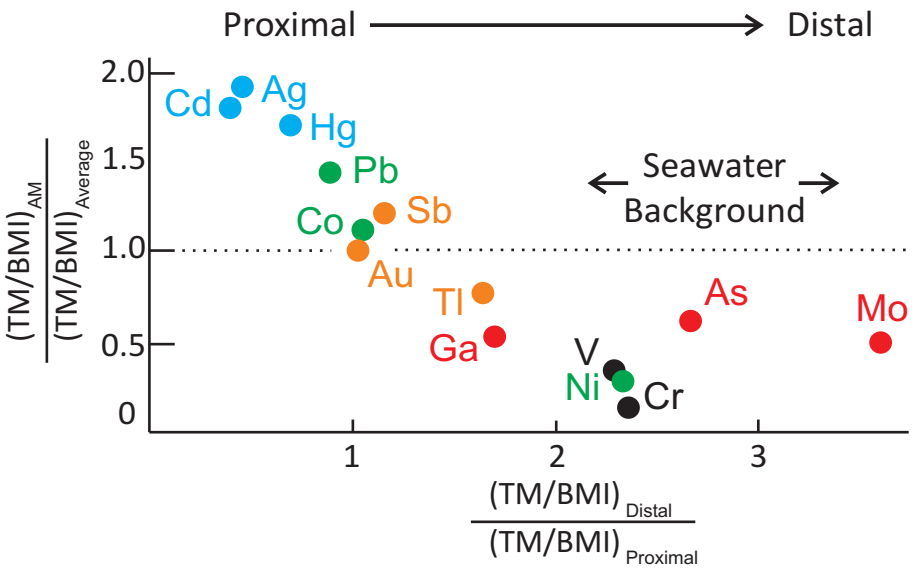
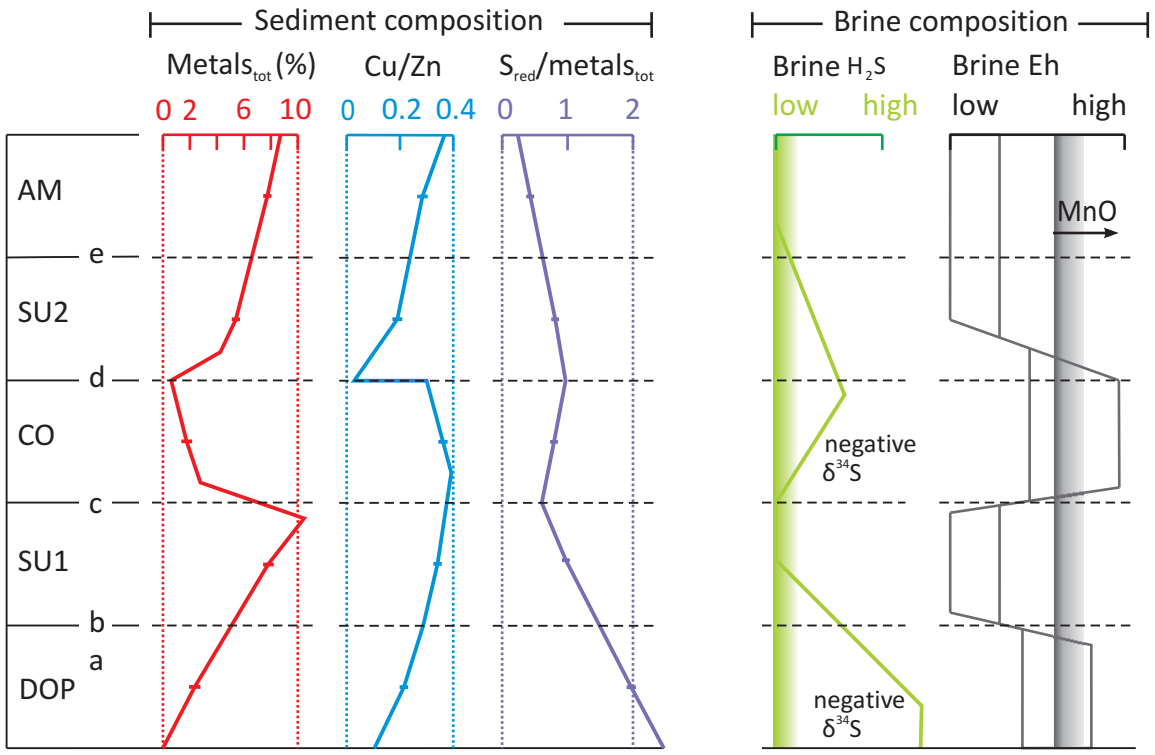

Proximal
Distal
2.0
1.5
1.0
0.5
0
Cd
Ag
Hg
Pb
Co
Sb
Au
Tl
Ga
As
Mo
V
Ni
Cr
Seawater
Background
1
2
3
(TM/BMI)AM / (TM/BMI)Average
(TM/BMI)Distal / (TM/BMI)Proximal

Figure 3.16


Sediment composition
Brine composition
Metals$_{tot}$ (%)
Cu/Zn
S$_{red}$/metals$_{tot}$
0 2 6 10
0 0.2 0.4
0 1 2
Brine H$_2$S
low high
Brine Eh
low high
AM
e
SU2
d
CO
c
SU1
b
a
DOP
MnO
negative δ$^{34}$S
negative δ$^{34}$S

Appendix 3.1. Summary statistics for major and trace elements in 100 samples of metalliferous sediment from the Atlantis II Deep (dry, salt-free basis).

| Element | Mo | As | Ga | Au | Tl | Sb | Hg | Ag | Cd | Pb | Co | Ni | Cr | V | Ge | In | Rb | Sc | Se | Sn |
|---|---|---|---|---|---|---|---|---|---|---|---|---|---|---|---|---|---|---|---|---|
| unit | ppm | ppm | ppm | ppb | ppm | ppm | ppb | ppm | ppm | ppm | ppm | ppm | ppm | ppm | ppm | ppm | ppm | ppm | ppm | ppm |
| method | 1 | 8 | 1 | 3 | 1 | 3 | 4 | 8 | 8 | 1 | 1 | 8 | 8 | 1 | 1 | 1 | 1 | 8 | 1 | 1 |
| det.lim. | 1 | 2 | 0.2 | 2 | 0.1 | 0.1 | 5 | 1 | 1 | 0.8 | 0.2 | 5 | 5 | 5 | 0.7 | 0.2 | 0.4 | 0.1 | 0.8 | 0.5 |
| mean | 121 | 215 | 14.1 | 765 | 14.8 | 25.0 | 1354 | 51 | 74 | 554 | 91 | 36 | 18.4 | 120 | 7.8 | 0.2 | 27 | 2.47 | 3.95 | 5.5 |
| minimum | 2.17 | 3.62 | 0.43 | b.d. | 0.11 | b.d. | 5 | b.d. | b.d. | b.d. | 1.85 | b.d. | b.d. | 2.57 | 0.38 | b.d. | 1.4 | 0.10 | b.d. | b.d. |
| median | 97 | 152 | 11.1 | 360 | 8.0 | 13.1 | 557 | 9 | 11 | 281 | 58 | 27 | 8.7 | 99 | 7.6 | 0.2 | 23 | 1.18 | 3.49 | 0.8 |
| maximum | 429 | 1145 | 53.7 | 3755 | 96.0 | 320 | 19455 | 850 | 1121 | 3398 | 358 | 198 | 87.7 | 746 | 24.5 | 1.2 | 127 | 11.53 | 15.96 | 109 |
| std.dev. | 102 | 226 | 11.0 | 908 | 20.1 | 40.6 | 2328 | 107 | 147 | 704 | 88 | 37 | 19.3 | 103 | 4.5 | 0.2 | 20 | 2.71 | 2.81 | 17.6 |
| std.d./mean | 0.84 | 1.05 | 0.78 | 1.19 | 1.35 | 1.63 | 1.72 | 2.10 | 1.98 | 1.27 | 0.97 | 1.04 | 1.05 | 0.86 | 0.58 | 0.72 | 0.74 | 1.10 | 0.71 | 3.22 |
| no of n.d. | | | | 15 | | 2 | 2 | 20 | 21 | 4 | | 21 | 48 | | | 92 | | 1 | 17 | 49 |
| Averages for different sample types: | | | | | | | | | | | | | | | | | | | | |
| Clay-rich | 160 | 215 | 8.8 | 322 | 7.5 | 12.0 | 606 | 6 | 10 | 221 | 55 | 14 | 7.6 | 71 | 9.5 | 0.3 | 40 | 0.88 | 3.25 | 4.4 |
| $CO_3$-rich | 72 | 81 | 9.9 | 195 | 4.2 | 8.2 | 470 | 12 | 16 | 172 | 49 | 41 | 35.5 | 127 | 5.0 | 0.2 | 30 | 4.95 | 3.10 | 1.2 |
| HSHM | 168 | 364 | 22.2 | 1575 | 31.2 | 51.6 | 3246 | 129 | 199 | 1219 | 179 | 55 | 12.4 | 130 | 11.0 | 0.3 | 24 | 1.64 | 5.77 | 4.4 |
| HSLM | 162 | 440 | 22.2 | 1545 | 27.6 | 49.9 | 679 | 54 | 45 | 541 | 48 | 32 | 20.8 | 234 | 6.5 | 0.2 | 21 | 2.43 | 5.29 | 16.7 |
| LSHM | 112 | 167 | 16.2 | 1261 | 20.1 | 25.5 | 2058 | 96 | 118 | 1297 | 198 | 24 | 7.3 | 78 | 8.9 | 0.2 | 20 | 0.95 | 4.75 | 26.9 |
| LSLM | 103 | 124 | 10.6 | 367 | 6.6 | 10.5 | 237 | 6 | 6 | 187 | 33 | 7 | 5.9 | 140 | 9.8 | 0.2 | 32 | 0.65 | 2.49 | 0.6 |
| anhy | 27 | 70 | 3.7 | 222 | 1.4 | 5.0 | 352 | 8 | 27 | 151 | 32 | 7 | 2.9 | 27 | 2.0 | 0.1 | 3 | 0.32 | 0.99 | 14.3 |

| Element | U | W | Y | Zr | Cu | Zn | Fe | $S_{red}$* | $SO_4$ | Mn | Si | Sr | Ba | Ca | $CO_2$ | $C_{org}$* |
|---|---|---|---|---|---|---|---|---|---|---|---|---|---|---|---|---|
| unit | ppm | ppm | ppm | ppm | ppm | ppm | wt.% | wt.% | wt.% | wt.% | wt.% | ppm | ppm | wt.% | wt.% | wt.% |
| method | 1 | 1 | 1 | 8 | 1 | 1 | 2 | 7/6 | 7 | 1 | 2 | 1 | 1 | 2 | 5 | 7/5 |
| det.lim. | 0.1 | 0.7 | 0.1 | 1 | 2 | 30 | 0.07 | 0.01 | 0.3 | 0.0004 | 0.02 | 3 | 3 | 0.01 | 0.01 | 0.01 |
| mean | 5.96 | 5.89 | 4.40 | 14.1 | 0.53 | 1.97 | 25.0 | 1.43 | 13.1 | 2.11 | 17.9 | 458 | 1432 | 11.0 | 7.0 | 0.16 |
| minimum | 0.05 | b.d. | b.d. | b.d. | 0.005 | 0.025 | 0.14 | b.d. | b.d. | 0.04 | 0.46 | 72.6 | b.d. | 1.33 | 0.01 | b.d. |
| median | 4.77 | 4.02 | 2.03 | 1.6 | 0.23 | 1.16 | 25.2 | 0.55 | 6.1 | 0.60 | 16.6 | 413 | 260 | 6.5 | 2.4 | 0.06 |
| maximum | 32.5 | 42.9 | 18.5 | 86.8 | 2.62 | 14.60 | 73.2 | 13.91 | 71.6 | 41.91 | 55.3 | 2009 | 16051 | 38.1 | 30.7 | 2.24 |
| std. | 4.96 | 6.68 | 4.70 | 21.0 | 0.65 | 2.42 | 16.8 | 2.14 | 16.0 | 5.51 | 9.7 | 312 | 2804 | 10.1 | 8.5 | 0.33 |
| std./mean | 0.83 | 1.13 | 1.07 | 1.48 | 1.22 | 1.23 | 0.67 | 1.50 | 1.22 | 2.61 | 0.54 | 0.68 | 1.96 | 0.92 | 1.22 | 2.09 |
| no of n.d. | | 27 | 1 | 52 | | | | 6 | 8 | | | 1 | | | 1 | 22 |
| Averages for different sample types | | | | | | | | | | | | | | | | |
| Clay-rich | 7.53 | 6.04 | 1.69 | 1.9 | 0.24 | 0.94 | 38.6 | 0.78 | 2.2 | 3.33 | 16.2 | 508 | 938 | 5.3 | 1.4 | 0.03 |

| | U | W | Y | Zr | Cu | Zn | Fe | $S_{red}$* | $SO_4$ | Mn | Si | Sr | Ba | Ca | $CO_2$ | $C_{org}$* |
|---|---|---|---|---|---|---|---|---|---|---|---|---|---|---|---|---|
| $CO_3$-rich | 5.87 | 1.45 | 8.89 | 33.4 | 0.25 | 0.70 | 19.7 | 0.47 | 2.6 | 3.63 | 19.0 | 420 | 638 | 15.9 | 16.5 | 0.28 |
| HSHM | 6.04 | 10.05 | 2.91 | 6.6 | 1.17 | 4.42 | 27.6 | 2.50 | 18.1 | 0.91 | 18.1 | 359 | 1074 | 6.2 | 3.5 | 0.10 |
| HSLM | 6.47 | 8.35 | 3.89 | 15.0 | 0.25 | 0.80 | 18.1 | 5.81 | 18.5 | 0.73 | 30.5 | 870 | 6579 | 6.4 | 2.4 | 0.17 |
| LSHM | 6.21 | 6.26 | 1.91 | 2.0 | 0.88 | 4.34 | 30.3 | 0.05 | 17.6 | 1.29 | 14.6 | 369 | 2692 | 8.7 | 2.9 | 0.41 |
| LSLM | 6.19 | 9.99 | 0.98 | 1.1 | 0.16 | 0.65 | 30.4 | 0.27 | 16.0 | 0.72 | 17.8 | 458 | 1532 | 8.9 | 2.2 | 0.08 |
| anhy | 0.85 | 1.85 | 0.52 | 0.6 | 0.18 | 0.80 | 4.1 | 0.08 | 61.3 | 0.16 | 3.0 | 584 | 1766 | 31.8 | 0.7 | 0.04 |

| Element | $Al_2O_3$ | Mg | $TiO_2$ | $K_2O$ | $P_2O_5$ | F | B | Br | Cs | Hf | Li | Nb | Ta | Th |
|---|---|---|---|---|---|---|---|---|---|---|---|---|---|---|
| unit | wt.% | wt.% | wt.% | wt.% | wt.% | wt.% | ppm | ppm | ppm | ppm | ppm | ppm | ppm | ppm |
| method | 9 | 2 | 9 | 9 | 9 | 10 | 1 | 3 | 8 | 8 | 8 | 8 | 8 | 8 |
| det.lim. | 0.01 | 0.01 | 0.0001 | 0.001 | 0.01 | 0.01 | 10 | 0.5 | 0.05 | 0.5 | 0.3 | 0.1 | 0.1 | 0.01 |
| mean | 2.22 | 1.81 | 0.14 | 1.63 | 0.28 | 0.02 | 103 | 343 | 1.80 | 0.66 | 20 | 2.04 | 0.16 | 0.83 |
| minimum | 0.03 | 0.03 | 0.0001 | 0.01 | b.d. | b.d. | 5.43 | 9.98 | 0.06 | b.d. | 2.57 | b.d. | b.d. | 0.01 |
| median | 1.32 | 1.42 | 0.06 | 1.46 | 0.27 | 0.01 | 88 | 268 | 1.35 | 0.53 | 20 | 0.97 | 0.11 | 0.44 |
| maximum | 9.52 | 8.17 | 0.68 | 5.18 | 0.77 | 0.13 | 278 | 1195 | 8.77 | 2.23 | 56 | 9.86 | 0.59 | 3.91 |
| std. | 2.13 | 1.39 | 0.16 | 1.06 | 0.16 | 0.02 | 63 | 246 | 1.66 | 0.42 | 9 | 2.32 | 0.12 | 0.89 |
| std./mean | 0.96 | 0.77 | 1.20 | 0.65 | 0.57 | 1.00 | 0.62 | 0.72 | 0.92 | 0.63 | 0.47 | 1.14 | 0.74 | 1.07 |
| no of n.d. | | | | | | 65 | | | | 80 | | 3 | 72 | |
| Averages for different sample types | | | | | | | | | | | | | | |
| Clay-rich | 0.82 | 1.44 | 0.04 | 2.62 | 0.18 | 0.01 | 167 | 526 | 2.46 | 0.59 | 26 | 0.68 | 0.12 | 0.31 |
| $CO_3$-rich | 4.03 | 2.35 | 0.28 | 1.38 | 0.30 | 0.04 | 97 | 213 | 2.16 | 0.96 | 19 | 4.15 | 0.26 | 1.63 |
| HSHM | 1.85 | 1.55 | 0.08 | 1.64 | 0.39 | 0.02 | 97 | 420 | 1.39 | 0.52 | 20 | 1.30 | 0.12 | 0.59 |
| HSLM | 2.22 | 1.95 | 0.15 | 1.37 | 0.26 | 0.01 | 58 | 282 | 1.82 | 0.59 | 16 | 2.15 | 0.15 | 0.86 |
| LSHM | 1.26 | 1.64 | 0.05 | 1.68 | 0.32 | 0.02 | 147 | 512 | 0.91 | 0.53 | 19 | 0.74 | 0.11 | 0.33 |
| LSLM | 0.62 | 2.55 | 0.02 | 2.10 | 0.15 | 0.01 | 96 | 421 | 2.29 | 0.47 | 26 | 0.49 | 0.09 | 0.25 |
| anhy | 0.33 | 0.36 | 0.01 | 0.10 | 0.08 | 0.01 | 13 | 61 | 0.12 | 0.29 | 8 | 0.21 | 0.06 | 0.09 |

The salt-free calculation is based on Na concentration, assuming all Na is in NaCl (conversion factors are given in Table 3.2). * $S_{red.}$ and $C_{org.}$ were calculated from total S and C (methods 8) minus sulfate sulfur (method 6) and carbonate carbon (method 5), respectively. Analytical methods: 1=ICP-MS after fusion with Na-peroxide and dissolution of the fused glass with nitric acid; 2=ICP-OES after fusion with Na-peroxide and dissolution of the fused glass with nitric acid; 3=Instrumental neutron activation (INAA), 4=cold vapour-flow injection mercury system (FIMS), 5=Coulometry, 6=Combustion at 550°C and infrared (IR) detection; 7=Combustion at 1800°C and thermal conductivity detection; 8=ICP-MS after

four-acid dissolution (HF-$HNO_3$-HCl-$HClO_4$-); 9=ICP-OES after four-acid dissolution (HF-$HNO_3$-HCl-$HClO_4$-); 10=Ion-specific electrode. Methods 1 to 6 and 10 were carried out by Activation Laboratories. Method 7 was carried out at the Hatch Laboratories at the University of Ottawa. Methods 8 and 9 were carried out at the University of Kiel. Be, Bi and Te were analyzed with detection limits of 3, 2 and 6 ppm respectively (method 1); Ir was analyzed with a detection limit 5 ppb (method 3). These elements were not detected, except one sample 334-312, which contained 6.3 ppm Bi. "no of n.d." equals the number of samples in which the element was not detected. "b.d."=Below detection. For the purpose of calculating averages, samples with elements below detection were assigned values of half the detection limit before correcting for the salt concentration. Reproducibility and standards: For ICP-OES, 8 duplicate samples were analyzed with average deviations of <5% for Al, Fe, Mn, Ca, K, Ti, Sr, Cu and Zn, and 5-20% for Mg, P and Ba. Standard NOD-A-1 was measured 7 times, Nod-P1 and GSPN-2 twice each, BHVO-1 four times and BHVO-2 three times. For ICP-MS, 8 duplicate samples were analyzed with average deviations of <5% and always <10% except once for Y, Zr, Te, Ta, La, Ce, Pr, Nd, Ba and Th. Standards NOD-A-1 was measured 4 times, Nod-P1 and GSPN-2 twice each, and BHVO-2 seven times. For INAA, standards GXR-1, CZN-3, MP-1b, and DMMAS 114 were measured twice each. For coulometry, 14 duplicates were measured with average deviations of 14.6% for samples with >0.02 wt.% $CO_2$, and typically <5% for samples with >1 wt.% $CO_2$. Standard SY-4 and calcium carbonate were measured 10 times each. For FUS-ISE, 6 duplicate samples were analyzed with deviations of <5% for two samples, excluding those with low concentrations or below detection limit. Standards GBW 07113, SCO-1, DR-N Cert, UB-N, W-2a, and SGR-1b were measured twice each. For FIMS, 6 duplicate samples were analyzed with deviations of <5%, except 15% for one sample. Standards GXR-1, GXR-4, and GXR-6 were measured twice each. For IR ($SO_4$), 10 duplicate samples were analyzed with deviations of <10% for samples with >1 wt.% $SO_4$, and 0-75% for concentration <1 wt.% $SO_4$, excluding those with concentration below detection limit. For fusion ICP-MS and ICP-OES, 10 duplicate samples were analyzed with deviations of <10%, except for Ag, Ce, Eu, Gd, La, Nd, Ni, Se, Sm, Sn and W, for which deviation was 10-30%, for Cs all duplicates had average deviation <10%, except one with concentrations 6.4 and 0.5 ppm. Standards GXR-1, DH-1a, MP-1a, GXR-4, CCU-1C, LKSD-4, NOD-A-1, NOD-P-1, NIST 696, GBW 07239, GBW 07238, NCS DC70014, NCS DC70009, GBW07241, MP-1b, CCU-1d, and CZN-4 were measured various times each to account for at least one element. For total sulfur, 10 duplicate samples were analyzed with deviations of <10%. Standard Sulfanilic Acid was measured 10 times and used for linear calibration twice.

Appendix 3.2. Comparison of average elemental concentrations in washed (Gurvich, 2006) and unwashed samples (this study, salt-free basis) in different stratigraphic units of the Atlantis II Deep.

| | | AM | | SU2 | | CO | | SU1 | | DOP | |
|---|---|---|---|---|---|---|---|---|---|---|---|
| | | Gurvich 2006 | this study | Gurvich 2006 | this study | Gurvich 2006 | this study | Gurvich 2006 | this study | Gurvich 2006 | this study |
| Fe | wt.% | 33.6 | 23.8 | 26.3 | 16.2 | 34.3 | 22.6 | 33.1 | 17.0 | 23.5 | 13.2 |
| Si | wt.% | 11.9 | 6.8 | 11.6 | 8.2 | 9.4 | 7.9 | 13.2 | 9.3 | 11.3 | 9.1 |
| Mn | wt.% | 0.70 | 0.72 | 0.88 | 0.63 | 4.7 | 4.3 | 1.77 | 1.3 | 1.7 | 1.3 |
| Cu | wt.% | 0.49 | 0.88 | 0.84 | 0.45 | 0.21 | 0.25 | 1.1 | 0.92 | 0.20 | 0.23 |
| Zn | wt.% | 2.3 | 3.2 | 5.1 | 2.3 | 0.47 | 0.69 | 3.5 | 2.7 | 0.71 | 1.1 |
| $S_{tot}$ | wt.% | 3.0 | 5.3 | 7.8 | 7.9 | 1.9 | 1.4 | 7.9 | 9.0 | 4.5 | 3.6 |
| $S_{red}$ | wt.% | | 1.63 | | 1.54 | | 0.61 | | 3.14 | | 1.79 |
| Ca | wt.% | 3.4 | 4.9 | 4.5 | 8.4 | 2.7 | 5.7 | 1.0 | 6.5 | 6.3 | 13.4 |
| Ba | wt.% | 0.10 | 0.08 | 0.15 | 0.16 | 0.12 | 0.15 | 0.12 | 0.22 | <0.03 | 0.08 |
| Al | wt.% | 0.95 | 0.57 | 1.09 | 0.70 | 1.47 | 1.27 | 1.37 | 1.15 | 2.50 | 2.36 |
| Mg | wt.% | 0.82 | 0.94 | 3.04 | 1.24 | 0.77 | 0.91 | 0.24 | 0.84 | 1.50 | 1.49 |
| Ti | wt.% | 0.06 | 0.02 | 0.06 | 0.03 | 0.10 | 0.07 | 0.05 | 0.05 | 0.19 | 0.14 |
| Na | wt.% | 2.00 | | 3.70 | | 1.80 | | 1.70 | | 1.00 | |
| K | wt.% | 0.93 | 1.73 | 0.31 | 1.54 | 0.28 | 1.56 | 0.30 | 0.93 | 0.88 | 1.08 |
| P | wt.% | 0.11 | 0.16 | 0.11 | 0.11 | 0.06 | 0.10 | 0.06 | 0.18 | 0.03 | 0.16 |
| $C_{tot}$ | wt.% | 1.1 | 0.49 | 1.5 | 0.88 | 2.2 | 1.80 | 2.9 | 2.18 | 4.9 | 4.50 |
| Mo | ppm | 140 | 130 | 270 | 87 | 182 | 153 | 116 | 165 | | 76 |
| As | ppm | 255 | 246 | 410 | 169 | 140 | 178 | | 360 | | 124 |
| Ga | ppm | | 14 | | 14 | | 10 | | 22 | | 10 |
| Au | ppb | 850 | 1168 | 1100 | 970 | 340 | 319 | | 1235 | | 452 |
| Tl | ppm | 10 | 19 | 17.3 | 11 | 6 | 5 | | 28 | | 11 |
| Sb | ppm | 295 | 49 | 223 | 19 | 59 | 12 | 33 | 42 | | 10 |
| Hg | ppb | 1370 | 3696 | 3100 | 1162 | | 484 | 1140 | 1687 | | 530 |
| Ag | ppm | 45 | 159 | 80 | 49 | 16 | 17 | 165 | 70 | <10 | 27 |
| Cd | ppm | 76 | 234 | 144 | 70 | 62 | 24 | 13.9 | 141 | | 29 |
| Pb | ppm | 480 | 1215 | 800 | 509 | 230 | 182 | 700 | 856 | 220 | 216 |
| Co | ppm | 116 | 174 | 113 | 107 | 31 | 41 | 45 | 100 | | 50 |
| Ni | ppm | 33 | 25 | 49 | 24 | 33 | 34 | 20 | 76 | | 52 |
| Cr | ppm | 18 | 13 | 23 | 20 | 20 | 40 | 13 | 20 | | 42 |
| V | ppm | 77 | 91 | 110 | 83 | 75 | 99 | 63 | 154 | | 189 |
| Ge | ppm | 8.2 | 10.3 | 7.5 | 8.5 | 2.7 | 7.6 | 7.8 | 8.3 | | 5.0 |
| Sc | ppm | 1.1 | 0.8 | 1.6 | 1.2 | 2.8 | 3.0 | 1.3 | 2.4 | 8.8 | 5.5 |
| U | ppm | 11.2 | 8.1 | 6.0 | 4.5 | 10.6 | 9.3 | 16.5 | 4.7 | 2.7 | 4.8 |
| Hf | ppm | 0.80 | n.d. | 1.20 | 0.98 | 1.30 | 1.52 | <0.75 | 1.36 | 2.90 | 1.37 |
| Li | ppm | 11.9 | 23.4 | 9.9 | 21.5 | 12.4 | 22.2 | 9.0 | 14.8 | | 19.8 |
| Th | ppm | 0.30 | 0.28 | 1.10 | 0.42 | 0.60 | 1.02 | 0.48 | 0.80 | 3.80 | 1.77 |
| La | ppm | 5.0 | 1.3 | 8.9 | 1.9 | 8.8 | 5.1 | 4.7 | 4.8 | 17.0 | 10.7 |
| Ce | ppm | 4.3 | 2.9 | 4.7 | 4.1 | 10.0 | 10.1 | 2.2 | 10.1 | 30.0 | 21.7 |
| Nd | ppm | 2.02 | 1.40 | 1.80 | 1.93 | 3.60 | 4.73 | 1.08 | 4.55 | | 9.98 |
| Sm | ppm | 0.47 | 0.31 | 0.45 | 0.42 | 0.93 | 1.00 | 0.30 | 0.92 | 3.50 | 2.04 |
| Eu | ppm | 0.20 | 0.17 | 0.26 | 0.17 | 0.31 | 0.33 | 0.28 | 0.62 | 1.30 | 0.84 |
| Tb | ppm | 0.07 | 0.04 | 0.06 | 0.06 | 0.10 | 0.14 | 0.03 | 0.13 | 0.50 | 0.29 |

| | | AM | | SU2 | | CO | | SU1 | | DOP | |
|---|---|---|---|---|---|---|---|---|---|---|---|
| | | Gurvich 2006 | this study | Gurvich 2006 | this study | Gurvich 2006 | this study | Gurvich 2006 | this study | Gurvich 2006 | this study |
| Yb | ppm | 0.17 | 0.13 | 0.23 | 0.18 | 0.27 | 0.43 | 0.08 | 0.40 | 1.60 | 0.87 |
| Lu | ppm | 0.08 | 0.02 | 0.09 | 0.03 | 0.05 | 0.08 | 0.01 | 0.06 | 0.27 | 0.13 |

Note: Ca was apparently lost due to washing of the samples and anhydrite dissolution, contributing to higher concentrations of the remaining elements. In AM, concentrations of Cu and Zn are significantly lower in the washed samples, suggesting losses of water-soluble metallic compounds or fine particles that would have passed the filters used in those studies.

Appendix 3.3. Pearson's correlation coefficient (r) in the Atlantis II sediments for all elements (excluding individual REE) in the whole data set (100 samples).

| | $S_{ox}$ | $S_{red}$ | Cu | Zn | Mo | As | Ga | Au | Tl | Sb | Hg | Ag | Cd | Pb |
|---|---|---|---|---|---|---|---|---|---|---|---|---|---|---|
| $S_{ox}$ | 1.00 | | | | | | | | | | | | | |
| $S_{red}$ | 0.16 | 1.00 | | | | | | | | | | | | |
| Cu | 0.21 | 0.40 | 1.00 | | | | | | | | | | | |
| Zn | 0.33 | 0.40 | 0.72 | 1.00 | | | | | | | | | | |
| Mo | 0.04 | 0.35 | 0.43 | 0.46 | 1.00 | | | | | | | | | |
| As | 0.23 | 0.54 | 0.58 | 0.54 | 0.72 | 1.00 | | | | | | | | |
| Ga | 0.20 | 0.54 | 0.72 | 0.67 | 0.57 | 0.71 | 1.00 | | | | | | | |
| Au | 0.32 | 0.51 | 0.72 | 0.75 | 0.53 | 0.71 | 0.86 | 1.00 | | | | | | |
| Tl | 0.24 | 0.65 | 0.74 | 0.62 | 0.54 | 0.71 | 0.81 | 0.75 | 1.00 | | | | | |
| Sb | 0.27 | 0.46 | 0.51 | 0.62 | 0.52 | 0.66 | 0.58 | 0.67 | 0.56 | 1.00 | | | | |
| Hg | 0.18 | 0.34 | 0.59 | 0.57 | 0.28 | 0.42 | 0.38 | 0.50 | 0.49 | 0.82 | 1.00 | | | |
| Ag | 0.23 | 0.41 | 0.54 | 0.61 | 0.36 | 0.48 | 0.47 | 0.58 | 0.56 | 0.88 | 0.92 | 1.00 | | |
| Cd | 0.28 | 0.40 | 0.57 | 0.72 | 0.39 | 0.51 | 0.50 | 0.60 | 0.55 | 0.88 | 0.87 | 0.91 | 1.00 | |
| Pb | 0.30 | 0.46 | 0.77 | 0.80 | 0.46 | 0.62 | 0.70 | 0.77 | 0.74 | 0.77 | 0.78 | 0.79 | 0.81 | 1.00 |
| Co | 0.21 | 0.31 | 0.78 | 0.72 | 0.32 | 0.42 | 0.60 | 0.66 | 0.65 | 0.47 | 0.62 | 0.61 | 0.60 | 0.78 |
| Ni | 0.13 | 0.45 | 0.70 | 0.54 | 0.40 | 0.55 | 0.68 | 0.48 | 0.70 | 0.41 | 0.31 | 0.33 | 0.41 | 0.53 |
| Se | 0.04 | 0.56 | 0.52 | 0.58 | 0.24 | 0.42 | 0.54 | 0.53 | 0.50 | 0.39 | 0.36 | 0.37 | 0.41 | 0.51 |
| W | 0.05 | 0.23 | 0.36 | 0.38 | 0.31 | 0.36 | 0.52 | 0.50 | 0.43 | 0.30 | 0.23 | 0.26 | 0.29 | 0.36 |
| Ge | -0.05 | 0.28 | 0.47 | 0.57 | 0.46 | 0.45 | 0.40 | 0.47 | 0.38 | 0.40 | 0.34 | 0.32 | 0.36 | 0.45 |
| U | -0.24 | 0.04 | 0.11 | -0.02 | 0.45 | 0.07 | 0.07 | 0.04 | -0.03 | 0.10 | 0.12 | 0.12 | 0.06 | 0.04 |
| Mn | -0.19 | -0.11 | -0.10 | -0.11 | 0.25 | -0.07 | 0.10 | -0.14 | -0.07 | -0.08 | -0.10 | -0.09 | -0.10 | -0.07 |
| V | -0.17 | 0.24 | -0.02 | 0.05 | 0.08 | 0.14 | 0.23 | 0.21 | 0.18 | 0.13 | -0.03 | 0.03 | 0.00 | 0.02 |
| Cr | -0.27 | 0.09 | -0.08 | -0.17 | -0.29 | -0.14 | 0.04 | -0.17 | -0.05 | -0.11 | -0.13 | -0.10 | -0.11 | -0.19 |
| Fe | -0.39 | -0.04 | 0.10 | -0.04 | 0.37 | 0.14 | -0.16 | -0.09 | -0.06 | -0.04 | 0.09 | -0.02 | -0.04 | 0.01 |
| Si | -0.25 | 0.33 | 0.11 | 0.07 | -0.08 | 0.16 | 0.33 | 0.26 | 0.27 | 0.12 | 0.01 | 0.08 | 0.07 | 0.06 |
| Ca | 0.33 | -0.32 | -0.38 | -0.28 | -0.55 | -0.40 | -0.36 | -0.35 | -0.35 | -0.24 | -0.24 | -0.19 | -0.18 | -0.31 |
| K | -0.42 | 0.01 | -0.08 | -0.02 | -0.08 | -0.14 | -0.08 | -0.06 | 0.01 | -0.11 | -0.05 | -0.09 | -0.12 | -0.03 |
| Mg | -0.24 | -0.13 | -0.15 | -0.17 | -0.38 | -0.28 | -0.06 | -0.15 | -0.22 | -0.17 | -0.09 | -0.11 | -0.13 | -0.20 |
| $CO_2$ | -0.34 | -0.20 | -0.15 | -0.24 | -0.37 | -0.25 | -0.11 | -0.29 | -0.17 | -0.19 | -0.17 | -0.17 | -0.18 | -0.23 |
| Ba | 0.21 | 0.19 | 0.01 | 0.02 | 0.16 | 0.24 | 0.26 | 0.31 | 0.18 | 0.24 | 0.00 | 0.14 | 0.13 | 0.14 |
| Sr | 0.11 | 0.05 | -0.17 | -0.15 | 0.00 | 0.03 | 0.09 | 0.09 | 0.06 | 0.08 | -0.13 | 0.01 | 0.00 | -0.06 |
| P | -0.36 | 0.09 | 0.14 | 0.03 | -0.03 | 0.03 | 0.17 | 0.11 | 0.14 | 0.02 | 0.05 | 0.02 | 0.00 | 0.02 |
| Rb | -0.41 | 0.00 | -0.13 | -0.10 | -0.18 | -0.18 | -0.09 | -0.15 | -0.02 | -0.11 | -0.11 | -0.11 | -0.13 | -0.14 |
| Te | -0.28 | 0.25 | 0.21 | 0.19 | 0.06 | 0.03 | 0.06 | 0.12 | 0.20 | 0.05 | 0.15 | 0.12 | 0.12 | 0.16 |
| Br | -0.29 | 0.02 | 0.08 | 0.19 | 0.04 | -0.07 | -0.01 | 0.18 | 0.04 | -0.05 | 0.12 | 0.05 | 0.03 | 0.16 |
| Cs | -0.35 | 0.10 | -0.11 | -0.11 | -0.16 | -0.11 | -0.05 | -0.13 | 0.02 | -0.08 | -0.13 | -0.11 | -0.12 | -0.16 |
| Li | -0.37 | 0.01 | -0.06 | -0.02 | -0.15 | -0.20 | -0.11 | -0.12 | -0.01 | -0.16 | -0.08 | -0.13 | -0.15 | -0.06 |
| B | -0.51 | -0.14 | -0.03 | -0.06 | 0.27 | 0.02 | -0.19 | -0.14 | -0.13 | -0.12 | -0.03 | -0.09 | -0.10 | -0.07 |
| Sn | 0.13 | 0.12 | 0.01 | 0.05 | 0.04 | 0.03 | -0.02 | 0.01 | 0.14 | 0.00 | -0.01 | 0.05 | 0.03 | 0.03 |
| Hf | -0.36 | 0.01 | -0.17 | -0.21 | -0.42 | -0.29 | -0.12 | -0.26 | -0.19 | -0.18 | -0.14 | -0.13 | -0.14 | -0.24 |
| Sc | -0.28 | 0.05 | -0.07 | -0.17 | -0.30 | -0.15 | 0.04 | -0.18 | -0.06 | -0.11 | -0.12 | -0.09 | -0.09 | -0.19 |
| Y | -0.30 | 0.03 | -0.07 | -0.18 | -0.30 | -0.16 | -0.01 | -0.22 | -0.08 | -0.13 | -0.12 | -0.10 | -0.11 | -0.19 |
| Zr | -0.25 | 0.05 | -0.10 | -0.20 | -0.32 | -0.17 | 0.00 | -0.20 | -0.08 | -0.13 | -0.15 | -0.11 | -0.12 | -0.21 |
| Al | -0.24 | 0.10 | 0.03 | -0.07 | -0.26 | -0.08 | 0.14 | -0.08 | 0.02 | -0.05 | -0.05 | -0.03 | -0.03 | -0.10 |
| Ti | -0.26 | 0.08 | -0.08 | -0.17 | -0.30 | -0.14 | 0.03 | -0.18 | -0.07 | -0.11 | -0.12 | -0.09 | -0.10 | -0.19 |
| Nb | -0.27 | 0.06 | -0.07 | -0.16 | -0.29 | -0.14 | 0.05 | -0.18 | -0.06 | -0.12 | -0.13 | -0.10 | -0.10 | -0.19 |
| Ta | -0.35 | 0.04 | -0.15 | -0.23 | -0.39 | -0.26 | -0.08 | -0.26 | -0.15 | -0.19 | -0.14 | -0.13 | -0.15 | -0.25 |
| Th | -0.26 | 0.08 | -0.04 | -0.14 | -0.28 | -0.12 | 0.07 | -0.16 | -0.03 | -0.08 | -0.10 | -0.06 | -0.07 | -0.15 |
| tot. REE | -0.28 | 0.10 | -0.03 | -0.17 | -0.22 | -0.10 | 0.04 | -0.18 | -0.01 | -0.09 | -0.11 | -0.09 | -0.09 | -0.15 |

Appendix 3.3. continuation (2/4).

| | Co | Ni | Se | W | Ge | U | Mn | V | Cr | Fe | Si | Ca | $K_2O$ | Mg |
|---|---|---|---|---|---|---|---|---|---|---|---|---|---|---|
| Co | 1.00 | | | | | | | | | | | | | |
| Ni | 0.48 | 1.00 | | | | | | | | | | | | |
| Se | 0.50 | 0.50 | 1.00 | | | | | | | | | | | |
| W | 0.33 | 0.12 | 0.28 | 1.00 | | | | | | | | | | |
| Ge | 0.39 | 0.19 | 0.40 | 0.59 | 1.00 | | | | | | | | | |
| U | 0.09 | -0.02 | 0.14 | 0.05 | 0.15 | 1.00 | | | | | | | | |
| Mn | 0.02 | 0.03 | -0.20 | -0.13 | -0.16 | 0.20 | 1.00 | | | | | | | |
| V | -0.08 | 0.15 | 0.25 | 0.14 | 0.05 | -0.05 | 0.01 | 1.00 | | | | | | |
| Cr | -0.21 | 0.40 | 0.20 | -0.30 | -0.37 | -0.04 | -0.04 | 0.29 | 1.00 | | | | | |
| Fe | 0.07 | -0.18 | 0.04 | 0.18 | 0.39 | 0.52 | -0.06 | -0.09 | -0.41 | 1.00 | | | | |
| Si | -0.01 | 0.25 | 0.29 | 0.17 | 0.16 | -0.17 | -0.20 | 0.44 | 0.48 | -0.32 | 1.00 | | | |
| Ca | -0.32 | -0.11 | -0.34 | -0.40 | -0.62 | -0.41 | -0.14 | -0.15 | 0.32 | -0.69 | -0.19 | 1.00 | | |
| K | 0.03 | -0.23 | 0.14 | 0.15 | 0.37 | -0.12 | -0.01 | 0.06 | -0.14 | 0.14 | 0.33 | -0.38 | 1.00 | |
| Mg | -0.10 | -0.02 | -0.08 | -0.05 | -0.12 | -0.14 | -0.04 | 0.06 | 0.39 | -0.27 | 0.32 | 0.17 | 0.04 | 1.00 |
| $CO_2$ | -0.21 | 0.27 | -0.17 | -0.35 | -0.46 | -0.16 | 0.02 | 0.06 | 0.65 | -0.35 | 0.08 | 0.55 | -0.27 | 0.32 |
| Ba | -0.03 | 0.05 | -0.02 | 0.14 | -0.11 | 0.02 | 0.07 | 0.13 | -0.03 | -0.24 | 0.33 | -0.05 | -0.20 | -0.21 |
| Sr | -0.11 | 0.00 | -0.10 | -0.04 | -0.28 | -0.17 | 0.27 | 0.11 | 0.07 | -0.48 | 0.24 | 0.24 | 0.01 | -0.08 |
| P | 0.01 | 0.32 | 0.22 | 0.08 | -0.01 | 0.01 | -0.03 | 0.73 | 0.47 | 0.08 | 0.36 | -0.17 | -0.05 | 0.21 |
| Rb | -0.15 | -0.07 | 0.07 | 0.07 | 0.25 | -0.21 | -0.06 | 0.20 | 0.17 | -0.06 | 0.54 | -0.19 | 0.83 | 0.13 |
| Te | 0.24 | -0.06 | 0.32 | 0.22 | 0.44 | 0.05 | -0.09 | 0.09 | -0.10 | 0.22 | 0.27 | -0.43 | 0.67 | -0.06 |
| Br | 0.26 | -0.35 | 0.21 | 0.33 | 0.49 | 0.07 | -0.05 | -0.01 | -0.44 | 0.33 | 0.08 | -0.49 | 0.70 | -0.01 |
| Cs | -0.22 | 0.03 | 0.08 | 0.05 | 0.20 | -0.20 | -0.05 | 0.35 | 0.28 | -0.11 | 0.62 | -0.18 | 0.64 | 0.11 |
| Li | 0.01 | -0.13 | 0.18 | 0.04 | 0.26 | -0.10 | -0.07 | 0.05 | 0.04 | 0.05 | 0.29 | -0.25 | 0.89 | 0.12 |
| B | -0.01 | -0.26 | 0.05 | 0.07 | 0.33 | 0.37 | 0.14 | -0.11 | -0.32 | 0.61 | -0.11 | -0.53 | 0.54 | -0.19 |
| Sn | 0.05 | -0.05 | 0.04 | 0.04 | 0.03 | -0.13 | -0.06 | 0.03 | -0.14 | 0.01 | -0.01 | -0.01 | 0.04 | -0.12 |
| Hf | -0.20 | 0.15 | 0.21 | -0.28 | -0.27 | -0.05 | -0.11 | 0.15 | 0.87 | -0.35 | 0.46 | 0.29 | 0.14 | 0.42 |
| Sc | -0.19 | 0.39 | 0.12 | -0.31 | -0.38 | -0.06 | -0.01 | 0.19 | 0.98 | -0.43 | 0.46 | 0.35 | -0.17 | 0.44 |
| Y | -0.20 | 0.40 | 0.12 | -0.35 | -0.40 | -0.06 | -0.01 | 0.20 | 0.97 | -0.34 | 0.38 | 0.31 | -0.20 | 0.41 |
| Zr | -0.22 | 0.38 | 0.14 | -0.34 | -0.41 | -0.05 | -0.05 | 0.19 | 0.98 | -0.45 | 0.44 | 0.39 | -0.17 | 0.39 |
| Al | -0.09 | 0.46 | 0.19 | -0.25 | -0.32 | -0.03 | -0.03 | 0.19 | 0.96 | -0.42 | 0.48 | 0.30 | -0.18 | 0.44 |
| Ti | -0.19 | 0.39 | 0.16 | -0.32 | -0.38 | -0.03 | -0.01 | 0.19 | 0.98 | -0.42 | 0.45 | 0.34 | -0.17 | 0.41 |
| Nb | -0.19 | 0.40 | 0.14 | -0.31 | -0.38 | -0.05 | -0.01 | 0.20 | 0.97 | -0.43 | 0.46 | 0.34 | -0.17 | 0.40 |
| Ta | -0.22 | 0.22 | 0.13 | -0.32 | -0.33 | -0.02 | -0.05 | 0.15 | 0.93 | -0.38 | 0.48 | 0.30 | 0.03 | 0.43 |
| Th | -0.16 | 0.43 | 0.16 | -0.31 | -0.36 | -0.06 | 0.00 | 0.21 | 0.98 | -0.44 | 0.47 | 0.32 | -0.15 | 0.41 |
| tot. REE | -0.19 | 0.44 | 0.15 | -0.31 | -0.35 | -0.06 | -0.01 | 0.26 | 0.92 | -0.26 | 0.37 | 0.23 | -0.22 | 0.33 |

Appendix 3.3. continuation (3/4)

| | $CO_2$ | Ba | Sr | $P_2O_5$ | Rb | Te | Br | Cs | Li | B | Sn |
|---|---|---|---|---|---|---|---|---|---|---|---|
| $CO_2$ | 1.00 | | | | | | | | | | |
| Ba | -0.16 | 1.00 | | | | | | | | | |
| Sr | 0.02 | 0.75 | 1.00 | | | | | | | | |
| P | 0.36 | -0.08 | -0.17 | 1.00 | | | | | | | |
| Rb | 0.00 | -0.20 | -0.03 | 0.14 | 1.00 | | | | | | |
| Te | -0.38 | -0.14 | -0.05 | 0.05 | 0.49 | 1.00 | | | | | |
| Br | -0.49 | -0.16 | -0.09 | -0.06 | 0.38 | 0.68 | 1.00 | | | | |
| Cs | 0.06 | -0.10 | 0.00 | 0.30 | 0.93 | 0.40 | 0.20 | 1.00 | | | |
| Li | -0.13 | -0.22 | 0.02 | 0.02 | 0.71 | 0.60 | 0.58 | 0.55 | 1.00 | | |
| B | -0.29 | -0.23 | -0.21 | -0.02 | 0.36 | 0.46 | 0.55 | 0.25 | 0.40 | 1.00 | |
| Sn | -0.17 | -0.06 | 0.00 | -0.06 | 0.01 | 0.05 | 0.00 | 0.04 | 0.01 | 0.06 | 1.00 |
| Hf | 0.50 | -0.15 | 0.05 | 0.32 | 0.34 | 0.16 | -0.13 | 0.37 | 0.31 | -0.14 | -0.09 |
| Sc | 0.67 | -0.04 | 0.07 | 0.41 | 0.14 | -0.14 | -0.47 | 0.26 | 0.02 | -0.33 | -0.15 |
| Y | 0.68 | -0.08 | 0.01 | 0.47 | 0.11 | -0.16 | -0.49 | 0.24 | -0.01 | -0.32 | -0.15 |
| Zr | 0.68 | -0.04 | 0.08 | 0.40 | 0.15 | -0.15 | -0.47 | 0.26 | 0.03 | -0.33 | -0.13 |
| Al | 0.64 | -0.03 | 0.04 | 0.42 | 0.12 | -0.12 | -0.44 | 0.23 | 0.01 | -0.34 | -0.15 |
| Ti | 0.65 | -0.03 | 0.06 | 0.41 | 0.14 | -0.13 | -0.46 | 0.26 | 0.02 | -0.32 | -0.14 |
| Nb | 0.66 | -0.03 | 0.08 | 0.42 | 0.14 | -0.13 | -0.46 | 0.26 | 0.02 | -0.32 | -0.15 |
| Ta | 0.57 | -0.12 | 0.03 | 0.36 | 0.29 | 0.07 | -0.25 | 0.35 | 0.22 | -0.19 | -0.12 |
| Th | 0.66 | -0.02 | 0.09 | 0.41 | 0.16 | -0.12 | -0.46 | 0.28 | 0.04 | -0.33 | -0.14 |
| tot. REE | 0.62 | -0.02 | 0.01 | 0.50 | 0.07 | -0.16 | -0.51 | 0.21 | -0.06 | -0.34 | -0.16 |

| | Hf | Sc | Y | Zr | $Al_2O_3$ | $TiO_2$ | Nb | Ta | Th | tot. REE |
|---|---|---|---|---|---|---|---|---|---|---|
| Hf | 1.00 | | | | | | | | | |
| Sc | 0.86 | 1.00 | | | | | | | | |
| Y | 0.83 | 0.97 | 1.00 | | | | | | | |
| Zr | 0.88 | 0.98 | 0.97 | 1.00 | | | | | | |
| Al | 0.85 | 0.99 | 0.96 | 0.97 | 1.00 | | | | | |
| Ti | 0.87 | 0.99 | 0.97 | 0.99 | 0.98 | 1.00 | | | | |
| Nb | 0.87 | 0.99 | 0.97 | 0.99 | 0.98 | 0.99 | 1.00 | | | |
| Ta | 0.96 | 0.94 | 0.90 | 0.95 | 0.92 | 0.95 | 0.94 | 1.00 | | |
| Th | 0.86 | 0.99 | 0.97 | 0.98 | 0.98 | 0.99 | 0.99 | 0.93 | 1.00 | |
| tot. REE | 0.75 | 0.92 | 0.97 | 0.91 | 0.90 | 0.92 | 0.92 | 0.82 | 0.91 | 1.00 |

Correlations with r >0.5 ($r^2$ >0.25) are significant at 99% confidence.

Appendix 3.4. Calculations of relative enrichments and depletions of selected trace metals in the different stratigraphic units, different sample types and different parts of the Deep (see Figures 3.7, 3.9, and 3.11).

| Average concentrations of metals in each stratigraphic unit (in ppm, except Hg and Au in ppb): | | | | | | | | | | | | | | | | |
|---|---|---|---|---|---|---|---|---|---|---|---|---|---|---|---|---|
| Stratigraphic unit | n | BMI | Mo | As | Ga | Au | Tl | Sb | Hg | Ag | Cd | Pb | Co | Ni | Cr | V |
| AM | 13 | 0.77 | 130 | 246 | 14 | 1168 | 19 | 49 | 3696 | 159 | 234 | 1215 | 174 | 25 | 13 | 91 |
| SU2 | 28 | 0.50 | 87 | 169 | 14 | 970 | 11 | 19 | 1162 | 49 | 70 | 509 | 107 | 24 | 20 | 83 |
| CO | 20 | 0.19 | 153 | 178 | 10 | 319 | 5 | 12 | 484 | 17 | 24 | 182 | 41 | 34 | 40 | 99 |
| SU1 | 22 | 0.71 | 165 | 360 | 22 | 1235 | 28 | 42 | 1687 | 70 | 141 | 856 | 100 | 76 | 20 | 154 |
| DOP | 17 | 0.23 | 76 | 124 | 10 | 452 | 11 | 10 | 530 | 27 | 29 | 216 | 50 | 52 | 42 | 189 |
| BMI-normalized average concentrations in each stratigraphic unit (BMI=2*Cu+Zn+Pb in moles). | | | | | | | | | | | | | | | | |
| AM | TM/BMI | | 169 | 321 | 18 | 1521 | 25 | 63 | 4812 | 207 | 305 | 1582 | 227 | 33 | 17 | 118 |
| SU2 | TM/BMI | | 175 | 340 | 27 | 1955 | 23 | 39 | 2342 | 99 | 141 | 1025 | 216 | 48 | 40 | 167 |
| CO | TM/BMI | | 824 | 958 | 53 | 1720 | 29 | 65 | 2609 | 92 | 129 | 981 | 222 | 183 | 216 | 534 |
| SU1 | TM/BMI | | 232 | 507 | 31 | 1740 | 40 | 60 | 2376 | 99 | 199 | 1206 | 140 | 107 | 28 | 217 |
| DOP | TM/BMI | | 324 | 527 | 44 | 1926 | 46 | 43 | 2258 | 115 | 124 | 920 | 214 | 222 | 179 | 805 |
| Average | | | 345 | 531 | 35 | 1772 | 33 | 54 | 2880 | 122 | 179 | 1143 | 204 | 119 | 96 | 368 |
| BMI-normalized concentrations in each stratigraphic unit compared to the average of all stratigraphic units: | | | | | | | | | | | | | | | | |
| AM | (TM/BMI)/Average | | 0.5 | 0.6 | 0.5 | 0.9 | 0.8 | 1.2 | 1.7 | 1.7 | 1.7 | 1.4 | 1.1 | 0.3 | 0.2 | 0.3 |
| SU2 | (TM/BMI)/Average | | 0.5 | 0.6 | 0.8 | 1.1 | 0.7 | 0.7 | 0.8 | 0.8 | 0.8 | 0.9 | 1.1 | 0.4 | 0.4 | 0.5 |
| CO | (TM/BMI)/Average | | 2.4 | 1.8 | 1.5 | 1.0 | 0.9 | 1.2 | 0.9 | 0.7 | 0.7 | 0.9 | 1.1 | 1.5 | 2.2 | 1.4 |
| SU1 | (TM/BMI)/Average | | 0.7 | 1.0 | 0.9 | 1.0 | 1.2 | 1.1 | 0.8 | 0.8 | 1.1 | 1.1 | 0.7 | 0.9 | 0.3 | 0.6 |
| DOP | (TM/BMI)/Average | | 0.9 | 1.0 | 1.3 | 1.1 | 1.4 | 0.8 | 0.8 | 0.9 | 0.7 | 0.8 | 1.0 | 1.9 | 1.9 | 2.2 |
| Average concentrations of metals in each sample type (in ppm, except Hg and Au in ppb): | | | | | | | | | | | | | | | | |
| Sample type | n | BMI | Mo | As | Ga | Au | Tl | Sb | Hg | Ag | Cd | Pb | Co | Ni | Cr | V |
| $SO_4$-rich; HSHM | 29 | 1.05 | 168 | 364 | 22 | 1575 | 31 | 52 | 3246 | 129 | 199 | 1219 | 179 | 55 | 12 | 130 |
| $SO_4$-rich; HSLM | 7 | 0.20 | 162 | 440 | 22 | 1545 | 28 | 50 | 679 | 54 | 45 | 541 | 48 | 32 | 21 | 234 |
| $SO_4$-rich; LSHM | 4 | 0.95 | 112 | 167 | 16 | 1261 | 20 | 25 | 2058 | 96 | 118 | 1297 | 198 | 24 | 7 | 78 |
| $SO_4$-rich; LSLM | 6 | 0.15 | 103 | 124 | 11 | 367 | 7 | 10 | 237 | 6 | 6 | 187 | 33 | 7 | 6 | 140 |
| $SO_4$-rich; anhy | 6 | 0.18 | 27 | 70 | 4 | 222 | 1 | 5 | 352 | 8 | 27 | 151 | 32 | 7 | 3 | 27 |
| Clay- and $CO_3$-rich | 48 | 0.20 | 101 | 126 | 10 | 237 | 5 | 9 | 515 | 10 | 14 | 188 | 51 | 32 | 26 | 109 |

| BMI-normalized average concentrations in each sample type (BMI=2*Cu+Zn+Pb in moles) | | | | | | | | | | | | | | | |
|---|---|---|---|---|---|---|---|---|---|---|---|---|---|---|---|
| | | Mo | As | Ga | Au | Tl | Sb | Hg | Ag | Cd | Pb | Co | Ni | Cr | V |
| $SO_4$-rich; HSHM | TM/BMI | 160 | 347 | 21 | 1501 | 30 | 49 | 3094 | 123 | 190 | 1162 | 170 | 53 | 12 | 124 |
| $SO_4$-rich; HSLM | TM/BMI | 794 | 2158 | 109 | 7569 | 135 | 245 | 3325 | 263 | 222 | 2650 | 233 | 159 | 102 | 1147 |
| $SO_4$-rich; LSHM | TM/BMI | 118 | 176 | 17 | 1331 | 21 | 27 | 2171 | 102 | 125 | 1369 | 209 | 25 | 8 | 83 |
| $SO_4$-rich; LSLM | TM/BMI | 681 | 815 | 70 | 2418 | 43 | 69 | 1560 | 42 | 40 | 1234 | 219 | 48 | 39 | 924 |
| $SO_4$-rich; anhy | TM/BMI | 153 | 392 | 21 | 1244 | 8 | 28 | 1968 | 46 | 153 | 842 | 177 | 41 | 16 | 150 |
| Clay- and $CO_3$-rich | TM/BMI | 508 | 631 | 48 | 1189 | 26 | 48 | 2585 | 50 | 69 | 943 | 255 | 162 | 131 | 545 |
| Average | | 402 | 753 | 48 | 2542 | 44 | 78 | 2450 | 105 | 133 | 1367 | 211 | 82 | 51 | 495 |
| BMI-normalized concentrations in each sample type compared to the average of all sample types: | | | | | | | | | | | | | | | |
| $SO_4$-rich; HSHM | (TM/BMI)/Average | 0.4 | 0.5 | 0.4 | 0.6 | 0.7 | 0.6 | 1.3 | 1.2 | 1.4 | 0.9 | 0.8 | 0.6 | 0.2 | 0.3 |
| $SO_4$-rich; HSLM | (TM/BMI)/Average | 2.0 | 2.9 | 2.3 | 3.0 | 3.1 | 3.2 | 1.4 | 2.5 | 1.7 | 1.9 | 1.1 | 2.0 | 2.0 | 2.3 |
| $SO_4$-rich; LSHM | (TM/BMI)/Average | 0.3 | 0.2 | 0.4 | 0.5 | 0.5 | 0.3 | 0.9 | 1.0 | 0.9 | 1.0 | 1.0 | 0.3 | 0.1 | 0.2 |
| $SO_4$-rich; LSLM | (TM/BMI)/Average | 1.7 | 1.1 | 1.5 | 1.0 | 1.0 | 0.9 | 0.6 | 0.4 | 0.3 | 0.9 | 1.0 | 0.6 | 0.8 | 1.9 |
| $SO_4$-rich; anhy | (TM/BMI)/Average | 0.4 | 0.5 | 0.4 | 0.5 | 0.2 | 0.4 | 0.8 | 0.4 | 1.1 | 0.6 | 0.8 | 0.5 | 0.3 | 0.3 |
| Clay- and $CO_3$-rich | (TM/BMI)/Average | 1.3 | 0.8 | 1.0 | 0.5 | 0.6 | 0.6 | 1.1 | 0.5 | 0.5 | 0.7 | 1.2 | 2.0 | 2.6 | 1.1 |

| Average concentrations of metals in different parts of the Deep (in ppm, except Hg and Au in ppb): | | | | | | | | | | | | | | | |
|---|---|---|---|---|---|---|---|---|---|---|---|---|---|---|---|
| Part of Deep | n | BMI | Mo | As | Ga | Au | Tl | Sb | Hg | Ag | Cd | Pb | Co | Ni | Cr | V |
| Distal | 35 | 0.27 | 134 | 192 | 10 | 455 | 9 | 15 | 691 | 19 | 23 | 303 | 62 | 20 | 12 | 86 |
| Proximal | 26 | 0.69 | 95 | 184 | 15 | 1126 | 14 | 33 | 2523 | 106 | 147 | 873 | 151 | 22 | 13 | 96 |
| BMI-normalized average concentrations in different parts of the Deep (BMI=2*Cu+Zn+Pb in moles) | | | | | | | | | | | | | | | | |
| Distal | | TM/BMI | 491 | 700 | 37 | 1663 | 33 | 56 | 2525 | 69 | 85 | 1107 | 225 | 74 | 44 | 313 |
| Proximal | | TM/BMI | 137 | 265 | 22 | 1625 | 20 | 47 | 3643 | 152 | 212 | 1261 | 218 | 32 | 19 | 139 |
| BMI-normalized trace metal enrichment in the different parts of the Deep (>1 indicates distal enrichment and <1 proximal enrichment): | | | | | | | | | | | | | | | | |
| Distal/proximal | | | 3.6 | 2.6 | 1.7 | 1.0 | 1.6 | 1.2 | 0.7 | 0.5 | 0.4 | 0.9 | 1.0 | 2.3 | 2.4 | 2.3 |

Calculations of relative enrichments and depletions of selected trace metals (TM) normalized to the base metal sulfide index (BMI=Cu*2+Zn+Pb in moles) in the different stratigraphic units different sample types and different parts of the Deep (see Figures 3.7, 3.9, and 3.1). TM refers to the average concentration of the metal in all samples from the unit or sample-type; BMI is the average base metal index for the unit, sample-type or

part of the Deep. Average is the BMI normalized average concentration of the metal in all units, sample types or whole Deep (calculated from the TM/BMI values). Stratigraphic units are according to Table 3.1, sample types are according to Table 3.2, and cores from vent proximal and vent distal parts of the Deep are indicated in Figure 3.1. Stratigraphic units: AM= Amorphous Siliceous unit; SU2= Upper Sulfidic unit; CO= Central Oxidic unit; SU1= Lower Sulfidic unit; DOP= Detrital Oxidic Pyritic unit. Sample types: HSHM= high S, high metals; LSHM=low S, high metals; HSLM= high S, low metals; LSLM=low S, low metals; anhy= >50% anhydrite, as discussed in the text. Clay- and $CO_3$-rich samples contain little sulfate or sulfide. The relative enrichments in the vent proximal and distal part of the Deep (less and more than 3 km from the inferred vent source, respectively: Fig. 3.1) are obtained by dividing average BMI-normalized trace metal concentrations in vent distal cores by BMI-normalized trace metal concentrations in the proximal cores. Values of 1 correspond to equal concentration in proximal and distal cores; values less than 1 correspond to relative enrichment proximal to the vent(s), and values greater than 1 correspond to relative enrichment distal to the vent(s). Data for vent proximal cores (334, 546, 557 and 617) and the distal cores (373, 387, 421, 495 and 503) are for the three uppermost stratigraphic units only because the two lower units are missing at the vent proximity.

# CHAPTER 4

# EARLY DEPOSITIONAL HISTORY OF METALLIFEROUS SEDIMENTS IN THE ATLANTIS II DEEP: EVIDENCE FROM RARE EARTH ELEMENT GEOCHEMISTRY

Published in Laurila, T. E., Hannington, M. D., Petersen, S. and Garbe-Schönberg, D., 2014, Geochimica Cosmochimica Acta 126, p. 146-168.

## 1. Introduction

Since the discovery of black smokers and accompanying hydrothermal plumes, our understanding of the formation of metalliferous sediments in the open ocean has greatly increased (Baker et al., 1985; German et al., 1993; Bennett et al., 2008; Adams et al., 2011; Yücel et al., 2011), informing genetic models for both ancient massive sulfide (VMS) deposits and banded iron formations (BIF). Most BIFs are thought to have formed from metal-enriched basinal fluids, some at the distal margins of VMS systems, in part from plume fallout analogous to that at present-day mid-ocean ridges (MOR) (Goodwin, 1962; Cloud, 1973; Grenne and Slack, 2003; Bekker et al., 2010; Planavsky et al., 2010). The particle load of hydrothermal plumes at MOR is composed mainly of hydrous Fe- and Mn-oxides and lesser sulfides that are deposited up to tens or even hundreds of kilometers away from the hydrothermal vent sites (Baker et al., 1985). The Fe- and Mn-(oxy)hydroxides have a high surface activity and, during both residence in the plume and after precipitation at the sea floor, scavenge many elements from seawater (German et al., 1990; Bau, 1999). During scavenging, the rare earth element (REE) pattern of the (oxy)hydroxides gradually changes from that resembling hydrothermal fluid (e.g., Michard et al., 1983) to more seawater-like (e.g., Klinkhammer et al., 1983). This is seen in the development of a stronger negative Ce anomaly, weaker positive Eu anomaly and decrease in La/Sm (German et al., 1990). The proximal facies of modern plume fallout is characterized by much higher concentrations of Cu, Zn, Pb and precious metals that are bound to sulfide minerals. These processes can be examined directly in the Red Sea, where active metal precipitation has been known since 1965 (Scholten et al., 2000).

The Atlantis II Deep is the most metal-enriched of several deeps within the axial valley of the Red Sea rift and is also by far the largest known hydrothermal metal deposit on the present-day seafloor. The total amount of metalliferous sediment in the Atlantis II Deep is estimated to be ~90 Mt of salt-free material with a cumulative thickness of 5 to 20 meters (Guney et al., 1988; Bertram et al., 2011). The processes leading to the formation of the stratified metalliferous sediment have been extensively discussed in the literature (Degens and Ross, 1969; Bäcker and Richter, 1973; Pottorf and Barnes, 1983; Zierenberg and Shanks, 1983; Anschutz and Blanc, 1995; Gurvich, 2006). Sedimentation rates have varied from ~20 cm/ky to ~10 times faster since the deposition of the oldest sediments less than 25 000 years ago. The general stratigraphy has been established by abundant sediment coring (about 10 cores/$km^2$), including 78 cores described by Bäcker and Richter (1973) and 486 cores logged during the MESEDA I-III projects (unpublished). Recent studies have concentrated mainly on the composition of the brine pool overlying the sediments (Blanc and Anschutz, 1995; Anschutz et al., 1998; Hartmann et al., 1998a; Pierret et al., 2001; Schmidt et al., 2003).

Oudin et al. (1984), Ramboz et al. (1988) and Winckler et al. (2000) showed that hydrothermal venting similar to that at mid-ocean ridges was the source of metals in the Deep and was responsible for anhydrite veining in the sediments. Positive Eu anomalies and LREE enrichment, typical of mid-ocean ridge hydrothermal fluids, have been reported in some layers of the Atlantis II sediments; however, a common feature is the lack of the

negative Ce anomaly of seawater (e.g., Butuzova and Lyapunov, 1995). This is related to the unusual fluid composition and environment of precipitation in the Atlantis II Deep that differ dramatically from open ocean systems. This study examines the REE geochemistry of chemically distinct layers of metalliferous sediment at the bottom of the Deep and the variations in terms of hydrothermal input, brine composition and possible mixing of the brine with seawater. We also consider what insights can be gained from the REE geochemistry of the Atlantis II sediments when compared to ancient metalliferous sediments.

**1.1 Geological setting**

The Atlantis II Deep is a 2200-m deep depression in the slowly spreading Red Sea rift zone (Figure 4.1). In total 26 deeps have been found along the Red Sea rift valley (Scholten et al., 2000), but they vary greatly in character. Some deeps are floored by basalt, some by evaporites; some have brine at the bottom, others do not. Some contain metalliferous sediments and even sulfide chimneys, but others have no mineralization (Gurvich, 2006). Thus, it appears that the deeps have developed independently of each other and in unique ways, unrelated to the maturity of the ridge axis on which they are located (Pierret et al., 2001).

The Atlantis II Deep covers an area of ~60 $km^2$ and is divided into 4 sub-basins, all of which are filled with brine but differ in some details (e.g., depth, metal concentrations and thickness of different sedimentary units). The brines are a very efficient trap for metals that

are being vented into the Deep, retaining ~85% of Fe from the hydrothermal fluids compared to <5% on mid-ocean ridges (Gurvich and Bogdanov, 1986; Gurvich, 2006). Venting is presently thought to be occurring in the Southwest Basin based on brine temperature (Schoell and Hartmann, 1973), epigenetic features (Zierenberg and Shanks, 1983), average thickness of the individual units, and average metal content of the whole sediment succession (Bäcker and Richter, 1973; Guney et al., 1988). Bäcker and Richter (1973) suggested, based on bulk chemistry of the cores, that the locus of venting shifted to its present location in the southwest after an initial period of venting in the north of the Deep, although the early history of sedimentation in the Southwest Basin cannot be confirmed due to the intrusion of a basaltic sill that has prevented coring of the lower strata (Hackett and Bischoff, 1973; Whitmarsh et al., 1974; Zierenberg and Shanks, 1983).

### 1.2. Depositional environment

The brine pool covering the Atlantis II Deep consists of five layers with different temperatures and salinities resulting from double-diffusive convection of heat and salt (salt migrates upwards at a different rate than heat: Anschutz et al., 1998). At the deepest part of the basin the vertical extent of the lower brine is 135 m, and it is overlying by ~50 m of upper brine (Swift et al., 2012). The lower brine layer (lower convective layer, LCL) has a volume of ~4 $km^3$ and is the most saline (~27 wt.% NaCl), anoxic and devoid of reduced sulfur (Anschutz et al., 1998). The temperature of the lower brine increased by 13°C during the last ~30 years and was ~67.2°C when last measured in 1995 (Hartmann et al., 1998b; Anschutz et al., 1998; Swift et al., 2012, reported 68.3°C in 2008). Between the lower brine

and the Red Sea deep water are multiple upper brine layers (upper convective layers, UCL-1 to UCL-3 according to Anschutz et al., 1998; although different authors identify different numbers of layers). They have temperatures from ~55°C to ~45°C, extend ~50 m above the upper surface of the LCL, and become less saline and increasingly oxic towards the interface with seawater. The chemical and isotopic compositions of the brines reflect different sources, including Red Sea deep water, fluids derived from leaching of surrounding Miocene evaporites, and hydrothermal fluids that have circulated through the underlying basalts and/or normal Red Sea sediments (Schoell and Faber, 1978; Zierenberg and Shanks, 1986; Pierret et al., 2001; Anschutz et al., 1995). Various attempts have been made to reconstruct the temperature and composition of the venting hydrothermal fluids based on the temperature and the amount of dissolved solids in the different brine layers (Ramboz and Danis, 1990; Anschutz and Blanc, 1995 and 1996). These studies concluded that the venting hydrothermal fluids had an average range of flow rate, temperature, and salinity of 670-1000 kg/s, 195-310°C, and 270-370‰, respectively.

The laterally extensive thin layers of metalliferous mud at the bottom of the Deep are formed by the settling of sulfides and Fe-(oxy)hydroxides during periods of hydrothermal venting into the Deep (Shanks and Bischoff, 1977; Shanks and Bischoff, 1980). Sulfides and Fe-(oxy)hydroxides precipitate in a number of ways. During periods of anoxic brine conditions, such as the present-day conditions, sulfides form from the hydrothermal fluids immediately after venting and are deposited proximal to the vent source (until reduced sulfur in the hydrothermal fluid is exhausted) and in a laterally more extensive “plume”

within the lower brine. Fe-(oxy)hydroxides form mainly just above the interface between the lower brine and upper brine, and manganese compounds precipitate mainly within the upper brine layers where oxygen becomes increasingly available (Butuzova et al., 1988a, b; Blanc et al., 1998; Garbe-Schönberg et al., 1998; Taitel-Goldman and Singer, 2002). Presently Mn-oxides and (oxy)hydroxides dissolve as they settle through the anoxic lower brine, but Fe-(oxy)hydroxides may settle through the lower brine as metastable phases (e.g., amorphous Fe-Si phases, ferrihydrite, goethite, nano-hematite: Schwertmann et al., 1998; Taitel-Goldman and Singer, 2001, 2002) and accumulate on the bottom of the deep (Hartmann, 1985; Butuzova et al., 1988a, b; Blanc et al., 1998). Particulate manganese (as Mn-oxides and Mn-(oxy)hydroxides) currently accumulates only on the flanks of the Atlantis II Deep, although Mn is also present in authigenic carbonates in sediment at the bottom of the Deep. Distinct Mn-rich layers are also found in some sections of the sedimentary strata at depth, indicating changes in the composition of the lower brine over time that allowed deposition of Mn-oxides at the bottom of the Deep. Diagenetic pyrite is also found in the sediment and may have formed by sulfate reduction (Shanks and Bischoff, 1980; Pottorf and Barnes, 1983).

The lower brine is highly enriched in metals (e.g., Brewer and Spencer, 1969; Anschutz et al., 2000) but devoid of reduced sulfur, so metals are co-precipitated with various amorphous phases like ferrihydrite. Extensive discussion of the characteristics of these particles is found in the literature (e.g., Badaut et al., 1992; Schwertmann et al., 1998; Taitel-Goldman and Singer; 2002, Taitel-Goldman et al., 2004). High Si concentrations,

which are typical of the Atlantis II lower brine, increase the stability of Fe-(oxy)hydroxides in the brine (Taitel-Goldman et al., 2004) by creating Fe-O-Si bonds that cause clustering of the surface active particles (e.g., Cornell et al., 1987). After deposition, the amorphous material gradually crystallizes to metal-bearing clays (Taitel-Goldman et al., 2004) and Fe-minerals like goethite, siderite and later to hematite and magnetite (Blanc et al., 1998; Zierenberg and Shanks, 1983). Diagenetic changes can also result from the advection of hydrothermal fluids through the sediments, as indicated by the composition of pore fluids near the inferred location of the current vent source (Anschutz et al., 2000). More concentrated fluid flow and epigenetic precipitation of metals is confirmed by the existence of minor sulfide minerals in anhydrite veins (Bischoff, 1969; Zierenberg and Shanks, 1983; Oudin et al., 1984); however, black smoker-type feeder veins (e.g., Humphris et al., 1995) have not yet been found.

### 1.3 Stratigraphy of the Atlantis II sediments

The stratigraphy of the Atlantis II sediments was defined by Bäcker and Richter (1973), who distinguished 5 units based on almost 100 sedimentary cores (Table 4.1). The different units range from 1 to 12 meters in thickness, and each unit is characterized by many beds and fine layering that range from centimeter to millimeter scale. An average hydrothermal sedimentation rate of ~1 m/Ka (Table 4.1) corresponds to accumulation of ~1 mm of sediment per year. However, a convincing model for the origin of these fine laminae has yet to emerge.

The major units appear to be related to changes in the location and intensity of hydrothermal activity and the amount of hydrothermal versus background sedimentation. The lowermost unit, referred to as the Detrital-Oxidic-Pyritic unit (DOP) was formed from ~25 Ka until ~12 Ka. It is composed mostly of a mixture of siliciclastic and biogenic detrital material with rare fragments of basalt. It has some limonitic and manganitic layers and disseminated sulfides, which become more abundant up stratigraphy, signaling the beginning of hydrothermal activity. The presence of manganite indicates formation during more oxidic brine conditions that allow Mn-oxides to accumulate at the bottom of the Deep, in contrast to the present situation in which Mn-oxides dissolve in the lower brine. In the northern parts of the Deep the DOP is cut by the vertical anhydrite veins that elsewhere are interpreted to have formed by high-temperature fluid flow through the sediments (e.g., Oudin et al., 1984; Zierenberg and Shanks, 1983). The presence of these veins indicates that hydrothermal venting was happening in this part of the Deep (North Passage or East Basin, Figure 4.1) during formation of the first sulfide- and metal-rich unit SU1 (~12-8.6 Ka), which directly overlies the DOP, and before hydrothermal venting shifted to its current location in the Southwest Basin (~8.6-5.9 Ka). SU1 is composed of silicates, Fe-bearing clays, oxides and (oxy)hydroxides, anhydrite, abundant sulfides, and rare barite. Anhydrite is found as crosscutting veins but also as sill-like bodies up to several meters thick. The horizontal extent of the anhydrite sills is poorly defined as they can be traced from core to core only in rare cases. The two lowermost units (DOP and SU1) are absent in the Southwest Basin or at least inaccessible due to intrusion of a basaltic sill (Hackett and Bischoff, 1973).

The Central-Oxidic (CO) unit (formed ~8.6-5.9 Ka), which consists mainly of hydrous and poorly crystalline Fe-oxide compounds, overlies the first sulfide-rich unit, SU1, with a sharp contact. Mn-oxides, Fe-, Mn- and Ca-carbonates, as well as anhydrite are found in varying but generally minor amounts in the CO, although locally these minerals may be the dominant phases. Due to presence of discrete Mn-oxide layers, the CO unit is thought to have formed during more oxidized conditions than the other predominantly hydrothermal units. However, disseminated sulfides are also found throughout the CO unit. Where sulfides are present at higher than average concentration (e.g., in vent proximal locations), this unit is referred to as the Central-Oxidic-Sulfidic unit (COS). In the Southwest Basin, the lower part of the CO unit is the only place where euhedral magnetite is found; it is thought to have formed as a result of heating of Fe-(oxy)hydroxides and/or hematite by the intruding basaltic sill (Zierenberg and Shanks, 1983).

The outbreak of hydrothermal activity in the Southwest Basin around 5.9 Ka marked the beginning of formation of the second sulfide- and metal-rich unit (SU2). Sulfides, including pyrite, sphalerite and chalcopyrite, are less common in SU2 than SU1, and the sphalerite/pyrite ratio is higher. Although chalcopyrite is present in both units, the Cu/Zn ratio decreases up stratigraphy from SU1 to SU2. Anhydrite is found as vertical veins and sill-like bodies, as in SU1, but horizontal layers are more common in SU2. Where sulfates are abundant (i.e., in vent proximal locations), SU2 is referred to as the Oxidic-Anhydritic unit (OAN) or Sulfidic-Oxidic-Anhydritic unit (SOAN).

The topmost unit is referred to as the Amorphous-Siliceous unit (AM), as it comprises mainly poorly crystalline Si-Fe phases and is saturated in brine. Mineralogically, the AM unit most closely resembles the CO unit, implying a similar origin (Taitel-Goldman and Singer, 2002), although it contains more metals and sulfide than the CO unit. In vent proximal locations, the AM unit has higher concentrations of sulfides and is referred to as the Sulfidic-Amorphous-Siliceous unit (SAM). The AM unit is separated almost basin-wide from SU2 by a few millimeters thick bright orange lepidocrocite horizon (Bäcker and Richter, 1973; Taitel-Goldman et al., 2002) that was formed at ~3.6 Ka; where this horizon is absent the contact is gradational.

All units are highly enriched in Fe (30-40 wt.%: Gurvich, 2006), but other metals are also present at high concentrations. Guney et al. (1988) estimated a bulk composition of the sediments based on more than 500 cores of ~2 wt.% Zn and ~0.5 wt.% Cu (~90 Mt of salt-free material). Some extremely high metal-concentrations have been found in some sections (e.g., Oudin, 1987). The concentrations of the major elements, S, Si and Ca, and some minor elements also vary between different stratigraphic units; however, the chemical variation between the fine layers in each unit has so far been little studied. Details of the main characteristics of the stratigraphic units are summarized in Table 4.1 (Bäcker and Richter, 1973).

## 2. Sampling and Methods

One hundred samples were taken from 9 brine-saturated sediment cores, the locations of which are shown in Figure 4.1. The samples here come from all 5 lithostratigraphic units and were selected to study the differences between sedimentary units, the variations within units relative to the location of the hydrothermal venting (distal vs. proximal), and different layer types (e.g., Fe-rich, S-rich, detrital). All samples are from sedimentary cores taken during the *R/V Valdivia* cruise 29 in 1980. Seven of the cores are from the deepest parts of the deep (≥2100 m depth); cores 495 and 546 are from shallower depths (2076 and 2013 m, respectively). The core lengths range from 5 to ~12 m. After recovery, the cores were split, with one half being sealed and stored in a cool warehouse. When reopened in 2010, the cores were in excellent condition and still moist, although the cut surfaces were, in many cases, encrusted with salt and had a thin layer of surface oxidation. This crystalline salt and surface oxidation were removed before logging and sampling of the cores. The core log for core Va29-387 shown in Figure 4.2 is an example of the material and the logs. Sampling sites are also indicated.

The layered and laminated structure of the Atlantis II sediments suggests that small-scale chemical changes are common and that all units comprise a mix of genetically different sediments, with one or more dominating (e.g., sulfide-rich layers are most common in SU1 and SU2 but oxide and detrital layers are still present). To observe the small-scale variations and to be able to study the possible formation mechanisms for different types of sediment, we sampled individual layers in which only one type of sediment was dominant. The different types of sediment have been grouped here according to major chemical

differences. This sampling is much more detailed than in previous studies of the Atlantis II cores that were focused on the bulk compositions of the sediments. Almost all of the published data on the compositions of the cores are based on composite samples of up to several 10s of cm, and commonly 1 m, in length. In this study, the analyzed samples consist of 2 cm-diameter minicores; in some cases even smaller samples were cut from the core with a spatula.

The samples were dried at 40°C, after which they were pulverized in an agate ball mill. The powders were dissolved in HF-$HNO_3$-HCl-$HClO_4$ in a multi-step table-top procedure, and analyzed by ICP-OES (Spectro Ciros SOP) for major elements and by ICP-MS (Agilent 7500cs) for trace elements at the University of Kiel. Sample preparation prior to analysis as well as calibration and interference correction procedures are from Garbe-Schönberg (1993) with only minor changes. The sample introduction system for the Agilent 7500cs is a freely aspirating PFA micronebulizer (ESI 100µL/min), and we use Pt cones. The instrument was operated in Standard mode without collision/ reaction gas. Procedural blanks, sample duplicates as well as certified reference materials (BHVO-2, NOD-A1, NOD-P-1, GSPN-2) were processed with each batch of 20 samples. Interferences of BaO on Eu (and CeO on Gd) were monitored and corrected for. We do this by calculating the actual BaO (and CeO) formation rate from synthetic solutions analyzed with each sample batch and correcting the measured Eu values accordingly. Ba was analyzed along with the REE in all samples. Precision as estimated from sample duplicates and replicate measurements was better than 5% for the majority of elements. Additional chemical data were obtained by ICP-OES and

ICP-MS at Activation Laboratories, Ancaster, Ontario, after fusion of the sample with sodium-peroxide and total dissolution of the fused sample. The methods used for each element are listed in Table 4.2, and analytical precision and standards are reported in Appendix 4.1.

## 3. Results

A major component of most of the samples was salt (3-70 wt.% NaCl), still contained in pore fluid brine in the sediment. This was generally greatest (50-70 wt.% NaCl) in samples from the top 1-3 m of the cores corresponding to the last ~2000 yrs of deposition (Table 4.1). Thus the measured concentrations of most elements, including REE, decrease up stratigraphy because of dilution by salt. All of the plotted data in this paper have been corrected to a salt-free basis according to the measured Na concentrations, assuming all Na is present as NaCl. This calculation has the potential to overestimate the amount of salt if samples have large amounts of other Na-bearing minerals like feldspar. However, all samples with abundant detrital material (and thus possibly significant amounts of feldspar) had low pore-water contents and also low sodium contents, so the percentage of Na-bearing minerals other than salt is insignificant. The overall variation in salt-free concentrations of different elements is large, with maximum values typically more than 100 times the minimum (Figure 4.3). These variations are interpreted to reflect temporal and spatial variations in deposition of different chemical components in the different layers. Below we discuss a number of aspects of the chemistry of the samples as a basis for

interpreting the REE geochemistry. Details of the major and trace element geochemistry are presented in Appendix C.

The lowermost mainly detrital unit in all sampled cores (DOP) is enriched in lithophile and high field strength elements (HFSE) (e.g., Al, Ti, Sc and Th), but has relatively low base metal content. The sulfidic units (SU1, SU2) and the currently forming amorphous unit (AM) are enriched in sulfur and metals (e.g., Cu, Zn, Pb, Cd), and the AM and the CO units are enriched in Fe (~23 wt.% $Fe_{tot}$) compared to other units (~16 wt.% $Fe_{tot}$). The CO unit is also highly enriched in Mn (>3x) compared to all other units. Both the CO unit and the AM unit have high concentrations of U (Table 4.3). The major elements, Si, Ca and P show no consistent pattern of enrichment between the different units.

Three geochemically distinct groups of samples can be distinguished among the different stratigraphic units (Figure 4.4A) and sedimentary layer types (Figure 4.4B). To investigate the chemistry of REE among these groups in more detail, sixty samples were selected to represent their compositions, each group containing ~20 samples.

Samples belonging to the Al-rich group (19 samples) have $Al_2O_3/(Al_2O_3+Fe_2O_3+Me)$ >0.6, where Me=(Cu+Zn+Pb*10+Cd*100)/1000. This group is characterized by high concentrations of $Al_2O_3$ (~4.5 wt.% versus 1.8 wt.% in the other groups) and is also highly enriched (~2.5x compared to other groups) in Ti, Sc and Th. As these elements are strongly

enriched in detrital compared to hydrothermal metalliferous sediments, we refer broadly to this group as “detrital”.

Samples belonging to the Fe-rich group (21 samples) have $Al_2O_3/(Al_2O_3+Fe_2O_3+Me)$ <0.5 and $Fe_2O_3/(Fe_2O_3+Me)$ >0.7. These samples, which consist mainly of Fe-oxides, are highly enriched in Fe but have low concentrations of other metals. Concentrations of U are >2x higher than the average value of all samples. One sample was excluded from this group due to very high Mn concentration (~32 wt.%).

Samples belonging to the S-rich group (20 samples) have $Al_2O_3/(Al_2O_3+ Fe_2O_3+Me)$ <0.5 and $Fe_2O_3/(Fe_2O_3+Me)$ <0.3. This group is characterized by high S contents (~12 wt.% total S versus <6 wt.% total S in all samples) and high concentrations of metals such as Cu, Zn, Pb and Cd (>2x the average of all samples), but relatively low concentrations of Fe. Samples with the high S and Fe but low base metal concentrations contain large amounts of pyrite that may have formed diagenetically; these samples were excluded from the present study. Two samples containing abundant calcium (>30 wt.% CaO as anhydrite) were also excluded from this group.

The selected samples are plotted on a Th-V-Sc triangular diagram in Figure 4.5, which shows the importance of detrital versus hydrothermal sources in the different sample groups (cf. Grenne and Slack, 2005). The samples span the range between pure Fe-(oxy)hydroxide precipitates and detrital sediments with the different stratigraphic units comprising

mixtures of these two sediment types (Fig. 4.5A), the groups selected to represent the different layer types above are more clearly discriminated (Fig. 4.5B).

**3.1 REE geochemistry of the stratigraphic units**

The concentrations of REE in the Atlantis II sediments are very low (average of 23 ppm ΣREE for all samples and only 5.5 ppm in 34 of 100 samples with <1% $Al_2O_3$). However, significant differences are seen between samples from the same sedimentary unit (Table 4.2). In order to investigate the behavior of the REE relative to the major and other trace elements, correlation coefficients of each element with ΣREE concentration were calculated using the whole data set of 100 analyses (Fig. 4.6). Aluminum, together with the lithophile and HFSE (e.g., Ti, Sc, Th) are strongly positively correlated with ΣREE in almost all of our samples. Elements with both hydrothermal and detrital sources (e.g., Si, Mg, Ca) are variably correlated with ΣREE in different units. Trace elements such as U, Mn and S that can be from seawater or hydrothermal sources do not correlate well with ΣREEs, except in the CO and AM units where r values up to 0.6 are found for some elements (Fig. 4.6).

The Al-rich layers (dominantly detrital) are by far the most important hosts for REE in all units (Figure 4.7). The AM unit is characterized by extremely low total REE (average 7.4 ppm; Table 4.3) and $Al_2O_3$ (average 1.1 wt.%: Table 4.2). Some of the increase in total REE in lower units can be explained by lower overall hydrothermal sedimentation during DOP and SU1 formation (Table 4.1) and a larger contribution from detrital sources. However, the two lowermost units (DOP and SU1) show a weaker correlation between $Al_2O_3$ and ΣREE than in

the SU2 and CO units, suggesting that not all REE increase is due to a larger input of detrital REE. The correlation between $P_2O_5$ and ΣREE in the Al-rich layers is moderate ($r$ =0.31).

Figure 4.7A shows shale-normalized REE plots for each of the different stratigraphic units, and Table 4.3 summarizes some of the main characteristics of the plots. All units are characterized by very similar REE patterns with positive europium anomalies but no Ce anomaly, even though they show major differences in their bulk composition (Table 4.2). Total REE, LREE enrichment (La/Yb) and LREE fractionation (La/Sm versus La/Gd) increase gradually down stratigraphy. No fractionation is seen in the HREE (Gd/Tb). The CO unit has the smallest Eu anomaly. Although the two sulfidic units (SU1 and SU2) are chemically similar, they are characterized by significantly different REE concentrations and positive Eu anomalies of different size.

To assess the amount of non-detrital REE in the samples, the influence of the detrital component can be subtracted by using Al, Th or Sc as a reference element and the REE concentrations in Atlantis II detrital material. The results using Sc as the reference material were the most consistent, with the lowest number of negative residual values (see also Pattan and Shane, 1999). Sixteen of 19 samples of the Al-rich layers (with $Eu^*_{PAAS}$<1.6) were used to determine the detrital REE pattern for the Atlantis II Deep. The average detrital REE concentrations determined in this way were subtracted from all other samples in proportion to the Sc concentrations of the samples. The results are plotted in Figure 4.7B and summarized in Table 4.3. Significantly negative residual REE concentrations calculated

by this method were common because of the low overall REE concentrations, and these were excluded from the averages.

All residual REE patterns (Fig. 4.7B) are strikingly similar to each other. All have significant positive Eu anomalies ($Eu^*_{PAAS}$ ~10), similar to black smoker fluids at mid-ocean ridges (e.g., Mitra et al., 1994; Fig. 4.9C) and effectively no Ce anomaly, similar to anoxic ocean waters (e.g., German et al., 1991). A major difference is the amount of residual ΣREE in the different units, which increases by a factor of about 10 with depth in the cores. The similar patterns suggest that all units have inherited their non-detrital REE from the same source(s), and the lowermost units are more influenced by that source than the topmost units. The anomalous pattern of non-detrital REE in the CO unit is due to very low total REE and correspondingly large analytical error close to the detection limits, especially for HREEs that are present at extremely low concentrations in these samples.

**3.2 REE geochemistry of the different layer types**

As seen for the different stratigraphic units (Fig. 4.8A), $Al_2O_3$ correlates well with ΣREE in the S- and Al-rich layers (Fig. 4.8C). Thus the detrital component dominates the REE distribution also in the S-rich layers. Fe-rich layers appear to have another major source or sources of REE. Figure 4.8D shows the correlation between $P_2O_5$ and ΣREE in the different sample types. In most of the samples, ΣREE correlates better with $Al_2O_3$ than $P_2O_5$, although when the concentration of $P_2O_5$ is more than 20% of the $Al_2O_3$ concentration the correlation of ΣREE with $P_2O_5$ is stronger (Table 4.4). Phosphorus does not correlate with $Al_2O_3$ at any

$Al_2O_3$ or $P_2O_5$ concentrations indicating that the phosphorus is contained within a phase unrelated to siliciclastic detrital material. This might be microcrystalline apatite and/or fish debris, which have been suggested by Oudin and Cocherie (1988) to be the main REE carriers in the Atlantis II Deep (see also Butuzova and Luapynov, 1995). However, Zr/Hf ratios > ~70, which are indicative of fish debris (Tlig, 1988), are not seen in our Atlantis II samples, and there is no correlation between Zr/Hf and ΣREE ($r^2$=0.16). As many Zr and Hf concentrations are below the detection limits, this may represent an analytical bias. Nevertheless, the concentrations of $P_2O_5$ in our samples never reach values as high as those reported by Oudin and Cocherie (1988) (~2 wt.% $P_2O_5$ with >1000 ppm ΣREE), suggesting that apatite or fish debris are not important components in our samples. Because detrital material is the main REE-bearing component in most samples, the increase in ΣREE with depth in the cores (Table 4.3) can therefore be attributed mainly to the increasing proportion of the Al-rich component. However, the amount of non-detrital REE also increases with depth (Table 4.3), which contributes to the ΣREE. Neither $P_2O_5$ nor REE scale with Fe in any of the layer types.

REE profiles for the different layer types are plotted in Figure 4.9A, and their characteristics are summarized in Table 4.5. The REE pattern for the Al-rich layers is very consistent and almost identical to that reported by Pierret et al. (2010) for biogenic and siliciclastic background sediments near the Thetis Deep (average of 10 samples from a 14-m long sediment core, also plotted in Figure 4.9A). The residual REE patterns were also computed for the different layer types (Figure 4.9B and Table 4.5). The proportion of non-detrital REE

in different layer types can be estimated by difference from the ΣREE. Al-rich layers contain only a minor proportion (~3%) of non-detrital REE, S-rich layers a significant proportion (~20%) and Fe-rich layers the largest proportion (~50%), although these vary between samples within one layer type, and all groups have some samples with negative residual REE. The differences in the REE profiles between the different layer types are now obvious (Fig. 4.9B); in the residual REE patterns, S-rich layers have >2 times larger Eu anomalies and higher La/Yb than Fe-rich layers (details in Table 4.5). The Al-rich layers, which have low residual REE, nevertheless have positive Eu anomalies in the residual that are similar to Eu anomalies in the Fe-rich layers. The residual REE pattern for the Al-rich layers also has a small negative Ce anomaly, which is an artifact of low REE concentrations. La anomalies in marine sediments can complicate the interpretation of Ce anomalies (Bau and Dulski, 1996), but the small positive La anomaly in Figure 4.9B is again an artifact of near detection concentrations and therefore unlikely to have led to a false Ce anomaly.

Pearson correlation coefficients (*r*) for La/Sm and Eu/Eu* in the different layer types and in the residual REE fraction of samples with Σresidual REE >1 ppm and Eu/Eu* >0 are given in Table 4.5. The correlation between these variables is good in the S-rich layers but weak in the Al-rich layers. The lack of correlation in the Fe-rich layers indicates REE enrichment from a source where La/Sm and Eu* are not correlated or a mixture of sources with different Eu* and/or La/Sm.

Yttrium concentrations were below detection (1 ppm) in almost half of the samples; the rest of the samples had Y concentrations at least an order of magnitude lower than in the modern open ocean water or metalliferous sediments at MOR. Average Y/Ho values for all samples are ~30, similar to MORB, chondrites and most shales (Bau, 1996), whereas seawater has significantly higher Y/Ho (44-74: Bau, 1996).

## 4. Discussion

### 4.1 Sources of REE in the Atlantis II sediments

Several different pathways are possible for enrichment of REE in the sediments of the Atlantis II Deep. Previous studies (Courtois and Treuil, 1977; Oudin and Cocherie, 1988; Calvez et al., 1988; Cocherie et al., 1994; Butuzova and Lyapunov, 1995) have suggested P-bearing phases that scavenged REEs during hydrothermal diagenesis are the main host for REE. The role of diagenesis is supported by Anschutz et al. (2000), who studied the composition of the pore water in sediments of the Atlantis II Deep and confirmed that advection of hydrothermal fluids through the sediments has transported elements upward in the vent proximal cores (although REE were not measured in the study). Advection could thus be a mechanism for replenishing the pore water with REE from the hydrothermal source. Butuzova and Lyapunov (1995) measured high REE concentrations (ΣREE of 130 ppm) in one Fe-rich layer (63 wt.% Fe) located low in the stratigraphy (SU1/DOP unit) and suggested that this layer was initially formed as Fe-(oxy)hydroxides that acquired REE by scavenging from the ambient environment following the outbreak of hydrothermal activity. In contrast to previous studies, our data suggest that the detrital component is by far the

most important source of REE in almost all sediments. Fe-rich layers, due to their abundance, are the main host for non-detrital REE. However, high REE concentrations in P-rich phases, as described by Oudin and Cocherie (1988), may be locally important.

The two main sources of non-detrital REE are hydrogenous and hydrothermal. The non-detrital REE pattern of the S-rich layers is dominated by hydrothermal REE. ΣREE, residual ΣREE and La/Sm all increase with depth from the topmost unit (AM) to the lowermost (DOP) (Fig. 4.7A; Table 4.3). In particular, there is an increase in residual ΣREE and weaker correlation of $Al_2O_3$ with ΣREE in the lowermost units (DOP and SU1) compared to the upper units (CO and SU2). The increase in La/Sm ratio down stratigraphy, the large residual (=non-detrital) ΣREE, and positive Eu anomaly in the lowermost unit (DOP) are consistent with the increasing influence of hydrothermal fluid with depth. The size of the Eu anomaly appears to be more closely related to proximity to the hydrothermal source, as S-rich layers (most common in the proximal part of the Deep) have larger Eu anomalies than the Fe-rich layers (Table 4.5 and Fig. 4.9B). In S-rich layers, La/Sm and Eu/Eu* are high and strongly correlated (Table 4.5), which is typical of MOR hydrothermal fluids (Klinkhammer et al., 1994). In contrast, Fe-rich layers have smaller Eu anomalies, and Eu/Eu* and La/Sm are poorly correlated. We interpret the non-detrital source of REE in the Fe-rich layers to include a component of seawater-derived REE and perhaps an additional minor source from surrounding Miocene evaporites.

Diffuse hydrothermal venting through the sediments as described by Anschutz et al. (2000) supports the suggestion that the lowermost Fe-(oxy)hydroxide layers acquired REE from diagenetic interaction with the hydrothermal fluid. Amorphous phases in the sediments are known to have undergone significant diagenetic transformation after deposition (Blanc et al., 1998; Butuzova and Lisitsyna, 1984). The lowermost units are likely to be most influenced by these diagenetic effects. For example, SU1 and SU2 are chemically similar, but SU1 has higher total REE and a larger Eu anomaly (Fig. 4.7A) that could be interpreted to reflect greater diagenetic interaction with hydrothermal fluids.

Hydrogenous sources (e.g., REE transported to the brine from seawater by adsorption to surface active particles) are mainly reflected in the Fe-rich layers. During formation at the interface between the lower brine and the upper brine and settling through the lower brine the Fe-(oxy)hydroxides scavenge REE (and other elements) from their surroundings according to their physical and chemical properties and the ambient conditions. These particles spend the longest time in the brine pool and are most likely to be enriched in hydrogenous REE. The Mn-(oxy)hydroxides also scavenge REE but dissolve in the present lower brine, thereby functioning as transport agents for REE from seawater to the lower brine but not enriching the sediments (Butuzova et al., 1988b; see also e.g., German et al., 1991 and De Lange et al., 1990a).

**4.2 Factors affecting the concentrations of REE in the Atlantis II sediments**

The degree of scavenging of REE by surface active particles likely varied with the ambient conditions in the brine pool. For example, scavenging of REE is much less efficient at low pH than at the pH of seawater (Bau, 1999). The pH of the current lower brine is ~5.4 (M. Schmidt, pers. comm.), and the mineralogical composition of the Atlantis II sediments is consistent with the pH of the lower brine having been stable and mostly ~5-6 throughout the history of hydrothermal sedimentation in the Atlantis II Deep (Hackett and Bischoff, 1973; Zierenberg and Shanks, 1983, Blanc et al., 1998). Bau (1999) found that Fe-(oxy)hydroxides that were stabilized in solutions at pH ~5.5 (similar to that of the current lower brine) had a negative Y anomaly, La/Sm and La/Yb of <1, no negative Ce anomaly and a flat HREE profile (Gd/Yb close to 1), similar to that observed in the Fe-rich layers of the present study. Thus, a low pH might be one of the reasons why brine-saturated sediments in the uppermost layers have low concentrations of REE despite the abundance of Fe-(oxy)hydroxides in these layers.

Despite the low total REE concentrations, the non-detrital component of the Fe-rich layers is relatively enriched in LREE. This could be due to hydrothermal input or transport of LREE from seawater to the brine by Mn-oxides. Experimental studies (Byrne and Kim, 1990; Koeppenkastrop and De Carlo, 1992) have shown that Mn- and Fe-oxides are likely to transport mostly LREE from seawater to the brine. This is supported by observations from the Mediterranean (Bau et al., 1997) and the Black Sea (German et al., 1991) that show LREE have the greatest mobility across the chemocline. Due to the lack of correlation

between La/Sm and the Eu anomaly in the Fe-rich layers, in contrast to the S-rich layers, the enrichment in LREE is unlikely to be a consequence of direct hydrothermal input.

A negative Ce anomaly, typical of precipitation from oxygenated seawater, is only seen in the non-detrital REE pattern of the Al-rich layers. These layers have extremely low residual REE, and therefore the Ce anomaly is probably an artifact of concentrations close to the detection limit. The absence of a negative Ce anomaly in most sediments suggests that there has been little direct influence of seawater in the composition of the brine at least since the formation of the upper DOP. This observation supports the conclusion of Schoell and Faber (1978) and Pierret et al. (2001), based on isotopic evidence, that the lower brine originated mainly from the dissolution of Miocene evaporites and has not mechanically mixed with seawater since the beginning of hydrothermal activity. Although $Ce^{3+}$ could have been remobilized during early diagenesis (Calvert and Pedersen, 1993; Wilde et al., 1996), the lack of any other trace element evidence of seawater influence (e.g., Y/Ho) supports the suggestion that mixing of seawater into the brine has not contributed significantly to the REE balance.

Even without mechanical mixing, a number of workers have shown that different elements can be transported between seawater and the anoxic part of a stratified water column (e.g., Tyro Basin: Bau et al., 1997; Framvaren Fjord: Swarzenski et al., 1999 and Cariaco Trench: De Baar et al., 1988). Swarzenski et al. (1999) studied uranium cycling across an $O_2/H_2S$ interface in a stratified water column and concluded that, in combination with Mn and S

cycling and with the aid of bacteria, U can be readily transported through the chemocline without mixing. REE, on the other hand, are transported at different rates through the chemocline (Bau et al., 1997). DOP, which marks the beginning of hydrothermal activity, has a low U concentration but high residual REE. CO, which formed during reduced hydrothermal activity, has a high U concentration but low REE. The lack of correlation between U and REE suggests that the amount of non-detrital REE is not directly linked to transport through the chemocline and must be influenced by other processes. However, experiments and plume studies have shown that the scavenging of REE by Fe-(oxy)hydroxides can happen rapidly, whereas U is removed from the water column more slowly by precipitation (Anderson et al., 1989). This also could explain the lack of correlation between U and REE enrichment in the Atlantis II sediments.

**4.3 Variations in sources of REE during the evolution of the brine pool**

The lowermost unit (DOP) has the highest concentration of non-detrital REE and smallest Eu anomaly of all units (Table 4.3), suggesting that the initial brine pool had high REE compared to the current situation. The abundant residual REE in the lower stratigraphy could be explained by rapid early removal of REE from the brine pool at the beginning of hydrothermal activity. The decrease in REE concentrations up stratigraphy suggests that REE deposition has decreased over time and that replenishment of the brine by hydrothermal venting and precipitation-dissolution processes across the chemoclines have not restored the original stock of REE. The rapid early uptake of REE in the brine pool by the first Fe-(oxy)hydroxides would also explain the lack of correlation between Eu/Eu* and

La/Sm (Table 4.5). However, even the lowermost sediments show a positive Eu anomaly (~7) suggesting that not all of the non-detrital REE was stripped from the initial brine pool. Diagenetic processes (addition of hydrothermal REE) must also have contributed to the REE enrichment.

Variations in the contribution of REE from different sources allow us to draw some conclusions about sedimentation throughout the history of the brine pool (Fig. 4.10). Before the onset of hydrothermal activity in the Atlantis II Deep, a thin layer of detrital sediments lying on the basaltic basement was covered by cold brine. The conditions at this time were likely similar to other well-known anoxic basins (e.g., Cariaco Trench: De Baar et al., 1988; Black Sea: German et al., 1991; Tyro and Bannock basins in the Mediterranean: De Lange et al., 1990b). We suggest that the earliest hydrothermal activity introduced Fe- and Mn-(oxy)hydroxides to the brine pool that quickly stripped the brine of REE and settled into DOP at the bottom of the Deep (4.10A). The (oxy)hydroxides, as well as $P_2O_5$-bearing phases(including fish debris, although not important in our samples as noted previously), continued to scavenge REE during diagenesis. The pore fluids were diffusively replenished with hydrothermal REE, as evidenced by positive Eu anomalies even in DOP. Eventually hydrothermal activity produced a hot, anoxic and metal-rich brine pool (4.10B). Sulfides precipitated in the vent proximal facies inherited the hydrothermal REE signature. At the same time Fe- and Mn-(oxy)hydroxides formed at the upper brine layers transported minor amounts of REE and U from seawater to the brine pool. Whereas Mn compounds dissolved in the lower bine and could be deposited only at the flanks of the deep, Fe-(oxy)hydroxides

settled through the brine pool in a metastable state before being deposited at the bottom of the Deep. They inherited their REE during settling through the different brine layers and by continued scavenging during diagenesis (4.10B). Sediments that formed during times of reduced hydrothermal activity (CO formation, 4.10C) have REE signatures and Y concentrations similar to the other sedimentary units indicating that voluminous mixing of seawater with the brine did not happen. These sediments have a high U content because of enhanced transport of U from the seawater through the chemocline to the lower brine rather than by mechanical mixing. The present configuration (4.10D) of the Atlantis II Deep is similar to that during SU1 formation (4.10B). The extremely low REE content in the uppermost sediments suggests that REE in upwelling hydrothermal fluids are stripped by the first (oxy)hydroxides (or $P_2O_5$-bearing phases) that they encounter in the sediments, and not all the REE are transported to the brine pool. Presently, sedimentation in the Atlantis II Deep seems to be in a transition from sulfidic (4.10B and D) to more oxidic (4.10C), indicated by the dominant mineralogy and high U content of the AM and CO units.

**4.4 Comparison with other modern and ancient hydrothermal systems**

The total amount of REE in the Atlantis II sediments is much lower than in metalliferous sediments deposited from plume fallout in open ocean settings. This is because the dominant source of REE in the brine pool is from Mn- and Fe-(oxy)hydroxide cycling, whereas the open ocean is almost an infinite source of REE. The negative Ce anomaly and high Y/Ho ratio, typical of seawater, are lacking from all Atlantis II sediments due to the anoxic conditions in the brine. However, the non-detrital REE pattern of the S-rich

component in the Atlantis II Deep resembles that of hydrothermal deposits formed at MOR black smokers (e.g., Mitra et al., 1994; Fig. 4.9C). The Fe-rich layers in the Atlantis II Deep have (non-detrital) Eu anomalies that are smaller than near-field plume fallout at MOR vents but larger than distal fallout (e.g., German, et al., 1993; Figures 4.9A and C) and reflect multiple sources of non-detrital REE. These mixed patterns are very like the TAG mound oxide patterns in Mills and Elderfield (1995) and bear resemblance to the peripheral Fe-oxides that precipitate from the most evolved low-temperature fluids, but the Atlantis II Fe-oxides have lower total REE concentrations. Unlike most modern metalliferous sediments at MORs, diffuse flow and associated diagenesis have strongly influenced the muds in the Atlantis II Deep, as previously suggested by Butuzova and Lyapunov (1995), especially in proximity to the vent source where upward diffusion of elements has been documented in pore waters (Anschutz et al., 2000). Advection of hydrothermal fluids through the lowermost sediments has contributed to their higher REE concentrations and larger Eu anomalies.

The thin silicate-, carbonate-, oxide- and sulfide-rich layers of the Atlantis II sediments are strikingly similar to those of Algoma-type BIF, although sediments in the Atlantis II Deep are much more enriched in Zn, Cu and many other trace metals due to proximity to the hydrothermal venting. Algoma-type BIF are interpreted to have been deposited under similar (anoxic) conditions and, like the Atlantis II sediments, the total concentrations of REE are small and mainly attributed to the detrital component (e.g., Slack et al., 2007; Bekker et al., 2010; Planavsky et al., 2010). Bau (1993) showed that only 1% of clastic material may

dominate the REE pattern in BIF, although many BIF samples are contaminated to lesser degree. However, the hydrothermal components of BIF and Atlantis II sediments always have positive Eu anomalies and low or completely absent negative Ce anomalies (Bau and Dulski, 1996; Planavsky et al., 2010; Bekker et al., 2010). The REE patterns of some BIF have higher HREE/LREE ratios and smaller Eu anomalies than the Atlantis II sediments, thus more closely resembling modern plume particles (Slack et al., 2007; Planavsky et al., 2010). Importantly, the Y/Ho values typical of BIF (and seawater) are not seen in the Atlantis II sediments and suggest stronger seawater influence in most BIF than in the Atlantis II precipitates.

Different authors have interpreted the variation in major element compositions and REE characteristics of BIF to reflect variation in the input from different sources (hydrothermal, volcaniclastic, terrigenous), variation in the pH of the local environment, or larger-scale changes in ocean chemistry (e.g., Manikyamba et al., 1993; Kato et al., 1998). Because most BIF are representative of the distal hydrothermal plume environment (Goodwin, 1962; Grenne and Slack, 2005), they are typically not influenced by diffuse venting of hydrothermal fluids through the sediments after deposition on the seafloor. This study suggests that some Fe-rich layers that are enriched in non-detrital REE may record early stages of hydrothermal activity in a confined, REE-enriched, anoxic basin, as suggested here for the Atlantis II sediments. In contrast to many BIF, a lack of Y/Ho anomalies and negative Ce anomalies, as well as higher LREE/HREE in the Atlantis II sediments can be attributed to the isolation of the brine pool from the surrounding seawater and possibly the lower pH of

the brines. However, Bau (1996) has noted that low Y/Ho values are not necessarily indicative of a lack of seawater influence or anoxic conditions but rather reflect fractionation of Y and Ho by Fe-oxides (see also Bau and Dulski, 1999). Moreover, Bau and Dulski (1996) suggested that variable Eu/Eu* reflect back-and-forth variations in the degree of hydrothermal contributions rather than secular evolution of BIF depositional environments.

## 5. Conclusions

The Atlantis II Deep contains a succession of about 20 m of finely-layered, metal-rich sediments. Three main components appear to be responsible for the major differences in REE between the different sedimentary layers. A small detrital component, which is rich in lithophile elements (e.g., Al, Ti, Sc, Th) is the major source of REE in the majority of the Atlantis II sediments. It is thought to be related to siliciclastic sediment input into the basin. Hydrothermal REE are most abundant in the proximal sulfur- and base metal-rich sediments. Although the lower brine is separated from seawater by an upper brine layer, REE from seawater have been transported to the Atlantis II brine pool via precipitation-dissolution cycling at the chemoclines. Seawater-derived REE are mainly taken up by Mn- and Fe-(oxy)hydroxides that are formed in the upper brine layers. Whereas the Mn-(oxy)hydroxides dissolve in the lower brine, the Fe-(oxy)hydroxides settle to the seafloor and deposit REE that are scavenged from the brine pool. The sediments formed at the beginning of hydrothermal activity have significantly more non-detrital REE and lower Eu anomalies than the younger sediments. We interpret this to indicate that REE were stripped

from the lower brine after the introduction of the first hydrothermal Fe- and Mn-(oxy)hydroxides. Further diagenetic enrichment of REE has been caused by scavenging from the ambient pore fluid that is replenished with hydrothermal REE by upward diffusion into the sediments. These findings suggest that similar changes in the REE chemistry of ancient chemical sedimentary rocks, such as BIF, may record important changes in basin evolution as well as more local variation in the input of REE from different sources.

## References


Adams, D. K., McGillicuddy Jr., D. J., Zamudio, L., Thurnherr, A. M., Liang, X., Rouxel, O., German, C. R. and Mullineaux, L. S., 2011, Surface-Generated Mesoscale Eddies Transport Deep-Sea Products from Hydrothermal Vents. *Science* 332, p. 580-582. DOI: 10.1126/science.1201066

Anderson, R. F., Fleisher, M. Q. and LeHuray, A. P., 1989, Concentration, oxidation state, and particulate flux of uranium in the Black Sea. *Geochim. Cosmochim. Acta* 53, p. 2215-2224.

Anschutz, P. and Blanc, G., 1995, Chemical mass balances in metalliferous deposits from the Atlantis II Deep (Red Sea). *Geochim. Cosmochim. Acta* 59, p. 4205-4218.

Anschutz, P. and Blanc, G., 1996, Heat and salt fluxes in the Atlantis II Deep (Red Sea). *Earth Planet. Sci. Lett.* 142, p. 147-159.

Anschutz, P., Blanc, G. and Stille, P., 1995, Origin of fluids and the evolution of the Atlantis II deep hydrothermal system, Red Sea: Strontium isotope study. *Geochim. Cosmochim. Acta* 59 (23), p. 4799-4808.

Anschutz, P., Turner, J. S. and Blanc, G., 1998, The development of layering, fluxes through double-diffusive interfaces, and location of hydrothermal sources of brines in the Atlantis II Deep: Red Sea. *Journ. Geophys. Res*. 103 (C12), p. 27809-27819.

Anschutz, P., Blank, G., Monnin, C. and Boulecue, J., 2000, Geochemical dynamics of the Atlantis II Deep (Red Sea): II. Composition of metalliferous sediment pore waters. *Geochim. Cosmochim. Acta* 64 (23), p. 3995–4006.

Badaut, D., Decarreau, A. and Besson, G., 1992, Ferripyrophyllite and Related $Fe^{3+}$-rich 2:1 Clays in Recent Deposits of Atlantis II Deep, Red Sea. *Clay miner*. 27, p. 227-244.

Baker E. T., Lavelle, J. W. and Massoth, G. J., 1985, Hydrothermal particle plumes over the southern Juan de Fuca Ridge. *Nature* 316 (6026), p. 342-344.

Bau, M., 1993, Effects of syn- and post-depositional processes on the rare-earth element distribution in Precambrian iron-formations, *Eur. J. Mineral*. 5, p. 257-267.

Bau, M., 1996, Controls on the fractionation of isovalent trace elements in magmatic and aqueous systems: evidence from Y/Ho, Zr/Hf, and lanthanide tetrad effect. *Contrib. Min. Petrol.* 123, p. 323-333.

Bau, M., 1999, Scavenging of dissolved yttrium and rare earths by precipitating iron oxyhydroxide: experimental evidence for Ce oxidation, Y–Ho fractionation, and lanthanide tetrad effect. *Geochim. Cosmochim. Act.* 63, 67–77.

Bau, M., and Dulski, P., 1996, Distribution of yttrium and rare-earth elements in the Penge and Kuruman Iron-Formations, Transvaal Supergroup, South Africa. *Precambrian Res.* 79, p. 37-55.

Bau, M. and Dulski, P., 1999, Comparing yttrium and rare earths in hydrothermal fluids from the Mid-Atlantic Ridge: implications for Y and REE behavior during near-vent mixing and for the Y/Ho ratio of Proterozoic seawater. *Chem. Geol.* 155, p. 77-90.

Bau, M., Möller, P. and Dulski, P., 1997, Yttrium and lanthanides in eastern Mediterranean seawater and their fractionation during redox-cycling. *Mar. Chem.* 56, p. 123-131.

Bekker A., Slack J., Planavsky N., Krapež B., Hofmann A., Konhauser K. O. and Rouxel O. J., 2010, Iron formation: The sedimentary product of a complex interplay among mantle, tectonic, oceanic, and biospheric processes. *Econ. Geol*. 105, p. 467-508.

Bennett, S. A., Achterberg, E. P., Connelly, D. P., Statham, P. J., Fones, G., R. and German, C. R., 2008, The distribution and stabilisation of dissolved iron (Fe) in deep-sea hydrothermal plumes. *Earth Planet. Sci. Lett*. 270 (3-4), p. 157-167.

Bertram, C., Krätschell, A., O'Brien, K., Brückmann, W., Proelss, A. and Rehdanz, K., 2011, Metalliferous sediments in the Atlantis II Deep—Assessing the geological and economic resource potential and legal constraints. *Res. Policy* 36, p. 315-329.

Bischoff, J. L., 1969, Red Sea Geothermal Brine Deposits: Their mineralogy, Chemistry and Genesis, *in* Degens, E. T. and Ross, D. A., eds., *Hot Brines and Recent Heavy Metal Deposits in the Red Sea*. Springer-Verlag, New York, p. 368-406.

Blanc, G. and Anschutz, P., 1995, New Stratification in the hydrothermal brine system of the Atlantis II Deep, Red Sea. *Geology* 23, p. 543-546.

Blanc, G., Anschutz, P. and Pierret, M-C., 1998, Metalliferous sedimentation in the Atlantis II Deep: a geochemical insight, *in* Purser, B. H. and Bosence Dan, W. J., eds., *Sedimentation and Tectonics in Rift Basins: Red Sea – Gulf of Aden*. Chapman & Hall, London, p. 505-520.

Brewer, P. G. and Spencer, D. W., 1969, A note on the chemical composition of the Red Sea Brines. *in* Degens, E. T. and Ross, D. A., eds., *Hot Brines and Recent Heavy Metal Deposits in the Red Sea*. Springer-Verlag, New York, p. 174-179.

Butuzova, G. Y. and Lisitsyna, N. A., 1984, Metal deposits in deep subbasins of the Red Sea; ore geochemistry and distribution pattern. *Lith. Min. Res. of USSR* 18, p. 224-238.

Butuzova G. and Lyapunov, S. M., 1995, Rare Earth elements in hydrothermal-sedimentary deposits from the Red Sea. *Lith. Min. Res.* 30 (1), p. 13-26.

Butuzova, G. Y., Gorshkov, A. I., Drits, V. A., Morozov, A. A. and Sivtsov, A. V., 1988a, Mineralogy and formation processes of oxidized Fe and Mn substances in the Red Sea rift zone. Part I, ore mineralogy. *Lith. Min. Res.* 23 (4), p. 318-329. (Translation from Litologiya i Poleznye Iskopaemye, 1988, vol. 4, p. 21-35).

Butuzova, G. Y., Morozov, A. A., Drits, V. A., and Gorshkov, A. I., 1988b, Mineralogy and formation of the oxides and hydroxide forms of iron and manganese in the rift zone of the Red Sea. *Lith. Min. Res.* 23 (6), p. 530-539. (Translation from Litologiya i Poleznye Iskopaemye, 1988, vol. 6, p. 17-30).

Byrne, R. H. and Kim, K-H., 1990, Rare earth element scavenging in seawater. *Geochim. Cosmochim. Acta* 54, p. 2645-2656.

Bäcker, H. and Richter, H., 1973, Die rezente hydrothermal-seidimentäre lagerstätte Atlantis II-tier im Roten Meer. *Geol. Rundsch.*62, p. 697-740.

Calvert, S. E. and Pedersen, T. F., 1993, Geochemistry of recent oxic and anoxic marine sediments: implications for the geological record. *Mar. Geol*. 113, p. 67-88.

Calvez, J. Y., Cocherie, A. and Oudin, E., 1988, Sr-Nd isotopes and REE signatures of the hydrothermal activity in the Red Sea. *Chem. Geol.* 70 (1-2), p. 133.

Cloud, P., 1973), Paleoecological significance of the banded iron-formation. *Econ. Geol*. 68, p. 1135-1143.

Cocherie, A., Calvez, J. T. and Oudin-Dunlop, E., 1994, Hydrothermal activity as recorded by Red Sea sediments: Sr-Nd isotopes and REE signatures. *Mar. Geol*. 118, p. 291-302.

Cornell, R. M, Giovanoli, R. and Schindler, P. W., 1987, Effect of silicate species on the transformation of ferrihydrite into goethite and hematite in alkaline media. *Clays Clay Miner.* 35, p. 21-28.

Courtois, C. and Treuil, M., 1977, Distribution des terres rares et de quelques éléments en traces dans les sédiments récents des fosses de la Mer Rouge. *Chem. Geol*. 20, p. 57-72.

De Baar, H. J. W., German, C. R., Elderfield, H. and van Gaans, P., 1988, Rare earth element distributions in anoxic waters of the Cariaco Trench. *Geochim. Cosmochim. Acta* 52, p. 1203-1219.

De Lange, G. J., Catalano, G., Klinkhammer, G. P. and Luther, G. W., 1990, The interface between oxic seawater and the anoxic Bannock brine; its sharpness and the consequences for the redox-related cycling of Mn and Ba. *Mar. Chem*. 31, p. 205-217.

De Lange, G. J., Middelburg, J. J., van der Weijden, C. H., Catalano, G., Luther, G. W., III, Hydes, D. J., Woittiez, J. R. W. and Klinkhammer, G. P., 1990b, Composition of anoxic hypersaline brines in the Tyro and Bannock Basins, eastern Mediterranean. *Mar. Chem.* 31, p. 63-88.

Degens, E. T. and Ross, D. A., 1969, *Hot brines and recent heavy metal deposits in the Red Sea*. Springer-Verlag Inc., New York, 600 p.

Garbe-Schönberg, D., 1993, Simultaneous determination of thirty-seven trace elements in twenty-eight international rock standards by ICP-MS. *Geostand. Newslett*. 17 (1), p. 81-97.

Garbe-Schönberg, D., Scholten, J. C. and Stoffers, P., 1998, Trace element chemistry of brines and brine-interfaces in the Atlantis-II, Chain, and Discovery Deeps in the Red Sea: first results, *Eos Trans. AGU*, 79 (45), Fall Meet. Suppl. V11B-05.

German, C. R., Klinkhammer, G. P., Edmond, J. M., Mitra, A. and Elderfield, H., 1990, Hydrothermal scavenging of rare-earth elements in the ocean. *Nature* 345, p. 516-518.

German, C. R., Holliday, B. P. and Elderfield, H., 1991, Redox cycling of rare earth elements in the suboxic zone of the Black Sea. *Geochim. Cosmochim. Acta* 55 (5), p. 3553-3558.

German, C. R., Higgs, N. C., Thomson, J., Mills, R., Elderfield, H., Blusztajn, J., Fleer, A. P. and Bacon, M. P., 1993, Geochemical study of metalliferous sediment from the TAG hydrothermal mound, 26°08'N, Mid-Atlantic Ridge*, J. Geophys. Res*. 98, p. 9683-9692.

Goodwin, A. M., 1962, Structure, stratigraphy and origin of iron formations, Michipicoten Area, Algoma District, Ontario, Canada, *Geol. Soc. Am. Bull.* 73, p. 561-586.

Grenne, T. and Slack, J. F., 2003, Bedded jaspers of the Ordovician Løkken ophiolite, Norway: seafloor deposition and diagenetic maturation of hydrothermal plume-derived silica-iron gels. *Miner. Deposita* 38, p. 625–639.

Grenne, T. and Slack, J. F., 2005, Geochemistry of jasper beds from the Ordovician Løkken ophiolite, Norway: origin of proximal and distal siliceous exhalites*, Econ. Geol*. 100, p. 1511-1527.

Guney, M., Al-Marhoun, M. A and Nawab, Z. A., 1988, Metalliferous sub-marine sediments of the Atlantis-II-Deep, Red Sea. *CIM Bulletin* 81, p. 33-39.

Gurvich, E. G. and Bogdanov, Y. A., 1986, Sediments of the AtlantisII Deep. Accumulation rates of the main components of the metal-bearing matter. Relationship to intensity of hydrothermal activity, *in* Lisitzin, A. P. and Bogdanow, Y. A., eds., *Metalliferous sediments of the Red Sea*. Nauka, Moscow, p. 138-145.

Gurvich, E. G., 2006, *Metalliferous Sediments of the World Ocean: Fundamental Theory of Deep-Sea Hydrothermal Sedimentation*. Springer, Heidelberg, DEU, 423 p.

Hackett, J. and Bischoff, J. L., 1973, New data on the stratigraphy, extent, and geologic history of the red sea geothermal deposits. *Econ. Geol.* 68, p. 553-564.

Hartmann, M., 1985, Atlantis-II-Deep geothermal brine system. Chemical processes between hydrothermal brines and red sea deep water. *Mar. Geol*. 64, p. 157-177.

Hartmann, M., Scholten, J. C., Stoffers, P. and Wehner, F., 1998a, Hydrographic structure of brine-filled deeps in the Red Sea – new results from the Shaban, Kebrit, Atlantis II, and Discovery Deep. *Mar. Geol*. 144, p. 311-330.

Hartmann M., Scholten J. C. and Stoffers P., 1998b, Hydrographic structure of brine-filled deeps in the Red Sea: Correction of Atlantis II deep temperatures. *Mar. Geol.* 144, p. 331-332.

Humphris, S. E., Herzig, P. M., Miller, D. J., Alt, J. C., Becker, K., Brown, D., Brügmann, G., Chiba, H., Fouquet, Y., Gemmell, J. B., Guerin, G., Hannington, M. D., Holm, N. G., Honnorez, J. J., Itturino, G. J., Knott, R., Ludwig, R., Nakamura, K., Petersen, S., Reysenbach, A.-L., Rona, P. A., Smith, S., Sturz, A. A., Tivey, M. K. and Zhao, X., 1995, The internal structure of an active sea-floor massive sulfide deposit. *Nature* 377, p. 713-716.

Kato, Y., Ohta, I., Tsunematsu, T., Watanabe, Y., Isozaki, Y., Maruyama, S and Imai, N., 1998, Rare earth element variations in mid-Archean banded iron formations: Implications for the chemistry of ocean and continent and plate tectonics. *Geochim. Cosmochim. Acta* 62 (21/22), p. 3475-3497.

Klinkhammer, G., Elderfield, H. and Hudson, A., 1983, Rare earth elements in seawater near hydrothermal vents, *Nature* 305, p. 185-188.

Klinkhammer G. P., Elderfield H., Edmond J. M. and Mitra A., 1994, Geochemical implications of rare earth element patterns in hydrothermal fluids from mid-ocean ridges. *Geochim. Cosmochim. Acta* 58 (23), p. 5105-5113.

Koeppenkastrop, D. and De Carlo, E. H., 1992, Sorption of rare-earth elements from seawater onto synthetic mineral particles: An experimental approach. *Chem. Geol*. 95, p. 251-263.

Manikyamba, C., Balaram, V. and Naqvi, S. M., 1993, Geochemical signatures of polygenetic origin of a banded iron formation (BIF) of the Archaean Sandur greenstone belt (schist belt) Karnataka nucleus, India. *Precambr. Res*. 61, p. 137-164.

Michard, A., Albaréde F., Michard G., Minster J. F. and Charlou J. L., 1983, Rare earth elements and uranium in high-temperature solutions from East Pacific Rise hydrothermal vent field (13°N). *Nature* 303, p. 795-797.

Mills, R. A. and Elderfield, H., 1995, Rare earth element geochemistry of hydrothermal deposits from the active TAG Mound, 26°N Mid-Atlantic Ridge. *Gechim. Cosmochim. Acta* 59 (17), p. 3511-3524.

Mitra, A., Elderfield, H. and Greaves, M. J., 1994, Rare earth elements in submarine hydrothermal fluids and plumes from the Mid-Atlantic Ridge. *Mar. Chem.* 46, p. 217-235.

Oudin, E., 1987, Trace element and precious metal concentrations in East Pacific Rise, Cyprus and Red Sea submarine sulfide deposits, *in* Teleki, P. G., ed., *Marine Minerals*. Reidel Publ., p. 349-362.

Oudin, E. and Cocherie, A., 1988, Fish debris record the hydrothermal activity in the Atlantis II deep sediments (Red Sea). *Geochim. Cosmochim. Acta* 52, p. 177-184.

Oudin, E., Thisse, Y. and Ramboz, C., 1984, Fluid inclusion and mineralogical evidence for high temperature saline hydrothermal circulation in the Red Sea metalliferous sediments: Preliminary results. *Mar. Mining* 5 (1), p. 3-31.

Pattan, J. N. and Shane P., 1999, Excess aluminum in deep-sea sediments of the Central Indian basin. *Mar. Geol*. 161, p. 247-255.

Pierret, M. C., Clauer, N., Bosch, D., Blanc, G. and France-Lanord, C., 2001, Chemical and isotopic ($^{87}Sr/^{86}Sr$, $\delta^{18}O$, $\delta D$) constraints to the formation processes of Red-Sea brines. *Geochim. Cosmochim. Acta* 65 (8), p. 1259-1275.

Pierret, M. C., Clauer, N., Bosch, D. and Blanc, G., 2010, Formation of Thetis Deep metal-rich sediments in the absence of brines, Red Sea. *Jour. Geochem. Exploration* 104, p. 12-26.

Planavsky, N., Bekker, A., Rouxel, O. J., Kamber, B., Hofmann, A., Knudsen, A. and Lyons, T. V., 2010, Rare earth element and yttrium compositions of Archean and Paleoproterozoic Fe formations revisited: New perspectives on the significance and mechanisms of deposition. *Geochim. Cosmochim. Acta* 74, p. 6387-6405.

Pottorf, R. J. and Barnes. H. L., 1983, Mineralogy, geochemistry, and ore genesis of hydrothermal sediments from the Atlantis II Deep, Red Sea. *Econ. Geol. Monograph* 5, p. 198-223.

Ramboz, C. and Danis, M., 1990, Superheating in the Red Sea? The heat-mass balance of the Atlantis II Deep revisited. *Earth Planet. Sci. Lett.* 97, p. 190-210.

Ramboz, C., Oudin, E. and Thisse, Y., 1988, Geyser-type discharge in Atlantis II Deep, Red Sea: Evidence of boiling from fluid inclusions in epigenetic anhydrite. *Can. Mineral.* 26, p. 765-786.

Schmidt, M., Botz, R., Faber, E., Schmitt, M., Poggenburg, J., Garbe-Schönberg, D. and Stoffers, P., 2003, High-resolution methane profiles across anoxic brine–seawater boundaries in the Atlantis-II, Discovery, and Kebrit Deeps (Red Sea). *Chem. Geol*. 200, p. 359-375.

Schoell, M. and Hartmann, M., 1973, Detailed temperature structure of the hot brines in the Atlantis II Deep area (Red Sea). *Mar. Geol*. 14, p. 1-14.

Schoell, M. and Faber, E., 1978, New isotopic evidence for the origin of Red Sea brines. *Nature* 275, p. 436-438.

Scholten, J. C., Stoffers, P., Garbe-Schönberg, D. and Moammar, M., 2000, Hydrothermal mineralization in the Red Sea, *in* Cronan, D. S., ed., *Handbook of Marine Mineral Deposits*. CRC-Press, Boca Raton, p. 369-395.

Schwertmann, U., Friedl, J., Stanjek, H., Murad, E. and Bender Koch, C., 1998, Iron oxides and smectites in sediments from the Atlantis II Deep, Red Sea. *Eur. J. Mineral.* 10, p. 953-967.

Shanks, W. C. and Bischoff, J. L., 1977, Ore transport and deposition in the Red Sea geothermal system: a geochemical model. *Geochim. Cosmochim. Acta* 41, p. 1507-1519.

Shanks, W. C. and Bischoff, J. L., 1980, Geochemistry, sulfur isotope composition and accumulation rates of Red Sea geothermal deposits. *Econ. Geol*. 75, p. 445-459.

Slack, J. F., Grenne, T., Bekker, A., Rouxel, O. J. and Lindberg, P. A., 2007, Suboxic deep seawater in the late Paleoproterozoic: Evidence from hematitic chert and iron formation related to seafloor-hydrothermal sulfide deposits, central Arizona, USA. *Earth Planet. Sci. Lett.* 255, p. 243-256.

Swarzenski, P. W., McKee, B. A., Skei, J. M. and Todd, J. F., 1999, Uranium biogeochemistry across the redox transition zone of a permanently stratified fjord: Framvaren, Norway. *Mar. Chem.* 67, p. 181-198.

Swift, S. A., Bower, A. S. and Schmitt, R. W., 2012, Vertical, horizontal, and temporal changes in temperature in the Atlantis II and Discovery hot brine pools, Red Sea. *Deep-Sea Res. I* 64, p. 118-128.

Taitel-Goldman, N. and Singer, A., 2001, High-resolution transmission electron microscopy study of newly formed sediments in the Atlantis II Deep, Red Sea. *Clay Clay Miner*. 49 (2), p. 174-182.

Taitel-Goldman, N. and Singer, A., 2002, Metastable Si-Fe phases in hydrothermal sediments of Atlantis II Deep, Red Sea. *Clay Miner.* 37, p. 235-248.

Taitel-Goldman, N., Koch, C. B. and Singer, A., 2002, Lepidocrocite in hydrothermal sediments of the Atlantis II and Thetis Deeps, Red Sea. *Clay Clay Miner.* 50 (2), p. 186-197.

Taitel-Goldman, N., Koch, C. B. and Singer, A., 2004, Si-associated goethite in hydrothermal sediments of the Atlantis II and Thetis Deeps, Red Sea. *Clay Clay Miner.* 52 (1), p. 115-129.

Taylor, S. R. and McLennan, S. M., 1985, *The Continental Crust: Its Composition and Evolution*. Blackwell, Oxford, 312 p.

Tlig, S., 1988, Fish debris as chemical scavengers of zirconium and lanthanum in oceanic environments - Zr and Hf fractionation in marine phosphates. *Chem. Geol.* 69, p. 59-71.

Whitmarsh, R. B., Weser, O. E., Ross, D. A., et al., 1974 *Initial Reports of the Deep Sea Drilling Project,* v. 23, Washington (U.S. Government Printing Office), p. 595-600.

Wilde, P., Quinby-Hunt, M. S. and Erdtmann, B. D., 1996, The whole-rock cerium anomaly: a potential indicator of eustatic sea-level changes in shales of the anoxic facies. *Sediment. Geol*. 101, p. 43-53.

Winckler, G., Kipfer, R., Aeschbach-hertig, W., Botz, R, Schmidt, M., Schuler, S and Bayer, R., 2000, Sub sea floor boiling of Red Sea brines: New indication from noble gas data. *Geochim. Cosmoch. Acta* 64 (9), p. 1567-1575.

Yücel, M., Gartman, A., Chan, C. S. and Luther, G. W., 2011, Hydrothermal vents as a kinetically stable source of iron-sulfide-bearing nanoparticles to the ocean. *Nat. geosci.* 4, p. 367-371.

Zierenberg, R. A. and Shanks, W. C., 1983, Mineralogy and geochemistry of epigenetic features in metalliferous sediments, Atlantis II Deep, Red Sea. *Econ. Geol.* 78, p. 57-72.

Zierenberg, R. A. and Shanks, W. C., 1986, Isotopic constraints on the origin of the Atlantis II, Suakin and Valdivia brines, Red Sea, *Geochim. Cosmochim. Acta* 50, p. 2205-2214.

## Figure Captions

Figure 4.1. Location of the Atlantis II Deep and some other well-studied deeps in the Red Sea rift axis. The deeps with hot (>30°C) brine are marked in red, and the deeps without brine are marked in green. On the left, the locations of cores sampled for this study are indicated. Triangles mark the pore-water sampling locations of Anschutz et al. (2000), and squares mark the locations of cores studied by Oudin and Cocherie (1988), Oudin et al. (1984) and Ramboz et al. (1988), which are referred to in the text.

Figure 4.2. An example of a core log (Va29-387) with stratigraphic units and sample locations marked, including the sample depth and sample type: D=detrital (Al-rich) F=Fe-rich; S=Sulfur- and base metal-rich; M=mixed sample; A=anhydrite. Logging was done according to layer thickness, color and structure of the mud. The characteristics of the major sediment types are indicated.

Figure 4.3. Major and selected trace element concentrations in the set of 100 samples analyzed for this study. 25th, 50th and 75th percentiles and minimum and maximum values (whiskers) are shown.

Figure 4.4. Triangular diagram in which different components of the Atlantis II muds are discriminated on the basis of $Fe_2O_3$ content (total Fe in %) and $Al_2O_3$ content (x10) and a metal index calculated from metal concentrations (in ppm) [(Cu+Zn+Pb*10+Cd*100)/1000]. A high metal index is an indication of proximal hydrothermal precipitation; a high $Fe_2O_3$

concentration (combined with low metals) is an indication of distal hydrothermal precipitation (analogous to “plume fall-out”), and a high $Al_2O_3$ concentration is an indication of the proportion of biogenic and siliciclastic detrital material in the sediment. (A) Sediment compositions plotted according to stratigraphic unit. (B) Sediment compositions plotted according to sample type described in the text. The different stratigraphic units include numerous layers of distinctly different chemical compositions and therefore are not well discriminated according to bulk composition.

Figure 4.5. Th-V-Sc triangular diagram used to discriminate detrital components from Fe-(oxy)hydroxides in metalliferous sediments (modified from Grenne and Slack, 2005). Our samples span the field of oceanic hydrothermal precipitates (Fe-(oxy)hydroxides) to marine detrital sediments, reflecting different mixtures of these two components. Data from the Atlantis II muds are labeled according to stratigraphic unit (A) and layer type (B). The data fall on a mixing line (in terms of the Th/Sc ratio) characteristic of the main source of detrital sediment in the Red Sea.

Figure 4.6. Values of Pearson's correlation coefficient (r) are for ΣREE versus individual elements for all analyzed samples (middle line); r values >0.4 or <-0.4 have p values <0.0001 (n=100 samples). The range represents the largest and smallest r value observed in any stratigraphic unit. Elements are grouped according to their source(s) and listed in order of decreasing correlation with REE. The full suite of trace element data used in this analysis are provided in Appendix C.

Figure 4.7. REE patterns (A) and residual REE patterns (B) for the different stratigraphic units (DOP=Detrital-Oxidic-Pyritic unit; SU=Sulfidic unit; CO=Central Oxidic unit; AM=Amorphous unit; sub-units are included). Residual REE patterns were calculated by subtracting the detrital component based on Sc (see Table 4.3 and text for details). All stratigraphic units have similar REE patterns with positive but varying Eu anomalies and no Ce anomalies. The total REE content, LREE fractionation (La/Sm), and LREE/HREE (La/Yb) increase with depth from the AM unit (top) to DOP (bottom). The residual profiles show that the non-detrital component has a larger Eu anomaly and higher La/Yb ratio than the detrital component.

Figure 4.8. ΣREE versus $Al_2O_3$ and $P_2O_5$ in different stratigraphic units (A and B) and in different layer types (C and D). Aluminum (along with other HFSE) is strongly correlated with total REE in all sediments of the Atlantis II Deep (see also Fig. 4.6). The plot of phosphorus, which was is not used to define the different depositional components, shows that detrital P-bearing phases are an important control on REE abundance, in addition to aluminosilicates. The $r^2$ value for ΣREE and $P_2O_5$ in the detrital-oxidic pyritic unit (B) is 0.25; in Al-rich (detrital) component (D) the $r^2$ is 0.63. The $r^2$ values for ΣREE and $P_2O_5$ in sulfidic units (SU1 and SU2) are 0.20 and 0.14, respectively; the $r^2$ value for the S-rich component is 0.53. Three samples with $P_2O_5$ concentration more than 0.7% (all <0.8%) were omitted from the dataset.

Figure 4.9. REE patterns (A) and the residual REE patterns (B) for the different layer types. A) The REE profiles for Al-rich layers closely resemble siliceous detrital and biogenic detrital background sediments near Thetis Deep (from Pierret et al., 2010; also plotted in 4.9C) and can be clearly distinguished from the two hydrothermal layer types; Eu/Eu* is somewhat larger in S-rich layers than in Fe-rich layers. B) Residual REE profiles were computed as in Figure 4.7. Fe-rich layers have the largest proportion of residual REE (about 50% vs. 20% in S-rich layers), lower La/Yb and a smaller Eu anomaly. The two different REE patterns suggest two different non-detrital sources of REE. See Table 4.5 for summary statistics. Note that the negative Ce anomaly for the Al-rich layers is an artifact of REE concentration close to their detection limits. C) REE patterns from the Atlantis II sediments mostly resemble Red Sea background sediments combined with a Eu anomaly inherited from REE in hydrothermal fluids. We have also plotted some reference REE patterns for comparison with the range found in the Atlantis II sediments (grey area). The hydrothermal sediments in the Atlantis II have lower ΣREE than open ocean (TAG) hydrothermal sediments sampled at the indicated depths below the seafloor (German et al., 1993). Seawater, black smoker (~360°C) and white smoker (~285°C) fluid concentrations are from TAG and multiplied by 1000 (Mitra et al., 1994).

Figure 4.10. Early depositional history of metalliferous sediments in the Atlantis II Deep of the Red Sea as suggested by REE geochemistry. (A) At the end of DOP (Detrital-Oxidic-Pyritic unit) hydrothermal venting begins adding Fe- and Mn-(oxy)hydroxides to cold brine that has a high concentration of extractable REE (with only a small Eu anomaly). Fe- (and perhaps

also Mn) particles settle through the brine and quickly strip the brine pool of REE. (B) During formation of the first sulfidic unit (SU1), venting occurs into an anoxic brine pool that is depleted in REE. REE are brought to the lower brine by 1) hydrothermal fluids and 2) precipitation-dissolution of surface active Mn (and Fe) particles that transport REE from seawater to the anoxic brine, and 3) non-hydrothermal brines from outside the deep. Sulfides precipitate in the proximal facies and Fe-(oxy)hydroxides in the distal facies, inheriting slightly different REE patterns. Secondary REE enrichment happens as hydrothermal fluids vent through the sediments; the first surface active particles encountered by the hydrothermal fluids (P-bearing or Fe-(oxy)hydroxides) adsorb the REE from the pore waters. This diagenetic REE enrichment only happens in the lowermost hydrothermal units. (C) Formation of the Central-Oxidic (CO) unit occurs during decreased hydrothermal activity; the anoxic brine layer is thinner and Mn-oxides can accumulate at the bottom of the deep (during active phases, B and D, Mn-oxides precipitate only at the flanks of the deep, which are covered by the transitional brine). Uranium concentrations show that some elements are transported from seawater to the brine pool, but there is no evidence in the REE data (such as high Y/Ho) of large-scale mixing of brine with seawater suggested by some earlier studies. (D) The outbreak of hydrothermal activity in the SW Basin marks the beginning of formation of the second sulfidic unit (SU2) during which the configuration of the brine pools is similar to (B). The currently forming Amorphous-Siliceous unit (AM) is continuous with SU2 formation. According to the high U concentrations and mineralogical similarity to CO, this unit appears to mark a time of more oxidic and/or less sulfidic conditions (e.g., Atlantis II may be transitioning to the configuration shown in C).

Table 4.1 Physical, chemical and mineralogical properties of the stratigraphic units of the Atlantis II metalliferous sediments (modified from Bäcker and Richter, 1973).

| Unit and thickness | Age (Ka) | Sedimentat-ion rate | Composition; mineralogy | Geochemical Enrichments |
|---|---|---|---|---|
| AM (*SAM)* Amorphous-Siliceous 3.5 (1-4) m | last 3.6 | 97 cm/ka ~4700 t/a tot. 17 Mt | Amorphous FeOOH and Si bearing compounds, Gt., Fe-Sme., Mn-Sd.; SW basin: sulfides, Fe-oxides, Anh.; elevated areas: MnOOH | Zn, Cd, Ag, Co, Sb, |
| Lepidocrocite horizon | | | | |
| SU2 (*SOAN/OAN*) Sulfidic 4 *(*2-12) m | 5.9-3.6 | 174 cm/ka ~8800 t/a tot. 20 Mt | Sp. common almost everywhere, rare Py., FeOOH minerals, green silicates, Anh., rare Brt., Fe & Mn carbonates. | Zn, Pb,As,Cd, Hg, Tl,Ba, Mo, V, Cr |
| Layer of anhydrite | | | | |
| CO *(COS*) Central Oxidic 6 (1-11) m | ~8.6-5.9 | 222 cm/ka ~12000 t/a tot. 32 Mt | Gt., Fe-(oxy)hydroxides, rare sulfides, carbonates, MnOOH minerals, Lm., Hem., some Anh. and euhedral Mag. | Mn, Fe, K, Ba, Mo, Rb, Cs; low S |
| Red silicate layers with Fe-oxides | | | | |
| SU1 Sulfidic* 3.8 (1-4) m | ~11.7-8.6 | 123 cm/ka ~5800 t/a tot. 18 Mt | Fe-clays, red-brown silicates with abundant sulfides: Py., Ccp., Sp. Mn-Sd., Hem., Anh., some Brt. | Si, Cu, Ag, As S, P, Ni, Tl, W |
| Pyrite much more abundant at the top of DOP than at the bottom | | | | |
| DOP Detrital-Oxidic-Pyritic* 2.5 (1-6) m | ~25-~11.7 | 19 cm/ka | Mixture of detrital-biogenic material with crystallization products of Fe- and Mn-(oxy)hydroxides, some sulfides, Anh., rare basalt fragments. | Ca, Al, Ti, Sr, Cr, Sc, Li, HFSE (REEs) |

The names of units in *italics* refer to sub-units that are mainly found in the Southwest Basin: SAM= Sulfidic-Amorphous-Siliceous unit; SOAN=Sulfidic-Oxidic-Anhydritic unit; OAN=Oxidic-Anhydritic unit; COS=Central-Oxidic-Silicatic unit

*=absent in SW basin

The ages of the units are derived from multiple sources (Hackett and Bischoff, 1973; Shanks and Bischoff, 1980). Thicknesses are averages from Bäcker and Richter (1973). Variation in thickness and annual tonnage are from Gurvich (2006). Sedimentation rates and total tonnage are calculated from average thickness/age. The sedimentation rates vary depending on location, depth and distance from the hydrothermal vent source.

Mineral abbreviations as follows: Anh.=anhydrite, Brt.=barite, Ccp.=chalcopyrite, Gt.=goethite, Hem.=hematite, Lm.=limonite, Mag.=magnetite, Py.=pyrite, Sd.=siderite, Sme.=smectite and Sp.=sphalerite.

Table 4.2. Major and trace element chemistry of 9 sedimentary cores from the Atlantis II Deep, Red Sea (salt-free basis).

| | | | $Fe_2O_3$[1] | $SiO_2$ | $Al_2O_3$ | $TiO_2$ | CaO | $P_2O_5$ | S | Zn | Cu | Pb | Cd | Mn | U | Th | Hf | Zr | Y | Sc | V | ΣREE[2] |
|---|---|---|---|---|---|---|---|---|---|---|---|---|---|---|---|---|---|---|---|---|---|---|
| Method | | | 2 | 2 | 4 | 4 | 2 | 4 | 2 | 1 | 1 | 1 | 3 | 1 | 1 | 3 | 3 | 3 | 3 | 3 | 3 | 3 |
| Detection limit | | | 0.05 | 0.01 | 0.01 | 0.0001 | 0.01 | 0.001 | 0.01 | 0.003 | 2 | 0.8 | 0.5 | 0.0003 | 0.1 | 0.01 | 0.5 | 1 | 1 | 0.05 | 10 | ** |
| Sample | Unit | | % | % | % | % | % | % | % | % | ppm | ppm | ppm | % | ppm | ppm | ppm | ppm | ppm | ppm | ppm | ppm |
| 334-83 | SAM | | 21.0 | 11.9 | 0.81 | 0.034 | 12.8 | 0.11 | 7.2 | 2.33 | 3423 | 432 | 78 | 0.25 | 4.8 | 0.22 | <0.5 | <1 | <1 | 0.73 | 64 | 4.9 |
| 334-312 | SAM | S | 34.5 | 14.2 | 1.14 | 0.043 | 9.2 | 0.25 | 8.4 | 4.61 | 7066 | 1050 | 155 | 0.17 | 7.3 | 0.32 | <0.5 | <1 | <1 | 0.78 | 77 | 6.8 |
| 334-513 | SAM | S | 27.6 | 11.4 | 1.21 | 0.046 | 9.4 | 0.27 | 12.9 | 7.25 | 8784 | 3398 | 1121 | 0.37 | 9.7 | 0.45 | <0.5 | <1 | <1 | 0.99 | 89 | 8.7 |
| 334-612 | SOAN | | 34.7 | 18.0 | 0.94 | 0.036 | 7.4 | 0.31 | 4.5 | 3.08 | 9525 | 794 | 94 | 0.10 | 7.8 | 0.22 | <0.5 | <1 | <1 | 0.72 | 93 | 6.2 |
| 334-757 | SOAN | S | 30.1 | 17.8 | 1.21 | 0.035 | 5.5 | 0.12 | 8.0 | 5.17 | 1232 | 504 | 251 | 0.10 | 5.5 | 0.30 | <0.5 | <1 | <1 | 0.76 | 78 | 6.2 |
| 373-8 | AM | | 27.1 | 18.1 | 1.13 | 0.066 | 8.1 | 0.29 | 1.5 | 1.75 | 3326 | 665 | 2 | 0.29 | 3.9 | 0.40 | <0.5 | <1 | <1 | 1.17 | 71 | 9.9 |
| 373-93 | SU2 | | 28.7 | 19.9 | 1.32 | 0.074 | 9.5 | 0.23 | 0.8 | 1.33 | 2763 | 248 | 2 | 0.26 | 4.8 | 0.47 | <0.5 | <1 | <1 | 1.43 | 70 | 11.4 |
| 373-210 | SU2 | | 24.8 | 28.8 | 0.50 | 0.013 | 5.8 | 0.07 | 1.4 | 0.25 | 1639 | 154 | <0.5 | 0.97 | 2.1 | 0.18 | <0.5 | <1 | <1 | 0.41 | 35 | 5.7 |
| 373-265 | CO | | 3.9 | 4.8 | 1.16 | 0.081 | 4.5 | 0.04 | 0.2 | 0.18 | 282 | 375 | <0.5 | 32.46 | 2.1 | 0.74 | <0.5 | <1 | 2.8 | 1.66 | 161 | 16.6 |
| 373-515 | COS | | 36.1 | 17.2 | 0.58 | 0.023 | 4.4 | 0.13 | 0.5 | 1.41 | 1305 | 193 | <0.5 | 2.40 | 6.3 | 0.31 | <0.5 | <1 | <1 | 0.71 | 59 | 9.5 |
| 373-555 | SU1 | S | 15.7 | 29.6 | 3.11 | 0.175 | 5.7 | 0.49 | 12.6 | 8.87 | 21498 | 2221 | 548 | 0.71 | 3.6 | 1.27 | <0.5 | 20 | 4.9 | 3.39 | 107 | 29.1 |
| 373-586 | SU1 | | 1.8 | 2.2 | 0.15 | 0.007 | 31.6 | 0.05 | 19.6 | 0.40 | 1350 | 143 | 16 | 0.03 | 0.1 | 0.06 | <0.5 | <1 | <1 | 0.17 | <10 | 1.4 |
| 373-672 | SU1 | F | 38.2 | 21.7 | 0.47 | 0.014 | 4.0 | 0.34 | 2.6 | 0.88 | 1336 | 218 | <0.5 | 1.03 | 1.6 | 0.22 | <0.5 | <1 | <1 | 0.48 | 298 | 4.4 |
| 373-751 | SU1 | S | 21.7 | 16.7 | 2.79 | 0.126 | 4.8 | 0.44 | 10.5 | 6.75 | 16767 | 1995 | 159 | 2.43 | 5.9 | 1.01 | <0.5 | 16 | 4.7 | 2.51 | 145 | 28.1 |
| 373-780 | DOP | A | 7.9 | 16.4 | 3.57 | 0.249 | 25.5 | 0.26 | 0.7 | 0.94 | 85 | 39 | 1 | 4.64 | 0.8 | 1.81 | 0.9 | 35 | 8.4 | 4.48 | 103 | 46.6 |
| 373-798 | DOP | F | 59.7 | 7.1 | 1.32 | 0.117 | 3.4 | 0.29 | 0.2 | 1.47 | 300 | 32 | 17 | 0.74 | 4.2 | 0.50 | <0.5 | 10 | 7.9 | 1.77 | 102 | 50.2 |
| 387-80 | SU2 | | 23.4 | 13.9 | 0.90 | 0.032 | 7.9 | 0.21 | 4.8 | 2.03 | 4662 | 414 | 34 | 0.19 | 4.1 | 0.26 | <0.5 | <1 | <1 | 0.74 | 51 | 5.3 |
| 387-174 | SU2 | | 30.8 | 37.6 | 0.42 | 0.024 | 6.4 | 0.06 | 1.8 | 1.40 | 657 | 56 | 61 | 0.36 | 1.2 | 0.17 | <0.5 | <1 | <1 | 0.48 | <10 | 2.7 |
| 387-261 | CO | A | 19.3 | 30.5 | 6.51 | 0.467 | 7.4 | 0.30 | 1.5 | 0.20 | 1302 | 67 | 1 | 1.76 | 4.8 | 2.76 | 1.4 | 56 | 12.4 | 7.99 | 143 | 64.4 |
| 387-302 | CO | F | 65.2 | 10.0 | 0.92 | 0.053 | 2.6 | 0.18 | 0.1 | 0.45 | 470 | 115 | 11 | 0.91 | 3.9 | 0.37 | <0.5 | <1 | 2.0 | 0.99 | 83 | 10.3 |
| 387-398 | SU1 | S | 13.1 | 30.5 | 3.38 | 0.173 | 5.8 | 0.49 | 14.6 | 7.95 | 25435 | 2277 | 491 | 0.37 | 3.0 | 1.23 | <0.5 | 18 | 4.7 | 3.42 | 134 | 26.4 |
| 387-466 | SU1 | S | 32.4 | 15.4 | 2.21 | 0.095 | 4.7 | 0.51 | 9.5 | 4.10 | 15873 | 909 | 167 | 1.62 | 5.2 | 0.67 | <0.5 | 7 | 3.3 | 2.16 | 106 | 28.5 |
| 387-490 | SU1 | F | 61.1 | 5.7 | 1.61 | 0.070 | 1.3 | 0.73 | 2.5 | 0.61 | 10837 | 442 | 23 | 0.76 | 6.9 | 0.54 | <0.5 | 5 | 4.8 | 1.73 | 92 | 33.3 |
| 387-502 | SU1 | | 1.5 | 0.7 | 0.03 | 0.002 | 32.5 | 0.03 | 19.9 | 0.21 | 395 | 7 | <0.5 | 0.06 | <0.1 | 0.06 | <0.5 | <1 | <1 | 0.10 | <10 | 0.5 |
| 387-575 | SU1 | S | 10.6 | 26.4 | 1.39 | 0.076 | 10.9 | 0.29 | 15.0 | 0.89 | 5057 | 938 | 98 | 0.38 | 4.4 | 0.53 | <0.5 | 8 | 1.8 | 1.45 | 261 | 16.9 |
| 421-80 | SU2 | | 34.1 | 14.5 | 0.93 | 0.028 | 5.5 | 0.40 | 3.5 | 2.36 | 12722 | 428 | 28 | 0.95 | 5.6 | 0.18 | <0.5 | <1 | <1 | 0.60 | 67 | 5.2 |
| 421-160 | SU2 | | 35.9 | 15.4 | 0.45 | 0.024 | 4.5 | 0.28 | 0.3 | 2.48 | 2951 | 318 | <0.5 | 2.22 | 2.3 | 0.14 | <0.5 | <1 | <1 | 0.51 | 36 | 4.5 |
| 421-223 | CO | F | 44.0 | 4.7 | 0.45 | 0.025 | 4.4 | 0.05 | 0.3 | 1.21 | 645 | 40 | 12 | 0.68 | 10.3 | 0.24 | <0.5 | <1 | <1 | 0.56 | 31 | 5.1 |
| 421-362 | COS | | 27.1 | 18.2 | 0.92 | 0.028 | 8.1 | 0.26 | 3.8 | 2.36 | 5784 | 605 | 41 | 0.61 | 3.8 | 0.18 | <0.5 | <1 | <1 | 0.68 | 69 | 6.2 |
| 421-496 | SU1 | F | 34.5 | 15.3 | 2.43 | 0.169 | 4.6 | 0.20 | 0.2 | 0.27 | 772 | 13 | <0.5 | 4.27 | 4.6 | 1.14 | <0.5 | 20 | 4.7 | 3.12 | 95 | 24.3 |
| 421-520 | SU1 | F | 33.3 | 16.4 | 1.10 | 0.071 | 7.4 | 0.18 | 0.2 | 0.37 | 1475 | 23 | <0.5 | 1.25 | 3.1 | 0.46 | <0.5 | 2 | 2.3 | 1.36 | 74 | 12.1 |
| 421-678 | DOP | S | 24.1 | 24.6 | 3.59 | 0.187 | 3.3 | 0.77 | 14.8 | 5.39 | 26218 | 1655 | 189 | 1.15 | 4.8 | 1.27 | <0.5 | 21 | 6.6 | 3.58 | 146 | 46.6 |
| 421-740 | DOP | | 24.5 | 30.4 | 0.64 | 0.031 | 2.0 | 0.76 | 2.8 | 3.73 | 1109 | 478 | 21 | 1.03 | 1.5 | 0.28 | <0.5 | <1 | <1 | 1.01 | 767 | 11.3 |
| 421-825 | DOP | A | 7.9 | 28.9 | 7.57 | 0.656 | 21.0 | 0.39 | 3.8 | 0.52 | 600 | 27 | 6 | 0.32 | 10.6 | 3.42 | 2.2 | 87 | 15.5 | 9.43 | 249 | 86.3 |
| 421-870 | DOP | F | 57.9 | 12.9 | 1.98 | 0.168 | 2.4 | 0.34 | 0.2 | 0.38 | 103 | 4 | 3 | 0.21 | 3.5 | 0.91 | <0.5 | 14 | 10.6 | 2.60 | 248 | 87.6 |
| 495-113 | AM | F | 42.2 | 14.3 | 0.73 | 0.029 | 6.5 | 0.26 | 2.1 | 1.37 | 1356 | 199 | <0.5 | 0.14 | 7.3 | 0.16 | <0.5 | <1 | <1 | 0.54 | 81 | 4.1 |

| Sample | Unit | | $Fe_2O_3$[1] | $SiO_2$ | $Al_2O_3$ | $TiO_2$ | CaO | $P_2O_5$ | S | Zn | Cu | Pb | Cd | Mn | U | Th | Hf | Zr | Y | Sc | V | ΣREE[2] |
|---|---|---|---|---|---|---|---|---|---|---|---|---|---|---|---|---|---|---|---|---|---|---|
| 495-240 | AM | | 43.0 | 12.8 | 1.01 | 0.053 | 6.2 | 0.51 | 2.6 | 1.50 | 14970 | 1284 | 241 | 0.29 | 8.8 | 0.32 | <0.5 | <1 | <1 | 1.01 | 83 | 11.5 |
| 495-362 | SU2 | | 35.7 | 15.7 | 0.83 | 0.040 | 7.4 | 0.24 | 2.4 | 1.33 | 5414 | 338 | 3 | 0.16 | 6.6 | 0.26 | <0.5 | <1 | <1 | 0.69 | 79 | 6.0 |
| 495-484 | SU2 | | 31.3 | 18.0 | 1.24 | 0.045 | 7.3 | 0.31 | 5.7 | 3.20 | 8663 | 748 | 31 | 0.22 | 5.9 | 0.31 | <0.5 | <1 | <1 | 0.79 | 86 | 6.9 |
| 495-548 | SU2 | F | 43.8 | 14.1 | 1.56 | 0.092 | 4.3 | 0.29 | 0.4 | 1.02 | 1841 | 211 | 1 | 2.92 | 9.7 | 0.51 | <0.5 | 5 | 3.1 | 1.63 | 114 | 17.1 |
| 495-557 | CO | F | 41.9 | 11.0 | 2.49 | 0.173 | 11.3 | 0.33 | 0.6 | 0.56 | 215 | 34 | 1 | 2.89 | 8.0 | 1.05 | <0.5 | 20 | 6.1 | 3.14 | 274 | 33.3 |
| 495-569 | CO | | 20.2 | 7.2 | 1.55 | 0.110 | 3.4 | 0.20 | 0.4 | 0.59 | 222 | 119 | <0.5 | 26.70 | 23.2 | 0.62 | <0.5 | 7 | 3.1 | 2.13 | 92 | 15.6 |
| 495-582 | CO | A | 3.0 | 14.5 | 3.81 | 0.287 | 33.1 | 0.15 | 0.4 | 0.11 | 53 | <0.8 | 1 | 3.23 | 4.6 | 1.98 | 1.0 | 34 | 8.1 | 5.06 | 82 | 40.7 |
| 495-599 | CO | | 19.8 | 19.1 | 2.98 | 0.210 | 16.8 | 0.37 | 0.4 | 0.36 | 296 | <0.8 | <0.5 | 3.76 | 7.7 | 1.19 | <0.5 | 23 | 6.0 | 3.75 | 103 | 29.8 |
| 495-693 | COS | F | 37.8 | 22.2 | 1.19 | 0.077 | 4.5 | 0.22 | 1.1 | 0.06 | 1703 | 58 | <0.5 | 0.25 | 8.5 | 0.53 | <0.5 | 4 | 2.3 | 1.63 | 116 | 12.7 |
| 495-757 | SU1 | A | 9.0 | 25.2 | 6.29 | 0.407 | 19.9 | 0.29 | 3.8 | 1.77 | 4755 | 406 | 66 | 0.77 | 4.1 | 2.27 | 1.3 | 46 | 11.3 | 7.43 | 109 | 60.7 |
| 495-777 | SU1 | S | 27.4 | 23.6 | 2.83 | 0.161 | 3.3 | 0.42 | 13.6 | 2.34 | 15019 | 2100 | 128 | 1.54 | 4.1 | 0.95 | <0.5 | 17 | 4.7 | 2.83 | 128 | 28.4 |
| 495-809 | SU1 | | 26.4 | 36.8 | 0.83 | 0.045 | 5.9 | 0.36 | 2.4 | 1.06 | 459 | 57 | <0.5 | 0.35 | 1.7 | 0.47 | <0.5 | <1 | <1 | 1.07 | 448 | 16.2 |
| 495-867 | SU1 | A | 9.5 | 22.8 | 5.89 | 0.421 | 25.4 | 0.35 | 1.7 | 0.76 | 2550 | 185 | 14 | 0.60 | 3.7 | 2.25 | 1.4 | 53 | 11.4 | 6.93 | 107 | 61.0 |
| 495-889 | DOP | | 31.2 | 16.2 | 3.61 | 0.246 | 10.5 | 0.29 | 2.4 | 1.24 | 3073 | 271 | 8 | 9.30 | 12.0 | 1.11 | <0.5 | 22 | 5.7 | 3.61 | 140 | 30.0 |
| 495-934 | DOP | A | 5.7 | 23.3 | 6.33 | 0.447 | 27.9 | 0.30 | 0.9 | 0.16 | 656 | 31 | 1 | 0.32 | 3.1 | 2.51 | 1.5 | 56 | 12.2 | 8.01 | 103 | 62.8 |
| 495-1088 | DOP | A | 5.8 | 26.9 | 7.24 | 0.431 | 22.8 | 0.20 | 1.5 | 0.27 | 383 | 36 | 1 | 0.22 | 4.9 | 2.45 | 1.5 | 54 | 12.9 | 8.90 | 105 | 64.4 |
| 495-1195 | DOP | A | 8.0 | 29.0 | 7.76 | 0.482 | 20.0 | 0.23 | 1.6 | 0.07 | 368 | 28 | <0.5 | 0.38 | 5.3 | 2.65 | 1.5 | 56 | 13.8 | 9.02 | 135 | 71.0 |
| 503-7 | SAM | | 36.9 | 13.1 | 0.80 | 0.029 | 8.2 | 0.20 | 4.4 | 2.02 | 4944 | 574 | 19 | 0.16 | 8.4 | 0.23 | <0.5 | <1 | <1 | 0.74 | 66 | 5.4 |
| 503-75 | OAN | S | 9.2 | 37.2 | 1.32 | 0.070 | 4.5 | 0.26 | 13.4 | 1.18 | 2328 | 737 | 148 | 0.70 | 7.9 | 0.53 | <0.5 | 8 | 1.7 | 1.23 | 287 | 22.2 |
| 503-140 | SOAN | | 20.1 | 17.4 | 0.55 | 0.009 | 8.7 | 0.03 | 7.5 | 1.88 | 2947 | 656 | 2 | 0.14 | 2.2 | 0.22 | <0.5 | <1 | <1 | 0.45 | 46 | 2.2 |
| 503-155 | SOAN | | 21.6 | 20.6 | 1.15 | 0.040 | 5.5 | 0.16 | 6.1 | 1.99 | 3390 | 748 | 2 | 0.13 | 3.9 | 0.66 | <0.5 | <1 | <1 | 0.90 | 58 | 7.2 |
| 503-235 | SOAN | | 0.2 | 0.5 | 0.03 | 0.000 | 38.1 | 0.03 | 23.8 | 0.33 | 212 | 44 | <0.5 | 0.07 | 0.4 | 0.01 | <0.5 | <1 | <1 | 0.12 | <10 | 0.3 |
| 503-266 | SOAN | | 4.8 | 1.2 | 0.10 | 0.003 | 29.3 | <.005 | 17.9 | 0.20 | 503 | 95 | 11 | 0.36 | 1.3 | 0.05 | <0.5 | <1 | <1 | 0.16 | <10 | 1.9 |
| 503-407 | COS | F | 73.3 | 3.5 | 0.45 | 0.011 | 1.8 | 0.21 | 0.2 | 0.16 | 1205 | 21 | <0.5 | 0.41 | 32.5 | 0.08 | <0.5 | <1 | <1 | 0.33 | 73 | 2.9 |
| 503-509 | COS | F | 35.4 | 11.7 | 0.36 | 0.008 | 10.9 | 0.12 | 4.4 | 0.40 | 1913 | 104 | <0.5 | 1.59 | 4.6 | 0.14 | <0.5 | <1 | <1 | 0.30 | 25 | 6.8 |
| 503-516 | COS | A | 7.4 | 47.4 | 9.52 | 0.683 | 3.2 | 0.58 | 3.7 | 1.62 | 18071 | 421 | 148 | 0.52 | 12.5 | 3.91 | 2.2 | 84 | 16.8 | 11.5 | 193 | 94.0 |
| 503-626 | COS | F | 58.6 | 6.0 | 0.36 | 0.008 | 3.0 | 0.09 | 0.4 | 0.15 | 1099 | 26 | 2 | 0.49 | 18.9 | 0.13 | <0.5 | <1 | <1 | 0.34 | 51 | 3.2 |
| 503-671 | COS | | 22.2 | 30.5 | 0.44 | 0.019 | 6.0 | 0.09 | 1.3 | 0.18 | 956 | 12 | <0.5 | 0.40 | 1.0 | 0.17 | <0.5 | <1 | <1 | 0.63 | 35 | 2.0 |
| 503-680 | COS | F | 42.1 | 20.0 | 0.71 | 0.036 | 4.3 | 0.21 | 0.6 | 0.37 | 7237 | 495 | 3 | 1.56 | 5.9 | 0.32 | <0.5 | <1 | <1 | 0.81 | 51 | 8.0 |
| 503-807 | SU1 | S | 15.4 | 30.0 | 1.82 | 0.089 | 5.0 | 0.28 | 11.8 | 0.70 | 7084 | 1514 | 53 | 0.97 | 4.0 | 0.63 | <0.5 | 10 | 2.7 | 1.91 | 254 | 35.4 |
| 503-889 | SU1 | F | 53.3 | 3.4 | 0.93 | 0.042 | 3.8 | 0.58 | 2.5 | 0.42 | 13323 | 430 | 17 | 2.53 | 10.0 | 0.42 | <0.5 | 3 | 3.4 | 0.91 | 54 | 16.9 |
| 503-912 | SU1 | S | 9.1 | 18.6 | 2.91 | 0.129 | 5.0 | 0.53 | 18.9 | 14.6 | 25201 | 2086 | 323 | 1.06 | 5.3 | 0.89 | <0.5 | 10 | 3.0 | 2.22 | 135 | 21.3 |
| 503-946 | DOP | | 31.5 | 10.3 | 1.65 | 0.053 | 8.1 | 0.31 | 7.9 | 2.42 | 3758 | 291 | 141 | 1.68 | 6.0 | 0.43 | <0.5 | 5 | 3.2 | 1.64 | 120 | 36.0 |
| 503-987 | DOP | A | 28.8 | 27.1 | 7.18 | 0.596 | 3.0 | 0.28 | 21.0 | 1.09 | 1160 | 328 | 10 | 0.38 | 13.2 | 3.05 | 1.7 | 64 | 14.0 | 8.67 | 183 | 82.2 |
| 546-5 | AM | | 45.1 | 14.4 | 1.62 | 0.040 | 1.6 | 0.56 | 2.5 | 3.39 | 16087 | 1153 | 152 | 1.74 | 12.4 | 0.19 | <0.5 | <1 | <1 | 0.72 | 186 | 6.1 |
| 546-92 | AM | | 37.6 | 17.7 | 1.10 | 0.029 | 2.7 | 0.40 | 1.7 | 3.31 | 9723 | 1415 | 137 | 2.60 | 7.8 | 0.23 | <0.5 | <1 | <1 | 0.52 | 91 | 5.1 |
| 546-180 | AM | | 34.6 | 17.9 | 0.78 | 0.032 | 2.7 | 0.24 | 0.8 | 1.14 | 2068 | 227 | 66 | 2.53 | 8.0 | 0.17 | <0.5 | <1 | <1 | 0.74 | 101 | 5.6 |
| 546-229 | SU2 | | 34.7 | 14.3 | 1.48 | 0.041 | 3.3 | 0.44 | 2.4 | 2.30 | 10403 | 1037 | 81 | 5.15 | 11.6 | 0.28 | <0.5 | <1 | 1.7 | 0.85 | 132 | 8.3 |
| 546-252 | CO | A | 7.6 | 27.2 | 6.83 | 0.506 | 23.7 | 0.25 | 0.7 | 0.65 | 77 | 4 | 16 | 1.08 | 1.4 | 2.91 | 1.6 | 62 | 14.0 | 8.95 | 95 | 73.6 |
| 546-267 | SU1 | F | 40.1 | 18.8 | 1.19 | 0.060 | 5.5 | 0.21 | 3.9 | 0.26 | 2452 | 254 | 28 | 0.65 | 7.9 | 0.36 | <0.5 | 2 | <1 | 1.31 | 117 | 9.4 |
| 546-311 | SU1 | F | 53.0 | 4.3 | 1.03 | 0.058 | 3.2 | 0.64 | 0.4 | 0.26 | 10394 | 819 | 4 | 4.57 | 4.9 | 0.38 | <0.5 | 4 | 6.4 | 1.13 | 57 | 47.2 |
| 546-318 | SU1 | A | 7.0 | 55.3 | 2.06 | 0.130 | 6.0 | 0.10 | 6.5 | 0.06 | 207 | 15 | 5 | 0.42 | 6.5 | 0.72 | <0.5 | 13 | 2.0 | 2.08 | 150 | 12.5 |

| Sample | Unit | | $Fe_2O_3$ [1] | $SiO_2$ | $Al_2O_3$ | $TiO_2$ | CaO | $P_2O_5$ | S | Zn | Cu | Pb | Cd | Mn | U | Th | Hf | Zr | Y | Sc | V | ΣREE [2] |
|---|---|---|---|---|---|---|---|---|---|---|---|---|---|---|---|---|---|---|---|---|---|---|
| 546-385 | DOP | A | 10.4 | 20.0 | 6.66 | 0.530 | 27.9 | 0.33 | 1.0 | 0.07 | 195 | 1 | 1 | 0.61 | 4.1 | 2.58 | 1.8 | 69 | 14.0 | 8.44 | 83 | 74.2 |
| 557-9 | SAM | S | 26.4 | 14.2 | 0.97 | 0.039 | 8.7 | 0.41 | 6.7 | 4.53 | 12929 | 2277 | 205 | 0.27 | 5.3 | 0.23 | <0.5 | <1 | <1 | 0.69 | 72 | 6.5 |
| 557-173 | SU2 | S | 26.6 | 22.7 | 1.70 | 0.058 | 5.5 | 0.40 | 8.2 | 8.01 | 11262 | 1596 | 289 | 0.18 | 3.6 | 0.40 | <0.5 | <1 | <1 | 1.02 | 98 | 8.4 |
| 557-227 | SU2 | S | 18.7 | 16.8 | 0.94 | 0.007 | 7.0 | 0.15 | 7.6 | 4.45 | 2226 | 530 | 58 | 0.75 | 2.7 | 0.18 | <0.5 | <1 | <1 | 0.47 | 154 | 3.1 |
| 557-255 | CO | | 24.1 | 27.0 | 6.06 | 0.433 | 3.6 | 0.29 | 1.4 | 1.61 | 2008 | 465 | 45 | 2.95 | 3.4 | 2.62 | 1.4 | 52 | 11.9 | 7.61 | 134 | 64.5 |
| 557-289 | CO | F | 58.1 | 4.0 | 0.63 | 0.010 | 2.3 | 0.16 | 1.1 | 1.23 | 5072 | 118 | 7 | 1.04 | 22.5 | 0.12 | <0.5 | <1 | <1 | 0.35 | 62 | 4.7 |
| 557-388 | SU1 | S | 22.0 | 20.7 | 3.33 | 0.186 | 4.9 | 0.51 | 13.6 | 6.29 | 20396 | 1775 | 262 | 2.10 | 7.0 | 1.09 | <0.5 | 18 | 4.6 | 2.84 | 102 | 28.1 |
| 557-502 | DOP | A | 3.5 | 19.3 | 5.30 | 0.408 | 33.3 | 0.21 | 0.5 | 0.18 | 211 | 16 | 2 | 0.42 | 1.5 | 2.36 | 1.3 | 50 | 10.7 | 6.81 | 87 | 53.5 |
| 557-608 | DOP | A | 5.4 | 12.6 | 3.91 | 0.259 | 36.6 | 0.24 | 0.3 | 0.03 | 61 | <0.8 | 1 | 0.40 | 1.0 | 1.59 | 0.9 | 34 | 8.4 | 5.13 | 73 | 39.5 |
| 557-753 | DOP | A | 3.6 | 15.2 | 4.26 | 0.276 | 35.0 | 0.19 | 0.3 | 0.04 | 317 | <0.8 | <0.5 | 0.43 | 3.7 | 1.88 | 1.0 | 41 | 9.4 | 5.59 | 346 | 44.1 |
| 557-795 | DOP | A | 5.6 | 11.4 | 3.17 | 0.262 | 37.3 | 0.19 | 0.3 | 0.03 | 45 | 7 | <0.5 | 0.37 | 0.9 | 1.27 | 0.8 | 33 | 7.0 | 4.33 | 81 | 34.0 |
| 617-9 | SAM | | 35.5 | 14.8 | 1.38 | 0.050 | 6.0 | 0.36 | 5.1 | 3.21 | 13176 | 847 | 131 | 0.31 | 9.5 | 0.26 | <0.5 | <1 | <1 | 0.96 | 87 | 6.6 |
| 617-148 | SAM | S | 30.2 | 15.3 | 1.25 | 0.044 | 7.1 | 0.39 | 10.6 | 4.81 | 16650 | 2272 | 271 | 0.23 | 12.2 | 0.44 | <0.5 | <1 | 3.0 | 0.82 | 81 | 14.9 |
| 617-220 | OAN | | 3.5 | 15.9 | 0.45 | 0.018 | 19.5 | 0.08 | 12.9 | 0.16 | 893 | 27 | 4 | 0.12 | 1.9 | 0.16 | <0.5 | <1 | <1 | 0.43 | 27 | 4.0 |
| 617-395 | OAN | F | 23.7 | 15.7 | 1.32 | 0.070 | 11.6 | 0.27 | 7.6 | 0.79 | 424 | 36 | 3 | 0.07 | 7.7 | 0.35 | <0.5 | <1 | <1 | 1.20 | 123 | 6.5 |
| 617-396 | OAN | | 25.4 | 31.1 | 5.00 | 0.323 | 4.8 | 0.38 | 2.2 | 0.81 | 10735 | 107 | 11 | 0.20 | 5.9 | 1.94 | 0.9 | 31 | 9.4 | 5.86 | 103 | 43.4 |
| 617-508 | SOAN | A | 15.6 | 26.1 | 5.46 | 0.384 | 22.2 | 0.22 | 1.2 | 0.62 | 1245 | 55 | 9 | 0.27 | 2.5 | 2.11 | 1.1 | 39 | 9.8 | 6.42 | 77 | 47.3 |
| 617-551 | SOAN | | 4.5 | 3.4 | 0.46 | 0.024 | 36.1 | 0.08 | 20.9 | 0.63 | 1389 | 139 | 13 | 0.09 | 1.1 | 0.12 | <0.5 | <1 | <1 | 0.45 | 21 | 3.2 |
| 617-650 | SOAN | S | 25.4 | 18.3 | 2.01 | 0.073 | 8.3 | 0.28 | 10.1 | 4.93 | 10786 | 760 | 136 | 0.24 | 4.7 | 0.46 | <0.5 | 4 | 2.2 | 1.43 | 106 | 10.8 |
| 617-787 | SOAN | | 31.0 | 14.8 | 1.40 | 0.056 | 11.7 | 0.21 | 10.2 | 2.48 | 2437 | 689 | 207 | 0.34 | 6.4 | 0.40 | <0.5 | <1 | <1 | 0.92 | 69 | 7.0 |
| 617-799 | SOAN | S | 16.3 | 12.1 | 1.90 | 0.108 | 17.4 | 0.22 | 12.4 | 7.07 | 5775 | 2294 | 152 | 0.27 | 4.1 | 0.60 | <0.5 | 4 | 3.5 | 1.88 | 53 | 16.4 |
| 617-875 | SOAN | S | 12.8 | 10.3 | 1.22 | 0.048 | 23.0 | 0.28 | 15.7 | 3.04 | 6722 | 476 | 124 | 0.11 | 2.1 | 0.26 | <0.5 | <1 | 1.9 | 0.90 | 98 | 11.1 |

Sample name refers to number of core (locations in Fig 4.1) and depth in core (in cm). Units are described in Table 4.1. Sample types are: A=Al-rich, F=Fe-rich, S=S-rich. [1] total Fe content given as $Fe_2O_3$. [2] Individual REE analyses are reported in Appendix 4.1. Analysis methods: 1=Fusion ICP-MS (Activation Laboratories), 2=Fusion ICP-OES (Activation Laboratories), 3=Four-acid leach ICP-MS (University of Kiel), 4=Four-acid leach ICP-OES (University of Kiel).

Table 4.3. Properties of total and residual REE profiles (PAAS normalized) and uranium concentration in different stratigraphic units of the Atlantis II Deep (abbreviations in Table 4.1).

| Average values | ΣREE (ppm) | La/Yb | La/Sm | Gd/Yb | Ce/Ce* | Eu/Eu* | U (ppm) |
|---|---|---|---|---|---|---|---|
| AM(+SAM) | 7.39 | 0.73 | 0.60 | 1.29 | 0.98 | 2.35 | 7.92 |
| SU2(+SOAN+OAN) | 10.0 | 0.73 | 0.60 | 1.31 | 0.97 | 2.32 | 4.30 |
| CO(+COS) | 25.2 | 0.82 | 0.70 | 1.30 | 0.98 | 2.04 | 9.08 |
| SU1 | 24.7 | 0.92 | 0.73 | 1.33 | 0.98 | 3.48 | 4.12 |
| DOP | 54.1 | 1.00 | 0.81 | 1.31 | 0.97 | 2.41 | 4.38 |
| Residual REE patterns | | | | | | | |
| AM(+SAM) | 0.86 | 1.6 | 0.73 | 2.1 | 0.89 | 9.65 | |
| SU2(+SOAN+OAN) | 0.57 | 2.8 | 1.0 | 2.3 | 0.93 | 9.68 | |
| CO(+COS) | 1.3 | -17 | 2.4 | -7.3 | 0.72 | 12.4 | |
| SU1 | 6.8 | 1.7 | 1.0 | 1.6 | 1.0 | 12.2 | |
| DOP | 14.9 | 3.3 | 1.6 | 2.2 | 0.87 | 7.0 | |

PAAS values are from Taylor and McLennan (1985). $Ce/Ce^* = Ce_N/((La_N+Pr_N)/2)$; $Eu/Eu^* = Eu_N/((Sm_N+Gd_N)/2)$. Residual REE profiles were calculated by subtracting the amount of each REE in proportion to the computed "Atlantis II detrital component" using Sc as reference element.

Table 4.4. Pearson correlation coefficients (*r*) for $Al_2O_3$ and $P_2O_5$ versus ΣREE in all samples according to $Al_2O_3/(5*P_2O_5)$.

| $Al_2O_3/(5*P_2O_5)$ | n | Al vs. ΣREE | P vs. ΣREE |
|---|---|---|---|
| All | 100 | 0.902 | 0.308 |
| <2 | 73 | 0.623 | 0.497 |
| <1 | 42 | 0.618 | 0.601 |
| <0.5 | 13 | 0.704 | 0.701 |

Table 4.5. Properties of total and residual REE profiles and uranium concentration in different layer types of the Atlantis II sediments (calculations as in Table 4.3).

| | ΣREE (ppm) | La/Yb | La/Sm | Gd/Yb | Ce/Ce* | Eu/Eu* | U (ppm) | La/Sm vs. Eu/Eu* |
|---|---|---|---|---|---|---|---|---|
| Fe-rich | 16.4 | 0.92 | 0.75 | 1.3 | 0.98 | 2.6 | 8.2 | 0.16 |
| S-rich | 18.4 | 0.96 | 0.73 | 1.3 | 0.99 | 3.2 | 5.2 | 0.62 |
| Al-rich | 58.6 | 0.75 | 0.67 | 1.2 | 0.98 | 1.4 | 4.3 | 0.38 |
| All | 23.4 | 0.83 | 0.69 | 1.3 | 0.97 | 2.5 | 5.7 | - |
| Residual REE patterns | | | | | | | | |
| Fe-rich | 8.11 | 3.0 | 1.6 | 2.2 | 0.86 | 6.0 | | 0.04 |
| S-rich | 4.02 | 6.2 | 1.3 | 3.3 | 0.98 | 18.0 | | 0.70 |
| Al-rich | 1.84 | 6.4 | 1.1 | 5.6 | 0.74 | 7.7 | | 0.14 |

The last column gives the Pearson correlation coefficients (r) for La/Sm versus Eu/Eu*.

Figure 4.1

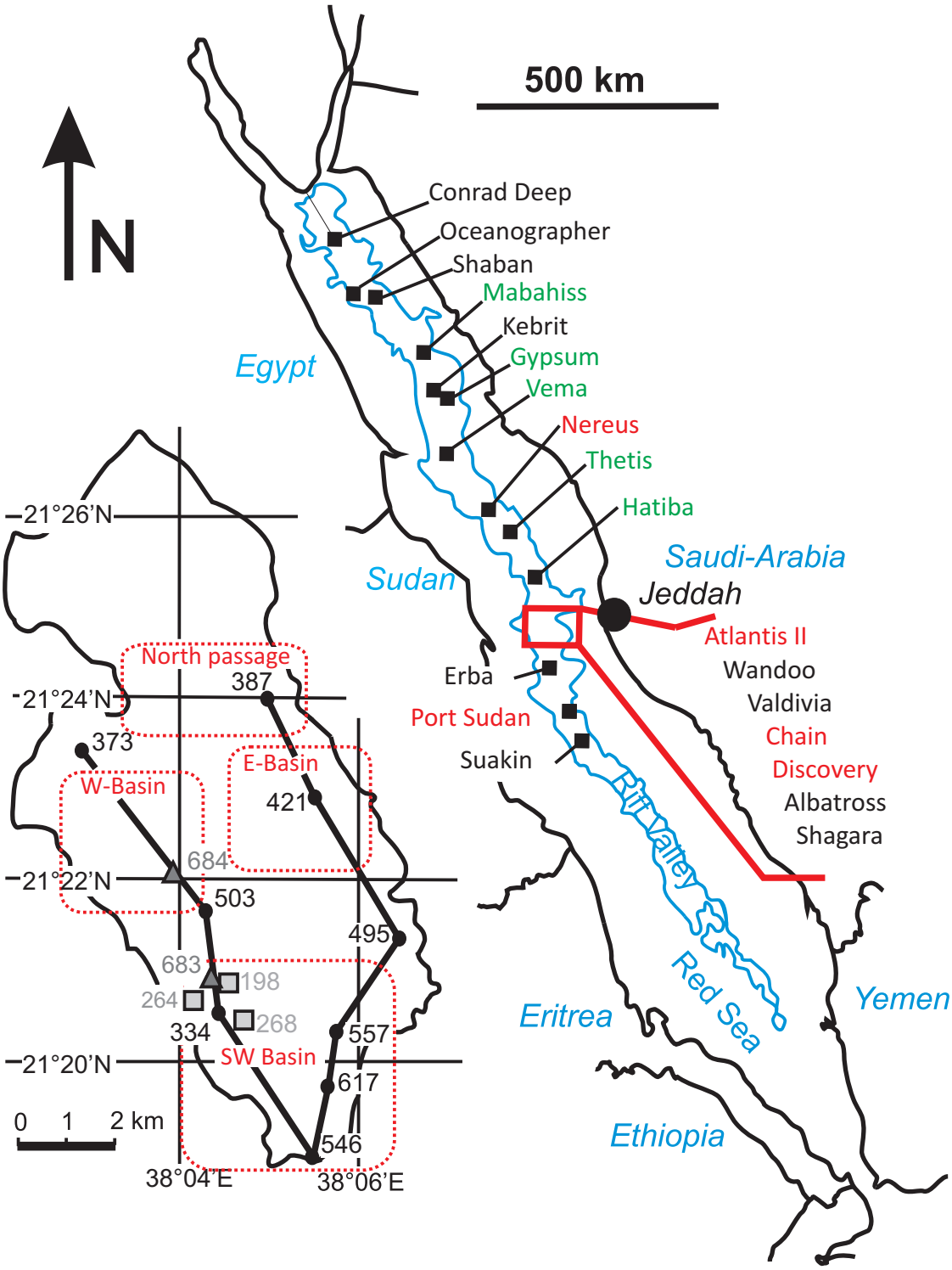

500 km
N
Conrad Deep
Oceanographer
Shaban
Mabahiss
Kebrit
Gypsum
Vema
Nereus
Thetis
Hatiba
Egypt
Sudan
Saudi-Arabia
Jeddah
Atlantis II
Wandoo
Valdivia
Chain
Discovery
Albatross
Shagara
Erba
Port Sudan
Suakin
Rift Valley
Red Sea
Eritrea
Yemen
Ethiopia
21°26'N
21°24'N
21°22'N
21°20'N
North passage
387
373
E-Basin
421
W-Basin
684
503
495
683
198
264
268
334
557
SW Basin
617
546
0 1 2 km
38°04'E
38°06'E

Figure 4.2

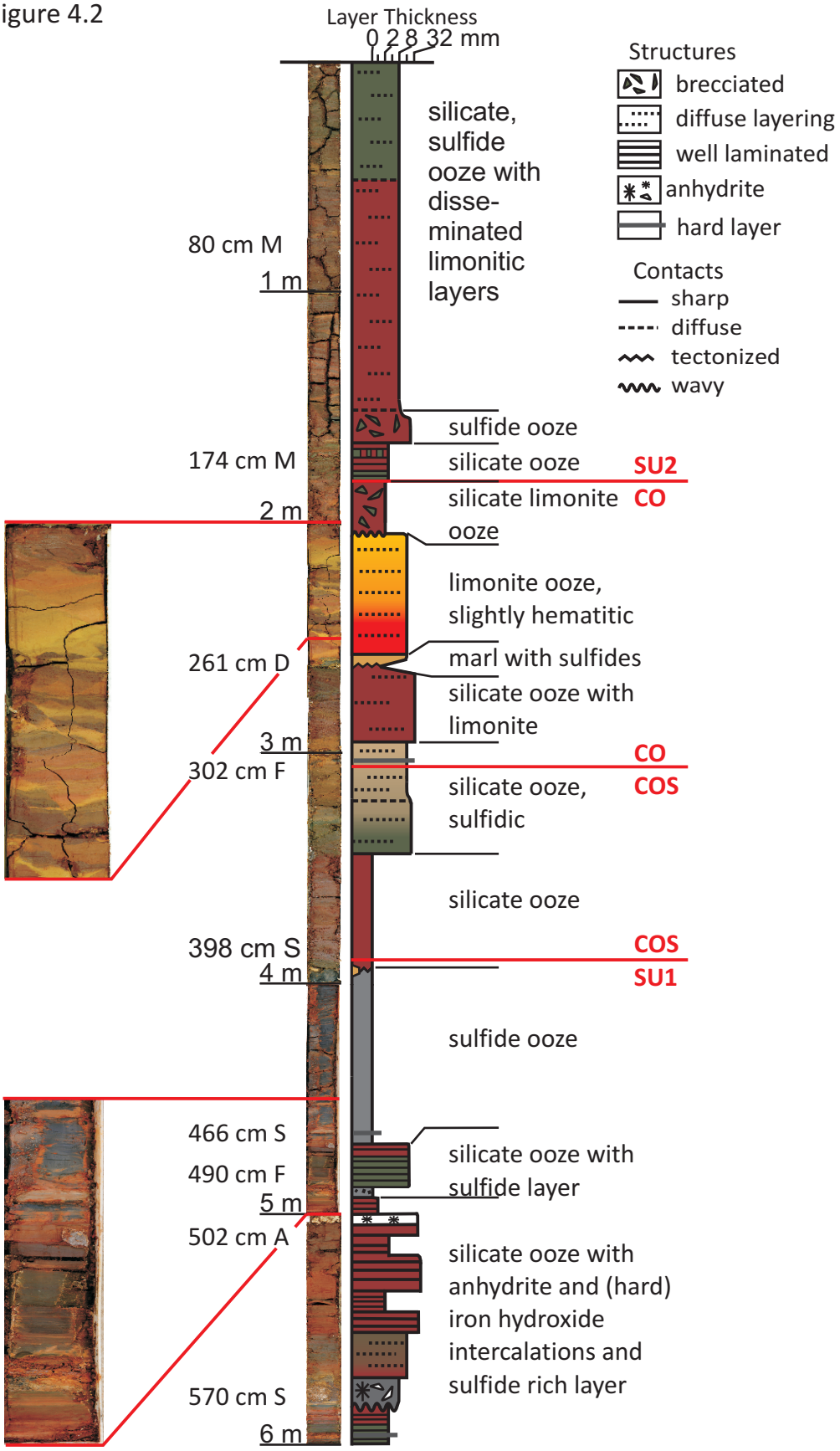

Layer Thickness
0 2 8 32 mm
Structures
brecciated
diffuse layering
well laminated
anhydrite
hard layer
Contacts
sharp
diffuse
tectonized
wavy
silicate, sulfide ooze with disse-minated limonitic layers
80 cm M
1 m
sulfide ooze
174 cm M
silicate ooze
SU2
2 m
silicate limonite ooze
CO
limonite ooze, slightly hematitic
261 cm D
marl with sulfides
silicate ooze with limonite
3 m
CO
302 cm F
COS
silicate ooze, sulfidic
silicate ooze
398 cm S
COS
4 m
SU1
sulfide ooze
466 cm S
silicate ooze with sulfide layer
490 cm F
5 m
502 cm A
silicate ooze with anhydrite and (hard) iron hydroxide intercalations and sulfide rich layer
570 cm S
6 m

Figure 4.3

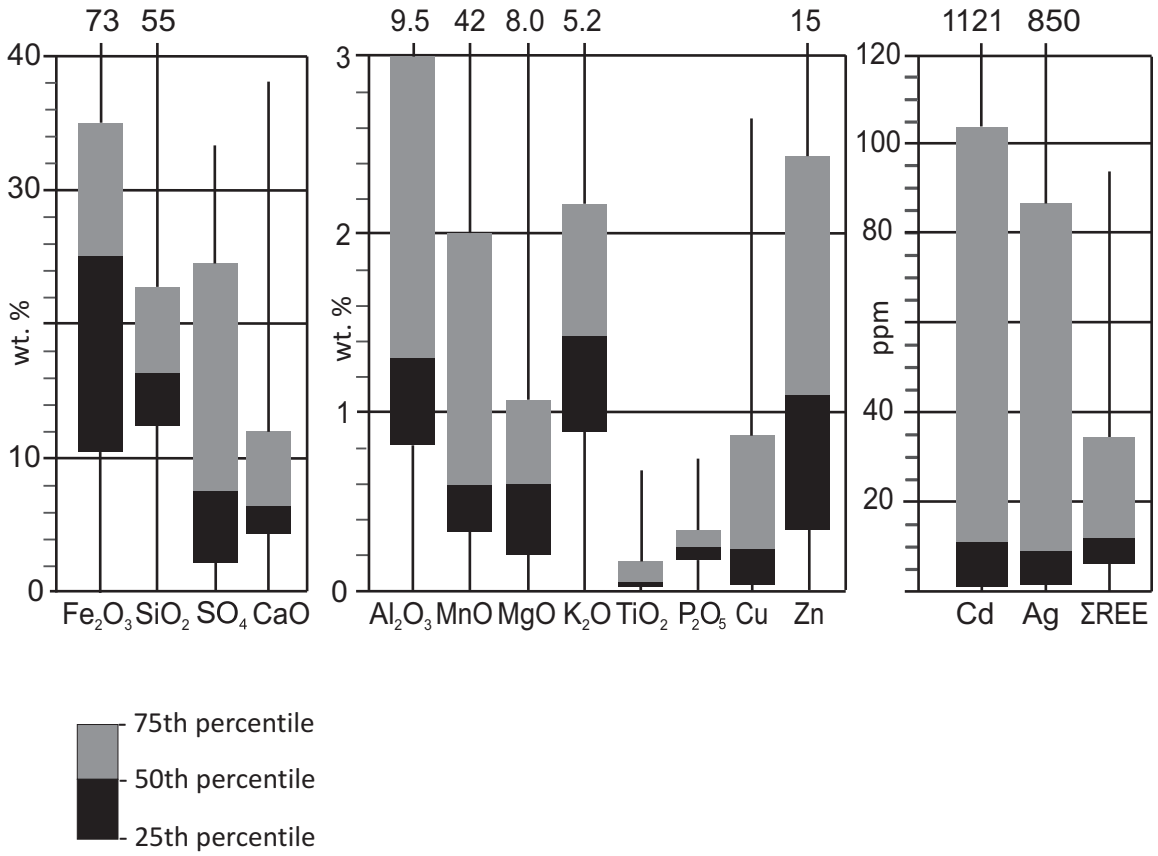
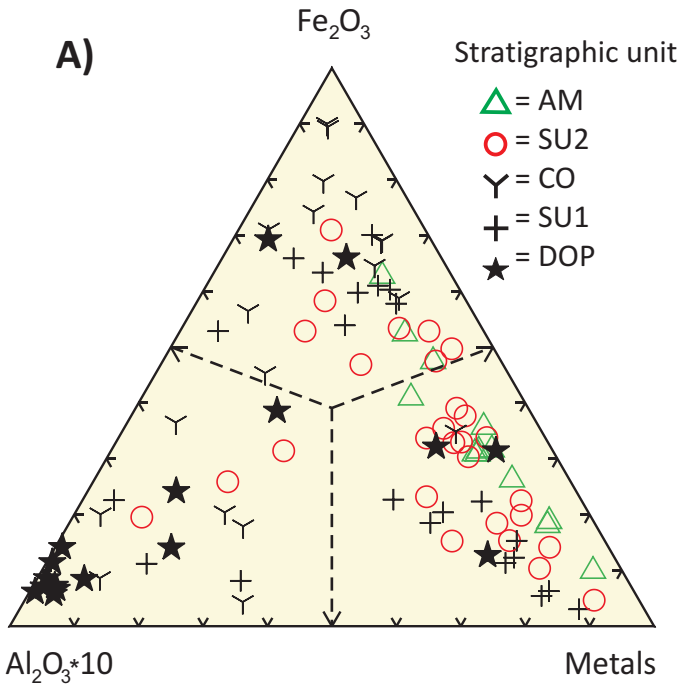

73
55
9.5
42
8.0
5.2
15
1121
850
wt. %
wt. %
ppm
Fe2O3
SiO2
SO4
CaO
Al2O3
MnO
MgO
K2O
TiO2
P2O5
Cu
Zn
Cd
Ag
ΣREE
75th percentile
50th percentile
25th percentile

Figure 4.4


A)
$Fe_2O_3$
Stratigraphic unit
= AM
= SU2
= CO
= SU1
= DOP
$Al_2O_3$*10
Metals

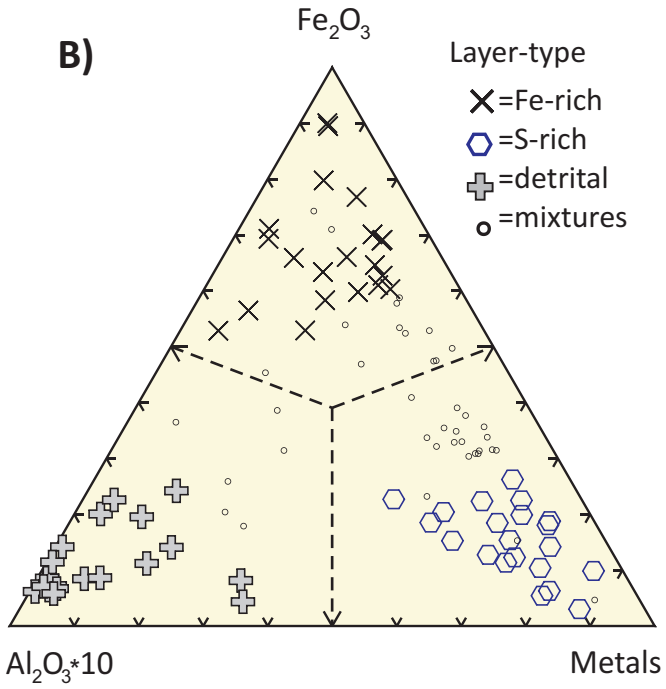
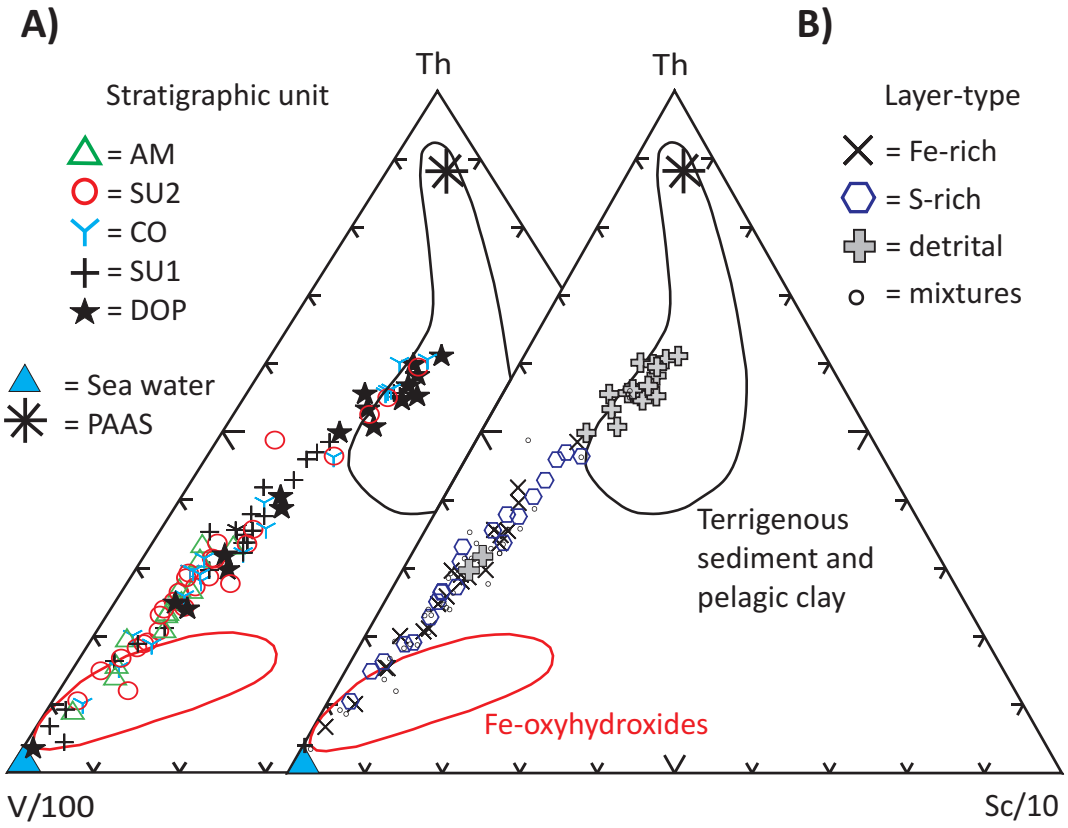

B)
$Fe_2O_3$
Layer-type
=Fe-rich
=S-rich
=detrital
=mixtures
$Al_2O_3$*10
Metals

Figure 4.5


A)
B)
Th
Th
Stratigraphic unit
= AM
= SU2
= CO
= SU1
= DOP
= Sea water
= PAAS
Layer-type
= Fe-rich
= S-rich
= detrital
= mixtures
Terrigenous
sediment and
pelagic clay
Fe-oxyhydroxides
V/100
Sc/10

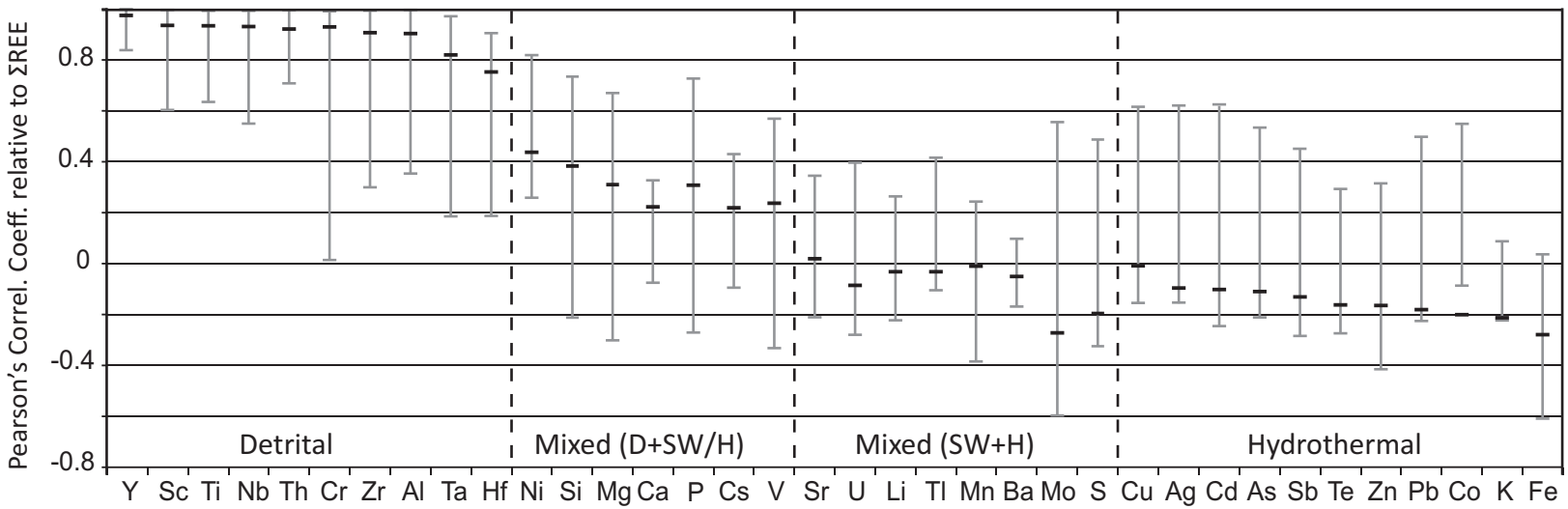

Pearson's Correl. Coeff. relative to ΣREE
0.8
0.4
0
-0.4
-0.8
Detrital
Mixed (D+SW/H)
Mixed (SW+H)
Hydrothermal
Y Sc Ti Nb Th Cr Zr Al Ta Hf Ni Si Mg Ca P Cs V Sr U Li Tl Mn Ba Mo S Cu Ag Cd As Sb Te Zn Pb Co K Fe

Figure 4.6

Figure 4.7

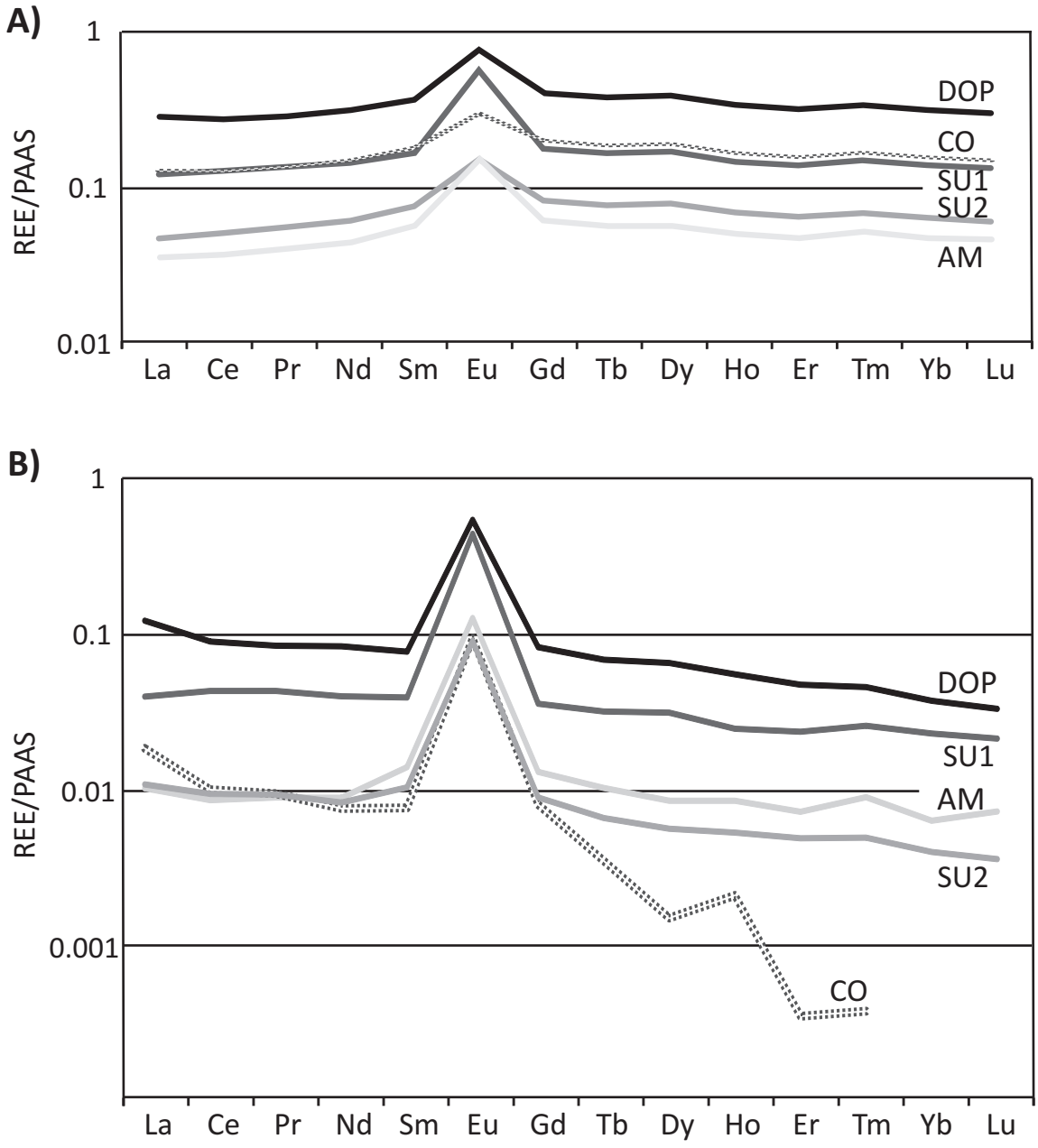

A)
1
0.1
0.01
REE/PAAS
DOP
CO
SU1
SU2
AM
La Ce Pr Nd Sm Eu Gd Tb Dy Ho Er Tm Yb Lu
B)
1
0.1
0.01
0.001
REE/PAAS
DOP
SU1
AM
SU2
CO
La Ce Pr Nd Sm Eu Gd Tb Dy Ho Er Tm Yb Lu

Figure 4.8

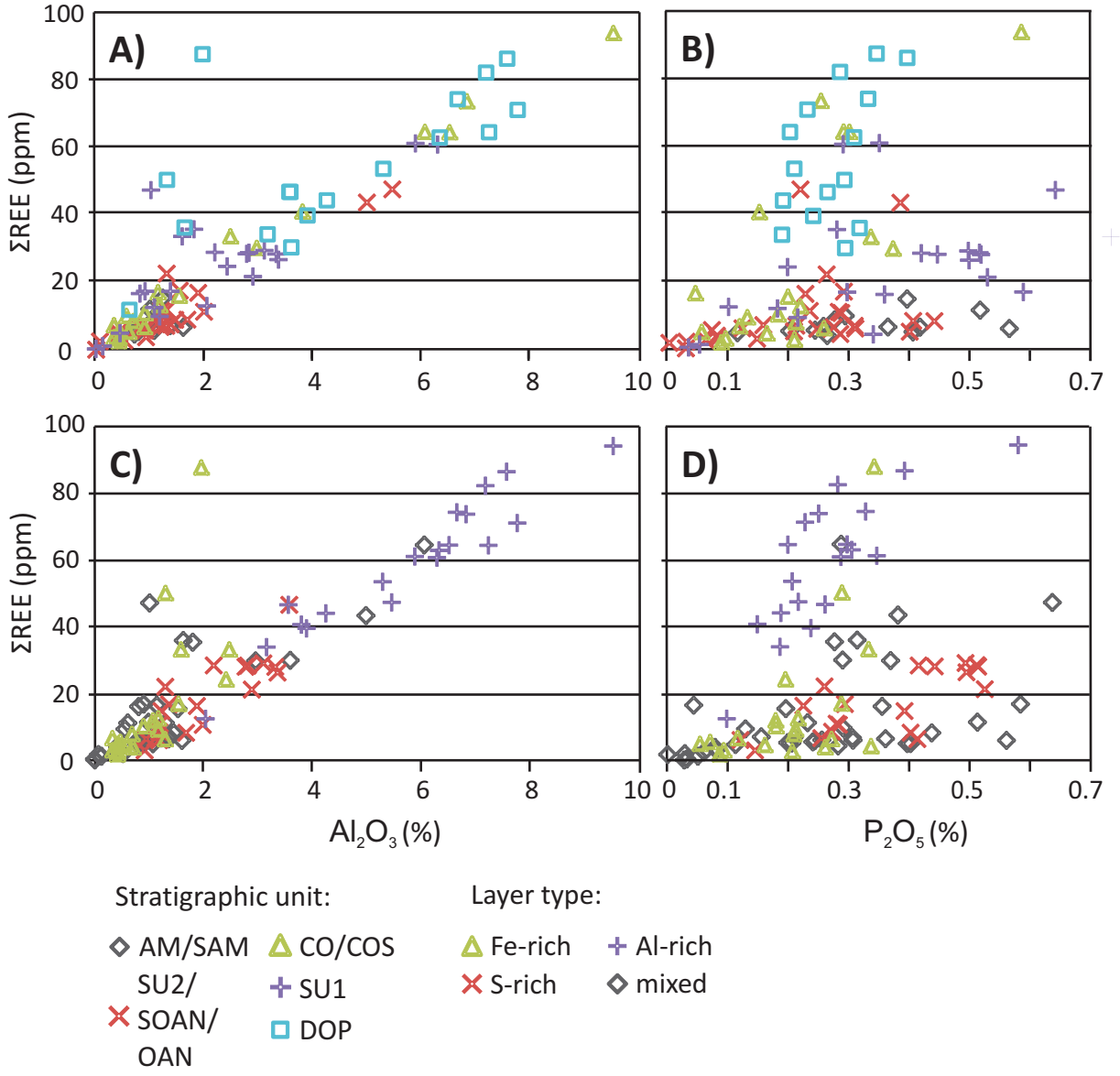
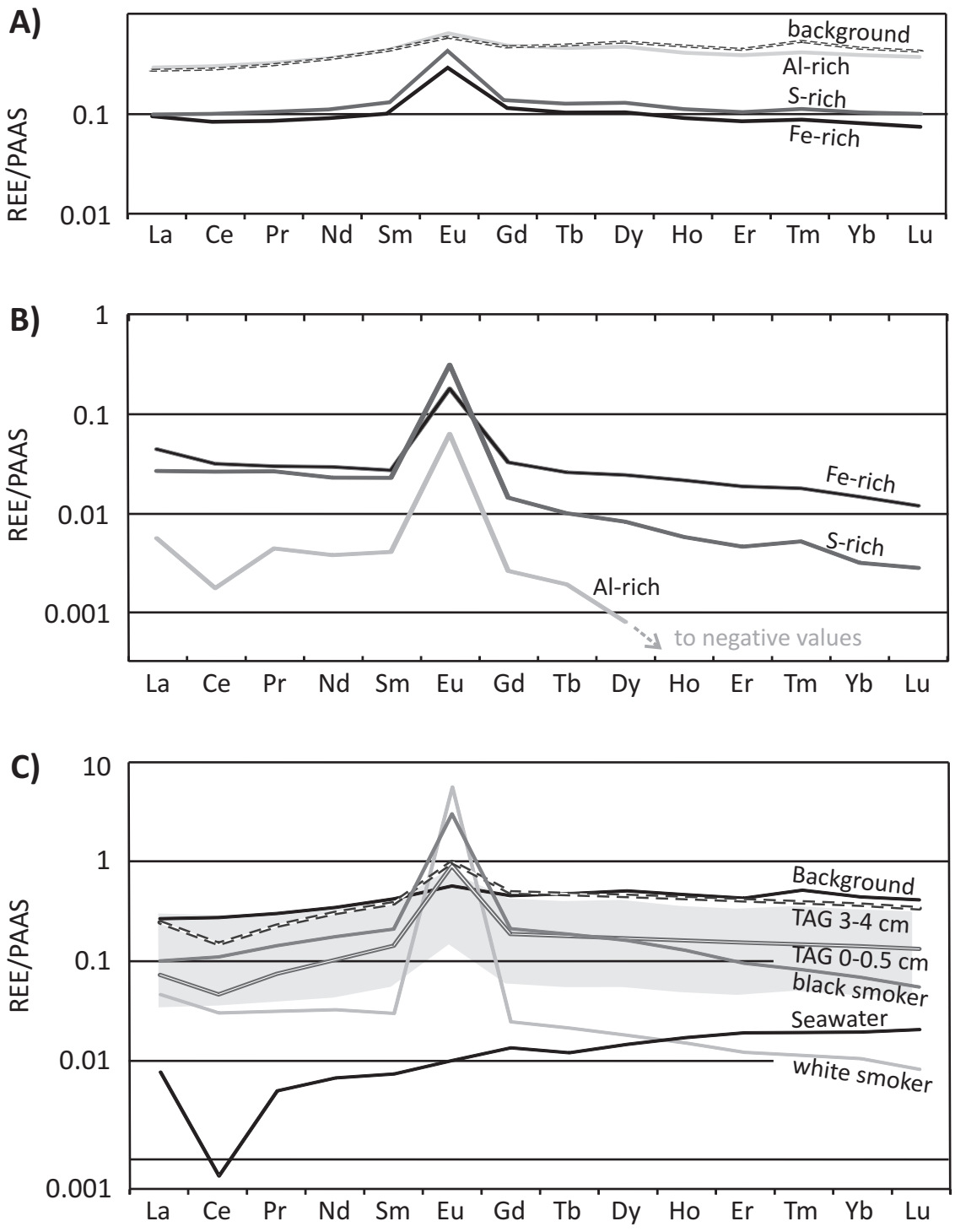

A)
B)
C)
D)
ΣREE (ppm)
ΣREE (ppm)
100
80
60
40
20
0
0
2
4
6
8
10
0
0.1
0.3
0.5
0.7
Al2O3 (%)
P2O5 (%)
Stratigraphic unit:
AM/SAM
CO/COS
SU2/ SOAN/ OAN
SU1
DOP
Layer type:
Fe-rich
Al-rich
S-rich
mixed

Figure 4.9


A)
REE/PAAS
0.1
0.01
background
Al-rich
S-rich
Fe-rich
La Ce Pr Nd Sm Eu Gd Tb Dy Ho Er Tm Yb Lu
B)
1
0.1
0.01
0.001
REE/PAAS
Fe-rich
S-rich
Al-rich
to negative values
La Ce Pr Nd Sm Eu Gd Tb Dy Ho Er Tm Yb Lu
C)
10
1
0.1
0.01
0.001
REE/PAAS
Background
TAG 3-4 cm
TAG 0-0.5 cm
black smoker
Seawater
white smoker
La Ce Pr Nd Sm Eu Gd Tb Dy Ho Er Tm Yb Lu

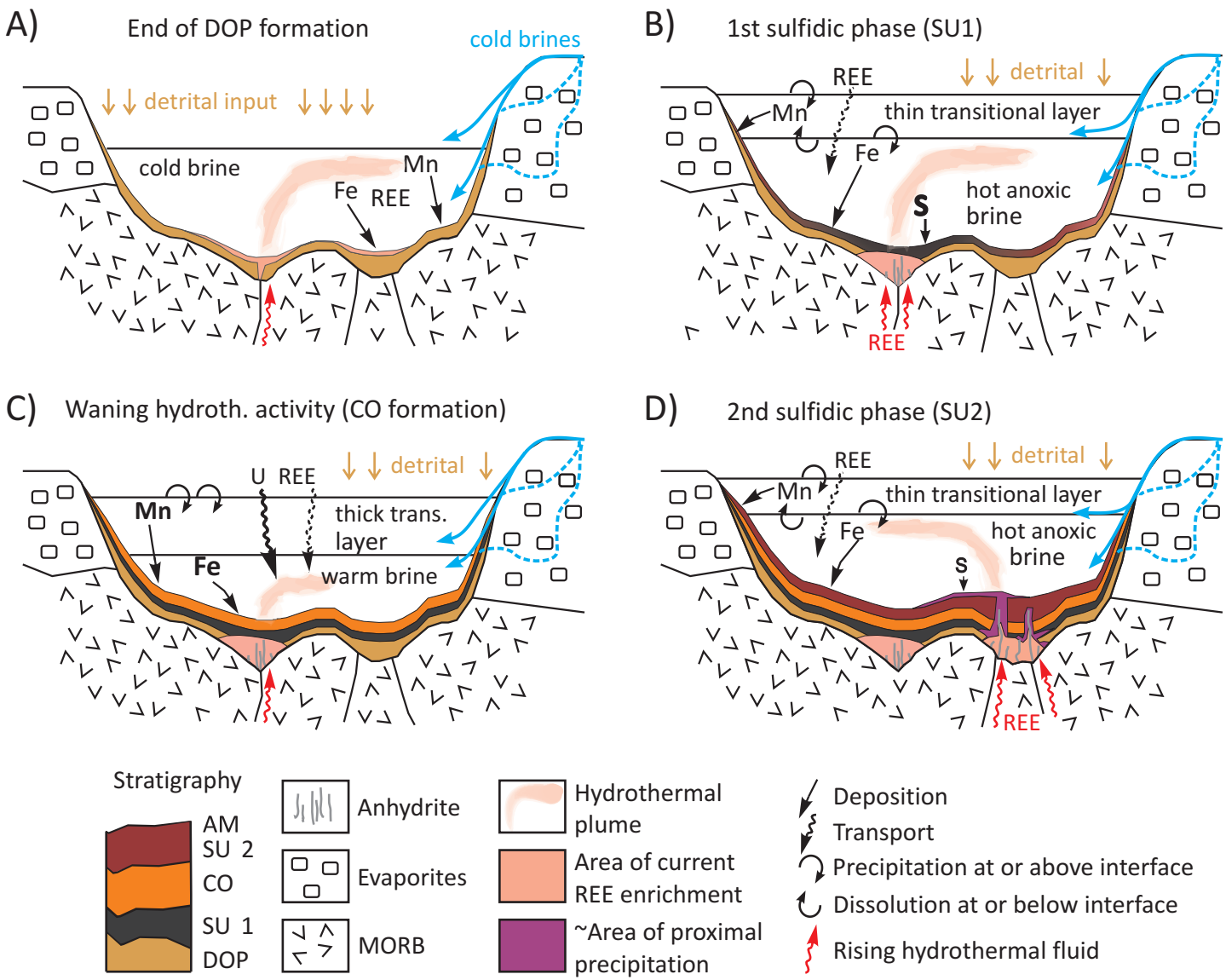

A)
End of DOP formation
cold brines
detrital input
cold brine
Mn
Fe
REE
B)
1st sulfidic phase (SU1)
REE
detrital
Mn
thin transitional layer
Fe
S
hot anoxic brine
REE
C)
Waning hydroth. activity (CO formation)
U
REE
detrital
Mn
thick trans. layer
Fe
warm brine
D)
2nd sulfidic phase (SU2)
REE
detrital
Mn
thin transitional layer
Fe
hot anoxic brine
S
REE
Stratigraphy
AM
SU 2
CO
SU 1
DOP
Anhydrite
Evaporites
MORB
Hydrothermal plume
Area of current REE enrichment
~Area of proximal precipitation
Deposition
Transport
Precipitation at or above interface
Dissolution at or below interface
Rising hydrothermal fluid

Figure 4.10

Appendix 4.1. Analyses of the individual REE for all samples considered in this study (dry, salt-free). Blanks, standards, accuracy and reproducibility for the analyses reported are summarized in the second table. All analyses were performed by ICP-MS at the University of Kiel after total dissolution of the sample by four-acid leach.

| | | La | Ce | Pr | Nd | Sm | Eu | Gd | Tb | Dy | Ho | Er | Tm | Yb | Lu |
|---|---|---|---|---|---|---|---|---|---|---|---|---|---|---|---|
| Det. limit | | 0.1 | 0.1 | 0.01 | 0.05 | 0.01 | 0.001 | 0.01 | 0.005 | 0.01 | 0.005 | 0.01 | 0.005 | 0.01 | 0.005 |
| Sample no. | corr. | ppm | ppm | ppm | ppm | ppm | ppm | ppm | ppm | ppm | ppm | ppm | ppm | ppm | ppm |
| 334-83 | 2.0 | 0.7 | 1.9 | 0.25 | 1.02 | 0.23 | 0.05 | 0.21 | 0.033 | 0.20 | 0.040 | 0.11 | 0.016 | 0.10 | 0.015 |
| 334-312 | 2.1 | 1.2 | 2.7 | 0.32 | 1.29 | 0.30 | 0.09 | 0.27 | 0.040 | 0.23 | 0.048 | 0.13 | 0.020 | 0.12 | 0.019 |
| 334-513 | 2.0 | 1.4 | 3.3 | 0.43 | 1.70 | 0.46 | 0.28 | 0.32 | 0.050 | 0.29 | 0.057 | 0.15 | 0.023 | 0.15 | 0.022 |
| 334-612 | 2.2 | 0.9 | 2.4 | 0.31 | 1.26 | 0.28 | 0.10 | 0.26 | 0.037 | 0.22 | 0.043 | 0.12 | 0.017 | 0.11 | 0.016 |
| 334-757 | 2.0 | 1.4 | 2.6 | 0.28 | 1.03 | 0.21 | 0.08 | 0.18 | 0.028 | 0.16 | 0.032 | 0.09 | 0.015 | 0.09 | 0.015 |
| 373-8 | 3.0 | 1.8 | 3.9 | 0.47 | 1.86 | 0.40 | 0.16 | 0.39 | 0.060 | 0.34 | 0.067 | 0.19 | 0.029 | 0.18 | 0.027 |
| 373-93 | 2.5 | 2.1 | 4.6 | 0.55 | 2.11 | 0.46 | 0.13 | 0.42 | 0.065 | 0.37 | 0.075 | 0.21 | 0.032 | 0.20 | 0.029 |
| 373-210 | 2.9 | 1.0 | 2.3 | 0.27 | 1.00 | 0.22 | 0.20 | 0.19 | 0.030 | 0.16 | 0.034 | 0.09 | <.005 | 0.09 | <.005 |
| 373-265 | 2.1 | 4.7 | 6.0 | 0.67 | 2.57 | 0.54 | 0.44 | 0.55 | 0.077 | 0.44 | 0.090 | 0.25 | 0.037 | 0.24 | 0.038 |
| 373-515 | 2.0 | 1.8 | 4.0 | 0.44 | 1.70 | 0.35 | 0.19 | 0.31 | 0.048 | 0.27 | 0.056 | 0.15 | 0.023 | 0.15 | 0.023 |
| 373-555 | 1.8 | 5.1 | 11.6 | 1.44 | 5.59 | 1.19 | 0.68 | 1.05 | 0.162 | 0.95 | 0.187 | 0.50 | 0.077 | 0.50 | 0.073 |
| 373-586 | 1.0 | 0.3 | 0.5 | 0.06 | 0.25 | 0.06 | 0.04 | 0.05 | 0.008 | 0.05 | 0.010 | 0.03 | <.005 | 0.03 | <.005 |
| 373-672 | 2.2 | 0.8 | 1.8 | 0.21 | 0.80 | 0.16 | 0.10 | 0.14 | 0.022 | 0.13 | 0.027 | 0.07 | 0.013 | 0.08 | 0.013 |
| 373-751 | 1.4 | 5.4 | 11.2 | 1.34 | 5.06 | 1.03 | 0.80 | 0.92 | 0.146 | 0.88 | 0.174 | 0.49 | 0.074 | 0.50 | 0.076 |
| 373-780 | 1.3 | 9.5 | 18.9 | 2.14 | 8.48 | 1.73 | 0.47 | 1.60 | 0.248 | 1.46 | 0.288 | 0.79 | 0.116 | 0.77 | 0.112 |
| 373-798 | 2.0 | 16.0 | 19.5 | 1.92 | 7.15 | 1.17 | 0.67 | 1.26 | 0.172 | 0.99 | 0.203 | 0.54 | 0.073 | 0.44 | 0.064 |
| 387-80 | 2.3 | 0.7 | 2.1 | 0.29 | 1.12 | 0.24 | 0.10 | 0.22 | 0.034 | 0.20 | 0.041 | 0.11 | 0.016 | 0.11 | 0.016 |
| 387-174 | 3.0 | <0.1 | 1.0 | 0.18 | 0.67 | 0.15 | 0.09 | 0.14 | 0.021 | 0.12 | 0.024 | 0.06 | <.005 | 0.06 | <.005 |
| 387-261 | 1.4 | 11.7 | 25.6 | 3.06 | 12.43 | 2.65 | 0.70 | 2.48 | 0.378 | 2.22 | 0.432 | 1.19 | 0.173 | 1.14 | 0.169 |
| 387-302 | 1.5 | 1.8 | 4.5 | 0.47 | 1.85 | 0.38 | 0.10 | 0.37 | 0.053 | 0.31 | 0.063 | 0.17 | 0.024 | 0.15 | 0.024 |
| 387-398 | 1.8 | 4.5 | 10.5 | 1.30 | 5.15 | 1.10 | 0.59 | 0.98 | 0.152 | 0.88 | 0.173 | 0.47 | 0.071 | 0.46 | 0.068 |
| 387-466 | 1.5 | 6.1 | 12.5 | 1.31 | 4.56 | 0.85 | 0.85 | 0.73 | 0.111 | 0.65 | 0.126 | 0.35 | 0.051 | 0.33 | 0.048 |
| 387-490 | 1.2 | 5.2 | 13.9 | 1.62 | 6.02 | 1.19 | 1.38 | 1.13 | 0.181 | 1.10 | 0.216 | 0.60 | 0.090 | 0.59 | 0.086 |
| 387-502 | 1.0 | <0.1 | 0.2 | 0.04 | 0.14 | 0.03 | 0.02 | 0.02 | <.005 | 0.02 | <.005 | <.01 | <.005 | <.01 | <.005 |
| 387-575 | 1.5 | 3.9 | 7.3 | 0.77 | 2.67 | 0.50 | 0.41 | 0.41 | 0.059 | 0.34 | 0.065 | 0.19 | 0.028 | 0.19 | 0.027 |
| 421-80 | 2.3 | 1.0 | 2.0 | 0.24 | 0.93 | 0.22 | 0.12 | 0.19 | 0.031 | 0.18 | 0.037 | 0.10 | 0.016 | 0.10 | 0.016 |
| 421-160 | 2.9 | 0.9 | 1.7 | 0.20 | 0.79 | 0.18 | 0.10 | 0.18 | 0.028 | 0.16 | 0.033 | 0.09 | 0.015 | 0.09 | 0.015 |
| 421-223 | 2.5 | 0.9 | 2.1 | 0.25 | 1.03 | 0.23 | 0.01 | 0.21 | 0.032 | 0.17 | 0.035 | 0.10 | 0.014 | 0.08 | 0.014 |
| 421-362 | 2.9 | 1.2 | 2.5 | 0.28 | 1.12 | 0.26 | 0.15 | 0.23 | 0.034 | 0.20 | 0.040 | 0.11 | 0.017 | 0.11 | 0.018 |
| 421-496 | 1.5 | 4.7 | 9.6 | 1.15 | 4.60 | 0.98 | 0.24 | 0.91 | 0.140 | 0.83 | 0.163 | 0.44 | 0.066 | 0.44 | 0.064 |
| 421-520 | 2.1 | 2.3 | 4.9 | 0.57 | 2.29 | 0.47 | 0.14 | 0.44 | 0.068 | 0.39 | 0.078 | 0.22 | 0.034 | 0.22 | 0.033 |
| 421-678 | 1.6 | 9.4 | 19.5 | 2.19 | 8.15 | 1.57 | 1.31 | 1.38 | 0.208 | 1.22 | 0.239 | 0.64 | 0.095 | 0.60 | 0.089 |
| 421-740 | 2.6 | 2.2 | 4.5 | 0.53 | 1.97 | 0.43 | 0.33 | 0.38 | 0.062 | 0.36 | 0.071 | 0.19 | 0.030 | 0.20 | 0.027 |
| 421-825 | 1.2 | 16.2 | 34.5 | 4.12 | 16.52 | 3.46 | 0.90 | 3.18 | 0.490 | 2.87 | 0.569 | 1.55 | 0.227 | 1.50 | 0.222 |
| 421-870 | 1.8 | 21.6 | 35.9 | 3.93 | 14.94 | 2.58 | 1.73 | 2.45 | 0.340 | 1.86 | 0.361 | 0.93 | 0.123 | 0.74 | 0.101 |
| 495-113 | 2.4 | 0.7 | 1.6 | 0.19 | 0.78 | 0.17 | 0.07 | 0.16 | 0.025 | 0.14 | 0.029 | 0.08 | 0.013 | 0.08 | 0.013 |
| 495-240 | 3.4 | 2.2 | 4.6 | 0.52 | 2.01 | 0.41 | 0.43 | 0.41 | 0.063 | 0.35 | 0.072 | 0.19 | 0.029 | 0.19 | 0.028 |
| 495-362 | 2.1 | 1.1 | 2.4 | 0.29 | 1.15 | 0.26 | 0.09 | 0.23 | 0.034 | 0.20 | 0.041 | 0.11 | 0.019 | 0.11 | 0.017 |
| 495-484 | 2.4 | 1.3 | 2.7 | 0.33 | 1.31 | 0.29 | 0.13 | 0.25 | 0.038 | 0.22 | 0.045 | 0.12 | 0.018 | 0.12 | 0.018 |
| 495-548 | 1.8 | 3.4 | 6.8 | 0.79 | 3.10 | 0.64 | 0.33 | 0.61 | 0.094 | 0.54 | 0.106 | 0.30 | 0.043 | 0.27 | 0.041 |
| 495-557 | 1.4 | 6.8 | 13.4 | 1.53 | 6.03 | 1.23 | 0.43 | 1.16 | 0.176 | 1.03 | 0.207 | 0.56 | 0.081 | 0.52 | 0.078 |
| 495-569 | 1.3 | 2.7 | 6.3 | 0.74 | 2.98 | 0.65 | 0.15 | 0.60 | 0.093 | 0.54 | 0.107 | 0.29 | 0.044 | 0.29 | 0.042 |
| 495-582 | 1.2 | 7.3 | 16.4 | 1.92 | 7.80 | 1.69 | 0.35 | 1.58 | 0.244 | 1.42 | 0.284 | 0.77 | 0.115 | 0.75 | 0.111 |
| 495-599 | 1.5 | 5.5 | 11.8 | 1.42 | 5.69 | 1.23 | 0.30 | 1.14 | 0.179 | 1.06 | 0.211 | 0.58 | 0.088 | 0.56 | 0.084 |
| 495-693 | 2.1 | 2.4 | 5.1 | 0.61 | 2.39 | 0.50 | 0.18 | 0.47 | 0.071 | 0.41 | 0.084 | 0.23 | 0.034 | 0.22 | 0.033 |
| 495-757 | 1.2 | 10.8 | 24.1 | 2.94 | 11.79 | 2.51 | 0.85 | 2.29 | 0.355 | 2.09 | 0.409 | 1.12 | 0.166 | 1.08 | 0.160 |
| 495-777 | 1.3 | 5.1 | 11.5 | 1.37 | 5.30 | 1.09 | 0.84 | 0.97 | 0.154 | 0.90 | 0.176 | 0.48 | 0.072 | 0.47 | 0.069 |
| 495-809 | 2.4 | 3.4 | 7.2 | 0.80 | 2.71 | 0.47 | 0.42 | 0.38 | 0.056 | 0.33 | 0.063 | 0.18 | 0.027 | 0.17 | 0.026 |
| 495-867 | 1.2 | 11.2 | 24.3 | 2.93 | 11.73 | 2.47 | 0.71 | 2.30 | 0.357 | 2.09 | 0.411 | 1.14 | 0.167 | 1.09 | 0.160 |
| 495-889 | 1.6 | 5.4 | 12.0 | 1.43 | 5.76 | 1.22 | 0.38 | 1.12 | 0.175 | 1.02 | 0.206 | 0.56 | 0.084 | 0.54 | 0.080 |

| Sample no. | corr. | La | Ce | Pr | Nd | Sm | Eu | Gd | Tb | Dy | Ho | Er | Tm | Yb | Lu |
|---|---|---|---|---|---|---|---|---|---|---|---|---|---|---|---|
| 495-934 | 1.1 | 11.5 | 24.9 | 3.00 | 12.06 | 2.57 | 0.69 | 2.37 | 0.371 | 2.19 | 0.438 | 1.19 | 0.177 | 1.17 | 0.171 |
| 495-1088 | 1.1 | 11.7 | 25.1 | 3.08 | 12.47 | 2.68 | 0.70 | 2.51 | 0.394 | 2.34 | 0.465 | 1.29 | 0.192 | 1.27 | 0.187 |
| 495-1195 | 1.2 | 12.7 | 27.9 | 3.43 | 13.82 | 2.95 | 0.88 | 2.75 | 0.430 | 2.54 | 0.499 | 1.38 | 0.201 | 1.32 | 0.193 |
| 503-7 | 2.4 | 0.8 | 2.1 | 0.29 | 1.16 | 0.25 | 0.10 | 0.24 | 0.034 | 0.20 | 0.039 | 0.11 | 0.016 | 0.11 | 0.017 |
| 503-75 | 1.7 | 5.5 | 9.7 | 1.01 | 3.49 | 0.65 | 0.53 | 0.44 | 0.062 | 0.33 | 0.064 | 0.18 | 0.027 | 0.17 | 0.025 |
| 503-140 | 2.2 | 0.3 | 0.8 | 0.13 | 0.52 | 0.10 | 0.03 | 0.10 | 0.015 | 0.09 | 0.019 | 0.05 | <.005 | 0.05 | <.005 |
| 503-155 | 2.2 | 1.3 | 2.8 | 0.38 | 1.44 | 0.27 | 0.07 | 0.24 | 0.037 | 0.22 | 0.045 | 0.13 | 0.020 | 0.13 | 0.021 |
| 503-235 | 1.1 | <0.1 | <0.1 | 0.02 | 0.07 | 0.02 | 0.01 | 0.02 | <.005 | 0.01 | <.005 | <.01 | <.005 | <.01 | <.005 |
| 503-266 | 1.2 | 0.4 | 0.8 | 0.10 | 0.33 | 0.06 | 0.08 | 0.06 | 0.008 | 0.05 | 0.009 | 0.02 | <.005 | 0.03 | <.005 |
| 503-407 | 1.6 | 0.5 | 1.1 | 0.14 | 0.55 | 0.12 | 0.10 | 0.11 | 0.017 | 0.10 | 0.021 | 0.06 | 0.009 | 0.06 | <.005 |
| 503-509 | 1.8 | 1.3 | 3.0 | 0.33 | 1.17 | 0.22 | 0.12 | 0.21 | 0.030 | 0.17 | 0.035 | 0.10 | 0.015 | 0.09 | 0.014 |
| 503-516 | 1.5 | 18.9 | 36.2 | 4.55 | 17.92 | 3.75 | 1.47 | 3.40 | 0.523 | 3.03 | 0.599 | 1.62 | 0.239 | 1.56 | 0.226 |
| 503-626 | 1.9 | 0.6 | 1.3 | 0.16 | 0.60 | 0.12 | 0.06 | 0.13 | 0.017 | 0.10 | 0.020 | 0.06 | <.005 | 0.06 | <.005 |
| 503-671 | 2.6 | <0.1 | 0.7 | 0.14 | 0.56 | 0.12 | 0.03 | 0.11 | 0.017 | 0.10 | 0.019 | 0.05 | <.005 | 0.06 | <.005 |
| 503-680 | 2.2 | 1.4 | 3.4 | 0.39 | 1.51 | 0.33 | 0.07 | 0.32 | 0.045 | 0.26 | 0.052 | 0.14 | 0.021 | 0.13 | 0.020 |
| 503-807 | 1.5 | 6.3 | 15.5 | 1.90 | 6.98 | 1.22 | 1.19 | 0.86 | 0.114 | 0.60 | 0.108 | 0.29 | 0.041 | 0.26 | 0.036 |
| 503-889 | 1.1 | 3.0 | 6.8 | 0.74 | 2.90 | 0.61 | 0.65 | 0.64 | 0.099 | 0.60 | 0.118 | 0.33 | 0.048 | 0.31 | 0.045 |
| 503-912 | 1.7 | 3.9 | 8.5 | 1.04 | 4.00 | 0.83 | 0.74 | 0.71 | 0.106 | 0.62 | 0.118 | 0.32 | 0.048 | 0.31 | 0.044 |
| 503-946 | 1.6 | 6.8 | 15.3 | 1.70 | 5.98 | 1.09 | 2.32 | 0.86 | 0.130 | 0.75 | 0.142 | 0.39 | 0.056 | 0.37 | 0.052 |
| 503-987 | 1.2 | 15.4 | 32.4 | 3.97 | 15.70 | 3.31 | 1.39 | 3.04 | 0.470 | 2.74 | 0.529 | 1.44 | 0.208 | 1.36 | 0.202 |
| 546-5 | 2.3 | 1.1 | 2.3 | 0.29 | 1.17 | 0.28 | 0.10 | 0.25 | 0.039 | 0.23 | 0.046 | 0.13 | 0.020 | 0.13 | 0.020 |
| 546-92 | 2.6 | 1.0 | 2.0 | 0.25 | 0.94 | 0.20 | 0.10 | 0.18 | 0.028 | 0.15 | 0.031 | 0.09 | 0.014 | 0.08 | 0.013 |
| 546-180 | 2.2 | 1.0 | 2.2 | 0.26 | 1.04 | 0.23 | 0.09 | 0.22 | 0.035 | 0.20 | 0.042 | 0.12 | 0.019 | 0.12 | 0.018 |
| 546-229 | 1.6 | 1.6 | 3.4 | 0.38 | 1.51 | 0.32 | 0.15 | 0.30 | 0.046 | 0.27 | 0.055 | 0.15 | 0.022 | 0.15 | 0.022 |
| 546-252 | 1.2 | 13.2 | 30.0 | 3.49 | 14.05 | 2.96 | 0.71 | 2.77 | 0.428 | 2.51 | 0.495 | 1.36 | 0.200 | 1.31 | 0.193 |
| 546-267 | 1.5 | 1.6 | 3.8 | 0.47 | 1.78 | 0.39 | 0.29 | 0.33 | 0.049 | 0.29 | 0.057 | 0.16 | 0.024 | 0.16 | 0.023 |
| 546-311 | 1.1 | 8.8 | 20.2 | 2.09 | 7.87 | 1.54 | 1.96 | 1.45 | 0.221 | 1.29 | 0.251 | 0.68 | 0.098 | 0.62 | 0.090 |
| 546-318 | 1.3 | 2.4 | 4.7 | 0.68 | 2.59 | 0.52 | 0.15 | 0.43 | 0.067 | 0.39 | 0.077 | 0.22 | 0.034 | 0.23 | 0.034 |
| 546-385 | 1.2 | 13.4 | 30.3 | 3.48 | 14.02 | 2.92 | 0.81 | 2.73 | 0.423 | 2.52 | 0.503 | 1.38 | 0.204 | 1.33 | 0.195 |
| 557-9 | 2.7 | 1.0 | 2.6 | 0.33 | 1.34 | 0.29 | 0.12 | 0.27 | 0.041 | 0.24 | 0.047 | 0.13 | 0.019 | 0.12 | 0.018 |
| 557-173 | 3.0 | 1.3 | 3.3 | 0.43 | 1.71 | 0.39 | 0.15 | 0.35 | 0.052 | 0.30 | 0.061 | 0.17 | 0.026 | 0.15 | 0.024 |
| 557-227 | 2.2 | 0.3 | 1.2 | 0.18 | 0.71 | 0.16 | 0.10 | 0.14 | 0.022 | 0.13 | 0.025 | 0.07 | 0.006 | 0.07 | 0.006 |
| 557-255 | 1.5 | 12.7 | 26.0 | 2.99 | 11.83 | 2.52 | 0.72 | 2.33 | 0.354 | 2.10 | 0.420 | 1.14 | 0.167 | 1.11 | 0.163 |
| 557-289 | 1.9 | 0.9 | 1.9 | 0.23 | 0.85 | 0.17 | 0.20 | 0.14 | 0.022 | 0.13 | 0.025 | 0.07 | 0.011 | 0.06 | 0.005 |
| 557-388 | 1.5 | 5.2 | 11.4 | 1.35 | 5.26 | 1.10 | 0.58 | 0.99 | 0.151 | 0.87 | 0.168 | 0.46 | 0.066 | 0.43 | 0.064 |
| 557-502 | 1.1 | 9.4 | 21.5 | 2.54 | 10.28 | 2.21 | 0.54 | 2.06 | 0.321 | 1.89 | 0.376 | 1.03 | 0.152 | 1.00 | 0.148 |
| 557-608 | 1.1 | 7.0 | 16.0 | 1.84 | 7.50 | 1.61 | 0.39 | 1.52 | 0.241 | 1.43 | 0.287 | 0.79 | 0.117 | 0.78 | 0.114 |
| 557-753 | 1.2 | 8.0 | 17.7 | 2.08 | 8.31 | 1.77 | 0.43 | 1.69 | 0.260 | 1.56 | 0.314 | 0.87 | 0.128 | 0.86 | 0.127 |
| 557-795 | 1.1 | 6.0 | 13.8 | 1.60 | 6.48 | 1.37 | 0.35 | 1.28 | 0.199 | 1.18 | 0.236 | 0.64 | 0.095 | 0.62 | 0.092 |
| 617-9 | 2.5 | 0.9 | 2.6 | 0.35 | 1.40 | 0.32 | 0.09 | 0.29 | 0.044 | 0.25 | 0.050 | 0.14 | 0.022 | 0.14 | 0.020 |
| 617-148 | 2.2 | 3.4 | 6.0 | 0.64 | 2.46 | 0.51 | 0.47 | 0.46 | 0.065 | 0.37 | 0.076 | 0.20 | 0.027 | 0.16 | 0.025 |
| 617-220 | 1.5 | 0.4 | 1.4 | 0.21 | 0.95 | 0.24 | 0.08 | 0.24 | 0.035 | 0.20 | 0.040 | 0.10 | 0.014 | 0.09 | 0.014 |
| 617-395 | 1.8 | 0.8 | 2.5 | 0.34 | 1.46 | 0.34 | 0.10 | 0.33 | 0.050 | 0.29 | 0.056 | 0.15 | 0.021 | 0.13 | 0.018 |
| 617-396 | 1.6 | 6.6 | 17.2 | 2.11 | 8.75 | 1.98 | 0.53 | 1.87 | 0.290 | 1.71 | 0.337 | 0.90 | 0.130 | 0.84 | 0.121 |
| 617-508 | 1.3 | 8.4 | 18.8 | 2.24 | 9.10 | 1.96 | 0.48 | 1.84 | 0.287 | 1.73 | 0.343 | 0.94 | 0.139 | 0.90 | 0.133 |
| 617-551 | 1.2 | 0.5 | 1.3 | 0.17 | 0.66 | 0.14 | 0.06 | 0.14 | 0.020 | 0.12 | 0.024 | 0.06 | 0.009 | 0.06 | 0.009 |
| 617-650 | 1.7 | 1.8 | 4.3 | 0.53 | 2.11 | 0.47 | 0.17 | 0.44 | 0.066 | 0.40 | 0.078 | 0.21 | 0.030 | 0.20 | 0.029 |
| 617-787 | 1.6 | 1.0 | 2.8 | 0.37 | 1.48 | 0.32 | 0.12 | 0.27 | 0.042 | 0.25 | 0.048 | 0.13 | 0.019 | 0.12 | 0.017 |
| 617-799 | 1.6 | 2.6 | 6.6 | 0.80 | 3.24 | 0.72 | 0.27 | 0.67 | 0.102 | 0.62 | 0.121 | 0.33 | 0.047 | 0.30 | 0.043 |
| 617-875 | 1.3 | 2.3 | 4.5 | 0.51 | 1.92 | 0.38 | 0.25 | 0.37 | 0.055 | 0.32 | 0.066 | 0.18 | 0.026 | 0.16 | 0.024 |

All data are calculated on a salt-free basis, assuming all Na is present as NaCl. The correction factor (corr.) is indicated. Measured NaCl concentrations are reported in Appendix C. The reported detection limits are for the bulk analyses, including salt; the practical limit of quantification can be calculated from the cited detection limit and the correction factor in the same way as the salt-free concentrations

Appendix 4.1 (continuation). Blanks, Standards, accuracy and reproducibility of the analyses.

| Blanks | | | | | | | | | |
|---|---|---|---|---|---|---|---|---|---|
| Results for 7.4.2011 | | | | | | | | | |
| Sample ID | Detection limit | Blank 1 | Blank 2 | blank 1 | blank 2 | Blank 1 | Blank 2 | blank 1 | blank 2 |
| Sc / 45 | 0.05 | 0.001 | 0.001 | 0.001 | 0.001 | 0.001 | 0.001 | 0.001 | 0.001 |
| V / 51 | 10 | -0.005 | 0.001 | 0.014 | -0.013 | -0.012 | 0.110 | -0.008 | -0.015 |
| Y / 89 | 1 | 0.007 | 0.009 | 0.002 | 0.001 | 0.001 | 0.000 | 0.000 | 0.000 |
| Zr / 90 | 1 | -0.067 | -0.067 | -0.065 | -0.068 | -0.068 | -0.068 | -0.070 | -0.070 |
| Cd / 114 | 0.5 | 0.002 | 0.002 | 0.004 | 0.002 | 0.003 | 0.002 | 0.002 | 0.002 |
| Ba / 138 | 10 | 0.007 | 0.052 | 0.058 | -0.013 | 0.073 | 0.058 | 0.020 | -0.014 |
| La / 139 | 0.1 | 0.000 | 0.000 | 0.000 | 0.000 | 0.000 | 0.000 | -0.001 | -0.001 |
| Ce / 140 | 0.1 | 0.000 | 0.000 | 0.000 | 0.000 | 0.000 | 0.000 | -0.001 | 0.000 |
| Pr / 141 | 0.01 | 0.000 | 0.000 | 0.000 | 0.000 | 0.000 | 0.000 | 0.000 | 0.000 |
| Nd / 146 | 0.05 | 0.000 | 0.000 | 0.000 | 0.001 | 0.000 | 0.000 | 0.000 | 0.000 |
| Sm / 147 | 0.01 | 0.000 | 0.000 | 0.000 | 0.000 | 0.000 | 0.000 | 0.000 | 0.000 |
| Eu / 151 | 0.001 | 0.000 | 0.000 | 0.000 | 0.000 | 0.000 | 0.000 | 0.000 | 0.000 |
| Gd / 157 | 0.01 | 0.000 | 0.000 | 0.000 | 0.000 | 0.000 | 0.000 | 0.000 | 0.000 |
| Tb / 159 | 0.005 | 0.000 | 0.000 | 0.000 | 0.000 | 0.000 | 0.000 | 0.000 | 0.000 |
| Dy / 163 | 0.01 | 0.000 | 0.000 | 0.000 | 0.000 | 0.000 | 0.000 | 0.000 | 0.000 |
| Ho / 165 | 0.005 | 0.000 | 0.000 | 0.000 | 0.000 | 0.000 | 0.000 | 0.000 | 0.000 |
| Er / 166 | 0.01 | 0.000 | 0.000 | 0.000 | 0.000 | 0.000 | 0.000 | 0.000 | 0.000 |
| Tm / 169 | 0.005 | 0.000 | 0.000 | 0.000 | 0.000 | 0.000 | 0.000 | 0.000 | 0.000 |
| Yb / 172 | 0.01 | 0.000 | 0.000 | 0.000 | 0.000 | 0.000 | 0.000 | 0.000 | 0.000 |
| Lu / 175 | 0.005 | 0.000 | 0.000 | 0.000 | 0.000 | 0.000 | 0.000 | 0.000 | 0.000 |
| Hf / 178 | 0.5 | 0.000 | 0.000 | 0.000 | 0.000 | 0.000 | 0.000 | 0.000 | 0.000 |
| Th / 232 | 0.01 | 0.000 | 0.000 | 0.000 | 0.000 | 0.000 | 0.000 | 0.000 | 0.000 |
| | | | | | | | | | |
| Results for 6.4.11 and 8.8.11 | | | | | | | | | |
| Sample ID | Detection limit | Blank | Blank | Blank | Blank | | | | |
| Sc / 45 | 0.05 | 0.001 | 0.001 | 0.001 | 0.001 | | | | |
| V / 51 | 10 | -0.004 | 0.116 | 0.000 | -0.006 | | | | |
| Y / 89 | 1 | 0.001 | 0.000 | 0.000 | 0.000 | | | | |
| Zr / 90 | 1 | -0.068 | -0.069 | -0.070 | -0.070 | | | | |
| Cd / 114 | 0.5 | 0.003 | 0.002 | 0.001 | 0.002 | | | | |
| Ba / 138 | 10 | 0.072 | 0.057 | 0.019 | -0.015 | | | | |
| La / 139 | 0.1 | -0.003 | -0.003 | -0.003 | -0.003 | | | | |
| Ce / 140 | 0.1 | -0.003 | -0.003 | -0.003 | -0.003 | | | | |
| Pr / 141 | 0.01 | 0.000 | 0.000 | 0.000 | 0.000 | | | | |
| Nd / 146 | 0.05 | 0.000 | 0.000 | 0.000 | 0.000 | | | | |
| Sm / 147 | 0.01 | 0.000 | 0.000 | 0.000 | 0.000 | | | | |
| Eu / 151 | 0.001 | 0.000 | 0.000 | 0.000 | 0.000 | | | | |
| Gd / 157 | 0.01 | 0.000 | 0.000 | 0.000 | 0.000 | | | | |
| Tb / 159 | 0.005 | 0.000 | 0.000 | 0.000 | 0.000 | | | | |
| Dy / 163 | 0.01 | 0.000 | 0.000 | 0.000 | 0.000 | | | | |
| Ho / 165 | 0.005 | 0.000 | 0.000 | 0.000 | 0.000 | | | | |
| Er / 166 | 0.01 | 0.000 | 0.000 | 0.000 | 0.000 | | | | |
| Tm / 169 | 0.005 | 0.000 | 0.000 | 0.000 | 0.000 | | | | |
| Yb / 172 | 0.01 | 0.000 | 0.000 | 0.000 | 0.000 | | | | |
| Lu / 175 | 0.005 | 0.000 | 0.000 | 0.000 | 0.000 | | | | |
| Hf / 178 | 0.5 | 0.000 | 0.000 | 0.000 | 0.000 | | | | |
| Th / 232 | 0.01 | 0.000 | 0.000 | 0.000 | 0.000 | | | | |

| Accuracy: Results for 7.4.2011 | | | | | | | | | | | | | | |
|---|---|---|---|---|---|---|---|---|---|---|---|---|---|---|
| | Recomm. | Measure | Measure | Measure | Measure | Measure | Recomm. | Measure | Measure | Measure | Recomm. | Measure | Recomm. | Measure |
| | BHVO-2 | BHVO-2 | BHVO-2 | BHVO-2 | BHVO-2 | BHVO-2 | NOD-A1 | NOD-A1 | Nod-A-1 | Nod-A-1 | NOD-P-1 | NOD-P1 | GSPN-2 | GSPN-2 |
| Sc | 31.8 | 32.3 | 32.1 | 31.8 | 31.9 | 31.7 | 12.4-15.7 | 12.2 | 11.9 | 12.0 | 9.7 | 10.0 | 13.0 | 13.7 |
| V | 317 | 324 | 318 | 318 | 321 | 320 | 770.0 | 612.3 | 592. 8 | 599.51 | 570 | 484 | 456.0 | 425.9 |
| Y | 25.5 | 25.6 | 25.5 | 25.3 | 25.5 | 25.4 | 116.0 | 125.1 | 121.0 | 120.79 | 94 | 92 | 144.0 | 136.6 |
| Zr | 174 | 174 | 174 | 172 | 174 | 173 | 233-436 | 328 | 312 | 317 | | 280 | 614.0 | 590.5 |
| Cd | | < 0.5 | < 0.5 | < 0.5 | < 0.5 | < 0.5 | 7.50 | 7.76 | 7.50 | 7.55 | 22.6 | 22.5 | 10.0 | 8.9 |
| Ba | 130 | 129 | 129 | 130 | 131 | 129 | 1670.0 | 1476.1 | 1451.2 | 1456.6 | 3350 | 2532 | 1800 | 1668 |
| La | 15.2 | 15.2 | 15.2 | 15.1 | 15.2 | 15.1 | 119.50 | 116.04 | 114.46 | 115.21 | 104 | 110 | 184.0 | 176.7 |
| Ce | 38 | 38 | 38 | 37 | 38 | 37 | 730.00 | 759.20 | 741.49 | 745.33 | 294 | 323 | 620.0 | 596.2 |
| Pr | 5.3 | 5.3 | 5.3 | 5.3 | 5.3 | 5.3 | 24.3-25 | 25.4 | 25.0 | 25.0 | 31 - 33 | 33 | 49.0 | 49.2 |
| Nd | 25 | 25 | 25 | 24 | 25 | 25 | 94.00 | 106.06 | 103.89 | 103.92 | 119 | 138 | 198.0 | 202.9 |
| Sm | 6.2 | 6.1 | 6.1 | 6.0 | 6.1 | 6.0 | 21.00 | 23.14 | 22.64 | 22.75 | 29.5 | 33.1 | 46.0 | 47.0 |
| Eu | 2.06 | 2.06 | 2.07 | 2.05 | 2.05 | 2.04 | 4.96 | 5.57 | 5.43 | 5.46 | 7.5 | 7.9 | 11.0 | 11.5 |
| Gd | 6.3 | 6.1 | 6.1 | 6.1 | 6.1 | 6.1 | 26 | 25 | 25 | 25 | 28.2 | 30.7 | 48.0 | 46.1 |
| Tb | 0.93 | 0.94 | 0.94 | 0.93 | 0.94 | 0.93 | 3.95 | 4.04 | 3.98 | 3.96 | 4.88-4.9 | 4.9 | 7.6 | 7.4 |
| Dy | 5.25 | 5.30 | 5.34 | 5.27 | 5.32 | 5.28 | 23.00 | 24.43 | 23.99 | 24.03 | 26.8 | 27.3 | 42.0 | 42.0 |
| Ho | 0.99 | 0.97 | 0.98 | 0.96 | 0.98 | 0.96 | 4.95 | 5.12 | 5.00 | 5.01 | 5 - 5.13 | 5.1 | 8.2 | 7.8 |
| Er | 2.5 | 2.4 | 2.4 | 2.4 | 2.4 | 2.4 | 12.00 | 14.39 | 14.07 | 14.11 | 12.5 | 13.2 | 21.0 | 20.5 |
| Tm | 0.34 | 0.33 | 0.33 | 0.32 | 0.32 | 0.32 | 2.05 | 2.18 | 2.14 | 2.15 | 1.9-2.03 | 2.0 | 3.1 | 3.0 |
| Yb | 2.00 | 1.98 | 1.99 | 1.97 | 1.99 | 1.98 | 14.00 | 14.25 | 13.98 | 13.96 | 12.7 | 13.2 | 20.0 | 20.3 |
| Lu | 0.28 | 0.27 | 0.28 | 0.27 | 0.27 | 0.27 | 2.20 | 2.25 | 2.19 | 2.20 | 1.78 | 1.93 | 2.9 | 3.0 |
| Hf | 4.074 | 4.396 | 4.417 | 4.357 | 4.383 | 4.371 | 4 - 5.8 | 6.3 | 6.1 | 6.2 | 4.2 | 4.0 | 10.0 | 9.5 |
| Th | 1.21 | 1.19 | 1.20 | 1.19 | 1.19 | 1.19 | 23.4-25.1 | 23.9 | 23.4 | 23.5 | 16.6-16.7 | 16.0 | 26.0 | 24.2 |
| Results for 6.4.11 and 8.8.11 | | | | | | | | | | | | | | |
| | BHVO-2 | BHVO-2 | BHVO-2 | | | | NOD-A1 | NOD-A-1 | | | NOD-P-1 | NOD-P1 | GSPN-2 | GSPN-2 |
| Sc | 31.8 | 31.9 | 31.5 | | | | 12.4-15.7 | 12.3 | | | 9.7 | 10.5 | 13.0 | 14.5 |
| V | 317 | 326 | 322 | | | | 770.0 | 619.75 | | | 570 | 501 | 456.0 | 452.3 |
| Y | 25.5 | 25.1 | 24.9 | | | | 116.0 | 123.64 | | | 94 | 94 | 144.0 | 142.4 |
| Zr | 174 | 175 | 173 | | | | 233-436 | 329 | | | | 294 | 614.0 | 629.0 |
| Cd | | 0.122 | 0.130 | | | | 7.50 | 7.98 | | | 22.6 | 23.3 | 10.0 | 9.6 |
| Ba | 130 | 132 | 131 | | | | 1670.0 | 1531.6 | | | 3350 | 2690 | 1800.0 | 1790.5 |
| La | 15.2 | 14.6 | 14.4 | | | | 119.50 | 115.75 | | | 104 | 111 | 184.0 | 183.5 |
| Ce | 38 | 36 | 36 | | | | 730.00 | 753.57 | | | 294 | 327 | 620.0 | 617.9 |
| Pr | 5.3 | 5.1 | 5.0 | | | | 24.3 - 25 | 24.8 | | | 31-33 | 33 | 49.0 | 49.8 |
| Nd | 25 | 23 | 23 | | | | 94.00 | 103.44 | | | 119 | 138 | 198.0 | 205.7 |
| Sm | 6.2 | 5.8 | 5.8 | | | | 21.00 | 22.76 | | | 29.5 | 33.3 | 46.0 | 48.2 |
| Eu | 2.06 | 1.97 | 1.95 | | | | 4.96 | 5.46 | | | 7.5 | 7.9 | 11.0 | 11.7 |
| Gd | 6.3 | 5.9 | 5.8 | | | | 26 | 25 | | | 28.2 | 31.2 | 48.0 | 47.0 |
| Tb | 0.93 | 0.89 | 0.89 | | | | 3.95 | 3.96 | | | 4.88-4.9 | 4.9 | 7.6 | 7.5 |
| Dy | 5.25 | 5.05 | 5.02 | | | | 23.00 | 23.85 | | | 26.8 | 27.3 | 42.0 | 42.3 |
| Ho | 0.99 | 0.92 | 0.92 | | | | 4.95 | 4.99 | | | 5-5.13 | 5.0 | 8.2 | 7.9 |
| Er | 2.5 | 2.3 | 2.3 | | | | 12.00 | 14.09 | | | 12.5 | 13.2 | 21.0 | 20.8 |
| Tm | 0.34 | 0.31 | 0.31 | | | | 2.05 | 2.11 | | | 1.9-2.03 | 2.0 | 3.1 | 3.1 |
| Yb | 2.00 | 1.88 | 1.88 | | | | 14.00 | 13.92 | | | 12.7 | 13.1 | 20.0 | 20.4 |
| Lu | 0.28 | 0.26 | 0.26 | | | | 2.20 | 2.19 | | | 1.78 | 1.93 | 2.9 | 3.0 |
| Hf | 4.074 | 4.182 | 4.149 | | | | 4 - 5.8 | 6.1 | | | 4.2 | 4.0 | 10.0 | 9.6 |
| Th | 1.21 | 1.20 | 1.19 | | | | 23.4-25.1 | 24.6 | | | 16.6-16.7 | 16.8 | 26.0 | 25.8 |

| Instrumental precision | | | | | | | | | | |
|---|---|---|---|---|---|---|---|---|---|---|
| Results for 7.4.2011 | | | | | | | | | | |
| | 546-92 | 546-92 | 546-92 | RSD % | 495-693 | 495-693 | 495-693 | 495-693 | 495-693 | RSD % |
| Sc | 0.198 | 0.19 | 0.19 | *2.2* | 0.77 | 0.74 | 0.73 | 0.74 | 0.74 | *1.9* |
| V | 35.0 | 34.4 | 34.2 | *1.0* | 54.8 | 55.1 | 54.5 | 55.6 | 55.4 | *0.7* |
| Y | < 1 | < 1 | < 1 | | 1.1 | 1.1 | 1.1 | 1.1 | 1.1 | *0.2* |
| Zr | < 1 | < 1 | < 1 | | 2.0 | < 1 | < 1 | 1.8 | 1.5 | *11.9* |
| Cd | 52.7 | 52.2 | 52.3 | *0.4* | < 0.5 | < 0.5 | < 0.5 | < 0.5 | < 0.5 | |
| Ba | 50.7 | 50.5 | 50.7 | *0.2* | 53.6 | 54.1 | 53.7 | 53.7 | 54.1 | *0.4* |
| La | 0.386 | 0.387 | 0.392 | *0.6* | 1.135 | 1.146 | 1.151 | 1.144 | 1.144 | *0.5* |
| Ce | 0.785 | 0.790 | 0.799 | *0.7* | 2.413 | 2.427 | 2.429 | 2.409 | 2.415 | *0.3* |
| Pr | 0.095 | 0.093 | 0.094 | *1.0* | 0.290 | 0.290 | 0.290 | 0.286 | 0.287 | *0.6* |
| Nd | 0.360 | 0.366 | 0.373 | *1.5* | 1.129 | 1.146 | 1.154 | 1.151 | 1.155 | *0.8* |
| Sm | 0.076 | 0.080 | 0.076 | *2.1* | 0.236 | 0.238 | 0.239 | 0.238 | 0.235 | *0.6* |
| Eu | 0.039 | 0.040 | 0.040 | *0.7* | 0.085 | 0.086 | 0.085 | 0.085 | 0.085 | *0.5* |
| Gd | 0.071 | 0.070 | 0.070 | *0.2* | 0.220 | 0.222 | 0.222 | 0.217 | 0.220 | *0.9* |
| Tb | 0.011 | 0.010 | 0.010 | *0.6* | 0.034 | 0.034 | 0.034 | 0.034 | 0.033 | *1.4* |
| Dy | 0.058 | 0.059 | 0.060 | *1.3* | 0.196 | 0.195 | 0.196 | 0.200 | 0.201 | *1.2* |
| Ho | 0.012 | 0.012 | 0.012 | *1.0* | 0.040 | 0.040 | 0.040 | 0.039 | 0.040 | *1.2* |
| Er | 0.033 | 0.033 | 0.032 | *1.2* | 0.107 | 0.107 | 0.109 | 0.105 | 0.107 | *1.2* |
| Tm | 0.005 | 0.005 | 0.005 | *0.2* | 0.016 | 0.016 | 0.017 | 0.016 | 0.016 | *1.2* |
| Yb | 0.033 | 0.030 | 0.032 | *3.3* | 0.104 | 0.106 | 0.107 | 0.108 | 0.106 | *1.4* |
| Lu | 0.005 | 0.005 | 0.005 | *1.2* | 0.016 | 0.016 | 0.016 | 0.016 | 0.015 | *1.3* |
| Hf | < 0.5 | < 0.5 | < 0.5 | | < 0.5 | < 0.5 | < 0.5 | < 0.5 | < 0.5 | |
| Th | 0.087 | 0.086 | 0.086 | *0.5* | 0.251 | 0.248 | 0.244 | 0.247 | 0.244 | *1.1* |
| | | | | | | | | | | |
| Results for 6.4.11 and 8.8.11 | | | | | | | | | | |
| | 503-140 dup1 | 503-140 dup1 | 503-140 dup1 | 503-140 dup1 | 503-140 dup1 | RSD % | | | | |
| Sc | 0.20 | 0.19 | 0.19 | 0.19 | 0.19 | *3.4* | | | | |
| V | 21.0 | 20.3 | 20.8 | 20.7 | 20.8 | *1.2* | | | | |
| Y | < 1 | < 1 | < 1 | < 1 | < 1 | | | | | |
| Zr | < 1 | < 1 | < 1 | < 1 | < 1 | | | | | |
| Cd | 1.1 | 1.2 | 1.1 | 1.2 | 1.2 | *1.9* | | | | |
| Ba | 18.8 | 19.3 | 19.5 | 19.5 | 19.3 | *1.4* | | | | |
| La | < 0.1 | < 0.1 | < 0.1 | < 0.1 | < 0.1 | | | | | |
| Ce | 0.314 | 0.307 | 0.304 | 0.307 | 0.311 | *1.2* | | | | |
| Pr | 0.052 | 0.054 | 0.054 | 0.054 | 0.055 | *1.6* | | | | |
| Nd | 0.207 | 0.205 | 0.209 | 0.210 | 0.202 | *1.4* | | | | |
| Sm | 0.043 | 0.043 | 0.044 | 0.043 | 0.042 | *0.9* | | | | |
| Eu | 0.015 | 0.016 | 0.015 | 0.015 | 0.015 | *1.5* | | | | |
| Gd | 0.043 | 0.044 | 0.044 | 0.043 | 0.045 | *2.1* | | | | |
| Tb | 0.007 | 0.007 | 0.007 | 0.007 | 0.007 | *1.8* | | | | |
| Dy | 0.042 | 0.042 | 0.040 | 0.041 | 0.041 | *1.7* | | | | |
| Ho | 0.009 | 0.009 | 0.009 | 0.009 | 0.009 | *1.4* | | | | |
| Er | 0.025 | 0.025 | 0.025 | 0.025 | 0.025 | *0.9* | | | | |
| Tm | < 0.005 | < 0.005 | < 0.005 | < 0.005 | < 0.005 | | | | | |
| Yb | 0.025 | 0.026 | 0.025 | 0.025 | 0.025 | *1.6* | | | | |
| Lu | < 0.005 | < 0.005 | < 0.005 | < 0.005 | < 0.005 | | | | | |
| Hf | < 0.5 | < 0.5 | < 0.5 | < 0.5 | < 0.5 | | | | | |
| Th | 0.068 | 0.066 | 0.066 | 0.066 | 0.067 | *1.1* | | | | |

BHVO-2 (Wilson, 1997) was analyzed 7 times. The average difference between analyzed and recommended values was calculated for each sample and each REE, with a deviation of 3.03% (maximum 10.0%). NOD-A1 (Flanagan and Gottfried, 1980; Govindaraju, 1994) was

analyzed 4 times with an average deviation of 5.26% (maximum 19.9%) between measured and recommended values. Instrumental precision (standard deviation between repeated analyses of the same solutions) for all REE was 0.93%. Analyses of duplicate samples (one every ten samples) had a precision for all REE of 2.99%. Numbers in italics refer to calculated values.

Govindaraju, K., 1994. 1994 Compilation of Working Values and Descriptions for 383 Geostandards, *Geostandards Newsletter* 18, p. 1-158.

Flanagan, F. J. and Gottfried, D., 1980. USGS Rock Standards, III: Manganese-Nodule Reference Samples USGS-Nod-A-1 and USGS-Nod-P-1, *U.S. Geological Survey Professional Paper* 1155, p. 39.

Wilson, S. A., 1997. Data compilation for USGS reference material BHVO-2, Hawaiian Basalt, U.S. Geological Survey Open-File Report xxxxx.

# CHAPTER 5

## SOURCES OF REDUCED SULFUR AND THE FORMATION OF SULFIDES IN THE ATLANTIS II SEDIMENTS: EVIDENCE FROM SULFUR ISOTOPE DATA

In preparation for Mineralium Deposita

## 1. Introduction

The existence of hydrothermal venting in the Atlantis II Deep has been known for more than half a century (Miller, 1964). The initial discovery was followed by extensive sampling campaigns as part of the attempt to make a resource estimate of the metalliferous sediments (Degens and Ross, 1969; Bäcker and Richter, 1973). Ultimately about 600 sedimentary cores were taken in the brine covered area (~10 cores/$km^2$). However, most of the recent research attention has focused on the composition of the brine pool (Anschutz et al., 2000; Pierret et al., 2001; Taitel-Goldman and Singer, 2002; Schmidt, et al., 2003; Swift et al., 2012). The origins of the metalliferous sediments and their major components (especially sulfur) have received little attention since the early studies of Bischoff (1696), Kaplan et al. (1969), Shanks and Bischoff (1980), Pottorf and Barnes (1983) and Zierenberg and Shanks (1988).

In general, sulfide minerals in exhalative ores may form by (1) precipitation from a single high-temperature hydrothermal fluid (i.e., as in modern black smokers and ancient VMS deposits: Hannington et al., 1995), (2) precipitation due to reaction between two fluids of different composition (i.e., as in some SEDEX deposits: Cooke et al., 2000), or (3) precipitation during diagenesis, due to reaction between sediments, pore fluids, and upwardly diffusing hydrothermal fluids. In the Atlantis II Deep, precipitation from a single fluid (e.g., Shanks and Bischoff, 1977), mixing of two fluids (Pottorf and Barnes, 1983), and bacterially mediated processes (Shanks and Bischoff, 1980) have all been suggested as possible causes of sulfide mineral precipitation. The sources of reduced sulfur include

bacterial sulfate reduction with $\delta^{34}S$ values down to about -35‰ (Kaplan et al., 1969; Sweeney and Kaplan, 1973), direct hydrothermal input with $\delta^{34}S$ values of ~5‰, and possible contributions from non-hydrothermal sources (e.g., Red Sea background shales) with $\delta^{34}S$ values of -12 to +22‰ (mean +3‰: Manheim, 1974). Shanks and Bischoff (1980) suggested that various non-equilibrium processes, such as kinetic isotope effects (due to retarded equilibration between $NaSO_4$ and $H_2S$ at low temperatures), might also contribute to variable $\delta^{34}S$ of reduced sulfur in the brine pool and sediments (see also studies by Grinenko et al., 1969; Igumnov, 1976; Sakai and Dickson, 1978). This study gives new insights into several questions that have prevailed about the formation of metalliferous sediments in the Atlantis II Deep since their discovery about half century ago, among them the unexpectedly uniform $\delta^{34}S$ values of the sulfides in the sulfide-rich units and apparent lack of diagenetic sulfate reduction (Kaplan et al., 1969; Sweeney and Kaplan, 1973; Shanks and Bischoff, 1980). Detailed sampling and analysis of different sediment layers in archived cores in this study show that different sources of reduced sulfur appear to have been important at different times during the evolution of the basin. In particular, we examine the role of early diagenetic transformation of metals to sulfides as a fundamental control on the distribution and isotopic composition of reduced sulfur in the sediments. Some of these processes were also likely important in the formation of ancient stratiform base metal ore deposits where the availability of reduced sulfur is thought to have been a limiting factor in metal deposition (Large et al., 1996; Johnson and Skinner, 2003; Huston et al., 2006).

## 2. Depositional Environments

**2.1 Characteristics of the brine pool**

The main processes involved in metal deposition and the possible sources of sulfur in the Atlantis II brine pool and sediment are summarized in Figure 5.1. The stratified brine pool is metal-rich, anoxic (no $H_2S$ detected), and hot (68.3°C when last measured in 2008: Swift et al., 2012), and the bottom layer is extremely saline (~28 wt.% NaCl). The Lower Brine has a mean thickness of ~76 m (Anschutz et al., 1998) and reaches ~135 m at the deepest parts in the Southwest Basin. It is overlain by a number of cooler, more oxidized, and less saline brine layers, which have a combined thickness of ~50 m. Swift et al. (2012) proposed 5 layers in the Upper Brine that have temperatures from ~57 to 43°C. The Lower Brine is devoid of dissolved reduced sulfur, but contains sulfate: measurements vary from as high as 850 ppm $SO_4$ (Anschutz et al., 2000) to as low as 450 ppm (Bougouffa et al., 2013), whereas the Red Sea Deep Water contains about 2,850 ppm $SO_4$. The Upper Brines have intermediate concentrations (~1,800 ppm: Bougouffa et al., 2013). The development of the brine pool and the composition of the hydrothermal fluid inferred from the brines are discussed in Schoell and Hartmann (1973), Schoell and Faber (1978), Oudin and Cocherie (1988), Ramboz et al. (1988), Ramboz and Danis (1990), Blanc et al. (1995), Anschutz et al. (1995, 1998), Anschutz and Blanc (1996), and Pierret et al. (2001). The compositions of the different brine layers are influenced by four main processes: 1) hydrothermal venting, which is the main source of metals and sulfur, 2) dissolution of components brought into the brine with silicic and biogenic pelagic detritus, 3) transport of trace elements from the Red Sea Deep Water into the brine pool with Mn- and Fe-(oxy)hydroxides that scavenge and release elements due to changes in redox conditions, 4) dissolution of evaporites and

influx of cold brines from above or below. These different processes are described in Hartmann and Nielsen (1966), Schoell and Faber (1978), Zierenberg and Shanks (1986, 1988), Dupré et al. (1988), Anschutz et al. (1995), Pierret et al. (2001), and Laurila et al. (2014b).

**2.2 Pathways of sulfur, and metal deposition**

The general characteristics of the Atlantis II sediments are summarized in Table 5.1. Significant variation in the mineralogy and bulk composition is seen with depth in the sediment (stratigraphic units defined by Bäcker and Richter, 1973), as well as with distance away from the inferred location of the vent source(s). The Lower Sulfidic unit (SU1), Upper Sulfidic unit (SU2) and Amorphous Siliceous unit (AM) are enriched in metals and sulfur, whereas the Detrital Oxidic Pyritic (DOP) unit and Central Oxidic (CO) unit, as well as sediment farther away from the vents source(s), have lower Cu, Zn and sulfur concentrations (Figure 5.2). The sulfur-rich sediments contain abundant anhydrite (high $Ca/CO_2$), whereas the sulfur-poor sediments are dominated by either carbonate and detrital components or Mn- and Fe-(oxy)-hydroxides and authigenic clays. Pore water content gradually decreases with depth.

Figure 5.3 shows the range of previously determined $\delta^{34}S$ values of sulfides and sulfates in the most metal- and sulfide-rich stratigraphic units (SU1, SU2 and AM) from Zierenberg and Shanks (1988). The sulfur isotope values generally match observations from other modern seafloor hydrothermal systems in which sulfide is mainly leached from basaltic basement by

hydrothermal fluids and sulfate (now in anhydrite and barite) is mainly from seawater. Sulfides precipitated from the brine pool are isotopically lighter than sulfides in epigenetic veins, whereas the opposite is observed in sulfate. Highly negative $\delta^{34}S$ values are found in sulfides deposited during times of no or low-temperature hydrothermal venting (Kaplan et al., 1969; Pottorf and Barnes, 1983), as well as in shallower parts of the Deep under the Upper Brines (Figure 5.1; Kaplan et al., 1969; Sval'nov et al., 1984). These data indicate that both hydrothermal and bacteriogenic sulfide contributed to the sulfur budget of the Deep and had important spatial and temporal variability.

Large variations in the mineralogy and bulk compositions between individual layers (cm-scale and lamina only a few mm thick: Laurila et al., 2014a,b) also reflect rapid changes in primary precipitation in the brine pool and diagenetic changes in the sediment during burial. By far most of the sedimentation is from the brine pool, which is responsible for deposition over large areas. The Lower Brine is the main precipitation environment for sulfides, whereas poorly crystalline oxide phases form in the Upper Brine. Mn-(oxy)hydroxides from the Upper Brine dissolve as they settle through the Lower Brine, but Fe-(oxy)hydroxides remain stable and are deposited in sediments below the Lower Brine. These are important transport agents for metals from the Lower Brine and are responsible for much of the geochemical and mineralogical variation in sediments currently accumulating at the bottom of the Deep. Although deposition as Fe-(oxy)hydroxides predominates in the brine pool, Fe- is also present in the sulfide and Zn in the nonsulfide particulate matter in the brine pool (Hartmann, 1973, 1985). Zn and Cu are mainly

deposited as sulfide minerals, but also via adsorption onto surface active particles: Cu adsorption is dominant in the Upper Brines, whereas Zn is adsorbed in during settling in the Lower Brine (Laurila et al., 2014a). Sulfides also precipitate directly from the cooling hydrothermal fluid in the vein conduits close to the vents source(s). Some large sulfide grains in the sediments are thought to have been formed at high temperature in the vein conduits (Missack et al., 1989) and mechanically transported away from the vents (Pottorf and Barnes, 1983).

Sulfides formed by these two pathways are characterized by dominantly hydrothermal $\delta^{34}S$ values (+2 to +10‰: Kaplan et al., 1969, Shanks and Bischoff, 1980 and Zierenberg and Shanks, 1988). Minor sulfides formed in the Upper Brines have negative $\delta^{34}S$ values, indicative of bacterially mediated sulfate reduction (Sweeney and Kaplan, 1973; Sval'nov et al, 1984). The presence of bacteria has been documented in the Upper Brine (Trüper, 1969; Fiala et al., 1990) and also at the chemocline separating the Upper Brine from the Lower Brine, where abundant Fe-(oxy)hydroxides form (Hartmann, 1973; Butuzova et al., 1990). Enhanced deposition of organic matter from the chemocline apparently coincided with the formation of the metal- and sulfide-rich sedimentary units (Shanks and Bischoff, 1980; see below), but evidence has been mostly lacking for abundant bacteriogenic sulfide in the sediments. Watson and Waterbury (1969) found no evidence of bacterial activity in the Lower Brine or the metalliferous sediment (although Siam et al., 2012, recently cultivated bacteria from the sediment, and Bougouffa et al, 2013 found rare bacteria in the Lower Brine), and early workers dismissed the possibility that sulfate reduction was an important

source of sulfide in the sediment (Kaplan et al., 1969; Sweeney and Kaplan, 1973; Shanks and Bischoff, 1977, 1980; Zierenberg and Shanks, 1988). Kaplan et al. (1969) and Shanks and Bischoff (1980) both found sulfides with $\delta^{34}S$ values less than -20‰ in sediment formed during low-temperature venting (CO formation) and under euxinic conditions (DOP formation), but not associated with the main sulfidic units.

**2.3 Diagenesis**

Pyrite is not stable in the Lower Brine (Shanks and Bischoff, 1977; Pottorf and Barnes, 1983), although Fe-monosulfide is a primary precipitate in the brine pool (Brockamp et al., 1978). However, pyrite is abundant in the sediment and therefore likely formed diagenetically (Pottorf and Barnes, 1983). Textural evidence for diagenetic sulfide formation (e.g., framboidal pyrite reported by Sweeney and Kaplan, 1973, Pottorf and Barnes, 1983, and this study; similar fine-grained sphalerite aggregates: Bignell et al., 1976; Sval'nov et al., 1984; zoned sulfide grains with highly variable chemistry: Stephens and Wittkopp, 1969) can be found in the sediments from the distal parts of the basin and especially in the shallower parts of the Deep under the Upper Brine. The amount of framboidal pyrite, in particular, increases with depth (Chapter 2); tiny pyrite grains are most common, but larger grains with diagenetic rims are also documented. Diagenetic sulfide growth is consistent with pore water concentrations of metal that decrease sharply with burial (Anschutz et al., 2000). Sweeney and Kaplan (1973) reported $\delta^{34}S$ distinctly lower values in framboidal than than in cubic pyrite, and Shanks and Bischoff (1980) noted that samples with large negative $\delta^{34}S$ values are dominated by pyrite, whereas samples with higher values are dominated by

sphalerite and chalcopyrite. However, clear evidence for the importance of diagenetic pyrite in the metal- and sulfur-rich sedimentary units was not reported by the early workers. Diagenetic sulfides are particularly abundant in the distal part of the basin, but there is little information available on the isotopic differences between the proximal and distal environments.

**2.4 Sulfate precipitation**

The $\delta^{34}S$ values of sulfate in the Atlantis II Deep are very close to those reported for seafloor hydrothermal systems at open ocean MORs (~20-22‰) and close to present-day seawater (~21‰). Moreover, little variation has been observed in the $\delta^{34}S$ of dissolved $SO_4$ in the different brine layers of the Atlantis II Deep, despite the ~4 times decrease in $SO_4$ concentration from the Red Sea Deep Water into the Lower Brine (Zierenberg and Shanks, 1986; Figure 5.1). Anhydrite occurs in the Atlantis II Deep as large sill-like bodies and as sub-vertical crosscutting veins that mark the locations of concentrated high-temperature hydrothermal upflow (Zierenberg and Shanks, 1983; Oudin et al., 1984). Zierenberg and Shanks (1988) found average $\delta^{34}S$ of about +22‰ in the vein anhydrite and +24‰ in the layer-type anhydrite (referred to as "brine pool precipitate" by these workers), suggesting different formation pathways. The highest $\delta^{34}S$ values in the layer-type anhydrite (+25‰) are much higher than sulfate in the Lower Brine (+21.5‰) and also higher than sulfate in the surrounding Miocene evaporites sampled during DSDP in 1973 (21.4-23.0‰: Zierenberg and Shanks, 1986).

Sval'nov et al. (1984) reported the presence of massive barite crusts on bathymetric highs in the central part of the Deep, where the seafloor directly underlies the Upper Brine. These crusts are similar to the "bathtub ring" barite deposits surrounding some ancient shale basins (e.g., Selwyn Basin: Goodfellow et al., 1993) and interpreted to form by reaction between Ba enriched in the lower water column with sulfate-enriched seawater (cf. Hanor and Baria, 1977; Koski and Hein, 2003). The bulk $\delta^{34}S$ of the barite crust is 14.3‰ (average of 10 bulk samples). The crusts contain up to 1.2 wt.% Zn and sphalerite with very low $\delta^{34}S$ values (-26‰).

## 3. Methodology

### 3.1 Sampling and geochemical analysis

In order to gain a better understanding of the spatial and temporal variations in sulfur sources in the accumulating sediments, $\delta^{34}S$ analyses were carried out on different phases in 46 samples from different layers in 9 sediment cores in the area of the Deep covered by the Lower Brine (Laurila et al., 2014a,b). The relevant mineralogical, chemical, and isotopic data for the samples considered in this study (n = 46) are provided in Table 5.2. The locations of the cores are shown in Figure 5.4 and full descriptions of the samples are presented in Appendix A. All cores were collected during the *R/V Valdivia* cruise 29 in 1980. After recovery, the cores were split, with one half being sealed and stored in a cool warehouse. When reopened in 2010, the archived cores were in excellent condition and still moist.

Samples were collected using <2 cm-diameter minicores or cut from the core box with a spatula along layering to attain visually homogenous samples. The samples were dried at 40°C, during which salt crystallized out of the pore water. After drying all samples contained variable amount of salt (from a few up to 70 wt.%). This contrasts with most earlier studies in which samples were washed to remove salt before chemical analyses; a process that undoubtedly influenced the mineralogy and bulk compositions (Laurila et al., 2014a). Dry samples were pulverized in an agate ball mill, and analyzed for geochemistry by multiple analytical methods described in Laurila et al. (2014a). Total sulfur was analyzed by thermal-conductivity (TCD) after combustion at 1800°C with VarioEL III at the University of Ottawa (Hatch Laboratories) and sulfate sulfur by infrared absorption spectroscopy (IR) after combustion at 550°C at the Activation Laboratories. The amount of reduced sulfur remaining in the samples was calculated from total S minus sulfate S. This is not the original $S_{red}$, owing to oxidation of sulfides during core storage (Laurila et al., 2014a), although the values correlate with the mineralogy of the cores determined shortly after they were sampled and our own re-logging. Because some sulfate has undoubtedly originated from oxidation of sulfide, the amount of reduced sulfur calculated in this way is a minimum value and the measured sulfate a maximum. For this reason, normative mineralogy is used for mineralogical characterization of the samples. The complete geochemical analyses and details of the analytical methods are presented in Appendix C.

### 3.2 Mineralogy

The mineralogy of the analyzed samples was reconstructed from a combination of detailed petrography and normative calculations from the bulk chemistry (Chapter 2 and Table 5.1). After correcting for the salt content, the siliciclastic detrital component was calculated according to immobile element concentrations (e.g., Al, Zr, Ti, Sc). Detrital layers contain about 35 wt.% siliciclastic material, on average. In all other layer types, the siliciclastic detrital component is typically less than 10 wt.% (and <5 wt.% in the clay-rich and anhydrite-rich layers). In samples with molar $CO_3$>$SO_4$, Ca was first attributed to calcite, then anhydrite; in samples with molar $SO_4$>$CO_3$, Ca was first attributed to anhydrite, then calcite. Any residual Ca was assumed to be present in clays. The amount of dolomite in these samples was estimated from the residual Mg concentration and reported as end-member $MgCO_3$; residual $CO_3$ after calcite and dolomite formation was first attributed to $MnCO_3$ (according to the bulk Mn content) and the remainder to $FeCO_3$. Residual Mn after forming Mn-carbonate was assumed to be present as Mn-(oxy)hydroxides, which are present in abundance only in the Mn-rich layers (indicative of formation under more oxic brine conditions).

The most metal-rich layers contain about 15 wt.% anhydrite. The amount of sulfate present as barite is never more than a few percent. Anhydrite and barite are the only known primary sulfates in the Atlantis II Deep, thus the higher molar amount of $SO_4$ than Ca and Ba in many of the samples, indicates the presence of other sulfates. These are mainly secondary sulfates formed during core storage, and for the purposes of the normative calculation are attributed to original metallic sulfides. The most metal-rich layers contain

about 15 wt.% sulfides, on average, with subequal amounts of pyrite, chalcopyrite, and Zn-sulfide. An important observation is that there is more Zn in the samples than can be accounted for by the residual sulfur after the formation of anhydrite, secondary metal sulfates, and other sulfides. This reflects the presence of locally abundant nonsulfidic Zn-bearing minerals. Because the samples have experienced varying degrees of sulfide oxidation (and formation of secondary sulfate), the $\delta^{34}S$ values of the primary minerals in mixtures were estimated from measurements of pure samples and from isotopic mass balances based on the reconstructed mineralogy. Importantly, large and euhedral sulfide grains, which are more resistant to dissolution due to their smaller surface area to volume ratio, have been the focus of many previous sulfur isotope studies, whereas fine-grained sulfides (e.g., fine-grained framboidal pyrite) appear to have been more readily oxidized (Chapter 2) and therefore account for a larger proportion of the secondary sulfates.

**3.3 Sulfur isotope analyses**

The topmost sample from each core was selected to study the spatial variation in $\delta^{34}S$ values within the Deep (n= 9; Figure 5.4). Because the samples from AM have experienced little or no diagenesis as a result of burial, these samples are considered to reflect the primary precipitation from the Lower Brine. They are all rather similar in terms of texture and mineralogy (e.g., high pore water content, small average grain size, high proportion of amorphous compounds) and likely had a similar post-depositional history, including after recovery of the cores. Additionally, a fence of 3 cores from the Southwest Basin to the West Basin (373, 503, 617) was sampled in greater detail (n=36; Figure 5.5) to study diagenetic

changes with depth and possible variations related to distance from the current vent source(s) in Southwest Basin. Also, one detrital sample from the lowermost DOP (495-1088) was included to study the end-member sulfide produced by sulfate reducing bacteria.

Sulfide and sulfate were extracted separately from the 46 samples at the University of Ottawa. In the first step, reduced sulfur in the sample was extracted with HCl. The sulfur gas was directed to zinc acetate dihydrate traps causing precipitation of zinc sulfide. Sulfur was stabilized as silver sulfate by adding silver nitrate, which reacts with sulfur from the zinc sulfide to form silver sulfide. Sulfate sulfur in the sample was extracted by addition of "Thode reagent", followed by zinc acetate dihydrate and silver nitrate as in step 1 (Thode et al., 1961; Gröger et al., 2009). In samples with >75 wt.% anhydrite and very little sulfide (373-586, 503-235, 617-551), sulfate was extracted directly by step 2. For some samples with low total sulfide (e.g., samples 373-751, 617-9), large sample sizes (up to 1 g) were required to extract enough reduced sulfur for isotopic analysis, resulting in poor precision in the analysis (see duplicates in Table 5.2).

Sulfur isotope measurements were conducted at the Hatch Laboratories at the University of Ottawa. ~0.8 mg of $Ag_2S$ was weighed into tin capsules with 5 mg of $WO_3$. Capsules were combusted on an Elementar Micro Elemental Analyzer followed by "trap and purge" separation and on-line analysis by continuous-flow with a Thermo Finnigan DeltaPlus XP isotope ratio mass spectrometer (IRMS) coupled with a ConFlo IV. One in ten samples was analyzed in duplicate to monitor sample homogeneity and analytical precision; duplicate

values deviated (absolute $\delta^{34}S$) <0.21‰ for sulfides and <1.44‰ for sulfates (Table 5.2). $\delta^{34}S$ values of sulfide are very consistent between different extractions; $\delta^{34}S$ of values of sulfate have a larger of variation.

To assess the possible cross-contamination of primary sulfate (in anhydrite) by secondary sulfate, we analyzed representative samples of pure anhydrite (373-586, 503-235, 617-551) to establish the end-member sulfate $\delta^{34}S$ values (Figure 5.6A). Estimates of the $\delta^{34}S$ values of the secondary sulfates were determined in Figure 5.6B. Sulfide oxidation in the cores is unlikely to fractionate sulfur isotopes (Nakai and Jensen, 1964; Rye et al., 1992; Seal, 2006), thus we interpret the low $\delta^{34}S$ of the samples with abundant metal-sulfate to reflect the primary sulfides. Sulfides that are still present in the samples represent only those minerals most resistant to post-depositional or post-recovery oxidation. The isotopic compositions of the preserved sulfides and the secondary metal-sulfates differ somewhat because the original minerals formed under somewhat different conditions (see below).

## 4. Results

All results are presented in Table 5.2. $\delta^{34}S$ in reduced sulfur has a range from -22 to +10‰, consistent with a range of diagenetic and hydrothermal sources. The average $\delta^{34}S$ value of the sulfide fraction is -7.0‰ in the DOP unit (formed before and during the beginning of hydrothermal venting), and +4.6‰ in the other units. However, negative $\delta^{34}S$ values of sulfide are also found in the sediment deposited during hydrothermally active periods, in particular in the CO unit, which was formed during a period of mainly low-temperature

hydrothermal activity (e.g., sample 503-516: Table 5.2). In contrast, in units SU1, SU2 and AM, formed during high-temperature hydrothermal activity, hydrothermal sulfide is predominant. The $\delta^{34}S$ in sulfate varies from that in pure anhydrite (~23‰) to as low as -12‰ in samples (e.g., 503-987; Table 5.3) with significant amount of sulfate but low anhydrite content (i.e., sulfate fraction dominated by secondary sulfates: Figure 5.7B). The low $\delta^{34}S$ values are interpreted to be due to oxidation of primary sulfides containing light sulfur, in particular diagenetic sulfides that were most susceptible to oxidation during core storage (Chapter 2). This is particularly common in the distal cores.

Throughout core 373, the $\delta^{34}S$ of sulfate is lower than the $\delta^{34}S$ of the preserved sulfide, consistent with the abundance of fine-grained framboidal pyrite that was oxidized after recovery. Sample 373-555 (unit SU1) is an example. It has high total sulfur concentration (40 wt.% $SO_4$), of which 25 wt.% is present as sulfate and the rest as sulfide. The $\delta^{34}S$ of the preserved $S_{red}$ is 2.7‰, whereas the sulfate fraction has a $\delta^{34}S$ value of -2.0‰. In this sample approximately 2.7 wt.% S is present in anhydrite (~11 wt.% anhydrite); 5.8 wt.% S is present as secondary metal-sulfates. Assuming $\delta^{34}S$ of 22‰ in pure anhydrite, isotopic mass balances indicate that the metal-sulfate fraction must have $\delta^{34}S$ value of -10 ‰. The greatest uncertainty in the calculation is the estimate of normative anhydrite (Chapter 2). The results for all samples indicate that sulfides with the largest negative $\delta^{34}S$ values contributed most of the secondary sulfates, consistent with petrographic observations (i.e., abundance of relict diagenetic sulfide grains).

The variations in the $\delta^{34}S$ values of sulfate and sulfide with depth in cores 373, 503 and 617 are shown in Figure 5.5. As noted in previous studies, there is little difference in the average $\delta^{34}S$ of sulfide between the different metal- and sulfur-rich units (+5.7‰, +5.0‰, and +6.5‰ in SU1, SU2 and AM, respectively). From this, it has been generally concluded that the preserved sulfide fraction in the samples is mainly hydrothermal in origin. $\delta^{34}S$ values for sulfide in the DOP and CO units (-6.1‰, and +3.1‰, respectively) have previously been interpreted in terms of bacteriogenic sulfide (Kaplan et al., 1969; Shanks and Bishoff, 1980), and one sample from this study (495-1088 from the lower part of DOP) has a $\delta^{34}S$ value in sulfide lower than -20‰ (Figure 5.7A).

The amount of anhydrite in all units increases with proximity to the vent source(s) in the Southwest Basin (from 3.2 wt.% in core 373 to 18 wt.% in core 503 and 25 wt.% in core 617), and there is a strong correlation ($r^2$=0.56) between the normative anhydrite and the $\delta^{34}S$ values in bulk sulfate (Figure 5.6A). The proximal core (617) appears to preserve the original sulfide/sulfate relationship (i.e., heavy sulfur in sulfate, light sulfur in sulfide). The difference of about 15‰ is similar to what one might expect in other seafloor hydrothermal systems (e.g., Shanks, 2001). Sample 503-235 is from a thick layer of anhydrite and contains 93 wt.% anhydrite; the $\delta^{34}S$ value of this sample (23.3‰, Table 5.2) is consistent with anhydrite precipitated in the brine pool (Zierenberg and Shanks, 1986, 1988; Figure 5.3). However, sulfur in the sill-like bodies of anhydrite is heavier than either local seawater $SO_4$ or Miocene evaporites. Lower $\delta^{34}S$ values in sulfate in the vein anhydrite than in the brine pool anhydrite (Figure 5.3: Zierenberg and Shanks, 1988) are interpreted to reflect

contributions of lighter sulfur from the hydrothermal fluids in the veins. Samples with abundant secondary sulfates and no anhydrite show little or no difference in $\delta^{34}S$ values between sulfide and sulfate sulfur. This appears to be the dominant case in the distal cores (503 and 373), which contained much less anhydrite.

The stratigraphic variation of $\delta^{34}S$ in sulfide is illustrated in Figures 5.7A, together with previously published data. $\delta^{34}S$ values of sulfides in the most metal- and sulfide-rich units (SU1, SU2 and AM) plot between +1 and +10‰ with few outliers. In contrast, samples from DOP show strong evidence for bacterial sulfate reduction with highly negative $\delta^{34}S$ values in some samples. One sample from the flanks of the Deep of unknown age also has very low $\delta^{34}S$ (bright yellow box in in Figure 5.7A: Sval'nov et al., 1984). Sulfides in CO have a similar range of values but fewer samples.

The spatial variation of the $\delta^{34}S$ values in the uppermost sample of each core (unit AM or SU2) is shown in Figure 5.4. For the samples analyzed in this study, the $\delta^{34}S$ values do not appear to vary significantly with proximity to the inferred location of the currently active venting in the Southwest Basin. However, published data from areas that are shallower than the Lower Brine have strongly negative $\delta^{34}S$ (<-25‰). This suggests that hydrothermal sulfide is limited to the Lower Brine, whereas sulfide formed in the Upper Brines has a strong contribution from bacterial sulfate reduction (see Trüper, 1969; Watson and Waterbury, 1969; and Fiala et al., 1990). According to our data (e.g., samples 373-93, 373-751 and 617-508 from units SU2, SU1 and SOAN, respectively: Table 5.3) bacteriogenic

sulfides exist as a minor phase also in the metal-rich stratigraphic units (SU1, SU2 and AM), even if they are more important in units DOP and CO and in more distal sediments.

## 5. Discussion

### 5.1 Sulfides

The sulfide fraction of the sediments has a narrow range of $\delta^{34}S$ values throughout the metal- and sulfide-rich units (SU1, SU2 and AM: total range from -2.9 to 9.7‰, with averages for the units of 5.0 and 6.5‰, Table 5.2). These data are consistent with earlier studies (Figure 5.7), and the spatial distribution confirms that hydrothermal sulfides were deposited throughout the Deep. The suggestion is that the hydrothermal plume source spread out laterally as far as the distal parts of the Deep (up to about 10 km). A similar conclusion can be drawn from the $\delta^{34}S$ values of sulfide in just the topmost sediment (Figure 5.4). Somewhat lower $\delta^{34}S$ values, on average, in the distal than proximal part of the Deep (Table 5.2) are mainly a consequence of the absence of unit DOP (with the largest negative $\delta^{34}S$ values) in the vent proximal cores.

The measured sulfide fraction does not include sulfides that were most susceptible to oxidation during core storage. These are now present as metal sulfates, which have consistently lower $\delta^{34}S$ values, suggesting that the oxidized sulfides were paragenetically distinct from those still preserved in the cores and the focus of earlier studies. The oxidized sulfides are interpreted to have been mainly fine-grained or framboidal pyrite that formed during diagenesis (e.g., Berner, 1984; Sweeney and Kaplan, 1973) and were abundant in the

sediments of the Atlantis II Deep, especially in the vent distal sediment and in the lower stratigraphic units (Chapter 2). Calculated $\delta^{34}S$ values for the oxidized sulfide fraction, based on normative mineralogy and end-member $\delta^{34}S$ values range from -55‰ to +37‰ (grey graph in Figure 5.7). Samples with sub-equal amount of anhydrite and metal-sulfates are characterized by lower $\delta^{34}S$ in AM and SU2 (upper strata) than in SU1 (lower strata) suggesting that the proportion of diagenetic sulfide increases with depth in the sediments. Negative $\delta^{34}S$ values measured in the sulfide fraction in samples 373-798, 495-1088, 503-516, 503-987 and 617-508 (Table 5.2) confirm that bacterial or chemical sulfate reduction is an important process in the sediments. Our data show that diagenetic sulfides are a minor but important component in all stratigraphic units (SU1, SU2 and AM), and not just in DOP and CO, as previously thought (Table 5.3). In other samples with much higher $\delta^{34}S$ values, we suggest that some of the samples originally contained sulfides with $\delta^{34}S$ values as low as -30‰ (Table 5.3), but the total sulfate is now only ~3‰ lighter than sulfides because of the presence of significant anhydrite ($\delta^{34}S$ always >+20‰).

According to Seal and Wandless (2003), conditions such as high sedimentation rate, limited supply of organic matter and sulfate, as well as low replenishment of the pore waters (e.g., conditions like those in the Atlantis II Deep during formation of the metal-rich units SU1, SU2 and AM) are favorable for bacterial sulfate reduction that produces sulfide with low $\delta^{34}S$. DOP and CO were formed at times of lower hydrothermal sulfide supply (with higher $SO_4$ content) and contain sulfides with large negative $\delta^{34}S$ values (Figure 5.7A and Table 5.2). They were deposited in shallower parts of the Deep that are currently under the more

oxic upper brine. Sval'nov et al. (1984) measured $\delta^{34}S$ values of -26.1‰ in sphalerite at station 407, and Kaplan et al. (1969) measured $\delta^{34}S$ values of -33.4‰ in sphalerite in their core 95K (locations shown in Figure 5.4). The latter is associated with a highly permeable fossiliferous layer, suggesting sphalerite precipitation below the seafloor and possibly facilitated by the presence of organic matter. Shanks and Bischoff (1980) estimated according to $C_{org}$ concentration and taking into account the dilution effect by total sedimentation rates that organic matter deposition rates were ~3 times higher during the period of abundant metal-sulfide deposition owing to enhanced bacterial growth at the chemocline overlying the Lower Brine. This may have been a major source of reduced carbon for bacterial sulfate reduction.

At times of high-temperature hydrothermal discharge (Figure 5.8A), reduced sulfur ($\delta^{34}S$ ~3 to 7‰) was incorporated in sulfides deposited basin-wide from the hydrothermal plume. Metals deposited mainly with Fe-(oxy)hydroxides during subsequent phases of reduced or lower-temperature hydrothermal activity (Figure 5.8B) were ultimately incorporated in diagenetic sulfides (Laurila et al. 2014a) with much lower $\delta^{34}S$ values. Bacteriogenic sulfide present in the Upper Brine might also have contributed to sulfide deposition in the distal part of the Deep and to the unexpected increase in the Cu/Zn ratio of the sediments with distance from the source (Figure 5.8) as discussed in Laurila et al. (2014a).

**5.2 Anhydrite and barite**

Experimental studies by Blount and Dickson (1969) show that the solubility of anhydrite in a fluid compositionally similar to the Lower Brine (and the inferred hydrothermal fluid) is at a minimum around 200-250°C, and thus anhydrite may precipitate either due to heating of the pore water (Brewer et al., 1971; Shanks and Bishoff, 1977; Cole, 1988; Monnin and Ramboz, 1996) or cooling the hydrothermal fluid (from ~400°C indicating by fluid inclusions in vein anhydrite: Oudin et al., 1984). The first likely explains the formation of the large sill-like bodies, and the latter formation of anhydrite in the vent fluid conduits (Zierenberg and Shanks, 1983; Oudin et al., 1984). Higher $\delta^{34}S$ values in the sill-like bodies of anhydrite than in either local seawater $SO_4$ or in Miocene evaporates suggest that light sulfur was depleted in the sedimentary pore water. This could be explained by bacterial reduction of the isotopically light fraction of $SO_4$ in the pore water, which would leave the remaining pore-water sulfate enriched in heavy sulfur.

Anschutz et al. (2000) observed an increase in the dissolved $SO_4$ concentration with depth in the pore waters of a proximal core (683; location in Figure 5.4) and a decrease in dissolved $SO_4$ concentration with depth in a distal core (684). Both cores had the same concentration in the uppermost sedimentary pore water (equivalent to that of the Lower Brine). Three possibilities have been considered for the increase in $SO_4$ concentration in the pore water close to the vent source(s). Hydrothermal fluids could entrain $SO_4$ in close proximity to the vents, a process that has been observed in MOR hydrothermal vents (Alt et al., 1996; Shanks, 2001). $SO_4$ could also have been introduced to the brine pool and pore water with cold brines from outside the Deep, but this would not explain the $SO_4$

enrichment being limited to the vent proximity. A third explanation for the increase in the $SO_4$ concentration of pore waters close to the vents is the dissolution of anhydrite during diagenesis. The temperature of the pore waters is expected to decrease rapidly away from the vent conduits; mineral thermometers confirm that temperatures drop below 100-150°C within <<1 km (Zierenberg and Shanks 1983, 1988; Cole, 1988). Thus, dissolution of anhydrite during cooling and burial is expected.

Kaplan et al. (1969) measured $\delta^{34}S$ of dissolved $SO_4$ in the interstitial waters. In general higher $\delta^{34}S$ values were measured in vent distal cores (core 120K: Figure 5.4) than in vent proximal cores (core 84K) suggesting a contribution of isotopically light sulfur from hydrothermal sources proximal to the known vents. The interpretation is that the pore water in proximity to the vents is replenished by hydrothermal input of $SO_4$ with low $\delta^{34}S$, whereas dissolved $SO_4$ in pore water distal to the vents gradually becomes heavier due to continuous sulfate reduction, explaining heavier sulfur in brine pool precipitates than in vein anhydrite (Figure 5.3: Zierenberg and Shanks, 1988).

Barite has been found in the sediments locally as delicate radial aggregates up to 30 μm in diameter (Figure 2.9D in Chapter 2). Textures and trace element geochemistry suggest that barite precipitation was associated with high-temperature hydrothermal activity (e.g., vent proximal alteration: Chapter 3), due to interaction between Ba in the hydrothermal fluid and $SO_4$ in the sedimentary pore water. Barite is undersaturated in the current Lower Brine (Shanks and Bischoff, 1977; Figure 2.19) despite the high dissolved Ba concentration (0.9

ppm: Manheim, 1974; 2.1 ppm: Pierret et al., 2001). Therefore, barite precipitation was most likely a consequence of local $SO_4$- or Ba- enrichment in the pore water caused by entrainment proximal to the vents, consistent with $\delta^{34}S$ values similar to those of anhydrite (Zierenberg and Shanks, 1988 results in Figure 5.7A are for sedimentary barite).

## 6. Conclusions

Abundant light sulfur in secondary sulfates in the cores from the Atlantis II Deep is derived from the oxidation of original diagenetic sulfides. High $\delta^{34}S$ values of anhydrite layers in the sediment also appear to reflect changes in the isotopic composition of $SO_4$ in the pore waters due to bacterial sulfate reduction (i.e., heavy sulfate remaining from bacterial sulfate reduction). Thus diagenetic processes, most probably within a few meters of burial (<5,000 years) have played an important role in formation of both sulfides and sulfates in the Atlantis II muds. These observations are also consistent with primary metal deposition as nonsulfidic particles, followed by rapid transformation to sulfides during early diagenesis (Chapter 2). In particular, most of the metal deposited with Fe-(oxy)hydroxides, representing up to 30% of the total Cu and Zn in the sediments (Chapter 2), is ultimately transformed to sulfides during burial and diagenesis. This is supported by the abundant framboidal textures and increase in reduced sulfur with depth in the sediments (Figure 2.11 in Chapter 2; Table 5.1).

The very large range of $\delta^{34}S$ values for sulfide in the Atlantis II Deep (from -25‰ to +10‰) is atypical of modern massive sulfides formed at open ocean hydrothermal systems (Figure

5.9) but more typical of sulfide deposits formed in sedimented environments, which are strongly influenced by bacteriogenic and diagenetic sources of sulfur (Shanks, 2001; Seal, 2006). The sulfide $\delta^{34}S$ values in the metal- and sulfide-rich layers of the Atlantis II Deep are very similar to MOR systems (e.g., TAG hydrothermal field: ~4.5‰ to 9‰: Gemmell and Sharpe, 1998; Petersen et al., 2000) suggesting leached basaltic sulfur is the main source of reduced sulfide. Likewise, anhydrite in the Atlantis II Deep has $\delta^{34}S$ values very close to contemporaneous seawater, similar to the anhydrite in MOR hydrothermal systems (e.g., 20-23‰: Chiba et al., 1998). However, the increase in diagenetic sulfide with depth in the cores more closely resembles that of other sediment-hosted massive sulfide deposits in which bacterially mediated sulfate reduction played a more important role (Hannington et al., 2005).

## References


Alt, J. C, Laverne, C., Vanko, D., Tartarotti, P., Teagle, D. A. H., Bach, W., Zuleger, E., Erzinger, J., Honnorez, J., Pezard, P. A., Becker, K., Salisbury, M. H. and Wilkens, R. H., 1996, Hydrothermal alteration of a section of upper oceanic crust in the eastern equatorial Pacific: a synthesis of results from Site 504 (DSDP Legs 69, 70, and 83, and ODP Legs 111, 137, 140, and 148)*, in* Alt, J. C., Kinoshita, H., Stokking, L. B. and Michael, P. J., eds., *Proc. ODP, Sci. Results* 148, p. 417-434.

Anschutz, P., Blanc, G. and Stille, P., 1995, Origin of fluids and the evolution of the Atlantis II deep hydrothermal system, Red Sea: Strontium isotope study. *Geochim. Cosmochim. Acta* 59 (23), p. 4799-4808.

Anschutz, P., Turner, J. S. and Blanc, G., 1998, The development of layering, fluxes through double-diffusive interfaces, and location of hydrothermal sources of brines in the Atlantis II Deep: Red Sea. *Jour. Geophys. Res.* 103 (C12), p. 27809-27819.

Anschutz, P. and Blanc, G., 1996, Heat and salt fluxes in the Atlantis II Deep (Red Sea). *Earth Planet. Sci. Lett.* 142, p. 147-159.

Anschutz, P., Blank, G., Monnin, C. and Boulècue, J., 2000, Geochemical dynamics of the Atlantis II Deep (Red Sea): II. Composition of metalliferous sediment pore waters. *Geochim. Cosmochim. Acta* 64 (23), p. 3995–4006.

Berner, R. A., 1984, Sedimentary pyrite formation: An update. *Geochim. Cosmochim. Acta* 48, p. 605-615.

Bertram, C., Krätschell, A., O'Brien, K., Brückmann, W., Proelss, A. and Rehdanz, K., 2011, Metalliferous sediments in the Atlantis II Deep—Assessing the geological and economic resource potential and legal constraints. *Res. Policy* 36, p. 315-329.

Bignell, R. D., Cronan, D. S. and Tooms, J. S., 1976, Metal dispersion in the Red Sea as an aid to marine geochemical exploration. *Inst. Mining Metall. Trans.* 84 (B), p. 274-278.

Blanc G., Boulègue J. and Michard A., 1995, Isotope compositions of the Red Sea hydrothermal end-member. *C. R. Acad. Sci.* 320, p. 1187-1193.

Blount, C. W. and Dickson, F. W., 1969, The solubility of anhydrite ($CaSO_4$) in NaCl-$H_2O$ from 100 to 450°C and 1 to 1000 bars. *Geochim. Cosmochim. Acta* 33, p. 227-245.

Brewer, P. G., Wilson, T. R. S., Murray, J. W., Munns, R. G., and Densmore, D. C., 1971, Hydrographic observations on the Red Sea brines indicate marked increase in temperature. *Nature* 231, p. 37-38.

Bougouffa, S., Yang, J. K., Lee, O. O., Wang, Y., Batang, Z., Al-Suwailem, A. and Qian, P. Y., 2013, Distinctive microbial community structure in highly stratified deep-sea brine water columns. *Appl. Environ. Microbiol.* 79 (11), p. 3425-3437.

Brockamp, O., Goulart, E., Harder, H. and Heydemann, A., 1978, Amorphous copper and zinc sulfides in the metalliferous sediments of the Red Sea. *Contr. Mineral. Petrol.* 68, p. 85-88.

Butuzova, G. Yu., Drits, V. A., Morozov, A. A. and Gorschkov, A. I., 1990, Process of formation of iron- manganese oxyhydroxides in the Atlantis-II and Thetis Deeps of the Red Sea. *Spec. Publs. int. Ass. Sediment.* 11, p. 57-72.

Bäcker, H. and Richter, H., 1973, Die rezente hydrothermal-seidimentärelagerstätte Atlantis II-tier im Roten Meer. *Geol. Rundsch.* 62, p. 697-740.

Chiba, H., Uchiyama, N. and Teagle, D. A. H., 1998, Stable isotope study of anhydrite and sulfide minerals at the TAG hydrothermal mound, Mid-Atlantic Ridge 26°N, *in* Herzig, P. M., Humphris, S. E. and Miller, J., eds., *Proc. ODP 158, Scientific Results*, College Station, TX, p. 85-90

Cole, T. G., 1988, The nature and origin of smectite in the Atlantis II Deep, Red Sea. *Can. Mineral*. 26, p. 755-763.

Cooke, D. R., Bull, S. W., Large, R. R. and McGoldrick, P. J., 2000, The Importance of Oxidized Brines for the Formation of Australian Proterozoic Stratiform Sediment-Hosted Pb-Zn (Sedex) Deposits. *Econ. Geol. Bull.* 95 (1), p. 1-18.

Degens, E. T. and Ross, D. A., 1969, *Hot Brines and Recent Heavy Metal Deposits in the Red Sea*. Springer-Verlag Inc., New York, 600 p.

Dupré, B., Blanc, G., Boulègue, J. and Allègre, J., 1988, Metal remobilization at a spreading centre studied using lead isotopes. *Nature* 333, p. 165-167.

Fiala, G., Woese, C. R., Langworthy, T. A. and Stetter, K. O., 1990, *Flexistipessinusarabici*, a novel genus and species of eubacteria occurring in the Atlantis II Deep brines of the Red Sea, *Arch. Microbiol*. 154, p. 120-126.

Gemmell, J. B. and Sharpe, R., 1998, Detailed sulfur-isotope investigation of the TAG hydrothermal mound and stockwork zone, 26°N, Mid-Atlantic Ridge, *in* Herzig, P. M., Humphris, S. E. and Miller, J., eds., *Proc. ODP 158, Scientific Results*, College Station, TX, p. 71-84

Goodfellow, W. D., Lydon, J. W. and Turner, R. J. W., 1993, Geology and genesis of stratiform sediment-hosted (SEDEX) zinc-lead-silver sulphide deposits, *in* Kirkham, R. V., Sinclair, W. D., Thorpe, R. I., and Duke, J. M., eds., *Mineral deposit modeling,* Geological Association of Canada Special Paper 40, p. 201-251.

Grinenko, V. A., Grinenko, L. N. and Zagryazhskaya, G. D., 1969, Kinetic isotope effect in high temperature reduction of sulfate. *Geokhimiya* 4, p. 484-491.

Gröger, J., Franke, J., Hamer, K. and Schulz, H. D., 2009, Quantitative recovery of elemental sulfur and improved selectivity in a chromium-reducible sulfur distillation. *Geostand. Geoanal. Res.* 33, p. 17-27.

Guney, M., Al-Marhoun, M. A and Nawab, Z. A., 1988, Metalliferous sub-marine sediments of the Atlantis II – Deep, Red Sea. *CIM Bulletin* 81, p. 33-39.

Hannington, M. D., de Ronde, C. E. J. and Petersen, S., 2005, Modern sea-floor tectonics and submarine hydrothermal systems, *in* Hedenquist, J. F., Thompson, J. F. H., Goldfarb, R. J. and Richards, J. P., eds., *100th Anniversary Volume of Econ. Geol.*, p. 111-142.

Hannington, M. D., Jonasson, I. R., Herzig, P. M. and Petersen, S., 1995, Physical and chemical processes of seafloor mineralization, *in* Humphris, S., Fornari, D. and Zierenberg, R., eds., *Physical, Chemical, Biological and Geological Interactions within Hydrothermal Systems*. AGU Monograph 91, p. 115-157.

Hanor, J. S. and Baria, L. R., 1977, Controls on the distribution of barite deposits in Arkansas, *in* Stone, C. G., Haley, B. R., Holbrook, D. F., Williams, N. F., Bush, W. V. and McFarland, J. D., eds., *Symposium on the geology of the Ouachita Mountains*, Little Rock, Arkansas Geological Commission, 2, p. 48–55.

Hartmann, M., 1973, Untersuchungen von suspendiertem Material in den Hydrothermallaugen des Atlantis-II-Tiefs, *Geol. Rundsch.* 62, p. 742-754.

Hartmann, M., 1985, Atlantis-II-Deep geothermal brine system: Chemical processes between hydrothermal brines and Red Sea deep water. *Mar. Geol.* 64, p. 157-177.
Hartmann, M. and Nielsen, H., 1966, Sulfur isotopes in the hot brine and sediment of Atlantis II Deep (Red Sea). *Mar. Geol.* 4, p. 305-306.
Huston, D. L., Stevens, B., Southgate, P. N., Muhling, P. and Wyborn, L., 2006, Australian Zn-Pb-Ag ore-forming systems: a review and analysis. *Econ. Geol*. 101, p. 1117-1157.
Igumnov, S. A., 1976, Sulfur isotope exchange between sulfide and sulfate in hydrothermal solutions. *Geochemistry Internat.* 13, p. 113-124.
Johnson, C. A. and Skinner, B. J., 2003, Geochemistry of the Furnace magnetite bed, Franklin, New Jersey, and the relationship between stratiform iron oxide ores and stratiform zinc oxide-silicate ores in the New Jersey Highlands. *Econ. Geol*. 98, p. 837-854.
Kaplan, I. R., Sweeney, R. E. and Nissenbaum, A., 1969, Sulfur isotope studies on Red Sea geothermal brines and sediments, *in* Degens, E. T. and Ross, D. A., eds., *Hot Brines and Recent Heavy Metal Deposits in the Red Sea,* Springer-Verlag, New York, p. 474-498.
Koski, R. S. and Hein, J. R., 2003, Stratiform barite deposition in the Roberts Mountains allochthon, Nevada: A review of potential analogs in modern sea-floor environments, *in* Bliss, J. D., Moyle, P. R. and Long, K. R., eds., *Contributions to Industrial-Minerals Research*. U.S. Geological Survey, Bulleting 2209-H.
Large, R. R., Bodon, S., Davidson, G. and Cooke, D., 1996, The chemistry of BHT ore formation—one of the keys to understanding differences be- tween SEDEX and BHT deposits. Centre for Ore Deposit and Exploration Studies Special Publ. 1, p. 105–112.
Laurila, T. E., Hannington, M. D., Petersen, S. and Garbe-Schönberg, D., 2014a, Trace metal distribution in the Atlantis II Deep (Red Sea) sediments. *Chem. Geol.* 386, p. 80-100.
Laurila, T. E., Hannington, M. D., Petersen, S. and Garbe-Schönberg, D., 2014b, Early depositional history of metalliferous sediments in the Atlantis II Deep of the Red Sea: Evidence from rare earth element geochemistry. *Geochim. Cosmochim. Acta* 126, p. 146-168.
Manheim, F. T., 1974, Red Sea geochemistry (ch. 38), *in* Whitmarsh, R. B., Weser, O. E., Ross, D. A., *et al.,* eds., *Initial Reports of the Deep Sea Drilling Project*, v. 23, Washington (U.S. Government Printing Office) p. 975-998.
Missack, E., Stoffers, P. and El Goresy, A., 1989, Mineralogy, parageneses, and phase relations of copper-iron sulfides in the Atlantis II Deep, Red Sea. *Mineral. Deposita* 24, p. 82-91.
Miller, A. R., 1964, Highest salinity in the world ocean? *Nature* 203, p. 590.
Monnin, C. and Ramboz, C., 1996, The anhydrite saturation index of the ponded brines and sediment pore waters of the Red Sea deep. *Chem. Geol.* 127, p. 141-159.
Nakai, N. and Jensen, M. L., 1964, The kinetic isotope effect in the bacterial reduction and oxidation of sulfur. *Geochim Cosmochim Acta* 28, p. 1893-1912
Oudin, E., Thisse, Y. and Ramboz, C., 1984, Fluid Inclusion and Mineralogical Evidence for High Temperature Saline Hydrothermal Circulation in the Red Sea Metalliferous Sediments: Preliminary Results. *Mar. Mining* 5 (1), p. 3-31.

Oudin, E. and Cocherie, A., 1988, Fish debris record the hydrothermal activity in the Atlantis II deep sediments (Red Sea). *Geochim. Cosmochim. Acta* 52, p. 177-184.

Petersen, S., Herzig, P.M. and Hannington, M.D., 2000, Third dimension of a presently forming VMS deposit: TAG hydrothermal mound, Mid-Atlantic Ridge, 26°N. *Mineralium Deposita* 35, p. 233-259.

Pierret, M. C., Clauer, N., Bosch, D., Blanc, G. and France-Lanord, C., 2001, Chemical and isotopic ($^{87}Sr/^{86}Sr$, $\delta^{18}O$, $\delta D$) constraints to the formation processes of Red-Sea brines. *Geochim. Cosmochim. Acta* 65 (8), p. 1259-1275.

Pottorf, R. J. and Barnes. H. L., 1983, Mineralogy, geochemistry, and ore genesis of hydrothermal sediments from the Atlantis II Deep, Red Sea. *Econ. Geol. Monograph* 5, p. 198-223.

Ramboz, C., Oudin, E. and Thisse, Y., 1988, Geyser-type discharge in Atlantis II Deep, Red Sea: Evidence of boiling from fluid inclusions in epigenetic anhydrite. *Can. Mineral.* 26, p. 765-786.

Ramboz, C. and Danis, M., 1990, Superheating in the Red Sea? The heat-mass balance of the Atlantis II Deep revisited. *Earth Planet. Sci. Lett.* 97, p. 190-210.

Rye R. O., Bethke, P. M. and Wasserman, M. D., 1992, The stable isotope geochemistry of acid sulfate alteration. *Econ. Geol.* 87, p. 225-262.

Sakai, H. and Dickson, F. W., 1978, Experimental determination of the rate and equilibrium fractionation factors of sulfur isotope exchange between sulfate and sulfide in slightly acid solutions at 300°C and 1,000 bars. *Earth and Planet. Sci. Lett*. 39, p. 151-161.

Schmidt, M., Botz, R., Faber, E., Schmitt, M., Poggenburg, J., Garbe-Schönberg, D. and Stoffers, P., 2003, High-resolution methane profiles across anoxic brine–seawater boundaries in the Atlantis-II, Discovery, and Kebrit Deeps (Red Sea). *Chem. Geol*. 200, p. 359-375.

Schoell, M., 1976, Heating and convection within the Atlantis II Deep geothermal system of the Red Sea. Proc. Second United Nations Symposium on the Development and Use of Geothermal Resources 1, p. 583-590.

Schoell, M. and Hartmann, M., 1973, Detailed temperature structure of the hot brines in the Atlantis II Deep area (Red Sea). *Mar. Geol*. 14, p. 1-14.

Schoell, M. and Faber, E., 1978, New isotopic evidence for the origin of Red Sea brines. *Nature* 275, p. 436-438.

Seal, R. R. II and Wandless, G. A., 2003, Sulfur isotope evidence for sea-floor mineralizing processes at the Bald Mountain and Mount Chase massive sulfide deposits, northern Maine. *Econ Geol. Monograph* 11, p. 567-587.

Seal, R. R. II, 2006, Sulfur Isotope geochemistry of sulfide minerals, *in* Vaughan D. V., ed., Sulfide Mineralogy and Geochemistry. *Rev. Mineral. Geochem.* 61, Min. Soc. Amer., p. 633-677.

Shanks III, W. C., 2001, Stable isotopes in seafloor hydrothermal systems: vent fluids, hydrothermal deposits, hydrothermal alteration, and microbial processes, *in* Valley, J. W. and Cole, D. R., eds., Stable Isotope Geochemistry. *Rev. Mineral*. 43. Mineralogical Society of America, Washington, D.C, p. 469-525.

Shanks, W. C. and Bischoff, J. L., 1977, Ore transport and deposition in the Red Sea geothermal system: a geochemical model. *Geochim. Cosmochim. Acta* 41, p. 1507-1519.

Shanks, W. C. and Bischoff, J. L., 1980, Geochemistry, sulfur isotope composition, and accumulation rates of the Red Sea geothermal deposits. *Econ. Geol.* 75, p. 445-459.

Shanks, W. C., Bischoff, J. L. and Kaplan, I. R., 1974, Sulfur isotope studies of evaporites and shales from sites 225, 227, and 228 in the Red Sea, *in* Whitmarsh, R. B., Weser, O. E., Ross, D. A., *et al.,* eds., *Initial Reports of the Deep Sea Drilling Project, v. 23*, Washington (U.S. Government Printing Office), p. 947-950.

Stephens, J. D. and Wittkopp, R. W., 1969, Microscopic and electron beam microprobe study of sulfide minerals in Red Sea mud samples, *in* Degens, E. T. and Ross, D. A., eds., *Hot Brines and Recent Heavy Metal Deposits in the Red Sea*, Springer-Verlag, New York, p. 441-447.

Sval'nov, V. N., Strizhov, V. P., Gogdanov, Yu. A. and Isayeva, A. B., 1984, Hydrothermal Barite Crust on Basalts in the Atlantis II Deep (Red Sea). *Oceanology* 24 (6), UDC 551.462 (268).

Sweeney, R. E. and Kaplan, I. R., 1973, Pyrite framboid formation: Laboratory synthesis and marine sediments. *Econ. Geol*. 68 (5), p. 618-634.

Swift, S. A., Bower, A. S. and Schmitt, R. W., 2012, Vertical, horizontal, and temporal changes in temperature in the Atlantis II and Discovery hot brine pools, Red Sea. *Deep-Sea Res. I* 64, p. 118-128.

Taitel-Goldman, N. and Singer, A., 2002, Metastable Si-Fe phases in hydrothermal sediments of Atlantis II Deep: Red Sea. *Clay Miner*. 37, p. 235-248.

Thode, H. G., Monster, J. and Dunford, H. B., 1961, Sulphur isotope geochemistry. *Geochim. Cosmochim. Acta* 25, p. 150-174.

Trüper, H. G., 1969, Bacterial sulfate reduction in the Red Sea hot brines, *in* Degens, E. T. and Ross, D. A., eds., *Hot Brines and Recent Heavy Metal Deposits in the Red Sea,* Springer-Verlag, New York, p. 263-271.

Turner, J. S., 1969, A physical interpretation of hot brine layers in the Red Sea, *in* Degens, E. T. and Ross, D. A., eds., *Hot Brines and Recent Heavy Metal Deposits in the Red Sea*, Springer-Verlag, New York, p. 164-173.

Siam, R., Mustafa, G. A., Sharaf, H., Moustafa, A., Ramadan, A. R., Antunes, A., Bajic, V. B., Stingl, U., Marsis, N. G. R., Coolen, M. J. L., Sogin, M., Ferreira, A. J. S. and Dorry, H. E., 2012, Unique prokaryotic consortia in geochemically distinct sediments from Red Sea Atlantis II and Discovery Deep brine pools. *PLoS ONE* 7 (8), e42872, 10 p.

Watson, S. W. and Waterbury, J. B., 1969, The Sterile Hot Brines of the Red Sea, *in* Degens, E. T. and Ross, D. A., eds., *Hot Brines and Recent Heavy Metal Deposits in the Red Sea*, Springer-Verlag, New York, p. 272-281.

Zierenberg, R. A. and Shanks, W. C., 1986, Isotopic constraints on the origin of the Atlantis II, Suakin and Valdivia brines, Red Sea. *Geochim. Cosmochim. Acta*. 50, p. 2205-2214.

Zierenberg, R. A. and Shanks, W. C., 1988, Isotopic studies of epigenetic features in metalliferous sediment, Atlantis II Deep, Red Sea. *Can. Mineral.* 26, p. 737-753.

## Figure Captions

Figure 5.1. Simplified cross section through the Atlantis II Deep sediment and brine pool. The sediments (~20 m thick sequence) directly overlie Red Sea MORB and are covered by a stratified brine pool with ~100 m thick anoxic lower layer (the Lower Brine) and gradually more seawater like Upper Brine layers (5 layers: Swift et al., 2012). There are four main sources of elements in the brine and the underlying sediments: hot hydrothermal fluid, background sedimentation, seawater (via Mn-Fe-(oxy)hydroxide precipitation-dissolution cycling), and possible cold brines that enter the deep either from above or below. Hydrothermal fluids are the main source of reduced sulfur, including possible upward diffusion from the hydrothermal system; other sources may include (in violet) bacterial activity at the chemocline, sinking cold brines from outside the Deep, and diagenetic (abiogenic or biogenic) sulfate reduction. A range of $\delta^{34}S$ values in sulfide minerals from different parts of the Deep are indicated in red, values in anhydrite are in black (from Zierenberg and Shanks, 1988). Average $\delta^{34}S$ values for sulfide in different stratigraphic units are from Shanks and Bischoff (1980). $\delta^{34}S$ values of dissolved $SO_4$ in different brine layers are from Zierenberg and Shanks (1986) and in the surrounding evaporites from Shanks et al. (1974).

Figure 5.2. Maps of the Atlantis II Deep showing the distribution of reduced sulfur and other selected elements measured in the three uppermost units (AM, SU2, CO) of 453 cores from the MESEDA project. The contoured data are average values of all samples taken at 1-m intervals in each core. The assays are based on salt-free, washed core samples (unpublished

data from the MESEDA I-III projects and Bertram et al., 2011). $S_{red}$ is acid-soluble sulfide extracted from washed samples with hydrochloric acid. $S_{red}$, Zn, and Cu are all enriched in the Southwest Basin, close to the inferred location of the currently active vents. Ca is present as sulfate proximal to the vents and as carbonate in the more distal parts of the basin (i.e., $Ca/CO_2$ is a proxy for the distribution of primary $SO_4$ in anhydrite).

Figure 5.3. Previously publish $\delta^{34}S$ values of sulfides and sulfates from the Atlantis II sulfides and sulfates from Zierenberg and Shanks (1988). Sulfide values are similar to those observed at many other sites of modern seafloor hydrothermal activity. Sulfate was interpreted to be mainly from the local seawater and Miocene evaporites. Samples were identified as “brine pool precipitate” and “epigenetic” according to either bedded or vein structures. Brine pool sulfides are isotopically lighter than vein sulfides, whereas the opposite was observed for sulfates.

Figure 5.4. Location of the cores analyzed in this study. $\delta^{34}S$ values for sulfide and sulfate in the uppermost sample of each core are indicated in brackets (sulfide/sulfate). The area covered by the Lower Brine (depth >2048 m) is indicated in blue; darker blue areas are deeper than 2100 m and 2200 m. The inferred location of the current vent source is situated in the deepest part of the Deep in the Southwest (the area outlined by the dashed line is referred to in this study as “vent proximal”).

Figure 5.5. Examples of the variation of $\delta^{34}S$ values of sulfate and sulfide from three cores along a line extending from Southwest Basin (vent proximal) to the West Basin (distal). There is little difference in the average $\delta^{34}S$ of sulfide (red dashed line) between the different metal- and sulfur-rich units (+5.7‰, +5.0‰, and +6.5‰ in SU1, SU2 and AM, respectively). From this, we conclude that the preserved sulfide fraction in the samples is mainly hydrothermal in origin. However, a clear trend of decreasing $\delta^{34}S$ in $SO_4$ (mainly secondary metal sulfates) is seen with distance away from the vent source (from about 10‰ to ~5‰ and to 0‰). In many samples (e.g., core 373), the $\delta^{34}S$ of sulfate is lower than the $\delta^{34}S$ of the preserved sulfide. This is interpreted to reflect a lower primary $\delta^{34}S$ of the sulfides that were most susceptible to oxidation after recovery (e.g., fine-grained, diagenetic sulfides) and the presence of little anhydrite. The proximal core (617) appears to preserve the original sulfide/sulfate relationship (i.e., heavy sulfur in sulfate, light sulfur in sulfide). The difference of about 15‰, is similar to what one would expect for high-temperature seafloor hydrothermal systems (e.g., Shanks, 2001).

Figure 5.6. Plots of $\delta^{34}S$ in sulfate and sulfide fractions versus normative abundance of anhydrite (A) and secondary metal sulfates (B). The maximum $\delta^{34}S$ of sulfate corresponds to end-member massive anhydrite; all other values are mixtures with secondary metal sulfates. The samples with the most abundant secondary metal sulfates are interpreted to reflect the isotopic composition of primary diagenetic sulfides that were oxidized during core storage.

Figure 5.7. Comparison of sulfur isotope data from the present study with previously published values on similar sample types. $\delta^{34}S$ values of sulfides still present in the cores (i.e., those minerals most resistant to oxidation during core storage) show little variation between the sulfide-rich units (SU1, SU2 and AM) or in samples considered to be from proximal versus distal parts of the basin. $\delta^{34}S$ values of sulfides of ~5-6‰ are typical of black smokers and suggest a dominantly hydrothermal origin for the sulfur (Shanks, 2001). A contribution of bacteriogenic sulfur (low $\delta^{34}S$) is clearly seen in units CO and DOP, which were formed during episodes of more oxidized and euxinic Lower Brine, respectively. $\delta^{34}S$ values of sulfates have a large range. Anhydrite values plot between +20 and +25‰; values up to about +22 can be explained by sulfate in seawater and the surrounding Miocene evaporites, but higher values suggest removal of light sulfur from the pore water during diagenesis. The abundant low $\delta^{34}S$ values of sulfate from this study reflect secondary metal-sulfates (together with anhydrite). Mass balances based on normative abundances of anhydrite and metal-sulfates in the samples indicate end-member values for the metal sulfides as low as -30‰ also in the metal- and sulfide-rich stratigraphic units (see text for discussion). $\delta^{34}S$ in sedimentary barite (Zierenberg and Shanks, 1988) is similar to that of anhydrite, whereas $\delta^{34}S$ values of barite crusts from the flank of the basin (Sval'nov et al., 1984) are lower, which may be due to contamination by bacteriogenic sulfides also reported from these samples.

Figure 5.8. Schematic illustrations of the distribution of metals and sulfur of different isotopic compositions, based on brine measurements during 1971 and 1977, from

Hartmann (1973, 1985). Pulses of high-temperature venting, such as that recorded in 1971 (A) led to deposition of abundant sulfide from a widespread neutrally buoyant plume (as observed by Turner, 1969; Schoell, 1976; Schoell and Hartmann, 1973; Zierenberg and Shanks, 1986). At times of high-temperature hydrothermal discharge, reduced sulfur ($\delta^{34}S$ ~3 to 7‰) was incorporated in sulfides deposited basin-wide from the hydrothermal plume. During a subsequent phase of reduced or lower-temperature hydrothermal activity in 1977 (B), Cu and Zn deposition was mainly with Fe-(oxy)hydroxides, with increasing Cu/Zn in the distal parts of the basin (Laurila et al., 2014a). These metals were ultimately incorporated in diagenetic sulfides with much lower $\delta^{34}S$ values. In the Upper Brine, bacteriogenic sulfide was present, and this is recorded in the $\delta^{34}S$ values of sulfides at the flanks (Sval'nov et al., 1984).

Figure 5.9. Isotopic composition of sulfides at various mid-ocean ridges on the modern seafloor (Hannington et al., 2005) compared to all samples from the Atlantis II Deep (colors indicate references, see Figure 5.7). Number of samples in the population (n) and average are given in brackets. Sedimented settings have broader variation in isotopic composition than the sediment-free ridges including significantly negative values consistent with sulfide from non-hydrothermal sources. At bare ridges, isotopic composition has narrower range and the average mainly reflects MORB composition consistent with dominantly hydrothermal source of sulfide. In the Atlantis II Deep, the isotopic compositions of sulfides in the metalliferous sediment are mainly dependent on the strength of hydrothermal activity, which was variable. During high-temperature venting, hydrothermal sulfide (~6‰)

predominates, whereas during low or absent hydrothermal activity sulfides have highly negative values down to less than -30‰.

Table 5.1. Mineralogy and bulk composition (salt-free) of the different stratigraphic units in the Atlantis II Deep.

| Unit [1] | thick-ness | Age | sed. rate | | S tot ($SO_4$) | $SO_4$ | S (red) | Ca | Fe | Zn | Cu | $CO_2$ | $Al_2O_3$ | Si | MnO |
|---|---|---|---|---|---|---|---|---|---|---|---|---|---|---|---|
| | m | Ka | cm/ka | | % | % | % | % | % | % | % | % | % | % | % |
| AM *(SAM)* | 3.5 (1-4) | <3.6 | 97 (17 Mt) | Amorphous Fe-Si-OOH, proto-clays, absorbed metals (Zn) | 16.0 | 11.9 | 1.4 | 4.9 | 23.8 | 3.17 | 0.88 | 1.8 | 1.1 | 6.8 | 0.93 |
| SU2 *(S)OAN* | 4.0 (2-12) | <5.9 (2.3) | 174 (20 Mt) | FeOOH, anhydrite, sphalerite, rare pyrite, green silicates | 23.9 | 20.1 | 1.3 | 8.4 | 16.2 | 2.30 | 0.45 | 3.2 | 1.3 | 8.2 | 0.81 |
| CO *COS* | 6.0 (1-11) | <8.6 (2.7) | 222 (32 Mt) | FeO(H), MnO(H), hydro-thermal clays, rare sulfide | 4.2 | 2.8 | 0.6 | 5.7 | 22.6 | 0.69 | 0.25 | 6.6 | 2.4 | 7.9 | 5.53 |
| SU1 | 3.8 (1-4) | <11.7 (3.1) | 123 (24 Mt) | Mn-Fe-Carbonates, clays, anhydrite, pyrite, chalcopyrite | 26.9 | 21.6 | 2.4 | 6.5 | 17.0 | 2.72 | 0.92 | 8.0 | 2.2 | 9.3 | 1.67 |
| DOP | 2.5 (1-6) | <~25 | 19 | Biogenic-silicic detritus, FeO, MnO, pyrite increase up | 10.9 | 7.8 | 1.5 | 13.4 | 13.2 | 1.06 | 0.23 | 16.5 | 4.5 | 9.1 | 1.72 |
| Spatial variation in reference to the vent source in the three units that are found basin wide | | | | | | | | | | | | | | | |
| Distal | AM, SU2, CO included | | | High Cu/Zn, pyrite>(Sph+Cpy) | 11.3 | 9.4 | 0.9 | 6.2 | 21.0 | 1.09 | 0.34 | 4.2 | 1.4 | 7.9 | 3.36 |
| Proximal | AM, SU2, CO included | | | Hot, metal-rich pore water | 21.7 | 17.8 | 1.3 | 7.5 | 18.4 | 3.14 | 0.66 | 3.8 | 1.9 | 7.7 | 1.07 |

[1] Sedimentary units: AM (subunit SAM) stands for (Sulfidic)-Amorphous-Siliceous unit; SU2 stand for sulfidic unit 2 and includes subunits SOAN, and OAN, which stand for (Sulfidic)-Oxidic-Anhydritic unit; CO (and subunit COS) stand for Central-Oxidic (-Sulfidic) unit; SU1 stand for sulfidic unit 1; DOP stands for Detrital-Oxidic-Pyritic unit. Units SU1 and DOP are absent in the SW Basin. Average thicknesses are from Bäcker and Richter (1973). The ages (start date of formation and total age in brackets) of the units are according to Hackett and Bischoff (1973) and Shanks and Bischoff (1980). Sedimentation rates are calculated according to average thickness and age. Total tonnages for each unit are based on estimates from Gurvich (2006). Average bulk compositions are based on 100 samples from Laurila et al. (2014b).

Table 5.2. Major chemical, isotopic and mineralogical composition of 46 sediment samples from the Atlantis II Deep.

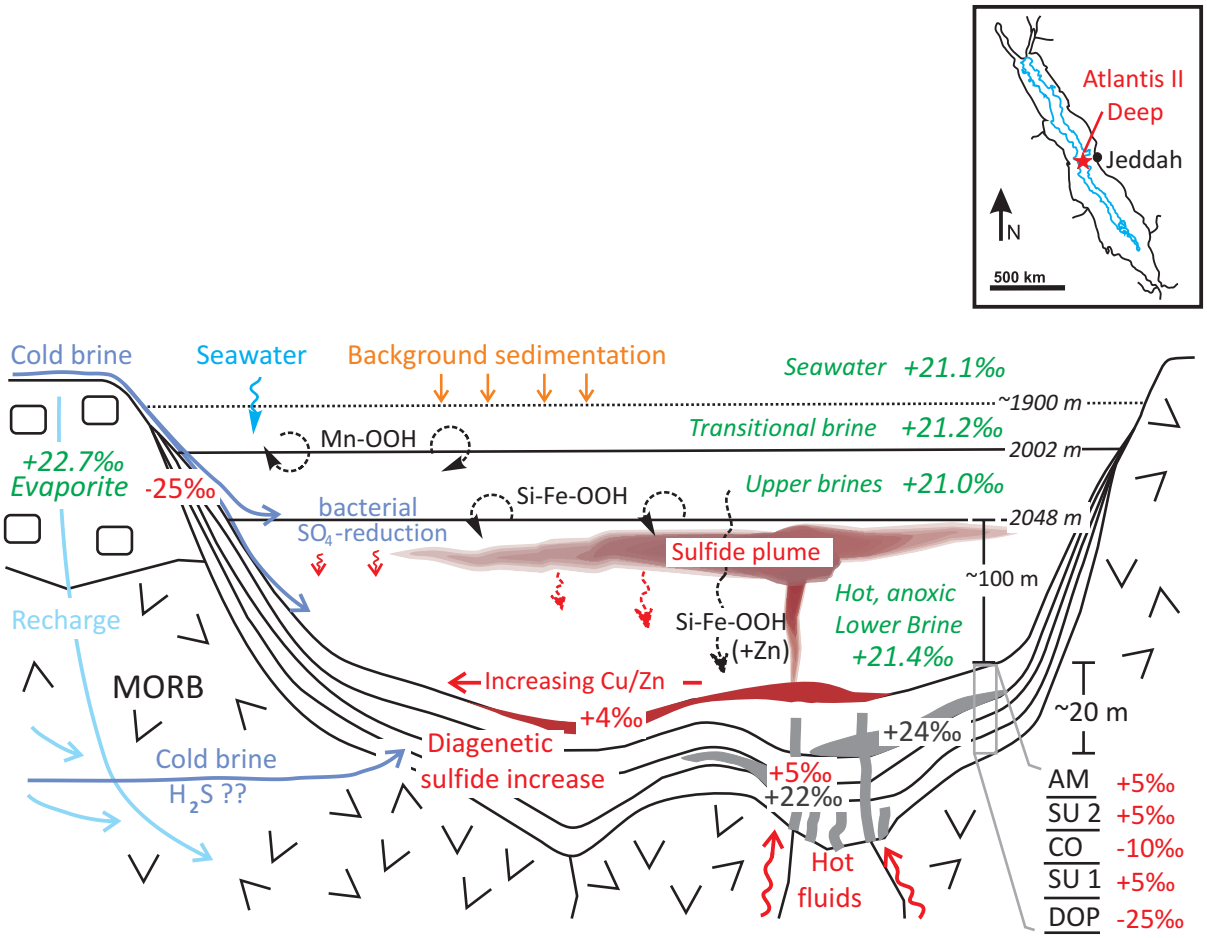
| | | $S_{tot}$ $SO_4$ | $SO_4$ | $S_{red}$ | Ca | Fe | Zn | Cu | Ba | $CO_2$ | $Al_2O_3$ | $\delta^{34}S$ $S_{red}$ | | $\delta^{34}S$ $SO_4$ | | det-rital | $CaCO_3$ | $CaSO_4$ | Cpy | Sph | Py |
|---|---|---|---|---|---|---|---|---|---|---|---|---|---|---|---|---|---|---|---|---|---|
| | | % | % | % | % | % | % | % | ppm | % | % | ‰ [1] | Repeats | ‰ [1] | Repeats | g/ kg | g/ kg | g/ kg | g/ kg | g/kg | g/kg |
| | | | 0.3 | | 0.01 | 0.05 | 30 ppm | 2 ppm | 3 | 0.01 | 0.01 | | | | | | | | | | |
| | | TCD | IR | calc. | F-OES | F-OES | F-MS | F-MS | F-MS | coul. | OES | | | | | | | | | | |
| 334-83 | SAM | 24.4 | 19.1 | 1.8 | 9.1 | 14.7 | 2.33 | 0.34 | 2249 | 1.0 | 0.8 | 5.6 | | 17.8 | | 35 | 130 | 271 | 10 | 0 | 10 |
| 373-8 | AM | 7.3 | 1.5 | 1.9 | 5.8 | 18.9 | 1.75 | 0.33 | 327 | 1.9 | 1.1 | 5.9 | | 6.5 | | 57 | 38 | 0 | 9 | 15 | 13 |
| 373-93 | SU2 | 3.7 | 0.8 | 1.0 | 6.8 | 20.1 | 1.33 | 0.28 | 1080 | 4.5 | 1.3 | 1.4 | | -1.9 | | 69 | 97 | 0 | 8 | 8 | 5 |
| 373-210 | SU2 | 5.4 | 2.6 | 0.9 | 4.1 | 17.3 | 0.25 | 0.16 | 115 | 0.5 | 0.5 | 9.7 | | 1.0 | | 20 | 0 | 37 | 4 | 0 | 6 |
| 373-265 | CO | 1.2 | n.d. | 0.4 | 3.2 | 2.8 | 0.18 | 0.03 | 5728 | 0.5 | 1.2 | | | 9.7 | | 81 | 11 | 0 | 1 | 1 | 55 |
| 373-515 | COS | 2.0 | 1.0 | 0.3 | 3.1 | 25.3 | 1.41 | 0.13 | 192 | 5.6 | 0.6 | 9.8 | | 5.5 | | 34 | 74 | 0 | 4 | 10 | 56 |
| 373-555 | SU1 | 40.3 | 25.2 | 5.0 | 4.1 | 11.0 | 8.87 | 2.15 | 6254 | 7.1 | 3.1 | 2.7 | | -2.0 | | 165 | 0 | 113 | 62 | 131 | 64 |
| *373-586* | *SU1* | *65.7* | *65.7* | *na* | *22.6* | *1.2* | *0.40* | *0.13* | *183* | *0.1* | *0.2* | | | *21.6* | | *8* | *0* | *766* | *0* | *6* | *0* |
| 373-672 | SU1 | 24.6 | 5.3 | 6.4 | 2.9 | 26.7 | 0.88 | 0.13 | 98 | 0.6 | 0.5 | 7.5 | 7.5, 6.9 | 1.4 | -3.7, 5.3 | 23 | 0 | 76 | 4 | 0 | 13 |
| 373-751 | SU1 | 30.8 | 25.9 | 1.6 | 3.5 | 15.2 | 6.75 | 1.68 | 256 | 13.1 | 2.8 | 5.1 | 5.1 | -5.9 | 3.2, 23.5 | 122 | 0 | 98 | 48 | 100 | 60 |
| 373-780 | DOP | 3.1 | 1.3 | 0.6 | 18.2 | 5.5 | 0.94 | 0.01 | 70 | 24.5 | 3.6 | -3.3 | 1.5 | 0.6 | | 218 | 430 | 0 | 0 | 13 | 5 |
| 373-798 | DOP | 4.6 | n.d. | 1.5 | 2.4 | 41.8 | 1.47 | 0.03 | 44 | 1.5 | 1.3 | -11.4 | | | | 86 | 20 | 0 | 1 | 3 | 1 |
| 387-80 | SU2 | 18.4 | 11.8 | 2.2 | 5.6 | 16.3 | 2.03 | 0.47 | 229 | 0.6 | 0.9 | 7.2 | **7.0** | 3.5 | **3.7** | 36 | 74 | 167 | 13 | 0 | 8 |
| 421-80 | SU2 | 6.1 | 6.1 | na | 3.9 | 23.9 | 2.36 | 1.27 | 176 | 4.9 | 0.9 | 7.9 | 9.0, 7.9 | 3.3 | | 29 | 168 | 86 | 37 | 0 | 3 |
| 495-113 | AM | 5.7 | 5.6 | 0.0 | 4.7 | 29.5 | 1.37 | 0.14 | 191 | 0.7 | 0.7 | 8.0 | | | | 26 | 0 | 79 | 4 | 0 | 2 |
| 495-1088 | DOP | 4.2 | 4.2 | na | 16.3 | 4.1 | 0.27 | 0.04 | 224 | 21.8 | 7.2 | -21.9 | | | | 433 | 358 | 0 | 1 | 4 | 25 |
| 503-7 | SAM | 13.4 | 10.9 | 0.9 | 5.8 | 25.8 | 2.02 | 0.49 | 381 | 1.0 | 0.8 | 5.9 | | 10.5 | | 36 | 151 | 154 | 14 | 0 | 6 |
| 503-75 | OAN | 39.6 | 26.2 | 4.5 | 3.2 | 6.4 | 1.18 | 0.23 | 15758 | 3.1 | 1.3 | 5.8 | | 2.7 | | 60 | 0 | 101 | 7 | 18 | 191 |
| 503-140 | SOAN | 22.4 | 22.4 | na | 6.2 | 14.0 | 1.88 | 0.29 | 58 | 0.6 | 0.5 | 8.0 | 7.8 | 11.8 | | 22 | 0 | 208 | 2 | 28 | 31 |
| 503-155 | SOAN | 18.2 | 16.4 | 0.6 | 3.9 | 15.1 | 1.99 | 0.34 | 107 | 0.9 | 1.2 | 6.4 | 8.9 | 10.2 | **10.2** | 44 | 0 | 126 | 10 | 30 | 35 |
| *503-235* | *SOAN* | *71.6* | *71.6* | *na* | *27.3* | *0.1* | *0.33* | *0.02* | *5028* | *0.0* | *0.0* | | | *23.3* | | *6* | *0* | *925* | *0* | *5* | *0* |
| 503-266 | SOAN | 55.7 | 54.3 | 0.5 | 20.9 | 3.3 | 0.20 | 0.05 | 4172 | 1.4 | 0.1 | 2.7 | | 17.1 | | 8 | 0 | 709 | 0 | 3 | 0 |
| 503-407 | COS | 1.4 | 0.5 | 0.3 | 1.3 | 51.3 | 0.16 | 0.12 | 125 | 0.8 | 0.4 | 7.3 | | 8.8 | | 16 | 10 | 0 | 3 | 2 | 2 |
| 503-509 | COS | 13.2 | 12.8 | 0.2 | 7.8 | 24.8 | 0.40 | 0.19 | 1620 | 8.1 | 0.4 | | | 22.2 | | 14 | 316 | 181 | 9 | 0 | 0 |
| 503-516 | COS | 11.2 | 0.8 | 3.5 | 2.3 | 5.2 | 1.62 | 1.81 | 4996 | 3.5 | 9.5 | -7.8 | | -3.8 | | 560 | 0 | 0 | 52 | 8 | 0 |
| 503-626 | COS | 7.3 | 7.3 | na | 2.1 | 41.0 | 0.15 | 0.11 | 3220 | 0.5 | 0.4 | 1.9 | | 0.0 | 3.7 | 16 | 0 | 70 | 0 | 2 | 13 |
| 503-671 | COS | 5.0 | 1.8 | 1.0 | 4.3 | 15.5 | 0.18 | 0.10 | 244 | 1.3 | 0.4 | 4.4 | | -2.3 | | 31 | 22 | 0 | 3 | 16 | 21 |
| 503-807 | SU1 | 34.0 | 9.8 | 8.1 | 3.6 | 10.8 | 0.70 | 0.71 | 6555 | 2.1 | 1.8 | 4.5 | 5.1, **4.9** | 6.5 | 6.1 | 93 | 0 | 107 | 20 | 10 | 154 |
| 503-889 | SU1 | 7.8 | 7.8 | na | 2.7 | 37.3 | 0.42 | 1.33 | 16 | 16.1 | 0.9 | 7.4 | 7.6 | 3.8 | 7.9 | 44 | 63 | 0 | 39 | 70 | 69 |
| 503-912 | SU1 | 59.3 | 47.2 | 4.0 | 3.6 | 6.4 | 14.60 | 2.52 | 117 | 2.0 | 2.9 | 6.9 | | 4.6 | | 108 | 0 | 105 | 73 | 216 | 125 |
| 503-946 | DOP | 24.8 | 20.4 | 1.5 | 5.8 | 22.1 | 2.42 | 0.38 | 7075 | 4.2 | 1.7 | 6.3 | | 14.4 | | 80 | 0 | 185 | 11 | 36 | 37 |

| | | $S_{tot}$ $SO_4$ | $SO_4$ | $S_{red}$ | Ca | Fe | Zn | Cu | Ba | $CO_2$ | $Al_2O_3$ | $\delta^{34}S$ $S_{red}$ | | $\delta^{34}S$ $SO_4$ | | det-rital | $CaCO_3$ | $CaSO_4$ | Cpy | Sph | Py |
|---|---|---|---|---|---|---|---|---|---|---|---|---|---|---|---|---|---|---|---|---|---|
| | | % | % | % | % | % | % | % | ppm | % | % | ‰ [1] | Repeats | ‰ [1] | Repeats | g/ kg | g/ kg | g/ kg | g/ kg | g/kg | g/kg |
| 503-987 | DOP | 64.9 | 23.1 | 13.9 | 2.1 | 20.1 | 1.09 | 0.12 | 567 | 4.6 | 7.2 | -4.9 | -3.4, -4.4 | -12.4 | -10.5 | 421 | 0 | 7 | 3 | 16 | 378 |
| 546-5 | AM | 9.4 | 5.3 | 1.4 | 1.1 | 31.6 | 3.39 | 1.61 | 851 | 3.2 | 1.6 | 4.5 | | 3.6 | | 35 | 0 | 33 | 41 | 29 | 0 |
| 546-92 | AM | 10.4 | 10.4 | na | 2.0 | 26.3 | 3.31 | 0.97 | 123 | 3.8 | 1.1 | 9.1 | | 8.3 | | 25 | 0 | 63 | 0 | 49 | 7 |
| 557-9 | SAM | 19.0 | 15.7 | 1.1 | 6.2 | 18.4 | 4.53 | 1.29 | 357 | 0.9 | 1.0 | 6.8 | | 3.6 | | 34 | 0 | 207 | 37 | 12 | 2 |
| 617-9 | SAM | 15.4 | 11.0 | 1.4 | 4.3 | 24.8 | 3.21 | 1.32 | 1395 | 0.5 | 1.4 | 6.5 | | 3.0 | 17.3, 10.6 | 46 | 0 | 139 | 38 | 12 | 2 |
| 617-148 | SAM | 31.9 | 19.2 | 4.2 | 5.1 | 21.2 | 4.81 | 1.66 | 1252 | 0.8 | 1.3 | 6.4 | | 7.3 | | 40 | 0 | 167 | 48 | 71 | 49 |
| 617-220 | OAN | 37.2 | 35.5 | 0.6 | 13.9 | 2.4 | 0.16 | 0.09 | n.d. | n.d. | 0.5 | 5.0 | | 20.1 | **18.6** | 21 | 0 | 470 | 3 | 2 | 31 |
| 617-395 | OAN | 23.7 | 18.3 | 1.8 | 8.3 | 16.6 | 0.79 | 0.04 | 32 | 1.2 | 1.3 | 4.9 | | 14.1 | **13.9** | 58 | 49 | 259 | 1 | 0 | 28 |
| 617-396 | OAN | 7.8 | 6.2 | 0.5 | 3.4 | 17.7 | 0.81 | 1.07 | 19 | 3.3 | 5.0 | 0.1 | | 9.0 | | 285 | 0 | 73 | 7 | 11 | 0 |
| 617-508 | SOAN | 4.2 | 2.9 | 0.4 | 15.9 | 10.9 | 0.62 | 0.12 | 240 | 17.2 | 5.5 | -2.9 | | 12.9 | | 312 | 361 | 0 | 4 | 9 | 14 |
| *617-551* | *SOAN* | *64.5* | *64.5* | *na* | *25.8* | *3.1* | *0.63* | *0.14* | *198* | *1.6* | *0.5* | | | *22.1* | ***22.7*** | *22* | *0* | *873* | *0* | *9* | *0* |
| 617-650 | SOAN | 30.4 | 24.2 | 2.1 | 6.0 | 17.8 | 4.93 | 1.08 | 105 | 1.3 | 2.0 | 4.6 | | -2.6 | | 70 | 0 | 192 | 31 | 73 | 39 |
| 617-787 | SOAN | 30.6 | 28.0 | 0.9 | 8.3 | 21.7 | 2.48 | 0.24 | 1426 | 0.8 | 1.4 | 6.8 | 6.8 | 11.9 | | 45 | 0 | 277 | 7 | 37 | 42 |
| 617-799 | SOAN | 36.8 | 36.2 | 0.2 | 12.4 | 11.4 | 7.07 | 0.58 | 9318 | 2.0 | 1.9 | 6.6 | **6.7** | 12.4 | | 91 | 0 | 408 | 18 | 75 | 0 |
| 617-875 | SOAN | 47.4 | 47.4 | na | 16.5 | 8.9 | 3.04 | 0.67 | 996 | 0.8 | 1.2 | 5.7 | 6.1, 5.7 | 20.3 | | 44 | 0 | 553 | 0 | 45 | 0 |
| Unit (subunit) | | $S_{tot}$ $SO_4$ | $SO_4$ | $S_{red}$ | Ca | Fe | Zn | Cu | Ba | $CO_2$ | $Al_2O_3$ | $\delta^{34}S$ $H_2S$ | Range $\delta^{34}S_{red}$ | $\delta^{34}S$ $SO_4$ | Range $\delta^{34}S_{ox}$ | det-rital | $CaCO_3$ | $CaSO_4$ | Cpy | Sph | Py |
| AM (SAM) | | 15.2 | 11.0 | 1.6 | 4.9 | 23.5 | 2.97 | 0.91 | 792 | 1.5 | 1.1 | 6.5 | 4.5-9.1 | 7.6 | 3.0-17.8 | 37 | 35 | 124 | 22 | 21 | 10 |
| SU2 (OAN/SOAN) | | 24.2 | 21.2 | 1.2 | 8.7 | 14.0 | 1.94 | 0.44 | 2255 | 2.9 | 1.6 | 5.0 | -2.9-9.7 | 9.1 | -2.6-20.3 | 76 | 47 | 229 | 10 | 21 | 29 |
| CO (COS) | | 5.9 | 4.0 | 1.0 | 3.4 | 23.7 | 0.59 | 0.35 | 2304 | 2.9 | 1.8 | 3.1 | -7.8-9.8 | 3.0 | -3.8-9.7 | 107 | 62 | 36 | 10 | 6 | 21 |
| SU1 | | 32.8 | 20.2 | 5.0 | 3.4 | 17.9 | 5.37 | 1.42 | 2216 | 6.8 | 2.0 | 5.7 | 2.7-7.5 | 1.4 | -5.9-6.5 | 93 | 11 | 83 | 41 | 88 | 81 |
| DOP | | 20.3 | 12.2 | 4.4 | 9.0 | 18.7 | 1.24 | 0.11 | 1596 | 11.3 | 4.2 | -6.1 | -21.9-6.3 | 0.9 | -12.4-14.4 | 248 | 162 | 38 | 3 | 14 | 89 |
| Distal | | 18.5 | 13.1 | 2.5 | 5.5 | 19.2 | 2.03 | 0.54 | 2069 | 4.8 | 1.9 | 3.3 | -21.9-9.8 | 4.5 | -12.4-22.2 | 102 | 63 | 90 | 15 | 26 | 48 |
| Proximal | | 23.5 | 20.0 | 1.4 | 8.0 | 17.5 | 2.96 | 0.79 | 1413 | 2.8 | 1.8 | 5.0 | -2.9-9.1 | 10.1 | -2.6-20.3 | 82 | 39 | 222 | 18 | 30 | 17 |

Sample numbers include core number and sampling depth (cm); see Figure 5.4 for core locations. Stratigraphic units are according to Table 5.1. Samples in italics comprise >75 wt.% anhydrite; these are omitted in the averages at the bottom of the Table. All data are calculated to a salt free basis (see Appendix C). Sulfide values were calculated according to total sulfur and sulfate sulfur; where indicated (na) sulfate sulfur was adjusted down where it exceeded $S_{tot.}$. N.d.= not detected. Analytical methods for major and trace

elements are reported in Appendix C. [1] Repeat analyses of $\delta^{34}S$ marked in **bold** font are splits of one sample, other values are analyses of the different sulfur extraction runs. Normative mineralogy is according to Chapter 2.

Figure 5.1


Atlantis II
Deep
Jeddah
N
500 km
Cold brine
Seawater
Background sedimentation
Seawater +21.1‰
~1900 m
Transitional brine +21.2‰
2002 m
Mn-OOH
+22.7‰
Evaporite
-25‰
bacterial
SO4-reduction
Si-Fe-OOH
Upper brines +21.0‰
2048 m
Sulfide plume
~100 m
Hot, anoxic
Lower Brine
+21.4‰
Recharge
Si-Fe-OOH
(+Zn)
MORB
Increasing Cu/Zn
+4‰
+24‰
~20 m
Diagenetic
sulfide increase
Cold brine
H2S ??
+5‰
+22‰
Hot
fluids
AM +5‰
SU 2 +5‰
CO -10‰
SU 1 +5‰
DOP -25‰

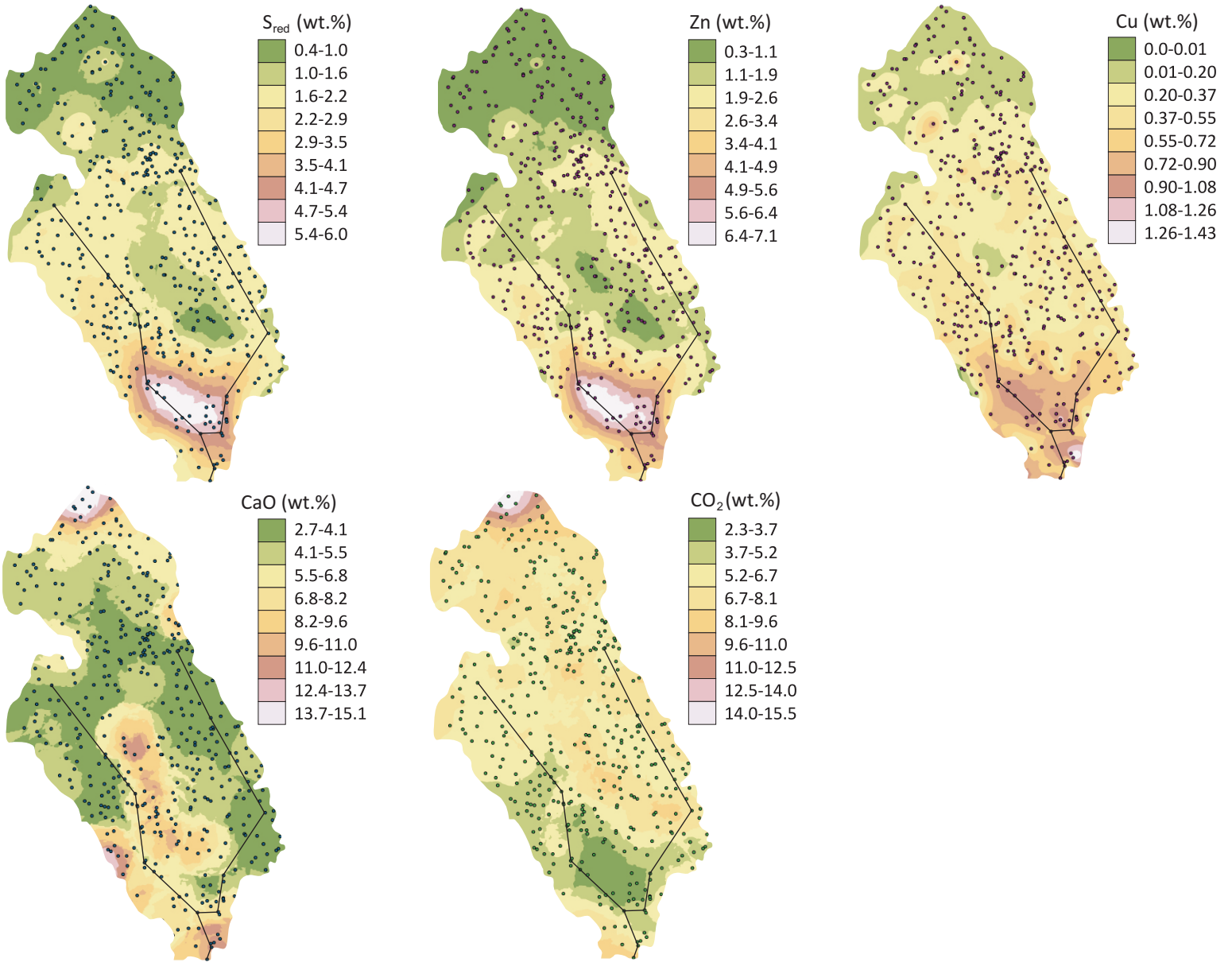

$S_{red}$ (wt.%)
0.4-1.0
1.0-1.6
1.6-2.2
2.2-2.9
2.9-3.5
3.5-4.1
4.1-4.7
4.7-5.4
5.4-6.0
Zn (wt.%)
0.3-1.1
1.1-1.9
1.9-2.6
2.6-3.4
3.4-4.1
4.1-4.9
4.9-5.6
5.6-6.4
6.4-7.1
Cu (wt.%)
0.0-0.01
0.01-0.20
0.20-0.37
0.37-0.55
0.55-0.72
0.72-0.90
0.90-1.08
1.08-1.26
1.26-1.43
CaO (wt.%)
2.7-4.1
4.1-5.5
5.5-6.8
6.8-8.2
8.2-9.6
9.6-11.0
11.0-12.4
12.4-13.7
13.7-15.1
$CO_2$(wt.%)
2.3-3.7
3.7-5.2
5.2-6.7
6.7-8.1
8.1-9.6
9.6-11.0
11.0-12.5
12.5-14.0
14.0-15.5

Figure 5.2

Figure 5.3

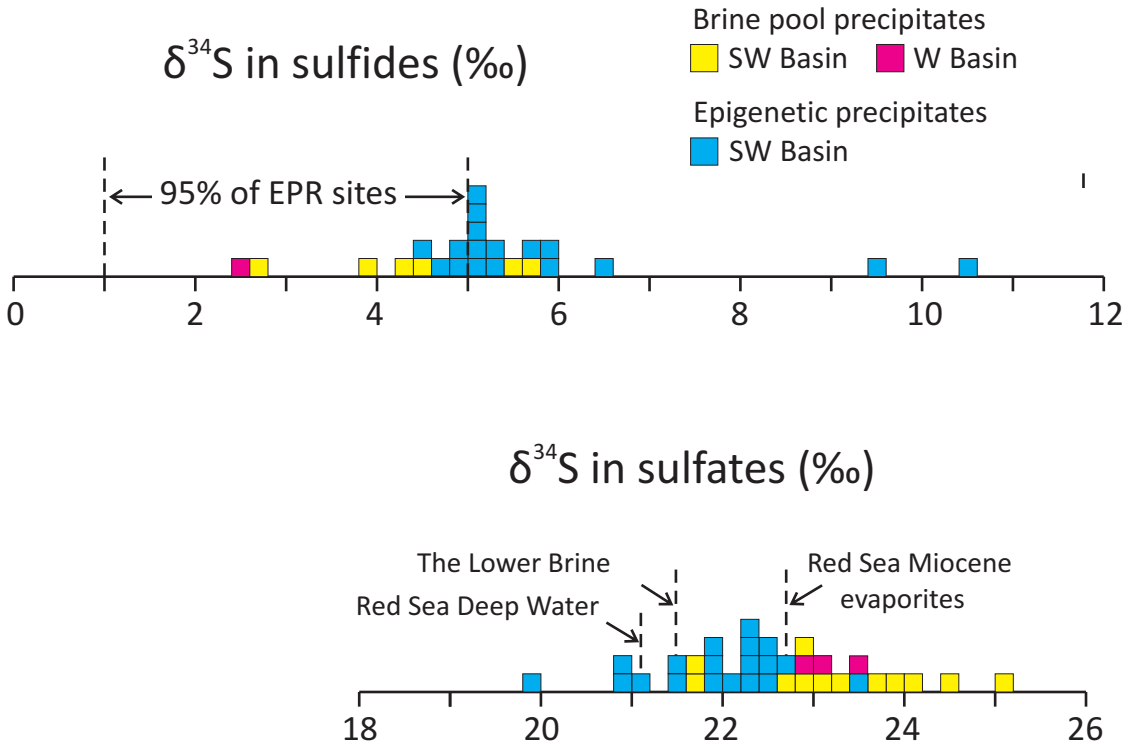
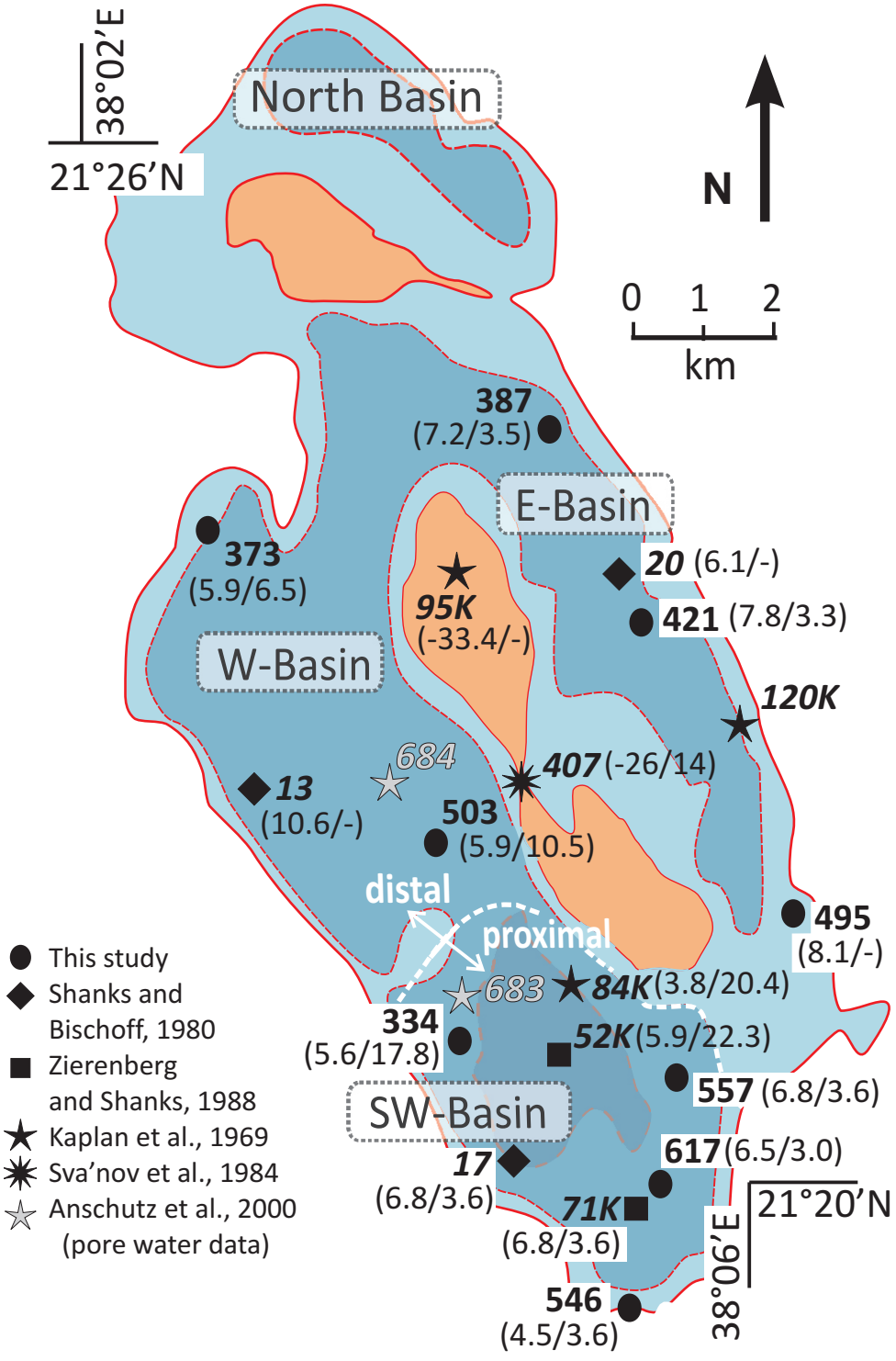

δ34S in sulfides (‰)
Brine pool precipitates
SW Basin
W Basin
Epigenetic precipitates
SW Basin
95% of EPR sites
0
2
4
6
8
10
12
δ34S in sulfates (‰)
The Lower Brine
Red Sea Deep Water
Red Sea Miocene
evaporites
18
20
22
24
26

Figure 5.4


38°02'E
21°26'N
North Basin
N
0 1 2
km
387
(7.2/3.5)
E-Basin
373
(5.9/6.5)
95K
(-33.4/-)
20 (6.1/-)
421 (7.8/3.3)
W-Basin
120K
684
407 (-26/14)
13
(10.6/-)
503
(5.9/10.5)
distal
proximal
495
(8.1/-)
683
84K (3.8/20.4)
334
(5.6/17.8)
52K (5.9/22.3)
557 (6.8/3.6)
SW-Basin
617 (6.5/3.0)
17
(6.8/3.6)
71K
(6.8/3.6)
21°20'N
38°06'E
546
(4.5/3.6)
This study
Shanks and Bischoff, 1980
Zierenberg and Shanks, 1988
Kaplan et al., 1969
Sva'nov et al., 1984
Anschutz et al., 2000 (pore water data)

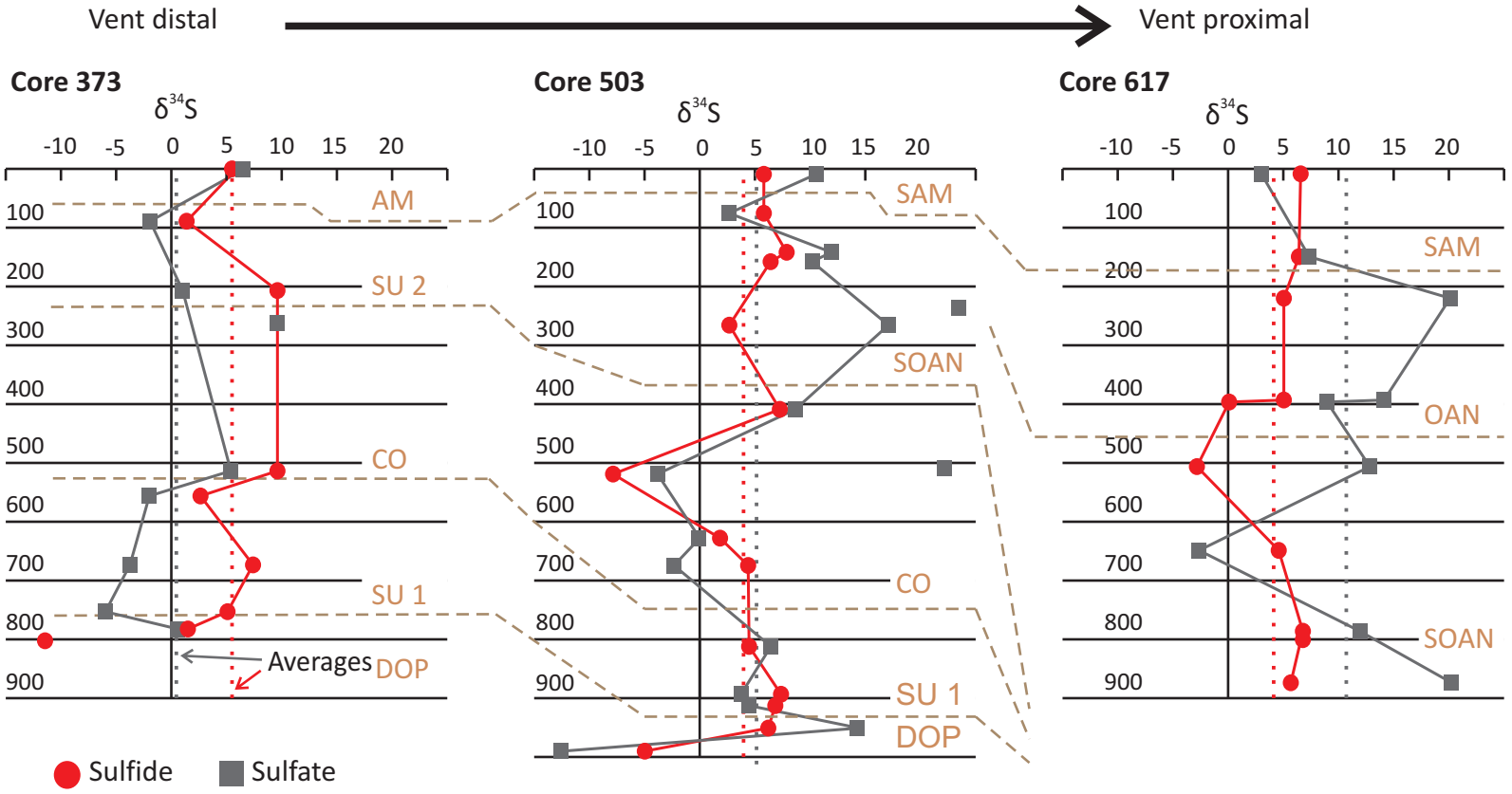

Vent distal
Vent proximal
Core 373
Core 503
Core 617
δ34S
-10 -5 0 5 10 15 20
100
200
300
400
500
600
700
800
900
AM
SU 2
CO
SU 1
DOP
Averages
SAM
SOAN
CO
SU 1
DOP
SAM
OAN
SOAN
Sulfide
Sulfate

Figure 5.5

Figure 5.6.

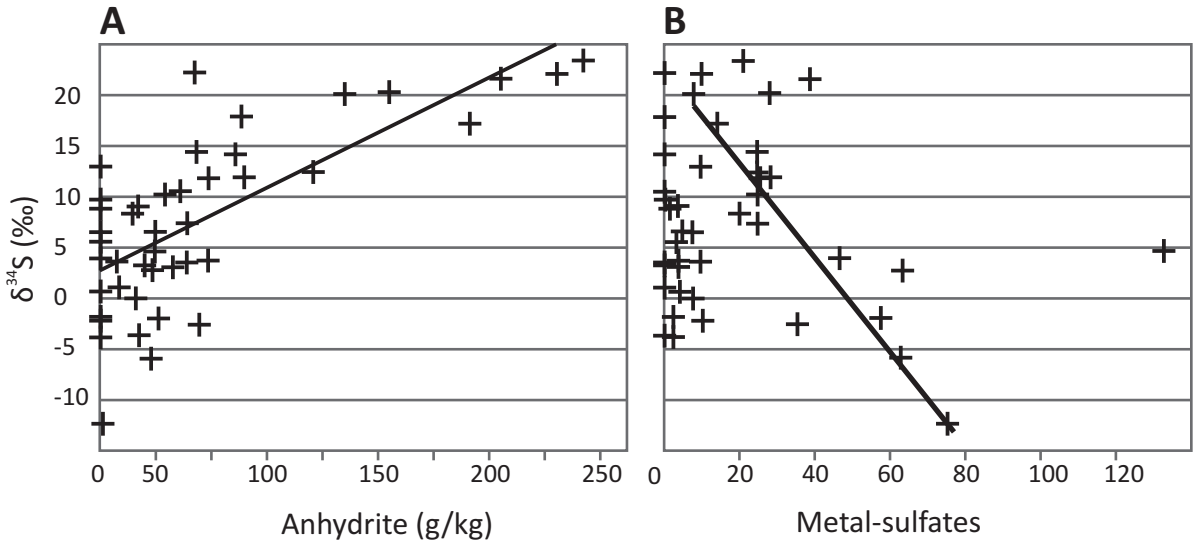

A
B
20
15
10
5
0
-5
-10
δ34S (‰)
0
50
100
150
200
250
Anhydrite (g/kg)
0
20
40
60
80
100
120
Metal-sulfates

Figure 5.7

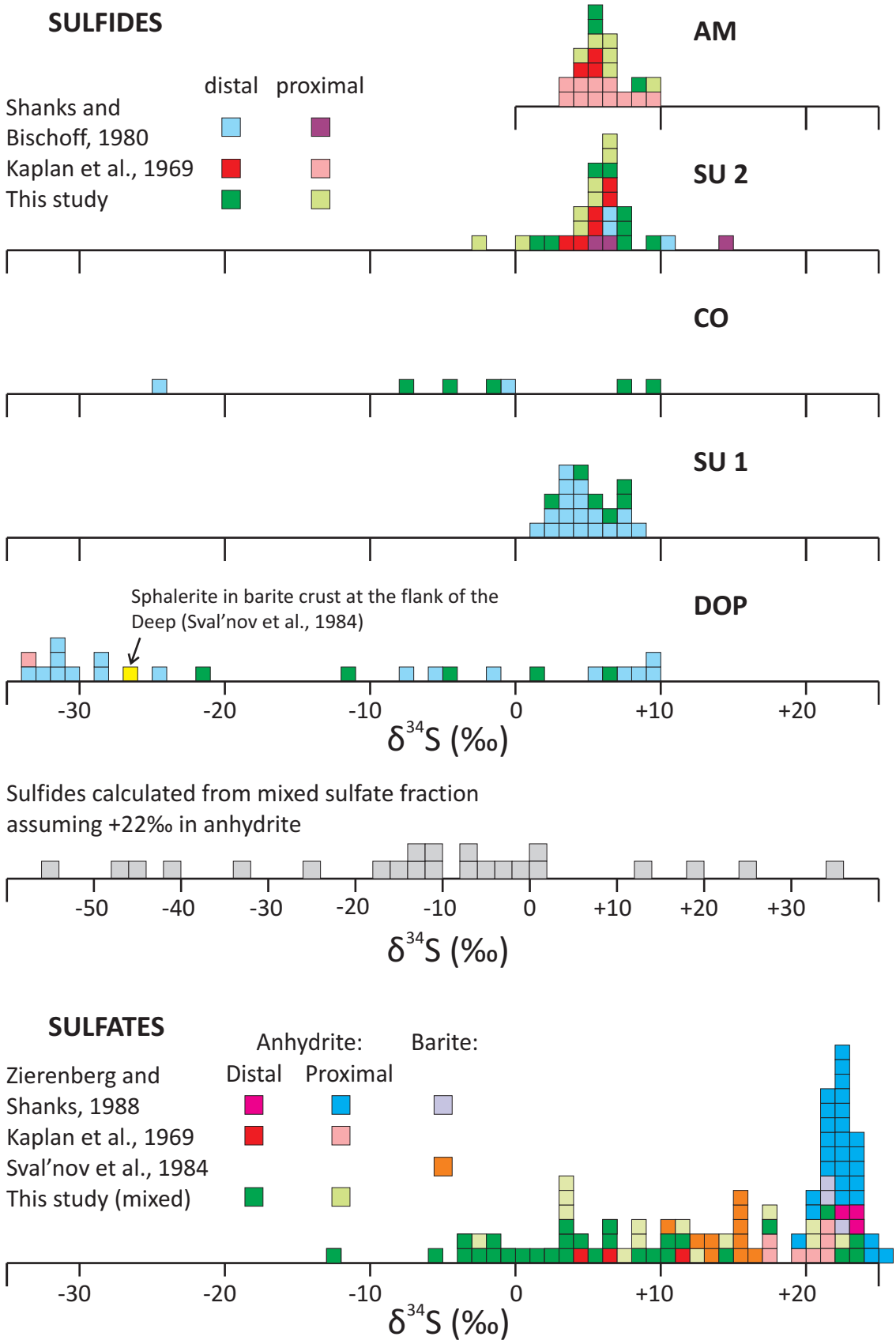

SULFIDES
distal proximal
Shanks and
Bischoff, 1980
Kaplan et al., 1969
This study
AM
SU 2
CO
SU 1
DOP
Sphalerite in barite crust at the flank of the
Deep (Sval'nov et al., 1984)
-30 -20 -10 0 +10 +20
δ34S (‰)
Sulfides calculated from mixed sulfate fraction
assuming +22‰ in anhydrite
-50 -40 -30 -20 -10 0 +10 +20 +30
δ34S (‰)
SULFATES
Anhydrite: Barite:
Distal Proximal
Zierenberg and
Shanks, 1988
Kaplan et al., 1969
Sval'nov et al., 1984
This study (mixed)
-30 -20 -10 0 +10 +20
δ34S (‰)

Figure 5.8

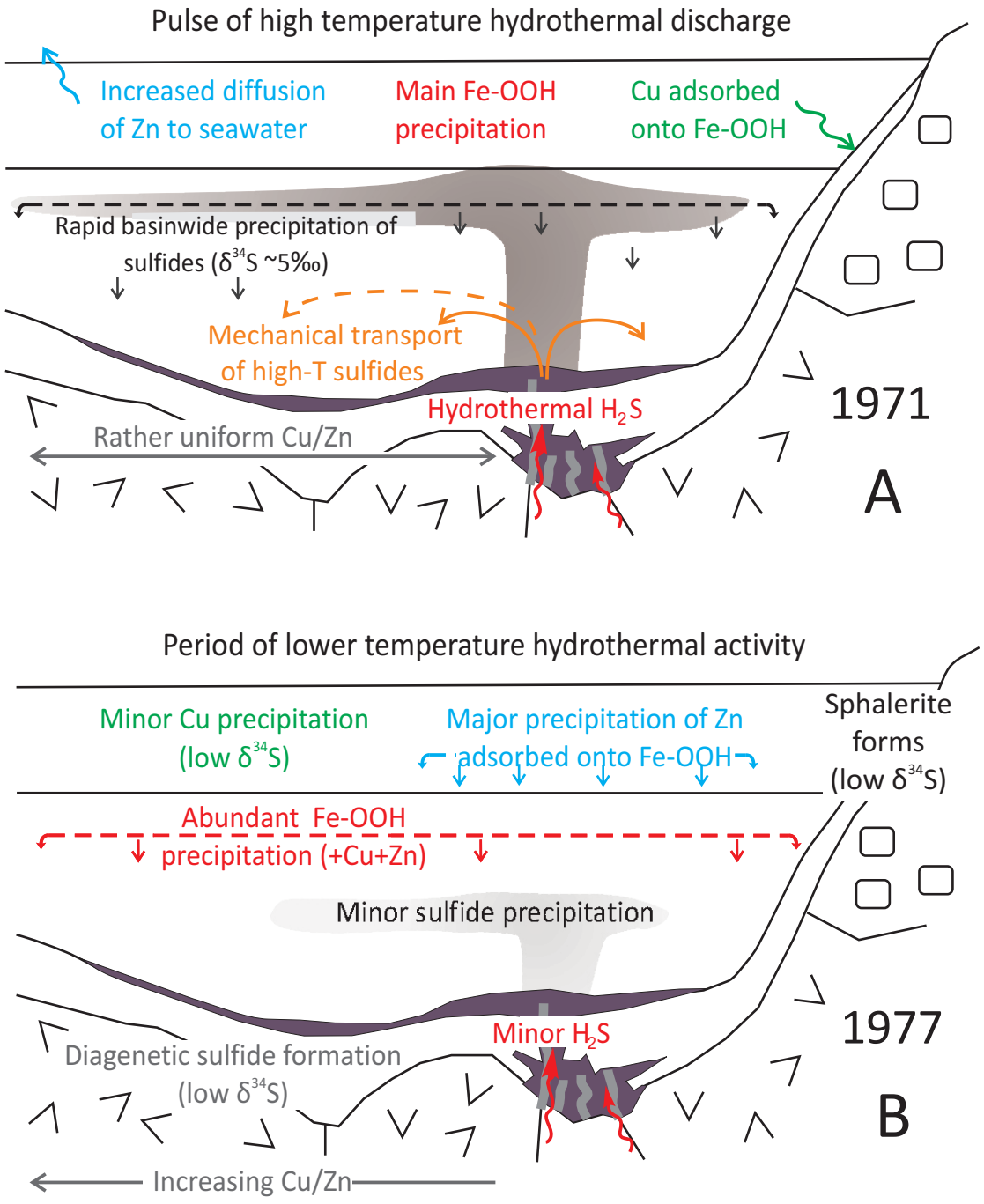
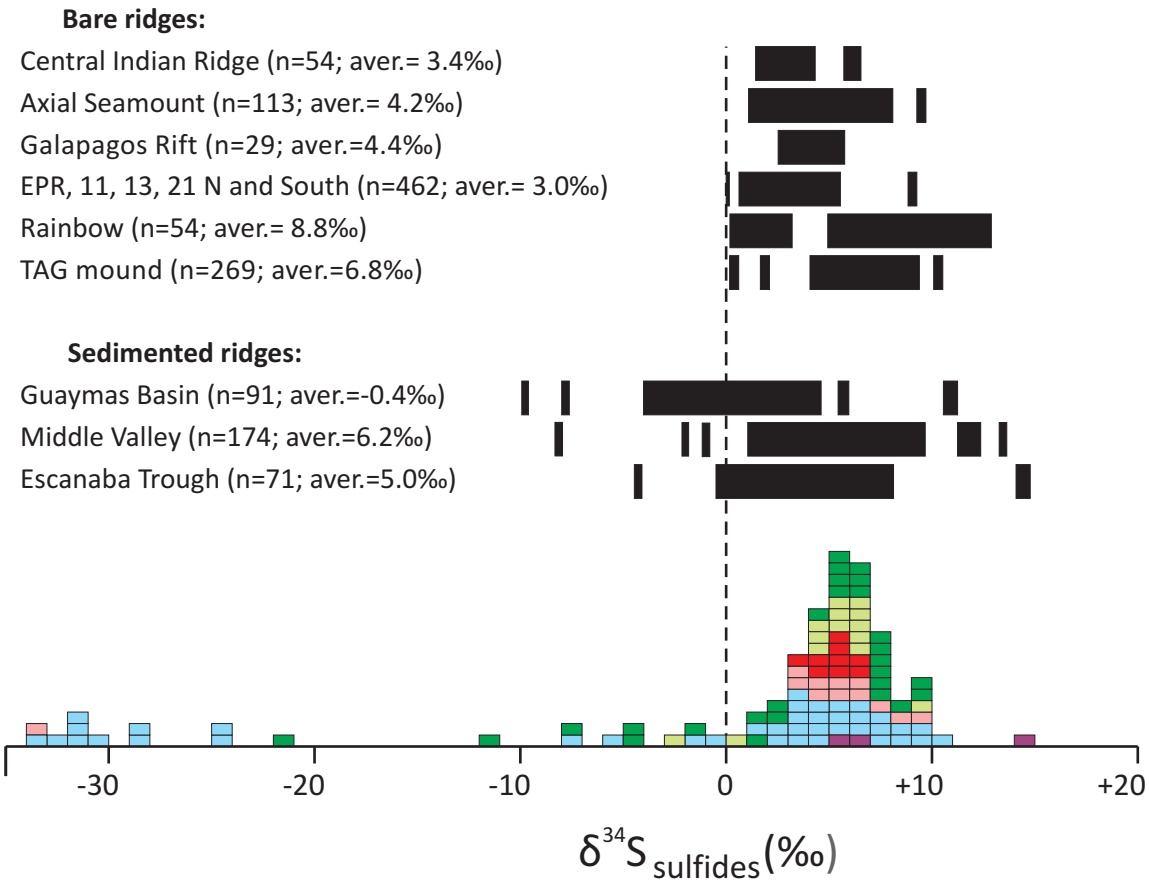

Pulse of high temperature hydrothermal discharge
Increased diffusion of Zn to seawater
Main Fe-OOH precipitation
Cu adsorbed onto Fe-OOH
Rapid basinwide precipitation of sulfides (δ34S ~5‰)
Mechanical transport of high-T sulfides
Hydrothermal H2S
Rather uniform Cu/Zn
1971
A
Period of lower temperature hydrothermal activity
Minor Cu precipitation (low δ34S)
Major precipitation of Zn adsorbed onto Fe-OOH
Sphalerite forms (low δ34S)
Abundant Fe-OOH precipitation (+Cu+Zn)
Minor sulfide precipitation
Minor H2S
Diagenetic sulfide formation (low δ34S)
Increasing Cu/Zn
1977
B

Figure 5.9.


Bare ridges:
Central Indian Ridge (n=54; aver.= 3.4‰)
Axial Seamount (n=113; aver.= 4.2‰)
Galapagos Rift (n=29; aver.=4.4‰)
EPR, 11, 13, 21 N and South (n=462; aver.= 3.0‰)
Rainbow (n=54; aver.= 8.8‰)
TAG mound (n=269; aver.=6.8‰)
Sedimented ridges:
Guaymas Basin (n=91; aver.=-0.4‰)
Middle Valley (n=174; aver.=6.2‰)
Escanaba Trough (n=71; aver.=5.0‰)
-30
-20
-10
0
+10
+20
δ34S sulfides (‰)

# CHAPTER 6

## COMPARISON OF THE ATLANTIS II DEEP TO ANCIENT STRATIFORM ORE

In preparation for Ore Geology Reviews

## 1. Introduction

This study has provided new insights into mineralizing processes in the Atlantis II Deep, the only site of modern hydrothermal activity in a brine pool with significant ore potential, and establishes the characteristics of the Atlantis II Deep as the type example of this style of mineralization. The new dataset combines the first comprehensive, high-precision chemical analysis of the metalliferous sediments with powerful microanalytical techniques to address the distribution of trace elements from basin-scale down to a few microns. In this chapter key features of the Atlantis II Deep are compared to a number of ancient stratiform base metal deposits that are widely considered to have formed in a similar brine pool environment (Tables 6.1 and 6.2). The following are considered in detail: 1) formation of the metal-bearing ore fluids, in particular their compositional variation, 2) transport and concentration of metals to the site of deposition, and 3) the physical and chemical changes causing precipitation and ultimate deposition of stratiform ores from the brine pool. The comparisons highlight profound genetic differences and similarities between the Atlantis II Deep, other sites of modern metal deposition on the seafloor, and a number of different stratiform sediment-hosted ore deposits in the rock record.

## 2. Summary: Setting and Conditions of Deposition in the Atlantis II Deep

### 2.1 Tectonic Setting

The Red Sea is a ~2000-km long (17-28°N) ocean basin created by wedge-like extension between the Arabian and African continental plates. It has evolved from early continental breakup (presently happening north of ~25°N, where spreading rates are ~0.5 cm/year), to

ocean spreading at rates of ~1-1.5 cm/year in the South (Cochran and Martinez, 1988; Chu and Gordon, 1998). The time of initiation of rifting and the transition from rifting to seafloor spreading is debated; estimates for the beginning of seafloor formation range from ~5 Ma (e.g., Cochran, 2005) to ~12 Ma (Izzeldin, 1987). The Atlantis II Deep is located on the slowly spreading rift axis, which began opening ~450,000 years ago, estimated from the width of the deep (~5 km) and a full spreading rate of ~1.1 cm/yr (Cochran and Martinez, 1988). This is a minimum age as evaporites outcropping at the flanks of the Deep may have flowed towards the axial trough and covered some of the earlier seafloor (Augustin et al., 2014).

The Atlantis II Deep is characterized by a deep axial rift zone and shallow flanks that transition to the continental shelf. It is symmetrically divided into a deeper eastern part and shallower western part with an axis-parallel tectonic ridge in the middle (Bäcker et al., 1975; Bignell, 1975). The deepest parts of the Atlantis II Deep (2,200 m) are overlain by about 200 m of stratified brine that is confined by the steep flanks of the valley. The sedimentary strata exposed on the flanks of the Deep vary greatly in thickness and comprise up to ~4 km of evaporites and shales with metal-enriched interlayers (Stoffers and Ross, 1974). Evaporites that outcrop at the flanks of the Atlantis II Deep are thought to have contributed to the formation of the highly saline brine pool (e.g., Anschutz et al., 1998; Pierret et al., 2001).

**2.2 Depositional environment and conditions of mineralization**

Despite the long history of rifting, the oldest sampled sediments in the Atlantis II Deep are only ~25,000 years old (Hackett and Bischoff, 1973). Sediments of this age have been cored in the Northeast of the Deep, but only much younger sediments (~6,000 years: Table 1.1; Ku, 1969) have been sampled in the Southwest Basin due to intrusion of a basaltic sill (DSDP drilling Leg 23 in 1972: Whitmarsh et al., 1974). The oldest sampled metalliferous sediments were deposited ~15,000 years ago, although older metalliferous sediment may be present below the recent basaltic sills. Background sedimentation in the Red Sea is ~15 cm/1,000 years, but only a thin layer of normal pelagic sediment is present between the youngest MORBs and the first metalliferous sediments. Therefore, despite the abundant sediments at the flanks of the rift, the basement in the Atlantis II Deep is mainly basaltic.

The sedimentary succession is divided into 5 different stratigraphic units that reflect major changes in the composition of the brine pool (Chapter 1). The lowermost unit DOP consists mainly of biogenic and silicic detrital sediments with an upward increase in the amount of authigenic material. SU1 is the lowermost metal- and sulfide-rich unit formed during an early phase of high-temperature venting, followed by the oxide-dominated CO unit formed during subdued hydrothermal activity. SU2 formed during a renewed episode of high-temperature venting. It has a gradational upper contact with the uppermost unit, AM, which also has high metal concentrations. In the current brine pool, sulfides are mainly precipitating in the Lower Brine; Fe-(oxy)hydroxides form at the chemocline between the Lower Brine the Upper Brine, where a small amount of oxygen is available, and settle into the currently-forming AM unit. Mn-(oxy)hydroxides precipitate at higher $fO_2$ and are only

deposited at the flanks of the Deep where the oxidized Upper Brine directly overlies the seafloor. Concentrations of some of the trace metals (e.g., Cu) in the dissolved and particulate fractions show significant (orders of magnitude) short-term variation in the brine pool, whereas other metals (e.g., Zn) have more constant concentrations (Hartmann, 1973, 1985), and this is reflected in the sediments.

The non-sulfidic, dominantly Fe-(oxy)hydroxide, components of the sediments are partly transformed to sulfides during diagenesis, but much of the Fe and some of the Zn and Cu remain bound to non-sulfidic minerals such as carbonates and clays (Chapter 2). The main sulfate mineral is anhydrite. Barite is a minor constituent throughout the sediments, but is locally abundant in barite crusts found at the flanks of the Deep under the Upper Brines (Sval'nov et al., 1984). Sulfides formed in the distal sediments and during times of reduced hydrothermal activity have lower $\delta^{34}S$ than the sulfides in the metal- and sulfide-rich units, consistent with significant bacterial sulfate reduction, most likely during diagenesis (Chapter 5). Sulfides in the main ore horizons (units SU1 and SU2) have a narrow range of $\delta^{34}S$ values (average of ~5‰) compared to the range for the Deep (-33‰ to +14‰). $\delta^{34}S$ values of anhydrite are typically close to that of Red Sea Deep Water and the Lower Brine (~21‰).

The current hydrothermal vent source is thought to be localized mainly within the central part of the Southwest Basin, based on epigenetic features in sediment cores (e.g., anhydrite veining: Zierenberg and Shanks, 1983), Cu and Zn grades (Appendix A), pore water

chemistry (Henricks et al., 1969; Anschutz et al., 2000), and the chemistry of the brine pool itself (Hartmann, 1973). High-temperature venting (up to ~400°C: Oudin et al., 1984; Ramboz et al., 1988) started at this location about 6,000 years ago (Table 1.1.). Thin subvertical epigenetic veins containing anhydrite and sulfides are the only direct physical evidence for paleo-venting. Because the anhydrite dissolves during cooling, these features may not be well preserved in the rock record.

The Lower Brine of the Atlantis II Deep is anoxic, hot and highly saline. It is enriched in dissolved metals (e.g., 5 ppm Zn, 65 ppm Fe and ~80 ppm Mn: Anschutz et al., 2000) but contains no reduced sulfur. $SO_4$ concentrations are between 470 and 850 ppm (Bougouffa et al., 2013, and Anschutz et al., 2000, respectively), corresponding to about 1/5 of that in the Red Sea Deep Water (Bougouffa et al., 2013). The metal concentrations are highly variable. Cu concentrations have varied by more than two orders of magnitude (Hartmann, 1973, 1985) but have been at least an order of magnitude lower than the Zn concentration at all times. The variations in the brine compositions are due to 1) hydrothermal venting, which is the main source of metals and sulfur, 2) dissolution of components brought into the brine with silicic and biogenic pelagic detritus, 3) transport of trace elements from the Red Sea Deep Water into the brine pool with Mn- and Fe-(oxy)hydroxides that adsorb and release elements as they descend through the brine, and 4) mixing with cold brines that enter the deep from above or below. These different processes are described in Schoell and Faber (1978), Zierenberg and Shanks (1986, 1988), Dupré et al. (1988), Anschutz et al. (1995), Pierret et al. (2001), and Laurila et al. (2014b).

The main ore horizons in the Atlantis II Deep (units SU2 and AM together, which have been deposited during the latest high-temperature hydrothermal activity, and the earlier SU1) vary in thickness from about 1 m to about 10 m. They are separated by unit CO, with low metal concentration. Combined, the whole succession has a thickness of about 20 m and is recognized basinwide (up to 10 km away from the vent source), resulting in an aspect ratio for the deposit of at least 500. However, the rate of deposition of metalliferous sediment and the metal grades decrease rapidly with distance away from the vent source (within < 2 km: Figure 3.10). The metal- and sulfide-rich sedimentary units are characterized by Fe/(Zn+Cu+Pb) of ~10, whereas units CO and DOP have much higher Fe/(Zn+Cu+Pb) ratios, closer to average shale and MORB (~300-600). Absolute Fe concentrations are highest in CO (~30 wt.% Fe), somewhat lower in SU1, SU2 and AM (~20 wt.% Fe) and down to background values in DOP. The Cu/Zn ratio is ~0.25 in the bulk of the Atlantis II sediments, which is considerably lower than average MORB or shale (~0.6-0.8); however, the Pb/Zn ratio is <0.01, which is more consistent with a metal source in MORB (Taylor and McLennan, 1985). The low $S_{red}$/(Fe+Zn+Cu+Pb) ratio of the sediment (<0.1) and low total $S_{red}$ concentration (~2.5 wt.%) reflect either a limited supply of reduced sulfur in the source or, more likely, high metal concentrations in the vent fluids due to the high salinity of the brines.

## 3. The Geological Record of Other Stratiform Base-Metal Ore Deposits

The processes involved in formation of the Atlantis II Deep metalliferous sediments also have been proposed for a number of different types of stratiform ore deposits. Brine pool deposition has been suggested for a number of volcanogenic massive sulfide deposits

(Solomon and Zaw, 1997; Tornos et al., 2008), sedimentary exhalative deposits (Large et al., 2001; Goodfellow and Lydon, 2007), and some atypical stratiform base metal deposits, such as Broken Hill and Sterling Hill (Large et al., 1996; Huston et al., 2006; Johnson et al., 1990). Fallout from hydrothermal plumes, similar to that inferred for sulfides in the Atlantis II Deep, also has been suggested as the depositional pathway for exhalite horizons found in association with some volcanogenic massive sulfide deposits (e.g., Spry et al., 2000; Grenne and Slack, 2005), and similar processes might be responsible for deposition of Algoma-type banded iron formations (Ohmoto et al., 2006). In some cases, finely laminated sediments have been interpreted to reflect deposition of fine particles formed at a chemocline in a stratified water column, similar to that for oxides in the Atlantis II Deep. Figures 6.1 and 6.2 are schematic illustrations of the main characteristics and processes involved in metal deposition suggested for some of these deposit types.

At open ocean MOR hydrothermal vents, two main end-member styles of venting have been identified: high-temperature (350°C) “black smoker” vents and lower temperature “white smoker” vents, dominated by sulfide- and sulfate deposition, respectively. In general, the MOR black smoker fluids are acidic (pH ~4), hot (>350°C) and reduced, allowing transport of both metals and $H_2S$ in the same fluid (i.e., $H_2S/\Sigma$metals ratio ~1), but at relatively low salinity (<1 to 8 wt.% NaCl; avg. 3.5 wt.%: Table 6.3, Hannington et al., 2005). Sulfides precipitate from the vent fluids due to rapid cooling and mixing with seawater, whereas anhydrite and barite precipitate due to reaction between Ca and Ba ions in the vent fluids and sulfate in seawater. Sulfide concentrations in the vent fluids closely matches

that of total metals (i.e., all metals are deposited as sulfides). Cu and Zn sulfides are deposited in order of the respective solubilities of chalcopyrite and sphalerite, whereas Fe (and Mn) are dispersed into the ocean as neutrally buoyant particle plumes (e.g., Baker et al., 1995), from which local Fe- and Mn-rich sediments may deposit on the seafloor (German et al., 1993). In these types of hydrothermal systems, only ~10% of the metals contained in the vent fluids are deposited as sulfide structures on the seafloor (Converse et al., 1984).

Metal contents in the hydrothermal fluids increase with increasing salinity (r=0.83) and temperature (r=0.61) (data for MAR sites from Hannington et al., 2005), but even at the highest salinities metals are rapidly precipitated from the fluids as the temperature decreases to <300°C. Salinities are never more than 10 wt.% NaCl, and high-salinity fluids are inferred to be a result of phase separation. However, even the most dense fluids are unlikely to rise to the seafloor (e.g., Fontaine et al., 2007). Only fluids with a salinity >10 wt.% will be more dense than seawater at ~2°C (Turner and Campbell, 1987), and venting of fluids that would pond at the seafloor is highly unlikely. Thus, brine pool deposits are only likely where an additional source of salinity is present (e.g., evaporites).

Some modern black smoker deposits have formed on sedimented ridges (e.g., Middle Valley, Escanaba Trough, Guaymas Basin: Goodfellow and Zierenberg, 1999). Due to the sediment cover, cooling and metal precipitation from the high temperature hydrothermal fluids happens largely below the seafloor. The seafloor vents generally have lower

temperatures and higher pH than black smokers, consistent with deposition of Cu mainly below the seafloor and overall low Cu/Zn ratios compared to black smoker deposits on sediment-free ridges (Table 6.1; Figure 6.3: modified from Hannington et al., 2005). Owing to the extensive subseafloor deposition, the accumulated massive sulfide is texturally and chemically distinct from that formed at open ocean MORs. Although sulfide is mainly hydrothermal in origin, a significant component of non-hydrothermal (bacteriogenic) sulfur may be formed in the host sediments (e.g., at Guaymas Basin; Chapter 5). In some cases the Pb content of the deposits is significant (0.1 wt.%) in comparison to MOR black smokers, reflecting the high Pb content of the sediments compared to MORB (Hannington et al., 2005, Hannington, 2014).

**3.1 Volcanogenic massive sulfide deposits**

Like MOR black smokers, the majority of ancient volcanogenic massive sulfide (VMS) deposits formed by metal-precipitation from high-temperature, moderately saline hydrothermal fluids with the metals sourced mainly from the volcanic rocks (e.g., Franklin et al., 2005; Hannington, 2014). A number of VMS deposits have been interpreted to be products of brine pool deposition, or at least to have formed beneath an anoxic brine pool: e.g., Hellyer in western Tasmania (Solomon and Zaw, 1997), Bathurst No. 12 in New Brunswick (Solomon, 2008a,b), and Tharsis in the Iberian Pyrite Belt (Tornos et al., 2008).

The Tharsis deposit in the Iberian Pyrite Belt (Figure 6.2; Tables 6.1, 6.2 and 6.4) is underlain by a thick succession (~2 km) of continental marine sediments, shales and volcanic rocks,

which is reflected in the relatively high Pb/Zn ratio and low Cu/Zn ratio (both ~0.4) of the ore compared to many other VMS deposits (Tornos and Heinrich, 2008). Due to efficient deposition of metals brought into the brine pool by the hydrothermal fluids, the Fe/(Zn+Cu+Pb) ratio in Tharsis is relatively high, and $H_2S$/(Fe+Zn+Cu+Pb) ratio is close to one. At least half of the reduced sulfur is thought to have been from non-hydrothermal sources, such as the shale horizons in the surrounding sediments and bacterial sulfate reduction in the brine pool (Tornos et al., 2008). Evaporites are not known in the footwall sediments, but high-salinity ore fluids (up to 14 wt.% NaCl) are interpreted to have formed by phase separation or magmatic contribution (Solomon et al., 2002; Tornos et al., 2008; cf. Nehlig et al., 1998). These fluids were considered to have been saline enough to have ponded at the seafloor forming a brine pool. Although the present Tharsis ore deposit comprises multiple stacked ore lenses, reconstruction of the pre-deformation shape shows that about 20 m of massive sulfides were deposited over large area of about ~2x4 km (Table 6.2). One of the more compelling aspects of the Tharsis deposit is the pervasive lamination of the ores, which have been interpreted as pulsed deposition from a brine pool or plume fall-out from an anoxic water column (process described in Goodfellow and Peter, 1996; Goodfellow et al., 2003). The former was favored by Tornos et al. (2008). The lack of zone refining or an obvious vent complex or chimney structures is consistent with deposition from the water column. Abundant diagenetically formed sulfides, with framboidal textures, are also present in the ores. Whether the sulfides at Tharsis precipitated directly from a brine pool or formed during diagenesis is uncertain. The presence of minor barite and the large range of $\delta^{34}S$ values are consistent with brine pool deposition (Solomon et al., 2004;

Table 6.4). The $\delta^{34}S$ values of the stockwork ore at Tharsis are ~5‰ higher than those of the massive banded ore; the latter is characterized by $\delta^{34}S$ around -5‰ and commonly as low as -10‰.

Many VMS deposits are spatially and genetically associated with chemical sediments (i.e., exhalite horizons) that closely resemble Algoma-type BIF (e.g., Sangster, 1978; Franklin et al., 1981; Peter and Goodfellow, 1996; Gross, 1996). Oxide facies BIF can be observed at the modern seafloor, where Fe- and Mn-(oxy)hydroxide-rich sediments of obvious hydrothermal origin are deposited at the distal margins of hydrothermal vent sites (e.g., Hein et al., 1997). Similar Fe(±Mn)-rich sedimentary horizons are found as distal equivalents of small VMS ore deposits in ophiolites (e.g., Høydal in the Løkken ophiolite, Norway: Grenne and Slack, 2005). A brine pool probably was not present at Høydal, and the vent proximal (sulfide-rich) and distal (jasper-rich) deposits more closely resemble modern black smoker deposits. The Si-Fe-OOH deposits are thought to have formed during white smoker venting (~100-280°C) and sulfide deposition during black smoker venting (>280°C) (Grenne and Slack, 2005). The distal Fe-rich sediments have mineralogical and chemical compositions that appear to reflect adsorption and deposition of metals (and other elements, esp. REE) on Fe-(oxy)hydroxide plume particles (e.g., Klein, 2005; Ohmoto et al., 2006; Bekker et al., 2004, 2006). At Høydal, trace metals such as As and Sb are enriched proximal to the hydrothermal vent source, which is considered to reflect more oxidized conditions in the water column during sedimentation. The fine laminations in the chemical sediments are interpreted to have formed during diagenesis (Grenne and Slack, 2003a) as in

other cherts (Murray et al., 1992; Lowe, 1999). This type of chemical precipitation may have been particularly common in the Mesozoic ocean and possibly Archean oceans, owing to anomalously Si-rich seawater at those times (Grenne and Slack, 2003b).

### 3.2 Sedimentary exhalative deposits

A number of sedimentary exhalative (SEDEX) massive sulfide deposits are considered to have formed from metal-rich pore waters expelled from compacting sedimentary basins during tectonic activity (e.g., Goodfellow and Lydon, 2007). Others may be hybrids formed by a combination of expulsion of basinal brines and hydrothermal convection driven either by the heat of rifting or by buried intrusions (Lydon, 2007; Tornos and Heinrich, 2008). SEDEX deposits derive a large part of their metals from the sedimentary basin, and the ore itself is typically hosted in sediments. Although they generally form at lower temperatures than most VMS, possibly with less effective metal leaching, the deposits are commonly large owing to the insulating properties of the thick pile of sedimentary strata. High salinity fluids are also common, formed from dissolution of evaporites, expulsion of connate brine, membrane diffusion or other diagenetic processes (Hanor, 1994), thus enhancing metal leaching even at low temperature. Modern SEDEX deposit formation (i.e., outflow of basinal brines on seafloor) is not known. However, brines are associated with fluid expulsion in the Gulf of Mexico (Lonsdale and Becker, 1985) and in the Mediterranean (Fitzsimons et al., 1997). Metalliferous basinal brines also have been sampled in deep wells (>1 km) in the Salton Sea geothermal system (Skinner et al., 1967; Williams and McKibben, 1989), possibly the closest modern examples of SEDEX-forming ore fluids in a continental setting. The

Salton Sea geothermal brines are highly saline (up to 30 wt.% NaCl), hot (up to ~350°C) and contain high concentrations of metals (e.g., 0.2 wt.% Fe, 800 ppm Zn) but little reduced sulfur.

Different types of sedimentary basins contain different types of SEDEX deposits (Cooke et al., 2000). The "McArthur River" type formed from $SO_4$-dominant ore fluids derived from sedimentary successions dominated by carbonates, evaporites, hematitic sandstones and mudstones; the “Selwyn Basin” type are interpreted to have formed from $H_2S$-dominant ore fluids in organic-rich shales basins.

The HYC deposit in the McArthur River Basin formed from oxidized brines that were characterized by high $aSO_4/aH_2S$ and near neutral or slightly acid pH (Tables 6.1, 6.2 and 6.3). The ore zone is ~80 m thick and composed of 8 mineralized shale horizons, each ~3-10 m thick. Large et al. (1998) suggested that each of the mineralized horizons formed from thousands of individual pulses of hydrothermal brine outflow, although the time span of the mineralizing events is not well-defined. The deposit lacks an obvious vent complex, although infilling of mass flows from the flanks of the basin was important (Large et al., 1998). Hydrothermal replacement textures are apparently minor. Some ores are interpreted to have formed by syn-sedimentary “rain-down”, although diagenetic replacement was also an important part of the ore-forming process (Large et al., 1998). The water column is thought to have been anoxic, with dominantly non-hydrothermal sources of reduced sulfur (e.g., in pore water: Large et al., 1998). To account for the metal

transport, the expelled basinal fluids were probably highly saline (~25 wt.% NaCl) and had temperatures of about 150°C (Cooke et al., 2000). Reaction with $H_2S$ or salinity decrease (dilution) were possible causes of metal precipitation. There is also extensive Mn-enrichment around the HYC deposit (Large et al., 2001).

The HYC model suggests that the ore-forming system was metal- rather than sulfide-limited. The $\delta^{34}S$ values of the main ore sulfides span a large range between -5‰ and +10‰, whereas early pyrite has slightly lower values down to -15‰ (Smith and Croxford, 1973; Eldridge et al., 1993). Late pyrite is heavier (average +10-15‰), with values up to +40‰ that increase gradually up stratigraphy. Large et al. (1998) interpreted the late pyrite to have formed from syngenetic sulfate deposits that underwent biogenic reduction during diagenesis (a process that might also occur in the Atlantis II sediments after the active phase is over).

A significant difference between HYC and other SEDEX deposits is a lack of distal barite. Barite is found as “bathtub ring” like deposits at the flanks of many SEDEX-hosting basins (e.g., Goodfellow et al., 1993), and extensive stratiform barite deposits are found in shale, siltstone and mudstone in the distal parts of the Pb-Zn deposits of the Selwyn Basin (Lydon et al., 1985). The stratiform barite is thought to have formed at the anoxic-oxic boundary from low temperature fluids emanating from basin-margin faults (Lydon et al., 1985).

Unlike the Selwyn Basin deposits, the Sullivan deposit in the Belt-Purcell Basin of southeastern British Columbia is characterized by a major feeder zone and vent complex with intense hydrothermal alteration dominated by chlorite and tourmaline (Lydon, 2007; Tables 6.1 and 6.2). A characteristic of the Sullivan deposit is that it formed during the early stages of emplacement of a sill-dike complex (Moyie Sills, that intruded unconsolidated sediments close to the seafloor), which is thought to have focused and possibly driven hydrothermal circulation (Lydon, 2007). The vent complex is surrounded by bedded sulfides that transition to distal hydrothermal sediments. Pyrrhotite is the main ore mineral, reflecting the reduced, low-sulfur nature of the hydrothermal fluids. The ores are Zn-rich, and the Pb/(Zn+Pb) ratio generally decreases away from the vent source from about 0.6 to <0.2 within a kilometer (Lydon, 2007). Cu is mainly found at the vent complex. $\delta^{34}S$ values of all sulfide minerals range from -10‰ to +5‰, with a mean of -2‰, and shift to heavier values in the ore zone, signifying greater input of hydrothermal fluids into the basin where metal-sulfides were being deposited (Campbell et al., 1978).

**3.3 Atypical stratiform base metal deposits**

A number of enigmatic stratiform base-metal deposits with characteristics of both VMS and SEDEX deposits or with unusual non-sulfidic mineral assemblages have been linked to brine pool deposition. The Broken Hill deposit in New South Wales, Australia, is one of the largest and richest stratiform ore deposits of this type on Earth (Tables 6.1 and 6.2). Its origin is highly debated, mainly because of the high-grade of metamorphism and because primary textures cannot be identified. A number of genetic models consider Broken Hill to have

formed as a volcanic-exhalative seafloor deposit (Parr and Plimer, 1993); others consider it to be a SEDEX deposit (Wright et al., 1987; Large, 2003) or entirely epigenetic and formed during peak metamorphism (Ehlers et al., 1996; Nutman and Ehlers, 1998). The similarity to SEDEX deposits and evidence for high-salinity ore fluids led Large and Davidson (1991) to suggest that Broken Hill was formed by deposition in a brine pool and that the main genetic difference between SEDEX and BHT deposits was the oxidation state of the brines (reduced, anoxic brines for most SEDEX basins and oxidized for BHT deposits).

The Broken Hill orebody included both Pb-rich and Zn-rich "lodes"; the Pb lodes have high Mn, whereas the Zn-lodes are Fe-rich. Large et al. (1996) suggested that variation in hydrothermal fluid composition is the main reason for formation of the compositionally different ore lenses: a shift towards less reduced and more alkaline fluids leading to the deposition of Pb-Mn lodes, and more reduced fluids responsible for formation of Zn-Fe lodes. Most of the non-ferrous metals are found as sulfides, but pyrite is subordinate to other sulfide minerals and a large part of the Fe is found in non-sulfides. The $S_{red}$/(Fe+Zn+Cu+Pb) ratio is around 0.6, and the Fe/(Cu+Zn+Pb) ratio is less than one. $\delta^{34}S$ values in sulfide minerals span a narrow range, with no significant variation between pyrite, sphalerite and galena (-3 to +7‰: Spry, 1987). Some orebodies are hosted in (meta)-exhalites, including coticules and tourmalinites (Spry and Wonder, 1989; Spry et al., 2000; Spry et al., 2007). They contain various non-sulfidic Cu- and especially Zn-rich minerals interpreted to have formed either by metamorphic desulfidation or representing primary non-sulfidic distal deposition (e.g., gahnite: Spry et al., 2000). The narrow range of $\delta^{34}S$

values may indicate that the hydrothermal fluids were the only major source of sulfide or may also be due to metamorphic desulfidation.

The Sterling Hill deposit in the New Jersey Highlands is an example of a stratiform Zn-oxide-silicate deposit. It was discovered and mined since the late 17$^{th}$ century until early 20$^{th}$ century (Ries and Bowen, 1922). The main ore minerals were willemite ($Zn_2SiO_4$), franklinite ($ZnFe_2O_4$), and zincite (ZnO) rather than sphalerite (Johnson et al., 1990). The deposit was highly metamorphosed during the Grenville orogeny (~1.0 Ga) obscuring important aspects of its genesis. However, it is clear that the metals were in place prior to the peak metamorphism; structural studies indicate that the orebody consists of continuous strata that experienced the same deformation as the host rock (Metsger, 1958; Metsger et al., 1969). The deposit is hosted in Franklin Marble, which is underlain by gneisses interpreted to be metamorphosed meta-sediments originally deposited in the rift basin before mineralization. Johnson and Skinner (2003) considered the non-sulfidic Zn ore to have formed syngenetically from oxidized brines devoid of reduced sulfur and that the primary deposition was as non-sulfidic particles that precipitated in a brine pool. Distal Fe mineralization was interpreted to have been deposited from an enriched water column associated with the Zn-rich hydrothermal system. Johnson and Skinner (2003) suggested that all Grenvillian stratiform deposits, from Sterling Hill to about 500 km north (cf. Buddington et al., 1969; deLorraine and Dill, 1982; Whelan et al., 1984; Gauthier and Brown, 1986; Gauthier et al., 1987), likely formed in similar brine pools.

## 4. Comparisons with the Atlantis II Deep

### 4.1 Geologic settings and sizes of deposits

The reconstructed tectonic histories of many SEDEX deposits suggest that they formed in intracontinental rifts at passive margins (e.g., HYC and Broken Hill: Huston et al., 2006), commonly with high sedimentation rates (e.g., ~57 cm/ka in the Belt-Purcell Basin: Lydon, 2007). Most ancient stratiform ores that are thought to have formed in brine pools are found in sedimentary basins with 2-7 km of sediment in the footwall (Table 6.2). This is a major difference between the Atlantis II Deep and other suspected brine-pool deposits and is clearly reflected in the metal ratios of the deposits (Table 6.1). The Red Sea rift is a young ocean basin and, despite the proximity of the continental landmasses, the sedimentation rate is <20 cm/ka; ore formation was preceded by no more than a few tens of thousands of years of sediment deposition. Solomon and Quesada (2003) suggested that brine-pool type VMS deposits, such as Tharsis, formed in collisional orogens; they considered that transcurrent faulting typical of compressional regimes was crucial for the rise of saline fluids and formation of brine pools.

All of the ancient ore deposits that are considered to have formed in a brine pool share one important characteristic in common with the Atlantis II Deep: their large size. Although the present Tharsis ore deposit comprises multiple stacked ore lenses, reconstruction of the pre-deformation shape shows that about 20 m of massive sulfides were deposited over an area of about ~2x4 km (Table 6.2). This is similar to the Atlantis II Deep, with a very similar total tonnage and ore grades. In both deposits the ore layers thin away from the vent

source, consistent with the highest depositional rates proximal to the vents. Sullivan, HYC and Broken Hill are all giant deposits (>150 Mt), highlighting the importance of a sedimentary host for trapping metals. Significantly lower Cu-grades than in Tharsis and Atlantis II are consistent with lower temperatures of the ore fluids.

The time required to form such large deposits is widely debated and generally poorly constrained. Large et al. (1998) suggested that the ore lenses at HYC formed during many discrete pulses of brine inflow. In the Atlantis II Deep, the equivalent thickness of ore (comparable to one ore lense at HYC) would have taken ~10,000 years to accumulate, taking into account the pore water content of the sediments. The main phase of hydrothermal activity in the Atlantis II Deep began ~15,000 years ago; at 90 Mt of ore, the average rate of deposition would have been ~6 Mt/ka; deposition of one unit (about 20-40 Mt) containing about 1 Mt of combined Cu and Zn would have taken approximately 5,000 years (Table 1.1). If we assume a similar mass accumulation rate for a deposit like HYC, it would have taken a minimum of ~100,000 years to deposit the 20 Mt of contained Zn+Pb+Cu. At these rates, even Broken Hill, one of the largest exhalative ore bodies on earth, could have formed within a million years. On modern mid-ocean ridges, slow spreading rates have been correlated with fewer but larger hydrothermal systems (Baker et al., 1995; Hannington et al., 2011). Even at slow rates of spreading, the Atlantis II Deep gets ~1.1 km wider every 100,000 years, raising questions about the long-term stability of the brine pool and whether it might eventually drain, thus terminating the formation of the deposit.

Solomon et al. (2004) considered that the lack of a distinct vent complex is one of the defining features of brine-pool type deposits, such as Tharsis. Both Sullivan and the deposits in the Selwyn Basin have notable vent complexes, although they lack chimneys and other constructional features that might have formed on the paleo seafloor. The McArthur River-type deposits lack an obvious vent complex (Cooke et al., 2000), although Goodfellow and Lydon (2007) noted that in many SEDEX deposits this may only reflect proximity to the source. For example in the Atlantis II Deep, the distal metalliferous sediments lack a clear relationship to the inferred vent complex.

A characteristic of many deposits, and a clear link to active rifting, is an association with emplacement of sill-dike complexes (e.g., Moyie Sills that intruded unconsolidated sediments close to the seafloor at Sullivan). The sills are thought to have focused and possibly driven hydrothermal circulation in some cases (e.g., Lydon, 2007). Syn-sedimentary emplacement of basaltic sills also occurred in the Atlantis II Deep and similar sub-seafloor sill complexes are present at Middle Valley and in the Guaymas Basin (Goodfellow and Zierenberg, 1999). The basaltic sill in the Southwest Basin of the Atlantis II Deep intruded very close to the seafloor (below <5 m of sediment) and caused extensive alteration and metamorphism in the immediate surrounding ore material (e.g., hematite transformation to magnetite and pyroxene formation). Intrusion of the sill also may have promoted the formation of anhydrite layers in the metalliferous sediment by heating of pore water.

However, it is unclear if they were deep enough or large enough to have driven hydrothermal circulation.

**4.2 Metal sources and hydrothermal deposition**

The documented resource of 90 Mt of dry, salt-free ore material in the Atlantis II Deep is an order of magnitude larger than any other known deposit on the sea floor (Hannington et al., 2010). In general, the sediment-hosted deposits are larger than open ocean black smoker deposits (Bent Hill at the Middle Valley is among the largest, with 9 Mt of massive sulfide material: Zierenberg et al., 1998), but average Cu and Zn grades are significantly lower. The Atlantis II sediments also have low Cu and Zn grades compared to other modern seafloor metal-deposits, but this reflects the large dilution by Fe-(oxy)hydroxides and other sediments. The Fe/(Zn+Cu+Pb) and Pb/(Zn+Pb) ratios of the Atlantis II sediments are similar to those of MOR black smoker fluids (e.g., Hannington et al., 2005) and consistent with a similar metal source, reflecting the dominant basaltic substrate. Except for a few meters of basal sediment, the metalliferous deposits in the Atlantis II Deep are directly underlain by mid-ocean ridge basalts (MORB). In contrast to the Atlantis II sediment, the massive sulfides deposited at open ocean black smokers have significantly lower Fe/(Zn+Cu+Pb) ratios than the hydrothermal fluids because Fe is less efficiently deposited than Cu and Zn. Most of the Fe contained in the high-temperature hydrothermal vent fluid is dispersed into the ocean (Converse et al., 1984; Baker et al., 1985). In the Atlantis II Deep, all of this Fe is efficiently deposited as Fe-(oxy)hydroxides in the metalliferous sediments.

The actual vent complex in the Atlantis II Deep has never been observed and no chimney deposits have been found, although Blum and Puchelt (1991) documented the presence of sulfide chimneys in the Kebrit Deep (24°43'N and 36°17'E: Figure 1.1). Subvertical anhydrite veins and breccias that are present in the cores from the Southwest Basin are considered to be the best evidence of a high-temperature hydrothermal upflow zone. Fluid inclusion data from the veins (at <10 m depth in the sediments) indicate black smoker temperatures (>350°C). However, black smoker fluids typically have a molar amount of reduced sulfur close to that of the total metals, and all of the metals in solution can be precipitated as sulfides. Black smoker sulfide deposits have $S_{red}$/(Fe+Cu+Zn+Pb) ratios typically around one, whereas the Atlantis II sediments have $S_{red}$/(Fe+Cu+Zn+Pb) <0.1 in all sedimentary units (Table 2.1). As the source of metals (MORB) is the same in the Red Sea as in typical MOR black smoker systems, the low $S_{red}$/(Fe+Cu+Zn+Pb) must be due to the significantly higher salinity and metal-carrying capacity of the ore fluids.

All of the SEDEX deposits considered above are interpreted to have formed from high-salinity fluids capable of leaching metals more efficiently than typical MOR hydrothermal fluids, even at relatively low temperatures. Abundant reduced sulfide and organic matter in the sedimentary footwall also differs from the Atlantis II Deep and may partly explain the much higher $S_{red}$/(Fe+Zn+Cu+Pb) and wider range of $\delta^{34}S$ values in those deposits. A characteristic of many of these deposits is a low Cu/Zn ratio, reflecting the strong temperature control on Cu solubility (e.g., Hannington, 2014). However, basinal brines have low Cu/Zn ratios even at high temperatures (e.g., Cu/Zn ratio ~0.01 in Salton Sea basinal

brines), suggesting that high-salinity favors Zn solubility (e.g., Yardley, 2005; Figure 6.4). Likewise, the high salinity of the Atlantis II fluids might contribute to the significantly lower Cu/Zn ratios in the Atlantis II sediments (0.23) than in black smoker fluids (~1.4: data for MAR sites from Hannington et al., 2005). Pottorf and Barnes (1983) concluded that anomalously low Cu/Zn in the Atlantis II Deep was due to pre-enrichment of Zn in the downwelling brine from leaching of metal out of the Red Sea evaporite-shale sequence, which is known to be enriched in Zn (Manheim, 1974). However, the Atlantis II sediments are low in other metals (e.g., vanadium) that are present at high concentrations in the Red Sea black shales (Stoffers and Ross, 1974; cf. Jedwab et al., 1989).

Pyrrhotite and pyrite, and to a lesser extent carbonates, are the dominant Fe minerals in ancient brine pool-type deposits, whereas oxy-hydroxides, clays and carbonates are dominant in the Atlantis II Deep. The latter more closely resemble BIF than SEDEX or VMS assemblages. At Broken Hill, the sulfide ores are partly hosted in BIF, resembling the transition between the SU units and CO unit in the Atlantis II Deep. In the absence of an additional source of reduced sulfur in brine pool-type deposits, the excess metals are deposited as non-sulfide phases. If non-hydrothermal sulfide is abundant, as documented at Tharsis, stratiform sulfide deposits will form (Solomon et al., 2004). In the Atlantis II Deep, abundant anhydrite was formed by heating of the Lower Brine, possibly enhanced by the highly saline, Ca- and $SO_4$-rich solutions (cf. Figure 2.20 in Chapter 2). The precipitation of abundant anhydrite in this manner may be evidence of brine pool conditions, but the

anhydrite is unlikely to be preserved in the geologic record, either because of dissolution or conversion to sulfide by bacteria as suggested for HYC (Large et al., 1998).

**4.3 Origins of the brines**

Although chloride concentrations up to ~8 wt.% equivalent NaCl have been measured in black smoker fluids (mainly related to phase separation: e.g., Butterfield et al., 1994; Fontaine et al., 2007), the average salinity is identical to seawater (Hannington et al., 2005). Even the most saline black smoker fluids (~8 wt.% NaCl at ~350°C) are buoyant in modern seawater (Turner and Campbell, 1987). Non-buoyant ("bottom-hugging") brines have not yet been observed at these high temperatures, and large density contrasts are unlikely to be maintained over long transport distances (Fontaine et al., 2007).

In SEDEX environments, like the Atlantis II Deep, evaporites are considered to be the most likely source of salt. Evaporites, or evidence of their dissolution are sometimes present in the sedimentary basins hosting significant SEDEX deposits. However, because of the solubility of evaporites in seawater their preservation in the recharge area of hydrothermal fluids is likely rare in most open ocean settings. Even in the Red Sea, evaporite outcrops at the flanks of the Atlantis II Deep are undergoing rapid mobilization (e.g., Augustin et al., 2014). Where exposed, the formation of cold brine pools in bathymetric depressions is common, but hot brines only develop where these fluids are circulated into the basement (e.g., Pierret et al., 2001). Laurila et al. (2014b) suggested that a cold (euxinic) brine pool was likely present in the Atlantis II Deep prior to the beginning of hydrothermal activity, and

the transformation of a cold to a hot brine pool may be the normal progression in rifted sedimentary basins.

**4.4 Role of anoxia and euxinia**

A number of authors have noted a strong correlation between the formation (and preservation) of exhalative ore deposits and times of global ocean anoxia (Goodfellow, 2004; Ohmoto et al., 2006). Goodfellow and Jonasson (1984) saw a strong correlation between secular variations in the $\delta^{34}S$ pyrite curve for the Selwyn Basin (Goodfellow, 1987) and the $\delta^{34}S$ in contemporaneous exhalative ore deposits (e.g., Howard Pass) and suggested formation of the massive sulfides during periods of seawater euxinia. Because similar trends were observed in other volcano-sedimentary basins (e.g., Bathurst mining camp, New Brunswick), the concept of global ocean anoxia was considered fundamental to the formation of large stratiform base metal ore deposits (Goodfellow and Peter, 1996). Solomon (1999, 2008a,b) argued that these conditions were likely confined to individual basins (cf. reply in Goodfellow and Peter, 1999) and suggested that these conditions were, in fact, developed only in local brine pools. Contemporaneous precipitation of exhalative sulfide ores and BIF (e.g., Ohmoto et al., 2006) is a strong argument against euxinia; all metals vented into an euxinic ocean would be deposited as sulfides, and massive deposition of Fe-(oxy)hydroxides in BIF would not have been possible. Gleeson et al. (2013) suggested that the sulfide minerals in the SEDEX deposits in the Selwyn Basin formed during early diagenesis due to a fluctuating chemocline in the host sediments, rather than as a consequence of long-term euxinia above the sediment water interface. This genetic model

is supported by observations in the Atlantis II Deep in which the formation of diagenetic sulfides from enriched pore waters can be observed and $\delta^{34}S$ of diagenetic sulfides reflect contributions of bacteriogenic sulfide in the sediments.

Stratified basins with euxinic bottom layers are common on the modern ocean floor and form from bacterial sulfate reduction without hydrothermal influence (e.g., Lyons and Severmann, 2006; Seal, 2006). This is thought to have been important for most SEDEX deposits (e.g., Sullivan: Taylor and Beaudoin, 2000) and some brine pool-type VMS (e.g., Tharsis: Tornos et al., 2008). However, it is less clear if the sulfate reduction happens in the water column or the sedimentary pore water. The current Atlantis II Lower Brine has sparse bacterial growth, but the overlying brine layers are inhabited by abundant bacteria that can reduce sulfate (Bougouffa et al., 2013). Bacteria were also recently incubated from the sediments (Siam et al., 2012), which were previously thought to be sterile (Trüper, 1969).

An alternative source of $H_2S$ in brine pool settings is contemporaneous hydrothermal activity. However, the accumulation of dissolved sulfide from a hydrothermal source requires that the total metal input is much less than that of the $S_{red}$. This is not the case in the Atlantis II Deep. In fact, the formation of wholly euxinic basins due to hydrothermal influence may be quite rare as the input of metal-rich hydrothermal brines would likely cause a massive decrease in the $H_2S$ content of the brine pool. Strongly negative $\delta^{34}S$ values in the initial sediments of the Atlantis II Deep also suggest that it evolved from an initially euxinic basin into an anoxic but $H_2S$-free brine pool early in its history, despite the large

input of hydrothermal fluid (Chapter 5). The evolution from sulfides with high bacterial influence (strongly negative $\delta^{34}S$ values) to mainly hydrothermal sulfides during main-stage ore formation ($\delta^{34}S$ ~+5‰) and back to negative is seen, for example, in the Red Dog Zn-Pb-Ag deposit (Kelley et al., 2004). Similar shifts in $\delta^{34}S$, from negative in the footwall to slightly positive are also seen at Sullivan (Campbell et al., 1978). It also seems unlikely that deposits with significant non-sulfidic metallic minerals or associated exhalite horizons could have formed in euxinic brine pools. For example, Johnson et al. (1990) and Johnson and Skinner (2003) suggested that both proximal and distal ores at Sterling Hill were formed in a stratified brine pool that contained almost no reduced sulfur, similar to the Atlantis II Deep.

A brine pool without dissolved sulfide also has been suggested as the depositional environment for Broken Hill (Large et al., 1996) based on the low $S_{red}$/(Fe+Zn+Cu+Pb) ratio and $\delta^{34}S$ values indicating little input of sulfide from non-hydrothermal sources. The narrow range of $\delta^{34}S$ values in Broken Hill suggests that the hydrothermal fluids were the only major source of sulfide. Large et al. (2001) and Campbell et al. (1978) suggested that HYC and Sullivan were also sulfide- rather than metal-limited systems, similar to the Atlantis II Deep. In some brine-pool models, $H_2S$ is thought to have diffused from the overlying euxinic water column into the brines (e.g., Goodfellow, 2004; Figure 6.5B). This is broadly similar to the present situation in the Atlantis II Deep, where bacterial sulfate reduction happens in the upper brines and the lower brine is anoxic (Figure 6.5C). Sulfide production by bacteria at the chemocline is limited, suggesting that formation of a significant stratiform sulfide lens typical of SEDEX environments is unlikely in the Atlantis II Deep. The source of

abundant reduced sulfur at Tharsis is less certain. The presence of minor barite and the large range of $\delta^{34}S$ values is similar to the Atlantis II Deep (Solomon et al., 2004; Table 6.4). However, the $\delta^{34}S$ values of the stockwork ore at Tharsis are ~5‰ higher than those of the massive banded ore; the latter is characterized by $\delta^{34}S$ around -5‰ and commonly as low as -10‰. Judging from the much more abundant pyrite at Tharsis, there was clearly a much larger input of reduced sulfur than in the Atlantis II Deep.

The abundant stratiform barite, commonly found as "bathtub ring" deposits at the flanks of many SEDEX-hosting basins (e.g., Lydon et al., 1985; Goodfellow et al., 1993), is thought to have formed at the anoxic-oxic boundary from low temperature fluids emanating from basin-margin faults. In the Atlantis II Deep, dissolved Ba is also precipitated at the shallow margins of the basin overlain by the Upper Brine (Sval'nov et al., 1984). Although the Lower Brine is undersaturated with respect to barite (Shanks and Bischoff, 1977), even at the high concentrations of barium and $SO_4$ (2.1 ppm Ba and 640 ppm $SO_4$: Pierret et al., 2001), the Upper Brine is more seawater-like with sufficient $SO_4$ to cause barite deposition. However, extensive deposits of stratiform barite, like those associated with some SEDEX deposits, have not been found.

**4.5 Fate of metals in the brine pool environment**

The Atlantis II Deep is very efficient in retaining metals, forming a significant ore deposit in less than 15,000 years. A drawback is dilution of the ore metals by abundant Fe-(oxy)-hydroxides. In open ocean conditions, metal loss is a major factor influencing the size and

grade of deposits forming on the seafloor (>90% of metals are lost: Converse et al., 1984). Metal loss before the hydrothermal fluids reach the seafloor is also significant in some cases and partly explains the low Cu/Zn in many massive sulfides deposits. Some high-temperature mineral deposition has occurred in the Atlantis II Deep proximal to the site of venting (Missack et al., 1989), but SEDEX deposits generally lack such high-temperature mineralization. The presence of permeable and/or reductive horizons in the sedimentary strata also may limit ore formation at the seafloor.

In contrast to Fe and other metals, the brine pool in the Atlantis II Deep is an inefficient trap for Mn. Whereas most other metals are retained within the brine-covered area, Mn-(oxy)hydroxides descending through the brine pool mainly dissolve before reaching the seafloor and are only deposited on the flanks of the basin. Thus, elements that diffuse out of a basin or to its margins (e.g., Mn and Ba) may be a good indicator of stratified brine-pool conditions with anoxic bottom layers. The distal Mn and Zn enrichment extends as much as 10 km away from the inferred source vents in the Atlantis II Deep (Bignell et al., 1976a; Figure 6.6). Fe, which is highly enriched in sediments within the brine-covered area, drops sharply to background values outside the brine-covered area (e.g., Bignell et al., 1976a; Figure 6.6). Only during the maximum extent of the Atlantis II Lower Brine, did the Fe- and Zn-rich Lower Brine spill over the bathymetric barriers of the depression leading to deposition of metal-rich layers on the surrounding seafloor (especially Discovery and Chain Deeps: Bischoff, 1969, Bignell et al., 1976a, b). Similar broad Mn and Zn enrichment halos are commonly found around many exhalative ore deposits and are well preserved in even

the most highly metamorphosed examples (e.g., Broken Hill: Spry et al., 2000). The extensive Mn-enrichment around the HYC deposit is similar to that observed in the Atlantis II Deep (Large et al., 2001). At the Lady Loretta deposit in Queensland, Australia, Zn- and Mn-enrichment extends only a few hundred meters away from the sulfide body (Large and McGoldrick, 1998). However, an inner "siderite halo" and an outer "ankerite halo" extend a few hundred meters away from the deposit. Similar mineralogical changes are seen in the Atlantis II Deep within ~2 km of the vent proximal area (Chapter 2).

Open ocean hydrothermal vent sites and similar ancient deposits (e.g., Høydal: Grenne and Slack, 2005) have much larger Fe- and Mn-enrichment haloes from distal plume fallout. At Høydal, trace metals such as As and Sb are enriched proximal to the hydrothermal vent source, whereas in the Atlantis II Deep, As is enriched in vent distal sediments. These differences are considered to reflect the more oxidized conditions in the water column during Høydal formation and rapid co-deposition of As with Fe-(oxy)hydroxides.

**4.6 Origin of banding in laminated ores**

Shortly after its discovery, James (1969) recognized the sedimentary succession of the Atlantis II Deep, with alternating layers of silicates, oxides, carbonates and sulfides, as essentially a banded iron formation with anomalously high Cu and Zn concentrations. The alternating chemically distinct layers in the sediment have generally been interpreted as reflecting temperature variations in the hydrothermal venting (e.g., Hofmann and Harris, 2008; Bekker et al., 2010). Although short-term changes in hydrothermal activity are

evident in the proportion of sulfidic components in the near-vent sediments of the Atlantis II Deep, the majority of the fine laminations appear to have formed after deposition. Among the key observations that support this interpretation are textural changes from poorly crystalline primary deposition with diffuse layering in AM to well-defined lamination and increasing chemical separation between the individual laminae with depth in the sedimentary cores. Similar diagenetic transformations are described for a number of ancient deposits (e.g., Large et al., 2007). The poorly crystalline clays in the Atlantis II sediments (Chapter 2) may also be precursors for aluminosilicates now present in many BIFs (e.g., Klein, 2005). Authigenic carbonates that also form diagenetically in the Atlantis II Deep (e.g., Bischoff, 1969; Blanc et al., 1998) are also compositionally similar to those found in BIFs (Klein, 2005). Unlike the very fine-grained chemical sediments that make up most Algoma-type BIFs, the Atlantis II Deep deposits are mainly chemical-clastic sediments, and some of the layering is related to clastic deposition. Rates of deposition in the Atlantis II Deep were generally high (~1-2m/1000 years: Table 1.1), but even higher rates of chemical sedimentation have been suggested for some BIF, such as the jasper beds in the Løkken ophiolite (e.g., >5m/1000 years: Grenne and Slack, 2003a, 2005).

## 5. Conclusions

The Atlantis II Deep has been widely suggested as a modern analog of stratiform base metal ore deposits formed in a brine pool. In a sediment-starved basin, such as the Red Sea rift, evaporites must be present in the surrounding strata to produce the high-salinity brines. Modern evaporites are rare except in enclosed basins at low latitudes, and an exact analog

of the Atlantis II Deep deposits have not yet been recognized in the geological record. This may be due to the rather unusual tectonic setting, with evaporites found directly associated with MORB.

The Tharsis deposit in the IPB is perhaps the best known example of a VMS deposit thought to have formed in a brine-pool. It is similar in size to the Atlantis II Deep, the massive sulfide lenses have a similar aspect ratio (thin and wide), and the metal grades are generally low compared to other VMS deposits. The "ores" in both deposits are well laminated, they lack well-developed vent complexes, and carbonate is abundant but barite is lacking. Framboidal textures and sulfur isotope data suggest that sulfide minerals formed in part diagenetically from bacteriogenic sulfate. Similar features are well known among the VMS deposits of the Bathurst Mining, although barite is more abundant in the Bathurst ores. A major difference between the Atlantis II Deposits and the IPB and Bathurst Mining Camp is the association with felsic volcanism and possible magmatic contributions of metals and sulfur to the VMS deposits (Solomon, 2008a).

The Atlantis II sediments closely resemble VMS-associated BIF and distal "exhalites" of some VMS deposits. The finely laminated texture and intercalation of Fe (± Mn) oxyhydroxide, carbonate, silicate and sulfide dominated sedimentary layers closely resemble the different facies of BIF. The main variations are in the Cu and Zn concentrations, reflecting proximity to the hydrothermal source. The dominantly stratigraphic rather than lateral facies variations in the Atlantis II Deep reflects the

confinement of the brines to a relatively small basin that limits the spatial separation between vent proximal and distal deposition. In both BIF and exhalites, precipitation at chemoclines is an important metal deposition pathway, similar to the Atlantis II Deep. A major difference is the higher metal content of the Atlantis II sediments, owing to the high salinity of the brines, but also the larger clastic component. In contrast to Atlantis II sediments and VMS-associated BIF, larger-scale Algoma-type BIF deposits usually lack a spatial association with a clearly established hydrothermal vent source (Bekker et al., 2010).

SEDEX deposits are among the closest analogs of the Red Sea metalliferous sediments. However, the MORB-dominated source rocks and lack of continent-derived sediment in the Atlantis II Deep is reflected in the higher Cu/Zn and lower Pb/Zn ratios compared to SEDEX deposits. Sulfur concentrations are also about an order of magnitude lower in the Atlantis II than in typical SEDEX deposits, reflecting limited input of non-hydrothermal sulfide. Bacterial sulfate reduction has played a critical role in formation of most SEDEX deposits (e.g., Large et al., 1998; Campbell et al., 1978; Smith and Croxford, 1973; Eldridge et al., 1993) and is clearly seen in the rather homogenous sulfur isotope record of SEDEX systems. Dramatic variations in $\delta^{34}S$ (>20‰) in the Atlantis II sediments are rarely seen in SEDEX deposits (e.g., absent in HYC). Instead, sulfide is produced in abundance by diagenetic processes and in the sedimentary pore water, as recently suggested for the Selwyn Basin (Gleeson et al., 2013). The finely laminated ores of many SEDEX deposits are strikingly similar to some of the sulfide facies of the Atlantis II sediments. In SEDEX systems, these are widely interpreted to be products of pulsed hydrothermal venting, which has also been

documented in the Atlantis II brine pool. However, this study shows that most of the fine layering in the sediments likely formed during diagenesis. Barite deposits are commonly spatially associated with SEDEX deposits hosted in reduced basins, but they are absent at McArthur River (Cooke et al., 2000). Barite crusts are found at the flanks of the Atlantis II Deep, but they are minor compared to the massive accumulations of barite at the margins of some reduced basins (e.g., Selwyn Basin). This may partly reflect the MORB source rocks in the Atlantis II Deep compared the to Ba-rich continent-derived sediments in the Selwyn Basin.

The Broken Hill deposits might have formed in a setting similar to that of the Atlantis II Deep. A number of important similarities are recognized: 1) the presence of non-sulfidic metallic minerals (i.e., total sulfur less than total metals), 2) sulfur-poor sulfide assemblages in which pyrite is not the dominant mineral, 3) host rocks containing various iron formation facies and oxidized clastic sediments, 4) strong Mn enrichment (more than few percent) in the surrounding strata and associated iron formation. Higher Pb/Zn and lower Cu/Zn at Broken Hill likely reflect lower temperatures of the vent fluids and the continental (felsic) substrate compared to the Atlantis II Deep. Elements such as Mn and Pb also may have been more efficiently precipitated in a more oxidized brine pool at Broken Hill. Mn oxides scavenge Pb about 10 times more efficiently that do Fe oxides (Dong et al., 2003) and this might partly account for the higher Pb content of the distal Broken Hill sediments.

## References


Anschutz, P., Blanc, G. and Stille, P., 1995,Origin of fluids and the evolution of the Atlantis II deep hydrothermal system, Red Sea: Strontium isotope study. *Geochim. Cosmochim. Acta* 59 (23), p. 4799-4808.

Ames, D. E., Franklin, J. M. and Hannington, M. D., 1993, Mineralogy and geochemistry of active and inactive chimneys and massive sulfide, Middle Valley, northern Juan de Fuca Ridge: An evolving hydrothermal system. *Can. Mineral.* 31, p. 997-1024.

Anschutz, P., Blanc, G. and Stille, P., 1995,Origin of fluids and the evolution of the Atlantis II deep hydrothermal system, Red Sea: Strontium isotope study. *Geochim. Cosmochim. Acta* 59 (23), p. 4799-4808.

Anschutz, P., Turner, J. S. and Blanc, G., 1998, The development of layering, fluxes through double-diffusive interfaces, and location of hydrothermal sources of brines in the Atlantis II Deep: Red Sea,*Jour. Geophys. Res*., 103 (C12), p. 27809-27819.

Anschutz, P., Blank, G., Monnin, C. and Boulècue, J., 2000, Geochemical dynamics of the Atlantis II Deep (Red Sea): II. Composition of metalliferous sediment pore waters. *Geochim. Cosmochim. Acta* 64 (23), p. 3995–4006.

Augustin, N., Devey, C. W., van der Zwan, F. M., Feldens, P., Tominaga, M., Bantan, R. A. and Kwasnitschka, T., 2014, The rifting to spreading transition in the Red Sea. *Earth Planet. Sci. Lett.* 395, p. 217-230.

Baker E. T., Lavelle, J. W. and Massoth, G. J., 1985, Hydrothermal particle plumes over the southern Juan de Fuca Ridge. *Nature* 316 (6026), p. 342-344.

Baker, E. T., German, C. R., and Elderfied, H., 1995, Hydrothermal plumes over spreading-center axes: global distributions and geological inferences, *in* Humphris, S. E., Zierenberg, R. A., Mullineaux, L. S. and Thomson, R. E., eds., *Seafloor Hydrothermal Systems: Physical, Chemical, Biological, and Geological Interactions*. AGU Monograph Ser. 91, American Geophysical Union, Washington, DC, p. 47-71.

Barrie, C. T. and Hannington, M. D., 1999, Classification of VMS deposits based on host rock compositions, *in* Barrie, C. T. and Hannington, M. D., eds., *Volcanic-Associated Massive Sulfide Deposits: Processes and Examples in Modern and Ancient Settings.* Rev. Econ. Geol. 8, p. 1-13.

Bekker, A., Holland, H. D., Wang, P. L., Rumble, D., Stein, H. J., Hannah, J. L., Coetzee, L. L., and Beukes, N. J., 2004, Dating the rise of atmospheric oxygen. *Nature* 427, p. 117-120.

Bekker A., Slack J., Planavsky N., Krapež B., Hofmann A., Konhauser K. O. and Rouxel O. J., 2010, Iron formation: The sedimentary product of a complex interplay among mantle, tectonic, oceanic, and biospheric processes. *Econ. Geol*. 105, p. 467–508.

Bignell, R. D., 1975, Timing, distribution and origin of submarine mineralization in the Red Sea. *Inst. Mining Metall. Trans*. 84 (B), p. 1-6

Bignell, R. D., Cronan, D. S. and Tooms, J. S., 1976a, Metal dispersion in the Red Sea as an aid to marine geochemical exploration. *Inst. Mining Metall. Trans.* 84 (B), p. 274-278.

Bignell, R. D., Cronan, D. S. and Tooms, J. S., 1976b, Red Sea metalliferous brine precipitates. *Geol. Ass. Canada. Spec. Paper* 14, p. 147-184.

Bischoff, J. L., 1969, Red Sea geothermal brine deposits: their mineralogy, chemistry and genesis, *in* Degens, E. T. and Ross, D. A., eds., *Hot Brines and Recent Heavy Metal Deposits in the Red Sea*. Springer-Verlag, New York, p. 368-406.

Blanc, G., Anschutz, P. and Pierret, M-C., 1998, Metalliferous sedimentation in the Atlantis II Deep: a geochemical insight, *in* Purser, B. H. and Bosence Dan, W. J., eds., *Sedimentation and Tectonics in Rift Basins: Red Sea – Gulf of Aden*, Springer, p. 505-520.

Blum, N. and Puchelt, H., 1991, Sedimentary-hosted polymetallic massive sulfide deposits of the Kebrit and Shaban Deeps, Red Sea. *Miner. Deposita* 26, p. 217-227.

Bougouffa, S., Yang, J. K., Lee, O. O., Wang, Y., Batang, Z., Al-Suwailem, A. and Qian, P. Y., 2013, Distinctive microbial community structure in highly stratified deep-sea brine water columns. *Appl. Environ. Microbiol.* 79 (11), p. 3425-3437.

Buddington, A. F., Jensen, M. L., and Mauger, R. L., 1969, Sulfur isotopes and origin of northwest Adirondacks sulfide deposits, in Igneous and metamorphic geology—A volume in honor of Arie Poldervaart. *Geol. Soc. America Memoir* 115, p. 423-451.

Butterfield, D. A., McDuff, R. E., Mottl, M. J., Lilley, M. D., Lupton, J. E., and Massoth, G. J., 1994, Gradients in the composition of hydrothermal fluids from the Endeavour segment vent field: phase separation and brine loss. *J. Geophys. Res.* 99, p. 9561-9584.

Bäcker, H., Lange, K. and Richter, H., 1975, Morphology of the Red Sea central graben between Subair Islands and Abul Kizaan. *Geol. Jahrb.* D13, p. 79-123.

Campbell, F. A., Ethier, V. G., Krouse, H. R. and Both, R. A., 1978, Isotopic composition of sulfur in the Sullivan orebody British Columbia. *Econ. Geol*. 73, p. 246-268.

Chu, D. and Gordon, R. G., 1998, Current plate motions across the Red Sea. *Geophys. J. Int.* 135, p. 313-328.

Claypool, G. E., Holser, W. T., Kaplan, I. R., Sakai, H. and Zak, I., 1980, The age curves of sulfur and oxygen isotopes in marine sulfate and their mutual interpretation. *Chem. Geol.* 28, p. 198-260.

Cochran, J. R., 2005, Northern Red Sea: Nucleation of an oceanic spreading center within a continental rift. *Geochem. Geophys. Geosyst.* 6 (3), Q03006, 34 p.

Cochran, J. R. and Martinez, F., 1988, Evidence from the northern Red Sea on the transition from continental to oceanic rifting, *in* Le Pichon, X. and Cochran, J. R, eds., *The Gulf of Suez and Red Sea Rifting*. Tectonophysics 153, p. 25-53.

Converse, D.R., Holland, H.D. and Edmond, J. M., 1984, Flow rates in the axial hot springs of the East Pacific Rise (21°N): implications for the heat budget and the formation of massive sulfides. *Earth Planet. Sci. Iett*. 69, p. 159-175.

Cooke, D. R., Bull, S. W., Large, R. R. and McGoldrick, P. J., 2000, The importance of oxidized brines for the formation of Australian proterozoic stratiform sediment-hosted Pb-Zn (Sedex) deposits. *Econ. Geol. Bull.* 95 (1), p. 1-18.

deLorraine, W. F. and Dill, D. B., 1982, Structure, stratigraphic controls, and genesis of the Balmat-Edwards zinc deposits, northwest Adirondacks, New York. *Geol. Ass. Canada* Special Paper 25, p. 571-596.

Dong, D., Derry, L. A. and Lion, L. W., 2003, Pb scavenging from a freshwater lake by Mn oxides in heterogeneous surface coating materials. *Water Res*. 37 (7), p. 1662-6.

Dupré, B., Blanc, G., Boulègue, J. and Allègre, J., 1988, Metal remobilization at a spreading centre studied using lead isotopes. *Nature* 333, p. 165-167.

Drake, A. A., Jr., 1990, The regional geologic setting of the Franklin-Sterling Hill district, *in* Character and origin of the Franklin-Sterling Hill orebodies, Proceedings volume, Lehigh Univ., Bethlehem, Pennsylvania, p. 14-31.

Ehlers, K., Foster, J., Nutman, A.P. and Giles, D., 1996, New constraints on Broken Hill geology and mineralization. *Centre for Ore Deposit and Exploration Studies Special Publication* 1, p. 73-87.

Eldridge C. S., Williams, N. and Walshe, J. L., 1993, Sulfur isotope variability in sediment-hosted massive sulfide deposits as determined using the ion microprobe SHRIMP II: A study of the HYC deposit at McArthur River, Northern Territory Australia, *Econ. Geol*. 88, p. 1-26.

Fernandes, N. A., 2011, *Geology and geochemistry of Late Devonian-Mississippian Sediment-Hosted barite sequences of the Selwyn Basin, NWT and Yukon, Canada*. M.Sc. Thesis, University of Alberta, 130 p.

Fitzsimons, M.F., Dando, P. R., Hughes, J. A. Thiermann, F. Akoumianaki, I. and Pratt S. M., 1997, Submarine hydrothermal brine seeps off Milos, Greece: Observations and geochemistry. *Mar. Chem.* 57, p. 325-340.

Fontaine, F. J., Wilcock, W. S. D. and Butterfield, D. A., 2007, Physical controls on the salinity of mid-ocean ridge hydrothermal vent fluids. *Earth Planet. Sci. Lett.* 257, p. 132-145.

Franklin, J. M., Gibson, H. L., Galley, A. G. and Jonasson, I. R., 2005, Volcanogenic massive sulfide deposits, *in* Hedenquist, J. F., Thompson, J. F. H., Goldfarb, R. J. and Richards, J. P., eds., *100th Anniversary Volume of Econ. Geol.,* p. 523-560.

Franklin, J. M., Lydon, J. M. and Sangster, D. F., 1981, Volcanic-associated massive sulfide deposits, *in* Skinner, B. J., ed., *Economic Geology 75$^{th}$ anniversary volume, 1905-1980.* Econ. Geol. Pub. Company, Littleton, CO, p. 485-627.

Gauthier, M., and Brown, A. C., 1986, Zinc and iron metallogeny in the Maniwaki-Gracefield district, southwestern Quebec. *Econ. Geol*. 81, p. 89-112.

Gauthier, M., Brown, A. C. and Morin, G., 1987, Small iron-formations as a guide to base- and precious-metal deposits in the Grenville province of southern Quebec, *in* Appel, P. W. U. and LaBerge, G. L., eds., *Precambrian iron-formations.* Theophrastus Publications, Athens, p. 297–327.

Gleeson, S., Paradis, S., Magnall, J. and Reynolds, M. A., 2013. Sedex deposits in the Northern Cordillera: Where are we in the basin, and what role does water column euxinia really play?. *Whistler 2013: Geoscience for Discovery, conference abstract volume*. Society of Economic Geologists, p. 20.

German, C. R., Higgs, N. C., Thomson, J., Mills, R., Elderfield, H., Blusztajn, J., Fleer, A. P. and Bacon, M. P., 1993, Geochemical study of metalliferous sediment from the TAG hydrothermal mound, 26°08'N, Mid-Atlantic Ridge. *J. Geophys. Res*. 98, p. 9683-9692.

Goodfellow, W. D., 1987, Anoxic stratified oceans as a source of sulphur in sediment-hosted stratiform Zn-Pb deposits (Selwyn Basin, Yukon, Canada). *Chem. Geol.* 65, p. 359-382.

Goodfellow, W. D., 2004, Geology, genesis, and exploration of SEDEX deposits, with emphasis on the Selwyn Basin, Canada, *in* Deb, M. and Goodfellow, W. D., eds.,

*Sediment-hosted Lead-zinc Sulphide Deposits: Attributes and Models of Some Major Deposits of India, Australia, and Canada*. Narosa Publ. House, Delhi, India, p. 24-99.

Goodfellow, W. D. and Franklin, J. M., 1993, Geology, mineralogy, and chemistry of sediment-hosted clastic massive sulfides in shallow cores, Middle Valley, northern Juande Fuca ridge. *Econ. Geol*. 88, p. 2037-2068.

Goodfellow, W. D. and Peter, J. M., 1996, Sulfur isotope composition of the Brunswick No. 12 massive sulfide deposit, Bathurst Mining camp, New Brunswick: implications for ambient environment, sulphur source, and ore genesis. *Can. J. Earth Sci.* 33, p. 231-251.

Goodfellow, W. D. and Peter, J. M., 1999, Reply: Sulphur isotope composition of the Brunswick No. 12 massive sulphide deposit, Bathurst Mining Camp, New Brunswick: implications for ambient environment, sulphur source, and ore genesis. *Can. J. Earth Sci*. 36, p. 127–134.

Goodfellow, W. D., and Jonasson, I. R., 1984, Ocean stagnation and ventilation defined by P S secular trends in pyrite and barite, Selwyn Basin, Yukon. *Geology* 12, p. 583-586.

Goodfellow, W.D. and Zierenberg, R. A., 1999, Massive sulphide deposits at sediment-covered spreading centers, *in* Barrie, C. T. and Hannington, M. D., eds., *Volcanic-Associated Massive Sulfide Deposits: Processes and Examples in Modern and Ancient Settings.* Rev. Econ. Geol. 8., p. 297-324.

Goodfellow, W. D. and Lydon, J. W., 2007, Sedimentary exhalative (SEDEX) deposits, *in* Goodfellow, W. D., ed., *Mineral deposits of Canada: A synthesis of Major Deposit Types, District Metallogeny, the Evolution of Geological Provinces, and Exploration Methods.* Geol. Ass. Canada Special Publ. 5, p. 163-183.

Goodfellow, W. D., Lydon, J.W. and Turner, R. J. W., 1993, Geology and genesis of stratiform sediment-hosted (SEDEX) zinc-lead-silver sulphide deposits, *in* Kirkham, R. V., Sinclair, W. D., Thorpe, R. I. and Duke, J. M., eds., *Mineral Deposit Modeling.* Geol. Ass. Canada Special Paper 40, p. 201-251.

Goodfellow, W. D., McCutcheon, S. R. and Peter, J. M., 2003, Massive sulfide deposits of the Bathurst Mining Camp, New Brunswick, and northern Maine: Introduction and summary of findings. *Econ. Geol. Monograph* 11, p. 1-16.

Grenne, T., 1989, Magmatic evolution of the Løkken SSZ ophiolite, Norwegian Caledonides: Relationships between anomalous lavas and high-level intrusions. *Geol. J.* 24, p. 251-274.

Grenne, T. and Slack, J. F., 2003a, Bedded jaspers of the Ordovician Løkken ophiolite, Norway: seafloor deposition and diagenetic maturation of hydrothermal plume-derived silica-iron gels. *Miner. Deposita* 38, p. 625-639.

Grenne, T. and Slack, J. F., 2003b, Paleozoic and Mesozoic silica-rich seawater: Evidence from hematitic chert (jasper) deposits. *Geology* 31, p. 319-322.

Grenne, T. and Slack, J. F., 2005, Geochemistry of jasper beds from the Ordovician Løkken ophiolite, Norway: Origin of proximal and distal siliceous exhalites*, Econ. Geol*. 100, p. 1511-1527.

Grenne, T., Ihlen, P. M. and Vokes, F. M., 1999, Scandinavian Caledonide metallogeny in a plate-tectonic perspective. *Miner. Deposita* 34, p. 422-471.

Gross, G. A., 1996, Algoma-type iron-formation, *in* Eckstrand, O. R., Sinclair, W. D. and Thorpe, R. I., eds., *Geology of Canadian Mineral Deposit Types.* Geology of Canada 8, Geological Survey of Canada, p. 66-73.

Guney, M., Al-Marhoun, M. A. and Nawab, Z. A., 1988, Metalliferous sub-marine sediments of the Atlantis-II-Deep, Red Sea. *CIM Bulletin* 81, p. 33-39.

Hackett, J. and Bischoff, J. L., 1973, New data on the stratigraphy, extent, and geologic history of the red sea geothermal deposits. *Econ. Geol*. 68, p. 553-564.

Hague, J. M., Baum, J. L., Herrmann, L. A. and Pickering, R. J., 1956, Geology and structure of the Sterling Hill area, N. J., *Geol. Soc. America Bull.* 67, p. 435-473.

Hamilton, J. M., Bishop, D. T., Morris, H. C. and Owens, O. E., 1982, Geology of the Sullivan orebody, Kimberley, B. C., Canada, *in* Hutchinson, R. W., Spence, C. D. and Franklin, J. M., eds., *Precambrian Sulphide Deposits*. Geol. Assoc. Canada, Special Paper 25, p. 597-665.

Hamilton, J. M., Delaney, G. D., Hauser, R. L. and Ransom, P. W., 1983, Geology of the Sullivan Deposit, Kimberley, B.C., Canada, *in* Sangster, D. F., ed., *Sediment-Hosted Stratiform Lead-Zinc Deposits*. Min. Assoc. Canada, Short Course Handbook 8, p. 31-83.

Hannington, M. D., 2014, Volcanogenic massive sulfide deposits, *in* Scott, S. D., ed., Chapter 13.18, *The Geochemistry of Ore Deposits*, *in* Holland, H. D. and Turekian, K. K., eds., *Treatise on Geochemistry* 28. Elsevier-Pergamon, Oxford, p. 463-488.

Hannington, M. D., de Ronde, C. E. J. and Petersen, S., 2005, Modern sea-floor tectonics and submarine hydrothermal systems, *in* Hedenquist, J. F., Thompson, J. F. H., Goldfarb, R. J. and Richards, J. P., eds., *100th Anniversary Volume of Econ. Geol.*, p. 111-142.

Hannington, M. D., Jamieson, J., Monecke, T. and Petersen, S., 2010, Modern seafloor massive sulfides and base metal resources: Towards an estimate of global seafloor massive sulfide potential. *Soc. Econ. Geol, Special Publication* 15, p. 317-338.

Hannington, M., Jamieson, J., Monecke, T., Petersen, S. and Beaulieu, S., 2011, The abundance of seafloor massive sulfide deposits. *Geology* 39 (12), p. 1155-1158.

Hanor, J. S. 1994, Origin of saline fluid in sedimentary basins. In Parnell, J. ed., *Geofluids: Origin, Migration and Evolution of Fluids in Sedimentary Basins*, Geological Society Special Publication 78, p. 151-174.

Hartmann, M., 1973, Untersuchungen von suspendiertem Material in den Hydrothermallaugen des Atlantis-II-Tiefs. *Geol. Rundsch.* 62, p. 742-754.

Hartmann, M., 1985, Atlantis-II-Deep geothermal brine system: Chemical processes between hydrothermal brines and Red Sea deep water. *Mar. Geol.*, v. 64, p. 157-177.

Hartmann, M. and Neilsen, H., 1966, Sulfur isotopes in the hot brine and sediments of Atlantis Il Deep (Red Sea). *Mar. Geol.* 4, p. 305-306.

Hein, J. S., Koschinsky, A., Halbach, P., Manheim, F. T., Bau, M., Kang, J-K. and Lubick N., 1997, Iron and manganese oxide mineralization in the Pacific, *in* Nicholson, K., Hein, J. R., Bühn, B. and Dasgupta, S., eds., *Manganese Mineralization: Geochemistry and Mineralogy of Terrestial and Marine Deposits*, Geol. Soc. Spec. Publ. 119, p. 123-138.

Henricks, R. L., Reisbick, F. B., Mahaffey, E. J., Roberts, D. B. and Peterson, M. N. A., 1969, Chemical composition of sediments and interstitial brines from the Atlantis II,

Discovery and Chain Deeps, *in* Degens, E. T. and Ross, D. A., eds., *Hot Brines and Recent Heavy Metal Deposits in the Red Sea*. Springer-Verlag, New York, p. 407-440.

Hofmann, A. and Harris, C., 2008, Silica alteration zones in the Barberton greenstone belt: A window into subseafloor processes 3.5–3.3 Ga ago. *Chem. Geol.* 257, p. 221–239.

Huston, D. L., Stevens, B., Southgate, P. N., Muhling, P. and Wyborn, L., 2006, Australian Zn-Pb-Ag ore-forming systems: a review and analysis. *Econ. Geol*. 101, p. 1117-1157.

Ireland, T., Large, R. R., McGoldrick, P. and Blake, M., 2004, Spatial distribution patterns of sulfur isotopes, nodular carbonate, and ore textures in the McArthur (HYC) Zn-Pb-Ag deposit, Northern Territory, Australia. *Econ. Geol.* 99, p. 1687-1710.

Izzeldin, A. Y., 1987, Seismic, gravity and magnetic surveys in the central part of the Red-Sea – their interpretation and implications for the structure and evolution of the Red-Sea. *Tectonophysics* 143, p. 269–306.

James, H. L., 1969. Comparison between Red Sea deposits and older ironstone and iron-formation, *in* Degens, E. T. and Ross, D. A., eds., *Hot Brines and Recent Heavy Metal Deposits in the Red Sea*. Springer-Verlag, New York, p. 525-532.

Jedwab, J., Blanc, G. and Boulegue, J., 1989, Vandiferous minerals from the Nereus Deep, Red Sea. *Terra Nova* 1, p. 188-194.

Johnson, C. A. and Skinner, B. J., 2003, Geochemistry of the Furnace magnetite bed, Franklin, New Jersey, and the relationship between stratiform iron oxide ores and stratiform zinc oxide-silicate ores in the New Jersey Highlands. *Econ. Geol*. 98, p. 837-854.

Johnson, C. A., Rye, D. M. and Skinner, B. J., 1990, Petrology and stable isotope geochemistry of the metamorphosed zinc-iron-manganese deposit at Sterling Hill, New Jersey. *Econ. Geol.* 85, p. 1133-1161.

Kaplan, I. R., Sweeney, R. E. and Nissenbaum, A., 1969, Sulfur isotope studies on Red Sea geothermal brines and sediments, *in* Degens, E. T. and Ross, D. A., eds., *Hot Brines and Recent Heavy Metal Deposits in the Red Sea*. Springer-Verlag, New York, p. 474-498.

Kase, K., Yamamoto, M., Nakamura, T. and Mitsuno, C., 1990, Ore mineralogy and sulfur isotope study of the massive sulfide deposit of Filon Norte, Tharsis mine, Spain. *Miner. Deposita* 25, p. 288-296.

Kelley, K. D., Leach, D. L., Johnson, C. A., Clark, J. L., Fayek, M., Slack, J. F., Anderson, V. M., Ayuso, R. A. and Ridley, W. I., 2004, Textural, compositional, and sulfur isotope variations of sulfide minerals in the Red Dog Zn-Pb-Ag deposits, Brooks Range, Alaska: Implications for ore formation. *Econ. Geol*. 99, p. 1509-1532.

Klein, C., 2005, Some Precambrian banded iron-formations (BIFs) from around the world: Their age, geologic setting, mineralogy, metamorphism, geochemistry, and origin. *Amer. Miner.* 90, p. 1473-1499.

Krasnov, S., Stepanova, T. and Stepanov, M., 1994, Chemical composition and formation of a massive sulfide deposit, Middle Valley, northern Juan de Fuca Ridge (Site 856). *Proc. ODP Sci. Res.* 139, p. 353-372.

Ku, T. L., 1969, Uranium series isotopes in sediments from the Red Sea hot brine area, *in* Degens, E. T. and Ross, D. A., eds., *Hot Brines and Recent Heavy Metal Deposits in the Red Sea*. Springer-Verlag, New York, p. 512-524.

Large, R. R., 2003, BHT deposits: Part of the spectrum of stratiform sediment hosted Zn-Pb-Ag deposits. *Australian Geol. Surv. Org. Record* 2000/10, p. 93-96.

Large, R. R. and Davidson, G. J., 1991, Controls of brine chemistry on the spectrum of Proterozoic sediment-hosted base metals deposits. Abstracts, Specialist Group in Economic Geology, Ore Fluids Conference, Canberra, Australia. *Bureau of Mineral Resources, Geology and Geophysics, Record* 1990/95, p. 50-51.

Large, R. R. and McGoldrick, P. J., 1998, Lithogeochemical halos and geochemical vectors to stratiform sediment hosted Zn– Pb–Ag deposits, Part 1. Lady Loretta deposit, Queensland. *J. Geochem. Explor*. 63, p. 37-56.

Large, R. R., Bodon, S., Davidson, G. J. and Cooke, D., 1996, The chemistry of BHT ore formation – one of the keys to understanding the difference between SEDEX and BHT deposits, *in* Pongratz, J. and Davidson, G. J., eds., *New Developments in Broken Hill Type Deposits*, CODES Special Publication 1, p. 105-111.

Large, R. R., Bull, S. W., Cooke, D. R. and McGoldrick, P. J., 1998, A genetic model for the HYC deposit, Australia: Based on regional sedimentology, geochemistry, and sulfide-sediment relationship. *Econ. Geol*. 93, p. 1345-1368.

Large, R. R., Bull, S. W. and McGoldrick, P. J., 2000, Lithogeochemical halos and geochemical vectors to stratiform sediment hosted Zn–Pb–Ag deposits Part 2. HYC deposit, McArthur River, Northern Territory. *J. Geochem. Explor.* 68, p. 105-126.

Large, R. R., Bull, S. W. and Winefield, P. R., 2001, Carbon and oxygen isotope halo in carbonates related to the McArthur River (HYC) Zn-Pb-Ag deposit, North Australia: Implications for sedimentation, ore genesis, and mineral exploration. *Econ. Geol.* 96, p. 1567-1593.

Large, R., Bull, S. W., McGoldrick, P. J., Walters, S., Derrick, G. M. and Carr, G. R., 2005, Stratiform and strata-bound Zn-Pb-Ag deposits in Proterozoic sedimentary basins, northern Australia, *in* Hedenquist, J. F., Thompson, J. F. H., Goldfarb, R. J. and Richards, J. P., eds., *100th Anniversary Volume of Econ. Geol.,* p. 931-963.

Large, R. R., Maslennikov, V. V., Robert, F., Danyushevsky, L. V. and Chang, Z. 2007, Multistage sedimentary and metamorphic origin of pyrite and gold in the Giant Sukhoi Log Deposit, Lena Gold Province, Russia. *Econ. Geol.* 102, p. 1233-1267.

Laurila, T. E., Hannington, M. D., Petersen, S. and Garbe-Schönberg, D., 2014a, Trace metal distribution in the Atlantis II Deep (Red Sea) sediments. *Chem. Geol.* 386, p. 80-100.

Laurila, T. E., Hannington, M. D., Petersen, S. and Garbe-Schönberg, D., 2014b, Early depositional history of metalliferous sediments in the Atlantis II Deep of the Red Sea: Evidence from rare earth element geochemistry. *Geochim. Cosmochim. Acta* 126, p. 146-168.

Leitch, C. H. B. and Lydon, J. W., 2000, Fluid inclusion petrography and microthermometry of the Sullivan Deposit and surrounding area, Chapter 33, *in* Lydon, J. W., Höy, T., Slack, J. F. and Knapp, M., eds., The Geological *Environment of the Sullivan Pb-Zn-Ag Deposit, British Columbia.* Geol. Assoc. Canada, Mineral Deposits Division, Spec. Publ. 1, p. 617-632.

Lonsdale, P. and Becker, K., 1985, Hydrothermal plumes, hot springs, and conductive heat flow in the southern trough of Guaymas basin. *Earth Planet. Sci. Lett.* 73, p. 211–225.

Lowe, D. R., 1999, Petrology and sedimentology of cherts and related silicified sedimentary rocks in the Swaziland Supergroup, *in* Lowe, D. R. and Byerly, G. R., eds., Geologic evolution of the Barberton Greenstone Belt, South Africa. *Geol. Soc. Am. Special Paper* 329, p. 83–114.

Lydon, J. W., 1996, Sedimentary exhalative sulphides (SEDEX), *in* Eckstrand, O. R., Sinclair, W. D. and Thorpe, R. I., eds., *Geology of Canadian Mineral Deposit Types.* Geology of Canada 8, Geological Survey of Canada, p. 130-152.

Lydon, J. W., Goodfellow, W. D. and Jonasson, I. R., 1985, A general genetic model for stratiform baritic deposits of the Selwyn Basin, Yukon Territory and District of Mackenzie. *Geol. Surv. Canada paper 85-1A*, p. 651-660.

Lydon, J. W., 2007, Geology and metallogeny of the Belt-Purcell Basin, *in* Goodfellow, W. D., ed., *Mineral Deposits of Canada: A Synthesis of Major Deposit- Types, District Metallogeny, the Evolution of Geological Provinces, and Exploration Methods.* Geol. Ass. Canada, Mineral Deposits Division, Spec. Publ. 5, p. 581-607.

Lyons, T. W. and Severmann, S., 2006, A critical look at iron paleoredox proxies: New insights from modern euxinic marine basins. *Geochim. Cosmochim. Acta* 70, p. 5698-5722.

Manheim, F. T., 1974, Red Sea geochemistry (ch. 38), *in*, Whitmarsh, R. B., Weser, O. E., Ross, D. A., *et al., Initial Reports of the Deep Sea Drilling Project*, v. 23, Washington (U.S. Government Printing Office) p. 975-998.

Missack, E., Stoffers, P. and El Goresy, A., 1989, Mineralogy, parageneses, and phase relations of copper-iron sulfides in the Atlantis II Deep, Red Sea, *Miner. Deposita* 24, p. 82-91.

Metsger, R. W., Tennant, C. B. and Rodda, J. L., 1958, Geochemistry of the Sterling Hill zinc deposit, Sussex Co., N. J. *Geol. Soc. Am. Bull.* 69, p. 775-788.

Metsger, R. W., Skinner, B. J. and Barton, P. B., Jr., 1969, Structural interpretation of the Sterling Hill ore body, Ogdensburg, N. J. (abs.). *Geol. Soc. Am. Abstracts with Programs* 7, p. 150.

Monnin, C. and Ramboz, C., 1996, The anhydrite saturation index of the ponded brines and sediment pore waters of the Red Sea deep. *Chem. Geol.* 127, p. 141-159.

Murray, R. W., Jones, D. L. and Buchholtz ten Brink, M. R., 1992, Diagenetic formation of bedded chert: Evidence from chemistry of the chert-shale couplet. *Geology* 20, p. 271-274.

Nehlig, P., Cassard, D. and Marcoux, E., 1998, Geometry and genesis of feeder zones of massive sulphide deposits: Constraints from the Rio Tinto ore deposit (Spain). *Miner. Deposita* 33, p. 137-149.

Nutman, A. P. and Ehlers, K., 1998, Evidence for multiple Paleoproterozoic thermal events and magmatism adjacent to the Broken Hill Pb-Zn-Ag ore body, Australia. *Precambrian Res.* 90, p. 203-238.

Ohmoto, H., Watanabe, Y., Yamaguchi, K. E., Naraoka, H., Haruna, M., Kakegawa, T., Hayashi, K. and Kato, Y., 2006, Chemical and biological evolution of early Earth: Constraints from banded iron formations, *in* Kesler, S. E. and Ohmoto, H., eds., *Evolution of Early Earth's Atmosphere, Hydrosphere, and Biosphere – Constraints from Ore Deposits.* Geol. Soc. Am. Memoir 198, p. 291-331.

Oudin, E., Thisse, Y. and Ramboz, C., 1984, Fluid inclusion and mineralogical evidence for high temperature saline hydrothermal circulation in the Red Sea metalliferous sediments: Preliminary results. *Mar. Mining* 5 (1), p. 3-31.

Parr, J. M. and Plimer, I. R., 1993, Models for Broken Hill Type lead-zinc-silver deposits, *in* Kirkham, R. V., Sinclair, W. D., Thorpe, R. I. and Duke, J. M., eds., *Mineral Deposit Modeling.* Geol. Ass. Canada Spec. Paper 40, p. 253-288

Peter, J. M. and Goodfellow, W. D., 1996, Mineralogy, bulk and rare earth element geochemistry of massive sulphide-associated hydrothermal sediments of the Brunswick Horizon, Bathurst Mining Camp, New Brunswick. *Can. J. Earth Sci*. 33, p. 252-283.

Pierret, M. C., Clauer, N., Bosch, D., Blanc, G. and France-Lanord, C., 2001, Chemical and isotopic ($^{87}Sr/^{86}Sr$, ä$^{18}O$, äD) constraints to the formation processes of Red-Sea brines. *Geochim. Cosmochim. Acta* 65 (8), p. 1259-1275.

Pottorf, R. J. and Barnes. H. L., 1983, Mineralogy, geochemistry, and ore genesis of hydrothermal sediments from the Atlantis II Deep, Red Sea. *Econ. Geol. Monograph* 5, p. 198-223.

Ramboz, C., Oudin, E. and Thisse, Y., 1988, Geyser-type discharge in Atlantis II Deep, Red Sea: Evidence of boiling from fluid inclusions in epigenetic anhydrite. *Can. Mineral*. 26, p. 765-786.

Ries, H. and Bowen, W. C., 1922, Origin of the zinc ores of Sussex county, New Jersey. *Econ. Geol.* 17, p. 517-571.

Sangster, D. F., 1978, Exhalites associated with Archaean volcanogenic massive sulphide deposits: Perth, Australia. *Univ. Western Australia, Geol. Dep. Publ.* 2, p. 70-81.

Schoell, M. and Faber, E., 1978, New isotopic evidence for the origin of Red Sea brines. *Nature* 275, p. 436-438.

Seal, R. R. II, 2006, Sulfur Isotope geochemistry of sulfide minerals, *in* Vaughan D. V., ed., *Sulfide Mineralogy and Geochemistry.* Rev. Mineral. Geochem. 61, Min. Soc. Am., p. 633-677.

Shanks, W. C. and Bischoff, J. L., 1977, Ore transport and deposition in the Red Sea geothermal system: A geochemical model. *Geochim. Cosmochim. Acta* 41, p. 1507-1519.

Siam, R., Mustafa, G. A., Sharaf, H., Moustafa, A., Ramadan, A. R., Antunes, A., Bajic, V. B., Stingl, U., Marsis, N. G. R., Coolen, M. J. L., Sogin, M., Ferreira, A. J. S. and Dorry, H. E., 2012, Unique prokaryotic consortia in geochemically distinct sediments from Red Sea Atlantis II and Discovery Deep brine pools. *PLoS ONE,* 7 (8), e42872, 10 p.

Skinner, B. J., White, D. E., Rose, H. J. and Mays, R. E., 1967, Sulfides associated with the Salton Sea geothermal brine. *Econ. Geol.* 62, p. 316-330.

Smith, J. W. and Croxford, N. E. J., 1973, Sulfur isotope ratios in the McArthur zinc-lead-silver deposit, *Nature Phys. Sci.* 245, p. 10-12.

Solomon, M., 1999, Discussion: Sulphur isotope composition of the Brunswick No. 12 massive sulphide deposit, Bathurst Mining Camp, New Brunswick: Implications for ambient environment, sulphur source, and ore genesis. *Can. J. Earth Sci.* 36, p. 121-125.

Solomon, M., 2008a, Brine pool deposition for the Zn–Pb–Cu massive sulphide deposits of the Bathurst mining camp, New Brunswick, Canada. I. Comparisons with the Iberian pyrite belt. *Ore Geol. Rev*. 33 (3-4), p. 329-351.

Solomon, M., 2008b, Brine pool deposition for the Zn–Pb–Cu massive sulphide deposits of the Bathurst mining camp, New Brunswick, Canada. II. Ocean anoxia during mineralization. *Ore Geol. Rev.* 33 (3-4), p. 352-360.

Solomon, M. and Zaw, K., 1997, Formation on the sea floor of the Hellyer volcanogenic massive sulfide deposit. *Econ. Geol.* 92, p. 686-695.

Solomon, M. and Quesada, C., 2003, Zn–Pb–Cu massive sulphide deposits: Brine pool types occur in collisional orogens, black smoker types in backarc and/or arc basins. *Geology* 31, p. 1029-1032.

Solomon, M., Tornos, F. and Gaspar, O. C., 2002, Explanation for many of the unusual features of the massive sulfide deposits of the Iberian Pyrite Belt. *Geology* 30, p. 87-90.

Solomon, M., Tornos, F., Large, R. R., Badham, J. N. P., Both, R. A. and Zaw, K., 2004, Zn-Pb-Cu volcanic-hosted massive sulphide deposits: Criteria for distinguishing brine pool-type from black smoker-type sulphide deposition. *Ore Geol. Rev.* 25, p. 259-283.

Spry, P. G., 1987, A sulfur isotope study of the Broken Hill deposits, New South Wales, Australia. *Miner. Deposita* 22, p. 109-115.

Spry, P. G. and Wonder, J. D., 1989, Manganese-rich rocks associate with the Broken Hill lead-zinc-silver deposit, New South Wales, Australia. *Can. Min*. 27, p. 275-292.

Spry, P. G., Peter, J. M. and Slack, J. F., 2000, Meta-exhalites as exploration guides to ore, *in* Spry, P. G., Marshall, B. and Vokes, F. M., eds., *Metamorphosed and Metamorphogenic Ore Deposits.* Rev. Econ Geol. 11, p. 163-201.

Spry, R. G., Heimann, A., Messerly, J. D. and Houk, R. S., 2007, Discrimination of metamorphic and metasomatic processes at the Broken Hill Pb-Zn-Ag deposit, Australia: Rare earth element signatures of garnet-rich rocks. *Econ. Geol*. 102, p. 471-494.

Steinkamp, K. and Schumann, D., 1974, The Chemical Composition of Sediment Cores Recovered During Valdivia Cruises VA01 and VA03 from the Atlantis II Deep (Red Sea). Unpublished cruise report 1.11.1974, Series CL, Preussag, Hannover, 155 p.

Stevens, B. P. J., Willis, I. L., Brown, R. E. and Stroud, W. J., 1983, The early Proterozoic Willyama Supergroup: Definitions of stratigraphic units from the Broken Hill Block, New South Wales. *New South Wales, Geological Survey records* 21 (2), p. 407-442.

Stoffers, P. and Ross, D. A., 1974, Sedimentary history of the Red Sea, (ch. 23), *in*, Whitmarsh, R. B., Weser, O. E., Ross, D. A*., et al., Initial Reports of the Deep Sea Drilling Project,* v. 23, Washington (U.S. Government Printing Office) p. 849-865.

Strauss, G. K. and Gray, K. G., 1986, Base metal deposits in the Iberian Pyrite Belt, *in* Friedrich, G. H., Genkin, A. D., Naldrett, A. J., Ridge, J. D., Sillitoe, R. H. and Vokes, F. M., eds., Geology and Metallogeny of Copper Deposits. Springer, Berlin-Heidelberg-New York, p. 304-324.

Sval'nov, V. N., Strizhov, V. P., Bogdanov, Y. A., and Isayeva, A. B., 1984, Hydrothermal barite crust on basalts in the Atlantis II Deep (Red Sea). *Oceanology* 24 (6), p. 716-720.

Taylor, S. R. and McLennan, S. M., 1985, *The Continental Crust: Its Composition and Evolution*. Blackwell, Oxford, 312 p.

Taylor B. E. and Beaudoin, G., 2000, Sulphur isotope stratigraphy of the Sullivan Pb-Zn-Ag deposit, B.C.: Evidence for hydrothermal sulphur, and bacterial and thermochemical sulphate reduction, Chapter 37. *In* Lydon, J. W., Höy, T., Slack, J. F. and Knapp, M. E., eds., *The Geological Environment of the Sullivan deposit, British Columbia.* Geol. Assoc. Canada, Spec. Publ. 1, p. 696-719.

Tornos, F. and Heinrich, C. A., 2008, Shale basins, sulfur-deficient ore brines and the formation of exhalative base metal deposits. *Chem. Geol.* 247, p. 195-207.

Tornos, F., González Clavijo, E. and Spiro, B. F., 1998, The Filón Norte ore-body (Tharsis, Iberian Pyrite Belt): A proximal low-temperature shale- hosted massive sulphide in a thin-skinned tectonic belt. *Miner. Deposita* 33, p. 150-169.

Tornos, F., Solomon, M., Conde, C. and Spiro, B. F., 2008, Formation of the Tharsis massive sulfide deposit, Iberian Pyrite Belt: Geological, lithogeochemical, and stable Isotope evidence for deposition in a brine pool. *Econ. Geol*. 100, p. 185-214.

Trüper, H. G., 1969, Bacterial sulfate reduction in the Red Sea hot brines, *in* Degens, E. T. and Ross, D. A., eds., Hot Brines and Recent Heavy Metal Deposits in the Red Sea. Springer-Verlag, New York, p. 263-271.

Turner, F. J. and Campbell, I. H., 1987, Temperature, density and buoyancy fluxes in ‘‘black smoker’’ plumes, and the criterion for buoyancy reversal. *Earth Planet. Sci. Lett*. 86, p. 85-92.

Turner, R. J. W., Leitch, C. H. B., Ross, K., Hoy, T., Delaney, G. D. and Hagen, A., 1996, Sullivan stratiform lead-zinc deposit, British Columbia, Canada: Rift setting, associated district-scale hydrothermal field, and comparison to BHT deposits*, in* Pongratz, J. and Davidson, G. J., eds., *New Developments in Broken Hill Type Deposits*, CODES Special Publication 1, p. 153-163.

Walters, S. and Bailey, A., 1998, Geology and mineralization of the Cannington Ag-Pb-Zn deposit: An example of Broken Hill-type mineralization in the Eastern succession, Mount Isa inlier, Australia. *Econ. Geol.* 93, p. 1307-1329.

Whelan, J. F., Rye, R. O. and deLorraine, W., 1984, The Balmat-Edwards zinc-lead deposits: Synsedimentary ore from Mississippi Valley-type fluids. *Econ Geol.* 79, p. 239-265.

Whitmarsh, R. B., Weser, O. E., Ross, D. A., *et al.,* 1974, *Initial Reports of the Deep Sea Drilling Project*, v. 23, Washington (U.S. Government Printing Office), 1180 p.

Williams, N., 1978, Studies of base metal sulfide deposits at McArthur River, Northern Territory, Australia: II. The sulfide-S and organic-C relationships of the concordant deposits and their significance. *Econ. Geol.* 73, p. 1036-1056.

Williams, A. E. and McKibben, M. A., 1989, A brine interface in the Salton Sea geothermal system, California: Fluid geochemical and isotopic characteristics. *Geochim. Cosmochim Acta* 53, p. 1905–1920.

Wright, J. V., Haydon, R. C. and McConachy, G. W., 1987, Sedimentary model for the giant Broken Hill Pb-Zn deposit, Australia. *Geology* 15, p. 598-602.

Yardley, B. W. D., 2005, 100th Anniversary Special Paper: Metal concentrations in crustal fluids and their relationship to ore formation. *Econ. Geol*. 100, p. 613-632.

Zierenberg, R. A. and Shanks, W. C., 1983, Mineralogy and geochemistry of epigenetic features in metalliferous sediments, Atlantis II Deep, Red Sea. *Econ. Geol.* 78, p. 57-72.

Zierenberg, R. A. and Shanks, W. C., 1986, Isotopic constraints on the origin of the Atlantis II, Suakin and Valdivia brines, Red Sea. *Geochim. Cosmochim. Acta* 50, p. 2205-2214.

Zierenberg, R. A. and Shanks, W. C., 1988, Isotopic studies of epigenetic features in metalliferous sediment, Atlantis II Deep, Red Sea. *Can. Mineral.* 26, p. 737-753.

Zierenberg, R. A., Fouquet, Y., Miller, D. J., Bahr, J. M., Baker, P. A., Bjerkgard, T., Brunner, C. A., Duckworth, R. C., Gable, R., Gieskes, J., Goodfellow, W. D., Gröschel-Becker, H. M., Guerin, G., Ishibashi, J., Iturrino, G., James, R. H., Lackschewitz, K. S., Marquez, L. L., Nehlig, P., Peter, J. M., Rigsby, C. A., Schultheiss, P., Shanks III, W. C., Simoneit, B. R. T., Summit, M., Teagle, D. A. H., Urbat, M. and Zuffa, G. G., 1998, The deep structure of a sea-floor hydrothermal deposit. *Nature* 392, p. 485-488.

## Figure Captions

Figure 6.1. Comparison of different settings for the formation of stratiform exhalative base metal ore deposits. A) MOR black smoker deposits: Fluids are characterized by (Fe+Cu+Zn+Pb)≥ $H_2S$ and Fe/(Cu+Zn+Pb) = ~10 and vent into oxic and low-T seawater. <10% of metals contained in the vent fluids accumulate proximal to the vent (resulting in low tonnage deposits). However, more of Fe than Cu, Zn and Pb disperses into the seawater increasing the grades of valuable metals.

B) Brine pool VMS: Venting of black smoker-like fluids occurs in an euxinic brine pool. A significant proportion of reduced sulfur in the brine pool is from non-hydrothermal sources (mainly bacteriogenic). Close to ~100% of metals deposit within the brine covered area, and the metal ratios in the deposition are the same as in the hydrothermal fluids. Some metals may escape the brine pool during exceptionally strong hydrothermal venting.

C-D) Current Atlantis II Deep: Venting of metal-rich brines occurs in an anoxic brine pool. Cu and Zn in the hydrothermal fluid precipitate on cooling from $H_2S$ in the fluid forming a hydrothermal plume. After $H_2S$ is exhausted metals start to accumulate in the brine and may be co-deposited with brine-pool particulates (adsorbed onto Si-Fe-(oxy)hydroxides). ~70% of metals deposit within the brine covered area; most Mn and a portion of the other metals (e.g., Zn) may escape the brine pool, especially during times when the redoxcline is situated above the boundaries of the pool (D).

E) Broken Hill: Hydrothermal fluids with (Fe+Cu+Zn+Pb)<$H_2S$ vent into an oxic brine pool with low $H_2S$-concentration causing efficient Mn- and Fe-(oxy)hydroxide precipitation. Some of the metals are deposited from the brine pool adsorbed onto (oxy)hydroxides and

are subsequently incorporated in sulfides during diagenesis. A large proportion of the Fe, Mn and Zn may also diffuse out of the brine pool and deposit as laterally extensive exhalite horizons.

F) Atlantis II during CO formation: Dominantly low-temperature hydrothermal venting of brines containing abundant Mn and Fe, but little other metal. Mn and Fe coprecipitate in the oxic brine pool as (oxy)hydroxides and settle within the brine covered area. This was a time of extensive tectonic activity, which might have caused increased ventilation of the brine pool. Non-hydrothermal reduced sulfide was more abundant in the brine pool than during high-temperature venting.

Figure 6.2. Schematic illustration of ore-forming environments of sediment-hosted exhalative base metal sulfide deposits.

A) “Selwyn-type” basins produce reduced ore fluids, which need high temperatures and moderate salinity (~10-15 wt.% NaCl) to transport metals. Addition of $H_2S$, decrease in salinity, cooling or pH increase will cause metal precipitation. Cooling and pH increase though to be the most important (Cooke et al., 2000). Selwyn-type ores typically have Zn-rich (and locally Cu-rich) vent complexes, commonly along basin-bounding faults, with metal deposition caused by cooling of the hydrothermal fluids in the conduits.

B) “McArthur-type” basins produce oxygenated ore fluids, which need high salinity for efficient metal dissolution. Temperatures are generally lower (~150°C), and metal deposition is caused by addition of $H_2S$ from external sources. Mineralized vent complexes are not common.

C) Iberian Pyrite Belt (IPB) ore forming systems are transitional in character between SEDEX and VMS systems. Metals are mainly leached from the underlying strata and deposited upon venting into an anoxic brine pool (Tornos and Heinrich, 2008).

Figure 6.3. Cu, Zn and Pb concentrations in some modern seafloor massive sulfides (circles and crosses) according to Hannington et al. (2005). The squares are average grades of ancient exhalative ore deposits (Table 6.1). Sediment-hosted deposits with higher Pb/Zn, but lower Cu/Zn compared to the deposits in sediment-free environments. Deposits in the Atlantis II Deep bear a closer resemblance to sediment-free mid-ocean ridge deposits in terms of Cu-Zn-Pb ratios because of the similar basaltic substrate.

Figure 6.4 Solubility of sphalerite and chalcopyrite as a function of salinity at 300°C, pH=4, $aH_2S$=0.001 and $aH_2S$>$aSO_4$ (modified from Hannington et al., 2014). The solubility of sphalerite increases by 2 log units (a factor of 100) for every log unit increase in salinity (a factor of 10), whereas the solubility of chalcopyrite increases by only 1 log unit, according to the reactions: $ZnS + 2Cl^- + 2H^+ = ZnCl_2$ *(aq)* + $H_2S$ and $CuFeS_2 + Cl^- + H^+ + 1/4O_2 = CuCl^o$ *(aq)* + $FeS_2 + 1/2H_2O$. This relationship is consistent with the generally high Zn concentrations and low Cu/Zn ratios of basinal brines in high-temperature geothermal systems (e.g., Salton Sea: Skinner et al., 1967; cf. Yardley, 2005).

Figure 6.5. Comparison of ore formation in different combinations of anoxic and euxinic bottom waters. A) SEDEX ore formation from buoyant hydrothermal fluids during a global stratified ocean with anoxic and euxinic bottom water (Goodfellow, 2004).
B) SEDEX ore formation from bottom-hugging oxic ore brines that pond on the seafloor after venting. Metals diffuse out of the oxic brine pool and precipitate on encountering $H_2S$ in the overlying euxinic seawater.
C) Ore formation in the current Atlantis II Deep. Sulfide minerals form mainly from hydrothermal $H_2S$ within the Lower Brine, but also due to bacterially reduced sulfur at the chemocline between Lower and Upper brine layers and in the sediments.

Figure 6.6. Schematic illustration of enrichment halos of Fe, Mn, Zn, Cu and Hg in sediments surrounding the Atlantis II Deep (Bignell et al., 1976a; see the upper right corner for detailed structure of the brine pool). Numbers indicate the enrichment factor of metals in the sediments compared to the average for background sediment samples recovered from the flanks of the axial valley sides (1100-1800 m depth) beyond the influence of rift-axis processes (3.2 wt.% Fe, 0.36 wt.% Mn, 200 ppm Zn, 60 ppm Cu and 30 ppb Hg; av. of 182 samples).

Table 6.1. Origin and composition of the Atlantis II Deep sediments and some selected stratiform base metal ore deposits (ref. in Table 6.3).

| | Location | Ore type | Age | S wt.% | Fe wt.% | Mn wt.% | Zn wt.% | Cu wt.% | Pb wt.% | Ag ppm | Au ppm | Cu/ Zn | Pb/ Zn | S/(Zn+ Cu+Pb) |
|---|---|---|---|---|---|---|---|---|---|---|---|---|---|---|
| Atlantis II | Red Sea | Modern brine pool | <15 ka | 2.3* | 29* | 2.2* | 2.1 | 0.5 | 0.01 | 41 | 0.51 | 0.23 | <0.01 | 0.08 |
| Bent Hill | Middle Valley | Sedimented MOR | <300 ka | 45 | 45 | 0.1 | 1.0 | 0.5 | 0.1 | 10 | 0.03 | 0.5 | 0.1 | 0.97 |
| Tharsis (Filon N) | IPB (Spain) | VMS (brine pool) | 0.35 Ga | 47 | ~40 | - | 1.8 | 0.5 | 0.8 | 22 | 0.7 | 0.4 | 0.4 | 1.09 |
| Sullivan | Belt-Purcell (BC, Can) | Sedex ("Selwyn Basin" type) | 1.47 Ga | ~30 | 28 | <1.3 | 5.9 | 0.03 | 6.1 | 67 | - | <0.01 | 1.0 | 0.75 |
| HYC | McArthur Basin (Aus) | Sedex ("McArthur Basin" type) | 1.64 Ga | ~20 | 10 | <1.3 | 9.2 | 0.2 | 4.1 | 41 | 0.01 | 0.02 | 0.45 | 0.85 |
| Broken Hill | Australia | Broken Hill type | 1.69 Ga | ~15 | 8 | 1-8 | 8.5 | 0.1 | 10 | 148 | 0.47 | 0.02 | 1.2 | 0.56 |
| Sterling Hill | New York state, US | Oxide-silicate Zn | >1.1 Ga | 0.2 | 16 | 8 | 20 | tr. | tr. | tr. | tr. | <0.01 | <0.01 | <0.01 |
| Løkken | Norway | VMS associated exhalite | ~0.45 Ga | <0.1 | 15 | <0.02 | <64 ppm | <30 ppm | <12 ppm | <0.3 ppm | <0.2 ppm | 0.5 | 0.2 | <0.01 |

* Values are averages of 3215 chemical analyses in the MESEDA database (1-m composites). The resource estimate of Guney et al. (1988) is used in this table for other elements and is consistent with averages from the MESEDA database (2.1 wt.% Zn, 0.4 wt.% Cu and 43 ppm Ag). Average grade for gold is based on chemical analyses of the flotation concentrates produced during the pre-pilot mining tests and recalculated to bulk ore (Guney et al., 1988).

Table 6.2. Physical properties of the Atlantis II Deep and representative stratiform metal deposits (ref. in Table 6.3).

| | Size (Mt) | Zn (Mt) | Form | Tectonic setting | Heat source | Structural control | Zoning |
|---|---|---|---|---|---|---|---|
| Atlantis II | 90 | 1.9 | 14x5km x20m | Nascent continental rift floored by basalt | Magmatic-hydrothermal | Rift bounding faults | Anhydrite proximal to vents, manganosiderite halo, Ba-crust on the flanks |
| Bent Hill | 9 | 0.09 | ~150m x>100m thick | Modern sediment-filled oceanic rift | Magmatic-hydrothermal | Rift-parallel faults | Proximal Q-(Fe-Chl)-Cpy with transition to Chl-Py, anhy-Py and distal calcite-Py. |
| Tharsis | 88 | 1.6 | 2x4km x20m | Continental marine basin in collisional orogen (~2 km of sediment) | High heat flow, igneous intrusions | Felsic volcanic center; syn-volcanic faults | Proximal siderite with increasing ankerite alteration away from the vents; barite absent |
| Sullivan | 162 | 9.5 | 2x1.6km x50m | Extensional sedimentary basin rift-fill sequence (6-7 km of sediment) | Geothermal gradient, sills | Syn-sedimentary faults overlain by black shale | Vent complex ore (70%) surrounded by bedded ore; Zn/Pb increases and Cu decreases away from vent complex; no barite (atypical for this ore type) |
| HYC | 227 | 20.9 | 10s of km horiz. | Extensional sedimentary basin, rift-sag sequence (~6.5 km of sediment) | Geothermal gradient | Basin-bounding faults | Carbonate alteration (Mn-Fe increase) halo up to 20 km away from the vents in pyritic shale; no barite |
| Broken Hill | 280 | 23.8 | 10s of km horiz. x2km | Ensialic rift, rift-fill sequence (6-7 km of sediment) | High heat flow associated with rifting | Syn-sedimen-tary faults, lithological contacts | Siliceous-Zn and calc-silicate-Mn-Ca-Fe-Pb-Ag-rich ore lenses; Zn/Pb decreases away from the vent source; distal Mn±BIF, barite, manganite and Fe-carbonate halos |
| Sterling Hill | ~11 | 2.2 | elongate (strong. metam.) | Rift basin with detrital-pelagic sediments and pillow lavas (multiple km of sediment) | Poorly defined (burial, rifting) | Stratigraphic control | Vent proximal ore surrounded by pyritic limestone, which transitions to banded zincite and finally to graphitic limestone |
| Løkken ex-halites | n.i. | n.i. | 1-2km x>1m | Oceanic back-arc | Magmatic hydrothermal | Distal to ophiolite-hosted VMS | Up to 1 km halo of high As/Fe and Sb/Fe around the vents; pyrite-rich exhalites found up to 10 km away from the vents |

Table 6.3. Fluid composition of the Atlantis II Deep and representative stratiform base metal deposits.

| | Salinity | T in hydroth. fluid | $H_2S$ in hydroth. fluid | Source of metals | T at precip. site | Site of precipitation | References |
|---|---|---|---|---|---|---|---|
| Atlantis II | Up to 32 wt.% NaCl (evaporite dissolution) | ~350°C | Low $S_{tot}$<Me | MORB | 70-140°C | Anoxic stratified brine pool devoid of $H_2S$ | Pottorf and Barnes, 1983; Oudin et al., 1984; Guney et al., 1988; Steinkamp and Schumann, 1974 |
| Bent Hill | "black smoker" <5 wt.% NaCl | > 350°C | $S_{tot}$~Me | Sediments, volcanics (sills), MORB | | Seafloor and sub-seafloor, confined by a silicified seal | Ames et al., 1993; Goodfellow and Franklin, 1993; Krasnov et al., 1994; Zierenberg et al., 1998 |
| Tharsis | Highly variable, up to 14 wt.% NaCl (basinal brines) | ~300°C, low $fO_2$ | $S_{tot}$≤Me | Sediments (shale, sand-stone), volc. sequence | 70-140°C | Variable conditions, euxinic-oxic, biogenic $H_2S$, mixing in brine pool | Strauss and Gray, 1986; Kase et al., 1990; Tornos et al., 1998, 2008; Solomon et al, 2002; Solomon et al., 2004; Solomon 2008a; Tornos and Heinrich, 2008 |
| Sullivan | ~10 (up to 32) wt.% NaCl (basinal brines, evaporites) | 250-300°C, low $fO_2$ | $S_{tot}$<Me | Argillaceous sediments | 100-250°C | Euxinic seawater or local basin containing black shales | Campbell et al., 1978; Hamilton et al., 1982, 1983; Turner et al., 1996; Leitch and Lydon, 2000; Lydon, 2007 |
| HYC | Up to 25 wt.% NaCl (basinal brines, evaporites) | 100-240°C, high $fO_2$ | $S_{tot}$<<Me | Volcanic-sedimentary sequence | | Sub-seafloor deposition in reactive ($S_{red}$-rich) sediments (aquicludes) | Williams, 1978; Lydon, 1996; Cooke et al., 2000; Large et al., 2000; Ireland et al., 2004; Large et al., 2005; Huston et al., 2006 |
| Broken Hill | Up to ~25 wt.%, (seawater, basinal brines, evaporites) | 100-200°C, low $fO_2$ | $S_{tot}$<Me ($aH_2S$> $aSO_4$) | Sediments | | Oxidized basin with $SO_4$; mixing in brine pool | Stevens et al., 1983; Parr and Plimer, 1993; Large et al., 1996; Walters and Bailey, 1998; Huston et al., 2006 |
| Sterling Hill | > seawater (evaporites) | ~150°C (min.) | $S_{tot}$<< Me | Oxidized sediments | ~120°C | Oxidized brine pool, metal absorption on (oxy)hydroxides | Ries and Bowen, 1922; Hague et al., 1956; Drake, 1990; Johnson et al., 1990; Johnson and skinner 2003 |
| Løkken | Presumably seawater-like | 100-250°C | Low | MORB | Sea-water | Plume fall-out in seawater | Grenne, 1989; Grenne et al., 1999; Grenne and Slack, 2005, 2003a,b |

Table 6.4. Evaluation of criteria for recognition of brine pool-type deposits (from Solomon et al., 2004): Tharsis, the Atlantis II Deep and Bent Hill.

| Criteria | Tharsis | Atlantis II | Bent Hill |
|---|---|---|---|
| Very large size | 88 Mt | 90 Mt | 9 Mt |
| High aspect ratio | >100 | >100 | ~1 |
| High Zn/Cu | 4 | 4 | 2 |
| High Fe/Cu | ~80 | ~60 | ~90 |
| Chimneys | Absent | Absent | Present |
| Pyrite content | >> sph+cpy | < sph+cpy | >> sph+cpy |
| Sulfide texture | Framboids dominate at vent distal | Framboids present at vent distal | Framboids rare |
| Fine lamination | Pervasive, primary | Pervasive, primary | Present locally, mainly replacement |
| Mineral assemblage | Reduced (py/apy/po) | Mainly oxides, locally reduced | Reduced |
| Barite (in the MS) | Rare | Rare | Minor |
| Carbonates | Bedded Fe(-Mn) | Bedded Fe-Mn | Not present |
| Zone refining | No major influence | No major influence | Present |
| Bacterial sulfate reduction | Ubiquitous at vent distal, rare proximal to vents | Present mainly in sediment with low sulfide content | Bacterial mats on top of the sulfide mound |
| References | Tornos et al., 2008 | This study | Goodfellow and Franklin, 1993; Ames et al., 1993; Zierenberg et al., 1998 |

Figure 6.1

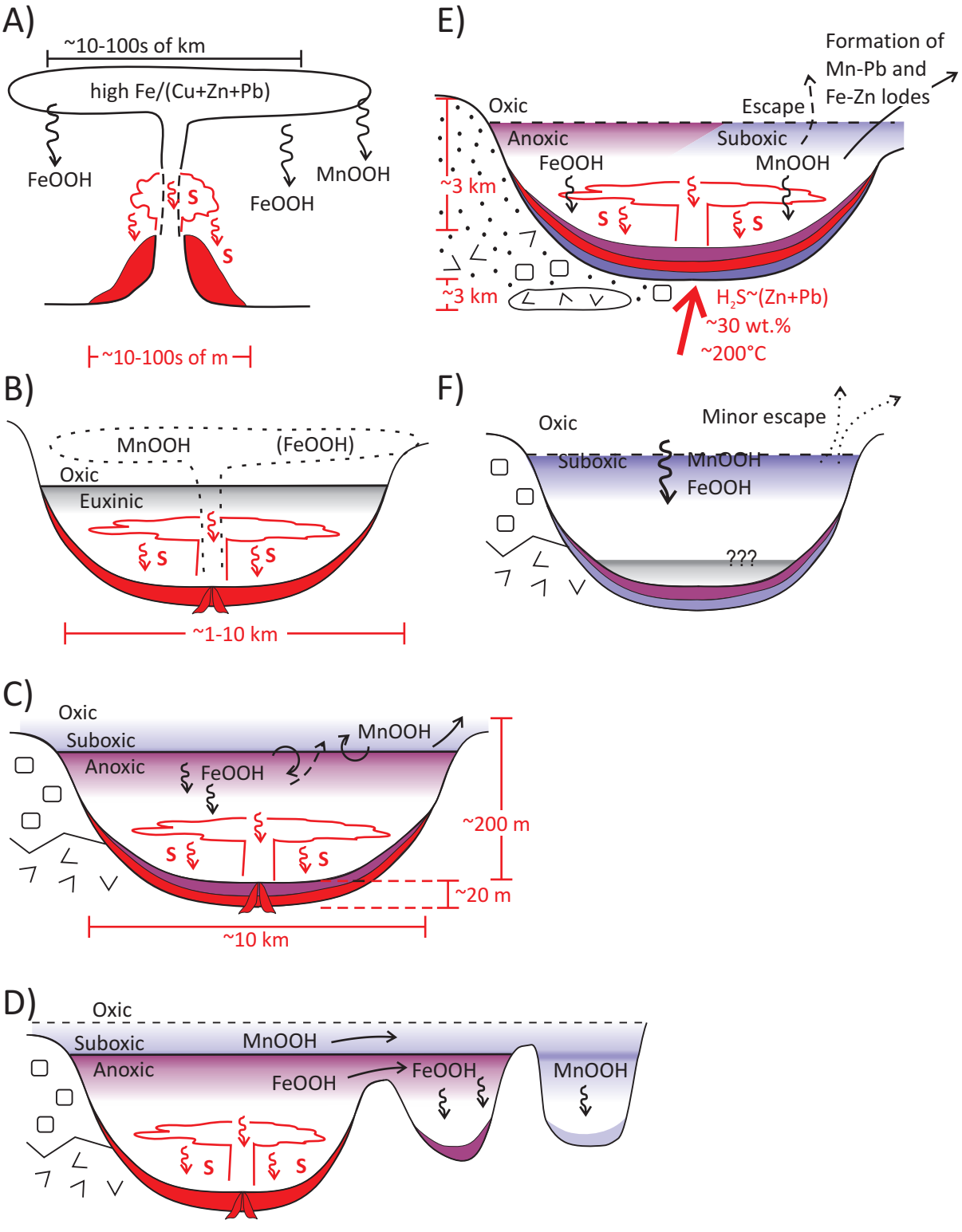

A)
~10-100s of km
high Fe/(Cu+Zn+Pb)
FeOOH
FeOOH
MnOOH
S
S
S
~10-100s of m
B)
MnOOH
(FeOOH)
Oxic
Euxinic
S
S
S
~1-10 km
C)
Oxic
Suboxic
Anoxic
MnOOH
FeOOH
S
S
S
~200 m
~20 m
~10 km
D)
Oxic
Suboxic
Anoxic
MnOOH
FeOOH
FeOOH
MnOOH
S
S
S
E)
Formation of
Mn-Pb and
Fe-Zn lodes
Oxic
Escape
Anoxic
Suboxic
FeOOH
MnOOH
~3 km
~3 km
S
S
S
H2S~(Zn+Pb)
~30 wt.%
~200°C
F)
Oxic
Minor escape
Suboxic
MnOOH
FeOOH
???

Figure 6.2

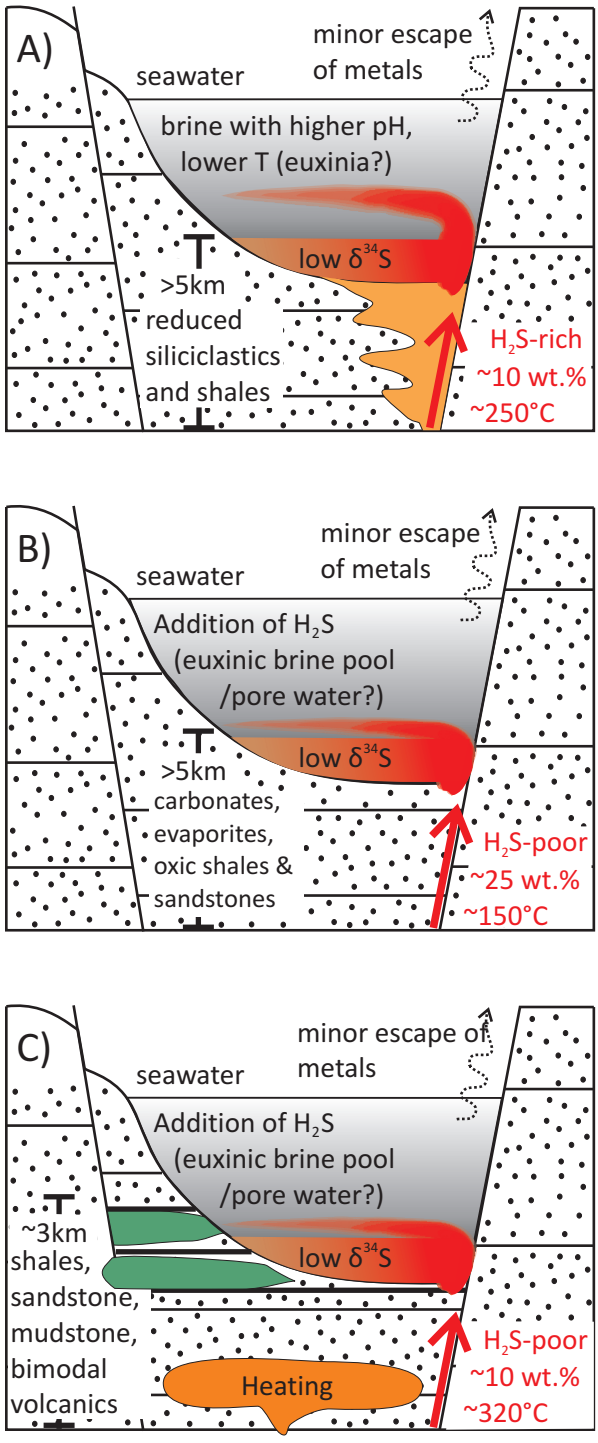
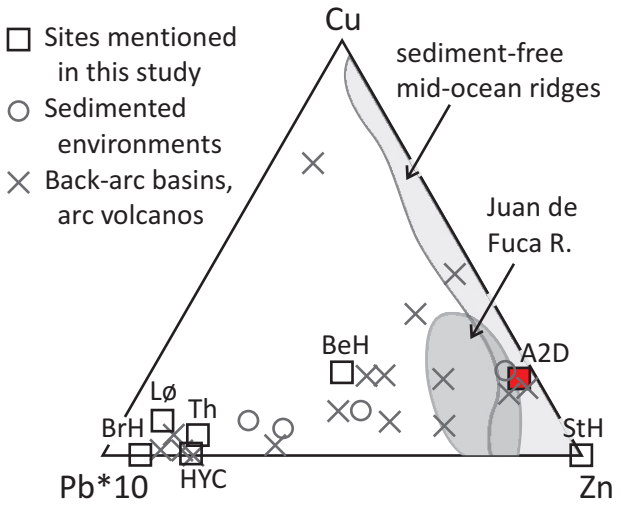

A)
seawater
minor escape
of metals
brine with higher pH,
lower T (euxinia?)
low δ34S
>5km
reduced
siliciclastics
and shales
H2S-rich
~10 wt.%
~250°C
B)
seawater
minor escape
of metals
Addition of H2S
(euxinic brine pool
/pore water?)
low δ34S
>5km
carbonates,
evaporites,
oxic shales &
sandstones
H2S-poor
~25 wt.%
~150°C
C)
seawater
minor escape of
metals
Addition of H2S
(euxinic brine pool
/pore water?)
low δ34S
~3km
shales,
sandstone,
mudstone,
bimodal
volcanics
Heating
H2S-poor
~10 wt.%
~320°C

Figure 6.3




Abbreviations

BrH = Broken Hill (BHT deposit)
Lø = Løkken (VMS related exhalites)
Th = Tharsis (brine pool VMS)
HYC = Here's your chance (SEDEX)
BeH = Bent Hill (modern VMS on sedimented ridge)
StH =Sterling Hill (stratiform Zn-oxide-silicate deposit)
A2D = Atlantis II Deep (modern brine pool)

Figure 6.4

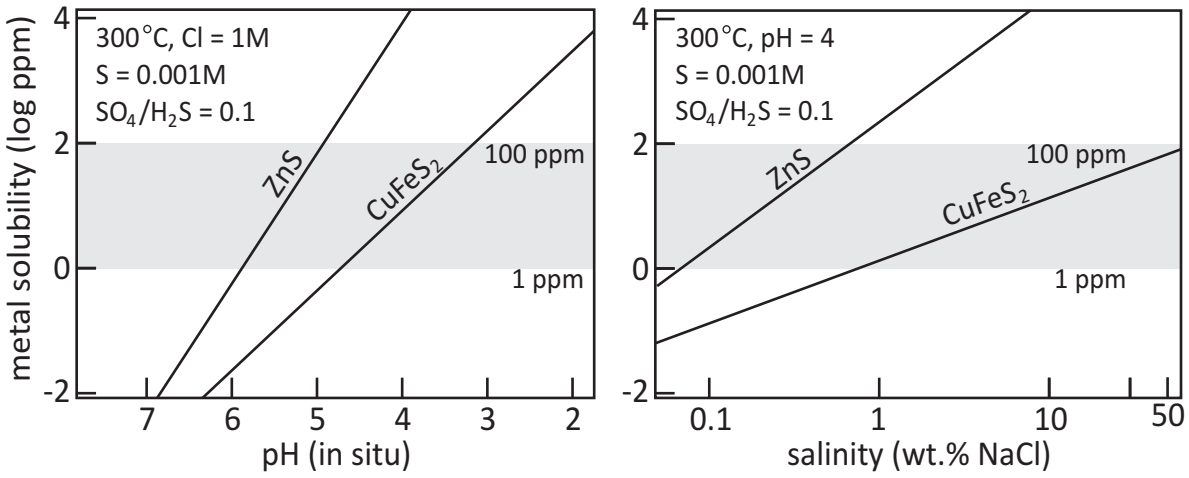

300°C, Cl = 1M
S = 0.001M
SO4/H2S = 0.1
ZnS
CuFeS2
100 ppm
1 ppm
metal solubility (log ppm)
4
2
0
-2
7
6
5
4
3
2
pH (in situ)
300°C, pH = 4
S = 0.001M
SO4/H2S = 0.1
ZnS
CuFeS2
100 ppm
1 ppm
0.1
1
10
50
salinity (wt.% NaCl)

Figure 6.5

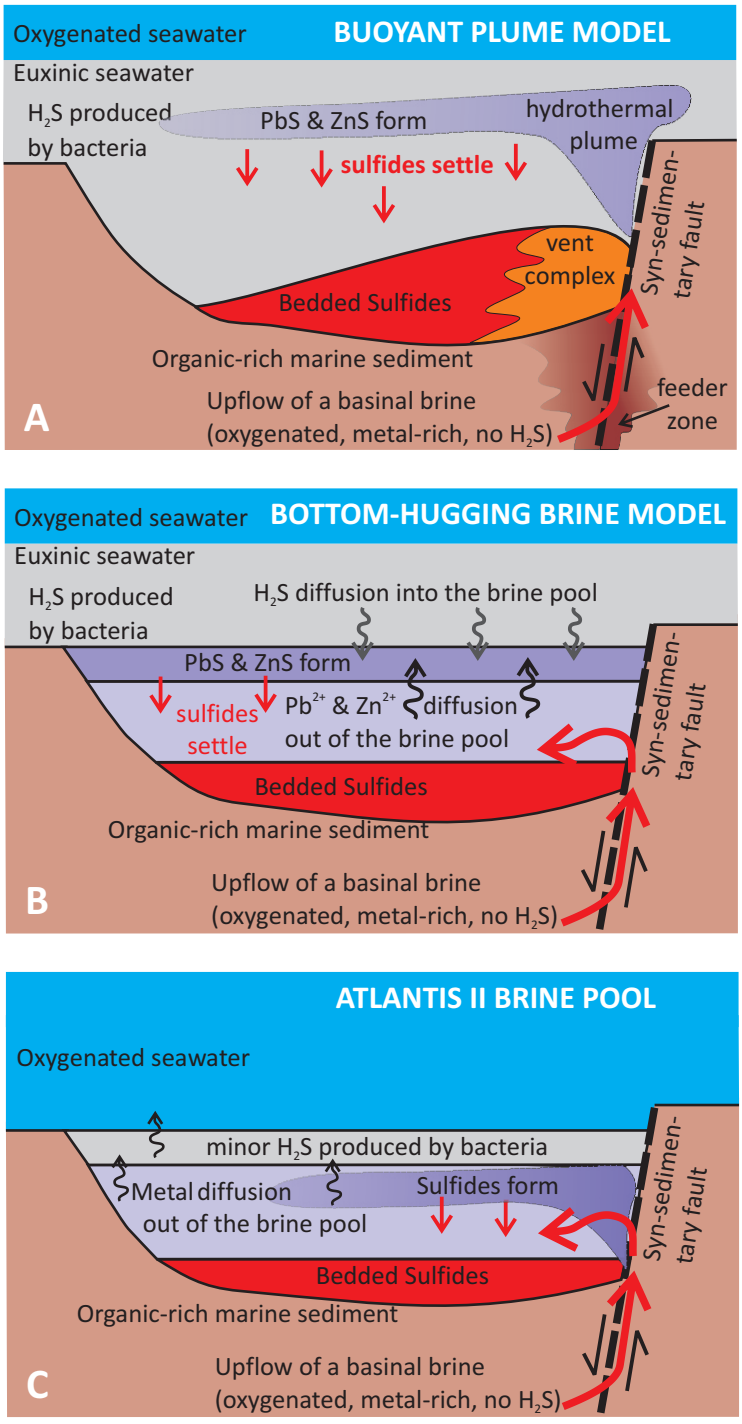
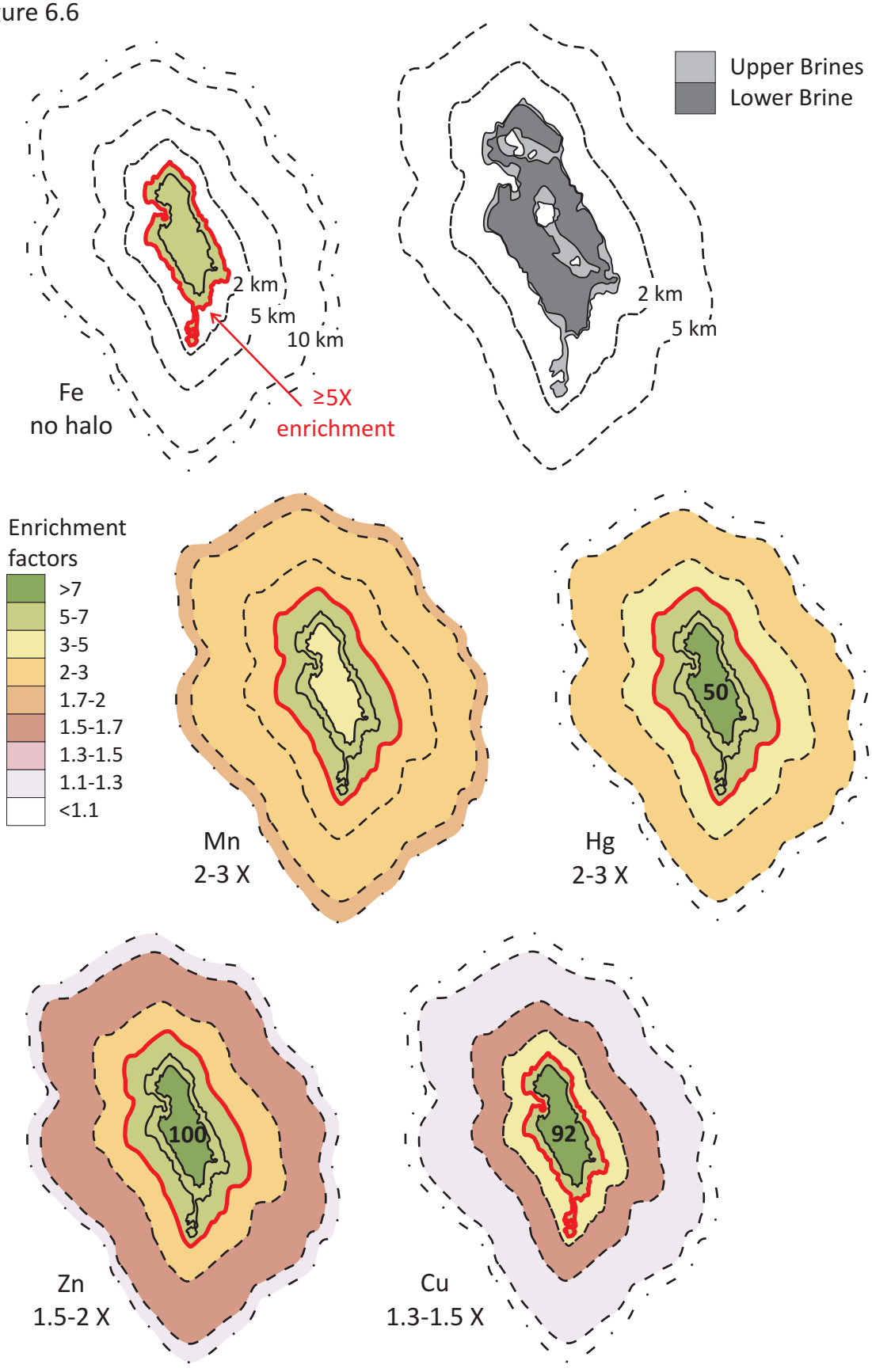

Oxygenated seawater
BUOYANT PLUME MODEL
Euxinic seawater
H2S produced by bacteria
PbS & ZnS form
hydrothermal plume
sulfides settle
vent complex
Syn-sedimen-tary fault
Bedded Sulfides
Organic-rich marine sediment
feeder zone
Upflow of a basinal brine (oxygenated, metal-rich, no H2S)
A
Oxygenated seawater
BOTTOM-HUGGING BRINE MODEL
Euxinic seawater
H2S produced by bacteria
H2S diffusion into the brine pool
PbS & ZnS form
sulfides settle
Pb2+ & Zn2+ diffusion out of the brine pool
Syn-sedimen-tary fault
Bedded Sulfides
Organic-rich marine sediment
Upflow of a basinal brine (oxygenated, metal-rich, no H2S)
B
ATLANTIS II BRINE POOL
Oxygenated seawater
minor H2S produced by bacteria
Metal diffusion out of the brine pool
Sulfides form
Syn-sedimen-tary fault
Bedded Sulfides
Organic-rich marine sediment
Upflow of a basinal brine (oxygenated, metal-rich, no H2S)
C

Figure 6.6


Upper Brines
Lower Brine
2 km
5 km
10 km
Fe
no halo
≥5X
enrichment
2 km
5 km
Enrichment
factors
>7
5-7
3-5
2-3
1.7-2
1.5-1.7
1.3-1.5
1.1-1.3
<1.1
Mn
2-3 X
50
Hg
2-3 X
100
Zn
1.5-2 X
92
Cu
1.3-1.5 X

# CHAPTER 7

## CONCLUSIONS

The Atlantis II Deep is the only known site of hydrothermal activity on the modern ocean floor where a large-tonnage stratiform base metal ore deposit is currently forming in a brine pool. A careful re-examination and re-analysis by modern techniques of the classic cores from the Atlantis II Deep has revealed a number of aspects that were previously unrecognized in studies from more than 30 years ago. A major problem in previous studies was the common practice of washing the samples before analysis. With the aid of modern analytical techniques we were able to use smaller sample sizes and samples with high salt-concentration without compromising the sample material by washing. Direct observation of the extremely fine-grained particles also has become possible with micro-imaging techniques that have become readily available since the early studies.

The sediments of the Atlantis II Deep comprise three main types: biogenic and silicic detrital background sediment, Fe-rich authigenic sediment, and sulfur-rich authigenic sediment. All three types are found throughout the basin and in all strata, but the proportions vary dramatically depending on conditions in the brine pool at the time of deposition and proximity to the hydrothermal vent sources. Deposition of Fe-rich sediments has dominated during times of low-temperature venting and in parts of the basin distal to the inferred vent sources, whereas sulfur-rich sediments (in particular, Cu- and Zn-rich sulfides and anhydrite) are most abundant during high-temperature venting and proximal to the vents. Finely-laminated sediments, with local brecciation, comprise the bulk of the sediment cores. The different laminae are dominated by silicates, oxides, carbonates or sulfides, similar to the facies described from banded iron formations. At the microscopic scale, it is

clear that even the finest layers are mixed chemical-clastic sediments (i.e., formed from particles of various sizes and compositions and from different sources). This contrasts with the formation of purely chemical sediments, such as chert or some BIF. Other components, for example authigenic barite, manganosiderite, and some sulfides clearly formed within the sediment by diagenetic growth from enriched pore fluids. The authigenic clays are compositionally Fe-rich nontronite, with subordinate Mg-rich clays proximal to the high-temperature vents. These clays may contain up to several weight percent Zn, making them one of the important sources of non-sulfide Zn in the sediments. Detrital carbonates are mainly fossiliferous biogenic calcite with minor dolomite. Close to the vent sources, the biogenic carbonate is dissolved by hydrothermal fluid and the carbonate reprecipitates as manganosiderite, which may also contain up to few percent Zn. The Fe content of the authigenic carbonates increases towards the vent source.

The stratified brine pool overlying the sediments includes an anoxic, hot and metal-rich Lower Brine and multiple, increasingly seawater-like, Upper Brine layers. The chemistry of the different layers determine the nature of precipitation from the brine pool. Sulfides form mainly in the anoxic, hot and metal-rich Lower Brine or from the sedimentary pore water. Fe-(oxy)hydroxides form at the chemocline between the Lower Brine and Upper Brine or in the Upper Brine. Mn-(oxy)hydroxides form in the upper parts of the Upper Brine where oxygen is readily available. The Fe-(oxy)hydroxides settle through the Lower Brine as metastable phases, basinwide, whereas Mn-(oxy)hydroxides accumulate only at the flanks of the Deep covered by the Upper Brine. Manganese that escapes from the brine pool is

found in the sediments at least 11 km away from the brine-covered area. Zn and Hg are also enriched in a halo around the brine pool.

The bulk metal grades of the sediments are variable, with the highest grades proximal to the current location of hydrothermal venting. Fe-sulfides are subordinate to other base metal sulfides, and in some parts of the sediment column, total Cu+Zn, on a molar basis, exceeds the amount of reduced S, highlighting the presence of non-sulfidic Cu- and Zn-rich compounds. Non-sulfides that have adsorbed metals from the Lower Brine during settling are most common in the brine-saturated and diffusively laminated uppermost sediments. Our samples contained abundant salt after drying (up to 75 wt.%), which reflects the degree of brine saturation of the primary sediments, especially in the uppermost layers. During diagenesis amorphous compounds recrystallize to Fe-oxides, clays and carbonates and the desorbed metals are incorporated in diagenetic sulfides, but also carbonates, clays and oxides. Much of the fine lamination of the sediments is developed diagenetically with burial (e.g., from AM to SU1), accompanied by increasing chemical differentiation between laminae. Because most of the non-sulfidic particles are transformed to sulfides during early diagenesis, evidence of the se processes is not well preserved, and their importance may not be recognized in similar ancient deposits.

Textural evidence for diagenetic sulfide formation has been long recognized throughout the Atlantis II Deep, but in this study isotopic evidence for bacterial sulfate reduction in the sedimentary pore waters was also found. Sulfides deposited in distal sediments are

characterized by isotopically light sulfur, consistent with bacteriogenic sulfate reduction in this environment. The distal sediments are also characterized by higher Cu/Zn ratios than in vent proximal sediments. This zonation contrasts with that of most seafloor hydrothermal systems where temperature is the dominant control on Cu and Zn solubility and may reflect more efficient deposition of Cu than Zn with Fe-(oxy)hydroxides in this environment. Precipitation and dissolution processes in the brine pool also play an important role in transport of elements from seawater into the Lower Brine and sediments in the distal part of the Deep.

The geochemical evolution of the brine pool over the last 15,000 years is recorded in the geochemistry of the different sediment types, in particular the trace elements and REEs. Both distal and proximal hydrothermal sediment have large positive Eu anomalies compared to background sediment, recording the hydrothermal input. Total REE concentrations increase dramatically with depth in the cores. This is interpreted to reflect rapid drawdown or stripping of REE from the early brine pool by the formation of the first Fe-(oxy)hydroxides and the inability to replenish that initial stock of REE during subsequent hydrothermal pulses.

Trace metals such as Cd, Ag and Hg are highly enriched in the uppermost sediment and especially close to the known vents with Cu- and Zn-sulfides. Other metals, such as Au, Sb and Tl are distributed more evenly throughout the Deep, deposited by a number of different pathways (as sulfides close to the vents but also in diagenetic pyrite and

authigenic clays farther from the vents). Mo and As (and Ga, to a lesser extent) are enriched in the distal part of the Deep and in some units with a larger detrital component: they are derived from a number of non-hydrothermal sources, especially scavenging from seawater. Diagenetic pyrite is almost always characterized by As-rich rims, which are interpreted to reflect scavenging of As from enriched pore waters during diagenetic growth. Au is co-enriched with As in diagenetic pyrite, enriched in authigenic clays (together with Ga ± Tl) and, especially at the vent proximity, deposited with hydrothermal sulfides. Possible evidence of enrichment of Au has been found by S-XRF analysis of several non-sulfide phases, but discrete particles of Au have not yet been found in the sediments.

The Atlantis II Deep is the largest accumulation of hydrothermal mineralization known on the modern seafloor and also the first site where commercial exploitation of a seafloor metal deposit has been assessed. The total resource of 1.9 Mt of Zn, 0.43 Mt of Cu, 3750 t of Ag and 47 t of Au rivals that of some of the largest VMS and SEDEX deposits on land. Importantly, the assay data from the pre-pilot mining test were based on samples that had been washed to remove salt prior to analysis, leading to partial loss of non-sulfide metals and any particles finer than the filters used.

The Atlantis II Deep has been widely acknowledged as a modern analog for a variety of stratiform ore deposit types, in particular sedimentary exhalative massive sulfide deposits (SEDEX) and some volcanic-hosted massive sulfide (VMS) deposits. Typical models of brine pool-type deposits consider that the brine pool was mainly a trap for exhaling metals,

resulting in broadly uniform deposition of all metals in the sediments. However, analysis of trace metal zoning in the Atlantis II sediments shows considerable variation related to processes taking place in the brine pool. Co-deposition of Zn with primary Si-Fe-OOH particles has been shown in this study to be an important process in the sulfide-deficient brine pool of the Atlantis II Deep, with implications for the formation of some stratiform Zn oxide-silicate deposits. Redox variations in the Atlantis II water column that cause efficient Fe deposition but allow Mn to diffuse into seawater may also explain the spatial separation between Fe-rich Zn-lodes and Mn-rich Pb-lodes in deposits like Broken Hill.

**Summary of Conclusions**

1) The study of sediment still containing its evaporated pore water has allowed the analysis of water-soluble and extremely fine-grained particles (0.45 μm filter mesh size) that were lost by washing in the previous studies.

2) Modern analytical techniques allowed the measurement of very low concentrations of all elements in small volume samples, revealing aspects of the geochemistry of the sediments at very fine scale that were not seen in previous studies.

3) Variable input from detrital, hydrogenic and hydrothermal sources were found to be the main control on the geochemistry of the sedimentary layers (Ch 4).

4) Different "pathways" of metal deposition have had a significant influence on basin-wide trace metal distribution (Ch 3).

5) Significant amounts of Cu and Zn are deposited with poorly crystalline or amorphous Si-Fe-(oxy)hydroxides and later incorporated into sulfides and clays during diagenesis (Ch 2 and 3).

6) Other trace metals are precipitated with high-temperature minerals (mainly sulfides) but are also scavenged from the brine pool by Si-Fe-(oxy)hydroxides and incorporated into diagenetically forming minerals (Ch 3).

7) Lack of sulfide in the pore waters leads to incorporation of some metals, including Cu and Zn, into diagenetic carbonates as well as clays (Ch 2 and 3).

8) Carbonate zoning is a result of dissolution of biogenic calcite and reprecipitation as Mn-Fe-(Ca) carbonate, with Fe/Mn increasing towards the vent source (Ch 2).

9) The Mg/Fe ratio of diagenetic clays also increases towards the vent source (Ch 2).

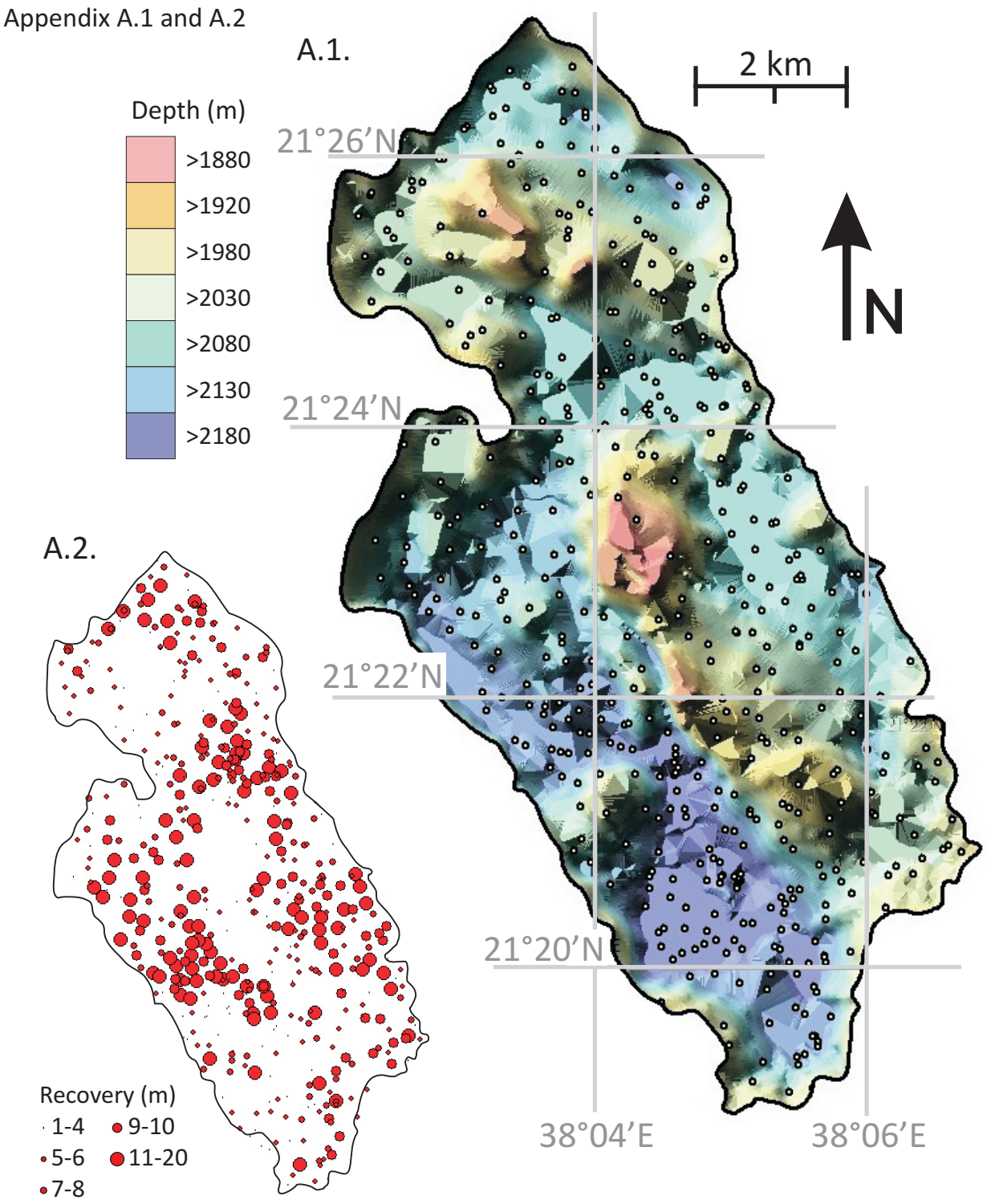
10) There is an unexpected inverse Cu/Zn zonation with respect to the location of the vents (due to non-sulfidic or bacteriogenic Cu deposition in the Upper Brines?) (Ch 3).

11) Sharply defined and very fine laminations in the sediments are mainly formed during diagenesis (Ch 2).

12) Mineralogical and geochemical changes with depth in the cores reflect the evolution from an early euxinic to a sulfide-deficient metal-rich brine pool (Ch 4).

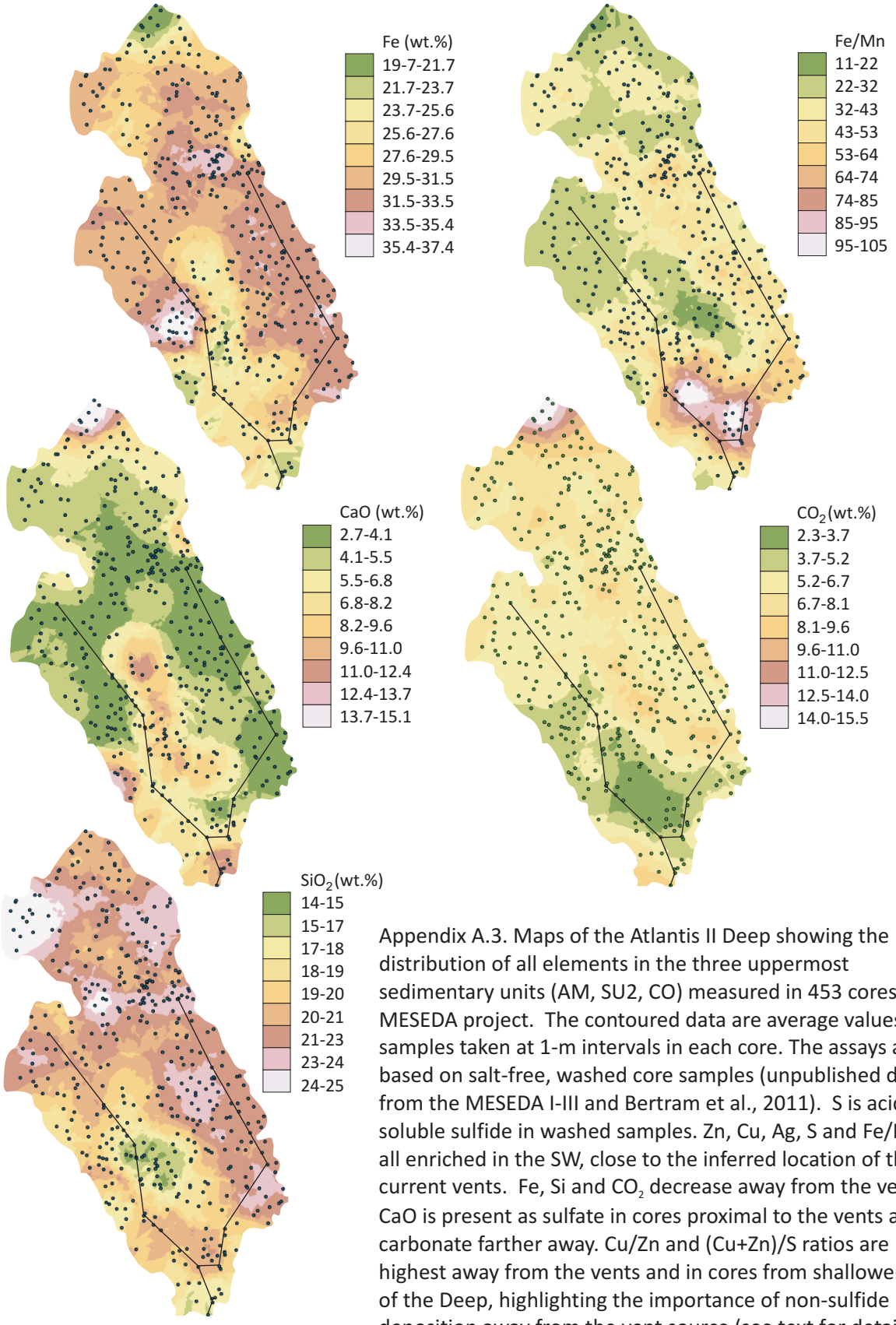
13) Negative $\delta^{34}S$ values in sulfides and metal-rich units indicate the role of bacterial sulfate reduction (Ch 5).

14) Processes controlling metal deposition are far more complex than suggested by earlier genetic models of brine-pool type deposits, in particular involving non-equilibrium processes and rapid diagenetic transformations (Ch 6).



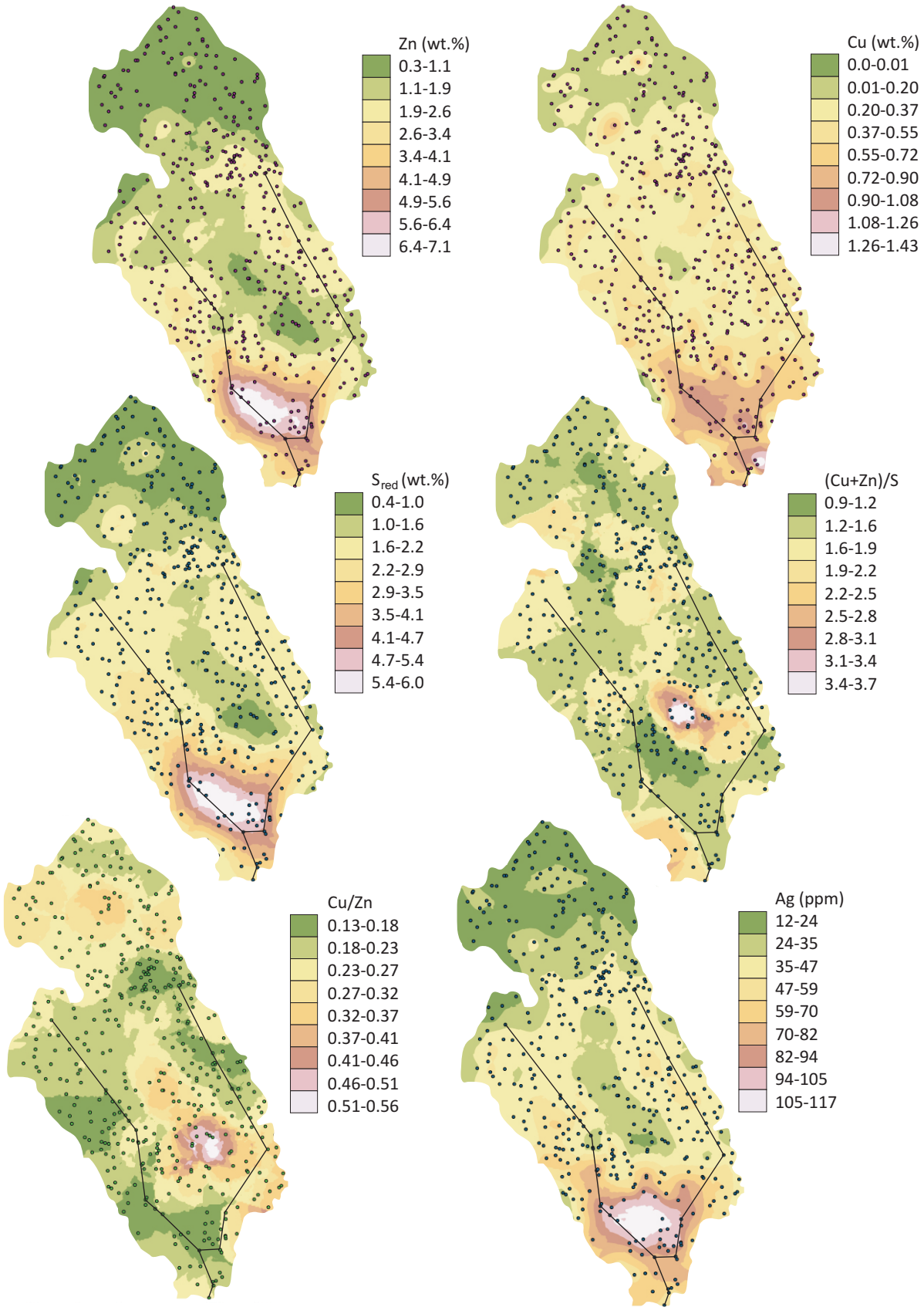

Appendix A.1) Location map of all the cores available for this study (upublished data from the MESEDA projects I, II and III; cf. Steinkamp and Schumann, 1974; Bertram et al., 2011). Appendix A.2) Thickness of recovered sediment in MESEDA cores; the sedimentary cover is thinnest within the Southwest Basin, where the lower sedimentary units (SU1 and DOP) are absent due to presence of a basaltic sill.

Appendix A.3 part 1/2

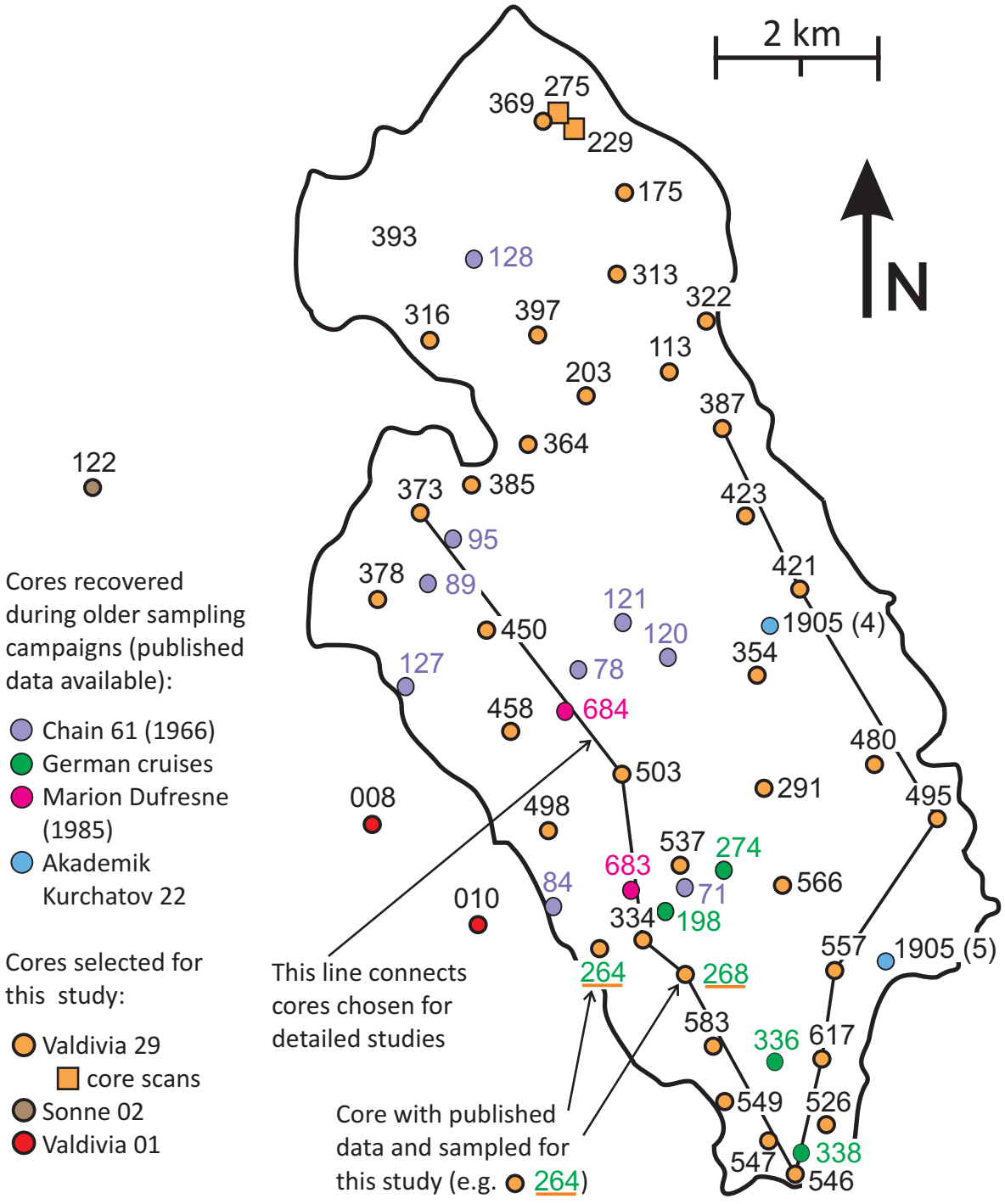



Appendix A.3. Maps of the Atlantis II Deep showing the distribution of all elements in the three uppermost sedimentary units (AM, SU2, CO) measured in 453 cores of the MESEDA project. The contoured data are average values of all samples taken at 1-m intervals in each core. The assays are based on salt-free, washed core samples (unpublished data from the MESEDA I-III and Bertram et al., 2011). S is acid-soluble sulfide in washed samples. Zn, Cu, Ag, S and Fe/Mn are all enriched in the SW, close to the inferred location of the current vents. Fe, Si and $CO_2$ decrease away from the vents. CaO is present as sulfate in cores proximal to the vents and as carbonate farther away. Cu/Zn and (Cu+Zn)/S ratios are highest away from the vents and in cores from shallower parts of the Deep, highlighting the importance of non-sulfide deposition away from the vent source (see text for details).

Appendix A.3 part 2/2



Appendix B.1




Appendix B.1. Location of cores sampled during this study and other cores with chemical data (published in English). German cruises are Valdivia 01, 02, 22 and 29, and Sonne 02. Cores sampled for this study are 334, 373, 387, 421, 495, 503, 546, 557, 617 (chemistry + mineralogy), 264 and 268 (mineralogy only).

Appendix B.2. Description of samples collected from cores in this study. Core locations are shown in Appendix B.1. The lengths of the sampled cores are according to Meseda archived information (the value in brackets indicates the amount of top loss, i.e., amount of unconsolidated sediment that was penetrated by the coring device and not recovered). Depth in the header is the water depth at the sampling site. For each sample, the sampling depth is given in cm below the beginning of the core (see photos in Appendix B.3). Unit refers to the sedimentary unit according to Bäcker and Richter (1973) and is assigned to each sample according to the original Meseda core logs. Color is the color at the time of sampling for this study (2010) and after drying and pulverizing of the sample. Color at the time of core recovery in 1979 is also recorded (original photos of the cores are included in Appendix B.3). R=Red, O=Orange, Y=Yellow, G=Green, H=Grey, B=Brown, letter preceding color are L=light, M= medium, D=Dark. Letters preceding hardness are m=moderate, v=very; other abbreviations are irr.=irregular, diff.=diffusive, comp.=compare to. Samples in bold were chosen for detailed mineralogical and chemical analysis; color is also given according to the Munsell color code.

| Valdivia 29_113; length 979 cm (275); depth 2101 m | | | |
|---|---|---|---|
| Depth | Unit | Color | Additional description |
| 13 | AM | R | |
| 21 | AM | O | |
| 47 | SU2 | DR | violet, relat. coarse grained, greasy, comp. 202 |
| 99 | SU2 | G | |
| 160 | SU2 | black | ~7cm thick sulfide layer |
| 165 | SU2 | mix | bright G and MR interlayers |
| 177 | SU2 | DG | brownish, greasy |
| 224 | SU2 | DR | violet, relat. coarse grained, greasy, named 202 |
| 271 | CO | black | named 250 |
| 285 | CO | Y | L/M Y, soft, named 363 |
| 389 | CO | B | lighter and darker brown, named 367 |
| 398 | CO | B | dark, mhard, named 376 |
| 487 | COS | black | mhard, coarse grain size, named 465 |
| 509 | COS | DG | mhard, diff. layered, named 486 |
| 629 | COS | R | msoft, diff. laminated, named 608 |
| 635 | SU1 | G | mhard, irr. Layered, named 613 |
| 652 | SU1 | black | msoft ooze with crystals, named 630 |
| 678 | SU1 | B | brownish interlayer in black ooze, named 656 |
| 804 | SU1 | MB | mhard, dessicated, ~homog, named 781 |
| 871 | DOP | LB | LB-MY-LH, mhard, irr. layered, named 849 |
| 915 | DOP | Y | homog., named 893 |
| 973 | DOP | MB | to DB with Y and G, dessicated, irr. and diff. layered, named 951 |

| Valdivia 29_175; length 835 cm (52); depth 2099 m | | | |
|---|---|---|---|
| Depth | Unit | Color | Additional description |
| 130 | AM | O | |
| 158 | AM | R | |
| 190 | SU2 | DG | |
| 203 | SU2 | G | |
| 256 | SU2 | DR | violet |
| 280 | SU2 | R | |
| 343 | CO | LB | coarser grained unit |
| 361 | CO | H | greenish-brownish, relat. coarse |
| 367 | CO | | |
| 410 | CO | B | reddish |
| 435 | CO | black | |
| 450 | COS | | |
| 574 | COS | | |
| 590 | SU1 | O | Silver tint, hard, interlayer |
| 596 | SU1 | G | Grass green, rather coarse |
| 609 | SU1 | B | coarse fraction |
| 636 | SU1 | B | marl interlayer in black S unit? |
| 643 | SU1 | black | brownish |
| 670 | SU1 | G | orange tint |
| 675 | SU1 | silver | interlayer below crystalline layer |
| 682 | SU1 | DR | violet, greasy ooze |
| 826 | DOP | Y | |
| Valdivia 29_203; length 725 cm (229); depth 2099 m | | | |
| Depth | Unit | Color | Additional description |
| 105 | AM | R | purplish, greasy |
| 108 | AM | O | bright, mix of O and R |
| 120 | AM | B | olive-greenish, greasy |
| 125 | AM | ? | |
| 158 | SU2 | black | very soft, fine grained |
| 174 | SU2 | B | reddish-greenish, red parts |
| 197 | CO | G | dark brownish, greasy |
| 217 | CO | black | soft, some hard parts |
| 230 | CO | Y | mustard |
| 243 | CO | LB | soft |
| 268 | CO | R | wine R, mixed R and O parts |
| 306 | CO | G | |
| 335 | COS | DR | purplish |
| 481 | COS | DR | purplish |
| 498 | SU1 | B | and black, crunchy |
| 538 | SU1 | Y | and grey mix, sandy |
| 539 | SU1 | R | brownish, muddy, mixed with above layer |
| 548 | SU1 | R | purplish |
| 577 | SU1 | B | greenish, msoft, crunchy, greasy “matrix” |
| 583 | SU1 | ? | piece of hard dark material in uncoherent light matrix |
| 594 | SU1 | silver | very hard, thin layer |
| 602 | SU1 | B | greenish with white needle shaped hard parts |
| 611 | DOP | B | sandy |
| 634 | DOP | Y | |
| 694 | DOP | Y | O-brownish |
| 696 | DOP | black | mhard, crunchy |
| 698 | DOP | LH | muddy |
| Valdivia 29_264; 1127 cm (0); 2143 m | | | |
| Depth | Unit | Color | Additional description |
| 58 | AM | black | violet, soft |
| 83 | AM | MR | lighter part in the core, soft, coarse |
| 192 | AM | R | brownish, soft |

| | | | |
|---|---|---|---|
| 250 | AM | R | greenish, soft |
| 309 | AM | R | wine R with orange layer, soft |
| 380 | AM | black | red |
| 403 | SU2 | R | violet |
| 474 | SU2 | DG | greasy |
| 508 | SU2 | black | soft |
| 513 | SU2 | G | bright |
| 538 | SU2 | DB | coarse |
| 550 | CO | B | bright, reddish |
| 559 | CO | DR | tint of violet |
| 579 | CO | DG | greasy |
| 586 | CO | G | olive G and yellowish grey layers |
| 604 | CO | G | bright G with white sandy interlaminae |
| 631 | COS | R | brownish |
| 647 | COS | B | light-forest brown |
| 704 | COS | DB | |
| 758 | COS | DR | purplish R with O interlayer |
| 795 | COS | DR | |
| 803 | COS | R | purplish with thin laminae of orange |
| 847 | SU1 | black | with grey and brown parts |
| 861 | SU1 | black | |
| 907 | SU1 | black | with brown (alteration) parts, muddy |
| 924 | DOP2 | black | with crunchy (gypsum?) crystals |
| 932 | DOP2 | LG | and Y |
| 941 | DOP2 | O | crunchy, comp. 980 |
| 972 | DOP2 | Y | comp. 932 |
| 980 | DOP2 | O | thinly laminated |
| 995 | DOP2 | black | and brown, firm, fine grained, thin laminated |
| 1008 | DOP2 | black | brownish (alteration?) surface |
| 1023 | DOP2 | B | greenish, finely laminated |
| 1046 | DOP2 | black | and yellow, sandy, finely laminated |
| 1061 | DOP2 | R | and orange |
| 1067 | DOP2 | black | layer of black in red mud (sample contains some red mud) |
| 1078 | DOP1 | black | crunchy, uncoherent |
| 1081 | DOP1 | | thin sections |
| 1089 | DOP1 | LB | muddy, but consolidated |
| 1094 | DOP1 | H | greenish, crunchy |
| 1098 | DOP1 | B | lighter and darker B, muddy |

Valdivia 29_268; 1125 cm (162); 2182 m

| Depth | Unit | Color | Additional description |
|---|---|---|---|
| 25 | SAM | DR | purplish, greasy |
| 143 | SAM | DR | dark, brownish |
| 221 | SAM | DG | greasy |
| 240 | OAN | G | mix of bluish with R parts, coarse |
| 269 | OAN | black | and violet, darker than surrounding |
| 297 | OAN | R | bright breccia with black and G "clasts" |
| 337 | OAN | R | bright, soft, homog. ooze |
| 389 | OAN | DR | to black, soft ooze |
| 415 | SOAN | black | soft, smooth |
| 499 | SOAN | DR | violet, soft |
| 513 | SOAN | DR | violet, soft, muddy ooze |
| 567 | SOAN | DB | to DG, ooze |
| 615 | SOAN | B | yellowish with irregular patches of B, uncoherent |
| 648 | SOAN | B | mix of hard greyish B mud with white needles |
| 661 | SOAN | DB | crunchy |
| 741 | SOAN | mix | B-G-Y-black, crunches |
| 765 | SOAN | black | some DB, crunchy |
| 830 | CO | H | hard, vein (horiz. & vertical) |
| 869 | CO | R | bright, soft, muddy |

| | | | |
|---|---|---|---|
| 904 | CO | R | bright, soft, muddy |
| 986 | CO | black | crunchy |
| 1027 | CO | G | mix of sandy and hard material |
| 1061 | CO | | details for precious metals? |
| 1070 | CO | | details for prec. metals? |
| 1072 | CO | R | bright, coherent, muddy, details for prec. Metals |
| 1076 | CO | | details for prec. metals? |
| 1086 | CO | LG | details for prec. metals? |
| 1099 | CO | | details for prec. metals? |
| Valdivia 29_291; 596 cm (0); 2019 m | | | |
| Depth | Unit | Color | Additional description |
| 28 | AM | DR | violet with black spots |
| 151 | AM | MB | reddish |
| 155 | AM | O | bright |
| 179 | AM | DR | violet |
| 196 | SU2 | O | thin O laminae in violet unit |
| 228 | SU2 | G | forest green and dark violet, greasy ~homog. |
| 298 | SU2 | mix | G, L yellowish brown and red laminae |
| 314 | CO | LG | forest color, thinly laminated with white hard parts |
| 349 | CO | black | uncoherent, sandy |
| 350 | CO | LH | to white, with hard parts |
| 373 | CO | black | soft, homogenous |
| 383 | CO | B | all tints of brown, thinly laminated |
| 404 | CO | DR | violet, thinly laminated, comp 426 |
| 426 | COS | R | similar to 404, but bit more reddish |
| 460 | COS | DR | violet, hard, coherent |
| 468 | SU1 | G | forest green, greasy |
| 477 | SU1 | G | bright, hard, muddy |
| 499 | SU1 | mix | mix of coherent black muddy and uncoherent white sandy layers |
| 509 | SU1 | H | with bright Y parts, very loose |
| 549 | SU1 | H | greenish grey and white, loose |
| 550 | SU1 | O | ~0.5 cm thick hard layer in irregular directions |
| 571 | SU1 | mix | black-orange-brown |
| 591 | DOP | DR | violet |
| Valdivia 29_313; 400 cm (0); 2031 m | | | |
| Depth | Unit | Color | Additional description |
| 7 | AM | R | with black spots |
| 57 | AM | R | coherent |
| 198 | AM | mix | O and Greenish Yellow grey |
| 249 | SU2 | DR | purple, greasy |
| 305 | SU2 | G | bright G and light/dark B, firm, thinly laminated |
| 332 | SU2 | DR | purple, firm |
| 340 | CO | B | crunchy and coarse grained |
| 357 | SU1 | B | rusty + black parts |
| 366 | SU1 | G | layer |
| 373 | SU1 | R | layer |
| 383 | SU1 | | |
| 395 | DOP | light | grey-brown and white |
| 396 | DOP | G | and other colors as mixture, greasy, laminated |
| Valdivia 29_316; 382 cm (43); 2032 m | | | |
| Depth | Unit | Color | Additional description |
| 76 | AM | DR | purple |
| 166 | AM | B | |
| 198 | AM | G | layer |
| 214 | AM | O | |
| 240 | SU2 | DB | upper (comp. to 242, 313) |
| 242 | SU2 | G | upper (comp. to 240, 313) |
| 313 | SU2 | G | lower level (comp. to 240, 242) |

| | | | |
|---|---|---|---|
| 326 | CO | B | orange tint, coarse |
| 331 | SU1 | silver | hard layer on top of salt layer |
| 334 | SU1 | R | dark, less greasy more muddy than AM (76) |
| 344 | SU1 | G | mhard, firm, greasy |
| 361 | SU1 | DB | |
| 369 | SU1 | DR | violet |
| 378 | DOP | H | light, greenish, coherent, as "clast" in O mud (380) |
| 380 | DOP | Y | light |
| Valdivia 29_334; 770 cm (0); 2184 m | | | |
| Depth | Unit | Color | Additional description |
| 13 | SAM | R | brown surface (alteration?), little black inside |
| **83** | **SAM** | **R** | **brownish on surface (alteration?), little black inside; [5YR 6/6]** |
| 121 | SAM | R | black inside |
| 172 | SAM | B | breccia |
| 191 | SAM | DR | very dark, clast in breccia |
| 223 | SAM | R | brighter and lighter R, harder than average, clast in breccia |
| 231 | SAM | DR | |
| 283 | SAM | R | bright |
| **312** | **SAM** | **black** | **[5YR 4/6]** |
| 378 | SAM | black | |
| 424 | SAM | R | DG material, "clast" in red |
| 443 | SAM | O | layer |
| 487 | SAM | DR | to black |
| **513** | **SAM** | **DR** | **black inside; [5YR 5/6]** |
| 531 | OAN | MR | brighter, LB inside in core |
| 559 | OAN | DG | layer |
| 595 | SOAN | R | black inside |
| **612** | **SOAN** | **R** | **black inside; [5YR 5/6]** |
| 646 | SOAN | R | |
| 691 | SOAN | DG | black inside |
| 705 | SOAN | MR | to DR, lots of hard pieces |
| 739 | SOAN | DR | wine R clast in breccia |
| 747 | SOAN | R | darker part in bright R material |
| **757** | **SOAN** | **MR** | **bright, firm; [10R 6/6]** |
| Valdivia 29_354; 1055 cm (39); 2061 m | | | |
| Depth | Unit | Color | Additional description |
| 10 | AM | MR | very soft |
| 108 | AM | MR | to DR, soft |
| 193 | AM | MR | to DR, soft |
| 251 | AM | O | soft |
| 258 | AM | MR | msoft, firmer than above, greasy |
| 294 | SU2 | dark | multi colored mix of diff. layered sedim., soft |
| 337 | SU2 | DR | soft |
| 377 | SU2 | B | medium B and G interlayer in R, soft |
| 433 | SU2 | MR | soft to msoft, laminated |
| 447 | CO | LB | soft to msoft, laminated |
| 461 | CO | black | with MR |
| 480 | CO | LB | to LH 2 cm interlayer in black matrix, mhard, silt |
| 517 | CO | DG | olive, soft to msoft, greasy |
| 539 | COS | DR | and black, soft to msoft, ~homog. |
| 622 | COS | DB | reddish, msoft to mhard, ~homog. |
| 638 | SU1 | black | soft with harder crystals |
| 666 | SU1 | LB | yellowish, mhard, greasy |
| 705 | SU1 | MR | to DR, msoft to mhard with hard parts |
| 733 | SU1 | mix | MY-MB-MH, crunchy |
| 764 | SU1 | black | to DB + white (anhy?) laminae, msoft to mhard |
| 770 | DOP | B | yellow-LB-DB, finely laminated, chem. +thin section |

| | | | |
|---|---|---|---|
| 786 | DOP | LH | mhard, silty |
| 805 | DOP | Y | mhard, homog. |
| 835 | DOP | DG | msoft harder parts, crunchy |
| 872 | DOP | MY | mhard, thin laminae, comp to 923 |
| 923 | DOP | mix | B+Y with black laminae, chem.+thin sections |
| 986 | DOP | LB | +tiny black laminae + white pieces of layers (~2 mm thick), chem. + thin section |
| Valdivia 29_364; 740 cm (389); 2091 m | | | |
| Depth | Unit | Color | Additional description |
| 20 | AM | DR | soft |
| 70 | SU2 | DR | black, Soft |
| 141 | SU2 | MG | to DG, msoft |
| 150 | SU2 | MG | olive tint, mhard/hard, diffusively layered sulphides comp. 151 |
| 151 | SU2 | MB | graded change between laminae, mhard/hard, diffusively layered sulphides |
| 155 | SU2 | MR | msoft, diff. laminated |
| 199 | CO | R | bright, soft |
| 207 | CO | black | soft with crystals (gypsum?), ooze |
| 220 | CO | MR | brownish |
| 260 | CO | black | interlayer |
| 263 | CO | R | mix of R and black soft ooze layers |
| 290 | CO | R | bright, soft |
| 299 | CO | mix | LB-LH-black |
| 305 | CO | MB | mhard, crunchy |
| 333 | COS | DG | brownish, mhard, lower part of an unconformity |
| 353 | COS | DR | msoft |
| 425 | SU1 | R | M to D, mhard, breccia, bulk sample |
| 438 | SU1 | black | soft ooze with crystals (gypsum?) comp. 474 |
| 474 | SU1 | black | comp. 438 |

| | | | |
|---|---|---|---|
| 539 | SU1 | R | |
| 555 | SU1 | MB | hard |
| 570 | SU1 | G | bright, yellowish, laminated |
| 604 | SU1 | black | mhard ooze, lamination on ox. surface |
| 616 | DOP | MB | to DB, hard, laminated |
| 633 | DOP | Y | mix of LH, O and black, mhard, top of Y layer |
| 649 | DOP | Y | mhard, comp. to 696 |
| 696 | DOP | Y | mhard, comp. to 649 |
| Valdivia 29_369; 683 cm (224); 2093 m | | | |
| Depth | Unit | Color | Additional description |
| 7 | AM | DR | to MR, soft |
| 53 | AM | MR | mhard ooze |
| 75 | AM | MY | |
| 94 | AM | R | M to D, ooze |
| 118 | SU2 | DR | msoft ooze |
| 152 | SU2 | MB | and greenish |
| 163 | SU2 | MG | black parts, mhard, silicic ooze |
| 256 | SU2 | DR | |
| 263 | SU2 | DB | to black, mhard |
| 267 | SU2 | L | to MB, layered |
| 296 | CO | Y | R and O, soft, layered |
| 307 | CO | black | soft ooze with crystals |
| 340 | CO | LB | mhard |
| 348 | CO | black | ooze, bottom of black unit |
| 359 | CO | | mhard, calcareous? laminated interlayer |
| 388 | CO | MB | mhard |
| 412 | CO | DG | to DB, mhard |
| 431 | COS | DR | to MR |
| 478 | COS | MB | to DB, layered, carb intercalations? |
| 505 | COS | DR | |

| | | | |
|---|---|---|---|
| 520 | SU1 | DR | mix of breccia material |
| 534 | SU1 | black | top of black unit |
| 568 | SU1 | black | bottom of black unit |
| 574 | SU1 | light | mhard layer within softer, dominantly black layer |
| 603 | SU1 | black | interlayer |
| 604 | SU1 | MG | to DG, comp. to 651 (same color, different look, bottom and top) |
| 626 | SU1 | MR | compare to 636, 651 |
| 636 | SU1 | DY | to yellowish MB, compare to 626, 651 |
| 651 | SU1 | MG | to DG, comp. to 626, 636, but also to 604 (same color, different look, bottom and top) |
| 663 | SU1 | DB | breccia, faulted contact |
| Valdivia 29_373; 970 cm (231); 2099 m | | | |
| Depth | Unit | Color | Additional description |
| **8** | **AM** | **MR** | **to DR, soft; [5YR 5/6]** |
| 45 | AM | MY | soft |
| **93** | **SU2** | **DR** | **msoft to soft ooze, diff. laminated; [10R 4/6]** |
| 117 | SU2 | DG | greener than surroundings |
| 162 | SU2 | DR | |
| 183 | SU2 | MG | |
| 197 | SU2 | black | |
| **210** | **SU2** | **G** | **dull, olive G, msoft, softer than DR material; [5Y 7/2]** |
| 236 | SU2 | MR | mhard |
| **265** | **CO** | **black** | **[5Y 3/1]** |
| 290 | CO | MY | to LB, soft |
| 305 | CO | mix | of R, L (Y) brown, mhard |
| 325 | COS | MD | to DR, mhard, comp. to 305 |
| 381 | COS | MR | to DR, mhard, comp. to 325 and 515 |
| 433 | COS | DH | with LB tiny inclusions |
| 469 | COS | MG | |
| 503 | COS | B | mix of LB and MB, "matrix" |
| **515** | **COS** | **DR** | **brownish; [5YR 5/5]** |
| 531 | SU1 | DG | olive, "lamination" as fractures |
| 547 | SU1 | Y | bright, mhard |
| **555** | **SU1** | **black** | **with harder crystals, upper part of layer; [N5]** |
| 580 | SU1 | LB | and Y oxid. surface, crunchy |
| **586** | **SU1** | **light** | **anhy clast on layer of MB and black material, shiny silver on oxid. surf., thin sect.; [10YR 8/4]** |
| 605 | SU1 | MB | inner lamination |
| 630 | SU1 | | mhard, lower part of layer |
| **672** | **SU1** | **MR** | **to DR, mhard, diffusively laminated [5YR 6/6]** |
| 716 | SU1 | MH | to LH with MY and MB, crunchy, contains very hard (anhy?) parts |
| 730 | SU1 | MG | mhard |
| 734 | SU1 | silver | hard, thin section? |
| **751** | **SU1** | **black** | **harder crystals (gypsum?) and harder white parts (anhy?) in msoft sedim.; [5Y 6/2]** |
| 769 | DOP | MB | to darker B, mhard to almost hard, sharply laminated |
| **780** | **DOP** | **LH** | **and yellowish, silt; [5Y 8/2]** |
| **798** | **DOP** | **Y** | **orange tint, soft to msoft; [10YR 6/6]** |
| Valdivia 29_378; 441 cm (285); 2112 m | | | |
| Depth | Unit | Color | Additional description |
| 7 | AM | DR | soft with tiny ball shaped clasts |
| 35 | SU2 | DR | soft, greasy |
| 59 | SU2 | DG | soft, greasy, harder than surroundings |
| 64 | SU2 | MB | to black, very soft but not greasy |
| 70 | SU2 | LB | harder layer |
| 90 | SU2 | L/MB | harder laminae |
| 93 | SU2 | black | bit of MB, soft ooze |

| | | | |
|---|---|---|---|
| 102 | CO | Y | and MR, soft, not greasy |
| 110 | CO | Y | to DB, with hard larger grained laminae |
| 118 | CO | black | msoft /soft, smooth, ooze |
| 154 | CO | MY | soft, upper, comp. 179 |
| 179 | CO | MR | soft, limonite with bit more hemat.? comp. to 154 |
| 197 | CO | MR | msoft, greasy, diffusively laminated |
| 250 | CO | DR | firm, greasy |
| 261 | CO | DG | to DB + LB, soft, not greasy, from tectonic contact |
| 261 | CO | DB | hard layer from inside the core |
| 284 | CO | black | soft ooze, very few crystals |
| 307 | CO | black | soft ooze, lots of crystals |
| 321 | CO | Y | and B mixed, hard with some soft parts |
| 340 | SU1 | MG | olive tint/brownish, mhard |
| 353 | SU1 | H | M/L H, Y + B mixed, soft |
| 366 | SU1 | MB | reddish, greasy and coherent material from a mixed unit |
| 380 | SU1 | dark | random pieces, harder than surroundings |
| 390 | SU1 | dark | very hard piece from somewhere, laying on the bottom of the box |
| Valdivia 29_387; 824 cm (377); 2110 m | | | |
| Depth | Unit | Color | Additional description |
| 20 | SU2 | DB | |
| **80** | **SU2** | **DR** | **[5YR 4/5]** |
| 143 | SU2 | DR | |
| **174** | **SU2** | **MG** | **[5Y 6/2]** |
| 239 | CO | B | and R |
| **261** | **CO** | **DG** | **to black; [10Y 6/2]** |
| 280 | CO | DR | |
| **302** | **CO** | **LB** | **yellowish, with harder parts; [10YR 6/6]** |
| 303 | CO | black | |
| 327 | COS | MG | yellowish, mhard |
| 381 | COS | DR | violet, mhard |
| **398** | **SU1** | **black** | **ooze with harder (gypsum?) crystals; [5GY 5/1]** |
| 404 | SU1 | black | soft with harder crystals, top of S layer, comp. 466 |
| **466** | **SU1** | **black** | **bottom of S layer, comp. 404; [10Y 6/2]** |
| 481 | SU1 | DB | mhard |
| **490** | **SU1** | **silver** | **violet, hard interlayer; [10YR 6/6]** |
| **502** | **SU1** | **white** | **hard (anhy clast?); [5Y 8/1]** |
| 508 | SU1 | DR | mhard |
| 550 | SU1 | R | bottom of R unit, lighter than 508 (comp) |
| **575** | **SU1** | **DH** | **with yellow parts, with big anhy clast; [10Y 7/2]** |
| 588 | SU1 | silver | hard interlayer, comp to 490 |
| 597 | SU1 | DG | to MG some DR, mhard, laminated to layered |
| Valdivia 29_393; 909 cm (238); 2061 m | | | |
| Depth | Unit | Color | Additional description |
| 8 | AM | DR | very soft |
| 61 | AM | DB | greenish, very soft |
| 79 | AM | DB | to DR, very soft |
| 116 | SU2 | DR | soft ooze |
| 162 | SU2 | G | M/D G, some B, diffusively layered |
| 185 | SU2 | LB | soft with harder parts |
| 190 | SU2 | DH | soft |
| 195 | SU2 | MB | soft |
| 204 | CO | R | D/M R and MY laminae |
| 239 | CO | black | with red stripe, soft with harder crystals |
| 266 | COS | DR | soft/msoft |
| 299 | COS | DR | msoft |
| 311 | SU1 | DR | almost black, msoft |
| 323 | SU1 | black | |
| 326 | SU1 | L/MB | msoft |

| | | | |
|---|---|---|---|
| 342 | SU1 | black | soft ooze with thick B layer on top |
| 352 | SU1 | LB | reddish, comp. to 323 and 342 (thicker alteration) |
| 368 | SU1 | DB | greenish, msoft |
| 396 | SU1 | R | D/M R, mhard |
| 436 | SU1 | black | hard ~1 mm thick layer, thin section |
| 438 | SU1 | | |
| 465 | DOP | L/DH | mhard with harder crystals |
| 499 | DOP | MY | and black, mhard, laminated, thin section |
| Valdivia 29_397; 620 cm (176); 2097 m | | | |
| Depth | Unit | Color | Additional description |
| 12 | AM | R | M/D very soft, with small dots |
| 82 | AM | O | and R contamination |
| 84 | AM | MR | soft |
| 96 | SU2? | MR | soft matrix of a breccia with DB clasts |
| 115 | SU2? | mix | brown matrix with G clasts, soft |
| 129 | SU2? | DG | soft, greasy, contains few laminae |
| 138 | CO | DG | and black, soft layer between DR material |
| 169 | CO | R | soft |
| 194 | CO | Y | soft |
| 199 | CO | MH | brownish, soft |
| 223 | CO | MY | |
| 239 | CO | B | M/D, mhard crunchy layer, harder than surroundings |
| 259 | CO | DR | smooth, homog. |
| 301 | COS | G | L/M |
| 305 | COS | R | MY-MR-DR, mhard, firm vertical vein |
| 342 | COS | DR | mhard, firm (more greasy than 259) |
| 386 | SU1 | MH | with MB alteration, crunchy sand-like |
| 398 | SU1 | mix | of black-brown and G mud, firm, somewhat crunchy |
| 409 | SU1 | MR | mhard, firm |
| 435 | SU1 | MG | to DG, brownish, greasy, inclined layering |
| 448 | SU1 | black | with a bit of white |
| 481 | DOP | Y | mhard, homog. |
| Valdivia 29_421; 785 cm (304); 2106 m | | | |
| Depth | Unit | Color | Additional description |
| 10 | AM | DR | soft breccia |
| **80** | **SU2** | **DR** | **to black, soft; [5YR 5/4]** |
| 120 | SU2 | MB | matrix of breccia wit DB clasts |
| 134 | SU2 | black | vsoft interlayer of ooze with crystals |
| **160** | **SU2** | **MB** | **and DB parts, mhard, sharp layering; [10YR 5/4]** |
| 182 | CO | MB | matrix (with R and black clasts), breccia |
| **223** | **CO** | **MY** | **bright, vsoft ooze; [5YR 4/5]** |
| 236 | CO | MR | with few Y and black parts as mixture |
| **362** | **COS** | **DR** | **to black, soft, lower part of R unit; [5YR 4/4]** |
| 391 | COS | MR | to MB (and DR), mhard, sharply layered |
| 408 | SU1 | MR | bright Y, soft, laminated, comp. to 433, 492 |
| 433 | SU1 | MR | bright Y, soft, laminated, comp. to 408, 493 |
| 492 | SU1 | MR | bright Y, soft, laminated, comp. to 433, 408 |
| **496** | **SU1** | **black** | **some Y from surroundings, soft ooze; [10YR 5/4]** |
| 509 | SU1 | LB | harder and softer parts |
| **520** | **SU1** | **MG** | **to MB, msoft, laminated; [10YR 6/5]** |
| 539 | SU1 | DR | to black, soft |
| 582 | SU1 | DR | to DG, mhard |
| 609 | SU1 | MG | bright, clast from breccia below (?), Comp. to 646, 667 |
| 614 | DOP | black | soft with harder parts, top of a black layer comp. 678 |
| 630 | DOP | silver | hard piece of a layer, thin section |
| 646 | DOP | MB | greyish, comp. to 656, 667, clast in breccia |

| | | | |
|---|---|---|---|
| 656 | DOP | MB | some greenish and yellowish, crunchy, comp. 646, 667, matrix of breccia |
| 667 | DOP | MG | bright, L/MG, msoft, comp. 656, 646, 609, clast in breccia |
| **678** | **DOP** | **black** | **comp. to 614; [5Y 5/1]** |
| 681 | DOP | LH | to M grey layer between 2 sulphide layers, thinly laminated |
| 694 | DOP | MG | layer |
| 710 | DOP | MR | to DR, mhard, top of R unit, ~homog. |
| 732 | DOP | MR | bottom of R unit, ~homog. |
| **740** | **DOP** | **DG** | **mhard; [5Y 7/4]** |
| 758 | DOP | | harder than surroundings, clast in a mixed (S rich?) unit |
| 763 | DOP | DH | to black, some LY mixed, crunchy |
| 782 | DOP | MG | mhard |
| 790 | DOP | silver | hard layer for thin sections, comp. to 776, 786, 790 |
| 799 | DOP | black | with white (anhy?) parts, uncoherent |
| 800 | DOP | | thin section |
| 807 | DOP | MB | reddish, thinly laminated |
| 820 | DOP | LY | to B, mhard, bit crunchy, top of Y layer |
| **825** | **DOP** | **DH** | **to black, mhard, homog.; [5Y 5/1]** |
| 827 | DOP | LH | within Y unit, msoft, under DH layer (825), homog. |
| 864 | DOP | LY | mhard, bottom of Y unit |
| **870** | **DOP** | **O** | **bright, comp. to 864; [10YR 7/6]** |
| 880 | DOP | | Thin ection |
| 884 | DOP | MH | bit greenish, mhard, thinly laminated |
| 899 | DOP | MY | to MB, mhard, thinly laminated |
| Valdivia 29_423; 980 cm (228); 2117 m | | | |
| Depth | Unit | Color | Additional description |
| 8 | AM | DR | soft |
| 76 | AM | DR | to black, soft, less soft than surroundings |

| | | | |
|---|---|---|---|
| 108 | SU2 | DR | soft, less soft than surroundings, irr. Laminated |
| 198 | SU2 | DB | to MG, DB softer, MG harder, greasy, layered |
| 219 | SU2 | DR | very dark, msoft, bit greasy |
| 257 | SU2 | R | MR-DR-B, laminated |
| 266 | CO | MB | soft to msoft |
| 311 | CO | Y | soft, very thin laminae |
| 366 | CO | LB | to white and some DG and DR from the layer above, soft |
| 378 | CO | DR | some MB as contamination, msoft, greasy, firm "piece of layer" |
| 391 | CO | black | and MB (alteration after black?), soft ooze |
| 418 | COS | DR | mhard, greasy, firm, inclined layering |
| 461 | COS | DR | mhard, firm |
| 485 | SU1 | black | mhard with crystals, laminated at oxid. surface |
| 506 | SU1 | light | hard |
| 513 | SU1 | MH | hard, lots of hard crystals, intense alteration |
| 518 | SU1 | DB | to MB (alteration), hard layer |
| 571 | SU1 | MH | L/MB on surface, harder parts |
| 612 | SU1 | H | L brownish H surface (darker inside), very fine laminae |
| 620 | SU1 | | mhard, harder than surroundings |
| 652 | SU1 | R | M/D, mhard, almost hard, firm |
| 675 | SU1 | MR | brownish, mhard almost hard, firm |
| 716 | SU1 | B | and G, very hard, firm |
| 753 | SU1 | MG | bright, mhard to hard, firm |
| 756 | SU1 | silver | hard, thin section + chem. |
| 773 | SU1 | black | mhard with crystals, laminated on oxid. surface |
| 793 | DOP | H | L and D, mhard to hard silt |
| 797 | DOP | Y | brownish, laminated, hardness varies between laminae |
| Valdivia 29_450; 760 cm (42); 2097 m | | | |

| Depth | Unit | Color | Additional description |
|---|---|---|---|
| 10 | AM | DR | soft |
| 91 | AM | DR | soft |
| 146 | AM | black | interlayer |
| 170 | SU2 | R | msoft |
| 190 | SU2 | | hardness varies among layers |
| 206 | CO | Y | bright, soft |
| 267 | CO | MR | brownish, soft |
| 279 | CO | LH | and white, harder than surrounding, "clast"" part of a layer |
| 286 | CO | black | soft to msoft ooze |
| 310 | COS | MB | to MG, laminated |
| 334 | COS | DG | DG/DB, mhard |
| 376 | COS | DR | ~homog. |
| 468 | COS | DR | to MR, mhard |
| 483 | SU1 | MB | matrix of breccia |
| 488 | SU1 | DG | mhard clast of breccia |
| 494 | SU1 | black | soft, ~homog. ooze |
| 513 | SU1 | black | mhard |
| 538 | SU1 | mix | bulk of breccia |
| 567 | SU1 | black | with yellow, crunchy ooze |
| 573 | SU1 | G | M/DG, mhard |
| 588 | SU1 | MY | with grey, dessicated "breccia" |
| 627 | DOP | H | D/M, layer |
| 663 | DOP | Y | and black, dessicated, sandy, may have been laminated in the beginning |
| 695 | DOP | LH | MY in lower unit, unequal grain size |
| Valdivia 29_458; 894 cm (259); 2147 m | | | |
| Depth | Unit | Color | Additional description |
| 6 | AM | DR | soft |
| 59 | AM | DR | soft |
| 72 | SU2 | DR | with some G and MY, soft |
| 144 | SU2 | mix | of MG-MB-black, soft |
| 196 | SU2 | DR | soft, diffusively laminated |
| 255 | SU2 | MG | to DG, clast in upper part of breccia |
| 277 | SU2 | LB | with LG clasts, lower part of breccia, matrix |
| 305 | SU2 | MB | and grey and all sorts of alteration |
| 312 | CO | MY | soft to msoft, comp. to 420 |
| 330 | CO | black | soft, smooth |
| 369 | COS | MR | mhard, firm |
| 410 | COS | MR | brownish, firm |
| 413 | COS | MH | greenish, silt, "unconformity", pieces of this found in R mud above |
| 420 | CO | MY | under unconformity, comp. to 312 |
| 445 | CO | mix | of MR-MB and Y, breccia |
| 466 | SU1 | black | laminated on oxid. surf., thin section + chem. |
| 496 | SU1 | black | soft with harder crystals, comp. to 466, which has no crystals |
| 516 | SU1 | DH | to black, smooth, lower level of black unit |
| 566 | SU1 | MR | firm |
| 604 | SU1 | DG | firm, greasy |
| 639 | SU1 | MH | greenish, thinly laminated (with no significant color changes) |
| 642 | SU1 | LG | firm, weak layering |
| 660 | SU1 | black | with white anhy., crunchy, ~homog. |
| | | | |
| Valdivia 29_480; 681 cm (321); 2125 m | | | |
| Depth | Unit | Color | Additional description |
| 4 | AM | DR | soft |

| | | | |
|---|---|---|---|
| 43 | AM | DR | soft |
| 53 | SU2 | DR | soft |
| 91 | SU2 | black | soft |
| 104 | SU2 | DG | brownish, soft greasy |
| 140 | SU2 | DR | soft, greasy |
| 152 | CO | DB | reddish, msoft to soft, laminated |
| 190 | CO | MB | with LB laminae, soft |
| 222 | COS | MR | msoft /hard |
| 232 | COS | R | msoft |
| 236 | COS | G | laminated, clast in breccia |
| 282 | COS | DG | msoft, greasy |
| 292 | SU1 | DR | msoft /mhard |
| 330 | SU1 | black | LB (alteration?) parts, soft with harder particles |
| 348 | SU1 | MH | brownish; orange and LB parts, soft, crunchy |
| 384 | SU1 | DG | homogenous, mhard, greasy, inclined layering |
| 414 | SU1 | R | M/D R, orange clasts, soft, crunchy |
| 446 | SU1 | DG | mhard |
| 468 | SU1 | black | B alteration |
| 473 | SU1 | white | hard |
| 478 | SU1 | L/MB | white, silt with black laminae |
| 484 | SU1 | DH | almost black |
| 498 | DOP | L/MB | |
| Valdivia 29_495; 1238 cm (26); 2076 m | | | |
| Depth | Unit | Color | Additional description |
| 13 | AM | DR | soft |
| **113** | **AM** | **DR** | **soft; [5YR 4/4]** |
| 192 | AM | DR | soft |
| **240** | **AM** | **MR** | **soft, more prominent lamination compared to surroundings; [10R 4/6]** |
| 296 | AM | DR | soft, firm |
| 338 | AM | DR | soft, firm |
| **362** | **SU2** | **DR** | **vsoft, less greasy, more prominent lamination compared to surroundings; [5YR 4/4]** |
| 405 | SU2 | DR | soft |
| **484** | **SU2** | **DR** | **soft, irregular lamination; [5YR 6/5]** |
| 528 | SU2 | DR | soft to msoft |
| **548** | **SU2** | **B** | **reddish, soft, lamination; [5YR 5/4]** |
| **557** | **CO** | **Y** | **mbrown tint, soft, lamination; [10YR 5/5]** |
| **569** | **CO** | **MR** | **with crunchy black layers, hardness varies; [10YR 5/3]** |
| **582** | **CO** | **white** | **to LB, sand/silt; [5Y 8/1]** |
| **599** | **CO** | **G** | **MB-H-G, lamination, thin sect. + chem.; [5Y 7/4]** |
| 622 | COS | DB | msoft to mhard, greasy |
| **693** | **COS** | **DR** | **firm, ~homog.; [5YR 4/4]** |
| 736 | COS | DR | mhard with hard parts, firm |
| **757** | **SU1** | **H** | **M/L/D grey, mhard, laminated, thin section + chem.; [5B 7/1]** |
| **777** | **SU1** | **black** | **msoft with few harder crystals; [5Y 4/1]** |
| **809** | **SU1** | **DG** | **olive G, firm, lamination on oxid. surface; [5Y 7/4]** |
| 848 | SU1 | black | some harder crystals, lamination on oxid. surface |
| 859 | SU1 | black | thin section, lamination |
| **867** | **SU1** | **G** | **light to dark G and LB, smooth, lamination; [5GY 8/1]** |
| **889** | **DOP** | **B** | **reddish, matrix of breccia (in which Y, G, black and R clasts); [10YR 5/4]** |
| **934** | **DOP** | **LB** | **hard to mhard, diff. Lamination; [5GY 8/1]** |
| 1000 | DOP | MH | to LH, brownish, hard with few white parts |
| **1088** | **DOP** | **MH** | **darker than above with few white parts, hard; [5B 7/1]** |
| 1118 | DOP | LB | to MG, hard, lamination |
| **1195** | **DOP** | **DG** | **mhard, ~homog.; [10Y 6/2]** |
| Valdivia 29_498; 1299 cm (164); 2147 m | | | |

| Depth | Unit | Color | Additional description |
|---|---|---|---|
| 15 | AM | MR | breccia with dark and G balls, soft |
| 107 | AM | MR | black inside, vsoft |
| 178 | AM | LR | vsoft |
| 207 | AM | DR | soft |
| 234 | SU2 | DR | black inside, soft |
| 321 | SU2 | DR | black inside, soft |
| 390 | SU2 | G | M to D, soft, greasy |
| 406 | SU2 | LB | LB matrix of breccia, soft, dark clasts, black inside |
| 411 | SU2 | LG | with LB layers, clast of breccia, inner lamination |
| 442 | SU2 | black | soft ooze |
| 472 | CO | MR | yellowish, soft, homog. |
| 503 | CO | black | soft, few hard parts |
| 538 | CO | MB | to DB, thinly laminated |
| 604 | CO | DR | mhard, firm |
| 650 | CO | MG | silty, thinly laminated |
| 713 | CO | black | ooze with harder parts |
| 734 | CO | R | clast in black matrix, msoft to soft, sharp contacts to matrix |
| 827 | CO | MR | mhard, colors create weak diff. lamination |
| 850 | COS | H | to DG, mhard |
| 888 | COS | DR | mhard, firm |
| 949 | COS | DR | mhard, diff. lamination |
| 962 | SU1 | DG | mhard, greasy |
| 990 | SU1 | black | soft with harder crystals (few) |
| 1024 | SU1 | MR | mhard, diff. lamination |
| 1053 | SU1 | DG | mhard, greasy |
| 1078 | SU1 | G | bright, mhard to msoft |
| 1105 | SU1 | black | and coarser MB parts, dessicated |
| 1132 | DOP | MG | greyish and Y parts |
| 1175 | DOP | black | ooze, with crystals, at tectonic contact |
| 1196 | DOP | mix | of Y and orange |
| 1206 | DOP | black | to DG, mhard, firm with few crystals |
| 1263 | DOP | O | with MB interlayers, mhard |

Valdivia 29_503; 1210 cm (217); 2159 m

| Depth | Unit | Color | Additional description |
|---|---|---|---|
| **7** | **SAM** | **DR** | **violet; [5YR 4/4]** |
| 73 | SAM | B | lighter than surroundings |
| **75** | **OAN** | **H** | **greenish grey; [10Y 8/2]** |
| 108 | OAN | DB | violet tint, crunchy |
| 123 | OAN | DR | violet, soft muddy |
| **140** | **SOAN** | **G** | **bright (in Yellow B matrix), clast in breccia; [10Y 8/4]** |
| 147 | SOAN | B | darker B and some green, matrix of breccia |
| **155** | **SOAN** | **Y** | **orange tint, matrix of breccia; [10Y 8/3]** |
| 199 | SOAN | white | crunchy |
| **235** | **SOAN** | **white** | **crunchy; [5Y 9/1]** |
| 254 | SOAN | white | thin section sample, hard |
| **266** | **SOAN** | **DB** | **hard, crunchy crystals; [10YR 8/4]** |
| 275 | SOAN | black | hard clast for thin section |
| 297 | SOAN | MB | to DB, uncoherent, sandy, heterog. |
| **407** | **CO/COS** | **Y** | **orange tint, muddy, coherent; [10YR 5/5]** |
| 470 | CO/COS | LH | greenish and some brown |
| **509** | **CO/COS** | **DB** | **reddish; [5YR 5/4]** |
| **516** | **CO/COS** | **DB** | **thinly laminated DB with black; [5Y 4/1]** |
| 575 | CO/COS | | thin section sample |
| 598 | CO/COS | B | reddish yellowish |
| **626** | **CO/COS** | **R** | **rather bright, muddy, coherent; [5YR 5/5]** |
| **671** | **COS** | **G** | **greasy, coherent; [10Y 6/2]** |
| **680** | **COS** | **DB** | **to black, coherent; [10YR 5/5]** |

| | | | |
|---|---|---|---|
| **807** | **SU1** | **H** | **greenish grey with some yellowish, uncoherent; [10Y 8/2]** |
| 860 | SU1 | DB | greenish, fine grained, coherent |
| **889** | **SU1** | **silver** | **violet, hard interlayer (~0.5 cm thick); [10YR 6/6]** |
| **912** | **SU1** | **DB** | **to black, crunchy; [10Y 6/2]** |
| **946** | **DOP** | **B** | **reddish B and some orange, crunchy; [10YR 6/6]** |
| 971 | DOP | LB | crunchy, muddy |
| 981 | DOP | | thin section, laminated |
| **987** | **DOP** | **black** | **smooth, coherent; [5Y 5/1]** |

Valdivia 29_526; 925 cm (0); 2180 m

| Depth | Unit | Color | Additional description |
|---|---|---|---|
| 48 | SAM | B | |
| 84 | SAM | B | more reddish than above |
| 114 | SAM | B | black inside |
| 162 | SAM | B | and black, harder than surroundings |
| 211 | SAM | B | Dreddish black inside |
| 269 | SAM | B | reddish, black inside |
| 316 | SAM | DB | reddish, black inside |
| 381 | SAM | black | and red (surface), crunchy layer |
| 412 | SAM | MR | |
| 443 | SAM | O | dull, black inside |
| 450 | SAM | R | brownish red; black inside, harder and firmer than surrounding, diff. laminated |
| 489 | SAM | MR | and Y, irr. laminated |
| 506 | SAM | DH | greenish Dgrey and orange sandy "spot" within a layer |
| 519 | SAM | R | and MY, diff. laminated |
| 572 | SOAN | DR | |
| 589 | SOAN | DR | and B and MY, shiny, sandy, layer |
| 608 | SOAN | MR | bright throughout |
| 644 | SOAN | R | bit of B, silt, abundant salt-crystals, layer |
| 698 | SOAN | DR | and almost black, firm, little salt |
| 725 | SOAN | R | brownish R (throughout) some G and black parts |
| 777 | SOAN | DR | and black, firm, abundant salt |
| 804 | SOAN | mix | DG+DO+B+R+black, soft part of layer |
| 805 | SOAN | mix | DG+DO+B+R+black, hard part of layer |
| 845 | SOAN | B | greenish and white, crunchy silt |
| 857 | SOAN | R | R+MR +black, quite firm |
| 878 | SOAN | B | greenish, reddish, silt, crunchy microfossils? |
| 888 | SOAN | DR | throughout DR, mhard harder than surroundings firm |

Valdivia 29_537; 1205 cm (269); 2186 m

| Depth | Unit | Color | Additional description |
|---|---|---|---|
| 2 | AM | DR | with MY, soft |
| 26 | SU2 | MB | greenish, soft |
| 33 | SU2 | H | |
| 46 | SU2 | G | brownish |
| 57 | SU2 | Y | |
| 59 | SU2 | silver | and white, white is hard, silver softer (not crystalline) |
| 108 | SU2 | MB | msoft, crunchy |
| 113 | SU2 | white | dull, hard, crystalline |
| 206 | SU2 | white | with black/DH, crystalline |
| 250 | SU2 | white | with black, soft white (anhy) and soft black mud |
| 256 | SU2 | DG | very hard |
| 260 | SU2 | black | soft |
| 307 | SU2 | mix | |
| 355 | SU2 | white | with B and black |
| 364 | SU2 | black | soft with harder parts |

| | | | |
|---|---|---|---|
| 370 | SU2 | MB | |
| 378 | SU2 | black | with MB, soft with harder parts |
| 398 | CO | MB | msoft with harder parts |
| 420 | CO | black | M/L, crunchy |
| 466 | CO | Y | msoft to mhard |
| 525 | CO | Y | msoft to mhard |
| 537 | CO | DR | |
| 544 | CO | G | yellowish |
| 599 | CO | G | brownish, mhard |
| 606 | CO | B | M/L, mhard |
| 626 | CO | black | |
| 631 | CO | H | LH to light pale green, tectonic lower contact |
| 664 | CO | LD | mhard |
| 713 | CO | MB | mhard, homog. |
| 780 | COS | | mhard, laminated |
| 799 | COS | MG | mhard, laminated |
| 835 | COS | DR | very dark, mhard |
| 871 | COS | DR | mhard |
| 890 | SU1 | black | mhard |
| 950 | SU1 | black | with Y/H alteration, soft ooze with crunchy alteration |
| 1003 | SU1 | DB | greenish, crunchy |
| 1037 | SU1 | MR | mhard |
| 1078 | SU1 | | hard layer for thin section |
| 1082 | SU1 | MG | under the hard layer |
| 1104 | SU1 | DG | to DB, crunchy anhy. spots |
| 1144 | DOP | MB | dessicated |
| Valdivia 29_546; 546 cm (91); 2013 m | | | |
| Depth | Unit | Color | Additional description |
| **5** | **AM** | **MR** | **to DR, msoft; [10YR 5/6]** |
| **92** | **AM** | **DG** | **some red, msoft greasy; [10YR 5/4]** |
| 137 | AM | DB | msoft |
| **180** | **AM** | **MB** | **reddish, msoft, layered; [10YR 5/5]** |
| 198 | SU2 | MB | DR+B, msoft, layered |
| **229** | **SU2** | **DB** | **mhard; [5Y 7/2]** |
| 241 | CO | MB | L/M, mhard, laminated |
| **252** | **CO** | **LB** | **to LG, mhard to hard; [5Y 8/2]** |
| **267** | **SU1** | **MR** | **hard, dry; [10YR 5/6]** |
| 280 | SU1 | MB | with O alteration, hard, dry |
| 295 | SU1 | DR | mhard, relat. homog. |
| **311** | **SU1** | **black** | **hard, ~0.5cm thick layer; chem. + thin section; [10YR 6/4]** |
| 316 | SU1 | MB | mhard |
| **318** | **SU1** | **white** | **with black interlayers, hard, dry; [5GY 8/1]** |
| 326 | DOP | MB | reddish, mhard to hard |
| 355 | DOP | LH | to MH and some white, hard, silty |
| 373 | DOP | MH | L to D grey |
| **385** | **DOP** | **white** | **hard, dry; [5GY 8/1]** |
| Valdivia 29_547; 1198 cm (0); 2135 m | | | |
| Depth | Unit | Color | Additional description |
| 12 | SAM/AM | MB | bulk of AM |
| 22 | SAM/AM | DG | clast |
| 59 | SAM/AM | MB | throughout |
| 120 | SAM/AM | O | little black inside |
| 150 | SAM/AM | DR | black inside, bulk |
| 157 | SAM/AM | black | and some red, bright (anhy) at oxid. surface |
| 219 | SAM/AM | DR | black inside, bulk |
| 254 | SAM/AM | black | and DR, with anhy crystals |
| 287 | SAM/AM | MR | throughout MR with G clasts, abundant |

| | | | |
|---|---|---|---|
| | | | salt |
| 296 | eq. OAN | R | bright; LB inside, top of brighter R unit |
| 317 | eq. OAN | R | bright; MB inside, abundant salt |
| 326 | eq. OAN | MB | throughout |
| 370 | SOAN/SU2 | DG | and black-Y-R, finely laminated |
| 395 | SOAN/SU2 | DG | breccia layer (~ 2 cm thick) |
| 408 | SOAN/SU2 | DR | with anhy |
| 437 | SOAN/SU2 | LB | greenish grey inside + some R |
| 454 | SOAN/SU2 | DR | some anhy and black |
| 505 | SOAN/SU2 | DB | and anhy + black + some DR |
| 547 | SOAN/SU2 | DR | black inside |
| 563 | SOAN/SU2 | black | shiny |
| 589 | SOAN/SU2 | black | with LB coarse grained shiny parts (anhy or fossils?) |
| 616 | SOAN/SU2 | DR | black inside |
| 638 | SOAN/SU2 | LH | black inside, vsoft, thin bright oxid. surface |
| 644 | SOAN/SU2 | MB | to LB, sandy |
| 675 | SOAN/SU2 | DR | black inside, abundant salt |
| 714 | SOAN/SU2 | DR | black inside |
| 728 | SOAN/SU2 | DG | DG on top, weird DH inside |
| 755 | SOAN/SU2 | MB | black inside |
| 769 | SOAN/SU2 | | layer of anhy in DB surroundings |
| 828 | SOAN/SU2 | MG | and some black inside, mhard, firm |
| 833 | SOAN/SU2 | black | with Y-MY-B alteration, diff. layering |
| 842 | SOAN/SU2 | white | and black hard part from inside the core, irregularly oriented, laminated |
| 845 | SOAN/SU2 | LB | firm, dry |
| 875 | SOAN/SU2 | B | reddish matrix of breccia, softer than surroundings |
| 905 | SOAN/SU2 | MB | thin MB surface, black inside |
| 913 | SOAN/SU2 | MB | reddish and greenish MB and white |
| 931 | SOAN/SU2 | LB | and shiny yellow, soft inside, but covered with very hard dark surface |
| 949 | SOAN/SU2 | MR | and MY, firm, laminated |
| 970 | CO | Y | and LR, laminated |
| 982 | CO | G | yellowish, silt included, laminated |
| 1027 | CO | MB | and MR and Y |
| 1027 | CO | Y | hard piece of layer inside the Y layer |
| 1043 | SOAN? | H | with white parts, silty |
| 1060 | SOAN? | black | and white, hard piece in the "marl", for thin section |
| 1066 | SOAN? | Y | one of Y hard pieces found in marl, for thin section |
| 1068 | SOAN? | black | dry, wedge shaped |
| 1093 | SOAN? | | hard part inside a softer layer, for thin section |
| 1111 | SOAN? | MB | dry |
| 1143 | COS | MR | bright, dry |
| Valdivia 29_549; 587 cm (207); 1996 m | | | |
| Depth | Unit | Color | Additional description |
| 16 | OAN | MB | MB top, lighter on the bottom |
| 84 | SU2 | MB | MB top, lighter on the bottom |
| 102 | CO/SOAN? | G | and R, hard, bulk of breccia |
| 114 | CO/SOAN? | MR | to DR, hard, laminae |
| 144 | SU1/SOAN | DB | reddish, hard, laminae |
| 162 | SU1/SOAN | G | olive G with DB with neo green (malachite alteration?), hard |
| 184 | DOP/CO | black | coherent, homog. |
| 226 | DOP | MY | with abundant dark laminae |
| 252 | DOP | Y | with black laminae |

| | | | |
|---|---|---|---|
| 275 | DOP | MH | coherent, silty surroundings |
| 288 | DOP | LB | with white particles |
| Valdivia 29_557; 856 cm (264); 2100 m | | | |
| **9** | **AM/SAM** | **DR** | **Soft; [5YR 4/4]** |
| 37 | eq. OAN | DR | soft |
| 49 | AM | DR | soft and firmer than above, beginning of inclined layering |
| 109 | SU2 | DR | soft |
| **173** | **SU2** | **DR** | **soft, irr. and diff. laminated; [10YR 5/4]** |
| 209 | SU2 | DG | greener part of red unit, msoft to mhard, firm |
| **227** | **SU2** | **MR** | **to DR, firm, greasy; [5YR 6/5]** |
| 245 | SU2 | MB | to LB, msoft, laminated |
| **255** | **CO** | **black** | **with DR laminae, no harder crystals; [5Y 5/2]** |
| 271 | CO | DR | msoft, laminated |
| **289** | **CO** | **Y** | **with rare thin R laminae; [10YR 5/6]** |
| 355 | CO | Y | mhard |
| **388** | **SU1** | **black** | **mhard with harder crystals; [10Y 5/2]** |
| 398 | SU1 | MH | to dark grey, few harder crystals, comp. to 388 |
| **502** | **DOP** | **H** | **silty, from vertical vein; [5Y 7/1]** |
| 554 | DOP | LB | to LR, hard, dried |
| **608** | **DOP** | **R** | **brownish (darker than surroundings), hard; [10YR 7/4]** |
| 694 | DOP | MR | to LR, hard |
| **753** | **DOP** | **H** | **D/M, hard, vein; [10Y 6/2]** |
| **795** | **DOP** | **MR** | **Hard; [10R 6/6]** |
| Valdivia 29_566; 634 cm (0); 2160 m | | | |
| Depth | Unit | Color | Additional description |
| 7 | AM | R | M/D with small dots of G and O, msoft to soft |
| 39 | AM | MB | reddish, msoft |
| 58 | SU2 | white | hard, anhy? |
| 90 | SU2 | black | and MB, msoft to soft |
| 131 | SU2 | G | M/D, comp. to 134, 136, clast in breccia |
| 134 | SU2 | black | comp. to 131, 136, clast in breccia |
| 139 | SU2 | MB | msoft, comp. to 131, 134, matrix of breccia |
| 204 | SU2 | MB | mhard, some harder parts |
| 215 | CO | R | bright, upper part of a R unit, comp. 316, 389, 340 |
| 316 | CO | MR | more Y than above, comp. 340, 215, 389 |
| 340 | CO | R | brownish, lower part of R unit, comp. 316, 215, 389 |
| 363 | COS | DG | upper contact of a tectonic interface |
| 381 | COS | black | hard, 1-0.5 cm thick interlayer |
| 389 | COS | DR | harder than the R samples above, comp. 316, 215, 340 |
| 410 | SU1 | black | and MB, mhard ooze |
| 427 | SU1 | mix | of MB, H and Y, mhard, crunchy |
| 452 | SU1 | MG | mhard, to hard, homog. |
| 469 | SU1 | White | and some brown, shiny |
| 484 | SU1 | | laminae, for thinsection |
| 517 | SU1 | DH | with Y particles |
| 544 | SU1 | mix | black-H-B, mhard to hard, thinly laminated |
| 561 | DOP | MH | to D grey, mhard to hard, thinly laminated |
| 564 | DOP | | hard, from above the L bright Y layer |
| 567 | DOP | LY | mhard, homog. |
| 583 | DOP | MB | inside M to L grey, mhard |
| Valdivia 29_583; 598 cm (153); 2173 m | | | |
| 5 | | DR | DR to black |
| 88 | | DR | lighter and coarser than surrounding |
| 145 | | DR | soft, bulk of all material around |
| 167 | | MB | msoft to mhard, layered, between mixed and R units |

| | | | |
|---|---|---|---|
| 180 | | R | bright R with darker clasts, soft, abundant salt, bulk matrix of breccia |
| 187 | | DR | to MH, soft, clast of breccia |
| 233 | | black | red parts, layered |
| 257 | | black | reddish and brownish, bulk of breccia |
| 310 | | R | bright R, soft to msoft |
| 320 | | H | hard, piece of a layer |
| 325 | | mix | R-B-black, msoft with crystals, bulk |
| 339 | | DR | mhard, firm |
| 360 | | G | M/D greyish, mixed material of breccia |
| 380 | | MH | to black, clastic |
| 393 | | LH | yellowish, falling into pieces |
| 419 | | MB | reddish, soft, irregularly laminated |
| 434 | | H | Mgreenish, uncoherent, marl? |
| 459 | | black | inflated |
| 459 | | MB | with white particles and black parts, inflated |
| 484 | | mix | all kinds of sediment |
| 499 | | DR | to black, mhard, sulfides? |
| 540 | | MR | cold tint, uncoherent |
| Valdivia 29_617; 929 cm (317); 2179 m | | | |
| Depth | Unit | Color | Additional description |
| **9** | **SAM** | **DR** | **[5YR 5/4]** |
| 92 | SAM | DR | |
| **148** | **SAM** | **DR** | **to black; [5YR 5/4]** |
| 156 | OAN | R | and grey, crunchy |
| 190 | OAN | LH | |
| **220** | **OAN** | **H** | **greenish grey with white parts; [5GY 8/1]** |
| 253 | OAN | MB | soft |
| 285 | OAN | R | bright, soft, bit mixed with other color mud |
| 296 | OAN | white | bright, anhy. clast |
| 319 | OAN | MR | brownish with black laminae, msoft, laminated |
| 362 | OAN | H | near vertical (anhy) vein, DH surrounding |
| **395** | **OAN** | **R** | **bright; [10R 5/5]** |
| **396** | **OAN** | **black** | **hard interlayer; [10YR 6/3]** |
| 426 | SOAN | DB | and black, hard |
| 478 | SOAN | R | brownish, mhard |
| 488 | SOAN | O | and white, shiny, sand |
| **508** | **SOAN** | **DB** | **and Dgrey, hard vertical crosscutting vein; [5Y 7/2]** |
| 513 | SOAN | R | brownish, mhard "matrix of breccia" |
| 545 | SOAN | R | layer |
| **551** | **SOAN** | **O** | **brownish, shiny, sand, interlayer; [10YR 8/3]** |
| 580 | SOAN | DB | hard clast |
| 586 | SOAN | R | brownish, matrix |
| **650** | **SOAN** | **B** | **to DB, greyish, soft; [10YR 5/5]** |
| 656 | SOAN | R | bright to brownish R, layer |
| 683 | SOAN | MB | mhard, layer |
| **787** | **SOAN** | **R** | **brownish; [10R 6/6]** |
| **799** | **SOAN** | **black** | **hard layer for chemistry and thin section; [10YR 6/2]** |
| 864 | SOAN | R | brownish, mhard to hard |
| **875** | **SOAN** | **DB** | **hard, inclined layering; [10YR 6/4]** |
| Sonne 02_122K; 595 cm (0); 2005 m | | | |
| Depth | Unit | Color | Additional description |
| 20 | n.d. | black | hard, dessicated, homog., upper part of box, lateral layering |
| 69 | n.d. | white | hard, dessicated, vertical and horizontal layering |
| 73 | n.d. | H | brownish, hard, dessicated lower part |
| 85 | n.d. | B | and white, crunchy |
| 104 | n.d. | LB | homog. |

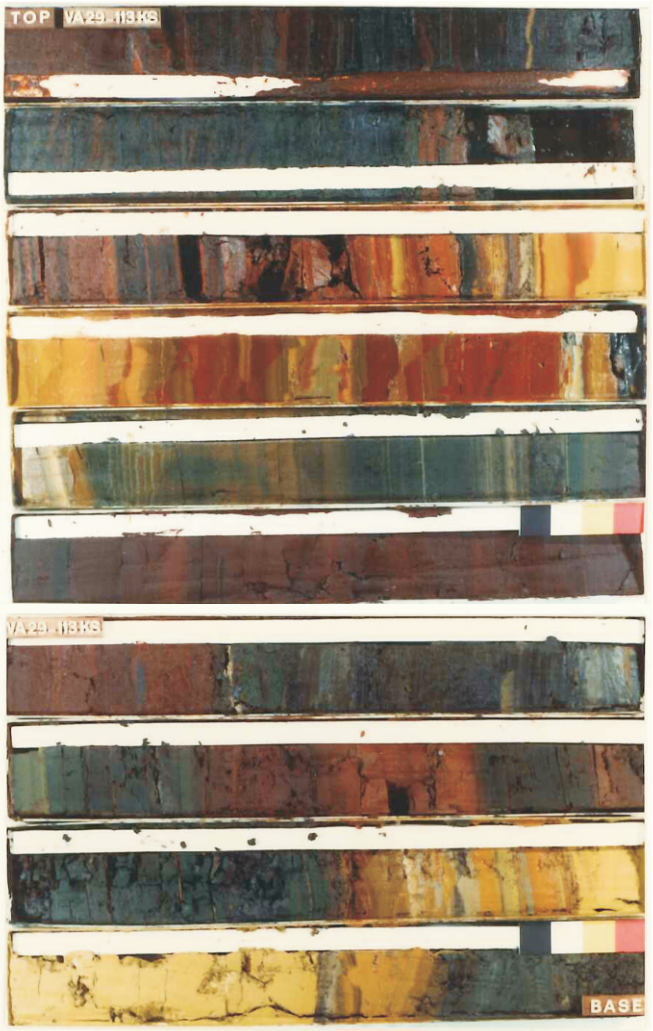
| | | | |
|---|---|---|---|
| 107 | n.d. | B | heterog., heavy |
| 111 | n.d. | LB | to white, uncoherent, sandy |
| 129 | n.d. | DH | sandy |
| 150 | n.d. | black | homog. ooze |
| 165 | n.d. | LB | homog. |
| 170 | n.d. | white | homog., sandy |
| 183 | n.d. | DB | and DG with yellow parts |
| 194 | n.d. | DB | rather homog. |
| 208 | n.d. | DB | layered |
| 230 | n.d. | MH | |
| 250 | n.d. | O | and black, laminated |
| 260 | n.d. | DH | to black |
| 280 | n.d. | white | and grey, sandy |
| 310 | n.d. | LB | to MB |
| 332 | n.d. | MH | with Y layer formed clast |
| 348 | n.d. | MB | with MR laminae |
| 358 | n.d. | MH | with light and LB hard sticks, sandy |
| 375 | n.d. | MB | thin laminae |
| 390 | n.d. | LH | sandy |
| 415 | n.d. | MH | sandy breccia with harder parts |
| 415 | n.d. | white | layer shape clast in breccia, comp. to above |
| 430 | n.d. | MR | darker and lighter layers and spots |
| 507 | n.d. | MR | darker and lighter layers and spots |
| 583 | n.d. | MR | darker and lighter layers and spots |
| Valdivia 01_08K; ~220 cm (?); 2000 m | | | |
| Depth | Unit | Color | Additional description |
| 20 | n.d. | LB | towards beige, homog., |
| 41 | n.d. | Y | and black, laminated |
| 64 | n.d. | black | uncoherent, layers |
| 77 | n.d. | LB | laminated |
| 88 | n.d. | DB | laminated |
| 97 | n.d. | DG | rather homog. |
| Valdivia 01_10K; ~210 cm (?); 1990 m | | | |
| Depth | Unit | Color | Additional description |
| 2 | n.d. | H | greenish |
| 11 | n.d. | black | Crunchy |
| 19 | n.d. | black | |
| 27 | n.d. | Y-O-black | laminated |
| 43 | n.d. | white | to LH, sandy |
| 61 | n.d. | O | to yellow |
| 74 | n.d. | Y | homog. |
| 81 | n.d. | B | |
| 90 | n.d. | DH | |
| 97 | n.d. | LG | rather homog., fossiliferous? |
| 110 | n.d. | black | hard, homog., Mn-rich? |
| 122 | n.d. | LB | and black, irr. contact to overlying layers |
| 134 | n.d. | LG | and grey, soft, uncoherent |
| 147 | n.d. | white | and LB, sandy |
| 153 | n.d. | LG | layered |
| 162 | n.d. | B | dried layers |
| 180 | n.d. | LB | no black parts included |
| 185 | n.d. | black | or DB, laminated |
| 191 | n.d. | O | bright, rusty |
| 195 | n.d. | B | dessicated, laminated? |

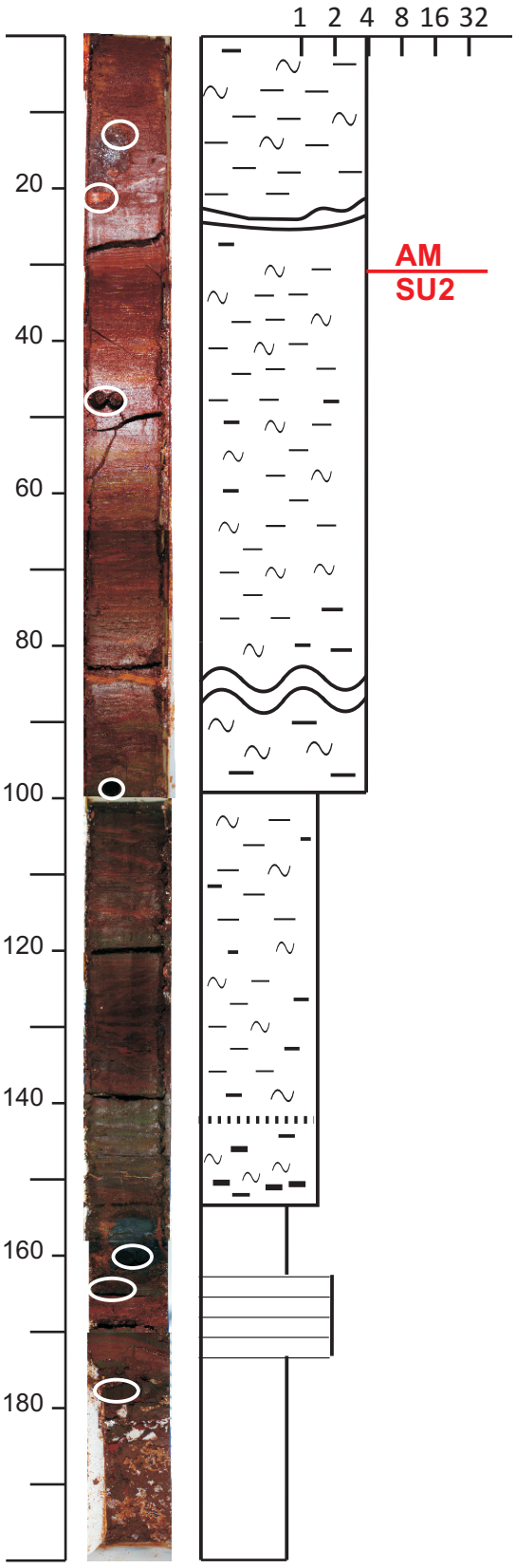
Appendix B.3.

Core: Va29_113 KS page 1/3

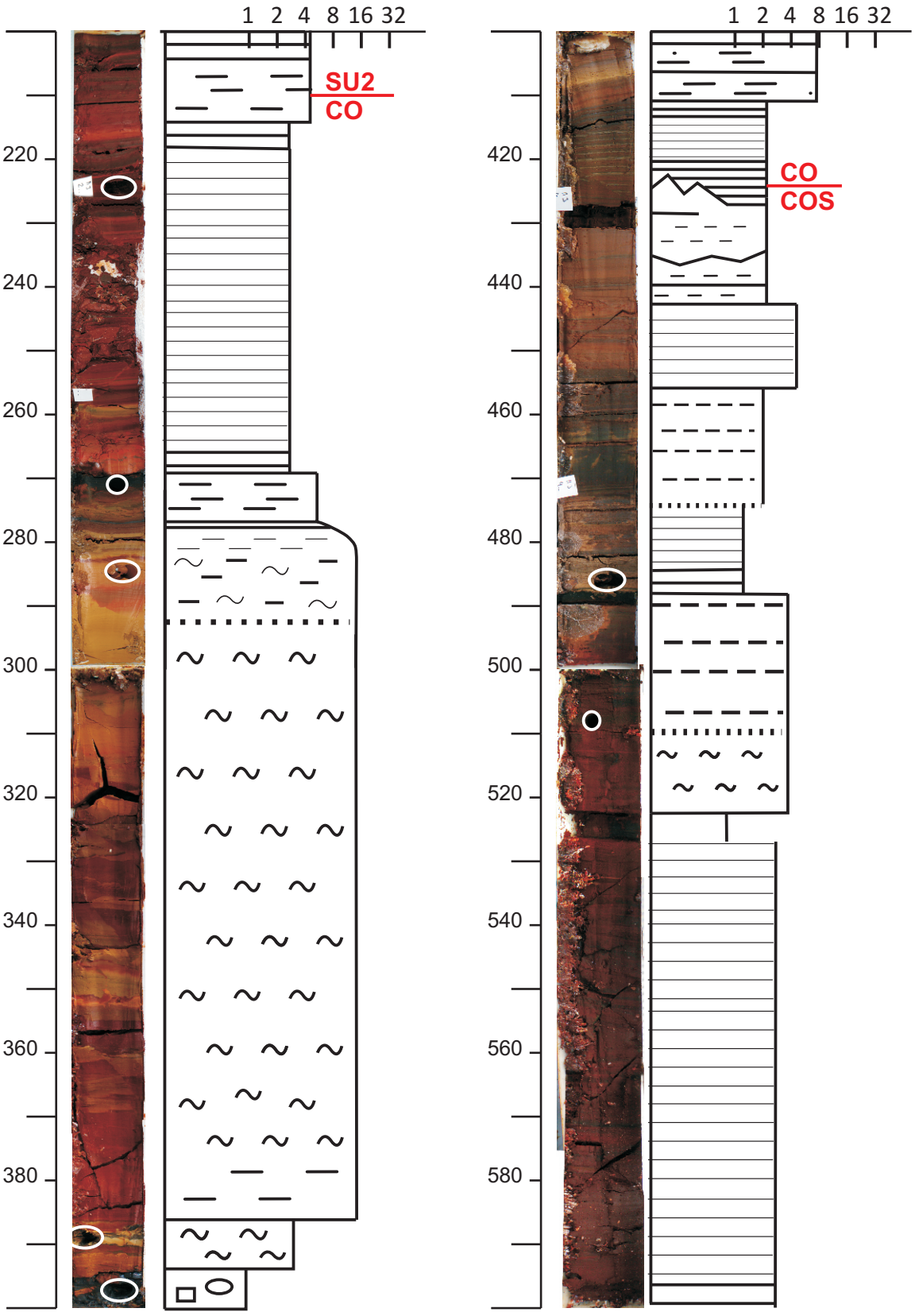
(N-Passage)
Water depth: 2101 m
Recovery: 9.79 m
Top loss: 2.75 m
Samples taken: 22

Samples were named differently than in the other boxes, thus deeper than 178 sample are taken at 22 cm deeper than their name

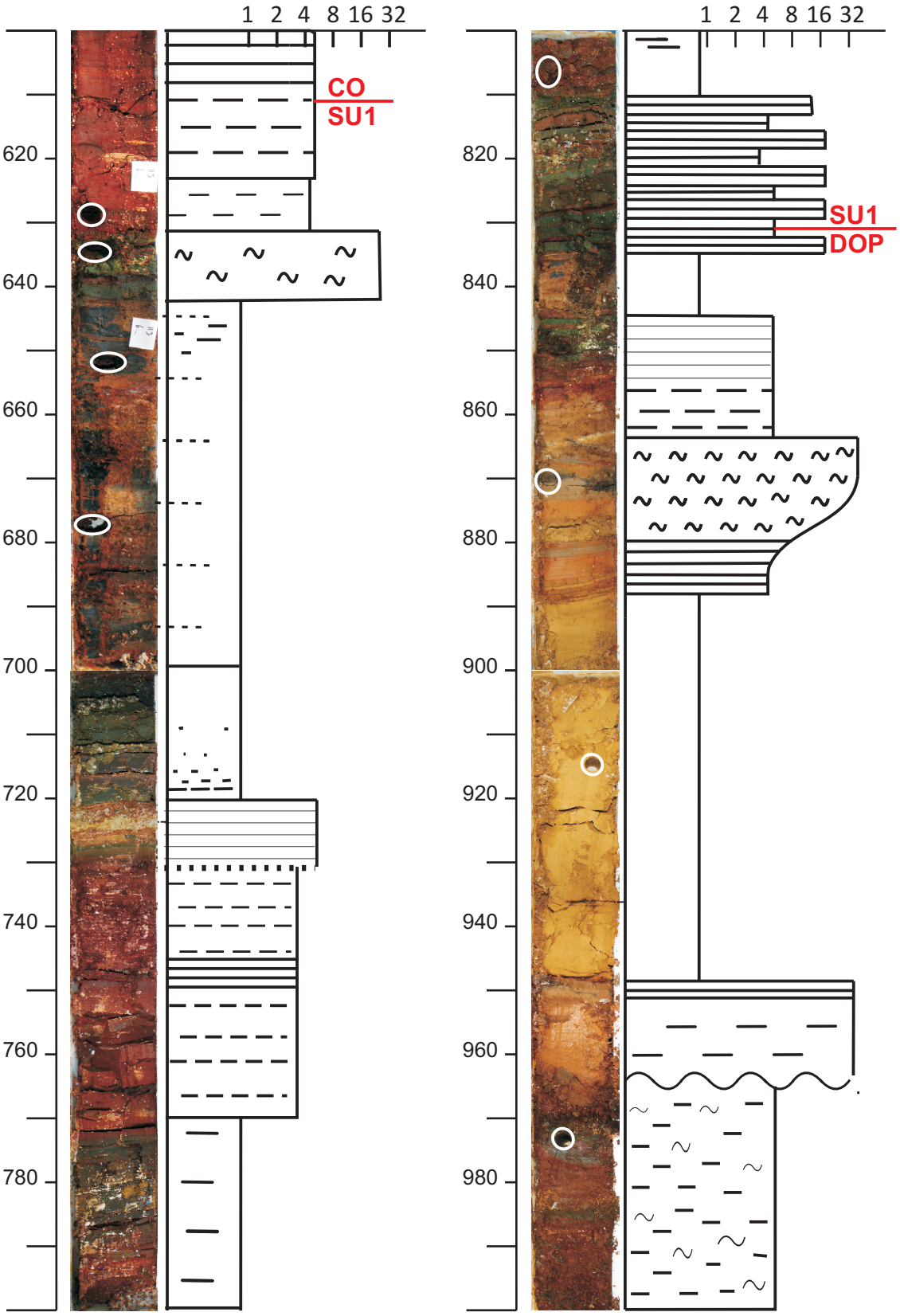


Core: Va29_113 KS page 2/3



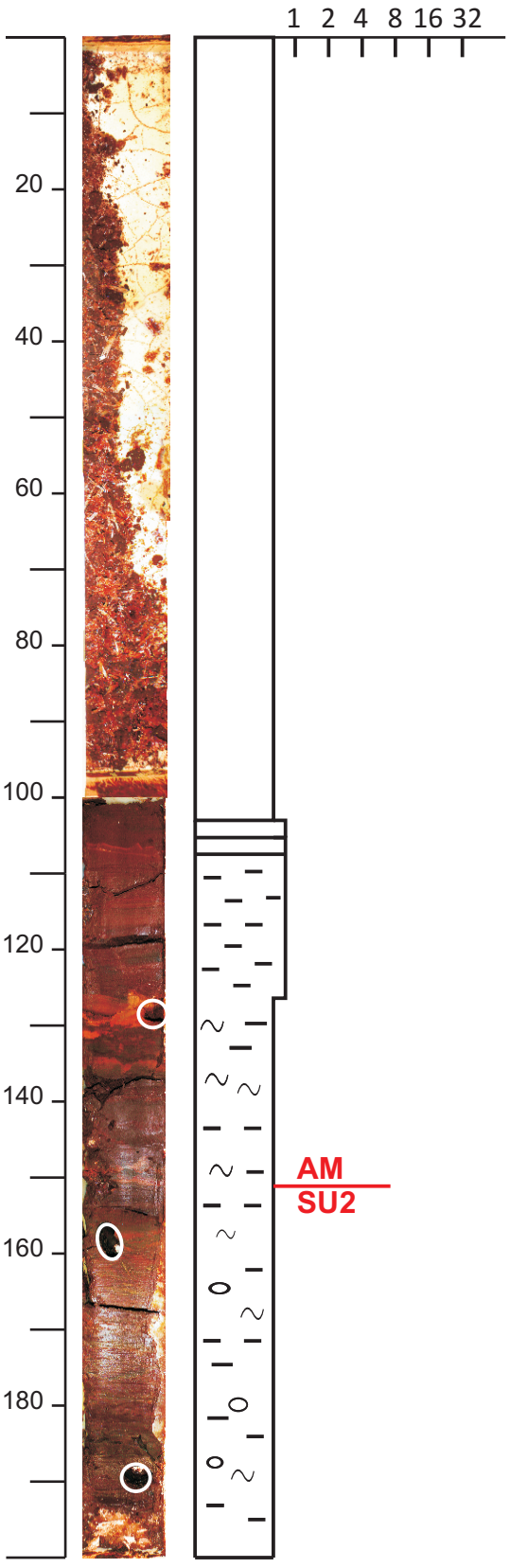
Core: Va29_113 KS page 3/3



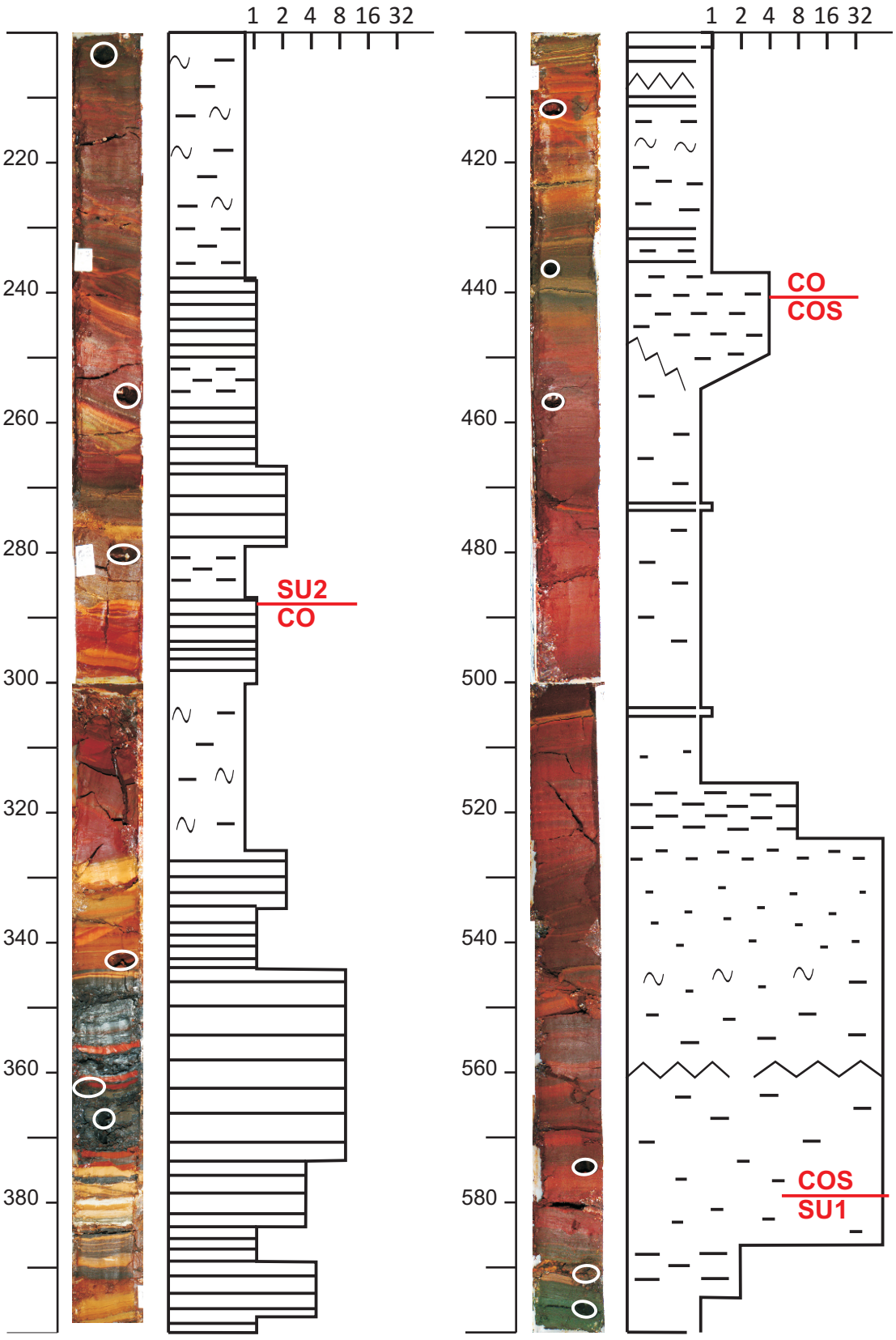
Appendix B.3.

Core: Va29_175 KS  page 1/3
(N-Basin)
Water depth: 2099 m
Recovery: 8.35 m
Top loss: 0.52 m
Samples taken: 22



Core: Va29_175 KS page 2/3



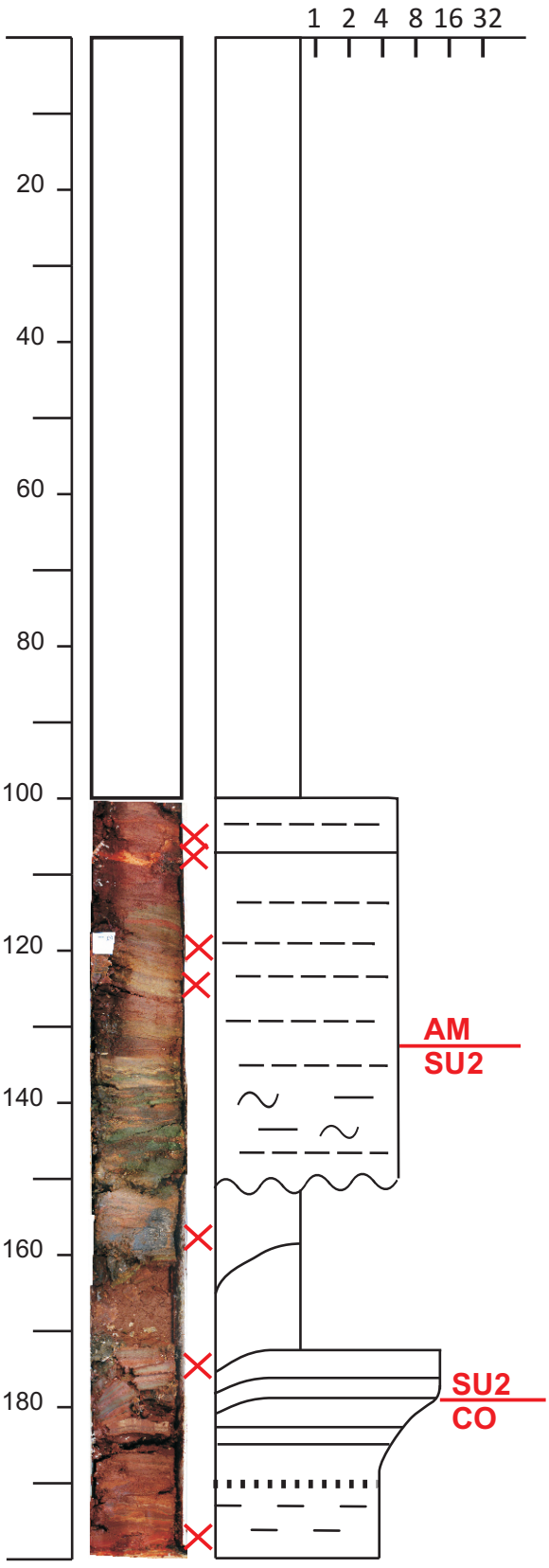
Core: Va29_175 KS page 3/3



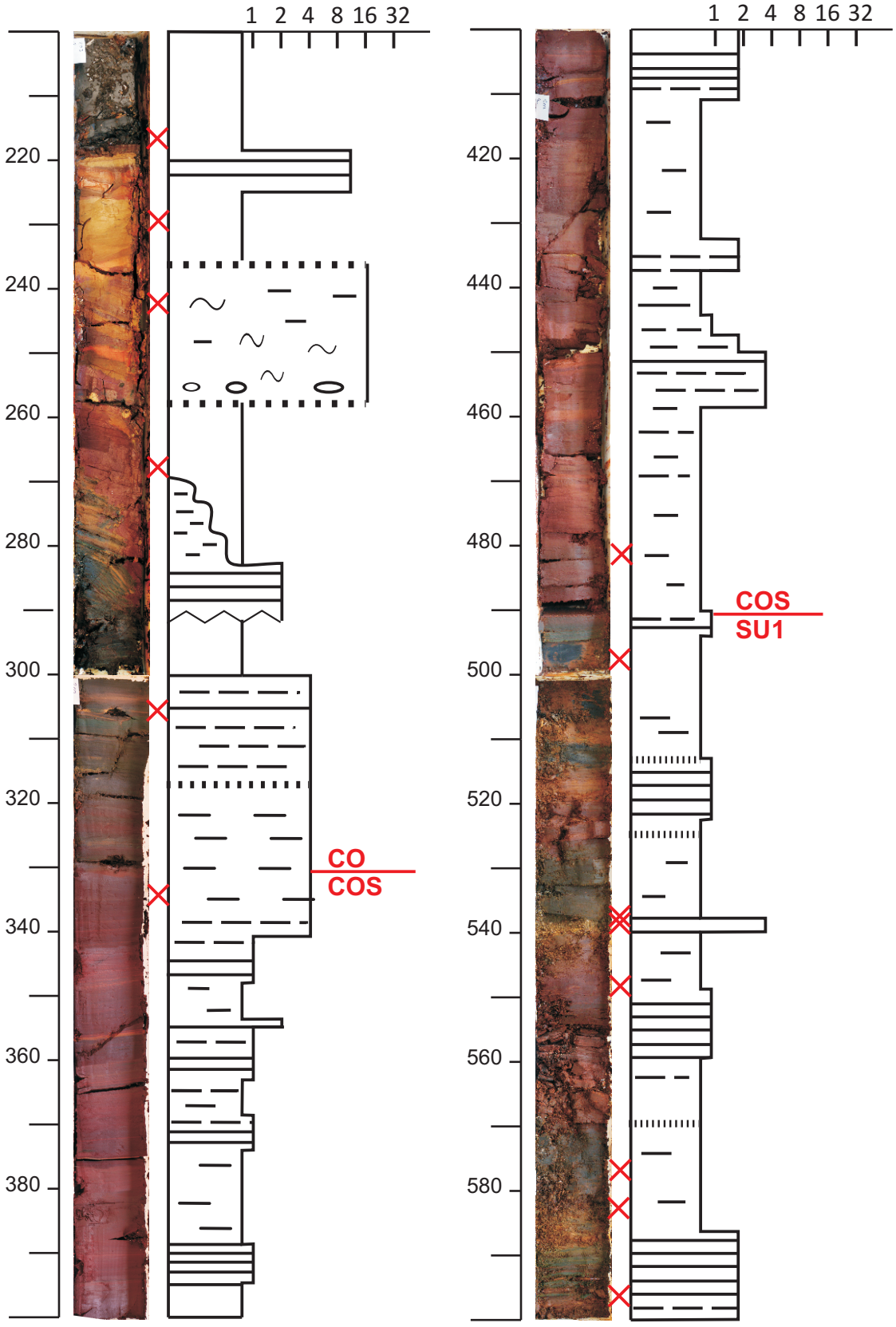
Appendix B.3.

Core: Va29_203 KS page 1/3
(N-Passage)
Water depth: 2099 m
Recovery: 7.25 m
Top loss: 2.29 m
Samples taken: 26

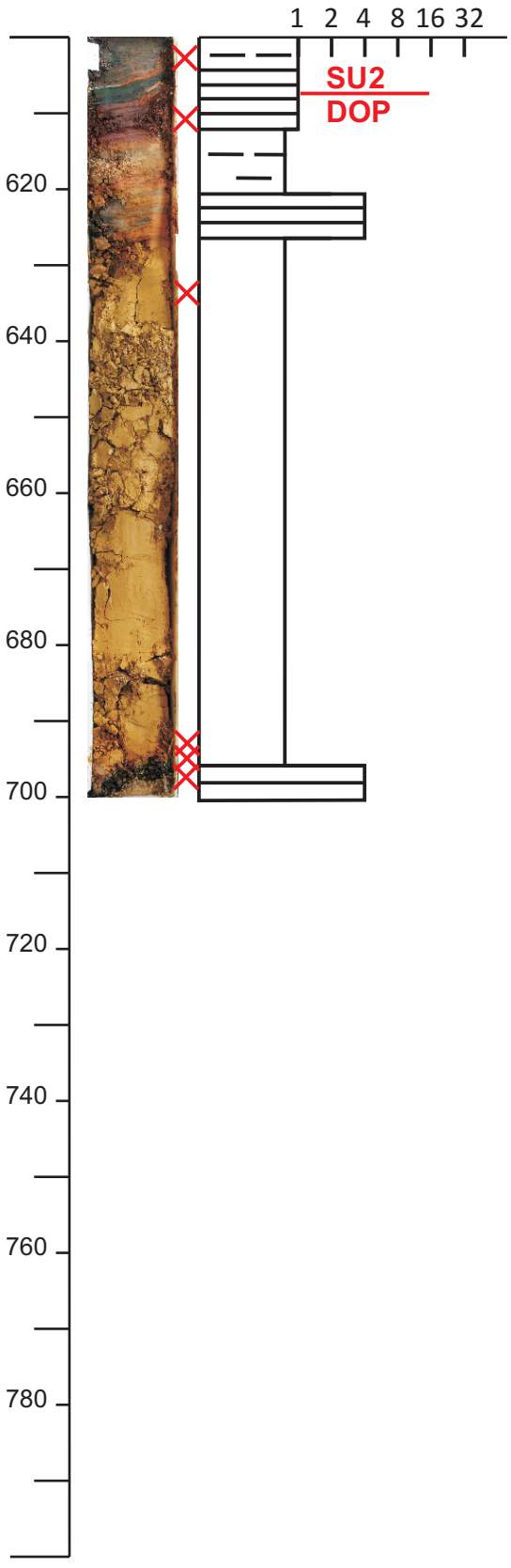


Core: Va29_203 KS page 2/3



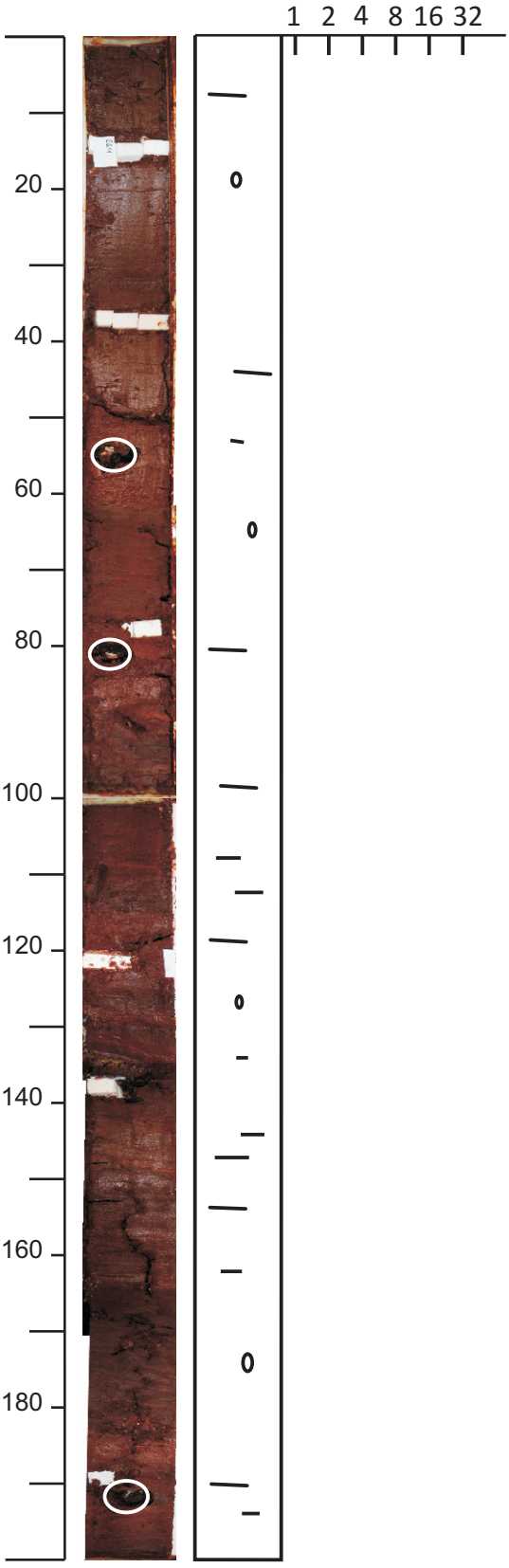
Core: Va29_203 KS  page 3/3



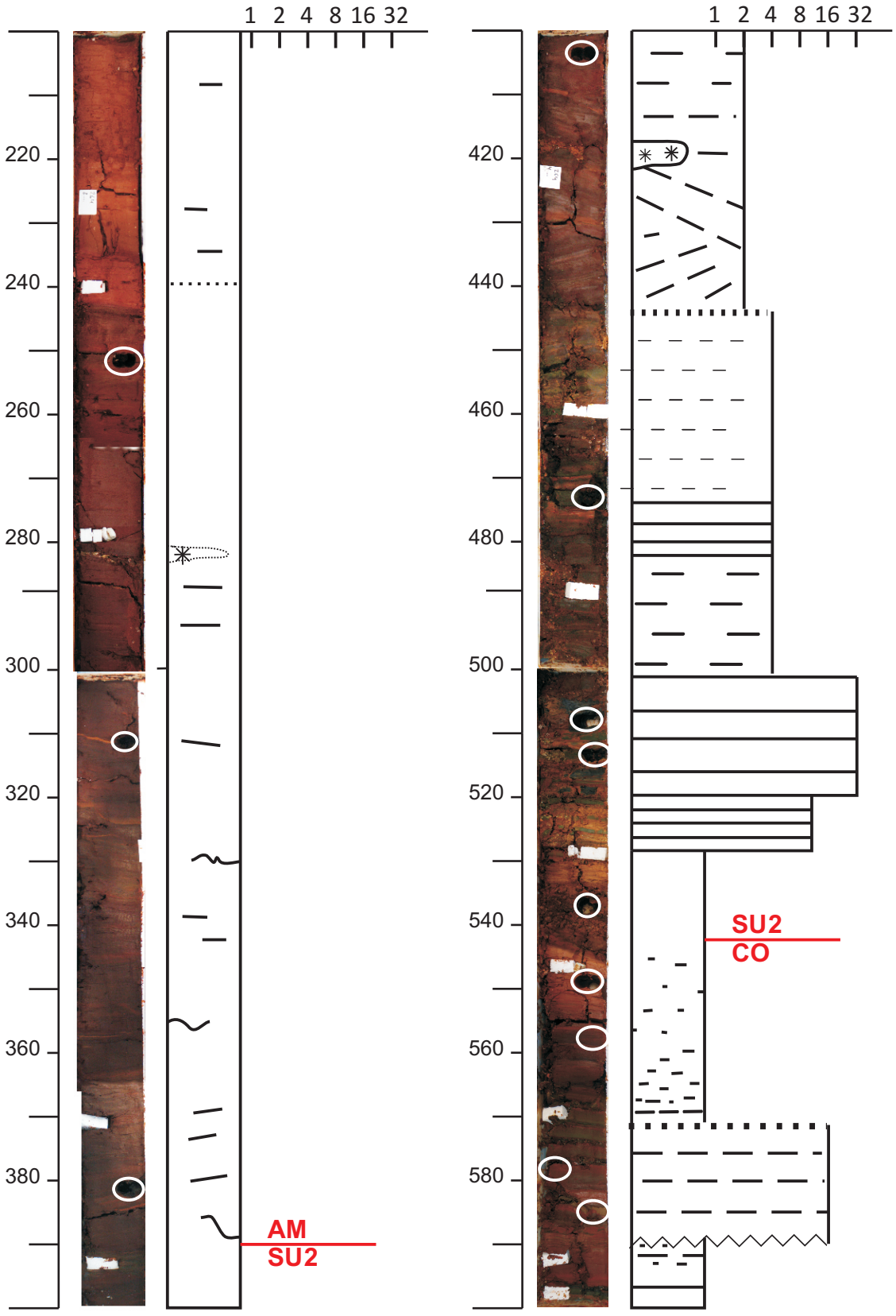
Appendix B.3.

Core: Va29_264 KS page 1/4
(SW-Passage)
Water depth: 2143 m
Recovery: 11.27 m
Top loss: 0 m
Samples taken: 41

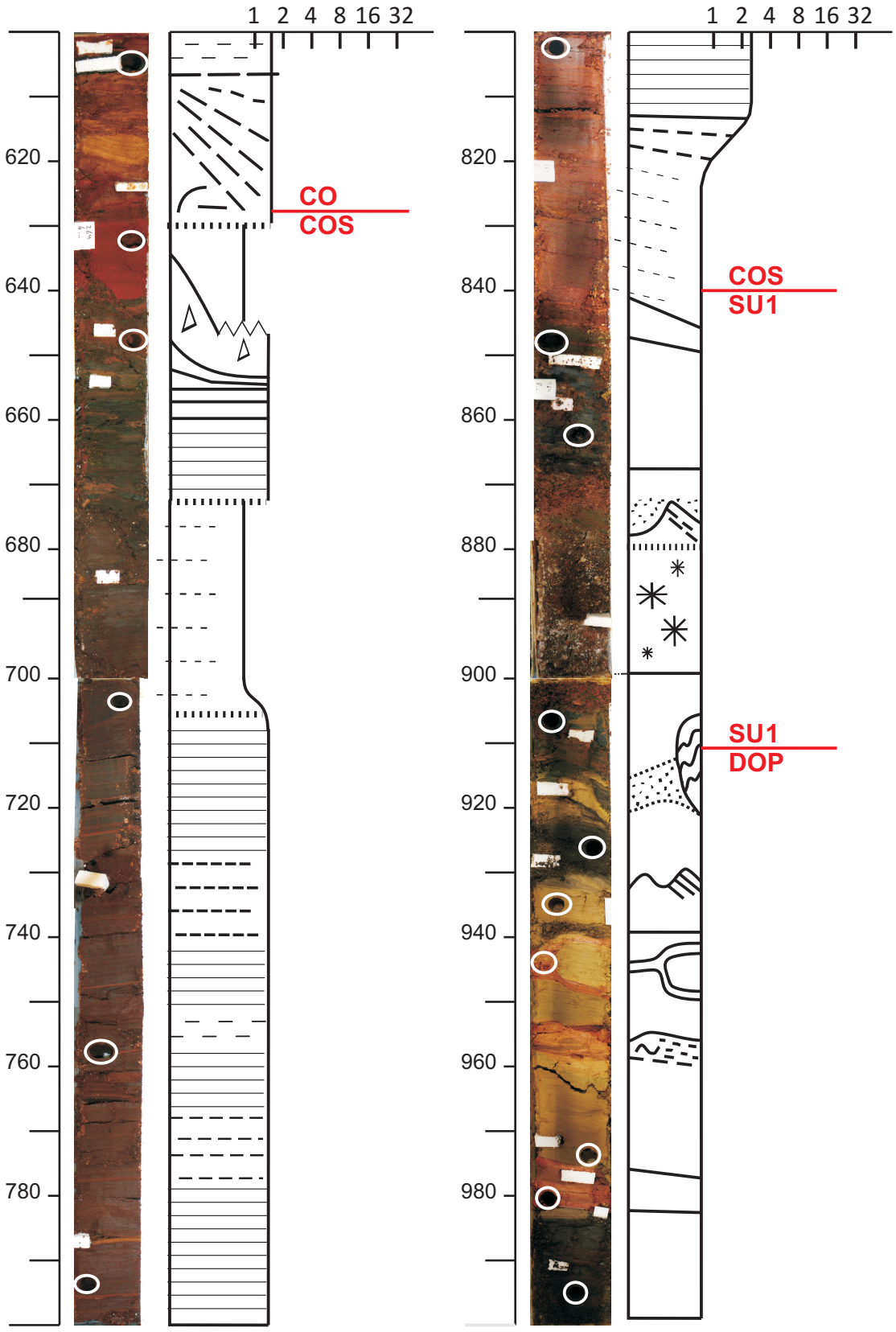


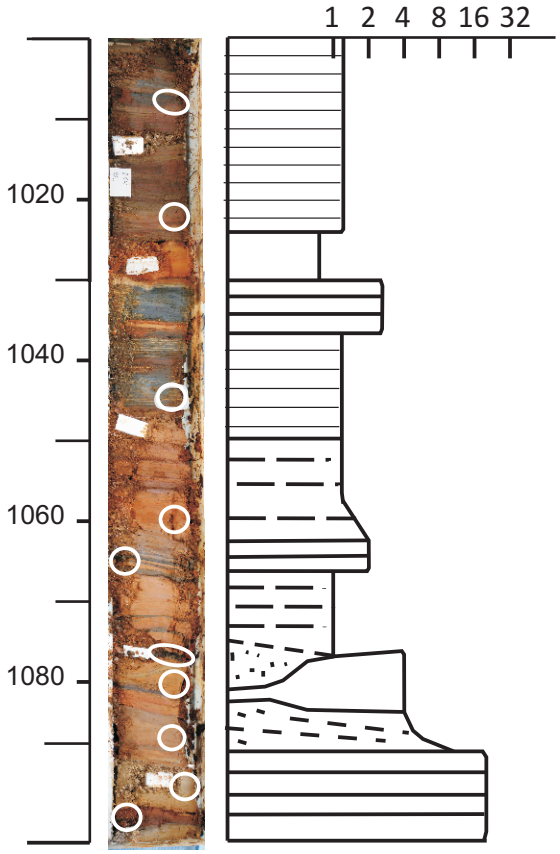
Core: Va29_264 KS page 2/4



Core: Va29_264 KS page 3/4



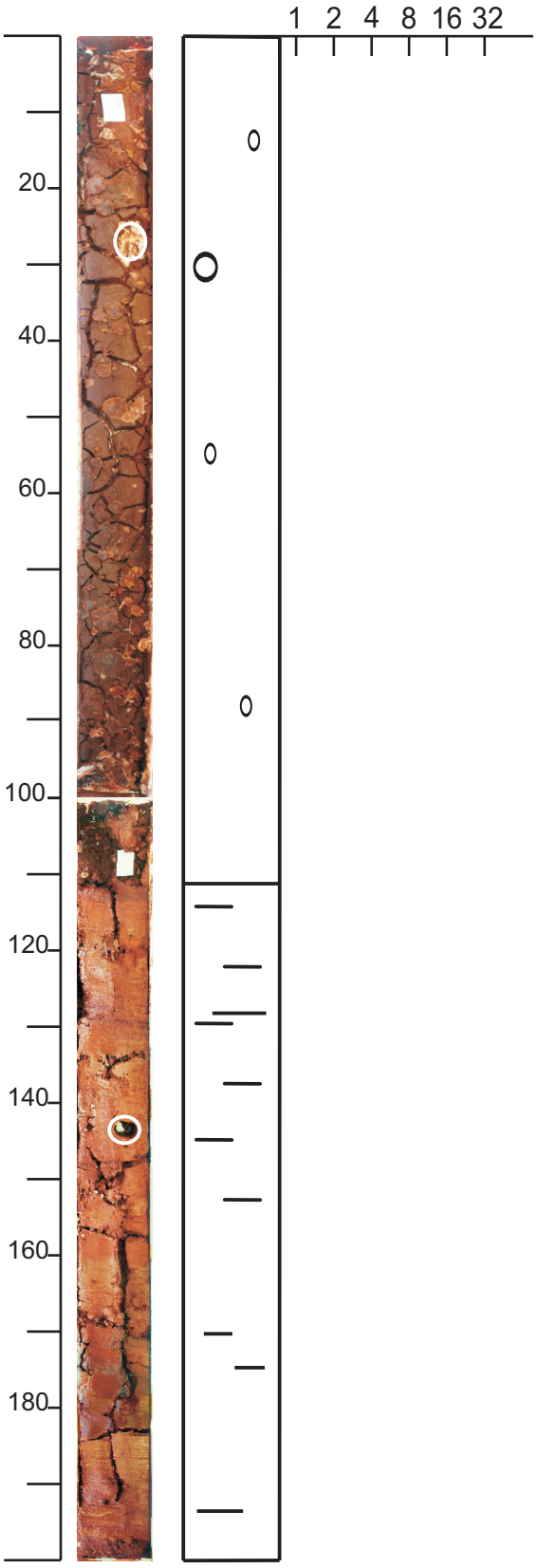
Core: Va29_264 KS  page 4/4



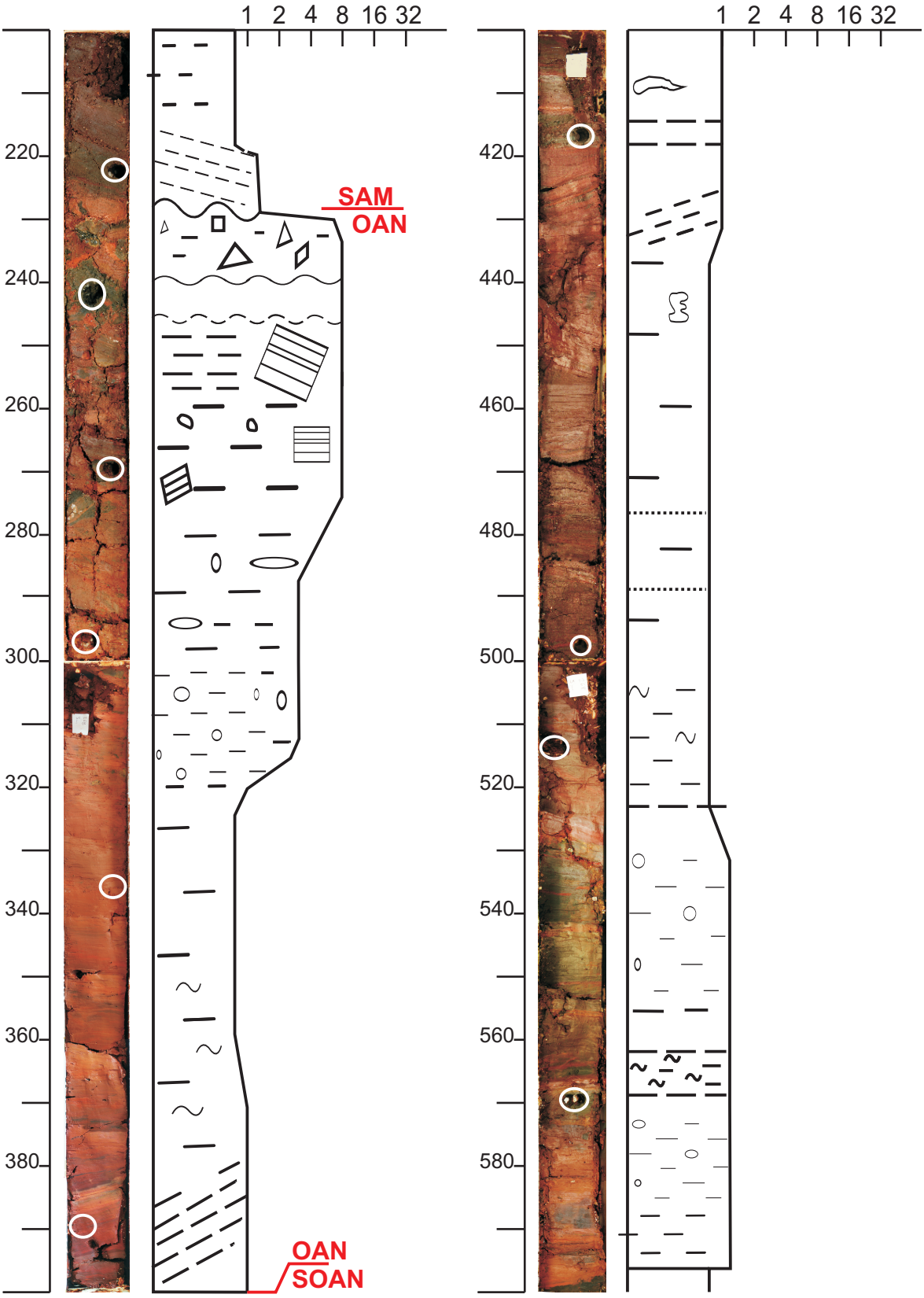
Appendix B.3.

Core: Va29_268 KS page 1/4
(SW-Basin)
Water depth: 2182 m
Recovery: 11.25 m
Top loss: 1.62 m
Samples taken: 28

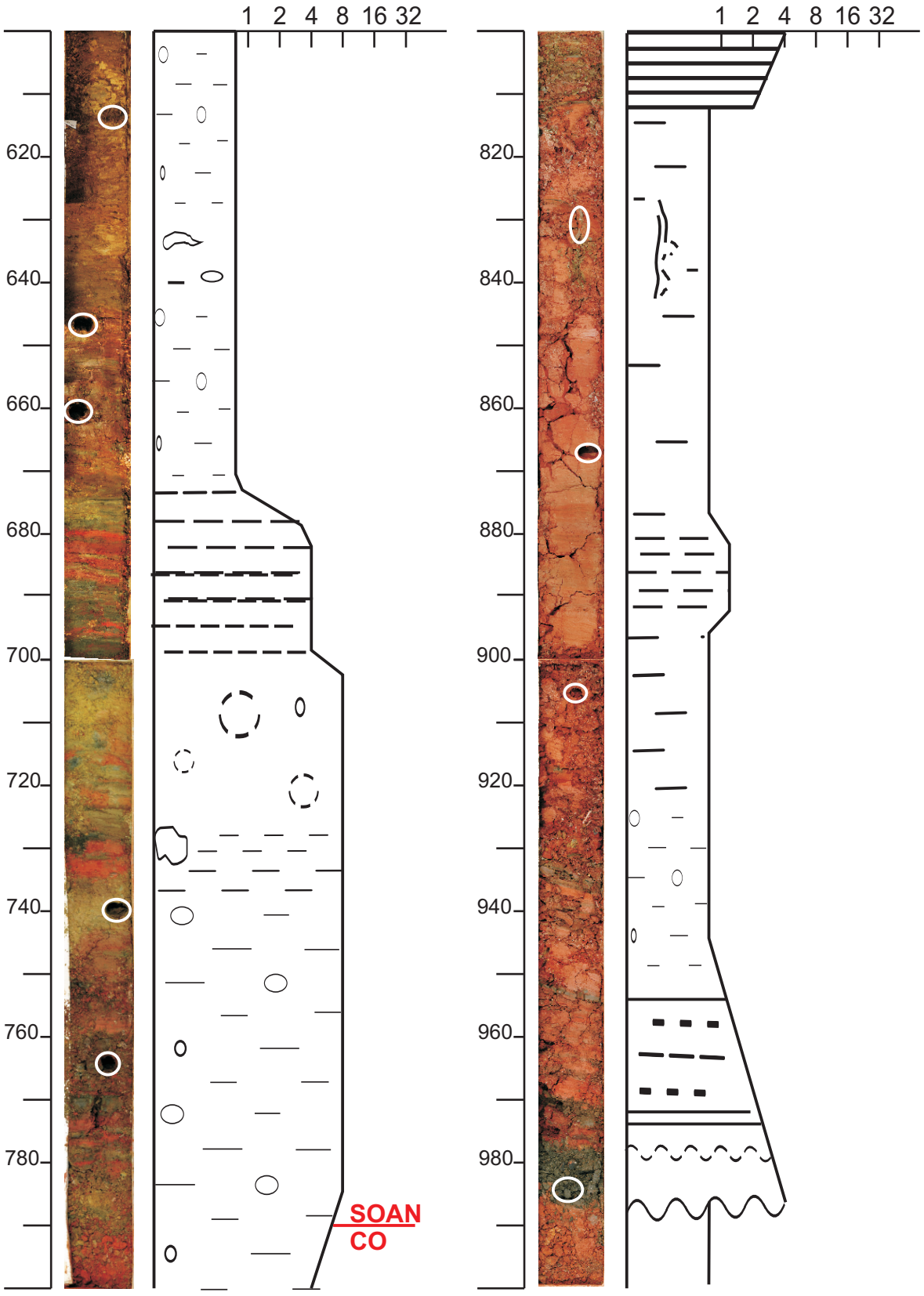


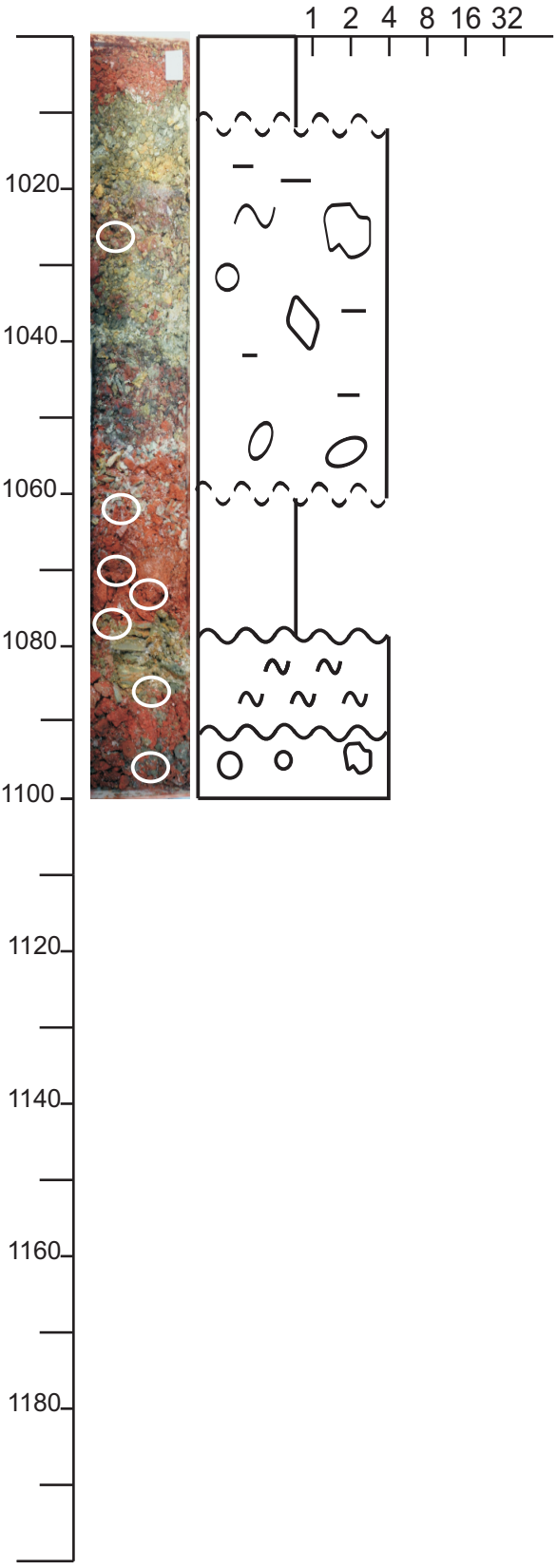
Core: Va29_268 KS page 2/4



Core: Va29_268 KS page 3/4

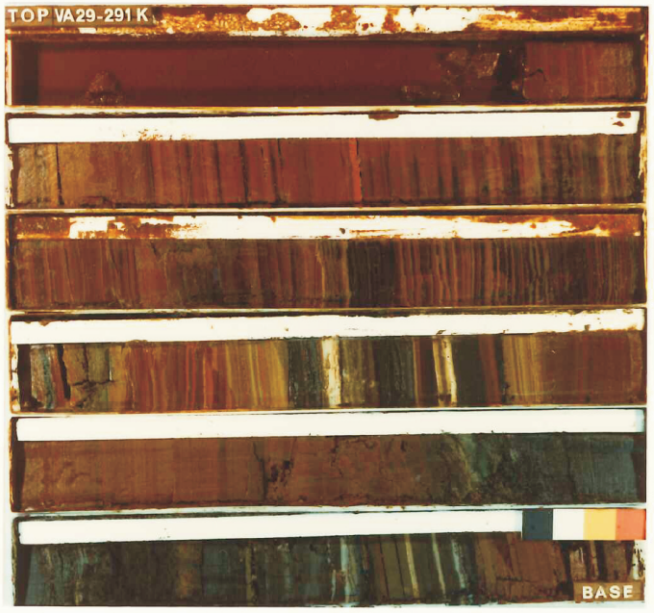


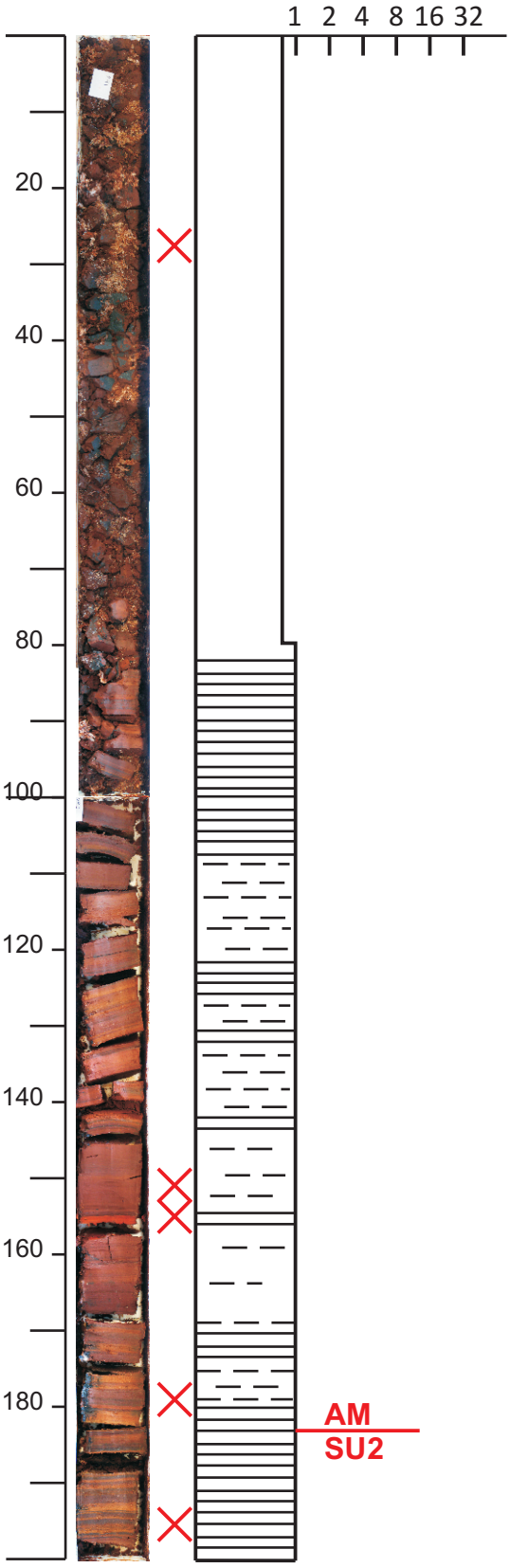
Core: Va29_268 KS  page 4/4



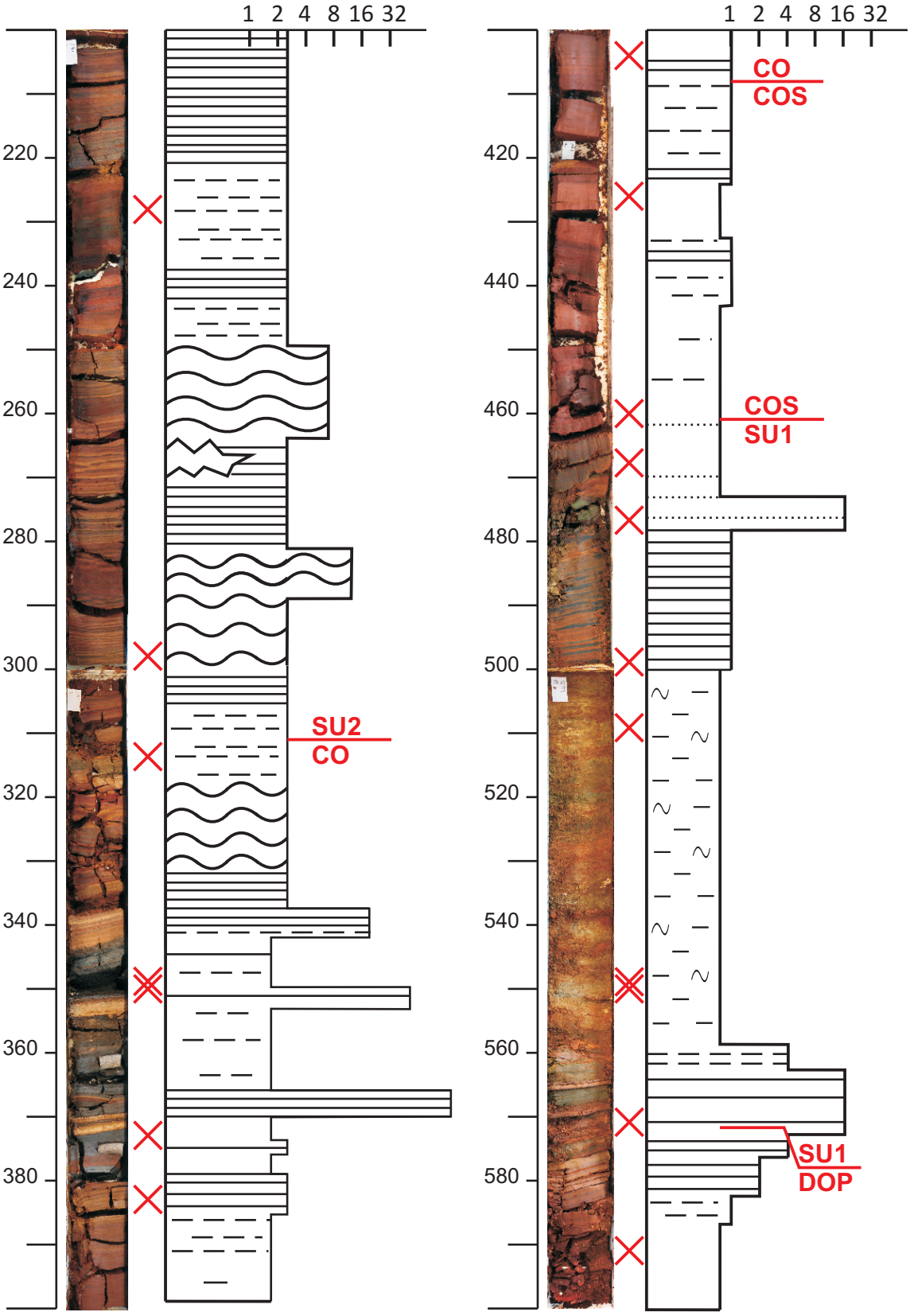
Appendix B.3.

Core: Va29_291 KS page 1/2
(Central-Sill)
Water depth: 2019 m
Recovery: 5.96 m
Top loss: 0 m
Samples taken: 23



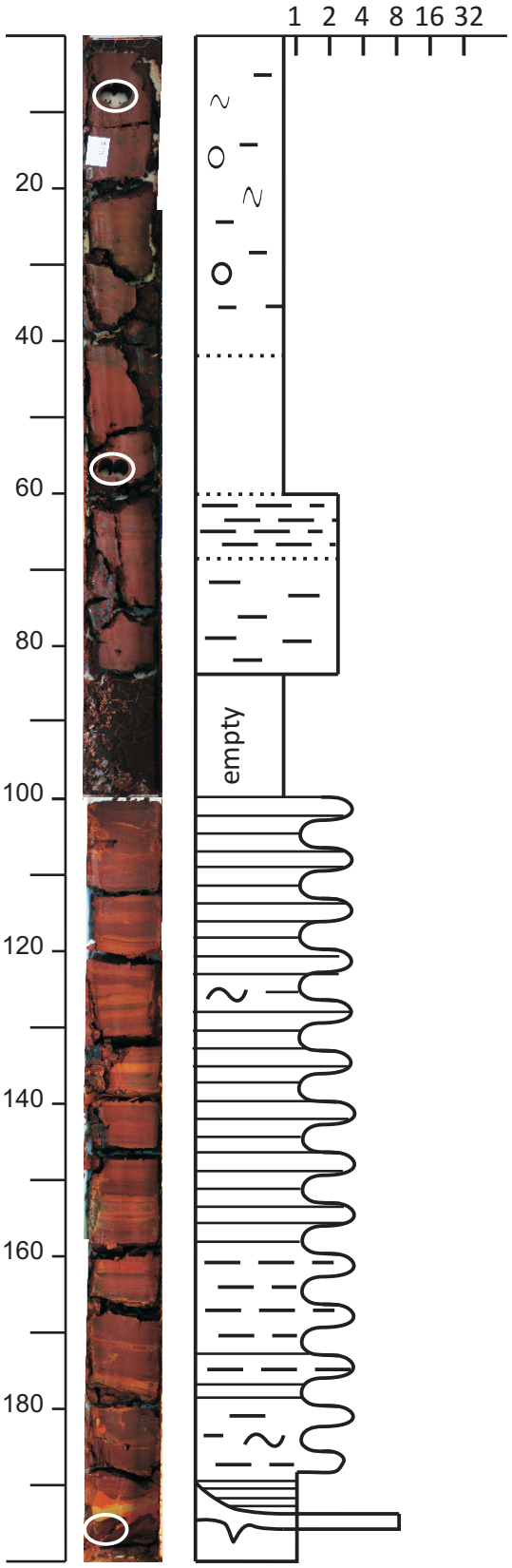
Core: Va29_291 KS  page 2/2



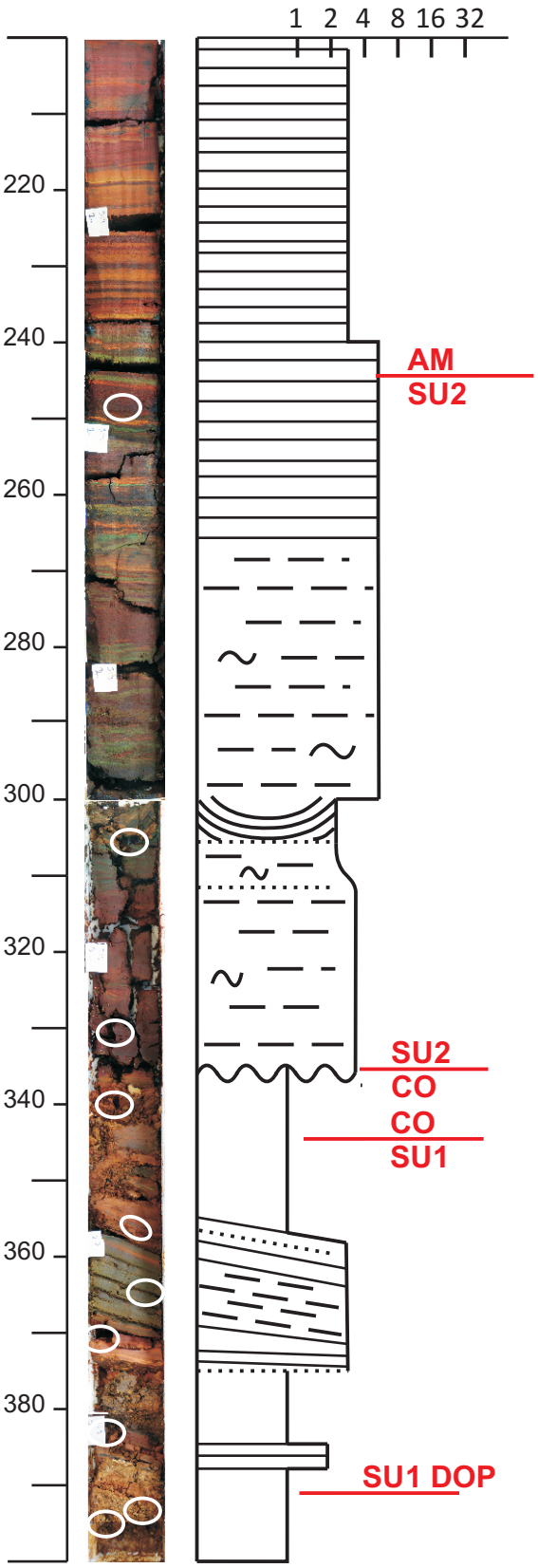
Appendix B.3.

Core: Va29_313 K page 1/2
(N-Basin)
Water depth: 2031 m
Recovery: 4.00 m
Top loss: 0 m
Samples taken: 13



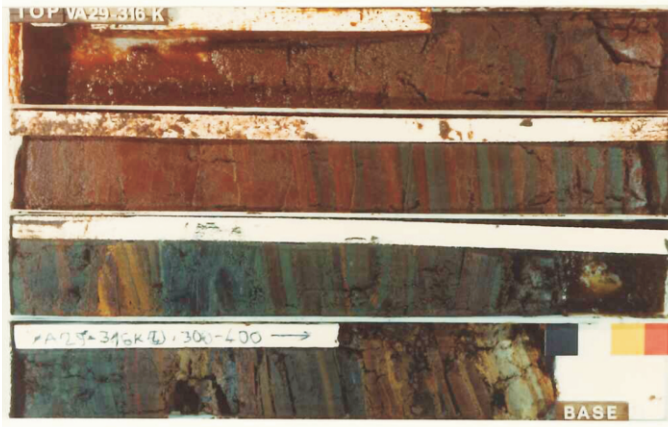



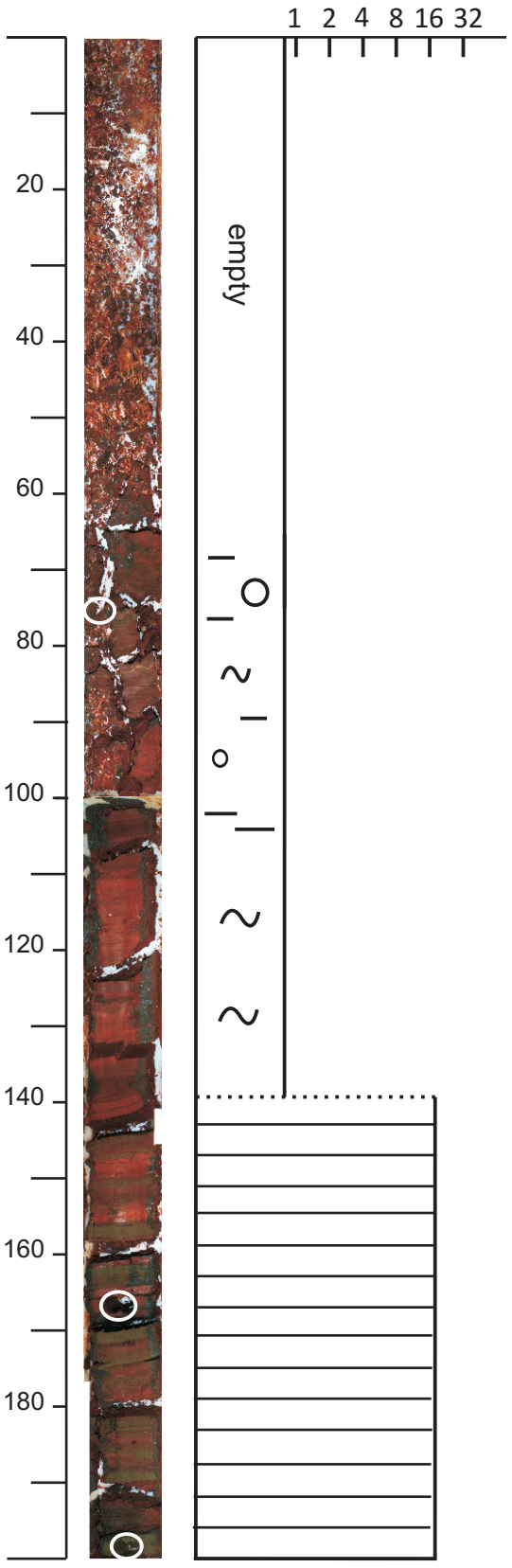
Core: Va29_583 KS  page 2/2



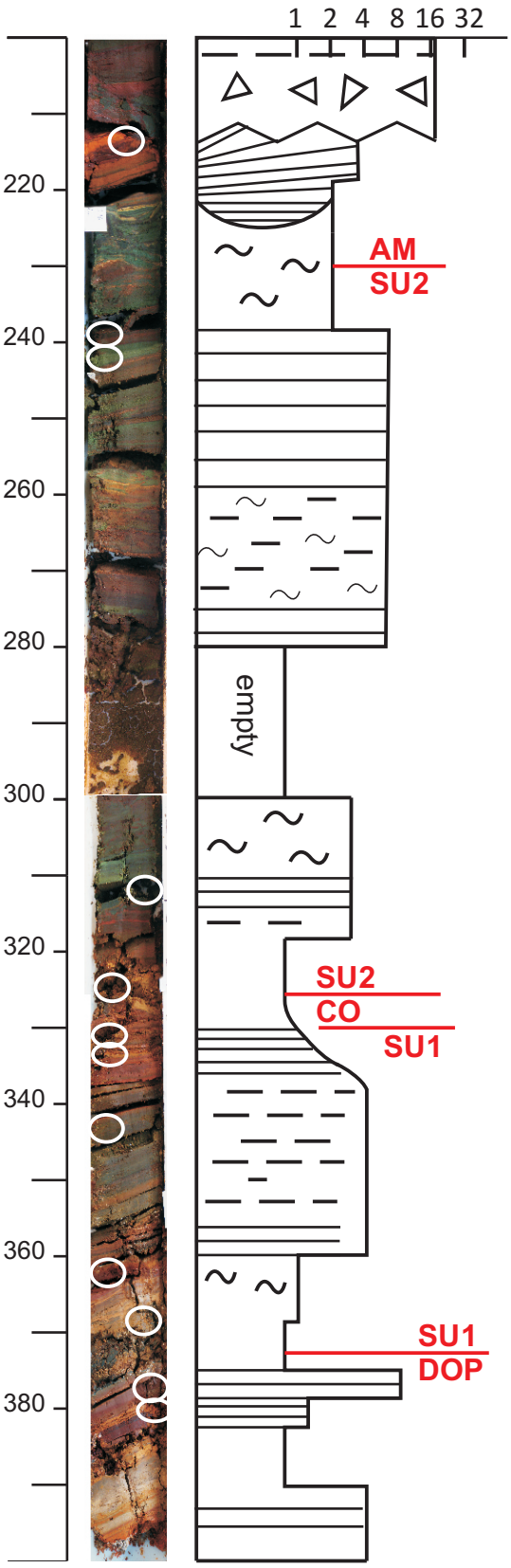
Appendix B.3.

Core: Va29_316 K page 1/2
(N-Passage)
Water depth: 2032 m
Recovery: 3.82 m
Top loss: 0.43 m
Samples taken: 15



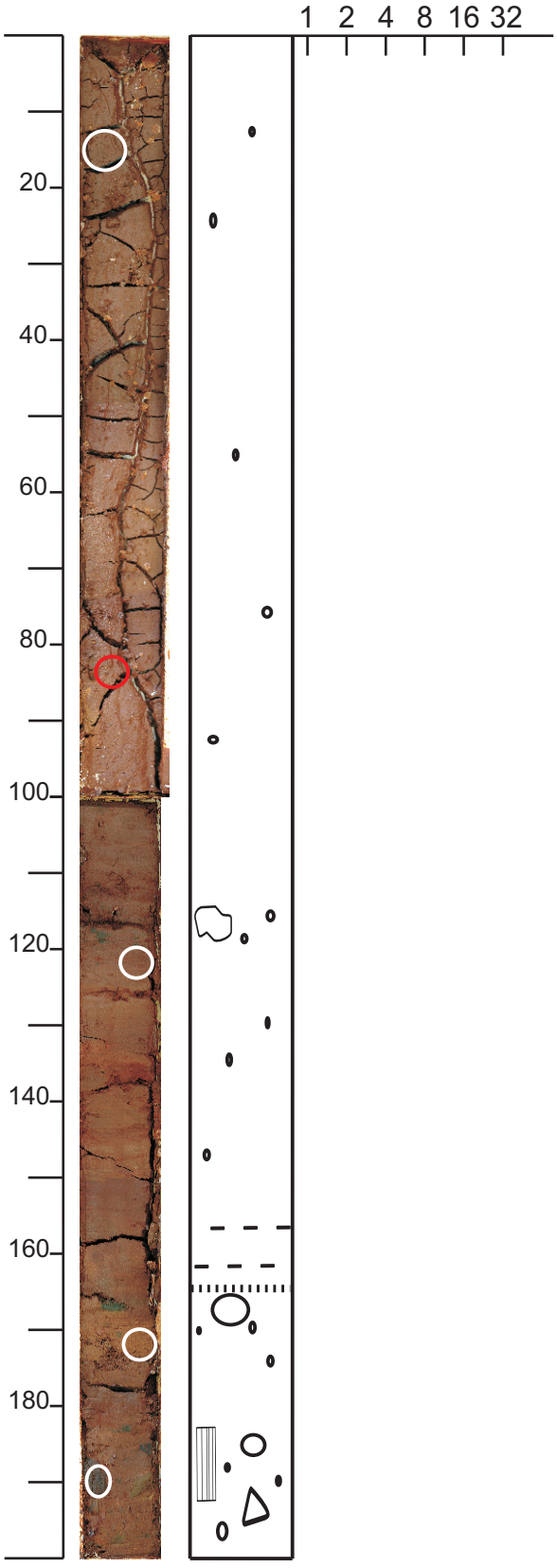
Core: Va29_316 KS page 2/2



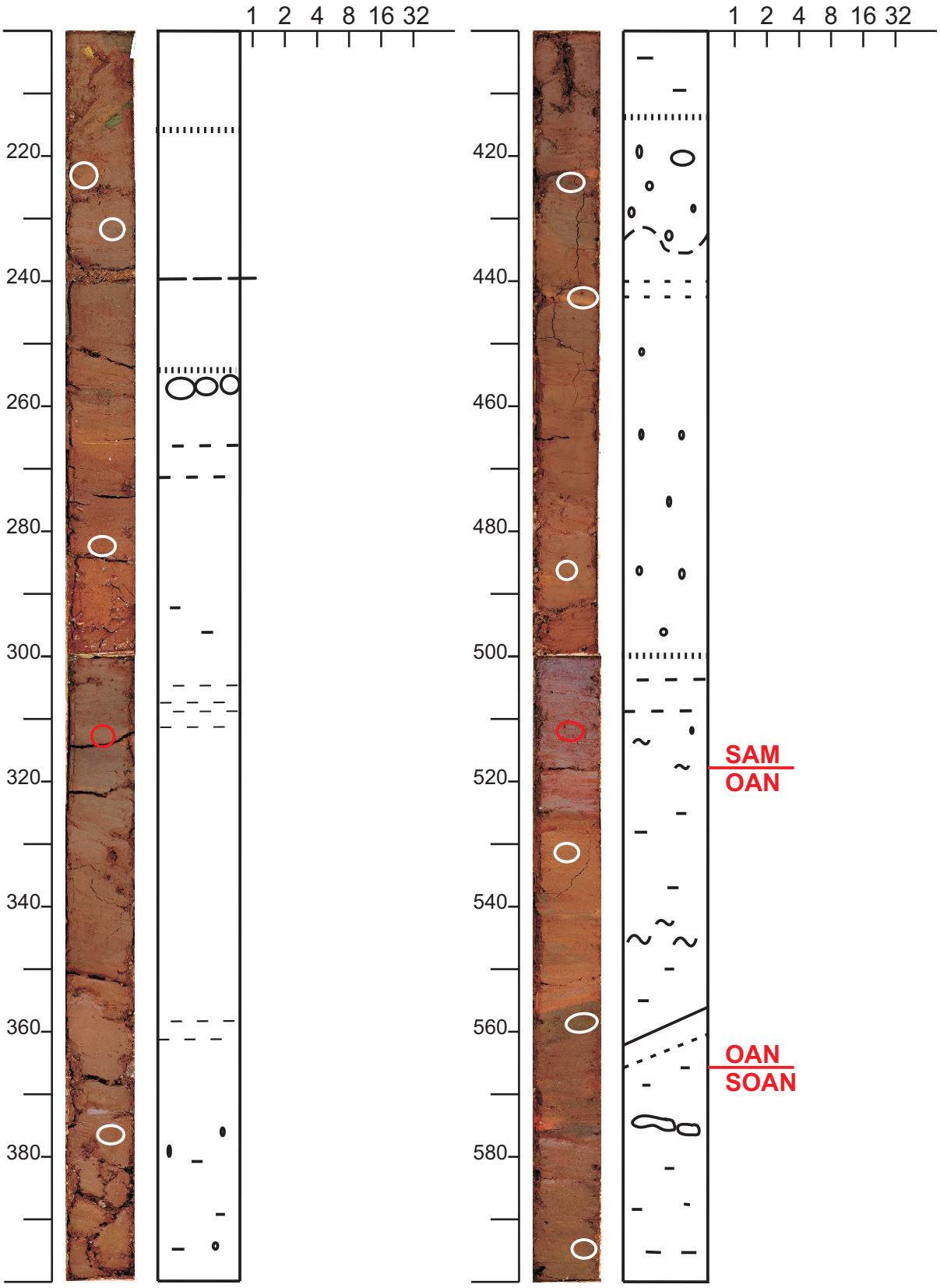
Appendix B.3.

Core: Va29_334 KS Page 1/3
(SW-Basin)
Water depth: 2184 m
Recovery: 7.70 m
Top loss: 0 m
Samples taken: 24

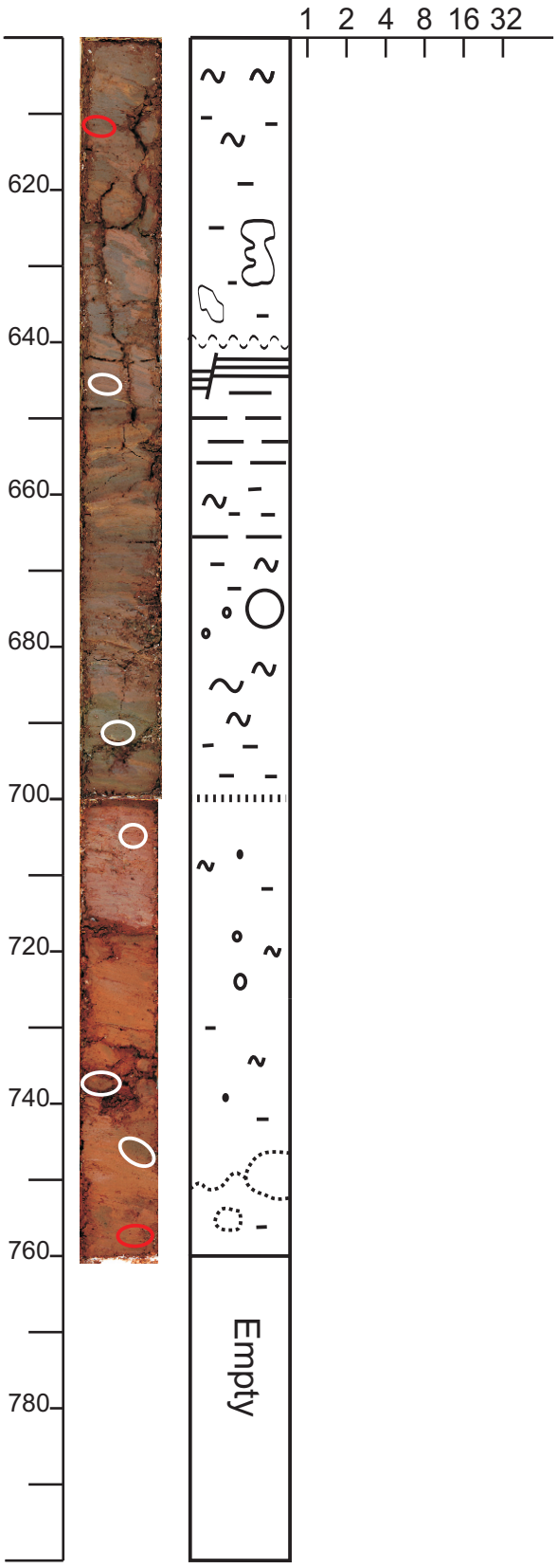


Core: Va29_334 KS page 2/3



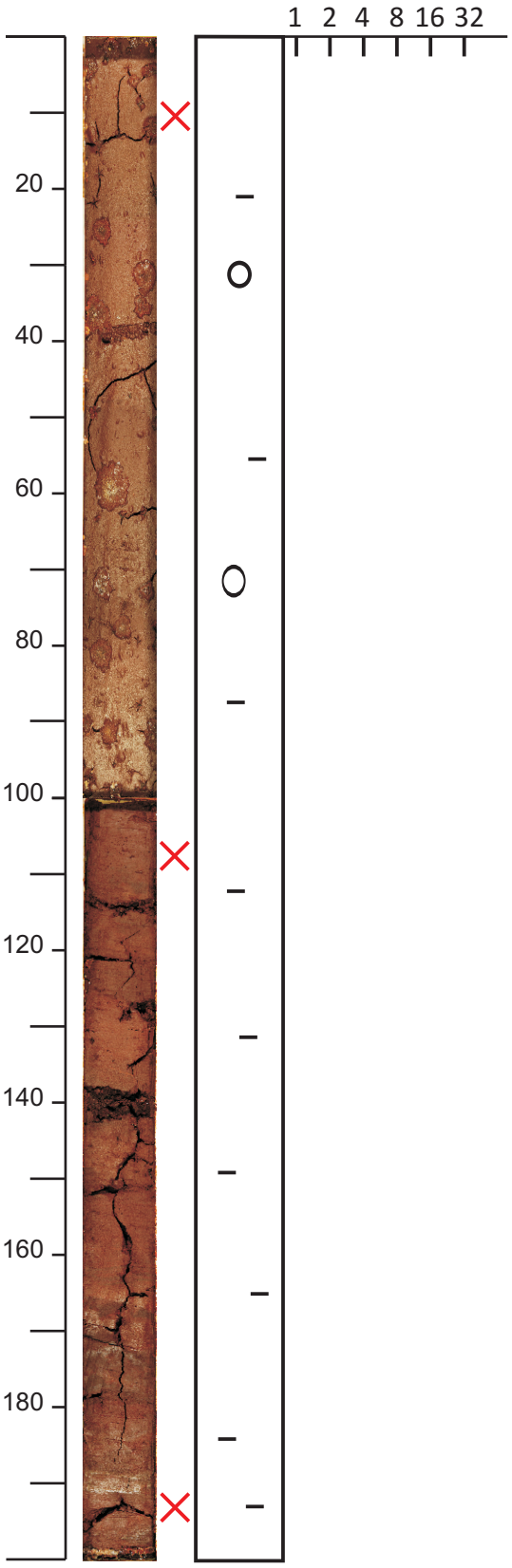
Core: Va29_334 KS page 3/3



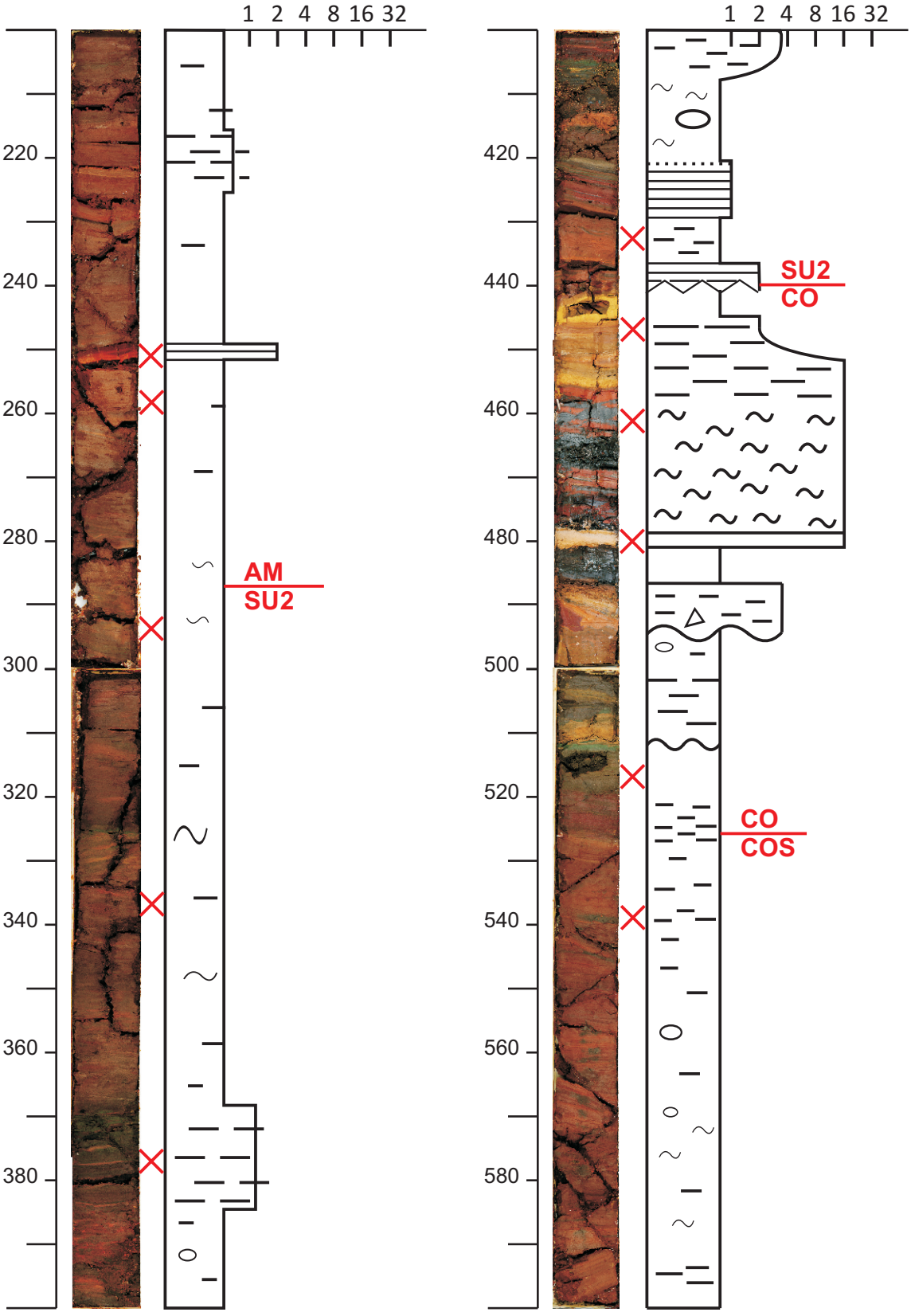
Appendix B.3.

Core: Va29_354 KS page 1/3
(E-Basin)
Water depth: 2061 m
Recovery: 10.55 m
Top loss: 0.39 m
Samples taken: 27

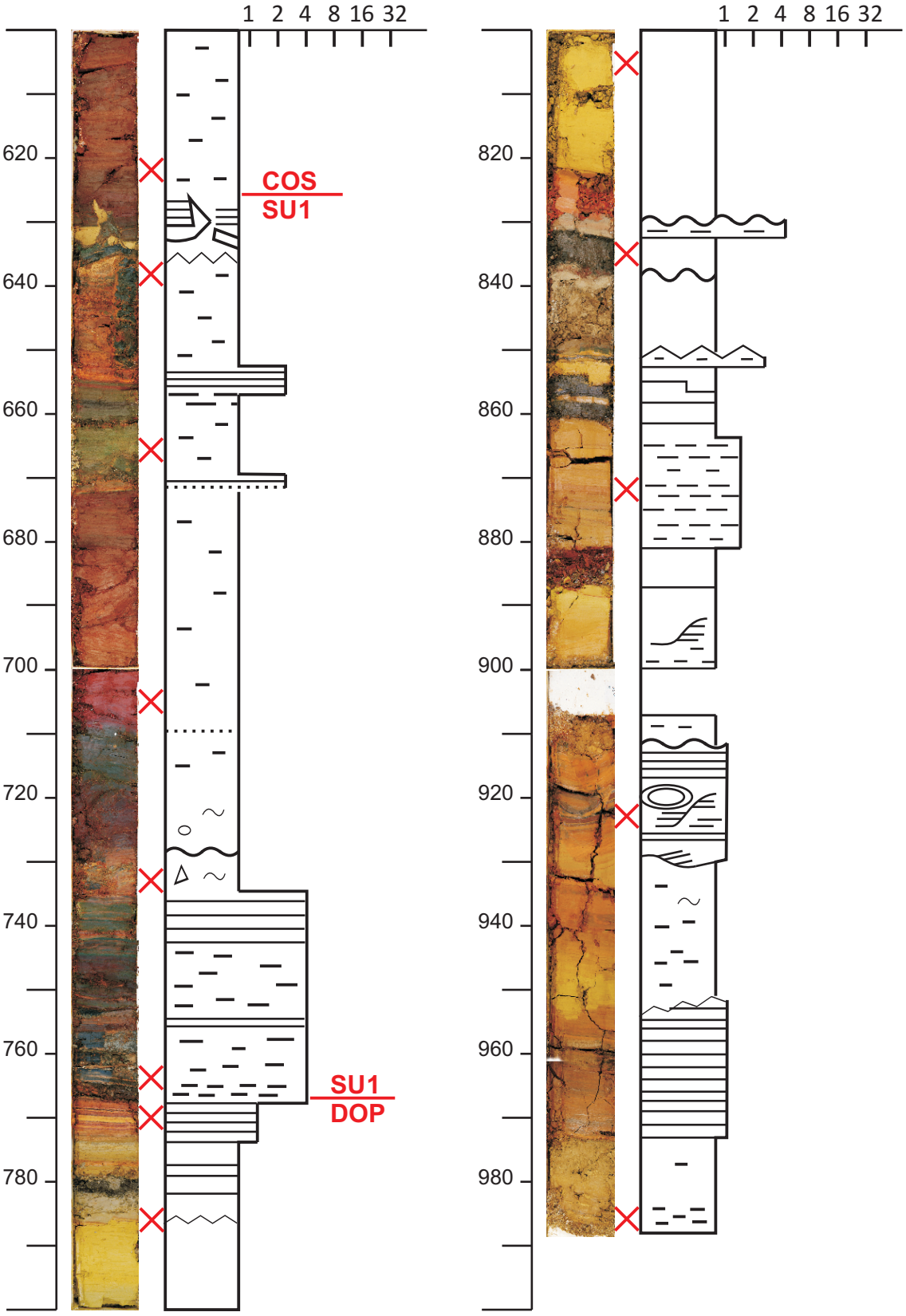


Core: Va29_354 KS page 2/3

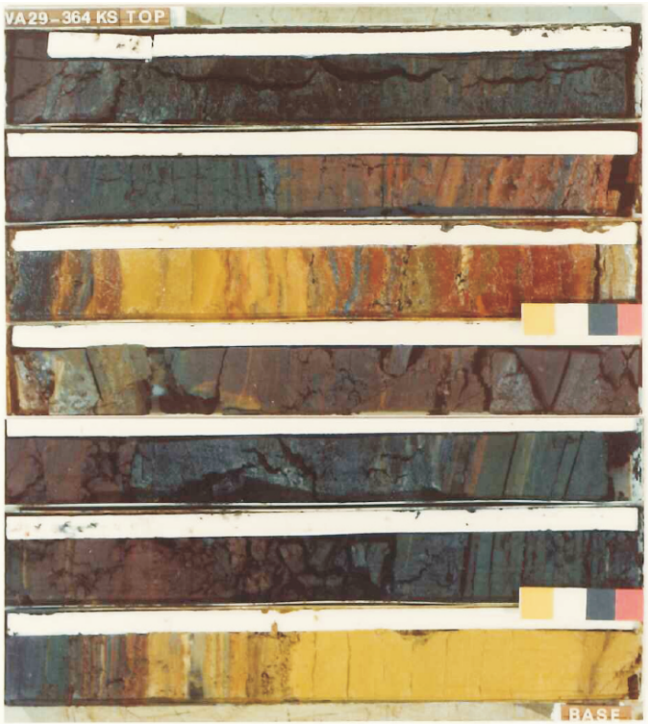


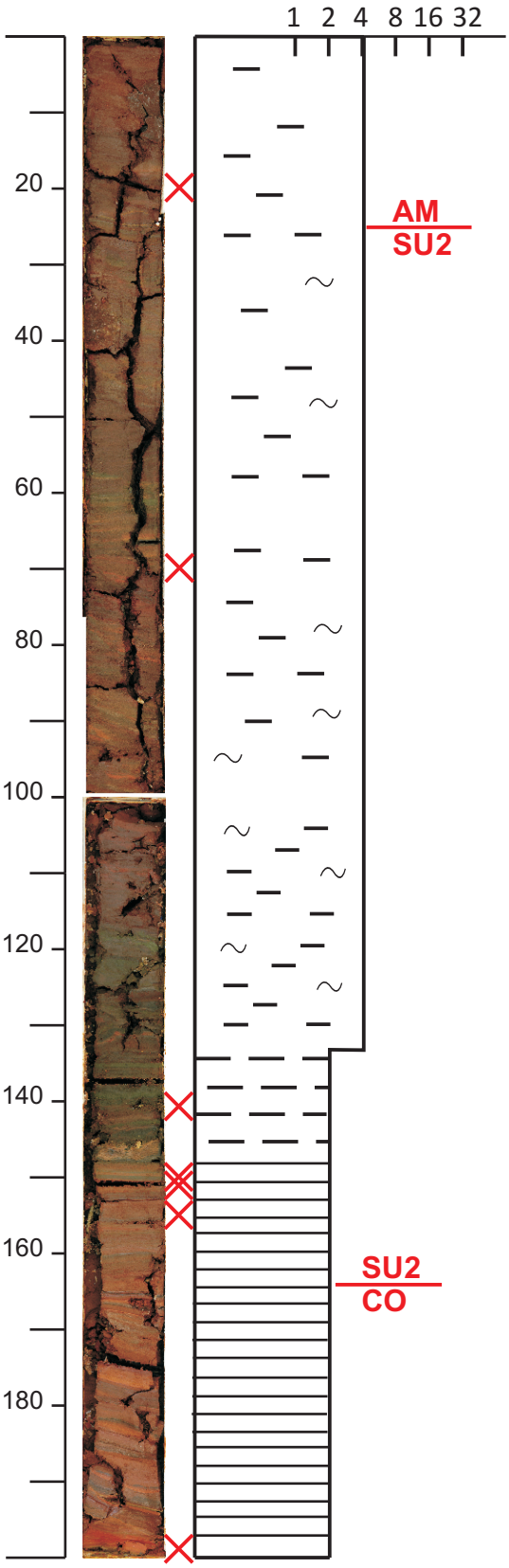
Core: Va29_354 KS page 3/3



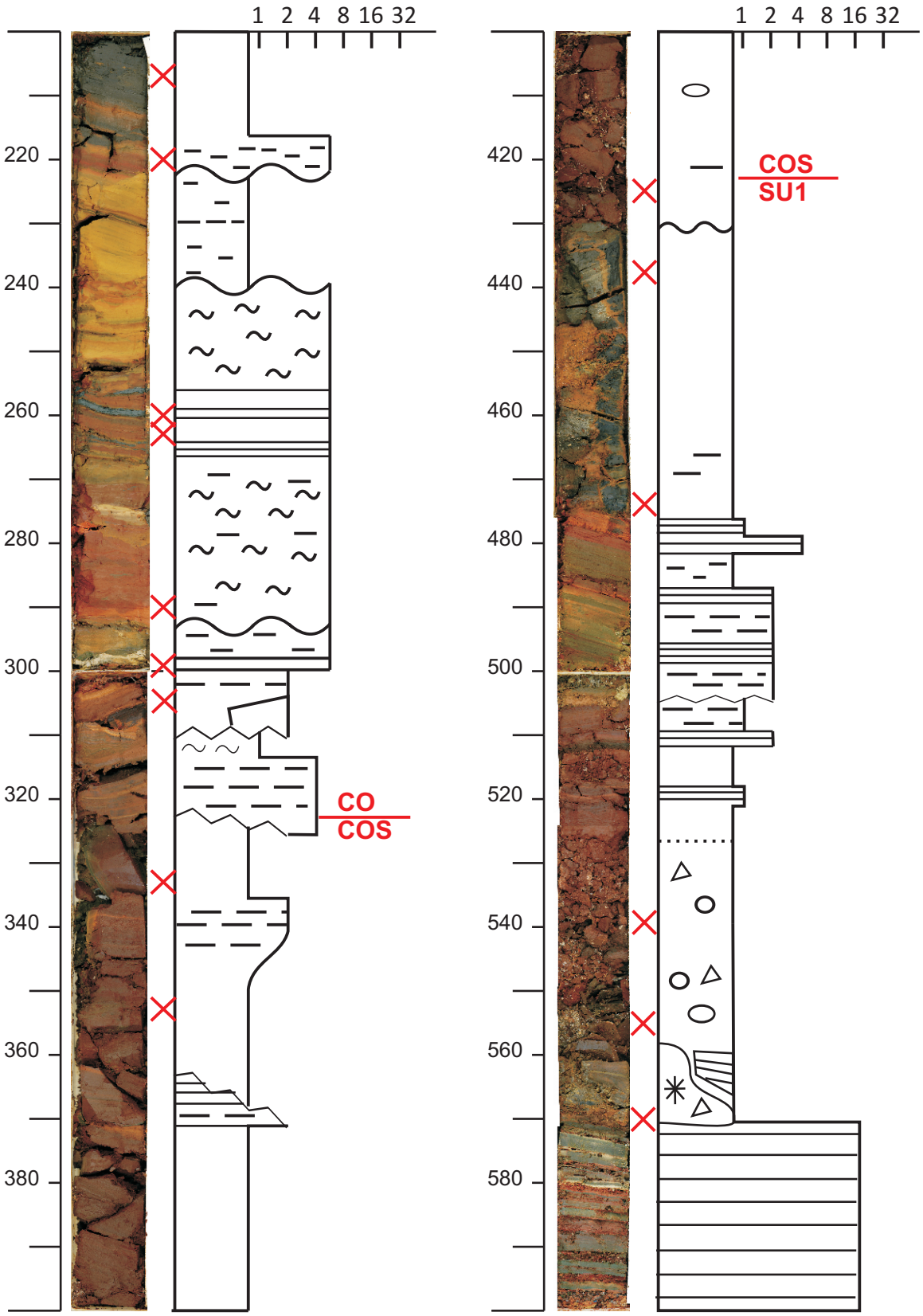
Appendix B.3.

Core: Va29_364 KS page 1/3
(N-Passage)
Water depth: 2091 m
Recovery: 7.40 m
Top loss: 3.89 m
Samples taken: 27

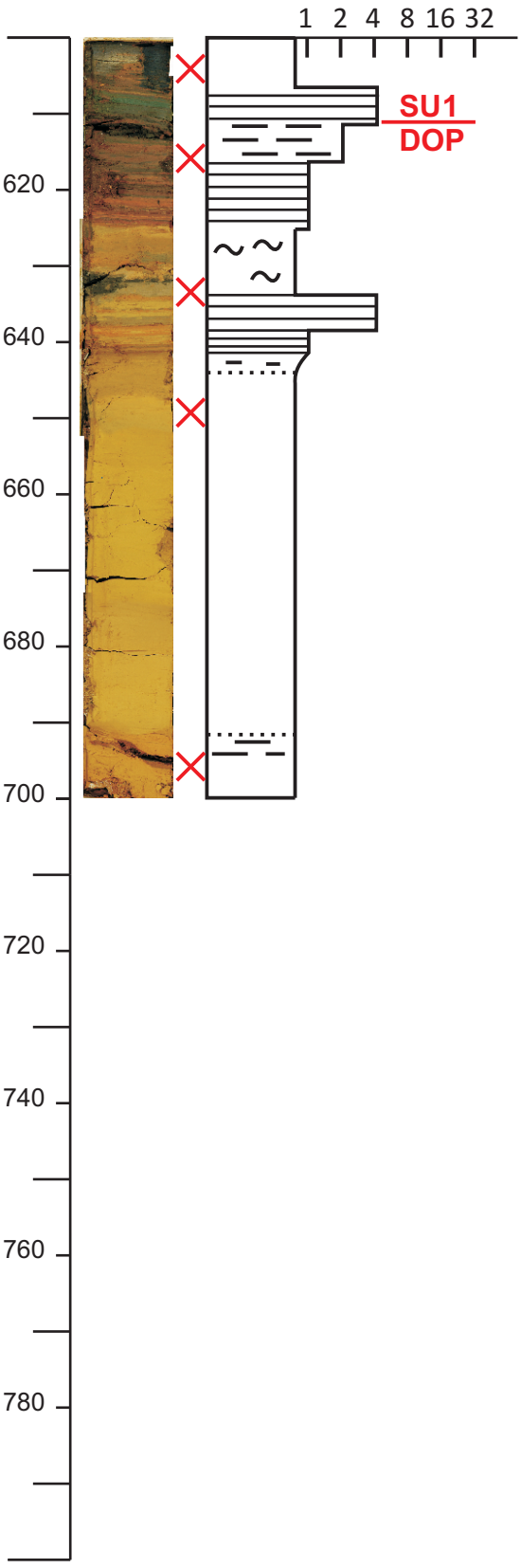


Core: Va29_364 KS page 2/3

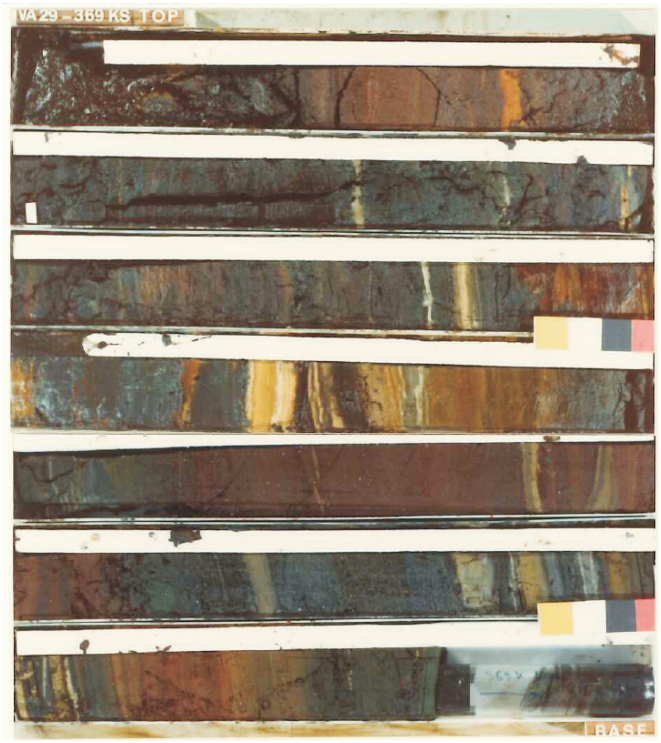


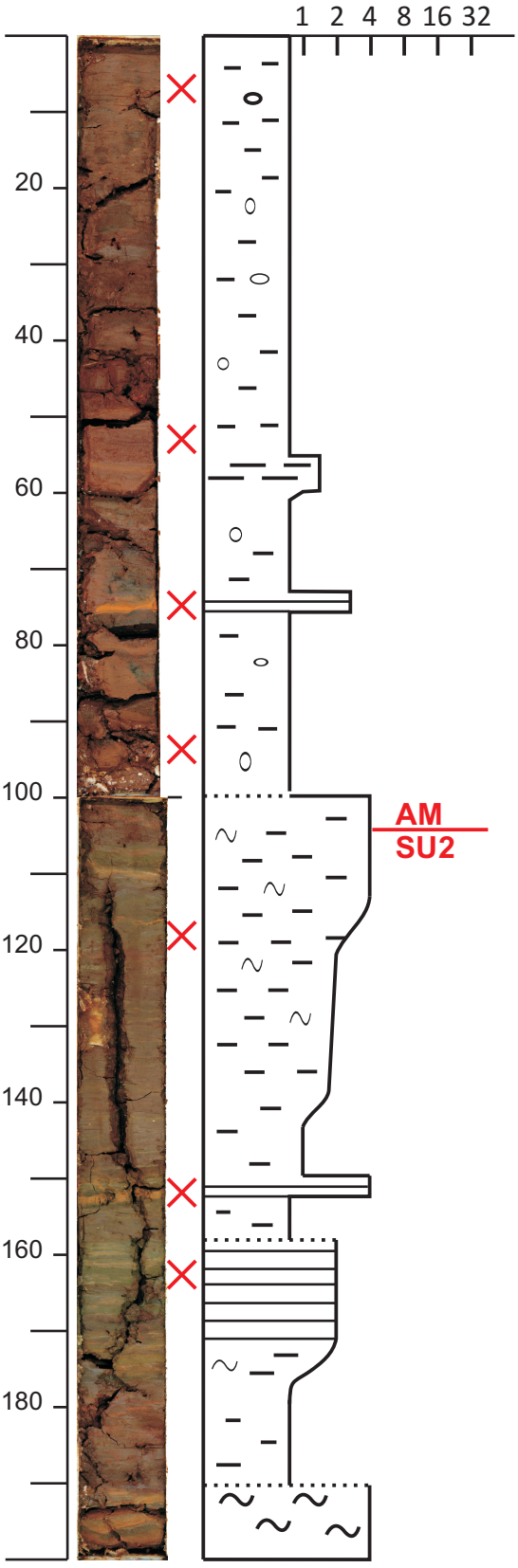
Core: Va29_364 KS  page 3/3



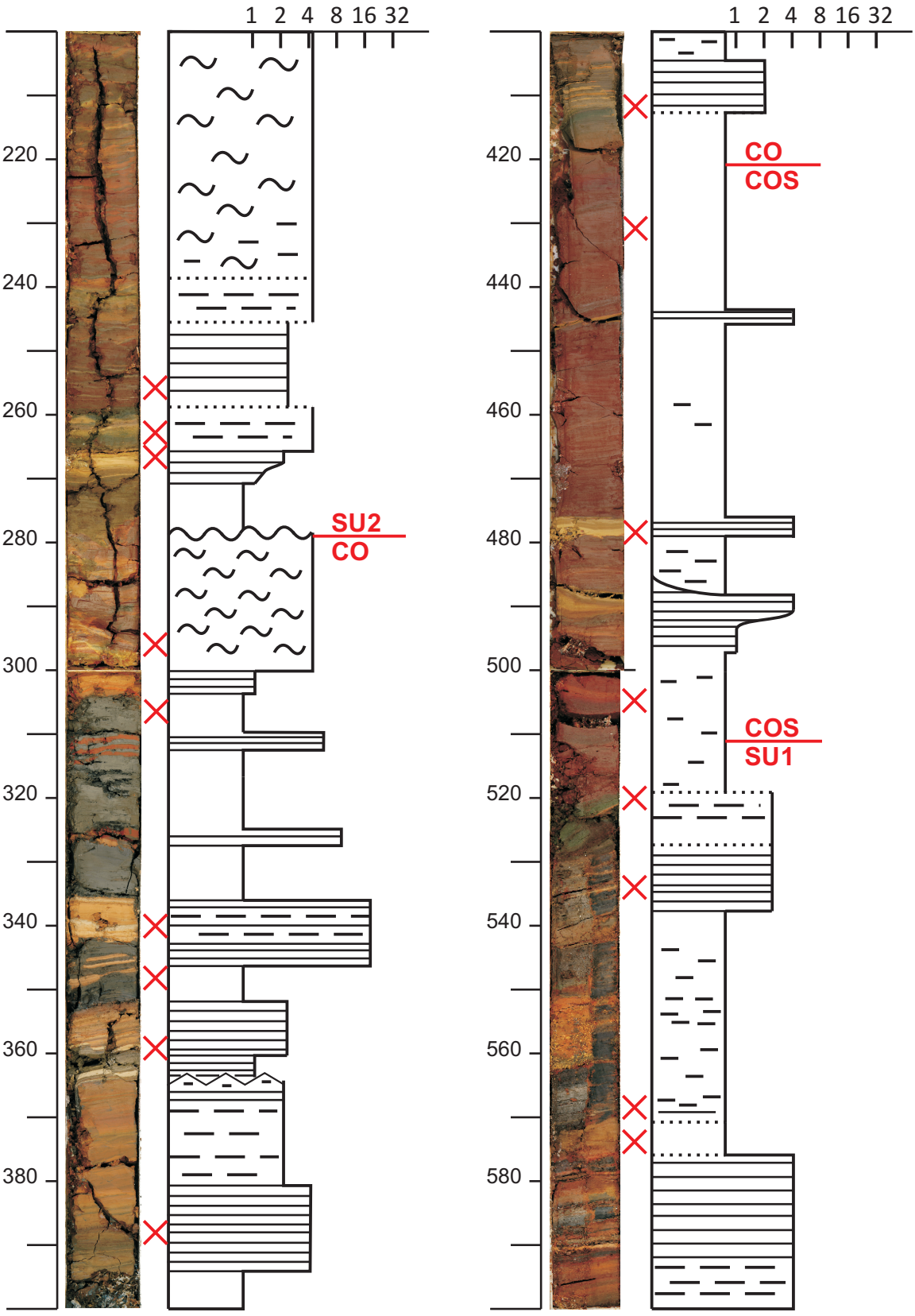
Appendix B.3.

Core: Va29_369 K  page 1/3
(N-Basin)
Water depth: 2093 m
Recovery: 6.83 m
Top loss: 2.24 m
Samples taken: 30

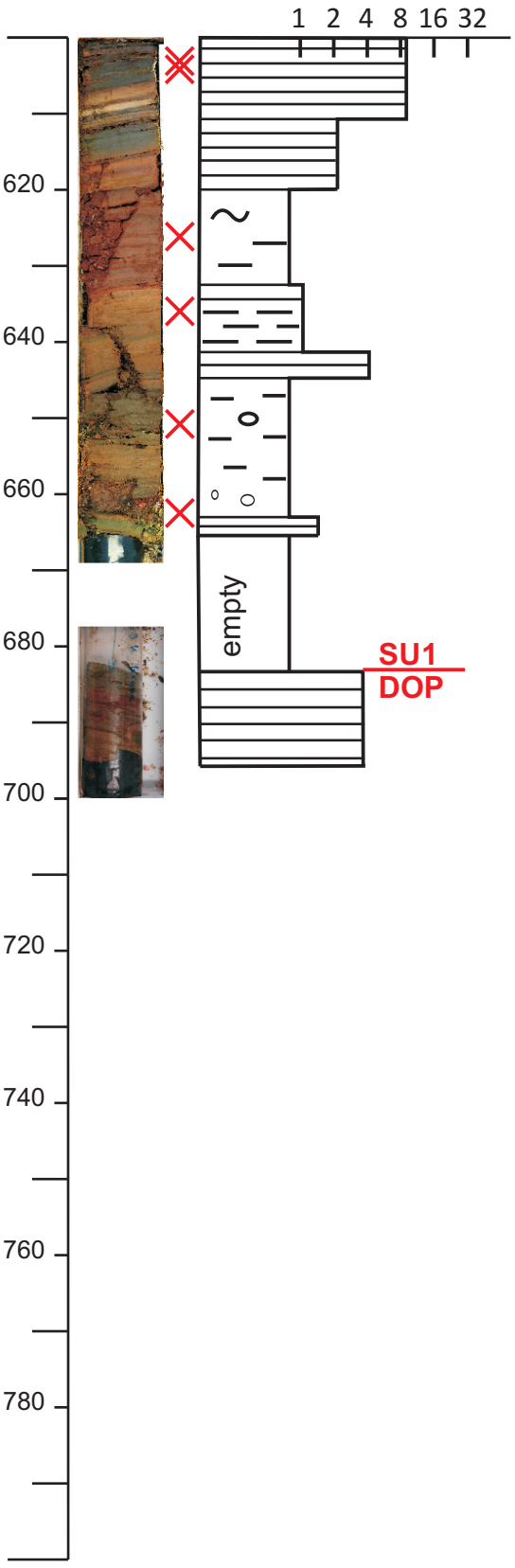


Core: Va29_369 KS page 2/3

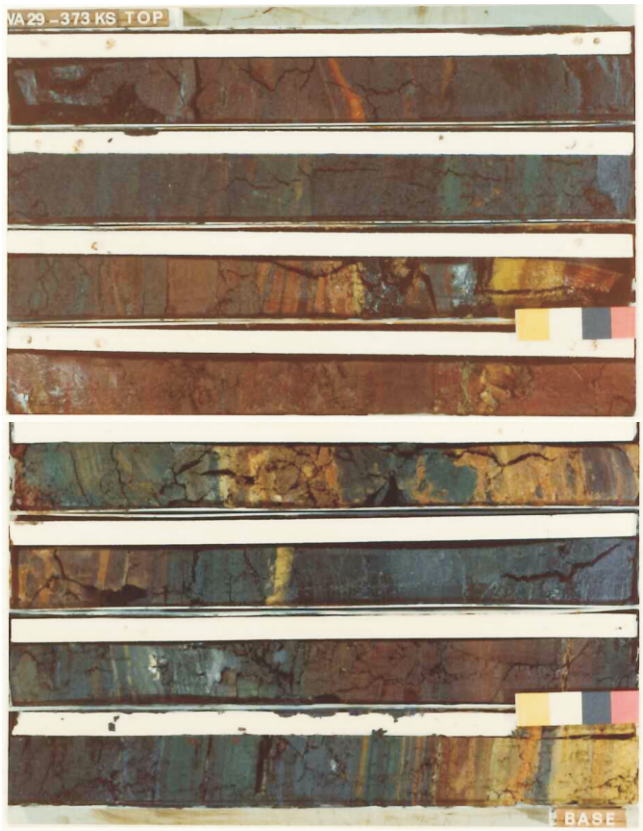


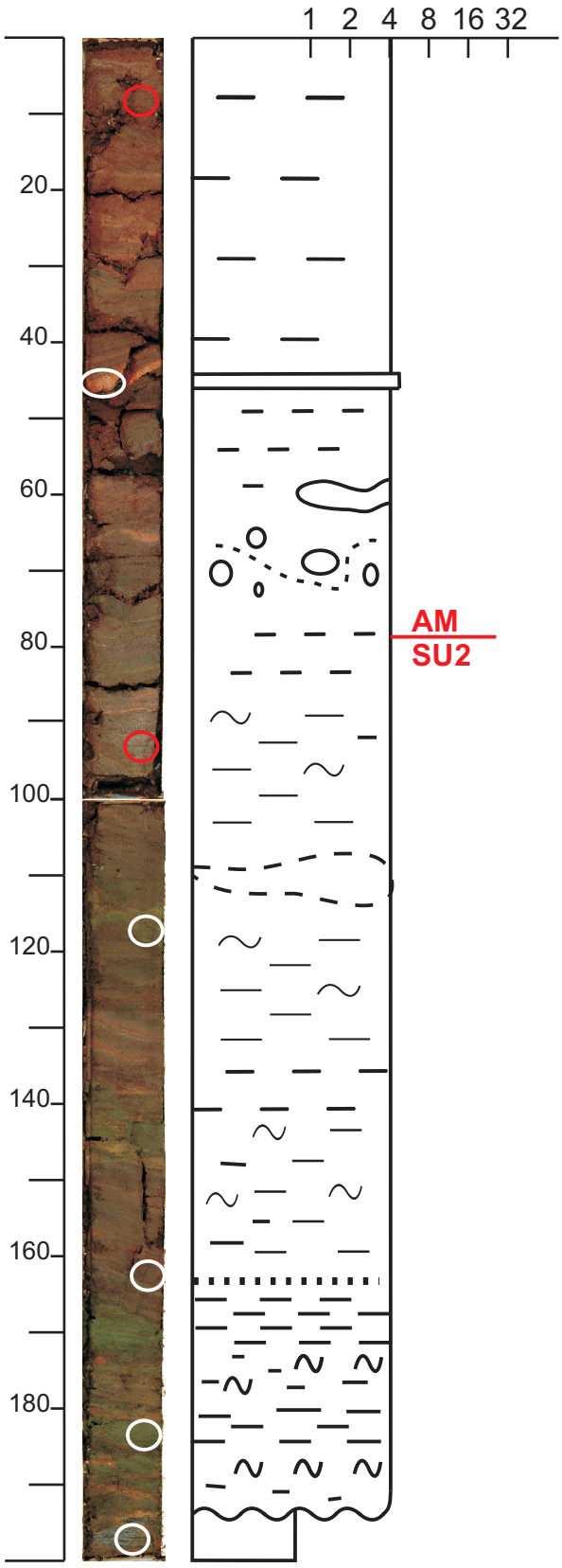
Core: Va29_369 KS page 3/3



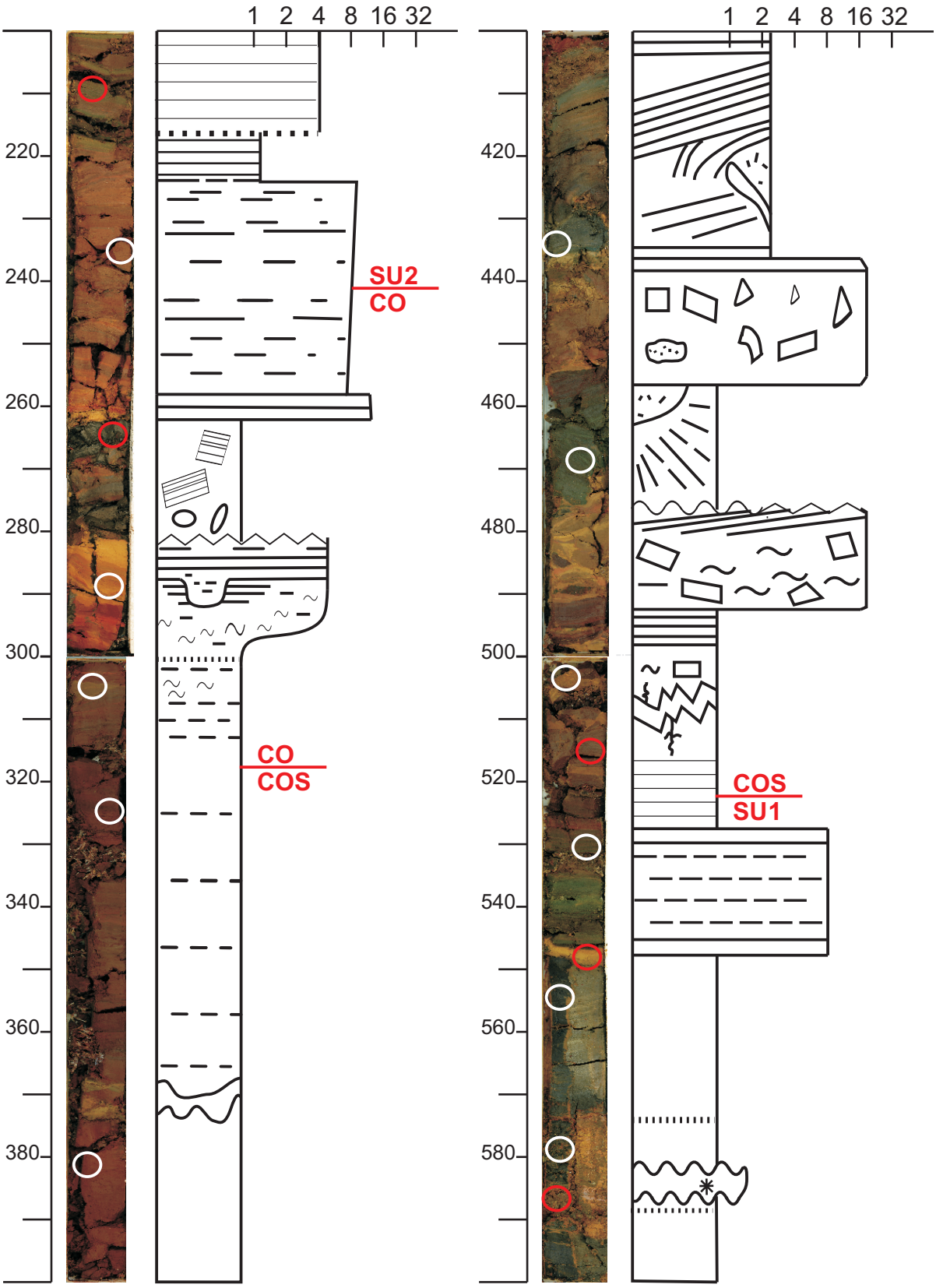
Appendix B.3.

Core: Va29_373 KS Page 1/3
(W-Basin)
Water depth: 2099 m
Recovery: 9.70 m
op loss: 2.31 m
Samples taken: 33

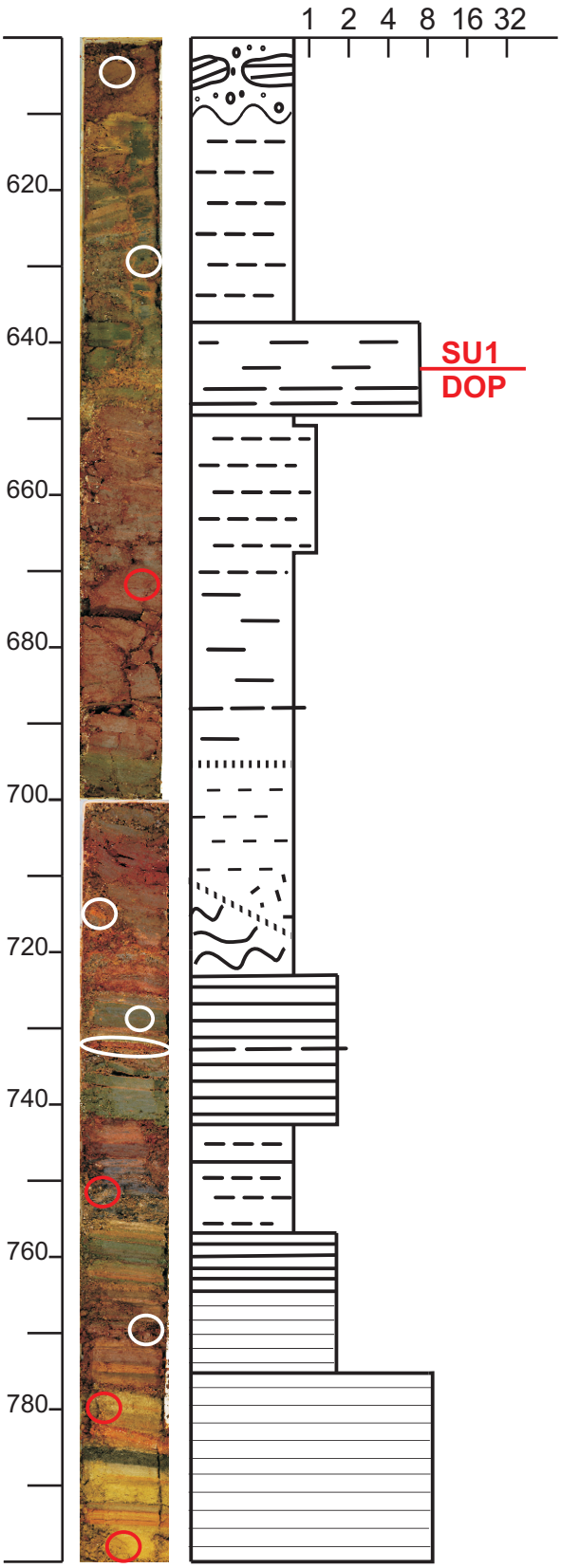


Core: Va29_373 KS page 2/3

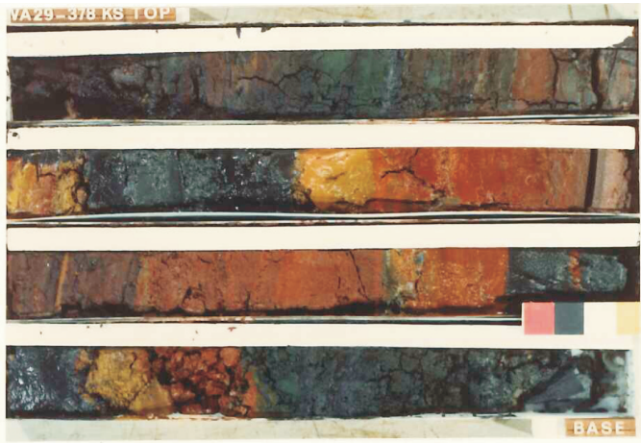


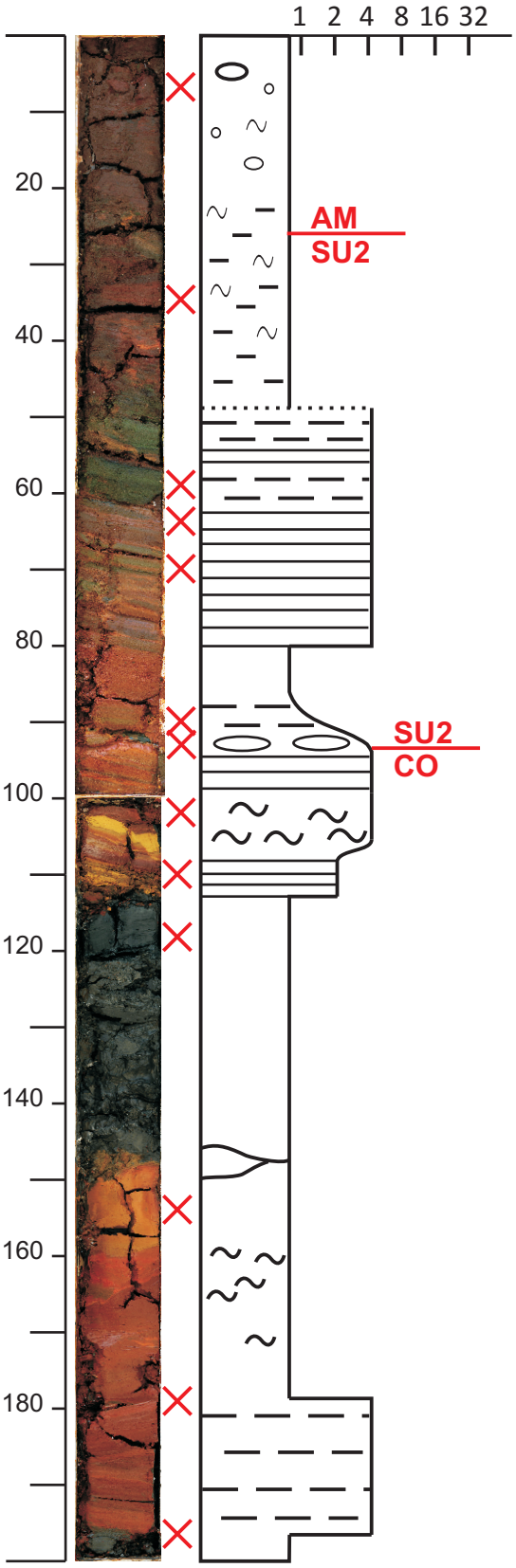
Core: Va29_373 KS  page 3/3



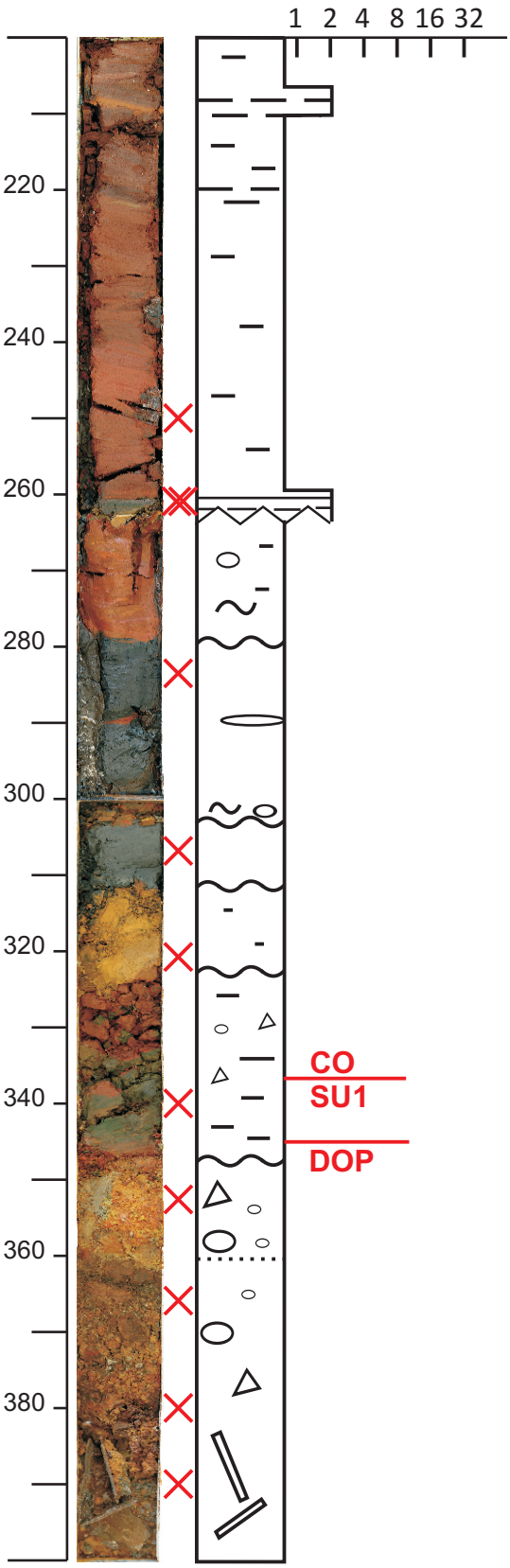
Appendix B.3.

Core: Va29_378 KS page 1/2
(W-Basin)
Water depth: 2112 m
Recovery: 4.41 m
Top loss: 2.85 m
Samples taken: 24



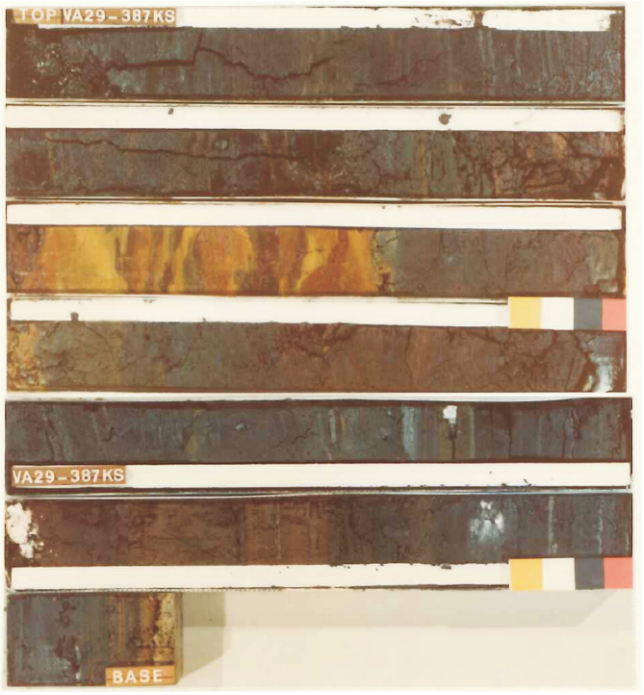



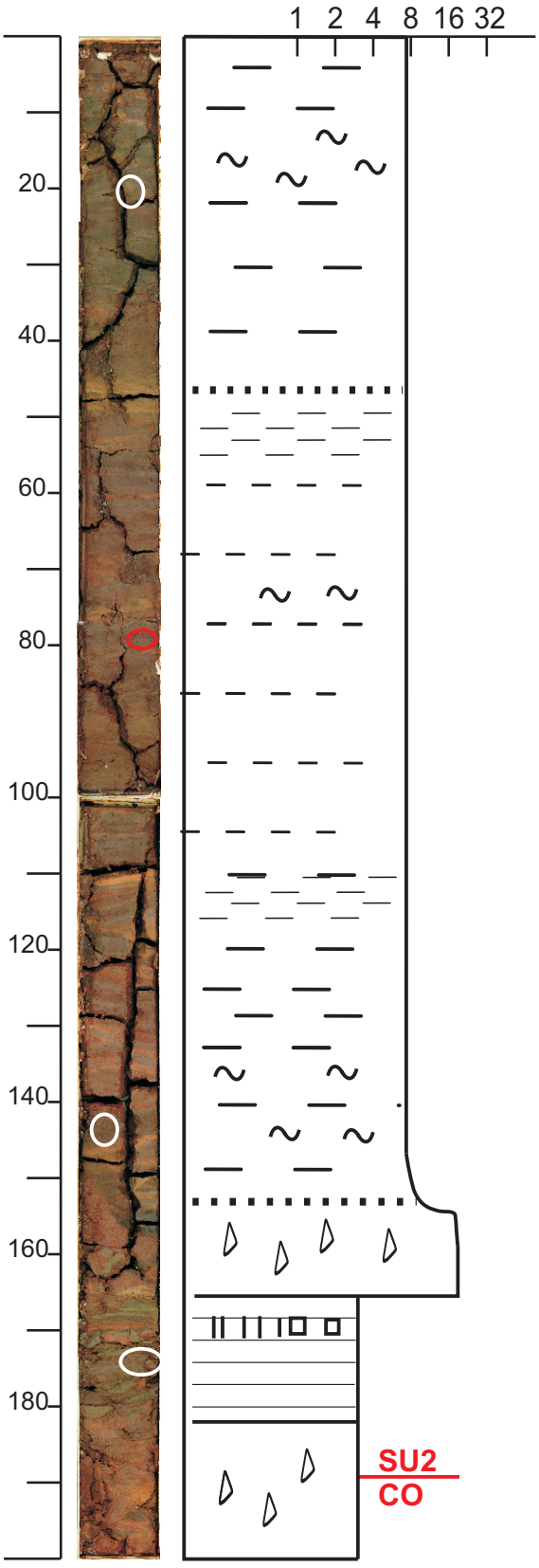
Core: Va29_378 KS page 2/2



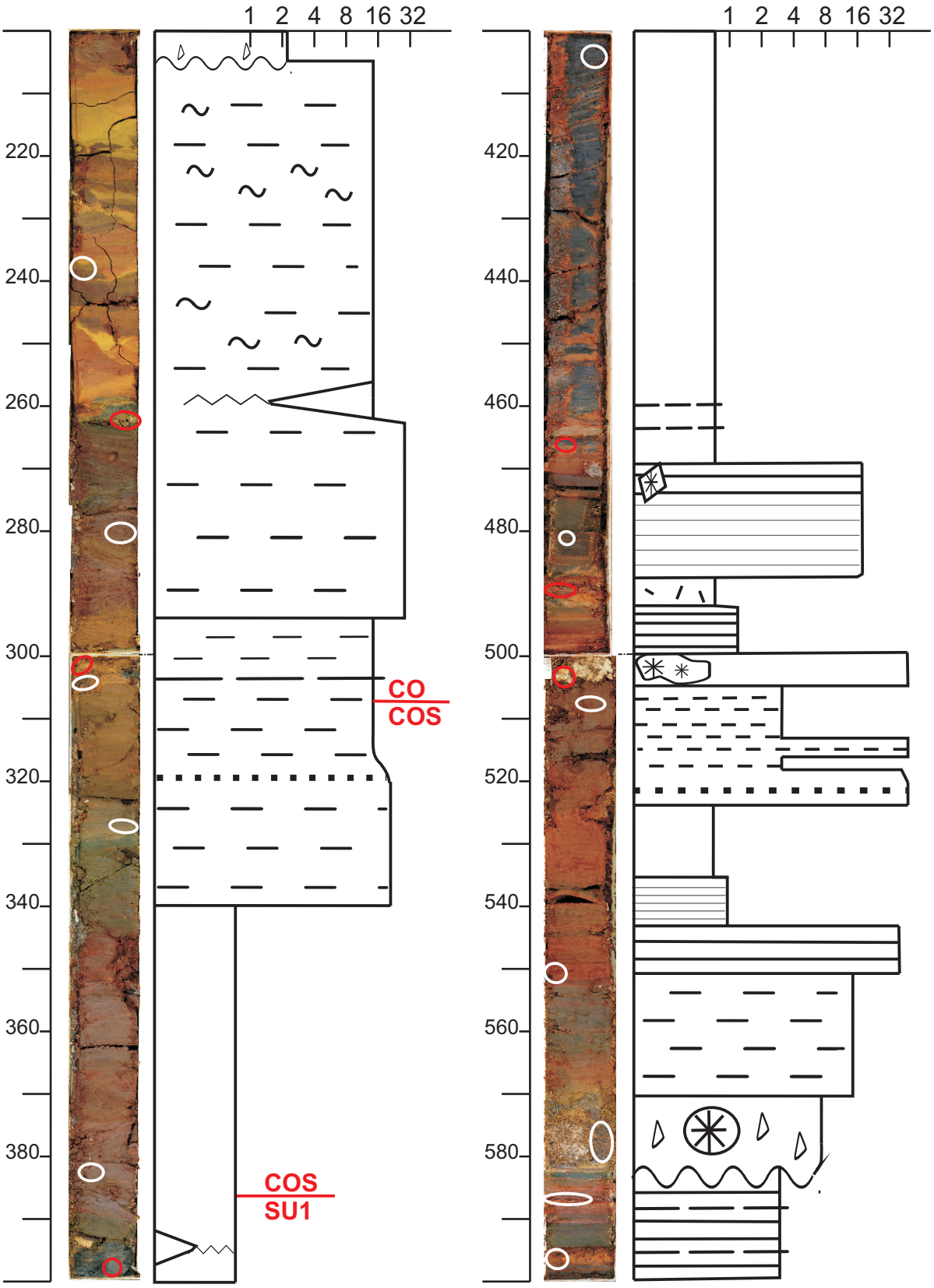
Appendix B.3.

Core: Va29_387 KS page 1/2
(N-Passage)
Water depth: 2110 m
Recovery: 8.24 m
Top loss: 3.77 m
Samples taken: 22



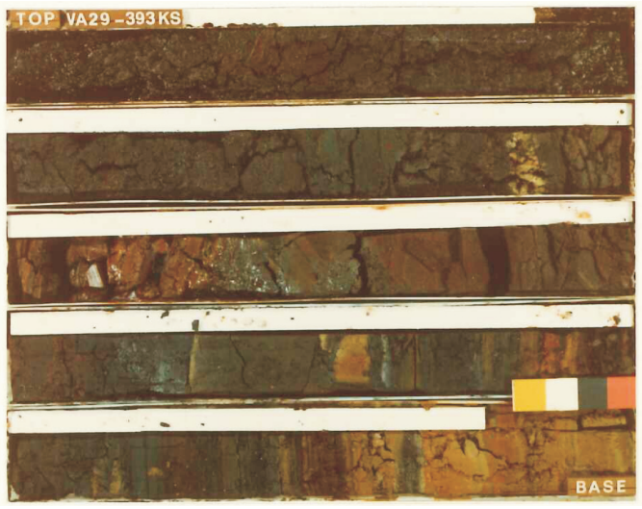



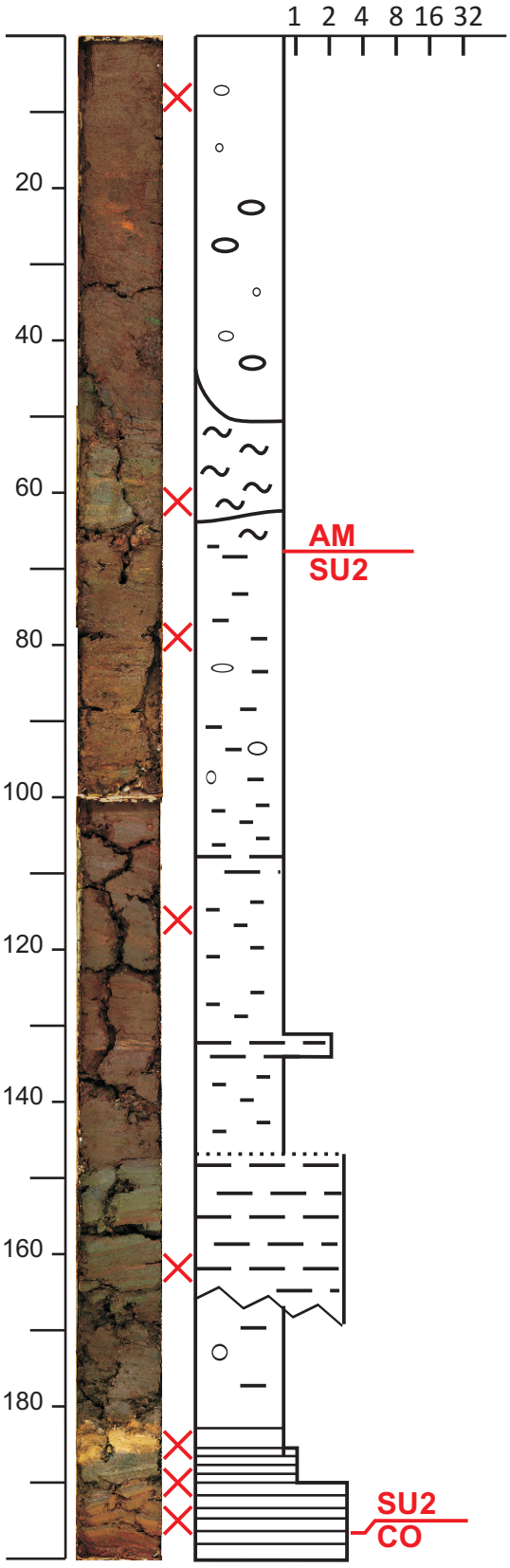
Core: Va29_387KS page 2/2



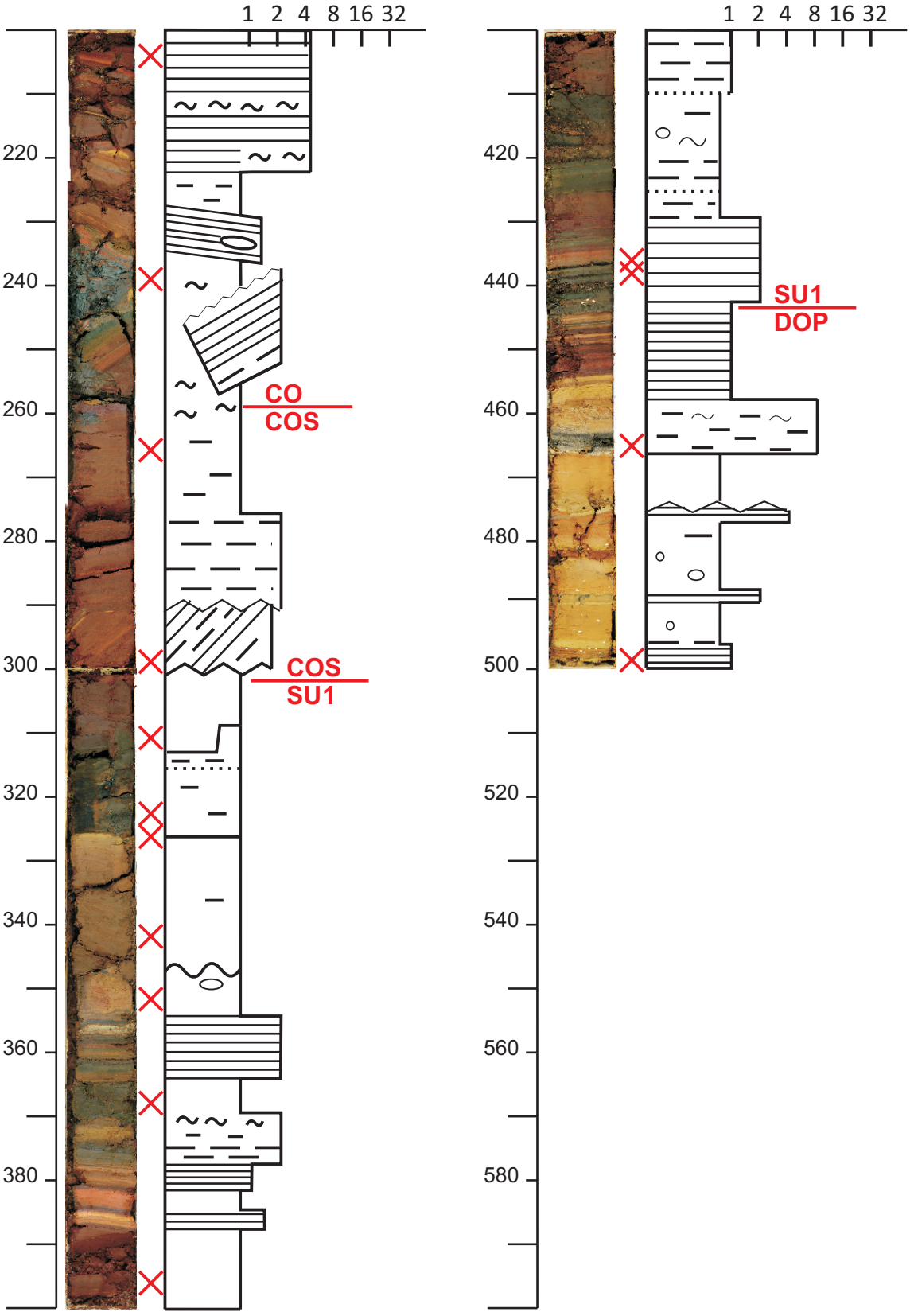
Appendix B.3.

Core: Va29_393 KS page 1 /2
(N-Passage)
Water depth: 2061 m
Recovery: 9.09 m
Top loss: 2.38 m
Samples taken: 23



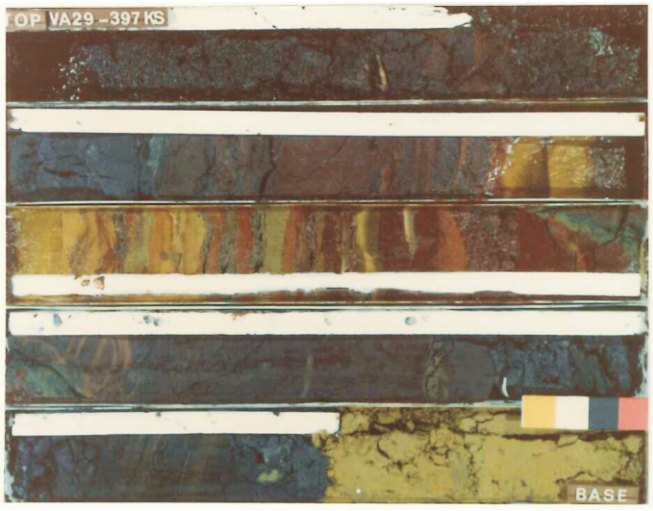



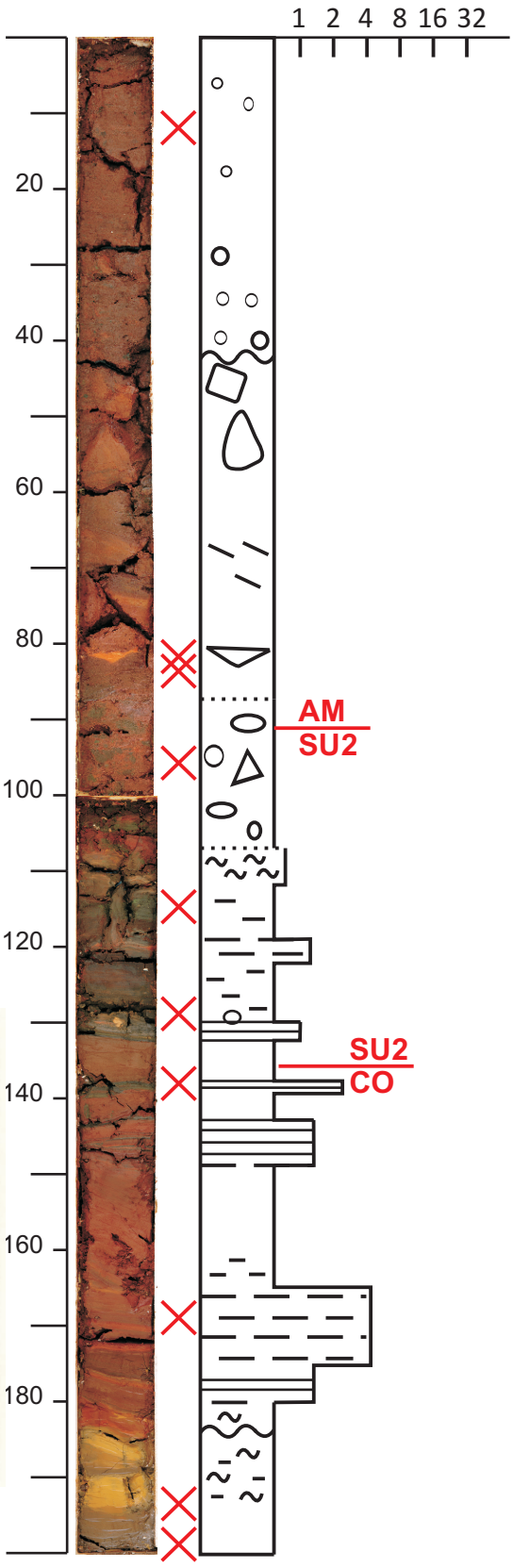
Core: Va29_393 KS  page 2/2



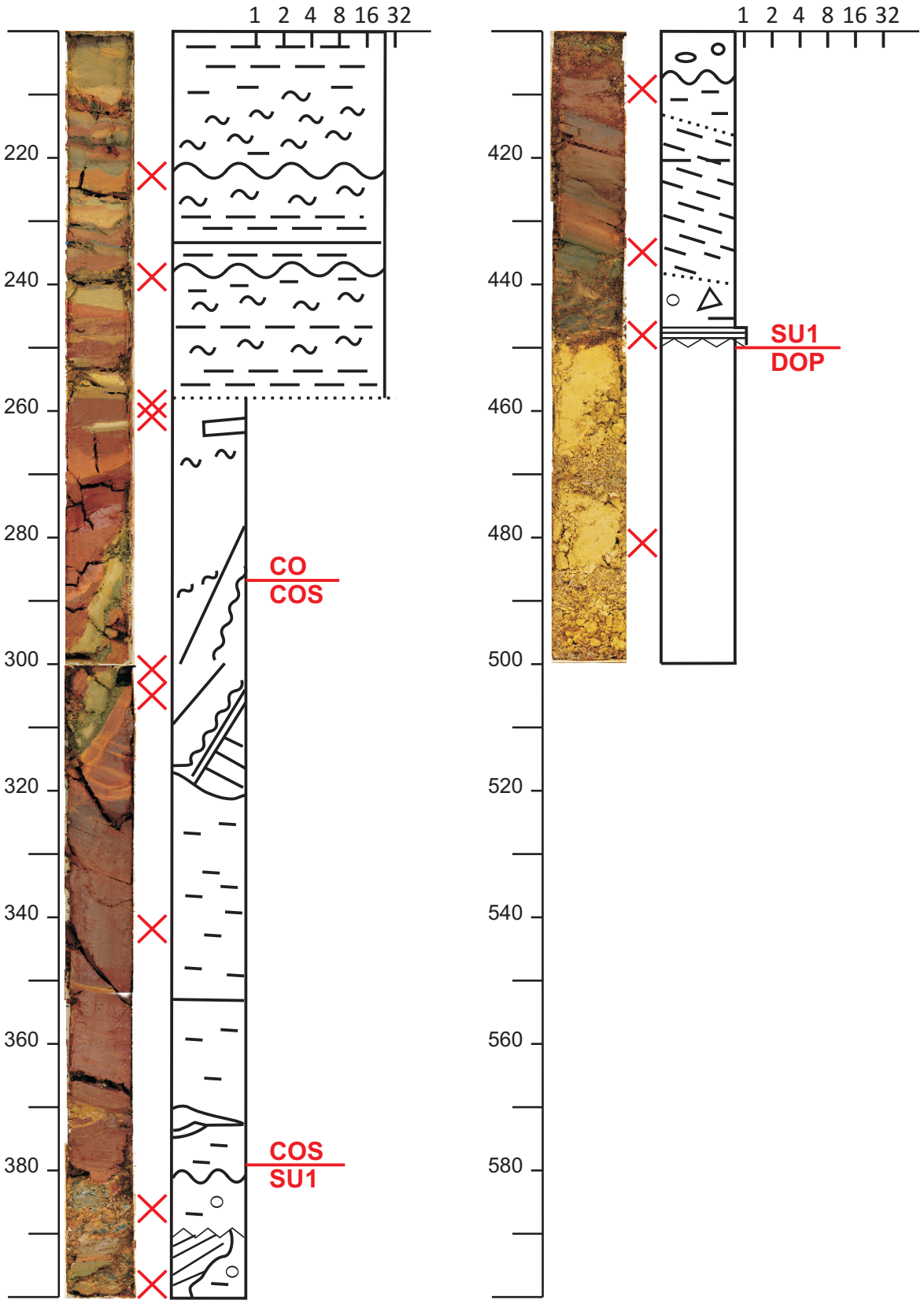
Appendix B.3.

Core: Va29_397 KS page 1 /2
(N-Basin)
Water depth: 2097 m
Recovery: 6.20 m
Top loss: 1.76 m
Samples taken: 22



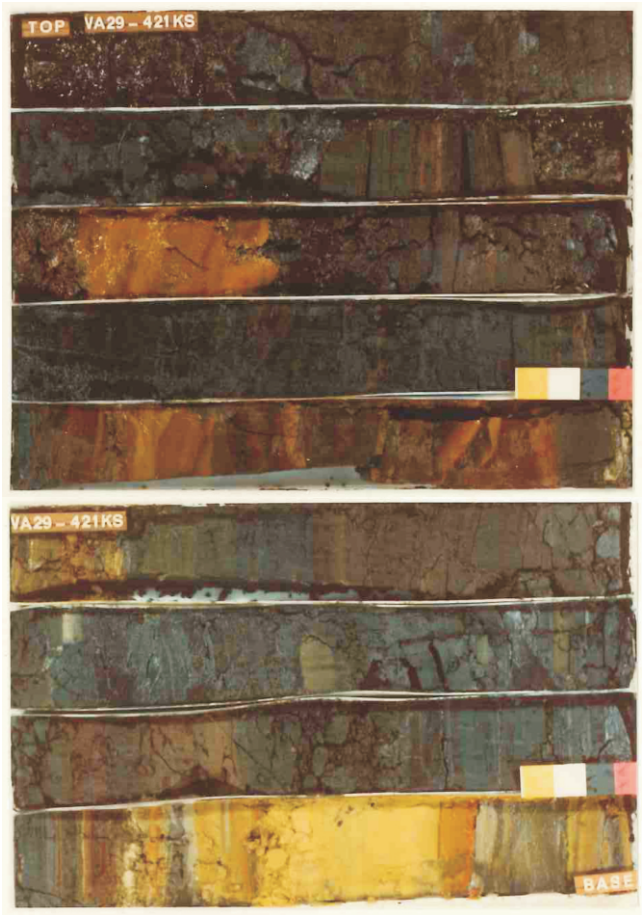



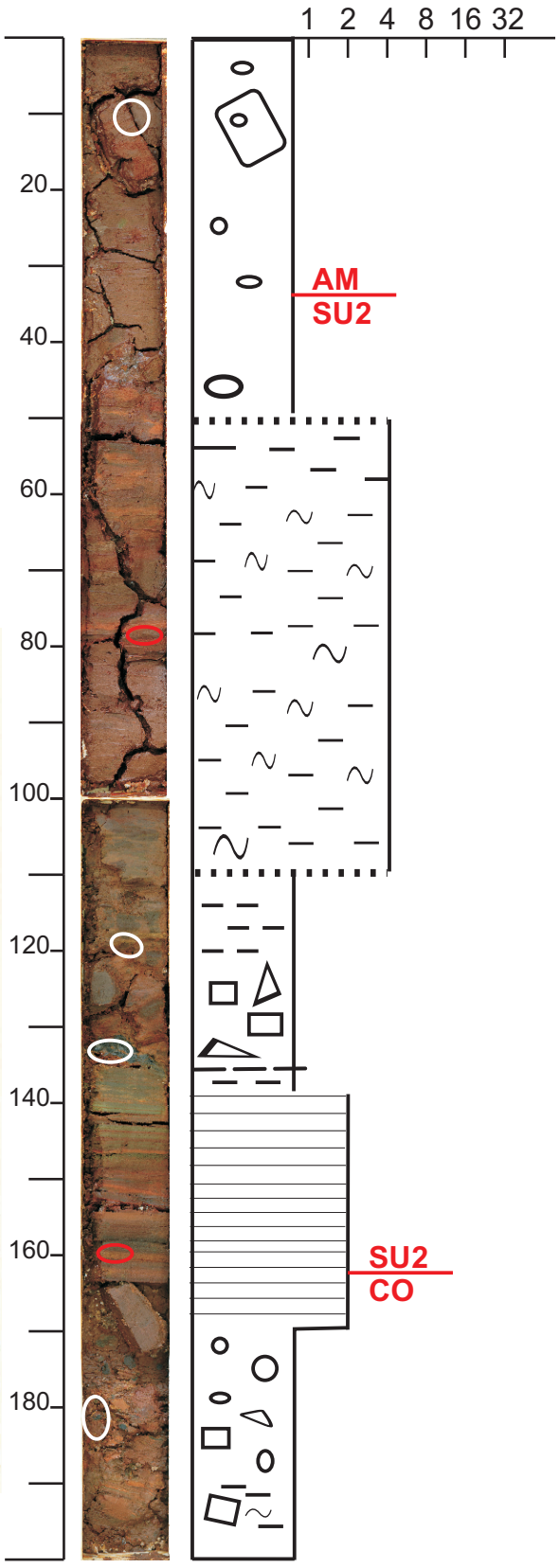
Core: Va29_397 KS page 2/2



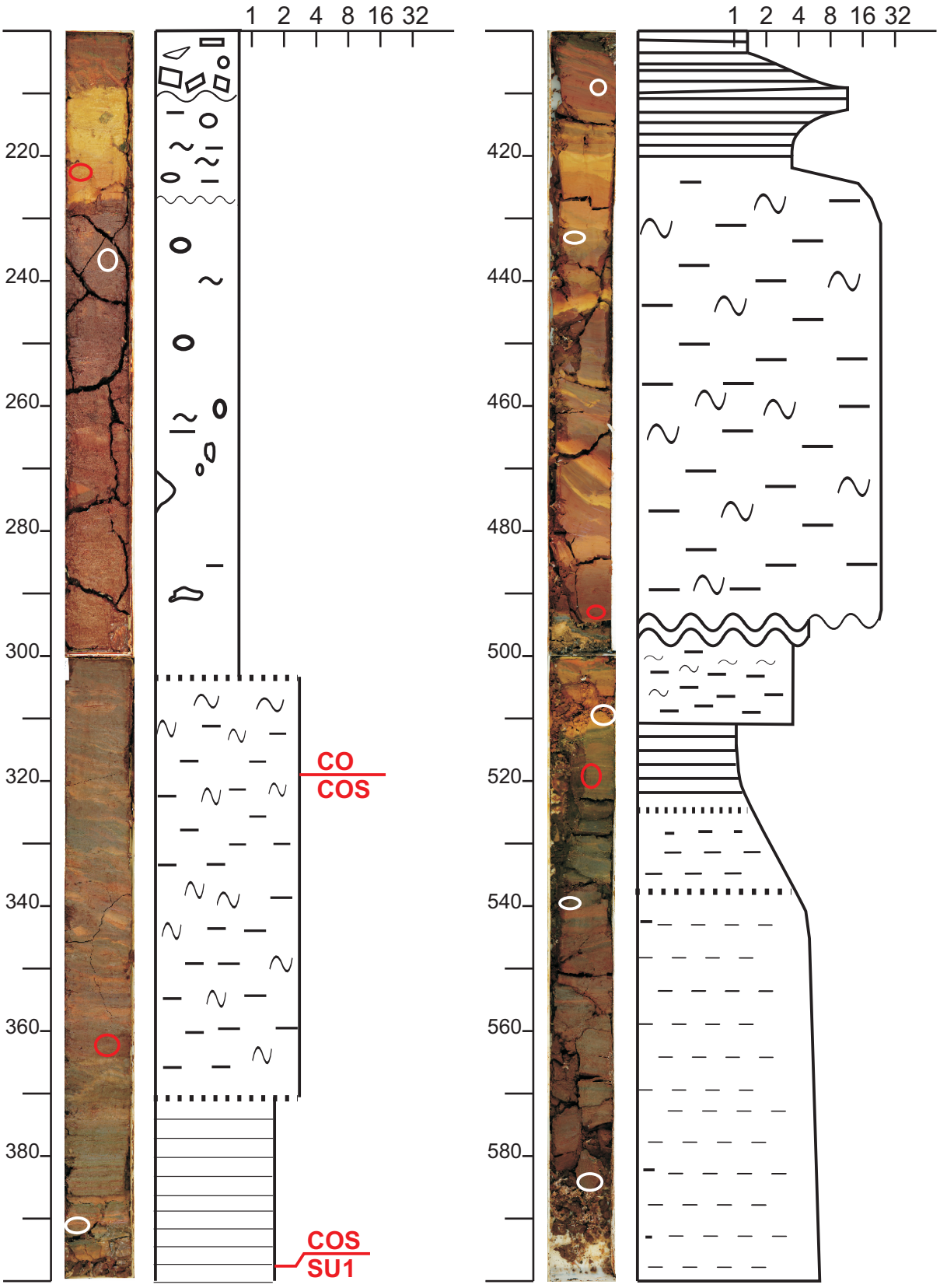
Appendix B.3.

Core: Va29_421 KS
page 1/3
(E-Basin)
Water depth: 2106 m
Recovery: 7.85 m
Top loss: 3.04 m
Samples taken: 45

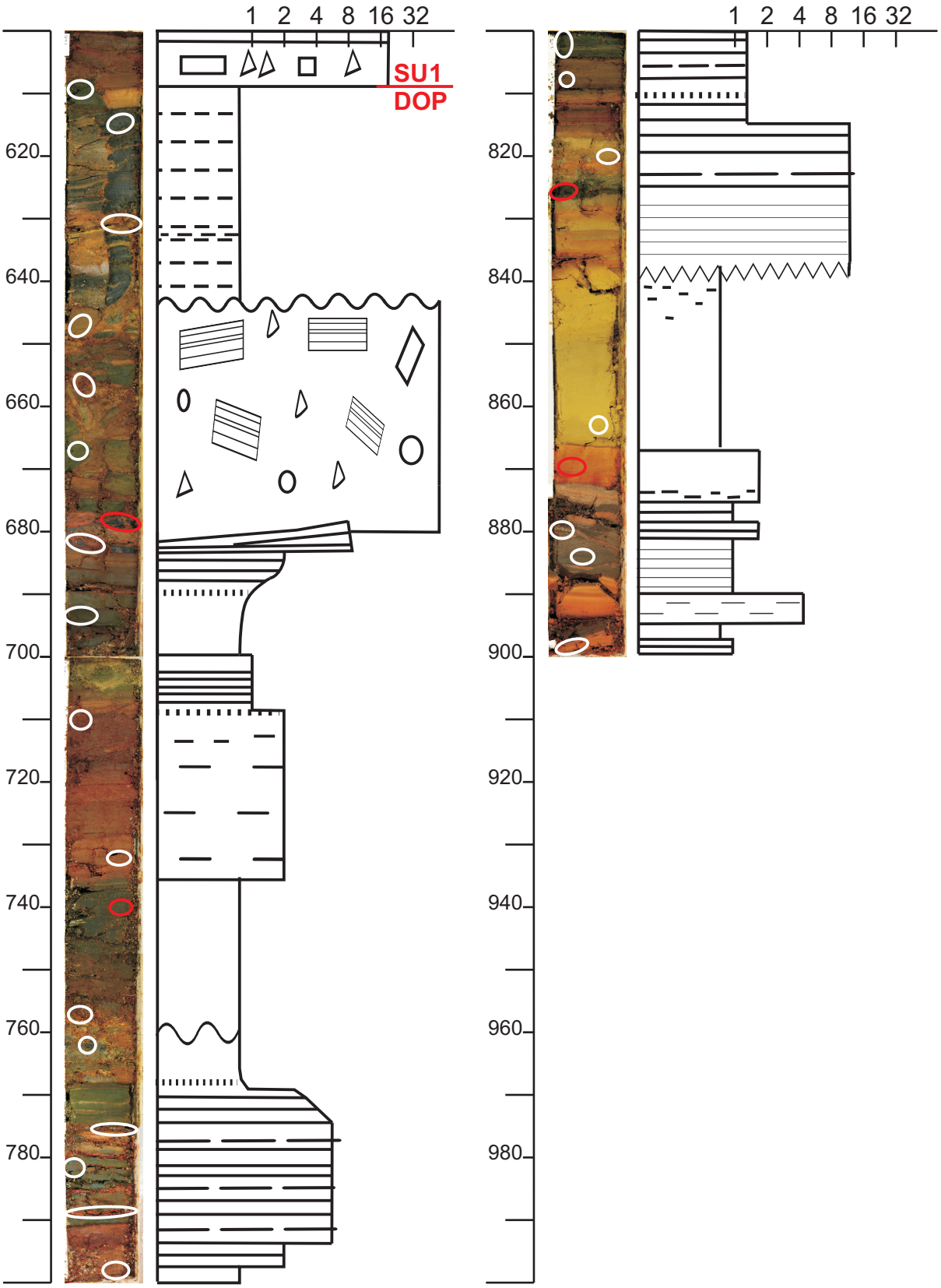


Core: Va29_421 KS page 2/3



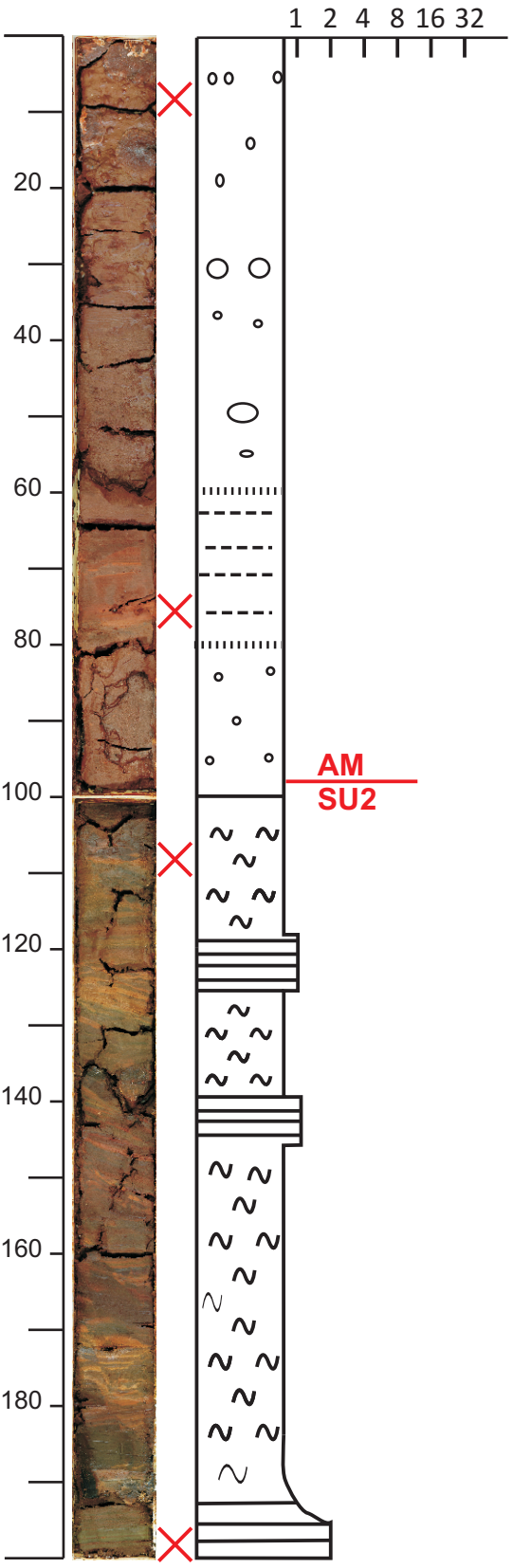
Core: Va29_421 KS page 3/3



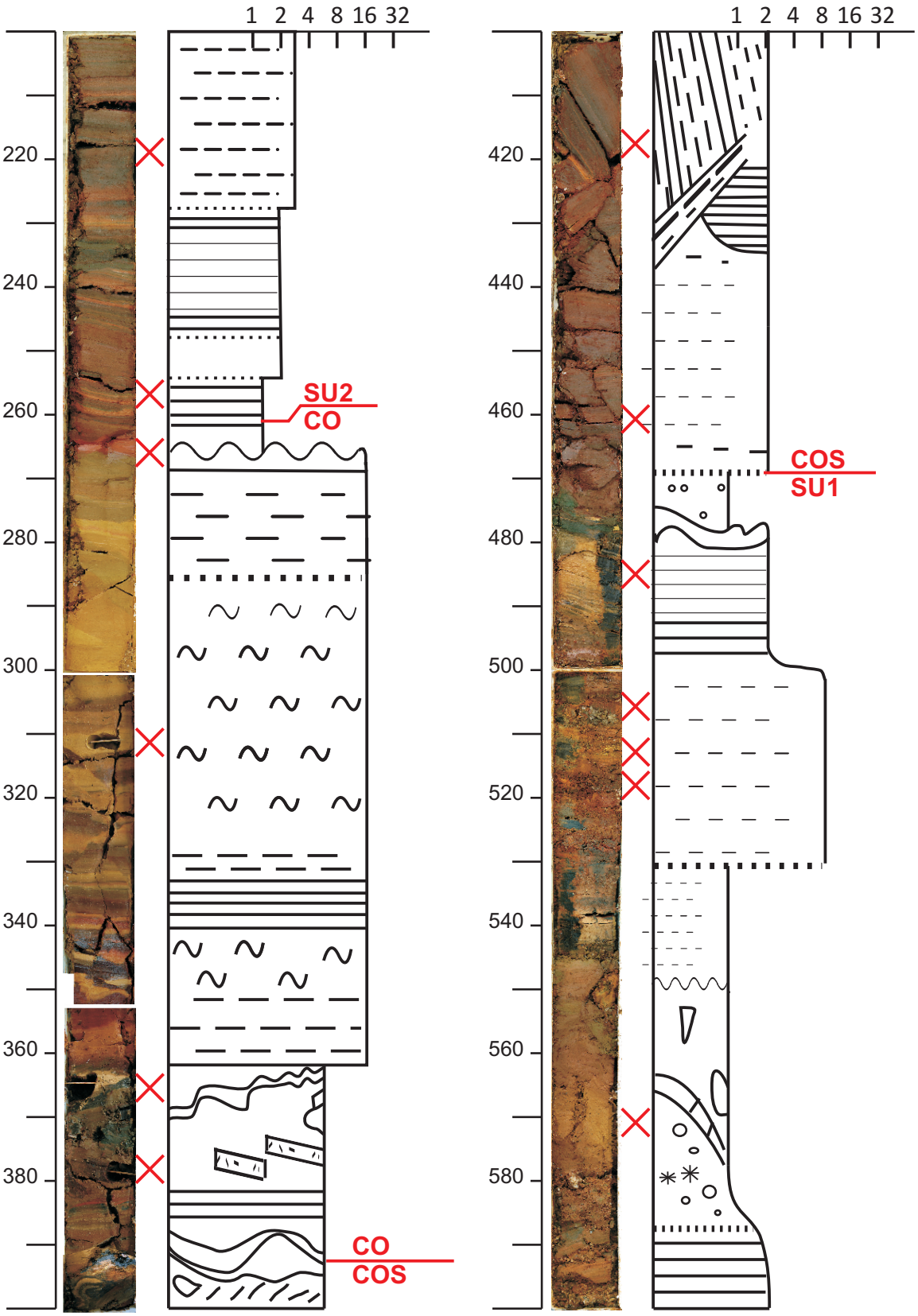
Appendix B.3.

Core: Va29_423 KS page 1/3
(E-Basin)
Water depth: 2117 m
Recovery: 9.80 m
Top loss: 2.28 m
Samples taken: 28

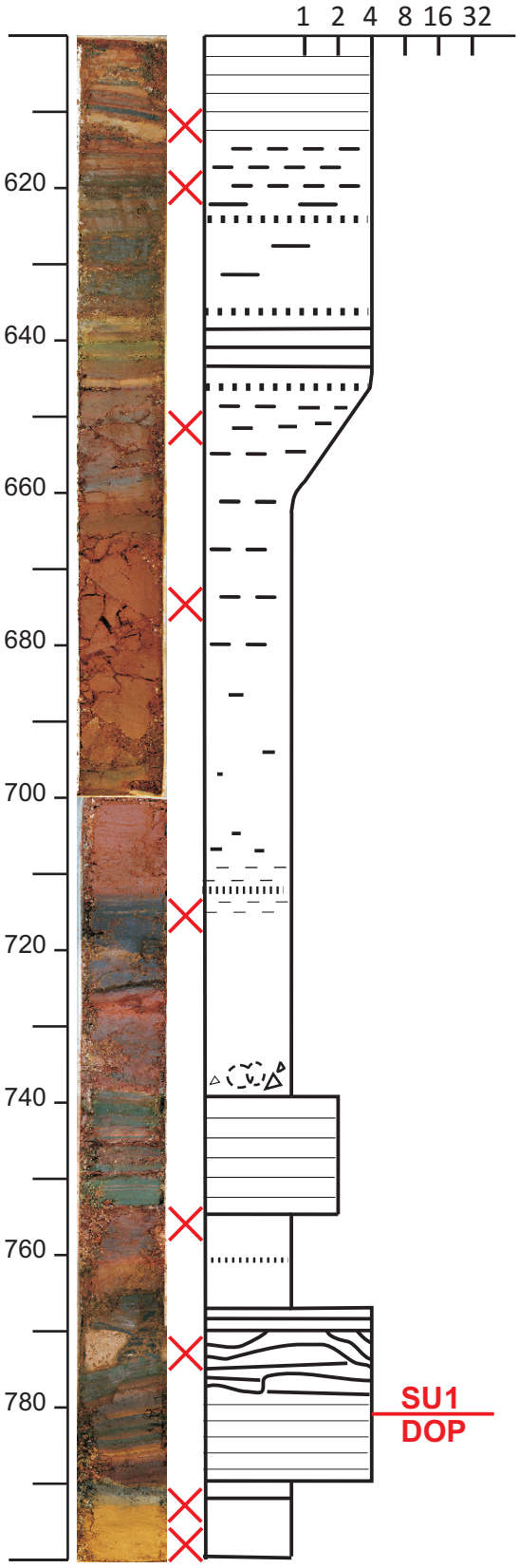


Core: Va29_423 KS page 2/3

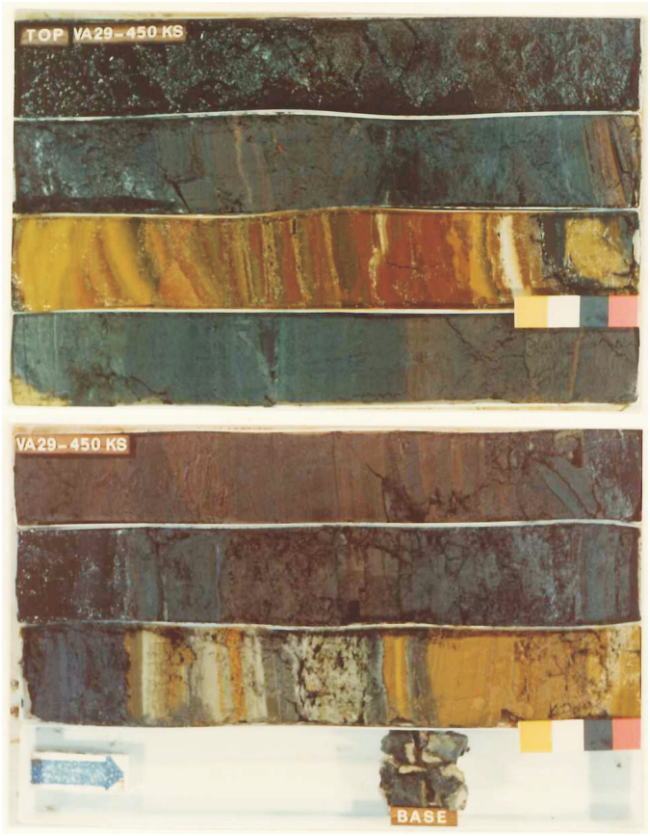


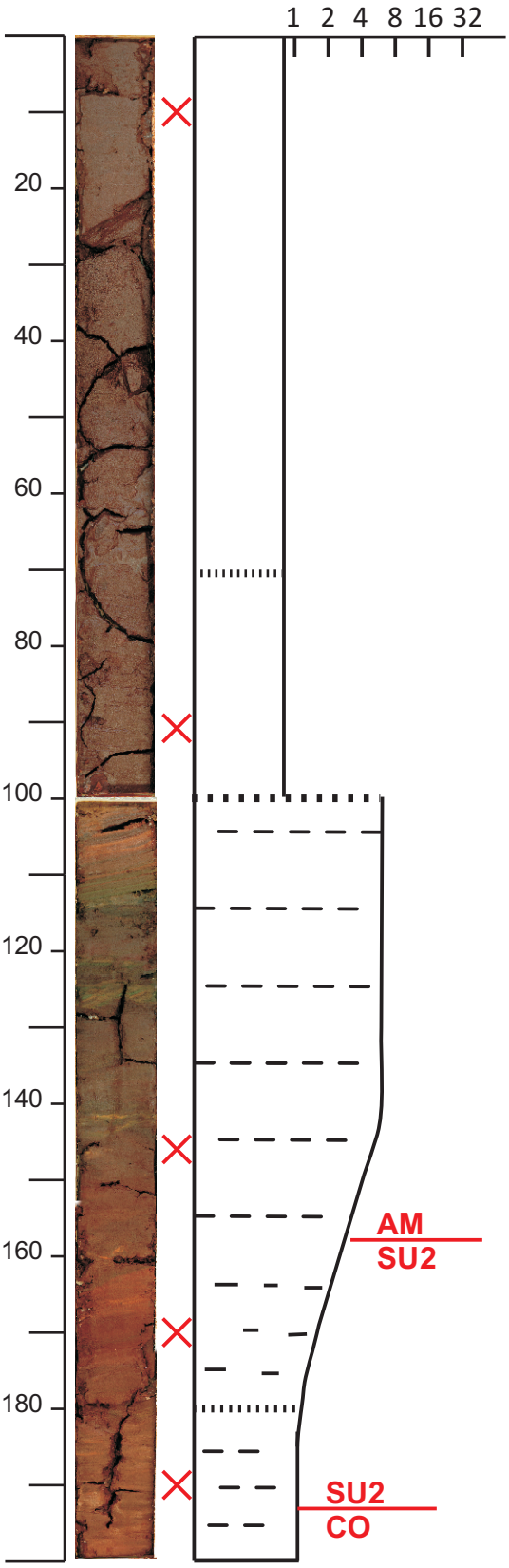
Core: Va29_423 KS page 3/3



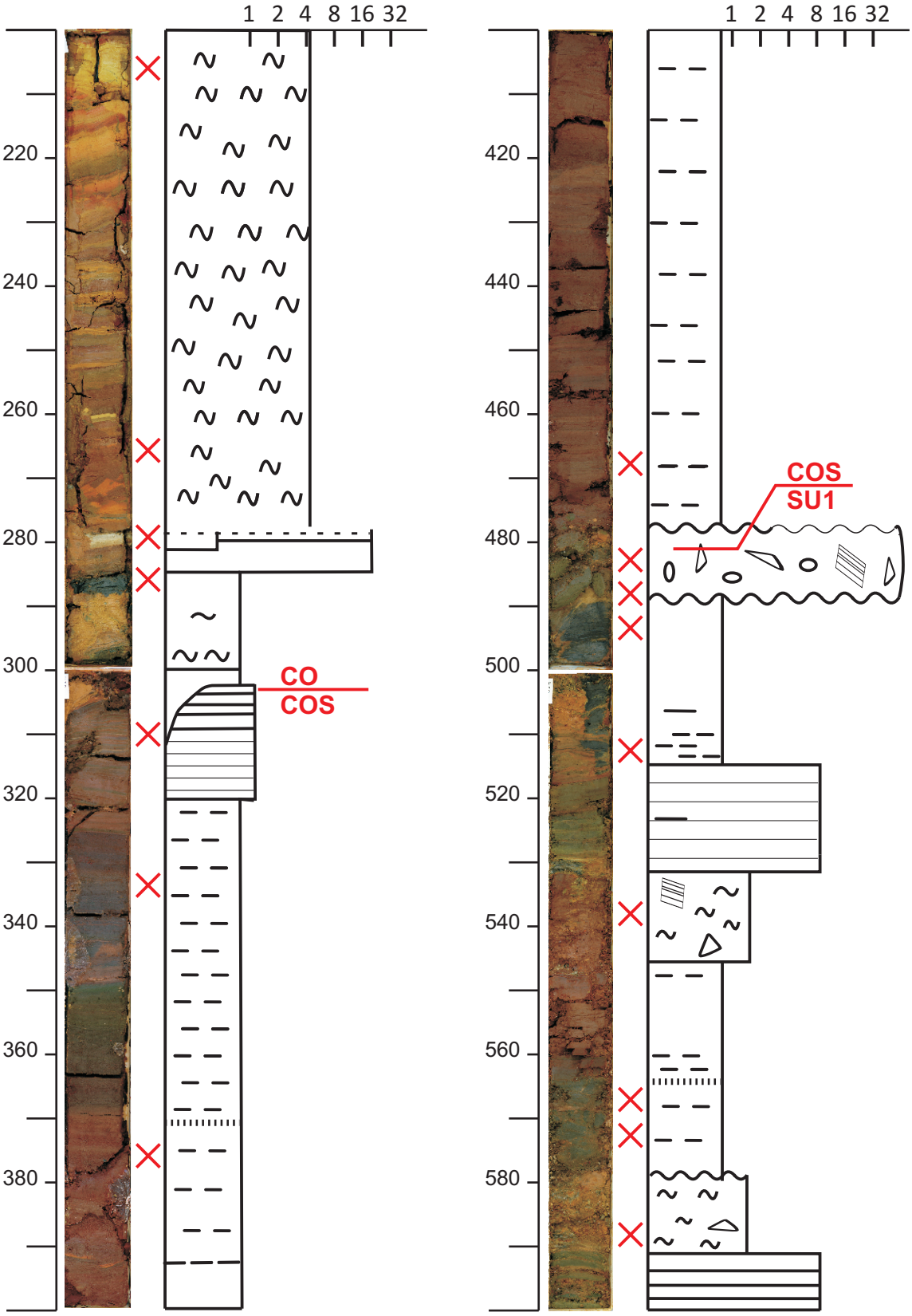
Appendix B.3.

Core: Va29_450 KS page 1/3
(W-Basin)
Water depth: 2097 m
Recovery: 7.60 m
Top loss: 0.42 m
Samples taken: 24

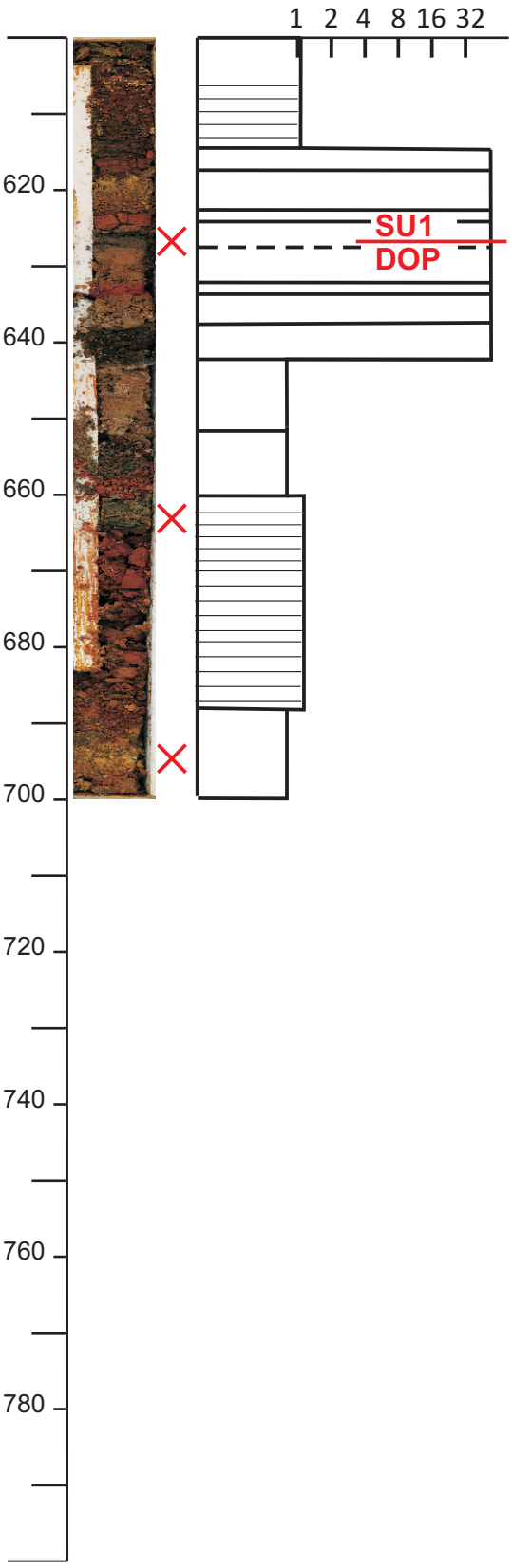


Core: Va29_450 KS page 2/3

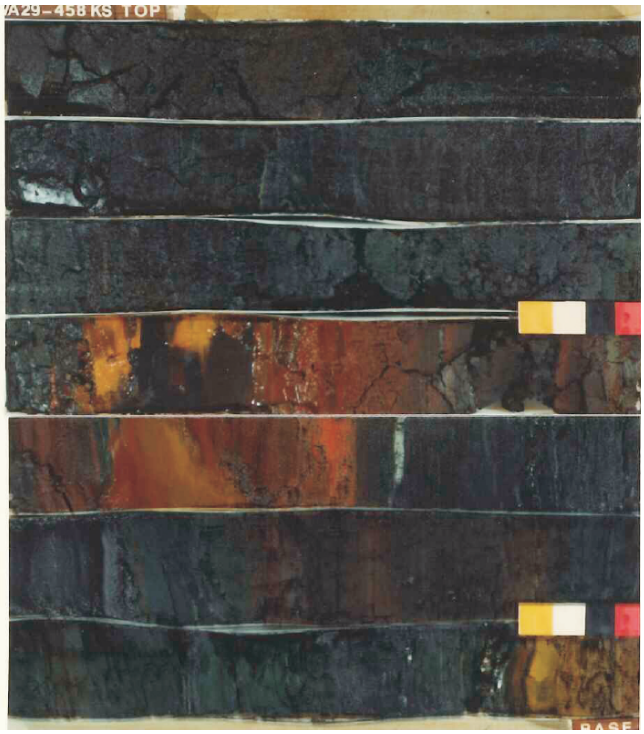


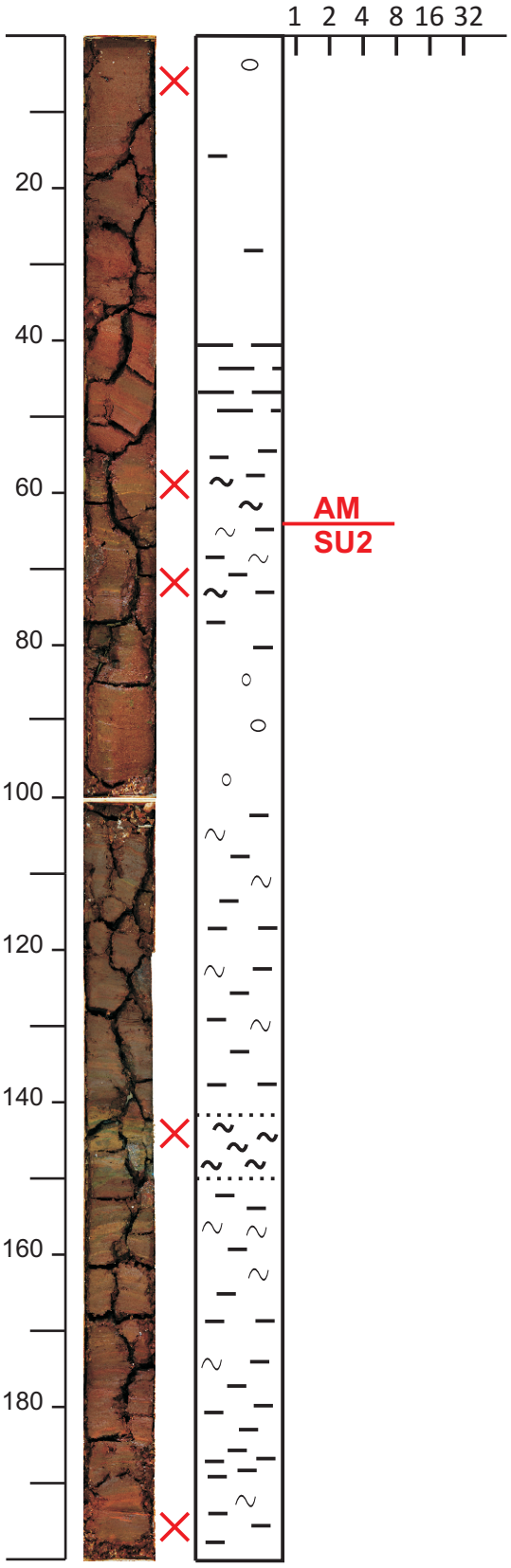
Core: Va29_450 KS page 3/3



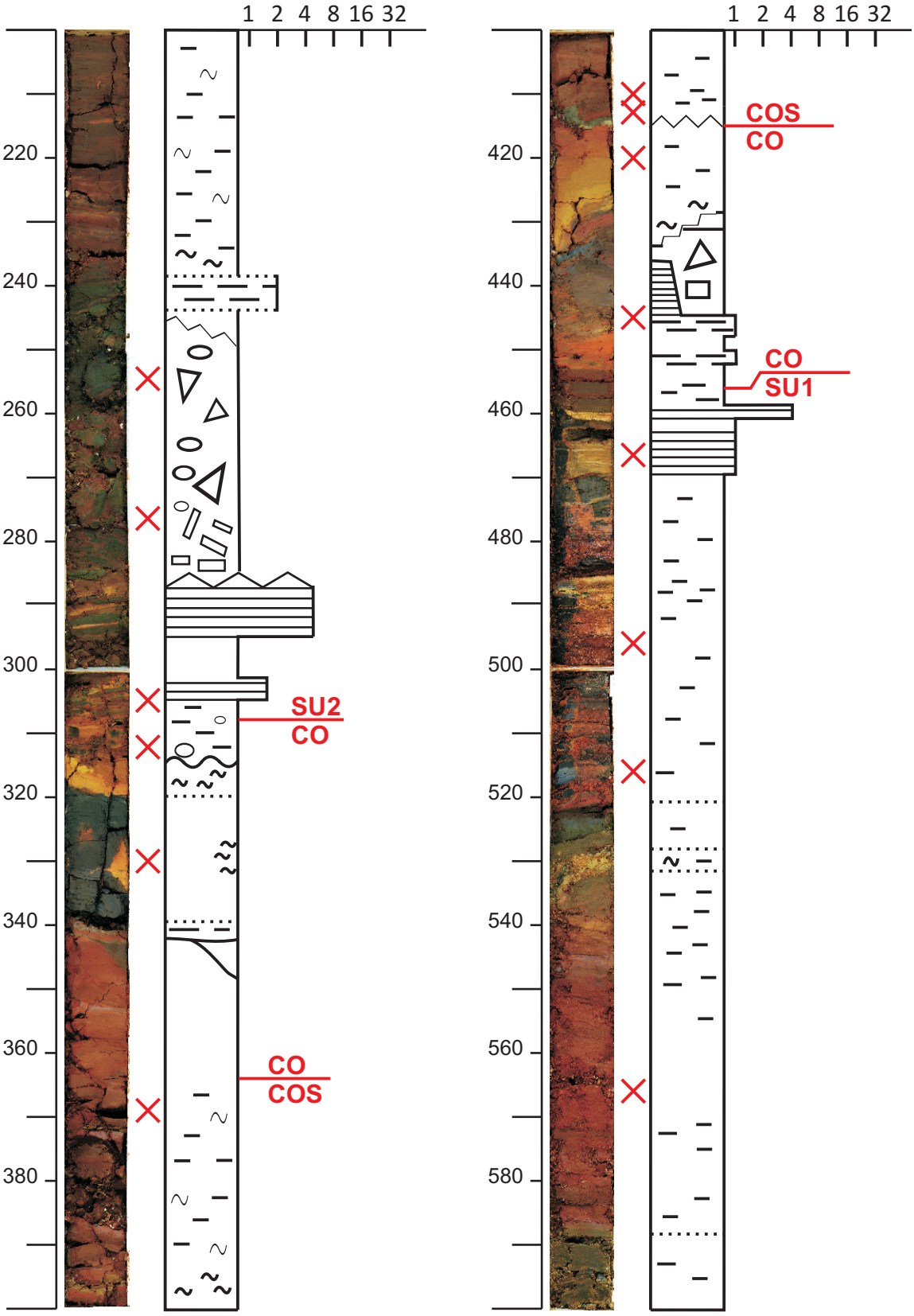
Appendix B.3.

Core: Va29_458 KS page 1/3
(W-Basin)
Water depth: 2147 m
Recovery: 8.94 m
Top loss: 2.59 m
Samples taken: 23

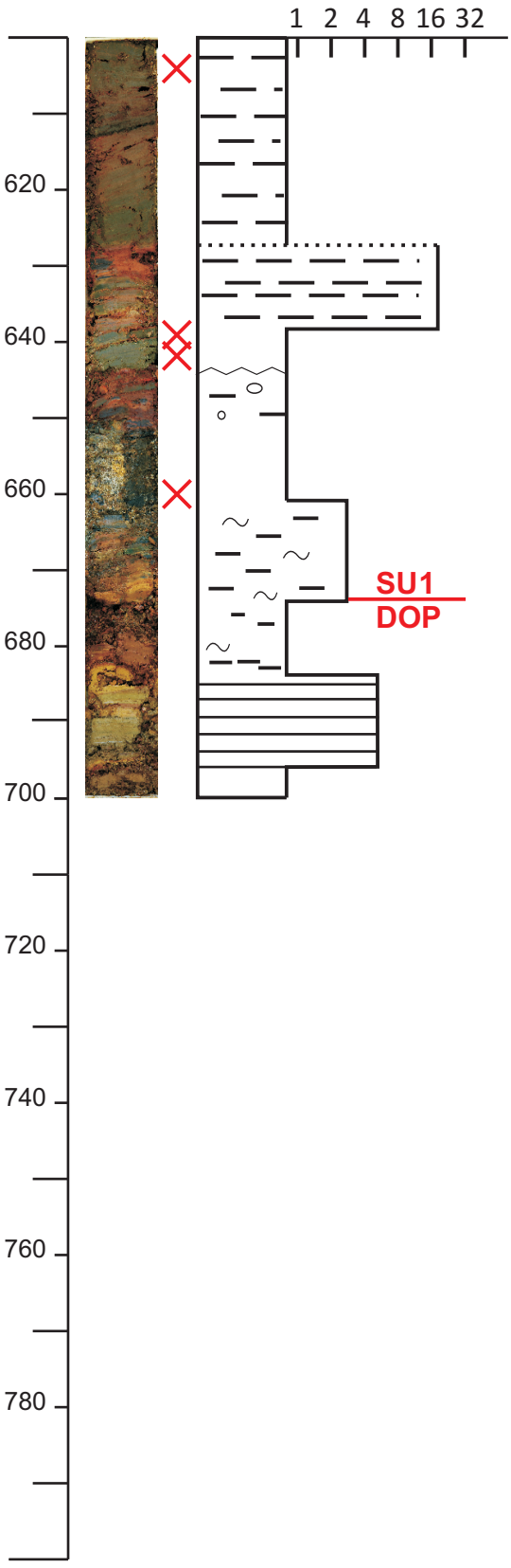


Core: Va29_458 KS page 2/3



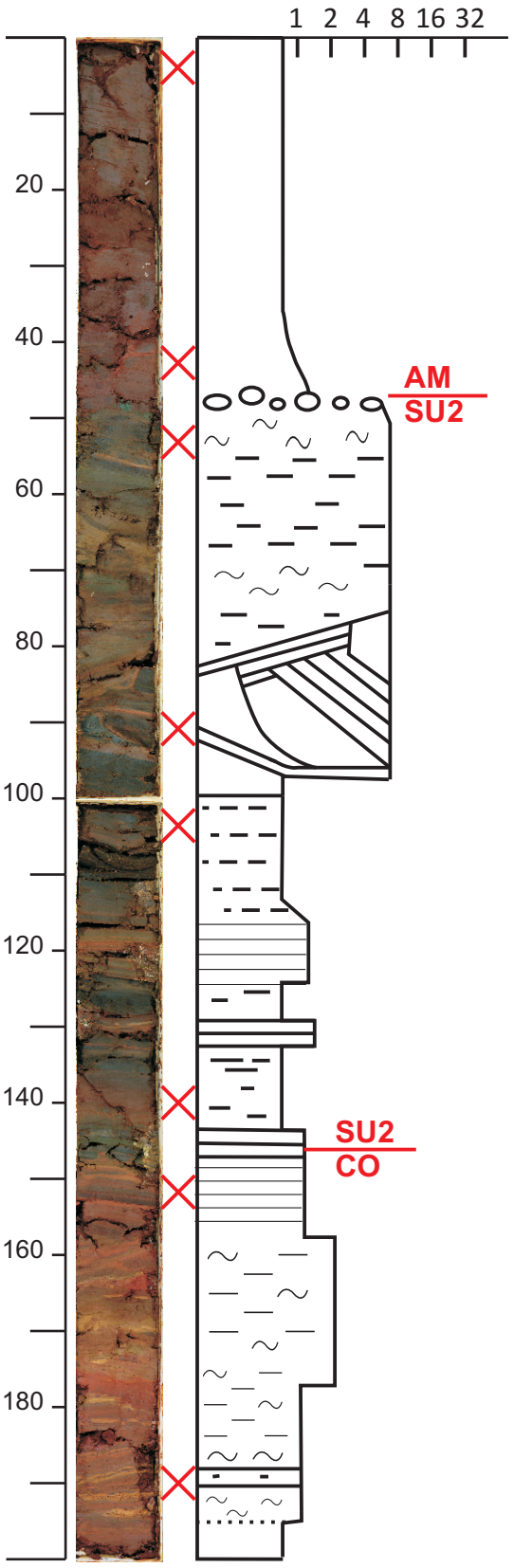
Core: Va29_458 KS  page 3/3



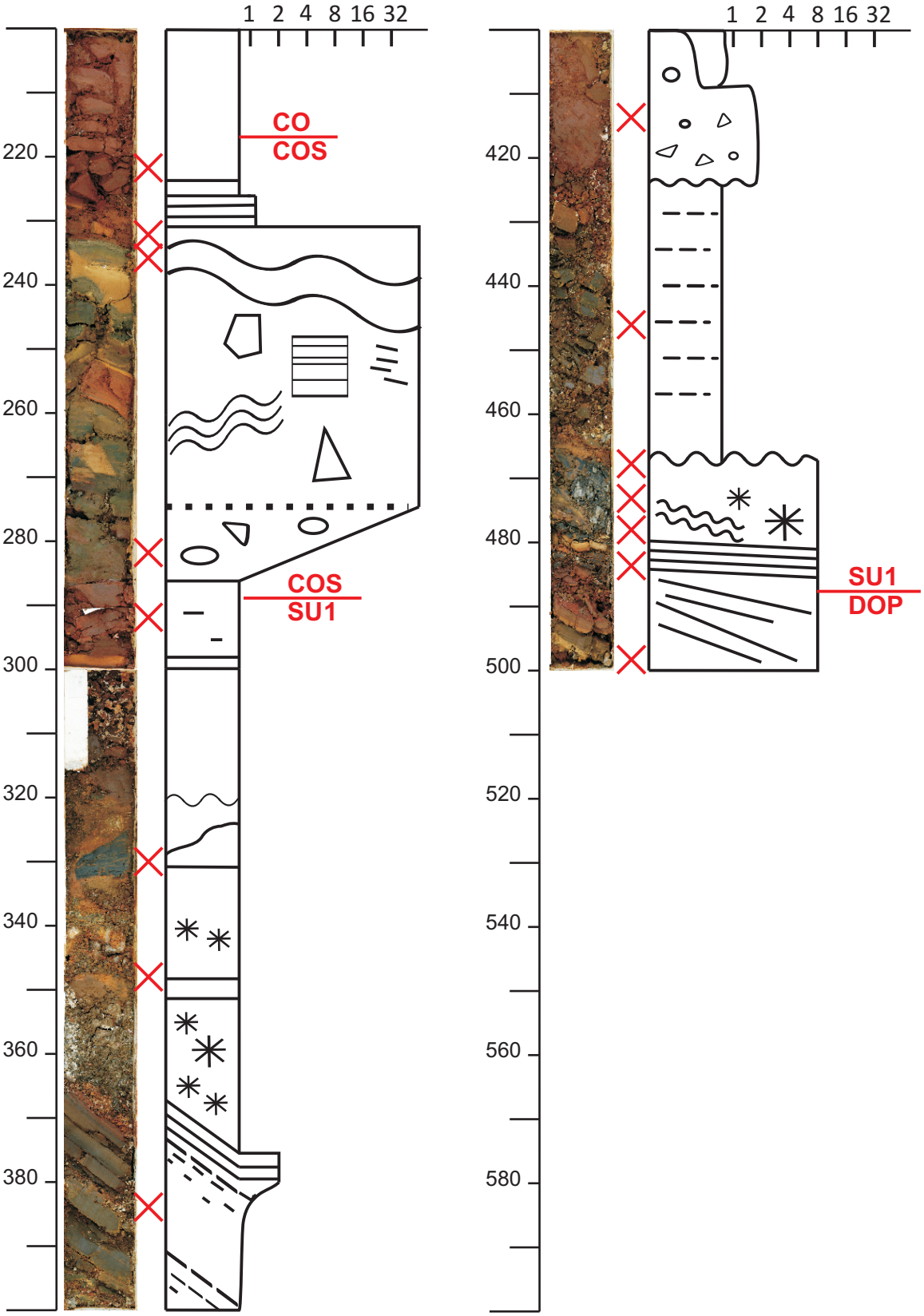
Appendix B.3.

Core: Va29_480 KS page 1/2
(N-Passage)
Water depth: 2125 m
Recovery: 6.80 m
Top loss: 3.21 m
Samples taken: 23



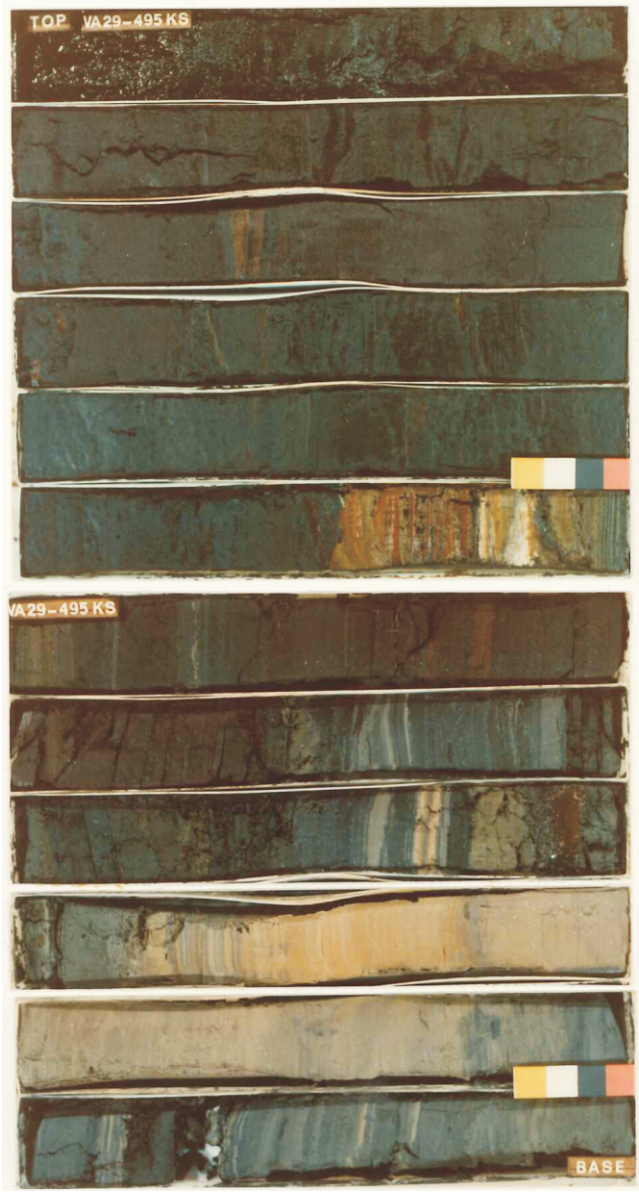



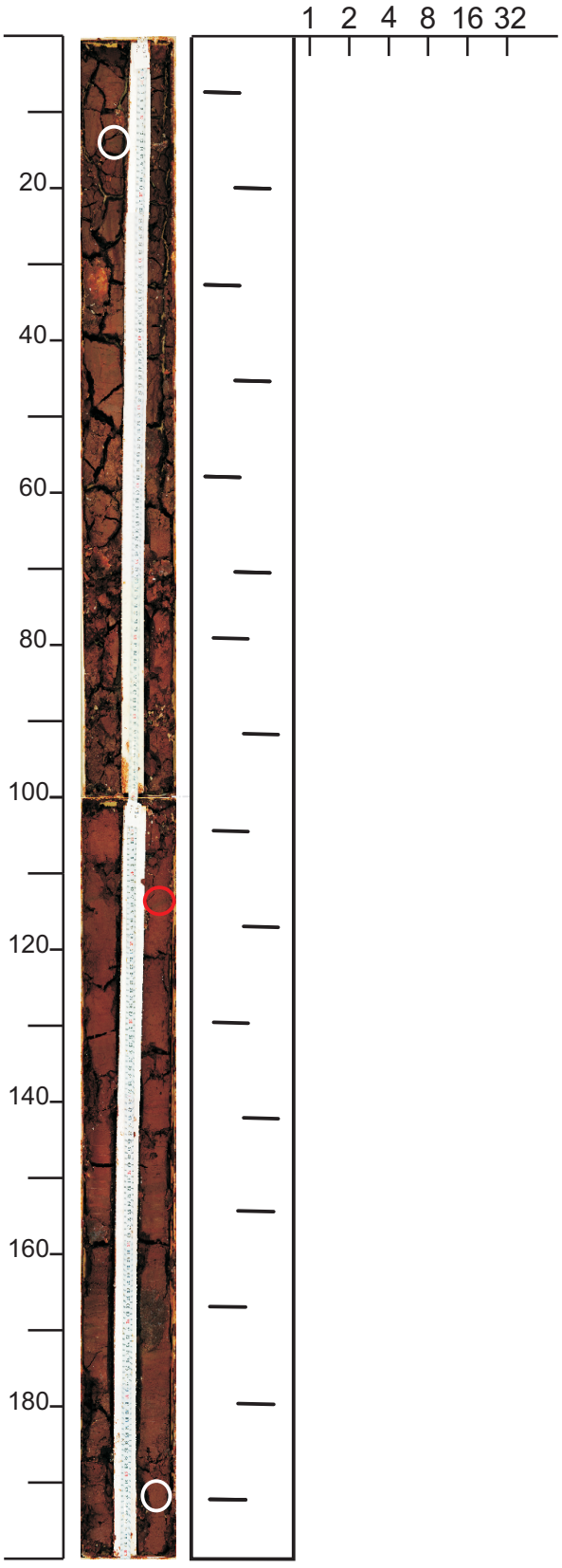
Core: Va29_480 KS page 2/2



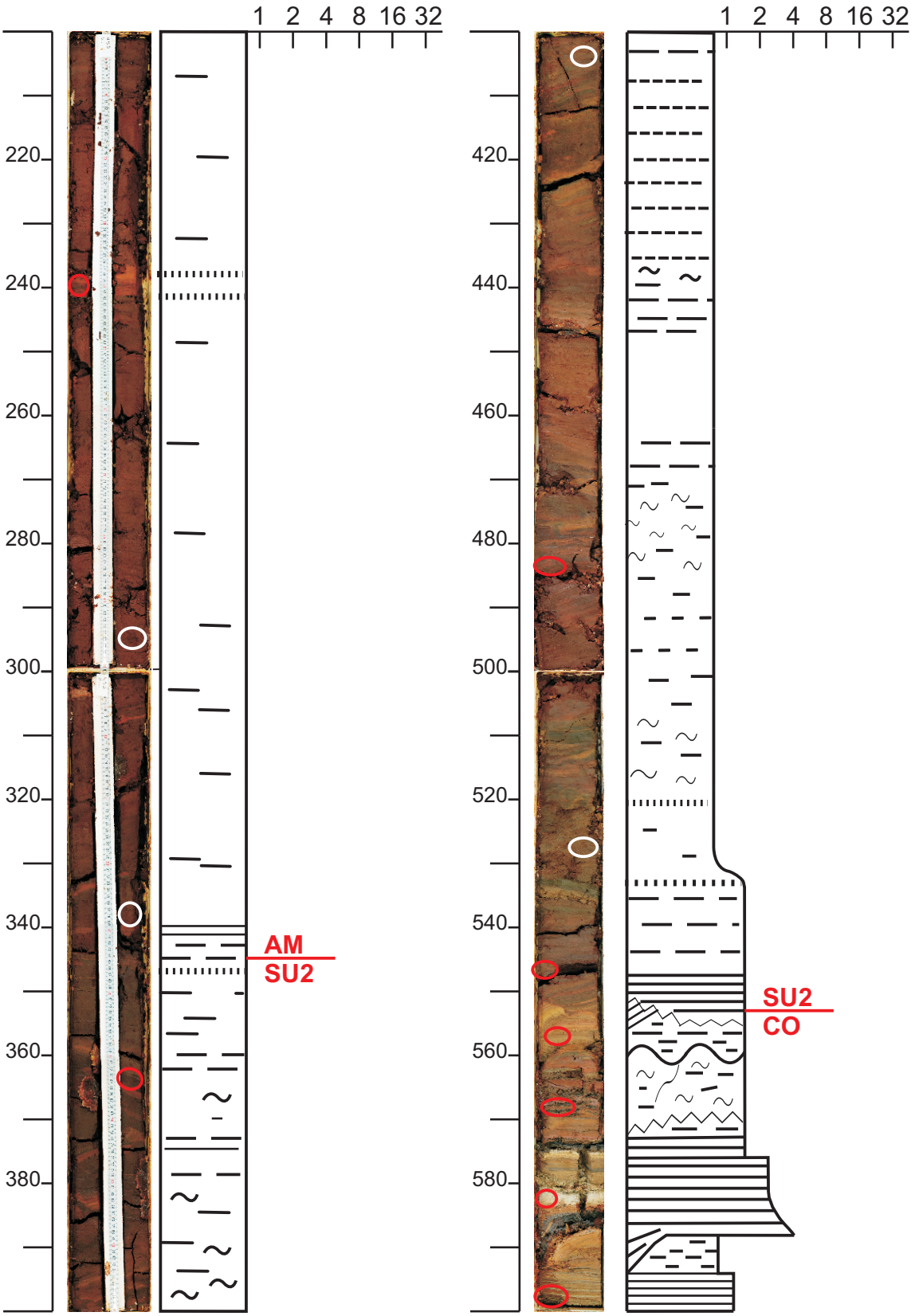
Appendix B.3.

Core: Va29_495 KS page 1/4
(E-Basin)
Water depth: 2076 m
Recovery: 12.38 m
Top loss: 0.26 m
Samples taken: 25

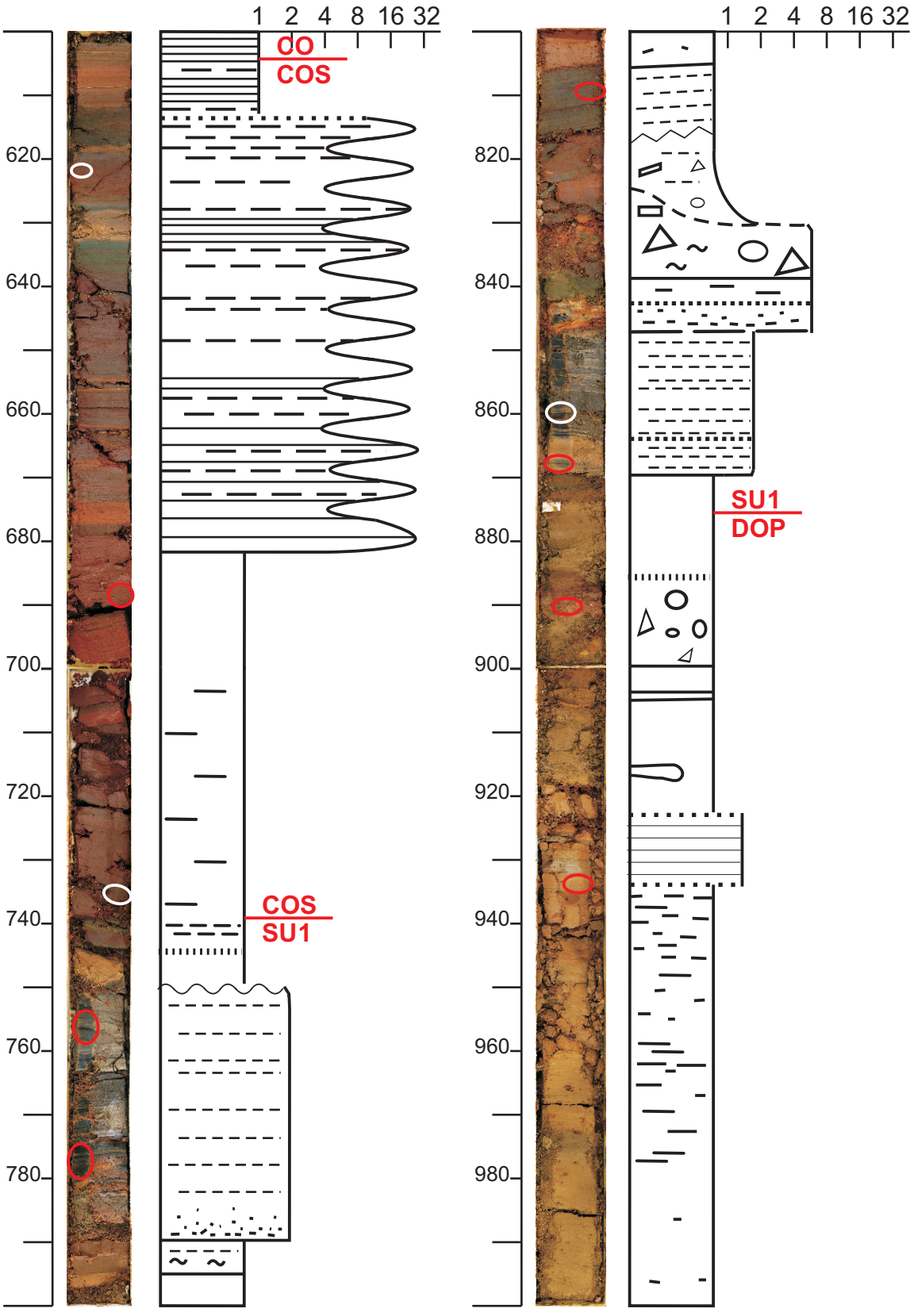


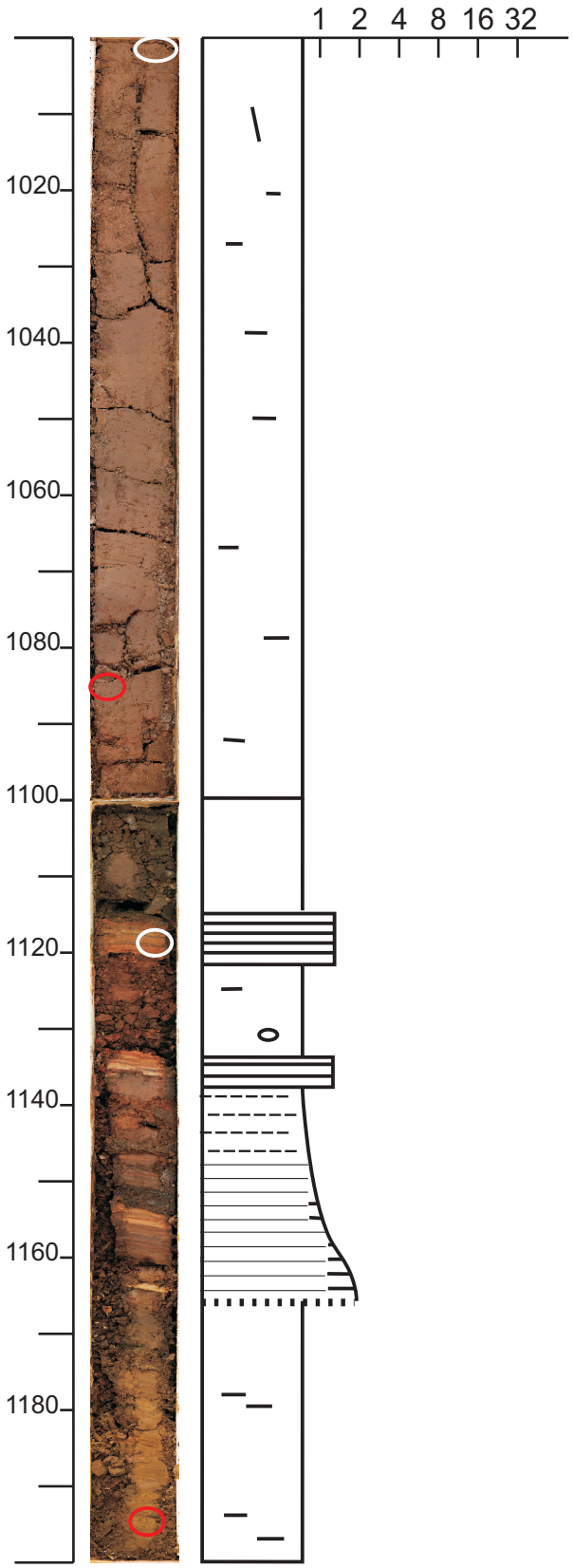
Core: Va29_494 KS page 2/4



Core: Va29_494 KS page 3/4

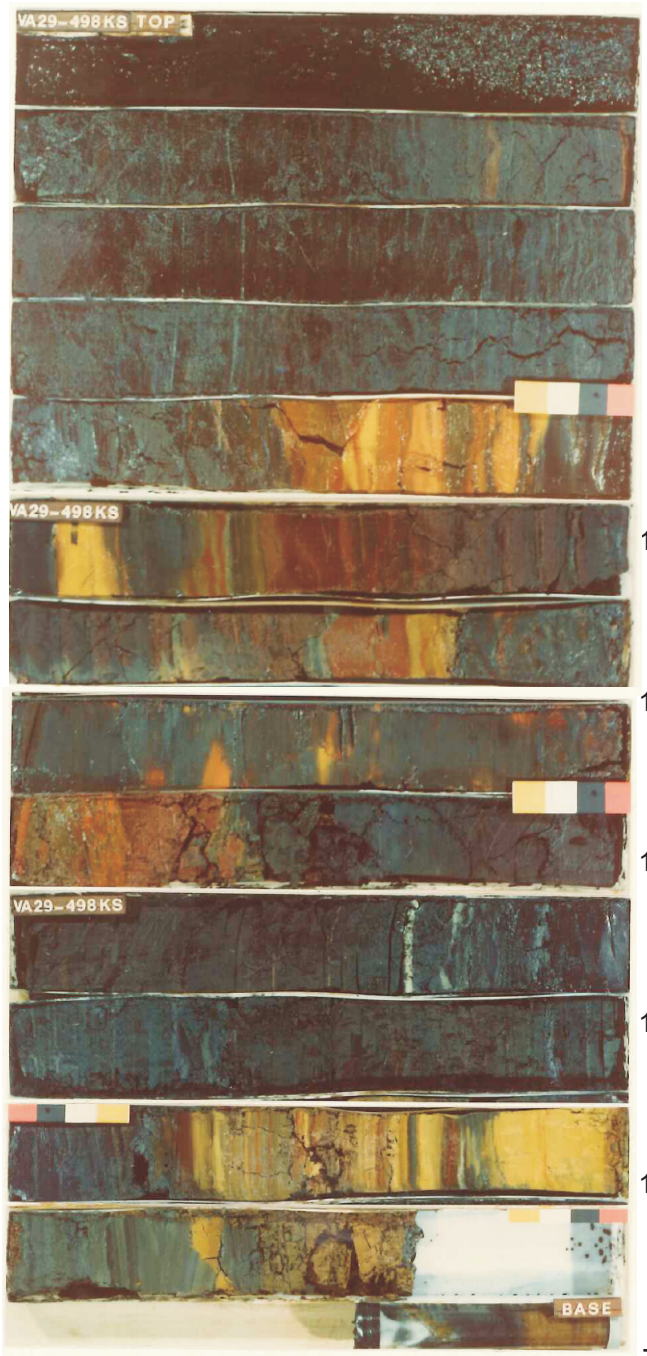


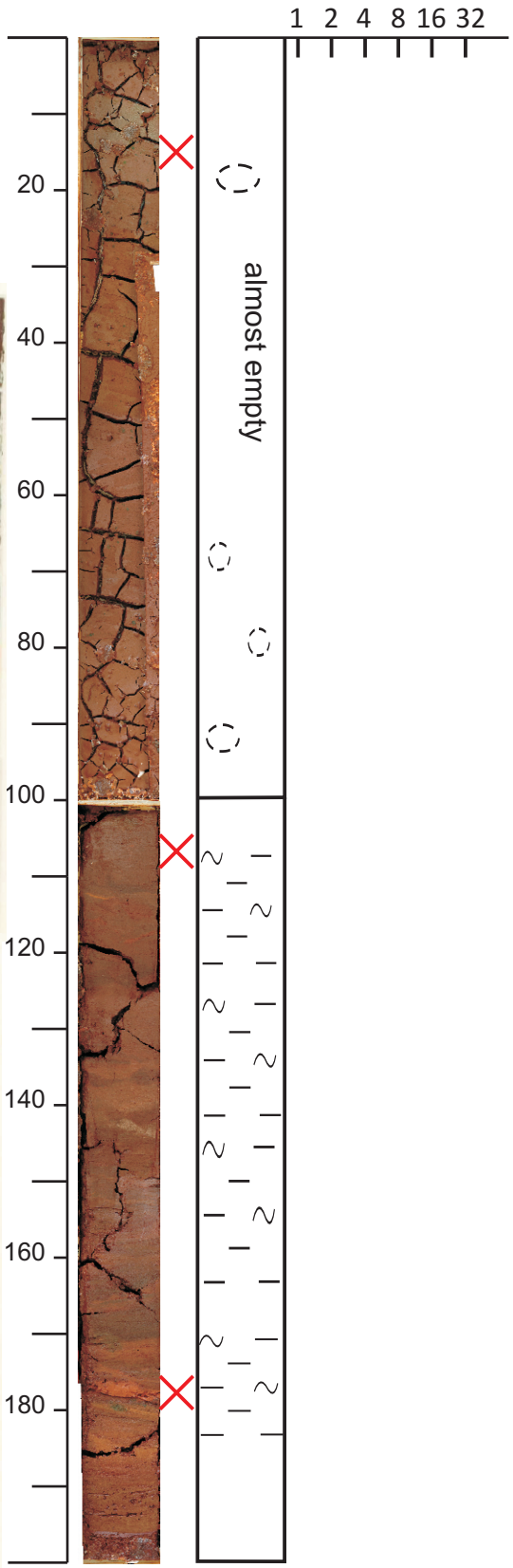
Core: Va29_494 KS  page 4/4



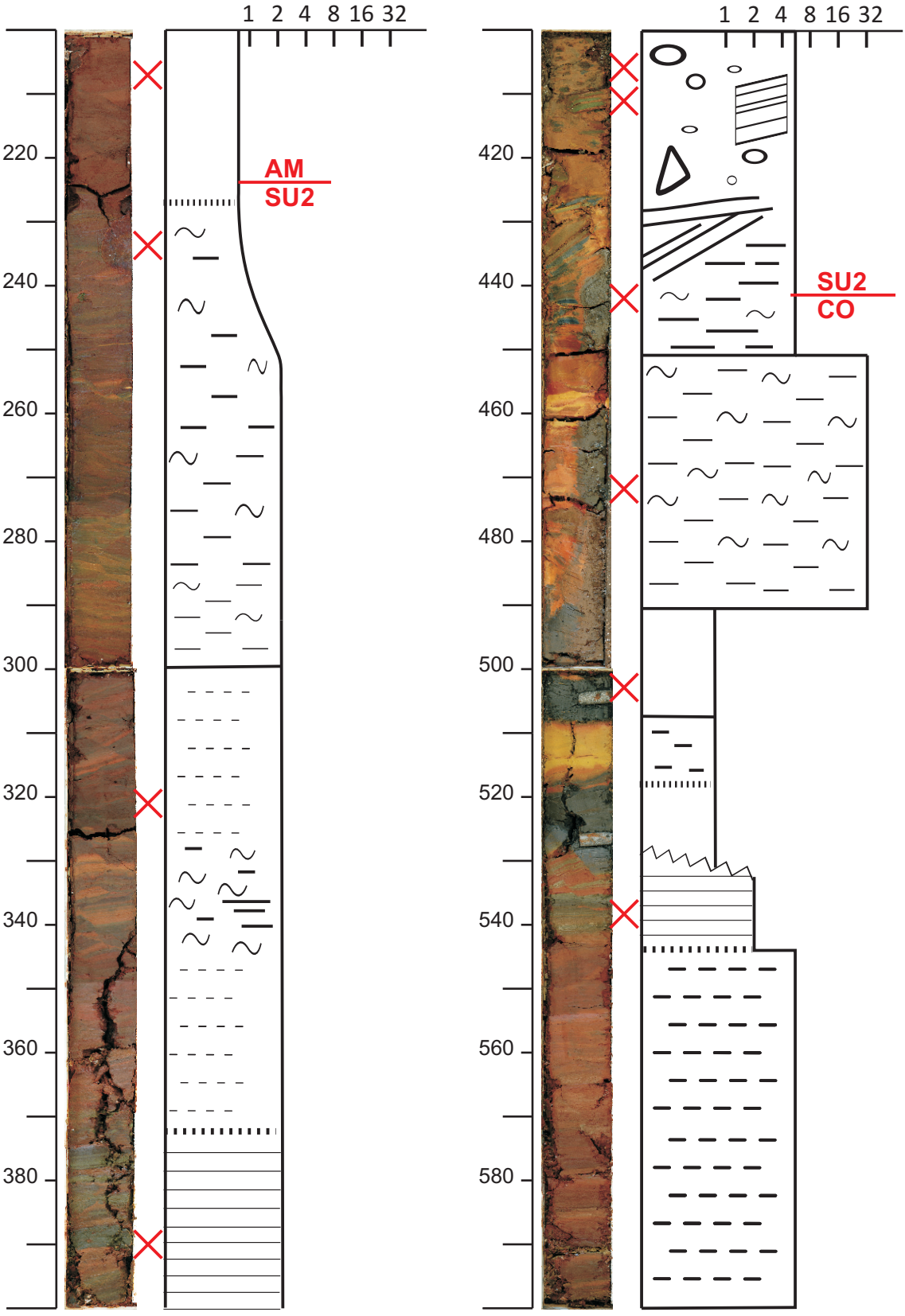
Appendix B.3.

Core: Va29_498 KS page 1/4
(N-Passage)
Water depth: 2147 m
Recovery: 12.99 m
Top loss: 1.64 m
Samples taken: 32

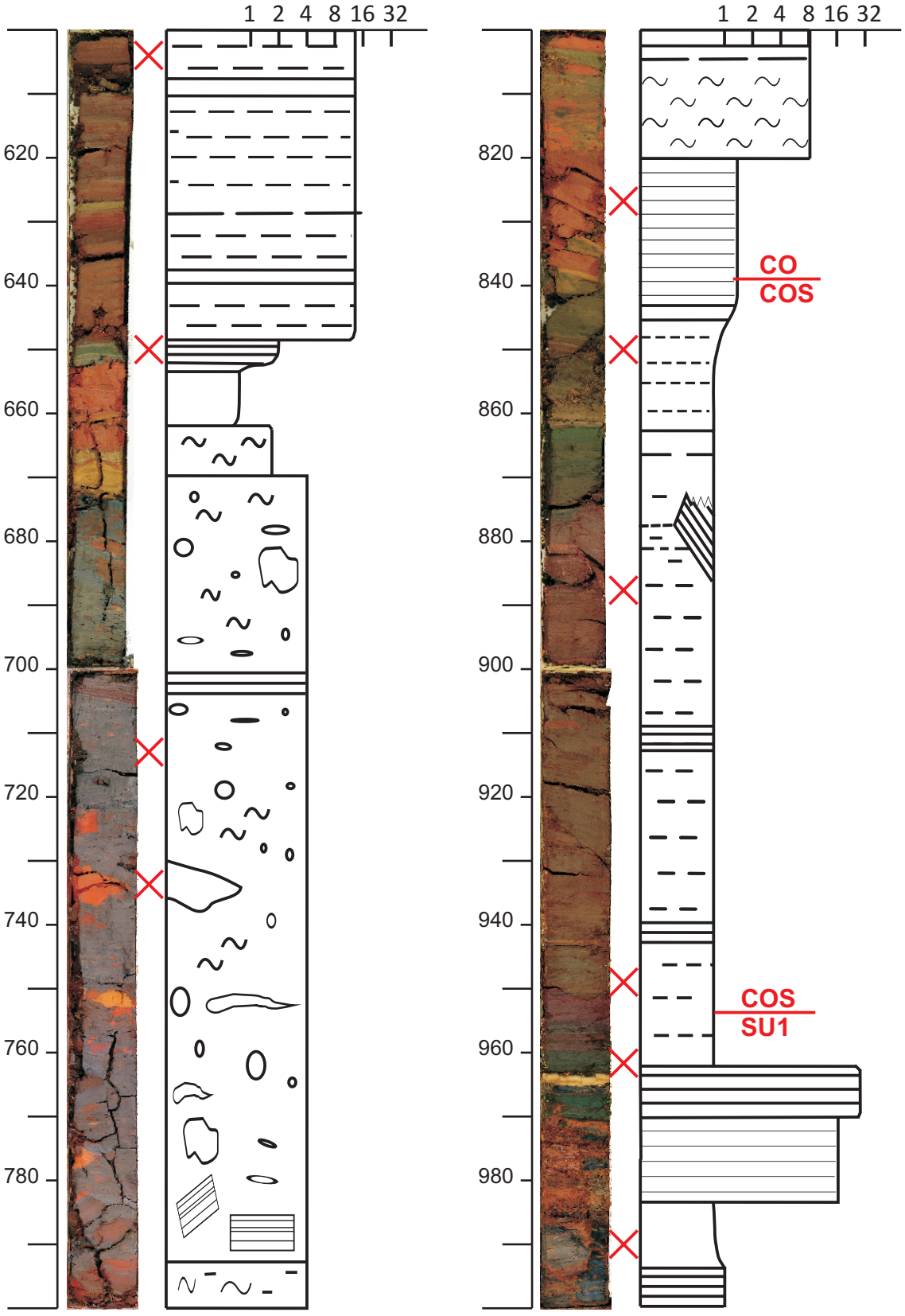


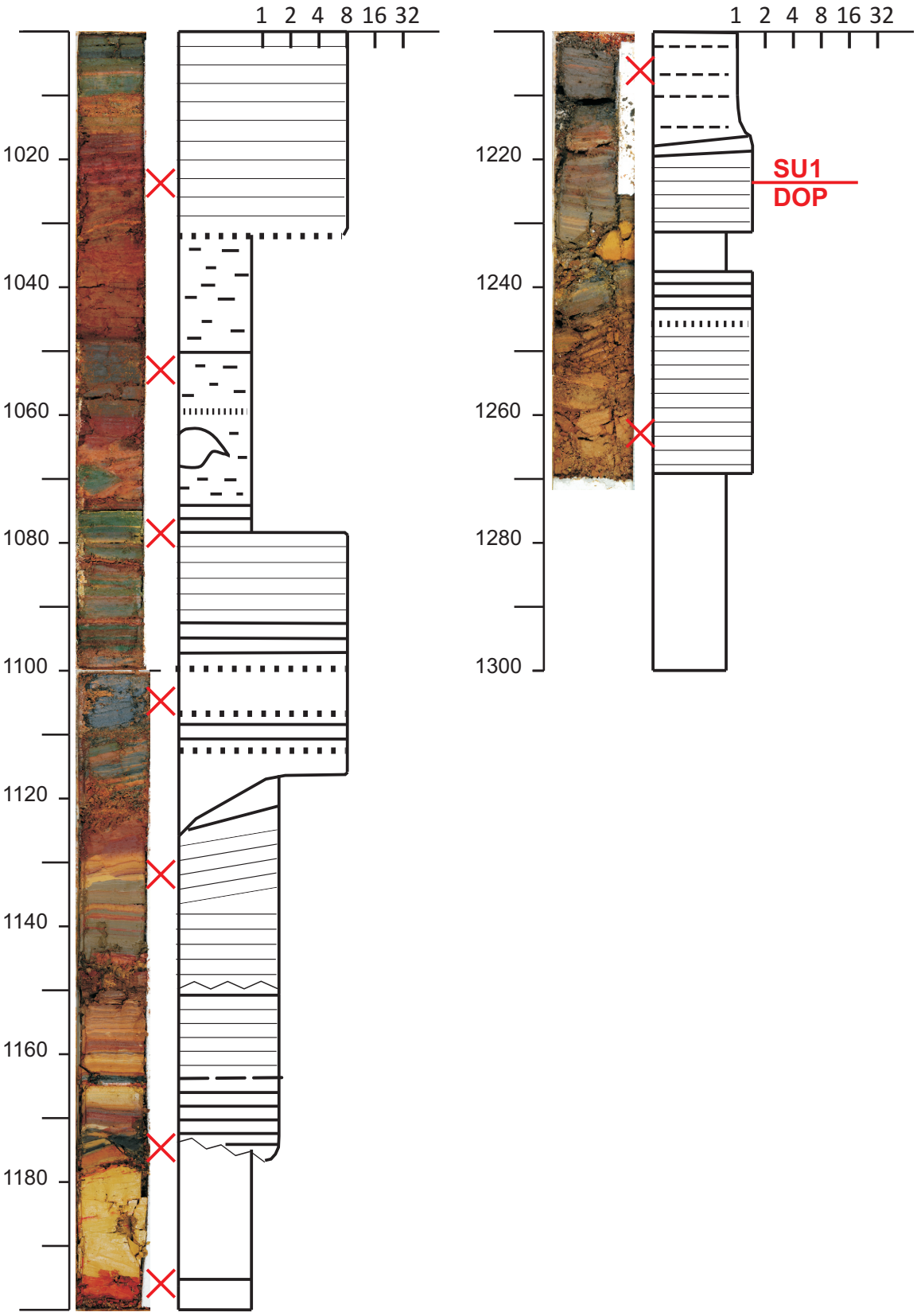
Core: Va29_498 KS page 2/4



Core: Va29_498 KS page 3/4

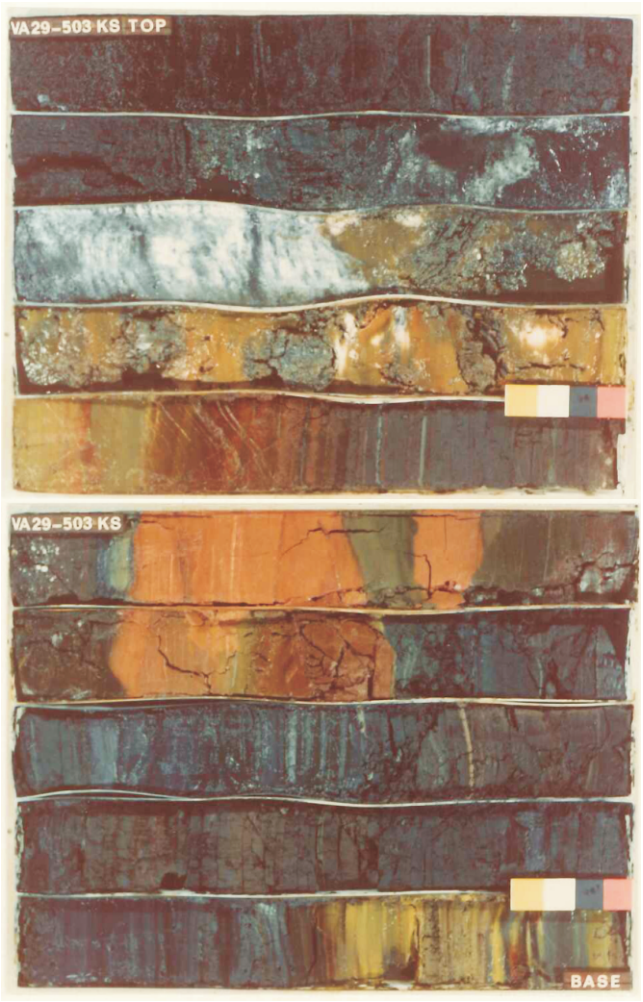


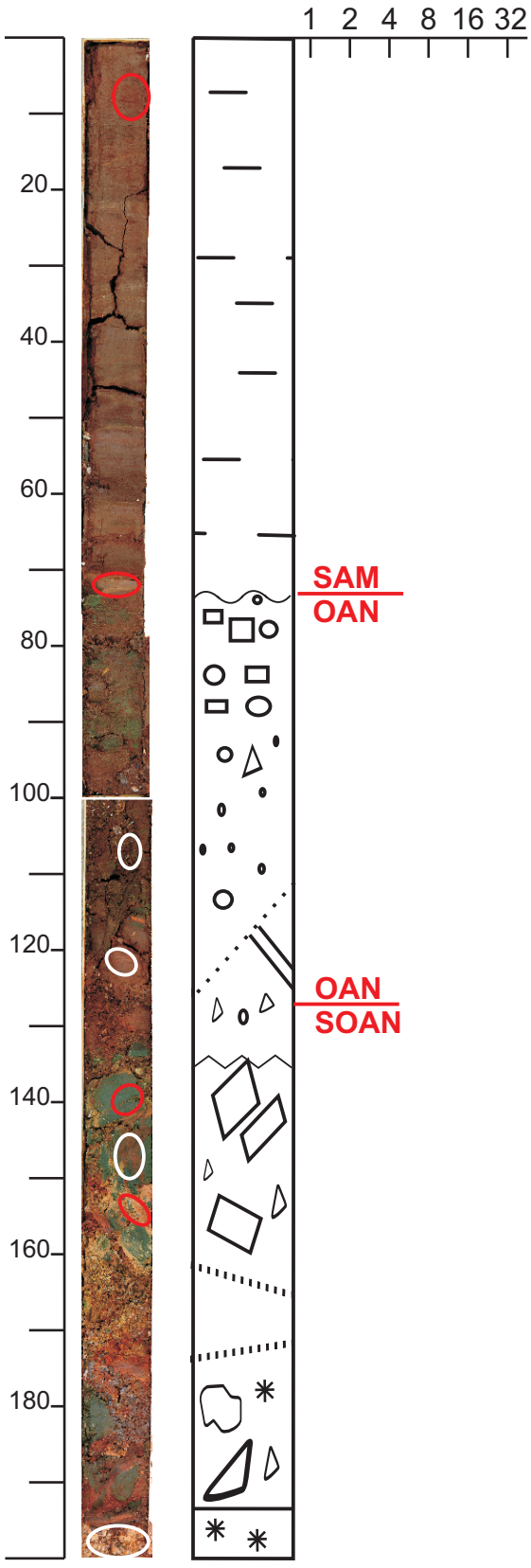
Core: Va29_498 KS page 4/4



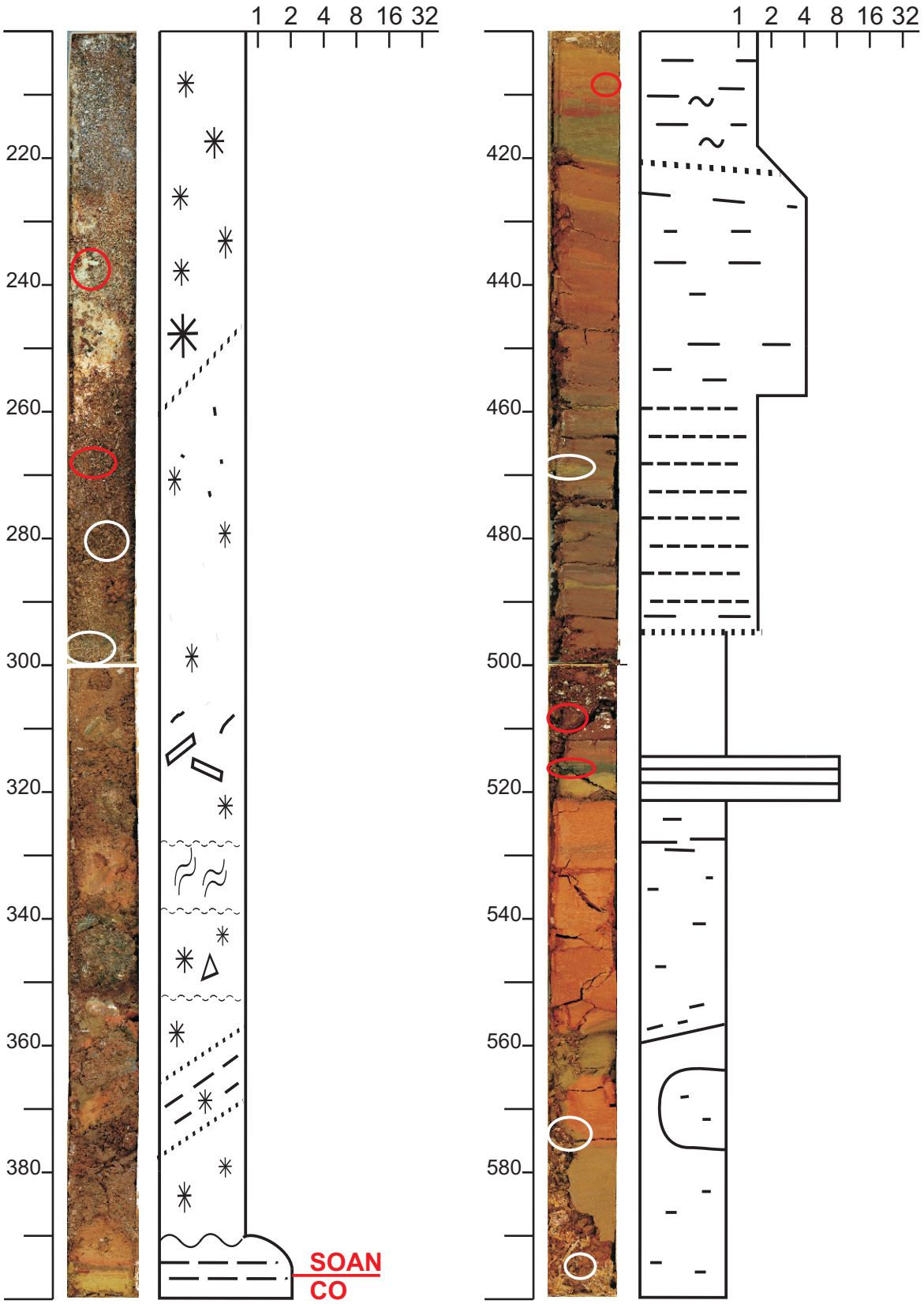
Appendix B.3.

Core: Va29_503KS page 1/3
(W-Basin)
Water depth: 2159 m
Recovery: 12.10 m
Top loss: 2.17 m
Samples taken: 31 (of which
17 analysed for chemistry)

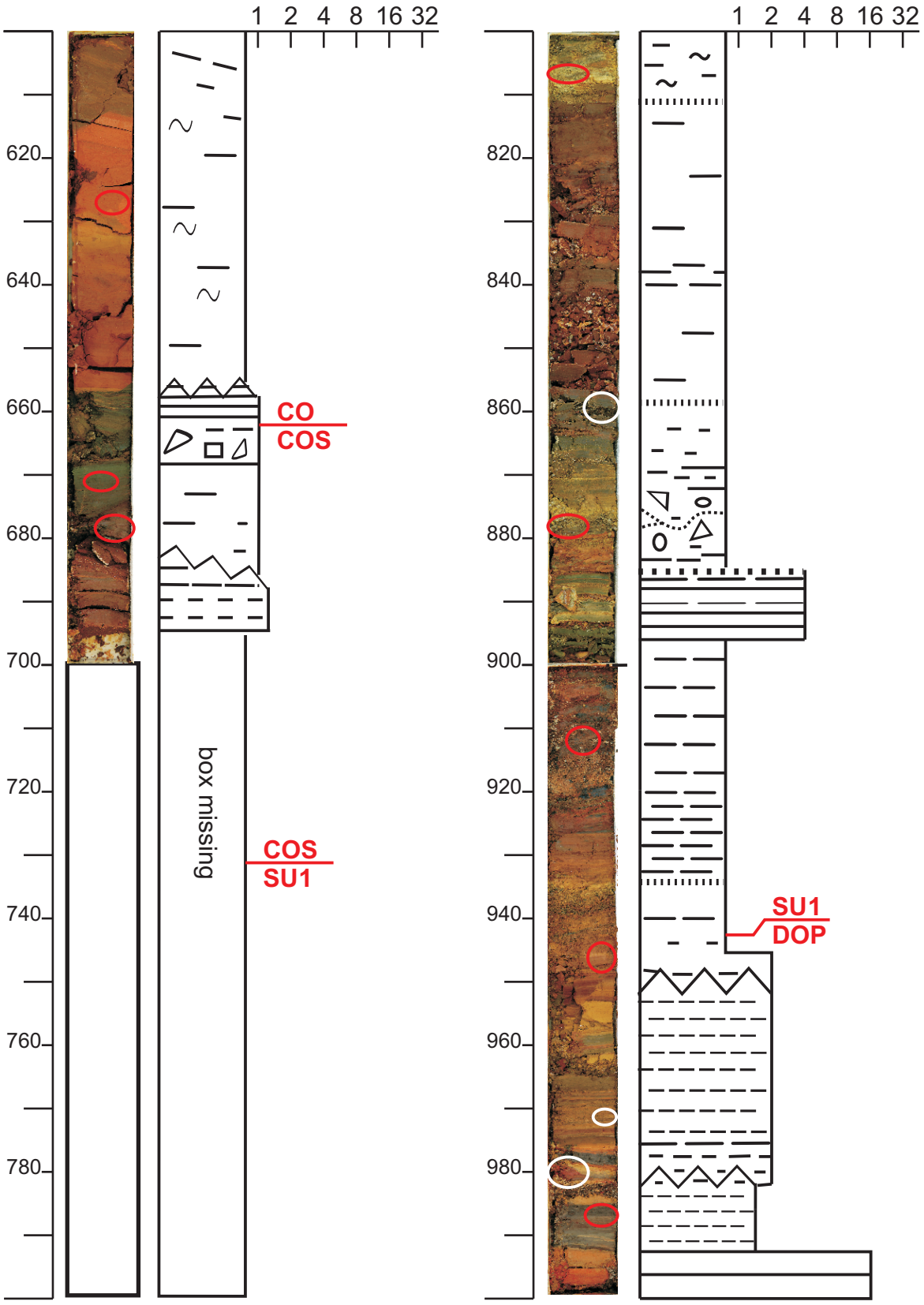


Core: Va29_503 KS page 2/3



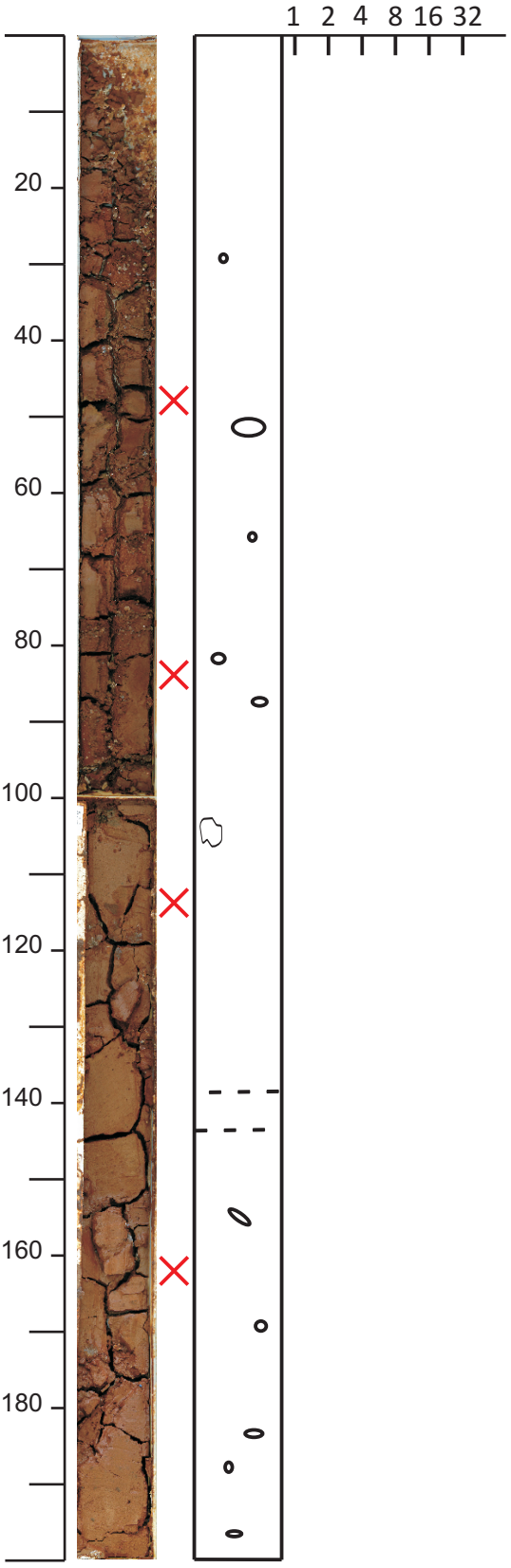
Core: Va29_503 KS page 2/3



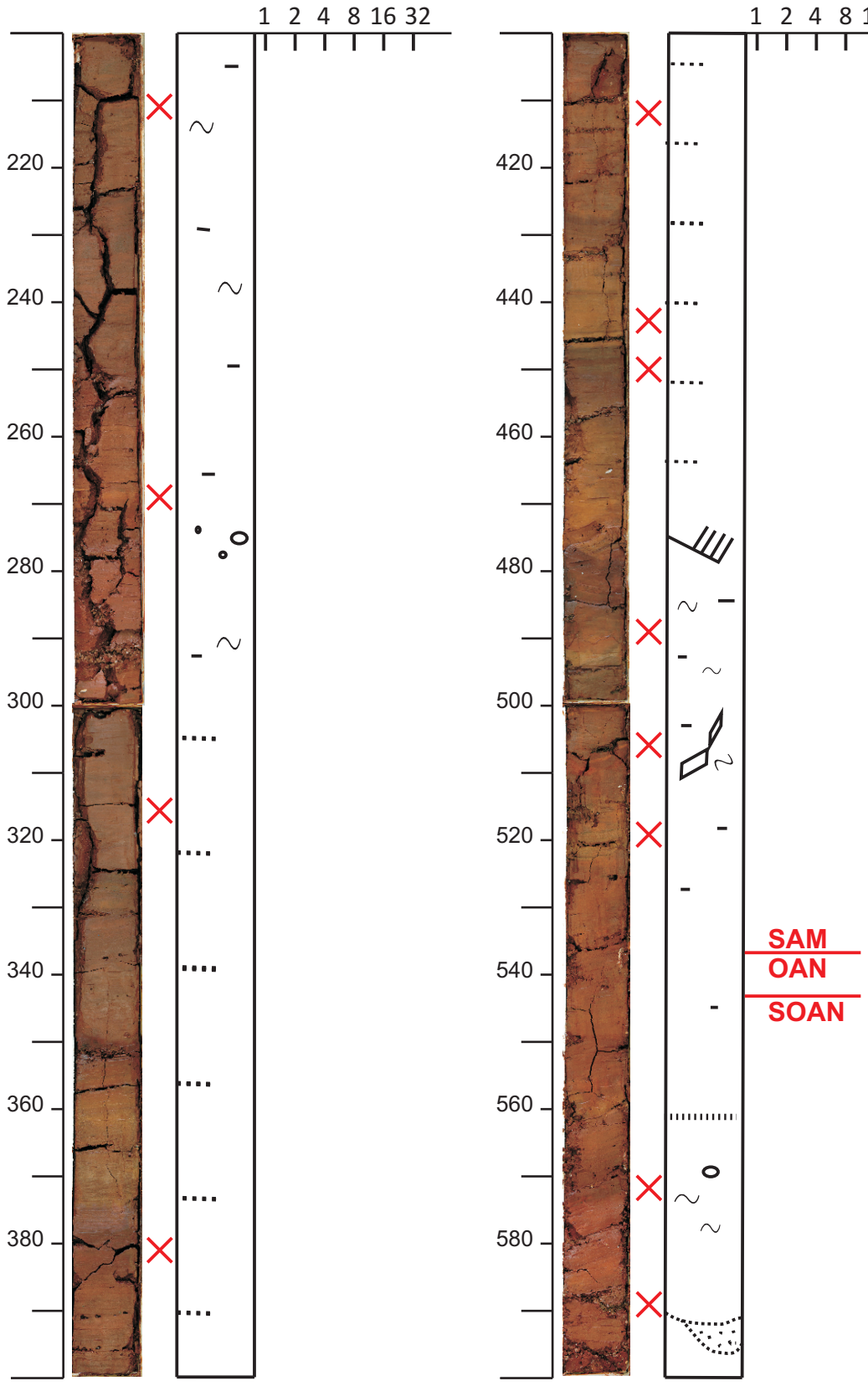
Appendix B.3.

Core: Va29_526 K page 1/3
(SW-Basin)
Water depth: 2180 m
Recovery: 9.25 m
Top loss: 0 m
Samples taken: 27

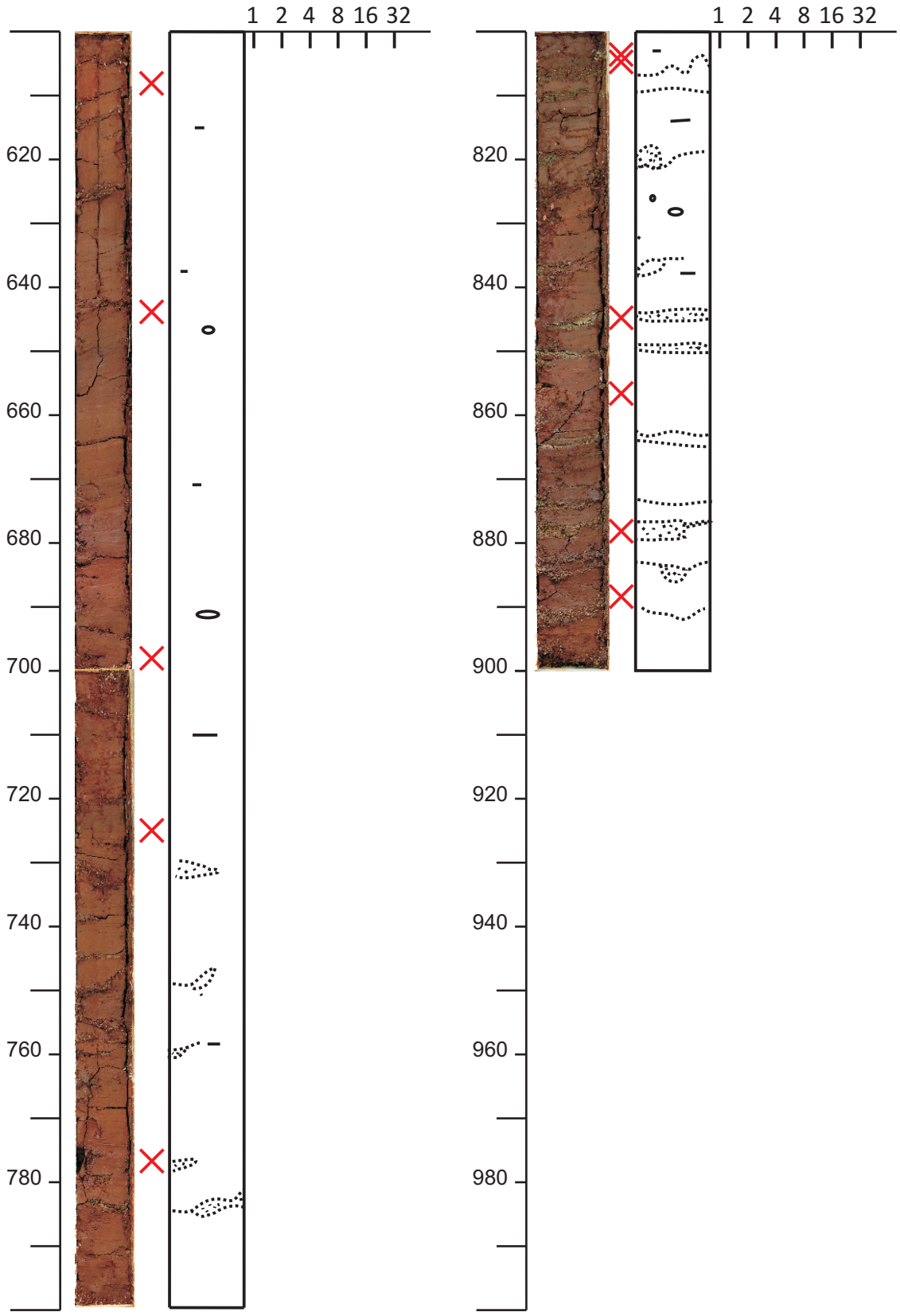


Core: Va29_526 KS page 2/3

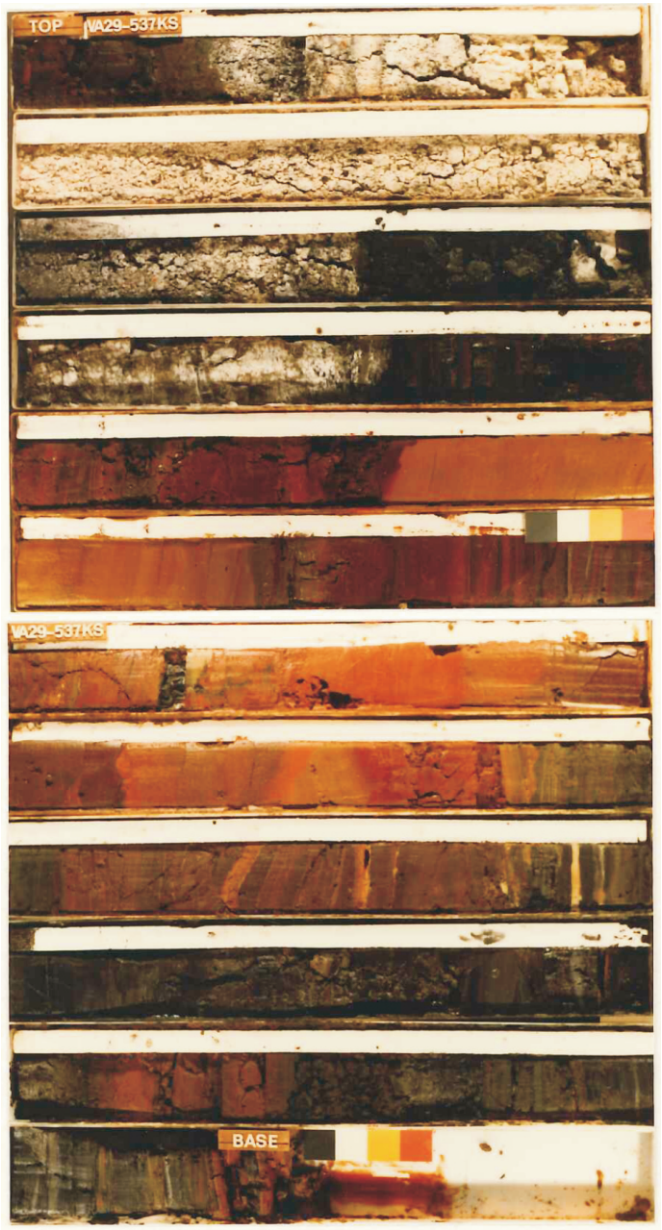


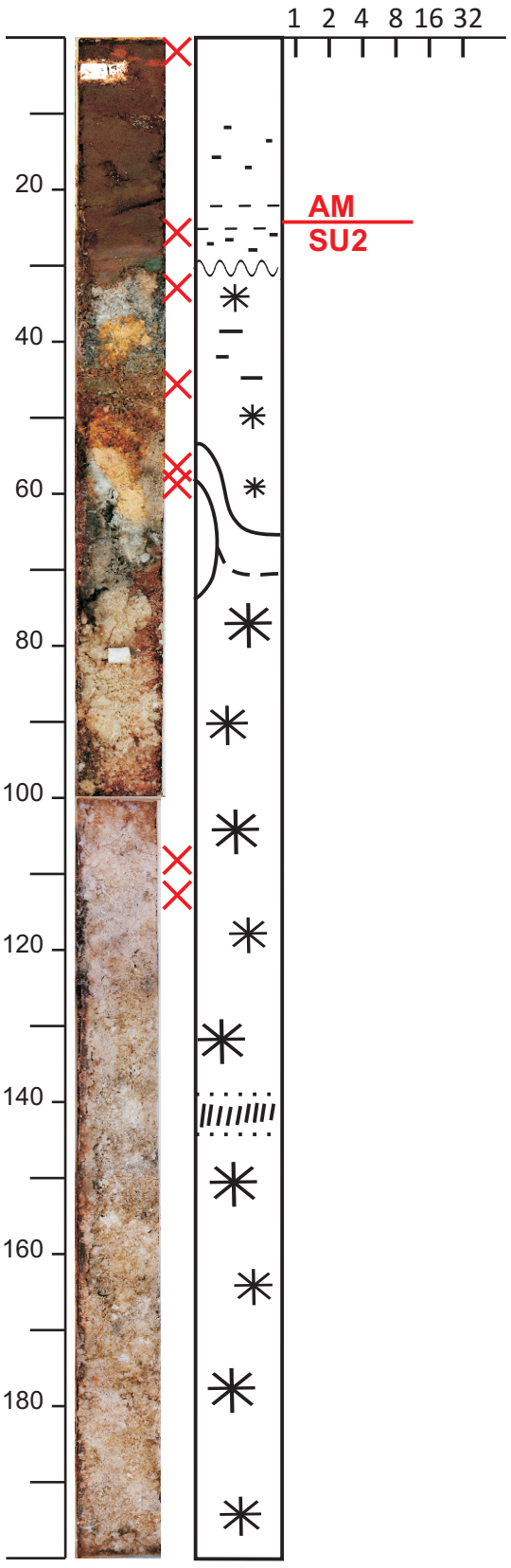
Core: Va29_526 KS page 3/3



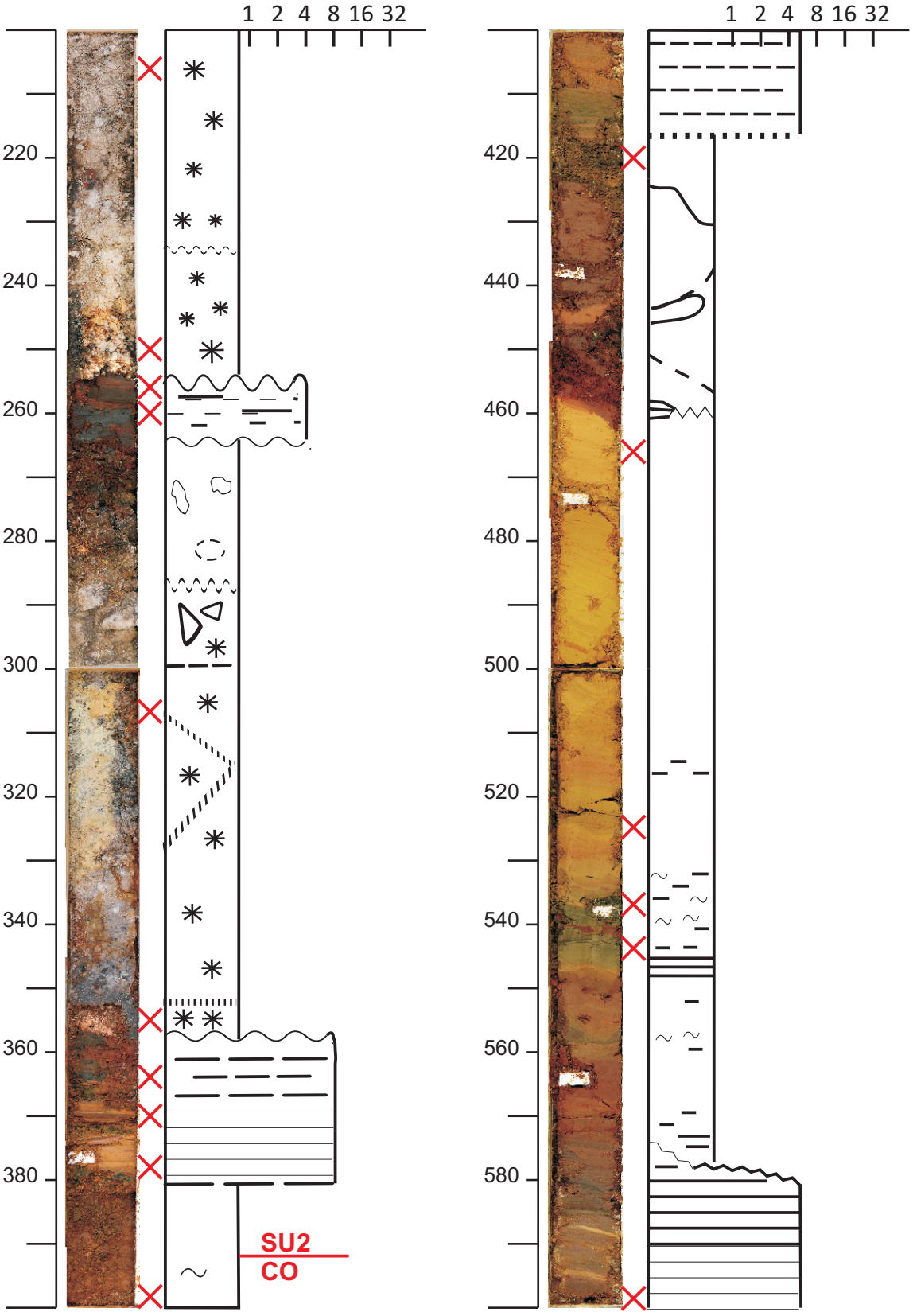
Appendix B.3.

Core: Va29_537 KS  Page 1/4
(SW-Passage)
Water depth: 2186 m
Recovery: 12.05 m
Top loss: 2.69 m
Samples taken: 41

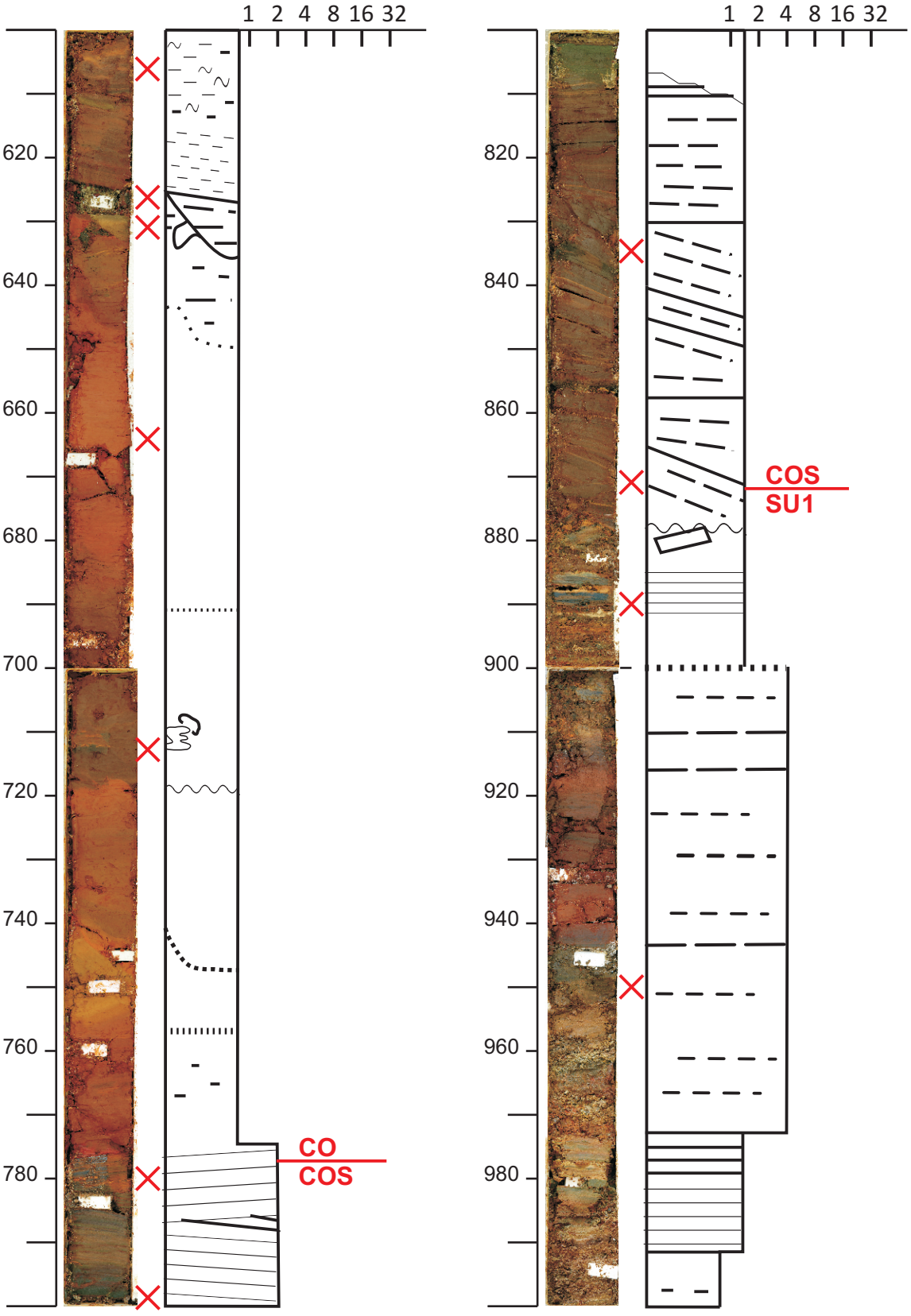


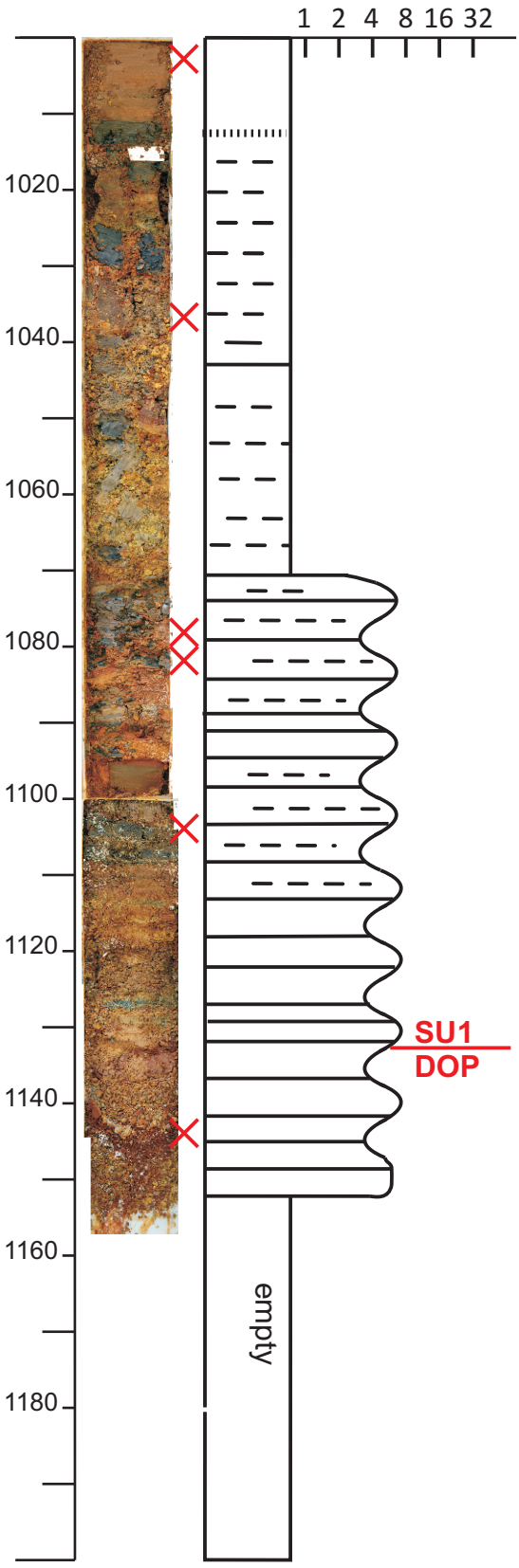
Core: Va29_537 KS page 2/4



Core: Va29_537 KS page 3/4

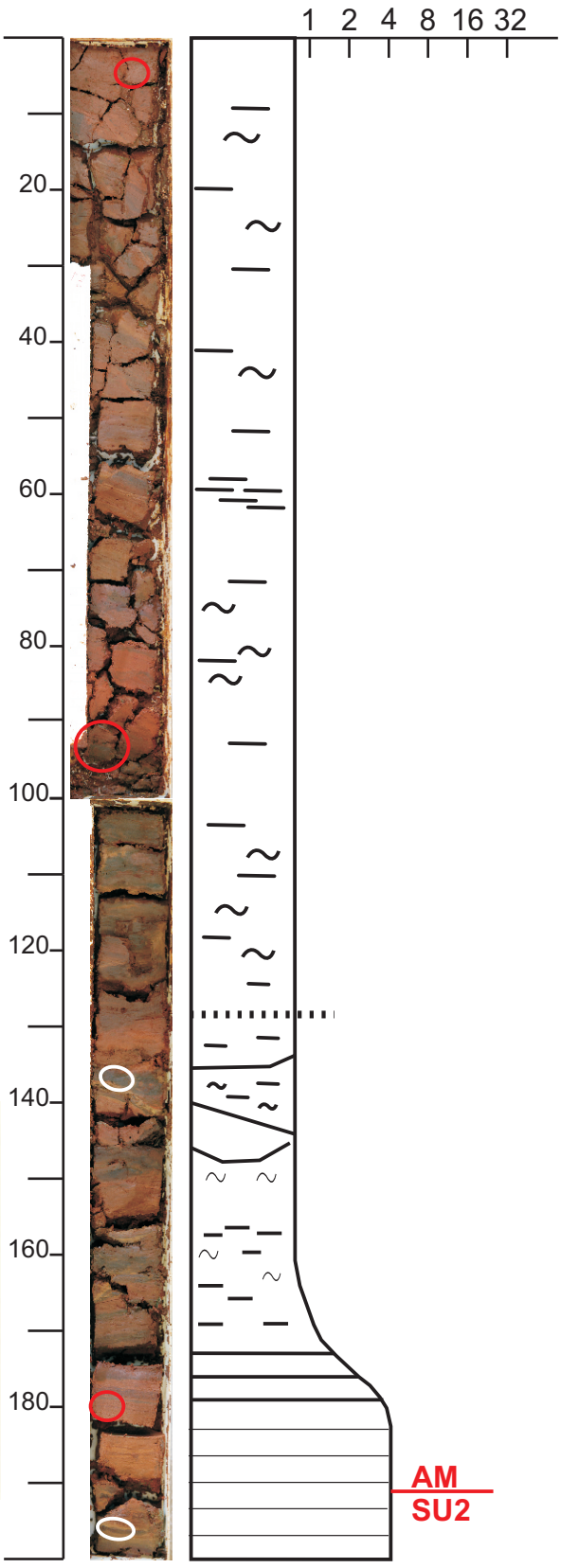


Core: Va29_537 KS  page 4/4



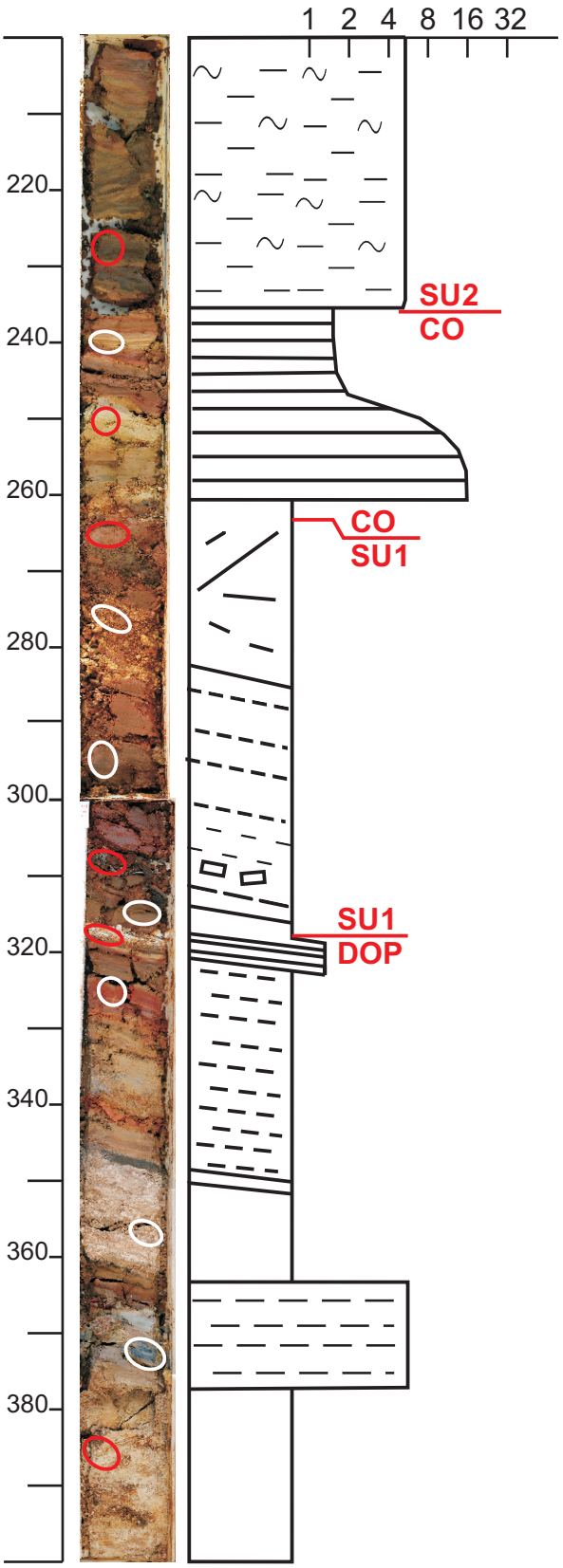
Appendix B.3.

Core: Va29_546 KS  Page 1/2
(S-Basin)
Water depth: 2013 m
Recovery: 5.46 m
Top loss: 0.91 m
Samples taken: 18



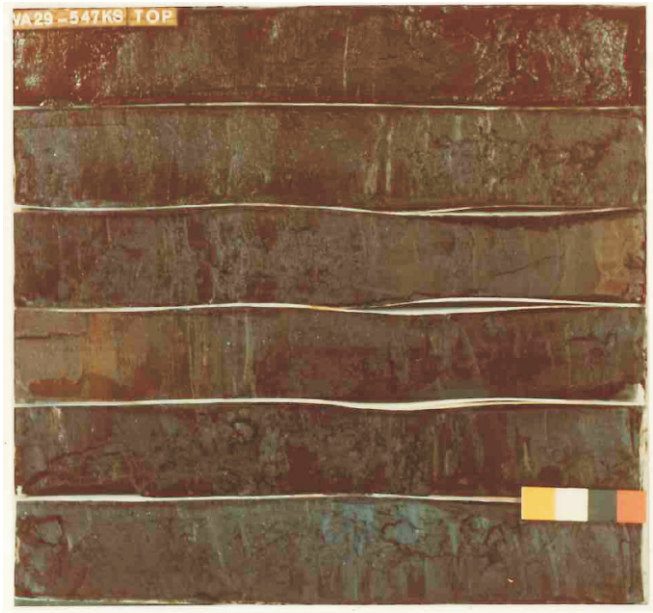



Core: Va29_546 KS  page 2/2



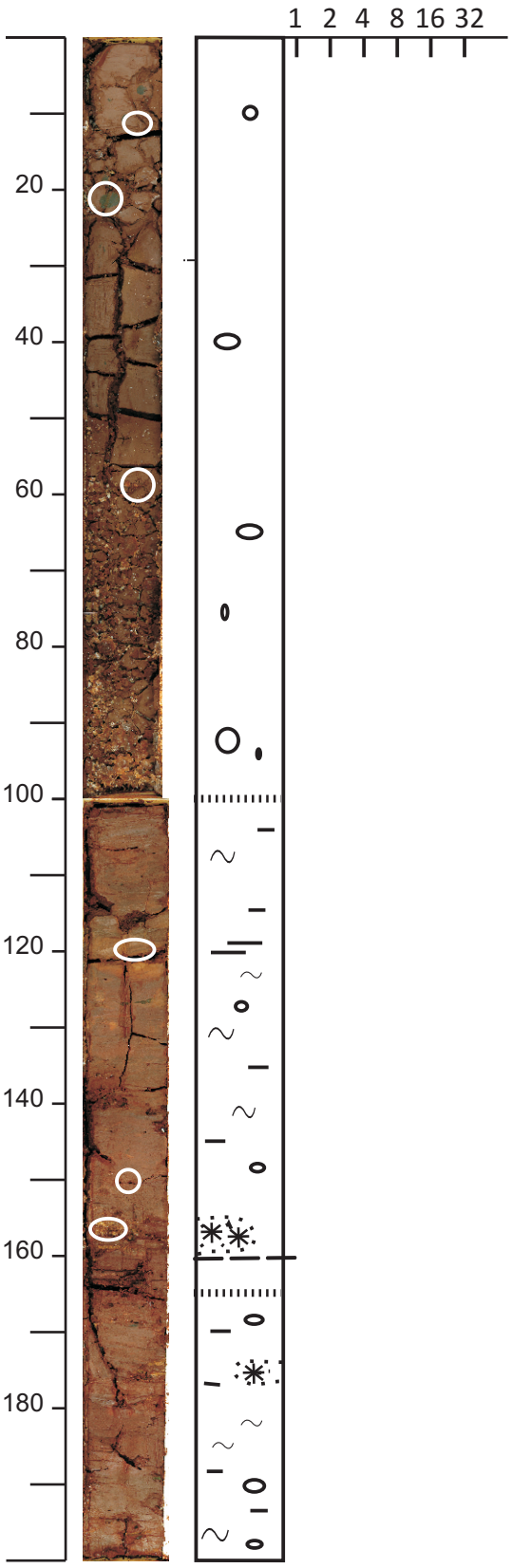
Appendix B.3.

Core: Va29_547 KS page 1/4
(S Basin)
Water depth: 2135 m
Recovery: 11.98 m
Top loss: 0 m
Samples taken: 49

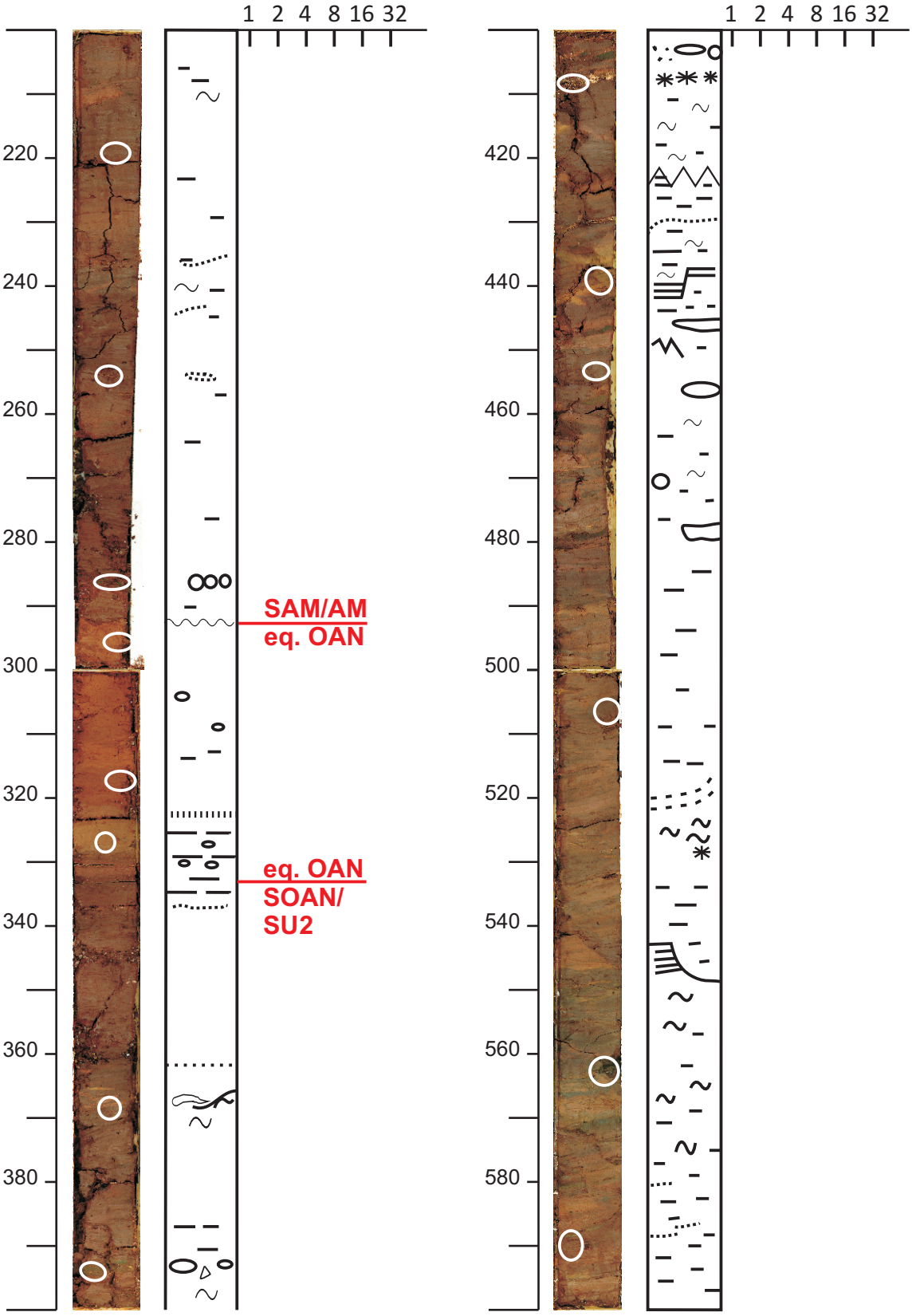




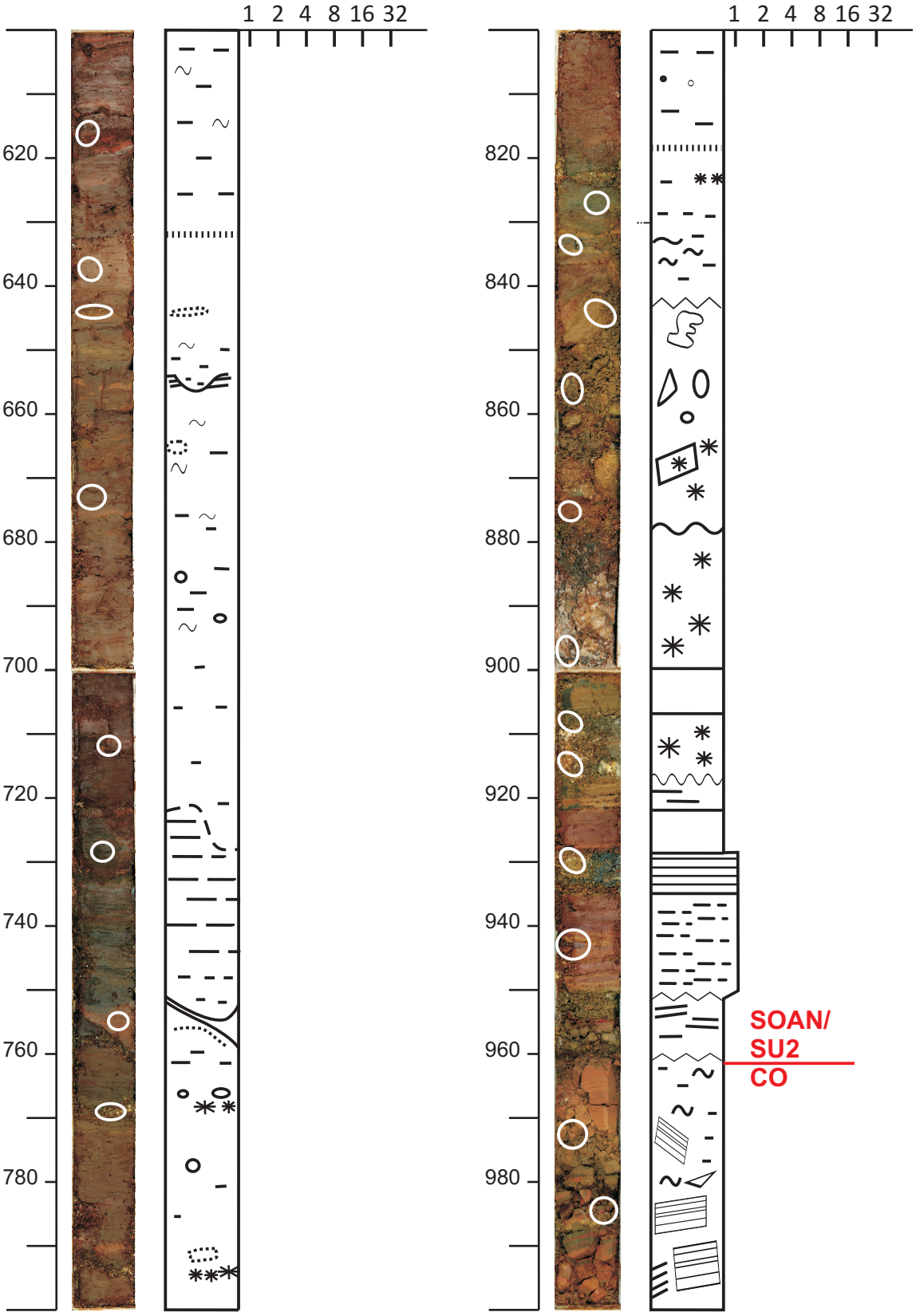




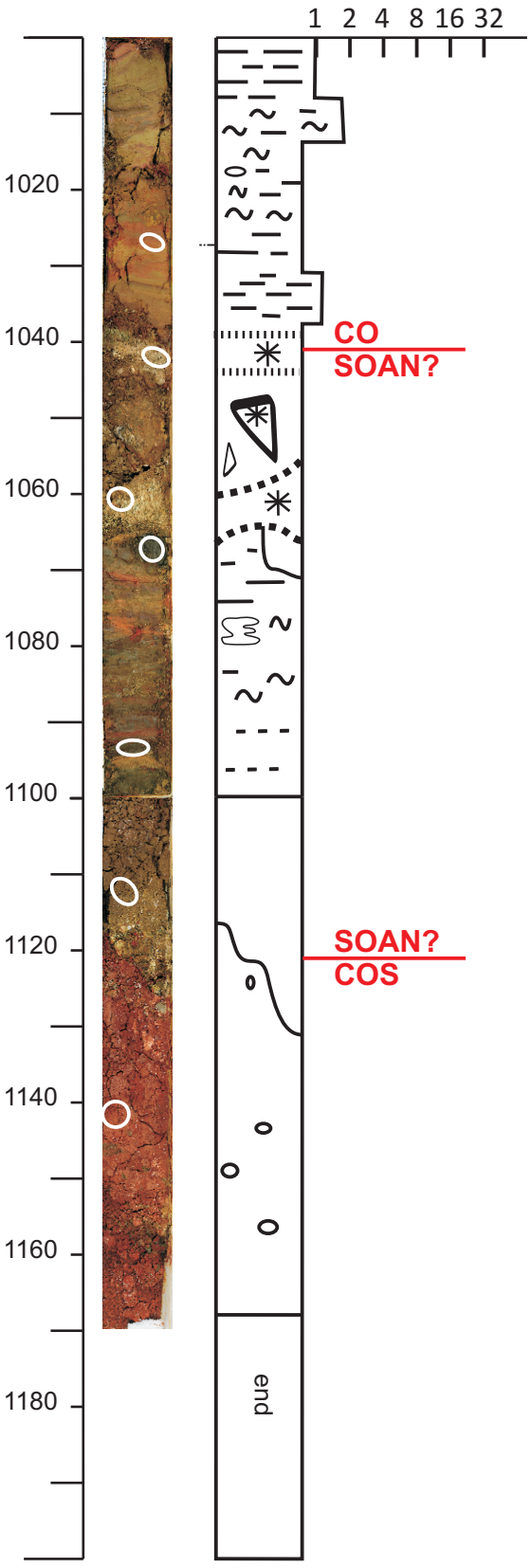
Core: Va29_547 KS page 2/4



Core: Va29_547 KS page 3/4



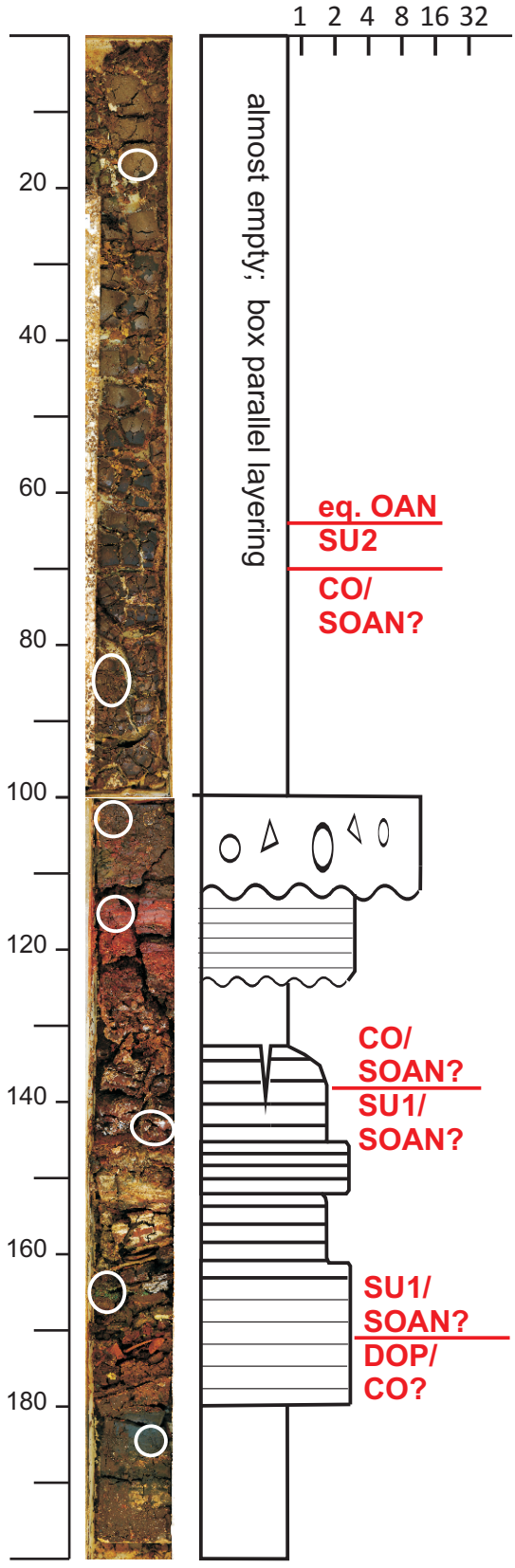
Core: Va29_547 KS page 4/4



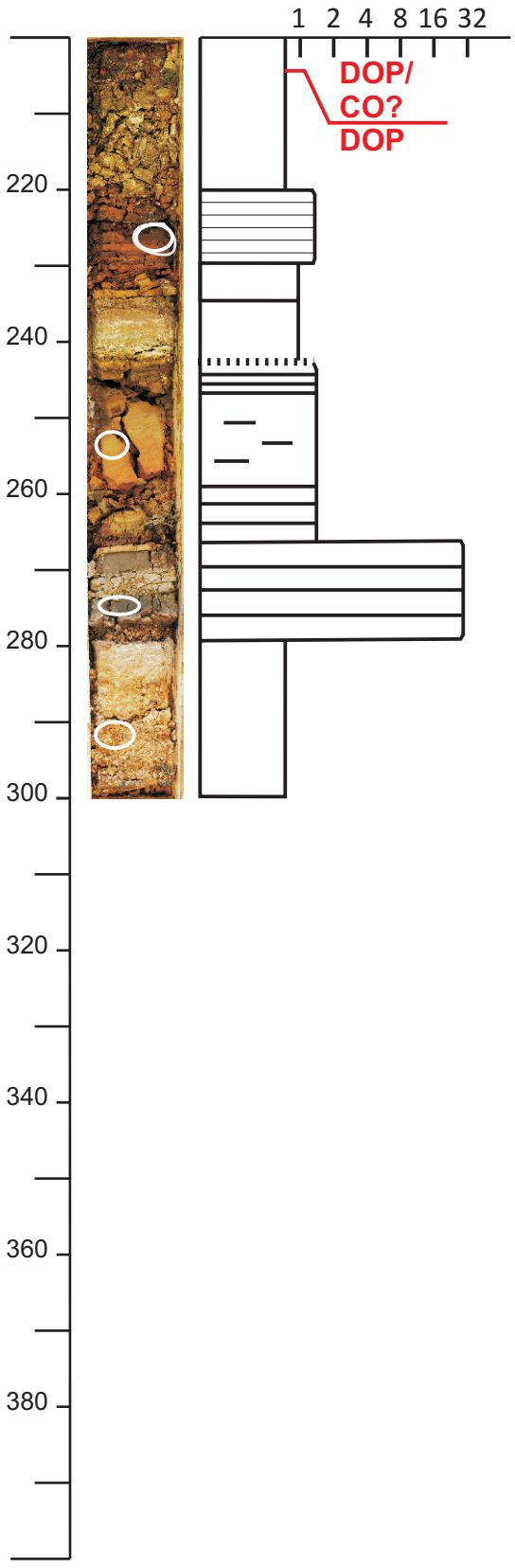
Appendix B.3.

Core: Va29_549 KS page 1/2
(S-Basin)
Water depth: 1996 m
Recovery: 5.87 m
Top loss: 2.07 m
Samples taken: 11

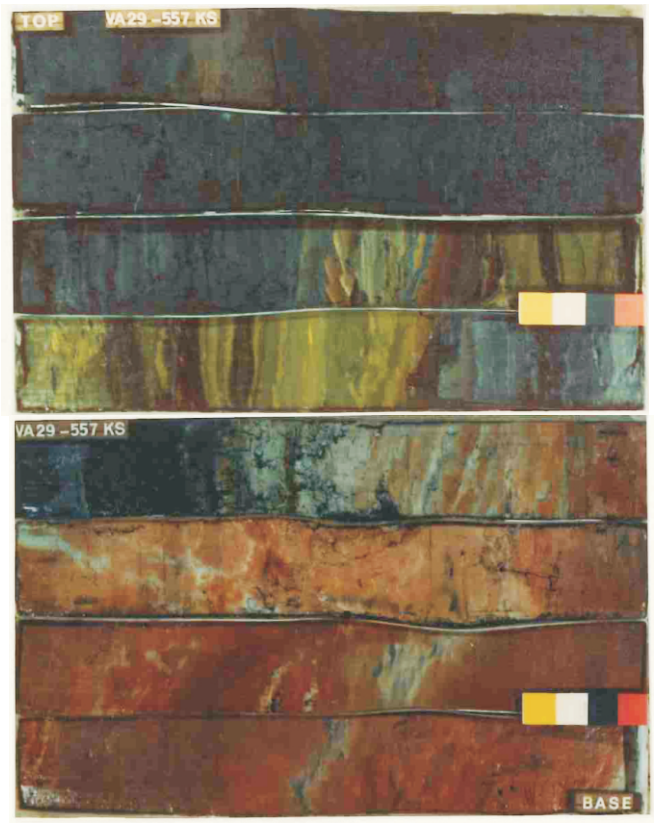


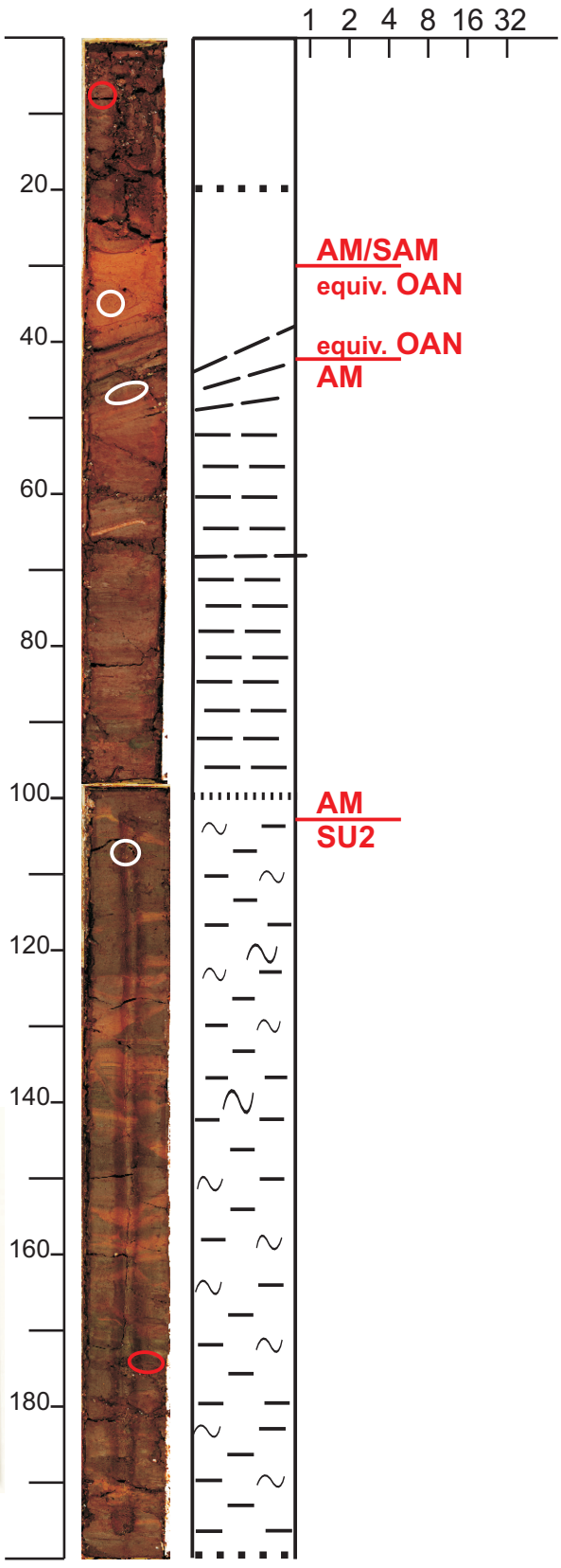



Core: Va29_549 KS  page 2/2

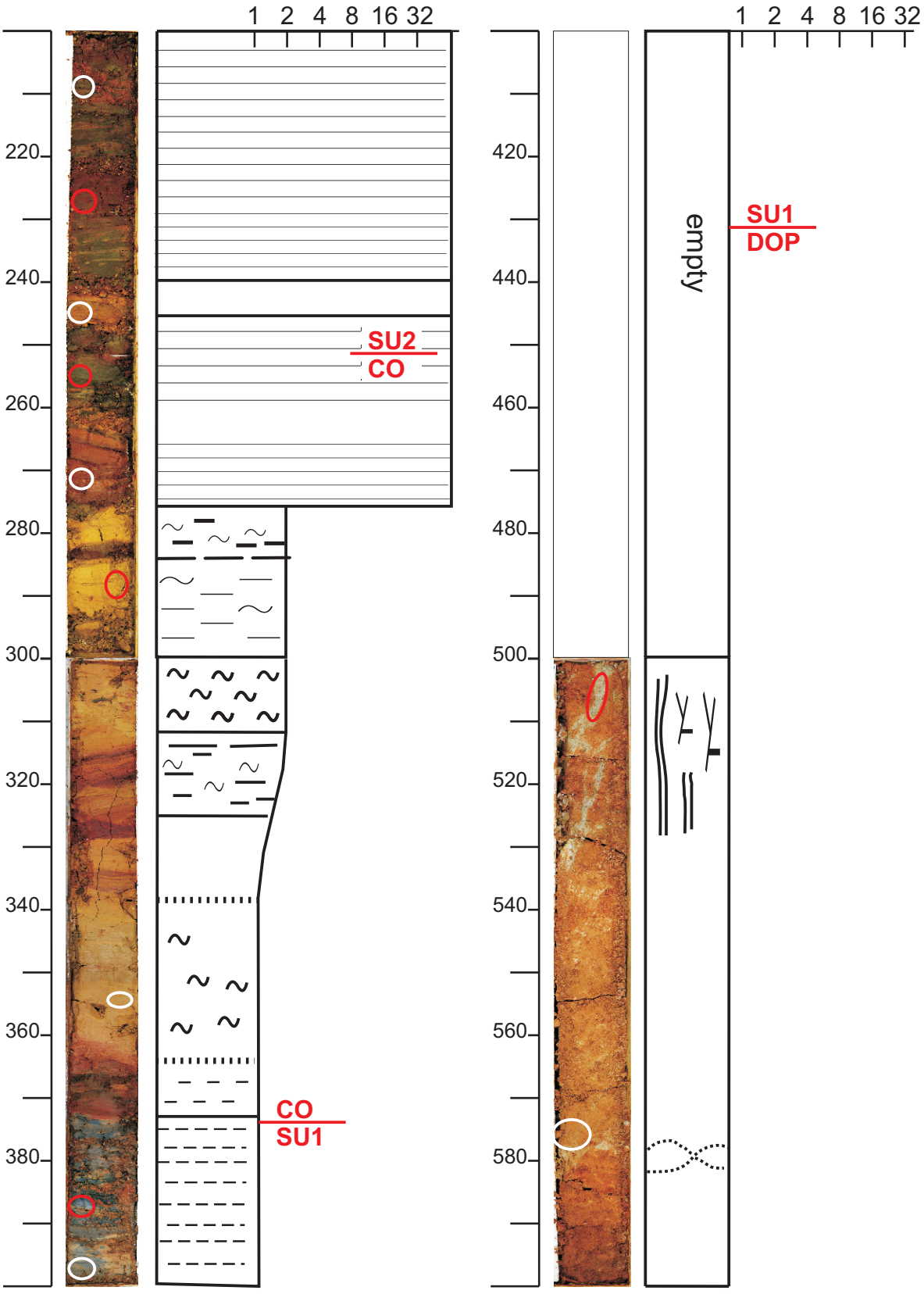


Core: Va29_557 KS page 1/2
(SE-Passage)
Water depth: 2100 m
Recovery: 8.56 m
Top loss: 2.64 m
Samples taken: 20

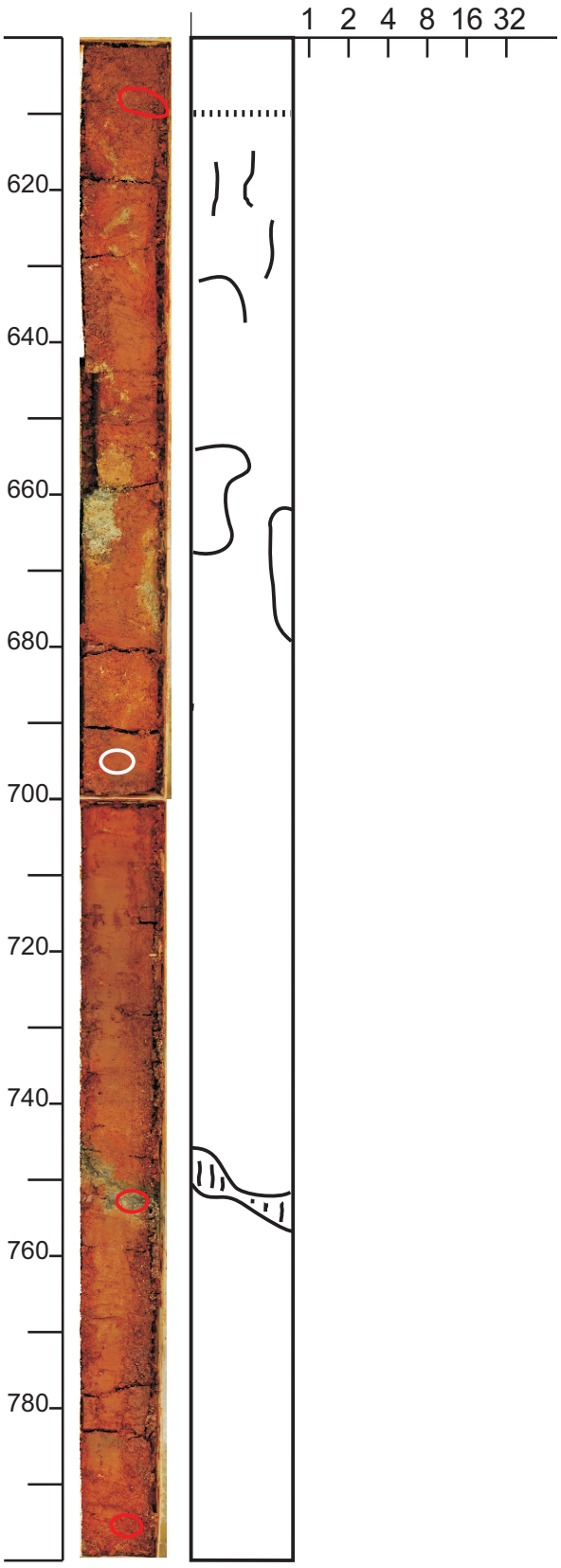


Core: Va29_557 KS page 2/3



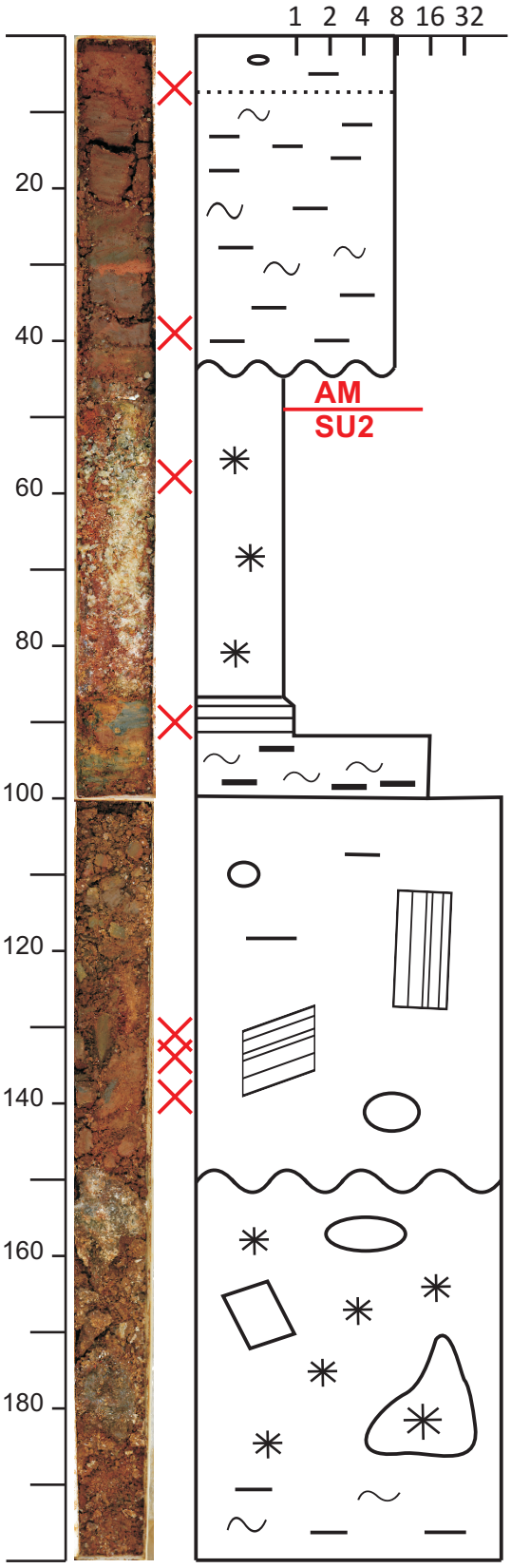
Core: Va29_557 KS  page 3/3



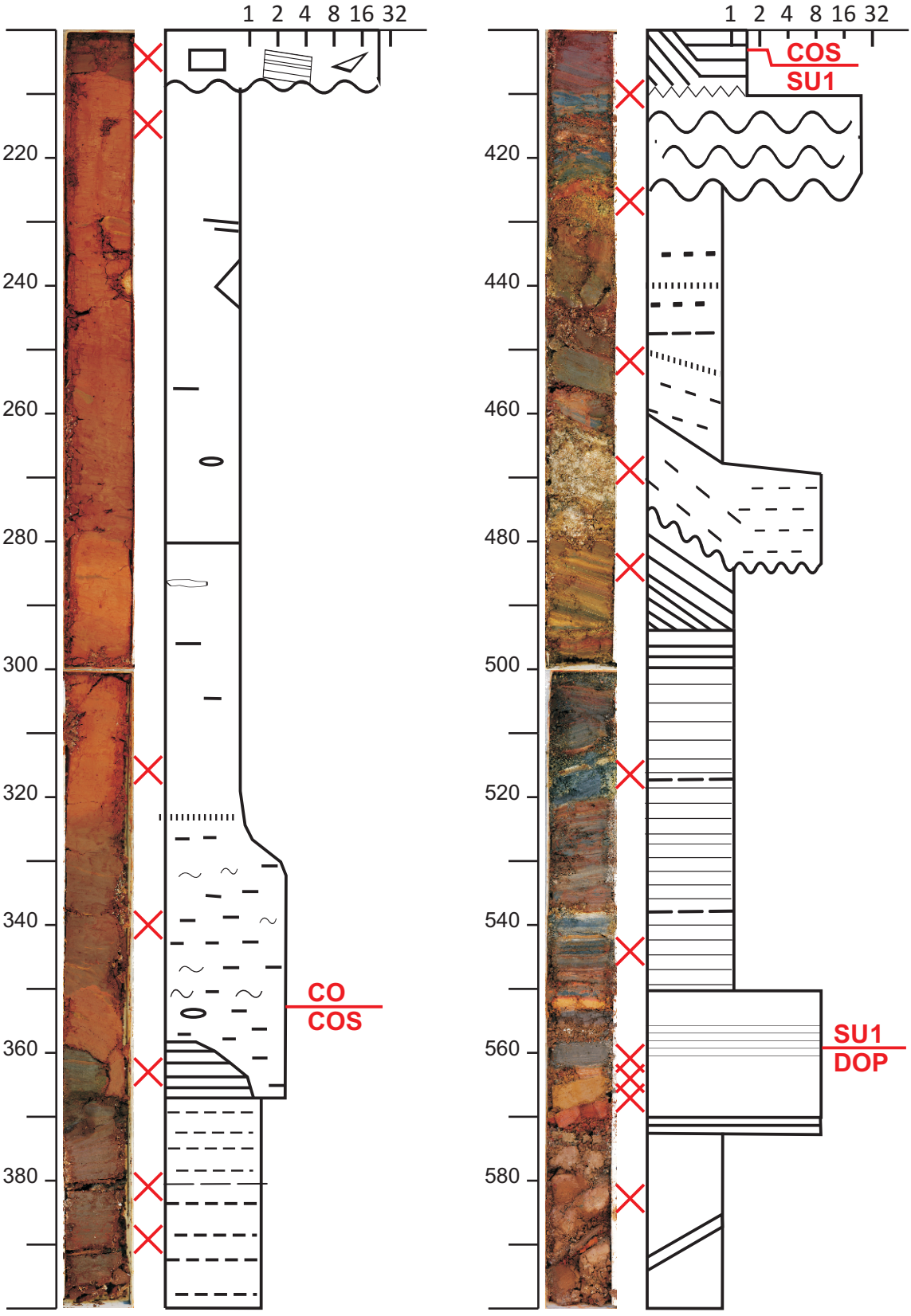
Appendix B.3.

Core: Va29_566 KS page 1/2
(SW-Passage)
Water depth: 2160 m
Recovery: 6.34 m
Top loss: 0 m
Samples taken: 25



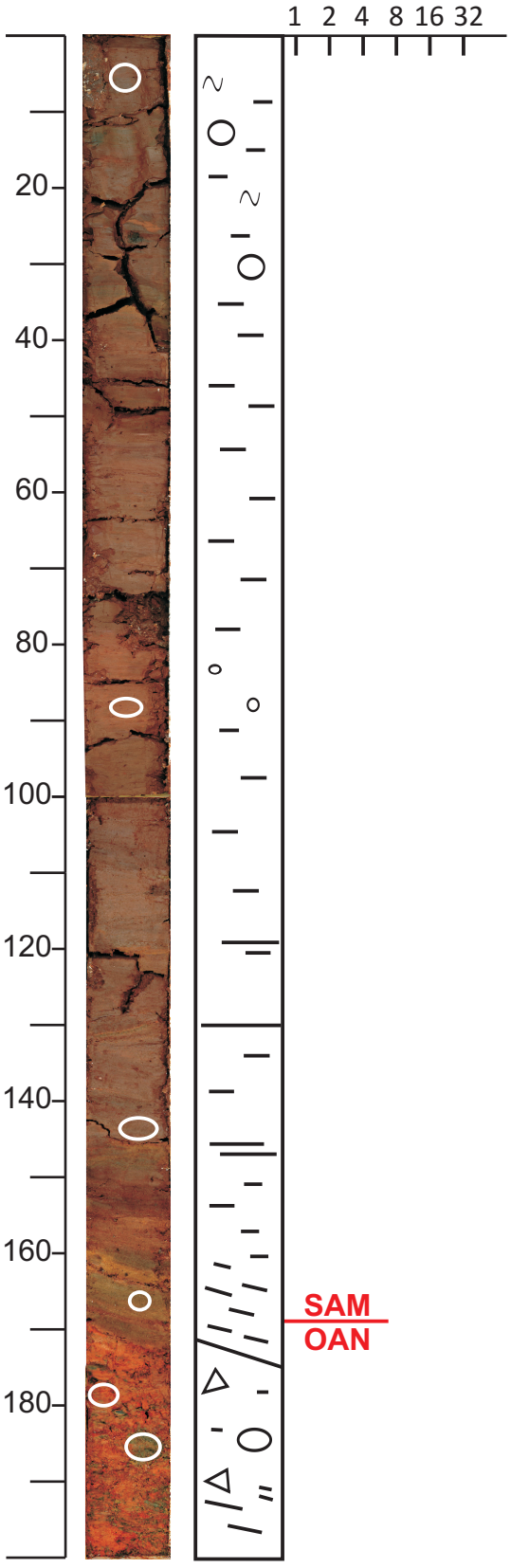
Core: Va29_566 KS page 2/2



Appendix B.3.

Core: Va29_583 KS
page 1 /2
(SW-Basin)
Water depth: 2173 m
Recovery: 5.98 m
Top loss: 1.53 m
Samples taken: 22



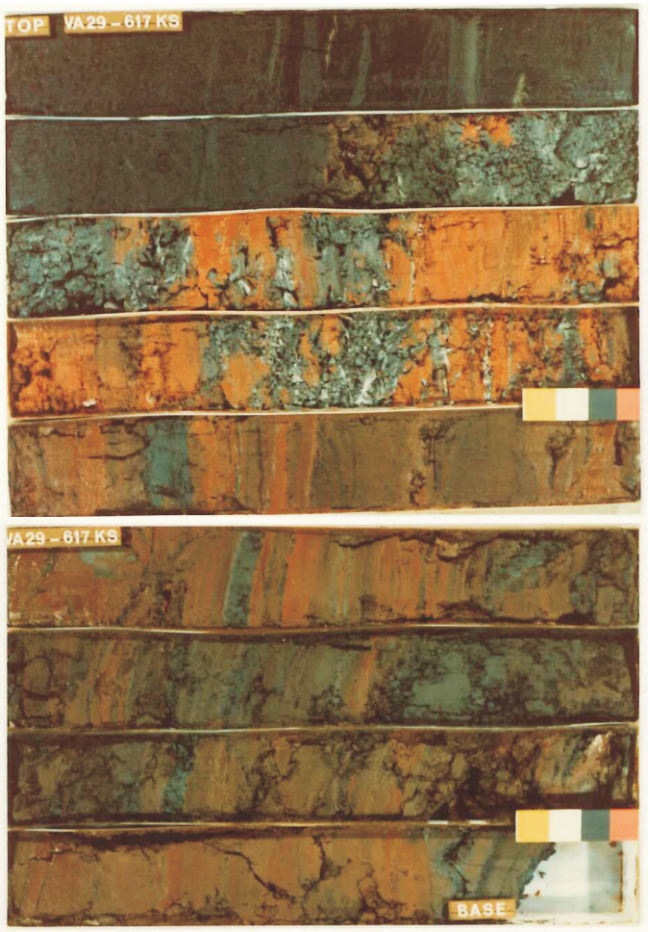



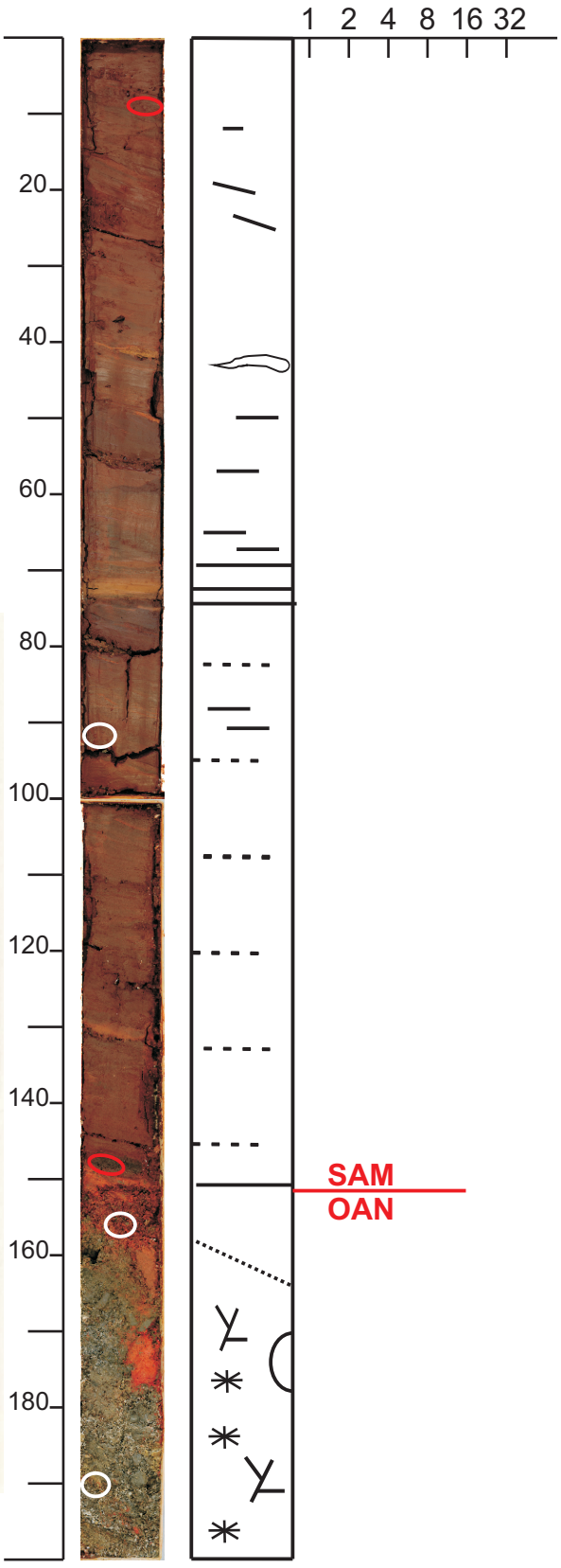
Core: Va29_583 KS page 2/2



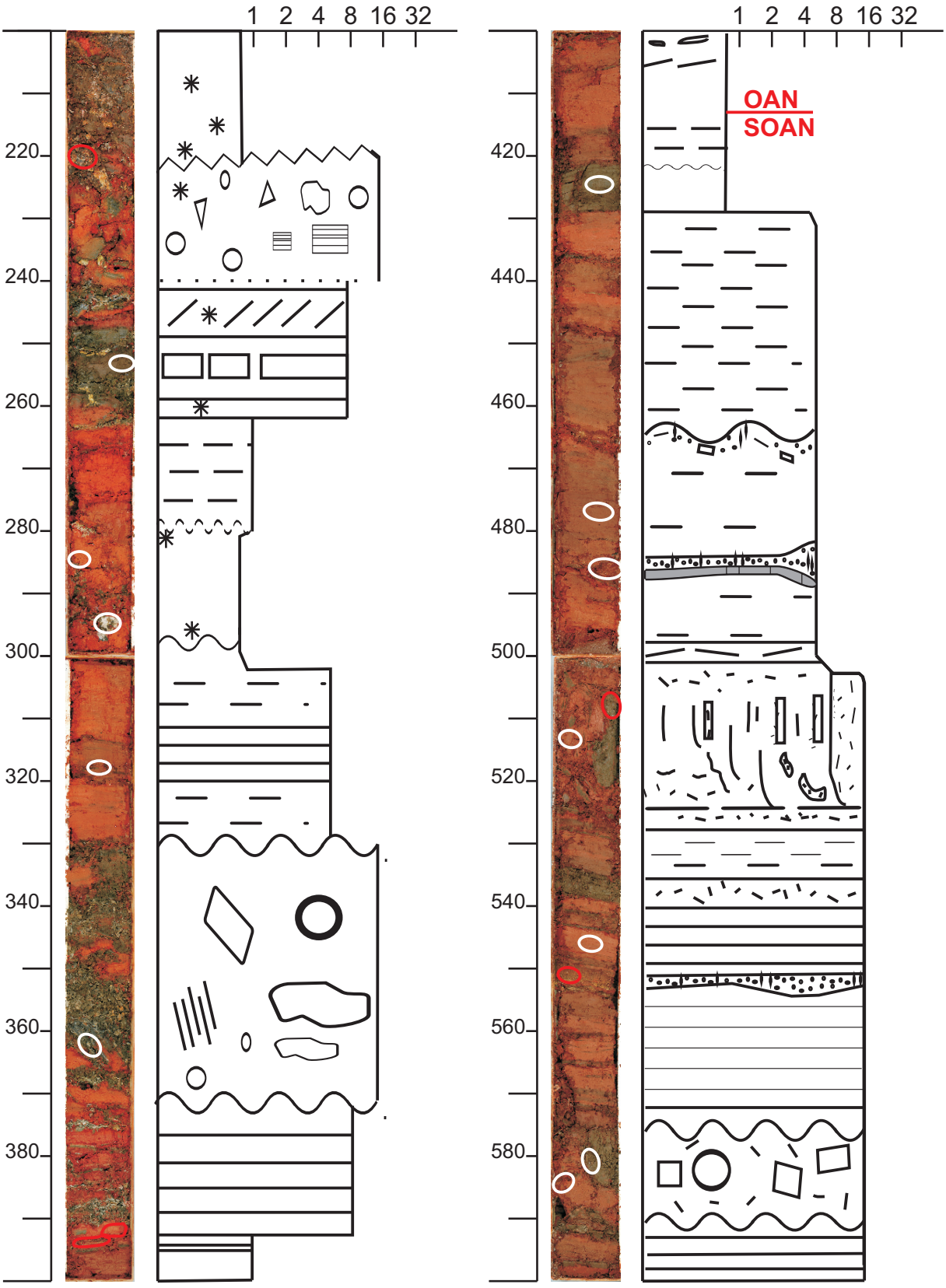
Appendix B.3.

Core: Va29_617 KS
Page 1/3
(S-Basin: 2179 m
Recovery: 9.29 m
Top loss: 3.17 m
Samples taken: 29



Core: Va29_617 KS page 2/3



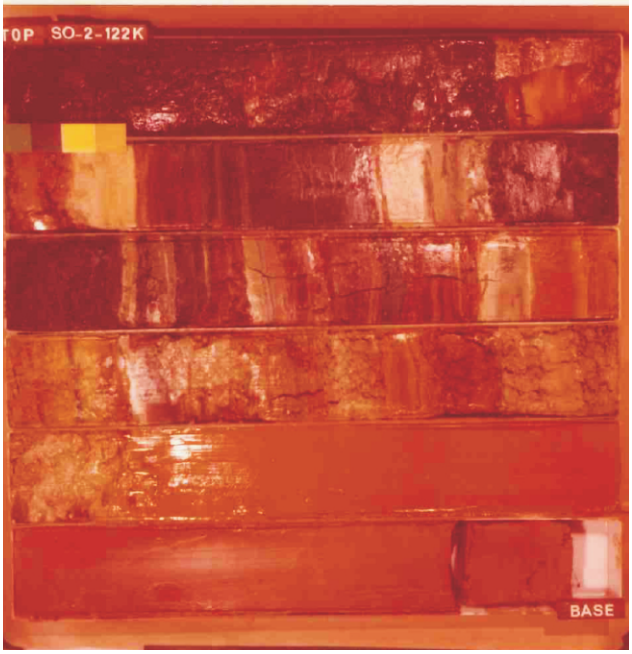
Core: Va29_617 KS page 3/3

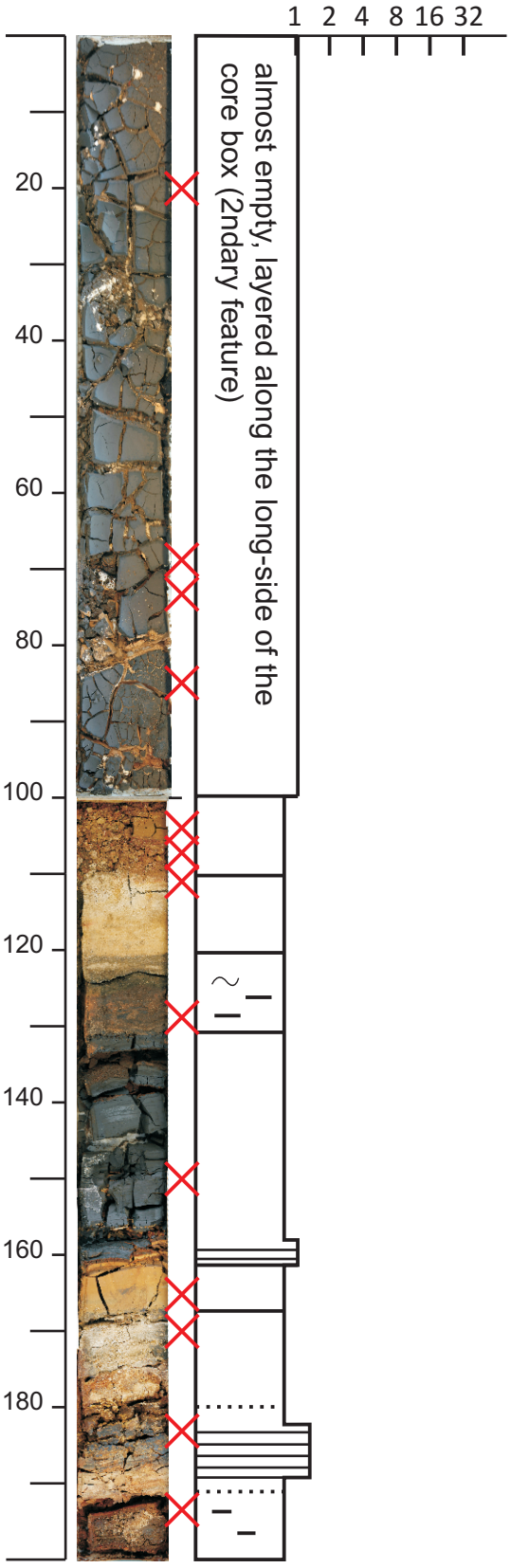


Appendix B.3.

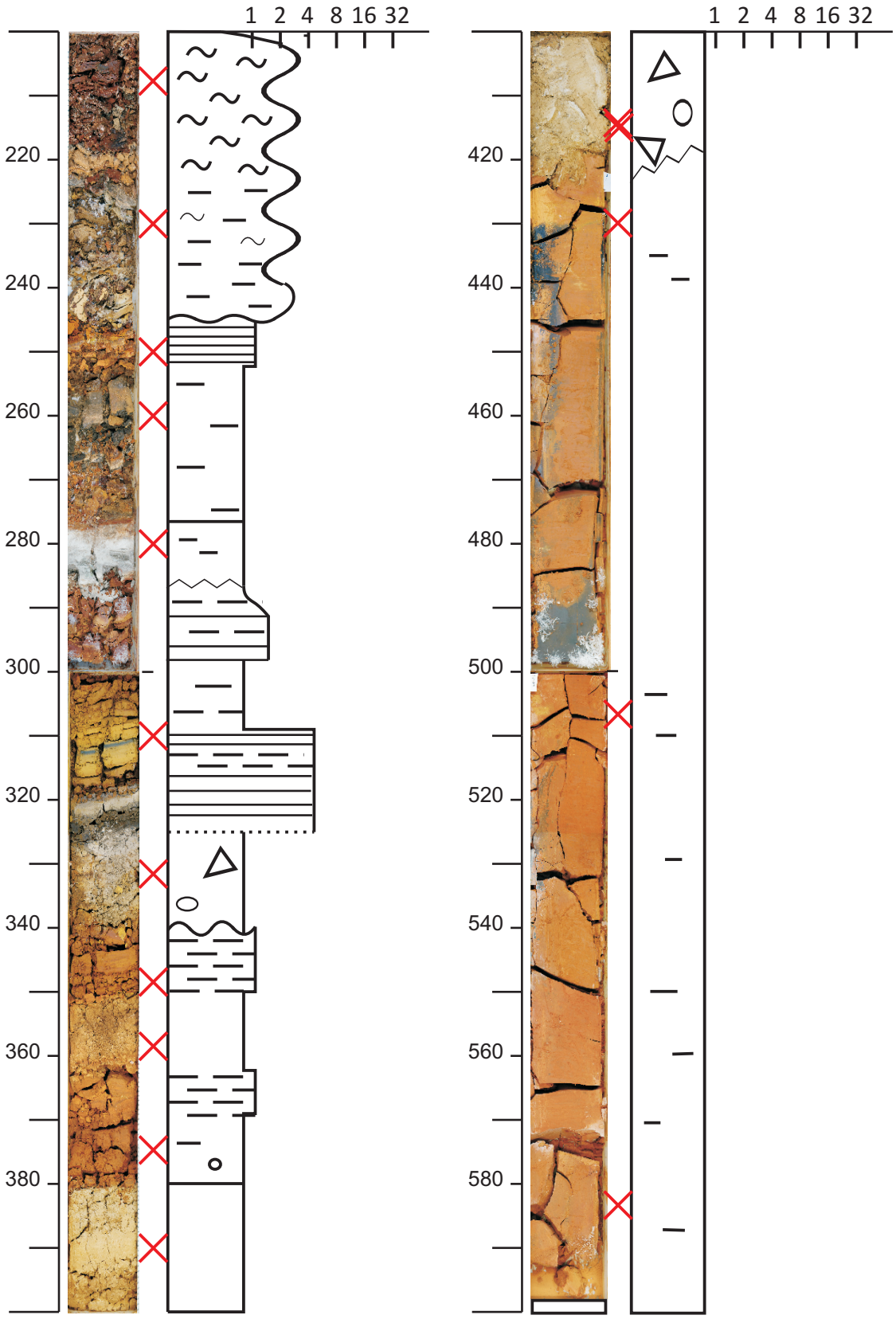
Core: SO-02-122K page 1/2

Water depth: 2005 m
Recovery: 5.95 m
Top loss: ? m
Samples taken: 29
Recovered ~3.5 km West of the brine covered area
Sedimentary units were not identified during this sampling campaign



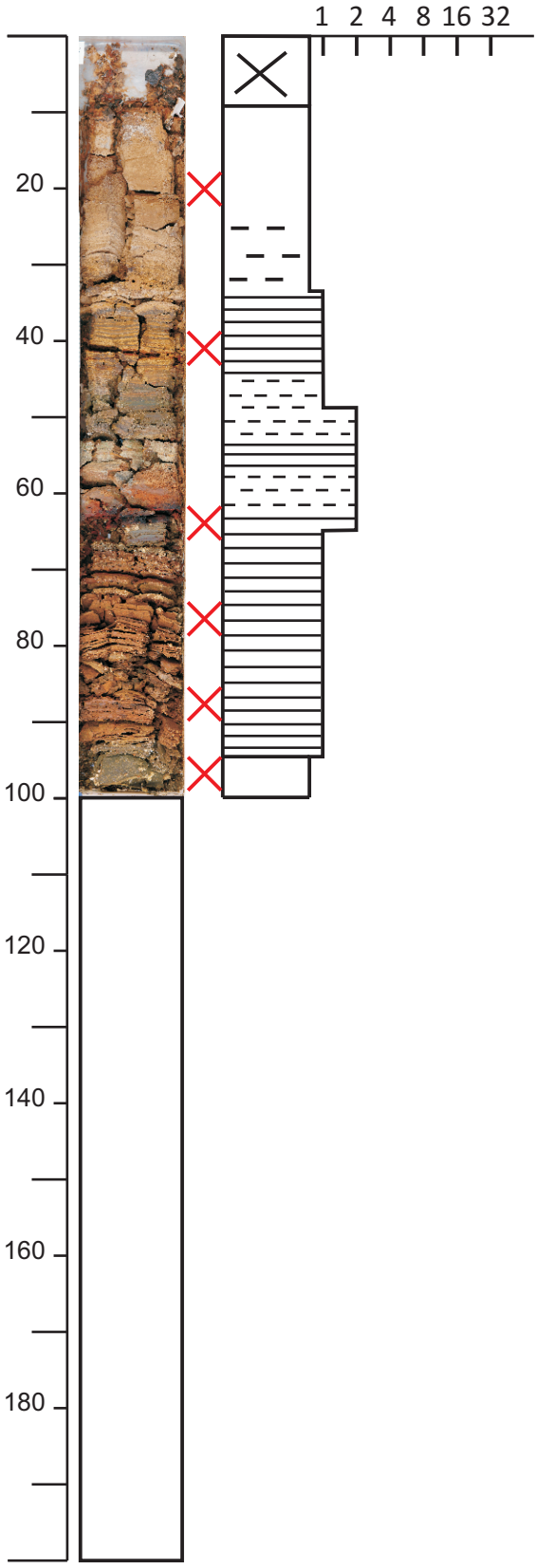
Core: SO-02-122K page 2/2



Appendix B.3.

Background core:
Va01_08K

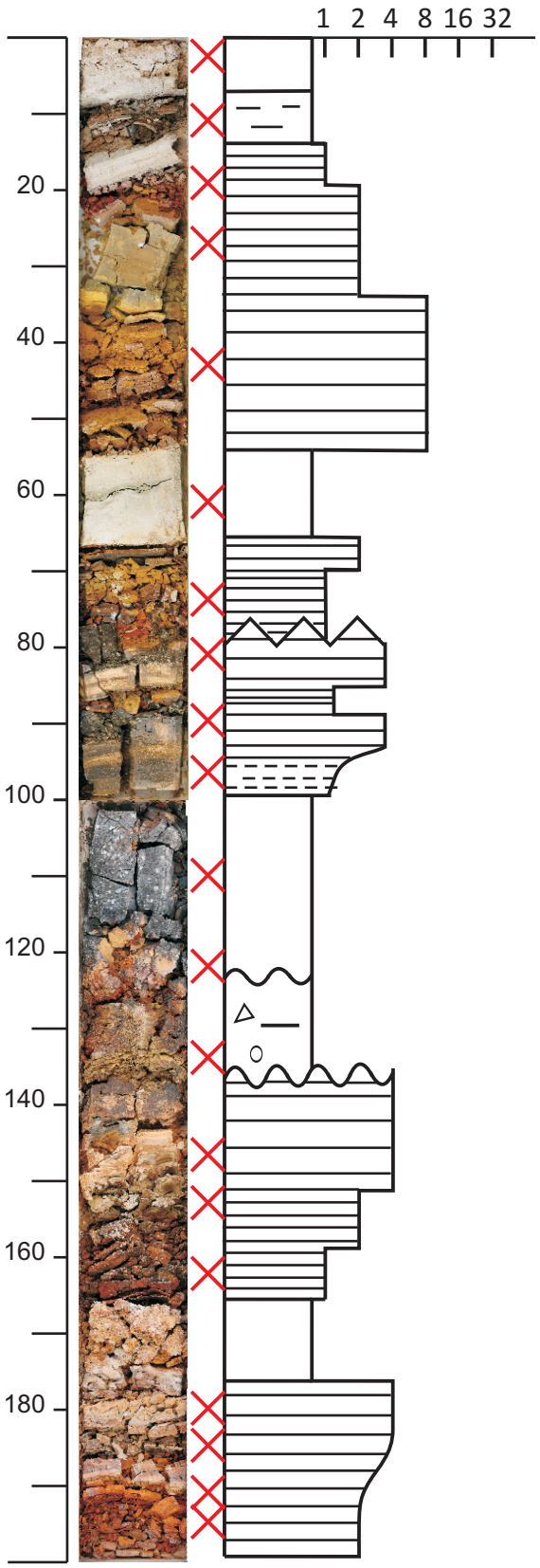
Situated in Wando Basin, ~1 km west of the South part of the West Basin
Water depth: 2000 m
Recovery: 2.20 m
Samples taken: 6



Appendix B.3.

## Background core: Va01_10K

Situated <1 km west of the North part of the Southwest Basin
Water depth: 1990 m
Recovery: ~2.1 m
Samples taken: 20



Appendix C.1. Complete bulk chemical data for 100 samples of metalliferous sediments from the Atlantis II Deep (salt-free basis).

| | | | | Element | | | Au | Ag | As | Cd | Co | Cr | Ga | Ge |
|---|---|---|---|---|---|---|---|---|---|---|---|---|---|---|
| | | | | Method | | | 3 | 8 | 8 | 8 | 1 | 8 | 1 | 1 |
| | | | | Detection limit | | | 2 | 1 | 2 | 1 | 0.2 | 5 | 0.2 | 0.7 |
| Sample ID | unit | SL | CH 2 | CH 3 | CH 4 | NaCl | ppb | ppm | ppm | ppm | ppm | ppm | ppm | ppm |
| 334-83 | SAM | x | HS-Zn | HSHM | n.c. | 49.8 | 484 | 23 | 119 | 78 | 123 | n.d. | 9 | 6 |
| 334-312 | SAM | x | LSHM | LSHM | S-rich | 52.3 | 1048 | 149 | 183 | 155 | 252 | n.d. | 14 | 8 |
| 334-513 | SAM | x | HS-Zn | HSHM | S-rich | 49.7 | 1727 | 850 | 604 | 1121 | 227 | n.d. | 17 | 11 |
| 334-612 | SOAN | | HS-Cu | HSHM | n.c. | 53.9 | 1018 | 115 | 231 | 94 | 148 | n.d. | 12 | 11 |
| 334-757 | SOAN | x | HS-Zn | HSHM | S-rich | 50.6 | 1157 | 57 | 168 | 251 | 125 | n.d. | 18 | 8 |
| 373-8 | AM | x | Clay-rich | Clay-rich | n.c. | 66.6 | 575 | 4 | 179 | n.d. | 105 | n.d. | 11 | 9 |
| 373-93 | SU2 | | Clay-rich | Clay-rich | n.c. | 60.6 | 357 | 13 | 178 | 2 | 61 | 14 | 8 | 9 |
| 373-210 | SU2 | | Clay-rich | Clay-rich | n.c. | 66.0 | 206 | n.d. | 123 | n.d. | 30 | n.d. | 9 | 11 |
| 373-265 | CO | | Mn-rich | Clay-rich | n.c. | 52.9 | n.d. | n.d. | 138 | n.d. | 173 | n.d. | 24 | 2 |
| 373-515 | COS | | $CO_3$-HC | $CO_3$-rich | n.c. | 50.5 | 449 | n.d. | 233 | n.d. | 38 | n.d. | 6 | 20 |
| 373-555 | SU1 | | HS-Zn | HSHM | S-rich | 43.7 | 2434 | 174 | 613 | 548 | 259 | 24 | 37 | 13 |
| 373-586 | SU1 | x | anhy | anhy | n.c. | 4.4 | 264 | 4 | 94 | 16 | 12 | n.d. | 4 | 1 |
| 373-672 | SU1 | | HSLM | HSLM | Fe-rich | 55.1 | 419 | 6 | 291 | n.d. | 17 | n.d. | 12 | 11 |
| 373-751 | SU1 | | HS-Zn | HSHM | S-rich | 30.8 | 2154 | 95 | 893 | 159 | 185 | 20 | 37 | 16 |
| 373-780 | DOP | | detrital | $CO_3$-rich | Al-rich | 22.6 | n.d. | n.d. | 24 | 1 | 19 | 33 | 8 | 3 |
| 373-798 | DOP | | Clay-rich | Clay-rich | Fe-rich | 49.9 | n.d. | 1 | 137 | 17 | 27 | 18 | 3 | 6 |
| 387-80 | SU2 | x | HS-Zn | HSHM | n.c. | 55.8 | 708 | 28 | 137 | 34 | 99 | n.d. | 11 | 7 |
| 387-174 | SU2 | | Clay-rich | Clay-rich | n.c. | 66.4 | n.d. | 11 | 112 | 61 | 18 | n.d. | 6 | 16 |
| 387-261 | CO | | $CO_3$-HC | $CO_3$-rich | Al-rich | 30.8 | 108 | 4 | 188 | 1 | 18 | 54 | 11 | 5 |
| 387-302 | CO | | Clay-rich | Clay-rich | Fe-rich | 35.3 | n.d. | 2 | 1145 | 11 | 9 | n.d. | 2 | 8 |
| 387-398 | SU1 | x | HS-Cu | HSHM | S-rich | 43.8 | 3166 | 306 | 703 | 491 | 288 | 24 | 44 | 13 |
| 387-466 | SU1 | x | HS-Cu | HSHM | S-rich | 35.1 | 1126 | 119 | 427 | 167 | 159 | 14 | 22 | 8 |
| 387-490 | SU1 | | HS-Cu | HSHM | Fe-rich | 14.5 | 249 | 8 | 280 | 23 | 53 | 9 | 10 | 6 |
| 387-502 | SU1 | | anhy | anhy | n.c. | 2.8 | 11 | n.d. | 12 | n.d. | 2 | n.d. | 1 | 2 |
| 387-575 | SU1 | x | HSLM | HSLM | S-rich | 32.2 | 3376 | 96 | 822 | 98 | 65 | 17 | 34 | 5 |
| 421-80 | SU2 | x | LSHM | LSHM | n.c. | 55.6 | 1277 | 66 | 185 | 28 | 147 | n.d. | 14 | 10 |
| 421-160 | SU2 | | $CO_3$-HC | $CO_3$-rich | n.c. | 65.4 | n.d. | 2 | 76 | n.d. | 43 | n.d. | 5 | 8 |
| 421-223 | CO | | Clay-rich | Clay-rich | Fe-rich | 60.0 | 90 | 4 | 71 | 12 | 28 | n.d. | 1 | 6 |
| 421-362 | COS | | Clay-rich | Clay-rich | n.c. | 65.9 | 719 | 22 | 147 | 41 | 119 | n.d. | 15 | 13 |
| 421-496 | SU1 | | $CO_3$-HC | $CO_3$-rich | Fe-rich | 32.8 | 59 | n.d. | 55 | n.d. | 19 | 22 | 6 | 4 |
| 421-520 | SU1 | | $CO_3$-HC | $CO_3$-rich | Fe-rich | 51.9 | 114 | 1 | 101 | n.d. | 15 | n.d. | 5 | 7 |
| 421-678 | DOP | | HS-Cu | HSHM | S-rich | 39.0 | 1753 | 199 | 647 | 189 | 315 | 27 | 37 | 12 |
| 421-740 | DOP | x | HS-Zn | HSHM | n.c. | 60.8 | 1318 | 10 | 96 | 21 | 30 | 21 | 13 | 10 |
| 421-825 | DOP | x | detrital | $CO_3$-rich | Al-rich | 18.6 | n.d. | 2 | 111 | 6 | 77 | 88 | 10 | 3 |
| 421-870 | DOP | | $CO_3$-HC | $CO_3$-rich | Fe-rich | 43.4 | n.d. | n.d. | 76 | 3 | 14 | 30 | 4 | 6 |
| 495-113 | AM | | Clay-rich | Clay-rich | Fe-rich | 58.7 | 375 | n.d. | 186 | n.d. | 36 | n.d. | 9 | 8 |
| 495-240 | AM | | Clay-rich | HSHM | n.c. | 70.4 | 777 | 40 | 416 | 241 | 164 | n.d. | 11 | 13 |
| 495-362 | SU2 | x | Clay-rich | Clay-rich | n.c. | 52.7 | 1041 | 16 | 187 | 3 | 60 | n.d. | 11 | 10 |
| 495-484 | SU2 | | HS-Zn | HSHM | n.c. | 57.9 | 923 | 77 | 194 | 31 | 214 | n.d. | 18 | 10 |
| 495-548 | SU2 | | $CO_3$-HC | $CO_3$-rich | Fe-rich | 45.1 | 115 | 5 | 198 | 1 | 37 | 12 | 16 | 10 |
| 495-557 | CO | x | $CO_3$-HC | $CO_3$-rich | Fe-rich | 27.3 | n.d. | 2 | 165 | 1 | 34 | 23 | 5 | 5 |
| 495-569 | CO | x | Mn-rich | $CO_3$-rich | n.c. | 25.1 | n.d. | n.d. | 67 | n.d. | 28 | 16 | 17 | 3 |
| 495-582 | CO | | detrital | $CO_3$-rich | Al-rich | 15.4 | 24 | n.d. | 6 | 1 | 9 | 34 | 8 | 1 |
| 495-599 | CO | | $CO_3$-HC | $CO_3$-rich | n.c. | 35.1 | 28 | n.d. | 38 | n.d. | 15 | 27 | 8 | 6 |
| 495-693 | COS | | Clay-rich | Clay-rich | Fe-rich | 52.7 | 362 | n.d. | 156 | n.d. | 24 | 12 | 9 | 12 |
| 495-757 | SU1 | | detrital | $CO_3$-rich | Al-rich | 19.7 | 458 | 26 | 108 | 66 | 70 | 51 | 14 | 5 |
| 495-777 | SU1 | | HS-Cu | HSHM | S-rich | 24.8 | 2047 | 130 | 802 | 128 | 157 | 22 | 48 | 8 |

| Sample ID | unit | SL | CH 2 | CH 3 | CH 4 | NaCl | Au | Ag | As | Cd | Co | Cr | Ga | Ge |
|---|---|---|---|---|---|---|---|---|---|---|---|---|---|---|
| 495-809 | SU1 | x | LSLM | LSLM | n.c. | 59.0 | 254 | 3 | 46 | n.d. | 15 | n.d. | 7 | 13 |
| 495-867 | SU1 | | detrital | $CO_3$-rich | Al-rich | 18.4 | 221 | 8 | 42 | 14 | 36 | 48 | 12 | 4 |
| 495-889 | DOP | | Mn-rich | $CO_3$-rich | n.c. | 35.9 | 334 | 18 | 194 | 8 | 83 | 27 | 15 | 7 |
| 495-934 | DOP | | detrital | $CO_3$-rich | Al-rich | 12.8 | 58 | 3 | 20 | 1 | 27 | 52 | 10 | 3 |
| 495-1088 | DOP | | detrital | $CO_3$-rich | Al-rich | 11.0 | n.d. | 2 | 21 | 1 | 25 | 55 | 10 | 3 |
| 495-1195 | DOP | | detrital | $CO_3$-rich | Al-rich | 13.8 | 41 | 2 | 30 | n.d. | 26 | 60 | 11 | 3 |
| 503-7 | SAM | | HS-Zn | HSHM | n.c. | 58.5 | 890 | 28 | 233 | 19 | 160 | n.d. | 9 | 10 |
| 503-75 | OAN | x | HSLM | HSLM | S-rich | 40.7 | 3678 | 183 | 773 | 148 | 65 | 14 | 36 | 7 |
| 503-140 | SOAN | x | LSLM | LSLM | n.c. | 54.9 | 328 | 1 | 77 | 2 | 114 | n.d. | 12 | 9 |
| 503-155 | SOAN | | HS-Zn | HSHM | n.c. | 54.3 | 717 | 1 | 121 | 2 | 131 | n.d. | 14 | 9 |
| 503-235 | SOAN | | anhy | anhy | n.c. | 7.9 | 40 | n.d. | 4 | n.d. | 14 | n.d. | 0 | n.d |
| 503-266 | SOAN | | anhy | anhy | n.c. | 16.4 | 56 | 6 | 18 | 11 | 20 | n.d. | 1 | 1 |
| 503-407 | COS | | Clay-rich | Clay-rich | Fe-rich | 37.6 | 85 | 1 | 153 | n.d. | 13 | n.d. | 3 | 11 |
| 503-509 | COS | | LSLM | LSLM | Fe-rich | 45.1 | 69 | n.d. | 169 | n.d. | 8 | n.d. | 4 | 9 |
| 503-516 | COS | x | $CO_3$-rich | $CO_3$-rich | Al-rich | 34.1 | 1300 | 130 | 151 | 148 | 45 | 78 | 27 | 5 |
| 503-626 | COS | | LSLM | LSLM | Fe-rich | 46.6 | 82 | 2 | 133 | 2 | 4 | n.d. | 2 | 7 |
| 503-671 | COS | x | Clay-rich | Clay-rich | n.c. | 61.5 | 185 | 3 | 54 | n.d. | 12 | n.d. | 6 | 11 |
| 503-680 | COS | x | Clay-rich | Clay-rich | Fe-rich | 54.5 | 352 | 2 | 295 | 3 | 67 | n.d. | 7 | 13 |
| 503-807 | SU1 | x | HSLM | HSLM | S-rich | 32.0 | 2146 | 67 | 524 | 53 | 77 | 14 | 39 | 6 |
| 503-889 | SU1 | x | $CO_3$-rich | $CO_3$-rich | Fe-rich | 7.7 | 253 | 19 | 132 | 17 | 236 | 6 | 6 | 5 |
| 503-912 | SU1 | x | HS-Zn | HSHM | S-rich | 40.1 | 3755 | 153 | 888 | 323 | 199 | 15 | 54 | 25 |
| 503-946 | DOP | | HS-Zn | HSHM | n.c. | 38.8 | 327 | 29 | 168 | 141 | 45 | 9 | 11 | 13 |
| 503-987 | DOP | | HSLM | HSLM | Al-rich | 19.6 | 167 | 9 | 373 | 10 | 45 | 72 | 13 | 9 |
| 546-5 | AM | | HS-Cu | HSHM | n.c. | 56.3 | 1654 | 168 | 259 | 152 | 122 | 13 | 23 | 11 |
| 546-92 | AM | x | LSHM | LSHM | n.c. | 61.6 | 1220 | 51 | 170 | 137 | 234 | n.d. | 19 | 10 |
| 546-180 | AM | x | $CO_3$-HC | $CO_3$-rich | n.c. | 53.8 | 673 | 31 | 139 | 66 | 68 | n.d. | 9 | 14 |
| 546-229 | SU2 | | $CO_3$-HC | $CO_3$-rich | n.c. | 38.2 | 1513 | 78 | 111 | 81 | 252 | 9 | 28 | 6 |
| 546-252 | CO | | detrital | $CO_3$-rich | Al-rich | 19.1 | n.d. | 9 | 14 | 16 | 45 | 58 | 10 | 3 |
| 546-267 | SU1 | x | LSLM | LSLM | Fe-rich | 35.2 | 1170 | 26 | 271 | 28 | 15 | 11 | 29 | 16 |
| 546-311 | SU1 | | $CO_3$-HC | $CO_3$-rich | Fe-rich | 10.2 | 96 | 3 | 17 | 4 | 66 | 8 | 5 | 5 |
| 546-318 | SU1 | | HSLM | HSLM | Al-rich | 20.3 | 440 | 12 | 191 | 5 | 3 | 19 | 8 | 2 |
| 546-385 | DOP | | detrital | $CO_3$-rich | Al-rich | 13.2 | n.d. | n.d. | 39 | 1 | 46 | 54 | 8 | 2 |
| 557-9 | SAM | | HS-Zn | HSHM | S-rich | 62.5 | 2460 | 90 | 198 | 205 | 187 | n.d. | 14 | 9 |
| 557-173 | SU2 | x | HS-Zn | HSHM | S-rich | 66.8 | 2388 | 209 | 275 | 289 | 328 | n.d. | 23 | 12 |
| 557-227 | SU2 | | HS-Zn | HSHM | S-rich | 55.1 | 1567 | 10 | 208 | 58 | 55 | n.d. | 19 | 16 |
| 557-255 | CO | | $CO_3$-HC | $CO_3$-rich | n.c. | 35.2 | 134 | 23 | 47 | 45 | 41 | 58 | 11 | 4 |
| 557-289 | CO | | LSLM | Clay-rich | Fe-rich | 46.6 | 795 | 16 | 185 | 7 | 94 | n.d. | 17 | 7 |
| 557-388 | SU1 | | HS-Cu | HSHM | S-rich | 31.8 | 2964 | 144 | 608 | 262 | 242 | 22 | 42 | 9 |
| 557-502 | DOP | | detrital | $CO_3$-rich | Al-rich | 8.7 | 34 | n.d. | 50 | 2 | 19 | 47 | 7 | 2 |
| 557-608 | DOP | | detrital | $CO_3$-rich | Al-rich | 12.0 | 39 | n.d. | 49 | 1 | 22 | 33 | 5 | 1 |
| 557-753 | DOP | | detrital | $CO_3$-rich | Al-rich | 13.2 | n.d. | n.d. | 19 | n.d. | 23 | 58 | 6 | 1 |
| 557-795 | DOP | | detrital | $CO_3$-rich | Al-rich | 11.1 | n.d. | n.d. | 46 | n.d. | 10 | 30 | 5 | 1 |
| 617-9 | SAM | | HS-Cu | HSHM | n.c. | 60.1 | 1448 | 67 | 185 | 131 | 232 | n.d. | 16 | 8 |
| 617-148 | SAM | x | HS-Cu | HSHM | S-rich | 54.2 | 1853 | 410 | 332 | 271 | 358 | n.d. | 19 | 18 |
| 617-220 | OAN | x | LSLM | LSLM | n.c. | 31.6 | 300 | 5 | 46 | 4 | 43 | n.d. | 8 | 4 |
| 617-395 | OAN | | HSLM | HSLM | Fe-rich | 44.3 | 589 | 4 | 108 | 3 | 61 | n.d. | 12 | 7 |
| 617-396 | OAN | | HS-Cu | HSHM | n.c. | 36.8 | 1381 | 36 | 143 | 11 | 138 | 41 | 16 | 11 |
| 617-508 | SOAN | | detrital | $CO_3$-rich | Al-rich | 20.7 | 161 | 9 | 22 | 9 | 60 | 45 | 9 | 7 |
| 617-551 | SOAN | | anhy | anhy | n.c. | 14.3 | 232 | 5 | 86 | 13 | 57 | n.d. | 3 | 1 |
| 617-650 | SOAN | | HS-Zn | HSHM | S-rich | 40.9 | 1998 | 98 | 312 | 136 | 317 | 11 | 24 | 9 |
| 617-787 | SOAN | | HS-Zn | HSHM | n.c. | 36.4 | 1236 | 76 | 293 | 207 | 122 | n.d. | 15 | 8 |
| 617-799 | SOAN | x | LSHM | LSHM | S-rich | 35.9 | 1498 | 119 | 131 | 152 | 161 | 12 | 17 | 8 |
| 617-875 | SOAN | x | anhy | anhy | S-rich | 24.7 | 731 | 34 | 207 | 124 | 86 | n.d. | 13 | 7 |

Appendix C.1. Complete bulk chemical data for 100 samples of metalliferous sediments from the Atlantis II Deep (salt-free basis).

| Element | Hg | In | MnO | Mo | Ni | Rb | Sb | Sc | Se | Sn | Sr | Tl |
|---|---|---|---|---|---|---|---|---|---|---|---|---|
| Method | 4 | 1 | 1 | 1 | 1 | 1 | 3 | 8 | 1 | 1 | 1 | 1 |
| Det. lim. | 5 | 0.2 | 0.001 | 1 | 10 | 0.4 | 0.1 | 0.50 | 0.8 | 0.5 | 3 | 0.1 |
| Sample ID | ppb | ppm | wt.% | ppm | ppm | ppm | ppm | ppm | ppm | ppm | ppm | ppm |
| 334-83 | 529 | n.d. | 0.32 | 86 | n.d. | 18 | 11 | 0.73 | 5.2 | 6.2 | 573 | 8.2 |
| 334-312 | 1522 | n.d. | 0.22 | 149 | 63 | 19 | 21 | 0.78 | 6.3 | 106.1 | 451 | 47.4 |
| 334-513 | 19455 | n.d. | 0.48 | 240 | 40 | 17 | 320 | 0.99 | 6.2 | 2.2 | 330 | 34.6 |
| 334-612 | 2734 | n.d. | 0.13 | 85 | 65 | 22 | 27 | 0.72 | 6.5 | 34.1 | 388 | 12.6 |
| 334-757 | 217 | n.d. | 0.13 | 152 | n.d. | 14 | 17 | 0.76 | 4.3 | 2.6 | 322 | 8.5 |
| 373-8 | 1546 | n.d. | 0.38 | 78 | 30 | 39 | 9 | 1.17 | 9.0 | 3.9 | 548 | 9.6 |
| 373-93 | 644 | 1.0 | 0.33 | 76 | n.d. | 34 | 11 | 1.43 | 4.6 | 4.6 | 598 | 4.3 |
| 373-210 | 241 | 1.2 | 1.25 | 79 | n.d. | 77 | 6 | 0.41 | n.d. | 41.4 | 499 | 17.0 |
| 373-265 | n.d. | n.d. | 41.91 | 216 | 42 | 23 | 9 | 1.66 | n.d. | 3.8 | 2009 | 12.1 |
| 373-515 | 649 | n.d. | 3.10 | 156 | 20 | 31 | 18 | 0.71 | 3.4 | n.d. | 408 | 3.2 |
| 373-555 | 4335 | n.d. | 0.92 | 288 | 213 | 24 | 104 | 3.39 | 8.4 | 4.4 | 988 | 64.7 |
| 373-586 | 72 | n.d. | 0.04 | 52 | 21 | 1 | 8 | 0.17 | 1.3 | 80.7 | 513 | 2.6 |
| 373-672 | 577 | n.d. | 1.33 | 147 | 156 | 39 | 22 | 0.48 | 3.8 | 108.9 | 301 | 12.9 |
| 373-751 | 2631 | 0.3 | 3.14 | 399 | 173 | 18 | 94 | 2.51 | 5.9 | 5.6 | 185 | 47.3 |
| 373-780 | 14 | n.d. | 5.99 | 12 | 39 | 30 | 2 | 4.48 | 1.2 | 2.6 | 530 | 1.7 |
| 373-798 | n.d. | n.d. | 0.96 | 268 | 40 | 17 | 7 | 1.77 | 5.2 | 3.4 | 288 | 3.2 |
| 387-80 | 1197 | n.d. | 0.25 | 111 | n.d. | 29 | 12 | 0.74 | 6.1 | 2.5 | 324 | 14.7 |
| 387-174 | 65 | n.d. | 0.47 | 119 | n.d. | 103 | 6 | 0.48 | 3.9 | 4.2 | 395 | 6.2 |
| 387-261 | 496 | n.d. | 2.28 | 32 | 58 | 57 | 3 | 7.99 | 3.2 | 3.3 | 386 | 3.8 |
| 387-302 | 119 | n.d. | 1.17 | 269 | 46 | 14 | 9 | 0.99 | 2.5 | 3.6 | 148 | 0.9 |
| 387-398 | 5034 | n.d. | 0.48 | 379 | 249 | 25 | 96 | 3.42 | 9.4 | 29.0 | 884 | 90.5 |
| 387-466 | 2681 | n.d. | 2.09 | 128 | 92 | 17 | 33 | 2.16 | 6.6 | 3.2 | 179 | 49.0 |
| 387-490 | 2820 | 0.6 | 0.98 | 82 | 59 | 8 | 37 | 1.73 | 2.8 | 1.4 | 83 | 8.5 |
| 387-502 | 11 | n.d. | 0.08 | 6 | n.d. | 2 | 1 | 0.10 | n.d. | n.d. | 471 | 0.2 |
| 387-575 | 650 | n.d. | 0.49 | 301 | 59 | 18 | 103 | 1.45 | 4.7 | 2.7 | 1253 | 44.8 |
| 421-80 | 3040 | n.d. | 1.22 | 173 | 563 | 36 | 20 | 0.60 | 2.7 | n.d. | 322 | 21.6 |
| 421-160 | 466 | n.d. | 2.87 | 119 | 29 | 27 | 3 | 0.51 | 3.8 | 4.6 | 408 | 13.3 |
| 421-223 | 115 | n.d. | 0.87 | 153 | n.d. | 18 | n.d. | 0.56 | n.d. | n.d. | 563 | 3.0 |
| 421-362 | 1412 | n.d. | 0.79 | 100 | 29 | 38 | 16 | 0.68 | 3.8 | n.d. | 470 | 18.2 |
| 421-496 | 118 | n.d. | 5.51 | 174 | 30 | 40 | 1 | 3.12 | n.d. | 3.7 | 187 | 0.4 |
| 421-520 | 260 | n.d. | 1.62 | 112 | n.d. | 49 | 11 | 1.36 | 2.7 | 3.1 | 330 | 2.5 |
| 421-678 | 4867 | n.d. | 1.49 | 203 | 180 | 24 | 39 | 3.58 | 5.2 | 4.4 | 233 | 96.0 |
| 421-740 | 659 | n.d. | 1.33 | 125 | n.d. | 59 | 24 | 1.01 | 3.1 | 6.1 | 250 | 19.4 |
| 421-825 | 293 | n.d. | 0.41 | 15 | 135 | 39 | 12 | 9.43 | 16.0 | 2.0 | 659 | 3.4 |
| 421-870 | 25 | n.d. | 0.28 | 175 | 18 | 21 | 4 | 2.60 | 4.1 | 1.2 | 170 | 0.5 |
| 495-113 | 242 | n.d. | 0.18 | 119 | n.d. | 28 | 8 | 0.54 | 3.1 | n.d. | 346 | 8.0 |
| 495-240 | 1723 | n.d. | 0.37 | 176 | 34 | 29 | 58 | 1.01 | 4.1 | 2.0 | 348 | 11.2 |
| 495-362 | 2348 | n.d. | 0.21 | 70 | n.d. | 28 | 17 | 0.69 | 4.2 | n.d. | 370 | 8.0 |
| 495-484 | 2034 | n.d. | 0.29 | 142 | 47 | 34 | 19 | 0.79 | 5.9 | n.d. | 370 | 24.7 |
| 495-548 | 144 | n.d. | 3.77 | 144 | 55 | 35 | 16 | 1.63 | 3.1 | n.d. | 321 | 2.9 |
| 495-557 | 51 | n.d. | 3.73 | 169 | 55 | 19 | 5 | 3.14 | 1.9 | 1.9 | 295 | 1.2 |
| 495-569 | 44 | n.d. | 34.46 | 390 | 27 | 11 | 5 | 2.13 | n.d. | 1.1 | 161 | 1.2 |
| 495-582 | 47 | n.d. | 4.17 | 7 | 24 | 22 | n.d. | 5.06 | n.d. | n.d. | 947 | 0.4 |
| 495-599 | 128 | n.d. | 4.85 | 59 | 46 | 55 | 4 | 3.75 | 1.5 | n.d. | 439 | 0.9 |
| 495-693 | 381 | n.d. | 0.32 | 127 | n.d. | 46 | 20 | 1.63 | 2.5 | 1.7 | 277 | 3.8 |
| 495-757 | 950 | n.d. | 0.99 | 54 | 75 | 35 | 22 | 7.43 | 2.4 | 0.9 | 466 | 11.5 |
| 495-777 | 3522 | 0.3 | 1.99 | 310 | 133 | 16 | 60 | 2.83 | 5.2 | 2.1 | 153 | 88.9 |

| Sample ID | Hg | In | MnO | Mo | Ni | Rb | Sb | Sc | Se | Sn | Sr | Tl |
|---|---|---|---|---|---|---|---|---|---|---|---|---|
| 495-809 | 193 | n.d. | 0.45 | 32 | n.d. | 73 | 9 | 1.07 | 3.9 | 1.5 | 430 | 12.7 |
| 495-867 | 293 | n.d. | 0.77 | 32 | 61 | 32 | 7 | 6.93 | 3.4 | 2.1 | 530 | 5.4 |
| 495-889 | 448 | n.d. | 12.00 | 215 | 62 | 26 | 19 | 3.61 | 2.5 | n.d. | 611 | 9.7 |
| 495-934 | 101 | n.d. | 0.42 | 14 | 57 | 33 | 3 | 8.01 | n.d. | 1.1 | 581 | 1.7 |
| 495-1088 | 75 | n.d. | 0.29 | 18 | 45 | 34 | 3 | 8.90 | 1.9 | 0.8 | 464 | 1.7 |
| 495-1195 | 91 | n.d. | 0.49 | 20 | 46 | 30 | 3 | 9.02 | 3.0 | 1.3 | 469 | 1.3 |
| 503-7 | 1380 | 0.5 | 0.21 | 183 | n.d. | 25 | 15 | 0.74 | 5.3 | 5.5 | 420 | 16.4 |
| 503-75 | 537 | n.d. | 0.91 | 307 | 51 | 13 | 119 | 1.23 | 3.4 | 1.3 | 1647 | 41.3 |
| 503-140 | 525 | n.d. | 0.18 | 33 | n.d. | 66 | 6 | 0.45 | 4.4 | n.d. | 461 | 13.1 |
| 503-155 | 632 | n.d. | 0.17 | 50 | 22 | 66 | 18 | 0.90 | 4.2 | n.d. | 435 | 14.9 |
| 503-235 | 24 | n.d. | 0.09 | 2 | n.d. | 6 | 1 | 0.12 | n.d. | n.d. | 1040 | 1.0 |
| 503-266 | 65 | n.d. | 0.47 | 17 | n.d. | 1 | 2 | 0.16 | n.d. | 3.8 | 614 | 1.1 |
| 503-407 | 32 | n.d. | 0.54 | 320 | n.d. | 7 | 6 | 0.33 | 2.7 | n.d. | 237 | 0.5 |
| 503-509 | 118 | n.d. | 2.05 | 128 | n.d. | 17 | 7 | 0.30 | 2.0 | n.d. | 579 | 0.7 |
| 503-516 | 1974 | 0.3 | 0.68 | 65 | 91 | 55 | 42 | 11.53 | 9.3 | n.d. | 661 | 17.0 |
| 503-626 | 56 | n.d. | 0.63 | 258 | n.d. | 11 | 6 | 0.34 | n.d. | n.d. | 489 | 1.3 |
| 503-671 | 312 | n.d. | 0.52 | 44 | n.d. | 127 | 14 | 0.63 | n.d. | n.d. | 416 | 7.0 |
| 503-680 | 1395 | n.d. | 2.02 | 213 | 22 | 36 | 32 | 0.81 | 3.1 | n.d. | 675 | 7.5 |
| 503-807 | 1232 | n.d. | 1.26 | 170 | 59 | 21 | 58 | 1.91 | 7.1 | 1.3 | 726 | 59.2 |
| 503-889 | 3618 | 0.2 | 3.27 | 89 | 108 | 6 | 21 | 0.91 | 1.9 | n.d. | 73 | 11.8 |
| 503-912 | 3321 | 0.7 | 1.36 | 429 | 200 | 18 | 149 | 2.22 | 11.0 | n.d. | 150 | 41.7 |
| 503-946 | 649 | n.d. | 2.17 | 87 | 49 | 12 | 22 | 1.64 | 3.8 | n.d. | 752 | 12.3 |
| 503-987 | 885 | n.d. | 0.49 | 94 | 99 | 34 | 26 | 8.67 | 12.2 | 1.2 | 216 | 30.1 |
| 546-5 | 4828 | n.d. | 2.24 | 105 | n.d. | 18 | 23 | 0.72 | 8.5 | n.d. | 309 | 11.7 |
| 546-92 | 1436 | n.d. | 3.36 | 70 | n.d. | 20 | 17 | 0.52 | 5.5 | n.d. | 268 | 6.5 |
| 546-180 | 597 | n.d. | 3.27 | 45 | n.d. | 23 | 14 | 0.74 | 5.0 | n.d. | 214 | 2.6 |
| 546-229 | 1699 | n.d. | 6.64 | 81 | 49 | 22 | 29 | 0.85 | 6.1 | n.d. | 120 | 13.1 |
| 546-252 | 36 | n.d. | 1.39 | 5 | 62 | 39 | 1 | 8.95 | 2.0 | 1.1 | 549 | 3.8 |
| 546-267 | 438 | n.d. | 0.84 | 140 | n.d. | 17 | 29 | 1.31 | 3.2 | n.d. | 484 | 11.1 |
| 546-311 | 900 | n.d. | 5.90 | 13 | 56 | 6 | 1 | 1.13 | 1.7 | n.d. | 96 | 3.7 |
| 546-318 | 804 | n.d. | 0.54 | 46 | n.d. | 14 | 11 | 2.08 | 1.6 | 1.3 | 1568 | 4.3 |
| 546-385 | 58 | n.d. | 0.79 | 30 | 115 | 28 | 1 | 8.44 | n.d. | 0.7 | 471 | 0.5 |
| 557-9 | 5198 | n.d. | 0.35 | 99 | 27 | 31 | 31 | 0.69 | 5.3 | n.d. | 427 | 28.3 |
| 557-173 | 3764 | n.d. | 0.23 | 81 | 60 | 41 | 44 | 1.02 | 9.0 | n.d. | 410 | 41.6 |
| 557-227 | 325 | n.d. | 0.96 | 109 | n.d. | 26 | 25 | 0.47 | 6.5 | n.d. | 218 | 23.8 |
| 557-255 | 996 | n.d. | 3.81 | 32 | 46 | 44 | 3 | 7.61 | 3.6 | n.d. | 188 | 11.9 |
| 557-289 | 835 | n.d. | 1.34 | 314 | n.d. | 12 | 22 | 0.35 | 3.4 | n.d. | 283 | 10.3 |
| 557-388 | 2656 | 0.3 | 2.71 | 247 | 132 | 20 | 52 | 2.84 | 7.5 | 1.0 | 135 | 50.6 |
| 557-502 | 32 | n.d. | 0.55 | 5 | 55 | 27 | 2 | 6.81 | 2.5 | n.d. | 492 | 1.0 |
| 557-608 | 17 | n.d. | 0.51 | 6 | 57 | 23 | 2 | 5.13 | 4.0 | n.d. | 596 | 0.2 |
| 557-753 | 251 | n.d. | 0.56 | 2 | 58 | 26 | 1 | 5.59 | 5.5 | n.d. | 750 | 0.3 |
| 557-795 | 12 | n.d. | 0.47 | 2 | 34 | 17 | 2 | 4.33 | n.d. | n.d. | 593 | 0.1 |
| 617-9 | 3081 | n.d. | 0.39 | 130 | 25 | 21 | 20 | 0.96 | 5.0 | n.d. | 448 | 26.6 |
| 617-148 | 6511 | n.d. | 0.30 | 208 | 66 | 29 | 83 | 0.82 | 4.8 | n.d. | 496 | 39.3 |
| 617-220 | 91 | n.d. | 0.16 | 29 | n.d. | 6 | 6 | 0.43 | n.d. | n.d. | 305 | 0.6 |
| 617-395 | 66 | n.d. | 0.10 | 68 | n.d. | 10 | 11 | 1.20 | 4.3 | n.d. | 377 | 0.7 |
| 617-396 | 3309 | n.d. | 0.26 | 13 | 47 | 16 | 6 | 5.86 | 2.2 | 7.1 | 272 | 3.2 |
| 617-508 | 160 | n.d. | 0.35 | 6 | 38 | 13 | 3 | 6.42 | n.d. | n.d. | 278 | 1.0 |
| 617-551 | 145 | n.d. | 0.12 | 16 | 12 | 2 | 6 | 0.45 | n.d. | n.d. | 495 | 0.7 |
| 617-650 | 2997 | n.d. | 0.31 | 68 | 34 | 9 | 35 | 1.43 | 7.5 | n.d. | 125 | 12.4 |
| 617-787 | 1050 | n.d. | 0.43 | 153 | 31 | 7 | 23 | 0.92 | 1.9 | n.d. | 206 | 4.7 |
| 617-799 | 2232 | n.d. | 0.35 | 55 | 47 | 5 | 44 | 1.88 | 4.5 | n.d. | 435 | 5.0 |
| 617-875 | 1793 | n.d. | 0.14 | 70 | 27 | 3 | 12 | 0.90 | 2.9 | n.d. | 371 | 2.7 |

Appendix C.1. Complete bulk chemical data for 100 samples of metalliferous sediments from the Atlantis II Deep (salt-free basis).

| Element | U | V | W | Y | Zr | Cu | Fe | Zn | Pb | S* | $SO_4$ | Ba | Ca |
|---|---|---|---|---|---|---|---|---|---|---|---|---|---|
| Method | 1 | 1 | 1 | 1 | 8 | 1 | 2 | 1 | 1 | 6 | 7 | 1 | 2 |
| Det. lim. | 0.1 | 5 | 0.7 | 0.1 | 1 | 2 | 0.05 | 30 | 0.8 | 0.01 | 0.3 | 3 | 0.01 |
| Sample ID | ppm | ppm | ppm | ppm | ppm | ppm | wt.% | ppm | ppm | wt.% | wt.% | ppm | wt.% |
| 334-83 | 4.8 | 78 | 6.6 | 1.4 | n.d. | 3423 | 14.7 | 23284 | 432 | 8.1 | 19.1 | 2249 | 9.1 |
| 334-312 | 7.3 | 90 | 7.8 | 1.5 | n.d. | 7066 | 24.1 | 46128 | 1050 | 5.9 | 17.8 | 1151 | 6.6 |
| 334-513 | 9.7 | 99 | 21.1 | 1.8 | n.d. | 8784 | 19.3 | 72535 | 3398 | 13.9 | 28.0 | 1061 | 6.7 |
| 334-612 | 7.8 | 102 | 10.4 | 1.3 | n.d. | 9525 | 24.3 | 30810 | 794 | 5.4 | 10.4 | 638 | 5.3 |
| 334-757 | 5.5 | 75 | 11.1 | 1.0 | n.d. | 1232 | 21.1 | 51659 | 504 | 8.5 | 16.8 | 407 | 4.0 |
| 373-8 | 3.9 | 69 | 7.2 | 1.8 | n.d. | 3326 | 18.9 | 17471 | 665 | 2.4 | 1.5 | 327 | 5.8 |
| 373-93 | 4.8 | 74 | 11.7 | 2.0 | n.d. | 2763 | 20.1 | 13258 | 248 | 1.2 | 0.8 | 1080 | 6.8 |
| 373-210 | 2.1 | 32 | 25.0 | 1.2 | n.d. | 1639 | 17.3 | 2468 | 154 | 1.8 | 2.6 | 115 | 4.1 |
| 373-265 | 2.1 | 140 | 3.8 | 2.8 | n.d. | 282 | 2.8 | 1782 | 375 | 0.4 | n.d. | 5728 | 3.2 |
| 373-515 | 6.3 | 51 | 6.9 | 1.4 | n.d. | 1305 | 25.3 | 14142 | 193 | 0.7 | 1.0 | 192 | 3.1 |
| 373-555 | 3.6 | 110 | 19.2 | 5.2 | 20 | 21498 | 11.0 | 88656 | 2221 | 13.4 | 25.2 | 6254 | 4.1 |
| 373-586 | 0.1 | 10 | 2.5 | 0.2 | n.d. | 1350 | 1.2 | 4038 | 143 | 21.9 | 65.7 | 183 | 22.6 |
| 373-672 | 1.6 | 287 | 8.0 | 0.7 | n.d. | 1336 | 26.7 | 8841 | 218 | 8.2 | 5.3 | 98 | 2.9 |
| 373-751 | 5.9 | 145 | 12.7 | 4.5 | 16 | 16767 | 15.2 | 67503 | 1995 | 10.3 | 25.9 | 256 | 3.5 |
| 373-780 | 0.8 | 101 | n.d. | 8.8 | 35 | 85 | 5.5 | 9379 | 39 | 1.0 | 1.3 | 70 | 18.2 |
| 373-798 | 4.2 | 98 | n.d. | 7.8 | 10 | 300 | 41.8 | 14704 | 32 | 1.5 | n.d. | 44 | 2.4 |
| 387-80 | 4.1 | 68 | 6.8 | 1.4 | n.d. | 4662 | 16.3 | 20279 | 414 | 6.1 | 11.8 | 229 | 5.6 |
| 387-174 | 1.2 | 39 | 7.4 | 0.6 | n.d. | 657 | 21.5 | 13968 | 56 | 2.4 | 4.2 | 247 | 4.5 |
| 387-261 | 4.8 | 158 | n.d. | 16.0 | 56 | 1302 | 13.5 | 1965 | 67 | 1.6 | 2.0 | 1590 | 5.3 |
| 387-302 | 3.9 | 88 | n.d. | 2.0 | n.d. | 470 | 45.6 | 4513 | 115 | 0.4 | n.d. | 80 | 1.9 |
| 387-398 | 3.0 | 146 | 20.3 | 5.2 | 18 | 25435 | 9.2 | 79505 | 2277 | 15.2 | 27.6 | 3842 | 4.1 |
| 387-466 | 5.2 | 117 | 8.9 | 3.9 | 7 | 15873 | 22.7 | 40991 | 909 | 10.4 | 16.2 | 381 | 3.3 |
| 387-490 | 6.9 | 101 | 1.3 | 5.1 | 5 | 10837 | 42.7 | 6050 | 442 | 2.3 | 5.5 | 99 | 0.9 |
| 387-502 | n.d. | n.d. | n.d. | n.d. | n.d. | 395 | 1.0 | 2069 | 7 | 21.4 | 64.2 | 17 | 23.3 |
| 387-575 | 4.4 | 279 | 4.0 | 2.1 | 8 | 5057 | 7.4 | 8935 | 938 | 15.1 | 32.1 | 6989 | 7.8 |
| 421-80 | 5.6 | 65 | 8.1 | 1.1 | n.d. | 12722 | 23.9 | 23643 | 428 | 2.0 | 6.1 | 176 | 3.9 |
| 421-160 | 2.3 | 38 | n.d. | 0.9 | n.d. | 2951 | 25.1 | 24797 | 318 | 5.1 | 1.2 | 61 | 3.2 |
| 421-223 | 10.3 | 28 | n.d. | 0.8 | n.d. | 645 | 30.8 | 12050 | 40 | 0.6 | n.d. | 2273 | 3.2 |
| 421-362 | 3.8 | 65 | 4.4 | 1.2 | n.d. | 5784 | 19.0 | 23607 | 605 | 3.6 | 5.0 | 358 | 5.8 |
| 421-496 | 4.6 | 88 | n.d. | 5.2 | 20 | 772 | 24.1 | 2722 | 13 | 0.3 | n.d. | 217 | 3.3 |
| 421-520 | 3.1 | 60 | 2.5 | 2.1 | n.d. | 1475 | 23.3 | 3678 | 23 | 0.4 | n.d. | 102 | 5.3 |
| 421-678 | 4.8 | 143 | 8.2 | 6.6 | 21 | 26218 | 16.9 | 53911 | 1655 | 14.0 | 28.8 | 456 | 2.4 |
| 421-740 | 1.5 | 746 | 11.5 | 1.8 | n.d. | 1109 | 17.2 | 37292 | 478 | 3.1 | 5.1 | 77 | 1.4 |
| 421-825 | 10.6 | 264 | n.d. | 17.4 | 87 | 600 | 5.5 | 5194 | 27 | 3.3 | 9.9 | 174 | 15.0 |
| 421-870 | 3.5 | 237 | n.d. | 10.3 | 14 | 103 | 40.5 | 3835 | 4 | 0.3 | 0.5 | 67 | 1.7 |
| 495-113 | 7.3 | 70 | 2.4 | 0.7 | n.d. | 1356 | 29.5 | 13706 | 199 | 1.9 | 5.6 | 191 | 4.7 |
| 495-240 | 8.8 | 71 | 4.1 | 2.0 | n.d. | 14970 | 30.0 | 15037 | 1284 | 2.6 | 6.8 | 392 | 4.5 |
| 495-362 | 6.6 | 78 | 3.2 | 1.1 | n.d. | 5414 | 25.0 | 13303 | 338 | 2.2 | 5.9 | 480 | 5.3 |
| 495-484 | 5.9 | 90 | 7.6 | 1.2 | n.d. | 8663 | 21.9 | 32041 | 748 | 5.5 | 11.6 | 218 | 5.2 |
| 495-548 | 9.7 | 109 | n.d. | 3.1 | 5 | 1841 | 30.6 | 10209 | 211 | 0.6 | 1.3 | 875 | 3.1 |
| 495-557 | 8.0 | 274 | n.d. | 6.3 | 20 | 215 | 29.3 | 5629 | 34 | 0.6 | 1.8 | 50 | 8.1 |
| 495-569 | 23.2 | 89 | n.d. | 3.2 | 7 | 222 | 14.1 | 5912 | 119 | 0.4 | 1.1 | 136 | 2.5 |
| 495-582 | 4.6 | 93 | n.d. | 8.9 | 34 | 53 | 2.1 | 1111 | n.d. | 0.3 | 0.7 | 3498 | 23.6 |
| 495-599 | 7.7 | 111 | n.d. | 6.5 | 23 | 296 | 13.8 | 3636 | n.d. | 0.4 | 0.9 | 311 | 12.0 |
| 495-693 | 8.5 | 127 | 5.5 | 2.1 | 4 | 1703 | 26.4 | 571 | 58 | 1.5 | 2.7 | 123 | 3.2 |
| 495-757 | 4.1 | 115 | 4.9 | 11.9 | 46 | 4755 | 6.3 | 17674 | 406 | 3.7 | 11.2 | 1456 | 14.2 |
| 495-777 | 4.1 | 141 | 19.3 | 4.9 | 17 | 15019 | 19.1 | 23393 | 2100 | 12.6 | 24.5 | 906 | 2.3 |

| Sample ID | U | V | W | Y | Zr | Cu | Fe | Zn | Pb | S* | $SO_4$ | Ba | Ca |
|---|---|---|---|---|---|---|---|---|---|---|---|---|---|
| 495-809 | 1.7 | 559 | 10.3 | 1.7 | n.d. | 459 | 18.5 | 10597 | 57 | 3.0 | 6.3 | 54 | 4.2 |
| 495-867 | 3.7 | 126 | 5.0 | 13.0 | 53 | 2550 | 6.6 | 7551 | 185 | 1.6 | 4.9 | 287 | 18.1 |
| 495-889 | 12.0 | 148 | n.d. | 6.2 | 22 | 3073 | 21.8 | 12384 | 271 | 2.4 | 6.1 | 3197 | 7.5 |
| 495-934 | 3.1 | 111 | 1.6 | 13.4 | 56 | 656 | 4.0 | 1594 | 31 | 0.8 | 1.9 | 163 | 20.0 |
| 495-1088 | 4.9 | 120 | 1.2 | 13.5 | 54 | 383 | 4.1 | 2652 | 36 | 1.4 | 4.2 | 224 | 16.3 |
| 495-1195 | 5.3 | 149 | 1.2 | 14.9 | 56 | 368 | 5.6 | 731 | 28 | 1.5 | 4.4 | 379 | 14.3 |
| 503-7 | 8.4 | 72 | 7.7 | 1.2 | n.d. | 4944 | 25.8 | 20236 | 574 | 4.5 | 10.9 | 381 | 5.8 |
| 503-75 | 7.9 | 305 | 16.4 | 2.0 | 8 | 2328 | 6.4 | 11844 | 737 | 13.2 | 26.2 | 15758 | 3.2 |
| 503-140 | 2.2 | 55 | n.d. | 0.4 | n.d. | 2947 | 14.0 | 18788 | 656 | 7.5 | 22.4 | 58 | 6.2 |
| 503-155 | 3.9 | 72 | 4.6 | 1.3 | n.d. | 3390 | 15.1 | 19925 | 748 | 6.1 | 16.4 | 107 | 3.9 |
| 503-235 | 0.4 | 7 | 1.0 | n.d. | n.d. | 212 | 0.1 | 3269 | 44 | 23.9 | 71.6 | 5028 | 27.3 |
| 503-266 | 1.3 | 12 | 1.3 | 0.2 | n.d. | 503 | 3.3 | 1984 | 95 | 18.6 | 54.3 | 4172 | 20.9 |
| 503-407 | 32.5 | 69 | n.d. | 0.6 | n.d. | 1205 | 51.3 | 1618 | 21 | 0.5 | 0.5 | 125 | 1.3 |
| 503-509 | 4.6 | 26 | 3.3 | 0.7 | n.d. | 1913 | 24.8 | 4045 | 104 | 4.4 | 12.8 | 1620 | 7.8 |
| 503-516 | 12.5 | 207 | 3.8 | 18.5 | 84 | 18071 | 5.2 | 16249 | 421 | 3.7 | 0.8 | 4996 | 2.3 |
| 503-626 | 18.9 | 51 | 2.2 | 0.6 | n.d. | 1099 | 41.0 | 1479 | 26 | 2.4 | 7.3 | 3220 | 2.1 |
| 503-671 | 1.0 | 44 | 9.4 | 0.5 | n.d. | 956 | 15.5 | 1767 | 12 | 1.7 | 1.8 | 244 | 4.3 |
| 503-680 | 5.9 | 57 | 5.9 | 1.3 | n.d. | 7237 | 29.5 | 3740 | 495 | 0.8 | 2.0 | 2970 | 3.1 |
| 503-807 | 4.0 | 284 | 10.0 | 2.9 | 10 | 7084 | 10.8 | 6952 | 1514 | 11.3 | 9.8 | 6555 | 3.6 |
| 503-889 | 10.0 | 53 | n.d. | 3.5 | 3 | 13323 | 37.3 | 4203 | 430 | 2.6 | 20.0 | 16 | 2.7 |
| 503-912 | 5.3 | 155 | 9.7 | 3.5 | 10 | 25201 | 6.4 | 146030 | 2086 | 19.8 | 47.2 | 117 | 3.6 |
| 503-946 | 6.0 | 132 | 17.3 | 3.3 | 5 | 3758 | 22.1 | 24182 | 291 | 8.3 | 20.4 | 7075 | 5.8 |
| 503-987 | 13.2 | 193 | n.d. | 15.5 | 64 | 1160 | 20.1 | 10915 | 328 | 21.6 | 23.1 | 567 | 2.1 |
| 546-5 | 12.4 | 183 | 7.6 | 1.4 | n.d. | 16087 | 31.6 | 33867 | 1153 | 3.1 | 5.3 | 851 | 1.1 |
| 546-92 | 7.8 | 96 | 4.2 | 1.3 | n.d. | 9723 | 26.3 | 33106 | 1415 | 3.5 | 10.4 | 123 | 2.0 |
| 546-180 | 8.0 | 100 | 2.6 | 1.1 | n.d. | 2068 | 24.2 | 11422 | 227 | 1.3 | 2.8 | 177 | 1.9 |
| 546-229 | 11.6 | 129 | 3.7 | 1.8 | n.d. | 10403 | 24.3 | 22975 | 1037 | 2.6 | 5.7 | 212 | 2.3 |
| 546-252 | 1.4 | 94 | n.d. | 14.7 | 62 | 77 | 5.3 | 6550 | 4 | 0.7 | 1.6 | 121 | 16.9 |
| 546-267 | 7.9 | 120 | 42.9 | 1.4 | 2 | 2452 | 28.1 | 2637 | 254 | 3.9 | 11.6 | 4241 | 3.9 |
| 546-311 | 4.9 | 56 | n.d. | 6.1 | 4 | 10394 | 37.1 | 2585 | 819 | 0.5 | 1.2 | 238 | 2.3 |
| 546-318 | 6.5 | 167 | 2.3 | 2.4 | 13 | 207 | 4.9 | 614 | 15 | 6.3 | 14.4 | 16051 | 4.3 |
| 546-385 | 4.1 | 120 | n.d. | 13.6 | 69 | 195 | 7.3 | 726 | 1 | 0.9 | 2.2 | 100 | 19.9 |
| 557-9 | 5.3 | 77 | 5.3 | 1.3 | n.d. | 12929 | 18.4 | 45318 | 2277 | 6.3 | 15.7 | 357 | 6.2 |
| 557-173 | 3.6 | 105 | 9.9 | 1.8 | n.d. | 11262 | 18.6 | 80097 | 1596 | 8.0 | 14.2 | 265 | 3.9 |
| 557-227 | 2.7 | 163 | 6.7 | 0.7 | n.d. | 2226 | 13.1 | 44529 | 530 | 7.9 | 16.9 | 47 | 5.0 |
| 557-255 | 3.4 | 145 | 1.2 | 13.6 | 52 | 2008 | 16.8 | 16061 | 465 | 1.6 | 3.9 | 789 | 2.6 |
| 557-289 | 22.5 | 66 | 8.0 | 0.6 | n.d. | 5072 | 40.6 | 12334 | 118 | 1.4 | 1.9 | 618 | 1.6 |
| 557-388 | 7.0 | 117 | 6.3 | 5.1 | 18 | 20396 | 15.4 | 62948 | 1775 | 13.2 | 25.5 | 292 | 3.5 |
| 557-502 | 1.5 | 100 | n.d. | 11.7 | 50 | 211 | 2.5 | 1829 | 16 | 0.6 | 1.0 | 215 | 23.8 |
| 557-608 | 1.0 | 81 | n.d. | 9.0 | 34 | 61 | 3.8 | 250 | n.d. | 0.3 | n.d. | 99 | 26.1 |
| 557-753 | 3.7 | 383 | n.d. | 10.1 | 41 | 317 | 2.5 | 415 | n.d. | 0.3 | 0.5 | 91 | 25.0 |
| 557-795 | 0.9 | 88 | 1.5 | 7.9 | 33 | 45 | 3.9 | 315 | 7 | 0.2 | n.d. | 57 | 26.7 |
| 617-9 | 9.5 | 90 | 8.5 | 1.5 | n.d. | 13176 | 24.8 | 32063 | 847 | 5.1 | 11.0 | 1395 | 4.3 |
| 617-148 | 12.2 | 90 | 11.6 | 2.8 | n.d. | 16650 | 21.2 | 48071 | 2272 | 10.6 | 19.2 | 1252 | 5.1 |
| 617-220 | 1.9 | 31 | n.d. | 1.0 | n.d. | 893 | 2.4 | 1578 | 27 | 12.4 | 35.5 | n.d. | 13.9 |
| 617-395 | 7.7 | 124 | 17.4 | 1.6 | n.d. | 424 | 16.6 | 7896 | 36 | 7.9 | 18.3 | 32 | 8.3 |
| 617-396 | 5.9 | 106 | 3.5 | 9.8 | 31 | 10735 | 17.7 | 8075 | 107 | 2.6 | 6.2 | 19 | 3.4 |
| 617-508 | 2.5 | 77 | 1.0 | 9.8 | 39 | 1245 | 10.9 | 6207 | 55 | 1.4 | 2.9 | 240 | 15.9 |
| 617-551 | 1.1 | 25 | 1.3 | 0.7 | n.d. | 1389 | 3.1 | 6291 | 139 | 21.5 | 64.5 | 198 | 25.8 |
| 617-650 | 4.7 | 113 | 12.7 | 2.2 | 4 | 10786 | 17.8 | 49274 | 760 | 10.1 | 24.2 | 105 | 6.0 |
| 617-787 | 6.4 | 75 | 11.2 | 1.3 | n.d. | 2437 | 21.7 | 24844 | 689 | 10.2 | 28.0 | 1426 | 8.3 |
| 617-799 | 4.1 | 61 | 5.0 | 3.7 | 4 | 5775 | 11.4 | 70702 | 2294 | 12.3 | 36.2 | 9318 | 12.4 |
| 617-875 | 2.1 | 105 | 4.6 | 1.9 | n.d. | 6722 | 8.9 | 30421 | 476 | 15.8 | 47.4 | 996 | 16.5 |

Appendix C.1. Complete bulk chemical data for 100 samples of metalliferous sediments from the Atlantis II Deep (salt-free basis).

| Element | $CO_2$ | Si | $Al_2O_3$ | Mg | $TiO_2$ | $K_2O$ | $P_2O_5$ | F | B | Br | Cs | Hf | Li |
|---|---|---|---|---|---|---|---|---|---|---|---|---|---|
| Method | 5 | 2 | 9 | 2 | 9 | 9 | 9 | 10 | 1 | 3 | 8 | 8 | 8 |
| Det. lim. | 0.01 | 0.01 | 0.01 | 0.01 | 0.0001 | 0.002 | 0.001 | 0.01 | 10 | 0.5 | 0.1 | 0.50 | 0.30 |
| Sample ID | wt.% | wt.% | wt.% | wt.% | wt.% | wt.% | wt.% | ppm | ppm | ppm | ppm | ppm | ppm |
| 334-83 | 1.0 | 5.6 | 0.81 | 0.56 | 0.034 | 1.54 | 0.113 | 0.040 | 159 | 370 | 0.8 | n.d. | 21 |
| 334-312 | 0.9 | 6.6 | 1.14 | 0.52 | 0.043 | 1.61 | 0.255 | n.d. | 168 | 346 | 0.9 | n.d. | 20 |
| 334-513 | 2.1 | 5.3 | 1.21 | 0.93 | 0.046 | 1.07 | 0.273 | n.d. | 79 | 233 | 0.8 | n.d. | 13 |
| 334-612 | 1.0 | 8.4 | 0.94 | 0.85 | 0.036 | 1.93 | 0.307 | n.d. | 152 | 382 | 1.1 | n.d. | 20 |
| 334-757 | 0.7 | 8.3 | 1.21 | 1.22 | 0.035 | 1.17 | 0.121 | n.d. | 81 | 282 | 0.5 | n.d. | 14 |
| 373-8 | 1.9 | 8.5 | 1.13 | 1.05 | 0.066 | 3.73 | 0.290 | n.d. | 240 | 734 | 2.4 | n.d. | 41 |
| 373-93 | 4.5 | 9.3 | 1.32 | 1.01 | 0.074 | 3.02 | 0.232 | n.d. | 152 | 535 | 1.8 | n.d. | 34 |
| 373-210 | 0.5 | 13.5 | 0.50 | 1.23 | 0.013 | 4.43 | 0.071 | n.d. | 176 | 685 | 5.2 | n.d. | 41 |
| 373-265 | 0.5 | 2.2 | 1.16 | 1.19 | 0.081 | 2.63 | 0.044 | n.d. | 106 | 441 | 1.1 | n.d. | 25 |
| 373-515 | 5.6 | 8.1 | 0.58 | 0.85 | 0.023 | 2.23 | 0.129 | n.d. | 141 | 495 | 2.6 | n.d. | 26 |
| 373-555 | 7.1 | 13.8 | 3.11 | 0.78 | 0.175 | 1.13 | 0.493 | 0.018 | 71 | 199 | 2.1 | n.d. | 17 |
| 373-586 | 0.1 | 1.0 | 0.15 | 0.04 | 0.007 | 0.01 | 0.050 | n.d. | 21 | 22 | 0.1 | n.d. | 3 |
| 373-672 | 0.6 | 10.1 | 0.47 | 0.85 | 0.014 | 2.32 | 0.337 | n.d. | 111 | 461 | 3.4 | n.d. | 27 |
| 373-751 | 13.1 | 7.8 | 2.79 | 0.88 | 0.126 | 0.79 | 0.442 | 0.029 | 72 | 126 | 1.5 | n.d. | 15 |
| 373-780 | 24.5 | 7.7 | 3.57 | 1.69 | 0.249 | 1.27 | 0.261 | 0.052 | 52 | 138 | 2.4 | 0.93 | 17 |
| 373-798 | 1.5 | 3.3 | 1.32 | 0.94 | 0.117 | 1.52 | 0.289 | n.d. | 140 | 352 | 0.6 | n.d. | 20 |
| 387-80 | 0.6 | 6.5 | 0.90 | 0.70 | 0.032 | 2.07 | 0.206 | n.d. | 113 | 444 | 1.4 | n.d. | 22 |
| 387-174 | 0.4 | 17.6 | 0.42 | 1.58 | 0.024 | 3.94 | 0.061 | n.d. | 119 | 609 | 7.0 | n.d. | 28 |
| 387-261 | 13.9 | 14.3 | 6.51 | 1.56 | 0.467 | 1.92 | 0.297 | 0.043 | 116 | 192 | 6.7 | 1.44 | 28 |
| 387-302 | 1.0 | 4.7 | 0.92 | 0.43 | 0.053 | 0.89 | 0.180 | n.d. | 278 | 202 | 0.8 | n.d. | 12 |
| 387-398 | 4.3 | 14.3 | 3.38 | 0.64 | 0.173 | 1.19 | 0.495 | 0.018 | 71 | 194 | 2.2 | n.d. | 16 |
| 387-466 | 16.3 | 7.2 | 2.21 | 0.85 | 0.095 | 0.91 | 0.512 | 0.031 | 62 | 171 | 1.5 | n.d. | 18 |
| 387-490 | 4.5 | 2.7 | 1.61 | 0.33 | 0.070 | 0.45 | 0.729 | 0.129 | 59 | 82 | 0.5 | n.d. | 7 |
| 387-502 | 0.2 | 0.3 | 0.03 | 0.02 | 0.002 | 0.04 | 0.032 | n.d. | 21 | 10 | 0.1 | n.d. | 3 |
| 387-575 | 3.1 | 12.3 | 1.39 | 0.35 | 0.076 | 1.48 | 0.294 | n.d. | 59 | 208 | 1.5 | n.d. | 11 |
| 421-80 | 4.9 | 6.8 | 0.93 | 0.68 | 0.028 | 2.44 | 0.397 | n.d. | 180 | 540 | 1.6 | n.d. | 24 |
| 421-160 | 6.9 | 7.2 | 0.45 | 0.87 | 0.024 | 2.81 | 0.282 | n.d. | 174 | 773 | 1.1 | n.d. | 33 |
| 421-223 | 2.5 | 2.2 | 0.45 | 0.53 | 0.025 | 2.13 | 0.054 | n.d. | 175 | 620 | 0.5 | n.d. | 23 |
| 421-362 | 2.4 | 8.5 | 0.92 | 0.85 | 0.028 | 2.78 | 0.256 | n.d. | 117 | 705 | 1.9 | n.d. | 29 |
| 421-496 | 13.2 | 7.2 | 2.43 | 1.12 | 0.169 | 1.50 | 0.195 | n.d. | 178 | 220 | 3.1 | n.d. | 18 |
| 421-520 | 6.0 | 7.6 | 1.10 | 0.94 | 0.071 | 2.54 | 0.179 | n.d. | 229 | 530 | 4.0 | n.d. | 24 |
| 421-678 | 7.8 | 11.5 | 3.59 | 0.70 | 0.187 | 1.23 | 0.772 | 0.049 | 66 | 215 | 2.1 | n.d. | 19 |
| 421-740 | 1.7 | 14.2 | 0.64 | 1.23 | 0.031 | 2.82 | 0.759 | n.d. | 102 | 613 | 5.6 | n.d. | 33 |
| 421-825 | 17.8 | 13.5 | 7.57 | 1.60 | 0.656 | 1.46 | 0.392 | 0.061 | 61 | 105 | 3.0 | 2.23 | 25 |
| 421-870 | 1.4 | 6.0 | 1.98 | 0.69 | 0.168 | 1.18 | 0.342 | n.d. | 88 | 210 | 1.4 | n.d. | 13 |
| 495-113 | 0.7 | 6.7 | 0.73 | 0.63 | 0.029 | 2.55 | 0.261 | n.d. | 145 | 513 | 1.1 | n.d. | 26 |
| 495-240 | 0.5 | 6.0 | 1.01 | 0.64 | 0.053 | 2.32 | 0.513 | n.d. | 203 | 453 | 1.3 | n.d. | 24 |
| 495-362 | 1.0 | 7.3 | 0.83 | 0.70 | 0.040 | 2.33 | 0.244 | n.d. | 169 | 472 | 1.2 | n.d. | 24 |
| 495-484 | 1.3 | 8.4 | 1.24 | 0.66 | 0.045 | 2.61 | 0.306 | n.d. | 166 | 529 | 1.6 | n.d. | 26 |
| 495-548 | 12.8 | 6.6 | 1.56 | 0.82 | 0.092 | 1.89 | 0.288 | n.d. | 146 | 314 | 2.0 | n.d. | 21 |
| 495-557 | 10.6 | 5.1 | 2.49 | 0.76 | 0.173 | 1.02 | 0.333 | 0.014 | 165 | 172 | 1.1 | n.d. | 14 |
| 495-569 | 2.3 | 3.4 | 1.55 | 0.47 | 0.110 | 0.66 | 0.196 | n.d. | 187 | 165 | 0.6 | n.d. | 9 |
| 495-582 | 29.7 | 6.8 | 3.81 | 1.48 | 0.287 | 0.81 | 0.149 | 0.047 | 47 | 92 | 1.5 | 0.96 | 14 |
| 495-599 | 17.9 | 8.9 | 2.98 | 1.11 | 0.210 | 2.16 | 0.369 | 0.031 | 246 | 260 | 4.8 | n.d. | 21 |
| 495-693 | 1.0 | 10.4 | 1.19 | 0.72 | 0.077 | 2.53 | 0.216 | n.d. | 106 | 514 | 3.3 | n.d. | 22 |
| 495-757 | 20.0 | 11.8 | 6.29 | 2.43 | 0.407 | 1.51 | 0.287 | 0.062 | 50 | 98 | 2.1 | 1.29 | 23 |
| 495-777 | 7.1 | 11.0 | 2.83 | 0.85 | 0.161 | 0.77 | 0.416 | 0.027 | 40 | 122 | 1.0 | n.d. | 13 |

| Sample ID | $CO_2$ | Si | $Al_2O_3$ | Mg | $TiO_2$ | $K_2O$ | $P_2O_5$ | F | B | Br | Cs | Hf | Li |
|---|---|---|---|---|---|---|---|---|---|---|---|---|---|
| 495-809 | 2.1 | 17.2 | 0.83 | 1.32 | 0.045 | 3.10 | 0.355 | 0.024 | 98 | 596 | 7.0 | n.d. | 29 |
| 495-867 | 23.3 | 10.7 | 5.89 | 2.15 | 0.421 | 1.37 | 0.347 | 0.061 | 49 | 95 | 1.9 | 1.44 | 21 |
| 495-889 | 11.2 | 7.5 | 3.61 | 1.01 | 0.246 | 1.62 | 0.290 | n.d. | 125 | 215 | 1.7 | n.d. | 18 |
| 495-934 | 23.3 | 10.9 | 6.33 | 2.34 | 0.447 | 1.36 | 0.305 | 0.057 | 46 | 70 | 2.0 | 1.49 | 23 |
| 495-1088 | 21.8 | 12.6 | 7.24 | 2.97 | 0.431 | 1.51 | 0.199 | 0.045 | 56 | 68 | 1.9 | 1.47 | 25 |
| 495-1195 | 21.1 | 13.6 | 7.76 | 3.08 | 0.482 | 1.34 | 0.228 | 0.046 | 35 | 65 | 1.7 | 1.53 | 20 |
| 503-7 | 1.0 | 6.1 | 0.80 | 0.70 | 0.029 | 2.33 | 0.199 | n.d. | 121 | 548 | 1.0 | n.d. | 26 |
| 503-75 | 3.1 | 17.4 | 1.32 | 0.35 | 0.070 | 0.88 | 0.260 | n.d. | 34 | 182 | 1.1 | n.d. | 9 |
| 503-140 | 0.6 | 8.1 | 0.55 | 0.86 | 0.009 | 4.92 | 0.029 | n.d. | 111 | 518 | 3.3 | n.d. | 55 |
| 503-155 | 0.9 | 9.6 | 1.15 | 0.90 | 0.040 | 5.18 | 0.155 | n.d. | 109 | 518 | 3.1 | n.d. | 56 |
| 503-235 | 0.0 | 0.2 | 0.03 | 0.07 | 0.000 | 0.18 | 0.028 | n.d. | n.d. | 82 | 0.1 | n.d. | 25 |
| 503-266 | 1.4 | 0.5 | 0.10 | 0.06 | 0.003 | 0.03 | 0.001 | n.d. | n.d. | 39 | 0.1 | n.d. | 8 |
| 503-407 | 0.8 | 1.6 | 0.45 | 0.26 | 0.011 | 0.78 | 0.207 | n.d. | 192 | 234 | 0.2 | n.d. | 13 |
| 503-509 | 8.1 | 5.5 | 0.36 | 0.60 | 0.008 | 1.69 | 0.116 | n.d. | 55 | 450 | 1.2 | n.d. | 30 |
| 503-516 | 3.5 | 22.2 | 9.52 | 1.18 | 0.683 | 2.09 | 0.580 | 0.046 | 91 | 240 | 5.8 | 2.15 | 33 |
| 503-626 | 0.5 | 2.8 | 0.36 | 0.34 | 0.008 | 1.23 | 0.093 | n.d. | 206 | 344 | 0.4 | n.d. | 18 |
| 503-671 | 1.3 | 14.3 | 0.44 | 1.25 | 0.019 | 4.88 | 0.086 | n.d. | 234 | 632 | 8.8 | n.d. | 34 |
| 503-680 | 1.8 | 9.3 | 0.71 | 0.90 | 0.036 | 2.44 | 0.209 | n.d. | 154 | 513 | 3.1 | n.d. | 28 |
| 503-807 | 2.1 | 14.0 | 1.82 | 0.44 | 0.089 | 1.60 | 0.277 | n.d. | 44 | 195 | 1.5 | n.d. | 12 |
| 503-889 | 16.1 | 1.6 | 0.93 | 0.54 | 0.042 | 0.21 | 0.584 | 0.032 | 76 | 40 | 0.4 | n.d. | 9 |
| 503-912 | 2.0 | 8.7 | 2.91 | 0.62 | 0.129 | 0.74 | 0.525 | n.d. | 83 | 159 | 1.3 | n.d. | 14 |
| 503-946 | 4.2 | 4.8 | 1.65 | 0.67 | 0.053 | 0.71 | 0.314 | n.d. | 98 | 196 | 0.7 | n.d. | 15 |
| 503-987 | 4.6 | 12.7 | 7.18 | 1.12 | 0.596 | 1.43 | 0.282 | 0.012 | 75 | 124 | 3.6 | 1.67 | 23 |
| 546-5 | 3.2 | 6.7 | 1.62 | 1.35 | 0.040 | 1.69 | 0.561 | n.d. | 206 | 730 | 0.5 | n.d. | 17 |
| 546-92 | 3.8 | 8.3 | 1.10 | 1.82 | 0.029 | 2.14 | 0.402 | n.d. | 209 | 923 | 0.8 | n.d. | 22 |
| 546-180 | 5.9 | 8.4 | 0.78 | 1.56 | 0.032 | 1.81 | 0.241 | n.d. | 173 | 671 | 1.4 | n.d. | 18 |
| 546-229 | 16.7 | 6.7 | 1.48 | 1.50 | 0.041 | 1.20 | 0.437 | 0.032 | 113 | 353 | 1.1 | n.d. | 13 |
| 546-252 | 19.8 | 12.7 | 6.83 | 1.69 | 0.506 | 1.45 | 0.250 | 0.025 | 62 | 148 | 3.4 | 1.63 | 19 |
| 546-267 | 2.0 | 8.8 | 1.19 | 1.17 | 0.060 | 1.03 | 0.212 | 0.015 | 77 | 344 | 1.6 | n.d. | 12 |
| 546-311 | 19.7 | 2.0 | 1.03 | 0.79 | 0.058 | 0.19 | 0.637 | 0.123 | 78 | 52 | 0.7 | n.d. | 9 |
| 546-318 | 2.1 | 25.8 | 2.06 | 0.63 | 0.130 | 0.64 | 0.098 | n.d. | 50 | 293 | 1.3 | n.d. | 9 |
| 546-385 | 24.5 | 9.3 | 6.66 | 1.58 | 0.530 | 1.04 | 0.328 | 0.046 | 46 | 104 | 1.9 | 1.76 | 22 |
| 557-9 | 0.9 | 6.6 | 0.97 | 0.77 | 0.039 | 2.52 | 0.414 | n.d. | 133 | 1077 | 1.1 | n.d. | 28 |
| 557-173 | 1.1 | 10.6 | 1.70 | 0.99 | 0.058 | 3.12 | 0.403 | n.d. | 120 | 1195 | 2.2 | n.d. | 29 |
| 557-227 | 0.6 | 7.8 | 0.94 | 0.78 | 0.007 | 1.97 | 0.145 | n.d. | 67 | 830 | 0.9 | n.d. | 26 |
| 557-255 | 7.9 | 12.6 | 6.06 | 1.34 | 0.433 | 1.83 | 0.288 | 0.046 | 77 | 326 | 2.7 | 1.42 | 25 |
| 557-289 | 0.8 | 1.9 | 0.63 | 0.60 | 0.010 | 1.32 | 0.161 | n.d. | 168 | 649 | 0.3 | n.d. | 22 |
| 557-388 | 10.5 | 9.7 | 3.33 | 0.85 | 0.186 | 0.99 | 0.514 | n.d. | 44 | 242 | 1.4 | n.d. | 16 |
| 557-502 | 27.1 | 9.0 | 5.30 | 1.84 | 0.408 | 1.01 | 0.207 | 0.044 | 44 | 102 | 1.7 | 1.33 | 18 |
| 557-608 | 29.3 | 5.9 | 3.91 | 1.36 | 0.259 | 0.88 | 0.238 | 0.034 | 45 | 148 | 1.3 | 0.85 | 16 |
| 557-753 | 27.4 | 7.1 | 4.26 | 1.20 | 0.276 | 1.01 | 0.188 | 0.046 | 46 | 137 | 1.5 | 1.05 | 17 |
| 557-795 | 30.7 | 5.3 | 3.17 | 1.36 | 0.262 | 0.72 | 0.186 | 0.045 | 45 | 103 | 0.9 | 0.81 | 13 |
| 617-9 | 0.5 | 6.9 | 1.38 | 0.83 | 0.050 | 2.01 | 0.361 | n.d. | 125 | 694 | 1.1 | n.d. | 26 |
| 617-148 | 0.8 | 7.2 | 1.25 | 0.87 | 0.044 | 1.84 | 0.392 | n.d. | 87 | 618 | 1.3 | n.d. | 23 |
| 617-220 | n.d. | 7.4 | 0.45 | 4.92 | 0.018 | 0.60 | 0.079 | n.d. | 29 | 275 | 0.2 | n.d. | 12 |
| 617-395 | 1.2 | 7.4 | 1.32 | 4.50 | 0.070 | 1.22 | 0.272 | n.d. | 36 | 511 | 0.3 | n.d. | 20 |
| 617-396 | 3.3 | 14.5 | 5.00 | 4.53 | 0.323 | 1.24 | 0.382 | n.d. | 63 | 394 | 0.8 | 0.89 | 20 |
| 617-508 | 17.2 | 12.2 | 5.46 | 1.44 | 0.384 | 0.73 | 0.217 | 0.025 | 25 | 130 | 0.6 | 1.07 | 9 |
| 617-551 | 1.6 | 1.6 | 0.46 | 0.29 | 0.024 | 0.13 | 0.081 | n.d. | 12 | 92 | 0.2 | n.d. | 4 |
| 617-650 | 1.3 | 8.6 | 2.01 | 0.81 | 0.073 | 0.84 | 0.284 | n.d. | 34 | 362 | 0.4 | n.d. | 10 |
| 617-787 | 0.8 | 6.9 | 1.40 | 0.58 | 0.056 | 0.42 | 0.210 | n.d. | 31 | 206 | 0.2 | n.d. | 6 |
| 617-799 | 2.0 | 5.7 | 1.90 | 0.92 | 0.108 | 0.54 | 0.225 | 0.031 | 31 | 239 | 0.3 | n.d. | 9 |
| 617-875 | 0.8 | 4.8 | 1.22 | 0.82 | 0.048 | 0.21 | 0.280 | n.d. | 13 | 119 | 0.2 | n.d. | 5 |

Appendix C.1. Complete bulk chemical data for 100 samples of metalliferous sediments from the Atlantis II Deep (salt-free basis). Complete REE composition is given in Chapter 4.

| Element | Nb | Ta | Th | Mo | Ni | U | V | W | REE | La | Ce | Nd | Eu | Gd |
|---|---|---|---|---|---|---|---|---|---|---|---|---|---|---|
| Method | 10 | 10 | 10 | 3 | 10 | 10 | 10 | 10 | sum | 10 | 10 | 10 | 10 | 10 |
| Det. lim. | 0.10 | 0.10 | 0.01 | 1 | 5 | 0.1 | 10 | 0.5 | | 0.1 | 0.1 | 0.1 | 0.001 | 0.01 |
| Sample ID | ppm | ppm | ppm | ppm | ppm | ppm | ppm | ppm | | ppm | ppm | ppm | ppm | ppm |
| 334-83 | 0.53 | n.d. | 0.22 | 62 | 12 | 4.3 | 64 | 6.1 | 4.9 | 0.7 | 1.9 | 1.0 | 0.050 | 0.21 |
| 334-312 | 0.59 | n.d. | 0.32 | 149 | 26 | 7.2 | 77 | 9.7 | 6.8 | 1.2 | 2.7 | 1.3 | 0.090 | 0.27 |
| 334-513 | 0.30 | n.d. | 0.45 | 203 | 28 | 8.9 | 89 | 7.4 | 8.7 | 1.4 | 3.3 | 1.7 | 0.275 | 0.32 |
| 334-612 | 0.57 | n.d. | 0.22 | 85 | 11 | 7.7 | 93 | 10.8 | 6.2 | 0.9 | 2.4 | 1.3 | 0.103 | 0.26 |
| 334-757 | 0.72 | n.d. | 0.30 | 101 | 14 | 5.2 | 78 | 13.3 | 6.2 | 1.4 | 2.6 | 1.0 | 0.078 | 0.18 |
| 373-8 | 1.12 | n.d. | 0.40 | n.d. | 23 | 4.2 | 71 | 8.4 | 9.9 | 1.8 | 3.9 | 1.9 | 0.162 | 0.39 |
| 373-93 | 1.22 | n.d. | 0.47 | 58 | n.d. | 4.8 | 70 | 10.4 | 11.4 | 2.1 | 4.6 | 2.1 | 0.128 | 0.42 |
| 373-210 | n.d. | n.d. | 0.18 | n.d. | n.d. | 2.2 | 35 | 11.9 | 5.7 | 1.0 | 2.3 | 1.0 | 0.201 | 0.19 |
| 373-265 | 1.28 | n.d. | 0.74 | 146 | 36 | 2.2 | 161 | 2.9 | 16.6 | 4.7 | 6.0 | 2.6 | 0.443 | 0.55 |
| 373-515 | 0.51 | n.d. | 0.31 | 133 | 20 | 6.2 | 59 | 7.9 | 9.5 | 1.8 | 4.0 | 1.7 | 0.186 | 0.31 |
| 373-555 | 2.87 | n.d. | 1.27 | 217 | 162 | 3.1 | 107 | 16.7 | 29.1 | 5.1 | 11.6 | 5.6 | 0.684 | 1.05 |
| 373-586 | 0.12 | n.d. | 0.06 | 52 | 7 | 0.3 | n.d. | 1.1 | 1.4 | 0.3 | 0.5 | 0.2 | 0.039 | 0.05 |
| 373-672 | 0.33 | n.d. | 0.22 | 122 | n.d. | 2.0 | 298 | 8.7 | 4.4 | 0.8 | 1.8 | 0.8 | 0.103 | 0.14 |
| 373-751 | 2.20 | n.d. | 1.01 | 364 | 130 | 5.6 | 145 | 12.5 | 28.1 | 5.4 | 11.2 | 5.1 | 0.800 | 0.92 |
| 373-780 | 4.27 | 0.25 | 1.81 | 16 | 29 | 0.9 | 103 | 0.7 | 46.6 | 9.5 | 18.9 | 8.5 | 0.473 | 1.60 |
| 373-798 | 1.49 | n.d. | 0.50 | 232 | 33 | 4.2 | 102 | n.d. | 50.2 | 16.0 | 19.5 | 7.1 | 0.674 | 1.26 |
| 387-80 | 0.64 | n.d. | 0.26 | 84 | 14 | 3.8 | 51 | 7.5 | 5.3 | 0.7 | 2.1 | 1.1 | 0.097 | 0.22 |
| 387-174 | 0.32 | n.d. | 0.17 | 59 | n.d. | 1.6 | n.d. | 10.4 | 2.5 | n.d. | 1.0 | 0.7 | 0.093 | 0.14 |
| 387-261 | 6.69 | 0.40 | 2.76 | 30 | 39 | 4.2 | 143 | n.d. | 64.4 | 11.7 | 25.6 | 12.4 | 0.704 | 2.48 |
| 387-302 | 0.76 | n.d. | 0.37 | 240 | 21 | 4.1 | 83 | 1.7 | 10.3 | 1.8 | 4.5 | 1.8 | 0.103 | 0.37 |
| 387-398 | 2.82 | n.d. | 1.23 | 327 | 198 | 2.9 | 134 | 18.1 | 26.4 | 4.5 | 10.5 | 5.2 | 0.591 | 0.98 |
| 387-466 | 1.53 | n.d. | 0.67 | 116 | 67 | 5.3 | 106 | 10.0 | 28.5 | 6.1 | 12.5 | 4.6 | 0.850 | 0.73 |
| 387-490 | 0.99 | n.d. | 0.54 | 92 | 51 | 6.5 | 92 | 4.0 | 33.3 | 5.2 | 13.9 | 6.0 | 1.383 | 1.13 |
| 387-502 | n.d. | n.d. | 0.06 | 13 | n.d. | n.d. | n.d. | 0.5 | 0.5 | n.d. | 0.2 | 0.1 | 0.016 | 0.02 |
| 387-575 | 1.26 | n.d. | 0.53 | 326 | 41 | 4.1 | 261 | 7.9 | 16.9 | 3.9 | 7.3 | 2.7 | 0.408 | 0.41 |
| 421-80 | 0.49 | n.d. | 0.18 | 108 | 22 | 5.2 | 67 | 12.6 | 5.2 | 1.0 | 2.0 | 0.9 | 0.118 | 0.19 |
| 421-160 | 0.35 | n.d. | 0.14 | 98 | 28 | 2.1 | 36 | 2.5 | 4.5 | 0.9 | 1.7 | 0.8 | 0.102 | 0.18 |
| 421-223 | 0.39 | n.d. | 0.24 | 105 | n.d. | 9.7 | 31 | n.d. | 5.1 | 0.9 | 2.1 | 1.0 | 0.012 | 0.21 |
| 421-362 | 0.51 | n.d. | 0.18 | n.d. | 28 | 3.4 | 69 | 10.4 | 6.2 | 1.2 | 2.5 | 1.1 | 0.152 | 0.23 |
| 421-496 | 2.76 | 0.16 | 1.14 | 153 | 22 | 4.0 | 95 | 2.7 | 24.3 | 4.7 | 9.6 | 4.6 | 0.241 | 0.91 |
| 421-520 | 1.13 | n.d. | 0.46 | 91 | 14 | 2.8 | 74 | 5.8 | 12.1 | 2.3 | 4.9 | 2.3 | 0.141 | 0.44 |
| 421-678 | 3.09 | 0.19 | 1.27 | 224 | 157 | 4.5 | 146 | 11.3 | 46.6 | 9.4 | 19.5 | 8.2 | 1.312 | 1.38 |
| 421-740 | 0.66 | n.d. | 0.28 | 107 | 17 | 1.2 | 767 | 17.7 | 11.3 | 2.2 | 4.5 | 2.0 | 0.333 | 0.38 |
| 421-825 | 8.87 | 0.50 | 3.42 | n.d. | 106 | 9.3 | 249 | n.d. | 86.3 | 16.2 | 34.5 | 16.5 | 0.904 | 3.18 |
| 421-870 | 2.45 | n.d. | 0.91 | 134 | 20 | 3.6 | 248 | 2.3 | 87.6 | 21.6 | 35.9 | 14.9 | 1.730 | 2.45 |
| 495-113 | 0.38 | n.d. | 0.16 | 136 | n.d. | 7.0 | 81 | 8.2 | 4.1 | 0.7 | 1.6 | 0.8 | 0.073 | 0.16 |
| 495-240 | 0.80 | n.d. | 0.32 | 128 | 32 | 8.5 | 83 | 10.5 | 11.5 | 2.2 | 4.6 | 2.0 | 0.425 | 0.41 |
| 495-362 | 0.52 | n.d. | 0.26 | 51 | n.d. | 6.1 | 79 | 8.5 | 6.0 | 1.1 | 2.4 | 1.1 | 0.087 | 0.23 |
| 495-484 | 0.66 | n.d. | 0.31 | 100 | 23 | 5.6 | 86 | 12.9 | 6.9 | 1.3 | 2.7 | 1.3 | 0.129 | 0.25 |
| 495-548 | 1.53 | n.d. | 0.51 | 133 | 40 | 9.3 | 114 | 9.2 | 17.1 | 3.4 | 6.8 | 3.1 | 0.332 | 0.61 |
| 495-557 | 2.68 | 0.16 | 1.05 | 147 | 47 | 7.5 | 274 | 2.2 | 33.3 | 6.8 | 13.4 | 6.0 | 0.432 | 1.16 |
| 495-569 | 1.83 | 0.14 | 0.62 | 311 | 22 | 21.7 | 92 | 0.8 | 15.6 | 2.7 | 6.3 | 3.0 | 0.153 | 0.60 |
| 495-582 | 4.07 | 0.24 | 1.98 | n.d. | 20 | 4.2 | 82 | n.d. | 40.7 | 7.3 | 16.4 | 7.8 | 0.348 | 1.58 |
| 495-599 | 3.06 | 0.18 | 1.19 | 32 | 29 | 7.3 | 103 | 2.4 | 29.8 | 5.5 | 11.8 | 5.7 | 0.305 | 1.14 |
| 495-693 | 1.24 | n.d. | 0.53 | 131 | n.d. | 8.0 | 116 | 6.7 | 12.7 | 2.4 | 5.1 | 2.4 | 0.181 | 0.47 |
| 495-757 | 5.73 | 0.35 | 2.27 | 56 | 60 | 3.7 | 109 | 5.5 | 60.7 | 10.8 | 24.1 | 11.8 | 0.846 | 2.29 |
| 495-777 | 2.37 | 0.14 | 0.95 | 283 | 113 | 3.8 | 128 | 20.4 | 28.4 | 5.1 | 11.5 | 5.3 | 0.835 | 0.97 |

| Sample ID | Nb | Ta | Th | Mo | Ni | U | V | W | REE | La | Ce | Nd | Eu | Gd |
|---|---|---|---|---|---|---|---|---|---|---|---|---|---|---|
| 495-809 | 0.89 | n.d. | 0.47 | 32 | n.d. | 1.3 | 448 | 8.3 | 16.2 | 3.4 | 7.2 | 2.7 | 0.416 | 0.38 |
| 495-867 | 6.28 | 0.41 | 2.25 | 27 | 47 | 3.2 | 107 | 3.3 | 61.0 | 11.2 | 24.3 | 11.7 | 0.708 | 2.30 |
| 495-889 | 3.01 | 0.18 | 1.11 | 197 | 55 | 10.9 | 140 | 5.0 | 30.0 | 5.4 | 12.0 | 5.8 | 0.378 | 1.12 |
| 495-934 | 6.66 | 0.40 | 2.51 | 15 | 50 | 2.7 | 103 | 1.4 | 62.8 | 11.5 | 24.9 | 12.1 | 0.694 | 2.37 |
| 495-1088 | 5.83 | 0.36 | 2.45 | 20 | 42 | 4.4 | 105 | 1.6 | 64.4 | 11.7 | 25.1 | 12.5 | 0.701 | 2.51 |
| 495-1195 | 6.67 | 0.41 | 2.65 | 19 | 44 | 4.9 | 135 | 1.6 | 71.0 | 12.7 | 27.9 | 13.8 | 0.881 | 2.75 |
| 503-7 | 0.55 | n.d. | 0.23 | 130 | 15 | 8.3 | 66 | 7.3 | 5.4 | 0.8 | 2.1 | 1.2 | 0.096 | 0.24 |
| 503-75 | 1.26 | n.d. | 0.53 | 262 | 37 | 6.8 | 287 | 11.3 | 22.2 | 5.5 | 9.7 | 3.5 | 0.530 | 0.44 |
| 503-140 | 0.27 | n.d. | 0.22 | n.d. | 17 | 2.0 | 46 | n.d. | 2.2 | 0.3 | 0.8 | 0.5 | 0.033 | 0.10 |
| 503-155 | 0.77 | n.d. | 0.66 | 35 | 20 | 4.0 | 58 | 6.8 | 7.2 | 1.3 | 2.8 | 1.4 | 0.065 | 0.24 |
| 503-235 | n.d. | n.d. | 0.01 | n.d. | n.d. | 0.3 | n.d. | n.d. | 0.1 | n.d. | n.d. | 0.1 | 0.008 | 0.02 |
| 503-266 | n.d. | n.d. | 0.05 | 10 | n.d. | 1.2 | n.d. | 1.3 | 1.9 | 0.4 | 0.8 | 0.3 | 0.076 | 0.06 |
| 503-407 | 0.21 | n.d. | 0.08 | 303 | n.d. | 34.8 | 73 | 2.2 | 2.9 | 0.5 | 1.1 | 0.5 | 0.105 | 0.11 |
| 503-509 | 0.20 | n.d. | 0.14 | 118 | n.d. | 4.6 | 25 | 3.7 | 6.8 | 1.3 | 3.0 | 1.2 | 0.122 | 0.21 |
| 503-516 | 9.86 | 0.59 | 3.91 | 67 | 79 | 11.9 | 193 | 4.9 | 94.0 | 18.9 | 36.2 | 17.9 | 1.473 | 3.40 |
| 503-626 | 0.24 | n.d. | 0.13 | 217 | n.d. | 19.3 | 51 | 2.8 | 3.2 | 0.6 | 1.3 | 0.6 | 0.057 | 0.13 |
| 503-671 | 0.39 | n.d. | 0.17 | n.d. | n.d. | 1.1 | 35 | 13.7 | 1.9 | n.d. | 0.7 | 0.6 | 0.032 | 0.11 |
| 503-680 | 0.61 | n.d. | 0.32 | 189 | 26 | 6.0 | 51 | 7.5 | 8.0 | 1.4 | 3.4 | 1.5 | 0.074 | 0.32 |
| 503-807 | 1.49 | n.d. | 0.63 | 170 | 50 | 3.7 | 254 | 11.4 | 35.4 | 6.3 | 15.5 | 7.0 | 1.185 | 0.86 |
| 503-889 | 0.69 | n.d. | 0.42 | 91 | 95 | 9.2 | 54 | 2.2 | 16.9 | 3.0 | 6.8 | 2.9 | 0.655 | 0.64 |
| 503-912 | 1.96 | n.d. | 0.89 | 456 | 154 | 5.0 | 135 | 13.5 | 21.3 | 3.9 | 8.5 | 4.0 | 0.739 | 0.71 |
| 503-946 | 0.99 | n.d. | 0.43 | 77 | 41 | 5.7 | 120 | 23.2 | 36.0 | 6.8 | 15.3 | 6.0 | 2.316 | 0.86 |
| 503-987 | 7.62 | 0.49 | 3.05 | 92 | 86 | 12.4 | 183 | 0.9 | 82.2 | 15.4 | 32.4 | 15.7 | 1.394 | 3.04 |
| 546-5 | 0.55 | n.d. | 0.19 | 85 | 13 | 11.8 | 186 | 13.7 | 6.1 | 1.1 | 2.3 | 1.2 | 0.103 | 0.25 |
| 546-92 | 0.38 | n.d. | 0.23 | n.d. | 19 | 7.7 | 91 | 8.9 | 5.1 | 1.0 | 2.0 | 0.9 | 0.103 | 0.18 |
| 546-180 | 0.52 | n.d. | 0.17 | 39 | n.d. | 8.0 | 101 | 7.1 | 5.6 | 1.0 | 2.2 | 1.0 | 0.095 | 0.22 |
| 546-229 | 0.72 | n.d. | 0.28 | 86 | 41 | 10.9 | 132 | 6.6 | 8.3 | 1.6 | 3.4 | 1.5 | 0.151 | 0.30 |
| 546-252 | 7.41 | 0.43 | 2.91 | n.d. | 38 | 1.1 | 95 | 0.8 | 73.6 | 13.2 | 30.0 | 14.0 | 0.715 | 2.77 |
| 546-267 | 0.99 | n.d. | 0.36 | 133 | 8 | 7.4 | 117 | 53.5 | 9.4 | 1.6 | 3.8 | 1.8 | 0.293 | 0.33 |
| 546-311 | 0.89 | n.d. | 0.38 | 22 | 49 | 4.7 | 57 | 0.6 | 47.2 | 8.8 | 20.2 | 7.9 | 1.961 | 1.45 |
| 546-318 | 2.11 | 0.13 | 0.72 | 64 | n.d. | 5.8 | 150 | 3.8 | 12.5 | 2.4 | 4.7 | 2.6 | 0.150 | 0.43 |
| 546-385 | 9.02 | 0.48 | 2.58 | 33 | 45 | 3.5 | 83 | 1.3 | 74.2 | 13.4 | 30.3 | 14.0 | 0.806 | 2.73 |
| 557-9 | 0.57 | n.d. | 0.23 | n.d. | 35 | 5.1 | 72 | 9.4 | 6.5 | 1.0 | 2.6 | 1.3 | 0.121 | 0.27 |
| 557-173 | 0.90 | n.d. | 0.40 | 126 | 30 | 3.4 | 98 | 16.3 | 8.4 | 1.3 | 3.3 | 1.7 | 0.149 | 0.35 |
| 557-227 | 0.35 | n.d. | 0.18 | 94 | 15 | 2.5 | 154 | 11.5 | 3.1 | 0.3 | 1.2 | 0.7 | 0.102 | 0.14 |
| 557-255 | 6.56 | 0.40 | 2.62 | n.d. | 36 | 3.0 | 134 | 3.6 | 64.5 | 12.7 | 26.0 | 11.8 | 0.723 | 2.33 |
| 557-289 | 0.27 | n.d. | 0.12 | 286 | n.d. | 21.2 | 62 | 13.2 | 4.7 | 0.9 | 1.9 | 0.9 | 0.205 | 0.14 |
| 557-388 | 2.63 | 0.16 | 1.09 | 277 | 106 | 6.3 | 102 | 9.5 | 28.1 | 5.2 | 11.4 | 5.3 | 0.580 | 0.99 |
| 557-502 | 5.47 | 0.33 | 2.36 | n.d. | 43 | 1.4 | 87 | 0.7 | 53.5 | 9.4 | 21.5 | 10.3 | 0.543 | 2.06 |
| 557-608 | 3.94 | 0.21 | 1.59 | n.d. | 46 | 0.9 | 73 | 1.7 | 39.5 | 7.0 | 16.0 | 7.5 | 0.385 | 1.52 |
| 557-753 | 4.38 | 0.25 | 1.88 | n.d. | 48 | 3.1 | 346 | n.d. | 44.1 | 8.0 | 17.7 | 8.3 | 0.433 | 1.69 |
| 557-795 | 3.90 | 0.22 | 1.27 | n.d. | 30 | 0.9 | 81 | 1.6 | 34.0 | 6.0 | 13.8 | 6.5 | 0.346 | 1.28 |
| 617-9 | 0.72 | n.d. | 0.26 | 70 | 25 | 9.5 | 87 | 9.8 | 6.6 | 0.9 | 2.6 | 1.4 | 0.093 | 0.29 |
| 617-148 | 0.72 | n.d. | 0.44 | 179 | 46 | 12.5 | 81 | 14.1 | 14.9 | 3.4 | 6.0 | 2.5 | 0.472 | 0.46 |
| 617-220 | 0.34 | n.d. | 0.16 | 56 | n.d. | 2.1 | 27 | n.d. | 4.0 | 0.4 | 1.4 | 0.9 | 0.082 | 0.24 |
| 617-395 | 0.95 | n.d. | 0.35 | 95 | n.d. | 6.9 | 123 | 21.8 | 6.5 | 0.8 | 2.5 | 1.5 | 0.097 | 0.33 |
| 617-396 | 4.54 | 0.28 | 1.94 | n.d. | 35 | 5.9 | 103 | 3.5 | 43.4 | 6.6 | 17.2 | 8.7 | 0.534 | 1.87 |
| 617-508 | 5.16 | 0.32 | 2.11 | 28 | 36 | 2.5 | 77 | 1.5 | 47.3 | 8.4 | 18.8 | 9.1 | 0.478 | 1.84 |
| 617-551 | 0.33 | n.d. | 0.12 | 29 | 7 | 1.0 | 21 | 1.5 | 3.2 | 0.5 | 1.3 | 0.7 | 0.063 | 0.14 |
| 617-650 | 1.06 | n.d. | 0.46 | 73 | 27 | 4.7 | 106 | 12.6 | 10.8 | 1.8 | 4.3 | 2.1 | 0.171 | 0.44 |
| 617-787 | 0.76 | n.d. | 0.40 | 170 | 18 | 6.4 | 69 | 11.7 | 7.0 | 1.0 | 2.8 | 1.5 | 0.116 | 0.27 |
| 617-799 | 1.49 | n.d. | 0.60 | 50 | 29 | 4.0 | 53 | 5.0 | 16.4 | 2.6 | 6.6 | 3.2 | 0.265 | 0.67 |
| 617-875 | 0.66 | n.d. | 0.26 | 60 | 22 | 2.1 | 98 | 5.2 | 11.1 | 2.3 | 4.5 | 1.9 | 0.250 | 0.37 |

Appendix C.1. Chemistry of the sediments from the Atlantis II Deep (Red Sea). Sample ID consists of the core number (locations in Appendix B.1) and sampling depth (cm below the top of the core). Units are according to the original core logging during MESEDA (Table 1.1 and Figure 1.3). Samples that were used for sequential leaches (column "SL") are indicated and the complete data for sequential leaches is given in Chapter 2 (Appendix 2.2). Sample classification is given according to Chapters 2, 3 and 4. Chapter 2 contains the most detailed division, whereas in Chapter 3 detrital and hydrothermal carbonate rich ($CO_3$-HC) samples (in Chapter 2) are grouped together as $CO_3$-rich samples, Mn-rich samples (Chapter 2) are divided between $CO_3$ and clay-rich samples in Chapter 3. Furthermore, high-sulfide high-metal samples (Chapter 3) are divided to Cu-rich (HS-Cu) and Zn-rich (HS-Zn) in Chapter 2. Chapter 4 used sub-set of samples with highest concentration of Al, Fe and metals (and sulphide); 39 samples that were not classified (n.c.) are indicated. The salt-free calculation is based on Na concentration, assuming all Na is in NaCl, amount of NaCl primary in the samples are also indicated. * S is total sulfur, amount of $S_{red}$ can be calculated as $S_{total}$ minus $S_{sulfate}$ (method 6). Analytical methods: 1=ICP-MS after fusion with Na-peroxide and dissolution of the fused glass with nitric acid; 2=ICP-OES after fusion with Na-peroxide and dissolution of the fused glass with nitric acid; 3=Instrumental neutron activation (INAA), 4=cold vapour-flow injection mercury system (FIMS), 5=Coulometry, 6=Combustion at 550°C and infrared (IR) detection; 7=Combustion at 1800°C and thermal conductivity detection; 8=ICP-MS after four-acid dissolution (HF-$HNO_3$-HCl-$HClO_4$-); 9=ICP-OES after four-acid dissolution (HF-$HNO_3$-HCl-$HClO_4$-); 10=Ion-specific electrode. Methods 1 to 6 and 10 were carried out by Activation Laboratories. Method 7 was carried out at the Hatch Laboratories at the University of Ottawa. Methods 8 and 9 were carried out at the University of Kiel. Be, Bi and Te were analyzed with detection limits of 3, 2 and 6 ppm respectively (method 1); Ir was analyzed with a detection limit 5 ppb (method 3). These elements were not detected, except one sample 334-312, which contained 6.3 ppm Bi. n.d.= not detected.

Appendix C.2. List of loadings for the first ten principal components of the PCA on the bulk geochemical data (salt-free) of 100 samples of metalliferous sediment from the Atlantis II Deep (Appendix C.1). The first three components account for 59.7 % of the total variance in the data set. All 10 components account for 86% of the total variance.

| Component | 1 | 2 | 3 | 4 | 5 | 6 | 7 | 8 | 9 | 10 |
|---|---|---|---|---|---|---|---|---|---|---|
| Initial Eigenvalue | 13.6 | 9.7 | 6.6 | 3.5 | 2.7 | 2.0 | 1.5 | 1.3 | 1.2 | 1.1 |
| % of variance | 27.2 | 19.3 | 13.2 | 7.0 | 5.3 | 3.9 | 3.0 | 2.6 | 2.5 | 2.1 |
| Zr | 0.88 | 0.42 | 0.11 | -0.04 | 0.00 | 0.06 | 0.06 | 0.07 | -0.07 | 0.01 |
| Sc | 0.87 | 0.44 | 0.12 | -0.05 | 0.01 | 0.07 | 0.05 | 0.02 | -0.05 | -0.03 |
| Y | 0.87 | 0.42 | 0.11 | -0.14 | 0.03 | 0.05 | 0.03 | 0.04 | -0.02 | 0.02 |
| Nb | 0.87 | 0.45 | 0.13 | -0.05 | 0.03 | 0.06 | 0.07 | 0.04 | -0.06 | -0.01 |
| Ti | 0.87 | 0.44 | 0.12 | -0.06 | 0.02 | 0.07 | 0.07 | 0.05 | -0.09 | 0.00 |
| Cr | 0.86 | 0.44 | 0.16 | -0.04 | 0.03 | 0.01 | 0.03 | 0.05 | -0.09 | 0.05 |
| Th | 0.85 | 0.47 | 0.13 | -0.03 | 0.02 | 0.07 | 0.06 | 0.05 | -0.04 | -0.02 |
| Al | 0.81 | 0.53 | 0.13 | -0.08 | 0.00 | 0.06 | 0.08 | -0.01 | -0.08 | -0.03 |
| $REE_{tot}$ | 0.81 | 0.44 | 0.09 | -0.15 | 0.11 | -0.02 | 0.01 | 0.06 | -0.02 | 0.03 |
| Hf | 0.78 | 0.26 | 0.37 | 0.03 | -0.14 | 0.18 | 0.06 | 0.04 | -0.20 | 0.10 |
| $CO_2$ | 0.73 | 0.17 | -0.11 | -0.17 | -0.01 | 0.07 | -0.06 | -0.19 | 0.36 | -0.08 |
| Ge | -0.63 | 0.22 | 0.46 | -0.10 | -0.05 | -0.17 | 0.01 | 0.00 | -0.09 | -0.24 |
| Mo | -0.56 | 0.35 | 0.00 | -0.17 | 0.54 | -0.02 | 0.14 | 0.22 | 0.08 | -0.14 |
| Ca | 0.55 | -0.11 | -0.54 | 0.21 | -0.41 | 0.09 | -0.01 | -0.03 | 0.11 | 0.03 |
| W | -0.50 | 0.24 | 0.21 | 0.10 | 0.07 | -0.30 | -0.12 | -0.28 | -0.15 | -0.18 |
| Ni | 0.05 | 0.83 | -0.03 | -0.11 | 0.10 | -0.14 | 0.31 | 0.03 | 0.23 | -0.05 |
| Ga | -0.35 | 0.78 | 0.02 | 0.11 | 0.20 | -0.20 | 0.19 | -0.19 | 0.06 | -0.11 |
| Tl | -0.43 | 0.73 | 0.05 | 0.12 | 0.05 | -0.17 | 0.18 | 0.04 | 0.16 | 0.05 |
| Pb | -0.57 | 0.71 | -0.02 | -0.03 | -0.13 | 0.17 | -0.02 | -0.06 | 0.10 | 0.03 |
| Cu | -0.45 | 0.70 | 0.06 | -0.18 | -0.06 | -0.04 | 0.24 | -0.13 | 0.07 | 0.02 |
| Au | -0.55 | 0.70 | -0.02 | 0.15 | 0.05 | -0.16 | 0.01 | -0.17 | -0.09 | -0.01 |
| Sb | -0.46 | 0.68 | -0.09 | 0.05 | -0.01 | 0.26 | -0.35 | 0.20 | 0.04 | -0.14 |
| Cd | -0.45 | 0.67 | -0.07 | -0.02 | -0.17 | 0.37 | -0.29 | 0.10 | 0.05 | -0.03 |
| Zn | -0.54 | 0.65 | 0.04 | -0.05 | -0.21 | 0.00 | 0.11 | -0.09 | 0.05 | 0.04 |
| Ag | -0.44 | 0.65 | -0.05 | -0.02 | -0.15 | 0.41 | -0.36 | 0.11 | 0.04 | 0.02 |
| Se | -0.20 | 0.62 | 0.32 | -0.05 | -0.08 | -0.08 | 0.18 | 0.02 | -0.28 | 0.29 |
| As | -0.48 | 0.61 | -0.06 | -0.02 | 0.26 | -0.18 | 0.06 | 0.21 | 0.01 | -0.18 |
| Hg | -0.45 | 0.58 | 0.00 | -0.16 | -0.22 | 0.44 | -0.35 | 0.05 | 0.07 | 0.02 |
| Co | -0.52 | 0.57 | 0.05 | -0.11 | -0.17 | 0.18 | 0.22 | -0.29 | 0.09 | 0.20 |
| K | -0.17 | -0.23 | 0.83 | 0.32 | -0.16 | 0.10 | 0.12 | 0.05 | 0.11 | -0.06 |
| Rb | 0.14 | -0.09 | 0.79 | 0.31 | -0.19 | -0.06 | -0.03 | 0.22 | 0.23 | -0.23 |
| Li | 0.00 | -0.15 | 0.77 | 0.27 | -0.22 | 0.13 | 0.21 | 0.03 | 0.03 | 0.02 |

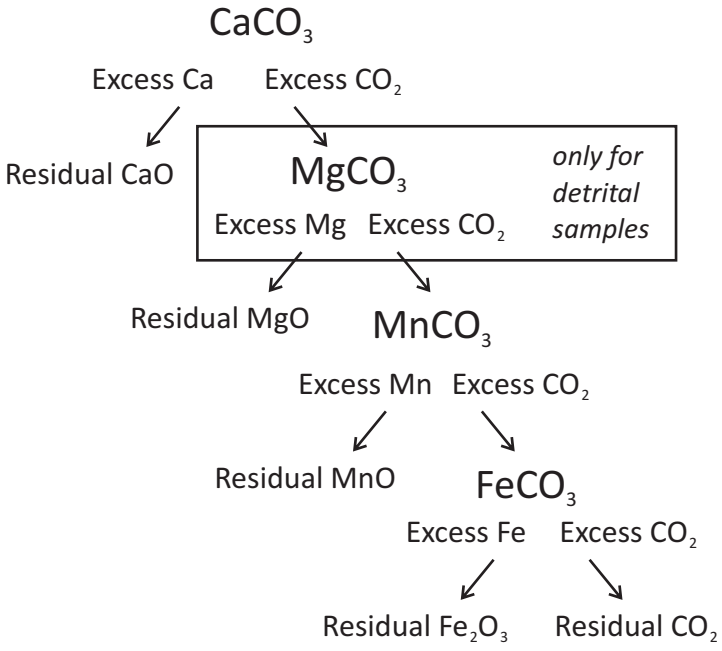
| | | | | | | | | | | |
|---|---|---|---|---|---|---|---|---|---|---|
| Te | -0.28 | 0.01 | 0.72 | 0.15 | -0.13 | 0.14 | 0.13 | 0.03 | -0.15 | 0.21 |
| Cs | 0.23 | 0.02 | 0.71 | 0.31 | -0.09 | -0.19 | -0.12 | 0.31 | 0.23 | -0.20 |
| $SO_4$ | -0.30 | 0.19 | -0.68 | 0.24 | -0.38 | -0.19 | 0.12 | 0.17 | -0.13 | 0.03 |
| Na | -0.64 | -0.15 | 0.68 | 0.12 | -0.01 | 0.12 | 0.01 | -0.08 | -0.08 | 0.08 |
| Br | -0.50 | -0.25 | 0.64 | 0.12 | -0.13 | 0.13 | 0.03 | -0.29 | -0.14 | 0.14 |
| B | -0.32 | -0.36 | 0.59 | -0.23 | 0.25 | 0.21 | 0.10 | 0.17 | 0.06 | 0.02 |
| Si | 0.28 | 0.43 | 0.50 | 0.45 | 0.06 | -0.22 | -0.17 | 0.01 | -0.16 | -0.16 |
| Sr | 0.11 | 0.06 | -0.21 | 0.82 | 0.38 | 0.26 | 0.02 | -0.05 | -0.03 | 0.08 |
| Fe | -0.43 | -0.29 | 0.31 | -0.62 | 0.31 | -0.02 | -0.08 | 0.12 | -0.14 | 0.04 |
| Ba | -0.08 | 0.19 | -0.29 | 0.62 | 0.49 | 0.05 | -0.14 | 0.02 | -0.30 | -0.04 |
| Mn | 0.02 | -0.10 | -0.06 | 0.06 | 0.53 | 0.31 | 0.24 | -0.18 | 0.46 | 0.04 |
| U | -0.16 | 0.01 | 0.09 | -0.48 | 0.50 | 0.26 | 0.04 | 0.09 | -0.36 | 0.03 |
| V | 0.14 | 0.27 | 0.27 | 0.18 | 0.28 | -0.46 | -0.48 | -0.04 | 0.12 | 0.34 |
| P | 0.32 | 0.35 | 0.34 | -0.21 | 0.22 | -0.36 | -0.41 | -0.19 | 0.18 | 0.30 |
| Mg | 0.45 | 0.06 | 0.18 | -0.03 | -0.23 | 0.02 | -0.15 | -0.52 | -0.07 | -0.19 |
| Sn | -0.14 | -0.05 | -0.02 | 0.10 | -0.12 | -0.17 | 0.05 | 0.35 | 0.20 | 0.53 |

PCA results are consistent with the interpretation of the correlation matrix in Figure 3.5. Principal components 1 and 2 represent the detrital and hydrothermal components of the samples, respectively. 3 represents the “evaporitic” or salt component (dominated by Na, K, Rb, Li, B, and Br), 4 is the barite component (strong loadings for Sr, K, and Rb), and 5 is the hydrogenous component (strong loadings for Mn, Mo, and U, and to a lesser extent for As, V, and P).

Appendix D. Normative Mineralogy.

Schematic illustration of the normative mineral calculation for carbonate minerals and sulfides (page 2/2) used to calculate Table 2.6. In samples with molar $CO_3$>$SO_4$, Ca was first attributed to calcite, then anhydrite; in samples with molar $SO_4$>$CO_3$, Ca was first attributed to anhydrite. In many carbonate-rich samples molar Ca is less than or equal to the molar $CO_3$. In the $CO_3$-rich (calcite and detrital silicate rich) samples (Table 2.6), the residual $CO_3$ correlates well with residual Mg ($r^2$=0.57), consistent with the presence of dolomite. The amount of dolomite in these samples is estimated from the residual Mg concentration and reported as end-member $MgCO_3$. Other samples contained minor dolomite. Any residual $CO_3$ after calcite (and dolomite) formation was first attributed to $MnCO_3$ (according to the bulk Mn content) and the remainder to $FeCO_3$. Residual elements are assumed to be present mainly in clays and (oxy)hydroxides.

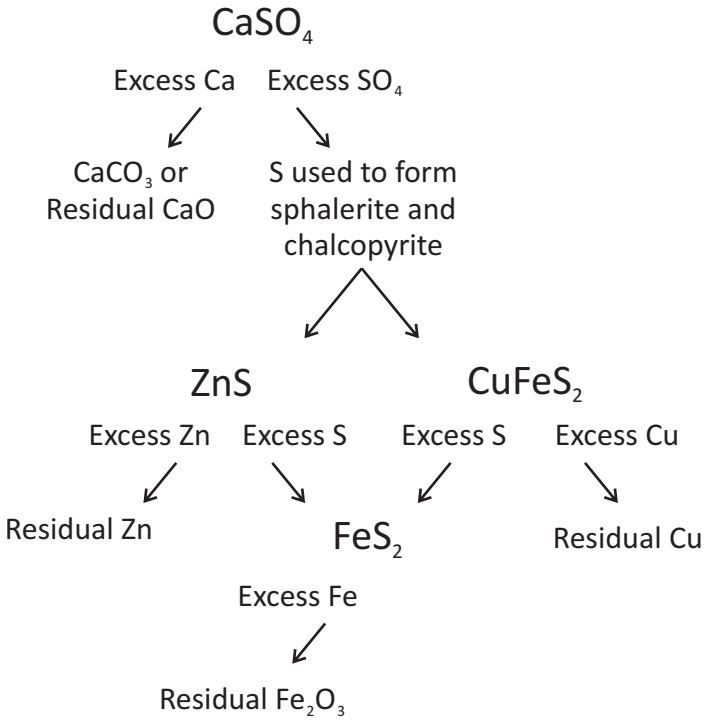
**Normative calculation for carbonate minerals**



Appendix D.

The reduced sulfur content of the samples is mainly present as pyrite and chalcopyrite, and was first attributed to $CuFeS_2$, then $FeS_2$. For the purposes of the normative calculation we assume that all Zn that is now present as secondary Zn-sulfates was originally deposited as sphalerite (cf. Chapter 2). Therefore, the sulfur in residual sulfate after the formation of anhydrite was attributed first to ZnS, and any remaining sulfur was attributed to pyrite. In a number of samples insufficient residual sulfate was present to account for all of the Zn, leaving a nontrivial component of residual Zn (Table 2.6).

**Normative calculation for sulfur minerals**



Appendix E. Mineral characterization and mineral chemistry.

This Appendix composes of summary descriptions of thin sections and polished blocks studied by Scanning Electron Microscope (SEM), Electron Microprobe (EPMA) and Synchrotron X-ray Fluorescence (S-XRF). Main interest was to study distribution of trace metals between the different mineralogical components and therefore absolute concentrations were determined in rare occasions (see Chapter 2). Maximum concentrations (in counts) for the individual grains mapped with EPMA-EDS are listed in Table E.1.

Table E.1. The count number corresponding to maximum on EPMA maps of individual sulfide and nonsulfide grains in Appendix E.

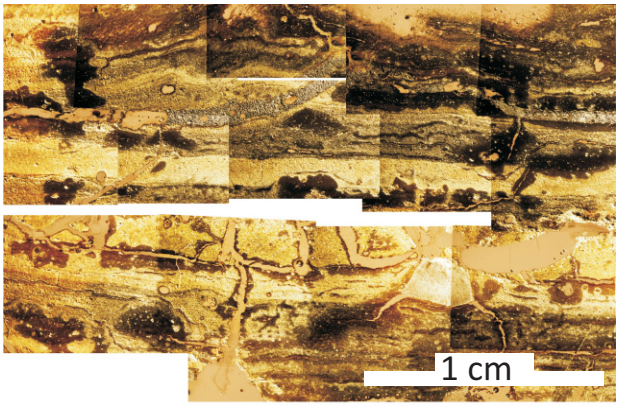
| Sample | Grain Mount (Figure) | Fe | Mo | Sb | Ag | As | Cu | Se | Cd | Zn | S |
|---|---|---|---|---|---|---|---|---|---|---|---|
| 268-985 | 1 (B3) | 3947 | 10 | 12 | 75 | 77 | 558 | 102 | 86 | 2050 | 254 |
| 268-985 | 3 (B3) | 7408 | 19 | 11 | 119 | 85 | 3188 | 112 | 94 | 275 | 1559 |
| 268-985 | 5 (C2) | 6233 | 21 | 26 | 283 | 82 | 3760 | 120 | 212 | 1638 | 1511 |
| 268-985 | 7 (B3) | 7479 | 19 | 10 | 112 | 84 | 2846 | 113 | 92 | 276 | 1778 |
| 268-985 | 10 (B2) | 1904 | 7 | 4 | 40 | 63 | 3115 | 59 | 125 | 298 | 120 |
| 268-985 | 12 (A2)[1] | 3366 | 10 | 11 | 80 | 53 | 1820 | 61 | 104 | 513 | 820 |
| 268-985 | 12 (A2)[2] | 6641 | 18 | 9 | 145 | 99 | 3234 | 119 | 87 | 361 | 1747 |
| 268-985 | 12 (B2) | 7504 | 21 | 17 | 172 | 88 | 3812 | 133 | 231 | 1789 | 1514 |
| 268-985 | 12 (B3) | 7738 | 21 | 14 | 200 | 87 | 3040 | 122 | 93 | 245 | 2021 |
| 268-985 | 13 (A2)[3] | 3810 | 45 | 12 | 21 | 57 | 72 | 30 | 30 | 306 | 2400 |
| 503-912 | 2 (A3) | 6451 | 425 | 17 | 95 | 180 | 1097 | 206 | 124 | 108 | 2415 |
| 503-912 | 4 (A1) | 5441 | 9 | 7 | 57 | 74 | 341 | 86 | 66 | 135 | 181 |
| 503-912 | 4 (B1) | 6456 | 22 | 6 | 66 | 108 | 179 | 104 | 73 | 76 | 2379 |
| 503-912 | 6 (B2) | 6538 | 22 | 9 | 63 | 206 | 274 | 118 | 78 | 138 | 2355 |
| 503-912 | 8 (A1) | 6456 | 22 | 6 | 66 | 108 | 179 | 104 | 73 | 76 | 2379 |
| 503-912 | 8 (C2) | 6172 | 13 | 21 | 62 | 92 | 4455 | 97 | 82 | 756 | 1736 |

The elemental map from sample 268-985 grain mount 12 (Figure A2) composes of two parts: [1]indicates the top part and [2] the lower part of the elemental map. [3]indicates the only grain that was mapped at the University of Ottawa with the same instrument and using same parameters as for the other grains, which were done at GEOMAR. Counts were calibrated to sulfur, but cannot be directly correlated between the different instruments.

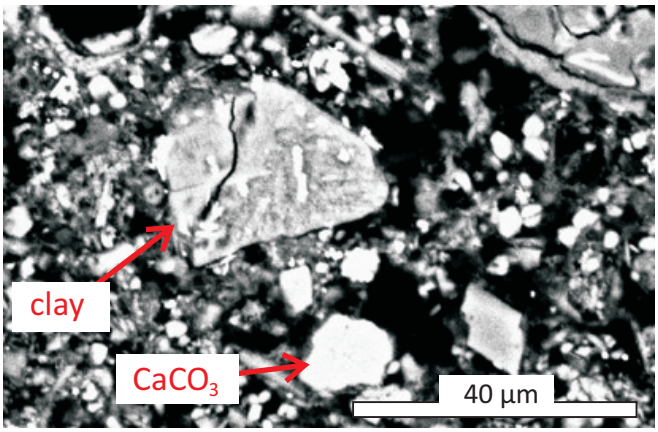
Appendix E. Summary description of sample 495-859.

This sample consists of alternating layers of sediment with variable hydrothermal components (Figure A). The light layers (Figure B) have larger detrital component than the dark layers (Figure C), which are dominated by authigenic components. The matrix is composed of clays, carbonates (mix of Fe, Mn, Ca carbonate and biogenic $CaCO_3$ locally), disseminated sulfides and anhydrite. The clasts are composed of carbonates (mainly of Fe, Mn, Ca carbonate), which are commonly euhedral, and pyrite (up to 10 μm), which may be rounded or angular. There is a large biogenic detrital component, mainly calcite, in the lighter areas (Fig. 2.8). Locally, radiolarian tests are filled with non-sulfidic, high-Zn material (see Fig. 2.9C). Fe-(oxy)hydroxide particles are up to 30 μm (Fig. 2.9E) and are commonly rimmed by amorphous Si-Fe-rich material that is also enriched in Zn and Cu. Element maps (C) show that the rims on the Fe-(oxy)hydroxide particles contain up to 10 wt.% Cu and Zn combined but less sulfur than would be required to bind all Cu and Zn as sulfide. Pyrite is found as relatively large sub- to euhedral grains. Chalcopyrite and sphalerite are found in the darker areas as small rounded particles (~1 μm diameter), and are rare in the lighter layers. Hydrothermal carbonates are found in both the lighter and darker areas but are more common in latter (small inset in B from a lighter band). Locally the hydrothermal carbonates have cores of Mg-Ca-carbonate (Fig. 2.9J).

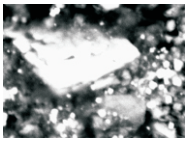
Appendix E. Sample 495-859



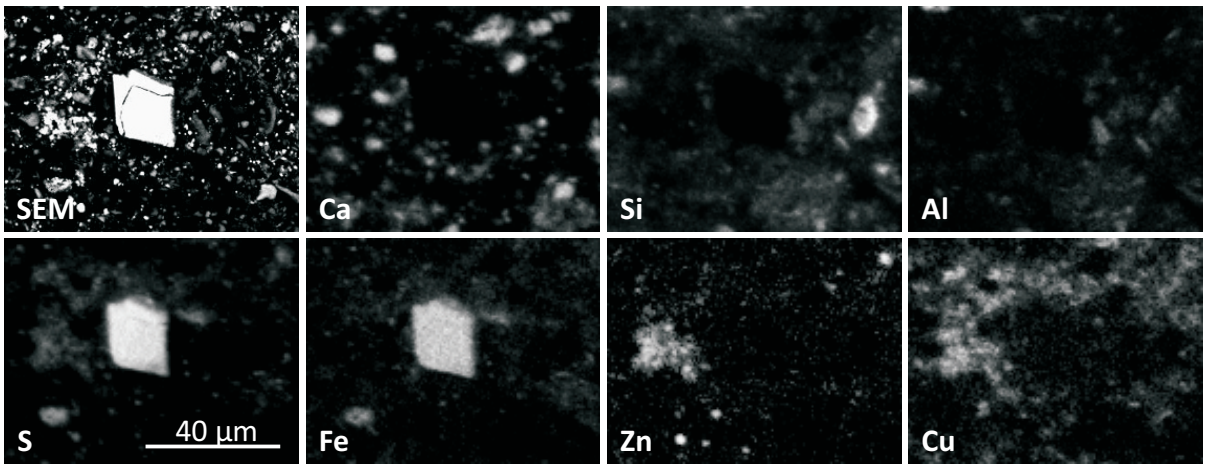

A) Photomicrograph in plane transmitted and reflected light showing the light and dark bands.




B) Backscattered electron SEM images show detrital (Ti-, Al-rich) clay and $CaCO_3$, and authigenic carbonate (on the right at the same scale).



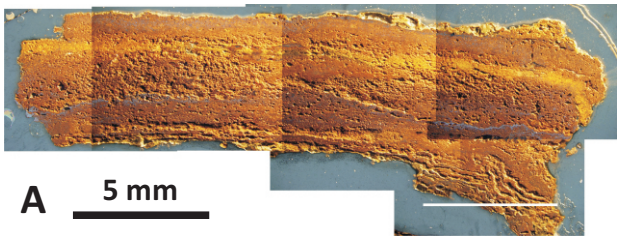
C) Element maps produced by SEM-EDS mapping showing the distribution of Ca, Si, Al, S, Fe, Zn and Cu in a dark band containing pyrite and non-sulfide Cu and Zn.



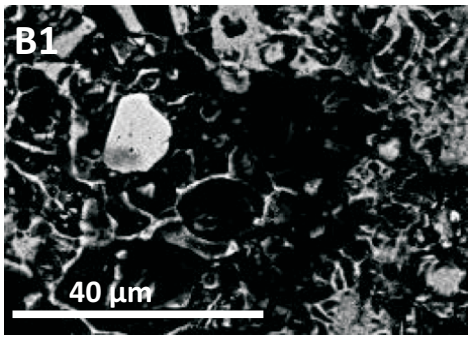
Appendix E. Summary description of sample 373-734.

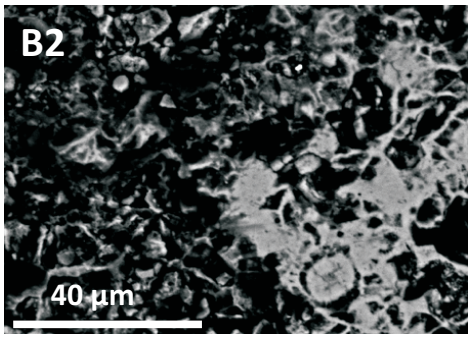
This sample is of a hard layer within unconsolidated brine-saturated sediment. It has macroscopic lamination with lighter and darker bands of yellow, orange, red and brown (A). The laminae comprise rounded particles (up to 20 μm) with a variable amount of matrix material. Color variation correlates with the abundance of authigenic clays (dark areas in SEM back-scatter images B1 and B2) versus Fe-(oxy)hydroxides (light matrix and light clasts in SEM images). The rounded particles resemble radiolaria tests but now comprise mostly Fe-Si and O. Abundant radiolaria are typical for SU1, and the radiolaria-rich horizons have high permeability, functioning as microaquifers for hydrothermal fluid flow. Many of the radiolarian tests have been pseudomorphed by Fe-(oxy)hydroxides. Sulfides and nonsulfide Zn or Cu are uncommon, although traces of pyrite are found. The diffuse boundaries of the laminae can be clearly distinguished in element maps of Fe, C, and O (C).

Appendix E. Sample 373-734

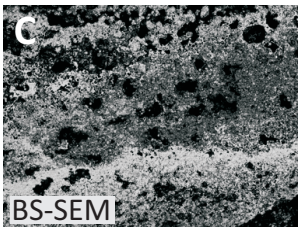


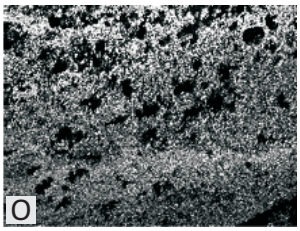

A) Photomicrograph in plane transmitted and reflected light showing light and dark bands. Lighter bands are composed mainly of Fe-OOH; darker bands are composed mainly of authigenic clays.

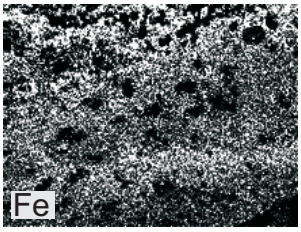


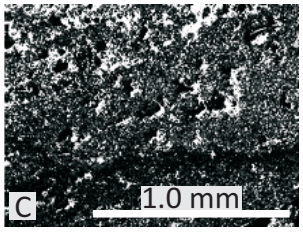




B) (above) Backscattered electron images of partly to completely pseudomorphed radiolaria, replaced by Fe-(oxy)hydroxides. The degree of replacement typically varies between coloured laminae.

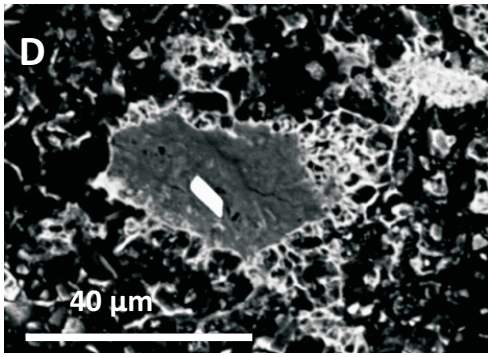



C) (left) Diffuse boundaries of the laminae are distinguished in back-scattered electron images by enrichment in Fe-O and depletion in C, reflecting enrichment of hydrothermal components in porous sublayers where biogenic carbonate was dissolved.

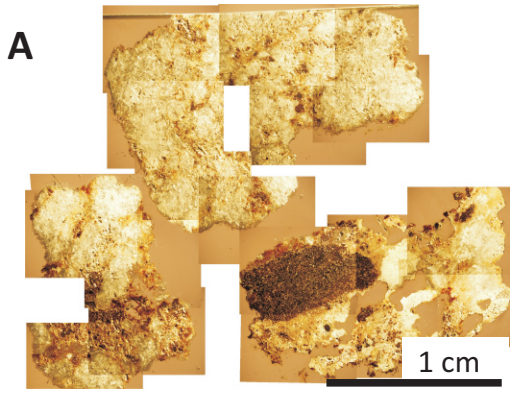



D) (right) Backscattered electron image of a large Fe-(oxy)hydroxide particle with an inclusion of a detrital grain (zircon). The larger particle is composed of Si, Fe and O with 2 wt.% Zn and 0.4 wt.% S. The lighter "rim" has a higher Fe-content.

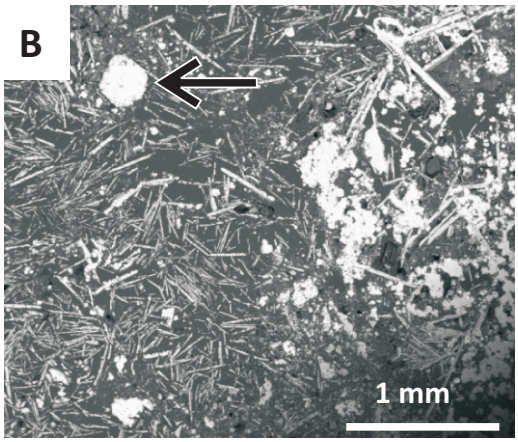
Appendix E. Summary description of sample 503-254.

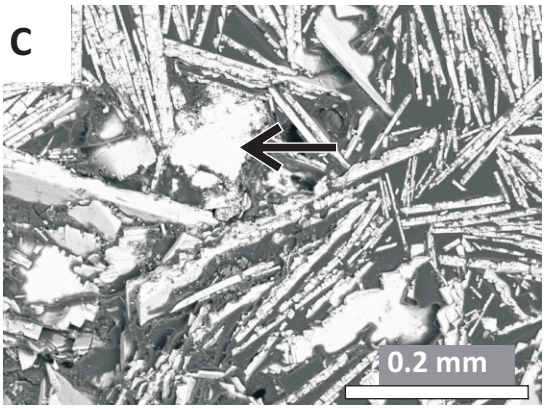
This sample is typical of massive anhydrite taken from a 1-m thick anhydrite bed in core 503 (unit SOAN). The mineralogy consists of anhydrite (white in image A), barite, Fe-Mn-carbonate and possible Fe-Mn (oxy)hydroxide (brown in image A). Anhydrite is commonly found as needles (B), but rectangular, platy crystals are also abundant (C). Rarely the grain borders are rounded (see Figure 2.9L). The anhydrite contains few minor elements (<1 wt.%). Barite typically occurs as rather large (50 um up to 0.2 mm) rounded particles with both sharp and indistinct grain boundaries (D and arrows in other images), but also as radial aggregates (Figure 2.9D). Barite contains ~4 wt.% Sr. Examples of Fe-Mn-carbonate and Fe-(oxy)hydroxides are shown in images E and F (the light rounded particles) and are the only mineral phase in which Cu or Zn was detected (up to 4 wt.% Cu+Zn).

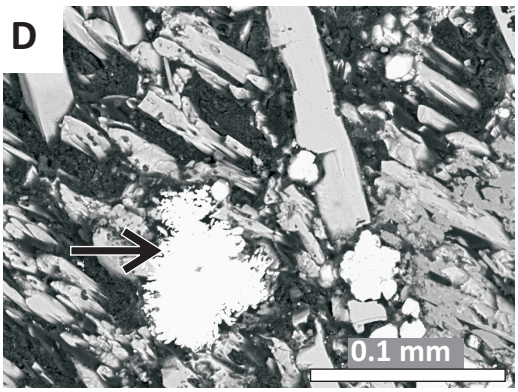
Appendix E. Sample 503-254



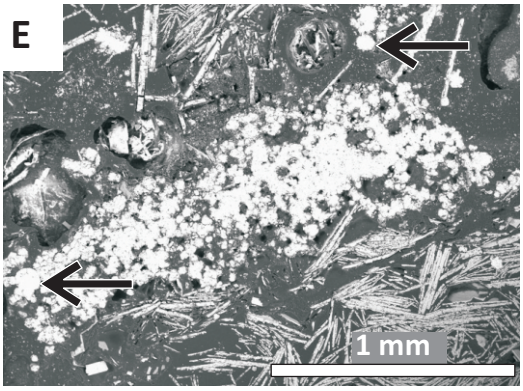

A) Anhydrite (white) and Fe-Mn carbonates and/or (oxy)hydroxides (brown) are the main mineral phases of this sample.

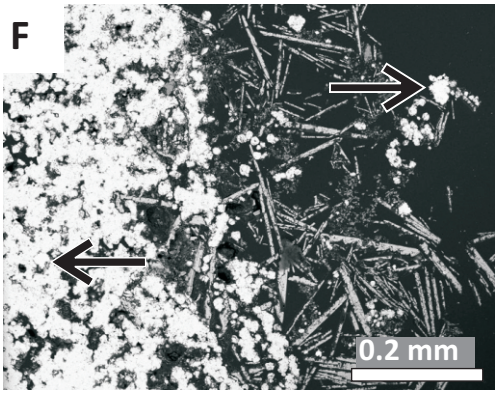



B-C) Anhydrite crystals are most often found as needle-shaped crystals, but angular platy grains are also common.
D) Barite crystals are typically rounded, they are indicated in all images with arrows.
E-F) Fe-Mn carbonates and/or (oxy)hydroxides (~40 wt.% Fe, ~10 wt.% Mn, minor Ca and Mg) are found as clusters of small rounded particles.

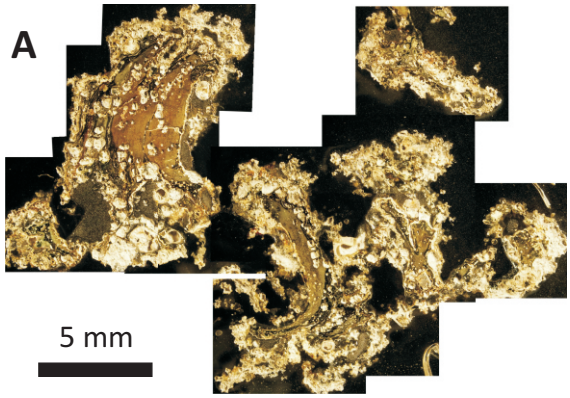


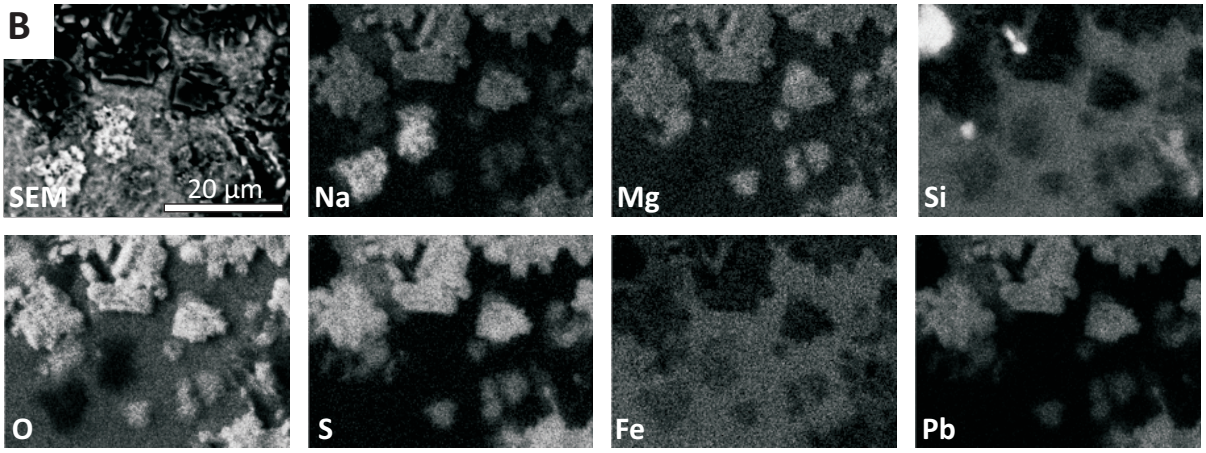
Appendix E. Summary description of sample 264-474.

This sample is of a green and authigenic clay-dominated layer with high metal, but low sulfide content. It had very high pore water content, which is now seen as abundant salt crystals with variable chemical composition (A, B). Zn is found in the matrix at high concentrations (~2-5 wt.%) with subordinate sulfur. High Zn concentrations (up to 45 wt.%, but typically 5-10 wt.%) are found in the small, bright angular grains (arrows pointing up in C and D). The grains contain less sulfur than would be expected for sphalerite and are interpreted to be either clays, Fe-(oxy)hydroxides with adsorbed Zn, or secondary sulfates (~35 wt.% Fe, ~8 wt.% Zn, few wt.% of Si, Mg, Cl or other elements, <1 wt.% S). Other Zn-rich grains had compositions corresponding to Cl-salt or oxide (e.g., 35 wt.% Cl, 20 wt.% O and 45 wt.% Zn in one grain and 20 wt.% Cl, 75 wt.% O and 6 wt.% Zn in another). Small barite grains are common (arrows pointing down in images C and D) and typically contain ~5 wt.% Sr. Cu was detected rarely and always accompanied by significant sulfur, likely in chalcopyrite.

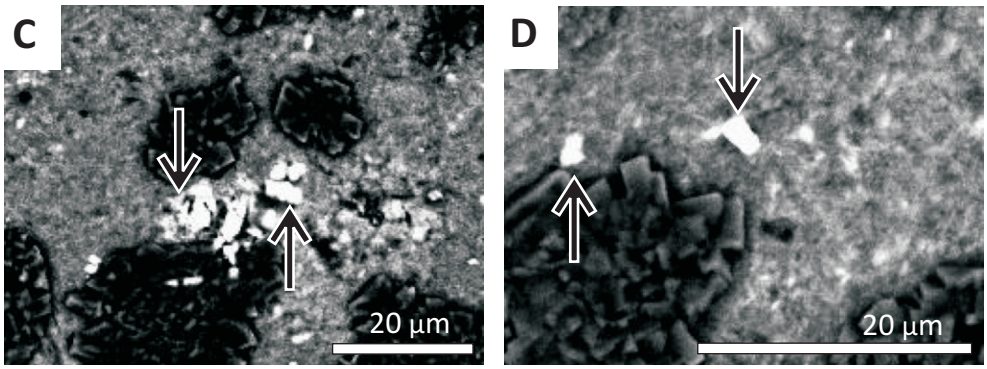
Appendix E. Sample 264-474




A) Photomicrograph in plane transmitted and reflected light shows the abundant salt crystallized from the abundant pore water in this metal-rich and sulfide-poor sample.




B) SEM-EDS element maps of various salts. White crystals are halite, whereas the black crystals are secondary Fe-Zn-sulfates (13 wt.% S, 8 wt.% Fe and Na, 5 wt.% Mg and Si, 2 wt.% Zn and Cl, 1 wt.% K and Mn, and ~55 wt.% O). The matrix is enriched in Fe (30 wt.%) and Zn (~5 wt.%; not shown).



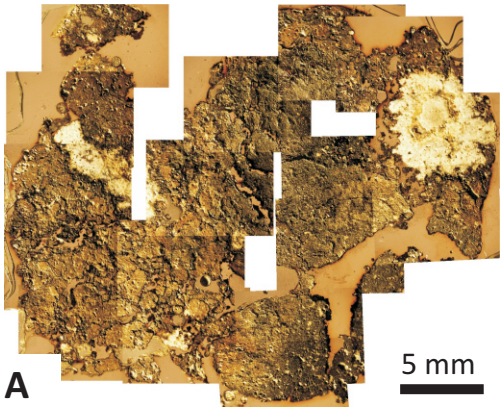

C-D) Backscattered SEM image of barite grains (arrows pointing down) and authigenic clays/(oxy)hydroxides with 8 wt.% Zn (arrows pointing up).

Appendix E. Summary description of sample 264-907.

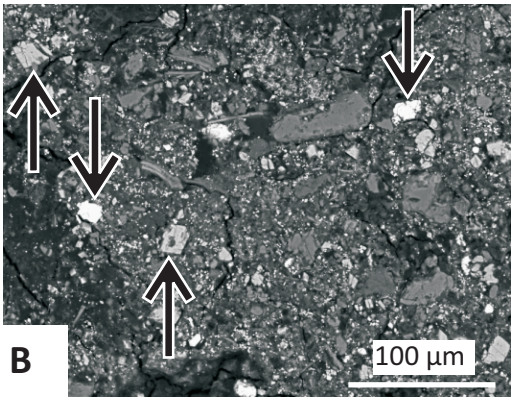
This is a sample of a dark grey layer with high sulfide content (A). It is dominated by granular authigenic components, mainly carbonates, sulfides and silicates. Anhydrite is found as large clusters of grains (white areas in A) rather than as small solitary grains mixed with other compounds, as in many other samples. Detrital silicates (high Al-concentration) are common suggesting that originally this sample had large detrital component, but most of the biogenic detritus was dissolved and replaced due to hydrothermal influence during diagenesis. Pseudomorphs after radiolaria tests show that the biogenic detritus has been partly dissolved and replaced by epigenetic clays and/or oxides, which may contain high Zn (Figure 2.9A). Calcite was not found suggesting that all biogenic calcite has been dissolved; instead authigenic (Fe-Mn-rich) carbonates are common. Carbonates vary in size up to ~20 µm and are found as sub- to euhedral grains (arrows pointing upwards in B and C). Their composition is homogenous and similar to those found in other samples containing abundant authigenic carbonate: ~40 wt.% Fe, ~8 wt.% Mn, ~5 wt.% Ca and minor amounts of Mg (± Si, S, Al and/or Zn). The matrix of this sample is composed of the same minerals than found as larger grains but with smaller grain size.

Pyrite and chalcopyrite are common (arrows pointing down in image B). Sphalerite was not found, except in composite chalcopyrite-sphalerite grains (image D; cf. Fig. 2.11C and Appendix D.2). Pyrite occurs as small (<5 µm), anhedral or framboidal grains with traces of other metals (~1- 5 wt.% Cu, Zn or Ni). Large, euhedral pyrite grains (E) are rare. The largest sulfide grains (up to ~50 µm) are chalcopyrite, which commonly have exsolution lamellae with variable Fe:Cu ratio (see also Figures 2.9K and 2.11B).

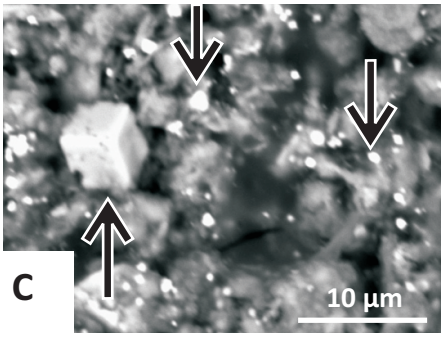
Appendix E. Sample 264-907




A) Photomicrograph in plane transmitted light showing the sulfide-rich sediment (grey) and large clusters of anhydrite (light).



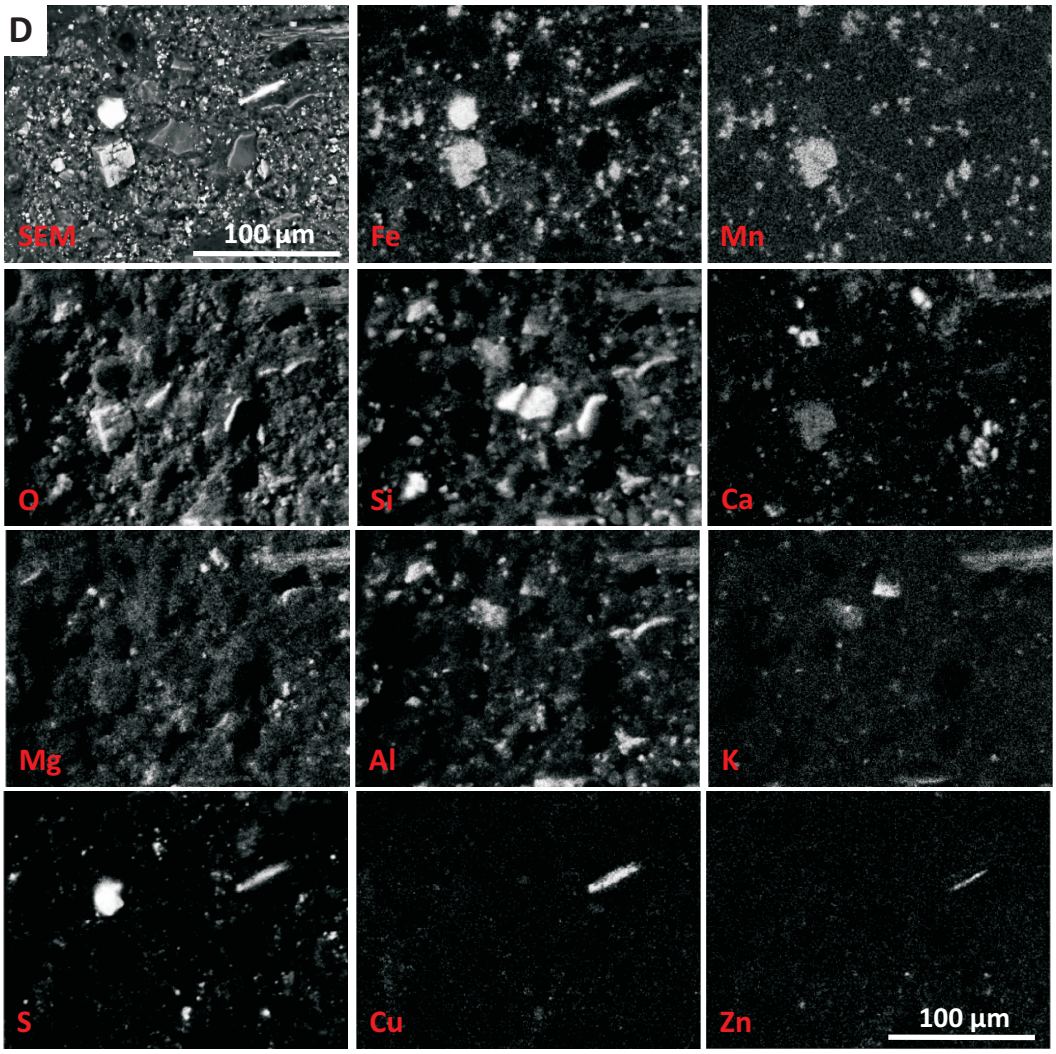

B) Backscattered SEM image (BSE) showing the typical granular texture of this sample, with grains of varying size. Authigenic carbonates (upward pointing arrows) are zoned with increasing Fe content towards the rim. The largest sulfide grains are chalcopyrite (downward pointing arrows).

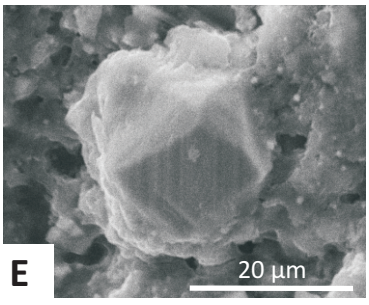



C) Secondary electron SEM image (SEI) showing detail of the authigenic carbonate (upward pointing arrow). In this sample, pyrite occurs as small, disseminated grains (downward pointing arrows). Anhedral, rounded and locally framboidal pyrite has high trace metal concentrations (up to few wt. % of Ni, As, Cu or Zn).

Appendix E. Sample 264-907

D) Element maps (SEM-EDS) show the distribution of the major elements in this sample. The highest Fe corresponds to pyrite, authigenic carbonates contain ~35 wt.% Fe (together with ~8 wt.% Mn and ~4 wt.% Ca); Fe is also abundant in the matrix. Silicates are composed of Fe, Mg, Si, Ca, K and Al; detrital silicates are high in Al, and the highest Si corresponds to amorphous silica. Pyrite and chalcopyrite are found throughout, whereas sphalerite is rare.




E) SEI image of the pyrite grain from the element maps in D. Such large pyrite grains are rather uncommon. They are characterized by sub- to euhedral shapes and have low trace metal concentrations.

multiple mineralogical components due to presence of a layer of amorphous material on all grains. The amorphous material composes typically of varying concentration of Fe (~25 wt.%), Si (~15 wt.%), S and Cl with subordinate Ca, Mg, Mn (±Na, Al, K) and ~5 wt.% Zn. This characteristic is illustrated in secondary electron image F1 and detail from it (F2). Backscattered SEM image F3 corresponds to F2.

Figure G shows synchrotron-XRF maps of an area covering the band of silica test including the area with high Cu-concentration (~50 wt.%). Ni is co-enriched with Cu (in some nonsulfide mineral phase, probably oxide). Zn is mainly found in nonsulfides (sulfate?) and does not correlate with Cu instead it is most enriched in areas that are low in almost all other elements. Ga correlates with Zn and Cu. Cd, Cr and Pb are most enriched outside the band of silica tests, which is also enriched in Fe and Mn. Fe and Mn are mainly found in authigenic carbonate (cf. Figure 2.10).

Appendix E. Summary description of sample 495-777.

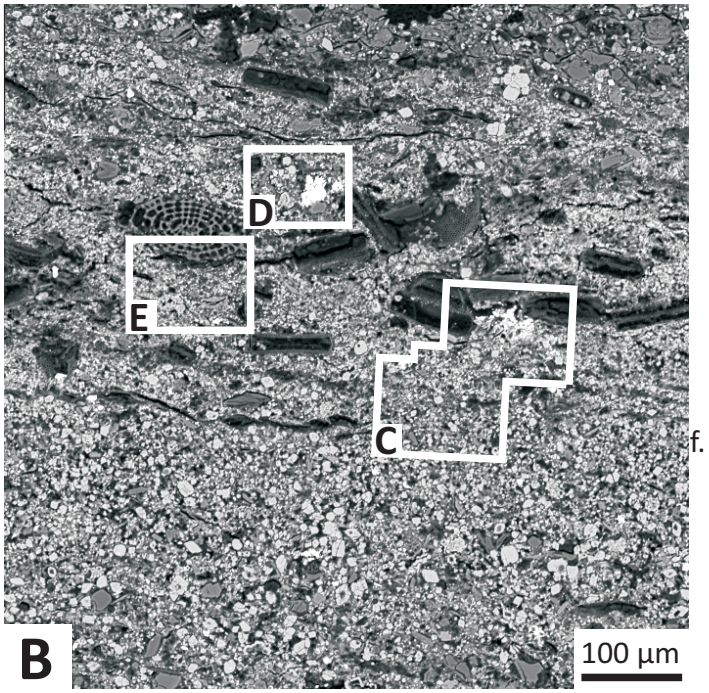
This sample is from a finely laminated sulfide-rich layer in unit SU1 (A). Area B (location indicated in A) comprising a band of silica tests was mapped with EPMA (results in Figure 2.10) and detailed backscattered SEM images from this area are shown in C, D and E.

Figure C1 illustrates the area with highest Cu-concentration close to a silica fossils (~50 wt.% Cu, ~25 wt.% O, ~15 wt.% Cl, <5 wt.% S, <5 wt.% Si and <2 wt.% Zn, corresponding to chloride or oxide). Authigenic (Fe-Mn-Ca) carbonates (examples indicated with upward pointing arrows) are often zoned with increasing Fe-concentration from core to rim. Authigenic carbonates and clays (examples indicated with downward pointing arrows) may contain several wt.% of Zn. Figure C2 (partly overlapping with C1) shows the difference between carbonate (grey), which is typically found as rather large grains and pyrite (light), which is typically present as very small granular grains. Three texturally different barite grains are indicated with arrows in backscattered SEM image D (cf. Figure 2.9A).

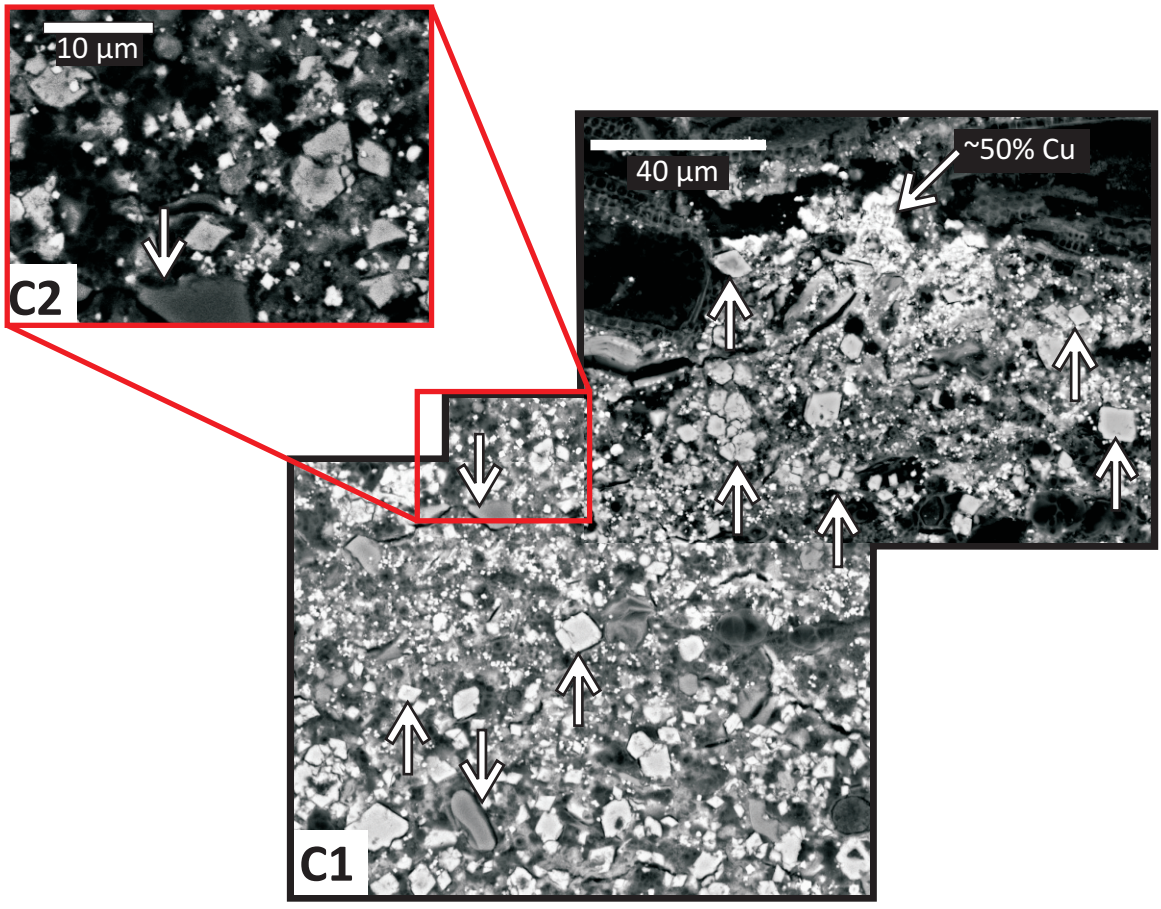
Backscattered SEM images in E1 and E2 are details from close proximity to a radiolaria fossil (37 wt.% Si; 62 wt.% O). Secondary electron image E3 corresponds exactly to E2. The brightest spots correspond most commonly to pyrite (with up to 2.5 wt.% As) and rarely to other sulfides. Downward pointing arrows indicate authigenic clays (rich in Mg, Fe, Si) and upward pointing arrows indicate authigenic (Fe-Mn-Ca) carbonates, both contain up to 7 wt.% combined Cu and Zn. Carbonate in E1 (arrow up) contains >2 wt.% Cu and Zn both, but only 1 wt.% S, excluding presence of Cu and Zn as sulfide. In some other clays and carbonates, high Cu and Zn might be due to intermixture of sulfide minerals in the spot analyze. Similarly, due to large spot size of SEM, most of the spot analyzes are mixtures of

Appendix E. Sample 495-777

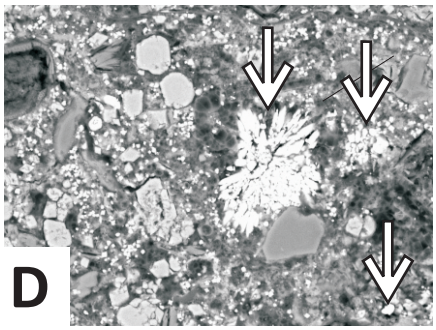


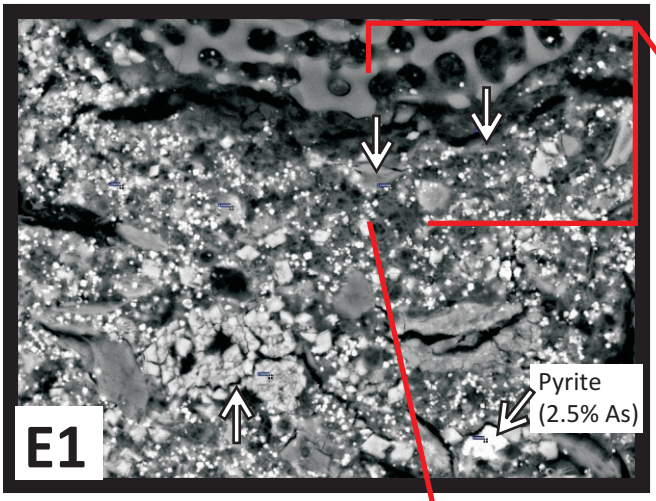



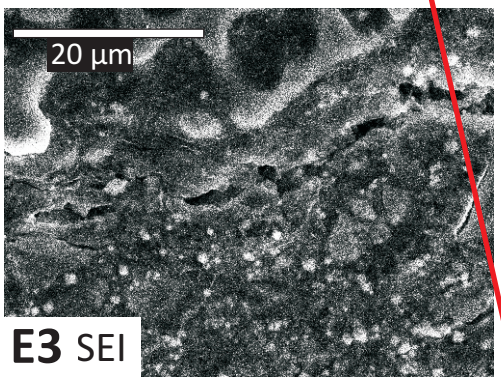

f.

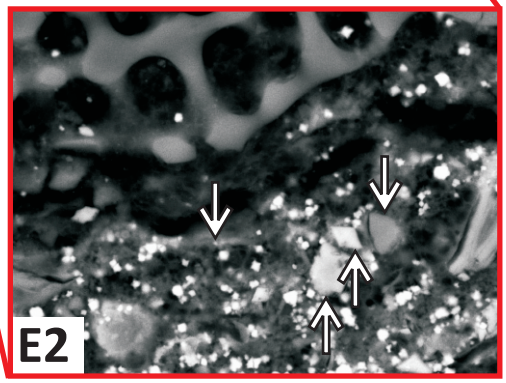


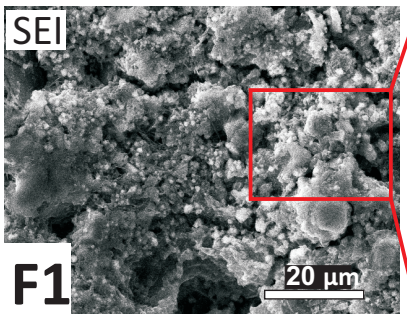
Appendix E. Sample 495-777

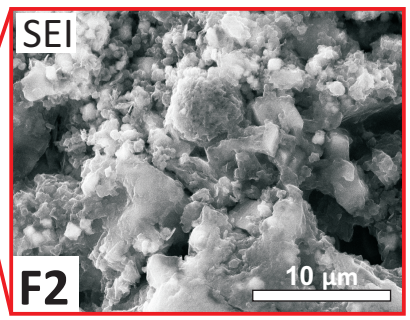


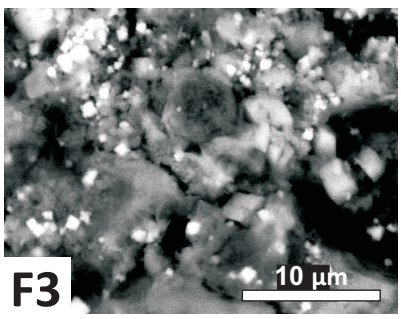



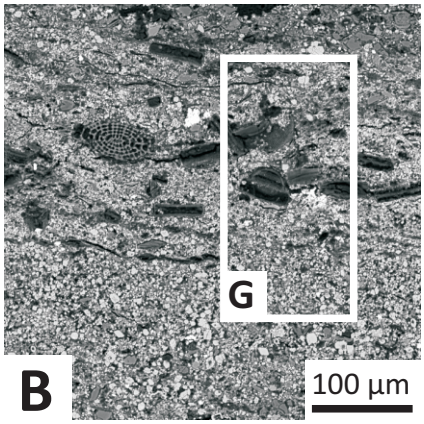



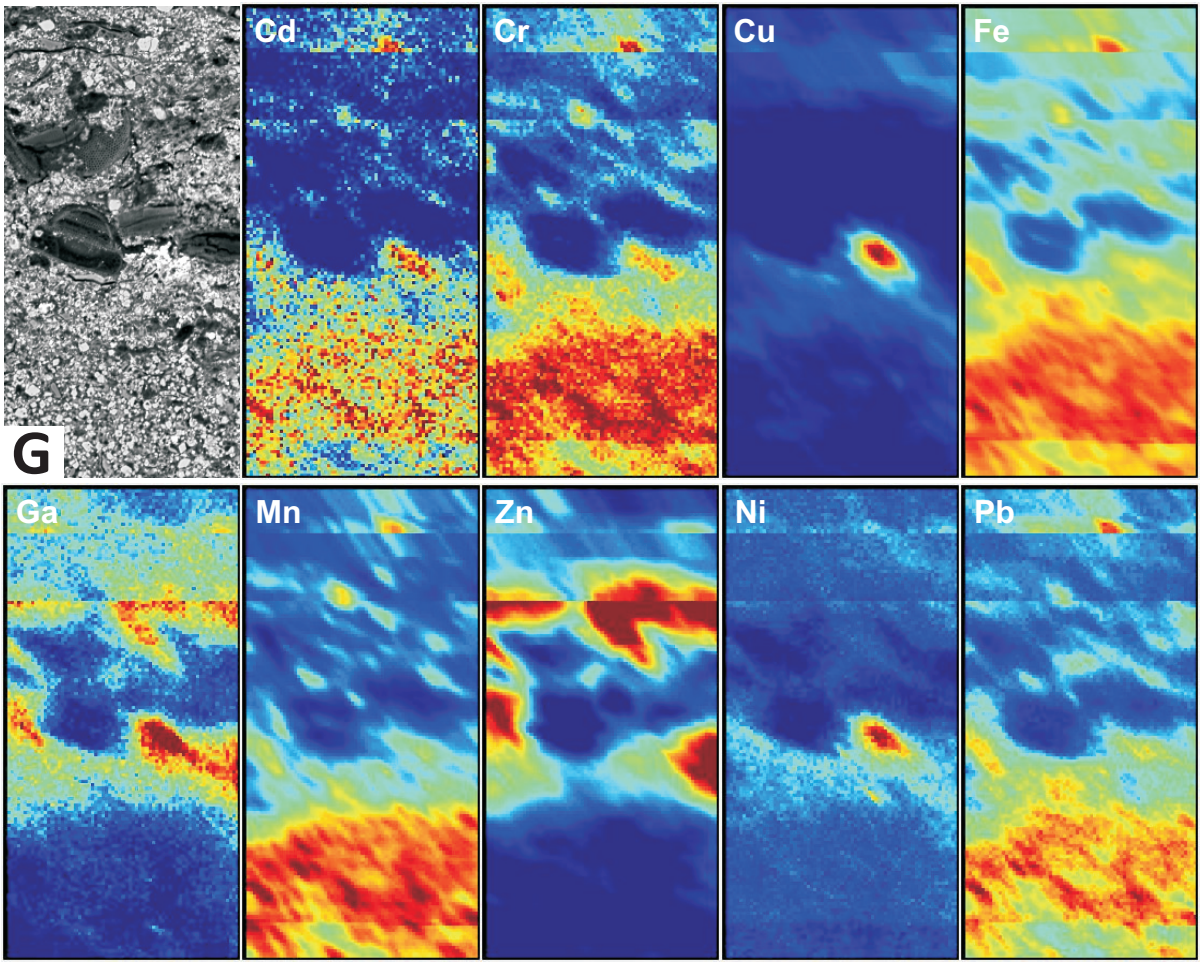



Appendix E. Sample 495-777

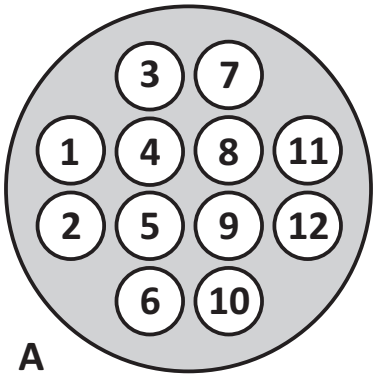


Appendix E. Analyses of Polished Block 503-912.

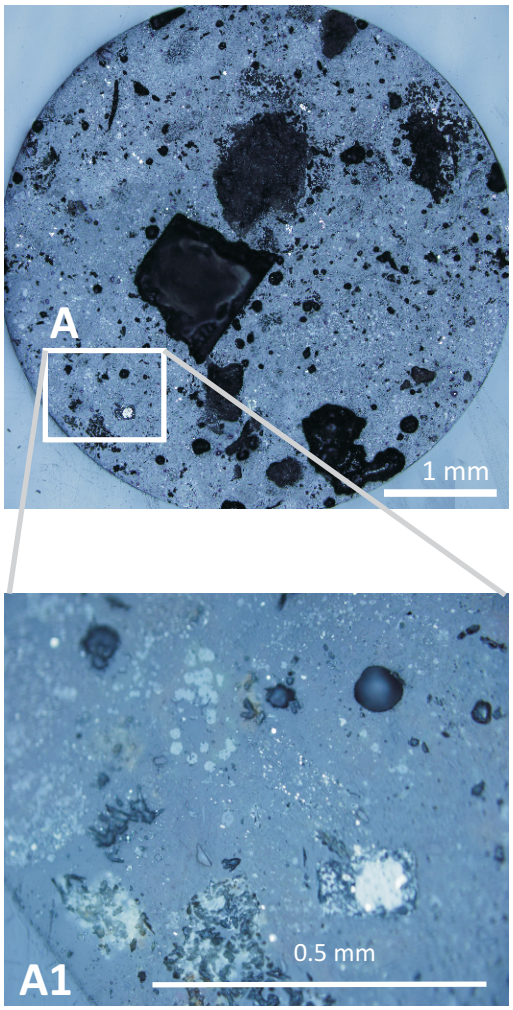
A polished block containing 12 separate grain mounts was prepared from sample 503-912 after slight washing (~5 min to remove the readily soluble salt). Attempts to create polished blocks without washing generally failed because of the high salt content of the samples. The sample is from unit SU1, just outside the vent proximal area (e.g., Figure 1.1). It has high Au and As concentrations (3.8 ppm and 888 ppm, respectively), as well as high base metal and sulfur contents (14.6 wt.% Zn, 2.5 wt.% Cu, 0.2 wt.% Pb, 19.8 wt.% $S_{tot}$, and 4.0 wt.% $S_{red}$). The most abundant sulfide mineral in the sample is pyrite; chalcopyrite is rare and most commonly occurs in composite chalcopyrite-sphalerite grains. Pyrite occurs mainly as clusters of small grains with textures indicating partial dissolution of the grains. Pyrite grains are typically zoned, with rims enriched in a number of different trace metals.

Different non-sulfidic particles with high non-ferrous metal contents (up to >50 wt.%) were identified; most likely formed during core storage, but primary textures were also recognized. Many had low sulfide concentrations typical of oxide or chloride phases; others are sulfates, including secondary metal-sulfates. However barite and anhydrite are rare (3.6 wt.% Ca and 117 ppm Ba in the bulk sample).



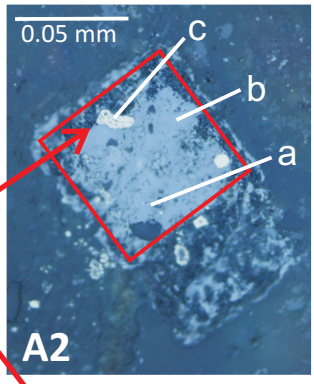

The following pages are descriptions of the selected grain mounts (1-12) from the polished block. Some grains were chosen for detailed chemical analysis by EPMA, FE-SEM (a high-magnification surface technique), and synchtrotron XRF (a deeply penetrating technique). Special samples were prepared for FE-SEM and S-XRF studies.

Grain Mount 2:




The area of interest in this grain mount is indicated in the image of the left in reflected light; images A1 and A2 are details of this area. Images A3 and A4 are EPMA and S-XRF maps (respectively) of the single grain in A2, and A5 shows the results of three spot S-XRF analyses (a, b, c) also indicated in A2.

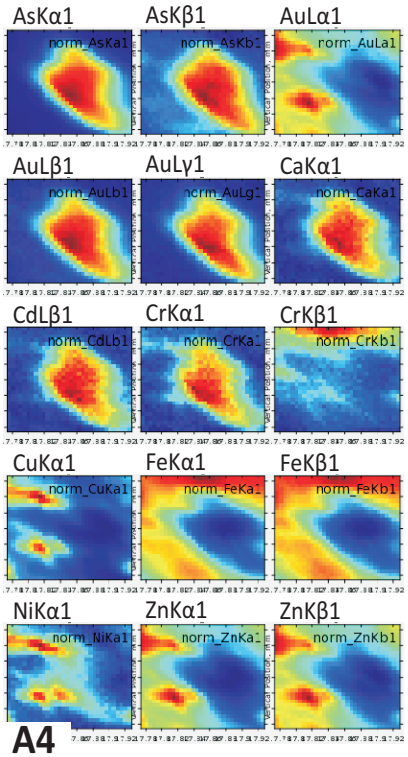
The light blue particle in A2 is a non-sulfide phase, containing little Cu, Zn and Fe (A3), but high Pb (A5). It is enriched in Mo, Ag, As, Se and Cd relative the matrix (A3). The S-XRF maps of the same area (A4) show high Zn and As, which interfere with Au (Lα) and Au (Lβ), but the Fe only partly overlaps with the Au (Lγ), which suggests that the Au enrichment may be real. The smaller white grains in A2 are pyrite; one with notably As-enriched rim.




Pyrite with As-rich rim

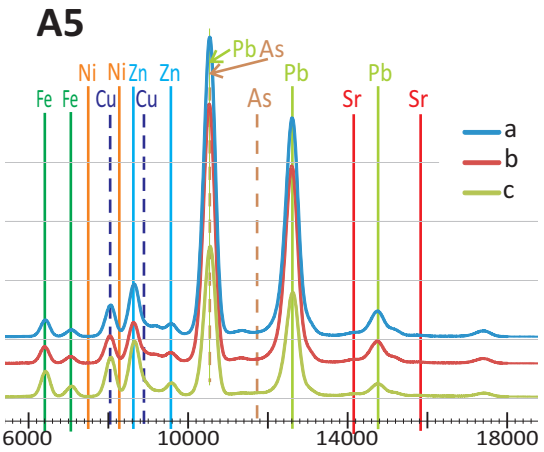
A3) EPMA maps of area indicated in A2 with red square.



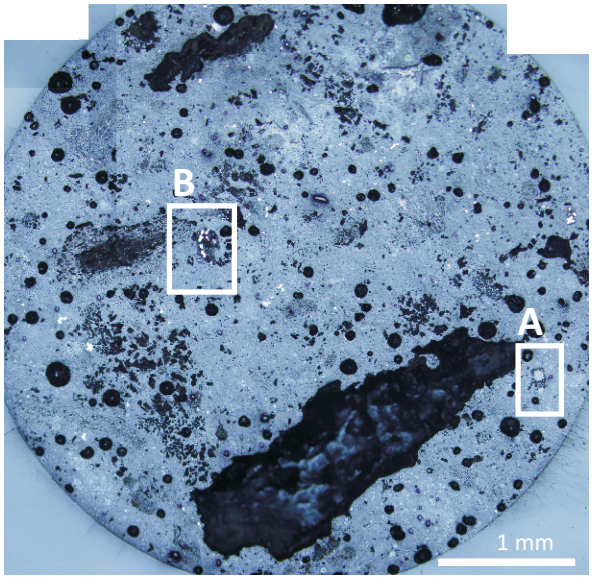




A4) S-XRF maps of the area covered by image A2.

A5) S-XRF spectra of spot analyses indicated in A2.

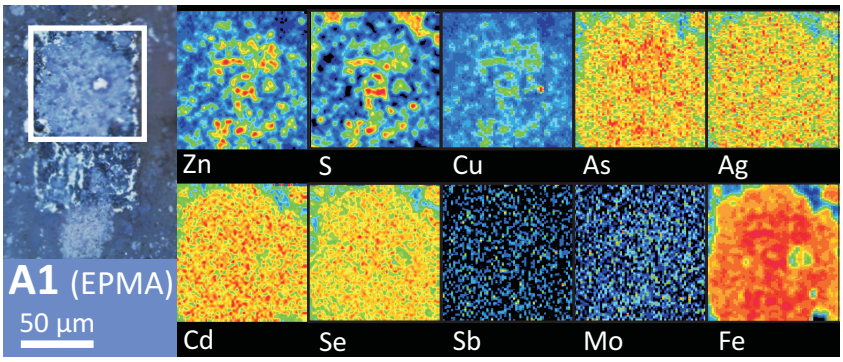


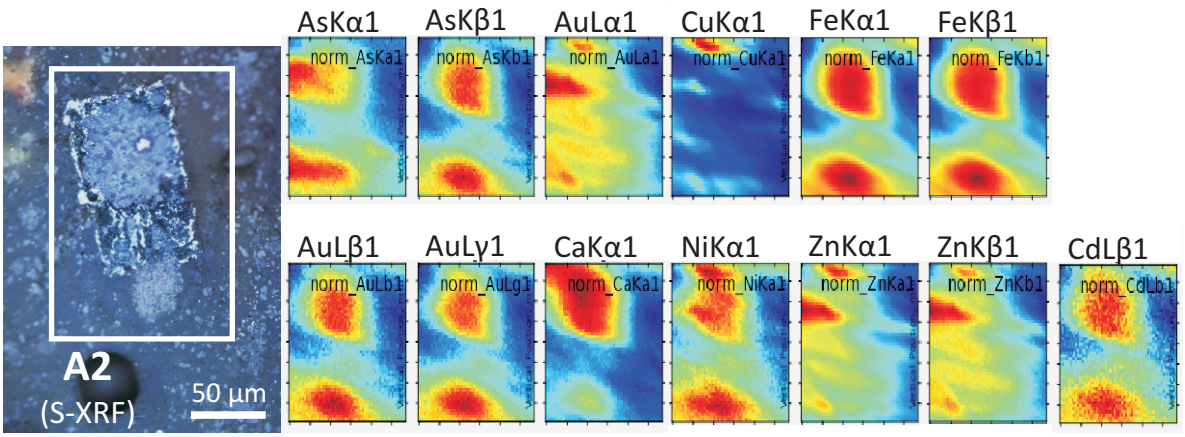
Grain Mount 4.

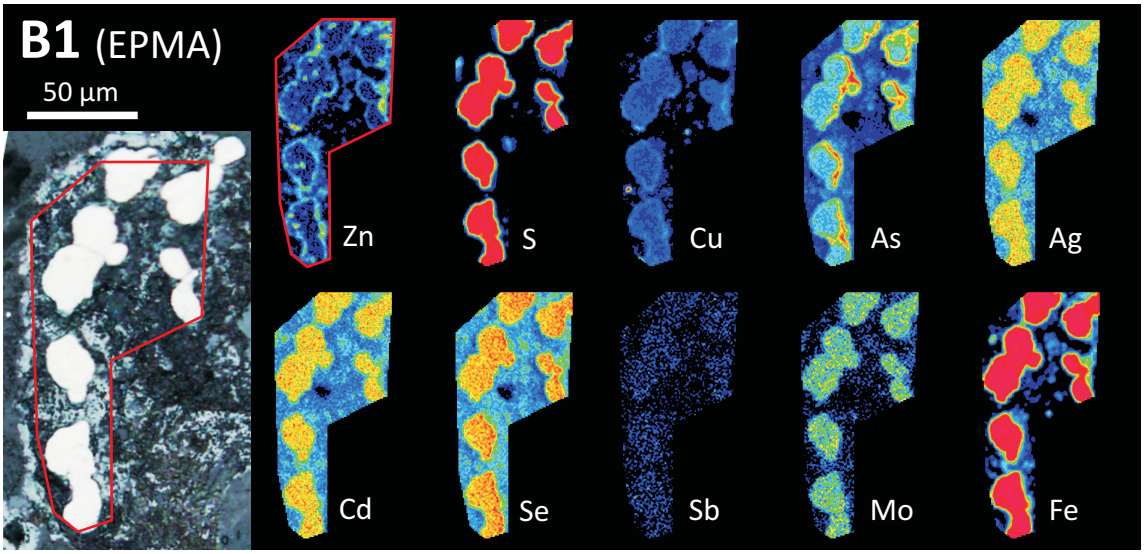


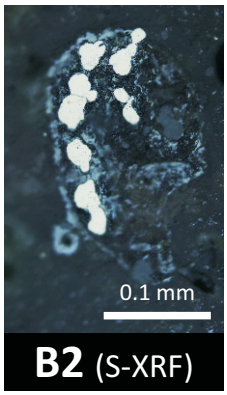

Two areas of interest (A and B) are indicated in the image on the left in reflected light. Area A shows a nonsulfide particle with a rectangular outline, similar to that shown in grain mount 2. Images A1 and A2 are details of this particle and indicate the areas shown in EPMA (A1) and S-XRF (A2) maps. The grain shown in A1 is Fe-rich (~40 wt.%) but has low Cu, Zn, and S, typical of the Fe-(oxy)hydroxides. Its low Pb content (S-XRF spot analyses, not shown) is the main difference compared to the nonsulfide in grain mount 2, but it also has significantly lower concentrations of Mo, As, Ag, Cd, Se and Sb. In the S-XRF maps (A2), Zn, As, and Fe peaks overlap with Au Lα, β and γ, respectively, suggesting that the latter are artifacts.

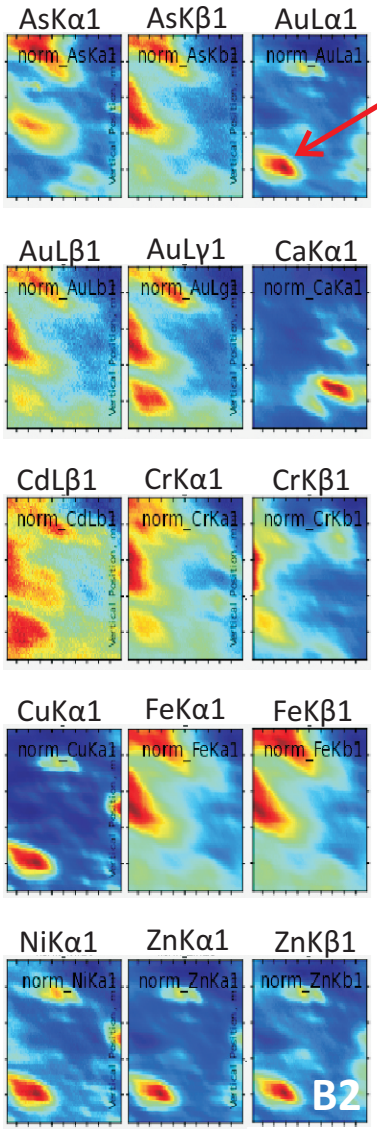
Area B shows a cluster of framboidal pyrite grains (details in B1, B2, B3) that are significantly enriched in As. Arsenic concentrations are up to 1.6 wt.% (Chapter 2 and Table 2.4) in the area of highest As (EPMA maps in Figure B1). Two S-XRF maps (B2 and B3) were acquired with different incidence angles of the X-rays (at 45°). In B2 AuLα correlates with Zn, but AuLβ and AuLγ do not correlate with As and Fe (respectively, in the area indicated with the red arrow) suggesting that the Au enrichment in this Cu- and Zn-rich nonsulfide phase may be real.


A1 (EPMA)
50 µm
Zn
S
Cu
As
Ag
Cd
Se
Sb
Mo
Fe

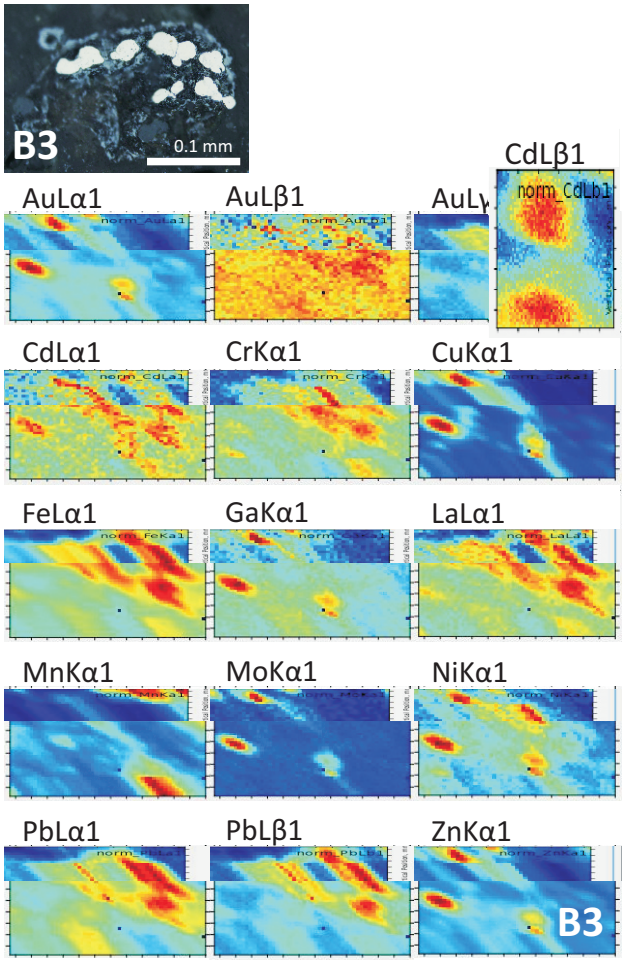

A2
(S-XRF)
50 µm
AsKα1
norm_AsKa1
AsKβ1
norm_AsKb1
AuLα1
norm_AuLa1
CuKα1
norm_CuKa1
FeKα1
norm_FeKa1
FeKβ1
norm_FeKb1
AuLβ1
norm_AuLb1
AuLγ1
norm_AuLg1
CaKα1
norm_CaKa1
NiKα1
norm_NiKa1
ZnKα1
norm_ZnKa1
ZnKβ1
norm_ZnKb1
CdLβ1
norm_CdLb1


B1 (EPMA)
50 µm
Zn
S
Cu
As
Ag
Cd
Se
Sb
Mo
Fe

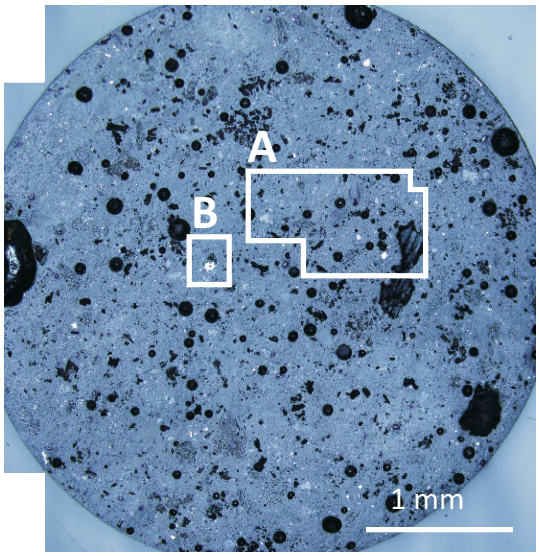



Area of Au-enrichment?

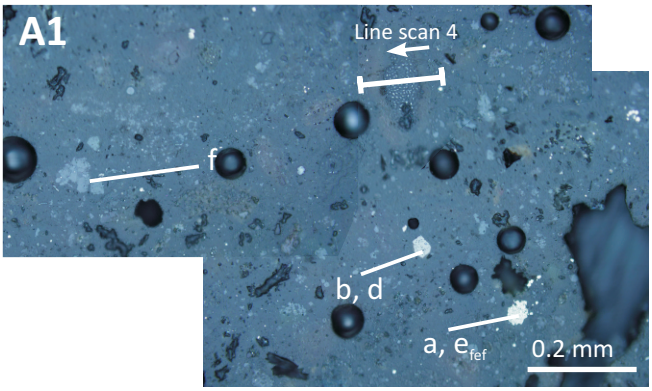


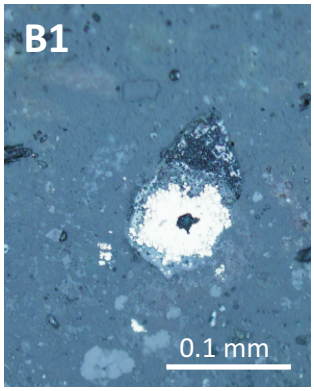
Grain Mount 6:

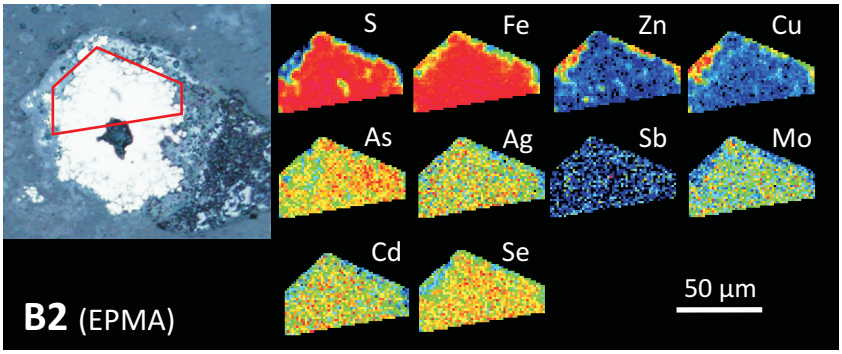


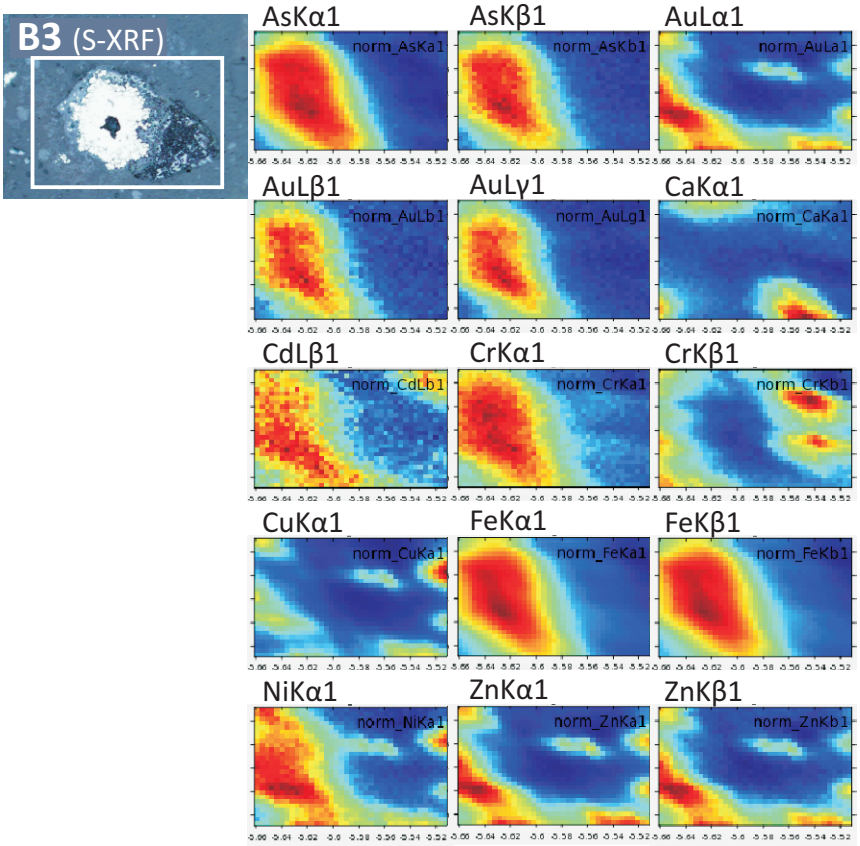

.

The areas of interest in this grain mount are indicated in the image on the left in reflected light. A1 shows abundant small nonsulfides and B1 shows a cluster of small framboidal pyrite grains with textural evidence for dissolution. EPMA element maps (B2) show clear As-enrichment of the pyrite grain. The S-XRF map shows an oblique view of the grain and AuLα, β and γ maps, which are likely due to interferences from Zn, As and Fe (respectively) in the area shown.

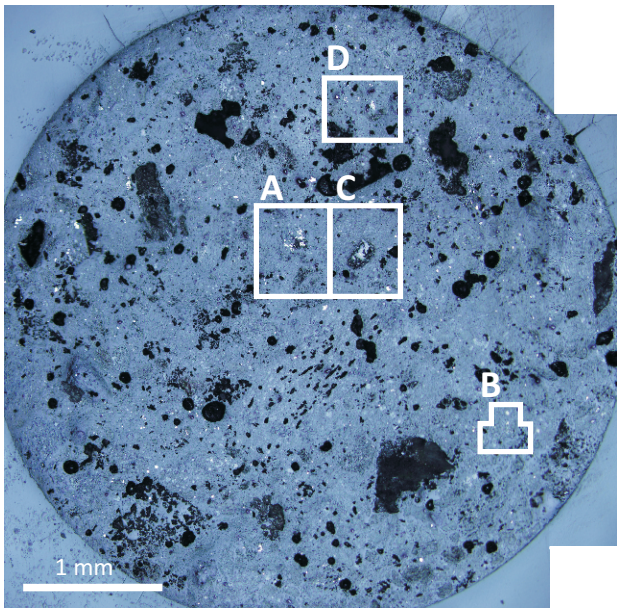

A1
Line scan 4
f
b, d
a, e
ref
0.2 mm


B1
0.1 mm


S
Fe
Zn
Cu
As
Ag
Sb
Mo
Cd
Se
50 µm
B2 (EPMA)


B3 (S-XRF)
AsKα1
norm_AsKa1
AsKβ1
norm_AsKb1
AuLα1
norm_AuLa1
AuLβ1
norm_AuLb1
AuLγ1
norm_AuLg1
CaKα1
norm_CaKa1
CdLβ1
norm_CdLb1
CrKα1
norm_CrKa1
CrKβ1
norm_CrKb1
CuKα1
norm_CuKa1
FeKα1
norm_FeKa1
FeKβ1
norm_FeKb1
NiKα1
norm_NiKa1
ZnKα1
norm_ZnKa1
ZnKβ1
norm_ZnKb1

Grain Mount 8:

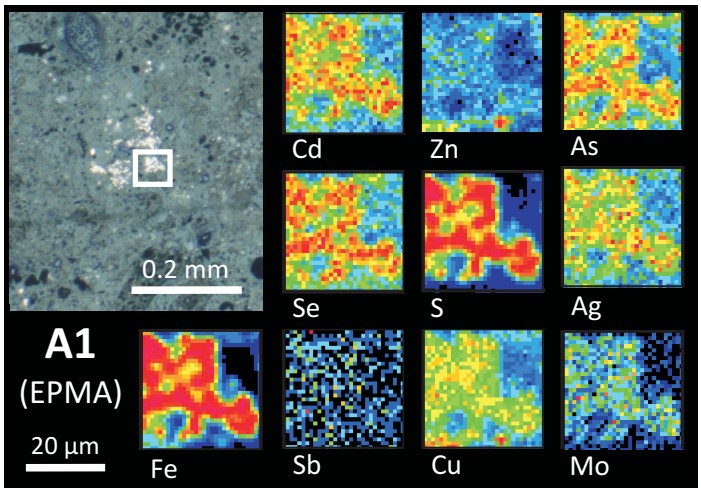


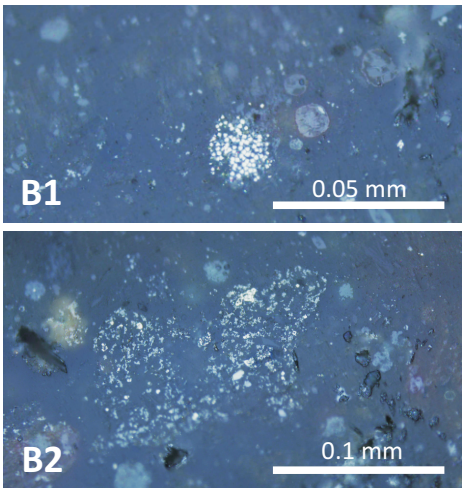

The areas of interest in this grain mount are indicated in reflected light in the image on the left, which shows clusters of diagenetic pyrite (A, B) and nonsulfides (C, D). Area A1 is a detail of area A showing the location of EPMA element maps. The EPMA maps show that the small pyrite grains have relatively low As content, whereas other trace metal concentrations are high (Table E.1).

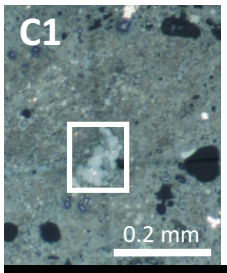
The pyrite cluster in B1 is tightly packed with small, uniformly sized grains showing evidence of moderate dissolution. The pyrite cluster in B2 is more sparse due to greater dissolution. The original borders of both pyrite clusters are still clearly seen.

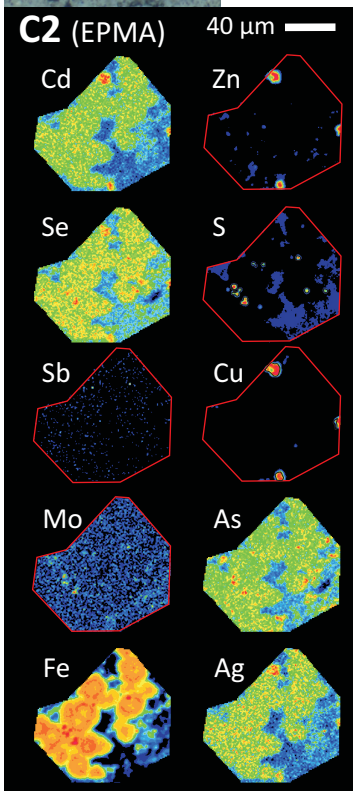
Image C1 is a detail of area C that contains a cluster of rounded and radially zoned Mn- and Fe-rich non-sulfides. EPMA element maps (C2) show that they are likely authigenic clays or oxy-hydroxides with adsorbed trace metals. The maximum S and Fe concentrations (~55 wt.% S; 45 wt.% Fe) in Figure C2 correspond to pyrite, which also contains the highest As and Se (As counts = 90, Se counts = 100). The highest Cu concentrations (~40 wt.%) and Zn concentrations (~30 wt.%) are found in small non-sulfide grains, which also contain the highest Ag and Cd (60 and 80 counts, respectively). S-XRF maps (C3) show no clear indication of Au due to interference with Zn (Au Lα), Fe (Au Lγ), and disagreement between the different peaks.

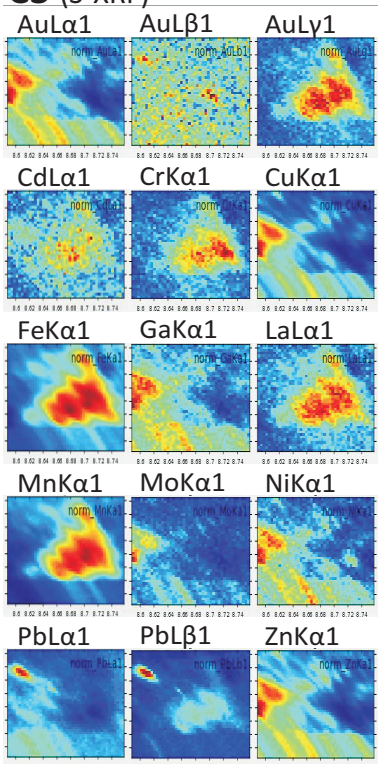
Another non-sulfide grain in D1 was mapped by S-XRF (D2). It is significantly enriched in Pb, Mo and Ga, and possibly also As (As Kα and Kβ are juxtaposed to the Pb Lα and Au Lβ lines, respectively), similar to the non-sulfide grains shown in mounts 2 and 4.

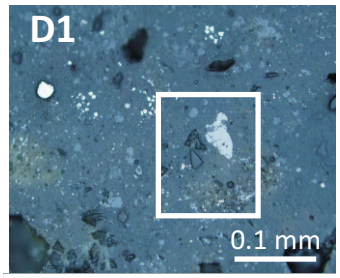

A1
(EPMA)
20 µm
0.2 mm
Cd
Zn
As
Se
S
Ag
Fe
Sb
Cu
Mo

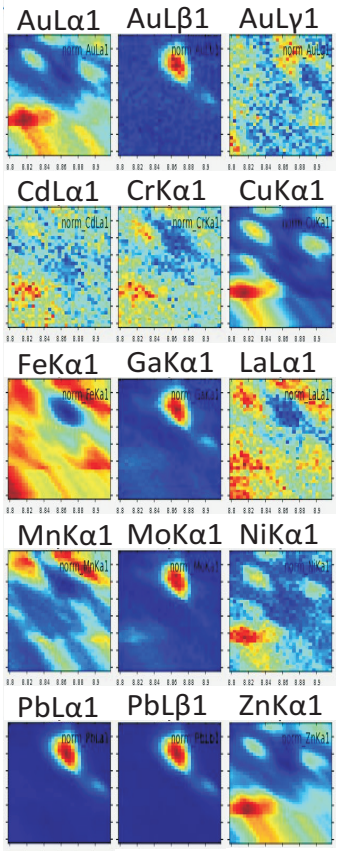

B1
0.05 mm
B2
0.1 mm


C1
0.2 mm

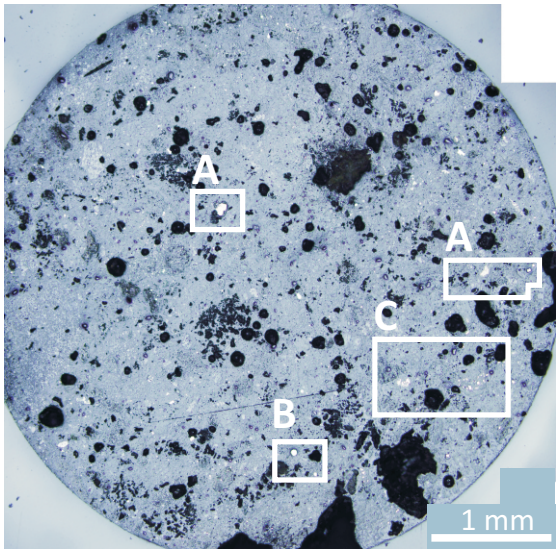

C2 (EPMA)
40 µm
Cd
Zn
Se
S
Sb
Cu
Mo
As
Fe
Ag


C3 (S-XRF)
AuLα1
AuLβ1
AuLγ1
CdLα1
CrKα1
CuKα1
FeKα1
GaKα1
LaLα1
MnKα1
MoKα1
NiKα1
PbLα1
PbLβ1
ZnKα1


D1
0.1 mm


AuLα1
AuLβ1
AuLγ1
CdLα1
CrKα1
CuKα1
FeKα1
GaKα1
LaLα1
MnKα1
MoKα1
NiKα1
PbLα1
PbLβ1
ZnKα1

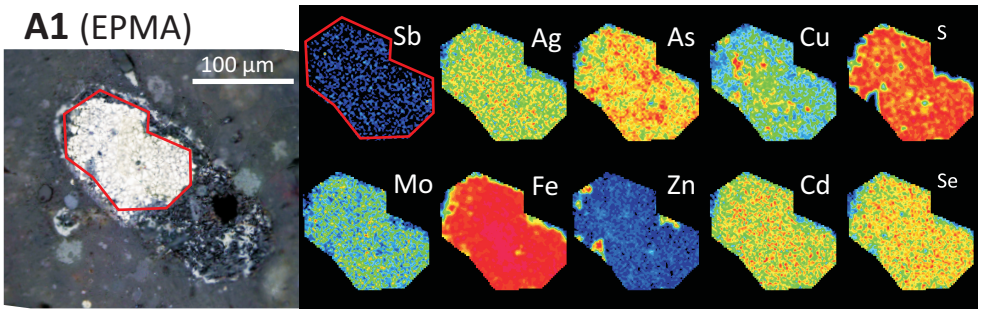
Grain Mount 10:

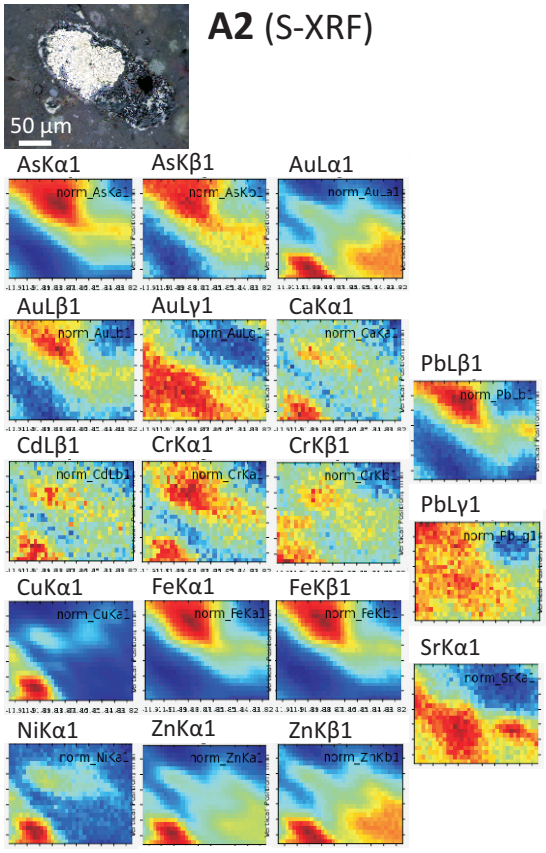


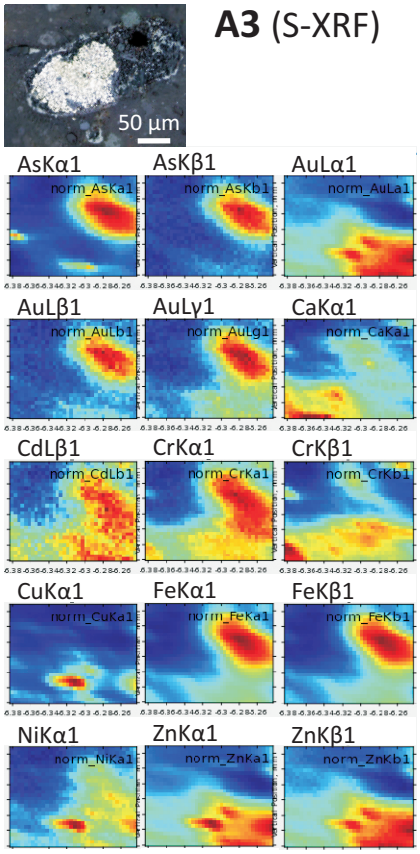

The areas of interest in this grain mount are indicated in the image on the left in reflected light and contain diagenetic pyrite clusters (A1 and B1) and a nonsulfide grain (C1). EPMA maps (A1) of a very tight cluster of intergrown pyrite show that the grains are highly enriched in As (As counts = ~200, corresponding to >1 wt.% As; cf. grain mount 4) and other trace metals (Table E.1). Two S-XRF maps (A2 and A3) were acquired with different incidence angles of the X-rays (at 45°).

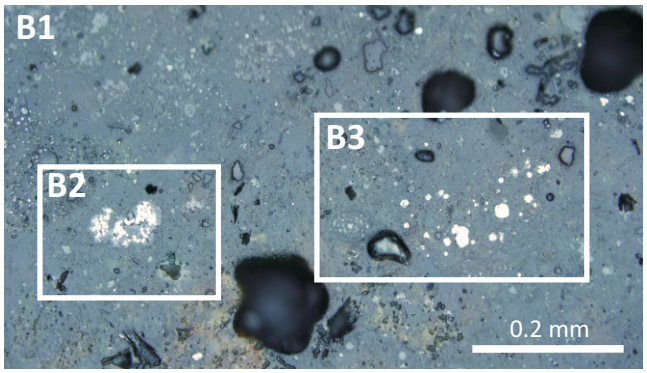
The textures of the pyrite clusters in B1 indicate significant dissolution. In B2, the original extent of the pyrite cluster is still clearly seen. In B3, the original "border" of the cluster is difficult to see, suggesting that the original sulfides might not have fully crystallized during diagenesis. Figure B3 also shows a pseudomorph after a radial fossil, which is now filled by nonsulfides. The sites of the S-XRF analyses in area B are shown in B2 and B3 (data not shown).

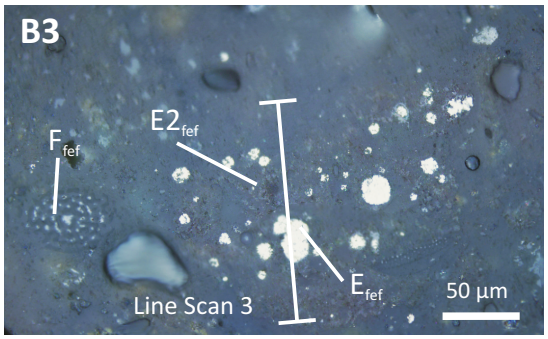
A bright, non-sulfide grain seen under reflected light in C1 is depleted in almost all mapped elements, except Sr. The Au Lγ peak in this grain does not correlate with Fe suggesting that this is not an interference and may reflect true Au enrichment. The only mineral with significant Sr in our samples is barite (cf. sample 503-254 in Appendix E), which has a similar appearance in other samples (cf. Chapter 2).

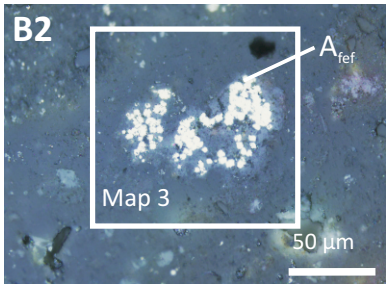

A1 (EPMA)
100 µm
Sb
Ag
As
Cu
S
Mo
Fe
Zn
Cd
Se

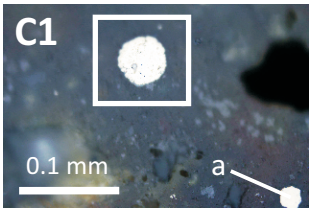

A2 (S-XRF)
50 µm
AsKα1
AsKβ1
AuLα1
AuLβ1
AuLγ1
CaKα1
CdLβ1
CrKα1
CrKβ1
CuKα1
FeKα1
FeKβ1
NiKα1
ZnKα1
ZnKβ1
PbLβ1
PbLγ1
SrKα1

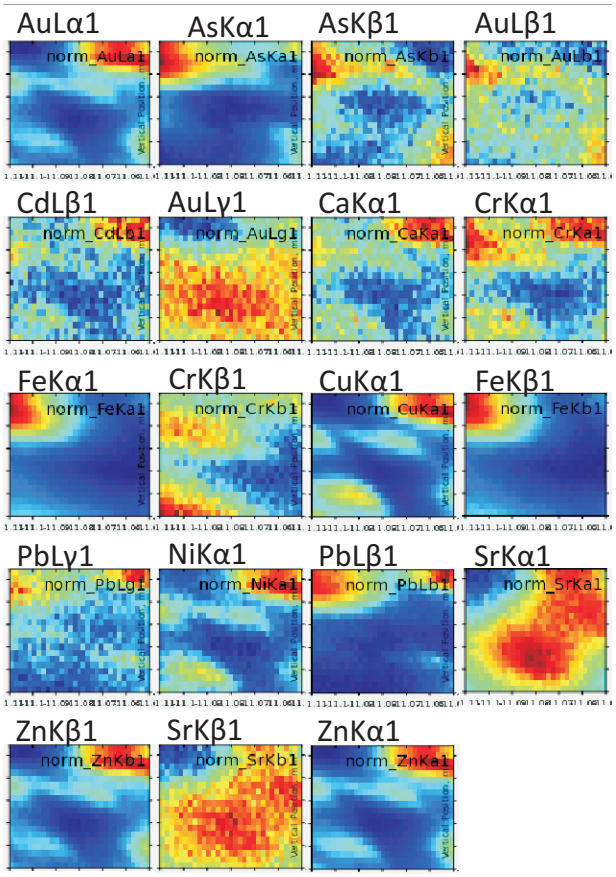

A3 (S-XRF)
50 µm
AsKα1
AsKβ1
AuLα1
AuLβ1
AuLγ1
CaKα1
CdLβ1
CrKα1
CrKβ1
CuKα1
FeKα1
FeKβ1
NiKα1
ZnKα1
ZnKβ1


B1
B2
B3
0.2 mm

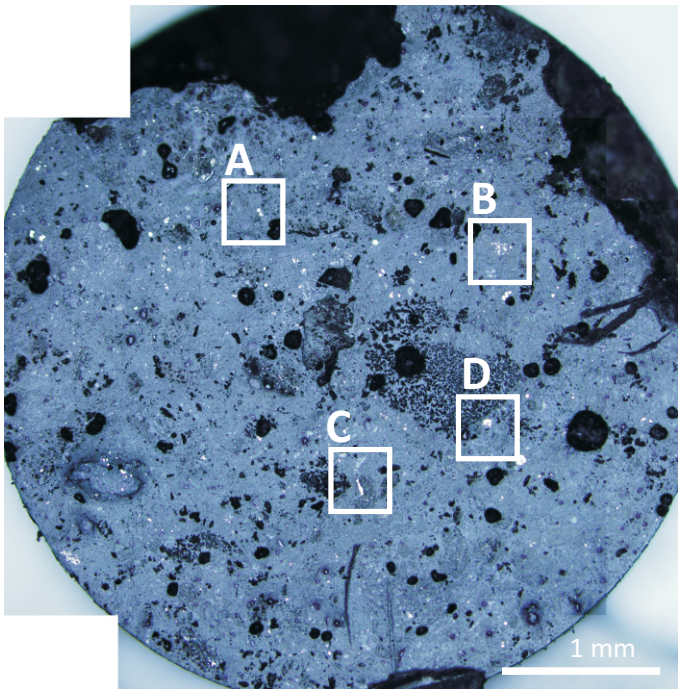

B3
F fef
E2 fef
E fef
Line Scan 3
50 µm


B2
A fef
Map 3
50 µm

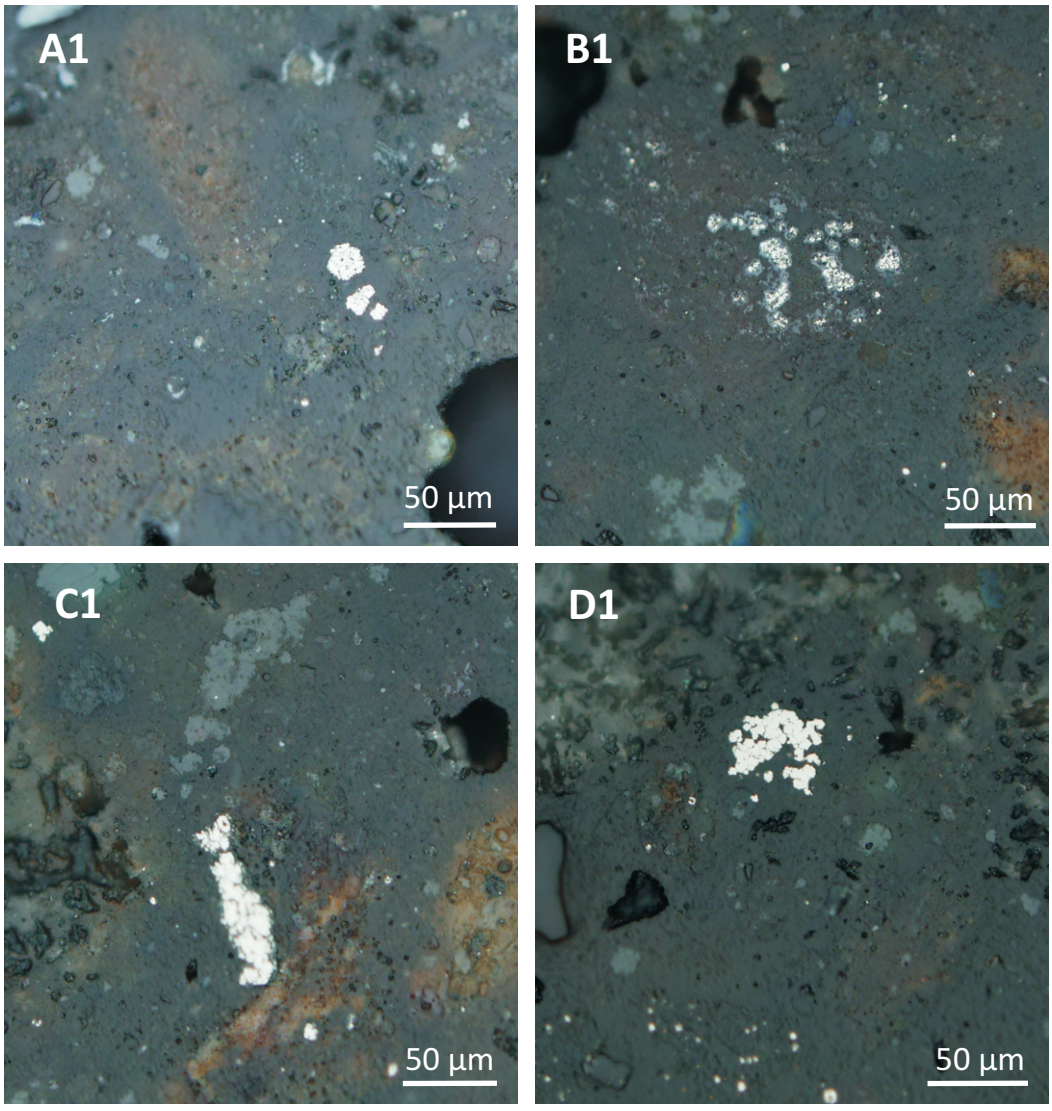

C1
0.1 mm
a


AuLα1
norm_AuLa1
AsKα1
norm_AsKa1
AsKβ1
norm_AsKb1
AuLβ1
norm_AuLb1
CdLβ1
norm_CdLb1
AuLγ1
norm_AuLg1
CaKα1
norm_CaKa1
CrKα1
norm_CrKa1
FeKα1
norm_FeKa1
CrKβ1
norm_CrKb1
CuKα1
norm_CuKa1
FeKβ1
norm_FeKb1
PbLγ1
norm_PbLg1
NiKα1
norm_NiKa1
PbLβ1
norm_PbLb1
SrKα1
norm_SrKa1
ZnKβ1
norm_ZnKb1
SrKβ1
norm_SrKb1
ZnKα1
norm_ZnKa1

Grain Mount 11:



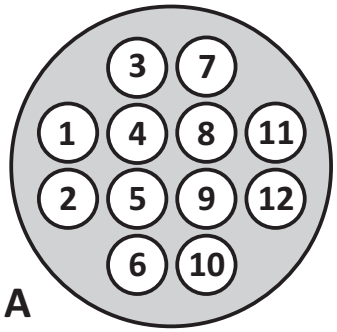

This grain mount was studied by FE-SEM. For sample preparation it was This grain mount was studied by FE-SEM. For sample preparation it was detached from the grain mount and attached to the FE-SEM sample holder and recoated with carbon. Pyrite grains shown in images A1, B1, C1 and D1 were imaged with high magnification but no signs of Au enrichment were detected. If nano-particles of Au had been present in this sample, they would most certainly have been imaged under the FE-SEM, suggesting no Au enrichment in the pyrite grains.


A1
50 µm
B1
50 µm
C1
50 µm
D1
50 µm

Appendix E. Analyses of Polished Block 268-985.

A polished block containing 12 separate grain mounts was prepared from sample 268-985 after slight washing (~5 min to remove the readily soluble salt), as for sample 503-912. The sample is from unit CO, proximal to the inferred location of venting in the SW Basin (Figure 1.1). The same section of core was studied by Oudin (1984), Oudin et al. (1987), and Ramboz et al. (1988). It has high Au, but low As concentrations (21 and 60 ppm, respectively: Oudin et al., 1987), as well as high base metal and sulfur contents (16.3 wt.% Zn, 0.4 wt.% Cu, 750 ppm Pb and 19.5 wt.% $S_{red}$).

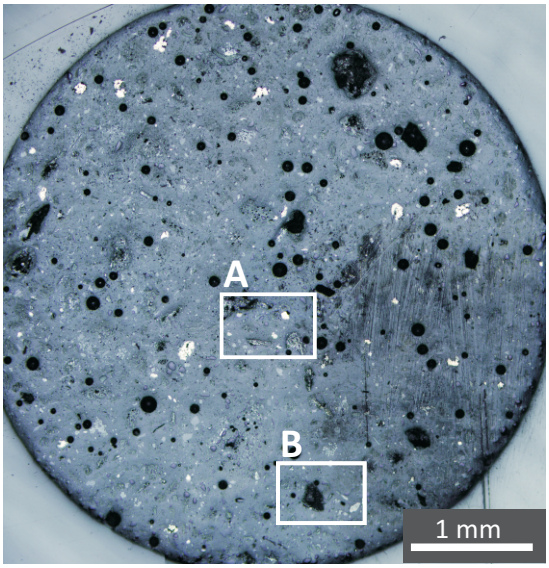
The most abundant sulfide mineral in the sample is chalcopyrite, which is found as large (up to 150 µm) grains that show variable amounts of fracturing and secondary alteration. Pyrite is rare and found as rather large, sub- to euhedral grains. Sphalerite was only detected in chalcopyrite-sphalerite aggregate grains. These observations are not consistent with the expected mineralogy according to the bulk chemistry, but probably reflect secondary alteration. The chalcopyrite grains are often surrounded by a Zn-enriched rim (~10 wt.% Zn) with subordinate low sulfide (<5 wt.%) but abundant Fe (>30 wt.%). These rims were typically formed by sulfide oxidation (e.g., mount 7), and more rarely preserve primary zoning (sharp interfaces, e.g., in grain mount 12). In many of the samples, similar Zn-rich nonsulfidic material was abundant in the matrix. Locally this (secondary?) phase has a distinctive rectangular outline surrounding a smaller sulfide grain. During polishing some of the grains disappeared; more commonly the rectangular outline was empty.



A

The following pages are descriptions of the selected grain mounts (1, 3, 5, 7, 10, 11 and 12: Figure A) from the polished block. Some grains were chosen for detailed chemical analysis by EPMA and synchtrotron XRF.

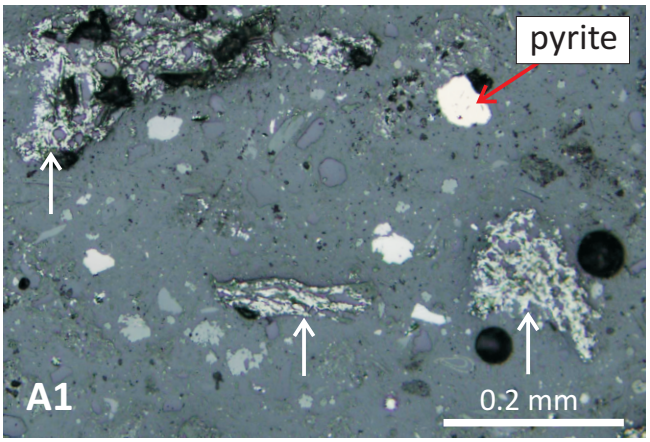
Grain Mount 1:

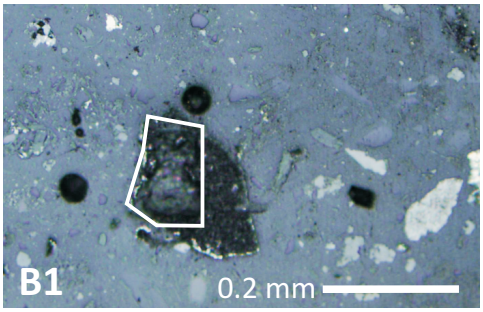


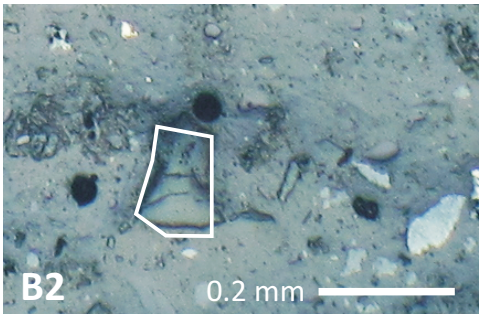

The areas of interest in this grain mount are indicated in the image on the left in reflected light; images A1 and B1 are details of these areas. Image B2 shows the same area as B1 before re-polishing. Image B3 is an EPMA map of the grain indicated in B2.

Various nonsulfides were identified in this mount (A1). They have darker and lighter grey to blue color, which is distinct from pyrite. The shapes may be angular or irregular, and the grain boundaries may be sharp or gradational. Nonsulfidic Cu, Zn and/or Pb enrichment is also found as irregular patches (arrows in image A1). The patchy texture strongly suggests a secondary origin, but the discrete grains may be primary.

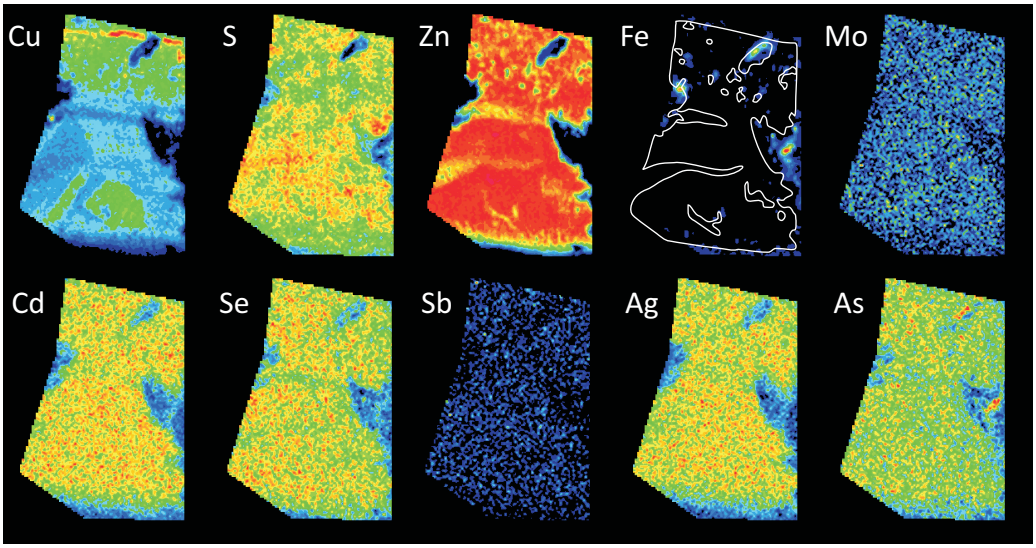
Comparison of the original (B2) and re-polished (B1) surfaces shows removal of the nonsulfide grain (and the areas around it). EPMA map (B3), made before re-polishing, shows that the original particle is extremely Zn-rich (~80 wt.% Zn by comparison with sphalerite), devoid of Fe, and has low sulfur (maximum about 5 wt.% S). The maximum Cu concentration is ~5 wt.%, and trace metal concentrations are relatively low (Table E.1).



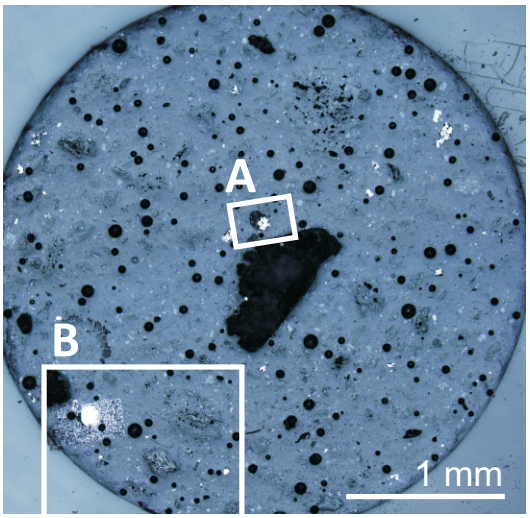




**B3** (EPMA)

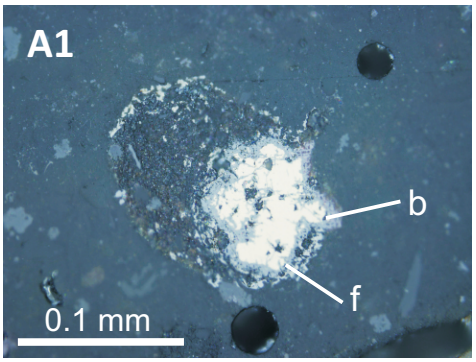


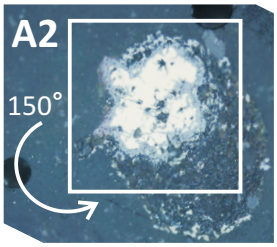
Grain Mount 3:

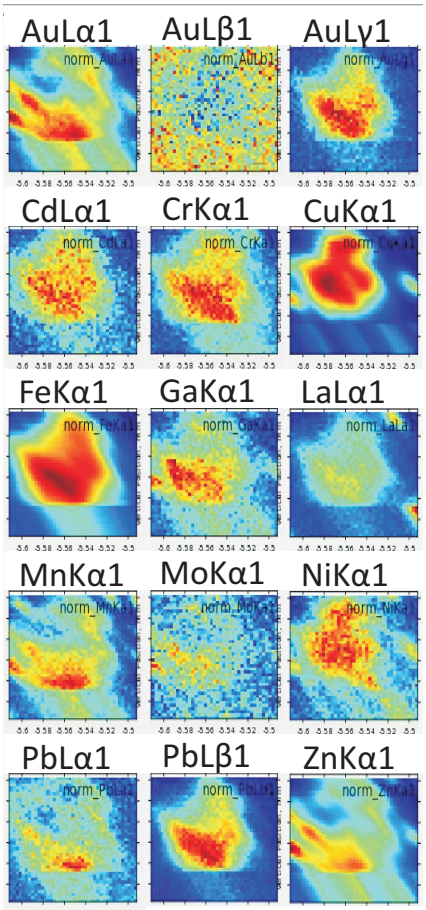


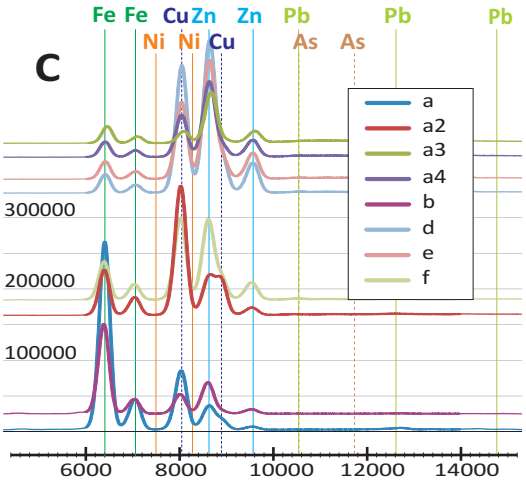

The areas of interest in this grain mount are indicated in the image on the left in reflected light; images A1 and B1 are details of these areas. Image A2 is a S-XRF map of the chalcopyrite grain in A1, and image C shows XRF-spectra from spot analyses (b, f) indicated in A1. The distribution of Cu (proxy for chalcopyrite) is coincides with that of Cd and Ni, whereas Zn (at the rim) coincides with Mn (A2). Fe-enrichment coincides with the highest Cu and Zn.

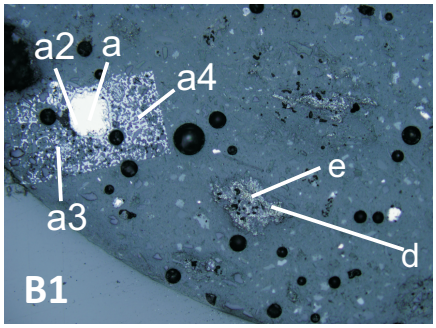
The image in reflected light of this area after re-polishing (B1) shows a rectangular alteration halo, which was not seen in before polishing (B2). The S-XRF spectra from spot analyses (a, a2, a3, a4, d, e) are shown in C and illustrate the variation in Fe, Cu and Zn. EPMA maps (B3) show that the bluish grey reflective network of secondary material has somewhat higher Fe concentration than chalcopyrite, much higher Zn content and low S concentration. Two S-XRF maps (B4 and B5) were acquired with different incidence angles of the X-rays (at 45°). The smaller map made with longer dwelling time (B4) shows similar results as the larger map (B5).

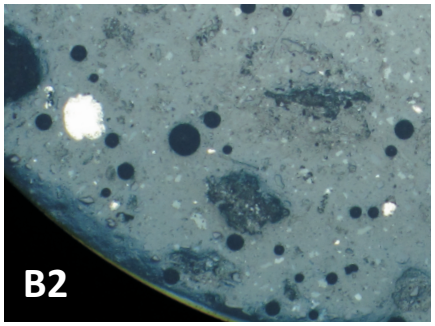

A1
b
f
0.1 mm

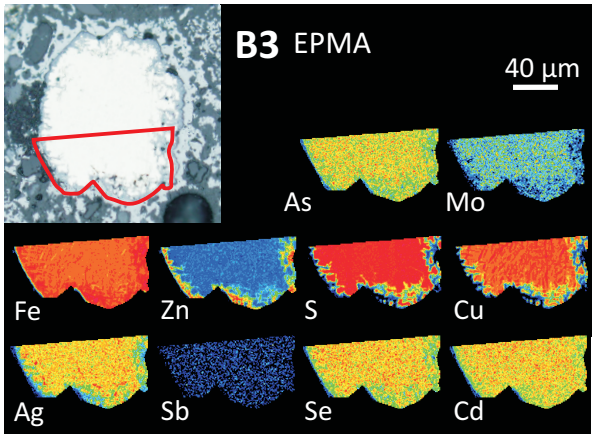

A2
150°

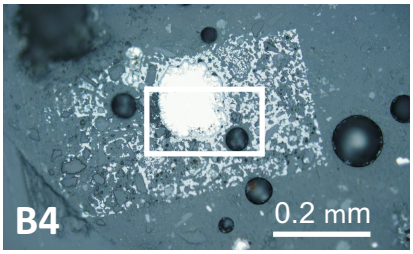

AuLα1
AuLβ1
AuLγ1
CdLα1
CrKα1
CuKα1
FeKα1
GaKα1
LaLα1
MnKα1
MoKα1
NiKα1
PbLα1
PbLβ1
ZnKα1

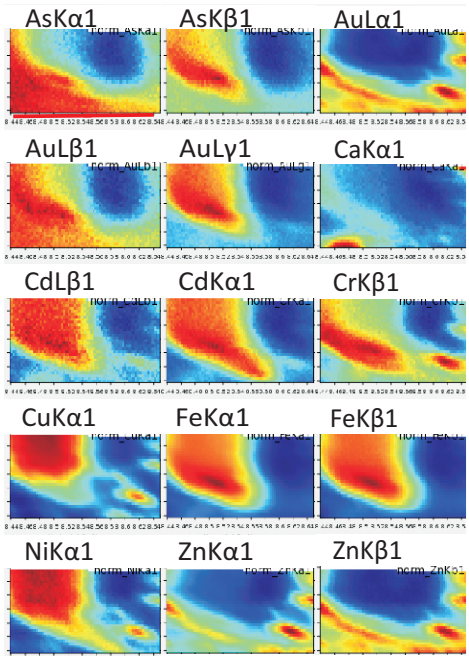

C
Fe Fe Cu Zn Zn Pb Pb Pb
Ni Ni Cu As As
a
a2
a3
a4
b
d
e
f
300000
200000
100000
6000
8000
10000
12000
14000

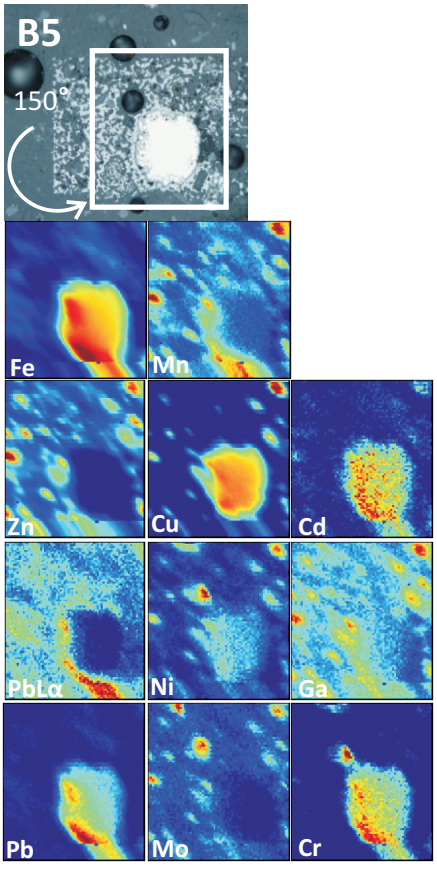

a2
a
a4
e
a3
d
B1


B2

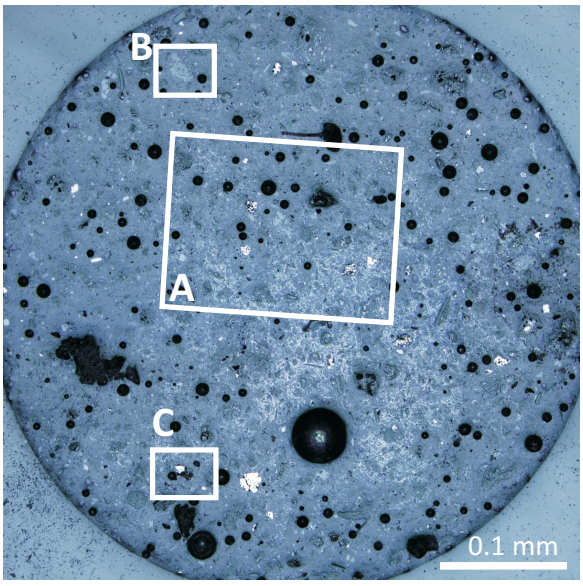

B3 EPMA
40 µm
As
Mo
Fe
Zn
S
Cu
Ag
Sb
Se
Cd


B4
0.2 mm


AsKα1
AsKβ1
AuLα1
AuLβ1
AuLγ1
CaKα1
CdLβ1
CdKα1
CrKβ1
CuKα1
FeKα1
FeKβ1
NiKα1
ZnKα1
ZnKβ1


B5
150°
Fe
Mn
Zn
Cu
Cd
PbLα
Ni
Ga
Pb
Mo
Cr

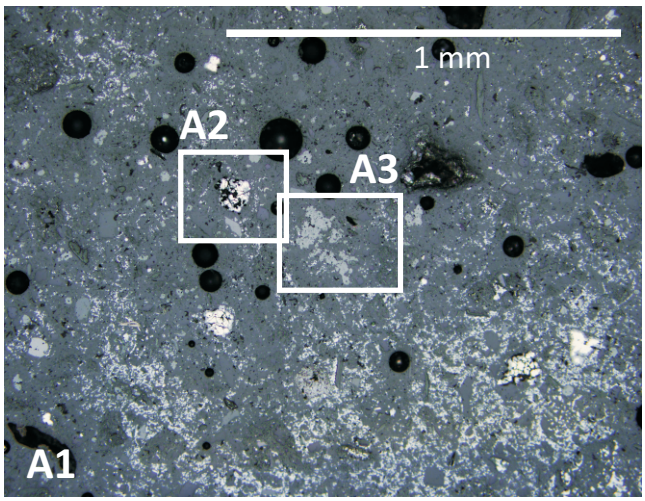
Grain Mount 5:

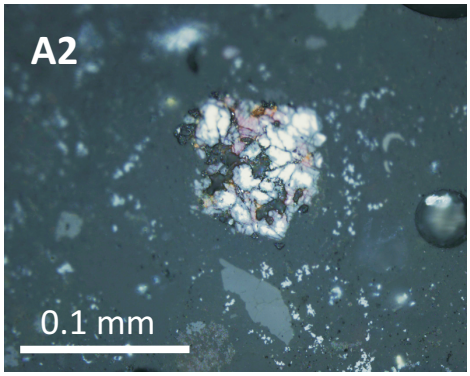


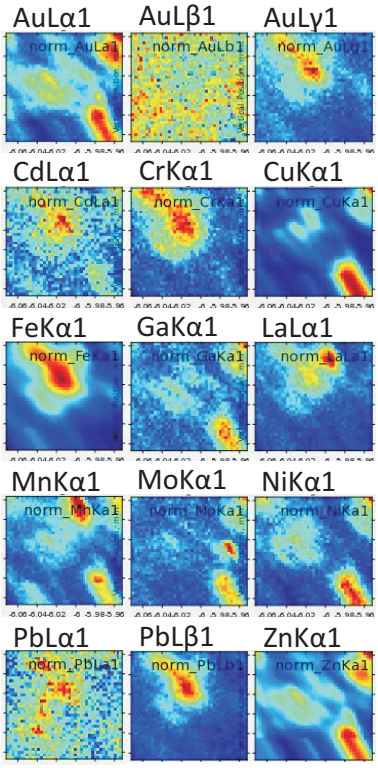

The areas of interest in this grain mount are indicated in the image on the left in reflected light; images A1, B1 and C1 are details of these areas.

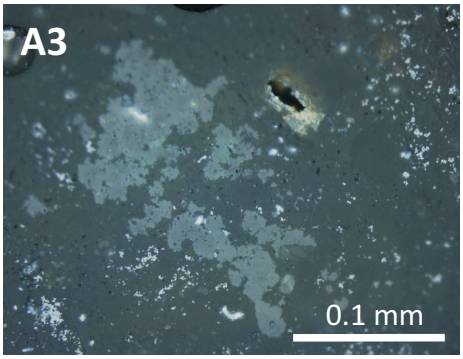
Four main types of nonsulfidic precipitates are identified in A1. 1) Secondary alteration related to dissolution of sulfides (A2); S-XRF maps of this area show that Cu-enrichment coincides more closely with Zn than with Fe suggesting that the original sulfide grain has been almost totally dissolved and only thin irregular patches are left (as seen on the surface in A2). 2) A cluster of rounded non-sulfide grains (A3), which are likely primary features. 3) Irregular patches of nonsulfides that resemble the matrix of the sample (especially abundant in the lower-right corner in A1; cf. mount 4 of this sample) and are almost certainly a secondary feature. 4) Discrete nonsulfide grains (e.g., dark grey grain in lower part of image A3; cf. mount 1 of this sample). The grain in B1 is composed mostly of Cu and Zn; it contains some trace metals (Cd, Cr, Ga, Mn, Mo, Ni), but is low in Fe and As (S-XRF maps in B1).

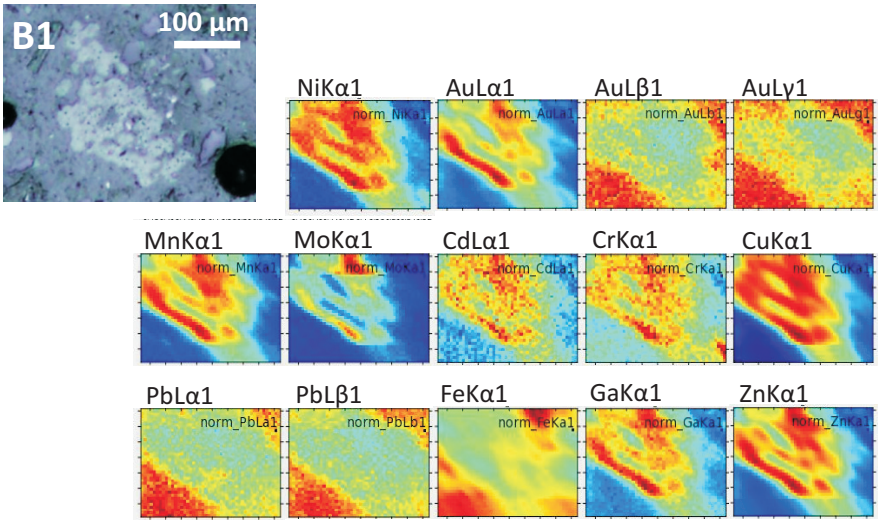
A sulfide grain in Figure C1 is composed of chalcopyrite (yellowish white lower part) and sphalerite (bluish grey top part). EPMA maps (C2) show exsolution laminae (varying Cu concentration) in chalcopyrite. Sphalerite is zoned with varying Fe concentrations, but in general the Fe concentration is low. Cd is almost entirely contained in sphalerite; the zone of highest Fe is significantly lower in Cd than the rest of the grain. Chalcopyrite is highly enriched in Ag and Cd, but Se, Sb, As and Mo are equally low in both minerals (Table E.1). S-XRF maps (C3) show that sphalerite is also enriched in Ga, Mn and Mo.

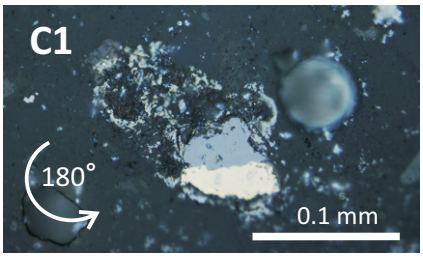

1 mm
A2
A3
A1

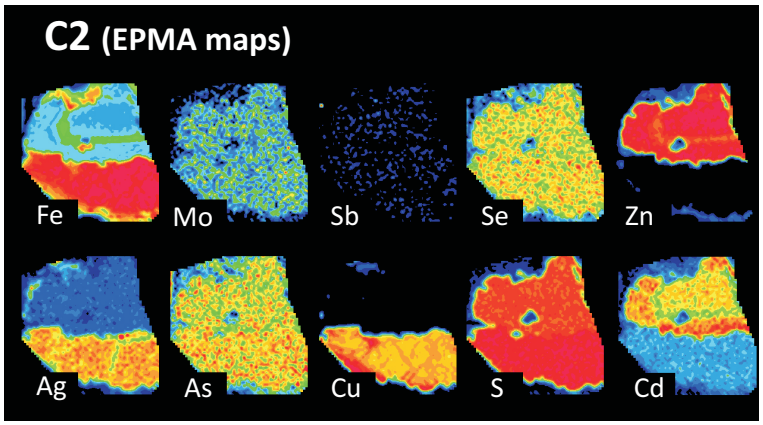

A2
0.1 mm

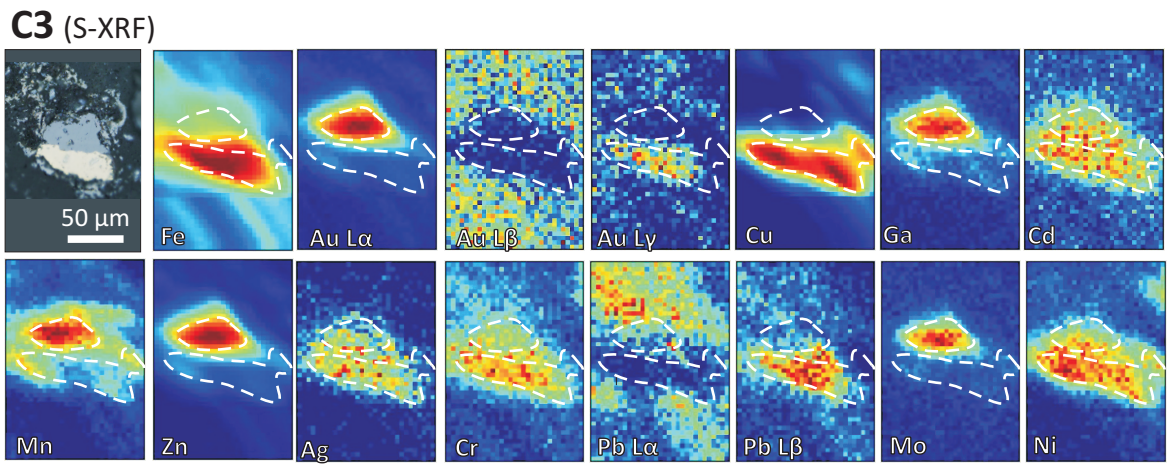

AuLα1
AuLβ1
AuLγ1
CdLα1
CrKα1
CuKα1
FeKα1
GaKα1
LaLα1
MnKα1
MoKα1
NiKα1
PbLα1
PbLβ1
ZnKα1


A3
0.1 mm

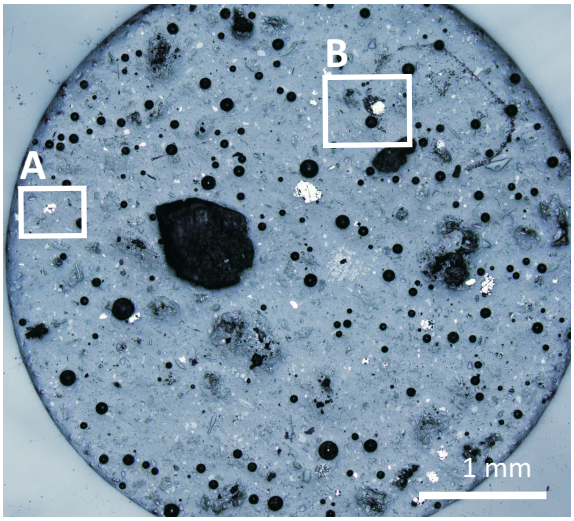

B1
100 µm
NiKα1
AuLα1
AuLβ1
AuLγ1
MnKα1
MoKα1
CdLα1
CrKα1
CuKα1
PbLα1
PbLβ1
FeKα1
GaKα1
ZnKα1


C1
180°
0.1 mm


C2 (EPMA maps)
Fe
Mo
Sb
Se
Zn
Ag
As
Cu
S
Cd

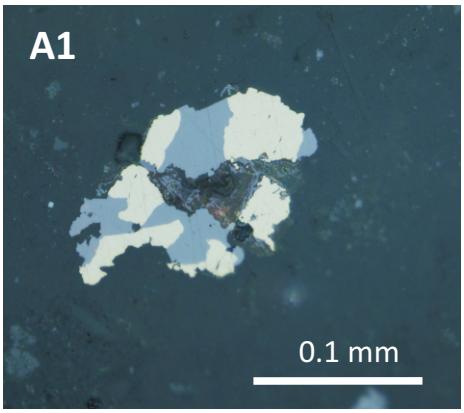

C3 (S-XRF)
50 µm
Fe
Au Lα
Au Lβ
Au Lγ
Cu
Ga
Cd
Mn
Zn
Ag
Cr
Pb Lα
Pb Lβ
Mo
Ni

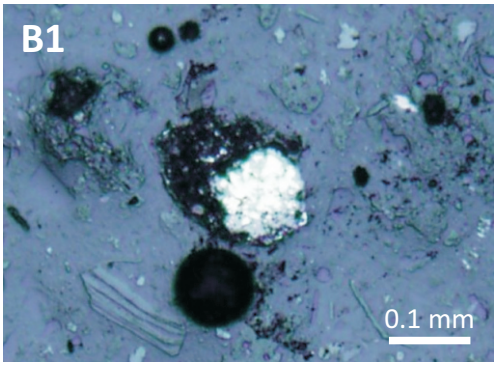
Grain Mount 7:

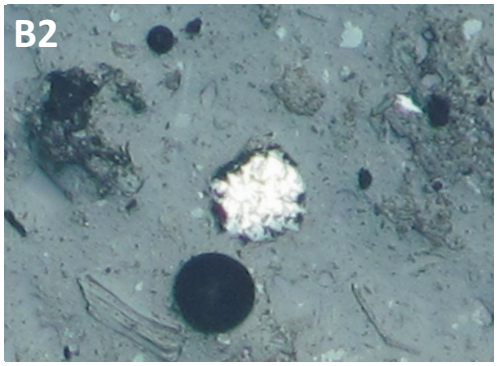


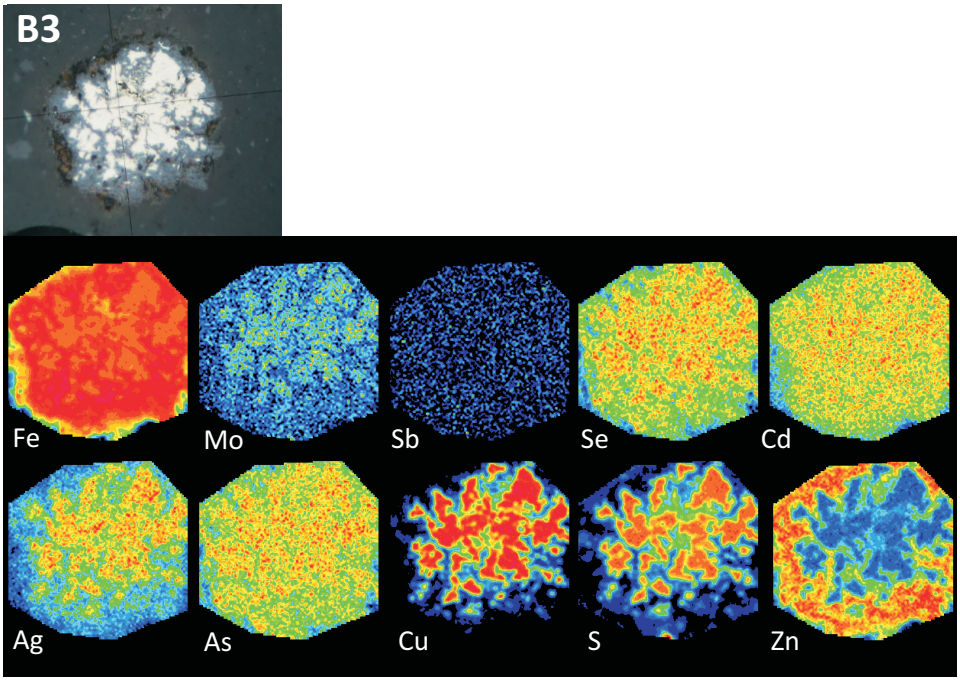

The areas of interest in this grain mount are indicated in the image on the left in reflected light; images A1 and B1 are details of these areas.

The texture of the sphalerite-chalcopyrite aggregate in A1 suggests rapid simultaneous precipitation of the two sulfide minerals. A chalcopyrite grain with a Zn-rich alteration halo (likely formed during core storage) was not influenced by re-polishing (reflected light image before re-polish in B2), but material around the grain was removed. The halo is composed of Fe (>35 wt.%), some Zn (~10 wt.%) and little sulfur (EPMA map in B3). Maximum trace metal concentrations are relatively low (Table E.1).

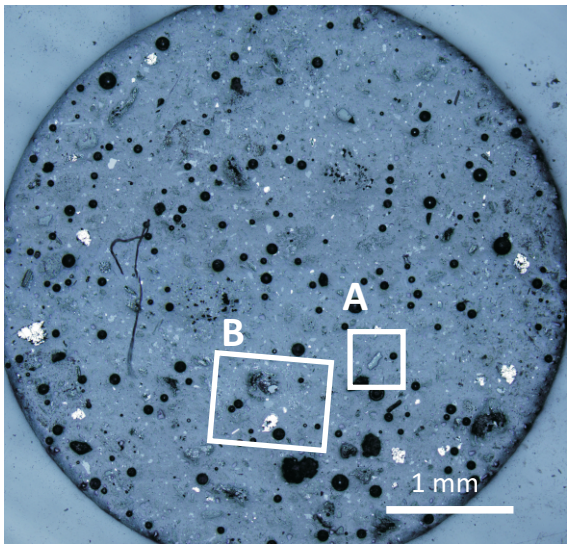

A1
0.1 mm


B1
0.1 mm


B2


B3
Fe
Mo
Sb
Se
Cd
Ag
As
Cu
S
Zn

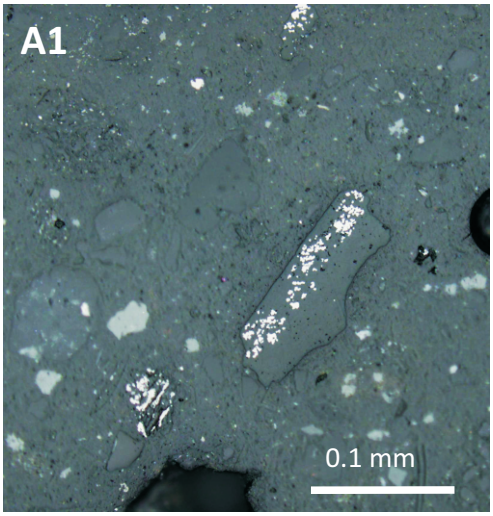
Grain Mount 10:

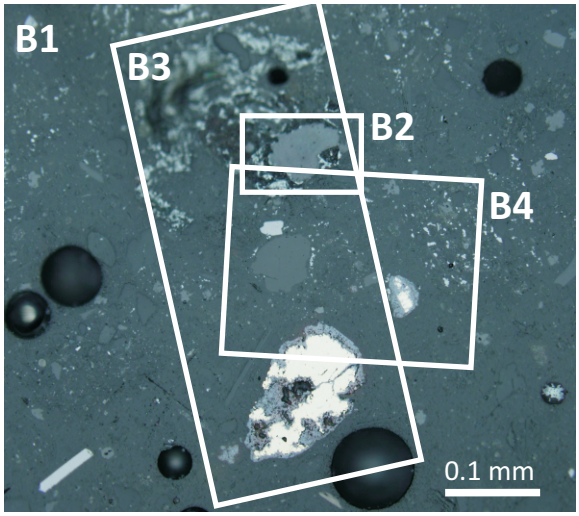


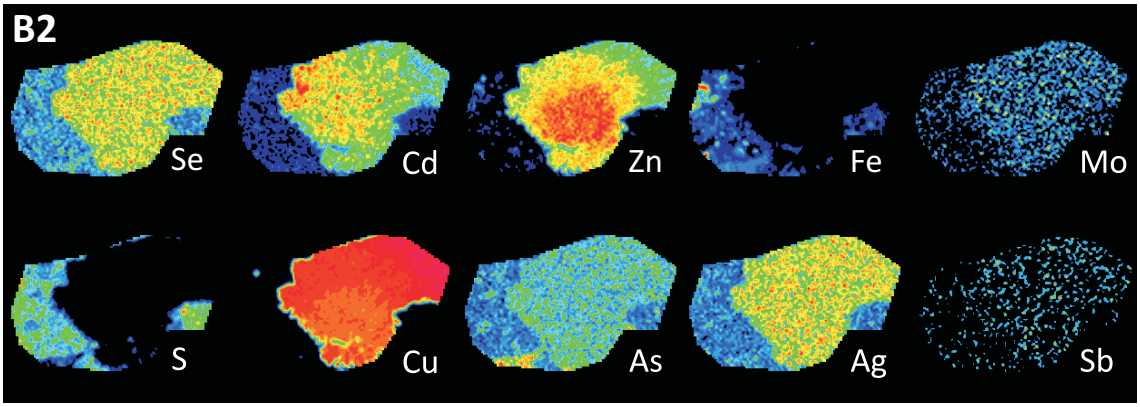

The areas of interest in this grain mount are indicated in the image on the left in reflected light; images A1 and B1 are details of these areas. Images B2 and B3 are EPMA and S-XRF maps (respectively) of the areas indicated in B1

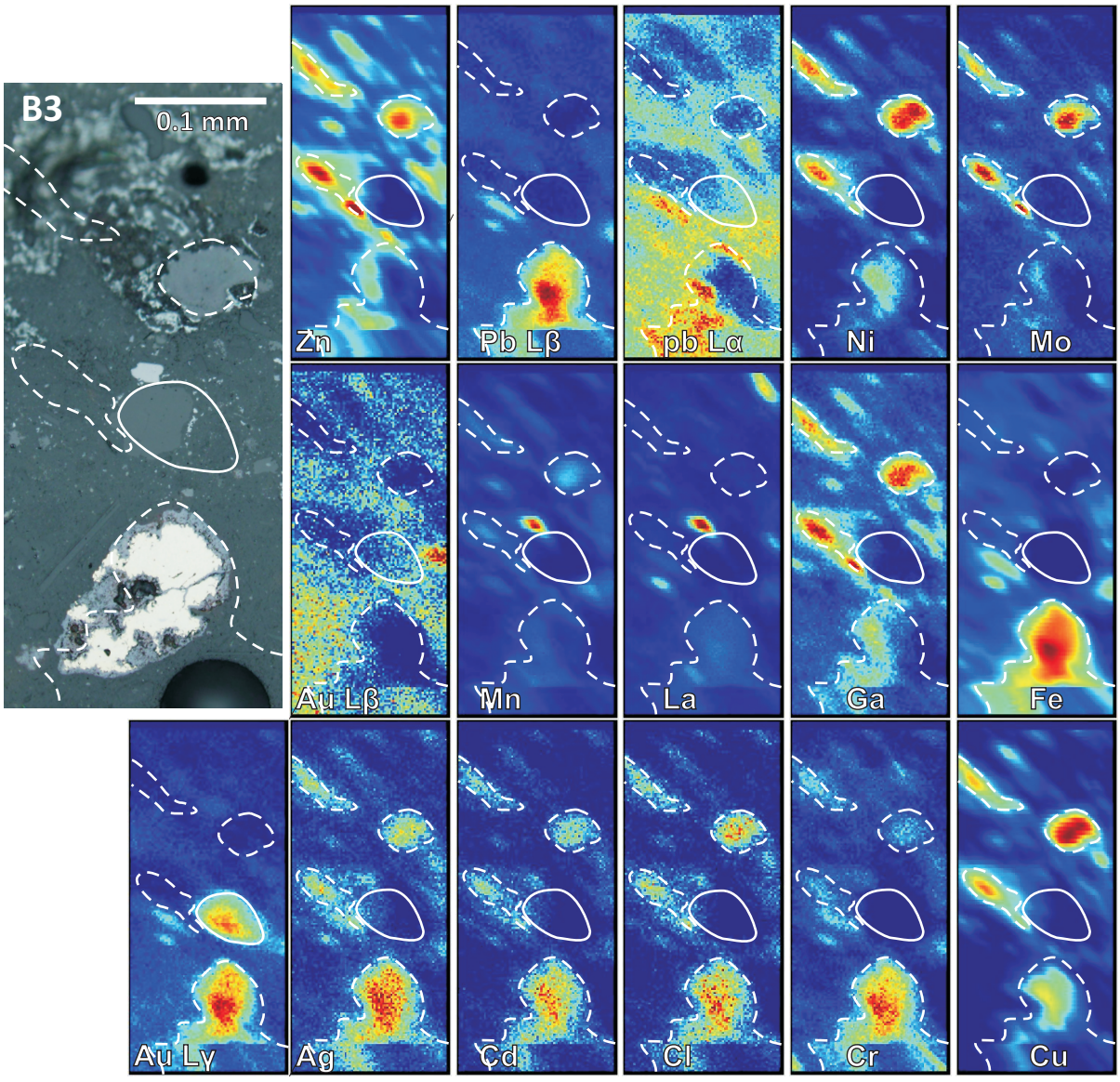
Intensely altered particles are discriminated from the matrix only by an obvious border outline (A1) and may be pseudomorphs after sphalerite, which has been completely dissolved and partly replaced by Zn-rich nonsulfide (the patchy, bright light blue infill). A clay or oxide in B2 (EPMA map) is composed of ~30 wt.% Cu with up to ~10 wt.% Zn, and is devoid of sulfur; maximum trace metal concentrations are low (Table E.1).

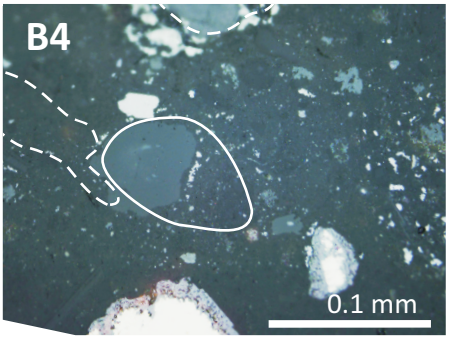
The S-XRF map of an area with a chalcopyrite grain and several nonsulfide phases (B3) shows that many of the grains have a poor surface expression. Au Lα correlates with Zn and Au Lβ with As, consistent with peak overlap, and Au Lγ interferes with the doubling peak of Fe in chalcopyrite. However, one particle in the middle of the mapped area does not correlate with these interfering peaks (detail in B4) and may reflect Au enrichment in an unidentified silicate phase.


A1
0.1 mm

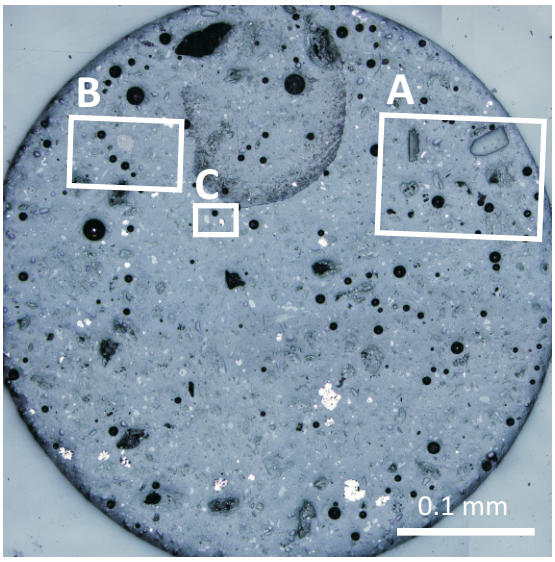

B1
B3
B2
B4
0.1 mm


B2
Se
Cd
Zn
Fe
Mo
S
Cu
As
Ag
Sb


B3
0.1 mm
Zn
Pb Lβ
pb Lα
Ni
Mo
Au Lβ
Mn
La
Ga
Fe
Au Lγ
Ag
Cd
Cl
Cr
Cu

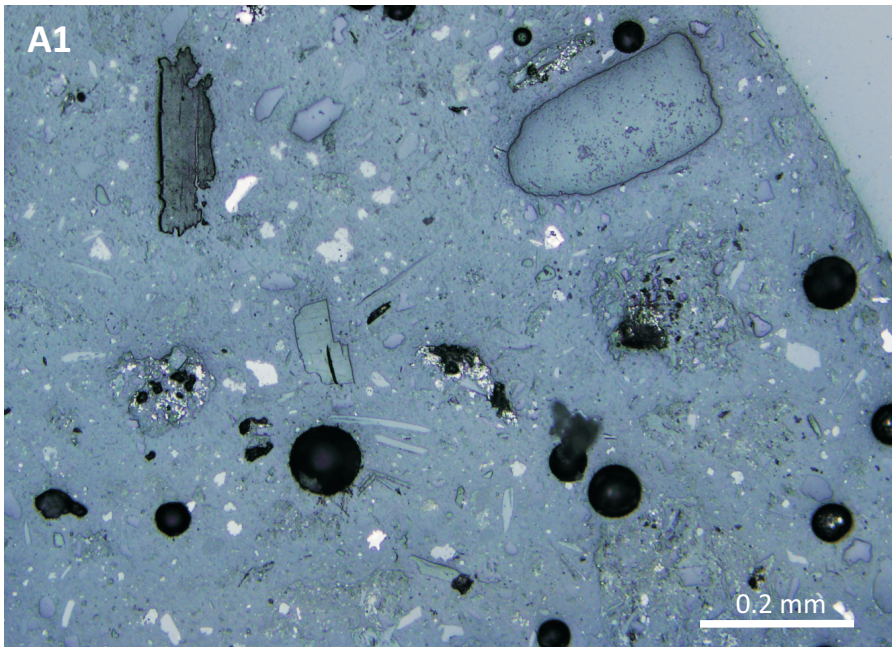

B4
0.1 mm

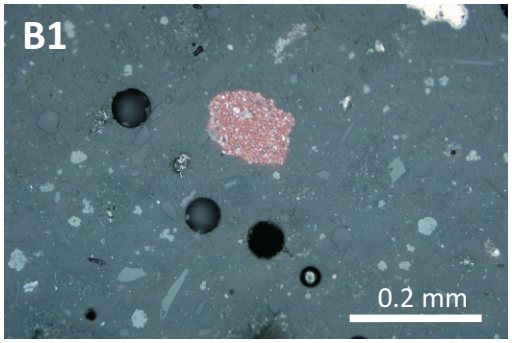
Grain Mount 11:

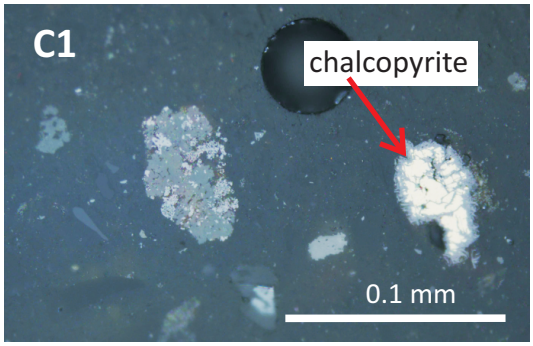



The areas of interest in this grain mount are indicated in the image on the left in reflected light; images A1, B1 and C1 are details of these areas.

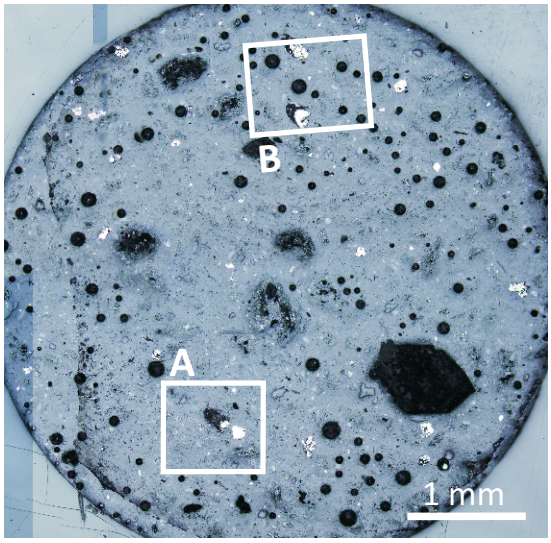
The detailed images show examples of nonsulfides that have been dissolved and variably replaced. These phases could not be positively identified. The nonsulfide grains have various forms, sizes, and colors and may have sharp or indistinct boundaries (A1). The red grain in B1 might be a relict chalcopyrite grain (compare to Figure A1 from mount 5 in this sample, which shows an earlier stage of the dissolution process). An example of a partly dissolved grain in which the original form is still clearly seen is shown in C1.


A1
0.2 mm


B1
0.2 mm


C1
chalcopyrite
0.1 mm

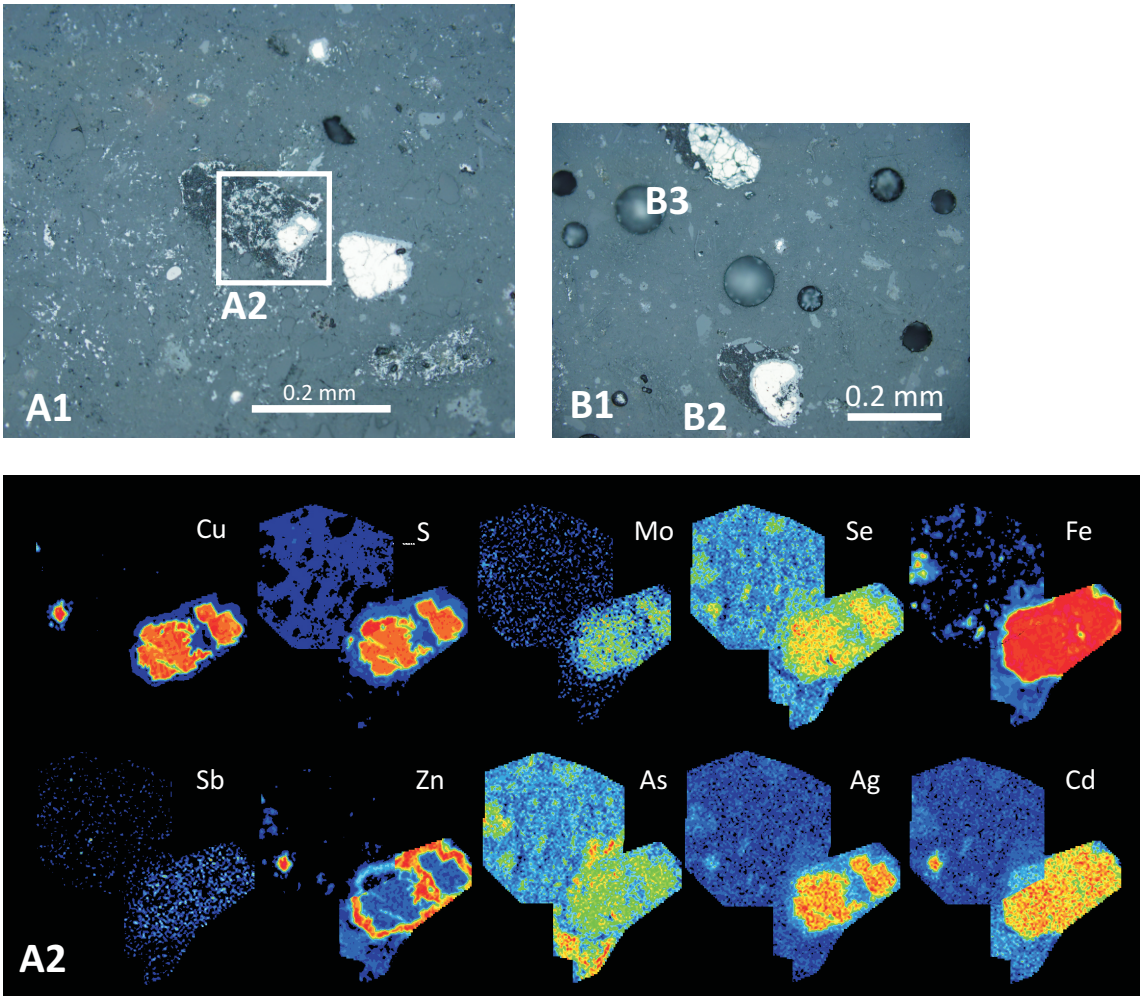
Grain Mount 12:



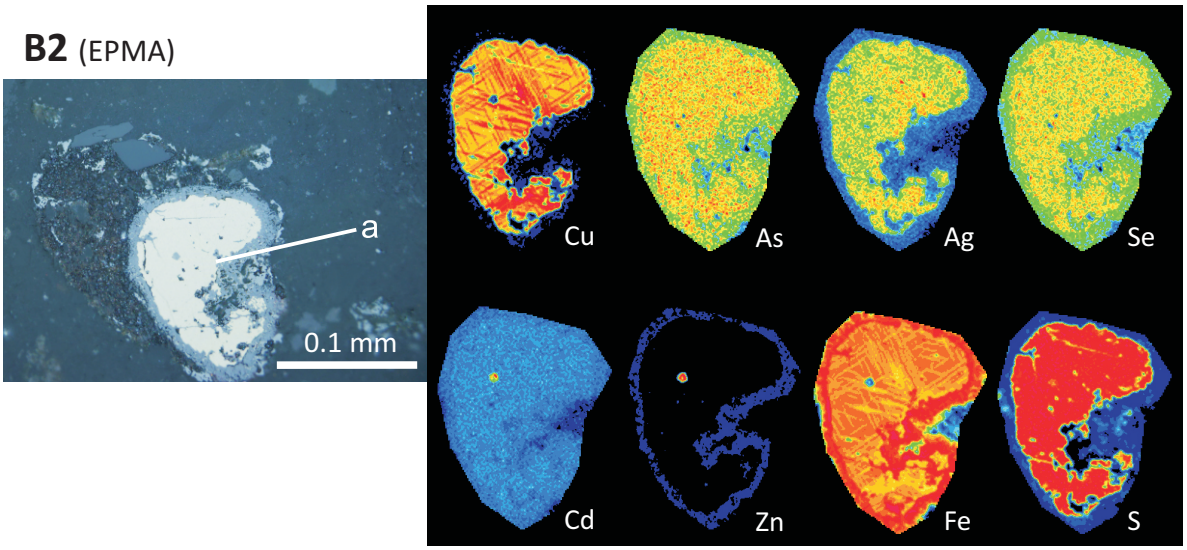

The areas of interest in this grain mount are indicated in the image on the left in reflected light; images A1 and B1 are details of these areas. Images A2, B2 and B3 are EPMA maps of texturally different chalcopyrite grains. All of the grains have Zn-enriched alteration haloes and are now surrounded by rounded areas of empty space, which emerged during re-polishing (all images taken after re-polishing). EPMA maps in A2 comprise two parts. The top-part covers a nonsulfide with high Zn and Cd concentrations (~40 wt.% Zn); the lower part is chalcopyrite (cf. Table E.1). Chalcopyrite is by far the most important host for Ag (max. 150 counts) and Se (120 counts). The alteration rim is high in Fe and contains ~10 wt.% Zn, but is low in trace metals.

Exsolution laminae are typical in chalcopyrite (EPMA maps in B2). The sharp interface between the chalcopyrite grain and the alteration halo suggests that this texture is not an artifact of sample preparation. The rim is chemically similar to the rim in A2, but in B2 the maximum Zn concentration corresponds to sphalerite (inclusion in chalcopyrite). The rim might be composed of Fe-(oxy)hydroxides as suggested by the high Fe-concentration (>chalcopyrite) and may have functioned as Fe-(oxy)hydroxide “armor” against dissolution (cf. Chapter 2). Sphalerite has high Cd concentration and chalcopyrite high Ag concentration (230 and 170 counts, respectively), similar to that observed in composite grains (mount 5 of this sample). Other trace metal concentrations are relatively low (Table E.1) and evenly distributed between sphalerite and chalcopyrite.

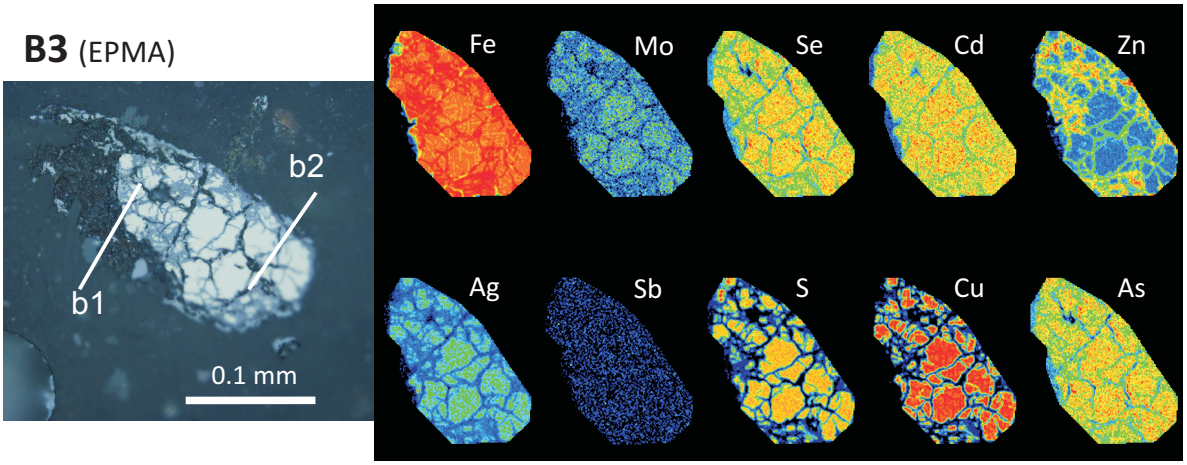
More intensive dissolution of chalcopyrite (B3) may be due to more abundant fracturing or other heterogeneity in the original sulfide grain. S-XRF spectra from spot analyses (a, b1, b2; locations indicated in images B2 and B3) are shown in image B4 and illustrate the variation in Cu, Zn and Fe concentrations between the cores and rims of the grains.



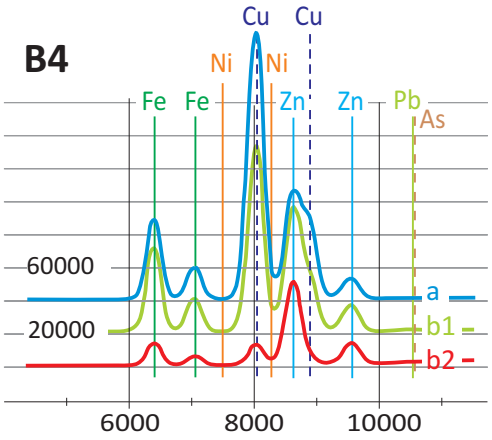
**B2** (EPMA)



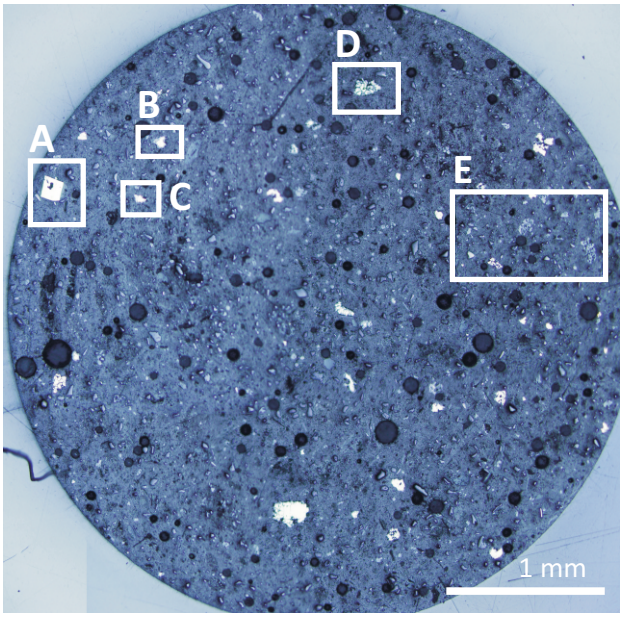

**B3** (EPMA)




**B4**



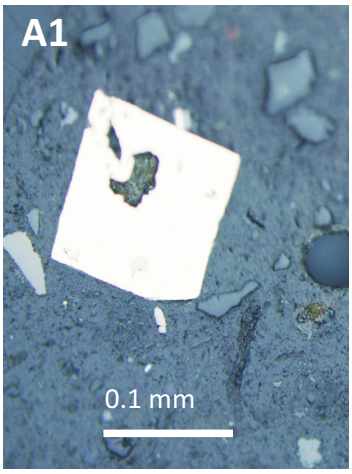
Grain Mount 13:

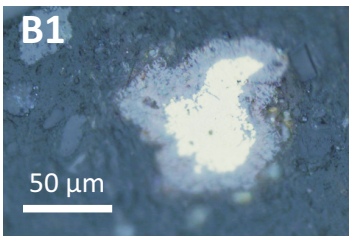


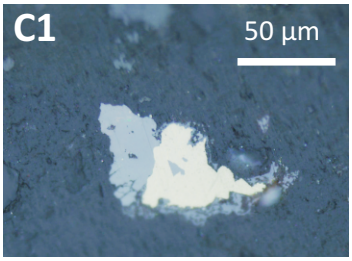

A second polished block from sample 268-985 was prepared, and one of the grain mounts is shown in reflected light on the left. The locations of detailed images A1, B1, C1, D1 and E1 are indicated. Images A2 and A3 are EPMA and S-XRF maps (respectively) of the large euhedral pyrite grain in A1

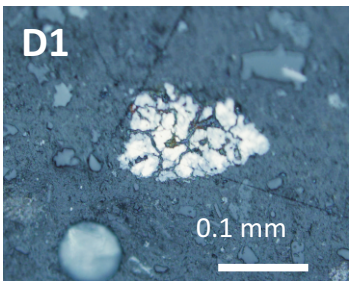
.

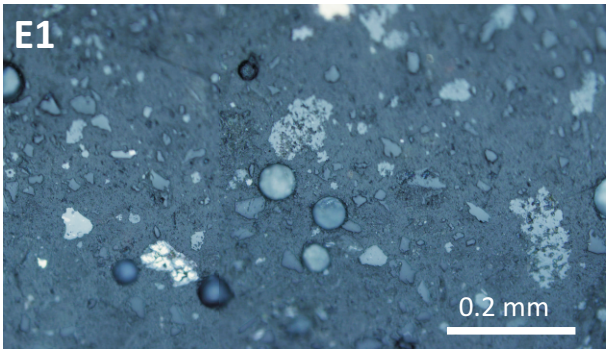
Almost all trace metal concentrations are exceptionally low in the euhedral pyrite grain (EPMA maps in A2) compared to the sub- to anhedral pyrite and especially the small framboids. Arsenic counts (~80) are >70% lower than in the rims of the framboidal pyrite (~1.6 wt.% As in sample 503-912 mount 4; cf. Chapter 2). Maximum concentrations of other metals (yellow) are <2 wt.% Cu and ~15 wt.% Zn, with very low Ag, Cd, Se, Sb, and Mo (Table E.1). Maps in A2 were done at the University of Ottawa using the same instrument and parameters as was used at GEOMAR for the other EPMA maps; counts can be directly compared between the two. Whereas correlation between the S-XRF maps and the surface expressions of the grains in A3 is clear, the spot of highest Cu, Zn, Ni and Cr has no surface expression. A Zn-rich alteration rim is clearly seen on chalcopyrite (B1), a sphalerite-chalcopyrite aggregate is seen in C1, and intense alteration along fractures in chalcopyrite is seen in D1. Various nonsulfides, some with little sulfide preserved in the core, are seen in E1.



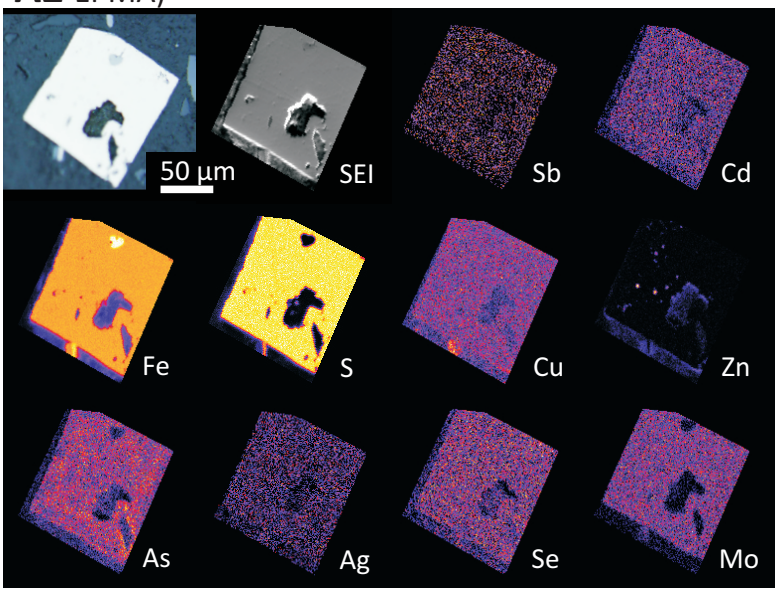



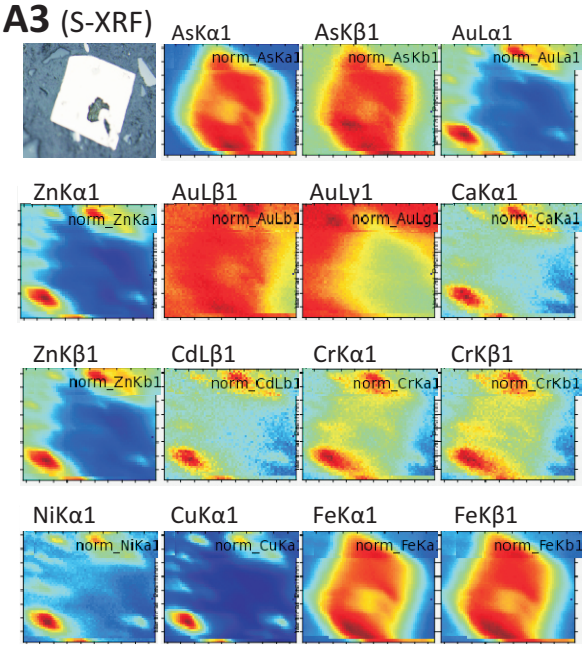




**A2** EPMA)

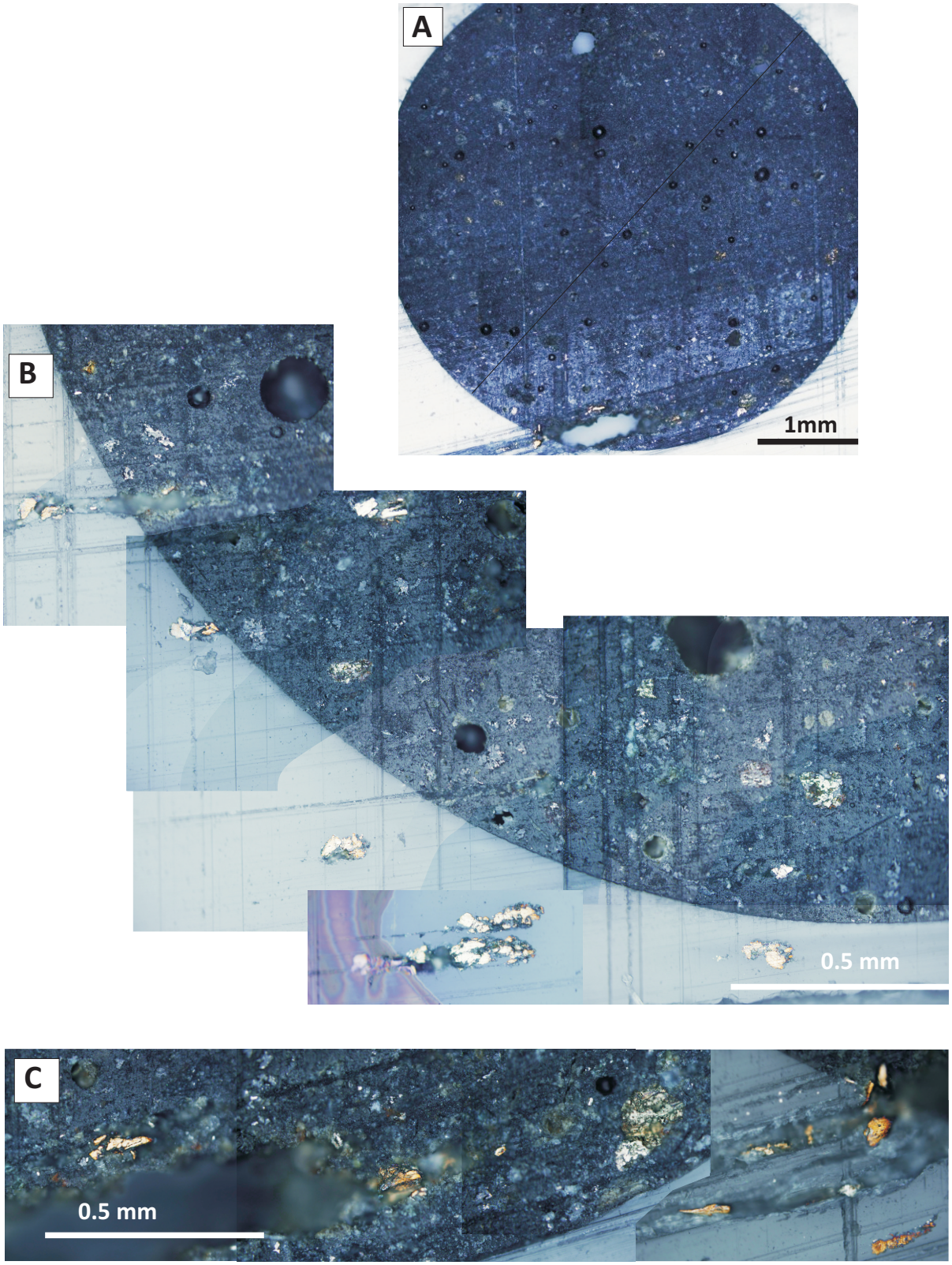



**A3** (S-XRF)



Appendix E. Ultrathin sections of Sample 268-985.

An ultrathin section of sample 268-985 was also prepared for S-XRF analyses (shown in A, with more detailed images in B and C). Multiple grains of pyrite and chalcopyrite were studied by elemental mapping, spot analyses and line scans, but no clear indication of trace metal enrichment was found (special attention was paid to Ga and Au). In these sections the correlation between elemental map and surface expression is more clear than in other S-XRF maps because the amount of material penetrated by the X-rays is small, thus decreasing the likelihood of finding discrete zones of Au enrichment. Some larger grains were mounted separately (solitary grains outside the original sample in B), but no Au-enrichment was detected.

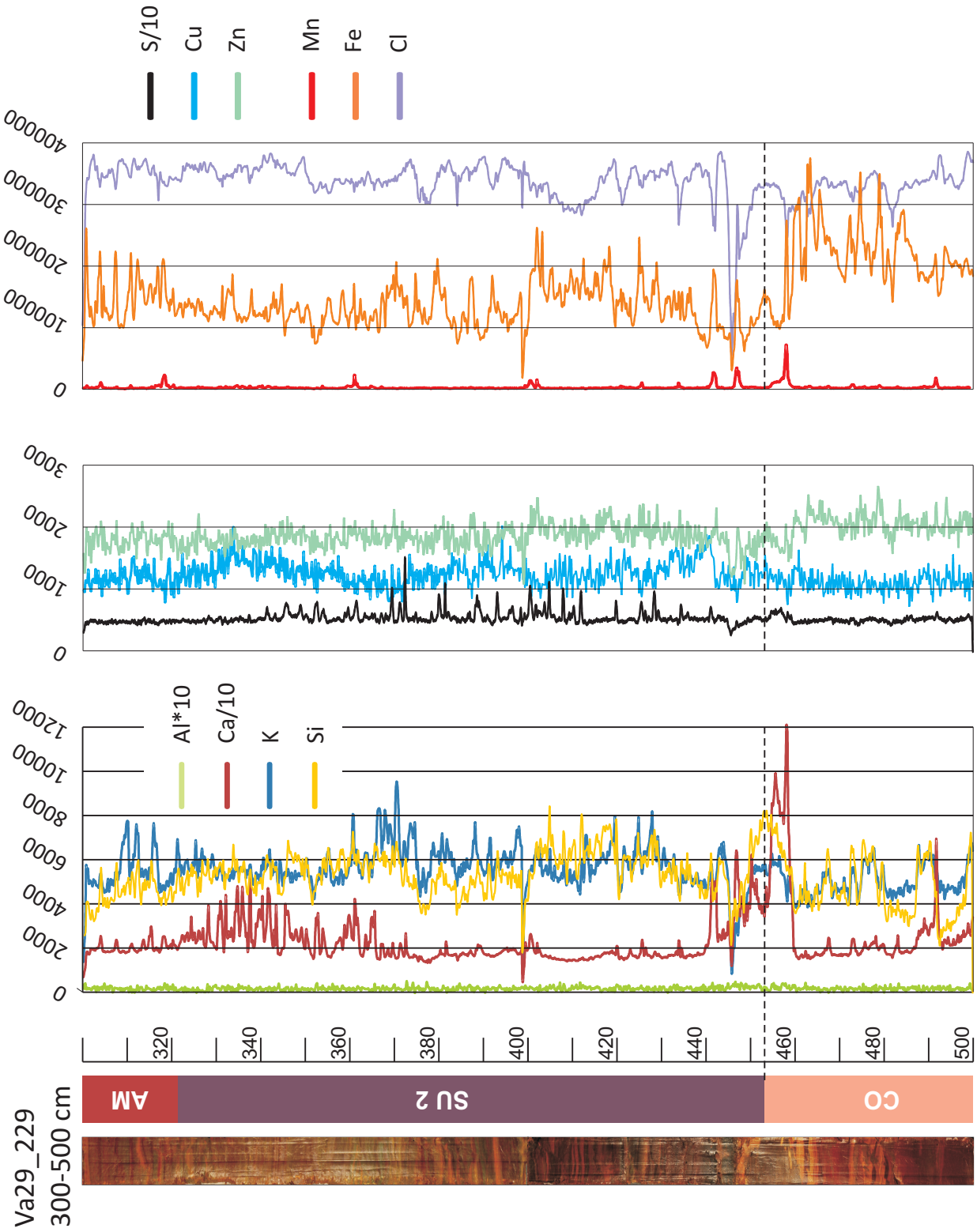

A
1mm
B
0.5 mm
C
0.5 mm

Appendix F. XRF core scans.

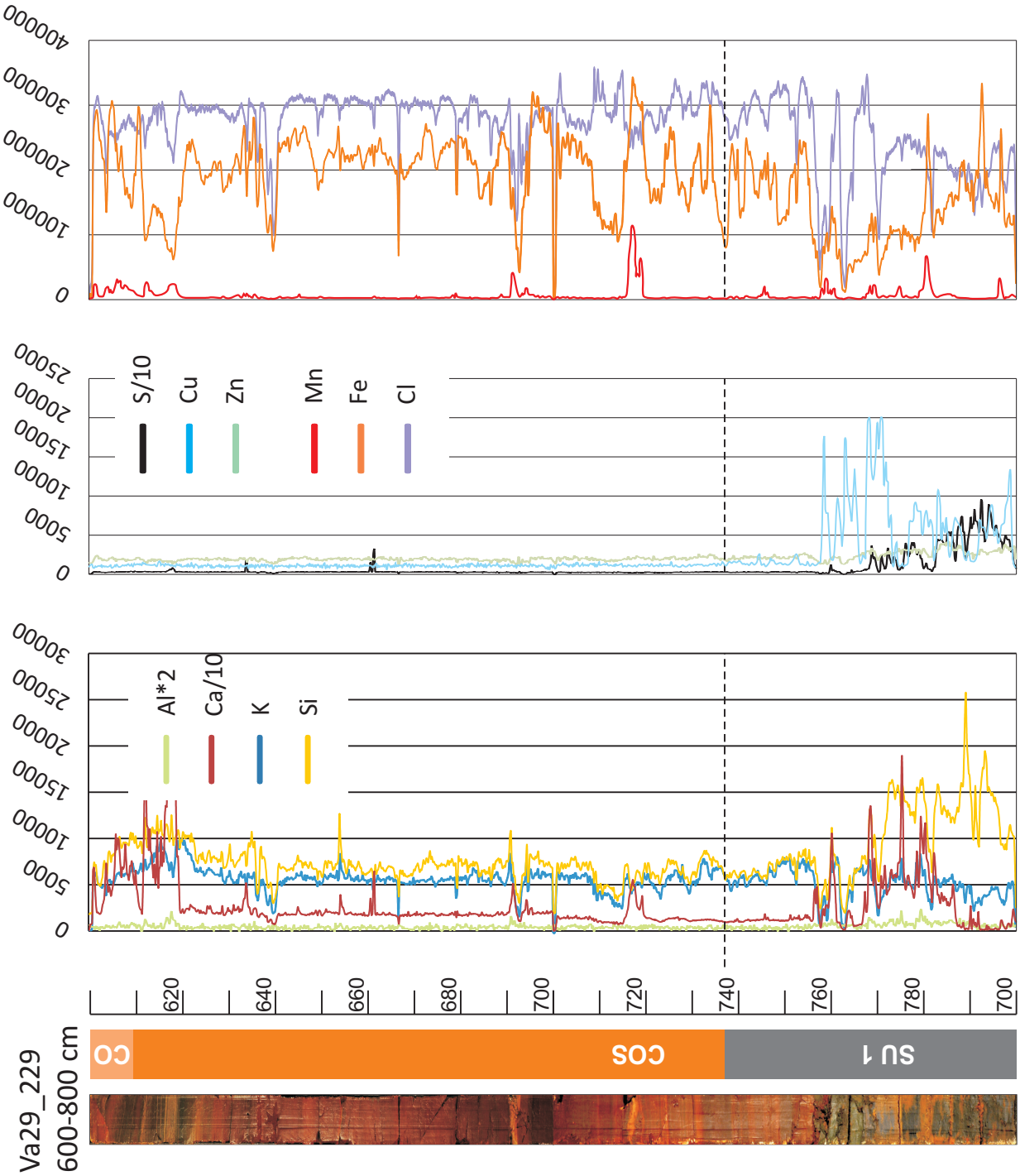
XRF core scans were performed at the University of Kiel as a part of Master's thesis project of Simon Jost. Both cores (Va29_229 and Va22_275) are located in the North of the Deep (cf. Appendix B.1), where the strata is more condensed. Both cores were in excellent condition with smooth surfaces required for the core scanning. Sections 300-500 cm and 600-800 cm in core Va29_229 cover stratigraphic units from SU1 to AM, and section 500-600 cm in core Va22_275 is at the border of units COS and SU2.

Scans of core Va29_229 illustrate the increase in amplitude of elemental variation between laminae with depth in the sediments, suggesting that the sharp lamination formed during diagenesis of poorly crystalline primary phases.

Scans of core Va22_275 show stratigraphic unit CO (and sub-unit COS), which is the only unit where abundant Mn-oxides have been observed. At high Mn concentrations, Fe and Mn are inversely correlated (separate Fe- and Mn-(oxy)hydroxide layers); elsewhere Fe and Mn correlate because both are present together in hydrothermal carbonate. See Chapters 2 and 3 for further discussion.


S/10
Cu
Zn
Mn
Fe
Cl
400000
300000
200000
100000
0
3000
2000
1000
0
Al*10
Ca/10
K
Si
12000
10000
8000
6000
4000
2000
0
320
340
360
380
400
420
440
460
480
500
AM
SU 2
CO
Va29_229
300-500 cm

Appendix F. XRF core scans.



Appendix F. XRF core scans.

